

Felix Binder

Luis A. Correa

Christian Gogolin

Janet Anders

Gerardo Adesso *Editors*

# Thermodynamics in the Quantum Regime

Fundamental Aspects and  
New Directions

# **Fundamental Theories of Physics**

## **Volume 195**

### **Series editors**

Henk van Beijeren, Utrecht, The Netherlands  
Philippe Blanchard, Bielefeld, Germany  
Bob Coecke, Oxford, UK  
Dennis Dieks, Utrecht, The Netherlands  
Bianca Dittrich, Waterloo, ON, Canada  
Detlef Dürr, Munich, Germany  
Ruth Durrer, Geneva, Switzerland  
Roman Frigg, London, UK  
Christopher Fuchs, Boston, MA, USA  
Domenico J. W. Giulini, Hanover, Germany  
Gregg Jaeger, Boston, MA, USA  
Claus Kiefer, Cologne, Germany  
Nicolaas P. Landsman, Nijmegen, The Netherlands  
Christian Maes, Leuven, Belgium  
Mio Murao, Tokyo, Japan  
Hermann Nicolai, Potsdam, Germany  
Vesselin Petkov, Montreal, QC, Canada  
Laura Ruetsche, Ann Arbor, MI, USA  
Mairi Sakellariadou, London, UK  
Alwyn van der Merwe, Denver, CO, USA  
Rainer Verch, Leipzig, Germany  
Reinhard F. Werner, Hanover, Germany  
Christian Wüthrich, Geneva, Switzerland  
Lai-Sang Young, New York City, NY, USA

The international monograph series “Fundamental Theories of Physics” aims to stretch the boundaries of mainstream physics by clarifying and developing the theoretical and conceptual framework of physics and by applying it to a wide range of interdisciplinary scientific fields. Original contributions in well-established fields such as Quantum Physics, Relativity Theory, Cosmology, Quantum Field Theory, Statistical Mechanics and Nonlinear Dynamics are welcome. The series also provides a forum for non-conventional approaches to these fields. Publications should present new and promising ideas, with prospects for their further development, and carefully show how they connect to conventional views of the topic. Although the aim of this series is to go beyond established mainstream physics, a high profile and open-minded Editorial Board will evaluate all contributions carefully to ensure a high scientific standard.

More information about this series at <http://www.springer.com/series/6001>

Felix Binder · Luis A. Correa  
Christian Gogolin · Janet Anders  
Gerardo Adesso  
Editors

# Thermodynamics in the Quantum Regime

Fundamental Aspects and New Directions



Springer

*Editors*

Felix Binder

School of Physical and Mathematical  
Sciences

Nanyang Technological University  
Singapore, Singapore

Luis A. Correa

School of Mathematical Sciences  
University of Nottingham  
Nottingham, UK

Christian Gogolin

ICFO: Institut de Ciencies Fotoniques  
Barcelona Institute of Science  
and Technology  
Castelldefels, Spain

Janet Anders

CEMPS, Physics and Astronomy  
University of Exeter  
Exeter, UK

Gerardo Adesso

School of Mathematical Sciences  
University of Nottingham  
Nottingham, UK

ISSN 0168-1222

Fundamental Theories of Physics

ISBN 978-3-319-99045-3

<https://doi.org/10.1007/978-3-319-99046-0>

ISSN 2365-6425 (electronic)

ISBN 978-3-319-99046-0 (eBook)

Library of Congress Control Number: 2018952905

© Springer Nature Switzerland AG 2018

This work is subject to copyright. All rights are reserved by the Publisher, whether the whole or part of the material is concerned, specifically the rights of translation, reprinting, reuse of illustrations, recitation, broadcasting, reproduction on microfilms or in any other physical way, and transmission or information storage and retrieval, electronic adaptation, computer software, or by similar or dissimilar methodology now known or hereafter developed.

The use of general descriptive names, registered names, trademarks, service marks, etc. in this publication does not imply, even in the absence of a specific statement, that such names are exempt from the relevant protective laws and regulations and therefore free for general use.

The publisher, the authors and the editors are safe to assume that the advice and information in this book are believed to be true and accurate at the date of publication. Neither the publisher nor the authors or the editors give a warranty, expressed or implied, with respect to the material contained herein or for any errors or omissions that may have been made. The publisher remains neutral with regard to jurisdictional claims in published maps and institutional affiliations.

This Springer imprint is published by the registered company Springer Nature Switzerland AG  
The registered company address is: Gewerbestrasse 11, 6330 Cham, Switzerland

# Preface

In the last two decades, experimental advances in quantum physics have made it possible to prepare and exquisitely control quantum systems that are increasingly large and complex. Today, tens of ions can be trapped and shuttled at will in segmented microtraps, clouds of cold bosons are routinely loaded into optical lattices and interfered, superconducting qubits in microwave cavities allow the observation of quantum trajectories, and nanoparticles can be levitated and cooled to low temperatures. Meanwhile, macroscopic thermodynamics and classical statistical physics, which predate quantum theory, have started to push towards smaller scales. Fluctuation relations now extend the second law of thermodynamics, originally phrased for processes between equilibrium states, to general non-equilibrium processes.

The field of *Quantum Thermodynamics* is concerned with closing the gap between the small world of quantum mechanics and the large classical equilibrium world of thermodynamics by bringing together these recent developments. It aims to build a new thermodynamic framework that goes beyond the conventional regime of validity of macroscopic thermodynamics to account for *finite size effects*, *non-equilibrium dynamics* and *quantum properties*.

Questions addressed in Quantum Thermodynamics include:

- How can process-dependent thermodynamic quantities, such as *work* and *heat*, be meaningfully defined and measured in quantum systems?
- What are the efficiencies of quantum engines and refrigerators? Are they *better* or *worse* than their classical counterparts?
- What opportunities and hurdles do quantum evolution of closed and open systems imply for finite-time thermodynamics?
- How do non-equilibrium fluctuation relations extend to the quantum regime?
- How does equilibrium of a closed or open quantum many-body system arise from microscopic dynamics and properties?
- Which corrections to standard thermodynamic laws and relations have to be made when considering systems that couple strongly to their surroundings?

- What implications does the link between information and thermodynamics, first established by Landauer, have in the quantum regime?
- Which are the thermodynamic resources required to generate certain quantum states?
- How can corrections to standard thermodynamics arising from quantum (non-equilibrium or finite size) properties, be measured?
- Do quantum phenomena, such as coherence, contextuality, non-commutativity, or correlations, result in thermodynamic advantages or barriers?

Over the past years, research in quantum thermodynamics has blossomed due to advances in theoretical concepts and experimental methods. It has been supported in no small part by the EU-funded research network “*Thermodynamics in the Quantum Regime*” (COST MP1209). The network has brought together a community of researchers with backgrounds in statistical mechanics, quantum information theory, quantum optics, mesoscopic physics and quantum many-body physics, fostering collaborative research across these fields. It also promoted and funded a series of meetings between 2013 and 2017, establishing the Quantum ThermoDynamics conference series (QTD). The first of these events were held in Berlin (2014), Palma de Mallorca (2015), Porquerolles (2015), Erice (2016), and Oxford (2017). In 2018, a successor conference was held in Santa Barbara.

In view of the many exciting developments within the COST network and beyond, we decided to put together this book in order to provide a global account of recent advances in the field, and to discuss the most promising future directions, both from the experimental and from the theoretical side. The book has six parts, each containing several autonomous chapters. These aim to be accessible introductions to each individual topic and, at the same time, to provide an updated overview of the state of the art. Connections between related chapters are frequently pointed out. Since this is an active and expanding area of research, the present book certainly cannot provide the final word on quantum thermodynamics. Instead, we hope that it will offer a stepping stone for researchers who are new to the field and wish to explore this frontier of modern physics, as well as a useful reference for experts.

**Introduction.** The book begins with a historical perspective on the development of the field written by Robert Alicki and Ronnie Kosloff, two pioneers in quantum thermodynamics (Chap. 1).

**Part I: Continuous and Discrete Quantum Heat Devices.** This part summarises recent research on energy-conversion cycles in the quantum regime, including continuous and discrete quantum thermodynamic cycles. The focus is placed on their performance optimisation (see Chaps. 2, 3 and 5) and the role of genuinely “quantum effects” in their operation (see Chaps. 4 and 9). Potential physical implementations (Chaps. 6 and 7), and the issue of energy storage and power (Chap. 8) are also covered.

**Part II: Fluctuating Work and Irreversibility in the Quantum Regime.** This part covers the fundamental issue of the identification of fluctuating thermodynamic variables in the quantum regime. Chapters 10 and 12 give an introduction to quantum fluctuation theorems. The elusive notion of fluctuating quantum “work” in the presence of quantum coherence is discussed in Chapter 11. As shown in Chapter 13, work statistics can encode relevant features of non-equilibrium many-body systems and they can be measured in practice (Chap. 14). Chapter 15 adopts an open-system viewpoint, permitting the definition of thermodynamics variables along the stochastic trajectories which unravel the dissipative dynamics. Finally, the characterisation of irreversible entropy production in open systems is addressed in Chapter 16.

**Part III: Equilibration and Thermalization.** This part focusses on the emergence of thermodynamic behaviour from a quantum many-body viewpoint. It revisits the notorious problem of determining the time scale over which quantum systems appear to reach equilibrium, and the onset of typical dynamical behaviour (Chaps. 17 and 18). Chapter 19 investigates to which extent the dynamics of a many-body system can be addressed by means of random matrix theory during equilibration. This part also includes a general overview of properties of many-body systems in thermal equilibrium and, in particular, correlations in their thermal states (Chap. 20). Finally, the emergent topic of quantum thermometry is introduced; special emphasis is placed on the potential role of genuinely quantum effects in the enhancement of thermometric precision (Chap. 21).

**Part IV: Thermodynamics of Strongly-Coupled Open Systems.** This part summarises new theoretical tools for the description of quantum systems strongly coupled to their baths that go beyond the standard open systems approach, predominant in the last four decades. Chapter 22 introduces the Hamiltonian of mean force and how this concept is used to extend thermodynamics and identify strong coupling corrections. Chapter 23 describes an effective “embedding” technique based on the reaction coordinate mapping, which allows to solve a system’s open dynamics beyond the limit of weak coupling. Chapter 24 describes the hierarchical equations of motion which allows numerical solutions to all orders in the coupling strength. This part ends with a discussion of the third law of thermodynamics and ultimate limits to cooling in Chapter 25.

**Part V: Information-Theoretic Approaches to Quantum Thermodynamics.** In this part, a modern approach to quantum thermodynamics is offered by the Thermal Operations framework which uses quantum information theory tools and treats non-thermal states as thermodynamic resources (Chap. 26). The role of information theoretic entropies in relation to single-shot thermodynamics is described in Chapter 27, while Chapter 32 takes error-tolerant, “smoothed” entropies as a starting point for an axiomatic approach to quantum thermodynamics. Chapter 28 takes a closer look at the Clausius formulation of the Second Law, stressing how various related inequalities can be derived and used in practical scenarios. Chapter 29 examines the fundamental thermodynamic role of quantum information itself in the

context of information erasure. Genuine quantum phenomena are addressed in the following two chapters: Chapter 30 examines the energetic value of quantum correlations, while non-commutativity of conserved charges is discussed in Chapter 31. Lastly, Chapter 33 takes information conservation as starting point for an axiomatic framework of quantum thermodynamics.

**Part VI: Experimental Platforms for Quantum Thermodynamics.** This part summarises recent advances in experimentally testing thermodynamics in the quantum regime, using a variety of platforms. One-dimensional atomic superfluids, a proven platform for the observation of equilibration dynamics, and single-electron boxes, which allow the detailed analysis of thermodynamic fluctuations, are introduced in Chapters 37 and 34, respectively. Levitated nanoparticles, which allow the exploration of single-particle thermodynamics with a macroscopic particle in the underdamped regime, are described in Chapter 35. The first realisation of a single atom heat engine in a tapered ion trap is summarised in Chapter 36 while experimental tests of quantum work fluctuation relations with trapped ions are described in Chapter 38. Photonic and superconducting circuit experiments that realise “Maxwell demons” and evidence the link between information and thermodynamics are discussed in Chapters 39 and 40. Lastly, NV centres in diamond (Chap. 41) are introduced as an experimental platform to test quantum thermodynamics in the laboratory.

We are grateful to Springer for making this book possible, to the reviewers for their constructive feedback, and, most of all, to all authors for their excellent contributions. We hope that readers will find this book useful as a reference and that the individual chapters will inspire future research in the exciting field of quantum thermodynamics.

Singapore, Singapore  
Nottingham, UK  
Barcelona, Spain  
Exeter, UK  
Nottingham, UK  
July 2018

Felix Binder  
Luis A. Correa  
Christian Gogolin  
Janet Anders  
Gerardo Adesso

# Contents

<b>1</b>	<b>Introduction to Quantum Thermodynamics: History and Prospects . . . . .</b>	1
	Robert Alicki and Ronnie Kosloff	
<b>Part I Continuous and Discrete Quantum Heat Devices</b>		
<b>2</b>	<b>Thermodynamic Principles and Implementations of Quantum Machines . . . . .</b>	37
	Arnab Ghosh, Wolfgang Niedenzu, Victor Mukherjee and Gershon Kurizki	
<b>3</b>	<b>Performance of Quantum Thermodynamic Cycles . . . . .</b>	67
	Tova Feldmann and José P. Palao	
<b>4</b>	<b>Quantum Features and Signatures of Quantum Thermal Machines . . . . .</b>	87
	Amikam Levy and David Gelbwaser-Klimovsky	
<b>5</b>	<b>Friction-Free Quantum Machines . . . . .</b>	127
	Adolfo del Campo, Aurélia Chenu, Shujin Deng and Haibin Wu	
<b>6</b>	<b>Physical Implementations of Quantum Absorption Refrigerators . . . . .</b>	149
	Mark T. Mitchison and Patrick P. Potts	
<b>7</b>	<b>Quantum Thermodynamics of Nanoscale Thermoelectrics and Electronic Devices . . . . .</b>	175
	Robert S. Whitney, Rafael Sánchez and Janine Splettstoesser	
<b>8</b>	<b>Quantum Batteries . . . . .</b>	207
	Francesco Campaioli, Felix A. Pollock and Sai Vinjanampathy	
<b>9</b>	<b>Quantum Rotor Engines . . . . .</b>	227
	Stella Seah, Stefan Nimmrichter, Alexandre Roulet and Valerio Scarani	

**Part II Fluctuating Work and Irreversibility in the Quantum Regime**

- 10** **Quantum Fluctuation Theorems** ..... 249  
Ken Funo, Masahito Ueda and Takahiro Sagawa
- 11** **Fluctuating Work in Coherent Quantum Systems: Proposals and Limitations** ..... 275  
Elisa Bäumer, Matteo Lostaglio, Martí Perarnau-Llobet and Rui Sampaio
- 12** **The Coherent Crooks Equality** ..... 301  
Zoe Holmes
- 13** **The Role of Quantum Work Statistics in Many-Body Physics** ..... 317  
John Goold, Francesco Plastina, Andrea Gambassi and Alessandro Silva
- 14** **Ancilla-Assisted Measurement of Quantum Work** ..... 337  
Gabriele De Chiara, Paolo Solinas, Federico Cerisola and Augusto J. Roncaglia
- 15** **Work, Heat and Entropy Production Along Quantum Trajectories** ..... 363  
Cyril Elouard and M. Hamed Mohammady
- 16** **Characterizing Irreversibility in Open Quantum Systems** ..... 395  
Tiago B. Batalhão, Stefano Gherardini, Jader P. Santos, Gabriel T. Landi and Mauro Paternostro

**Part III Equilibration and Thermalization**

- 17** **Dynamical Typicality for Initial States with a Preset Measurement Statistics of Several Commuting Observables** ..... 413  
Ben N. Balz, Jonas Richter, Jochen Gemmer, Robin Steinigeweg and Peter Reimann
- 18** **Equilibration Times in Closed Quantum Many-Body Systems** ..... 435  
Henrik Wilming, Thiago R. de Oliveira, Anthony J. Short and Jens Eisert
- 19** **Nonequilibrium Many-Body Quantum Dynamics: From Full Random Matrices to Real Systems** ..... 457  
Lea F. Santos and Eduardo Jonathan Torres-Herrera
- 20** **Properties of Thermal Quantum States: Locality of Temperature, Decay of Correlations, and More** ..... 481  
Martin Kliesch and Arnaud Riera
- 21** **Quantum Thermometry** ..... 503  
Antonella De Pasquale and Thomas M. Stace

**Part IV Thermodynamics of Strongly-Coupled Open Systems**

- 22 Hamiltonian of Mean Force for Strongly-Coupled Systems . . . . .** 531  
Harry J. D. Miller
- 23 The Reaction Coordinate Mapping in Quantum Thermodynamics . . . . .** 551  
Ahsan Nazir and Gernot Schaller
- 24 Hierarchical Equations of Motion Approach to Quantum Thermodynamics . . . . .** 579  
Akihito Kato and Yoshitaka Tanimura
- 25 Cooling to Absolute Zero: The Unattainability Principle . . . . .** 597  
Nahuel Freitas, Rodrigo Gallego, Lluís Masanes and Juan Pablo Paz

**Part V Information-Theoretic Approaches to Quantum Thermodynamics**

- 26 Resource Theory of Quantum Thermodynamics: Thermal Operations and Second Laws . . . . .** 625  
Nelly Huei Ying Ng and Mischa Prebin Woods
- 27 One-Shot Information-Theoretical Approaches to Fluctuation Theorems . . . . .** 651  
Andrew J. P. Garner
- 28 The Second Law and Beyond in Microscopic Quantum Setups . . . . .** 681  
Raam Uzdin
- 29 Information Erasure . . . . .** 713  
Toshio Croucher, Jackson Wright, André R. R. Carvalho,  
Stephen M. Barnett and Joan A. Vaccaro
- 30 Trade-Off Between Work and Correlations in Quantum Thermodynamics . . . . .** 731  
Giuseppe Vitagliano, Claude Klöckl, Marcus Huber and Nicolai Friis
- 31 Quantum Thermodynamics with Multiple Conserved Quantities . . . . .** 751  
Erick Hinds Mingo, Yelena Guryanova, Philippe Faist  
and David Jennings
- 32 Smooth Entropy in Axiomatic Thermodynamics . . . . .** 773  
Mirjam Weilenmann, Lea Krämer and Renato Renner
- 33 Thermodynamics from Information . . . . .** 799  
Manabendra Nath Bera, Andreas Winter and Maciej Lewenstein

**Part VI Experimental Platforms for Quantum Thermodynamics**

<b>34 One-Dimensional Atomic Superfluids as a Model System for Quantum Thermodynamics . . . . .</b>	823
Jörg Schmiedmayer	
<b>35 Single Particle Thermodynamics with Levitated Nanoparticles . . . . .</b>	853
James Millen and Jan Gieseler	
<b>36 Single Atom Heat Engine in a Tapered Ion Trap . . . . .</b>	887
Samuel T. Dawkins, Obinna Abah, Kilian Singer and Sebastian Deffner	
<b>37 Quantum Thermodynamics in a Single-Electron Box . . . . .</b>	897
Jonne V. Koski and Jukka P. Pekola	
<b>38 Probing Quantum Fluctuations of Work with a Trapped Ion . . . . .</b>	917
Yao Lu, Shuoming An, Jing-Ning Zhang and Kihwan Kim	
<b>39 Maxwell's Demon in Photonic Systems . . . . .</b>	939
Luca Mancino, Mario A. Ciampini, Mihai D. Vidrighin, Marco Sbroscia, Ilaria Gianani and Marco Barbieri	
<b>40 Maxwell's Demon in Superconducting Circuits . . . . .</b>	959
Nathanaël Cottet and Benjamin Huard	
<b>41 NV Color Centers in Diamond as a Platform for Quantum Thermodynamics . . . . .</b>	983
Nir Bar-Gill	

# Chapter 1

# Introduction to Quantum Thermodynamics: History and Prospects



Robert Alicki and Ronnie Kosloff

Quantum Thermodynamics is a continuous dialogue between two independent theories: Thermodynamics and Quantum Mechanics. Whenever the two theories have addressed the same phenomena new insight has emerged. We follow the dialogue from equilibrium Quantum Thermodynamics and the notion of entropy and entropy inequalities which are the base of the II-law. Dynamical considerations lead to non-equilibrium thermodynamics of quantum Open Systems. The central part played by completely positive maps is discussed leading to the Gorini–Kossakowski–Lindblad–Sudarshan “GKLS” equation. We address the connection to thermodynamics through the system-bath weak-coupling-limit WCL leading to dynamical versions of the I-law. The dialogue has developed through the analysis of quantum engines and refrigerators. Reciprocating and continuous engines are discussed. The autonomous quantum absorption refrigerator is employed to illustrate the III-law. Finally, we describe some open questions and perspectives.

## 1.1 Introduction

Quantum mechanics was conceived from a consistency argument on the nature of thermal emitted light. In 1900, Planck, as an act of despair, introduced a fix to the frequency distribution law of black body radiation [1]. In 1905 Einstein reanalysed the problem, based on consistency with thermodynamics, he writes: *In terms of heat theory monochromatic radiation of low density (within the realm of validity of Wien’s radiation formula) behaves as if it consisted of independent energy quanta*

---

R. Alicki

Institute of Theoretical Physics and Astrophysics, University of Gdańsk, Gdańsk, Poland

R. Kosloff (✉)

The Fritz Haber Research Center for Molecular Dynamics, The Institute of Chemistry,  
The Hebrew University of Jerusalem, 91904 Jerusalem, Israel

e-mail: ronnie@fh.huji.ac.il

of the magnitude  $h\nu$ . Einstein's conclusion is a quantised electromagnetic field [2] the dawn of quantum mechanics. From this point on, quantum mechanics developed independently eventually setting its own set of assumptions [3]. Currently, the consistency argument is used in reverse, deriving the laws of thermodynamics from the established quantum principles. This approach allows naturally the addition of dynamical out of equilibrium considerations.

In 1916 Einstein examined the relation between stimulated emission and radiation absorption using thermodynamical equilibrium arguments [4]. This paper addressing the light matter interaction is the prerequisite for the theory of lasers. Lasers represent a non equilibrium phenomena where amplified light is generated from a non equilibrium distribution of matter. In 1959, during the early development of solid state lasers, Scovil and Schulz-DuBois realized the equivalence of a three-level maser with a Carnot heat engine [5]. This is a seminal paper in contemporary quantum thermodynamics. They identified the amplified light as work and the kinetic process that establishes the population inversion as heat generated by a hot and cold bath of different temperatures. The well known thermodynamical viewpoint that an engine can be reversed to a heat pump led Geusic, Scovil and Schulz-DuBios to suggest Maser cooling [6] and in 1967 Laser cooling in the summarizing paper *quantum equivalence of Carnot cycle* [7]. These studies preceded the work of Wineland and Hänsch which reinvented laser cooling in 1975 [8, 9] which was not based on thermodynamical arguments.

Thermodynamics is usually viewed as a theory of large scale macroscopic processes. In view of the trend toward miniaturization, how far down can thermodynamics be applicable? J. von Neumann set the foundation for quantum theory on a probabilistic footing relevant for a single particle. Thus quantum mechanics enables thermodynamical ideas to be applicable on any scale.

## 1.2 Equilibrium Quantum Thermodynamics

### 1.2.1 *The von Neumann Mathematical Formalism of Quantum Statistical Physics*

A mathematically precise framework of quantum mechanics for systems of finite number of degrees of freedom has been developed by J. von Neumann in his book [3]. He synthesized the contribution of E. Schrödinger, W. Heisenberg and P.A.M. Dirac in the language of Hilbert spaces and linear operators acting on them [10–12]. von Neumann established the following fundamental structure of *quantum probability* [3]:

- (i) quantum observables are self-adjoint (Hermitian) operators (denoted by  $\hat{A}, \hat{B}, \dots$ ) acting on the Hilbert space  $\mathcal{H}$ ,
- (ii) quantum events are the particular *yes-no* observables described by projectors ( $\hat{P} = \hat{P}^2$ ),

- (iii) quantum probability measures are represented by density matrices, i.e. positive operators with trace one (denoted by  $\hat{\rho}, \hat{\sigma}, \dots$ ),
- (iv) probability of the event  $\hat{P}$  for the state  $\hat{\rho}$  is given by

$$\mathcal{P} = \text{Tr}(\hat{\rho}\hat{P}), \quad (1.1)$$

- (v) an averaged value of the observable  $\hat{A}$  at the state  $\hat{\rho}$  is equal to

$$\langle \hat{A} \rangle_{\rho} = \text{Tr}(\hat{\rho}\hat{A}). \quad (1.2)$$

The reversible dynamics of a quantum system formulated in terms of density matrices is governed by the von Neumann evolution equation with the generally time-dependent Hamiltonian  $\hat{H}(t)$

$$\frac{d}{dt}\hat{\rho}(t) = -\frac{i}{\hbar}[\hat{H}(t), \hat{\rho}(t)], \quad (1.3)$$

with the solution in terms of the unitary propagator  $\hat{U}(t, t_0)$

$$\hat{\rho}(t) = \hat{U}(t, t_0)\hat{\rho}(t_0)\hat{U}(t, t_0)^{\dagger}, \quad \hat{U}(t, t_0) = \mathbb{T} \exp\left\{-\frac{i}{\hbar} \int_{t_0}^t \hat{H}(t') dt'\right\}. \quad (1.4)$$

where  $\mathbb{T}$  is the time ordering operator. von Neumann introduced also the notion of entropy of the density matrix, called now von Neumann entropy and defined by the expression

$$S_{vn}(\hat{\rho}) = -k_B \text{Tr}(\hat{\rho} \ln \hat{\rho}) = -k_B \sum_j \lambda_j \ln \lambda_j \quad (1.5)$$

where  $\hat{\rho} = \sum_j \lambda_j |j\rangle\langle j|$  is a spectral decomposition of the density matrix. Notice, that this entropy is well-defined and non-negative (albeit can be infinite) in contrast to the generally ill-defined Boltzmann entropy for classical probability distributions on phase-spaces. The von Neumann entropy is an invariant of the state  $\hat{\rho}$  and is the lower bound for  $S_A(\hat{\rho}) \geq S_{vn}(\hat{\rho})$  where  $S_A = -k_B \sum_j p_j \ln p_j$  is the Shannon entropy defined by the probability distribution obtained by a complete measurement of the operator  $\hat{A}$ .

The quantum counterpart of the canonical (Gibbs) ensemble, corresponding to the thermodynamic equilibrium state at the temperature  $T$ , for the system with the Hamiltonian  $\hat{H}$ , is described by the density matrix of the form

$$\hat{\rho}_{\beta} = \frac{1}{Z} e^{-\beta \hat{H}}, \quad \beta = \frac{1}{k_B T}, \quad Z = \text{Tr} e^{-\beta \hat{H}}. \quad (1.6)$$

The Gibbs state maximizes entropy under the condition of a fixed mean energy (internal energy in thermodynamic language)  $E = \text{Tr}(\hat{\rho}\hat{H})$  or minimizes  $E$  for a fixed entropy  $S_{vn}$ . In this case  $S_{vn} = S_H$ .

Similarly to the classical Hamiltonian evolution the reversible dynamics given by (1.3) preserves entropy and hence cannot describe the equilibration process for an isolated quantum system without additional coarse-graining procedures. In particular, a pure state represented in the Hamiltonian eigenbasis by  $|\psi\rangle = \sum_j c_j |j\rangle$  remains a pure state. von Neumann proposed as a first step towards thermalization the time-averaging procedure leading from  $|\psi\rangle$  to the following density matrix (for a generic case of a non-degenerated Hamiltonian spectrum).

$$\hat{\rho}_D = \lim_{\tau \rightarrow \infty} \frac{1}{\tau} \int_0^\tau e^{-i/\hbar \hat{H}t} |\psi\rangle \langle \psi| e^{-i/\hbar \hat{H}t} d\tau = \sum_j |c_j|^2 |j\rangle \langle j|. \quad (1.7)$$

The problem of thermalization mechanism for closed, complex quantum system is still open [13].

### 1.2.2 Finite Quantum Systems

To avoid mathematical problems we begin with the discussion of equilibrium states for quantum systems with finite-dimensional Hilbert spaces. The basic property of an equilibrium system is related to the Kelvin formulation of the Second Law: *It is not possible to extract work from a single heat source at a fixed temperature in a cyclic process* [14]. This leads to the notion of a *passive state* [15–17] for a given system with a Hamiltonian  $\hat{H}$  as the state  $\hat{\rho}$  for which

$$\text{Tr}(\hat{\rho}\hat{H}) \leq \text{Tr}(\hat{U}\hat{\rho}\hat{U}^\dagger \hat{H}) \quad (1.8)$$

for any unitary  $\hat{U}$ . This arbitrary unitary map represents any reversible external driving applied to the system and the inequality (1.8) means impossibility of extracting work by such a procedure. It is not difficult to show that any passive state  $\hat{\rho}_p$  is diagonal in the Hamiltonian eigenbasis which can be ordered in such a way that

$$\hat{\rho}_p = \sum_{j=1}^n \lambda_j |j\rangle \langle j|, \quad E_j \leq E_{j+1}, \quad \lambda_{j+1} \leq \lambda_j \quad (1.9)$$

where  $\hat{H}|j\rangle = E_j |j\rangle$ .

Gibbs states (1.6) are obviously passive, but there exist many others, like for instance a variant of microcanonical ensemble determined by the energy scale  $E$  and defined as

$$\hat{\rho}[E] = \frac{1}{\#\{j; E_j \leq E\}} \sum_{\{j; E_j \leq E\}} |j\rangle \langle j|. \quad (1.10)$$

However, only Gibbs states possess the property of *complete passivity* which means that also its  $n$ -fold product  $\hat{\rho}^{\otimes n}$  is passive with respect to  $n$ -fold sum of its Hamiltonian, for arbitrary  $n = 1, 2, 3, \dots$ . No energy can be extracted by a unitary even from the  $n$ -fold product completely passive state, which is a quantum version of Kelvin's II-law.

Any density matrix  $\hat{\rho}$  can be transformed into a unique passive state  $\hat{\rho}_p = \hat{U} \hat{\rho} \hat{U}^\dagger$  by a unitary  $\hat{U}$  which maps the eigenvectors of  $\hat{\rho}$  into the eigenvectors of  $\hat{H}$  with the proper ordering.

Kubo introduced multi-time correlation functions (called Green functions) at the equilibrium states as a link between quantum statistical mechanics and nonequilibrium dynamics [18]. Generalizing an idea by Einstein on the relation between drag and restoring force of a brownian particle Green and Kubo [19] expressed the transport coefficients in terms of integrals of equilibrium time correlation functions. As an illustration consider a two-point correlation function for finite system at the Gibbs state corresponding to the Hamiltonian  $\hat{H}$

$$F_{AB}(t) = \text{Tr}(\hat{\rho}_\beta \hat{A}(t) \hat{B}), \quad \hat{A}(t) = e^{\frac{i}{\hbar} \hat{H} t} \hat{A} e^{-\frac{i}{\hbar} \hat{H} t} \quad (1.11)$$

for two observables  $\hat{A}$  and  $\hat{B}$ . Discreteness of the Hamiltonian spectrum implies that  $F_{AB}(t)$  is a *quasi-periodic function*, i.e. after sufficient time its value returns arbitrarily close to the initial one, which corresponds to Poincare recurrences in classical mechanics.

By analytic continuation the functions  $F_{AB}(t)$  can be extended to a complex domain ( $t \rightarrow z$ ) and one can show that Gibbs states are completely characterized by the following the Kubo–Martin–Schwinger (KMS) condition [18, 20]

$$F_{AB}(-t) = F_{BA}(t - i\hbar\beta) \quad (1.12)$$

valid for any pair of observables and arbitrary time.

### 1.2.3 Infinite Quantum Systems and KMS States

Large, many-particle quantum systems are important in quantum thermodynamics for studying physical properties of bulk matter or models of heat baths in the context of nonequilibrium theory of open systems. A very useful idealization called the *thermodynamic limit* is a mathematical procedure replacing a system of  $N$  particles in a volume  $V$  by its infinite volume limit with a fixed density  $N/V$ . The mathematically rigorous theory of infinite quantum systems has been developed in the Sixties and Seventies and allowed to study, for example, decay of spatial and temporal correlations or define precisely the notion of phase transition and spontaneous symmetry breaking.

The original Hilbert space description in terms of density matrices and Hermitian operators loses its meaning in the thermodynamic limit and must be replaced by

a more abstract algebraic formalism. However, one can use an alternative approach involving Green functions, for which their thermodynamic limit can be well-defined.

As an example, consider a free Bose or Fermi gas confined in a finite volume and described by a set of annihilation and creation operators  $\hat{a}_k, \hat{a}_k^\dagger$  labeled a discrete set of quantum numbers  $\{k\}$  and satisfying canonical commutation and anticommutation relations, respectively. The Hamiltonian is given by

$$\hat{H} = \sum_k \epsilon_k \hat{a}_k^\dagger \hat{a}_k, \quad (1.13)$$

and the thermal equilibrium state by the *grand canonical ensemble*

$$\hat{\rho}_{\beta,\mu} = Z^{-1}(\beta, \mu) e^{-\beta \hat{H}_\mu}, \quad Z(\beta, \mu) = \text{Tr} e^{-\beta \hat{H}_\mu} \quad (1.14)$$

which can be treated as a Gibbs state with the modified Hamiltonian

$$\hat{H}_\mu = \hat{H} - \mu \hat{N} = \sum_k (\epsilon_k - \mu) \hat{a}_k^\dagger \hat{a}_k. \quad (1.15)$$

where  $\mu$  is a chemical potential.

For a pair of observables  $A = \sum_k (f_k \hat{a}_k + \bar{f}_k \hat{a}_k^\dagger)$  and  $B = \sum_k (g_k \hat{a}_k + \bar{g}_k \hat{a}_k^\dagger)$  the Green function in the thermodynamic limit can be computed replacing the discrete energy levels  $\epsilon_k$  by the continuous variable  $\hbar|\omega|$  and  $f_k, g_k$  by functions  $f(|\omega|, \alpha)$ ,  $g(|\omega|, \alpha)$  where  $\alpha$  denotes additional (discrete and continuous) quantum numbers. Then

$$F_{AB}(t) = \int_{-\infty}^{+\infty} d\omega e^{-i\omega t} \int d\alpha \{ \bar{f}(|\omega|, \alpha) g(|\omega|, \alpha) [1 - (\mp)n(\hbar|\omega|)] \Theta(\omega) \\ + [f(|\omega|, \alpha) \bar{g}(|\omega|, \alpha) n(\hbar|\omega|) \Theta(-\omega)] \}, \quad (1.16)$$

where  $\int d\alpha$  denotes integral and sum over continuous or discrete  $\alpha$ -s,  $\Theta(\cdot)$  is the Heaviside function and

$$n(x) = \frac{1}{e^{\beta(x-\mu)} \mp 1}, \quad (1.17)$$

with the convention that in  $\mp$  the minus sign corresponds to bosons and the plus sign to fermions. The Green function (1.16) has an explicit structure of a Fourier transform that illustrates the fact that in the thermodynamic limit time correlations decay to zero for long times without Poincare recurrences. Moreover, one can expect that in the generic case of infinite systems the inverse Fourier transforms  $\tilde{F}_{AB}(\omega)$  are meaningful and then the KMS condition (1.12) implies the relation [18, 20]

$$\tilde{F}_{BA}(-\omega) = e^{-\hbar\beta\omega} \tilde{F}_{AB}(\omega), \quad (1.18)$$

which plays an important role in the quantum theory of open systems.

The KMS condition in the form (1.12) has been proposed to define thermal equilibrium states for infinite systems [18, 20]. It has been subsequently proved that KMS states possess desired stability properties with respect to local perturbations. Moreover, passivity (originally introduced in context of infinite systems [21]) combined with a certain clustering property, which excludes long-range order, implies the KMS condition [17].

For finite systems at the given temperature the corresponding Gibbs state is unique. In the case of an infinite system at the given temperature many KMS states can coexist, usually below a certain critical temperature. This is exactly the mechanism of *phase transition*, the notion which can be precisely defined only in the thermodynamic limit (see Chap. 20).

### 1.3 Non-equilibrium Thermodynamics of Quantum Open Systems

The progress in the field of quantum optics and laser physics in the Sixties and Seventies stimulated efforts to develop a mathematically sound theory of irreversible quantum dynamics. As noticed by Kraus [22], the mathematical theory of completely positive (CP) maps [23] provided a natural framework for both, the dynamics of open quantum systems and quantum measurement theory. The general form of CP and trace preserving map reads

$$\Lambda \hat{\rho} = \sum_j \hat{W}_j^\dagger \hat{\rho} \hat{W}_j, \quad (1.19)$$

where  $\hat{W}_j$  are called *Kraus operators* and satisfy the condition  $\sum_j \hat{W}_j \hat{W}_j^\dagger = I$ .

For any CP dynamical map  $\Lambda$ , Lindblad proved a kind of *H-theorem* [24]

$$S(\Lambda \hat{\rho} | \Lambda \hat{\sigma}) \leq S(\hat{\rho} | \hat{\sigma}) \quad (1.20)$$

valid for the *relative entropy* of an arbitrary pair of density matrices

$$S(\hat{\rho} | \hat{\sigma}) = \text{Tr}(\hat{\rho} \ln \hat{\rho} - \hat{\rho} \ln \hat{\sigma}). \quad (1.21)$$

The highlight of this period was the discovery in 1976 of the general form of the Markovian Master Equation (MME) satisfying CP condition

$$\frac{d}{dt} \hat{\rho} = -\frac{i}{\hbar} [\hat{H}, \hat{\rho}] + \frac{1}{2} \sum_j ([\hat{V}_j \hat{\rho}, \hat{V}_j^\dagger] + [\hat{V}_j, \hat{\rho} \hat{V}_j^\dagger]) \equiv -\frac{i}{\hbar} [\hat{H}, \hat{\rho}] + \mathcal{L} \hat{\rho}. \quad (1.22)$$

called the Gorini–Kossakowski–Lindblad–Sudarshan (GKLS) equation [25].

While in [26] finite-dimensional Hilbert spaces were considered, the case of bounded generators  $\mathcal{L}$  for open systems with infinite-dimensional spectrum was independently proved in [27]. For a recent discussion of the still open unbounded case see [28].

### 1.3.1 Quantum Thermodynamics in the Markovian Regime

Two years before the appearance of the GKLS equation Davies presented a rigorous derivation of MME for a  $N$ -level system weakly coupled to a heat bath represented by an ideal fermionic gas at the thermodynamic limit [29]. The derivation incorporates in a single mathematical procedure, called weak coupling limit (WCL), which includes the heuristic ideas of Born, Markovian and secular approximations, previously applied to various examples of open systems such as nuclear magnetic resonance by Bloch [30] and later Redfield [31]. Other approaches to the MME include the projection technique of Nakajima–Zwanzig [32, 33].

Adding to the WCL method a kind of renormalization procedure which allows to use the physical Hamiltonian  $\hat{H}$  of the system, containing lowest order Lamb corrections, and parametrizing the system-bath interaction as  $\hat{H}_{int} = \sum_k \hat{S}_k \otimes \hat{R}_k$  one obtains the following structure of MME which is in the GKLS form

$$\frac{d}{dt} \hat{\rho} = -i[\hat{H}, \hat{\rho}] + \mathcal{L}\hat{\rho}, \quad \mathcal{L}\hat{\rho} = \sum_{k,l} \sum_{\{\omega\}} \mathcal{L}_{lk}^{\omega} \hat{\rho} \quad (1.23)$$

where

$$\mathcal{L}_{lk}^{\omega} \hat{\rho} = \frac{1}{2\hbar^2} \tilde{R}_{kl}(\omega) \left\{ [\hat{S}_l(\omega)\hat{\rho}, \hat{S}_k^{\dagger}(\omega)] + [\hat{S}_l(\omega), \hat{\rho}\hat{S}_k^{\dagger}(\omega)] \right\}. \quad (1.24)$$

Here, the operators  $\hat{S}_k(\omega)$  originate from the Fourier decomposition ( $\{\omega\}$  denotes the set of Bohr frequencies of  $\hat{H}$ ).

$$e^{i/\hbar \hat{H}t} \hat{S}_k e^{-i/\hbar \hat{H}t} = \sum_{\{\omega\}} e^{-i\omega t} \hat{S}_k(\omega), \quad (1.25)$$

and  $\tilde{R}_{kl}(\omega)$  is the Fourier transform of the bath correlation function  $\langle \hat{R}_k(t)\hat{R}_l \rangle_{bath}$  computed in the thermodynamic limit  $\tilde{R}_{kl}(\omega) = \int_{-\infty}^{+\infty} e^{i\omega t} \langle \hat{R}_k(t)\hat{R}_l \rangle_{bath} dt$ . The derivation of (1.23) and (1.24) makes sense for a generic stationary state of the bath and implies two properties:

- (1) the Hamiltonian part  $[\hat{H}, \cdot]$  commutes with the dissipative part  $\mathcal{L}$ ,
- (2) the diagonal (in the  $\hat{H}$ -basis) matrix elements of  $\hat{\rho}$  evolve (independently of the off-diagonal ones) according to the Pauli Master Equation with transition rates given by the Fermi Golden Rule [34, 35].

If additionally the bath is a heat bath, i.e. an infinite system in a KMS state the additional relation (1.12) implies that:

- (3) Gibbs state  $\hat{\rho}_{\beta} = Z^{-1} \exp -\beta \hat{H}$  is a stationary solution of (1.23),
- (4) under the condition that only scalar operators commute with all  $\{\hat{S}_k(\omega), \hat{S}_k^{\dagger}(\omega)\}$ , any initial state relaxes asymptotically to the Gibbs state: *The 0-Law of Thermodynamics* [36].

The derivation of (1.23) and (1.24) can be extended to slowly varying time-dependent Hamiltonian (within the range of validity of the adiabatic theorem) [37]

$\hat{H}(t)$  and an open system coupled to several heat baths at the inverse temperatures  $\{\beta_k = 1/k_B T_k\}$ . The MME takes form

$$\frac{d}{dt}\hat{\rho}(t) = -i[\hat{H}(t), \hat{\rho}(t)] + \mathcal{L}(t)\hat{\rho}(t), \quad \mathcal{L}(t) = \sum_k \mathcal{L}_k(t). \quad (1.26)$$

Each  $\mathcal{L}_k(t)$  is derived using a temporal Hamiltonian  $\hat{H}(t)$ ,  $\mathcal{L}_k(t)\hat{\rho}_j(t) = 0$  with a temporary Gibbs state  $\hat{\rho}_j(t) = Z_j^{-1}(t) \exp\{-\beta_j \hat{H}(t)\}$ . The energy conservation in this case is the First Law of Thermodynamics [38]

$$\frac{d}{dt}E(t) = \mathcal{J}(t) - \mathcal{P}(t). \quad (1.27)$$

Here

$$E(t) = \text{Tr}\left(\hat{\rho}(t)\hat{H}(t)\right) \quad (1.28)$$

is the internal energy of the system,

$$\mathcal{P}(t) \equiv -\text{Tr}\left(\hat{\rho}(t)\frac{d\hat{H}(t)}{dt}\right), \quad (1.29)$$

is the power provided by the system, and

$$\mathcal{J}(t) \equiv \text{Tr}\left(\hat{H}(t)\frac{d}{dt}\hat{\rho}(t)\right) = \sum_k \mathcal{J}_k(t), \quad \mathcal{J}_k(t) = \text{Tr}\left(\hat{H}(t)\mathcal{L}_k(t)\hat{\rho}(t)\right). \quad (1.30)$$

is the sum of net heat currents supplied by the individual heat baths.

The  $H$ -theorem (1.20) directly implies the following mathematical identity [39, 40]

$$-\text{Tr}\left[\mathcal{L}\hat{\rho}(t)(\ln \hat{\rho}(t) - \ln \hat{\rho}_{st})\right] \geq 0, \text{ for } \mathcal{L}\hat{\rho}_{st} = 0, \quad (1.31)$$

which applied to individual generators  $\mathcal{L}_k(t)$  reproduces the Second Law of Thermodynamics in the form

$$\frac{d}{dt}S_{vn}(t) - \sum_k \frac{1}{T_k} \mathcal{J}_k(t) \geq 0. \quad (1.32)$$

obtained first for the constant  $\hat{H}$  in [41] and ultimately generalized in [38].

For external periodic modulation of the Hamiltonian  $\hat{H}(t) = \hat{H}(t + \tau)$ , a very similar WCL formalism for open systems has been developed [42–45]. One assumes that modulation is fast, i.e. its angular frequency  $\Omega = 2\pi/\tau$  is comparable to the relevant Bohr frequencies of the Hamiltonian, therefore the previous adiabatic approximation is not appropriate. According to the Floquet theory the unitary propagator (1.4)  $\hat{U}(t) \equiv \hat{U}(t, 0)$  can be written as

$$\hat{U}(t) = \hat{U}_p(t)e^{-\frac{i}{\hbar}\hat{H}_{av}t} \quad (1.33)$$

where  $\hat{U}_p(t) = \hat{U}_p(t + \tau)$  is a periodic propagator and  $\hat{H}_{av}$  can be called *averaged Hamiltonian*. Under similar assumptions as before one can derive, using the WCL procedure, the Floquet- Markovian ME in the *interaction picture*

$$\frac{d}{dt}\hat{\rho}^{int}(t) = \mathcal{L}\hat{\rho}^{int}(t), \quad \mathcal{L}\hat{\rho} = \sum_{k,l} \sum_{\{\omega_q\}} \mathcal{L}_{lk}^{\omega_q} \hat{\rho} \quad (1.34)$$

where

$$\mathcal{L}_{lk}^{\omega_q} \hat{\rho} = \frac{1}{2\hbar^2} \tilde{R}_{kl}(\omega_q) \left\{ [\hat{S}_l(\omega_q)\hat{\rho}, \hat{S}_k^\dagger(\omega_q)] + [\hat{S}_l(\omega_q), \hat{\rho}\hat{S}_k^\dagger(\omega_q)] \right\}. \quad (1.35)$$

Now, the summation in (1.34) is taken over the set of *extended Bohr frequencies*  $\{\omega_q = \omega_{av} + q\Omega \mid \omega_{av} - \text{Bohr frequencies of } \hat{H}_{av}, q \in \mathbf{Z}\}$ , which takes into account the exchange processes of energy quanta  $\hbar|q|\Omega$  with the source of external modulation. Here again the operators  $\hat{S}_k(\omega_q)$  originate from the Fourier decomposition

$$\hat{U}^\dagger(t)\hat{S}_k\hat{U}(t) = \sum_{\{\omega_q\}} e^{-i\omega_q t} \hat{S}_k(\omega_q). \quad (1.36)$$

Notice, that the interaction picture generator is time-independent and the Schrödinger picture dynamics is given by the composition  $\hat{\rho} \mapsto \hat{U}(t)(e^{\mathcal{L}t}\hat{\rho})\hat{U}^\dagger(t)$ . Typically,  $\mathcal{L}$  possesses a single stationary state  $\hat{\rho}_0$  and then for any initial state  $\hat{\rho}(0)$  the Schrödinger evolution drives the system to a limit cycle  $\hat{\rho}_{lc}(t) = \hat{U}_p(t)\hat{\rho}_0\hat{U}_p^\dagger(t)$ .

Heat currents corresponding to different baths can be defined for any time. As a result the Second Law is satisfied for this definition, nevertheless the form of the First Law is problematic. Namely, for fast modulation the instantaneous decomposition of energy into work and internal energy of the system is not clear. Only in the limit cycle, where the system's internal energy and entropy are constant, and the heat currents are time independent we can write the First Law as

$$\mathcal{P} = \sum_j \mathcal{J}_j, \quad (1.37)$$

and the Second Law as

$$\sum_j \frac{1}{T_j} \mathcal{J}_j \leq 0. \quad (1.38)$$

Here, the heat current associated with the  $j$  bath is given in terms of the corresponding interaction picture generator

$$\mathcal{J}_j = \sum_{l,k \in I_j} \sum_{\{\omega_q\}} \frac{\omega_q}{\omega_{av}} \text{Tr}(\hat{H}_{av} \mathcal{L}_{lk}^{\omega_q} \hat{\rho}_0), \quad (1.39)$$

and  $I_j$  denotes the subset of indices corresponding to the interaction with the  $j$ th heat bath. The above scheme has been extended to non-equilibrium stationary baths in [46], with possible applications to non-thermal radiation baths, rotating heat baths, etc. [47, 48].

### 1.3.2 Beyond the WCL Markovian Approximation

The theory of open quantum systems together with the Davies construction supplies a consistent framework of Thermodynamics where the basic laws have a quantum dynamical framework [49]. This framework is quite restrictive and therefore one may ask if some of the assumptions can be relaxed without compromising the consistency with thermodynamics.

Many suggestions have been proposed:

- Challenging complete positivity.
- Local versus Non Local GKLS equation.
- Non Markovian dynamics.
- Strong system-bath coupling.

The complete positivity structure assumes that initially the system and bath are uncorrelated [22]. This has been challenged by Pechukas [50] who claimed that positivity of the dynamical map is sufficient. Alicki responded that one should stress that beyond the weak coupling regime there exists no unique definition of the quantum reduced dynamics [51]. A similar answer was given by Lindblad [52]. It has been claimed that the second law of thermodynamics is violated by a non-CP dynamics [53, 54].

An alternative approach to open system dynamics has been proposed by Caldeira, and Leggett, based on a path integrals formalism, generating a QME for quantum Brownian motion [55]. The equation is not guaranteed to be positive in particular at low temperature. A fix to the problem has been suggested by Diosi adding terms to the equation to obtain a GKLS format [56]. For a Brownian particle one would expect that the friction is isotropic meaning that the dissipation equations should be translationally invariant. It has been noticed by Tannor and Kohen that complete positivity, translational invariance and detailed balance cannot be satisfied simultaneously [57, 58]. This is also true for the fix of Diosi which adds a diffusion-like term in position.

The Davies construction of the GKLS equation Eq. (1.23) requires that the jump operators Eq. (1.24) are generated from the complete system Hamiltonian Eq. (1.36). What happens when the system can be deconstructed into segments which are weakly coupled to each other? Can one use a local GKLS equation for each segment and then linking together to construct a network? Careful analysis has shown that such

a construction can violate the II-law: Heat can flow from the cold to the hot bath spontaneously [59]. In degenerate networks when the links are identical the secular approximation may fail for vanishing small links. In these cases local GKLS equations give the correct heat current with respect to numerical converged approaches [60–62]. General conditions of adding up consistently GKLS generators have been suggested [63].

A violation of the II-law has also been identified if the Floquet GKLS equation Eq. (1.39) is replaced by the standard stationary GKLS. This is even true for the well known two-level Bloch equation [42] and for the three-level amplifier [64].

It is customary to start the non-Markovian investigation from the second order integro-differential equation [32, 33, 65–67]:

$$\frac{d}{dt}\hat{\rho}_s = -i[\hat{H}_{eff}, \hat{\rho}_s] + \int_0^t dt' \mathcal{K}(t, t')\hat{\rho}_s(t') \quad (1.40)$$

where  $\hat{H}_{eff}$  is an effective system Hamiltonian and  $\mathcal{K}(t, t')$  is termed a memory kernel.

Different approaches can be classified by the type of approximation to the memory kernel. One option is to generate a time local kernel [68, 69] which can lead to a GKLS-like equations with time dependent coefficients. Complete positivity is not ensured which manifests itself by negative coefficients.

Another option is termed the Hierarchical Equations of Motion Approach [66, 70–73] which decomposes the kernel to exponentially decaying functions (see Chap. 24). One then adds a set of auxiliary variables which leads to a hierarchy of coupled differential equations. This is equivalent to a Markovian description embedded in a larger Hilbert space. The thermodynamical consequence of non-Markovian dynamics has recently been addressed [74]. It has been observed that in the absence of the semigroup property, if the reduced dynamics has a thermal asymptotic state, this need not be stationary. Then even the integrated entropy production becomes negative. These observations imply that, when the conditions leading to reduced dynamics of semigroup type are relaxed, a consistent formulation of the second law of thermodynamics requires that the environment contribution to the entropy balance be explicitly taken into account [75].

An alternative theory of quantum thermodynamics in the framework of the nonequilibrium Green's functions has been proposed by Esposito and Galperin [76, 77]. The theory was applied to noninteracting open quantum systems strongly coupled to their reservoirs. The theory is non-Markovian and nonlocal in time. As a consequence the particle number, energy, and entropy of the system are redefined as energy-resolved versions of the standard weak coupling definitions. The approach has been criticised as failing, already at equilibrium, to describe correctly the energy fluctuations [78].

Strong system bath coupling is another challenge that has been met by embedding in a larger system. The main idea is to move the system bath partition further into the bath (see Chap. 23). The polaron transformation is such an example. It incorporates

part of the bath degrees of freedom in a modified system [79–87]. If weak coupling is incorporated on the new system bath boundary, consistency with thermodynamics is maintained.

Another approach to strong coupling is to embed the system in a finite surrogate spin bath which represents the true infinite bath. The total system and bath are described by unitary dynamics. To model the infinite bath thermal boundary conditions are imposed between a thermal secondary bath and the primary bath. A random swap operation is employed for this task. Each individual realization is unitary. Averaging the individual realizations is equivalent to a Poisson type GKLS equation on the boundary of the primary bath. Thermodynamic properties can be obtained by evaluating the currents through the device [88]. Consistency with thermodynamics has been obtained for the case of heat transfer from a hot to a cold bath irrespective of the system-bath coupling [88, 89].

## 1.4 Models of Quantum Engines and Refrigerators

Since the pioneering work of Carnot [90], learning from example has been a major theme in thermodynamical studies. This is also true in Quantum Thermodynamics (QT) where the issues of heat and work obtain a concrete meaning [38]. In addition the tradeoff between efficiency and finite power can be explored. The trend toward miniaturisation has led to the construction of quantum heat devices composed from a microscopic working entity, for example a single ion in a Paul trap [91] (see also Chap. 36). This macroscopic scale raises the question: What quantum effects to expect? Is there a role for coherence or entanglement? Can we expect quantum supremacy?

Models of heat engines and refrigerators can lead to new insight in QT. They can be broadly classified as reciprocating and continuous.

### 1.4.1 Reciprocating Engines and Refrigerators

Reciprocating engines are composed of a series of strokes which combine to a cyclic operation. The different cycles are defined by the individual stroke operations and their order. In QT a reciprocating engine can be defined by a product of CP maps Eq. (1.19), which operate on the working medium:

$$\mathcal{U}_{cyc} = \prod_j \mathcal{U}_j \quad (1.41)$$

where  $\mathcal{U}_{cyc}$  is the cycle propagator and  $\mathcal{U}_j$  are stroke propagators. The steady state operation is an invariant of the cycle propagator  $\mathcal{U}_{cyc} \hat{\rho}_{st} = \hat{\rho}_{st}$ . For cycles that have

a single non-degenerate invariant the CP character of  $\mathcal{U}_{cyc}$ , Eq. (1.21) guarantees a monotonic convergence to the steady state cycle, termed the limit cycle [92].

The four stroke Otto cycle is a primary example (see Chaps. 3 and 5). It is composed of two unitary strokes and two thermalization strokes: The Hamiltonian of the working medium is parametrically externally controlled:  $\hat{H}(\omega)$  where  $\omega$  is an external parameter which changes the energy scale. For example  $\hat{H} = \frac{1}{2m}\hat{P}^2 + \frac{m\omega(t)^2}{2}\hat{X}^2$  for the harmonic working medium [93] and  $\hat{H} = \omega(t)\hat{S}_z + J\hat{S}_x$  for a spin system [94, 95].

The quantum Otto cycle is therefore described as:

1. The hot *isochore*: heat is transferred from the hot bath to the working medium without change in the external parameter  $\omega_h$ . The stroke is described by the propagator  $\mathcal{U}_h$ .
2. The expansion *adiabat*: the working medium reduces its energy scale from  $\omega_h$  to  $\omega_c$ , with  $\omega_h > \omega_c$ , producing work while isolated from the hot and cold reservoirs. The stroke is described by the propagator  $\mathcal{U}_{hc}$ .
3. The cold *isochore*: heat is transferred from the working medium to the cold bath without change in the external parameter  $\omega_c$ . The stroke is described by the propagator  $\mathcal{U}_c$ .
4. The compression *adiabat*: the working medium increases its energy scale from  $\omega_c$  to  $\omega_h$ , consuming power while isolated from the hot and cold reservoirs. The stroke is described by the propagator  $\mathcal{U}_{ch}$ .

The cycle propagator becomes the product of the segment propagators:

$$\mathcal{U}_{cyc} = \mathcal{U}_{ch}\mathcal{U}_c\mathcal{U}_{hc}\mathcal{U}_h . \quad (1.42)$$

It should be mentioned that the stroke propagators do not commute for example:  $[\mathcal{U}_{hc}, \mathcal{U}_h] \neq 0$ . The Otto cycle can operate in two extreme protocols, adiabatic and sudden.

In the adiabatic cycle the working medium state is diagonal in the energy representation throughout the cycle. Such cycles are called stochastic [96, 97]. The efficiency becomes  $\eta_o = 1 - \frac{\omega_c}{\omega_h} \leq \eta_c$  where  $\eta_c = 1 - \frac{T_c}{T_h}$  is the Carnot efficiency.

To obtain finite power the time allocated to the propagators  $\mathcal{U}_{hc}$  and  $\mathcal{U}_{ch}$  should be shortened. For the unitary strokes this means deviating from the adiabatic limit. Whenever  $[\hat{H}(t), \hat{H}(t')] \neq 0$  coherence will be generated and  $\hat{\rho}$  will not be diagonal in the energy basis  $S_H > S_{vn}$ . Generating coherence will always cost additional external work. This phenomena has been termed quantum friction [95, 98]. Quantum friction can be understood using the notion of passivity Eq. (1.8). In the adiabatic limit the eigenvalues of the density operator remain passive in the energy basis. The minimum work can be associated to the change in energy scale. Any nonadiabatic deviation will increase the required work.

The price of generating coherence can be reduced if at the end of the adiabatic stroke the state is restored to be passive in the energy basis. Such protocols are termed shortcuts to adiabaticity or frictionless [99–101] (see also Chap. 5). These protocols

allow to achieve adiabatic like solutions in finite time for the propagators  $\mathcal{U}_{hc}$  and  $\mathcal{U}_{ch}$ . The fast shortcut solutions raise the question what is the shortest time allocation for frictionless adiabatic strokes. This issue is in the realm of the quantum speed limit [102, 103] with the caveat that the energy scale of the Hamiltonian also changes. The transformation can be made faster if temporary energy is stored in the working fluid. Optimal control protocols that constrain the stored energy in the working fluid lead to a scaling of the time allocation as  $\tau \propto \frac{1}{\sqrt{\omega_c \omega_h}}$  for  $\omega_c \rightarrow 0$  [99, 104].

Coherence can also be introduced as a resource by employing a non-thermal bath. Even a single bath is sufficient to extract work [105]. Nevertheless there is no violation of the II-law if accounting is done properly [106].

For finite power also the time allocated to thermalization  $\mathcal{U}_c$  and  $\mathcal{U}_h$  should be restricted. Typically in most studies the generator of thermalization  $\mathcal{L}$  is the GKLS equation (1.22) [94]. Finite time allocation is obtained by avoiding the infinite time full thermalization. Optimizing the time allocation in the stochastic limit leads to a finite power engine. The efficiency at maximum power at high temperature becomes [93]:

$$\eta_{ca} = 1 - \sqrt{\frac{T_c}{T_h}} \quad (1.43)$$

which is known as the Novikov–Curzon–Ahlborn efficiency [107, 108]. The importance of Eq. (1.43) is that it points to the tradeoff between efficiency and power. For the Otto cycle at high temperature the efficiency at maximum power is limited by the energy level structure of the working medium with the leading term  $\eta \approx \frac{1}{2}\eta_c + \dots$  [109]. This result has been obtained from general considerations in the adiabatic limit [110].

In QT the Carnot cycle has received less attention than the Otto cycle. The reason is that the hot and cold isochores are replaced by isotherms where the thermalization takes place with a time dependent Hamiltonian. In the adiabatic limit of slow change GKLS equations of motion can be obtained [94]. Beyond the adiabatic limit deriving GKLS equations is complicated due to the non-periodic driving. The original motivation for the study of QT cycles was to supply a more fundamental justification for the empirical Finite-Time-Thermodynamics approach [111, 112]. In the infinitely slow cycle limit, the efficiency converges to the ideal Carnot efficiency  $\eta_c$ . Optimizing power leads to the Novikov–Curzon–Ahlborn efficiency  $\eta_{ca}$ , which is universal in the stochastic low dissipation limit [113, 114]. In this limit the irreversibility can be associated to heat transport, thus termed endo-reversible.

A two stroke engine has been suggested where  $\mathcal{U}_{cyc} = \mathcal{U}_T \mathcal{U}_S$  [115, 116]. One that resembles the Otto cycle is composed of a four level working medium. Thermalization,  $\mathcal{U}_T$  is conducted in parallel where two-levels are connected to the hot bath and the other two-levels to the cold bath. The unitary  $\mathcal{U}_S$  stroke is composed of a swap propagator between these two sets of levels. The efficiency of this engine is equivalent to the Otto efficiency  $\eta_o$ .

The other extreme operational limit is the sudden limit where a limited action is performed on each stroke. The work per cycle then decreases but the power which

is the work divided by cycle time can reach a constant. In this limit each stroke can be expressed as  $\mathcal{U}_j = \exp \mathcal{L}_j \tau$ , where  $\mathcal{L}_j$  is the generator and  $\tau$  the time allocation. Then a four stroke cycle becomes equivalent to a continuous engine with finite power [117] (see also Chap. 4). In the limit of  $\tau \rightarrow 0$ :

$$\mathcal{U}_{cyc} = \mathcal{U}_{ch}\mathcal{U}_c\mathcal{U}_{hc}\mathcal{U}_h = e^{\mathcal{L}_{ch}\frac{1}{2}\tau}e^{\mathcal{L}_c\tau}e^{\mathcal{L}_{hc}\tau}e^{\mathcal{L}_h\tau}e^{\mathcal{L}_{ch}\frac{1}{2}\tau} \approx e^{(\mathcal{L}_{ch}+\mathcal{L}_c+\mathcal{L}_{hc}+\mathcal{L}_h)\tau} \quad (1.44)$$

which is correct up to  $O(\tau^3)$  based on the cyclic property of the engine and Trotter formula [118]. Moreover the work extraction mechanism employs coherence [117]. Adding pure dephasing to the engine will null the power which is a signature of a quantum device.

Reversing the sequence of a reciprocating cycle leads to a quantum refrigerator:  $\mathcal{U}_{cyc}^{ref} = \mathcal{U}_{hc}\mathcal{U}_c\mathcal{U}_{ch}\mathcal{U}_h$ .

A prerequisite for such a device is that the working medium temperature is lower than the cold bath temperature at the end of the expansion stroke  $\omega_h \rightarrow \omega_c$ . Reciprocating refrigeration cycles were used to gain insight on the dynamical approach to the III-law of thermodynamics the vanishing of the cooling power when  $T_c \rightarrow 0$  [119]. Optimizing the cooling performance requires that the energy gap of the system  $\hbar\omega_c$  will match the cold bath temperature  $k_B T_c$  [120]. The cooling power can either be restricted by the thermalization or by the adiabatic propagator. The energy quantum removed from the cold bath per cycle becomes  $\hbar\omega_c$ . Considering the optimal frictionless solution, a scaling of  $\mathcal{J}_c \propto T_c^{\frac{3}{2}}$  is obtained as  $T_c \rightarrow 0$ .

### 1.4.2 Continuous Time Quantum Machines

The three-level engine was the first QT example studied by Scovil et al. [5, 7]. The principle of operation is to convert population inversion into output power in the form of light. A hot reservoir characterised by temperature  $T_h$  induces transitions between the ground state  $\epsilon_0$  and the excited state  $\epsilon_2$ . The cold reservoir at temperature  $T_c$  couples level  $\epsilon_0$  and level  $\epsilon_1$ . The amplifier operates by coupling the energy levels  $\epsilon_3$  and  $\epsilon_2$  to the radiation field generating an output frequency which on resonance is  $\nu = (\epsilon_3 - \epsilon_2)/\hbar$ . The necessary condition for amplification is positive gain or population inversion defined by:

$$\mathcal{G} = p_2 - p_1 \geq 0. \quad (1.45)$$

The positive gain condition dictates:

$$\frac{\omega_c}{\omega_h} \equiv \frac{\omega_{10}}{\omega_{20}} \geq \frac{T_c}{T_h}, \quad (1.46)$$

The efficiency of the amplifier becomes the Otto efficiency:  $\eta_o = \frac{\nu}{\omega_{20}} = 1 - \frac{\omega_c}{\omega_h}$ . Inserting the positive gain condition Eqs. (1.45) and (1.46) the efficiency is lim-

ited by Carnot:  $\eta_o \leq \eta_c$ . This result connecting the efficiency of a quantum amplifier to the Carnot efficiency was first obtained by Scovil et al. [5, 7].

The above description of the 3-level amplifier is based on a static quasi-equilibrium viewpoint. Real engines which produce power operate far from equilibrium conditions. Typically, their performance is restricted by friction, heat transport and heat leaks. A dynamical viewpoint is therefore the next required step [121].

Engines or refrigerators can be classified as either autonomous or driven. A continuous autonomous device operates by connecting to three or more heat baths simultaneously either heating the hottest bath or cooling the coldest bath. Such a device operates without any external intervention [122–124]. A driven system is connected to an external power source or to a more elaborate measurement and feedback device, which syncronizes the engine [125].

The tricycle model is the template for almost all continuous autonomous engines [126] (see also Chap. 6). It can also be viewed as a heat transistor [79, 127]. Surprisingly very simple models exhibit the same features of engines generating finite power. Their efficiency at operating conditions is lower than the Carnot efficiency. In addition, heat leaks restrict the performance meaning that reversible operation is unattainable.

- The basic model consists of three thermal baths: a hot bath with temperature  $T_h$ , a cold bath with temperature  $T_c$  and a work bath with temperature  $T_w$ .
- Each bath is connected to the engine via a frequency filter modelled by three oscillators or three qubits:

$$\hat{H}_F = \hbar\omega_h \hat{a}^\dagger \hat{a} + \hbar\omega_c \hat{b}^\dagger \hat{b} + \hbar\omega_w \hat{c}^\dagger \hat{c}, \quad (1.47)$$

where  $\omega_h$ ,  $\omega_c$  and  $\omega_w$  are the filter frequencies on resonance  $\omega_w = \omega_h - \omega_c$ .

- The device operates as an engine by removing an excitation from the hot bath and generating excitations on the cold and work reservoirs. In second quantization formalism the Hamiltonian describing such an interaction becomes:

$$\hat{H}_I = \hbar\epsilon (\hat{a}\hat{b}^\dagger \hat{c}^\dagger + \hat{a}^\dagger \hat{b}\hat{c}), \quad (1.48)$$

where  $\epsilon$  is the coupling strength.

- The device operates as a refrigerator by removing an excitation from the cold bath as well as from the work bath and generating an excitation in the hot bath. The term  $\hat{a}^\dagger \hat{b}\hat{c}$  in the Hamiltonian of Eq. (1.48) describes this action.

Different types of heat baths can be employed which can include bosonic baths composed of phonons or photons, or fermionic baths composed of electrons. The frequency filters select from the continuous spectrum of the bath the working component to be employed in the tricycle. These frequency filters can be constructed also from two-level-systems (TLS) or formulated as qubits [44, 128–130]. A direct realization of Eq. (1.48) has been performed by an absorption refrigerator constructed from three ions in a Paul trap [131].

The interaction term is strictly non-linear, incorporating three heat currents simultaneously. This crucial fact has important consequences. A linear device cannot operate as a heat engine or refrigerator [132]. A linear device is constructed from a network of harmonic oscillators with linear connections of the type  $\hbar\mu_{ij}(\hat{a}_i\hat{a}_j^\dagger + \hat{a}_i^\dagger\hat{a}_j)$  with additional connections to heat baths constructed from harmonic oscillators. In such a device the hottest bath always cools down and the coldest bath always heats up. Thus, this construction can transport heat but not generate power since power is equivalent to transporting heat to an infinitely hot reservoir. Another flaw in a linear model is that the different bath modes do not equilibrate with each other. A generic bath should equilibrate any system Hamiltonian irrespective of its frequency.

Many nonlinear interaction Hamiltonians of the type  $\hat{H}_I = \hat{A} \otimes \hat{B} \otimes \hat{C}$  can lead to a working heat engine. These Hamiltonians can be reduced to the form of Eq. (1.48) which captures the essence of such interactions.

The first-law of thermodynamics represents the energy balance of heat currents originating from the three baths and collimating on the system:

$$\frac{dE_s}{dt} = \mathcal{J}_h + \mathcal{J}_c + \mathcal{J}_w . \quad (1.49)$$

At steady state no heat is accumulated in the tricycle, thus  $\frac{dE_s}{dt} = 0$ . In addition, in steady state the entropy is only generated in the baths, leading to the second-law of thermodynamics:

$$\frac{d}{dt}\Delta S_u = -\frac{\mathcal{J}_h}{T_h} - \frac{\mathcal{J}_c}{T_c} - \frac{\mathcal{J}_w}{T_w} \geq 0 . \quad (1.50)$$

This version of the second-law is a generalisation of the statement of Clausius; heat does not flow spontaneously from cold to hot bodies [133]. When the temperature  $T_w \rightarrow \infty$ , no entropy is generated in the power bath. An energy current with no accompanying entropy production is equivalent to generating pure power:  $\mathcal{P} = \mathcal{J}_w$ , where  $\mathcal{P}$  is the output power.

The evaluation of the currents  $\mathcal{J}_j$  in the tricycle model requires dynamical equations of motion. A thermodynamical idealisation assumes that the tricycle system and the baths are uncorrelated, meaning that the total state of the combined system becomes a tensor product at all times [49]:

$$\hat{\rho} = \hat{\rho}_s \otimes \hat{\rho}_H \otimes \hat{\rho}_C \otimes \hat{\rho}_W . \quad (1.51)$$

Under these conditions the dynamical equations of motion for the tricycle become:

$$\frac{d}{dt}\hat{\rho}_s = \mathcal{L}\hat{\rho}_s , \quad (1.52)$$

where  $\mathcal{L}$  is the GKLS Markovian generator Eq. (1.23). The derivation of  $\mathcal{L}$  is complicated due to the nonlinearity of the interaction Eq. (1.48). Solutions can be obtained in the case when  $T_w \rightarrow \infty$  or a singular bath [126]. Equivalent solutions for  $\mathcal{L}$

can be obtained for the 3-level [122], 2-qubit and 3-qubit absorption refrigerator [134, 135].

The autonomous absorption refrigerator has been a major model in the study of the dynamical version of the III-law of thermodynamics (see Chap. 25). Examining the II-law Eq. (1.50) as  $T_c \rightarrow 0$ , to avoid divergence of  $\Delta S_u \mathcal{J}_c$  should scale as at least linearly with  $T_c$ . A stronger version associated to Nernst Heat Theorem [136, 137] demands that  $\mathcal{J}_c \propto T_c^{1+\epsilon}$  which ensures the vanishing of entropy production from the cold bath as  $T_c \rightarrow 0$  [138]. For generic refrigerator models as  $T_c \rightarrow 0$  the cold bath current obtains the universal form:

$$\mathcal{J}_c = \hbar \omega_c \mathcal{K} \mathcal{G} \quad (1.53)$$

where  $\mathcal{K}$  is a heat conductance term. When  $T_c \rightarrow 0$  the gain  $\mathcal{G}$  is finite only if  $\omega_c \propto T_c$ . This leaves the issue: How does the conductance  $\mathcal{K}$  scale with  $\omega_c$ , which is model dependent. For example for a Bose Einstein Condensate (BEC), the conductance is proportional to the uncondensed fraction leading to  $\mathcal{J}_c \propto T_c^3$  [49, 138].

The unattainability principle [139], a different formulation of the III-law states: *The zero temperature can be reached only if infinite resources are invested.* In quantum mechanics a zero temperature system is in a pure state. This is only possible if at  $T_c \rightarrow 0$ ,  $\hat{\rho}_s \otimes \hat{\rho}_B$ . In addition since  $\hat{\rho}_B = |0\rangle\langle 0|$ , the system-bath interaction energy will vanish, meaning that when the bath approaches its ground state the mechanism of extracting energy ceases to operate. One can consider two scenarios. Cooling an infinite cold bath and cooling a finite system. Considering an infinite bath the change in temperature becomes  $\frac{dT_c}{dt} = \frac{\mathcal{J}_c}{C}$  where  $C$  is the heat capacity. This leads to a scaling of  $\frac{dT_c}{dt} \propto T_c^{3/2}$  as  $T_c \rightarrow 0$  for both degenerate Bose and Fermi gases [138].

A different perspective on the III-law can be obtained from quantum resource theory. Using quite general arguments the following scaling relation was obtained  $\frac{dT_c}{dt} \propto T_c^{1+\frac{1}{\gamma}}$  [140]. Addition of noise can further restrict the minimum achievable temperature [141].

Driven continuous devices require an external power source typically  $\hat{H}_s(t) = \hat{H}_0 + \hat{V} f(t)$  where  $f(t)$  is a periodic function. The most direct connection to a driven system is to replace the excitation of the power reservoir by its semiclassical expectation value  $\hat{c} \sim \bar{c} e^{-i\omega_w t}$  [121]. A derivation of a thermodynamical consistent GKLS equation requires to use Floquet theory (1.34) [45, 64]. Strong driving alters the system excitations and frequencies Eq. (1.36) which can change the operation conditions from an engine to a dissipator and to a refrigerator [64, 142].

Optimizing the performance of continuous devices leads to the tradeoff between efficiency and power. For an engine constructed from two coupled harmonic oscillators the efficiency at high temperature at maximum power becomes again  $\eta_{ca}$  Eq. (1.43) [121]. Universal features of the maximum power efficiency have been obtained by information theory considerations [143].

Driven systems are prototype models of quantum amplifiers and lasers [144]. Such a treatment ignores the entropy carried away by the amplified light. This can be solved by incorporating the emitted light as a single mode harmonic oscillator [145].

A more complete derivation of the 3-level laser has been derived recently including the entropy dissipated by light [146].

## 1.5 Open Problems and Prospects

In this section we discuss some controversial or unsolved questions of QT of fundamental nature.

### 1.5.1 Work Generation: Steady-State or Thermodynamic Cycles

One believes that the energy convertors like photovoltaic, thermoelectric and fuel cells, and their biological counterparts can directly transform light, heat or chemical energy into work carried by electric current. It is assumed that they do not need any moving parts and operate at non-equilibrium steady-states. A recent review of this approach mostly concentrated on the conversion of heat at the nanoscale is given in [147]. The phenomenological picture of heat to electric current conversion is based on the coupled equations for charge and heat local current densities  $j_e, j_h$

$$\begin{aligned} j_e &= \lambda_{ee}(\Delta\mu/eT) + \lambda_{eh}(\Delta T/T^2) \\ j_h &= \lambda_{he}(\Delta\mu/eT) + \lambda_{hh}(\Delta T/T^2) \end{aligned} \quad (1.54)$$

with local temperature  $T$ , local chemical potential  $\mu$  and the Onsager matrix  $[\lambda_{ab}]$ .

The importance of nanoscale devices and the fact that the energy conversion is based on microscopic quantum processes stimulates the development of more fundamental microscopic theories (see Chap. 7). The most popular is stochastic thermodynamics reviewed in [97]. Here, the force driving charge carriers is a phenomenological nonconservative force corresponding to a kind of negative friction powered by the external gradients of temperature and chemical potential.

Recently, the steady-state picture has been challenged in a series of papers, where models of cyclic classical [148] and quantum engines [149, 150] have been proposed. This work was motivated by an apparent inconsistency of (1.54) when applied to the devices generating electric current flowing in a closed circuit. Namely, the integral of the steady electric current over its closed path should be different from zero, while the similar integration over the RHS of (1.54) yields always zero.

The “moving parts” in the cyclic models correspond to collective delocalized charge oscillations at the interface of two different materials. For semiconductor devices they are THz plasma oscillations, while for organic photovoltaic or photosynthetic complexes delocalized and infrared sensitive phonon modes play the role of a “piston”. The cyclic models predict two types of phenomena: emission of coherent radiation by oscillating “pistons” and reverse effect—enhancement of the generated

electric current by coherent resonant radiation stimulating the “piston”. In fact, both effects were observed in organic photovoltaic systems [151, 152] and the role of selected phonon modes in photosynthesis has also been discussed [153]. However, those phenomena were considered as auxiliary effects improving the efficiency of energy converters and not as the necessary elements of their operation principle.

### 1.5.2 *Information and Thermodynamics*

The idea of representing physical processes as computation processes or more generally as information processing is quite popular in the rapidly developing field of quantum information [154]. For example, one believes that an acquired bit of information can be traded-off for a  $k_B T \ln 2$  of work extracted from the bath at temperature  $T$ . This leads to the Landauer formula [155, 156] which puts the lower limit equal to  $k_B T \ln 2$  for the work needed to reset a bit of information in a memory (see Chap. 10). The reasoning is based on the idea of Szilard [157, 158] who proposed a model of an engine which consists of a box with a single gas particle, in thermal contact with a heat bath, and a partition. The partition can be inserted into the box, dividing it into two equal volumes, and can slide without friction along the box. To extract  $k_B T \ln 2$  of work in an isothermal process of gas expansion one connects up the partition to a pulley. Szilard assumed that in order to realize work extraction it is necessary to know “which side the molecule is on” which corresponds to one bit of information. This model was generalized in various directions including the quantum case, [159] and claimed to be realized experimentally in the classical [160, 161] and the quantum domain [162].

However, the very idea of the equivalence between information and thermodynamics remains controversial [163–165]. As noticed already by Popper and Feyerabend [166] there exist procedures of extracting work without knowing the position of the particle and, on the other hand the mechanism of inserting a partition can provide a necessary amount of work to avoid the conflict with the Kelvin formulation of the Second Law.

The recently developed resource theory of quantum thermodynamics is another example of the interplay between information theory and thermodynamics [167–170] (see also Chaps. 26 and 33). The theory is an axiomatic approach with a mathematical structure motivated by the theory of entanglement. The resource in this theory are states with informational nonequilibrium. Resource theories in quantum information identify a set of restrictive operations that can act on valuable resource states. For a given initial state these restrictive operations then define a set of states that are reachable. For example energy conserving unitaries on the system bath and work repository. The single shot regime refers to operating on a single quantum system, which can be a highly correlated system of many subsystems, rather than on an infinite ensemble of identical and independently distributed copies of a quantum system [170–173]. The idea is to find additional restrictions on possible thermodynamical transformation on finite systems. For example single shot II-laws based on properties

of Rényi divergence [173, 174] which in the thermodynamical limit converge to the standard II-law. The drawback of the theory is that there is no dynamics so there is no reference to a fast or slow operation.

### 1.5.3 Work and Heat

One of the great discoveries in the history of science was the recognition that heat is a form of energy. This allowed to interpret the phenomenological First Law of Thermodynamics

$$dE = \delta Q - \delta W \quad (1.55)$$

as the instance of *energy conservation principle*. However, in contrast to internal energy  $E$ , identified with the total energy of the system, work  $W$  and heat  $Q$  are path-dependent and are therefore *thermodynamic process functions*. In quantum language it means that there are neither described by Hermitian operators [175] nor by nonlinear functions of density matrices like e.g. von Neumann entropy.

It seems that, generally, the instantaneous decomposition corresponding to (1.55) may be even impossible as one needs certain time-scale to decide which part of energy is related to a random motion (heat) or to a deterministic one (work). It seems also that heat, which is transported by irreversible processes can be determined easier than work. The case of Markovian dynamics illustrates very well this problem. Only for slow driving there exists a natural “instantaneous” analogue of (1.55) given by (1.27), while for fast periodic driving only temporal heat currents are well-defined and the unique form of the I-Law is known in the limit cycle only (1.37).

There exists a number of proposals in the literature to define work and heat beyond the Markovian approximation:

1. Work defined in terms of two measurements [176, 177] (useful for Hamiltonian dynamics, fluctuation theorems and full counting statistics, see Chaps. 11 and 15).
2. Heat as the energy exchanged with a bath (including the assumptions of good ergodic properties of the bath and weak influence on the bath by the system).
3. Work reservoir represented by a sink (e.g. low lying level) in Markovian Master equations. Here, the applied standard entropy balance suggests that the energy flow  $J_{\text{sink}}$  dumped in a sink is accompanied by a large flow of entropy  $J_{\text{en}} = J_{\text{sink}}/T_{\text{sink}}$  with the effective sink temperature usually close or even equal to zero. It suggests that  $J_{\text{sink}}$  should be rather interpreted as a heat flow, as work is “energy with negligible entropy”. Otherwise violation of the second law can occur [178].
4. Work reservoir represented by a quantum system (e.g. harmonic oscillator). Treating the whole transferred energy as work one can violate the Carnot bound [179]. The proper procedure seems to be using ergentropy as a measure of work stored in the work reservoir [180] (see also Chaps. 2 and 8).

5. Work measured by *wits* (qubits in excited state), resource theory, analogy to qubits, [167].

### 1.5.4 Thermalization

Considering a finite quantum system: What are the properties that it can serve as a bath? How large does it have to be? What should be its spectrum? How should it couple to the system? Does the system bath dynamics mimic the Markovian GKLS dynamics?

Thermalization can be described as a process where the system loses its memory partly or completely of its initial state and the system settles to a steady state. In classical mechanics chaotic dynamics even in a finite system are sufficient to lead to thermalization. On the contrary, an isolated quantum system has a discrete spectrum and therefore its dynamics is quasiperiodic. Thus strictly speaking, in terms of positive Kolmogorov entropy isolated quantum systems are non chaotic [181]. Another property should lead to quantum thermalization.

The eigenvalue thermalization hypothesis (ETH) [182, 183] (see also Chaps. 17 and 19), applies for strongly coupled quantum systems which therefore possess a Wigner-Dyson distribution of energy gaps [184]. The conjecture is that the expectation value of any operator  $\hat{A}$  will relax asymptotically to its microcanonical value, with the notation of Eq. (1.7) and  $A_{jj} = \langle j | \hat{A} | j \rangle$  [13]:

$$\sum_j |c_j|^2 A_{jj} = \langle A \rangle_{\text{microcan}}(E_0) = \frac{1}{\mathcal{N}_{E_0 \Delta E}} \sum_{|E_0 - E_j| < \Delta E}^j A_{jj} \quad (1.56)$$

where  $E_0$  is the mean energy of the initial state,  $\Delta E$  is the half-width of an appropriately chosen energy window centred at  $E_0$ , and  $\mathcal{N}_{E_0 \Delta E}$  the normalization. The ETH hypothesis has been extensively tested numerically and has been found to apply in sufficiently large and complex systems [13, 185–188]. One should comment that the popular bath composed of noninteracting harmonic oscillators does not fulfil the requirements of the eigenvalue thermalization hypothesis, its ergodic properties being weak because it is a quasi-free system with additional constants of motion.

We can now apply the ETH to a small quantum system coupled to a finite strongly coupled bath. In this case we expect the system to converge to a canonical state. The operators of interest are local in the system. Therefore according to the ETH we expect them to relax to a value which is determined by the bath mean energy with a correction to the finite heat capacity of the bath. This idea has been tested for a system consisting of a one and two qubits and a bath consisting of 32 or 34 strongly and randomly coupled spins. The initial state of the bath was a random phase thermal wavefunction. A Hilbert size of  $\sim 10^{11}$  employed for the study is on the limit of simulation by currently available classical computers. The ETH proved to be correct with respect to the asymptotic system expectation values [189, 190]. In addition, for

the one qubit case a Bloch-type equation with time-dependent coefficients provides a simple and accurate description of the dynamics of a spin particle in contact with a thermal bath. A similar result was found for the 2-qubit system with a variety of bath models.

### 1.5.5 Concluding Remarks

The recent rapid development in the field of quantum thermodynamics is intimately connected to the quantum theory of open systems and strongly influenced by the ideas and methods of quantum information. The new directions of theoretical research are stimulated by the fast technological progress in construction and precise control of micro(meso)scopic devices for information processing and energy transduction. The implementations cover a vast spectrum of physical systems including quantum optical, superconducting, solid state or based on organic molecules devices. The operation conditions for all these systems require refrigeration.

These emerging technologies pose problems of reliability, scalability and efficiency, related to the fundamental principles of thermodynamics, which have to be properly extended to the quantum domain. This extension is a highly nontrivial and controversial task because the standard simplifications used for macroscopic systems are generally not valid at micro(meso)scopic scale, short time-scales and at the presence of strong correlations. Therefore, even the unique definitions of fundamental notions like heat, work and entropy are available only in the limiting cases. Although most of the results suggest that the laws of thermodynamics are still valid in the averaged sense, the role of quantum effects remains an open problem.

One can expect that the further analysis of particular models like quantum heat/chemical engines, quantum pumps, quantum clocks or quantum switches, including mechanisms of feedback and self-oscillations should provide new inputs for improvement and new designs of quantum thermodynamic machines.

**Acknowledgements** We want to thank Amikam Levi and Raam Uzdin for their helpful comments. The work was partially supported by the Israeli Science Foundation: Grant 2244/14.

## References

1. M.K.E.L. Planck, Zur theorie des gesetzes der energieverteilung im normalspectrum. Verhandl. Dtsc. Phys. Ges. **2**, 237 (1900)
2. A. Einstein, Über einen die erzeugung und verwandlung des lichtes betreffenden heuristischen gesichtspunkt. Annalen der physik **322**(6), 132–148 (1905). <https://doi.org/10.1002/andp.19053220607>
3. J. Von Neumann, *Mathematical Foundations of Quantum Mechanics*, vol. 2 (Princeton university press, Princeton, 1955). <https://doi.org/10.1090/s0002-9904-1958-10206-2>
4. A. Einstein, Strahlungs-emission und absorption nach der quantentheorie. Deutsche Physikalische Gesellschaft, 18 (1916)

5. H.E.D. Scovil, E.O. Schulz-DuBois, Three-level masers as heat engines. *Phys. Rev. Lett.* **2**(6), 262 (1959). <https://doi.org/10.1103/PhysRevLett.2.262>
6. J.E. Geusic, B.O. Schulz-DuBois, R.W. De Grasse, H.E.D. Scovil, Three level spin refrigeration and maser action at 1500 mc/sec. *J. Appl. Phys.* **30**(7), 1113–1114 (1959). <https://doi.org/10.1063/1.1776991>
7. J.E. Geusic, E.O. Schulz-DuBios, H.E.D. Scovil, Quantum equivalent of the carnot cycle. *Phys. Rev.* **156**(2), 343 (1967). <https://doi.org/10.1103/PhysRev.156.343>
8. D.J. Wineland, R.E. Drullinger, F.L. Walls, Radiation-pressure cooling of bound resonant absorbers. *Phys. Rev. Lett.* **40**(25), 1639 (1978). <https://doi.org/10.1103/PhysRevLett.40.1639>
9. T.W. Hänsch, A.L. Schawlow, Cooling of gases by laser radiation. *Optics Commun.* **13**(1), 68–69 (1975). [https://doi.org/10.1016/0030-4018\(75\)90159-5](https://doi.org/10.1016/0030-4018(75)90159-5)
10. W. Heisenberg, *The Physical Principles of the Quantum Theory* (Courier Corporation, North Chelmsford, 1949)
11. E. Schrödinger, An undulatory theory of the mechanics of atoms and molecules. *Phys. Rev.* **28**(6), 1049 (1926). <https://doi.org/10.1103/PhysRev.28.1049>
12. P.A.M. Dirac, *The Principles of Quantum Mechanics*, vol. 27 (Oxford university press, Oxford, 1981)
13. M. Rigol, V. Dunjko, M. Olshanii, Thermalization and its mechanism for generic isolated quantum systems. *Nature* **452**(7189), 854–858 (2008). <https://doi.org/10.1038/nature06838>
14. H.B. Callen, *Thermodynamics and An Introduction to Thermostatistics* (University of Pennsylvania, Philadelphia, 1998)
15. R. Haag, D. Kastler, E.B. Trych-Pohlmeyer, Stability and equilibrium states. *Commun. Math. Phys.* **38**(3), 173–193 (1974). <https://doi.org/10.1007/BF01651541>
16. A. Lenard, Thermodynamical proof of the gibbs formula for elementary quantum systems. *J. Stat. Phys.* **19**(6), 575–586 (1978). <https://doi.org/10.1007/BF01011769>
17. W. Pusz, S.L. Woronowicz, Passive states and kms states for general quantum systems. *Commun. Math. Phys.* **58**(3), 273–290 (1978). <https://doi.org/10.1007/BF01614224>
18. R. Kubo, Statistical-mechanical theory of irreversible processes. i. general theory and simple applications to magnetic and conduction problems. *J. Phys. Soc. Jpn.* **12**(6), 570–586 (1957). <https://doi.org/10.1143/JPSJ.12.570>
19. M.S. Green, Markoff random processes and the statistical mechanics of time-dependent phenomena. ii. irreversible processes in fluids. *J. Chem. Phys.* **22**(3), 398–413 (1954). <https://doi.org/10.1063/1.1740082>
20. P.C. Martin, J. Schwinger, Theory of many-particle systems. i. *Phys. Rev.* **115**(6), 1342 (1959). <https://doi.org/10.1103/PhysRev.115.1342>
21. O. Bratteli, D.W. Robinson, Operator algebras and quantum statistical mechanics. vol. 2: Equilibrium states. models in quantum statistical mechanics (1996)
22. K. Kraus, General state changes in quantum theory. *Ann. Phys.* **64**(2), 311–335 (1971). [https://doi.org/10.1016/0003-4916\(71\)90108-4](https://doi.org/10.1016/0003-4916(71)90108-4)
23. W.F. Stinespring, Mr0069403 (16, 1033b) 46.0 x. *Proc. Am. Math. Soc.* **6**, 211–216 (1955)
24. G. Lindblad, Completely positive maps and entropy inequalities. *Commun. Math. Phys.* **40**, 147 (1975). <https://doi.org/10.1007/BF01609396>
25. D. Chruściński, S. Pascazio, A brief history of the gkls equation. *Open Syst. Inf. Dyn.* **24**(03), 1740001 (2017). <https://doi.org/10.1142/S1230161217400017>
26. V. Gorini, A. Kossakowski, E.C.G. Sudarshan, Completely positive dynamical semigroups of n-level systems. *J. Math. Phys.* **17**(5), 821–825 (1976). <https://doi.org/10.1063/1.522979>
27. G. Lindblad, On the generators of quantum dynamical semigroups. *Commun. Math. Phys.* **48**(2), 119–130 (1976). <https://doi.org/10.1007/BF01608499>
28. I. Siemon, A.S. Holevo, R.F. Werner, Unbounded generators of dynamical semigroups. *Open Syst. Inf. Dyn.* **24**(04), 1740015 (2017). <https://doi.org/10.1142/S1230161217400157>
29. E.B. Davies, Markovian master equations. *Commun. Math. Phys.* **39**(2), 91–110 (1974). <https://doi.org/10.1007/BF01608399>

30. R.K. Wangsness, F. Bloch, The dynamical theory of nuclear induction. *Phys. Rev.* **89**(4), 728 (1953). <https://doi.org/10.1103/PhysRev.89.728>
31. A.G. Redfield, On the theory of relaxation processes. *IBM J. Res. Dev.* **1**(1), 19–31 (1957). <https://doi.org/10.1147/rd.11.0019>
32. S. Nakajima, On quantum theory of transport phenomena: steady diffusion. *Prog. Theor. Phys.* **20**(6), 948–959 (1958). <https://doi.org/10.1143/PTP.20.948>
33. R. Zwanzig, Ensemble method in the theory of irreversibility. *J. Chem. Phys.* **33**(5), 1338–1341 (1960). <https://doi.org/10.1063/1.1731409>
34. E. Fermi, *Nuclear Physics: A Course Given by Enrico Fermi at the University of Chicago* (University of Chicago Press, Chicago, 1950)
35. R. Alicki, The markov master equations and the fermi golden rule. *Int. J. Theor. Phys.* **16**(5), 351–355 (1977). <https://doi.org/10.1007/BF01807150>
36. A. Frigerio, Quantum dynamical semigroups and approach to equilibrium. *Lett. Math. Phys.* **2**(2), 79–87 (1977). <https://doi.org/10.1007/BF00398571>
37. E.B. Davies, H. Spohn, Open quantum systems with time-dependent hamiltonians and their linear response. *J. Stat. Phys.* **19**(5), 511–523 (1978). <https://doi.org/10.1007/BF01011696>
38. R. Alicki, The quantum open system as a model of the heat engine. *J. Phys. A: Math. General* **12**(5), L103 (1979). <https://doi.org/10.1088/0305-4470/12/5/007>
39. H. Spohn, Entropy production for quantum dynamical semigroups. *J. Math. Phys.* **19**(5), 1227–1230 (1978). <https://doi.org/10.1063/1.523789>
40. R.T. McAdory Jr., W.C. Schieve, On entropy production in a stochastic model of open systems. *J. Chem. Phys.* **67**(5), 1899–1903 (1977). <https://doi.org/10.1063/1.435120>
41. H. Spohn, J.L. Lebowitz, Irreversible thermodynamics for quantum systems weakly coupled to thermal reservoirs. *Adv. Chem. Phys.* **38**, 109–142 (1978). <https://doi.org/10.1002/9780470142578.ch2>
42. E. Geva, R. Kosloff, J.L. Skinner, On the relaxation of a two-level system driven by a strong electromagnetic field. *J. Chem. Phys.* **102**(21), 8541–8561 (1995). <https://doi.org/10.1063/1.468844>
43. S. Kohler, T. Dittrich, P. Hänggi, Floquet-markovian description of the parametrically driven, dissipative harmonic quantum oscillator. *Phys. Rev. E* **55**(1), 300 (1997). <https://doi.org/10.1103/PhysRevE.55.300>
44. A. Levy, R. Alicki, R. Kosloff, Quantum refrigerators and the third law of thermodynamics. *Phys. Rev. E* **85**, 061126 (2012). <https://doi.org/10.1103/PhysRevE.85.061126>
45. K. Szczęgielski, D. Gelbwaser-Klimovsky, R. Alicki, Markovian master equation and thermodynamics of a two-level system in a strong laser field. *Phys. Rev. E* **87**(1), 012120 (2013). <https://doi.org/10.1103/PhysRevE.87.012120>
46. R. Alicki, D. Gelbwaser-Klimovsky, Non-equilibrium quantum heat machines. *New J. Phys.* **17**(11), 115012 (2015). <https://doi.org/10.1088/1367-2630/17/11/115012>
47. J. Roßnagel, O. Abah, F. Schmidt-Kaler, K. Singer, E. Lutz, Nanoscale heat engine beyond the cannot limit. *Phys. Rev. Lett.* **112**(3), 030602 (2014). <https://doi.org/10.1103/PhysRevLett.112.030602>
48. W. Niedenzu, V. Mukherjee, A. Ghosh, A.G. Kofman, G. Kurizki, Universal thermodynamic limit of quantum engine efficiency, *Nat. Commun.* **9**, 165 (2018). <https://doi.org/10.1038/s41467-017-01991-6>
49. R. Kosloff, Quantum thermodynamics: a dynamical viewpoint. *Entropy* **15**(6), 2100–2128 (2013). <https://doi.org/10.3390/e15062100>
50. P. Pechukas, Reduced dynamics need not be completely positive. *Phys. Rev. Lett.* **73**(8), 1060 (1994). <https://doi.org/10.1103/PhysRevLett.73.1060>
51. R. Alicki, Comment on reduced dynamics: need not be completely positive. *Phys. Rev. Lett.* **75**(16), 3020 (1995). <https://doi.org/10.1103/PhysRevLett.75.3020>
52. G. Lindblad, On the existence of quantum subdynamics. *J. Phys. A: Math. General* **29**(14), 4197 (1996). <https://doi.org/10.1088/0305-4470/29/14/037>
53. G. Argentieri, F. Benatti, R. Floreanini, M. Pezzutto, Violations of the second law of thermodynamics by a non-completely positive dynamics. *EPL (Europhys. Lett.)* **107**(5), 50007 (2014). <https://doi.org/10.1209/0295-5075/107/50007>

54. G. Argentieri, F. Benatti, R. Floreanini, M. Pezzutto, Complete positivity and thermodynamics in a driven open quantum system. *J. Stat. Phys.* **159**(5), 1127–1153 (2015). <https://doi.org/10.1007/s10955-015-1210-4>
55. A.O. Caldeira, A.J. Leggett, Path integral approach to quantum brownian motion. *Phys. A: Stat. Mech. Appl.* **121**(3), 587–616 (1983). [https://doi.org/10.1016/0378-4371\(83\)90013-4](https://doi.org/10.1016/0378-4371(83)90013-4)
56. L. Diósi, Caldera-leggett master equation and medium temperatures. *Phys. A: Stat. Mech. Appl.* **199**(3–4), 517–526 (1993). [https://doi.org/10.1016/0378-4371\(93\)90065-C](https://doi.org/10.1016/0378-4371(93)90065-C)
57. D. Kohen, C. Clay Marston, D.J. Tannor, Phase space approach to theories of quantum dissipation. *J. Chem. Phys.* **107**(13), 5236–5253 (1997). <https://doi.org/10.1063/1.474887>
58. G. Lindblad, Brownian motion of a quantum harmonic oscillator. *Rep. Math. Phys.* **10**(3), 393–406 (1976). [https://doi.org/10.1016/0034-4877\(76\)90029-X](https://doi.org/10.1016/0034-4877(76)90029-X)
59. A. Levy, R. Kosloff, The local approach to quantum transport may violate the second law of thermodynamics. *EPL (Europhys. Lett.)* **107**(2), 20004 (2014). <https://doi.org/10.1209/0295-5075/107/20004>
60. P.P. Hofer, M. Perarnau-Llobet, L.D.M. Miranda, G. Haack, R. Silva, J.B. Brask, N. Brunner, Markovian master equations for quantum thermal machines: local vs global approach. *New J. Phys.* **19**, 123037 (2017). <https://doi.org/10.1088/1367-2630/aa964f>
61. M.T. Mitchison, M.B. Plenio, Non-additive dissipation in open quantum networks out of equilibrium. *New J. Phys.* **20**, 033005 (2018). <https://doi.org/10.1088/1367-2630/aa9f70>
62. J.O. González, L.A. Correa, G. Nocerino, J.P. Palao, D. Alonso, G. Adesso, Testing the validity of the localand globalgkls master equations on an exactly solvable model. *Open Syst. Inf. Dyn.* **24**(04), 1740010 (2017). <https://doi.org/10.1142/S1230161217400108>
63. J.B. Brask, J. Kołodyński, M. Perarnau-Llobet, B. Bylicka, Additivity of dynamical generators for quantum master equations. *Phys. Rev. A* **97**, 062124 (2018). <https://doi.org/10.1103/PhysRevA.97.062124>
64. E. Geva, R. Kosloff, The quantum heat engine and heat pump: an irreversible thermodynamic analysis of the three-level amplifier. *J. Chem. Phys.* **104**(19), 7681–7699 (1996). <https://doi.org/10.1063/1.471453>
65. F. Haake, Statistical treatment of open systems by generalized master equations, in *Springer Tracts in Modern Physics* (Springer, Berlin, 1973), pp. 98–168. [https://doi.org/10.1007/978-3-662-40468-3\\_2](https://doi.org/10.1007/978-3-662-40468-3_2)
66. U. Kleinekathöfer, Non-markovian theories based on a decomposition of the spectral density. *J. Chem. Phys.* **121**(6), 2505–2514 (2004). <https://doi.org/10.1063/1.1770619>
67. I. de Vega, D. Alonso, Dynamics of non-markovian open quantum systems. *Rev. Mod. Phys.* **89**(1), 015001 (2017). <https://doi.org/10.1103/RevModPhys.89.15001>
68. F. Shibata, Y. Takahashi, N. Hashitsume, A generalized stochastic liouville equation. non-markovian versus memoryless master equations. *J. Stat. Phys.* **17**(4), 171–187 (1977). <https://doi.org/10.1007/BF01040100>
69. A.G. Kofman, G. Kurizki, Unified theory of dynamically suppressed qubit decoherence in thermal baths. *Phys. Rev. Lett.* **93**(13), 130406 (2004). <https://doi.org/10.1103/PhysRevLett.93.130406>
70. Y. Tanimura, R. Kubo, Time evolution of a quantum system in contact with a nearly gaussian-markoffian noise bath. *J. Phys. Soc. Jpn.* **58**(1), 101–114 (1989). <https://doi.org/10.1143/JPSJ.58.101>
71. C. Meier, D.J. Tannor, Non-markovian evolution of the density operator in the presence of strong laser fields. *J. Chem. Phys.* **111**(8), 3365–3376 (1999). <https://doi.org/10.1063/1.479669>
72. J. Jin, X. Zheng, Y. Yan, Exact dynamics of dissipative electronic systems and quantum transport: Hierarchical equations of motion approach. *J. Chem. Phys.* **128**(23), 234703 (2008). <https://doi.org/10.1063/1.2938087>
73. A. Ishizaki, G.R. Fleming, Unified treatment of quantum coherent and incoherent hopping dynamics in electronic energy transfer: Reduced hierarchy equation approach. *J. Chem. Phys.* **130**(23), 234111 (2009). <https://doi.org/10.1063/1.3155372>

74. S. Marcantoni, S. Alipour, F. Benatti, R. Floreanini, A.T. Rezakhani, Entropy production and non-markovian dynamical maps. *Sci. Rep.* **7**(1), 12447 (2017). <https://doi.org/10.1038/s41598-017-12595-x>
75. S. Alipour, F. Benatti, F. Bakhshinezhad, M. Afsary, S. Marcantoni, A.T. Rezakhani, Correlations in quantum thermodynamics: heat, work, and entropy production. *Sci. Rep.* **6** (2016). <https://doi.org/10.1038/srep35568>
76. M. Esposito, M.A. Ochoa, M. Galperin, Quantum thermodynamics: a nonequilibrium green's function approach. *Phys. Rev. Lett.* **114**(8), 080602 (2015). <https://doi.org/10.1103/PhysRevLett.114.080602>
77. M.F. Ludovico, M. Moskalets, D. Sánchez, L. Arrachea, Dynamics of energy transport and entropy production in ac-driven quantum electron systems. *Phys. Rev. B* **94**(3), 035436 (2016). <https://doi.org/10.1103/PhysRevB.94.035436>
78. M.A. Ochoa, A. Bruch, A. Nitzan, Energy distribution and local fluctuations in strongly coupled open quantum systems: the extended resonant level model. *Phys. Rev. B* **94**(3), 035420 (2016). <https://doi.org/10.1103/PhysRevB.94.035420>
79. G. Schaller, T. Krause, T. Brandes, M. Esposito, Single-electron transistor strongly coupled to vibrations: counting statistics and fluctuation theorem. *New J. Phys.* **15**(3), 033032 (2013). <https://doi.org/10.1088/1367-2630/15/3/033032>
80. D. Segal, Two-level system in spin baths: Non-adiabatic dynamics and heat transport. *J. Chem. Phys.* **140**(16), 164110 (2014). <https://doi.org/10.1063/1.4871874>
81. X. Dazhi, C. Wang, Y. Zhao, J. Cao, Polaron effects on the performance of light-harvesting systems: a quantum heat engine perspective. *New J. Phys.* **18**(2), 023003 (2016). <https://doi.org/10.1088/1367-2630/18/2/023003>
82. C. Wang, J. Ren, J. Cao, Unifying quantum heat transfer in a nonequilibrium spin-boson model with full counting statistics. *Phys. Rev. A* **95**(2), 023610 (2017). <https://doi.org/10.1103/PhysRevA.95.023610>
83. D. Gelbwaser-Klimovsky, A. Aspuru-Guzik, Strongly coupled quantum heat machines. *J. Phys. Chem. Lett.* **6**(17), 3477–3482 (2015). <https://doi.org/10.1021/acs.jpclett.5b01404>
84. A. Bruch, M. Thomas, S.V. Kusminskiy, F. von Oppen, A. Nitzan, Quantum thermodynamics of the driven resonant level model. *Phys. Rev. B* **93**(11), 115318 (2016). <https://doi.org/10.1103/PhysRevB.93.115318>
85. P. Strasberg, G. Schaller, N. Lambert, T. Brandes, Nonequilibrium thermodynamics in the strong coupling and non-markovian regime based on a reaction coordinate mapping. *New J. Phys.* **18**(7), 073007 (2016). <https://doi.org/10.1088/1367-2630/18/7/073007>
86. D. Newman, F. Mintert, A. Nazir, Performance of a quantum heat engine at strong reservoir coupling. *Phys. Rev. E* **95**(3), 032139 (2017). <https://doi.org/10.1103/PhysRevE.95.032139>
87. M. Perarnau-Llobet, H. Wimling, A. Riera, R. Gallego, J. Eisert, Strong coupling corrections in quantum thermodynamics. *Phys. Rev. Lett.* **120**(12), 120602 (2018). <https://doi.org/10.1103/PhysRevLett.120.120602>
88. G. Katz, R. Kosloff, Quantum thermodynamics in strong coupling: heat transport and refrigeration. *Entropy* **18**(5), 186 (2016). <https://doi.org/10.3390/e18050186>
89. R. Uzdin, A. Levy, R. Kosloff, Quantum heat machines equivalence and work extraction beyond markovianity, and strong coupling via heat exchangers. *Entropy* **18**, 124 (2016). <https://doi.org/10.3390/e18040124>
90. S. Carnot, Réflexions sur la puissance motrice du feu et sur les machines propres à développer cette puissance. *Annales scientifiques de l'Ecole normale* (1872). <https://doi.org/10.24033/asens.88>
91. J. Roßnagel, S.T. Dawkins, K.N. Tolazzi, O. Abah, E. Lutz, F. Schmidt-Kaler, K. Singer, A single-atom heat engine. *Science* **352**(6283), 325–329 (2016). <https://doi.org/10.1126/science.aad6320>
92. T. Feldmann, R. Kosloff, Characteristics of the limit cycle of a reciprocating quantum heat engine. *Phys. Rev. E* **70**(4), 046110 (2004). <https://doi.org/10.1103/PhysRevE.70.046110>
93. Y. Rezek, R. Kosloff, Irreversible performance of a quantum harmonic heat engine. *New J. Phys.* **8**(5), 83 (2006). <https://doi.org/10.1088/1367-2630/8/5/083>

94. E. Geva, R. Kosloff, A quantum-mechanical heat engine operating in finite time. a model consisting of spin-1/2 systems as the working fluid. *The J. Chem. Phys.* **96**(4), 3054–3067 (1992). <https://doi.org/10.1063/1.461951>
95. T. Feldmann, R. Kosloff, Quantum four-stroke heat engine: thermodynamic observables in a model with intrinsic friction. *Phys. Rev. E* **68**(1), 016101 (2003). <https://doi.org/10.1103/PhysRevE.68.016101>
96. M. Esposito, Stochastic thermodynamics under coarse graining. *Phys. Rev. E* **85**(4), 041125 (2012). <https://doi.org/10.1103/PhysRevE.85.041125>
97. U. Seifert, Stochastic thermodynamics, fluctuation theorems and molecular machines. *Rep. Prog. Phys.* **75**(12), 126001 (2012). <https://doi.org/10.1088/0034-4885/75/12/126001>
98. F. Plastina, A. Alecce, T.J.G. Apollaro, G. Falcone, G. Francica, F. Galve, N. Lo Gullo, R. Zambrini, Irreversible work and inner friction in quantum thermodynamic processes. *Phys. Rev. Lett.* **113**(26), 260601 (2014). <https://doi.org/10.1103/PhysRevLett.113.260601>
99. A. Xi Chen, S. Ruschhaupt, A. Del Campo, D. Guéry-Odelin, J.G. Muga, Fast optimal frictionless atom cooling in harmonic traps: shortcut to adiabaticity. *Phys. Rev. Lett.* **104**(6), 063002 (2010). <https://doi.org/10.1103/PhysRevLett.104.063002>
100. E. Torrontegui, S. Ibáñez, S. Martínez-Garaot, M. Modugno, A. del Campo, D. Guéry-Odelin, A. Ruschhaupt, X. Chen, J.G. Muga, Shortcuts to adiabaticity. *Adv. At. Mol. Opt. Phys.* **62**, 117–169 (2013). <https://doi.org/10.1016/B978-0-12-408090-4.00002-5>
101. A. Del Campo, J. Goold, M. Paternostro, More bang for your buck: Super-adiabatic quantum engines. *Sci. Rep.* **4** (2014). <https://doi.org/10.1038/srep06208>
102. J. Anandan, Y. Aharonov, Geometry of quantum evolution. *Phys. Rev. Lett.* **65**(14), 1697 (1990). <https://doi.org/10.1103/PhysRevLett.65.1697>
103. S. Deffner, E. Lutz, Energy-time uncertainty relation for driven quantum systems. *J. Phys. A: Math. Theor.* **46**(33), 335302 (2013). <https://doi.org/10.1088/1751-8113/46/33/335302>
104. D. Stefanatos, Minimum-time transitions between thermal and fixed average energy states of the quantum parametric oscillator. *SIAM J. Control Optim.* **55**(3), 1429–1451 (2017). <https://doi.org/10.1137/16M1088697>
105. M.O. Scully, M.S. Zubairy, G.S. Agarwal, H. Walther, Extracting work from a single heat bath via vanishing quantum coherence. *Science* **299**(5608), 862–864 (2003). <https://doi.org/10.1126/science.1078955>
106. W. Niedenzu, D. Gelbwaser-Klimovsky, A.G. Kofman, G. Kurizki, On the operation of machines powered by quantum non-thermal baths. *New J. Phys.* **18**(8), 083012 (2016). <https://doi.org/10.1088/1367-2630/18/8/083012>
107. I.I. Novikov, The efficiency of atomic power stations (a review). *J. Nucl. Energy* **7**(1), 125–128 (1954). [https://doi.org/10.1016/0891-3919\(58\)90244-4](https://doi.org/10.1016/0891-3919(58)90244-4)
108. F.L. Curzon, B. Ahlborn, Efficiency of a carnot engine at maximum power output. *Am. J. Phys.* **43**(1), 22–24 (1975). <https://doi.org/10.1119/1.10023>
109. R. Uzdin, R. Kosloff, Universal features in the efficiency at maximal work of hot quantum otto engines. *EPL (Europhys. Lett.)* **108**(4), 40001 (2014). <https://doi.org/10.1209/0295-5075-108/40001>
110. V. Cavina, A. Mari, V. Giovannetti, Slow dynamics and thermodynamics of open quantum systems. *Phys. Rev. Lett.* **119**(5), 050601 (2017). <https://doi.org/10.1103/PhysRevLett.119.050601>
111. B. Andresen, R.S. Berry, A. Nitzan, P. Salamon, Thermodynamics in finite time. i. the step-carnot cycle. *Phys. Rev. A* **15**(5), 2086 (1977). <https://doi.org/10.1103/PhysRevA.15.2086>
112. P. Salamon, J.D. Nulton, G. Siragusa, T.R. Andersen, A. Limon, Principles of control thermodynamics. *Energy* **26**(3), 307–319 (2001). [https://doi.org/10.1016/S0360-5442\(00\)00059-1](https://doi.org/10.1016/S0360-5442(00)00059-1)
113. E. Geva, R. Kosloff, On the classical limit of quantum thermodynamics in finite time. *J. Chem. Phys.* **97**(6), 4398–4412 (1992). <https://doi.org/10.1063/1.463909>
114. M. Esposito, R. Kawai, K. Lindenberg, C. Van den Broeck, Efficiency at maximum power of low-dissipation carnot engines. *Phys. Rev. Lett.* **105**(15), 150603 (2010). <https://doi.org/10.1103/PhysRevLett.105.150603>

115. H.T. Quan, Y.-x. Liu, C.P. Sun, F. Nori, Quantum thermodynamic cycles and quantum heat engines. *Phys. Rev. E* **76**(3), 031105 (2007). <https://doi.org/10.1103/PhysRevE.76.031105>
116. A.E. Allahverdyan, R.S. Johal, G. Mahler, Work extremum principle: Structure and function of quantum heat engines. *Phys. Rev. E* **77**(4), 041118 (2008). <https://doi.org/10.1103/PhysRevE.77.041118>
117. R. Uzdin, A. Levy, R. Kosloff, Quantum equivalence and quantum signatures in heat engines. *Phys. Rev. X* **5**, 031044 (2015). <https://doi.org/10.1103/PhysRevX.5.031044>
118. P.R. Chernoff, *Product Formulas, Nonlinear Semigroups, and Addition of Unbounded Operators*, vol. 140 (American Mathematical Soc., 1974)
119. T. Feldmann, R. Kosloff, Performance of discrete heat engines and heat pumps in finite time. *Phys. Rev. E* **61**(5), 4774 (2000). <https://doi.org/10.1103/PhysRevE.61.4774>
120. Y. Rezek, P. Salamon, K.H. Homann, R. Kosloff, The quantum refrigerator: the quest for absolute zero. *EPL (Europhys. Lett.)* **85**(3), 30008 (2009). <https://doi.org/10.1209/0295-5075/85/30008>
121. R. Kosloff, A quantum mechanical open system as a model of a heat engine. *J. Chem. Phys.* **80**(4), 1625–1631 (1984). <https://doi.org/10.1063/1.446862>
122. J.P. Palao, R. Kosloff, J.M. Gordon, Quantum thermodynamic cooling cycle. *Phys. Rev. E* **64**(5), 056130 (2001). <https://doi.org/10.1103/PhysRevE.64.056130>
123. F. Tonner, G. Mahler, Autonomous quantum thermodynamic machines. *Phys. Rev. E* **72**(6), 066118 (2005). <https://doi.org/10.1103/PhysRevE.72.066118>
124. N. Linden, S. Popescu, P. Skrzypczyk, How small can thermal machines be? the smallest possible refrigerator. *Phys. Rev. Lett.* **105**(13), 130401 (2010). <https://doi.org/10.1103/PhysRevLett.105.130401>
125. A. Levy, L. Diósi, R. Kosloff, Quantum flywheel. *Phys. Rev. A* **93**, 052119 (2016). <https://doi.org/10.1103/PhysRevA.93.052119>
126. A. Levy, R. Kosloff, Quantum absorption refrigerator. *Physical Review Letters* **108**, 070604 (2012). <https://doi.org/10.1103/PhysRevLett.108.070604>
127. O.-P. Saira, M. Meschke, F. Giazotto, A.M. Savin, M. Möttönen, J.P. Pekola, Heat transistor: demonstration of gate-controlled electronic refrigeration. *Phys. Rev. Lett.* **99**(2), 027203 (2007). <https://doi.org/10.1103/PhysRevLett.99.027203>
128. P. Skrzypczyk, N. Brunner, N. Linden, S. Popescu, The smallest refrigerators can reach maximal efficiency. *J. Phys. A: Math. Theor.* **44**(49), 492002 (2011). <https://doi.org/10.1088/1751-8113/44/49/492002>
129. L.A. Correa, J.P. Palao, G. Adesso, D. Alonso, Performance bound for quantum absorption refrigerators. *Phys. Rev. E* **87**(4), 042131 (2013). <https://doi.org/10.1103/PhysRevE.87.042131>
130. R. Kosloff, A. Levy, Quantum heat engines and refrigerators: continuous devices. *Ann. Rev. Phys. Chem.* **65**, 365–393 (2014). <https://doi.org/10.1146/annurev-physchem-040513-103724>
131. G. Maslennikov, S. Ding, R. Hablutzel, J. Gan, A. Roulet, S. Nimmrichter, J. Dai, V. Scarani, D. Matsukevich, Quantum absorption refrigerator with trapped ions (2017). <https://doi.org/10.1109/CLEOE-EQEC.2017.8087335>
132. E.A. Martinez, J.P. Paz, Dynamics and thermodynamics of linear quantum open systems. *Phys. Rev. Lett.* **110**(13), 130406 (2013). <https://doi.org/10.1103/PhysRevLett.110.130406>
133. R. Clausius, Über die bewegende kraft der wärme und die gesetze, welche sich daraus für die wärmelehre selbst ableiten lassen. *Annalen der Physik* **155**(3), 368–397 (1850). <https://doi.org/10.1002/andp.18501550306>
134. L.A. Correa, J.P. Palao, D. Alonso, G. Adesso, Quantum-enhanced absorption refrigerators. *Sci. Rep.* **4**, srep03949 (2014). <https://doi.org/10.1038/srep03949>
135. A. Mu, B.K. Agarwalla, G. Schaller, D. Segal, Qubit absorption refrigerator at strong coupling. *New J. Phys.* **19**(12), 123034 (2017). <https://doi.org/10.1088/1367-2630/aa9b75>
136. W. Nernst, Ueber die Berechnung chemischer Gleichgewichte aus thermischen Messungen. *Nachr. Kgl. Ges. Wiss. Gött.* **1**, 40 (1906)

137. P.T. Landsberg, A comment on nernst's theorem. *J. Phys A: Math. Gen.* **22**, 139 (1989). <https://doi.org/10.1088/0305-4470/22/1/021>
138. A. Levy, R. Alicki, R. Kosloff, Comment on cooling by heating: refrigeration powered by photons. *Phys. Rev. Lett.* **109**, 248901 (2012). <https://doi.org/10.1103/PhysRevLett.109.248901>
139. W. Nernst, *The theoretical and experimental bases of the New Heat Theorem Ger, Die theoretischen und experimentellen Grundlagen des neuen Wärmesatzes*. W. Knapp, Halle, 1918
140. L. Masanes, J. Oppenheim, A general derivation and quantification of the third law of thermodynamics. *Nat. Commun.* **8** (2017). <https://doi.org/10.1038/ncomms14538>
141. N. Freitas, J.P. Paz, Fundamental limits for cooling of linear quantum refrigerators. *Phys. Rev. E* **95**(1), 012146 (2017). <https://doi.org/10.1103/PhysRevE.95.012146>
142. D. Gelbwaser-Klimovsky, R. Alicki, G. Kurizki, Minimal universal quantum heat machine. *Phys. Rev. E* **87**(1), 012140 (2013). <https://doi.org/10.1103/PhysRevE.87.012140>
143. Y. Zhou, D. Segal, Minimal model of a heat engine: information theory approach. *Phys. Rev. E* **82**(1), 011120 (2010). <https://doi.org/10.1103/PhysRevE.82.011120>
144. D. Gelbwaser-Klimovsky, R. Alicki, G. Kurizki, Work and energy gain of heat-pumped quantized amplifiers. *EPL (Europhys. Lett.)* **103**(6), 60005 (2013). <https://doi.org/10.1209/0295-5075/103/60005>
145. E. Boukobza, D.J. Tannor, Three-level systems as amplifiers and attenuators: a thermodynamic analysis. *Phys. Rev. Lett.* **98**(24), 240601 (2007). <https://doi.org/10.1103/PhysRevLett.98.240601>
146. S.-W. Li, M.B. Kim, G.S. Agarwal, M.O. Scully, Quantum statistics of a single-atom Scovil-Schulz-DuBois heat engine. *Phys. Rev. A* **96**(6), 063806 (2017). <https://doi.org/10.1103/PhysRevA.96.063806>
147. G. Benenti, G. Casati, K. Saito, R.S. Whitney, Fundamental aspects of steady-state conversion of heat to work at the nanoscale. *Phys. Rep.* **694**, 1 (2017). <https://doi.org/10.1016/j.physrep.2017.05.008>
148. R. Alicki, D. Gelbwaser-Klimovsky, A. Jenkins, A thermodynamic cycle for the solar cell. *Ann. Phys.* **378**, 71–87 (2017). <https://doi.org/10.1016/j.aop.2017.01.003>
149. R. Alicki, D. Gelbwaser-Klimovsky, K. Szczygielski, Solar cell as a self-oscillating heat engine. *J. Phys. A: Math. Theor.* **49**(1), 015002 (2015). <https://doi.org/10.1088/1751-8113/49/1/015002>
150. R. Alicki, Thermoelectric generators as self-oscillating heat engines. *J. Phys. A: Math. Theor.* **49**(8), 085001 (2016). <https://doi.org/10.1088/1751-8113/49/8/085001>
151. H. Lee, J. Wu, J. Barbe, S.M. Jain, S. Wood, E. Speller, Z. Li, F.A. de Castro, J. Durrant, W. Tsai, Organic photovoltaic cell—a promising indoor light harvester for self-sustainable electronics. *J. Mater. Chem. A* (2017). <https://doi.org/10.1039/C7TA10875C>
152. A.A. Bakulin, R. Lovrincic, X. Yu, O. Selig, H.J. Bakker, Yves L.A. Rezus, P.K. Nayak, A. Fonari, V. Coropceanu, J.-L. Brédas et al., Mode-selective vibrational modulation of charge transport in organic electronic devices. *Nat. Commun.* **6** (2015). <https://doi.org/10.1038/ncomms8880>
153. A.W. Chin, J. Prior, R. Rosenbach, F. Caycedo-Soler, S.F. Huelga, M.B. Plenio, The role of non-equilibrium vibrational structures in electronic coherence and decoherence in pigment-protein complexes. *Nat. Phys.* **9**(2), 113–118 (2013). <https://doi.org/10.1038/nphys2515>
154. M.A. Nielsen, I. Chuang, *Quantum Computation and Quantum Information* (2002). <https://doi.org/10.1119/1.1463744>
155. R. Landauer, Irreversibility and heat generation in the computing process. *IBM J. Res. Dev.* **5**(3), 183–191 (1961). <https://doi.org/10.1147/rd.53.0183>
156. C.H. Bennett, Notes on landauer's principle, reversible computation, and maxwell's demon. *Stud. Hist. Philos. Sci. Part B: Stud. Hist. Philos. Mod. Phys.* **34**(3), 501–510 (2003). [https://doi.org/10.1016/S1355-2198\(03\)00039-X](https://doi.org/10.1016/S1355-2198(03)00039-X)
157. L. Szilard, Über die ausdehnung der phänomenologischen thermodynamik auf die schwankungsscheinungen. *Zeitschrift für Physik A Hadrons and Nuclei* **32**(1), 753–788 (1925). <https://doi.org/10.1007/BF01331713>

158. L. Szilard, Über die entropieverminderung in einem thermodynamischen system bei eingriffen intelligenter wesen. *Zeitschrift für Physik A Hadrons and Nuclei* **53**(11), 840–856 (1929). <https://doi.org/10.1007/BF01341281>
159. T. Sagawa, Thermodynamics of information processing in small system. *Prog. Theor. Phys.* **127**(1), 1–56 (2012). <https://doi.org/10.1143/PTP.127.1>
160. S. Toyabe, T. Sagawa, M. Ueda, E. Muneyuki, M. Sano, Experimental demonstration of information-to-energy conversion and validation of the generalized jarzynski equality. *Nat. Phys.* **6**(12), 988–992 (2010). <https://doi.org/10.1038/nphys1821>
161. A. Bérut, A. Arakelyan, A. Petrosyan, S. Ciliberto, R. Dillenschneider, E. Lutz, Experimental verification of landauer's principle linking information and thermodynamics. *Nature* **483**(7388), 187–189 (2012). <https://doi.org/10.1038/nature10872>
162. P. Jukka, J.P. Pekola, Towards quantum thermodynamics in electronic circuits. *Nat. Phys.* **11**(2), 118–123 (2015). <https://doi.org/10.1038/nphys3169>
163. J.D. Norton, Eaters of the lotus: Landauer's principle and the return of maxwell's demon. *Stud. Hist. Philos. Sci. Part B: Stud. Hist. Philos. Mod. Phys.* **36**(2), 375–411 (2005). <https://doi.org/10.1016/j.shpsb.2004.12.002>
164. O.R. Shenker, Logic and Entropy (2000). <http://philsci-archive.pitt.edu/id/eprint/115>
165. R. Alicki, Information is not physical (2014). [arXiv:1402.2414](https://arxiv.org/abs/1402.2414)
166. P. Feyerabend, Consolations for the specialist. *Crit. Growth Knowl.* **4**, 197–229 (1970). <https://doi.org/10.1017/CBO9781139171434.010>
167. M. Horodecki, J. Oppenheim, Fundamental limitations for quantum and nanoscale thermodynamics. *Nat. Commun.* **4**, 2059 (2013). <https://doi.org/10.1038/ncomms3059>
168. G. Gour, M.P. Müller, V. Narasimhachar, R.W. Spekkens, N.Y. Halpern, The resource theory of informational nonequilibrium in thermodynamics. *Phys. Rep.* **583**, 1–58 (2015). <https://doi.org/10.1016/j.physrep.2015.04.003>
169. J. Goold, M. Huber, A. Riera, L. del Rio, P. Skrzypczyk, The role of quantum information in thermodynamics? a topical review. *J. Phys. A: Math. Theor.* **49**(14), 143001 (2016). <https://doi.org/10.1088/1751-8113/49/14/143001>
170. S. Vinjanampathy, J. Anders, Quantum thermodynamics. *Contemp. Phys.* **57**(4), 545–579 (2016). <https://doi.org/10.1080/00107514.2016.1201896>
171. K. Korzekwa, M. Lostaglio, J. Oppenheim, D. Jennings, The extraction of work from quantum coherence. *New J. Phys.* **18**(2), 023045 (2016). <https://doi.org/10.1088/1367-2630/18/2/023045>
172. J. Goold, M. Huber, A. Riera, L. del Rio, P. Skrzypczyk, The role of quantum information in thermodynamics: a topical review. *J. Phys. A: Math. Theor.* **49**(14), 143001 (2016). <https://doi.org/10.1088/1751-8113/49/14/143001>
173. F. Brandao, M. Horodecki, N. Ng, J. Oppenheim, S. Wehner, The second laws of quantum thermodynamics. *Proc. Natl. Acad. Sci.* **112**(11), 3275–3279 (2015). <https://doi.org/10.1073/pnas.1411728112>
174. A. Rényi et al., On measures of entropy and information. in *Proceedings of the Fourth Berkeley Symposium on Mathematical Statistics and Probability, Volume 1: Contributions to the Theory of Statistics* (The Regents of the University of California, 1961). <https://projecteuclid.org/euclid.bsmsp/1200512181>
175. P. Talkner, E. Lutz, P. Hänggi, Fluctuation theorems: work is not an observable. *Phys. Rev. E* **75**(5), 050102 (2007). <https://doi.org/10.1103/PhysRevE.75.050102>
176. A.J. Roncaglia, F. Cerisola, J.P. Paz, Work measurement as a generalized quantum measurement. *Phys. Rev. Lett.* **113**(25), 250601 (2014). <https://doi.org/10.1103/PhysRevLett.113.250601>
177. R. Sampaio, S. Suomela, T. Ala-Nissila, J. Anders, T. Philbin, The impossible quantum work distribution (2017). *Phys. Rev. A* **97**, 012131 (2018)
178. D. Gelbwaser-Klimovsky, A. Aspuru-Guzik, On thermodynamic inconsistencies in several photosynthetic and solar cell models and how to fix them. *Chem. Sci.* **8**(2), 1008–1014 (2017). <https://doi.org/10.1039/C6SC04350J>

179. E. Boukobza, H. Ritsch, Breaking the carnot limit without violating the second law: a thermodynamic analysis of off-resonant quantum light generation. *Phys. Rev. A* **87**(6), 063845 (2013). <https://doi.org/10.1103/PhysRevA.87.063845>
180. R. Alicki, From the gkls equation to the theory of solar and fuel cells. *Open Syst. Inf. Dyn.* **24**(03), 1740007 (2017). <https://doi.org/10.1142/S1230161217400078>
181. R. Kosloff, S.A. Rice, The influence of quantization on the onset of chaos in hamiltonian systems: the kolmogorov entropy interpretation. *J. Chem. Phys.* **74**(2), 1340–1349 (1981). <https://doi.org/10.1063/1.441196>
182. J.M. Deutsch, Quantum statistical mechanics in a closed system. *Phys. Rev. A* **43**(4), 2046 (1991). <https://doi.org/10.1103/PhysRevA.43.2046>
183. M. Srednicki, Chaos and quantum thermalization. *Phys. Rev. E* **50**(2), 888 (1994). <https://doi.org/10.1103/PhysRevE.50.888>
184. F.J. Dyson, Statistical theory of the energy levels of complex systems. i. *J. Math. Phys.* **3**(1), 140–156 (1962)
185. H. Kim, T.N. Ikeda, D.A. Huse, Testing whether all eigenstates obey the eigenstate thermalization hypothesis. *Phys. Rev. E* **90**(5), 052105 (2014). <https://doi.org/10.1103/PhysRevE.90.052105>
186. R. Steinigeweg, A. Khodja, H. Niemeyer, C. Gogolin, J. Gemmer, Pushing the limits of the eigenstate thermalization hypothesis towards mesoscopic quantum systems. *Phys. Rev. Lett.* **112**(13), 130403 (2014). <https://doi.org/10.1103/PhysRevLett.112.130403>
187. T.N. Ikeda, Y. Watanabe, M. Ueda, Finite-size scaling analysis of the eigenstate thermalization hypothesis in a one-dimensional interacting bose gas. *Phys. Rev. E* **87**(1), 012125 (2013). <https://doi.org/10.1103/PhysRevE.87.012125>
188. V. Alba, Eigenstate thermalization hypothesis and integrability in quantum spin chains. *Phys. Rev. B* **91**(15), 155123 (2015). <https://doi.org/10.1103/PhysRevB.91.155123>
189. P. Zhao, H. De Raedt, S. Miyashita, F. Jin, K. Michielsen, Dynamics of open quantum spin systems: An assessment of the quantum master equation approach. *Phys. Rev. E* **94**(2), 022126 (2016). <https://doi.org/10.1103/PhysRevE.94.022126>
190. H. De Raedt, F. Jin, M.I. Katsnelson, K. Michielsen, Relaxation, thermalization, and markovian dynamics of two spins coupled to a spin bath. *Phys. Rev. E* **96**(5), 053306 (2017). <https://doi.org/10.1103/PhysRevE.96.053306>

**Part I**

**Continuous and Discrete Quantum Heat  
Devices**

# Chapter 2

## Thermodynamic Principles and Implementations of Quantum Machines



**Arnab Ghosh, Wolfgang Niedenzu, Victor Mukherjee  
and Gershon Kurizki**

The efficiency of cyclic heat engines is limited by the Carnot bound. This bound follows from the second law of thermodynamics and is attained by engines that operate between two thermal baths under the reversibility condition whereby the total entropy does not increase. By contrast, the efficiency of engines powered by quantum non-thermal baths has been claimed to surpass the thermodynamic Carnot bound. The key to understanding the performance of such engines is a proper division of the energy supplied by the bath to the system into heat and work, depending on the associated change in the system entropy and ergentropy. Due to their hybrid character, the efficiency bound for quantum engines powered by a non-thermal bath does not solely follow from the laws of thermodynamics. Hence, the thermodynamic Carnot bound is inapplicable to such hybrid engines. Yet, they do not violate the principles of thermodynamics. An alternative means of boosting machine performance is the concept of heat-to-work conversion catalysis by quantum non-linear (squeezed) pumping of the piston mode. This enhancement is due to the increased ability of the squeezed piston to store ergentropy. Since the catalyzed machine is fueled by thermal baths, it adheres to the Carnot bound. We conclude by arguing that it is not quantumness per se that improves the machine performance, but rather the properties of the baths, the working fluid and the piston that boost the ergentropy and minimize the wasted heat in both the input and the output.

---

A. Ghosh · W. Niedenzu · V. Mukherjee · G. Kurizki (✉)  
Department of Chemical and Biological Physics, Weizmann Institute of Science,  
7610001 Rehovot, Israel  
e-mail: gershon.kurizki@weizmann.ac.il

W. Niedenzu  
Institut für Theoretische Physik, Universität Innsbruck, Technikerstraße 21a,  
A-6020 Innsbruck, Austria

## 2.1 Introduction

Engines transform some form of energy, such as thermal, chemical, mechanical, or electrical energy into useful work. Their efficiency, namely, the ratio of the output work to the input energy, is restricted to 1 at most by energy conservation. Engines converting mechanical (potential, kinetic or rotational) energy into work may, in principle, approach unit efficiency. By contrast, the efficiency of heat-to-work conversion in a cyclic heat engine that operates between cold and hot thermal baths with temperature ratio  $T_c/T_h$  is independent of the specific design and limited by the universal Carnot bound [1]. This bound follows from the second law of thermodynamics under the *reversibility* condition, whereby the total (combined) entropy of the engine and the two baths is unaltered over a cycle [2].

As opposed to standard heat engines (HE) conforming to the above description, diverse models of cyclic engines energized by *quantum non-thermal* baths have been suggested to *surpass* the Carnot bound [3–12]. Until recently, there has been no clear, rigorously founded answer to the questions: Is there a common mechanism for such surpassing? And if there is, does it not violate the second law? The issue is even broader: In many models the engine comprises quantum-mechanical ingredients whose purpose is to provide a “quantum advantage” or “quantum supremacy” [3–31]. What are, if any, their common operational principles and their impact on the performance? In particular, can we assess their maximum efficiency from the second law via the reversibility condition as in standard HE?

Here we present an overview of our recent endeavor [9, 32–34] to resolve the foregoing principle issues of cyclic quantum machines fuelled by arbitrary baths: The fundamental aspect of this endeavor has been the understanding of the role played by the first and second laws in quantum dissipative processes that characterize bath-powered engines. It is widely accepted [10, 13, 20, 25, 26, 29, 35–44] that the second law applied to quantum relaxation processes is faithfully rendered by Spohn’s inequality [45]. According to this inequality, the entropy change of a system that interacts with a thermal bath is bounded from below by the exchanged energy divided by the bath temperature. We have shown [33], however, that the bound on entropy change in quantum dissipative processes crucially depends on whether the state of the system is non-passive. The definition of a non-passive state [46–48] is that its energy can be unitarily reduced until the state becomes passive, thereby extracting work. The maximum amount of work extractable from such states (their “work capacity”) has been dubbed “ergotropy” in Ref. [48]. Non-passive states may thus be thought of as “quantum batteries” [49–51]. Examples of non-passive states are squeezed or coherent states of a harmonic oscillator [9, 22, 52].

The significance of non-passivity [9, 25, 26, 29, 32, 46–56] as a work resource in bath-powered engines has been demonstrated by us in our classification [9, 32, 33] of such machines according to their operation principle, as discussed below:

- *Machines of the first kind* are fuelled by a non-thermal bath, such as a squeezed thermal [7] or coherently-displaced thermal bath [55], that render the working fluid (WF) steady-state *non-passive* [22, 25, 26, 46–48, 52]. We have pointed out [9, 32,

[33] that in such machines the energy imparted by the non-thermal bath consists of a part that increases the ergotropy of the WF and an entropy-changing part that changes the WF's passive energy. This division of the transferred energy into work-like and heat-like contributions implies that the efficiency of machines of the first kind *does not have a thermodynamic bound that may be deduced from the reversibility condition expressed by the second law*. This becomes clear when the energy of the non-thermal bath has no thermal component and is pure ergotropy: The engine can then deliver work without heat input. Hence, such machines may be thought of as *hybrid thermo-mechanical engines*. Their efficiency bound cannot be properly compared with the Carnot bound, since the latter is a restriction imposed by the second law on heat [2] but not on work imparted by the bath.

- *Machines of the second kind* are heat engines wherein the WF is *thermalized*, i.e., is rendered passive by the bath, be it thermal or non-thermal. Hence, the entire energy transfer from the bath to the WF corresponds to heat. In addition to standard HE, machines of the second kind are exemplified by the pioneering model introduced by Scully and co-workers [3] of a Carnot heat engine powered by partly-coherent three-level atoms (dubbed “phaseonium”) that interact with a cavity-mode WF as they cross the cavity. The surprising finding [3] was that a beam of such “phaseonium” atoms may be treated as a non-thermal, quantum-coherent bath that, for an appropriate phase  $\varphi$  of the interlevel coherence, can thermalize the cavity field to a temperature  $T_\varphi > T$ , where the latter is the atoms' temperature without coherence. Machines of the second kind act as a genuine heat engine, whose efficiency is limited by the Carnot bound, but the one corresponding to the *real* temperature of the WF, i.e.,  $T_\varphi$ .

Instead of quantum machines fueled by non-thermal baths [9, 32], which adhere to rules that differ from those of quantum heat engines, we may also consider machines fueled by thermal baths but still allow for an enhanced ergotropy of the piston state. We show that the non-linear pumping of the piston mode provides a powerful boost on the performance of the machine [34], i.e., its output power and efficiency which is determined by the capacity of the piston state to store work, i.e., its ergotropy. Finally, we discuss the question: Is the engine performance in the above scenarios determined by quantumness, i.e., the quantum features of the setup? The topics outlined above are to be discussed in detail in the sections that follow.

## 2.2 Energy Exchange Between a Driven System and a Bath

The distinction discussed above between machines of first and second kind is due to the different nature of their system-energy exchange in the quantum domain. Consider an initially prepared state  $\rho_0$  of a quantum system that evolves into a state  $\rho(t)$  under the action of a Hamiltonian  $H(t)$  and a bath. In general, the bath and/or the system may be in a non-thermal state. The change in the system energy  $E(t) = \text{Tr}[\rho(t)H(t)]$  is decomposed as follows [35, 36],

$$\Delta E(t) = W(t) + \mathcal{E}_d(t). \quad (2.1)$$

Here the first term

$$W(t) := \int_0^t \text{Tr}[\rho(t') \dot{H}(t')] dt' \quad (2.2a)$$

is the work [46] that is either extracted or invested by an external source, as in driven engines [26]. The second term

$$\mathcal{E}_d(t) := \int_0^t \text{Tr}[\dot{\rho}(t') H(t')] dt' \quad (2.2b)$$

is the energy change of the system due to its dissipative interaction with the bath.

We now further decompose  $\mathcal{E}_d(t)$  according to the associated entropy change, which naturally relates to the concept of non-passive states and ergotropy [46–48]: The energy  $E$  of a state  $\rho$  can be decomposed into *ergotropy*  $\mathcal{W} \geq 0$  and *passive energy*  $E_{\text{pas}}$ . Ergotropy is defined as the maximum amount of work extractable from  $\rho$  by means of unitary transformations and reads

$$\mathcal{W}(\rho, H) := \text{Tr}(\rho H) - \min_U \text{Tr}(U \rho U^\dagger H) \geq 0, \quad (2.3)$$

where the minimization is over all possible unitary transformations  $U$ . Passive energy, by contrast, cannot be extracted as useful work in a cyclic, unitary, fashion. For a state  $\rho$ , there is a passive state  $\pi = V \rho V^\dagger$  that only contains passive energy, where  $V$  is the unitary that minimizes the second term on the r.h.s. of Eq. (2.3). The corresponding passive energy is  $E_{\text{pas}} = \text{Tr}[V \rho V^\dagger H] = \text{Tr}[\pi H]$  such that the energy of the state  $\rho$  can be written as

$$E = E_{\text{pas}} + \mathcal{W} = \text{Tr}[\pi H] + \text{Tr}[(\rho - \pi)H]. \quad (2.4)$$

Since  $\rho$  and  $\pi$  are related by a unitary transformation, their entropies  $\mathcal{S}(\rho) = \mathcal{S}(\pi)$  coincide. Here  $\mathcal{S}(p) = -k_B \text{Tr}[p \ln p]$  is the von Neumann entropy of the state  $p$ . This observation motivates the decomposition of the dissipative energy change (2.2b) as

$$\mathcal{E}_d(t) = \mathcal{Q}(t) + \Delta \mathcal{W}|_d(t). \quad (2.5)$$

Here

$$\mathcal{Q}(t) := \int_0^t \text{Tr}[\dot{\pi}(t') H(t')] dt' \quad (2.6a)$$

is associated with a change in the passive state and thus a change in entropy. In analogy to thermodynamics, due to its entropy-changing character, we refer to Eq. (2.6a) as *heat*. While  $\mathcal{Q}(t)$  is the dissipative (non-unitary) change in *passive energy*, the second contribution in Eq. (2.5),

$$\Delta\mathcal{W}|_d(t) := \int_0^t \text{Tr} \left[ (\dot{\rho}(t') - \dot{\pi}(t')) H(t') \right] dt', \quad (2.6b)$$

is the dissipative (non-unitary) change in the system *ergotropy* due to its interaction with the bath. If the system state is always passive, Eqs. (2.6a) and (2.2b) coincide.

Hence, the system ergotropy may increase in a non-unitary fashion due to interaction with a bath and be subsequently extracted from the system in the form of work via a suitable unitary process [57]. Any *unitary* change in passive energy due to the time-dependence of the Hamiltonian contributes to the work (2.2a). The decomposition of the exchanged energy (2.5) into dissipative changes in passive energy (2.6a) and ergotropy (2.6b), is a new unraveling of the first law of thermodynamics for quantum systems [33].

The energies (2.6) are, in general, process variables and thus depend on the evolution path. By contrast, for a constant Hamiltonian, they become path-independent and reduce to the change in passive energy

$$\mathcal{Q}(t) = \Delta E_{\text{pas}}(t) = \text{Tr}[\pi(t)H] - \text{Tr}[\pi_0H], \quad (2.7a)$$

and the change in system ergotropy,

$$\Delta\mathcal{W}|_d(t) = \Delta\mathcal{W}(t) = \mathcal{W}(\rho(t)) - \mathcal{W}(\rho_0), \quad (2.7b)$$

respectively.

## 2.3 Reversibility and Entropy Production

In this section we derive the bound on the entropy change of a quantum system that is in contact with a (thermal or non-thermal) bath [33] based on our above analysis (see Chap. 28). A tight estimate of entropy change is required to deduce the maximum work obtainable from cyclic quantum machines. We use the division (2.6) discussed above to derive a bound that is much tighter than that obtained from the second law (non-negative entropy production) [2] in scenarios where non-passive states of the WF are involved.

In non-equilibrium thermodynamics, a dissipative processes is irreversible if the total entropy of the system and the bath combined increases (positivity of its entropy production) [2]. This criterion translates into Spohn's inequality for the entropy production rate [45] by quantum systems that are weakly coupled to thermal or non-thermal baths,

$$\sigma := -\frac{d}{dt} S(\rho(t)||\rho_{ss}) \geq 0, \quad (2.8)$$

where  $S(\rho(t)||\rho_{ss}) := k_B \text{Tr}[\rho(t)(\ln \rho(t) - \ln \rho_{ss})]$  is the system entropy relative to its steady state  $\rho_{ss}$ . Inequality (2.8) holds for any  $\rho(t)$  that evolves according to a Markovian master equation [44]

$$\dot{\rho} = \mathcal{L}\rho, \quad (2.9)$$

where  $\mathcal{L}$  is a Lindblad operator, the steady-state solution obeying  $\mathcal{L}\rho_{ss} = 0$ . The time-integrated ( $t \rightarrow \infty$ ) inequality (2.8) then yields the entropy production

$$\Sigma = S(\rho(t) || \rho_{ss}) \geq 0 \quad (2.10)$$

for the relaxation  $\rho_0 \mapsto \rho_{ss}$ . Note that inequality (2.8) may not hold in the non-Markovian [58] and/or strong-coupling regimes, where correlations or entanglement between the system and the bath may be appreciable [44]. By contrast, since the relative entropy is non-negative, Eq. (2.10) is valid for any system-bath coupling, not only in the Born-Markov regime [39, 59].

For a Hamiltonian  $H(t)$  that varies slowly compared to the thermalization time [35], the corresponding master equation is

$$\dot{\rho}(t) = \mathcal{L}(t)\rho(t), \quad (2.11)$$

where  $\mathcal{L}(t)$  is the same Lindblad operator as in Eq. (2.9), but with time-dependent coefficients (cf. Ref. [35]), and an invariant state  $\rho_{ss}(t)$  that satisfies  $\mathcal{L}(t)\rho_{ss}(t) = 0$ . The generalization of inequality (2.8) to the case of (2.11) then leads, following integration, to

$$\Delta\mathcal{S} = \mathcal{S}(\rho_{ss}(\infty)) - \mathcal{S}(\rho_0) \geq -k_B \int_0^\infty \text{Tr} \left[ (\mathcal{L}(t)\rho(t)) \ln \rho_{ss}(t) \right] dt. \quad (2.12)$$

If the time-dependent interaction is with a thermal bath at temperature  $T$ , then

$$\rho_{ss}(t) = \rho_{th}(t) = \frac{1}{Z(t)} \exp \left( -\frac{H(t)}{k_B T} \right) \quad (2.13)$$

is a thermal state for  $H(t)$ . Inequality (2.12) then yields

$$\Delta\mathcal{S} \geq \frac{1}{T} \int_0^\infty \text{Tr} [\dot{\rho}(t)H(t)] dt = \frac{\mathcal{E}_d}{T}, \quad (2.14)$$

$\mathcal{E}_d$  being the long-time limit ( $t \rightarrow \infty$ ) of the energy dissipated by the thermal bath.

We have pointed out [33] that the second law (non-negative entropy production) may overestimate the actual system entropy change. This can be seen upon examining the relaxation of an initially non-passive state  $\rho_0$  to a (passive) thermal state  $\rho_{th}$  through its interaction with a thermal bath at temperature  $T$ . According to the decomposition (2.5) of  $\mathcal{E}_d$ , Eq. (2.14) can be written as

$$\Delta\mathcal{S} \geq \frac{\mathcal{E}_d}{T} = \frac{\mathcal{Q} + \Delta\mathcal{W}|_d}{T}. \quad (2.15)$$

The second law thus reflects the entropy change bound to the total exchanged energy (2.2b). However, as pointed out before, this energy can be decomposed into the two contributions (2.6), where only (2.6a) is associated to a change in entropy. Therefore, we contend that Eq. (2.15) ought to be replaced by a much tighter inequality that does not account for dissipated ergotropy, as explained below for different cases.

### 2.3.1 Entropy Change in a Thermal Bath: Constant Hamiltonian

Entropy is a state variable [2], hence  $\Delta S = S(\rho_{\text{th}}) - S(\rho_0)$  is only determined by the initial state  $\rho_0$  and the (passive) thermal steady state  $\rho_{\text{th}}$ . Yet, Spohn's inequality (2.10) applied to *alternative evolution paths* from  $\rho_0$  to  $\rho_{\text{th}}$ , *may give rise to different inequalities for the same  $\Delta S$* . In particular, we can choose a path that *does not involve any dissipation of ergotropy* to the bath, i.e., it corresponds to first performing a unitary transformation to the passive state,  $\rho_0 \mapsto \pi_0$ , then bringing this state in contact with the thermal bath, where it relaxes to the thermal steady-state  $\rho_{\text{th}}$ . Inequality (2.10) applied on this path yields [33]

$$\Delta S \geq \frac{\mathcal{Q}}{T}, \quad (2.16)$$

where  $\mathcal{Q}$  is the same heat exchange as in Eq. (2.15).

In case of actual evolution, the system ergotropy decreases as a result of the relaxation caused by the thermal bath, from  $\mathcal{W}_0 \geq 0$ , the ergotropy of the initial state  $\rho_0$ , down to vanishing ergotropy in the thermal steady state, so that

$$\Delta \mathcal{W}|_{\text{d}} = -\mathcal{W}_0 \leq 0. \quad (2.17)$$

Hence, inequality (2.16) implies inequality (2.15).

### 2.3.2 Entropy Change of a System in a Thermal Bath: Time-Dependent Hamiltonian

As mentioned above,  $\mathcal{Q}$  and  $\Delta \mathcal{W}|_{\text{d}}$  on the r.h.s. of Eq. (2.15) are *path-dependent* if the Hamiltonian  $H(t)$  slowly varies [35]. This means that they depend not only on the initial state  $\rho_0$  and the steady state  $\rho_{\text{th}}(\infty)$ , which is a thermal state under the Hamiltonian  $H(\infty)$ . In particular, the path may be such that the time-dependent Hamiltonian generates a non-passive state at some point, even if the initial state is passive and the bath is thermal. Accordingly, we may choose a path void of *initial ergotropy* by extracting the ergotropy of the initial state by a unitary process *prior* to the interaction with the bath, thus resulting in the passive state  $\pi_0$ . If subsequently,

this passive state is placed into contact with the thermal bath, it results in the steady state  $\rho_{\text{th}}(\infty)$ . Our revised inequality for the latter step yields [33]

$$\Delta S \geq \frac{\mathcal{Q}'}{T}, \quad (2.18)$$

where

$$\mathcal{Q}' := \int_0^\infty \text{Tr}[\dot{\varrho}(t)H(t)]dt \quad (2.19)$$

is the heat exchanged with the bath along the chosen path. Here  $\varrho(t)$  is the solution of the same thermal master equation that governs  $\rho(t)$  but with the passive initial condition  $\varrho_0 = \pi_0$ . For a constant Hamiltonian, Eq. (2.18) coincides with Eq. (2.16).

### 2.3.3 Entropy Change of a System in a Non-thermal Bath

We next consider the case of a system that interacts with a non-thermal bath while its Hamiltonian is kept constant. Due to this interaction, the system relaxes to the non-passive steady state

$$\rho_{\text{ss}} = U\pi_{\text{ss}}U^\dagger. \quad (2.20)$$

The entropy production (2.10) during the relaxation process  $\rho_0 \mapsto \rho_{\text{ss}}$  then evaluates to

$$S(\rho_0||\rho_{\text{ss}}) = S(\tilde{\rho}_0||\pi_{\text{ss}}) \geq 0, \quad (2.21)$$

which equals the entropy production during the fictitious relaxation process  $\tilde{\rho}_0 \mapsto \pi_{\text{ss}}$ , where  $\tilde{\rho}_0 := U^\dagger \rho_0 U$ .

In order to obtain the tightest inequality for the entropy change  $\Delta S$ , we here, instead of (2.10), propose the following relative-entropy inequality,

$$S(\pi_0||\pi_{\text{ss}}) \geq 0. \quad (2.22)$$

As before, the motivation for Eq. (2.22) is that the entropy of any state  $\rho$  is the same as its passive counterpart  $\pi$ . A general proof that Eq. (2.22) is indeed a tighter inequality for  $\Delta S$  than Eq. (2.21) can be found in Ref. [33].

We now consider the situation when the working fluid is a single-mode harmonic oscillator in a Gaussian state, i.e., an experimentally relevant [11] special case where the passive steady state is thermal,  $\pi_{\text{ss}} = \rho_{\text{th}}$ . As shown in Ref. [60], the system evolution (determined by a Markovian master equation [44] with Liouvillian  $\mathcal{L}_U$ ) is then unitarily equivalent to the interaction of a transformed state  $\tilde{\rho}(t)$  with a *thermal* bath, which is described by the Liouvillian  $\mathcal{L}_{\text{th}}$  (Fig. 2.1). Inequality (2.21) then yields

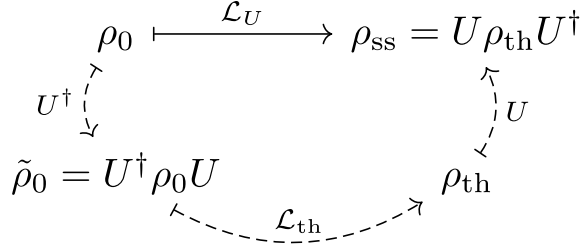


**Fig. 2.1** Two alternative evolution paths between  $\rho_0$  and  $\rho_{ss}$ . The underlying assumptions and the equivalence between the two paths are given in [33]: The solid (physical) path corresponds to the interaction of the system with a non-thermal bath whereas the dashed path consists of two unitary transformations and the interaction with a thermal bath. Figure adapted from [33].

$$\Delta S \geq \frac{\tilde{\mathcal{E}}_d}{T}, \quad (2.23)$$

where  $\tilde{\mathcal{E}}_d$  is the change in the energy  $\tilde{E} = \text{Tr}[\tilde{\rho}H]$  of the unitarily transformed state  $\tilde{\rho}$ , as it relaxes from  $\tilde{\rho}_0$  to  $\rho_{th}$  (second step in the dashed path in Fig. 2.1). By contrast, inequality (2.22) keeps track of the initial ergotropy and evaluates to Eq. (2.16).

Hence, inequalities (2.16) and (2.18) also apply to the situation where the non-thermal bath relaxes the system to a state of the form  $\rho_{ss} = U \rho_{th} U^\dagger$  [33]. The latter state naturally arises in machines of the first kind fuelled by a squeezed thermal bath [7].

## 2.4 Efficiency Bound of Cyclic Quantum Engines Powered by Thermal or Non-thermal Baths

Based on the results of the previous section, we here show that reversible operation according to the second law does not yield a proper efficiency bound of cyclic engines fuelled by non-thermal baths whenever such baths impart both heat and ergotropy to the WF. This inadequacy, as discussed above, is due to the fact that the second law does not discern between dissipative changes in passive energy and ergotropy.

Here we consider a broad class of cyclic quantum engines (Fig. 2.2) that operate between a cold thermal bath (at temperature  $T_c$ ) and a hot (thermal or non-thermal) bath, while being subject to a *time-dependent* drive (the “piston” [35]). The “hot” non-thermal bath is assumed to produce a non-passive state of the WF whose passive counterpart is thermal with temperature  $T_h > T_c$ . For a harmonic-oscillator (HO) WF interacting with a squeezed thermal bath [44, 61],  $T_h$  is the temperature that the bath had before its squeezing. We allow the WF Hamiltonian to slowly change during the interaction with the baths [35]. We only require that the WF attains its steady state by the end of the energizing stroke where it interacts with the hot bath and the stroke where it interacts with the cold bath.

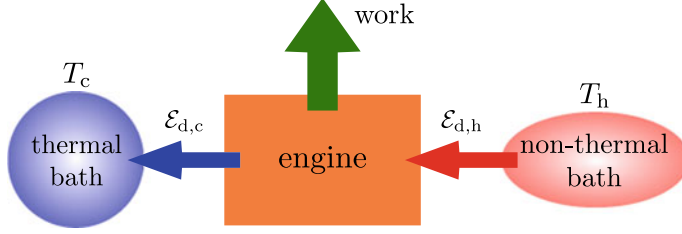


**Fig. 2.2** A quantum engine cyclically converts energy obtained from a non-thermal (e.g., squeezed thermal) bath into useful work that is extracted by a piston. In each cycle, the non-thermal bath provides the energy  $\mathcal{E}_{d,h}$ . A fraction thereof is converted into work and an amount  $\mathcal{E}_{d,c}$  is dumped into the cold thermal bath. Figure adapted from [33].

The energizing stroke is described by a master equation [44] that evolves the WF to a non-passive state  $\rho_{ss}(\infty) = U\rho_{th}(\infty)U^\dagger$ . To obtain the efficiency bound, we need to extract the ergotropy from the WF (by the piston via a suitable unitary transformation) before its interaction with the cold bath. In continuous cycles where both baths are simultaneously coupled to the WF [19, 26, 62], part of the ergotropy may then be dissipated into the cold bath, so that such cycles are inherently less efficient than stroke cycles. For time-dependent Hamiltonians, the requirement that  $H(t)$  commutes with itself at all times, e.g., a HO with time-independent eigenstates, will be adopted in this chapter for any interaction of a system with a bath, since Hamiltonians that do not commute with themselves at different times reduce the efficiency via “quantum friction” [20, 63].

The entropy changes in the two strokes of the WF-bath interactions obey

$$\Delta S_c \geq \frac{\mathcal{E}_{d,c}}{T_c} \quad (2.24a)$$

$$\Delta S_h \geq \frac{\mathcal{Q}'_h}{T_h}. \quad (2.24b)$$

Here  $\mathcal{E}_{d,c} \leq 0$  is the change in the WF energy due to its interaction with the cold (thermal) bath and  $\mathcal{Q}'_h \geq 0$  is the heat that the WF would have received, if the initial state was passive and the non-thermal bath were thermal (as in Eq. (2.19) and Fig. 2.1). The WF cyclically returns to its initial state, therefore  $\Delta S = \Delta S_c + \Delta S_h = 0$  over a cycle. These two conditions yield the inequality

$$\frac{\mathcal{E}_{d,c}}{T_c} + \frac{\mathcal{Q}'_h}{T_h} \leq 0. \quad (2.25)$$

Correspondingly, energy conservation over a cycle yields

$$\mathcal{E}_{d,c} + \mathcal{E}_{d,h} + W = 0, \quad (2.26)$$

where  $\mathcal{E}_{d,h}$  is the dissipative energy change of the WF due to its interaction with the hot non-thermal bath (Fig. 2.2).

The engine efficiency is defined as the ratio of the extracted work to the *total energy* (heat and ergotropy)  $\mathcal{E}_{d,h}$  imparted by the hot (non-thermal or thermal) bath. Here we assume  $\mathcal{E}_{d,c} \leq 0$  and  $\mathcal{E}_{d,h} \geq 0$ . The efficiency then reads

$$\eta := \frac{-W}{\mathcal{E}_{d,h}} = 1 + \frac{\mathcal{E}_{d,c}}{\mathcal{E}_{d,h}}. \quad (2.27)$$

From condition (2.25) it then follows that

$$\mathcal{E}_{d,c} \leq -\frac{T_c}{T_h} \mathcal{Q}'_{d,h}, \quad (2.28)$$

which restricts the efficiency to

$$\eta \leq 1 - \frac{T_c}{T_h} \frac{\mathcal{Q}'_h}{\mathcal{E}_{d,h}} =: \eta_{\max}. \quad (2.29)$$

The efficiency bound (2.29) does not only depend on the two temperatures [33]. The bath characteristics (e.g., its squeezing parameter) determine the ratio  $\mathcal{Q}'_h/\mathcal{E}_{d,h}$  of the heat (2.19) to the total energy input from the hot bath. Eq. (2.29) holds in the regime where the hot bath supplies energy and increases the WF entropy,  $\mathcal{Q}'_h \geq 0$  and  $\mathcal{E}_{d,h} > 0$ . The bound (2.29) is then limited by unity,  $\eta_{\max} \leq 1$ . Unity efficiency is reached in the “mechanical”-engine limit,  $\mathcal{Q}'_h \rightarrow 0$ , where the hot non-thermal bath only provides ergotropy. In the heat-engine limit,  $\mathcal{Q}'_h \rightarrow \mathcal{E}_{d,h}$ , where only heat but no ergotropy is supplied by the hot bath, Eq. (2.29) reduces to the Carnot bound  $\eta_{\text{Carnot}} = 1 - T_c/T_h$ .

By contrast, the bound  $\eta_\Sigma$  that follows from the non-negativity of the entropy production may *surpass* 1 which is unphysical (see Ref. [10]). This can be seen from the second-law condition on entropy change over a cycle,

$$\frac{\mathcal{E}_{d,c}}{T_c} + \frac{\tilde{\mathcal{E}}_{d,h}}{T_h} \leq 0. \quad (2.30)$$

Here  $\tilde{\mathcal{E}}_{d,h}$  is the energy change during the interaction with the thermal bath along the dashed path in Fig. 2.1, so that

$$\eta \leq 1 - \frac{T_c}{T_h} \frac{\tilde{\mathcal{E}}_{d,h}}{\mathcal{E}_{d,h}} =: \eta_\Sigma. \quad (2.31)$$

The bound in (2.31) exceeds 1 if  $\tilde{\mathcal{E}}_{d,h} < 0$ , which occurs under *excessive bath squeezing*, as explained below. The interaction with the effective thermal bath, which proceeds along the dashed path in Fig. 2.1, then *reduces* the WF energy, whereas the

interaction with the non-thermal bath along the solid path *increases* the WF energy. By contrast,  $\eta_{\max}$  in (2.29) advocated by us does not exceed 1.

The reason for the unphysicality of (2.31) becomes clear when the Hamiltonian is constant during the hot-bath stroke. Then

$$\tilde{\mathcal{E}}_{d,h} = \tilde{\mathcal{Q}} + \widetilde{\Delta\mathcal{W}|_d}, \quad (2.32)$$

where  $\widetilde{\Delta\mathcal{W}|_d} \leq 0$  is the ergotropy lost to the effective thermal bath in the second stage of the dashed path (Fig. 2.1). The more we squeeze the non-thermal bath, the more ergotropy is lost to the effective thermal bath, until the regime  $\tilde{\mathcal{E}}_{d,h} < 0$  is attained, causing Eq. (2.31) to exceed 1.

There exists a regime [9], wherein such a machine of the first kind acts simultaneously as an engine and a refrigerator that cools the cold bath. In this regime  $\mathcal{E}_{d,c} > 0$  and  $\mathcal{Q}'_{d,h} < 0$ . Then also the cold bath provides energy to the WF and the efficiency becomes

$$\eta = \frac{-W}{\mathcal{E}_{d,h} + \mathcal{E}_{d,c}} = \frac{\mathcal{E}_{d,h} + \mathcal{E}_{d,c}}{\mathcal{E}_{d,h} + \mathcal{E}_{d,c}} = 1. \quad (2.33)$$

Namely, it is not restricted by any condition on  $\Delta\mathcal{S}$  and hence by the second law.

## 2.5 Stroke-Based Quantum Engines Powered by Non-thermal Baths

### 2.5.1 Machines of the First Kind

We now consider explicit examples of stroke-based (“reciprocal”) bath-powered engine cycles which are not restricted by the second law, but by other constraints on their entropy. These cycles conform to the classification of the engine as a *machine of the first kind* in the introduction.

#### 2.5.1.1 Modified Otto Cycle Powered by a Squeezed Thermal Bath

We first consider machines powered by a squeezed thermal bath that obey the modified Otto cycle proposed in [9]. In addition to the two isentropic strokes (adiabatic compression and decompression of the WF) and the two isochoric strokes (interaction with the baths under a fixed Hamiltonian) of the standard quantum Otto cycle [64], we add one additional *ergotropy-extraction stroke*. The latter may be implemented by abruptly ramping up the HO frequency and then gradually ramping this frequency down [65–67]. This cycle is schematically shown in Fig. 2.3a.

As the interaction of the WF with the bath is isochoric, we have  $\mathcal{Q}'_h = \Delta E_{pas,h}$  and  $\mathcal{E}_{d,h} = \Delta E_{pas,h} + \Delta\mathcal{W}_h$ , where  $\Delta E_{pas,h}$  is the passive energy change and  $\Delta\mathcal{W}_h$

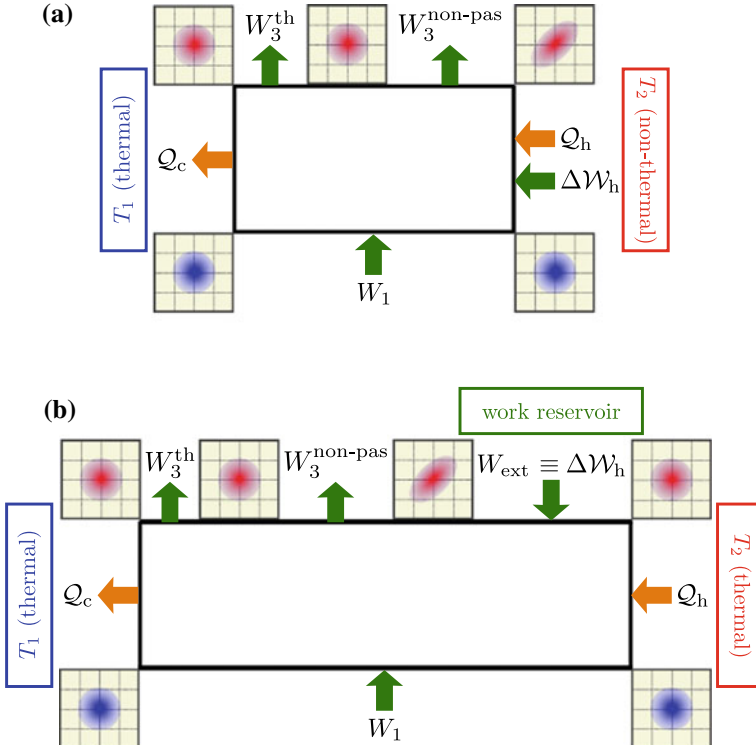


**Fig. 2.3** **a** Modified Otto cycle for an oscillator WF and a squeezed thermal bath: In the first stroke the work  $W_1$  is invested by the piston to compress the (thermal) WF. The second stroke consists of the interaction of the WF with a squeezed thermal bath, from which passive energy  $Q_h$  and ergotropy  $\Delta\mathcal{W}_h$  is imparted to the WF. As a modification of the standard Otto cycle, now a unitary transformation is performed on the WF to extract its ergotropy in the form of work  $W_3^{\text{non-pas}}$ . The WF is now passive (thermal) and the work  $W_3^{\text{th}}$  is extracted by the piston by expanding the WF, as in the standard Otto cycle. Finally, the cycle is closed by the interaction of the WF with a cold thermal bath at temperature  $T_c$  to which the heat  $Q_c$  is released. **b** Equivalent hybrid machine yielding the same work and efficiency as the modified Otto cycle in **a**: Instead of being fuelled by a squeezed thermal bath, the WF first interacts with a hot thermal bath at temperature  $T_h$  that provides the heat  $Q_c$ . Afterwards, an external work reservoir (e.g., a battery) investes the work  $W_{\text{ext}}$  to squeeze the WF. This increases the WF ergotropy by the same amount  $\Delta\mathcal{W}_h$  that the squeezed thermal bath produced in **a**. This demonstrates the hybrid character of machines of the first kind. Figure adapted from [9].

is the ergotropy change, respectively. The efficiency bound (2.29) of this Otto-like cycle then reads

$$\eta_{\max} = 1 - \frac{T_c}{T_h} \frac{\Delta E_{\text{pas,h}}}{\Delta E_{\text{pas,h}} + \Delta \mathcal{W}_h}. \quad (2.34)$$

In general, any engine cycle wherein the interaction with the hot bath is isochoric and sufficiently long (for the WF to reach steady state) abides by the bound (2.34).

The interaction of the WF with the squeezed thermal bath is governed by the master equation [61]

$$\dot{\rho} = \kappa(N + 1)\mathcal{D}(a, a^\dagger)[\rho] + \kappa N\mathcal{D}(a^\dagger, a)[\rho] - \kappa M\mathcal{D}(a, a)[\rho] - \kappa M\mathcal{D}(a^\dagger, a^\dagger)[\rho]. \quad (2.35)$$

Here the dissipator is defined as  $\mathcal{D}(A, B)[\rho] := 2A\rho B - BA\rho - \rho BA$ ,  $a$  and  $a^\dagger$  are the WF creation and annihilation operators,  $\kappa$  denotes the decay rate and (w.l.o.g. the squeezing phase is zero)

$$N := \bar{n}_h(\cosh^2 r + \sinh^2 r) + \sinh^2 r \quad (2.36a)$$

$$M := -\cosh r \sinh r(2\bar{n}_h + 1), \quad (2.36b)$$

$\bar{n}_h = [\exp(\hbar\omega/[k_B T_h]) - 1]^{-1}$  being the thermal excitation number of the bath at the WF-oscillator frequency  $\omega$  and  $r$  the squeezing parameter.

The steady state of Eq. (2.35) is a squeezed thermal state of the WF. The deviation of the squeezed WF's excitation number from thermal equilibrium is [61]

$$\Delta\bar{n}_h = (2\bar{n}_h + 1) \sinh^2(r) > 0. \quad (2.37)$$

The efficiency bounds  $\eta_\Sigma$  [Eq. (2.31)] and  $\eta_{\max}$  [Eq. (2.34)] then evaluate to [33]

$$\eta_\Sigma = 1 - \frac{T_c}{T_h} \frac{\bar{n}_h - \bar{n}_c - \Delta\bar{n}_c}{\bar{n}_h + \Delta\bar{n}_h - \bar{n}_c} \quad (2.38)$$

and

$$\eta_{\max} = 1 - \frac{T_c}{T_h} \frac{\bar{n}_h - \bar{n}_c}{\bar{n}_h + \Delta\bar{n}_h - \bar{n}_c}. \quad (2.39)$$

The efficiency of the modified Otto cycle evaluates to [9]

$$\eta = 1 - \frac{(\bar{n}_h - \bar{n}_c)\omega_c}{(\bar{n}_h + \Delta\bar{n}_h - \bar{n}_c)\omega_h}. \quad (2.40)$$

Equation (2.40) holds for  $\mathcal{E}_{d,c} \leq 0$ ; for  $\mathcal{E}_{d,c} \geq 0$  the machine operates as an engine and a refrigerator for the cold bath with  $\eta = 1$  [Eq. (2.33)]. The machine acts as an engine for  $\mathcal{E}_{d,h} \geq 0$ , i.e., it delivers work for  $\bar{n}_h + \Delta\bar{n}_h \geq \bar{n}_c$ . In Fig. 2.4 we compare  $\eta_\Sigma$  [Eq. (2.38)] obtained from the reversibility condition with the physical bound  $\eta_{\max}$  [Eq. (2.39)] discussed above.

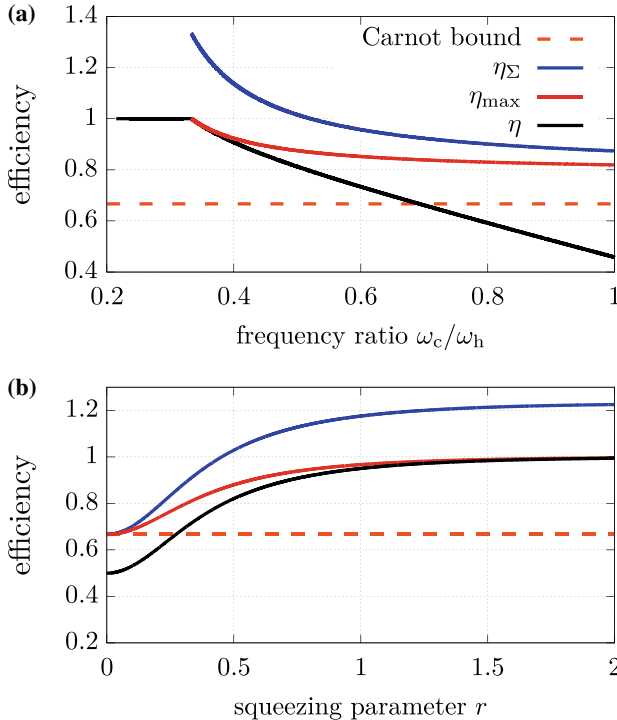


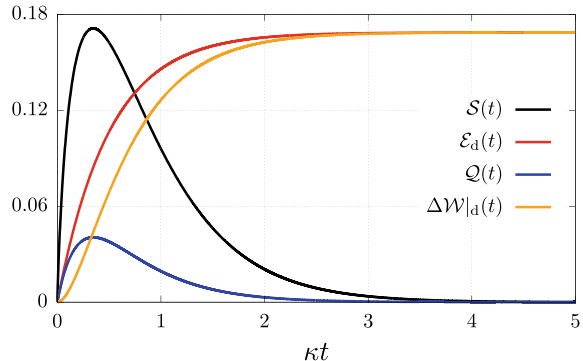
**Fig. 2.4** Efficiency (2.40) of the modified Otto cycle as a function of **a** the frequency ratio and **b** the squeezing parameter. The second-law bound  $\eta_\Sigma$  [Eq. (2.38)] does not limit the efficiency and may even surpass 1. By contrast, the bound (2.39) interpolates between the Carnot bound (in the heat-engine limit) and unity (in the mechanical-engine limit). Parameters:  $T_h = 3T_c$  and **a**  $r = 0.5$  and **b**  $\omega_c = \omega_h/2$ . Figure adapted from [33].

The difference between a standard heat engine (which, by definition, is energized exclusively by heat) and this hybrid (thermo-mechanical) *machine of the first kind* becomes apparent in the extreme case  $T_c = T_h = 0$  ( $\bar{n}_c = \bar{n}_h = 0$ ). A machine of the first kind can then still deliver work,

$$W = -\hbar(\omega_h - \omega_c)\Delta\bar{n}_h < 0, \quad (2.41)$$

although no heat is imparted to the WF by the (pure-state) bath. The machine is then an *effectively mechanical* engine, energized by  $\mathcal{E}_{d,h} = \hbar\omega_h\Delta\bar{n}_h > 0$ , which is pure ergotropy transfer from the zero-temperature bath. The WF energy increase in the second stroke is then *effectively isentropic* and does not involve any net heat exchange with the bath (Fig. 2.5).

**Fig. 2.5** Entropy, energy, passive-energy, and ergotropy changes for a harmonic oscillator initialized in the vacuum state that interacts with a squeezed-vacuum bath according to the master equation (2.35). Figure adapted from [33].



### 2.5.1.2 An Equivalent Hybrid Cycle

The above modified Otto cycle (Fig. 2.3a) may be replaced by an equivalent cycle (Fig. 2.3b) involving a hot thermal bath at temperature  $T_h$  and an external work source (which is *not the piston*) [9]. After the second stroke this external work source performs a unitary transformation on the thermal WF state that transforms it into the same non-passive state that it would become via contact with a non-thermal bath. The amount of work invested by this device is the same ergotropy of the WF state that a non-thermal bath would provide. This equivalent cycle demonstrates the *hybrid thermo-mechanical* nature of the engine. The equivalence of this cycle and the modified Otto cycle follows from our analysis, whereby the heat provided by the non-thermal bath is the *same* as the heat that a thermal bath at temperature  $T_h$  would have provided [cf. Eq. (2.25)]. The energy surplus imparted by the non-thermal bath was identified to be the work obtained from ergotropy. This equivalence supports our conclusion that the maximum efficiency of this cycle is not a thermodynamic bound, since the work imparted by the auxiliary work reservoir is not bounded by the second law of thermodynamics, whereas the heat exchanges are.

### 2.5.1.3 Modified Carnot Cycle Powered by a Squeezed Thermal Bath

We finally consider a cycle powered by a squeezed thermal bath that comprises the four strokes of the ordinary thermal Carnot cycle [1, 2] and an additional ergotropy-extraction stroke (stroke 3 in Fig. 2.6). Stroke 2 is isothermal expansion wherein the state  $\varrho(t)$  is always in thermal equilibrium. Hence, from Eq. (2.18) we have  $Q'_h = T_h \Delta S_h$  (Fig. 2.7). Stroke 5 is isothermal compression, i.e.,  $E_{d,c} = T_c \Delta S_c$ . The condition of vanishing entropy change over a cycle corresponds to the equality sign in condition (2.25). Hence, the efficiency of this cycle is the bound  $\eta_{\max}$  in Eq. (2.29).

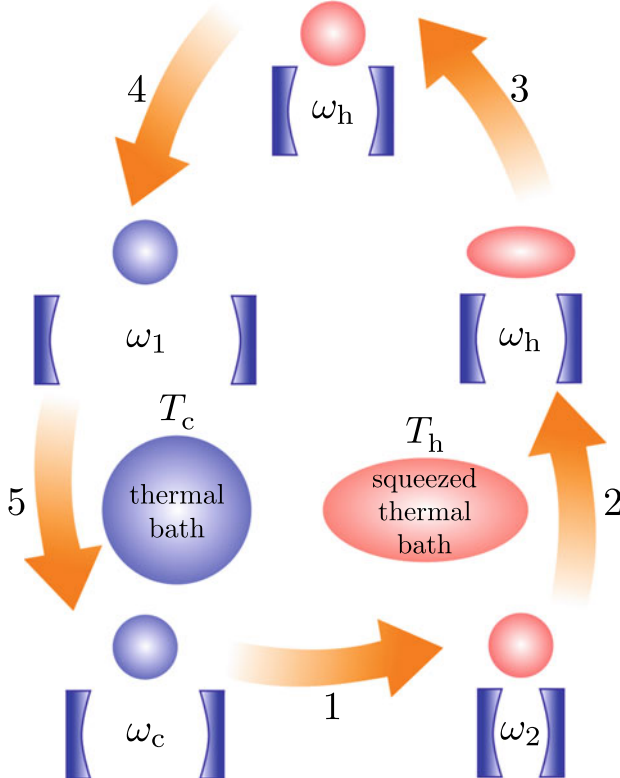


**Fig. 2.6** The modified Carnot cycle starts with a thermal state with frequency  $\omega_c$  and temperature  $T_c$  (lower left corner). In stroke 1, the mode undergoes an adiabatic compression to frequency  $\omega_2 = \omega_c T_h / T_c$  and temperature  $T_h > T_c$ . Thereafter, in the energizing stroke 2, the frequency is slowly reduced to  $\omega_h \leq \omega_2$  while the mode is connected to the squeezed thermal bath, yielding a squeezed thermal steady state. Its ergotropy is extracted in stroke 3 by an “unsqueezing” unitary operation, resulting in a thermal state with temperature  $T_h$ . In stroke 4, the frequency is again adiabatically reduced to  $\omega_1 = \omega_h T_c / T_h$  such that the mode attains the temperature  $T_c$ . Finally, stroke 5 is an isothermal compression back to the initial state. Figure adapted from [33].

We conclude that the bound  $\eta_{\max}$  is lower than  $\eta_{\Sigma}$  [33] for all possible engine cycles that contain a “Carnot-like” energizing stroke, namely, a stroke characterized by a slowly-changing Hamiltonian and an initial thermal state at temperature  $T_h$ , such that  $\mathcal{Q}'_h = T_h \Delta S_h$ . The Carnot-like cycle always operates at the maximum efficiency (2.29), even when both passive thermal energy and ergotropy are imparted by this bath.

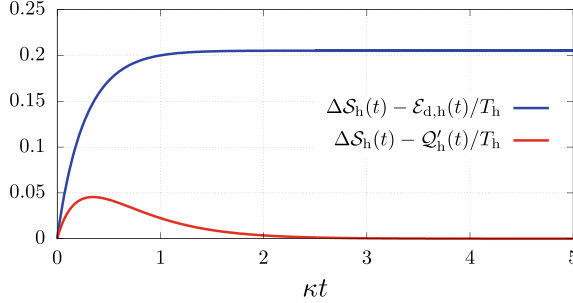


**Fig. 2.7** Change in entropy (in units of  $k_B$ ) during stroke 2 of the modified Carnot cycle in Fig. 2.6 as a function of the stroke duration obtained by a numerical integration of the master equation. The upper (blue) curve corresponds to the second-law inequality (2.14) which is far from being saturated. By contrast, our proposed inequality (2.18) is saturated (i.e., the equality sign applies) for sufficiently long stroke duration (red lower curve); here  $\Delta S_h(t) = S(\rho(t)) - S(\rho_0)$ . Parameters:  $\omega(t) = (25 - 0.05\kappa t)\kappa$ ,  $k_B T_h = 5\hbar\kappa$  and  $r = 0.2$ ,  $\kappa$  being the decay rate of the cavity-mode WF. Figure adapted from [33].

### 2.5.2 Machines of the Second Kind

There are machines wherein the WF does not draw both work and heat from the non-thermal bath, but is instead thermalized by this bath, in spite of the bath being non-thermal. Then, the excitation  $\bar{n}_h + \Delta\bar{n}_h$  corresponds to a *real* temperature  $T_{\text{real}}$  (the WF relaxes to a thermal state with this temperature if left in contact with the non-thermal bath) of the WF [68], such that [9]

$$\mathcal{Q}_c + \mathcal{Q}_h + W = 0 \quad (2.42a)$$

and

$$\frac{\mathcal{Q}_h}{T_{\text{real}}} + \frac{\mathcal{Q}_c}{T_c} \leq 0. \quad (2.42b)$$

Thus, in this regime the machine operates as a genuine heat engine whose efficiency is restricted by the Carnot bound

$$\eta = \frac{-W}{\mathcal{Q}_h} \leq 1 - \frac{T_c}{T_{\text{real}}} \equiv \eta_{\text{Carnot}} \quad (2.43)$$

corresponding to this real temperature. The (“original”) temperature  $T_h$  of the bath, prior to its transformation into a non-thermal state, plays no role; the only temperatures that matter are  $T_c$  and  $T_{\text{real}}$ . These temperatures appear in (2.42b), which, together with the first law (2.42a), gives rise to the Carnot bound (2.43).

For a HO WF, such a machine of the second kind can be realized, e.g., for a cavity being fuelled by a phaseonium bath where  $T_{\text{real}} = T_\varphi$  [3], by its  $N$ -level generalization [69], or by a beam of entangled atom dimers [70]. The non-thermal character

of the bath presents an advantage to engine operation only if  $T_{\text{real}} > T_h$ , which corresponds to  $\Delta\bar{n}_h > 0$ . Contrary to machines of the first kind, in machines of the second kind  $\Delta\bar{n}_h$  may, in principle, become negative. This case is exemplified by a phaseonium bath with the wrong choice of phase  $\varphi$  [3].

## 2.6 Catalysis of Heat-to-Work Conversion in Quantum Machines

We have recently shown [34] that under non-linear (quadratic) pumping the piston mode of a quantum heat engine evolves into a squeezed thermal state that strongly enhances its work capacity (ergotropy) compared to its linearly-pumped or unpumped counterparts. The resulting effects are that the output power and efficiency of heat-to-work conversion are drastically enhanced. Yet, since the engine is fueled by thermal baths, its efficiency is limited by the Carnot bound [2]. In describing the enhanced performance of the engine we resort to the concept of *catalysis*, whereby a small amount of catalyst (here a weak pump) strongly enhances the heat-to-work conversion.

### 2.6.1 Model of Catalyzed Quantum Heat Engine

Our model of a catalyzed quantum heat engine is shown in Fig. 2.8a. The Hamiltonian has the form ( $\hbar = 1$ )

$$H_{\text{tot}} = \sum_{j=h,c} (H_{\text{SB}}^j + H_B^j) + H_{\text{S+P}} + H_{\text{pump}}(t), \quad (2.44)$$

where,  $H_B^j$  is the free Hamiltonian of the cold (c) and hot (h) baths and  $H_{\text{SB}}^j = \sigma_X B_j$  is their coupling to the WF. The S-P interaction is described by

$$\begin{aligned} H_{\text{S+P}} &= H_{\text{S}} + H_{\text{P}} + H_{\text{SP}}, \\ H_{\text{S}} &= \frac{1}{2}\omega_0\sigma_Z; \quad H_{\text{P}} = \nu a^\dagger a; \quad H_{\text{SP}} = g\sigma_Z \otimes (a + a^\dagger). \end{aligned} \quad (2.45)$$

The P mode is isolated from the baths. Yet, the latter still modify its energy and entropy (Fig. 2.8) indirectly via S. This implies that the state of the piston cannot be fully cyclic, it must inevitably keep changing.

The catalysis is induced by the coupling of P to a (degenerate) parametric amplifier [61] via the Hamiltonian

$$H_{\text{pump}}(t) = \frac{i}{2}\kappa e^{-2i\nu t} a^{\dagger 2} + \text{h.c.} \quad (2.46)$$

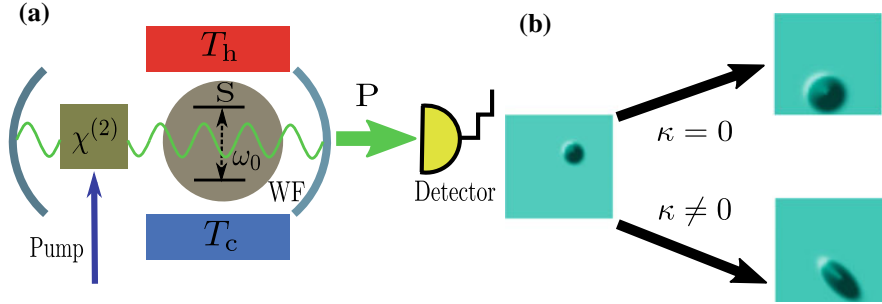


**Fig. 2.8** **a** A schematic diagram of a catalyzed quantum heat engine: The two-level WF, S is continuously coupled to cold and hot thermal baths and to a non-linearly-pumped piston mode P. **b** Evolution of the Wigner phase-space distribution function of an initial coherent state in the presence ( $\kappa \neq 0$ ) and absence ( $\kappa = 0$ ) of a non-linear pump.

where  $|\kappa|$  ( $0 < |\kappa| \leq 1$ ) is the undepleted pumping rate, taken to be real. The quadratic form of  $H_{\text{pump}}(t)$  generates squeezing [61]. We show that two *not-additive* processes may reinforce each other, thereby producing the catalysis: The enhancement of the ergotropy of P and the amplification of P by the S-B coupling.

The present model is realizable by a cavity-based non-linear parametric amplifier [61] that couples to two heat baths with different temperatures and spectra. S can be a superconducting flux qubit that is dispersively coupled to P which can be realized by a phonon mode of a nano-mechanical cantilever [71] or by a field mode [72]. In either realization, the quantized quadrature  $a + a^\dagger$  of the P-mode acts on the flux qubit energy  $\sigma_Z$  [19].

### 2.6.2 Model Analysis: Derivation of the Lindblad Master Equation

In order to derive a Lindblad master equation, we first diagonalize the Hamiltonian (2.45) by the unitary transformation

$$a \mapsto b = \mathcal{U}^\dagger a \mathcal{U}, \quad \sigma_k \mapsto \tilde{\sigma}_k = \mathcal{U}^\dagger \sigma_k \mathcal{U}; \quad \mathcal{U} = \exp \left[ \frac{g}{\nu} (a^\dagger - a) \sigma_Z \right]; \quad (k = X, Y, Z). \quad (2.47)$$

In terms of these new operators, the evolution of the piston mode is found to be [34]

$$\dot{\rho}_P = \frac{\Gamma + D}{2} ([b, \rho_P b^\dagger] + [b \rho_P, b^\dagger]) + \frac{D}{2} ([b^\dagger, \rho_P b] + [b^\dagger \rho_P, b]) + \frac{\kappa}{2} [b^\dagger]^2 \rho_P(t) - \frac{\kappa^*}{2} [b^2] \rho_P(t). \quad (2.48)$$

Here both the drift (gain or amplification) and diffusion (thermalization) rates

$$\begin{aligned}\Gamma &= \left(\frac{g}{\nu}\right)^2 \left((G(\omega_+) - G(\omega_-))\rho_{11} + (G(-\omega_-) - G(-\omega_+))\rho_{00}\right); \\ D &= \left(\frac{g}{\nu}\right)^2 ((G(\omega_-)\rho_{11} + G(-\omega_+)\rho_{00})),\end{aligned}\quad (2.49)$$

depend on the sum of the baths' response spectra  $G(\omega) = \sum_{j=h,c} G_j(\omega)$  evaluated at frequencies  $\omega_{\pm} = \omega_0 \pm \nu$ . They satisfy the Kubo-Martin-Schwinger (KMS) condition [44]  $G_j(\omega) = e^{\omega/T_j} G_j(-\omega)$ , and  $\rho_{11}, \rho_{00}$  are the populations of the upper and lower states of S. One may verify that even with the original operators (cf. Eq. (2.47)), the master equation for P to second order in  $g/\nu$  does not change the qualitative nature of our results [34]. Hence, in the following we consider Eq. (2.48) as our starting equation.

For appropriate values of  $G_j(\omega_{\pm})$  one can achieve gain, i.e.,  $\Gamma < 0$ . The following choice is optimal for a heat engine [19, 22]:  $G_h(\omega_0 - \nu) = G_c(\omega_0 - \nu) = 0$ ,  $G_h(\omega_0 + \nu) \gg G_c(\omega_0 + \nu)$ ,  $G_c(\omega_0) \gg G_h(\omega_0)$ . Namely, the spectral densities of the baths nearly non-overlapping, the cold bath spectral density is centered around  $\omega_0$  and the hot bath spectral density around  $\omega_0 + \nu$ . The sum  $D + \Gamma \geq 0$ , so that  $\Gamma < 0$ , implies  $D/|\Gamma| \geq 1$ .

Equation (2.48) is equivalent to a Fokker-Planck equation for the Wigner quasiprobability distribution function  $\mathbf{W}(\alpha)$  [34],

$$\frac{\partial \mathbf{W}}{\partial t} = \left( \frac{\partial}{\partial \alpha} d_{\alpha} + \frac{\partial}{\partial \alpha^*} d_{\alpha}^* \right) \mathbf{W} + \left( D + \frac{\Gamma}{2} \right) \frac{\partial^2 \mathbf{W}}{\partial \alpha \partial \alpha^*}, \quad (2.50)$$

where  $d_{\alpha} = \frac{\Gamma}{2}\alpha - \kappa\alpha^*$ . For an initial coherent state  $|\alpha(0)\rangle$  of P, corresponding to the Wigner distribution  $\mathbf{W}(\alpha, \alpha^*, 0) = \frac{2}{\pi}e^{-2|\alpha-\alpha(0)|^2}$ , the solution reads

$$\mathbf{W}(x_1, x_2, t) = \frac{1}{2\pi\sqrt{f_+ f_-}} \exp \left\{ -\frac{1}{2f_+ f_-} \left[ f_-(x_1 - x_{10}e^{\Gamma_+ t})^2 + f_+(x_2 - x_{20}e^{\Gamma_- t})^2 \right] \right\}, \quad (2.51)$$

where  $\Gamma_{\pm} = -\Gamma/2 \pm |\kappa|$ . Here the real variables  $x_1, x_2$  are defined by  $\alpha = x_1 + ix_2$ ,  $x_{10} = \text{Re}[\alpha(0)]$ ,  $x_{20} = \text{Im}[\alpha(0)]$ , and the coefficients  $f_{\pm}$  are the Gaussian widths

$$f_{\pm} = \frac{e^{2\Gamma_{\pm} t}}{4} + \frac{(D + \frac{\Gamma}{2})}{4\Gamma_{\pm}} (e^{2\Gamma_{\pm} t} - 1). \quad (2.52)$$

Hence under quadratic pumping in the gain regime  $\Gamma < 0$ , the initial coherent-state distribution evolves to a Gaussian with maximal and minimal widths  $f_+$  and  $f_-$  along the orthogonal axes  $x_1$  and  $x_2$  that are determined by the phase of the pump. The maximal width  $f_+$  grows much faster than the minimal width  $f_-$  (Fig. 2.8b), resulting in enhanced squeezing of the distribution.

### 2.6.3 Work Extraction Under Non-linear Pumping

The maximum extractable work from  $\rho_P$  is its ergotropy

$$\mathcal{W}(\rho_P) = \langle H_P(\rho_P) \rangle - \langle H_P(\pi_P) \rangle. \quad (2.53)$$

Here  $\pi_P$  is the corresponding passive state of P. The passive state  $\pi_P$  corresponding to the Gaussian  $\rho_P$  is the thermal (Gibbs) state

$$\pi_P(t) = Z^{-1} e^{-\frac{H_P}{T_P(t)}} \quad (2.54)$$

with slowly varying temperature  $T_P(t)$ . We then find from Eqs. (2.53) and (2.54) the maximal power

$$\mathcal{P}_{\max} = \dot{\mathcal{W}} - \dot{W}_{\text{pump}} = \langle \dot{H}_P \rangle - T_P(t) \dot{S}_P(t) - \dot{W}_{\text{pump}}. \quad (2.55)$$

Equation (2.55) is the net rate of extractable work converted from heat. The first term  $\langle \dot{H}_P \rangle$  is the power obtained for a perfectly non-passive state, the second term  $-T_P(t) \dot{S}_P$  in (2.55) expresses its passivity increase due to the rise of the temperature  $T_P(t)$  and the entropy  $S_P$  of P, and the third term is the subtracted power supplied by the pump.

As we show, the power may be strongly catalyzed by the pump squeezing (Fig. 2.9a). To obtain a better insight into this catalysis, we compute the engine efficiency bound which is defined as the ratio of the maximal net power output to the heat flux input  $\dot{Q}_{\text{SP/h}}$ ,

$$\eta_{\max} = \frac{\dot{\mathcal{W}} - \dot{W}_{\text{pump}}}{\dot{Q}_{\text{SP/h}}} = \frac{\langle \dot{H}_P \rangle - T_P \dot{S}_P - \dot{W}_{\text{pump}}}{\dot{Q}_{\text{SP/h}}}, \quad (2.56)$$

where the heat current from the hot bath to S+P is given by [34]

$$\dot{Q}_{\text{SP/h}} = -\omega_+ \Gamma \langle b^\dagger b \rangle + \omega_+ D. \quad (2.57)$$

Using Eq. (2.48) one finds

$$\langle \dot{H}_P \rangle = \nu \text{Tr}[\dot{\rho}_P b^\dagger b] = -\nu \Gamma \langle b^\dagger b \rangle + \nu D + \nu \kappa \langle b^{\dagger 2} \rangle + \text{c.c.}, \quad (2.58)$$

$$\dot{W}_{\text{pump}}(t) = \text{Tr}[\rho_P \frac{d}{dt} H_{\text{pump}}(t)] = \nu \kappa \langle b^{\dagger 2} \rangle + \text{c.c.} \quad (2.59)$$

Combining Eqs. (2.57)–(2.59), we finally arrive at

$$\langle \dot{H}_P \rangle - \dot{W}_{\text{pump}} = \frac{\nu}{\omega_+} \dot{Q}_{\text{SP/h}}. \quad (2.60)$$

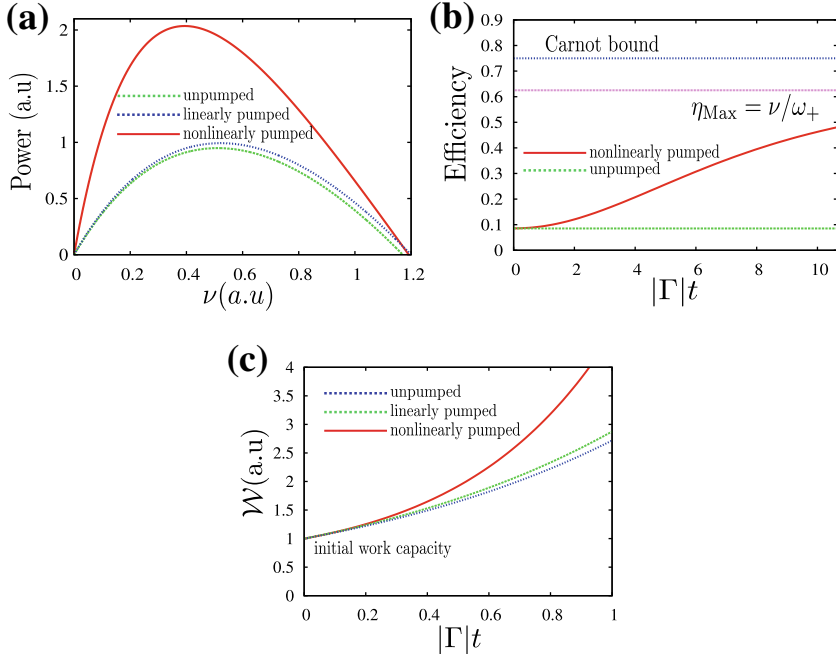


**Fig. 2.9** **a** Output power as a function of the piston frequency for quadratic pumping, linear pumping and without pumping, respectively for  $T_c = 0.6T_h$ . **b** Comparison of efficiency in the presence of weak non-linear pumping ( $\kappa \neq 0$ , and  $|\kappa|/|\Gamma| \sim 0.1$ ) and in absence of any pumping ( $\kappa = 0$ ). **c** The maximal extractable work (ergotropy) drastically increases in the presence of quadratic pumping compared to its linear and unpumped counterparts (normalized by the initial work capacity) as a function of  $|\Gamma|t$  for an initial coherent state with  $|\alpha(0)|^2 \sim 1$ .

### 2.6.4 Efficiency Boost

From Eqs. (2.56) and (2.60), the efficiency bound can be expressed as

$$\eta_{\max} = \frac{\nu}{\omega_+} - \frac{\nu \dot{n}_{\text{pas}}}{\dot{Q}_{\text{SP/h}}}, \quad (2.61)$$

where we have used the identity  $T_p \dot{S}_p = \nu \dot{n}_{\text{pas}}$  for Gaussian states that relates the entropy increase to  $n_{\text{pas}} = (e^{\nu/T_p} - 1)^{-1}$ , the thermal excitation of the passive state (2.54). Equation (2.61) shows that the efficiency depends on the *ratio of  $\nu \dot{n}_{\text{pas}}$  to the incoming heat flow*. In turn,  $\nu \dot{n}_{\text{pas}}$  and  $\dot{Q}_{\text{SP/h}}$  depend on the evolving  $T_p(t)$  and squeezing parameter  $r(t)$  [34] of P, and on the expectation values  $x_{10}$ ,  $x_{20}$ , of the quadrature operators  $\hat{x}_1$  and  $\hat{x}_2$  in the initial state of P.

We can simplify the exact expression of  $\eta_{\max}$  using the parametrization of Gaussian states in terms of the squeezing parameter  $r(t)$  [34] which relates to the quadrature widths  $f_{\pm}$  [cf. (2.52)] of the distribution (2.51),

$$(n_{\text{pas}} + 1/2) \cosh 2r(t) = f_+ + f_- \quad (2.62)$$

Then one obtains [34]

$$\begin{aligned} \dot{n}_{\text{pas}} &= -\Gamma(n_{\text{pas}} + 1/2) + (D + \Gamma/2) \cosh 2r(t), \\ \dot{Q}_{\text{SP/h}} &= \omega_+(D + \Gamma/2) - \omega_+\Gamma \left[ (n_{\text{pas}} + 1/2) \cosh 2r(t) + x_{10}^2 e^{2\Gamma_+ t} + x_{20}^2 e^{2\Gamma_- t} \right]. \end{aligned} \quad (2.63)$$

Both  $\dot{n}_{\text{pas}}$  and the heat flow are enhanced by the squeezing, but remarkably, the heat flow  $\dot{Q}_{\text{SP/h}}$  is more strongly enhanced, which yields an ergotropy increase along with an efficiency increase.

Assuming that  $n_{\text{pas}} \gg D/|\Gamma|$ , for any Gaussian (squeezed) state the efficiency can be computed as [34]

$$\eta(t) \simeq \frac{\nu}{\omega_+} \left[ 1 - \frac{n_{\text{pas}} + 1/2}{(n_{\text{pas}} + 1/2) \cosh 2r(t) + (x_{10}^2 e^{2\Gamma_+ t} + x_{20}^2 e^{2\Gamma_- t})} \right]. \quad (2.64)$$

The efficiency reaches the maximal attainable efficiency  $\eta_{\max}$ , bounded by the Carnot efficiency [34],

$$\eta_{\max} := \frac{\nu}{\omega_+} \leq \eta_{\text{Carnot}} = 1 - \frac{T_c}{T_h}. \quad (2.65)$$

It is seen from Fig. 2.9b and the analysis of the expression (2.64) that  $\eta$  tends to  $\eta_{\max} = \frac{\nu}{\omega_+}$  as the pumping rate  $\kappa$  increases. Thus  $\eta_{\max}$  can approach the Carnot efficiency by choosing  $T_h/T_c = \omega_+/\omega_0$ .

When the pumping is off ( $\kappa = r(t) = 0$ ), the passivity term that limits the ergotropy (2.53) or the power (2.55) becomes small only in the semiclassical limit  $x_{10}^2 + x_{20}^2 = |\alpha(0)|^2 \gg 1$  and under the weak coupling condition  $(g/\nu)|\alpha(0)| \ll 1$ . The efficiency in the unpumped gain regime  $\Gamma < 0$  is then

$$\eta_0 = \frac{\nu}{\omega_+} \left[ \frac{|\alpha(0)|^2}{|\alpha(0)|^2 - D/\Gamma} \right] = \frac{\nu}{\omega_+} \frac{1}{1 + \frac{D}{|\Gamma||\alpha(0)|^2}}. \quad (2.66)$$

A comparison between the unpumped case (2.66) and the pumped case (2.64) and (2.65) shows that quadratic pumping may dramatically enhance the efficiency (Fig. 2.9b) and the ergotropy as shown in Fig. 2.9c for an initial piston charging  $|\alpha(0)|^2 \sim 1$ . The reason is that when the non-linear pumping is on, any heat input in  $P$  is amplified by the squeezing as  $\nu(n_{\text{pas}} + 1/2) \cosh 2r(t)$  which enhances the leading term in the denominator of (2.64). On the other hand, the terms depending on

$\Gamma_{\pm}$  therein [cf. (2.51)] and the passive energy,  $\nu n_{\text{pas}}$ , are unaffected by the squeezing. As a consequence, the stronger the squeezing, the higher the efficiency.

Similar calculations lead to the following work capacity for its *linear pumping* counterpart (pump Hamiltonian  $H_{\text{pump}}(t) = i\kappa b^\dagger e^{-i\nu t} + \text{h.c.}$ ),

$$\mathcal{W}_{\text{L}} = \nu |\alpha(t)|^2, \quad (2.67)$$

where  $\alpha(t)$  is the generated phase-space displacement  $\alpha(t) := \alpha(0)e^{-\frac{\Gamma t}{2}} + \frac{2\kappa}{|\Gamma|}(e^{-\frac{\Gamma t}{2}} - 1)$ . Linear pumping generates an energy contribution which is additive to the passive energy,  $\nu n_{\text{pas}} + \nu |\alpha(t)|$ . The efficiency for linear pumping is found to be limited by

$$\eta_{\text{L}} \xrightarrow[t \gg |\Gamma|^{-1}]{\nu}{\omega_+} \frac{|\alpha(0) + 2\frac{\kappa}{|\Gamma|}|^2}{|\alpha(0) + 2\frac{\kappa}{|\Gamma|}|^2 + n_{\text{pas}}(0) + D/|\Gamma|}. \quad (2.68)$$

This efficiency never approaches  $\eta_{\text{max}} = \frac{\nu}{\omega_+}$  if  $|\alpha(0)|$  is much smaller than  $n_{\text{pas}}(0) + D/|\Gamma|$ . Consequently, the ergotropy increase generated by heat input for linear pumping is much less significant than for non-linear pumping resulting in much lower power.

## 2.7 Discussion: Quantumness and Engine Performance

We have shown that the operation of machines powered by quantum-coherent (non-thermal) baths or catalyzed by quantum-non-linear pumping of the piston crucially depends on whether the working fluid (WF) or the piston are in a passive or non-passive state. However, non-passivity also exists in a classical context [73–75] which prompts the question: To what extent is the performance of these machines truly affected by quantum features of the bath, the WF and (or) the piston? This question requires the clarification of two points: (i) What are the relevant criteria for the bath, WF or piston quantumness? (ii) Is there a compelling link between such quantumness and the machine performance? (iii) Conversely, does the fact that a machine with quantum ingredients is fueled by a heat bath imply that the machine conforms to the rules of thermal (heat) engines?

As long as the dynamics of the harmonic-oscillator (HO) WF or piston is described by linear or quadratic operators, the Gaussian character of their state is preserved [76]. A Gaussian HO state is non-classical if its  $P$ -function is negative [61, 77, 78]. According to this criterion, a squeezed thermal distribution with thermal photon number  $\bar{n}$  and squeezing parameter  $r > 0$  is non-classical only if its fluctuations are below the minimum uncertainty limit. This holds if  $\bar{n} < (e^{2r} - 1)/2$  [61, 79].

Whether or not the WF or the piston are in a non-classical state, however, has no direct impact on the machine's operation —only the energy and ergotropy of their state play a role. The highest (near-unity) efficiency is attained by nearly mechanical

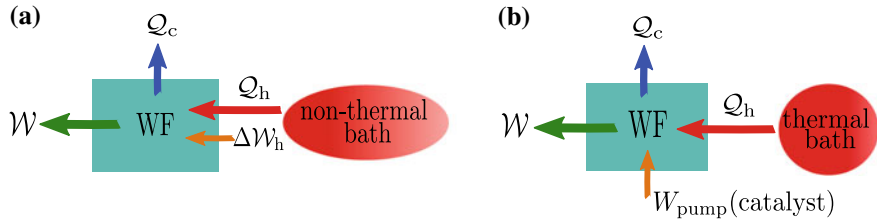


**Fig. 2.10** **a** Scheme of a machine powered by a squeezed (non-thermal) bath [7, 9, 32]. **b** Scheme of a catalyzed quantum heat machine.

*operation* of the machine. It is effected by the ergotropy imparted by a squeezed bath to the WF or by a non-linear pump to the piston (Fig. 2.10). Thus the possibility of strong catalysis of heat-to-work conversion arises from ergotropy enhancement as the piston undergoes squeezing after it is initialized in any nearly-coherent state and subjected to quadratic pumping. Yet, non-classicality and non-passivity do not generally go hand-in-hand: Coherent thermal states are classical but non-passive, whereas squeezed thermal states may be either classical or non-classical.

In general for Gaussian and non-Gaussian states alike, the machine performance is optimized for a WF or piston state with the highest possible ergotropy allowed for its energy. Equivalently, the quantumness of an engine and bath may be deemed useful, if given a certain energy to transfer (eg. squeeze) a thermal bath, the unitary transformation that maximizes the ergotropy of the bath has no classical counterpart. Thus, neither the *operational principles* of a cyclic machine nor its performance demand the non-classicality of the state of its ingredients. The extracted work and efficiency are optimized by maximizing the ergotropy and minimizing the passive (thermal) energy of the WF and/or the piston, but are not necessarily related to the non-classicality of their state.

**Acknowledgements** We acknowledge discussions with A. G. Kofman and support from ISF, DFG and VATAT. W.N. acknowledges support from an ESQ fellowship of the Austrian Academy of Sciences (ÖAW).

## References

1. S. Carnot, *Réflexions sur la puissance motrice du feu et sur les machines propres à développer cette puissance* (Bachelier, Paris, 1824). <https://doi.org/10.3931/e-rara-9118>
2. D. Kondepudi, I. Prigogine, *Modern Thermodynamics*, 2nd ed. (Wiley, Chichester, 2015). <https://doi.org/10.1002/9781118698723>
3. M.O. Scully, M.S. Zubairy, G.S. Agarwal, H. Walther, Extracting work from a single heat bath via vanishing quantum coherence. *Science* **299**, 862 (2003). <https://doi.org/10.1126/science.1078955>
4. R. Dillenschneider, E. Lutz, Energetics of quantum correlations. *EPL (Europhys. Lett.)* **88**, 50003 (2009). <https://doi.org/10.1209/0295-5075/88/50003>

5. X.L. Huang, T. Wang, X.X. Yi, Effects of reservoir squeezing on quantum systems and work extraction. *Phys. Rev. E* **86**, 051105 (2012). <https://doi.org/10.1103/PhysRevE.86.051105>
6. O. Abah, E. Lutz, Efficiency of heat engines coupled to nonequilibrium reservoirs. *EPL (Europhys. Lett.)* **106**, 20001 (2014). <https://doi.org/10.1209/0295-5075/106/20001>
7. J. Roßnagel, O. Abah, F. Schmidt-Kaler, K. Singer, E. Lutz, Nanoscale heat engine beyond the carnot limit. *Phys. Rev. Lett.* **112**, 030602 (2014). <https://doi.org/10.1103/PhysRevLett.112.030602>
8. A.Ü.C. Hardal, Ö.E. Müstecaplıoğlu, Superradiant quantum heat engine. *Sci. Rep.* **5**, 12953 (2015). <https://doi.org/10.1038/srep12953>
9. W. Niedenzu, D. Gelbwaser-Klimovsky, A.G. Kofman, G. Kurizki, On the operation of machines powered by quantum non-thermal baths. *New J. Phys.* **18**, 083012 (2016). <https://doi.org/10.1088/1367-2630/18/8/083012>
10. G. Manzano, F. Galve, R. Zambrini, J.M.R. Parrondo, Entropy production and thermodynamic power of the squeezed thermal reservoir. *Phys. Rev. E* **93**, 052120 (2016). <https://doi.org/10.1103/PhysRevE.93.052120>
11. J. Klaers, S. Faelt, A. Imamoglu, E. Togan, Squeezed thermal reservoirs as a resource for a nanomechanical engine beyond the carnot limit. *Phys. Rev. X* **7**, 031044 (2017). <https://doi.org/10.1103/PhysRevX.7.031044>
12. B.K. Agarwalla, J.-H. Jiang, D. Segal, Quantum efficiency bound for continuous heat engines coupled to noncanonical reservoirs. *Phys. Rev. B* **96**, 104304 (2017). <https://doi.org/10.1103/PhysRevB.96.104304>
13. R. Alicki, M. Horodecki, P. Horodecki, R. Horodecki, Thermodynamics of quantum information systems –Hamiltonian description. *Open Syst. Inf. Dyn.* **11**, 205 (2004). <https://doi.org/10.1023/B:OPSY.0000047566.72717.71>
14. H.T. Quan, Y. Liu, C.P. Sun, F. Nori, Quantum thermodynamic cycles and quantum heat engines. *Phys. Rev. E* **76**, 031105 (2007). <https://doi.org/10.1103/PhysRevE.76.031105>
15. J. Gemmer, M. Michel, G. Mahler, *Quantum Thermodynamics*, 2nd ed. (Springer, Berlin, 2009). <https://doi.org/10.1007/978-3-540-70510-9>
16. N. Linden, S. Popescu, P. Skrzypczyk, How small can thermal machines be? The smallest possible refrigerator. *Phys. Rev. Lett.* **105**, 130401 (2010). <https://doi.org/10.1103/PhysRevLett.105.130401>
17. R. Dorner, J. Goold, C. Cormick, M. Paternostro, V. Vedral, Emergent thermodynamics in a quenched quantum many-body system. *Phys. Rev. Lett.* **109**, 160601 (2012). <https://doi.org/10.1103/PhysRevLett.109.160601>
18. O. Abah, J. Roßnagel, G. Jacob, S. Deffner, F. Schmidt-Kaler, K. Singer, E. Lutz, Single-ion heat engine at maximum power. *Phys. Rev. Lett.* **109**, 203006 (2012). <https://doi.org/10.1103/PhysRevLett.109.203006>
19. D. Gelbwaser-Klimovsky, R. Alicki, G. Kurizki, Minimal universal quantum heat machine. *Phys. Rev. E* **87**, 012140 (2013a). <https://doi.org/10.1103/PhysRevE.87.012140>
20. R. Kosloff, Quantum thermodynamics: a dynamical viewpoint. *Entropy* **15**, 2100 (2013). <https://doi.org/10.3390/e15062100>
21. A. del Campo, J. Goold, M. Paternostro, More bang for your buck: super-adiabatic quantum engines. *Sci. Rep.* **4**, 6208 (2014). <https://doi.org/10.1038/srep06208>
22. D. Gelbwaser-Klimovsky, G. Kurizki, Heat-machine control by quantum-state preparation: from quantum engines to refrigerators. *Phys. Rev. E* **90**, 022102 (2014). <https://doi.org/10.1103/PhysRevE.90.022102>
23. R. Kosloff, A. Levy, Quantum heat engines and refrigerators: continuous devices. *Annu. Rev. Phys. Chem.* **65**, 365 (2014). <https://doi.org/10.1146/annurev-physchem-040513-103724>
24. P. Skrzypczyk, A.J. Short, S. Popescu, Work extraction and thermodynamics for individual quantum systems. *Nat. Commun.* **5**, 4185 (2014). <https://doi.org/10.1038/ncomms5185>
25. F. Binder, S. Vinjanampathy, K. Modi, J. Goold, Quantum thermodynamics of general quantum processes. *Phys. Rev. E* **91**, 032119 (2015). <https://doi.org/10.1103/PhysRevE.91.032119>
26. D. Gelbwaser-Klimovsky, W. Niedenzu, G. Kurizki, Thermodynamics of quantum systems under dynamical control. *Adv. At. Mol. Opt. Phys.* **64**, 329 (2015). <https://doi.org/10.1016/bs.aamop.2015.07.002>

27. R. Uzdin, A. Levy, R. Kosloff, Equivalence of quantum heat machines, and quantum-thermodynamic signatures. *Phys. Rev. X* **5**, 031044 (2015). <https://doi.org/10.1103/PhysRevX.5.031044>
28. R. Uzdin, A. Levy, R. Kosloff, Quantum heat machines equivalence, work extraction beyond markovianity, and strong coupling via heat exchangers. *Entropy* **18**, 124 (2016). <https://doi.org/10.3390/e18040124>
29. S. Vinjanampathy, J. Anders, Quantum thermodynamics. *Contemp. Phys.* **57**, 1 (2016). <https://doi.org/10.1080/00107514.2016.1201896>
30. J. Roßnagel, S.T. Dawkins, K.N. Tolazzi, O. Abah, E. Lutz, F. Schmidt-Kaler, K. Singer, A single-atom heat engine. *Science* **352**, 325 (2016). <https://doi.org/10.1126/science.aad6320>
31. J. Klatzow, J.N. Becker, P.M. Ledingham, C. Weinzel, K.T. Kaczmarek, D.J. Saunders, J. Nunn, I.A. Walmsley, R. Uzdin, E. Poem, Experimental demonstration of quantum effects in the operation of microscopic heat engines (2017). [arXiv:1710.08716](https://arxiv.org/abs/1710.08716)
32. C.B. Dağ, W. Niedenzu, Ö.E. Müstecaplıoğlu, G. Kurizki, Multiatom quantum coherences in micromasers as fuel for thermal and nonthermal machines. *Entropy* **18**, 244 (2016). <https://doi.org/10.3390/e18070244>
33. W. Niedenzu, V. Mukherjee, A. Ghosh, A.G. Kofman, G. Kurizki, Quantum engine efficiency bound beyond the second law of thermodynamics. *Nat. Commun.* **9**, 165 (2018). <https://doi.org/10.1038/s41467-017-01991-6>
34. A. Ghosh, C.L. Latune, L. Davidovich, G. Kurizki, Catalysis of heat-to-work conversion in quantum machines. *Proc. Natl. Acad. Sci. U.S.A.* **114**, 12156 (2017). <https://doi.org/10.1073/pnas.1711381114>
35. R. Alicki, The quantum open system as a model of the heat engine. *J. Phys. A* **12**, L103 (1979). <https://doi.org/10.1088/0305-4470/12/5/007>
36. R. Kosloff, A quantum mechanical open system as a model of a heat engine. *J. Chem. Phys.* **80**, 1625 (1984). <https://doi.org/10.1063/1.446862>
37. E. Boukobza, D.J. Tannor, Three-level systems as amplifiers and attenuators: a thermodynamic analysis. *Phys. Rev. Lett.* **98**, 240601 (2007). <https://doi.org/10.1103/PhysRevLett.98.240601>
38. J.M.R. Parrondo, C.V. den Broeck, R. Kawai, Entropy production and the arrow of time. *New J. Phys.* **11**, 073008 (2009). <https://doi.org/10.1088/1367-2630/11/7/073008>
39. S. Deffner, E. Lutz, Nonequilibrium entropy production for open quantum systems. *Phys. Rev. Lett.* **107**, 140404 (2011). <https://doi.org/10.1103/PhysRevLett.107.140404>
40. E. Boukobza, H. Ritsch, Breaking the carnot limit without violating the second law: a thermodynamic analysis of off-resonant quantum light generation. *Phys. Rev. A* **87**, 063845 (2013). <https://doi.org/10.1103/PhysRevA.87.063845>
41. T. Sagawa, in *Lectures on Quantum Computing, Thermodynamics and Statistical Physics*, ed. by M. Nakahara, S. Tanaka (World Scientific, Singapore, 2013), pp. 125–190. [https://doi.org/10.1142/9789814425193\\_0003](https://doi.org/10.1142/9789814425193_0003)
42. G. Argentieri, F. Benatti, R. Floreanini, M. Pezzutto, Violations of the second law of thermodynamics by a non-completely positive dynamics. *EPL (Europhys. Lett.)* **107**, 50007 (2014). <https://doi.org/10.1209/0295-5075/107/50007>
43. K. Brandner, U. Seifert, Periodic thermodynamics of open quantum systems. *Phys. Rev. E* **93**, 062134 (2016). <https://doi.org/10.1103/PhysRevE.93.062134>
44. H.-P. Breuer, F. Petruccione, *The Theory of Open Quantum Systems* (Oxford University Press, Oxford, 2002)
45. H. Spohn, Entropy production for quantum dynamical semigroups. *J. Math. Phys.* **19**, 1227 (1978). <https://doi.org/10.1063/1.523789>
46. W. Pusz, S.L. Woronowicz, Passive states and KMS states for general quantum systems. *Commun. Math. Phys.* **58**, 273 (1978). <https://doi.org/10.1007/BF01614224>
47. A. Lenard, Thermodynamical proof of the Gibbs formula for elementary quantum systems. *J. Stat. Phys.* **19**, 575 (1978). <https://doi.org/10.1007/BF01011769>
48. A.E. Allahverdyan, R. Balian, T.M. Nieuwenhuizen, Maximal work extraction from finite quantum systems. *EPL (Europhys. Lett.)* **67**, 565 (2004). <https://doi.org/10.1209/epl/i2004-10101-2>

49. R. Alicki, M. Fannes, Entanglement boost for extractable work from ensembles of quantum batteries. *Phys. Rev. E* **87**, 042123 (2013). <https://doi.org/10.1103/PhysRevE.87.042123>
50. F.C. Binder, S. Vinjanampathy, K. Modi, J. Goold, Quantacell: powerful charging of quantum batteries. *New J. Phys.* **17**, 075015 (2015b). <https://doi.org/10.1088/1367-2630/17/7/075015>
51. N. Friis, M. Huber, Precision and work fluctuations in gaussian battery charging. *Quantum* **2**, 61 (2018). <https://doi.org/10.22331/q-2018-04-23-61>
52. D. Gelbwaser-Klimovsky, R. Alicki, G. Kurizki, Work and energy gain of heat-pumped quantized amplifiers. *EPL (Europhys. Lett.)* **103**, 60005 (2013). <https://doi.org/10.1209/0295-5075/103/60005>
53. J. Anders, V. Giovannetti, Thermodynamics of discrete quantum processes. *New J. Phys.* **15**, 033022 (2013). <https://doi.org/10.1088/1367-2630/15/3/033022>
54. P. Skrzypczyk, R. Silva, N. Brunner, Passivity, complete passivity, and virtual temperatures. *Phys. Rev. E* **91**, 052133 (2015). <https://doi.org/10.1103/PhysRevE.91.052133>
55. E.G. Brown, N. Friis, M. Huber, Passivity and practical work extraction using Gaussian operations. *New J. Phys.* **18**, 113028 (2016). <https://doi.org/10.1088/1367-2630/18/11/113028>
56. G. De Palma, A. Mari, S. Lloyd, V. Giovannetti, Passive states as optimal inputs for single-jump lossy quantum channels. *Phys. Rev. A* **93**, 062328 (2016). <https://doi.org/10.1103/PhysRevA.93.062328>
57. R. Alicki, From the GKLS equation to the theory of solar and fuel cells. *Open Syst. Inf. Dyn.* **24**, 1740007 (2017). <https://doi.org/10.1142/S1230161217400078>
58. N. Erez, G. Gordon, M. Nest, G. Kurizki, Thermodynamic control by frequent quantum measurements. *Nature* **452**, 724 (2008). <https://doi.org/10.1038/nature06873>
59. F. Schrögl, Zur statistischen Theorie der Entropieproduktion in nicht abgeschlossenen Systemen. *Z. Phys.* **191**, 81 (1966). <https://doi.org/10.1007/BF01362471>
60. A.K. Ekert, P.L. Knight, Canonical transformation and decay into phase-sensitive reservoirs. *Phys. Rev. A* **42**, 487 (1990). <https://doi.org/10.1103/PhysRevA.42.487>
61. C.W. Gardiner, P. Zoller, *Quantum Noise*, 2nd ed. (Springer, Berlin, 2000)
62. V. Mukherjee, W. Niedenzu, A.G. Kofman, G. Kurizki, Speed and efficiency limits of multilevel incoherent heat engines. *Phys. Rev. E* **94**, 062109 (2016). <https://doi.org/10.1103/PhysRevE.94.062109>
63. T. Feldmann, R. Kosloff, Quantum lubrication: suppression of friction in a first-principles four-stroke heat engine. *Phys. Rev. E* **73**, 025107 (2006). <https://doi.org/10.1103/PhysRevE.73.025107>
64. R. Kosloff, Y. Rezek, The quantum harmonic otto cycle. *Entropy* **19**, 136 (2017). <https://doi.org/10.3390/e19040136>
65. R. Graham, Squeezing and frequency changes in harmonic oscillations. *J. Mod. Opt.* **34**, 873 (1987). <https://doi.org/10.1080/09500348714550801>
66. G.S. Agarwal, S.A. Kumar, Exact quantum-statistical dynamics of an oscillator with time-dependent frequency and generation of nonclassical states. *Phys. Rev. Lett.* **67**, 3665 (1991). <https://doi.org/10.1103/PhysRevLett.67.3665>
67. I. Averbukh, B. Sherman, G. Kurizki, Enhanced squeezing by periodic frequency modulation under parametric instability conditions. *Phys. Rev. A* **50**, 5301 (1994). <https://doi.org/10.1103/PhysRevA.50.5301>
68. R. Alicki, D. Gelbwaser-Klimovsky, Non-equilibrium quantum heat machines. *New J. Phys.* **17**, 115012 (2015). <https://doi.org/10.1088/1367-2630/17/11/115012>
69. D. Türkpençe, Ö.E. Müstecaplıoğlu, Quantum fuel with multilevel atomic coherence for ultra-high specific work in a photonic Carnot engine. *Phys. Rev. E* **93**, 012145 (2016). <https://doi.org/10.1103/PhysRevE.93.012145>
70. C. B. Dağ, W. Niedenzu, F. Ozaydin, Ö.E. Müstecaplıoğlu, G. Kurizki, Temperature Control in Dissipative Cavities by Entangled Dimers. *J. Phys. Chem. C* (accepted, 2019 in press). <https://doi.org/10.1021/acs.jpcc.8b11445>
71. M. Aspelmeyer, T.J. Kippenberg, F. Marquardt, Cavity optomechanics. *Rev. Mod. Phys.* **86**, 1391 (2014). <https://doi.org/10.1103/RevModPhys.86.1391>

72. A. Ghosh, D. Gelbwaser-Klimovsky, W. Niedenzu, A.I. Lvovsky, I. Mazets, M.O. Scully, G. Kurizki, Two-level masers as heat-to-work converters. *Proc. Natl. Acad. Sci. U.S.A.* **115**, 9941 (2018). <https://doi.org/10.1073/pnas.1805354115>
73. J. Górecki, W. Pusz, Passive states for finite classical systems. *Lett. Math. Phys.* **4**, 433 (1980). <https://doi.org/10.1007/BF00943428>
74. H.A.M. Daniëls, Passivity and equilibrium for classical Hamiltonian systems. *J. Math. Phys.* **22**, 843 (1981). <https://doi.org/10.1063/1.524949>
75. J. da Providência, C. Fiolhais, Variational formulation of the Vlasov equation. *J. Phys. A: Math. Gen.* **20**, 3877 (1987). <https://doi.org/10.1088/0305-4470/20/12/034>
76. M. Wallquist, K. Hammerer, P. Zoller, C. Genes, M. Ludwig, F. Marquardt, P. Treutlein, J. Ye, H.J. Kimble, Single-atom cavity QED and optomechanics. *Phys. Rev. A* **81**, 023816 (2010). <https://doi.org/10.1103/PhysRevA.81.023816>
77. R.J. Glauber, Coherent and Incoherent States of the Radiation Field. *Phys. Rev.* **131**, 2766 (1963). <https://doi.org/10.1103/PhysRev.131.2766>
78. V.V. Dodonov, ‘Nonclassical’ states in quantum optics: a ‘squeezed’ review of the first 75 years. *J. Opt. B: Quantum Semiclass. Opt.* **4**, R1 (2002). <https://doi.org/10.1088/1464-4266/4/1/201>
79. M.S. Kim, F.A.M. de Oliveira, P.L. Knight, Properties of squeezed number states and squeezed thermal states. *Phys. Rev. A* **40**, 2494 (1989). <https://doi.org/10.1103/PhysRevA.40.2494>

# Chapter 3

## Performance of Quantum Thermodynamic Cycles



Tova Feldmann and José P. Palao

Quantum cycles are the microscopic version of the macroscopic thermodynamic cycles, such as the Carnot cycle or the Otto cycle. The quantum Otto cycle consists of four-strokes, two *adiabats* and two *isochores*. The equations for the dynamics on the *adiabats* and *isochores* are derived from first principles and illustrated for a working medium consisting of spins. We review a frictionlike behaviour due to the noncommutability of the external and internal Hamiltonians. The performance of the engine cycle and the refrigerator cycle are illustrated using a simple model of an ensemble of spin pairs with an effective interaction.

### 3.1 Introduction

The task of a quantum heat engine is to transform heat into useful work using the spontaneous heat flow from a hot to a cold reservoir. Quantum heat engines are either continuous (see Chaps. 1, 2 and 9) or discrete. Examples of the latter are four-stroke engines [1, 2] and two-stroke engines [3–5]. The cycle operation in four-stroke quantum engines is similar to their classical counterparts, either the Carnot cycle or the Otto cycle [1, 6]. In this chapter we focus on the quantum version of the Otto cycle. The working medium consists of an ensemble of quantum systems, for example two-level systems (TLS's) [7, 8] or harmonic oscillators [9, 10]. The energy scale of the working medium can be modified by an external control parameter  $\omega(t)$ . All

---

T. Feldmann  
Institute of Chemistry, Hebrew University of Jerusalem,  
91904 Jerusalem, Israel  
e-mail: tovaf@huji.ac.il

J. P. Palao (✉)  
Departamento de Física and IUDEA, Universidad de La Laguna,  
E-38204 La Laguna, Spain  
e-mail: jppalao@ull.es

branches can be described by quantum equations of motion and the thermodynamic variables can be derived from first principles.

The construction of the quantum Otto cycle requires two kind of processes in the working medium: (a) processes in which the external control  $\omega$  varies when the medium is isolated from the environment, termed *adiabats* since only work is consumed or produced. (b) Processes in which the external control remains constant, but the working medium is in contact with a heat bath. Only heat is exchanged with the environment, and the process is termed *isochore* by analogy with the classical ones. The cycle is described as [10]:

1. The compression *adiabat*: the system frequency increases from  $\omega_c$  to  $\omega_h$  in a time period  $\tau_{ch}$ , while the working medium is isolated from the heat baths.
2. The hot *isochore*: the working medium is coupled to the hot bath at temperature  $T_h$  in a time period  $\tau_h$  while  $\omega_h$  remains constant.
3. The expansion *adiabat*: the working medium is isolated from the heat baths in a time period  $\tau_{hc}$  and the frequency decreases from  $\omega_h$  to  $\omega_c$ .
4. The cold *isochore*: the working medium is coupled to the cold bath at temperature  $T_c$  in a time period  $\tau_c$  while  $\omega_c$  remains constant.

The useful work is obtained at the cost of the heat absorbed from the hot bath. In order to close the cycle, the surplus energy is rejected from the working medium to the environment, represented by the cold heat bath.

A refrigerator cycle can be obtained by reversing the sequence of the branches [11, 12]. Here the objective is to remove heat from a cold bath at temperature  $T_c$  at the expenses of external work performed on the system. The surplus energy is rejected to the environment represented by a hot bath at temperature  $T_h$ . Some interesting questions arise when approaching low temperatures. For example, what are the conditions for optimizing the cooling rate for small  $T_c$ ? or whether there is a minimum temperature below which the refrigerator cycle stops working [13–16].

The performance of classical cycles is limited by the rate of heat transport, friction and heat leaks, which become more important when the cycle time is reduced. The miniaturization of the engines from the macroscopic to the quantum regime raises the questions whether the same limitations scale down, and whether the quantum origin of the macroscopic phenomena can be identified. The first attempts to answer these questions studied the heat transport in cycles using the framework of open quantum systems. For example, a model of the Otto cycle with spins as a working medium was used to explore the performance of a quantum engine only limited by heat transfer [17]. The maximum power for this engine was obtained for the unrealistic case of zero time allocation on the *adiabats*, the bang-bang solution. An improved model [11], in which *friction* was added phenomenally, already shows some realistic features of heat engines and refrigerators, as for example minimum cycle time and reduced efficiency for finite power. The frictionlike phenomena appears naturally in quantum models when the “nonadiabatic” dynamics generates coherences on the *adiabats* since the cycle requires an additional energy cost when they are dissipated on the *isochores*. This “nonadiabatic” effect has been termed as *inner friction* or *quantum friction* [7, 8, 18]. (Notice that we use “nonadiabatic” and *adiabat* in the

quantum and thermodynamic sense respectively). This apparent friction is traced back to the noncommutability of the external control field Hamiltonian and the internal Hamiltonian of the working fluid [15]. Optimising performance then leads to two different strategies for the optimal protocol of changing the control parameter  $\omega$  on the *adiabats*. One strategy is to find a frictionless protocol [15, 19]. The other strategy is to shorten the cycle time such that coherence is maintained throughout [20].

This chapter has two parts. In the first one we introduce the equations for the dynamics of the working medium, either driven by an external control or in contact with a heat bath, and identify work and heat by the change of the working medium energy in each case (see Chap. 1). Next, we describe two models of the working medium, noninteracting spins with effective inner *friction* and interacting spins, where we discuss in detail the origin of quantum *friction*. Although we mainly consider spin systems, we also briefly introduce the harmonic working medium. In the second part we study the engine and refrigerator cycles. In order to get some insight based on simple analytical expressions, we describe them for the model of noninteracting spins with effective inner *friction*. Finally, we discuss the concept of limit cycle. In the following, we use units for which  $\hbar = 1$  and  $k_B = 1$ .

## 3.2 Dynamics of the Working Medium

The working medium consists of an ensemble of quantum systems and is described by the density operator  $\hat{\rho}$  with the Hamiltonian

$$\hat{\mathbf{H}}(\omega) = \hat{\mathbf{H}}_0 + \hat{\mathbf{H}}_{ext}(\omega) + \hat{\mathbf{H}}_{int}, \quad (3.1)$$

where  $\hat{\mathbf{H}}_0$  is the free Hamiltonian,  $\hat{\mathbf{H}}_{ext}(\omega)$  incorporates the external time-dependent control field  $\omega$  and  $\hat{\mathbf{H}}_{int}$  represents the internal interaction in the ensemble. In general  $[\hat{\mathbf{H}}(t), \hat{\mathbf{H}}(t')] \neq 0$ .

### 3.2.1 Dynamics on the Adiabats

The evolution of the density operator is given by

$$\frac{d\hat{\rho}}{dt} = -i[\hat{\mathbf{H}}(\omega), \hat{\rho}]. \quad (3.2)$$

The change of the energy  $\langle E \rangle = \text{Tr}\{\hat{\mathbf{H}}(\omega)\hat{\rho}\}$  due to the explicit time dependence of  $\omega$  on the *adiabats* becomes

$$\frac{d}{dt}\langle E \rangle_a = \text{Tr} \left\{ \left( \frac{d}{dt}\hat{\mathbf{H}}(\omega) \right) \hat{\rho} \right\}. \quad (3.3)$$

The work in a time period  $t$  is then

$$W(t) = \int_0^t \frac{d}{dt'} \langle E \rangle_a dt' = \langle E(t) \rangle_a - \langle E(0) \rangle_a. \quad (3.4)$$

Notice that  $W > 0$  when the system energy increases, and  $W < 0$  when the cycle realizes useful work on the environment.

### 3.2.2 Dynamics on the Isochores

The system is in contact with a heat bath at temperature  $T_\alpha$  while the external control is equal to  $\omega_\alpha$ , with  $\alpha = c, h$ . When the working medium couples weakly to a heat bath, the Markovian relaxation towards thermal equilibrium [21] is described by the Gorini–Kossakowski–Lindblad–Sudarshan (GKLS) equation [22, 23] (see also Chap. 1),

$$\frac{d\hat{\rho}}{dt} = -i[\hat{\mathbf{H}}(\omega_\alpha), \hat{\rho}] + \mathcal{L}_\alpha(\hat{\rho}), \quad (3.5)$$

where

$$\mathcal{L}_\alpha(\hat{\rho}) = \sum_j \kappa_j \left( \hat{\mathbf{A}}_j \hat{\rho} \hat{\mathbf{A}}_j^\dagger - \frac{1}{2} \{ \hat{\mathbf{A}}_j^\dagger \hat{\mathbf{A}}_j, \hat{\rho} \} \right). \quad (3.6)$$

In this expression,  $\hat{\mathbf{A}}_j$  are transition operators between neighboring energy levels of  $\hat{\mathbf{H}}$  and  $\kappa_j$  the corresponding transition rates. Pure dephasing can be considered by adding to Eq. (3.5) a term

$$\mathcal{L}_D(\hat{\rho}) = -\gamma_\alpha [\hat{\mathbf{H}}(\omega_\alpha), [\hat{\mathbf{H}}(\omega_\alpha), \hat{\rho}]]. \quad (3.7)$$

This term has been also considered on the *adiabats* in order to suppress quantum friction [24]. The energy change on the *isochore* is

$$\frac{d}{dt} \langle E \rangle_i = \text{Tr}\{\hat{\mathbf{H}}(\omega_\alpha) \mathcal{L}_\alpha(\hat{\rho})\}. \quad (3.8)$$

The heat exchange with the baths in a time period  $t$  is then

$$\mathcal{Q}_\alpha(t) = \int_0^t \frac{d}{dt'} \langle E \rangle_i dt' = \langle E(t) \rangle_i - \langle E(0) \rangle_i, \quad (3.9)$$

which is positive when energy flows towards the system.

### 3.2.3 Entropy and Internal Temperature

In addition to the von Neumann entropy,  $s_{VN} = -\text{Tr}\{\hat{\rho} \ln \hat{\rho}\}$ , we consider the energy entropy  $s_E = -\sum_i p_i \ln p_i$ , where  $p_i$  are the diagonal elements of the density operator in the energy basis. In general  $s_E \geq s_{VN}$ . The equality holds when  $\hat{\rho}$  is diagonal in the energy basis. The difference between the von Neumann entropy and the energy entropy is one of the possible measures of coherence [25]. Besides, the energy entropy appears in the definition of a dynamical temperature when the working medium is not in thermal equilibrium,  $T_{dyn} = (\partial \langle E \rangle / \partial t) / (\partial s_E / \partial t)$ , where the derivative is taken with constant external field [26].

## 3.3 Models of the Working Medium

### 3.3.1 Noninteracting Spins with Effective Inner Friction

In the analysis of a working medium with effective internal interaction, we must consider the dynamics of a single component. To be more concrete, we consider a spin 1/2 system with Hamiltonian  $\hat{\mathbf{H}}_{ext}(\omega) = \omega \hat{\sigma}_z / 2$ , where the frequency is determined by the longitudinal component of an external magnetic field,  $\omega = -\gamma B_z$  [1, 11, 17]. The energy is then

$$\langle E \rangle = \text{Tr}\{\hat{\mathbf{H}}_{ext}(\omega) \hat{\rho}\} = \omega \mathcal{S}, \quad (3.10)$$

and depends only on the polarization  $\mathcal{S} = (p_+ - p_-)/2$ , where  $p_\pm$  are the populations in the eigenstates of  $\hat{\mathbf{H}}_{ext}$  with energies  $\pm\omega/2$ . The internal temperature  $T$  is defined via the relation

$$\mathcal{S} = -\frac{1}{2} \tanh\left(\frac{\omega}{2T}\right). \quad (3.11)$$

Let us first analyse the dynamics on the *adiabats*. The interaction between spins is described effectively by a constant speed polarization change,  $d\mathcal{S}/dt = (\sigma/\tau_a)^2$ , where  $\tau_a$  is the duration of the process on the *adiabat* and  $\sigma$  the *friction coefficient* [11]. The validity of this assumption is discussed below. The polarization as a function of time becomes

$$\mathcal{S}(t) = \mathcal{S}(0) + \left(\frac{\sigma}{\tau_a}\right)^2 t, \quad (3.12)$$

and the work on a period of time  $t$ , Eqs. (3.4) and (3.10), results in

$$W(t) = [\omega(t) - \omega(0)]\mathcal{S}(0) + \omega(t) \left(\frac{\sigma}{\tau_a}\right)^2 t. \quad (3.13)$$

The second term corresponds to the additional work on the system associated with *friction*.

The spin is in contact with a bath at temperature  $T_\alpha$  on the *isochores*. The Liouville operator Eq. (3.6) includes two terms, with rates  $\kappa_{\downarrow}^{(\alpha)}$  for transitions from the upper to the lower level and  $\kappa_{\uparrow}^{(\alpha)}$  from the lower to the upper level. The corresponding operators are  $\hat{\mathbf{A}}_{\downarrow} = (\hat{\sigma}_x - i\hat{\sigma}_y)/2$  and  $\hat{\mathbf{A}}_{\uparrow} = (\hat{\sigma}_x + i\hat{\sigma}_y)/2$ . The rate coefficients and the bath temperature are related by detailed balance,  $\kappa_{\uparrow}^{(\alpha)}/\kappa_{\downarrow}^{(\alpha)} = \exp(-\omega_\alpha/T_\alpha)$ . The rate equations for the populations are obtained using Eq. (3.6), from which one achieves the equation of motion for the polarization

$$\frac{dS}{dt} = -\Gamma_\alpha(S - S_\alpha^{eq}), \quad (3.14)$$

where  $\Gamma_\alpha = \kappa_{\downarrow}^{(\alpha)} + \kappa_{\uparrow}^{(\alpha)}$ , and

$$S_\alpha^{eq} = -\frac{1}{2} \frac{\kappa_{\downarrow}^{(\alpha)} - \kappa_{\uparrow}^{(\alpha)}}{\kappa_{\downarrow}^{(\alpha)} + \kappa_{\uparrow}^{(\alpha)}} = -\frac{1}{2} \tanh\left(\frac{\omega_\alpha}{2T_\alpha}\right) \quad (3.15)$$

is the value of the polarization when the spin reaches thermal equilibrium with the bath. Then, the polarization changes on the *isochore* are given by [11]

$$S(t) = S(0)e^{-\Gamma_\alpha t} + S_\alpha^{eq}(1 - e^{-\Gamma_\alpha t}). \quad (3.16)$$

Using Eq. (3.9), the heat exchange with the bath on an *isochore* after a time period  $t$  is

$$Q_\alpha(t) = \omega_\alpha[S(t) - S(0)]. \quad (3.17)$$

### 3.3.2 Pairs of Interacting Spins

The model consists of an ensemble of spin atoms, in which the internal interaction only couples a given atom with another one, while each pair of atoms does not interact with any other pair [7, 8]. As a consequence, we need to consider only one pair of interacting spins to describe the medium dynamics. The Hamiltonian is given by

$$\hat{\mathbf{H}}(\omega) = \hat{\mathbf{H}}_{ext}(\omega) + \hat{\mathbf{H}}_{int}(J) = \omega\hat{\mathbf{B}}_1 + J\hat{\mathbf{B}}_2, \quad (3.18)$$

where  $\hat{\mathbf{B}}_1 = (\hat{\sigma}_z^{(1)} \otimes \hat{\mathbf{I}}^{(2)} + \hat{\mathbf{I}}^{(1)} \otimes \hat{\sigma}_z^{(2)})/2$ ,  $\hat{\mathbf{B}}_2 = (\hat{\sigma}_x^{(1)} \otimes \hat{\sigma}_x^{(2)} - \hat{\sigma}_y^{(1)} \otimes \hat{\sigma}_y^{(2)})/2$ , and  $\hat{\sigma}_{x,y,z}^{(i)}$  are the Pauli matrices corresponding to each spin. Notice that  $[\hat{\mathbf{H}}_{ext}(\omega), \hat{\mathbf{H}}_{int}(J)] \neq 0$ . The parameter  $J$  scales the strength of the internal interaction. The thermodynamic quantities and the system state can be determined from the expecta-

tion values of the subset  $\{\hat{\mathbf{B}}_1, \hat{\mathbf{B}}_2, \hat{\mathbf{B}}_3 = i[\hat{\mathbf{B}}_1, \hat{\mathbf{B}}_2] = (\hat{\sigma}_x^{(1)} \otimes \hat{\sigma}_y^{(2)} + \hat{\sigma}_y^{(1)} \otimes \hat{\sigma}_x^{(2)})/2\}$  of the operator algebra of the system, which is a closed Lie subalgebra [8].

We denote by  $(p_1, p_2, p_3, p_4)$  the populations of the eigenstates of  $\hat{\mathbf{H}}(\omega)$  with energies  $(\Omega, 0, 0, -\Omega)$ , where  $\Omega = \pm\sqrt{\omega^2 + J^2}$ , and introduce  $\mathcal{S} = (p_1 - p_4)/2$ . The system energy is given by

$$\langle E \rangle = 2\Omega \mathcal{S} = \omega \langle b_1 \rangle + J \langle b_2 \rangle, \quad (3.19)$$

where  $\langle b_i \rangle = \text{Tr}\{\hat{\mathbf{B}}_i \hat{\rho}\}$ .

Let us now consider the system dynamics on the *adiabats*. As mentioned above, the system density matrix can be constructed from the expectation values of the operators  $\hat{\mathbf{B}}_1, \hat{\mathbf{B}}_2$  and  $\hat{\mathbf{B}}_3$ , since the internal interaction only connects the states  $|++\rangle$  and  $|--\rangle$  in the polarization basis [7]. Notice that  $p_1 + p_4, p_2$  and  $p_3$  remain constant in these processes. Using Eq. (3.2) with the Hamiltonian Eq. (3.18), the evolution of the expectation values of these operators is given by the coupled differential equations

$$\frac{d}{dt} \langle b_1 \rangle_a = 2J \langle b_3 \rangle_a, \quad \frac{d}{dt} \langle b_2 \rangle_a = -2\omega \langle b_3 \rangle_a, \quad \frac{d}{dt} \langle b_3 \rangle_a = 2\omega \langle b_2 \rangle_a - 2J \langle b_1 \rangle_a. \quad (3.20)$$

Closed-form solutions for these equations can be obtained for constant “adiabatic” parameter  $\mu_s = J\Omega^{-3}(d\omega/dt)$  [15].

When  $\omega$  changes slowly, the populations in the energy basis follow the external control field and the energy is given by  $\langle E(t) \rangle_a^{ad} = 2\Omega(t)\mathcal{S}(0)$ . However, in a fast process, the “nonadiabatic” dynamics may lead to the generation of coherences and a population transfer between states. Then, an additional term must be considered in the energy,  $\langle E(t) \rangle_a^{na} = 2\Omega(t)[\mathcal{S}(t) - \mathcal{S}(0)]$ . Using Eq. (3.4), the work on the *adiabat* after a period  $t$  results in  $W = W^{ad} + W^{na}$ , where  $W^{ad} = 2[\Omega(t) - \Omega(0)]\mathcal{S}(0)$  and

$$W^{na}(t) = 2\Omega(t)[\mathcal{S}(t) - \mathcal{S}(0)]. \quad (3.21)$$

The “nonadiabatic” effects are reflected in the energy entropy  $s_E$ . For an initial thermal state (as expected after a long enough *isochore*)  $s_E(0) = s_{VN} \leq s_E(t)$ , which implies that  $\mathcal{S}(0) \leq \mathcal{S}(t)$ . Then  $W^{na}$  is positive, that is, it implies an additional cost in external work to drive the system on the *adiabats*. We remark that this conclusion is valid if the initial state is a thermal state,  $\mathcal{S} < 0$ . The additional cost reduces in general the cycle performance. This is the origin of quantum *friction*. The same effect may appear for any working medium whenever  $[\hat{\mathbf{H}}(t), \hat{\mathbf{H}}(t')] \neq 0$ . However, it depends on the particular time scheduling for  $\omega$ . When the populations in the energy basis coincide at time  $t = 0$  and  $t$ , the additional work  $W^{na}(t) = 0$ , irrespective of the time employed on the process. Those protocols, termed frictionless solutions or shortcuts to “adiabaticity” [19, 27], are the subject of Chap. 5. Other possible strategies to avoid the frictionlike mechanism consist in adding noise on the *adiabats* [24] or the multilevel embedding scheme [28].

The close relation between the energy entropy, the coherences, and the additional work in “nonadiabatic” processes is illustrated in Fig. 3.1 for a linear scheduling of

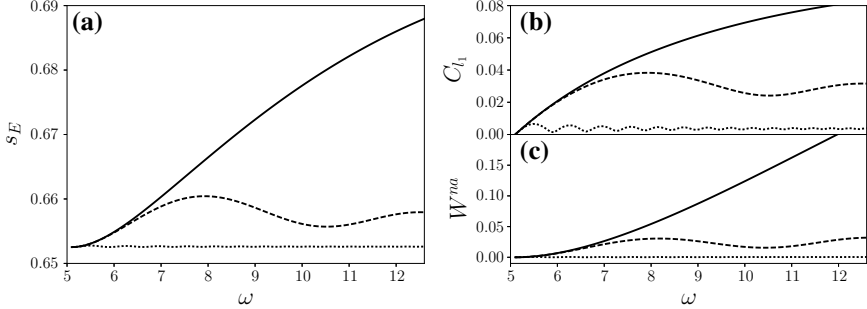


**Fig. 3.1** **a** Energy entropy  $s_E$  vs. control field  $\omega$  on the *adiabat* when the frequency changes linearly from  $\omega_c$  to  $\omega_h$ . **b** Coherence  $C_{l_1}(t) = |\langle 1 | \hat{\rho} | 4 \rangle|$  in the energy basis and **c** the “nonadiabatic” work  $W^{na}(t)$  during the process. The time periods are  $\tau_{ch} = \tau_1$  (solid lines),  $\tau_{ch} = 10\tau_1$  (dashed lines) and  $\tau_{ch} = 100\tau_1$  (dotted lines). The parameters are  $\tau_1 = 0.05$ ,  $\omega_c = 5.1$ ,  $\omega_h = 12.6$ ,  $J = 2$ . The initial state is a thermal state at temperature  $T = 2.5$ .

$\omega(t)$ . Three different time periods are considered. For large time periods, they show an oscillating behaviour while the magnitude of the “nonadiabatic” effects decrease. Frictionless solutions take advantage of this oscillating behaviour, since the initial energy entropy is recovered for some protocols after a specific time period [15].

The super-operator  $\mathcal{L}$  for the dynamics on the *isochores* is constructed taking  $\{\hat{A}\}$  as a set of transition operators between the energy eigenstates, with the condition that any two states are connected by a sequence of transitions. The corresponding evolution operator can be obtained explicitly [8]. However, the complete cycle dynamics must be obtained numerically except when considering protocols with analytical solutions on the *adiabats*.

A simple effective model can be constructed considering the TLS formed by states 1 and 4. The starting point is the change of the TLS “polarization” on the *adiabats*. Using Eqs. (3.19) and (3.20), it is given by

$$\frac{dS}{dt} = v_s = \frac{J}{\omega^2} \left( \frac{d\omega}{dt} \right) (-\text{Re}\{\langle 1 | \hat{\rho} | 4 \rangle\}). \quad (3.22)$$

In order to simplify the model we will consider a constant speed change of  $S$  and initial thermal states for which  $S(0) \leq S(t)$ . Qualitatively, the coherences increase with  $J$  but decrease with the time period  $\tau_a$  of the *adiabat*. Assuming a linear change of the field  $(d\omega/dt) \propto 1/\tau_a$ , we set the speed  $v_s = \sigma^2/\tau_a^2$ , where the *friction* coefficient  $\sigma$  is proportional to  $J$  [11]. Besides, all the coherences and the populations in the other states are neglected. As a consequence, the only frictionless solutions are slow processes. In this way, the model of noninteracting spins with effective *inner* friction is obtained. We remark that the effective model does not incorporate the oscillating behaviour shown in Fig. 3.1, and neither additional effects of the coherences along a cycle.

### 3.3.3 Harmonic Oscillators

We briefly introduce the harmonic working medium. Two different models have been studied: (a) systems with Hamiltonian  $\hat{\mathbf{H}}(\omega) = \omega \hat{\mathbf{a}}_0^\dagger \hat{\mathbf{a}}_0$ , where  $\hat{\mathbf{a}}_0^\dagger$  and  $\hat{\mathbf{a}}_0$  are time independent creation and annihilation operators respectively [2]. This model is free of quantum *friction* and the results are similar to those obtained for noninteracting spins [17]. (b) Systems where the external control is the curvature of the potential well [9]. The Hamiltonian is

$$\hat{\mathbf{H}}(\omega) = \frac{\hat{\mathbf{P}}^2}{2m} + \frac{1}{2}m\omega^2\hat{\mathbf{X}}^2. \quad (3.23)$$

As a consequence,  $[\hat{\mathbf{H}}(t), \hat{\mathbf{H}}(t')] \neq 0$  and the system may be subject to quantum *friction*. The Liouville operator Eq. (3.6) includes two terms, with  $\hat{\mathbf{A}}_\downarrow = \hat{\mathbf{a}}$  for transitions from the upper to the lower level and  $\hat{\mathbf{A}}_\uparrow = \hat{\mathbf{a}}^\dagger$  from the lower to the upper level, with  $\hat{\mathbf{a}} = \sqrt{m\omega/2}\hat{\mathbf{X}} + i\hat{\mathbf{P}}/\sqrt{2m\omega}$ . Closed-form solutions for the dynamics can be obtained when the “nonadiabatic” parameter  $\mu_o = \omega^{-2}(d\omega/dt)$  is constant, including frictionless solutions [10].

## 3.4 Performance of Heat Engine Cycle

The main quantities of interest in the analysis of the engine performance are the work per cycle  $W_{cyc}$ , the averaged power per cycle  $\mathcal{P}_{cyc} = W_{cyc}/\tau$ , where  $\tau$  is the time period of the cycle, and the efficiency

$$\eta = \frac{-W_{cyc}}{\mathcal{Q}_h}, \quad (3.24)$$

where  $\mathcal{Q}_h$  is the heat absorbed from the hot bath. For very slow cycles  $\eta_{ad} = 1 - \frac{\omega_c}{\omega_h} \leq \eta_{Carnot}$  [1]. We have introduced the Carnot efficiency  $\eta_{Carnot} = 1 - T_c/T_h$ . However, the power is negligible in this regime. In order to obtain finite power output, the cycle time  $\tau$  should be shortened, at the price of introducing possible “nonadiabatic” effects. We assume that those effects, which can be avoided by using the appropriate protocol, are detrimental for the engine performance,  $\eta_{na} \leq \eta_{ad} \leq \eta_{Carnot}$ . The special case of very short time periods is discussed in the last section. The engine performance for low temperatures,  $\omega_\alpha/T_\alpha \gg 1$ , is similar for spin systems and harmonic oscillators. For high temperatures,  $\omega_\alpha/T_\alpha \ll 1$ , the efficiency at maximum power of the engine with a working medium consisting of harmonic oscillators is given by  $\eta_{o,ht} = 1 - \sqrt{T_c/T_h} = \eta_{CA}$  [9, 29], which is the efficiency at maximum power of endoreversible engines [30–32]. A similar result is shown below for spins. These results highlight the connection between the analysis of quantum models and the finite-time analysis of macroscopic engines [33].

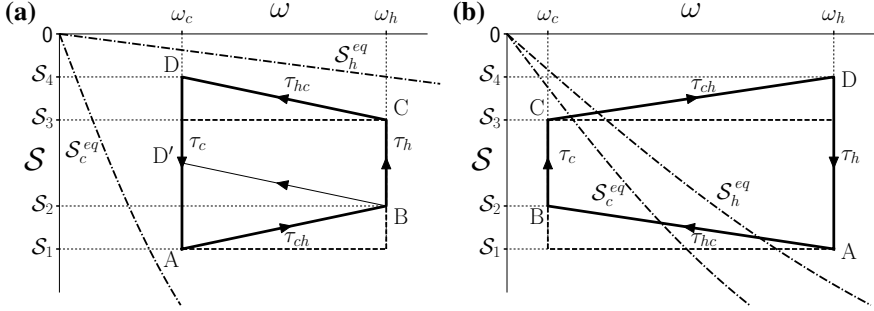


**Fig. 3.2** Schematic representation of **a** the engine and **b** refrigerator Otto cycles in the external control  $\omega$  and polarization  $S$  plane for spins with effective *friction*. Notice that for thermal states  $S < 0$ ,  $\tau_h$  and  $\tau_c$  are the time periods on the hot and cold *isochores*, and  $\tau_{ch}$  and  $\tau_{hc}$  on *adiabats*. The equilibrium polarizations  $S_c^{eq}$  and  $S_h^{eq}$  as a function of the external field (dashed-dotted lines) and the cycles without *friction* with the same points  $A$  and  $C$  (dashed lines) are also shown.

As an illustrative example, we consider the engine Otto cycle for noninteracting spins with effective *friction*. The cycle was described in the introduction and is schematically represented in Fig. 3.2a. Using Eqs. (3.12), (3.13), (3.15), (3.16) and (3.17), the polarization, work and heat involved in each branch are given by

$$\begin{aligned} \text{Compression adiabat } AB : \quad & S_2 = S_1 + \sigma^2/\tau_{ch}, & W_{AB} = (\omega_h - \omega_c)S_1 + \omega_h\sigma^2/\tau_{ch}. \\ \text{Hot isochore } BC : \quad & S_3 = yS_2 + (1-y)S_h^{eq}, & Q_{h,BC} = \omega_h(S_3 - S_2). \\ \text{Expansion adiabat } CD : \quad & S_4 = S_3 + \sigma^2/\tau_{hc}, & W_{CD} = (\omega_c - \omega_h)S_3 + \omega_c\sigma^2/\tau_{hc}. \\ \text{Cold isochore } DA : \quad & S_1 = xS_4 + (1-x)S_c^{eq}, & Q_{c,DA} = \omega_c(S_1 - S_4), \end{aligned} \quad (3.25)$$

where  $x = e^{-\Gamma_c \tau_c}$  and  $y = e^{-\Gamma_h \tau_h}$ . In the spin system the useful work is realized on the *adiabat*  $AB$  ( $W_{AB} < 0$ ). As an effect of *friction*, the work output on the *adiabat*  $AB$  and the heat absorbed on the *isochore*  $BC$  are reduced, whereas the work on the *adiabat*  $CD$  and the heat rejected on the *isochore*  $DA$  become higher than in the ideal cycle. The results for the cycle without *friction* [17] are obtained setting  $\sigma = 0$ ,  $S_2 = S_1$  and  $S_4 = S_3$ . The relation between the polarizations along the cycle restrict the possible values of some of the parameters. For example, the internal temperature of the working medium is always lower than  $T_h$  and higher than  $T_c$ , and therefore  $S_3 < S_h^{eq}$  and  $S_1 > S_c^{eq}$ . Besides  $S_3 > S_1$ , and using Eq. (3.11)

$$\frac{\omega_h}{T_h} < \frac{\omega_c}{T_c}. \quad (3.26)$$

Equation (3.25) determines completely the polarizations along the cycle. For example

$$S_1 = \frac{(1-x)S_c^{eq} + x(1-y)S_h^{eq}}{1-xy} + \sigma^2 \frac{x(1/\tau_{hc} + y/\tau_{ch})}{1-xy}, \quad (3.27)$$

and the polarization change in the hot *isochore* is

$$\mathcal{S}_3 - \mathcal{S}_2 = \Delta\mathcal{S}^{eq} \frac{(1-x)(1-y)}{1-xy} - \sigma^2 \frac{(1-y)(x/\tau_{hc} + 1/\tau_{ch})}{1-xy}, \quad (3.28)$$

where  $\Delta\mathcal{S}^{eq} = \mathcal{S}_h^{eq} - \mathcal{S}_c^{eq}$ . The total work per cycle is the sum of the work on each *adiabat*,

$$W_{cyc} = W_{AB} + W_{CD} = -(\omega_h - \omega_c)(\mathcal{S}_3 - \mathcal{S}_2) + \sigma^2 \omega_c (1/\tau_{ch} + 1/\tau_{hc}). \quad (3.29)$$

We recall that  $W_{cyc} < 0$  when the cycle realizes useful work on the environment. In the same way, the heat exchanged with the baths per cycle is  $\mathcal{Q}_{cyc} = \mathcal{Q}_{BC} + \mathcal{Q}_{DA} = -W_{cyc}$ , showing the consistency of the model with the first law of thermodynamics. Considering that after a cycle the working medium reaches again the initial state, the total entropy production is only associated with the heat exchanged with the baths on the *isochores*,

$$\Delta s_{cyc}^u = -\mathcal{Q}_{BC}/T_h - \mathcal{Q}_{DA}/T_c = (\omega_c/T_c - \omega_h/T_h)(\mathcal{S}_3 - \mathcal{S}_2) + \sigma^2 \omega_c (1/\tau_{ch} + 1/\tau_{hc})/T_c, \quad (3.30)$$

and, therefore, the model can be classified as endoreversible. The entropy production and the work per cycle have a reciprocal relation as the entropy production increases with  $\sigma$ , whereas the work output decreases. The efficiency of the engine cycle is given by

$$\eta = \frac{-W_{cyc}}{\mathcal{Q}_{h,BC}} = 1 - \frac{\omega_c}{\omega_h} - \sigma^2 \frac{\omega_c (1/\tau_{ch} + 1/\tau_{hc})}{\omega_h (\mathcal{S}_3 - \mathcal{S}_2)} \quad (3.31)$$

For slow processes ( $\tau_{ch}, \tau_{hc} \gg 1$ ), the contribution of the third term is negligible, and then  $\eta \leq \eta_{ad} \leq \eta_{Carnot}$ , where we have used Eq. (3.26).

The cycle time is the sum of the time period in each branch,  $\tau = \tau_{ch} + \tau_h + \tau_{hc} + \tau_c$ . The minimum value of  $\tau$  required to close the cycle is given by the condition  $\mathcal{S}_3 - \mathcal{S}_2 = 0$ , see cycle ABD' in Fig. 3.2a. Using Eq. (3.28), the corresponding maximum value of  $x$  is

$$x_{max} = \frac{\Delta\mathcal{S}^{eq} - \sigma^2/\tau_{ch}}{\Delta\mathcal{S}^{eq} + \sigma^2/\tau_{hc}}. \quad (3.32)$$

Then, the minimum time on the cold branch is  $\tau_{c,min} = -\ln(x_{max})/\Gamma_c$  and the minimum cycle time is  $\tau_{min} = \tau_{ch} + \tau_{c,min} + \tau_{hc} = 1$ ,  $\tau_{c,min} = 0$  and  $W_{cyc} < 0$  for any cycle time, which is not realistic due to the unavoidable noise in the process. But when subject to quantum *friction*, the work output  $W_{cyc}$  is the sum of a negative (useful work) and a positive (work against friction) contribution. The minimum time for which they are balanced is denoted by  $\tau_0 \geq \tau_{min}$ . The condition  $W_{cyc} = 0$  is not sufficient to determine  $\tau_0 = \tau_{ch} + \tau_{h,0} + \tau_{hc} + \tau_{c,0}$ , but it establishes a relation between the time allocation in each segment of the cycle,

$$y_0 = \frac{(x_{max} - x_0) - R}{(x_{max} - x_0) - Rx_0}, \quad (3.33)$$

where  $x_0 = \exp(-\Gamma_c \tau_{c,0})$ ,  $y_0 = \exp(-\Gamma_h \tau_{h,0})$ , and  $R = \sigma^2 \omega_c (1/\tau_{ch} + 1/\tau_{hc}) / [(\omega_h - \omega_c)(\Delta S^{eq} + \sigma^2/\tau_{hc})]$ .

### 3.4.1 Optimization of Power

Different optimization problems can be considered, for example the optimization of power with respect to time allocation in each branch, with respect to external fields, or even with respect to all control parameters [11]. For fixed cycle time, the optimization power is equivalent to the optimization of work.

First, we discuss the optimization of work with respect to time allocation on the *isochores*, for fixed  $\tau$ ,  $\tau_{ch}$ ,  $\tau_{hc}$ ,  $\omega_c$  and  $\omega_h$ . The Lagrangian for the work becomes

$$L(x, y, \lambda) = W_{cycle}(x, y) + \lambda \left( \tau + \frac{\ln x}{\Gamma_c} + \frac{\ln y}{\Gamma_h} - \tau_{ch} - \tau_{hc} \right), \quad (3.34)$$

where  $x$  and  $y$  are the optimization variables and  $\lambda$  is the Lagrange multiplier associated with the constraint of constant total cycle time. Equating the partial derivatives of  $L$  with respect to  $x$  and  $y$ , the following relation is found

$$\Gamma_c x [(1-y)(1-yx_{max})] = \Gamma_h y [(1-x)(x_{max}-x)]. \quad (3.35)$$

For slow processes ( $\tau_c, \tau_h \gg 1$ ),  $\Gamma_c x = \Gamma_h y$ , which leads to the optimal ratio  $\tau_c/\tau_h = \Gamma_h/\Gamma_c$ , that is, the time period in each *isochore* is inversely proportional to the dissipation rate [17]. In the cases of equal relaxation rates,  $\Gamma_c = \Gamma_h$ , the relation becomes  $x = x_{max}y$ : The time allocated on the cold segment becomes larger than the time allocated on the hot segment, as the additional work due to inner *friction* must be dissipated in the cold bath [11].

For optimal time allocation on the *isochores* and fixed  $\tau_{ch}$  and  $\tau_{hc}$ , the minimum cycle time  $\tau_0$  required to obtain useful work ( $W_{cycle} < 0$ ) can be derived from Eqs. (3.33) and (3.35). After some algebra, the problem reduces to determining  $x_0$  solving the quadratic equation  $Ax_0^2 + Bx_0 + C = 0$ , with coefficients  $A = \Gamma_h(1+R)$ ,  $B = -\Gamma_c R(R - x_{max} + 1) - \Gamma_h[2x_{max} - R(1 - x_{max}) - R^2]$ , and  $C = \Gamma_h x_{max} (x_{max} - R)$ .

The dependence of the cycle times  $\tau_{min}$  and  $\tau_0$  on the *friction* coefficient is illustrated in Fig. 3.3a for optimal time allocation on the *isochores*. Both times increase with  $\sigma$ , but  $\tau_0$  diverges at a much lower value. Above this *friction* coefficient no useful work can be obtained from the engine. The divergence of  $\tau_{min}$  corresponds to a value of the *friction* parameter beyond which the cycle cannot be closed. The optimal work and power per cycle as a function of the cycle time are shown in Fig. 3.3b. The maximum useful work ( $W_{cyc} < 0$ ) is obtained for very slow cycles. However, the maximum power is obtained for a finite time, which is larger as the *friction* coefficient increases. In the idealized case of infinitely fast adiabats and  $\sigma = 0$ , maximum power is obtained in the limit  $\tau = 0$  corresponding to the bang-bang solution [17].

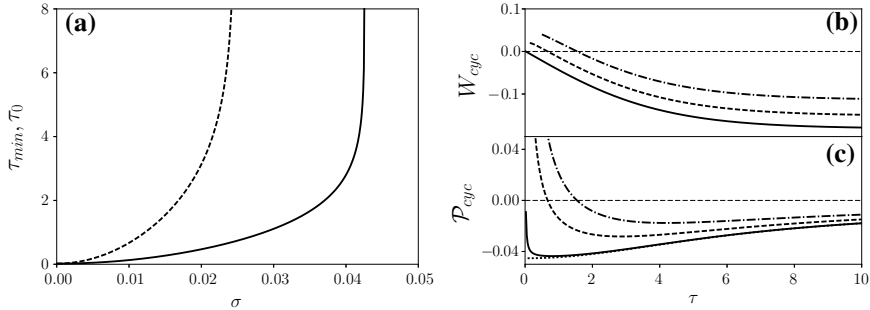


**Fig. 3.3** **a** Minimum time  $\tau_{min}$  required to close the cycle (solid line) and minimum time  $\tau_0$  for obtaining useful work (dashed line) as a function of the *friction* coefficient  $\sigma$ . **b** Optimal work and **c** optimal power with respect to time allocation on the *isochores* as a function of the cycle time  $\tau$  for different *friction* coefficients:  $\sigma = 0$  (solid lines),  $\sigma = 0.010$  (dashed lines),  $\sigma = 0.015$  (dashed-dotted lines). The parameters used are  $\omega_c = 1$ ,  $T_c = 1$ ,  $\Gamma_c = 1$ ,  $\omega_h = 2$ ,  $T_h = 10$ ,  $\Gamma_h = 1$ ,  $\tau_{ch} = \tau_{hc} = 0.01$ . The optimal power for  $\sigma = 0$  and infinite fast *adiabats* ( $\tau_{ch} = \tau_{hc} = 0$ ) is also shown (dotted line).

This result arises the question: Which is the minimum cycle time for a frictionless protocol in an arbitrary working medium? [34].

Let us consider now the optimization of work with respect to the external fields in the high temperature limit. We assume in addition “adiabatic” processes, and then  $W_{cyc}^{ht} = -(\omega_h - \omega_c)\Delta\mathcal{S}^{ht}F(x, y)$ , where  $\Delta\mathcal{S}^{ht} = (\omega_c/T_c - \omega_h/T_h)$  and  $F(x, y) = (1-x)(1-y)/[4(1-xy)]$ . The optimal frequency  $\omega_c^{opt} = \omega_h(T_c + T_h)/(2T_h)$  is obtained by equating to zero the derivative of  $W_{cyc}^{ht}$  with respect to  $\omega_c$ . The work  $W_{cyc}^{ht}(\omega_c^{opt}, \omega_h)$  grows monotonically with  $\omega_h$  in this limit since the rates for upward and downward transitions are equal. However, the efficiency Eq. (3.31) remains constant,

$$\eta_{s,ht} = \frac{\eta_{Carnot}}{2}, \quad (3.36)$$

which is the efficiency at maximum power for engines found in linear response (in this case, high temperatures) and “strong coupling” between work and heat flow (in this case,  $\eta = 1 - \omega_c/\omega_h$ ) [32, 35].

### 3.5 Refrigerator Cycle

Reversing the sequence of the engine cycle leads to a refrigeration cycle, schematically represented in Fig. 3.2b for the spin system with inner *friction* [11]. The objective is to absorb heat from a cold bath at temperature  $T_c$ . The cycle starts with an adiabatic compression  $AB$ , during which the working medium is isolated from the heat baths and the control frequency changes from  $\omega_h$  to  $\omega_c$  in a time period  $\tau_{hc}$ .

The final polarization  $\mathcal{S}_2$  corresponds to an internal temperature lower than  $T_c$ . On the cold *isochore BC*, the working medium is coupled to the cold bath for a time  $\tau_c$ . In this process the polarization changes from  $\mathcal{S}_2$  to  $\mathcal{S}_3 < -\tanh(\omega_c/2T_c)/2$  and the heat absorbed by the working medium is

$$\mathcal{Q}_{BC} = \omega_c(\mathcal{S}_3 - \mathcal{S}_2). \quad (3.37)$$

In the adiabatic expansion *CD*, the energy gap changes from  $\omega_c$  to  $\omega_h$  in a period  $\tau_{ch}$ . Finally, on the hot *isochore DA*, surplus heat is rejected to the hot bath and the polarization changes from  $\mathcal{S}_4$  to the initial value  $\mathcal{S}_1 > -\tanh(\omega_h/2T_h)/2$ . From  $\mathcal{S}_1 < \mathcal{S}_3$ , the working condition for the refrigerator cycle is

$$\frac{\omega_c}{T_c} < \frac{\omega_h}{T_h}. \quad (3.38)$$

In a similar analysis to the one for heat engine cycles, the polarization change on the cold branch is given by

$$\mathcal{S}_3 - \mathcal{S}_2 = -\Delta\mathcal{S}^{eq} \frac{(1-x)(1-y)}{1-xy} - \sigma^2 \frac{(1-x)(1/\tau_{hc} + y/\tau_{ch})}{1-xy}. \quad (3.39)$$

Notice that in the refrigerator cycle  $\Delta\mathcal{S}^{eq} < 0$ . The work per cycle is in this case

$$W_{cyc} = (\omega_h - \omega_c)(\mathcal{S}_3 - \mathcal{S}_2) + \sigma^2 \omega_h(1/\tau_{ch} + 1/\tau_{hc}), \quad (3.40)$$

and the coefficient of performance (COP) [11, 36]

$$\varepsilon = \frac{\mathcal{Q}_{BC}}{W_{cyc}} \leq \frac{\omega_c}{\omega_h - \omega_c} \leq \varepsilon_{Carnot}, \quad (3.41)$$

where  $\varepsilon_{Carnot} = T_c/(T_h - T_c)$  is the Carnot COP. Here, the variable to be optimized is the cycle cooling rate,  $\dot{\mathcal{Q}}_{BC} = \mathcal{Q}_{BC}/\tau$ , and different optimization strategies can be adopted. For example, the numerical optimization with respect to time allocation between all segments in the refrigerator gives a point of optimal operation [11], which coincides with the universal plot for commercial chillers [37].

We consider the optimization with respect to the field frequencies  $\omega_c$ , since the cooling rate is monotonic with respect to  $\omega_h$  [11]. From the condition  $\partial\dot{\mathcal{Q}}_{BC}/\partial\omega_c = 0$ , the optimal cooling rate results in

$$\dot{\mathcal{Q}}_{BC}^{opt} = \frac{(1-x)(1-y)}{4(1-xy)\tau} \left( \frac{\omega_c}{T_c} \right)^2 \frac{T_c}{\cosh^2[\omega_c/(2T_c)]}, \quad (3.42)$$

with the upper bound

$$\dot{Q}_{BC}^{opt} \leq \frac{(1-x)(1-y)}{4(1-xy)\tau} \left( \frac{\omega_c}{T_c} \right)^2 T_c. \quad (3.43)$$

Equation (3.38) implies that the ratio  $\omega_c/T_c$  remains bounded when the temperature of the cold bath decreases. Therefore, the cooling rate vanishes at least linearly with temperature for fixed cycle time [11]. In particular, for a working medium consisting of harmonic oscillators and frictionless protocols, an optimization with respect to all cycle parameters gives a cooling rate proportional to  $T_c^{3/2}$  [13]. Those results lead to a possible dynamical interpretation of the third law of thermodynamics (see Chap. 25), the absolute zero cannot be reached because the maximum cooling rate of the cycle vanishes at least linearly with temperature [11]. In interacting spin systems, the cooling rate for frictionless protocols degrades with any noise in the controls. Then, the refrigerator cycle works down to a minimum temperature  $T_{c,min}$ , which scales linearly with the interaction strength  $J$  [14, 15]. However, for harmonic oscillators  $T_{c,min} = 0$  [16], although the cooling rate vanishes as stated before. The conclusion is that any refrigerator constructed with a working medium possessing an uncontrolled energy gap will reach a minimum operating temperature of the order of the minimum energy gap.

### 3.6 The Limit Cycle

Let us consider a heat engine or refrigerator in an arbitrary initial state and with fixed values of the cycle parameters (external frequencies and time allocations). In general, after a short transitory, it settles to a steady state regime, the limit cycle [38]. In order to analyze it, we introduce the propagator of the cycle  $\hat{U}_{cyc}$ , a completely positive map constructed as the product of the individual propagators on the different branches (see Chap. 1),

$$\hat{U}_{cyc} = \hat{U}_c \hat{U}_{hc} \hat{U}_h \hat{U}_{ch}. \quad (3.44)$$

The propagators on the *adiabats*,  $\hat{U}_{ch}$  and  $\hat{U}_{hc}$ , and on the *isochores*,  $\hat{U}_c$  and  $\hat{U}_h$ , can be obtained from Eqs. (3.2) and (3.5) respectively. The approach to the limit cycle has similarities to the approach to thermodynamic equilibrium of an initially displaced state. The limit cycle  $\hat{\rho}_{lc}$  is a single nondegenerate invariant state of  $\hat{U}_{cyc}$ ,

$$\hat{U}_{cyc} \hat{\rho}_{lc} = 1 \hat{\rho}_{lc}. \quad (3.45)$$

If  $\hat{\rho}_{lc}$  is found, any initial state will approach monotonically to it by the repeated application of the cycle [38]. The limit cycle can be found for every possible choice of parameters when the working medium consists of spin systems [39], except when no time is allocated on the *isochores*. Then, the evolution is unitary, the modulus of all eigenvalues of  $\hat{U}_{cyc}$  are one, and there is no unique limit cycle [38]. In the case of harmonic oscillators, the modulus of one eigenvalue may be larger than one for

specific values of the parameters. As a consequence, the system is unable to reach the steady state regime [39, 40].

The analysis of the approach to the limit cycle requires a symmetric distance measure, for example Wooter's distance [41]

$$\mathcal{D}(\hat{\rho}, \hat{\rho}_{lc}) = \sqrt{N[1 - \text{Tr}\{\sqrt{\hat{\rho}^{1/2} \hat{\rho}_{lc} \hat{\rho}^{1/2}}\}]}, \quad (3.46)$$

where  $N$  is the size of the Hilbert space. The rate of approach to the limit cycle is determined by the remaining eigenvalues of the propagator, which are smaller than one and proportional to  $\exp\{-\Gamma_c \tau_c - \Gamma_h \tau_h\}$  [38].

The limit cycle can be easily obtained for noninteracting spins with effective *friction*. Let us assume an arbitrary initial polarization  $\mathcal{S}_1^{(0)}$  and fixed  $\omega_c$  and  $\omega_h$ , time allocations, bath temperatures and rate coefficients. Using Eq. (3.25), the polarization after  $n$  cycles is [17]

$$\mathcal{S}_1^{(n)} = (xy)^n \mathcal{S}_1^{(0)} + (b + ax) \sum_{n'=0}^n (xy)^{n'}, \quad (3.47)$$

where  $a = (1 - y)\mathcal{S}_h^{eq} + y\sigma^2/\tau_{ch}$  and  $b = (1 - x)\mathcal{S}_c^{eq} + x\sigma^2/\tau_{hc}$ . In the limit of a large number of applications  $\mathcal{S}_1^{(n \rightarrow \infty)} = \mathcal{S}_1$ , see Eq. (3.27). Therefore, regardless of the initial polarization, the limit cycle is identical to the one described in Fig. 3.2a. Notice the dependence on  $xy = \exp\{-\Gamma_c \tau_c - \Gamma_h \tau_h\}$ .

### 3.7 Concluding Remarks

Quantum thermodynamic cycles, and in particular the quantum Otto cycle, allow for a rigorous dynamical description of the processes in the working medium, and in consequence, supply a fundamental explanation for the empirical finite-time thermodynamics. In this chapter, we have illustrated that for “adiabatic” cycles, in which the density matrix of the working medium remains diagonal in the energy basis, the performance of the quantum cycles closely resembles their macroscopic counterpart. In this regime the cycles can be described by the rate equations for the populations, such as in the framework of stochastic thermodynamics [42, 43]. When the cycle time is shortened, “nonadiabatic” effects may appear, generating coherences and reducing the performance. For *sudden* cycles, corresponding to cycle times shorter than the internal timescale of the working fluid, significant coherence remains in all branches. *Sudden* cycles show additional differences from regular cycles. For example, the branches are interrelated, the limit cycle is reached after a large number of iterations and it strongly depends on the parameters. Besides, a maximum in the cooling rate is found depending on  $J/T_c$  for refrigerator cycles [20]. The performance degrades as the cycle time is further shortened until eventually the device stops working. But a

different picture emerges when very short *sudden* cycles ( $\tau \rightarrow 0$ ) are considered. For example, for refrigerator cycles, finite cooling power is obtained once again [44]. In this case, the “nonadiabatic” work  $W^{na}$  does not necessarily reduces the cycle output and the work extraction mechanism may benefit from the coherences [28, 45]. This effect is one of the subjects of the following Chap. 4. The exciting prospect of the experimental implementation of quantum cycles, for example using ions [46], is discussed in the last part of this volume.

**Acknowledgements** Tova Feldmann thanks Prof. Ronnie Kosloff the collaboration for over twenty years, during which Ronnie taught her new ways of thinking in science. Tova Feldmann also thanks Amikam Levy for many interesting conversations. José P. Palao thanks Ronnie Kosloff, Antonia Ruiz and J. Onam González for useful discussions, and acknowledges financial support by the Spanish MINECO (FIS2013-4132-P, FIS2017-82855-P).

## References

1. E. Geva, R. Kosloff, A quantum-mechanical heat engine operating in finite time. A model consisting of spin-1/2 systems as the working fluid. *J. Chem. Phys.* **96**, 3054 (1992). <https://doi.org/10.1063/1.461951>
2. E. Geva, R. Kosloff, On the classical limit of quantum thermodynamics in finite time. *J. Chem. Phys.* **97**, 4398 (1992). <https://doi.org/10.1063/1.463909>
3. H.T. Quan, Y. Liu, C.P. Sun, F. Nori, Quantum thermodynamic cycles and quantum heat engines. *Phys. Rev. E* **76**, 031105 (2007). <https://doi.org/10.1103/PhysRevE.76.031105>
4. A.E. Allahverdyan, E. Armen, R.S. Johal, G. Mahler, Work extremum principle: structure and function of quantum heat engines. *Phys. Rev. E* **77**, 041118 (2008). <https://doi.org/10.1103/PhysRevE.77.041118>
5. R. Silva, G. Manzano, P. Skrzypczyk, N. Brunner, Performance of autonomous quantum thermal machines: Hilbert space dimension as a thermodynamical resource. *Phys. Rev. E* **94**, 032120 (2016). <https://doi.org/10.1103/PhysRevE.94.032120>
6. M. Esposito, R. Kawai, K. Lindenberg, C. Van den Broeck, Efficiency at maximum power of low-dissipation Carnot engines. *Phys. Rev. Lett.* **105**, 150603 (2010). <https://doi.org/10.1103/PhysRevLett.105.150603>
7. R. Kosloff, T. Feldmann, Discrete four-stroke quantum heat engine exploring the origin of friction. *Phys. Rev. E* **65**, 055102 (2002). <https://doi.org/10.1103/PhysRevE.65.055102>
8. T. Feldmann, R. Kosloff, Quantum four-stroke heat engine: thermodynamic observables in a model with intrinsic friction. *Phys. Rev. E* **68**, 016101 (2003). <https://doi.org/10.1103/PhysRevE.68.016101>
9. Y. Rezek, R. Kosloff, Irreversible performance of a quantum harmonic heat engine. *New J. Phys.* **8**, 83 (2006). <https://doi.org/10.1088/1367-2630/8/5/083>
10. R. Kosloff, Y. Rezek, The quantum harmonic Otto cycle. *Entropy* **19**, 136 (2017). <https://doi.org/10.3390/e19040136>
11. T. Feldmann, R. Kosloff, Performance of discrete heat engines and heat pumps in finite time. *Phys. Rev. E* **61**, 4774 (2000). <https://doi.org/10.1103/PhysRevE.61.4774>
12. J. He, J. Chen, B. Hua, Quantum refrigeration cycles using spin-1/2 systems as working substance. *Phys. Rev. E* **65**, 036145 (2002). <https://doi.org/10.1103/PhysRevE.65.036145>
13. Y. Rezek, P. Salamon, K.H. Hoffmann, R. Kosloff, The quantum refrigerator: the quest for absolute zero. *Europhys. Lett.* **85**, 30008 (2009). <https://doi.org/10.1209/0295-5075/85/30008>
14. T. Feldmann, R. Kosloff, Minimal temperature of quantum refrigerators. *Europhys. Lett.* **89**, 20004 (2010). <https://doi.org/10.1209/0295-5075/89/20004>

15. R. Kosloff, T. Feldmann, Optimal performance of reciprocating demagnetization quantum refrigerators. *Phys. Rev. E* **82**, 011134 (2010). <https://doi.org/10.1103/PhysRevE.82.011134>
16. E. Torrontegui, R. Kosloff, Quest for absolute zero in the presence of external noise. *Phys. Rev. E* **88**, 032103 (2013). <https://doi.org/10.1103/PhysRevE.88.032103>
17. T. Feldmann, E. Geva, R. Kosloff, P. Salomon, Heat engines in finite time governed by master equations. *Am. J. Phys.* **64**, 485 (1996). <https://doi.org/10.1119/1.18197>
18. F. Plastina, A. Alecce, T.J.G. Apollaro, G. Falcone, G. Francica, G. Galve, N. Lo Gullo, R. Zambrini, Irreversible work and inner friction in quantum thermodynamic processes. *Phys. Rev. Lett.* **113**, 260601 (2014). <https://doi.org/10.1103/PhysRevLett.113.260601>
19. X. Chen, A. Ruschhaupt, S. Schmidt, A. del Campo, D. Guéry-Odelin, J.G. Muga, Fast optimal frictionless atom cooling in harmonic traps: shortcut to adiabaticity. *Phys. Rev. Lett.* **104**, 063002 (2010). <https://doi.org/10.1103/PhysRevLett.104.063002>
20. T. Feldmann, R. Kosloff, Short time cycles of purely quantum refrigerators. *Phys. Rev. E* **85**, 051114 (2012). <https://doi.org/10.1103/PhysRevE.85.051114>
21. H. Breuer, F. Petruccione, *The Theory of Open Quantum Systems* (Oxford University Press, New York, 2002). <https://doi.org/10.1093/acprof:oso/9780199213900.001.0001>
22. G. Lindblad, On the generators of quantum dynamical semigroups. *Commun. Math. Phys.* **48**, 119 (1976). <https://doi.org/10.1007/BF01608499>
23. V. Gorini, A. Kossakowski, E. Sudarshan, Completely positive dynamical semigroups of n-level systems. *J. Math. Phys.* **17**, 821 (1976). <https://doi.org/10.1063/1.522979>
24. T. Feldmann, R. Kosloff, Quantum lubrication: suppression of friction in a first-principles four-stroke heat engine. *Phys. Rev. E* **73**, 025107(R) (2006). <https://doi.org/10.1103/PhysRevE.73.025107>
25. T. Baumgratz, M. Cramer, M.B. Plenio, Quantifying coherence. *Phys. Rev. Lett.* **113**, 140401 (2014). <https://doi.org/10.1103/PhysRevLett.113.140401>
26. A. Bartana, R. Kosloff, D. Tannor, Laser cooling of molecular internal degrees of freedom by a series of shaped pulses. *J. Chem. Phys.* **99**, 196 (1993). <https://doi.org/10.1063/1.465797>
27. A. del Campo, J. Goold, M. Paternostro, More bang for your buck: super-adiabatic quantum engines. *Sci. Rep.* **4**, 6208 (2014). <https://doi.org/10.1038/srep06208>
28. R. Uzdin, A. Levy, R. Kosloff, Equivalence of quantum heat machines, and quantum-thermodynamics signatures. *Phys. Rev. X* **5**, 031044 (2015). <https://doi.org/10.1103/PhysRevX.5.031044>
29. R. Uzdin, R. Kosloff, Universal features in the efficiency at maximal work of hot quantum Otto engines. *Europhys. Lett.* **108**, 40001 (2014). <https://doi.org/10.1209/0295-5075/108/40001>
30. I.I. Novikov, Efficiency of an atomic power generating installation. *At. Energy* **3**, 1269 (1957). <https://doi.org/10.1007/BF01507240>
31. F.L. Curzon, B. Ahlborn, Efficiency of a Carnot engine at maximum power output. *Am. J. Phys.* **43**, 22 (1975). <https://doi.org/10.1119/1.10023>
32. C. Van den Broeck, Thermodynamic efficiency at maximum power. *Phys. Rev. Lett.* **95**, 190602 (2005). <https://doi.org/10.1103/PhysRevLett.95.190602>
33. P. Salamon, J.D. Nulton, G. Siragusa, T.R. Andersen, A. Limon, Principles of control thermodynamics. *Energy* **26**, 307 (2001). [https://doi.org/10.1016/S0360-5442\(00\)00059-1](https://doi.org/10.1016/S0360-5442(00)00059-1)
34. P. Salamon, K.H. Hoffmann, Y. Rezek, R. Kosloff, Maximum work in minimum time from a conservative quantum system. *Phys. Chem. Chem. Phys.* **11**, 1027 (2009). <https://doi.org/10.1039/b816102j>
35. J.P. Palao, L.A. Correa, G. Adesso, D. Alonso, Efficiency of inefficient endoreversible thermal machines. *Braz. J. Phys.* **46**, 282 (2016). <https://doi.org/10.1007/s13538-015-0396-x>
36. O. Abah, E. Lutz, Optimal performance of a quantum Otto refrigerator. *Europhys. Lett.* **113**, 60002 (2016). <https://doi.org/10.1209/0295-5075/113/60002>
37. J.M. Gordon, K.C. Ng, H.T. Chua, Optimizing chiller operation based on finite-time thermodynamics: universal modeling and experimental confirmation. *Int. J. Refrig.* **20**, 191 (1997). [https://doi.org/10.1016/S0140-7007\(96\)00074-6](https://doi.org/10.1016/S0140-7007(96)00074-6)
38. T. Feldmann, R. Kosloff, Characteristics of the limit cycle of a reciprocating quantum heat engine. *Phys. Rev. E* **70**, 046110 (2004). <https://doi.org/10.1103/PhysRevE.70.046110>

39. A. Insinga, B. Andresen, P. Salamon, R. Kosloff, Quantum heat engines: limit cycles and exceptional points. *Phys. Rev. E* **97**, 062153 (2018). <https://doi.org/10.1103/PhysRevE.97.062153>
40. A. Insinga, B. Andresen, P. Salamon, Thermodynamical analysis of a quantum heat engine based on harmonic oscillator. *Phys. Rev. E* **94**, 012119 (2016). <https://doi.org/10.1103/PhysRevE.94.012119>
41. M. Hübner, Explicit computation of the Bures distance for density matrices. *Phys. Lett. A* **163**, 239 (1992). [https://doi.org/10.1016/0375-9601\(92\)91004-B](https://doi.org/10.1016/0375-9601(92)91004-B)
42. U. Seifert, Stochastic thermodynamics, fluctuation theorems and molecular machines. *Rep. Prog. Phys.* **75**, 126001 (2012). <https://doi.org/10.1088/0034-4885/75/12/126001>
43. J.O. González, J.P. Palao, D. Alonso, Relation between topology and heat currents in multilevel absorption machines. *New J. Phys.* **19**, 113037 (2017). <https://doi.org/10.1088/1367-2630/aa8647>
44. T. Feldmann, R. Kosloff, Transitions between refrigeration regions in extremely short quantum cycles. *Phys. Rev. E* **93**, 052150 (2016). <https://doi.org/10.1103/PhysRevE.93.052150>
45. R. Uzdin, A. Levy, R. Kosloff, Quantum heat machines equivalence, work extraction beyond Markovianity, and strong coupling via heat exchangers. *Entropy* **18**, 124 (2016). <https://doi.org/10.3390/e18040124>
46. J. Rosnagel, S.T. Dawkins, K.N. Tolazzi, O. Abah, E. Lutz, F. Schmidt-Kaler, K. Singer, A single-atom heat engine. *Science* **352**, 325 (2016). <https://doi.org/10.1126/science.aad6320>

# Chapter 4

## Quantum Features and Signatures of Quantum Thermal Machines



Amikam Levy and David Gelbwaser-Klimovsky

The aim of this book chapter is to indicate how quantum phenomena are affecting the operation of microscopic thermal machines, such as engines and refrigerators. As converting heat to work is one of the fundamental concerns in thermodynamics, the platform of quantum thermal machines sheds light on thermodynamics in the quantum regime. This chapter focuses on the basic features of quantum mechanics, such as energy quantization, the uncertainty principle, quantum coherence and correlations, and their manifestation in microscopic thermal devices. In addition to indicating the peculiar behaviors of thermal-machines due to their non-classical aspects, we present quantum-thermodynamic signatures of these machines. Any violation of the classical thermodynamic bounds observed in the outcome of measurements on these machines is a sufficient condition to conclude that quantum effects are present in the operation of that thermal machine. Experimental setups demonstrating some of these results are also presented.

### 4.1 Introduction

Quantum mechanics is one of the greatest revolutions in the history of science. It changed the way we understand the world and demonstrates that the microscopic

---

A. Levy (✉)

Department of Chemistry, University of California Berkeley, Berkeley, CA 94720, USA  
e-mail: amikamlevy@gmail.com

A. Levy

The Sackler Center for Computational Molecular Science, Tel Aviv University,  
69978 Tel Aviv, Israel

D. Gelbwaser-Klimovsky

Department of Chemistry and Chemical Biology, Harvard University, Cambridge,  
MA 02138, USA  
e-mail: dgelbi@yahoo.com.mx

realm is governed by a theory that is fundamentally different from classical mechanics. Classical mechanics is formulated on the phase-space and treats particles as points whereas quantum mechanics is described by wave functions and operators acting in Hilbert space. In the quantum framework, the classical perception of certainty is replaced by probability, and instead of being continuous, physical quantities are generally quantized. These significant differences result in peculiar phenomena that are observed only in the quantum regime.

Since the beginning, the development of quantum mechanics has been influenced by thermodynamics. Planck initiated the quantum era by introducing the quantization hypothesis to describe thermal radiation emitted from a black body; Einstein discovered stimulated emission while studying thermal equilibration between light and matter. In spite of the close historical relationship between quantum mechanics and thermodynamics, one could wonder if the quantum revolution would eventually shake the foundations of thermodynamics as it did with classical mechanics. Some of the early works in this direction studied the behavior of heat machines, which, besides their technological applications, were used to test the compliance with the laws of thermodynamics. Despite the effort focused on this direction, as of today, the fundamental laws and bounds of thermodynamics hold also in the quantum regime.

Even though quantum mechanics complies with the laws of thermodynamics, classical and quantum heat machines still differ in a non trivial way. As we show in this chapter, not only are classical and quantum heat machines fundamentally different, but quantum mechanics allows the realization of classically inconceivable heat machines.

In order to identify the appearance and effects of quantum features in thermal machines, one should first have a clear notion of classical thermal machines. Throughout this chapter, we will use different notions or levels of classicality, starting from the purest definitions, (i.e., a system is classical only if it is precisely described by classical mechanics), and working toward less strict definitions, which consider systems governed by quantum Hamiltonians as classical as long as either their coherences or quantum correlations are zero. In this manner we obtain a thorough understanding of how different quantum features influence thermal devices.

The chapter is divided into three sections concerning three main quantum features and their corresponding thermodynamic signatures. In the first section, classicality will be considered as it is in classical thermodynamics, where the probability distribution is fully described by a phase-space distribution without any constraint aside from normalization. In this section, quantum effects result only from the quantization of energy levels and the uncertainty principle, which set some limitations on the probability distributions. These features alone lead to discrepancies in the behavior of classical and quantum heat machines.

The second section describes the effects of quantum coherence in thermal machines. Both the positive and negative implications of coherence are discussed. Furthermore, we present a recent experiment demonstrating some of these results. In these scenarios thermal machines that are governed by a quantum Hamiltonian, but can be fully described by their populations are considered classical (stochastic). In this context it's also important to note that the preferred basis to describe thermal

machine is the one in which measurements are preformed, typically, this will be the energy basis.

In the last section, we discuss the role of correlations in the operation of thermal machines. We demonstrate that quantum correlations can induce anomalous heat flow from a colder body to a hotter body, that can not be explained classically. Here, classicality refers to separable quantum states with zero discord, (i.e., only classical correlations are allowed). The chapter is structured so that each of the three main section are independent of the others.

## 4.2 Energy Quantization and Uncertainty Principle

Classical and quantum mechanics provide different descriptions of the same physical system. This is true even for the simplest cases. As an example, consider a harmonic oscillator with mass  $m$  and frequency  $\omega$ , in a thermal state at temperature  $T$ . Classically, its phase-space distribution is given by the following Gaussian:

$$P_{HO}^{clas}(x, p) = \frac{\omega}{2\pi k_B T} e^{-\left(\frac{m\omega^2 x^2}{2k_B T} + \frac{p^2}{2mk_B T}\right)}. \quad (4.1)$$

Strictly speaking, phase-space distributions are not part of the quantum mechanical framework, as it is impossible to simultaneously determine the position and momentum of a system. Nevertheless, quasi-probability distributions, such as the Wigner function, share many properties with phase-space distributions [1, 2] and are considered the “closest quantum equivalent” to a phase-space distribution. The Wigner function for the same harmonic oscillator at the same state is

$$P_{HO}^{quan}(x, p) = \frac{\tanh[\frac{\hbar\omega}{2k_B T}]}{\hbar\pi} e^{-\tanh[\frac{\hbar\omega}{2k_B T}]\left(\frac{m\omega x^2}{\hbar} + \frac{p^2}{\hbar m\omega}\right)}. \quad (4.2)$$

These two distributions coincide at the regime where the thermal energy is much larger than the quantization energy, i.e.,  $\frac{\hbar\omega}{k_B T} \ll 1$ . In this limit, the classical description is very precise, so quantum effects can be neglected. Nevertheless, the distributions diverge at low temperatures (see Fig. 4.1), where classical mechanics predicts a smaller and smaller position and momentum uncertainties, in contradiction with the uncertainty principle. In contrast, the Wigner distribution, Eq. (4.2), obeys the uncertainty principle at any temperature.

This is the main difference between quantum and classical distributions [2]. Moreover, confining potentials impose boundary conditions that quantize the energy state, create a zero point energy, and establish a dependence of the system energy on the boundary conditions. The combination of all these effects results on different energy, heat capacity and other thermal properties [3] relative to the ones predicted by classical mechanics and thermodynamics that neglect boundary effects [4]. In this section of the chapter we will explore how those differences affect the performance of thermal

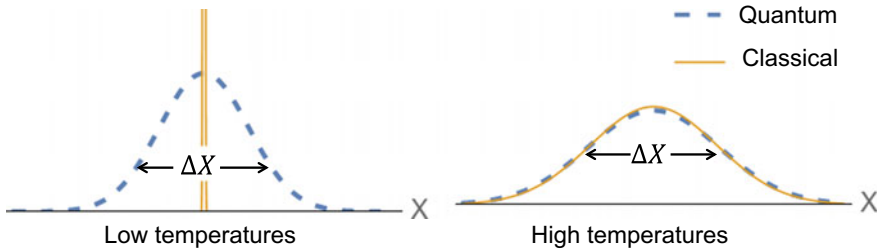


**Fig. 4.1** Position projection of the classical (yellow continuous line) and quantum (blue dashed line) phase-space distributions for a harmonic oscillator in a thermal state. Both distributions coincide at high temperatures (right), but at low temperatures (left) the quantum Wigner distribution, in contrast with the classical one, has to comply with the uncertainty principle, forcing the distributions to diverge.

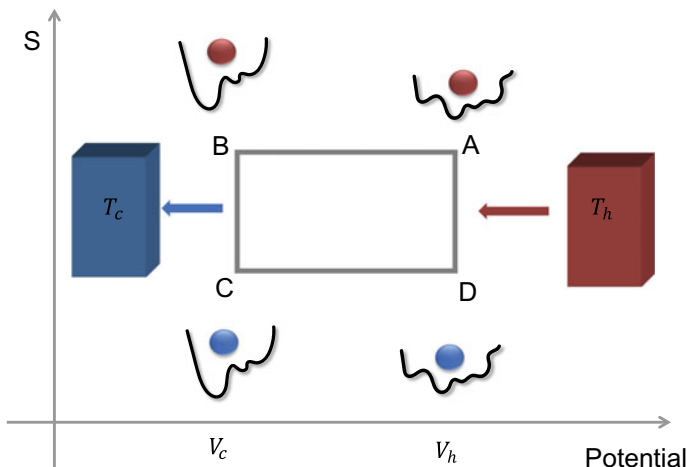


**Fig. 4.2** Otto cycle. The x-axis represents a parameter that controls the working medium potential and the y-axis represents its Von Neumann entropy.

heat machines. We will compare exactly the same heat machine, i.e., same working medium, same baths, same temperatures, etc., where in one case the behavior of the working medium is dictated by classical mechanics and in the other by quantum mechanics. In this section we do not consider the effects of quantum coherences or quantum correlations. These are left for subsequent sections of this chapter.

In particular, we consider an Otto heat machine [5–7] operating with a M-dimensional working medium, but a similar analysis can be done for other cycles. The Otto cycle is composed of the following four strokes (see Fig. 4.2): At point A of the cycle the working medium potential is  $V_h(x_1, \dots, x_M) \equiv V_h$ . Its Hamiltonian is  $H_h$  and its energy levels are  $\{E_n^h\}$ . The working medium is in thermal equilibrium with a hot bath at temperature  $T_h$ , so its state in the Hamiltonian energy basis is

$\rho_A = Z_{T_h}^{-1} \sum_n e^{-\frac{E_n^h}{k_B T_h}} |n\rangle \langle n|$ , where  $Z_{T_h}$  is the partition function. At A, the adiabatic stroke starts: the working medium is decoupled from the hot bath and the potential is slowly deformed until point B, where it reaches  $V_c(x_1, \dots, x_M) \equiv V_c$ . Here, the Hamiltonian is  $H_c$ , and its energy levels are  $\{E_n^c\}$ . The deformation is slow enough for the process to fulfill the assumptions of the quantum adiabatic theorem [8], so the levels populations are the same  $\rho_B = \rho_A$ . At B, the system is coupled to the cold thermal bath at temperature  $T_c$ , initiating the cold isochoric stage. The system relaxes, achieving thermal equilibrium at C, i.e.,  $\rho_C = Z_{T_c}^{-1} \sum_n e^{-\frac{E_n^c}{k_B T_c}} |n\rangle \langle n|$ , where  $Z_{T_c}$  is the partition function. Then, the working medium undergoes the second adiabatic stroke: it is decoupled from the bath and the potential is again slowly transformed back, reaching  $V_h$  at D. Here too, we apply the quantum adiabatic theorem so  $\rho_D = \rho_C$ . Finally, at this point, the second isochoric phase starts: the working medium is coupled again to the hot bath and equilibrates with it, returning to point A.

One useful feature of the Otto cycle is that work and heat are exchanged during different parts of the cycle: work is transferred during the adiabatic processes and heat over the isochoric strokes. The heat flow from the hot bath is

$$Q_h = \langle H_h \rangle_A - \langle H_h \rangle_D = \sum_n E_n^h \left( \frac{e^{-\frac{E_n^h}{k_B T_h}}}{Z_{T_h}} - \frac{e^{-\frac{E_n^h}{k_B T_c}}}{Z_{T_c}} \right) \quad (4.3)$$

and from the cold bath is

$$Q_c = \langle H_c \rangle_C - \langle H_c \rangle_B = \sum_n E_n^c \left( \frac{e^{-\frac{E_n^c}{k_B T_c}}}{Z_{T_c}} - \frac{e^{-\frac{E_n^c}{k_B T_h}}}{Z_{T_h}} \right). \quad (4.4)$$

Using the first law of thermodynamics, the expression for the work can be obtained,

$$W = -Q_h - Q_c = (E_n^c - E_n^h) \left( \frac{e^{-\frac{E_n^h}{k_B T_h}}}{Z_{T_h}} - \frac{e^{-\frac{E_n^c}{k_B T_c}}}{Z_{T_c}} \right). \quad (4.5)$$

Here, we use the sign convention that energy flowing to the working medium is positive and flowing from the working medium is negative. The heat machine has several operating modes: for  $W < 0$  and  $Q_h > 0$ , it is a heat engine and its thermal efficiency quantifies the amount of work extracted per unit of incoming heat, i.e.,  $\eta = \frac{-W}{Q_h}$ ; for  $W > 0$  and  $Q_c > 0$ , it is a refrigerator and its efficiency or coefficient of performance measures how much energy flows from the cold bath per unit of invested work  $COP = \frac{Q_c}{W}$ .

For a classical Otto heat machine, whose working medium is an ideal gas, the operation mode is determined by the compression ratio  $r = \frac{Vol_c}{Vol_h}$ , ( $Vol_c$  is the container volume at point C and  $Vol_h$  is the container volume at point A): for

$r > r_{Car} = \left(\frac{T_h}{T_c}\right)^{\frac{1}{\gamma-1}}$ , it operates as a refrigerator and for  $1 < r < r_{Car}$  the classical Otto heat machine operates as an engine with an efficiency

$$\eta = 1 - \frac{1}{r^{\gamma-1}} \leq 1 - \frac{1}{r_{Car}^{\gamma-1}} = \eta_{Car}, \quad (4.6)$$

where  $\eta_{Car}$  is the Carnot efficiency for an engine and  $\gamma = \frac{C_p}{C_v}$  is the ratio of heat capacities. An important property of the classical Otto machine is that, in order to extract work or extract heat from the cold bath, the working medium has to be compressible [4, 9–12]. Otherwise,  $r = 1$  and  $\eta = 0$ , precluding work extraction. This compression ratio is smaller than  $r_{Car}$ , hindering also the refrigerator operation. Here, quantum mechanics provides heat machines with an advantage over their classical counterparts. As it was shown on [5] and we explain below, once the working medium is governed by quantum laws instead of classical mechanics, compressibility is no longer required for work extraction or for cooling down the cold bath. Quantum mechanics allows the realization of heat machines with incompressible working media, opening the possibility for creating classically inconceivable heat machines.

One feature of a classical ideal gas undergoing an Otto cycle is that it is always at equilibrium, so at every point of the cycle it is possible to define the ideal gas temperature. This is not always true for a quantum working medium. For example, at  $B$ , the working medium is at the state  $\rho_B = Z_{T_h}^{-1} \sum_n e^{-\frac{E_n^h}{k_B T_h}} |n\rangle\langle n|$ , which is a Boltzmann distribution of the energy levels at point  $A$  ( $\{E_n^h\}$ ) instead of point  $B$  ( $\{E_n^c\}$ ). So, in general, the state  $\rho_B$  is not a thermal equilibrium state with respect to the Hamiltonian at point  $B$ . The only exception is if the transformation homogeneously scales the energy levels i.e.,  $E_n^c = q E_n^h$ , where  $q$  is independent of  $n$ . Under this condition we can rewrite the state at  $B$  as  $\rho_B = Z_{q T_h}^{-1} \sum_n e^{-\frac{E_n^c}{k_B q T_h}} |n\rangle\langle n|$ , which is a Boltzmann distribution at temperature  $q T_h$  of the energy levels at point  $B$ . In a similar way, the state at  $D$ ,  $\rho_D = Z_{T_c}^{-1} \sum_n e^{-\frac{E_n^c}{k_B T_c}} |n\rangle\langle n| = Z_{T_c/q}^{-1} \sum_n e^{-\frac{q E_n^h}{k_B T_c}} |n\rangle\langle n|$  is a Boltzmann distribution at temperature  $T_c/q$  of the energy levels at point  $D$ . Most of the research on quantum Otto cycles has focused on this type of transformations [6, 7] which includes the length change of a 1D infinite well [13], frequency shift of a 1D harmonic oscillator [14] or any other scale invariant transformation [15]. We will first study the differences between classical and quantum heat machines undergoing homogeneously energy scaling, which allows the working medium to be in a thermal state during the whole cycle. Then, we will explore the regime of inhomogeneous energy scaling, which has been seldom studied, with few exceptions [16, 17]. For an inhomogeneous energy scaling, the working medium deviates from a thermal state during the adiabatic strokes, resulting on more striking discrepancies between the operation of classical and quantum heat machines, and providing the later with more noteworthy advantages.

### 4.2.1 Homogeneous Energy Scaling: Work and Heat Corrections

In the case of the homogeneous energy scaling, the working medium is in a thermal state during the whole cycle. So we can use Wigner's original computation to calculate the quantum corrections to the performance of a heat machine. In 1932, Wigner calculated the quantum corrections to the quasiprobability distribution of an  $M$ -dimensional system in a potential  $V$  at thermal equilibrium at temperature  $T$  [2]. After integrating the momentum, the unnormalized position distribution is given by a series expansion on  $\hbar$ :

$$\int \dots \int dp_1 \dots dp_M P^{quan}(x_1, \dots, x_n; p_1, \dots, p_M) = P^{clas} + \hbar^2 P_2^{quan} + \hbar^4 P_4^{quan} + O(\hbar^6), \quad (4.7)$$

where

$$P^{clas} = e^{-\frac{V}{k_B T}} \quad (4.8)$$

is the classical phase-space distribution and  $P_{2n}^{quan}$  are quantum corrections that depend on the potential and its derivatives but not on  $\hbar$ . For example, the first quantum correction is

$$P_2^{quan} = e^{-\frac{V}{k_B T}} \left[ -\frac{1}{12(k_B T)^2} \sum_k \frac{1}{m_k} \frac{\partial^2 V}{\partial x_k^2} + \frac{1}{24(k_B T)^3} \sum_k \frac{1}{m_k} \left( \frac{\partial V}{\partial x_k} \right)^2 \right]. \quad (4.9)$$

At high temperatures, the Wigner function tends to the classical phase space distribution, i.e.,  $\int \dots \int dp_1 \dots dp_M P^{quan}(x_1, \dots, x_n; p_1, \dots, p_M) \approx e^{-\frac{V}{k_B T}}$ . But as the temperature decreases, quantum corrections need to be included to prevent the violation of the uncertainty principle. These corrections change the expectation value of the energy,

$$\langle H \rangle_T = E_{clas}(V, T) + \hbar^2 E_{2,QC}(V, T) + O(\hbar^4), \quad (4.10)$$

where  $E_{clas}(V, T)$  corresponds to the system energy predicted by classical mechanics and  $E_{2,QC}(V, T)$  is the first quantum correction

$$E_{2,QC}(V, T) = \frac{1}{\int P^{clas}} \left[ \frac{1}{24k_B T} \int \sum_k \frac{1}{m_k} \frac{\partial^2 V}{\partial x_k^2} P^{clas} + \int V \times P_2^{quan} - \frac{\int V \times P^{clas} \int P_2^{quan}}{\int P^{clas}} \right], \quad (4.11)$$

where all the integrals are over all the positions,  $x_1, \dots, x_M$ . The quantum corrections to the energy affect the output of a heat machine. For example, the heat exchanged with the hot bath, including quantum corrections of the order  $\hbar^2$  is

$$Q_h = Q_h^{clas} + \hbar^2 (E_{2,QC}(V_h, T_h) - E_{2,QC}(V_h, T_c/q)) + O(\hbar^4), \quad (4.12)$$

where  $Q_h^{clas}$  corresponds to the heat that a classical working medium would exchange with the hot bath during the Otto cycle, and the other terms are corrections that have to be included for a quantum working medium. In the same way, we can calculate the exchanged work,

$$W = W^{clas} - \hbar^2 (E_{2,QC}(V_h, T_h) - E_{2,QC}(V_h, T_c/q) + E_{2,QC}(V_c, T_c) - E_{2,QC}(V_c, qT_h)) + O(\hbar^4), \quad (4.13)$$

where  $W^{clas}$  corresponds to the work exchange by a classical Otto engine and the rest are the quantum corrections. As we explain later (see Eq. (4.17)), in order to extract work, i.e.,  $W < 0$ , the scaling factor of the energy levels has to comply with the following inequality:  $\frac{T_c}{T_h} < q < 1$ .

For 1D systems in an Otto cycle with potentials  $V_c = a_c x^{2n}$  and  $V_h = a_h x^{2n}$ , the scaling factor between energy levels is  $q = \left(\frac{a_c}{a_h}\right)^{\frac{1}{1+2n}}$  [7] and the correction of order  $\hbar^2$  to the exchanged work can be analytically calculated. It is equal to

$$-\frac{\hbar^2 \pi (2n^2 + n - 1) \csc[\frac{\pi}{2n}]}{12m(\Gamma[\frac{1}{2n}])^2} \left( \frac{a_c}{k_B T_c} \right)^{\frac{1}{n}} \left( 1 - \frac{1}{q} \right) \left( 1 - \left( \frac{T_c}{q T_h} \right)^{\frac{1}{n}} \right), \quad (4.14)$$

where  $\Gamma$  is the gamma function. The correction can be positive or negative, but in the regime of work extraction,  $W < 0$ , it is always positive, i.e., it always reduces the work extraction.

The first quantum correction starts being relevant when the operation temperatures are not so high and any of the Wigner functions during the cycle deviate from the classical phase-space distribution. As temperatures decrease even more, higher order corrections should be considered. At least for 1D systems, there are recursive formulas that could be used to calculate any  $P_{2n}^{quan}$  [18], from which the full quantum corrections to the work and heat could be calculated. Nevertheless, this is not a practical approach and we will now introduce a simpler strategy that is exact at any temperature.

Using the fact that the energy levels are homogeneously scaled,  $E_n^h = q E_n^h$ , the expressions for the exchanged heat and work, Eqs. (4.3)–(4.5), can be rewritten. Consider for example  $Q_h$  (Eq. (4.3)). Using the relation between the energy levels this equation becomes

$$\begin{aligned} Q_h &= \sum_n E_n^h \left( \frac{e^{-\frac{E_n^h}{k_B T_h}}}{Z_{T_h}} - \frac{e^{-\frac{q E_n^h}{k_B T_c}}}{Z_{T_c/q}} \right) \\ &= \int_{T_c/q}^{T_h} \frac{d}{dT} \left( \sum_n E_n^h \frac{e^{-\frac{E_n^h}{k_B T}}}{Z_T} \right) dT = \int_{T_c/q}^{T_h} \frac{d\langle H_h \rangle_T}{dT} dT = \int_{T_c/q}^{T_h} C_v dT, \end{aligned} \quad (4.15)$$

where we have used the fundamental theorem of calculus and  $C_v$  is the heat capacity of a thermal state at temperature  $T$  with Hamiltonian  $H_h$ . In the same way, we can rewrite the equations for  $Q_c$  and  $W$  as:

$$Q_c = -q \int_{T_c/q}^{T_h} C_v dT, \quad (4.16)$$

$$W = (q - 1) \int_{T_c/q}^{T_h} C_v dT. \quad (4.17)$$

Because the heat capacity is always positive, work is extracted only if  $\frac{T_c}{T_h} < q < 1$ . We leave the readers to prove this as an exercise. All the information about the nature of the working medium is contained only on the heat capacity,  $C_v$ . If the working medium is a classical system, classical mechanics should be used to compute  $C_v$ . If the working medium is a quantum system, quantum mechanics should be used instead. Consider for example a working medium composed of  $N$  independent harmonic oscillators at thermal equilibrium at temperature  $T$ . A classical description, based on the equipartition theorem, assigns a contribution of  $\frac{k_B}{2}$  for each quadratic degree of freedom of the Hamiltonian. There are two quadratic degrees of freedom for each harmonic oscillator,  $x$  and  $p$ . Therefore, classically  $C_v^{HO,clas} = Nk_B$  at any  $T$ . In contrast, if we use quantum mechanics for calculating the heat capacity, we will get  $C_v^{HO,quan} = Nk_B \left( \frac{\hbar\omega}{2k_B T} \operatorname{csch} \left[ \frac{\hbar\omega}{2k_B T} \right] \right)^2$ , which is temperature dependent (see Fig. 4.3-left). Because,  $C_v^{HO,quan} \leq C_v^{HO,clas}$ , the heat and work exchanged by a heat machine made of a quantum harmonic oscillator working medium is always less than its classical counterpart, turning the classical heat machine into a better choice if we want to increase the heat or work exchange.

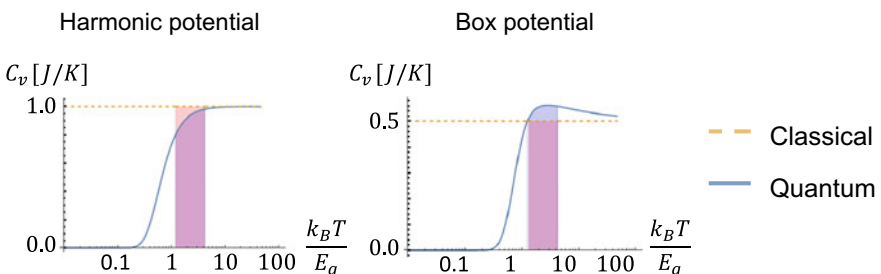


**Fig. 4.3** Classical (yellow dashed line) and quantum (blue continuous line) heat capacities as function of the temperature normalized by the working medium ground state energy. The area below the curves, enclosed by the temperatures  $T_c/q$  and  $T_h$ , is proportional to the work and heat exchange by a classical or a quantum heat machine. For 1D harmonic oscillator potentials (left), the classical heat machine has a larger output than its quantum counterpart (see red area above the quantum curve). In contrast, for a particle in a 1D box (right), the output of the quantum heat machine is larger (see blue area above the classical curve).

Nevertheless, the advantage of the classical heat machine is not a general feature and depends on the type of working medium, which is determined by the potentials, and the temperature range. As an example consider a working medium composed of particles of mass  $m$  in a one dimensional box of length  $L$ . The quantum heat capacity is larger than its classical counterpart at not so low temperatures, i.e.,  $k_B T \gtrsim \frac{\hbar^2 \pi^2}{2mL^2}$  (see Fig. 4.3-right). Thus, for a one dimensional box potential, a quantum heat machine may have a larger output than its classical counterpart, i.e., extracts more work and exchanges more heat with the thermal baths. Which are the required features for a potential in order to boost the heat machine output and how they relate with other quantum effects, such as the Wigner function negativity, are still open questions that should be further investigated.

Up to this point we have talked about the work and heat exchange. But what about the thermal efficiencies, such as the engine efficiency or the coefficient of performance of a refrigerator? Because these quantities are rates of the exchanged work and the heat from one of the baths,

$$\eta = -\frac{W}{Q_h} = 1 - q; \quad COP = \frac{Q_c}{W} = \frac{q}{1 - q}, \quad (4.18)$$

they do not depend on the heat capacity, and therefore they do not depend on the quantum or classical nature of the working medium. Thus,  $\eta^{quan} = \eta^{clas}$  and  $COP^{quan} = COP^{clas}$ . The efficiencies only depend on the potential deformation, which is characterized by the energy levels scaling factor,  $q$ .

#### 4.2.2 Inhomogeneous Energy Scaling and the Efficiency Divergence

Could the efficiency of a quantum heat machine be greater than or at least different from its classical counterpart? Do quantum heat machines have any fundamental advantage over their classical counterparts? The answer to both questions is yes, but the potential transformation should be such that the energy levels are not homogeneously scaled, i.e.,  $E_n^c \neq q E_n^h$ . As we show below, not only the performance is different, but energy quantization enables the realization of classically inconceivable heat machines, such as those operating with an incompressible working medium [5].

We exemplify these effects in a particular 2D example, but a similar analysis can be done for higher dimensions, such as 3D, or other potentials [5]. Here, we consider a working medium contained in a two dimensional box. At points  $D$  and  $A$  of the cycle, the dimensions of the box are  $L_x^h$  and  $L_y^h$ . At points  $B$  and  $C$ , they are  $L_x^c$  and  $L_y^c$ . If the working medium is incompressible, the box transformations during the adiabatic strokes have to keep the area constant: if the length along  $x$  is increased by a factor  $j$ ,  $L_x^c = j L_x^h$ , then the size along  $y$  has to be scaled by a factor  $\frac{1}{j}$ ,  $L_y^c = \frac{1}{j} L_y^h$ . These transformations correspond to the red lines on the plots on Fig. 4.4.

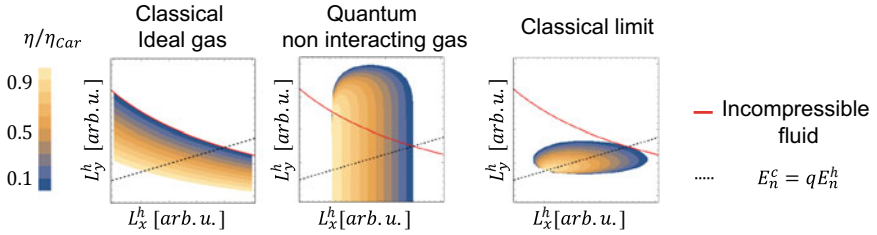


**Fig. 4.4** Heat engine efficiency for a 2D potential box normalized by the Carnot efficiency. At point  $B$  and  $C$  of the cycle, the box lengths are such that  $L_y^c/L_x^c = 0.25$  and the temperature ratio is  $T_h/T_c = 2$ . The plots show the results for different values of the box lengths at points  $D$  and  $A$  of the cycle, i.e.,  $L_x^h$  and  $L_y^h$ . An incompressible working medium can only undergo area preserving transformations, here indicated by the red line. For these transformations there is no work extraction for a classical working medium, independently if it is an ideal gas (left) or the classical limit  $\hbar \rightarrow 0$  (right) of a quantum particle in a box. In contrast, a quantum working medium (center) can be highly efficient,  $\eta/\eta_{Car} > 0.9$ , even for area preserving transformations. The dashed black line indicates transformations where the energy levels are homogeneously scaled and the quantum and classical efficiency coincide.

During the adiabatic strokes, the adiabatic invariants have to be constant. The adiabatic invariant for a classical particle of mass  $m$  and energy  $E$  in a two dimensional box of area  $A$  is [19]

$$\mu = 2\pi m EA, \quad (4.19)$$

which implies that during the adiabatic transformation  $mEA$  is constant. So, for a constant area adiabatic transformation, the energy of the classical working medium does not change, precluding the work extraction. This is true for any classical non-interacting system, from an ideal gas to a single particle. Furthermore, the lack of work extraction is confirmed by taking the classical limit ( $\hbar \rightarrow 0$ ) of the quantum calculation for the work, (see Eq. (4.5) and Fig. 4.4-center).

For a quantum working medium, one has to consider the energy levels, which are given by

$$E_{n_x, n_y}^i = \frac{\hbar^2 \pi^2}{2m} \left( \left( \frac{n_x}{L_x^i} \right)^2 + \left( \frac{n_y}{L_y^i} \right)^2 \right), \quad (4.20)$$

where  $n_x$  and  $n_y$  are integers, and  $i = \{h, c\}$ . For the constant area transformations, as long as  $j \neq 1$ , the energy levels scaling is inhomogeneous and the classical and quantum efficiencies differ. Moreover, Eq. (4.19) is not an adiabatic invariant at the quantum regime, where constant level populations is enough to warrant adiabaticity. As stated by the quantum adiabatic theorem, adiabaticity is achieved by performing the transformation slowly enough. This can be realized for constant area deformations that change the energy of the working medium. For simplicity, here we are assuming that the quantum working medium is composed of distinguishable particles.

In contrast to the classical heat machine, a quantum heat machine can be highly efficient, i.e., operate close to the Carnot limit, even for constant area transformations (see red line on Fig. 4.4-center). This opens the possibility of creating heat machines using incompressible working media, which classically would be impossible. Despite the increase in efficiency, quantum heat machines are always limited by the Carnot bound and fully comply with the second law of thermodynamics.

The quantum model of a particle in a two dimensional box is not the exact counterpart of a classical ideal gas heat machine. For an ideal gas, changes on one of the directions affect the other, redistributing the energy. In contrast, our quantum model is composed of two independent degrees of freedom that do not interact between themselves. Its classical limit,  $\hbar \rightarrow 0$ , corresponds to a different performance than the ideal gas heat machine (see Fig. 4.4 right and left, respectively). In any case, for a classical working medium contained in a two dimensional box, either an ideal gas or one composed of two independent degrees of freedom, classical adiabatic invariants forbid the work extraction for constant area transformations. This differs from the quantum case where quantum adiabatic invariants still allow work extraction. Further extension of this work should confirm if, for constant area transformations, work can be extracted using a “quantum ideal gas”. The gas Hamiltonian should include non-trivial interactions among its degrees of freedom, i.e., non-linear couplings, in order to avoid the formation of normal modes and to achieve full thermalization. Further works should also consider the effects of different quantum statistics, such as Fermi–Dirac or Bose–Einstein statistics.

In summary, in this section we have analyzed the differences between heat machines with a working medium governed either by classical or quantum mechanics. The difference in their operation is determined by the type of Hamiltonian transformation: if the energy levels are homogeneously scaled, the work and heat exchange may diverge, but the efficiencies are the same. In contrast, for inhomogeneous energy level scaling, the efficiencies also diverge, allowing the extraction of work with incompressible working fluids and opening for the realization of classically impossible heat machines. Future research should focus on finding other fundamental differences between the operation of classical and quantum heat machines. In this section, we have not studied quantum coherences or correlations. All the quantum effects that have been considered are the basic ones of a confined system: energy quantization and the uncertainty principle. Nevertheless, as we showed, this is enough for heat machines to have fundamentally different performances.

### 4.3 Coherence and Small Action Regime

Quantum coherence is one of the underlying principles of quantum mechanics that allows us to distinguish between classical and quantum phenomena. Historically, quantum coherence clarified the basic aspect of wave-particle duality in physical objects. Nowadays, scientists are trying to reveal the role of quantum coherence in biological, chemical, and physical systems and learn how to exploit it as a resource [20, 21].

In recent years, the role of coherence in quantum thermodynamics has been studied extensively. One fundamental question is how, if at all, quantum coherence can be extracted as thermodynamic work [22–28]. The role of coherence in the operation of quantum thermal machines is another area of investigation. For example, it has been shown that noise-induced coherence can break detailed balance and enable the removal of additional power from a laser or a photocell heat engine [29]. It has also been shown that coherence enhances heat flow between a quantum engine and the thermal bath, implying that coherence plays an important role in the operation of quantum refrigerators [30–33]. Engines subject to coherent and squeezed thermal baths have also been studied [34–36]. While such engines can exceed the Carnot efficiency or even extract work from a single bath [37, 38], they do not break the second-law of thermodynamics as useful work is hidden in the bath [39]. In this context, it is important to note, that the Carnot bound is a relevant reference point only when thermal bath are considered.

However, the existence of coherence in quantum thermal machines is not always beneficial for their operation. In [40] it was shown that for slow driving in the linear response of a Stirling-type engine coherence leads to power loss. This detraction in the performance of the engine is related to the phenomenon of quantum friction [41–44] (see also Chap. 3). In this section we will discuss both positive and negative implications of coherence. In particular, we will present a study by Uzdin et al. [45, 46] that reveals the thermodynamic equivalence of different types of engines in the small action regime. In this regime it has further been shown that coherence enhances power extraction. We further present a recent experiment [47] that demonstrate these two findings. At the end of this section we will discuss the origin of quantum friction which degrades the performance of thermal machines.

### 4.3.1 Heat Machines Types and the Mathematical Description

#### 4.3.1.1 Heat Machine Types

In this section, we will consider the three most common types of heat engines: the continuous engine, the two-stroke engine, and the four-stroke engine (see Fig. 4.5). The elementary components for assembling a quantum heat engine are two heat baths at different temperatures,  $T_h$  and  $T_c$ , where the subscripts  $h(c)$  correspond to hot(cold), such that  $T_h > T_c$ , a work source, which is used for consuming/extracting energy in/out of the engine, and as the working medium, a quantum system, that couples the different components of the engine.

As was discussed in the previous chapters and in Refs. [48–52], the working medium can be described by different types of quantum systems. Here, we treat the working medium as a three-level system. The three-level setup was first studied by Scovil and Schulz-DuBois [53] and is considered the pioneering work in the field. This model was later studied by Kosloff et al. [48, 54, 55] who employed a quantum

dynamical description, which reveals the significance of quantum effects in the study of thermodynamics of microscopic heat engines. Besides being an elementary model, the three-level engine has demonstrated quantum signatures in a nitrogen-vacancy centers experimental setup [47]. This will be discussed in more detail in Sect. 4.3.4. In Fig. 4.5 the three types of quantum heat engines that are comprised of three-level systems are described schematically. The Hamiltonian of the system, including the driving Hamiltonian, takes the form  $H(t) = H_o + H_w(t)$  with

$$\begin{aligned} H_o &= \hbar\omega|2\rangle\langle 2| + \hbar\omega_h|3\rangle\langle 3|, \\ H_w &= \epsilon(t)\exp(i\omega t)|1\rangle\langle 2| + \text{H.c..} \end{aligned} \quad (4.21)$$

Here,  $H_o$  is the bare Hamiltonian, where the energy of level one is assumed to be zero. The system is periodically driven with the frequency  $\omega = \omega_h - \omega_c$  which is in resonance with the transition frequency between the first and second levels. The driving Hamiltonian,  $H_w(t)$ , is expressed after performing the rotating wave approximation (assuming  $\epsilon \ll \omega$ ), and H.c. stands for the Hermitian conjugate. The interaction with the bath will be described explicitly below for both the Markovian and non-Markovian regimes.

*Continuous engines* are machines in which all components of the engine are simultaneously coupled through the working medium [48, 56–58], attaining a steady-state operation. The hot bath couples the first and third levels while the cold bath couples the second and third levels. The coupling to the heat baths generates a population inversion between the first and second levels, which is used to extract work by amplifying a driving field connecting the two levels. In the weak driving limit, the condition for population inversion can be simplified to  $\frac{T_h}{T_c} > \frac{\omega_h}{\omega_c} > 1$ . The device can operate as a refrigerator by simply changing the direction of the inequality  $\frac{T_h}{T_c} < \frac{\omega_h}{\omega_c}$  [59]. We remark that population inversion is not the only mechanism to gain power from a quantum heat engine. In Ref. [60] electromagnetically induced transparency mechanism was suggested to obtain bright narrow emission light without population inversion, and this was later demonstrated experimentally [61] with cold Rb atoms.

*Two-stroke engines* operate in a two stage mode [6, 62]. In the first stroke, the quantum system is coupled to both the cold and hot baths, whereas in the second stroke, after the system is decoupled from the heat baths, work is extracted from the quantum system via a coupling to an external field. In the example of the three level system, at the end of the first stroke population inversion between the first and second levels is created, and in the second stroke this population inversion is exploited to extract useful work from the engine (see Fig. 4.5).

*Four-stroke engines* are perhaps the most familiar types of engines, as they include the Otto and Carnot engines. The Otto cycle, which was already introduced in Sect. 4.2 is comprised of four strokes, two isochores and two adiabats [14, 41, 63]. In Fig. 4.5, we describe the quantum analogue of the four-stroke Otto engine. In the first stroke, levels one and three are coupled to the hot bath, and heat flows into the working medium. In the second stroke, work is invested without any transfer of heat,

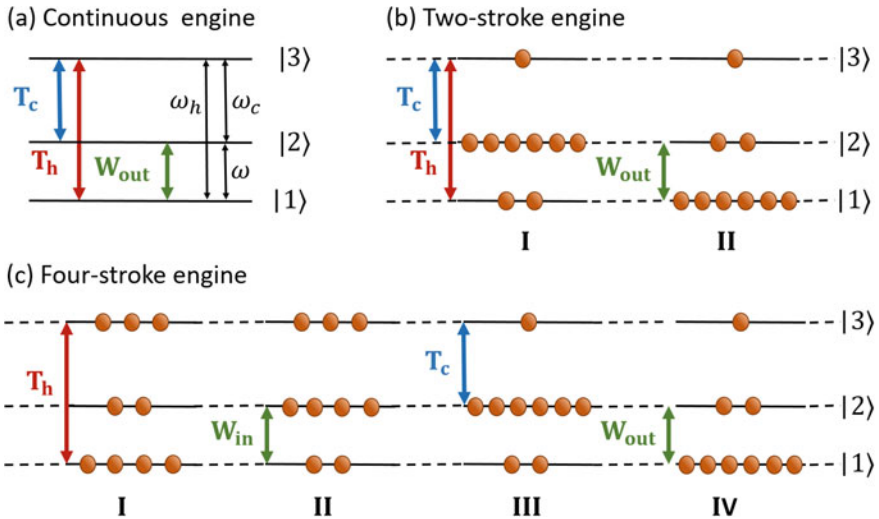


**Fig. 4.5** Scheme of three different types of heat engines: **a** a continuous engine, **b** a two-stroke engine, and **c** a four-stroke engine.

and in the third stroke levels three and two are coupled to the cold bath, and heat flows out of the working medium. In the last stroke, the working medium is again decoupled from the heat bath and work is extracted from the engine, completing a full cycle.

The stroke-type engines operate repeatedly, and each cycle takes a certain amount of time  $\tau_{cyc}$ . Defining where the cycle begins is arbitrary, as long as all four stroke are completed. Unlike the continuous engines, the stroke-type engines do not reach a steady state operation, but rather, they reach a limit cycle, where at the end of each cycle the state of the quantum system is the same. The efficiencies for all of the engines described in Fig. 4.5 are given by  $\eta_{otto} = 1 - \frac{\omega_c}{\omega_h}$ , which is termed the quantum otto efficiency [14, 41, 48]. We leave the readers to prove this as an exercise. For simplicity, the description of the stroke-engines above is based solely on population inversion and does not require description of quantum coherence. In this sense, these engines describe a stochastic (classical) operation of the engines. In the following sections we will see that the presence of quantum coherence will have an influence on the thermodynamics of these thermal devices.

The mathematical description of these engines requires tools from the theory of open quantum systems. While the work strokes are described using a unitary propagator  $U$  which preserves the entropy of the quantum system, the coupling to the bath introduces irreversible dynamics accompanied with entropy generation. The dynamics of the engine is described by a completely-positive and trace-preserving map. In the Markovian regime this can be achieved using the Lindblad-Gorini-Kossakowski-Sudarshan (LGKS) master equation [64, 65], which is described in detail in the next section. Extending the study of quantum heat machines beyond the Markovian

regime and the weak system-bath coupling limit can be preformed using Green's functions [66], the polaron transformation [67–69], the reaction coordinate mapping [70–72] or using simulations based on the stochastic surrogate Hamiltonian [73]. Here, we will take a different approach based on the idea of heat exchangers [46], which will be described in detail in Sect. 4.3.1.3.

#### 4.3.1.2 Markovian Regime and Liouville Space

In the Markovian regime, the dynamics of the system (the working medium) is described by a reduced description for the density operator  $\rho$  and takes the form of the LGKS Markovian master equation [64, 65, 74] (see also Chap. 1):

$$i\hbar \frac{d}{dt}\rho = L(\rho) \equiv [H_s, \rho] + i \sum_k S_k \rho S_k^\dagger - \frac{1}{2} S_k^\dagger S_k \rho - \frac{1}{2} \rho S_k^\dagger S_k. \quad (4.22)$$

The  $S_k$  operators depend on the system-bath coupling and on the properties of the bath, including the temperature and the correlations [74]. In following, we concentrate on thermal generators  $L$  that asymptotically induce the system to evolve into a Gibbs state,  $\rho_{th} = \exp(-\beta H_s)/Z$ , with the inverse bath temperature  $\beta = 1/k_B T$  and the partition function  $Z$ . This type of generator can be derived from a microscopic Hamiltonian description in the weak system-bath coupling limit [74, 75] and for a collision model in the low density limit [76]. The necessity of a microscopic derivation was discussed in [77], where it was shown that a local phenomenological description may lead to a violation of the second law of thermodynamics. Further discussion on this topic is found in [78, 79].

To derive the results of this chapter, we analyze the dynamics in the extended Liouville space. In this space, any matrix representation of an operator acting in a Hilbert space is mapped to a vector. That is, for a general matrix  $B$  acting in Hilbert space:  $B_{N \times N} \rightarrow |B\rangle_{1 \times N^2}$ . Given this index mapping, the master equation (4.22) in Liouville space reads:

$$i\hbar \frac{d}{dt}|\rho\rangle \equiv \mathcal{L}|\rho\rangle \equiv (\mathcal{H}_s + \mathcal{L}^d)|\rho\rangle. \quad (4.23)$$

The super-operator  $\mathcal{H}_s$  is represented by a Hermitian  $N^2 \times N^2$  matrix that corresponds to the first term on the right hand side of (4.22), and the super-operator  $\mathcal{L}^d$  is a non-Hermitian  $N^2 \times N^2$  matrix that corresponds to the dissipative terms in (4.22). In this chapter, we use calligraphic letters to describe super-operators acting in Liouville space and ordinary letters for operators acting on a Hilbert space. We also chose a specific map known as the “vec-ing”. More details on the Liouville-space representation of quantum mechanics are presented in Box 1.

The LGKS operators in Hilbert space that describes the coupling of the system to the hot bath are expressed as

$$\begin{aligned} S_1^h &= \sqrt{\gamma_h} e^{-\hbar\omega_h\beta_h} |3\rangle\langle 1|, \\ S_2^h &= \sqrt{\gamma_h} |1\rangle\langle 3|. \end{aligned} \quad (4.24)$$

and those to the cold bath as

$$\begin{aligned} S_1^c &= \sqrt{\gamma_c} e^{-\hbar\omega_c\beta_c} |3\rangle\langle 2|, \\ S_2^c &= \sqrt{\gamma_c} |2\rangle\langle 3|. \end{aligned} \quad (4.25)$$

These operators form the dissipators  $\mathcal{L}_h$  and  $\mathcal{L}_c$  respectively. In the weak coupling limit, the parameters  $\gamma_h$  and  $\gamma_c$  are given by the Fourier-transforms of the baths correlation functions [74]. Without any external driving, the coupling to the baths will lead asymptotically to a Boltzmann factor ratio of the populations,  $p_3/p_1 = e^{-\hbar\omega_h\beta_h}$  and  $p_3/p_2 = e^{-\hbar\omega_c\beta_c}$ . However, when driving is incorporated to the process, the behavior of the state is changing, and different engine-types will differ from one another. With these building blocks a full description in the Markovian regime of the different engines can be obtained.

### Box 1: Liouville-space representation of quantum mechanics

Quantum dynamics is traditionally described in Hilbert space. However, it is convenient, particularly, for open quantum systems, to introduce an extended space where the density operator is represented by a vector and the time evolution of a quantum system is generated by a Schrödinger-like equation. This space is usually referred to as Liouville space [80]. We denote the “density vector” by  $|\rho\rangle \in \mathbb{C}^{1 \times N^2}$ , which is obtained by reshaping the density matrix  $\rho$  into a larger vector with index  $\alpha \in \{1, 2, \dots, N^2\}$ . The one-to-one mapping of the two matrix indices into a single vector index  $\{i, j\} \rightarrow \alpha$  is arbitrary, but has to be used consistently. In general, the vector  $|\rho\rangle$  is not normalized to unity. Its norm is equal to the purity,  $\mathcal{P} = \text{tr}(\rho^2) = \langle \rho | \rho \rangle$ , where  $\langle \rho | = |\rho\rangle^\dagger$ . The equation of motion of the density vector in Liouville space follows from

$$d_t \rho_\alpha = \sum_{\beta} \rho_{\beta} \partial(d_t \rho_{\alpha}) / \partial \rho_{\beta}. \quad (4.26)$$

Using this equation, one can verify that the dynamics of the density vector  $|\rho\rangle$  is governed by a Schrödinger-like equation in the new space,

$$i\hbar \partial_t |\rho\rangle = \mathcal{L} |\rho\rangle, \quad (4.27)$$

where the super-operator  $\mathcal{L} \in \mathbb{C}^{N^2 \times N^2}$  is given by

$$\mathcal{L}_{\alpha\beta} = i\hbar \frac{\partial(d_t \rho_{\alpha})}{\partial \rho_{\beta}}. \quad (4.28)$$

A particularly useful index mapping is the “vec-ing” maping [81–83] that provides a simple form for  $\mathcal{L}$  in terms of original Hilbert-space Hamiltonian and Lindblad operators. In this mapping, the density vector  $|\rho\rangle$  is ordered row by row, i.e.,  $\alpha = \text{col}+N(\text{row}-1)$ , and the following relations hold:

$$\begin{aligned}[H, \rho] &\rightarrow (H \otimes I - I \otimes H^T) |\rho\rangle, \\ A\rho A^\dagger &\rightarrow (A \otimes A^*) |\rho\rangle, \\ A^\dagger A\rho &\rightarrow (A^\dagger A \otimes I) |\rho\rangle, \\ \rho A A^\dagger &\rightarrow \left( I \otimes (A^\dagger A)^T \right) |\rho\rangle,\end{aligned}\tag{4.29}$$

where  ${}^T$  denotes the transpose and  ${}^*$  denotes the complex conjugate. Using these relations the generator  $\mathcal{L}$  can easily be expressed in a matrix form. The dynamical map generated by the Lindblad super-operator can also be expressed in a matrix form  $\Lambda = \exp(-i\mathcal{L}t/\hbar)$ . This matrix has a single eigenvalue which is equal to one and it’s eigenvector is associated with the stationary state of the system. For standard thermalization dynamics, this state is the Gibbs (thermal) state with the temperature of the bath.

The inner product of two operators  $A$  and  $B$  in Hilbert space is mapped to Liouville-space as

$$\text{tr}(A^\dagger B) \rightarrow \langle A | B \rangle.\tag{4.30}$$

Since  $\rho$  is Hermitian, (4.30) implies that the expectation value of an operator  $A$  in Liouville space is given by the inner product of  $\rho$  and  $A$ ,

$$\langle A \rangle = \langle \rho | A \rangle.\tag{4.31}$$

The dynamics of the expectation value  $\langle A \rangle$  can then be expressed as

$$\frac{d}{dt} \langle A \rangle = \frac{i}{\hbar} \langle \rho | \mathcal{L}^\dagger | A \rangle + \langle \rho | \partial_t A \rangle.\tag{4.32}$$

Another useful relation for the Hamiltonian part

$$\mathcal{H}|H\rangle = \langle H | \mathcal{H} = 0,\tag{4.33}$$

where we mapped  $H \rightarrow |H\rangle$  and  $[H, \cdot] \rightarrow \mathcal{H}$ . This relation follows from the fact that the Hamiltonian commutes with itself.

### 4.3.1.3 Non-Markovian and Strong Coupling Regime

Generally, treating non-Markovian dynamics and a strong system-bath coupling can be challenging. Here we adopt the idea developed in [46] of heat exchangers that captures the effects of non-Markovianity and strong coupling on the quantum thermal machines equivalence principle which will be discussed in Sect. 4.3.2.

Heat exchangers are widely used in engineering to pump heat out of a system. For example, computer chips interact strongly with a metal that conducts the heat and then is cooled by the surrounding air. In the context of the engines described in Fig. 4.5, the quantum system interacts with heat exchangers that are modeled by two level particles. There are  $N_h$  and  $N_c$  particles in the hot and the cold heat exchangers, respectively. We assume that in each stroke, the working medium interacts with a single particle of the heat exchangers. Before the interaction, each of the particles in the exchangers is in a thermal state with temperature  $T_{h,c}$ . During the interaction, heat is exchanged with the quantum system and the states of the particle and the working medium change. After the interaction, the particle relaxes back to its original thermal state via a coupling to a thermal bath. Thus, each particle will interact with the working medium cyclically with a period  $N_{h,c}\tau_{\text{cyc}}$ .

The advantage of the above description is that it is independent of the properties of the thermal bath (the interaction can be described in the weak coupling and Markovian limits). On the other hand, the particles may interact strongly with the working medium and in a non-Markovian manner, imposing the effects of strong and non-Markovianity on the equivalence principle.

In this scheme, the work source is modeled by a set of qubits or qutrits interacting with the working medium. After a complete cycle of the engine, energy is stored in the work repository which can later be extracted, similar to the function of a battery. The concepts of quantum batteries and quantum flywheels (see Chap. 8), where energy is stored and extracted from internal degrees of a quantum system were studied in different contexts [46, 84–88].

When the work repository is quantized, the exchange of energy with the working medium cannot necessarily be considered as pure work, since entropy may be generated in the battery and the working medium [46, 84, 89–91]. This phenomenon is ignored when the work repository is modeled as a semi-classical field. The field is typically considered large enough that the entropy generated in the field is negligible, and since its operation on the quantum system is unitary the entropy of the quantum system does not change as well. This generation of entropy in the battery can be resolved using a feedback scheme [84] or by applying a specific procedure that guarantees that entropy will be produced in the working medium while the entropy of the battery is not changing or even reduced (super-charging) [46].

The interaction of the working medium with the work repository and the heat exchangers can be modeled by unitary dynamics evolving from a Hamiltonian description. The initial states of the heat exchangers, the work repository, and the working medium in each cycle are uncorrelated, i.e.,  $\rho_{\text{tot}}(0) = \rho_c \otimes \rho_h \otimes \rho_w \otimes \rho$ . Here  $\rho$  is the engine (working medium) state and  $\rho_{c,h,w}$  are the heat exchangers and

work repository states. The coupling between the engine and the rest of the particles takes the form

$$H_{int} = \sum_{k=c,h,w} f_k(t) H_{ok}, \quad (4.34)$$

where  $f_k(t)$  is a periodic function that controls the timing of the interaction. We further require that the interactions will be energy conserving. Thus the energy in the exchangers, the work repository, and the engine are not effected by  $H_{ok}$  but only redistributed. Mathematically this requirement is translated to  $[H_{ok}, H_o + H_k] = 0$ , where the index  $k$  stands for  $c, h, w$ , and  $H_o$  is defined by Eq. (4.21). The interaction Hamiltonian takes the form,

$$H_{ok} = a_k^\dagger a_{ok} + a_k a_{ok}^\dagger, \quad (4.35)$$

where  $a_k$  is the annihilation operator of the  $k$  particle of the exchangers and battery, and  $a_{ok}$  is the annihilation operator of the  $k$  manifold of the working medium (the three-level system, see Fig. 4.5). This type of interaction generates a partial or full swap between the  $k$  manifold of the engine and the corresponding  $k$  particle of the exchangers and battery. Since the swap operation may significantly change both the states of the heat exchangers particles and the engine and form quantum correlations, this simplified model captures non-Markovian and strong coupling effects.

### 4.3.2 Quantum Thermal Machines Equivalence

A peculiar phenomenon in the thermodynamic behavior of the different engine-types described above occurs in a quantum regime where the action over a cycle is small compared to  $\hbar$  [45]. In this regime of operation, the four-stroke, two-stroke, and continuous engines have the same thermodynamic properties for both transient and steady state operation. At the end of each cycle, the power, heat and efficiency becomes equivalent. This phenomenon can be traced back to the coherent mechanisms of the engines that become dominant in the small action regime. The action is defined as the integral over a cycle time of the spectral norm of the generator of the dynamics:

$$s = \int_0^\tau \| \mathcal{L}(t) \| dt. \quad (4.36)$$

The spectral norm (operator norm) is simply given by the square root of the largest eigenvalue of  $\| \mathcal{L} \| = \max \sqrt{\text{eig}(\mathcal{L}^\dagger \mathcal{L})}$ . For a non-Hermitian operator, this magnitude is the largest singular value of the operator  $\mathcal{L}$ . The action norm Eq. (4.36) has been used before to obtain quantum speed limits and distance bounds for quantum states [92, 93] and the distance between protocols in the context of quantum control [94]. As an example [45], the action norm limits the maximal state change during time  $\tau$ , such that  $\max (\| |\rho(\tau)\rangle - |\rho(0)\rangle \|) \leq s/\hbar$ .

The derivation of the equivalence is based on the Strang decomposition [95, 96] for two non-commuting operators  $\mathcal{A}$  and  $\mathcal{B}$ ,

$$e^{(\mathcal{A}+\mathcal{B})dt/\hbar} = e^{\frac{1}{2}\mathcal{A}dt/\hbar} e^{\mathcal{B}dt/\hbar} e^{\frac{1}{2}\mathcal{A}dt/\hbar} + O(\bar{s}^3) \cong e^{\frac{1}{2}\mathcal{A}dt/\hbar} e^{\mathcal{B}dt/\hbar} e^{\frac{1}{2}\mathcal{A}dt/\hbar}. \quad (4.37)$$

Here we define  $\bar{s} \equiv s/\hbar$ , which is the norm action  $s = (\|\mathcal{A}\| + \|\mathcal{B}\|)dt$  divided by  $\hbar$  that must be small parameter for the expansion to hold, i.e.  $\bar{s} \ll 1$  [45].

#### 4.3.2.1 Equivalence in the Markovian Regime

To derive the engines' equivalence we start with the dynamical description of the continuous engine. The following calculations are carried out in a rotating frame, according to the transformation  $\mathcal{U} = e^{-i\mathcal{H}_o t/\hbar}$ . Since  $\mathcal{L}_h$  and  $\mathcal{L}_c$  commute with  $\mathcal{H}_o$  the transformation will not affect these generators. The interaction Hamiltonian is now time independent  $H_w \rightarrow \tilde{H}_w = \epsilon|1\rangle\langle 2| + \text{H.c.}$  (see Eq.(4.21)), and the generator of the dynamics reads,

$$\tilde{\mathcal{L}} = \mathcal{L}_h + \mathcal{L}_c + \tilde{\mathcal{H}}_w. \quad (4.38)$$

We chose the cycle time  $\tau_{\text{cyc}} = 6m\tau_d$ , where  $\tau_d$  is the external drive cycle and  $m \in \mathbb{Z}^+$ . The propagator of the continuous engine over time  $\tau_{\text{cyc}}$  is

$$\Lambda^{\text{cont}} = \exp \left[ -i(\mathcal{L}_h + \mathcal{L}_c + \tilde{\mathcal{H}}_w) \frac{\tau_{\text{cyc}}}{\hbar} \right]. \quad (4.39)$$

Applying the Strang splitting Eq.(4.37) on  $\mathcal{L}_h + \mathcal{L}_c$  we obtain the two-stroke propagator over one cycle,

$$\Lambda^{2st} = \exp \left[ -i\frac{3}{2}(\mathcal{L}_h + \mathcal{L}_c) \frac{\tau_{\text{cyc}}}{3\hbar} \right] \exp \left[ -i3\tilde{\mathcal{H}}_w \frac{\tau_{\text{cyc}}}{3\hbar} \right] \exp \left[ -i\frac{3}{2}(\mathcal{L}_h + \mathcal{L}_c) \frac{\tau_{\text{cyc}}}{3\hbar} \right]. \quad (4.40)$$

Here we rescaled the cycle time and the couplings to the bath and the external field such that the total cycle time will remain  $\tau_{\text{cyc}}$ . Moreover, we set the fraction time of the work stroke to be 1/3 of the cycle time, in agreement with the experiment [47] described in Sect. 4.3.4. We can repeat this procedure and obtain the four-stroke propagator over one cycle. First we split  $\mathcal{L}_c$  in Eq.(4.39) and then split  $\mathcal{H}_w$ ,

$$\Lambda^{4st} = \exp \left[ -i3\mathcal{L}_c \frac{\tau_{\text{cyc}}}{6\hbar} \right] \exp \left[ -i3\tilde{\mathcal{H}}_w \frac{\tau_{\text{cyc}}}{6\hbar} \right] \exp \left[ -i3\mathcal{L}_h \frac{\tau_{\text{cyc}}}{3\hbar} \right] \exp \left[ -i3\tilde{\mathcal{H}}_w \frac{\tau_{\text{cyc}}}{6\hbar} \right] \exp \left[ -i3\mathcal{L}_c \frac{\tau_{\text{cyc}}}{6\hbar} \right]. \quad (4.41)$$

Also here, the cycle time and couplings are rescaled to maintain a similar  $\tau_{\text{cyc}}$  for all engines. According to Eq.(4.37), given  $\bar{s} \ll 1$ , all engine-types propagators over a cycle are equivalent to order  $O(\bar{s}^3)$ , that is

$$\Lambda^{\text{cont}} \cong \Lambda^{2st} \cong \Lambda^{4st}. \quad (4.42)$$

The equivalence holds also for the average work and heat over a cycle:

$$\begin{aligned} W^{cont} &\cong W^{2st} \cong W^{4st}, \\ Q_{c,h}^{cont} &\cong Q_{c,h}^{2st} \cong Q_{c,h}^{4st}. \end{aligned} \quad (4.43)$$

As heat and work are process-dependent, and since the states of the different engines differ significantly from one another during the cycle, Eq. (4.43) should be proved. The rigorous proof can be found in [45] and is based on the symmetric rearrangement theorem. Here we will explicitly show how work equivalence can be derived for the continuous and the two-stroke engines. In steady state, the work performed over one cycle of the continuous engine is given by the steady state power multiplied by the cycle time [45],

$$W^{cont} = \frac{-i}{\hbar} \langle H_o | \tilde{\mathcal{H}}_w | \tilde{\rho}_s \rangle \tau_{cyc}. \quad (4.44)$$

Here  $\tilde{\rho}_s$  is the steady state density matrix of the continuous engine in the rotating frame. The work output over a single cycle of the two-stroke engine is simply given by the energy difference between the end and beginning of the work stroke. Assuming that the engine operates in the limit cycle and that the cycle (4.40) starts at a state  $|\tilde{\rho}(t_o - \tau_{cyc}/2)\rangle$ , we have,  $|\tilde{\rho}(t_o - \tau_{cyc}/2)\rangle = |\tilde{\rho}(t_o + \tau_{cyc}/2)\rangle$ . The work in this cycle is then given by

$$W^{2st} = \langle H_o | \tilde{\rho}(t_o + \frac{\tau_{cyc}}{6}) \rangle - \langle H_o | \tilde{\rho}(t_o - \frac{\tau_{cyc}}{6}) \rangle = \frac{-i}{\hbar} \langle H_o | \tilde{\mathcal{H}}_w | \tilde{\rho}(t_o) \rangle \tau_{cyc} + O(\tilde{s}^3). \quad (4.45)$$

The second equality in Eq. (4.45) follows from the fact that in the small action regime we can expand the states  $|\tilde{\rho}(t_o \pm \tau_{cyc}/6)\rangle = |\tilde{\rho}(t_o)\rangle \mp i3\tilde{H}_w \frac{\tau_{cyc}}{6\hbar} |\tilde{\rho}(t_o)\rangle + O(\tilde{s}^2)$ . Because of symmetry, the second order term vanishes and we are left with correction of the order  $O(\tilde{s}^3)$ . Using Eq. (4.42), we have  $|\tilde{\rho}(t_o \pm \tau_{cyc}/2)\rangle = |\tilde{\rho}_s\rangle + O(\tilde{s}^3)$ , and  $|\tilde{\rho}(t_o \pm \tau_{cyc}/2)\rangle = |\tilde{\rho}(t_o)\rangle \mp i\tilde{\mathcal{L}} \frac{\tau_{cyc}}{2\hbar} |\tilde{\rho}(t_o)\rangle + O(\tilde{s}^2)$ , which implies  $|\tilde{\rho}(t_o)\rangle = |\tilde{\rho}_s\rangle + O(\tilde{s}^2)$ . Inserting this last relation into the right hand side of Eq. (4.44), we obtain  $W^{cont} = W^{2st} + O(\tilde{s}^3)$ . In a similar manner, one can show the equivalence of the heat which is defined as

$$Q_{c,h}^{cont} = \frac{-i}{\hbar} \langle H_o | \mathcal{L}_{c,h} | \tilde{\rho}_s \rangle \tau_{cyc}. \quad (4.46)$$

The proof above assumes operation in the limit cycle. However, note that the equivalence holds also for transients and can be shown to hold for the four stroke engine without explicit calculation. To show this, the symmetric rearrangement theorem [45] should be applied.

The average power and heat flow are given by  $P = W/\tau_{cyc}$  and  $J_{c,h} = Q_{c,h}/\tau_{cyc}$ . The power and heat flows of the continuous engine is independent of the cycle time  $\tau_{cyc}$ . Thus, according to the proof of the equivalence for the work and heat, the power and heat flow of the two-stroke and four-stroke engines will deviate quadratically from the power of the continuous one,

$$P^i = P^{cont} + \alpha_i \bar{s}^2 \quad \text{for } i = 2st, 4st. \quad (4.47)$$

This result can be observed in Fig. 4.7b and will be discussed in detail in Sect. 4.3.4.

### 4.3.2.2 Equivalence in the Strong-Coupling and Non-Markovian Regime

The thermodynamic equivalence of heat machines can be extended to the non-Markovian and strong coupling regime. Adapting the setup introduced in Sect. 4.3.1.3 and applying the Strang decomposition Eq. (4.37), one can show the equivalence principle for small action in a similar manner to the Markovian regime. Yet, the equivalence work and heat in this setup is of the order of  $O(\bar{s}^4)$ , instead of  $O(\bar{s}^3)$  as it is in the Markovian regime. The dynamics of the engine and its interaction with the heat exchangers and the battery are described by a unitary transformation. By choosing the energy gaps in the engine manifold  $k$  to match those of the  $k$ -th heat exchanger and battery, we have the condition  $[H_o + \sum_{k=h,c,w} H_k, H_{int}] = 0$ . This condition implies that a transformation to a rotated frame according to  $U_0 = \exp[-i(H_o + \sum_{k=h,c,w} H_k)t/\hbar]$  will not affect  $H_{int}$ . Thus, in the rotated frame, the propagators in Hilbert space of continuous,<sup>1</sup> two-stroke, and four-stroke engines over a cycle time read:

$$\begin{aligned} U^{cont} &= \exp[-i(H_{oh} + H_{oc} + H_{ow})\frac{\tau_{cyc}}{\hbar}], \\ U^{2st} &= \exp[-i\frac{3}{2}H_{ow}\frac{\tau_{cyc}}{3\hbar}] \exp[-i3(H_{oh} + H_{oc})\frac{\tau_{cyc}}{3\hbar}] \exp[-i\frac{3}{2}H_{ow}\frac{\tau_{cyc}}{3\hbar}], \\ U^{4st} &= \exp[-i3H_{oc}\frac{\tau_{cyc}}{6\hbar}] \exp[-i3H_{ow}\frac{\tau_{cyc}}{6\hbar}] \exp[-i3H_{oh}\frac{\tau_{cyc}}{3\hbar}] \exp[-i3H_{ow}\frac{\tau_{cyc}}{6\hbar}] \exp[-i3H_{oc}\frac{\tau_{cyc}}{6\hbar}]. \end{aligned} \quad (4.48)$$

Applying the Strang decomposition in a similar manner to Sect. 4.3.2.1 results in

$$U^{cont}(\tau_{cyc}) \cong U^{2st}(\tau_{cyc}) \cong U^{4st}(\tau_{cyc}), \quad (4.49)$$

up to order  $O(\bar{s}^3)$ . If the engines start in the same initial condition, then their states at time  $m\tau_{cyc}$  for  $m \in \mathbb{Z}^+$  will differ at most by  $O(\bar{s}^3)$ , while at other times, they will differ in the strongest order possible  $O(\bar{s})$ . The heat and the work over one cycle are given by the energy of the heat exchanger particle and the energy stored in the battery after this cycle,

$$\begin{aligned} W^j &= \text{tr} \left[ (U^j(\tau_{cyc})\rho_{tot}(0)U^j(\tau_{cyc})^\dagger - \rho_{tot}(0)) H_w \right] \quad (4.50) \\ Q_{c,h}^j &= \text{tr} \left[ (U^j(\tau_{cyc})\rho_{tot}(0)U^j(\tau_{cyc})^\dagger - \rho_{tot}(0)) H_{c,h} \right], \quad j = cont, 2st, 4st. \end{aligned}$$

---

<sup>1</sup>The proper name for this type of engine would be the simultaneous engine, as all the interactions occur within one stroke. After this stroke, some energy is stored in the battery and the engine will subsequently interact with a new set of particles. However, for consistency with previous sections we will refer to this engine as continuous.

Equations (4.49) and (4.50) imply immediately, without the need of the symmetric rearrangement theorem, the equivalence of heat and work for the different heat engine types.

Since at every cycle the engine interacts with new particles of the battery and the heat exchangers, and no initial correlation is present, the equivalence of heat and work hold up to order  $O(\tilde{s}^4)$ . The  $O(\tilde{s}^3)$  corrections contribute only to inter-particle coherence generation and not to population changes. The inter-particle coherence should be distinguished from the single particle coherence, which is manifested by local operations on the single particles. The inter-particle coherence represents the interaction between degenerate states. In the model described above, we have three pairs of degenerate states  $\{|0_w 2\rangle, |1_w 1\rangle\}$ ,  $\{|0_h 3\rangle, |1_h 1\rangle\}$ , and  $\{|0_c 3\rangle, |1_c 2\rangle\}$ , which are essential for the engine operation. Suppression of these coherences will lead to a Zeno effect, where the engine will not evolve in time.

Here, we assumed that the initial states of all the engines are the same, which implies that the equivalence also holds in the transient dynamics. However, the equivalence holds also in the limit cycle regardless of the initial state of the engines. To show this one should look at the reduced state of one of the engine types at the limit cycle and apply the evolution operator of a different engine and see how the state changes.

### 4.3.3 Quantum-Thermodynamic Signatures

Much like in quantum information theory, where entanglement witness are identified in order to distinguish between entangled and separable states, it is desirable to identify quantum thermodynamic signatures in the operation of quantum thermal machines. We define a quantum-thermodynamic signature as a thermodynamic measurement, such as power or heat flow, that confirms the presence of quantum effects, such as coherence or quantum correlations, in the operation of the device. In this section, we will focus on the presence of coherence (interference) in the operation of quantum heat engines and its signature [45].

A quantum-thermodynamic signature is constructed by setting a bound on a thermodynamic measurement of a classical engine. In this section we define a classical engine as a device that can be fully described by its population dynamics. Considering, for example, the two-stroke engine described in Sect. 4.3.2.1, the work done in the work stroke is given by  $W = \langle H_o | \exp[-\frac{i}{\hbar} \tilde{\mathcal{H}}_w \tau_w] | \tilde{\rho} \rangle - \langle H_o | \tilde{\rho} \rangle$ , where  $\tau_w$  is the work stroke duration. Splitting the state into the diagonal (population) contribution and to off-diagonal (coherence) contribution such that  $|\tilde{\rho}\rangle = |\tilde{\rho}_{pop}\rangle + |\tilde{\rho}_{coh}\rangle$ , we can express the work as

$$W = \langle H_o | \sum_{n=1} \frac{(-\frac{i}{\hbar} \tilde{\mathcal{H}}_w \tau_w)^{2n}}{2n!} |\tilde{\rho}_{pop}\rangle + \langle H_o | \sum_{n=1} \frac{(-\frac{i}{\hbar} \tilde{\mathcal{H}}_w \tau_w)^{2n-1}}{(2n-1)!} |\tilde{\rho}_{coh}\rangle. \quad (4.51)$$

The above splitting is possible because of two reasons. First, note that  $\tilde{H}_w$  in Hilbert space only has off-diagonal terms in the energy basis of  $H_o$ . This implies that in Liouville space, the super-operator and the state will have the structure<sup>2</sup>

$$\tilde{\mathcal{H}}_w = \begin{pmatrix} 0 & h \\ h^\dagger & 0 \end{pmatrix} \quad |\tilde{\rho}\rangle = \begin{pmatrix} pop \\ coh \end{pmatrix}. \quad (4.52)$$

This means that  $\tilde{\mathcal{H}}_w$  couples only coherences to populations and populations to coherences. Second, since in Hilbert space  $H_o$  is diagonal,  $\langle H_o |$  projects the state on the population space in Liouville space. Thus, contributions to the work will come from odd powers of  $\tilde{\mathcal{H}}_w$  operating on coherences and from even powers operating on populations.

To construct classical (stochastic) engines based on our previous description of the two-stroke and the four-stroke quantum engines, we introduce a dephasing operator  $\mathcal{D}$  that will eliminate coherences in the engine. This is achieved by operating with  $\mathcal{D}$  at the beginning and at the end of each stroke. We require that the operator  $\mathcal{D}$  dephases the system in the energy basis such that it does not change the energy population. This is referred as pure dephasing, which means that before and after the operation of  $\mathcal{D}$ , the energy of the engine and the population in the energy basis are the same. Conceptually this operator can be described as a projection operator on the population space  $\mathcal{D} = |pop\rangle\langle pop|$ . In practice, this operator can be expressed in Hilbert space, for example, as  $D(\rho) = -\eta[H_o, [H_o, \rho]]$  with the dephasing rate  $\eta > 0$ . This term may arise in different physical scenarios [94, 97, 98]. Since  $\mathcal{D}$  commutes with  $\mathcal{L}_{h,c}$ , the effect of  $\mathcal{D}$  on the dynamics and the work is reduced to its influence on the unitary strokes. The work of the stochastic engine can now be expressed as  $W^{stoch} = \langle H_o | \mathcal{D}(\exp[-\frac{i}{\hbar} \tilde{\mathcal{H}}_w \tau_w] - \mathbb{I}) \mathcal{D} | \tilde{\rho} \rangle = \langle H_o | (\exp[-\frac{i}{\hbar} \tilde{\mathcal{H}}_w \tau_w] - \mathbb{I}) | \tilde{\rho}_{pop} \rangle$ , where we used the relation  $\langle H_o | \mathcal{D} = \langle H_o |$ . In the small action regime the leading order to the work is quadratic in  $\tilde{\mathcal{H}}_w$ ,

$$W^{stoch} = -\frac{\tau_w^2}{2\hbar^2} \langle H_o | \tilde{\mathcal{H}}_w^2 | \tilde{\rho}_{pop} \rangle + O(\tilde{s}^4). \quad (4.53)$$

Energy leaving the system is always negative, hence we will bound the absolute value of the work produced by the engine. Applying Hölder's inequality we obtain  $|\langle H_o | \tilde{\mathcal{H}}_w^2 | \tilde{\rho}_{pop} \rangle| \leq \|\langle H_o | \tilde{\mathcal{H}}_w^2 \|_\infty \| \tilde{\rho}_{pop} \|_1$ . Since  $\| \tilde{\rho}_{pop} \|_1 = 1$ , the upper bound on the work and power is independent of the state of the engine and is determined solely by the configuration of the engine,

$$\begin{aligned} |W^{stoch}| &\leq \frac{\tau_w^2}{2\hbar^2} \|\langle H_o | \tilde{\mathcal{H}}_w^2 \|_\infty \\ |P^{stoch}| &\leq \frac{d^2 \tau_{cyc}}{2\hbar^2} \|\langle H_o | \tilde{\mathcal{H}}_w^2 \|_\infty. \end{aligned} \quad (4.54)$$

---

<sup>2</sup>In the more general case where  $\tilde{H}_w$  also has diagonal terms, there will be an additional entry to the matrix that does not vanish, (i.e.,  $\tilde{H}_w[2, 2] \neq 0$ ) and couples coherences to coherences.

Here  $d = \frac{\tau_w}{\tau_{cyc}}$  is the partial duration of the work stroke. The upper bound (4.54) is tighter than the one introduced in [45] as the norm  $\|\cdot\|_\infty \leq \|\cdot\|_2$ . For the Hamiltonian (4.21) the two-stroke stochastic engine upper bound is then given by

$$|P^{stoch}| \leq \hbar\omega|\epsilon|^2 d^2 \tau_{cyc}. \quad (4.55)$$

Any power measurement that exceeds the stochastic bound  $|P| > |P^{stoch}|$  is considered a quantum-thermodynamic signature, indicating the existence of interference in the engine (see Fig. 4.7a). Thus, exceeding the classical bound is a sufficient (but not necessary) condition that the engine incorporates coherence in its operation. Two immediate results can be derived from the above construction. First, continuous engines with the Hamiltonian structure (4.52), only have a coherent work extraction mechanism, which is a result of Eq. (4.44) and the splitting (4.51). Thus, complete dephasing nulls the power. Second, given the same thermodynamic resources, in the small action regime, a coherent quantum engine will outperform a stochastic (classical) engine, resulting in higher power output (see Fig. 4.7a).

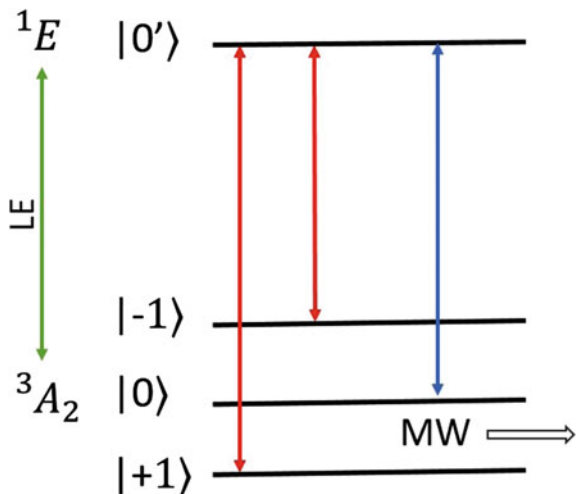
#### 4.3.4 Experimental Realization

Major advances in realizing microscopic thermal machines have been made in recent years. Experimental demonstration of such devices have been implemented with trapped ions [99, 100], superconducting circuits [101, 102], and quantum dots [103]. In this section we will concentrate on the pioneering experiment by Klatzow et al. [47] in nitrogen-vacancy centers in diamonds, which clearly demonstrates the contrast between classical and quantum heat engines. In particular, Klatzow et al. have demonstrated both the equivalence of two-stroke and continuous engines and the violation of the stochastic power bound discussed in previous sections.

The working medium of the engine is an ensemble of negatively charged nitrogen vacancy ( $NV^-$ ) centers in diamond. The  $NV^-$  center consist of a ground state spin triplet  ${}^3A_2$   $\{| -1 \rangle, | 0 \rangle, | +1 \rangle\}$  in which degeneracy can be removed by applying a magnetic field. The excited states consist of two spin triplets and three singlets. Due to fast decay rates and time averaging at room temperature, the excited states can be considered as a meta-stable spin singlet state  ${}^1E$  denoted  $| 0' \rangle$ . Optical excitation, de-excitation (fluorescence) and non-radiative decay through the state  $| 0' \rangle$  mimic the effect of the couplings to the thermal baths. The system approaches a steady state with population inversion between the states  $| 0 \rangle$  and  $| +1 \rangle$ . Schematic description of the system is introduced in Fig. 4.6.

A microwave (MW) field set in resonance with the  $| +1 \rangle \leftrightarrow | 0 \rangle$  transition is then amplified, and power in the form of stimulated emission of MW radiation (maser) is extracted from the engine. The power is determined from a direct measurement of the fluorescence intensity change once the MW field is applied. This setup can be mapped to the three-level continuous engine discussed in detail in Sect. 4.3.1.1.

**Fig. 4.6** Scheme of NV<sup>-</sup> center levels and the effective couplings. The ground state triplet and the meta-stable excited singlet state are coupled through a 532 nm laser field. The collective effects of optical excitation, de-excitation and non-radiative decay are similar to coupling the NV<sup>-</sup> to hot (red arrows) and cold (blue arrow) thermal baths. Work is extracted in the form of amplifying a MW field that is in resonance with the transition  $|+1\rangle \leftrightarrow |0\rangle$ .



Since the level  $| -1 \rangle$  is off-resonance with the MW field, it will not contribute to work extraction. Then the states  $\{| +1 \rangle, | 0 \rangle, | 0' \rangle\}$  in Fig. 4.6 can be mapped to states  $\{| 1 \rangle, | 2 \rangle, | 3 \rangle\}$  of Fig. 4.5, where the level  $| -1 \rangle$  only contributes to population transfer through level  $| 0' \rangle$ . Switching on and off the MW field allows for the realization of a two-stroke engine and its comparison to the continuous engine.

The normalized action in this case [47] is given by  $\bar{s} = [\frac{\epsilon}{2}d + \gamma(1-d)]\tau_{cyc}$ , where  $\epsilon$  in Eq. (4.21) is twice the Rabi frequency,  $\gamma$  is the total coupling rates to the baths and  $d$  is the fraction of time of the work stroke out of the full cycle. Figure 4.7a presents a power measurement of a two-stroke engine that exceeds the stochastic bound set by Eq. (4.55). This is a clear indication of a quantum-thermodynamic signature in the operation of the engine. The stochastic bound, plotted in the purple line, was calculated for the parameters  $\omega = 2\pi \times 2600$  MHz,  $\epsilon = 3.2$  Mrad/s,  $\gamma = 0.41$  MHz, and  $d = 1/3$  while changing the cycle time  $\tau_{cyc}$ . The bound is violated by 2.4 standard deviations. Figure 4.7b demonstrates the equivalence principle in the form of Eq. (4.47). The powers of the two-stroke and continuous engines coincide in the small action regime. We also notice that, as predicted, the power of the continuous engine is independent of the cycle time. That is, for  $\tau_{cyc} \rightarrow 0$  the power does not vanish as it would for a stochastic engine in the small action regime. This indicates that a continuous engine with the Hamiltonian structure (4.52) requires coherence in order to operate. In this experiment  $\epsilon = 5$  Mrad/s.

This experiment demonstrated the existence of quantum phenomena in microscopic thermal machines for the first time. In the small action regime, quantum coherence plays an important role in the operation of the engine. In this regime, the extracted power is enhanced, and thermodynamic properties of different types of engines coincide.

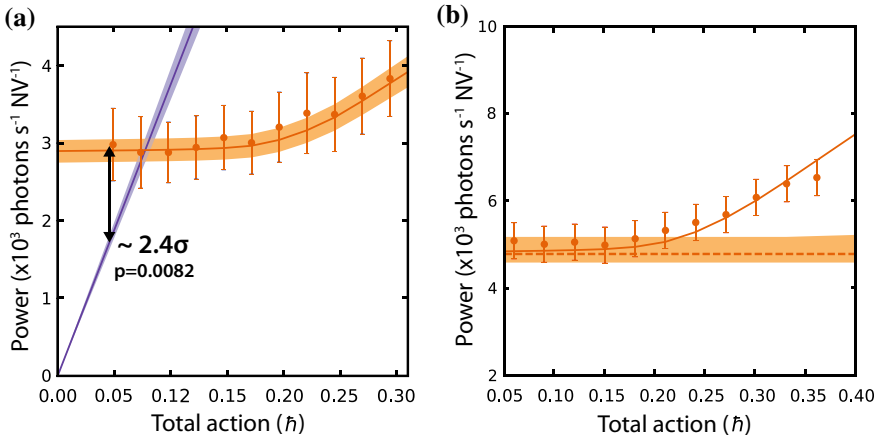


**Fig. 4.7** Power per NV<sup>-</sup> center versus the normalized action  $\bar{s}$ . **a** Quantum-thermodynamic signature: the orange line and data points present the theoretical and measured power of the two-stroke engine, respectively. The purple straight line is the upper stochastic bound on the power. In the small action regime, a clear violation of the stochastic bound (2.4 standard deviation) is observed. **b** The equivalence principle: The data points and the shaded region present power measurements of the two-stroke and continuous engines, respectively. The theoretical predictions for the two-stroke and continuous engines are given by the solid and dashed line, respectively. In the small action regime, the two measurements coincide. Figure courtesy of J. Klatzow, J. N. Becker, and E. Poem.

### 4.3.5 Quantum Friction

Quantum friction is a quantum phenomenon that influences the operation of quantum thermal machines. It is related to the generation of coherences and excitations along a finite-time unitary evolution, and its dissipation when coupled to a thermal environment. Quantum friction in the context of quantum-thermodynamics was termed by Feldmann and Kosloff [41, 42] and is often referred as intrinsic or internal quantum friction. To understand this phenomenon intuitively, we will consider a specific example. We will compare two thermodynamic processes that will reveal the amount of energy lost to friction. The first process is an ideal quantum adiabatic process, where the initial state of the system is a thermal state  $\rho_i = \exp[-\beta_i H_i] Z_i^{-1}$  with the initial inverse temperature  $\beta_i$  and the initial Hamiltonian  $H_i = H(0)$ . The system is then driven adiabatically by changing the system energy scale and keeping its population constant. We require the final state to be expressed as  $\rho_f = \exp[-\beta_f H_f] Z_f^{-1}$  such that  $\beta_f$  is the inverse final temperature,  $H_f = H(t_f)$ , and the final populations satisfy  $P_n^i = P_n^f$ . This requirement implies that for all  $n$ -levels, the compression ratio is given by  $\epsilon_n^f / \epsilon_n^i = \beta_i / \beta_f$ , where  $\epsilon_n^{f,i}$  are the eigenvalues of  $H_{f,i}$ . This condition corresponds to homogeneous energy scaling of Sect. 4.2.

In real, finite-time processes, the adiabatic limit does not hold in general. Because of the non-commutativity of the Hamiltonian at different times,  $[H(t), H(t')] \neq 0$ , coherences and excitations will be generated in the final state. Thus, we will consider

a second, more real process. In the first stage the system is driven non-adiabatically by changing the Hamiltonian  $H_i \rightarrow H_f$  so that at the end of this stage the system is found in some state  $\rho_\tau$ . In the second stage, the system is brought to equilibrium via coupling to a thermal bath at inverse temperature  $\beta_f$  such that the final state is  $\rho_f = \exp[-\beta_f H_f] Z_f^{-1}$ . Such a process is elementary when studying quantum thermal machines, such as in the study of Carnot and Otto cycles. The energy that was invested in the creation of coherences and excitations and that was later dissipated to the thermal bath is the amount of energy lost to quantum friction.

In this sense, the effect of the non-adiabatic driving resembles the effect of friction in classical mechanics. Extra energy is needed to complete the process, which is then dissipated to the environment. The energy lost to friction is evaluated by the difference between the work invested in the real non-adiabatic stage and the work of the ideal adiabatic process,

$$W_{fric} = W_{re} - W_{ad}. \quad (4.56)$$

This amount of work is exactly the amount of energy dissipated (irreversibly) to the bath during the second stage of the second process. The work in the adiabatic process is  $W_{ad} = \text{tr}(\rho_f H_f) - \text{tr}(\rho_i H_i) = \sum_n P_n^i (\epsilon_n^f - \epsilon_n^i)$ . For the non-adiabatic stage in the second process we have,  $W_{re} = \text{tr}(\rho_\tau H_f) - \text{tr}(\rho_i H_i)$ , implying that

$$W_{fric} = \sum_n \epsilon_n^f (\langle \epsilon_n^f | \rho_\tau | \epsilon_n^f \rangle - P_n^f). \quad (4.57)$$

The work (4.57) can be related to the relative entropy of the final state  $\rho_\tau$  at the end of stage one with the final thermal state  $\rho_f$  at the end of stage two [43],

$$W_{fric} = \beta_f^{-1} S(\rho_\tau \| \rho_f). \quad (4.58)$$

To show this we, consider the the definition of the relative entropy

$$\begin{aligned} S(\rho_\tau \| \rho_f) &= \text{tr}(\rho_\tau \ln \rho_\tau) - \text{tr}(\rho_\tau \ln \rho_f) \\ &= \sum_n P_n^i \ln P_n^i - (\langle \epsilon_n^f | \rho_\tau | \epsilon_n^f \rangle \times \ln P_n^f) \\ &= \sum_n \beta_f \epsilon_n^f (\langle \epsilon_n^f | \rho_\tau | \epsilon_n^f \rangle - P_n^f). \end{aligned} \quad (4.59)$$

Here we used the fact that the von-Neumann entropy is invariant under unitary transformations, the relation  $P_n^i = P_n^f$ , and that  $\ln P_n^f = -\beta_f \epsilon_n^f - \ln Z_f$ . Since the relative entropy is non-negative, Eq.(4.58) implies that  $W_{fric} \geq 0$ . Applying arguments from [104] it was shown in [43] that a tighter bound for  $W_{fric}$  can be obtained using the Bures length

$$W_{fric} \geq \frac{8\beta_f^{-1}}{\pi} L^2(\rho_\tau, \rho_f), \quad (4.60)$$

where  $L(\rho_\tau, \rho_f) = \arccos(\sqrt{F(\rho_\tau, \rho_f)})$ , with the fidelity  $F(\rho_\tau, \rho_f) = [tr(\sqrt{\sqrt{\rho_\tau}\rho_f\sqrt{\rho_\tau}})]^2$ .

More generally (i.e., not limited to the process above), the power along the work stroke of a thermal machine can be divided into classical and coherent extraction mechanisms [40]

$$P \equiv tr \left( \frac{dH(t)}{dt} \rho(t) \right) = \sum_n \dot{\epsilon}_n(t) \langle \epsilon_n(t) | \rho(t) | \epsilon_n(t) \rangle + \langle \epsilon_n(t) | [H(t), \rho(t)] | \dot{\epsilon}_n(t) \rangle. \quad (4.61)$$

The first term can be associated with classical power,

$$P_{clas} = \sum_n \dot{\epsilon}_n(t) \langle \epsilon_n(t) | \rho(t) | \epsilon_n(t) \rangle = \sum_n \dot{\epsilon}_n(t) \rho_{nn}(t), \quad (4.62)$$

and the second term with the coherent power,

$$P_{coh} = \sum_n \langle \epsilon_n(t) | [H(t), \rho(t)] | \dot{\epsilon}_n(t) \rangle = \sum_{n,l} (\epsilon_n - \epsilon_l) \langle \epsilon_l | \dot{\epsilon}_n \rangle \rho_{nl}(t), \quad (4.63)$$

where  $\rho$  is expressed in the instantaneous eigenbasis of  $H(t)$ . Here, the term classical power is referred to power generated by changes in the energy levels of the engine and the contribution comes only from the diagonal terms of the density matrix in the energy basis. The contribution to the coherent power, however, arises only from the off-diagonal terms. The average classical and coherent work can be calculated by taking the time integral over the power. For the adiabatic process described above,  $P_{coh}$  vanishes and the population  $\rho_{nn}$  is fixed in time. Thus, the average work is again given by  $\sum_n P_n^i (\epsilon_n^f - \epsilon_n^i)$ . Starting with a diagonal state in the energy basis, which often occurs after a full thermalization stroke, coherence will be generated once  $[H(t), H(t')] \neq 0$ . Thus,  $P_{coh} \neq 0$ , and in general, the average coherent work will be non-zero. The terms “classical” and “coherent” in Eqs. (4.62) and (4.63) should be used carefully. As we saw in the previous section, coherences and populations are coupled to each other during the dynamical evolution, so the distinction between the two may become ambiguous.

As long as dissipation is not introduced, friction is absent from the process, since the dynamic is reversible. In principle, one can extract all of the work from the state before it interacts with the thermal bath. By introducing a unitary cyclic process that transforms the state to a passive state<sup>3</sup> [105], work can be extracted without changing the energy levels. This is the maximal amount of extractable work from a quantum state, and is sometimes referred to as ergotropy [106]. This procedure assumes that we have access to a semi-classical field and that the unitary operation can be implemented in practice.

<sup>3</sup>A passive state  $\rho_{pas}$  is a state for which no work can be extracted by a cyclic unitary operation, thus  $tr(\rho_{pas} H) \leq tr(U \rho_{pas} U^\dagger H)$ . It was shown by Pusz and Woronowicz that a state is passive if and only if it is diagonal in the energy eigenbasis and its eigenvalues are non-increasing with energy.

Extracting work from coherences before they dissipate is one way to avoid friction. Other strategies to avoid friction in finite-time processes employ different control methods. Quantum lubrication [107] is a method that minimizes  $S(\rho_\tau \parallel \rho_f)$  in Eq. (4.58) by adding pure dephasing noise to the unitary stage. This additional noise can be considered as an instantaneous quantum Zeno effect, where the state of the system is projected to the instantaneous eigenstates of the time dependent Hamiltonian, eliminating the generation of coherence [94]. Shortcuts to adiabaticity [108] are other useful control methods that can be used in order to find frictionless control Hamiltonians [109, 110], which speed up adiabatic processes. For a given final time, the state of the system is an eigenstate of the final Hamiltonian  $H_f$ , but during the process, the state is subject to the generation of coherences and excitations. These control processes can be executed on very short time scales with high fidelity. If one assumes that the unitary evolution is not subject to noise from the control fields or from the environment, an exact frictionless Hamiltonian for finite time can be found. In a more realistic scenario where noise is present in the unitary process, one should aim to find a control Hamiltonian that minimizes the effect of noise [111].

The average work measured by the energy difference between the end and the beginning of the process is the same for the shortcut to adiabaticity protocol and the regular adiabatic process, which implies that frictionless protocols can in principle be implemented. However, in the shortcut protocol the instantaneous power can become very large and will require different resources in order to be implemented. Very fast protocols may require infinite resources. This is the manifestation of the time-power trade-off [111] or the speed-cost trade-off [112]. This feature was also recently studied by examining the growth of work fluctuations in shortcut protocols [113].

## 4.4 Quantum Correlations in the Operation of Thermal Machines

The existence of quantum correlations is one of the most powerful signatures of non-classicality in quantum systems, as seen in recent reviews [114, 115] and references therein. In this context, thermodynamic approaches play a major role in witnessing and quantifying the existence of quantum correlations [116–121]. Many studies relating thermodynamics with quantum correlation have focused on the amount of work extractable from correlations [85, 87, 122, 123] or the thermodynamic cost of creating correlations [124].

Quantum correlations have also been considered in the study of quantum thermal machines such as engines and refrigerators. In [125], entanglement between three qubits that form a quantum absorption refrigerator was studied. It was shown that near the Carnot bound entanglement is absent, nevertheless, in other regimes entanglement enhanced cooling and energy transport in the device. On the other hand, in a similar setup, that employed a different dynamical description of the refrigerator [126], it was shown that bipartite entanglement is absent between the qubits and correlations in the form of quantum discord which always exist in the system, do not influence the stationary heat flows. Entanglement in the working medium of

quantum engines has mainly been investigated in the form of thermal-entanglement of two spins in Heisenberg types of models [127–130]. In these studies, the heat and the work produced by the engines are expressed in terms of the concurrence that measure the amount of entanglement in the system. Existence of temporal quantum correlations in a single two-level system Otto engine was also considered [131]. It was shown that in some regimes of the engine operations, the Leggett–Garg function exceeds its maximal classical value, which is a signature of non-classical behavior.

However, in most of the studies referred above, quantum correlations do not play a major role in the thermodynamic operation of the devices. The correlations were not exploited to gain power, and no clear quantum-thermodynamic signature is obtained. Instead, these studies only indicate that quantum correlations are present in the working medium when setting carefully the parameters of the problem. Next, we review a quantum-thermodynamic signature in the form of heat exchange. We believe this work will motivate further study on whether and how correlation can be exploited in the repeated operation of quantum thermal machines. A detailed discussion on correlations in quantum thermodynamics can be found in Chap. 30.

#### 4.4.1 Quantum-Thermodynamic Signatures

Here we derive a result obtained by Jennings and Rudolph [118] on the average heat exchange between two local correlated thermal states. This study was motivated by the work of Parović on the disappearance of the thermodynamic arrow in highly correlated environments [132]. Although the setup is not a standard<sup>4</sup> thermal machine, which is the focus of this chapter, it can be considered as a single-shot cooling process where no external work is invested. Instead, correlations are exploited (as fuel) in order to cool the system. Moreover, this study presents an important thermodynamic signature of quantum-mechanical features that goes beyond what is possible classically. In the language of quantum information, the signature is called an entanglement witness. In particular, a bound on the amount of heat that can flow from a cold local thermal state to a hot local thermal state due to classical correlations is obtained. It is further shown that quantum correlations may violate this bound.

The Clausius statement of the second law of thermodynamics implies that when no work is done on the system, heat can only flow from a hotter body to colder body. This statement holds when no initial correlations are present between the two bodies. To show this, we consider two initially uncorrelated systems  $A$  and  $B$ . The global initial state is thus represented by the product of the states of the two subsystems,  $\rho_{AB}(0) = \rho_A(0) \otimes \rho_B(0)$ . This is known as Boltzmann’s assumption of molecular chaos. We further assume that each subsystem is initially in a thermal state,  $\rho_X(0) = \exp[-\beta_X H_X]$ , where  $X \in \{A, B\}$ . Next we let the two subsystems interact via a global unitary interaction  $U(\tau, 0)$  for time  $\tau$  that couples the two subsystems. As we wish to preserve the average energy of  $\rho_{AB}$ , and thus not perform any work on the system from external sources, we require that the transformation

---

<sup>4</sup>Here we consider a “standard” thermal machine to be a device that has specific functioning, such as heat engines and refrigerators, and that operates in the limit cycle/steady state.

uphold  $\text{tr} [\rho_{AB}(0)(H_A + H_B)] = \text{tr} [\rho_{AB}(\tau)(H_A + H_B)]$ . After the interaction, the local reduced states are  $\rho_{A,B} = \text{tr}_{B,A}(\rho_{AB})$  and the corresponding internal energy and entropy will change by the amount  $\Delta E_X$  and  $\Delta S_X$ , where

$$\begin{aligned}\Delta E_X &= \text{tr} [(\rho_X(\tau) - \rho_X(0))H_X], \\ \Delta S_X &= S_X(\tau) - S_X(0),\end{aligned}\tag{4.64}$$

and  $S_X = -\text{tr}(\rho_X \ln \rho_X)$  is the von-Neumann entropy. Since the thermal state minimizes the free energy,  $F(\rho_X) = \text{tr} [\rho_X H_X] - S(\rho_X)/\beta_X$ , we obtain,  $\text{tr} [\rho_X(0)H_X] - S(\rho_X(0))/\beta_X \leq \text{tr} [\rho_X(\tau)H_X] - S(\rho_X(\tau))/\beta_X$ , which can be cast into<sup>5</sup> [133]

$$\beta_X \Delta E_X - \Delta S_X \geq 0.\tag{4.65}$$

To quantify the amount of correlations present between the two subsystems  $A$  and  $B$  we will use the quantum mutual information for bipartite systems:

$$I_q[\rho_{AB}] \equiv S(\rho_{AB} \parallel \rho_A \otimes \rho_B) = S_A + S_B - S_{AB}.\tag{4.66}$$

This function is always non-negative [134] and accounts for both classical and quantum correlations. For product states, like the one considered in the process above, the mutual information vanishes,  $I_q[\rho_{AB}(0)] = 0$ . This implies that at time  $\tau$  the change in the mutual information is  $\Delta I_q[\rho_{AB}] = I_q[\rho_{AB}(\tau)] \geq 0$ . On the other hand since  $S_{AB}$  is invariant under the unitary transformation  $U(\tau, 0)$  we obtain  $\Delta I_q[\rho_{AB}] = \Delta S_A + \Delta S_B$  which is true irrespective of the initial conditions. Applying these relation to (4.65) we obtain

$$\beta_A Q_A + \beta_B Q_B \geq \Delta I_q(\rho_{AB}) \geq 0,\tag{4.67}$$

where we identified the heat transferred to system  $X$  as the change in its internal energy,  $Q_X = \Delta E_X$ . Since  $Q_A = -Q_B$ , relation (4.67) implies that heat will always flow from hot to cold. Note, however, if the assumption of initial product state is removed then  $\Delta I_q[\rho_{AB}]$  can become negative, which opens up the possibility of “anomalous heat flow” namely heat flowing from the colder body to the hotter body. In this case Eq. (4.67) reads

$$\beta_A Q_A + \beta_B Q_B \geq -|\Delta I_q(\rho_{AB})|.\tag{4.68}$$

The initial correlations present in the system, which can be either classical, quantum, or both, are the source of this backward flow. In order to derive a clear quantum-thermodynamic signature, a bound on the maximal backward flow that could occur from just classical correlations is set. The classical mutual information of a quantum

<sup>5</sup>Note that the von-Neumann entropy for nonequilibrium states cannot be associated with the thermodynamic entropy. However, the inequality can be derived directly from the relative entropy  $S(\rho(\tau) \parallel \rho(0))$ , where  $\rho(0)$  is a thermal state.

state is given by taking the maximum over all POVMs  $M_A \otimes M_B$ , which are the most general kind of quantum measurements possible on  $A$  and  $B$  [135]:

$$I_c(\rho_{AB}) = \max_{M_A \otimes M_B} [H(P_A) + H(P_B) - H(P_{AB})], \quad (4.69)$$

where  $H(P)$  is the Shannon entropy of the measurement statistics  $P$ . The classical mutual information satisfies<sup>6</sup>  $0 \leq I_c(\rho_{AB}) \leq I_q(\rho_{AB})$  [136], which implies that  $\max |\Delta I_c(\rho_{AB})| \leq \max |\Delta I_q(\rho_{AB})|$ . To obtain a bound on  $\max |\Delta I_c(\rho_{AB})|$  that is independent of the specific details of the states, we note that  $I_c(\rho_{AB}) \leq \ln D$ , where  $D = \min\{\text{Dim}(\rho_A), \text{Dim}(\rho_B)\}$  is the dimension of the smaller system. This bound is a result of the monotonicity property of the Shannon entropy under partial trace,  $H(P_{AB}) \geq H(P_A), H(P_B)$ . The same argument applies for the von-Neumann entropy for separable states  $S(\rho_{AB}|_{\text{sep}}) \geq S(\rho_A), S(\rho_B)$  [137]. The upper bound,  $\ln D$ , is saturated for perfectly correlated, zero discord, separable states  $\rho_{AB} = \frac{1}{D} \sum_k |e_k\rangle\langle e_k|_A |f_k\rangle\langle f_k|_B$ , where  $|e_k\rangle$  and  $|f_k\rangle$  are orthonormal bases for  $A$  and  $B$ . Assuming that the initial state  $\rho_{AB}$  is the perfectly correlated state above and that at the final time it is a product state, the maximal violation of heat transfer from cold to hot due to classical correlations is

$$Q_{\text{clas}} = \frac{\ln D}{|\beta_A - \beta_B|}. \quad (4.70)$$

Since for entangled states the mutual entropy can exceed  $\ln D$ , and in fact, go to  $2 \ln D$  for maximally entangled states, the violation of heat transfer can exceed  $Q_{\text{clas}}$ . Thus, any measurement of heat exchange that gives  $Q > Q_{\text{clas}}$  indicates that the initial state  $\rho_{AB}$  was necessarily entangled. Therefore the heat-flow pattern acts as a “witness” that reveals genuine non-classicality in the thermodynamic system. Moreover, this quantum resource can be exploited in a cooling process, removing heat from a colder body and transferring it to a hotter one. This phenomenon was recently demonstrated in a NMR experiment [138], where it was shown that heat is transferred from a colder nuclear spin to a hotter one due to correlations. The result presented here was later extended to derive an exchange fluctuation theorem for energy exchange between thermal quantum systems beyond the assumption of molecular chaos [139].

## 4.5 Conclusions

In this chapter we have presented a short review about some of the studies that compare the performance of classical and quantum heat machines. In particular, we have focused on three main quantum features, energy quantization, quantum coherence, quantum correlations, and their manifestation in the operation of quantum thermal machines. All of these features boil down to the mathematical structure of quantum mechanics, which is represented by wave functions and operators acting in Hilbert space. However, we showed that the manifestation of particular quantum

---

<sup>6</sup>The relative entropy is monotonically decreasing under completely positive maps.

phenomena can be distinguished from one another. Specifically, we saw that energy quantization and the uncertainty principle alone lead to differences in the behavior of heat engines. Moreover, quantum mechanics enables the realization of thermal-machines with incompressible working medium which is classically impossible.

The role of quantum coherence was also studied. Since the generation of coherences for interacting quantum systems is typically unavoidable, and since coherences have thermodynamic cost, dephasing leads to quantum friction. Working in the small action regime, complete dephasing can be suppressed. In this regime, coherences survive the couplings to the thermal baths, and quantum engines outperform stochastic engines, which incorporate only populations in their operation. This phenomenon can be observed experimentally by setting a bound on the maximal power obtained by a stochastic engine. A violation of this bound is a signature of a quantum-thermodynamic behavior. Furthermore, in the small action regime, the thermodynamic properties of different types of engines coincide, since coherent work extraction becomes dominant.

Quantum correlations are obviously closely related to the existence of coherence between particles, however, by investigating bounds on classically correlated systems, it is possible to isolate the effects of quantum correlations. Here, we demonstrated that the presence of quantum correlations can explain anomalous heat flow that cannot be achieved classically.

As we have shown, operating in the quantum regime is not always advantageous. Thus it is important to understand the quantum behavior of thermal-machines in order to avoid undesired reductions in the performance. We believe that the results presented here represent only some initial results that require further investigation, such as:

- What are the features needed on the potentials for providing a quantum boost to the work and heat exchange and how do these features relate to other quantum properties?
- One possible manner of obtaining an efficiency divergence between classical and quantum heat machines is by performing a thermal cycle that involves an inhomogeneous energy level scaling. As of today, there are only a small number of studies concerned with this type of cycle, calling for further research in this direction.
- Since coupling to a thermal source is an unavoidable process in thermal devices, innovative methods to exploit quantum coherences and correlations before they decay are essential for obtaining quantum supremacy. Possible approaches are: identifying and operating in the regime where the quantum effects are still relevant; applying quantum control methods, such as feedback control, in order to maintain the quantum properties.
- The main results concerning the relationship between thermodynamics and quantum correlations are focused on single-shot processes. A desired goal would be to exploit correlations in the repeated operation of a device.
- Can the quantum thermal machines be scaled up in size and maintain their quantum nature? Can we deduce from these models something about energy transfer and quantum behavior of more complex systems, such as biological systems?

As we have shown, the actual performances of classical and quantum heat machine diverge, even though both are limited by the same fundamental thermodynamic bounds, such as the Carnot efficiency. Nevertheless, the difference between them is noteworthy and should be studied further, especially considering the fast experimental progress that has already succeeded in demonstrating quantum behavior of thermal-machines.

**Acknowledgements** We thank R. Kosloff, R. Uzdin, D. Jennings, M. Lostaglio, D. Jasrasaria, A. Bylinskii, D. Gangloff, R. Islam, A. Aspuru-Guzik and V. Vuletic for useful comments and for sharing their wisdom. We also acknowledge J. Klatzow, J. N. Becker and E. Poem, for sharing their experimental results and preparing Fig. 4.7.

## References

1. W.B. Case, Am. J. Phys. **76**, 937 (2008). <https://doi.org/10.1119/1.2957889>
2. E. Wigner, Phys. Rev. **40**, 749 (1932). <https://doi.org/10.1103/PhysRev.40.749>
3. V. Sundar, D. Gelbwaser-Klimovsky, A. Aspuru-Guzik (2017), [arXiv:1712.06649](https://arxiv.org/abs/1712.06649)
4. H.B. Callen, *Thermodynamics and an Introduction to Thermostatistics* (Wiley, New York, 1985)
5. D. Gelbwaser-Klimovsky, A. Bylinskii, D. Gangloff, R. Islam, A. Aspuru-Guzik, V. Vuletic, Phys. Rev. Lett. **120**, 170601 (2018). <https://doi.org/10.1103/PhysRevLett.120.170601>
6. H. Quan, Y.-X. Liu, C. Sun, F. Nori, Phys. Rev. E **76**, 031105 (2007). <https://doi.org/10.1103/PhysRevE.76.031105>
7. Y. Zheng, D. Poletti, Phys. Rev. E **90**, 012145 (2014). <https://doi.org/10.1103/PhysRevE.90.012145>
8. D.J. Griffiths, *Introduction to Quantum Mechanics* (Cambridge University Press, Cambridge, 2016)
9. R.J. Farris, Rubber Chem. Technol. **52**, 159 (1979). <https://doi.org/10.5254/1.3535199>
10. J. Mullen, G.W. Look, J. Konkel, Am. J. Phys. **43**, 349 (1975). <https://doi.org/10.1119/1.9852>
11. S. Paolucci, *Continuum Mechanics and Thermodynamics of Matter* (Cambridge University Press, Cambridge, 2016). <https://doi.org/10.1017/CBO9781316106167>
12. M.E. Gurtin, E. Fried, L. Anand, *The Mechanics and Thermodynamics of Continua* (Cambridge University Press, Cambridge, 2010). <https://doi.org/10.1017/CBO9780511762956>
13. H.T. Quan, Phys. Rev. E **79**, 041129 (2009). <https://doi.org/10.1103/PhysRevE.79.041129>
14. R. Kosloff, Y. Rezek, Entropy **19**, 136 (2017). <https://doi.org/10.3390/e19040136>
15. Y. Zheng, D. Poletti, Phys. Rev. E **92**, 012110 (2015). <https://doi.org/10.1103/PhysRevE.92.012110>
16. R. Uzdin, R. Kosloff, New J. Phys. **16**, 095003 (2014). <https://doi.org/10.1088/1367-2630/16/9/095003>
17. H. Quan, P. Zhang, C. Sun, Phys. Rev. E **72**, 056110 (2005). <https://doi.org/10.1103/PhysRevE.72.056110>
18. W. Coffey, Y.P. Kalmykov, S. Titov, B. Mulligan, Phys. Chem. Chem. Phys. **9**, 3361 (2007). <https://doi.org/10.1039/B614554J>
19. R. Brown, E. Ott, C. Grebogi, J. Stat. Phys. **49**, 511 (1987). <https://doi.org/10.1007/BF01009347>
20. A. Streltsov, G. Adesso, M.B. Plenio, Rev. Mod. Phys. **89**, 041003 (2017). <https://doi.org/10.1103/RevModPhys.89.041003>
21. D. Gelbwaser-Klimovsky, A. Aspuru-Guzik, Chem. Sci. **8**, 1008 (2017). <https://doi.org/10.1039/C6SC04350J>

22. M. Lostaglio, D. Jennings, T. Rudolph, *Nat. Commun.* **6** (2015). <https://doi.org/10.1038/ncomms7383>
23. K. Korzekwa, M. Lostaglio, J. Oppenheim, D. Jennings, *New J. Phys.* **18**, 023045 (2016). <https://doi.org/10.1088/1367-2630/18/2/023045>
24. P. Skrzypczyk, A.J. Short, S. Popescu (2013), <arXiv:1302.2811>
25. J. Åberg, *Phys. Rev. Lett.* **113**, 150402 (2014). <https://doi.org/10.1103/PhysRevLett.113.150402>
26. M. Horodecki, J. Oppenheim, *Nat. Commun.* **4** (2013). <https://doi.org/10.1038/ncomms3059>
27. W. Niedenzu, D. Gelbwaser-Klimovsky, G. Kurizki, *Phys. Rev. E* **92**, 042123 (2015). <https://doi.org/10.1038/srep07809>
28. D. Gelbwaser-Klimovsky, G. Kurizki, *Sci. Rep.* **5** (2015). <https://doi.org/10.1038/srep07809>
29. M.O. Scully, K.R. Chapin, K.E. Dorfman, M.B. Kim, A. Svidzinsky, *Proc. Natl. Acad. Sci.* **108**, 15097 (2011). <https://doi.org/10.1073/pnas.1110234108>
30. S. Rahav, U. Harbola, S. Mukamel, *Phys. Rev. A* **86**, 043843 (2012). <https://doi.org/10.1103/PhysRevA.86.043843>
31. M.T. Mitchison, M.P. Woods, J. Prior, M. Huber, *New J. Phys.* **17**, 115013 (2015). <https://doi.org/10.1088/1367-2630/17/11/115013>
32. C. Latune, I. Sinayskiy, F. Petruccione (2018), <arXiv:1801.10113>
33. J.B. Brask, N. Brunner, *Phys. Rev. E* **92**, 062101 (2015). <https://doi.org/10.1103/PhysRevE.92.062101>
34. J. Roßnagel, O. Abah, F. Schmidt-Kaler, K. Singer, E. Lutz, *Phys. Rev. Lett.* **112**, 030602 (2014). <https://doi.org/10.1103/PhysRevLett.112.030602>
35. G. Manzano, F. Galve, R. Zambrini, J.M. Parrondo, *Phys. Rev. E* **93**, 052120 (2016). <https://doi.org/10.1103/PhysRevE.93.052120>
36. R. Alicki, D. Gelbwaser-Klimovsky, *New J. Phys.* **17**, 115012 (2015). <https://doi.org/10.1088/1367-2630/17/11/115012>
37. M.O. Scully, M.S. Zubairy, G.S. Agarwal, H. Walther, *Science* **299**, 862 (2003). <https://doi.org/10.1126/science.1078955>
38. D. Gelbwaser-Klimovsky, N. Erez, R. Alicki, G. Kurizki, *Phys. Rev. A* **88**, 022112 (2013). <https://doi.org/10.1103/PhysRevA.88.022112>
39. W. Niedenzu, D. Gelbwaser-Klimovsky, A.G. Kofman, G. Kurizki, *New J. Phys.* **18**, 083012 (2016). <https://doi.org/10.1088/1367-2630/18/8/083012>
40. K. Brandner, M. Bauer, U. Seifert, *Phys. Rev. Lett.* **119**, 170602 (2017). <https://doi.org/10.1103/PhysRevLett.119.170602>
41. T. Feldmann, R. Kosloff, *Phys. Rev. E* **61**, 4774 (2000). <https://doi.org/10.1103/PhysRevE.61.4774>
42. R. Kosloff, T. Feldmann, *Phys. Rev. E* **65**, 055102 (2002). <https://doi.org/10.1103/PhysRevE.65.055102>
43. F. Plastina, A. Alecce, T.J.G. Apollaro, G. Falcone, G. Francica, F. Galve, N. Lo Gullo, R. Zambrini, *Phys. Rev. Lett.* **113**, 260601 (2014). <https://doi.org/10.1103/PhysRevLett.113.260601>
44. A. Alecce, F. Galve, N.L. Gullo, L. Dell'Anna, F. Plastina, R. Zambrini, *New J. Phys.* **17**, 075007 (2015). <https://doi.org/10.1088/1367-2630/17/7/075007>
45. R. Uzdin, A. Levy, R. Kosloff, *Phys. Rev. X* **5**, 031044 (2015). <https://doi.org/10.1103/PhysRevX.5.031044>
46. R. Uzdin, A. Levy, R. Kosloff, *Entropy* **18** (2016). <https://doi.org/10.3390/e18040124>
47. J. Klatzow, C. Weinzel, P.M. Ledingham, J.N. Becker, D.J. Saunders, J. Nunn, I.A. Walmsley, R. Uzdin, E. Poem (2017), <arXiv:1710.08716>
48. R. Kosloff, A. Levy, *Annu. Rev. Phys. Chem.* **65**, 365 (2014). <https://doi.org/10.1146/annurev-physchem-040513-103724>
49. F. Chen, Y. Gao, M. Galperin, *Entropy* **19** (2017). <https://doi.org/10.3390/e19090472>
50. E. Geva, R. Kosloff, *J. Chem. Phys.* **96**, 3054 (1992). <https://doi.org/10.1063/1.461951>
51. L.A. Correa, *Phys. Rev. E* **89**, 042128 (2014). <https://doi.org/10.1103/PhysRevE.89.042128>

52. M. Esposito, R. Kawai, K. Lindenberg, C. Van den Broeck, Phys. Rev. E **81**, 041106 (2010). <https://doi.org/10.1103/PhysRevE.81.041106>
53. H. Scovil, E. Schulz-DuBois, Phys. Rev. Lett. **2**, 262 (1959). <https://doi.org/10.1103/PhysRevLett.2.262>
54. E. Geva, R. Kosloff, Phys. Rev. E **49**, 3903 (1994). <https://doi.org/10.1103/PhysRevE.49.3903>
55. J.P. Palao, R. Kosloff, J.M. Gordon, Phys. Rev. E **64**, 056130 (2001). <https://doi.org/10.1103/PhysRevE.64.056130>
56. A. Levy, R. Kosloff, Phys. Rev. Lett. **108**, 070604 (2012). <https://doi.org/10.1103/PhysRevLett.108.070604>
57. D. Gelbwaser-Klimovsky, R. Alicki, G. Kurizki, Phys. Rev. E **87**, 012140 (2013). <https://doi.org/10.1103/PhysRevE.87.012140>
58. D. Gelbwaser-Klimovsky, W. Niedenzu, G. Kurizki, *Advances In Atomic, Molecular, and Optical Physics*, vol. 64 (Elsevier, Amsterdam, 2015), pp. 329–407. <https://doi.org/10.1016/bs.aamop.2015.07.002>
59. A. Levy, R. Alicki, R. Kosloff, Phys. Rev. E **85**, 061126 (2012). <https://doi.org/10.1103/PhysRevE.85.061126>
60. S.E. Harris, Phys. Rev. A **94**, 053859 (2016). <https://doi.org/10.1103/PhysRevA.94.053859>
61. Y. Zou, Y. Jiang, Y. Mei, X. Guo, S. Du, Phys. Rev. Lett. **119**, 050602 (2017). <https://doi.org/10.1103/PhysRevLett.119.050602>
62. A.E. Allahverdyan, R.S. Johal, G. Mahler, Phys. Rev. E **77**, 041118 (2008). <https://doi.org/10.1103/PhysRevE.77.041118>
63. J. Zhang, Y.-X. Liu, R.-B. Wu, K. Jacobs, F. Nori, Phys. Rep. **679**, 1–60 (2017). <https://doi.org/10.1016/j.physrep.2017.02.003>
64. G. Lindblad, J. Phys. A: Math. Gen. **48**, 119 (1976). <https://doi.org/10.1088/0305-4470/29/14/037>
65. V. Gorini, A. Kossakowski, E.C.G. Sudarshan, J. Math. Phys. **17**, 821 (1976). <https://doi.org/10.1063/1.522979>
66. M. Esposito, M.A. Ochoa, M. Galperin, Phys. Rev. Lett. **114**, 080602 (2015). <https://doi.org/10.1103/PhysRevLett.114.080602>
67. D. Gelbwaser-Klimovsky, A. Aspuru-Guzik, J. Phys. Chem. Lett. **6**, 3477 (2015). <https://doi.org/10.1021/acs.jpclett.5b01404>
68. D. Segal, J. Chem. Phys. **140**, 164110 (2014). <https://doi.org/10.1063/1.4871874>
69. D. Xu, C. Wang, Y. Zhao, J. Cao, New J. Phys. **18**, 023003 (2016). <https://doi.org/10.1088/1367-2630/18/2/023003>
70. P. Strasberg, G. Schaller, N. Lambert, T. Brandes, New J. Phys. **18**, 073007 (2016). <https://doi.org/10.1088/1367-2630/18/7/073007>
71. D. Newman, F. Mintert, A. Nazir, Phys. Rev. E **95**, 032139 (2017). <https://doi.org/10.1103/PhysRevE.95.032139>
72. P. Strasberg, G. Schaller, T.L. Schmidt, M. Esposito, Phys. Rev. B **97**, 205405 (2018). <https://doi.org/10.1103/PhysRevB.97.205405>
73. G. Katz, D. Gelman, M.A. Ratner, R. Kosloff, J. Chem. Phys. **129**, 034108 (2008). <https://doi.org/10.1063/1.2946703>
74. H.-P. Breuer, F. Petruccione, *Open Quantum Systems* (Oxford University Press, Oxford, 2002)
75. E. Davies, Commun. Math. Phys. **39**, 91 (1974). <https://doi.org/10.1007/BF01608389>
76. R. Dumcke, Commun. Math. Phys. **97**, 331 (1985). <https://doi.org/10.1007/BF01213401>
77. A. Levy, R. Kosloff, EPL (Europhys. Lett.) **107**, 20004 (2014). <https://doi.org/10.1209/0295-5075/107/20004>
78. P.P. Hofer, M. Perarnau-Llobet, L.D.M. Miranda, G. Haack, R. Silva, J.B. Brask, N. Brunner, New J. Phys. **19**, 123037 (2017). <https://doi.org/10.1088/1367-2630/aa964f>
79. J.O. González, L.A. Correa, G. Nocerino, J.P. Palao, D. Alonso, G. Adesso, Open Syst. Inf. Dyn. **24**, 1740010 (2017). <https://doi.org/10.1142/S1230161217400108>
80. S. Mukamel, *Principles of Nonlinear Optical Spectroscopy*, vol. 6 (Oxford University Press, Oxford, 1999)

81. S. Machnes, M.B. Penio (2014), [arXiv:1408.3056v1](https://arxiv.org/abs/1408.3056v1)
82. H. Roger, R.J. Charles, *Topics in Matrix Analysis* (Cambridge University Press, Cambridge, 1994)
83. M. Am-Shallem, A. Levy, I. Schaefer, R. Kosloff (2015), [arXiv:1510.08634](https://arxiv.org/abs/1510.08634)
84. A. Levy, L. Diósi, R. Kosloff, Phys. Rev. A **93**, 052119 (2016). <https://doi.org/10.1103/PhysRevA.93.052119>
85. R. Alicki, M. Fannes, Phys. Rev. E **87**, 042123 (2013). <https://doi.org/10.1103/PhysRevE.87.042123>
86. F.C. Binder, S. Vinjanampathy, K. Modi, J. Goold, New J. Phys. **17**, 075015 (2015). <https://doi.org/10.1088/1367-2630/17/7/075015>
87. M. Perarnau-Llobet, K.V. Hovhannисyan, M. Huber, P. Skrzypczyk, N. Brunner, A. Acín, Phys. Rev. X **5**, 041011 (2015). <https://doi.org/10.1103/PhysRevX.5.041011>
88. K. Korzekwa, M. Lostaglio, J. Oppenheim, D. Jennings, New J. Phys. **18**, 023045 (2016). <https://doi.org/10.1088/1367-2630/18/2/023045>
89. M.P. Woods, N. Ng, S. Wehner (2015), [arXiv:1506.02322](https://arxiv.org/abs/1506.02322)
90. D. Gelbwaser-Klimovsky, G. Kurizki, Phys. Rev. E **90**, 022102 (2014). <https://doi.org/10.1103/PhysRevE.90.022102>
91. D. Gelbwaser-Klimovsky, R. Alicki, G. Kurizki, EPL (Europhys. Lett.) **103**, 60005 (2013). <https://doi.org/10.1209/0295-5075/103/60005>
92. R. Uzdin, R. Kosloff, EPL (Europhys. Lett.) **115**, 40003 (2016). <https://doi.org/10.1209/0295-5075/115/40003>
93. D.A. Lidar, P. Zanardi, K. Khodjasteh, Phys. Rev. A **78**, 012308 (2008). <https://doi.org/10.1103/PhysRevA.78.012308>
94. A. Levy, E. Torrontegui, R. Kosloff, Phys. Rev. A **96**, 033417 (2017). <https://doi.org/10.1103/PhysRevA.96.033417>
95. T. Jahnke, C. Lubich, BIT Numer. Math. **40**, 735 (2000). <https://doi.org/10.1023/A:1022396519656>
96. G. Strang, SIAM J. Numer. Anal. **5**, 506 (1968). <https://doi.org/10.1137/0705041>
97. G.J. Milburn, Phys. Rev. A **44**, 5401 (1991). <https://doi.org/10.1103/PhysRevA.44.5401>
98. L. Diósi, Phys. Lett. A **129**, 419 (1988). [https://doi.org/10.1016/0375-9601\(88\)90309-X](https://doi.org/10.1016/0375-9601(88)90309-X)
99. J. Roßnagel, S.T. Dawkins, K.N. Tolazzi, O. Abah, E. Lutz, F. Schmidt-Kaler, K. Singer, Science **352**, 325 (2016). <https://doi.org/10.1126/science.aad6320>
100. G. Maslennikov, S. Ding, R. Hablitzel, J. Gan, A. Roulet, S. Nimmrichter, J. Dai, V. Scarani, D. Matsukevich (2017). <https://doi.org/10.1038/s41467-018-08090-0>
101. J.P. Pekola, F.W.J. Hekking, Phys. Rev. Lett. **98**, 210604 (2007). <https://doi.org/10.1103/PhysRevLett.98.210604>
102. A. Fornieri, C. Blanc, R. Bosisio, S. D'ambrosio, F. Giazotto, Nat. Nanotechnol. **11**, 258 (2016). <https://doi.org/10.1038/nnano.2015.281>
103. H. Thierschmann, R. Sánchez, B. Sothmann, F. Arnold, C. Heyn, W. Hansen, H. Buhmann, L.W. Molenkamp, Nat. Nanotechnol. **10**, 854 (2015). <https://doi.org/10.1038/nnano.2015.176>
104. S. Deffner, E. Lutz, Phys. Rev. Lett. **105**, 170402 (2010). <https://doi.org/10.1103/PhysRevLett.105.170402>
105. W. Pusz, S. Wornwicz, Commun. Math. Phys. **58**, 273 (1978). <https://projecteuclid.org/euclid.cmp/1103901491>
106. A.E. Allahverdyan, R. Balian, Th.M. Nieuwenhuizen, Eur. Phys. Lett. **67**, 565 (2004). <https://doi.org/10.1209/epl/i2004-10101-2>
107. T. Feldmann, R. Kosloff, Phys. Rev. E **73**, 025107(R) (2006). <https://doi.org/10.1103/PhysRevE.73.025107>
108. E. Torrontegui, S. Ibáñez, S. Martínez-Garaot, M. Modugno, A. del Campo, D. Guéry-Odelin, A. Ruschhaupt, X. Chen, J.G. Muga, Adv. At. Mol. Opt. Phys. **62**, 117 (2013). <https://doi.org/10.1016/B978-0-12-408090-4.00002-5>
109. X. Chen, A. Ruschhaupt, S. Schmidt, A. del Campo, D. Guery-Odelin, J.G. Muga, Phys. Rev. Lett. **104**, 063002 (2010). <https://doi.org/10.1103/PhysRevLett.104.063002>

110. A. Del Campo, J. Goold, M. Paternostro, Sci. Rep. **4**, 6208 (2014). <https://doi.org/10.1038/srep06208>
111. A. Levy, A. Kiely, J.G. Muga, R. Kosloff, E. Torrontegui, New J. Phys. **20**, 025006 (2018). <https://doi.org/10.1088/1367-2630/aaa9e5>
112. S. Campbell, S. Deffner, Phys. Rev. Lett. **118**, 100601 (2017). <https://doi.org/10.1103/PhysRevLett.118.100601>
113. K. Funo, J.-N. Zhang, C. Chatou, K. Kim, M. Ueda, A. del Campo, Phys. Rev. Lett. **118**, 100602 (2017). <https://doi.org/10.1103/PhysRevLett.118.100602>
114. K. Modi, A. Brodutch, H. Cable, T. Paterek, V. Vedral, Rev. Mod. Phys. **84**, 1655 (2012). <https://doi.org/10.1103/RevModPhys.84.1655>
115. R. Horodecki, P. Horodecki, M. Horodecki, K. Horodecki, Rev. Mod. Phys. **81**, 865 (2009). <https://doi.org/10.1103/RevModPhys.81.865>
116. J. Oppenheim, M. Horodecki, P. Horodecki, R. Horodecki, Phys. Rev. Lett. **89**, 180402 (2002). <https://doi.org/10.1103/PhysRevLett.89.180402>
117. W.H. Zurek, Phys. Rev. A **67**, 012320 (2003). <https://doi.org/10.1103/PhysRevA.67.012320>
118. D. Jennings, T. Rudolph, Phys. Rev. E **81**, 061130 (2010). <https://doi.org/10.1103/PhysRevE.81.061130>
119. A. Brodutch, D.R. Terno, Phys. Rev. A **81**, 062103 (2010). <https://doi.org/10.1103/PhysRevA.81.062103>
120. S. Popescu, D. Rohrlich, Phys. Rev. A **56**, R3319 (1997). <https://doi.org/10.1103/PhysRevA.56.R3319>
121. J. Goold, M. Huber, A. Riera, L. del Rio, P. Skrzypczyk, J. Phys. A: Math. Theor. **49**, 143001 (2016). <https://doi.org/10.1088/1751-8113/49/14/143001>
122. K.V. Hovhannisyan, M. Perarnau-Llobet, M. Huber, A. Acín, Phys. Rev. Lett. **111**, 240401 (2013). <https://doi.org/10.1103/PhysRevLett.111.240401>
123. G.L. Giorgi, S. Campbell, J. Phys. B: At. Mol. Opt. Phys. **48**, 035501 (2015). <https://doi.org/10.1088/0953-4075/48/3/035501>
124. M. Huber, M. Perarnau-Llobet, K.V. Hovhannisyan, P. Skrzypczyk, C. Klöckl, N. Brunner, A. Acín, New J. Phys. **17**, 065008 (2015). <https://doi.org/10.1088/1367-2630/17/6/065008>
125. N. Brunner, M. Huber, N. Linden, S. Popescu, R. Silva, P. Skrzypczyk, Phys. Rev. E **89**, 032115 (2014). <https://doi.org/10.1103/PhysRevE.89.032115>
126. L.A. Correa, J.P. Palao, D. Alonso, G. Adesso, Phys. Rev. E **87**, 042131 (2013). <https://doi.org/10.1103/PhysRevE.87.042131>
127. T. Zhang, W.-T. Liu, P.-X. Chen, C.-Z. Li, Phys. Rev. A **75**, 062102 (2007). <https://doi.org/10.1103/PhysRevA.75.062102>
128. F. Altintas, A.Ü. Hardal, Ö.E. Müstecaplıoğlu, Phys. Rev. E **90**, 032102 (2014). <https://doi.org/10.1103/PhysRevE.90.032102>
129. H. Wang, S. Liu, J. He, Phys. Rev. E **79**, 041113 (2009). <https://doi.org/10.1103/PhysRevE.79.041113>
130. X.L. Huang, T. Wang, X.X. Yi, Phys. Rev. E **86**, 051105 (2012). <https://doi.org/10.1103/PhysRevE.86.051105>
131. A. Friedenberger, E. Lutz, EPL (Europhys. Lett.) **120**, 10002 (2017). <https://doi.org/10.1209/0295-5075/120/10002>
132. M.H. Partovi, Phys. Rev. E **77**, 021110 (2008). <https://doi.org/10.1103/PhysRevE.77.021110>
133. A. Peres, *Quantum Theory: Concepts and Methods*, vol. 57 (Springer Science & Business Media, Berlin, 2006). <https://doi.org/10.1007/0-306-47120-5>
134. A. Wehr, Rev. Mod. Phys. **50**, 221 (1978). <https://doi.org/10.1103/RevModPhys.50.221>
135. B.M. Terhal, M. Horodecki, D.W. Leung, D.P. DiVincenzo, J. Math. Phys. **43**, 4286 (2002). <https://doi.org/10.1063/1.1498001>
136. G. Lindblad, Commun. Math. Phys. **39**, 111 (1974). <https://doi.org/10.1007/BF01608390>
137. R. Horodecki, P. Horodecki, Phys. Lett. A **194**, 147 (1994). [https://doi.org/10.1016/0375-9601\(94\)91275-0](https://doi.org/10.1016/0375-9601(94)91275-0)
138. K. Micadei, J.P. Peterson, A.M. Souza, R.S. Sarthour, I.S. Oliveira, G.T. Landi, T.B. Batalhão, R.M. Serra, E. Lutz (2017), arXiv:1711.03323
139. S. Jevtic, T. Rudolph, D. Jennings, Y. Hirono, S. Nakayama, M. Murao, Phys. Rev. E **92**, 042113 (2015). <https://doi.org/10.1103/PhysRevE.92.042113>

# Chapter 5

## Friction-Free Quantum Machines



Adolfo del Campo, Aurélia Chenu, Shujin Deng and Haibin Wu

The operation of a quantum heat engine in finite time generally faces a trade-off between efficiency and power. Using shortcuts to adiabaticity (STA), this trade off can be avoided to engineer thermal machines that operate at maximum efficiency and tunable output power. We demonstrate the use of STA to engineer a scalable superadiabatic quantum Otto cycle and report recent experimental progress to tailor quantum friction in finite-time quantum thermodynamics. In the presence of quantum friction, it is also shown that the use of a many-particle working medium can boost the performance of the quantum machines with respect to an ensemble of single-particle thermal machines.

### 5.1 Heat Engines Today

Catalyzing the industrial revolution, heat engines have played a decisive role in the history of humankind. Their study also led to a paradigm shift that transformed physics, setting the ground for a new type of science beyond Newtonian mechanics in the nineteenth century. Together with the study of heat conduction by Fourier, heat engines led to the birth of thermodynamics. The quantification of the efficiency of

---

A. del Campo (✉)

Department of Physics, University of Massachusetts, Boston, MA 02125, USA  
e-mail: adolfo.delcampo@umb.edu

A. del Campo · A. Chenu

Theory Division, Los Alamos National Laboratory, MS-B213,  
Los Alamos, NM 87545, USA

S. Deng · H. Wu

State Key Laboratory of Precision Spectroscopy, East China Normal University,  
Shanghai 200062, People's Republic of China

an engine driven through a thermodynamic cycle led to the notion of irreversibility, which has been described as the most original contribution of this field [1].

Over the last two centuries, technological advances have motivated the thermodynamic description of increasingly smaller systems, including chemical processes, single biomolecules and simple quantum systems. At the nanoscale, thermal and quantum fluctuations appear as a dominant new ingredient.

In parallel with these developments, a number of fundamental problems, ranging from blackhole physics to the cost of computation, have unravelled the role of information. Quantum thermodynamics flourishes currently in this context merging notions of foundations of physics, information theory and statistical mechanics [2–4].

In the quantum domain, the study of heat engines keeps facilitating further advances, building on the dialogue between fundamental questions and applied science. A full quantum description of heat engines was first put forward in [5, 6]. It is now understood that information can be used as a resource from which to extract work, leading to the notion of information-driven heat engines such as that proposed by Szilard [7, 8]. Quantum optical devices including masers and lasers [9], together with physical processes such as light harvesting in natural and artificial systems [10–13], can be analyzed in terms of quantum thermodynamic cycles. One may therefore hope for an interplay between quantum thermodynamics and energy science.

A central result in thermodynamics is that the efficiency of any heat engine run using two equilibrium thermal reservoirs with inverse temperatures  $\beta_c$  and  $\beta_h$  (satisfying  $\beta_c > \beta_h$ ) has as a universal upper bound the Carnot efficiency  $\eta_C = 1 - \beta_h/\beta_c$ . This bound however may be reached only in engines that run infinitely slowly. From the macroscale to quantum world, realistic heat engines are expected to operate in finite time. This necessity comes from an observed trade-off between efficiency and power, that has sometimes been referred to as “the tragedy of finite-time thermodynamics”. While the maximum efficiency of a thermodynamic cycle,  $\eta_{\max} \leq \eta_C$ , can be reached in principle under sufficiently slow driving, the practical desideratum of a finite output power sets an upper bound to the operation time. As a result, an attempt to increase the output power by reducing the cycle operation time leads to the emergence of friction and the reduction of the cycle efficiency. The optimization of this tradeoff has motivated a substantial body of literature. Pioneering works on the finite-time thermodynamics of classical heat engines established that the performance at maximum power is characterized by the so-called Curzon–Ahlborn efficiency  $\eta_{CA} = 1 - \sqrt{1 - \eta_C}$  [14]. Finite-time thermodynamics was consolidated as an important subject area of research, see, e.g., [15, 16]. In the quantum domain, following the work by Scovil and Schulz-DuBois [9], early descriptions of quantum heat engines emphasized their operation in finite time. Subsequent works accumulated evidence indicating that the trade off between efficiency and power holds as well in the quantum realm [17–24].

Over the last few years, however, it has been shown that this tradeoff is not fundamental and can be avoided. Even more, it is possible in principle to operate a heat engine at maximum efficiency and high output power [25–31]. Such a friction-

less quantum heat engine may be engineered using shortcuts to adiabaticity (STA): nonadiabatic protocols that lead to the same final state that would be achieved under slow adiabatic driving [32]. In addition, nonadiabatic many-particle effects have been shown to boost the performance of quantum thermal machines [33]. This chapter summarizes these developments, focusing on the description of quantum heat engines (QHEs) with an emphasis on their operation in finite time.

## 5.2 Trapped Quantum Fluids as Working Media

The substance that performs work and on which work is also done in different stages of a thermodynamic cycle is generally referred to as the working substance or working medium. In classical thermodynamics, the performance of a heat engine is largely independent of its choice. Theoretical models of quantum heat engines have shown that this conclusion often holds in the quantum domain under slow driving, but not generally [34, 35]. In addition, the operation of the engine away from equilibrium generally exhibits specific signatures of the working medium. This may result from using nonthermal reservoirs or operating the cycle in finite-time, i.e., in a non-adiabatic fashion. The quest for quantum effects that boost the performance in heat engines arises in this scenario as a natural pursuit. The choice of the working substance is further guided by the range of available quantum platforms, simplicity and aesthetic appeal. Quantum systems with discrete energy levels or a continuous spectra can be considered.

In what follows, we shall focus on the realization of heat engines with confined particles in a time-dependent harmonic trap as a working medium [33]. In particular, we consider the family of quantum many-body systems with Hamiltonian

$$\hat{H}(t) = \sum_{i=1}^N \left[ -\frac{\hbar^2}{2m} \nabla_i^2 + \frac{1}{2} m \omega(t)^2 \mathbf{r}_i^2 \right] + \sum_{i < j} V(\mathbf{r}_i - \mathbf{r}_j), \quad (5.1)$$

that describes  $N$  particles of equal mass  $m$  in an isotropic harmonic trap with frequency  $\omega(t)$ . It will prove convenient to choose the pairwise interaction  $V(\mathbf{r})$  as a homogeneous function of degree  $-2$ , satisfying,

$$V(b\mathbf{r}) = b^{-2} V(\mathbf{r}). \quad (5.2)$$

This choice accounts for a variety of many-body systems including free noninteracting gases, quantum fluids with hard-core interactions, inverse-square interactions models, as well as Bose gases with s-wave contact interactions in two spatial dimensions, among other examples. It further simplifies the dynamics under a modulation of the trapping frequency  $\omega(t)$ , due to the emergence of scale-invariance as a dynamical symmetry [36–40].

In the adiabatic limit achieved under slow driving of  $\omega(t)$ , scale invariance determines the instantaneous mean energy

$$\langle \hat{H}(t) \rangle_{\text{ad}} = \frac{1}{b_{\text{ad}}^2} \langle \hat{H}(0) \rangle , \quad (5.3)$$

where the adiabatic scaling factor is given by

$$b_{\text{ad}} = \sqrt{\omega(0)/\omega(t)} . \quad (5.4)$$

Under arbitrary driving, the nonadiabatic mean energy is fixed by the initial mean energy, particle position fluctuations and squeezing according to [33]

$$\langle \hat{H}(t) \rangle = \frac{1}{b^2} \langle \hat{H}(0) \rangle - \frac{m}{2} (b\ddot{b} - \dot{b}^2) \sum_{i=1}^N \langle \mathbf{r}_i^2(0) \rangle + \frac{\dot{b}}{2b} \sum_{i=1}^N \langle \{\mathbf{r}_i, \mathbf{p}_i\}(0) \rangle . \quad (5.5)$$

Here, the time-dependent coefficients are fixed by the scaling factor, that is a solution of the Ermakov equation

$$\ddot{b} + \omega(t)^2 b = \omega_0^2 b^{-3} . \quad (5.6)$$

Provided that the initial state is at thermal equilibrium, so that the squeezing term vanishes, the nonadiabatic mean-energy following a variation of the trapping frequency  $\omega(t)$  is given by the relation

$$\langle \hat{H}(t) \rangle = Q^*(t) \langle \hat{H}(t) \rangle_{\text{ad}} , \quad (5.7)$$

where the nonadiabatic factor  $Q^* \geq 1$  reads

$$Q^*(t) = \frac{\omega_0}{\omega(t)} \left( \frac{1}{2b^2} + \frac{\omega(t)^2}{2\omega_0^2} b^2 + \frac{\dot{b}^2}{2\omega_0^2} \right) . \quad (5.8)$$

Here  $b(t)$  is the solution of (5.6) subject to the boundary conditions  $b(0) = 1$  and  $\dot{b}(0) = 0$ , to account for the initial equilibrium state. The nonadiabatic factor  $Q^*$  was first discussed by Husimi in the study of a single-particle driven oscillator [41]. As we shall see, values of  $Q^* > 1$  limit the finite-time efficiency of thermodynamic cycles. We note that in the adiabatic limit time derivatives of the scaling factor can be ignored and

$$b(t) \rightarrow b_{\text{ad}} = \sqrt{\omega_0/\omega(t)} , \quad (5.9)$$

$$Q^*(t) \rightarrow Q_{\text{ad}}^*(t) = 1 . \quad (5.10)$$

In the next section, we shall describe a many-particle QHE based on an Otto cycle and consider thermal equilibrium states in the canonical ensemble at (inverse) temperature  $\beta$  described by a density matrix of the form

$$\hat{\rho} = \frac{e^{-\beta \hat{H}}}{\text{tr}(e^{-\beta \hat{H}})} . \quad (5.11)$$

### 5.3 The Quantum Otto Cycle: Finite-Time Thermodynamics

The quantum Otto cycle consists of four consecutive strokes performed on a quantum system that acts as a working substance [42], as shown in Fig. 5.1:

(1) In a first isentropic stroke ( $A \rightarrow B$ ), the working substance prepared in an equilibrium state at low temperature undergoes a compression induced by increasing the trap frequency  $\omega(t)$ . In this stroke the dynamics is unitary as there is no coupling to the environment. Thus, there is no heat exchange and entropy is conserved. The change in the internal energy constitutes the work input. Upon completion of the stroke, the final state is generally nonthermal and out of equilibrium.

(2) Subsequently, the system is heated up at constant volume to a new thermal state at high temperature ( $B \rightarrow C$ ). As the Hamiltonian of the working substance is kept constant, the change of internal energy is exclusively given by the heat absorbed, and no work is done in this stroke. Once at equilibrium the system is decoupled from the hot reservoir. This assumes that no work is done by coupling and decoupling the working substance to and from the hot reservoir, an approximation which can be called into question beyond the weak coupling limit.

(3) The equilibrium state at inverse temperature  $\beta_h$  is taken as the starting point of an expansion stroke ( $C \rightarrow D$ ) in which the dynamics is unitary and the work output

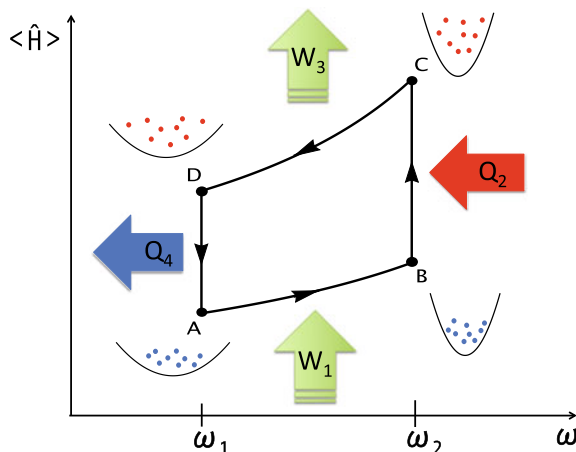


**Fig. 5.1 Many-particle quantum heat engine.** A quantum Otto cycle realized by a quantum fluid as a working medium involves expansion and compression processes in which the frequency of the harmonic trap varies between  $\omega_1$  and  $\omega_2$ . These strokes in which the dynamics is unitary are alternated with heating and cooling processes in which the system Hamiltonian is kept constant and heat is either absorbed or released.

is set by the change in the internal energy of the working substance, that is found in a nonequilibrium state upon completion of the stroke.

(4) The cycle is then completed by a second isochoric stroke ( $D \rightarrow A$ ) in which the working substance thermalizes to the low-temperature equilibrium state at  $\beta_c$ . Again, in this stroke it is assumed that the work done by putting in contact the working substance with the cold reservoir is negligible. The Hamiltonian of the working substance can then be considered constant and the heat released is therefore given by the change in the energy of the working substance.

The efficiency of a heat engine is defined as the total output work per input heat

$$\eta = -\frac{\langle W_1 \rangle + \langle W_3 \rangle}{\langle Q_2 \rangle}, \quad (5.12)$$

where  $\langle W_{1(3)} \rangle = \langle \hat{H} \rangle_{B(D)} - \langle \hat{H} \rangle_{A(C)}$  and  $\langle Q_{2(4)} \rangle = \langle \hat{H} \rangle_{C(A)} - \langle \hat{H} \rangle_{B(D)}$ . As the working substance is decoupled from the thermal reservoir during the isentropic strokes, when the dynamics is unitary, we use the scaling dynamics (5.1) to predict the mean energy according to (5.7). Direct computation yields

$$\langle W_1 \rangle = \langle \hat{H} \rangle_B - \langle \hat{H} \rangle_A = \left( Q_{AB}^* \frac{\omega_2}{\omega_1} - 1 \right) \langle \hat{H} \rangle_A, \quad (5.13a)$$

$$\langle W_3 \rangle = \langle \hat{H} \rangle_D - \langle \hat{H} \rangle_C = \left( Q_{CD}^* \frac{\omega_1}{\omega_2} - 1 \right) \langle \hat{H} \rangle_C, \quad (5.13b)$$

$$\langle Q_2 \rangle = \langle \hat{H} \rangle_C - \langle \hat{H} \rangle_B = \langle \hat{H} \rangle_C - Q_{AB}^* \frac{\omega_2}{\omega_1} \langle \hat{H} \rangle_A, \quad (5.13c)$$

$$\langle Q_4 \rangle = \langle \hat{H} \rangle_D - \langle \hat{H} \rangle_A = Q_{CD}^* \frac{\omega_1}{\omega_2} \langle \hat{H} \rangle_C - \langle \hat{H} \rangle_A, \quad (5.13d)$$

where  $\langle \hat{H} \rangle_A$  and  $\langle \hat{H} \rangle_C$  denote the equilibrium energies of the thermal states parameterized by  $(\omega_1, \beta_c)$  and  $(\omega_2, \beta_h)$ , respectively. A similar analysis was first reported in the study of a quantum heat engine with a single-particle harmonic oscillator as a working medium [20, 23]. Equations (5.13) hold however for the family of many-particle quantum systems described by the Hamiltonian class (5.1) [27, 33]. Further,  $Q_{AB}^*$  and  $Q_{CD}^*$  denote the nonadiabatic factors at the end of the compression and expansion strokes, respectively. Expressions (5.13) assume that no work is done by coupling and decoupling the working medium to and from the heat reservoirs, e.g., in the limit of weak coupling between the working substance and the heat reservoirs. The efficiency of the many-particle quantum heat engine run in finite time is then given by

$$\eta = 1 - \frac{\omega_1}{\omega_2} \left( \frac{Q_{CD}^* \langle \hat{H} \rangle_C - \frac{\omega_2}{\omega_1} \langle \hat{H} \rangle_A}{\langle \hat{H} \rangle_C - Q_{AB}^* \frac{\omega_2}{\omega_1} \langle \hat{H} \rangle_A} \right). \quad (5.14)$$

In the adiabatic limit ( $Q_{AB(CD)}^* \rightarrow 1$ ) the engine operates at the maximum Otto efficiency

$$\eta_{\max} = \eta_O = 1 - \frac{\omega_1}{\omega_2}, \quad (5.15)$$

which is shared as an upper bound by both single- and many-particle quantum and classical Otto cycles. Another relevant limit corresponds to the sudden quench of the trapping frequency between  $\omega_1$  and  $\omega_2$ . The nonadiabatic factor  $Q_{\text{sq}}^* = (\omega_1^2 + \omega_2^2)/(2\omega_1\omega_2)$  [41] is symmetric on  $\omega_1$  and  $\omega_2$ . As a result, it describes both a sudden compression and expansion strokes.

When a compression (expansion) of finite duration  $\tau$  is considered in which the frequency varies monotonically as a function of time we have  $Q_{AB(CD)}^* \leq Q_{\text{sq}}^*$ . Equation (5.14) then implies that the finite-time efficiency  $\eta$  is bounded from below and above as [33]

$$\eta_{\text{sq}} \leq \eta \leq \eta_O, \quad (5.16)$$

where  $\eta_{\text{sq}}$  is the efficiency under a sudden quench. For a monotonic frequency modulation, we have that  $Q^*(\tau) \rightarrow Q_{\text{sq}}^*$  in the sudden-quench limit  $\tau \rightarrow 0$ . In addition, as proved in [33], the efficiency (5.14) is bounded from above by a non-adiabatic Otto limit,

$$\eta \leq 1 - Q_{CD}^* \frac{\omega_1}{\omega_2}, \quad (5.17)$$

that is independent of the number of particles  $N$  and interaction potential  $V$ .

This formula encodes the “tragedy of finite-time thermodynamics” in the many-particle setting: The maximum efficiency is achieved under slow driving, in the adiabatic limit, when the QHE operates at vanishing output power  $-(\langle W_1 \rangle + \langle W_3 \rangle)/\tau_c$  as a result of the requirement for a long cycle time  $\tau_c$ . By contrast, realistic engines operated in finite time achieve a finite output power at the cost of introducing nonadiabatic energy excitations that represent quantum friction and lower the efficiency of the cycle. Note that for the characterization of the engine performance, energy excitations can be associated with friction even if the dynamics along the expansion and compression strokes is unitary. That nonadiabatic effects generally decrease the engine efficiency follows from the fact that  $Q_{AB(CD)}^* \geq 1$  and the expression for the finite-time efficiency (5.14). However, we will show that this trade-off is not fundamental in nature and can be avoided.

## 5.4 Shortcuts to Adiabaticity: Towards a Superadiabatic Otto Cycle

The efficiency of a quantum Otto cycle is limited by the presence of quantum friction generated in the nonadiabatic dynamics of the isentropic strokes. However, there exist

nonadiabatic protocols in which the quantum friction vanishes upon completion of the stroke. To demonstrate this we consider the dynamics of an isentropic stroke in which the working substance is described by the Hamiltonian (5.1). At the beginning of the stroke, the working substance is in equilibrium and  $Q^*(0) = 1$ . We consider the duration of the stroke to be  $\tau$  and look for a shortcut protocol for which quantum friction vanishes upon completion of the stroke, this is,  $Q^*(\tau) = 1$ . We shall refer to such a protocol as a shortcut to adiabaticity (STA) [32]. More generally, a STA is any fast nonadiabatic protocol that provides an alternative to adiabatic evolution, leading to the same final state without the requirement of slow driving.

Whenever the evolution of the working substance exhibits scale invariance, it is possible to design a STA by reverse engineering the dynamics. This approach was first discussed for the single-particle harmonic oscillator in [43] and extended to driven quantum fluids in [37]. Our strategy to design STA, however, focuses on the analysis of the nonadiabatic factor  $Q^*$  in Eq. (5.8) that plays the role of quantum friction. One first singles out a trajectory of the scaling factor  $b(t)$  connecting the initial and final states, both at equilibrium. From the explicit expression for  $Q^*$ , Eq. (5.8), we identify the boundary conditions,

$$b(0) = 1, \quad b(\tau) = b_\tau, \quad (5.18)$$

$$\dot{b}(0) = 0, \quad \dot{b}(\tau) = 0, \quad (5.19)$$

$$\ddot{b}(0) = 0, \quad \ddot{b}(\tau) = 0, \quad (5.20)$$

where the vanishing of  $\ddot{b}$  at the end points  $t = \{0, \tau\}$  is optional and imposed for smoothness of the associated frequency modulation, to be determined. Here,  $b_\tau$  is the expansion or compression scaling factor upon completion of the stroke. Making use of Eqs. (5.18)–(5.20) it is possible to fix the form of an interpolating ansatz of the form  $b(t) = \sum_{n=0}^5 c_n \left(\frac{t}{\tau}\right)^n$ , i.e.,

$$b(t) = 1 + 10(b_\tau - 1) \left(\frac{t}{\tau}\right)^3 - 15(b_\tau - 1) \left(\frac{t}{\tau}\right)^4 + 6(b_\tau - 1) \left(\frac{t}{\tau}\right)^5. \quad (5.21)$$

Having found a trajectory  $b(t)$  of the scaling factor associated with a STA with  $Q^*(\tau) = 1$ , we determine the required modulation of the driving frequency from the Ermakov equation (5.6), as

$$\omega^2(t) = \frac{\omega_0^2}{b^4(t)} - \frac{\ddot{b}(t)}{b(t)}. \quad (5.22)$$

Thus, a nonadiabatic isentropic stroke with this modulation of the trapping frequency is free from friction.

There are closely related approaches to engineer STA. One strategy involves choosing a reference modulation of the trapping frequency  $\omega(t)$  assuming adiabatic dynamics. Setting  $\ddot{b} = 0$  in the Ermakov equation one finds the corresponding adiabatic scaling factor to be given by  $b_{\text{ad}} = [\omega(0)/\omega(t)]^{1/2}$ . A STA by local coun-

terdiabatic driving can then be implemented by changing the trap with the modified frequency [39, 40, 44]

$$\Omega(t)^2 = \omega(t)^2 - \frac{\ddot{b}_{\text{ad}}}{b_{\text{ad}}} = \omega(t)^2 - \frac{3}{4} \left[ \frac{\dot{\omega}(t)}{\omega(t)} \right]^2 + \frac{\ddot{\omega}(t)}{2\omega(t)} . \quad (5.23)$$

For completeness, we also note that scaling laws are not restricted to harmonic traps and can occur in other confinements with specific space and time dependencies [40]. For instance, in a box-like trap, scaling invariance occurs provided that a time-dependent harmonic trap is superimposed during the expansion of the box trap [38]. Currently, there is a variety of experimental techniques that allow for the engineering of arbitrary trapping potentials  $V(\mathbf{r}, t)$  for ultracold atoms, including the use of time-averaged potentials [45, 46] and digital micromirror devices (DMDs) [47].

Superadiabatic strokes have been demonstrated in the laboratory using a unitary Fermi gas confined in an anisotropic harmonic trap as a working medium [30, 48]. The Hamiltonian describing the system is

$$\hat{\mathcal{H}}(t) = \sum_{\sigma=\uparrow,\downarrow} \int d^3\mathbf{r} \hat{\psi}_\sigma^\dagger(\mathbf{r}) \left[ -\frac{\hbar^2}{2m} \nabla^2 + V(\mathbf{r}, t) \right] \hat{\psi}_\sigma(\mathbf{r}) + g \hat{\psi}_\uparrow^\dagger(\mathbf{r}) \hat{\psi}_\downarrow^\dagger(\mathbf{r}) \hat{\psi}_\downarrow(\mathbf{r}) \hat{\psi}_\uparrow(\mathbf{r}) , \quad (5.24)$$

where

$$V(\mathbf{r}, t) = \frac{1}{2} m (\omega_x^2 x^2 + \omega_y^2 y^2 + \omega_z^2 z^2) . \quad (5.25)$$

Here,  $\hat{\psi}_\sigma(\mathbf{r})$  denotes the annihilation field operator for the spin state  $\sigma = \{\uparrow, \downarrow\}$ ,  $g$  is the coupling strength of the s-wave interactions and  $\omega_j$  ( $j = x, y, z$ ) the trap frequencies along the different axes. For finite value of the interaction strength  $g$ , the system lacks scale invariance. However, the unitary limit (in which  $g \rightarrow \infty$ ) can be reached by tuning the interaction strength, i.e., via a Feshbach resonance. The system is then described by a nonrelativistic conformal field theory, with an associated scaling symmetry [49], that can be exploited to implement superadiabatic expansion and compression strokes, as those used in a quantum Otto cycle. Their implementation in the laboratory was reported in [30], that we briefly summarize next. The spin-1/2 unitary Fermi gas was prepared using a balanced mixture of  ${}^6\text{Li}$  fermions in the lowest hyperfine states. By bringing the atomic cloud at resonance, the scattering length governing the pairwise interactions can be tuned to exceed the interparticle distance and reach the unitary regime. A sketch of the experimental setup is shown in Fig. 5.2. The effectively harmonic confinement in three dimensions was specially designed for an accurate and easy control of the trapping frequencies and their modulation in time. The theoretical analysis presented in the preceding sections for the isotropic trap can be extended to account for the anisotropy of the trap [30]. Indeed, despite the anisotropy of the trap, it is possible to engineer an isotropic expansion factor  $b(t)$  that is common to all axes (x, y and z). Figure 5.2 reports the time evolution of the nonadiabatic factor during an expansion and a compression.

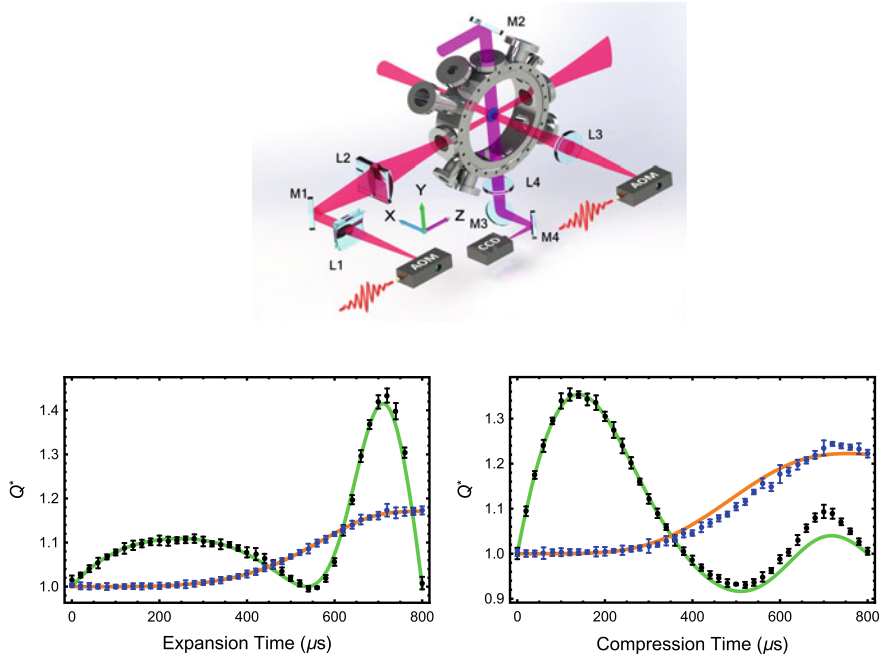


**Fig. 5.2 Friction-free superadiabatic strokes.** Top: Experimental setup. The optical dipole trap is specially designed for a flexible control of the trap frequencies and consists of two orthogonal far-off resonance laser beams. One beam is focused only in one spatial direction (x), i.e., providing confinement along this axis. A second, perpendicular laser beam confines the 3D unitary Fermi gas along the y and z axes. The frequency in the x direction mostly depends on the power of the first beam. Similarly, the second beam determines the frequencies in the y and z directions. The frequency aspect ratio of the trap can be simply controlled by precisely adjusting the power ratio of the two beams. Bottom left: Evolution of the nonadiabatic factor  $Q^*$  along an expansion stroke with the unitary Fermi gas as a working substance. In the course of the superadiabatic stroke,  $Q^*$  fluctuates reaching the value  $Q^* = 1$  at the end of the expansion. The green solid line corresponds to the theoretical prediction and accurately matches the experimental data, in black. By contrast, a nonadiabatic expansion stroke  $Q^*$  grows monotonically as a function of time and acquires final values  $Q^* > 1$  associated with quantum friction. The theoretical prediction is plotted as a red solid line, in agreement with the experimental data, in blue. See [30] for details of the experiment and the parameters used. Bottom right: Evolution of the nonadiabatic factor  $Q^*$  along a superadiabatic compression stroke with the unitary Fermi gas as a working substance. The final value of  $Q^* = 1$  in a superadiabatic compression but takes values  $Q^* > 1$  in a general nonadiabatic stroke. Small discrepancies are observed in the transient fluctuations between the theoretical prediction (solid lines) and experimental data (symbols).

In both cases, the final value of the nonadiabatic factor  $Q^*$  reduces to the identity upon the completion of the superadiabatic stroke. By contrast, a generic nonadiabatic stroke results in values of  $Q^*(\tau) > 1$ , that are associated with quantum friction.

Note that the above analysis does not make reference to the isochoric strokes, that are assumed to be ideal (friction free) leading to the perfect thermalization of the working substance. By combining the superadiabatic expansion and compression demonstrated in [30] with the isochoric heating and cooling strokes, one can then envision the realization of a superadiabatic Otto cycle.

## 5.5 Shortcuts to Adiabaticity by Counterdiabatic Driving

In the preceding sections we have focused on the use of quantum fluids as a working medium. The realization of STA in this context is greatly simplified due to the presence of scale invariance. In what follows we introduce a universal technique to design STA in arbitrary quantum systems. It involves acting on a system Hamiltonian (e.g., describing the working medium) with auxiliary controls. Determining the later requires knowledge of the spectral properties of the system, which may be unavailable in complex many-body cases such as the quantum fluids we have discussed.

Consider a time-dependent Hamiltonian  $\hat{H}(t)$  with instantaneous eigenvalues  $\{\varepsilon_n(t)\}$  and eigenstates  $\{|n(t)\rangle\}$ , so that

$$\hat{H}(t)|n(t)\rangle = \varepsilon_n(t)|n(t)\rangle . \quad (5.26)$$

We pose the problem of driving an initial state  $|n(0)\rangle$  to  $|n(\tau)\rangle$  in a given finite time,  $\tau$ , generally short enough for the dynamics to remain adiabatic. A technique which achieves this goal is the so-called counterdiabatic driving (CD) technique [50, 51], also known as transitionless quantum driving [52].

Whenever  $\hat{H}(t)$  is slowly-varying, the adiabatic approximation provides an approximate solution  $|\psi_n^{\text{ad}}(t)\rangle$  of the time-dependent Schrödinger equation, i.e.,

$$i\hbar \frac{d}{dt} |\psi_n^{\text{ad}}(t)\rangle \approx \hat{H}(t) |\psi_n^{\text{ad}}(t)\rangle . \quad (5.27)$$

Specifically, when the system is initialized in the  $n$ th eigenstate  $|n(0)\rangle$ , the evolution follows the instantaneous eigenstate  $|n(t)\rangle$  as

$$|\psi_n^{\text{ad}}(t)\rangle = \exp \left( -i \int_0^t \frac{\varepsilon_n(s)}{\hbar} ds - \int_0^t \langle n(s) | \frac{d}{ds} |n(s)\rangle ds \right) |n(t)\rangle , \quad (5.28)$$

where the exponential term includes the dynamical and geometric phases [53].

The central goal of CD is to find the so-called counterdiabatic Hamiltonian  $\hat{H}_{\text{CD}}$  such that the adiabatic approximation  $|\psi_n^{\text{ad}}(t)\rangle$  to the dynamic generated by  $\hat{H}$  becomes the exact solution of the time-dependent Schrödinger equation with  $\hat{H}_{\text{CD}}$

$$i\hbar \frac{d}{dt} |\psi_n^{\text{ad}}(t)\rangle = \hat{H}_{\text{CD}} |\psi_n^{\text{ad}}(t)\rangle , \quad (5.29)$$

without the requirement of slow driving.

We assume that  $\hat{H}_{\text{CD}}$  is self-adjoint and look for the unitary time-evolution operator,  $\hat{U}_{\text{CD}}(t, t' = 0)$  that guides the dynamics through the adiabatic reference trajectory

$$|\psi_n^{\text{ad}}(t)\rangle = \hat{U}_{\text{CD}}(t, 0)|n(0)\rangle \quad (5.30)$$

for all  $|n(0)\rangle$ . As a result,  $\hat{U}_{\text{CD}}(t, 0)$  also obeys the time-dependent Schrödinger equation (TDSE)

$$i\hbar \frac{d}{dt} \hat{U}_{\text{CD}}(t, 0) = \hat{H}_{\text{CD}} \hat{U}_{\text{CD}}(t, 0) . \quad (5.31)$$

The desired Hamiltonian can then be obtained from the time-evolution operator using the identity

$$\hat{H}_{\text{CD}} = i\hbar \left[ \frac{d}{dt} \hat{U}_{\text{CD}}(t, 0) \right] \hat{U}_{\text{CD}}(t, 0)^{\dagger} . \quad (5.32)$$

By construction, the time evolution operator is given by

$$\hat{U}_{\text{CD}}(t, 0) = \sum_n |\psi_n^{\text{ad}}(t)\rangle \langle n(0)| , \quad (5.33)$$

whence it follows that the counterdiabatic Hamiltonian can be expressed as the sum

$$\hat{H}_{\text{CD}}(t) = \hat{H}(t) + \hat{H}_1(t) \quad (5.34)$$

of the uncontrolled system Hamiltonian  $\hat{H}(t)$  and an auxiliary counterdiabatic term

$$\hat{H}_1(t) = i\hbar \sum_n (|d_t n\rangle \langle n| - \langle n| d_t n\rangle |n\rangle \langle n|) . \quad (5.35)$$

The first term in the right hand side in Eq. (5.35) is responsible for suppressing excitations away from the  $n$ th mode while the second one accounts for the Berry phase. We notice that whenever the spectrum of the driven Hamiltonian  $\hat{H}(t)$  is nondegenerate, we can rewrite the auxiliary term as

$$\hat{H}_1 = i\hbar \sum_n \sum_{m \neq n} \frac{|m\rangle \langle m| \dot{\hat{H}} |n\rangle \langle n|}{\varepsilon_n - \varepsilon_m} , \quad (5.36)$$

where the sum is restricted to values of  $m \neq n$  as the diagonal term is cancelled by the term that generates the Berry phase. This expression is physically very intuitive as it suggests that under the condition for adiabaticity the counterdiabatic driving explicitly vanishes, as it should. Further, it shows that the counterdiabatic term is off-

diagonal in the energy eigenbasis of the system Hamiltonian  $\hat{H}$ . One can thus expect that the physical implementation of the full auxiliary term might be challenging in the laboratory, as it requires carefully tuned matrix elements  $|m\rangle\langle n|$ .

The experimental demonstration of the CD technique has by now been reported in a range of platforms for quantum technologies in quantum systems with simple energy spectra [54–57]. It can be extended to many-body spin systems undergoing a quantum phase transition, at the cost of implementing  $n$ -body interactions [58], which are necessary to suppress the universal formation of excitations and defects [59].

We close this section by emphasizing the nonadiabatic nature of shortcuts to adiabaticity, such as the driving protocols engineered using the counterdiabatic driving technique. We recall that  $|\psi_n^{\text{ad}}(t)\rangle$  is the adiabatic approximation to the TDSE associated with  $\hat{H}$ . At the same time, it is the exact solution of the TDSE associated with  $\hat{H}_{\text{CD}}$ . Given that  $[\hat{H}, \hat{H}_{\text{CD}}] = [\hat{H}, \hat{H}_1] \neq 0$ , these two Hamiltonians do not share a common spectrum and cannot be diagonalized in the same basis. Said differently,  $|\psi_n^{\text{ad}}(t)\rangle$  is diagonal in the eigenbasis of  $\hat{H}$  but not in that of  $\hat{H}_{\text{CD}}$ . As a result, we conclude that  $|\psi_n^{\text{ad}}(t)\rangle$  describes a nonadiabatic trajectory with respect to the instantaneous full counterdiabatic Hamiltonian, including transitions among its instantaneous eigenstates.

## 5.6 Cost of Counterdiabatic Driving

Provided an arbitrary counterdiabatic driving can be implemented, the duration of a STA can be made arbitrarily short. One can try to quantify the cost of implementing a CD scheme by analyzing the amplitude of the auxiliary driving fields as function of the (prescheduled) duration of the process  $\tau$ . Rescaling the time of evolution  $s = t/\tau \in [0, 1]$ , the spectral decomposition of the system Hamiltonian can be written as  $\hat{H}(s) = \sum_n \varepsilon_n(s) \hat{P}_n(s)$  in terms of the projector  $\hat{P}_n(s) = |n(s)\rangle\langle n(s)|$ , where  $|n(s)\rangle$  is the instantaneous energy eigenstate. The auxiliary counterdiabatic term can then be written as

$$\hat{H}_1 = \frac{i\hbar}{\tau} \sum_n \frac{d\hat{P}_n(s)}{ds} \hat{P}_n(s). \quad (5.37)$$

Demirplak and Rice [60] used the Hilbert–Schmidt norm of the auxiliary term  $\hat{H}_1$  to quantify the time-energy cost of counterdiabatic driving, finding

$$\|\hat{H}_1\|^2 = \frac{\hbar^2}{2\tau^2} \sum_n \text{tr} \dot{\hat{P}}_n^2. \quad (5.38)$$

The authors also considered the time-integral of the norm, an analysis that has been further elaborated in [61, 62].

An alternative characterization of the time-energy cost of STA resorts to the study of the energy fluctuations involved along the process [58]. In particular, the energy variance

$$\Delta H_{\text{CD}}^2 = \langle \hat{H}_{\text{CD}}^2 \rangle - \langle \hat{H}_{\text{CD}} \rangle^2 \quad (5.39)$$

is constrained by a time-energy uncertainty relation, and provides an upper bound to the speed of evolution in Hilbert space. For the total Hamiltonian of the system given by the sum of the system Hamiltonian and the auxiliary control fields, it was found that the energy variance equals the second moment of the control field. In particular, for the driving of a single eigenstate

$$\Delta H_{\text{CD}}^2(t) = \langle n(t) | \hat{H}_1^2(t) | n(t) \rangle . \quad (5.40)$$

In turn, the later acquires a geometric interpretation in terms of the fidelity susceptibility  $\chi_f^{(n)}(\lambda)$  that rules the decay of the overlap between an eigenstate of the Hamiltonian  $\hat{H}(t) = \hat{H}[\lambda(t)]$  and the adiabatically continued eigenstate under a small variation of the parameter  $\lambda$  [63]

$$|\langle n(\lambda) | n(\lambda + \delta) \rangle|^2 = 1 - \delta^2 \chi_f^{(n)}(\lambda) + \mathcal{O}(\lambda^3) . \quad (5.41)$$

This is indeed the case as [58]

$$\begin{aligned} \langle n(t) | \hat{H}_1^2(t) | n(t) \rangle &= \dot{\lambda}^2 \chi_f^{(n)}(\lambda) \\ &= \dot{\lambda}^2 \sum_{m \neq n} \frac{|\langle m(\lambda) | \frac{d}{d\lambda} \hat{H}_0 | n(\lambda) \rangle|^2}{|\varepsilon_m - \varepsilon_n|^2} . \end{aligned} \quad (5.42)$$

More recently, the thermodynamic cost of STA was analyzed by studying quantum work fluctuations [64, 65]. For systems undergoing unitary dynamics, a possible definition of the work involved in driving the system from an initial Hamiltonian  $\hat{H}(0)$  to a final one  $\hat{H}(t)$  requires two energy measurements, one at the beginning of the process ( $t' = 0$ ) and a second one upon its completion ( $t' = t$ ) [66–68]. Denoting the spectral decomposition of the instantaneous CD Hamiltonian by  $\hat{H}_{\text{CD}}(t) = \sum_n E_n(t) |E_n(t)\rangle \langle E_n(t)|$ , the explicit expression for the work probability distribution  $P[W(t)]$  associated with the CD is given by

$$P[W(t)] := \sum_{k,n} p_n^0 p_{n \rightarrow k}^t \delta[W(t) - (E_k(t) - E_n(0))] . \quad (5.43)$$

The probability for the initial state  $\hat{\rho}$  to be found in the  $n$ th eigenmode is thus given by  $p_n^0 = \langle E_n(0) | \hat{\rho} | E_n(0) \rangle$ , while the transition probability from the  $n$ th mode at  $t = 0$  to the  $k$ th mode at time  $t$  is given by  $p_{n \rightarrow k}^t = |\langle E_k(t) | \hat{U}_{\text{CD}}(t, 0) | E_n(0) \rangle|^2$ . In the implementation of CD, one is generally interested in the case in which the auxiliary

control field  $\hat{H}_1$  vanishes at the beginning and end of the driving protocol so that  $\hat{H}_{\text{CD}} = \hat{H}$  at  $t = \{0, \tau\}$ . As a result, at these two instances of time (and only then),  $E_n(t) = \varepsilon_n(t)$  and  $|E_n(t)\rangle = |\varepsilon_n(t)\rangle$ .

We first note the work statistics in the adiabatic limit. Then,  $H_1$  strictly vanishes,  $\hat{H}_{\text{CD}}(t) = \hat{H}(t)$ , and the transition probability becomes the Kronecker delta,  $p_{n \rightarrow k}^t = \delta_{k,n}$  for all  $t$ . The work probability distribution under adiabatic evolution is thus

$$P_{\text{ad}}[W(t)] = \sum_n p_n^0 \delta[W(t) - W_{\text{ad}}^{(n)}(t)], \quad (5.44)$$

where  $W_{\text{ad}}^{(n)}(t) := \varepsilon_n(t) - \varepsilon_n(0)$  is the work cost along the adiabatic trajectory of the  $n$ th eigenmode. In particular, the mean work is given by

$$\langle W(t) \rangle_{\text{ad}} := \int dW P_{\text{ad}}[W] W(t) = \sum_n p_n^0 [\varepsilon_n(t) - \varepsilon_n(0)]. \quad (5.45)$$

In a STA, given that upon completion of the protocol  $\hat{H}(\tau)$  remains constant and  $\hat{H}_1(\tau)$  vanishes, the work probability distribution reads

$$P_{\text{CD}}[W(\tau)] = P_{\text{ad}}[W(\tau)]. \quad (5.46)$$

Therefore, CD successfully reproduces the work statistics under slow driving, and in this sense, it has no thermodynamic cost.

Along the STA ( $0 < t < \tau$ ), however, CD does modify the work statistics, i.e.,  $P_{\text{CD}}(W)$  differs from  $P_{\text{ad}}[W(t)]$ . Nonetheless, it satisfies two remarkable properties. First, the mean work identically matches the adiabatic value

$$\langle W(t) \rangle = \langle W(t) \rangle_{\text{ad}}. \quad (5.47)$$

Said differently, the mean work done by the auxiliary counterdiabatic term vanishes for all  $0 \leq t \leq \tau$ .

Second, CD enhances work fluctuations. If the system Hamiltonian  $\hat{H}(\lambda)$  depends explicitly on a set of parameters  $\lambda = (\lambda^1, \dots, \lambda^N)$ , the excess of the work variance over the adiabatic value is precisely given by

$$\text{Var}[W(t)] - \text{Var}[W(t)]_{\text{ad}} = \hbar^2 \sum_n p_n^0 g_{\mu\nu}^{(n)} \dot{\lambda}^\mu \dot{\lambda}^\nu. \quad (5.48)$$

The term in the right hand side is the average of the quantity  $g_{\mu\nu}^{(n)}$  weighted with the occupation  $p_n^0$  of the energy levels following the first projective energy measurement. As  $g_{\mu\nu}^{(n)}$  is the real part of the quantum geometric tensor  $Q_{\mu\nu}^{(n)}$  of the  $|n(t)\rangle$ -state manifold [69],

$$Q_{\mu\nu}^{(n)} := \langle \partial_\mu n(t) | [1 - |n(t)\rangle \langle n(t)|] | \partial_\nu n(t) \rangle, \quad (5.49)$$

the broadening of the work distribution is dictated by the geometry of the Hilbert space. When the system Hamiltonian is modulated by a single parameter,  $g_{\mu\mu}^{(n)} = \chi_f^{(n)}$ . Using the identity (5.49) and analyzing the time-average excess of work fluctuations, it is also possible to derive work-time uncertainty relations [64, 65]. The excess of work fluctuations induced by CD, Eq. (5.48), has recently been verified experimentally using a superconducting Xmon qubit [70].

We conclude this section by pointing out that a common feature among the different approaches to quantify the cost of STA is that  $\|\hat{H}_1\|^2$ ,  $\Delta H_{\text{CD}}^2(t)$  and  $\text{Var}[W(t)] - \text{Var}[W(t)]_{\text{ad}}$  all diverge as  $1/\tau^2$  as the protocol duration  $\tau$  is reduced. This is consistent with the fact that the above quantities are ultimately quadratic in the auxiliary control term  $\hat{H}_1$ . This scaling with the duration  $\tau$  is specific of counterdiabatic driving and can differ from that in related STA protocols in which the evolution is generated by a unitarily equivalent Hamiltonian, an approach often referred to as local counterdiabatic driving [30, 57], see as well [61]. In addition, counterdiabatic driving generates coherence in the instantaneous energy eigenbasis along the STA. In the presence of decoherence, the work input and output associated with the compression and expansion strokes can be thus affected [71].

## 5.7 Choice of Working Medium, Many-Particle Quantum Effects and Quantum Supremacy

We have seen that by using STA, an Otto cycle can be operated in finite-time without friction (assuming friction associated with the heating and cooling strokes to be negligible). In this section we focus on the finite-time thermodynamics in the presence of friction, e.g., with an efficiency below the maximum value. The performance of the engine can then exhibit a dependence on the nature of the working medium. Which kind of substance would be optimal?

Jaramillo et al. [33] considered a fixed number of particles  $N$  for the working medium and compared the performance of one single many-particle heat engine with an ensemble of  $N$  single-particle heat engines. In doing so, it was shown that it is possible to find scenarios characterized by quantum supremacy, a many-particle quantum enhancement of the performance with no classical counterpart.

This effect was illustrated with a working medium consisting of  $N$  bosons in an effectively one-dimensional harmonic trap and subject to inverse-square pairwise interactions [72, 73],

$$\hat{H}(t) = \sum_{i=1}^N \left[ -\frac{\hbar^2}{2m} \frac{\partial^2}{\partial z_i^2} + \frac{1}{2} m\omega(t)^2 z_i^2 \right] + \frac{\hbar^2}{m} \sum_{i < j} \frac{\lambda(\lambda-1)}{(z_i - z_j)^2}, \quad (5.50)$$

where  $\lambda \geq 0$  is the interaction strength. This instance of (5.1) is the (rational) Calogero-Sutherland model that reduces to an ideal Bose gas for  $\lambda = 0$  and to the Tonks-Girardeau gas (hard-core bosons) for  $\lambda = 1$  [74, 75], the thermodynamics

of which is equivalent to that of polarized fermions. For arbitrary  $\lambda$ , the Calogero-Sutherland model can be interpreted as an ideal gas of particles obeying generalized-exclusion statistics [76–78].

The comparative performance in both scenarios can be assessed via the power and efficiency ratios, defined respectively by

$$\frac{P^{(N,\lambda)}}{N \times P^{(1,\lambda)}}, \quad \frac{\eta^{(N,\lambda)}}{\eta^{(1,\lambda)}}. \quad (5.51)$$

In an ample regime of parameters, it was shown that both ratios can simultaneously increase and surpass unity. The enhancement of the efficiency is maximum for an ideal Bose gas ( $\lambda = 0$ ). While the effect is robust in the presence of interactions, the ensemble of single-particle engines can however outperform the many-particle one for moderate values of  $\lambda$ , e.g., for hard-core bosons (fermions).

Bengtsson et al. have identified a similar many-particle boost in the average work output in the adiabatic limit of a quantum Szilard engine, when an attractive Bose gas is chosen as a working medium [35]. Zheng and Poletti have uncovered quantum statistical effects in the performance of an adiabatic Otto cycle for a given working medium (ideal Bose and Fermi gases), confined in non-harmonic traps [34]. It has further been shown that the performance of an Otto cycle can also be enhanced whenever the working substance exhibits critical behavior [79]. An analysis of this cycle with a working medium exhibiting many-body localization has also been reported [80].

Overall, the optimal choice of the working substance for a given quantum cycle seems to be largely unexplored. Further, this choice may depend on the assessment of the performance as the characterization of a quantum thermodynamic cycle does not necessarily carry over many cycles when work is measured via projective energy measurements [81]. Nonetheless, it seems that a rich variety of scenarios can be found in which many-particle quantum effects can lead to an improvement of the performance over classical many-particle cycles as well as ensembles of single-particle quantum machines.

## 5.8 Quo Vadis?

The time of writing is particularly exciting concerning experimental progress towards the realization of quantum heat engines at the nanoscale. Using trapped-ion technology a single atom heat engine has been realized [82]. A quantum heat engine based on an Otto cycle has been implemented using a spin-1/2 system and nuclear magnetic resonance techniques [83]. Quantum refrigerators have as well been reported using superconducting circuits [84] and trapped ions [85]. The possibility of combining these setups with superadiabatic strokes such as those reported in [30] suggest that the realization of friction-free thermal machines may be feasible in the near future.

This prospect is enhanced by the fact that superadiabatic machines are not necessarily restricted to the quantum domain and can be envisioned in classical systems as well, such as colloidal heat engines [86].

The current description of quantum heat engines based on a thermodynamic cycle consisting of multiple strokes disregards the explicit mechanism for work outcoupling, this is, the coupling between the working medium and an external work storage. As a result, work is merely associated with a change of a parameter of the working-medium Hamiltonian, such as the frequency of the trap in the quantum Otto cycle. A direct implementation of such scheme can be envisioned via external active control, inducing a given modulation in time of the Hamiltonian parameter.

Useful heat engines are expected to run autonomously without the requirement for external controls. With an eye on experimental implementations, it is therefore necessary to transcend the current description. This is likely to require a quantum description of the full engine including the fuel, working substance, and work storage. Such description will no doubt be less universal, but is likely to be a highly fruitful pursuit. Encouraging steps in this direction include an account of the dynamics of quantum machine that lifts a weight against gravitational field [87] and tilted potentials [88], an autonomous absorption refrigerator in atom-cavity systems [89] as well as an autonomous rotor heat engine [90], discussed in Chap. 9.

We anticipate that the engineering of superadiabatic quantum machines will be at reach in the presence of external active control. By contrast, their autonomous counterpart is likely to prove more challenging. The ultimate cost of STA may therefore arise from its practical implementation. The study of STA has however shown that they can be implemented following simple principles, such as slow driving at the beginning and end of a process [39, 43].

In addition, our discussion of superadiabatic heat engines has focused on the Otto cycle. This choice is motivated by the presence of strokes governed by unitary dynamics, for which STA techniques are well developed. In general thermodynamic cycles (e.g., the Carnot cycle) the dynamics is open (in contact with a heat reservoir) in all stages. The engineering of superadiabatic engines based on such cycles would require the use of STA for open quantum systems, which is an open problem. This challenge would also be faced in continuously driven cycles.

**Acknowledgements** This chapter reports on joint work with Shuoming An, Mathieu Beau, Cyril Chatou, Ivan Coulamy, Pengpeng Diao, Ken Funo, John Goold, Juan Diego Jaramillo, Kihwan Kim, Fang Li, Mauro Paternostro, Marek M. Rams, Masahito Ueda, Shi Yu and Jing-Ning Zhang, and Wojciech H. Zurek. It has further benefited from discussions with Obinna Abah, Sebastian Deffner, Luis Pedro García-Pintos, Fernando J. Gómez-Ruiz, Jiangbin Gong, Christopher Jarzynski, Ronnie Kosloff, Peter Hägggi, Eric Lutz, Doha M. Mesnoui, Victor Mukherjee, José Pascual Palao, Dario Poletti, Stuart A. Rice, Peter Talkner, B. Prasanna Venkatesh, Gentaro Watanabe, and Zhenyu Xu. We acknowledge funding support from the John Templeton Foundation, and UMass Boston (project P20150000029279).

## References

1. I. Prigogine, I. Stengers, *Order out of chaos* (Verso Books, London, 1984)
2. J. Gemmer, G. Mahler, M. Michel, *Quantum Thermo-dynamics: Emergence of Thermodynamic Behavior within Composite Quantum Systems*, LNP 657 (Springer, Berlin, 2004). <https://doi.org/10.1007/b98082>
3. S. Vinjanampathy, J. Anders, *Contemp. Phys.* **57**, 545 (2016). <https://doi.org/10.1080/00107514.2016.1201896>
4. J. Goold, M. Huber, A. Riera, L. del Rio, P. Skrzypczyk, *J. Phys. A: Math. Theor.* **49**, 143001 (2016). <https://doi.org/10.1088/1751-8113/49/14/143001>
5. R. Alicki, *J. Phys. A* **12**, L103 (1979). <https://doi.org/10.1088/0305-4470/12/5/007>
6. R. Kosloff, *J. Chem. Phys.* **80**, 1625 (1984). <https://doi.org/10.1063/1.446862>
7. H.S. Leff, A.F. Rex, *Maxwell's Demon 2: Entropy, Classical and Quantum Information, Computing* (Institute of Physics, Bristol, 2003)
8. S.W. Kim, T. Sagawa, S. De Liberato, M. Ueda, *Phys. Rev. Lett.* **106**, 070401 (2011). <https://doi.org/10.1103/PhysRevLett.106.070401>
9. H. Scovil, E. Schulz-DuBois, *Phys. Rev. Lett.* **2**, 262 (1959). <https://doi.org/10.1103/PhysRevLett.2.262>
10. K.E. Dorfman, D.V. Voronine, S. Mukamel, M.O. Scully, *PNAS* **110**, 2751 (2013). <https://doi.org/10.1073/pnas.1212666110>
11. M.O. Scully, *Phys. Rev. Lett.* **104**, 207701 (2010). <https://doi.org/10.1103/PhysRevLett.104.207701>
12. M.O. Scully, K.R. Chapin, K.E. Dorfman, M. Barnabas Kim, A. Svidzinsky, *PNAS* **108**, 15097 (2011). <https://doi.org/10.1073/pnas.1110234108>
13. C. Creatore, M.A. Parker, S. Emmott, A.W. Chin, *Phys. Rev. Lett.* **111**, 253601 (2013). <https://doi.org/10.1103/PhysRevLett.111.253601>
14. F.L. Curzon, B. Ahlborn, *Am. J. Phys.* **43**, 22 (1975). <https://doi.org/10.1119/1.10023>
15. R.S. Berry, V. Kazakov, S. Sieniutycz, Z. Szwest, A.M. Tsirlin, *Thermodynamic Optimization of Finite-Time Processes*, 1st edn. (Wiley, New York, 2000)
16. P. Salamon, J. Nulton, G. Siragusa, T.R. Andersen, A. Limon, *Energy* **26**, 307 (2001). [https://doi.org/10.1016/S0360-5442\(00\)00059-1](https://doi.org/10.1016/S0360-5442(00)00059-1)
17. E. Geva, R. Kosloff, *J. Chem. Phys.* **96**, 3054 (1992). <https://doi.org/10.1063/1.461951>
18. R. Kosloff, T. Feldmann, *Phys. Rev. E* **65**, 055102(R) (2002). <https://doi.org/10.1103/PhysRevE.65.055102>
19. T. Feldmann, R. Kosloff, *Phys. Rev. E* **68**, 016101 (2003). <https://doi.org/10.1103/PhysRevE.68.016101>
20. Y. Rezek, R. Kosloff, *New J. Phys.* **8**, 83 (2006). <https://doi.org/10.1088/1367-2630/8/5/083>
21. P. Salamon, K.H. Hoffmann, Y. Rezek, R. Kosloff, *Phys. Chem. Chem. Phys.* **11**, 1027 (2009). <https://doi.org/10.1039/B816102J>
22. Y. Rezek, P. Salamon, K.H. Hoffmann, R. Kosloff, *EPL* **85**, 30008 (2009). <https://doi.org/10.1209/0295-5075/85/30008>
23. O. Abah, J. Roßnagel, G. Jacob, S. Deffner, F. Schmidt-Kaler, K. Singer, E. Lutz, *Phys. Rev. Lett.* **109**, 203006 (2012). <https://doi.org/10.1103/PhysRevLett.109.203006>
24. O. Abah, E. Lutz, *EPL* **113**, 60002 (2016). <https://doi.org/10.1209/0295-5075/113/60002>
25. J. Deng, Q. Wang, Z. Liu, P. Hänggi, J. Gong, *Phys. Rev. E* **88**, 062122 (2013). <https://doi.org/10.1103/PhysRevE.88.062122>
26. A. del Campo, J. Goold, M. Paternostro, *Sci. Rep.* **4**, 6208 (2014). <https://doi.org/10.1038/srep06208>
27. M. Beau, J. Jaramillo, A. del Campo, *Entropy* **18**, 168 (2016). <https://doi.org/10.3390/e18050168>
28. L. Chotorlishvili, M. Azimi, S. Stagraczyński, Z. Toklikishvili, M. Schüller, J. Berakdar, *Phys. Rev. E* **94**, 032116 (2016). <https://doi.org/10.1103/PhysRevE.94.032116>
29. O. Abah, E. Lutz, *EPL* **118**, 40005 (2017). <https://doi.org/10.1209/0295-5075/118/40005>

30. S. Deng, A. Chenu, P. Diao, F. Li, S. Yu, I. Coulamy, A. del Campo, H. Wu, Sci. Adv. **4**, eaar5909 (2018). <https://doi.org/10.1126/sciadv.aar5909>
31. J. Li, T. Fogarty, S. Campbell, X. Chen, T. Busch, New J. Phys. **20**, 015005 (2018). <https://doi.org/10.1088/1367-2630/aa9cd8>
32. E. Torrontegui, S. Ibáñez, S. Martínez-Garaot, M. Modugno, A. del Campo, D. Guéry-Odelin, A. Ruschhaupt, X. Chen, J.G. Muga, Adv. At. Mol. Opt. Phys. **62**, 117 (2013). <https://doi.org/10.1016/B978-0-12-408090-4.00002-5>
33. J. Jaramillo, M. Beau, A. del Campo, New J. Phys. **18**, 075019 (2016). <https://doi.org/10.1088/1367-2630/18/7/075019>
34. Y. Zheng, D. Poletti, Phys. Rev. E **92**, 012110 (2015). <https://doi.org/10.1103/PhysRevE.92.012110>
35. J. Bengtsson, M. Nilsson Tengstrand, A. Wacker, P. Samuelsson, M. Ueda, H. Linke, S.M. Reimann, Phys. Rev. Lett. **120**, 100601 (2018). <https://doi.org/10.1103/PhysRevLett.120.100601>
36. P.J. Gambardella, J. Math. Phys. **16**, 1172 (1975). <https://doi.org/10.1063/1.522651>
37. A. del Campo, Phys. Rev. A **84**, 031606(R) (2011). <https://doi.org/10.1103/PhysRevA.84.031606>
38. A. del Campo, M.G. Boshier, Sci. Rep. **2**, 648 (2012). <https://doi.org/10.1038/srep00648>
39. A. del Campo, Phys. Rev. Lett. **111**, 100502 (2013). <https://doi.org/10.1103/PhysRevLett.111.100502>
40. S. Deffner, C. Jarzynski, A. del Campo, Phys. Rev. X **4**, 021013 (2014). <https://doi.org/10.1103/PhysRevX.4.021013>
41. K. Husimi, Prog. Theor. Phys. **9**, 381 (1953). <https://doi.org/10.1143/ptp/9.4.381>
42. R. Kosloff, Y. Rezek, Entropy **19**, 136 (2017). <https://doi.org/10.3390/e19040136>
43. X. Chen, A. Ruschhaupt, S. Schmidt, A. del Campo, D. Guéry-Odelin, J.G. Muga, Phys. Rev. Lett. **104**, 063002 (2010). <https://doi.org/10.1103/PhysRevLett.104.063002>
44. A. del Campo, EPL **96**, 60005 (2011). <https://doi.org/10.1209/0295-5075/96/60005>
45. K. Henderson, C. Ryu, C. MacCormick, M.G. Boshier, New J. Phys. **11**, 043030 (2009). <https://doi.org/10.1088/1367-2630/11/4/043030>
46. T.A. Bell, J.A.P. Glidden, L. Humbert, M.W.J. Bromley, S.A. Haine, M.J. Davis, T.W. Neely, M.A. Baker, H. Rubinsztein-Dunlop, New J. Phys. **18**, 035003 (2016). <https://doi.org/10.1088/1367-2630/18/3/035003>
47. G. Gauthier, I. Lenton, N. McKay Parry, M. Baker, M.J. Davis, H. Rubinsztein-Dunlop, T.W. Neely, Optica **3**, 1136 (2016). <https://doi.org/10.1364/OPTICA.3.001136>
48. S. Deng, P. Diao, Q. Yu, A. del Campo, H. Wu, Phys. Rev. A **97**, 013628 (2018). <https://doi.org/10.1103/PhysRevA.97.013628>
49. Y. Castin, F. Werner, *The BCS-BEC Crossover and the Unitary Fermi Gas*. Lecture Notes in Physics, vol. 836, ed. by W. Zwerger (Springer, Berlin, 2012). <https://doi.org/10.1007/978-3-642-21978-8>
50. M. Demirplak, S.A. Rice, J. Phys. Chem. A **107**, 9937 (2003). <https://doi.org/10.1021/jp030708a>
51. M. Demirplak, S.A. Rice, J. Phys. Chem. B **109**, 6838 (2005). <https://doi.org/10.1021/jp040647w>
52. M.V. Berry, J. Phys. A: Math. Theor. **42**, 365303 (2009). <https://doi.org/10.1088/1751-8113/42/36/365303>
53. M.V. Berry, Proc. R. Soc. Lond. **392**, 45 (1984). <https://doi.org/10.1098/rspa.1984.0023>
54. M.G. Bason, M. Viteau, N. Malossi, P. Huillery, E. Arimondo, D. Ciampini, R. Fazio, V. Giovannetti, R. Mannella, O. Morsch, Nat. Phys. **8**, 147 (2012). <https://doi.org/10.1038/nphys2170>
55. J. Zhang, J. Hyun Shim, I. Niemeyer, T. Taniguchi, T. Teraji, H. Abe, S. Onoda, T. Yamamoto, T. Ohshima, J. Isoya, D. Suter, Phys. Rev. Lett. **110**, 240501 (2013). <https://doi.org/10.1103/PhysRevLett.110.240501>
56. Y.-X. Du, Z.-T. Liang, Y.-C. Li, X.-X. Yue, Q.-X. Lv, W. Huang, X. Chen, H. Yan, S.-L. Zhum, Nat. Commun. **7**, 12479 (2016). <https://doi.org/10.1038/ncomms12479>

57. S. An, S. Lv, A. del Campo, K. Kim, Nat. Commun. **7**, 12999 (2016). <https://doi.org/10.1038/ncomms12999>
58. A. del Campo, M.M. Rams, W.H. Zurek, Phys. Rev. Lett. **109**, 115703 (2012). <https://doi.org/10.1103/PhysRevLett.109.115703>
59. A. del Campo, W.H. Zurek, Int. J. Mod. Phys. A **29**, 1430018 (2014). <https://doi.org/10.1142/S0217751X1430018X>
60. M. Demirplak, S.A. Rice, J. Chem. Phys. **129**, 154111 (2008). <https://doi.org/10.1063/1.2992152>
61. Y. Zheng, S. Campbell, G. De Chiara, D. Poletti, Phys. Rev. A **94**, 042132 (2016). <https://doi.org/10.1103/PhysRevA.94.042132>
62. S. Campbell, S. Deffner, Phys. Rev. Lett. **118**, 100601 (2017). <https://doi.org/10.1103/PhysRevLett.118.100601>
63. S.-J. Gu, Int. J. Mod. Phys. B **24**, 4371 (2010). <https://doi.org/10.1142/S0217979210056335>
64. K. Funo, J.-N. Zhang, C. Chatou, K. Kim, M. Ueda, A. del Campo, Phys. Rev. Lett. **118**, 100602 (2017). <https://doi.org/10.1103/PhysRevLett.118.100602>
65. A. Bravetti, D. Tapias, Phys. Rev. E **96**, 052107 (2017). <https://doi.org/10.1103/PhysRevE.96.052107>
66. H. Tasaki, (2000), <arXiv:cond-mat/0009244>
67. J. Kurchan, (2000), <arXiv:cond-mat/0007360>
68. M. Campisi, P. Hänggi, P. Talkner, Rev. Mod. Phys. **83**, 771 (2011). <https://doi.org/10.1103/RevModPhys.83.771>
69. P. Provost, G. Vallee, Commun. Math. Phys. **76**, 289 (1980). <https://doi.org/10.1007/BF02193559>
70. Z. Zhang, T. Wang, L. Xiang, Z. Jia, P. Duan, W. Cai, Z. Zhan, Z. Zong, J. Wu, L. Sun, Y. Yin, G. Guo, New J. Phys. **20**, 085001 (2018). <https://doi.org/10.1088/1367-2630/aad4e7>
71. A. Levy, A. Kiely, J.G. Muga, R. Kosloff, E. Torrontegui, New J. Phys. **20**, 025006 (2018). <https://doi.org/10.1088/1367-2630/aaa9e5>
72. F. Calogero, J. Math. Phys. **12**, 419 (1971). <https://doi.org/10.1063/1.1665604>
73. B. Sutherland, J. Math. Phys. **12**, 246 (1971). <https://doi.org/10.1063/1.1665584>
74. M.D. Girardeau, J. Math. Phys. **1**, 516 (1960). <https://doi.org/10.1063/1.1703687>
75. M.D. Girardeau, E.M. Wright, J.M. Triscari, Phys. Rev. A **63**, 033601 (2001). <https://doi.org/10.1103/PhysRevA.63.033601>
76. F.D.M. Haldane, Phys. Rev. Lett. **67**, 937 (1991). <https://doi.org/10.1103/PhysRevLett.67.937>
77. Y.-S. Wu, Phys. Rev. Lett. **73**, 922 (1994). <https://doi.org/10.1103/PhysRevLett.73.922>
78. M.V.N. Murthy, R. Shankar, Phys. Rev. Lett. **73**, 3331 (1994). <https://doi.org/10.1103/PhysRevLett.73.3331>
79. M. Campisi, R. Fazio, Nat. Commun. **7**, 11895 (2016). <https://doi.org/10.1038/ncomms11895>
80. N. Yunger Halpern, C. David White, S. Gopalakrishnan, G. Refael, Phys. Rev. B **99**, 024203 (2019). <https://doi.org/10.1103/PhysRevB.99.024203>
81. G. Watanabe, B.P. Venkatesh, P. Talkner, A. del Campo, Phys. Rev. Lett. **118**, 050601 (2017). <https://doi.org/10.1103/PhysRevLett.118.050601>
82. J. Roßnagel, S.T. Dawkins, K.N. Tolazzi, O. Abah, E. Lutz, F. Schmidt-Kaler, K. Singer, Science **352**, 325 (2016). <https://doi.org/10.1126/science.aad6320>
83. J.P.S. Peterson, T.B. Batalhão, M. Herrera, A.M. Souza, R.S. Sarthour, I.S. Oliveira, R.M. Serra (2018), <arXiv:1803.06021>
84. K.Y. Tan, M. Partanen, R.E. Lake, J. Govenius, S. Masuda, M. Möttönen, Nat. Commun. **8**, 15189 (2017). <https://doi.org/10.1038/ncomms15189>
85. G. Maslennikov, S. Ding, R. Hablitzel, J. Gan, A. Roulet, S. Nimmrichter, J. Dai, V. Scarani, D. Matsukevich (2017). <https://doi.org/10.1038/s41467-018-08090-0>
86. I.A. Martínez, E. Roldán, L. Dinis, R.A. Rica, Soft Matter **13**, 22 (2017). <https://doi.org/10.1039/C6SM00923A>
87. L. Gilz, E.P. Thesing, J.R. Anglin, Phys. Rev. E **94**, 042127 (2016). <https://doi.org/10.1103/PhysRevE.94.042127>

88. C. Teo, U. Bissbort, D. Poletti, Phys. Rev. E **95**, 030102(R) (2017). <https://doi.org/10.1103/PhysRevE.95.030102>
89. M.T. Mitchison, M. Huber, J. Prior, M.P. Woods, M.B. Plenio, Quantum Sci. Technol. **1**, 015001 (2016). <https://doi.org/10.1088/2058-9565/1/1/015001>
90. A. Roulet, S. Nimmrichter, J.M. Arrazola, S. Seah, V. Scarani, Phys. Rev. E **95**, 062131 (2017). <https://doi.org/10.1103/PhysRevE.95.062131>

# Chapter 6

## Physical Implementations of Quantum Absorption Refrigerators



Mark T. Mitchison and Patrick P. Potts

The investigation of quantum thermal machines is a subfield of quantum thermodynamics which is of particular practical relevance. A thermal machine is a device which utilizes a temperature bias to achieve some useful task (for recent reviews see e.g. [1–6] as well as Chap. 1, Part I). The nature of this task can vary, with the most prominent example being the production of work in heat engines. Further examples include the creation of entanglement [7], the estimation of temperature [8] and the measurement of time [9].

This chapter discusses physical implementations of quantum absorption refrigerators. There are two compelling reasons which motivate the pursuit of implementing exactly this thermal machine. First, the absorption refrigerator is an autonomous thermal machine. Autonomous machines only require static biases of temperature and/or chemical potential and do not require any time-dependent control. Therefore, they dispense of any controversy over the definition of work in the quantum regime (see also Part II) as well as the energetic cost of maintaining control over time-dependent fields [9–11]. Furthermore, autonomous machines connect to naturally occurring processes (e.g., photosynthesis [12–14]), where no external control

---

Author, Patrick P. Potts, is formerly known as Patrick P. Hofer.

---

M. T. Mitchison (✉)

Institut für Theoretische Physik, Universität Ulm, Albert-Einstein Allee 11, 89069 Ulm, Germany

e-mail: markTmitchison@gmail.com

P. P. Potts

Department of Applied Physics, University of Geneva, Chemin de Pinchat 22, 1211 Geneva, Switzerland

e-mail: patrick.hofer@teorfys.lu.se

P. P. Potts

Physics Department and NanoLund, Lund University, 22100 Lund, Sweden

is needed to harness energy. They are thus promising candidates for harvesting waste heat from other processes or naturally abundant (thermal) energy sources. The second reason why the quantum absorption refrigerator is of great practical relevance is the fact that it is a refrigerator. As discussed below, the quantum absorption refrigerator can stabilize single degrees of freedom in low-entropy states. The ability to initiate a quantum system in a low-entropy state is crucial for most experiments in the quantum regime. In addition to performing state preparation, implementing a quantum absorption refrigerator allows for investigating the fundamental physics of this important process, illuminating its capabilities and limitations.

Since the initial theoretical conception of quantum absorption refrigerators [15–17], several experimental proposals have been put forward [18–22], with one experiment having realized a quantum absorption refrigerator in a trapped-ion system [23]. Here, we focus on the setups described in Refs. [21, 22], in the context of cavity and circuit quantum electrodynamics (QED). These involve different physical degrees of freedom and operate in distinct regimes of energy, temperature, and cooling performance. Nevertheless, as we shall explain, both can be understood in terms of the concept of *virtual temperature* [24, 25], which provides a unifying framework for understanding autonomous thermal machines.

The rest of this chapter is structured as follows: In Sect. 6.1, the theory of the quantum absorption refrigerator and the relevant concepts and mechanisms are reviewed. Physical implementations in the setting of cavity and circuit QED are then discussed in Sects. 6.2 and 6.3. The chapter concludes with a comparison of the two implementations and an outlook in Sect. 6.4.

## 6.1 The Quantum Absorption Refrigerator

Unlike the refrigerator found in a typical kitchen, an absorption refrigerator does not rely on energy in the form of mechanical work. Instead, an absorption refrigerator harnesses the spontaneous flow of heat from a hot bath into the environment in order to perform cooling. Let us first analyze the thermodynamics of a generic absorption refrigerator before introducing its quantum realization.

An absorption refrigerator interacts with three thermal reservoirs: a cold one at temperature  $T_c$  representing the body to be cooled, a reservoir at room temperature  $T_r$  representing the environment, and a hot reservoir at temperature  $T_h$  which provides a source of free energy (see Fig. 6.1), with  $T_c \leq T_r < T_h$ . Suppose that the refrigerator absorbs quantities of heat  $\delta Q_h$  from the hot reservoir and  $\delta Q_c$  from the cold reservoir, while dumping  $\delta Q_r$  heat into the environment. Under steady-state conditions, and assuming the ideal case where the internal mechanism of the refrigerator is frictionless and without heat leaks [26], the first law of thermodynamics reads as

$$\delta Q_c + \delta Q_h = \delta Q_r. \quad (6.1)$$

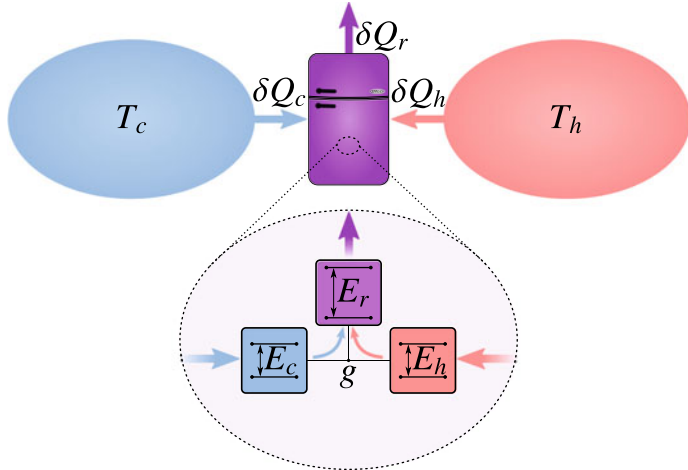


**Fig. 6.1** An absorption refrigerator removes heat simultaneously from a hot ( $T_h$ ) and a cold ( $T_c$ ) body and dumps it into the environment at ambient temperature  $T_r$ . We consider quantum absorption refrigerators comprising three subsystems with transitions of energy  $E_c$ ,  $E_h$  and  $E_r = E_c + E_h$ , coupled by a three-body interaction of strength  $g$ .

If we also assume idealized heat reservoirs then the total entropy change of this process is

$$\delta S = \frac{\delta Q_r}{T_r} - \frac{\delta Q_h}{T_h} - \frac{\delta Q_c}{T_c} \geq 0. \quad (6.2)$$

According to the second law of thermodynamics, such a process is physically permissible so long as the entropy change is non-negative.

In order to design a *quantum* absorption refrigerator, we need to model a dynamical process that transfers heat between three reservoirs in the manner described above. A simple example of such a model comprises three components or subsystems [16, 17], referred to as  $c$ ,  $r$  and  $h$ , each of which is connected to one of the three reservoirs. We use the subscripts  $c$ ,  $r$  or  $h$  to denote quantities associated to the subsystem coupled to the corresponding bath.

The refrigerator Hamiltonian  $\hat{H} = \sum_j \hat{H}_j + \hat{H}_{\text{int}}$  can be resolved into the local energy  $\hat{H}_j$  of each component, for  $j = c, r, h$ , together with the interaction between them,  $\hat{H}_{\text{int}}$ . We assume that the energy spectrum of each subsystem consists of an equally spaced (possibly infinite) ladder of states separated in energy by an amount  $E_j$ , i.e.

$$\hat{H}_j = E_j \sum_n n |n\rangle_j \langle n|, \quad (6.3)$$

where the integer  $n \geq 0$  labels the energy eigenstates. Such a Hamiltonian describes, for example, a two-level atom, a spin in a static magnetic field, or a harmonic oscillator. The interaction between the subsystems is governed by the three-body Hamiltonian

$$\hat{H}_{\text{int}} = g \left( \hat{L}_c \hat{L}_r^\dagger \hat{L}_h + \hat{L}_c^\dagger \hat{L}_r \hat{L}_h^\dagger \right). \quad (6.4)$$

Here,  $g$  is a coupling constant that is assumed to be small in comparison to the local energies  $E_j$ , while  $\hat{L}_j$  is a lowering operator with respect to the corresponding local Hamiltonian, i.e.

$$[\hat{H}_j, \hat{L}_j] = -E_j \hat{L}_j. \quad (6.5)$$

In other words, the nonzero matrix elements of  $\hat{L}_j$  connect states  $|n\rangle_j$  and  $|n+1\rangle_j$  separated in energy by  $E_j$ . Therefore, the interaction (6.5) induces transitions between the states

$$|l+1\rangle_c |m\rangle_r |n+1\rangle_h \longleftrightarrow |l\rangle_c |m+1\rangle_r |n\rangle_h. \quad (6.6)$$

This provides a channel for energy to flow from subsystem  $h$  to  $r$ , but only by simultaneously extracting some energy from  $c$ . At the same time, each component of the refrigerator continuously absorbs or dissipates heat due to its contact with the corresponding bath. The net effect is a cooperative flow of heat from the cold and hot reservoirs into the room-temperature environment.

In order for  $\hat{H}_{\text{int}}$  to have an appreciable effect for small  $g$ , the transition (6.6) should be resonant, which is enforced by the condition

$$E_c + E_h = E_r. \quad (6.7)$$

Since  $E_j$  is the smallest quantity of heat which can be absorbed by each subsystem, this represents a direct analogue of the first law (6.1) at the level of individual energy quanta. Note that here, in identifying  $\delta Q_j = E_j$ , we are again implicitly assuming steady-state operation and the absence of heat leaks in the transfer of energy between the baths mediated by the interaction (6.4), which is valid so long as the coupling  $g$  is sufficiently weak [27–30]. If we similarly set  $\delta Q_j = E_j$  in the second law (6.2), we obtain the condition

$$T_c \geq \frac{E_r - E_h}{E_r/T_r - E_h/T_h} \equiv T_v. \quad (6.8)$$

Thus, the ability of the refrigerator to cool is determined by a new temperature scale,  $T_v$ , the *virtual temperature* [24].

In order to understand what the virtual temperature represents microscopically, consider the pairs of states  $|0_{mn}\rangle_v = |m\rangle_r |n+1\rangle_h$  and  $|1_{mn}\rangle_v = |m+1\rangle_r |n\rangle_h$ , each of which constitutes a *virtual qubit*. The difference in energy between the virtual qubit's states is  $E_r - E_h = E_c$  by virtue of the constraint (6.7). Suppose that initially the interaction is switched off and each subsystem equilibrates with its corresponding bath. The equilibrium populations  $p_n^{(j)}$  of the energy eigenstates  $|n\rangle_j$  of each subsystem are given by the Boltzmann distribution, so that

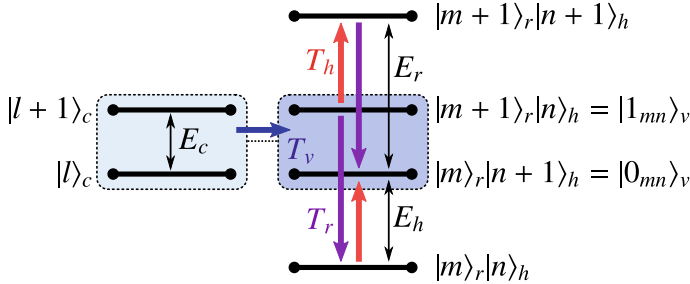


**Fig. 6.2** A virtual qubit is a pair of states in the composite Hilbert space of a quantum absorption refrigerator, which is resonant with the target object to be cooled. Transitions driven by physical baths at temperatures  $T_r$  and  $T_h$  drive population into the lower-energy virtual-qubit state. The resulting population imbalance is described by a cold virtual temperature  $T_v$ , thus inducing heat to flow out of the target.

$$\frac{p_{n+1}^{(j)}}{p_n^{(j)}} = e^{-E_j/k_B T_j}. \quad (6.9)$$

It follows immediately that the virtual qubit populations are Boltzmann-distributed at the virtual temperature, i.e.,

$$\frac{p_{1_{mn}}^{(v)}}{p_{0_{mn}}^{(v)}} = \frac{p_{m+1}^{(r)} p_n^{(h)}}{p_m^{(r)} p_{n+1}^{(h)}} = e^{-E_c/k_B T_v}. \quad (6.10)$$

Now, switching on the interaction  $\hat{H}_{\text{int}}$  causes resonant transitions according to Eq. (6.6) or, equivalently,

$$|l+1\rangle_c |0_{mn}\rangle_v \longleftrightarrow |l\rangle_c |1_{mn}\rangle_v, \quad (6.11)$$

leading to thermalization of  $c$  with the virtual qubits. Meanwhile, exchange of heat with the hot and room-temperature reservoirs acts to maintain the virtual qubits at temperature  $T_v$  (see Fig. 6.2). A net heat flux out of  $c$  is therefore established so long as the virtual qubits are effectively colder, i.e., if  $T_c \geq T_v \geq 0$ , which is precisely the result obtained in Eq. (6.8) from purely thermodynamic arguments. This condition is also sometimes equivalently expressed in terms of the cooling window for the energy splitting  $E_c$ ,

$$0 \leq E_c \leq \frac{(T_h - T_r)T_c}{(T_r - T_c)T_h} E_h. \quad (6.12)$$

In order to analyze the performance of the refrigerator, we need to choose appropriate figures of merit according to the specific task at hand. One possibility is that, by analogy with the classical case, the purpose of the refrigerator is to extract heat from the *macroscopic bath* at temperature  $T_c$ . In this case, performance can be measured in terms of the steady-state heat currents  $J_j = \partial Q_j / \partial t$ , which we define as the rate

at which heat flows *into* the system from baths  $j = c, h$ , and the rate at which heat flows *out of* the system to the room-temperature bath for  $j = r$ . The cooling power is defined by  $J_c$ , while the coefficient of performance (COP)  $\varepsilon = J_c/J_h$  gives a measure of efficiency. We assume, as above, that each quantity of heat  $E_r$  dumped into the environment corresponds to precisely one quantum of energy  $E_c$  and  $E_h$  absorbed from each of the cold and hot baths, respectively. Therefore, the heat currents must satisfy  $J_j = \chi E_j$ , with  $\chi$  a common proportionality factor, and we obtain the very simple expression

$$\varepsilon = \frac{E_c}{E_h}. \quad (6.13)$$

This universal result is valid under the assumption of ideal heat transfer between the baths [31].

Combining the first and second laws of thermodynamics, Eqs. (6.1) and (6.2), one obtains the Carnot bound [15, 32]

$$\varepsilon \leq \varepsilon_C = \frac{1 - T_r/T_h}{T_r/T_c - 1}. \quad (6.14)$$

Note that this bound is consistent with Eqs. (6.12) and (6.13). The Carnot point  $\varepsilon = \varepsilon_C$  corresponds to reversible operation, with  $\delta S = 0$ . The cooling power is clearly zero at the Carnot point because  $T_v = T_c$  and thus the effective temperature difference driving the heat current vanishes. Note that, unlike the efficiency of a heat engine, the COP can be greater than unity. Indeed, in the limit  $T_r \rightarrow T_c$ , we have that  $\varepsilon_C \rightarrow \infty$  and the COP can be arbitrarily large. This makes sense, since heat can be transferred between two baths at equal temperatures without entropic cost, in principle.

A different approach is to consider the refrigerator as a machine designed to cool down the *quantum system*  $c$  itself. In this case, the achievable temperature is a more relevant figure of merit. More generally, since the final state of  $c$  will generally be out of equilibrium, one can consider the achievable energy or entropy instead. This situation is frequently encountered in practice, since the objective of refrigeration is often to *prepare* the quantum system in a low-entropy state as a precursor to some experiment. It is clearly additionally advantageous to reach the minimum temperature as quickly as possible, which opens up interesting possibilities for engineering the transient behavior of the refrigerator to gain some enhancement. In particular, since the dynamics induced by the interaction (6.4) may be oscillatory, the minimum temperature may be reached in a finite time [33, 34]. In order for this to be useful, there must exist some mechanism to switch off the interaction at the appropriate moment. The superconducting-circuit refrigerator discussed in Sect. 6.3 represents an example where this is the case.

We finally mention that, by a judicious choice of the physical energies and temperatures, the virtual temperature can be made to take any desired value. For example, if  $T_v > T_c$ , then the system operates as a heat pump that transfers energy from  $r$  to  $h$ . Indeed, even negative values for  $T_v$  are possible. In this case, the dynamics induces population inversion in the states of subsystem  $c$ , raising its energy in an analogous manner to a heat engine lifting a weight. If the autonomous machine acts

on a more complex system that possesses multiple transitions at different energies, then the machine itself must also be more complex, having at least one virtual qubit (and associated virtual temperature) resonantly coupled to each of these transitions. The most efficient machines (the ones reaching Carnot efficiency) make use of a single virtual temperature only [24]. Therefore, the virtual temperature provides a unified description of autonomous quantum thermal machines, from refrigerators to engines.

## 6.2 Optomechanical Coupling in Cavity QED

One important application of refrigeration in the quantum regime is the cooling of atomic motion. Indeed, the development of laser-cooling techniques laid the foundation for much of the research on controlled quantum dynamics that is carried out today. This includes the field of cavity QED, which is a mature experimental platform for investigating the interaction of light and matter at the atomic level (see, for example, Refs. [35–37] and references therein). In this section, we will discuss a physical realization of a quantum absorption refrigerator designed to cool the motion of a trapped atom inside two optical cavities [21]. The scheme is very closely related to conventional laser sideband cooling [38], which allows us to draw a connection between modern developments in quantum thermodynamics and standard refrigeration methods in atomic physics.

### 6.2.1 Origin of the Optomechanical Interaction

To illustrate the physical principles underlying the atom-cavity refrigerator, we first consider a two-level atom or ion of mass  $m$  confined by a harmonic trap that is placed inside an optical cavity aligned parallel to the  $x$  axis, as depicted in Fig. 6.3a. Let us focus on a particular vibrational mode with angular frequency  $E_c$ , corresponding to motion parallel to the cavity axis, and an optical mode with angular frequency  $E_h$  and wavelength  $\lambda_h = 2\pi c/E_h$ , with  $c$  the speed of light. We set  $\hbar = 1$  throughout. The internal electronic levels  $|\uparrow\rangle_\sigma$  and  $|\downarrow\rangle_\sigma$  are separated by an energy  $E_\sigma$ . The free Hamiltonian is thus

$$\hat{H}_0 = E_c \hat{a}_c^\dagger \hat{a}_c + E_\sigma \hat{\sigma}^\dagger \hat{\sigma} + E_h \hat{a}_h^\dagger \hat{a}_h. \quad (6.15)$$

Here,  $\hat{a}_c$  and  $\hat{a}_h$  are bosonic ladder operators that annihilate vibrational quanta (phonons) and cavity photons, respectively, while  $\hat{\sigma} = |\downarrow\rangle_\sigma \langle \uparrow|$  is a lowering operator for the electronic levels. For typical vibrational and optical frequencies, we have that  $E_c \ll E_\sigma, E_h$ . Taking the electronic and vibrational degrees of freedom together, the spectrum of transition frequencies of the atomic system consists of a central (carrier) frequency  $E_\sigma$  split into closely spaced sidebands separated in frequency by  $E_c$ .

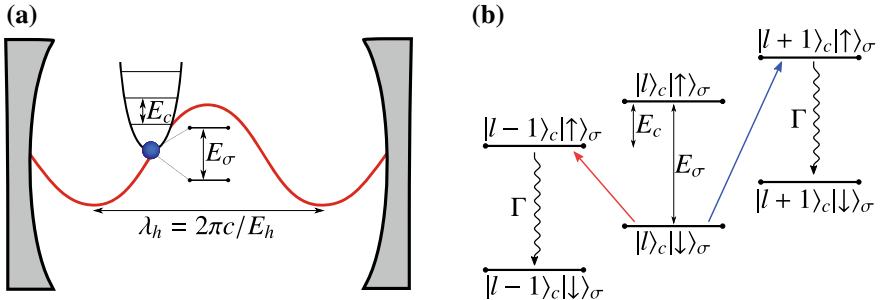


**Fig. 6.3** **a** Trapping a two-level atom near the node of a cavity mode gives rise to an optomechanical coupling. **b** The atomic motion splits the electronic transition into sidebands separated by frequency  $E_c$ . Red and blue arrows show the corresponding (first) sideband transitions. Driving transitions on the red sideband leads to cooling by converting phonons into spontaneously emitted photons (wavy line), while blue sideband transitions lead to heating.

The light-matter interaction Hamiltonian in the dipole approximation is given by  $\hat{H}_{\text{int}} = -\hat{\mathbf{d}} \cdot \hat{\mathbf{E}}(\hat{\mathbf{r}})$ , with  $\hat{\mathbf{d}}$  the dipole moment operator and  $\hat{\mathbf{E}}(\hat{\mathbf{r}})$  the electric field operator of the cavity mode evaluated at the atom's center of mass  $\hat{\mathbf{r}} = (\hat{x}, \hat{y}, \hat{z})$ . Neglecting the slow spatial variation of the field in the  $y$  and  $z$  directions, we have [39, 40]

$$\hat{H}_{\text{int}} = g_0 \sin\left(\frac{2\pi\hat{x}}{\lambda_h}\right) \left( \hat{\sigma} \hat{a}_h^\dagger + \hat{\sigma}^\dagger \hat{a}_h \right), \quad (6.16)$$

where the cavity coupling constant  $g_0$  is determined by the product of the transition dipole moment and the electric-field strength per photon. Here we have made a rotating-wave approximation by neglecting counter-rotating terms such as  $\hat{\sigma}^\dagger \hat{a}_h^\dagger$ , which is valid so long as  $g_0 \ll E_\sigma + E_h$ .

The center-of-mass coordinate can be written as  $\hat{x} = x_0 + x_{\text{zp}}(\hat{a}_c + \hat{a}_c^\dagger)$ , with  $x_0$  the minimum of the trap potential and  $x_{\text{zp}} = 1/\sqrt{2mE_c}$  the width of the vibrational ground-state wavefunction (zero-point motion). The optomechanical interaction is then characterized by the dimensionless phase  $\phi = 2\pi x_0/\lambda_h$  and Lamb-Dicke parameter  $\eta = 2\pi x_{\text{zp}}/\lambda_h = E_h/\sqrt{mc^2 E_c}$ . In particular, we may write  $\hat{H}_{\text{int}} = \cos(\phi)\hat{H}_{\text{node}} + \sin(\phi)\hat{H}_{\text{anti}}$ , where

$$\hat{H}_{\text{node}} = g_0 \sin[\eta(\hat{a}_c + \hat{a}_c^\dagger)] \left( \hat{\sigma} \hat{a}_h^\dagger + \hat{\sigma}^\dagger \hat{a}_h \right), \quad (6.17)$$

$$\hat{H}_{\text{anti}} = g_0 \cos[\eta(\hat{a}_c + \hat{a}_c^\dagger)] \left( \hat{\sigma} \hat{a}_h^\dagger + \hat{\sigma}^\dagger \hat{a}_h \right). \quad (6.18)$$

These two Hamiltonians describe the light-matter interaction when the minimum of the trap potential coincides either with a node of the cavity field, where  $\phi = n\pi$  for integer  $n$ , or with an anti-node, where  $\phi = (n + \frac{1}{2})\pi$ .

At the node, we see that the emission and absorption of cavity photons must be associated with a change in the motional state. This can be understood from

symmetry: The electric field switches sign under a parity transformation  $(\hat{x} - x_0) \rightarrow -(\hat{x} - x_0)$ , and therefore the matrix elements of  $\hat{H}_{\text{int}}$  vanish between states of the same parity. Furthermore, the motional energy eigenstates  $|l\rangle_c$ , with  $l$  the integer phonon number, have definite parity  $(-1)^l$ . This gives rise to a selection rule  $\Delta l = 2m - 1$ , where the state must change by an odd number of phonons. Conversely, at the anti-node the electric field is parity-invariant and thus couples states with the same parity, leading to the selection rule  $\Delta l = 2m$ .

Typically,  $\lambda_h \lesssim 1 \mu\text{m}$  while  $x_{\text{zp}} \lesssim 10 \text{ nm}$ , so that  $\eta$  is a small parameter. In the Lamb-Dicke regime where  $\eta\sqrt{n_c} \ll 1$ , with  $n_c = \langle \hat{a}_c^\dagger \hat{a}_c \rangle$  the mean phonon number, we may expand the Hamiltonian up to first order in  $\eta$  (Lamb-Dicke approximation). First, consider the case where the potential minimum is placed at a node and the cavity frequency is tuned to the first red sideband,  $E_h = E_\sigma - E_c$ . Neglecting terms that do not commute with  $\hat{H}_0$ , the interaction Hamiltonian can be approximated as  $\hat{H}_{\text{node}} \approx \hat{H}_{\text{red}}$ , where

$$\hat{H}_{\text{red}} = g_0 \eta \left( \hat{a}_c \hat{\sigma}^\dagger \hat{a}_h + \hat{a}_c^\dagger \hat{\sigma} \hat{a}_h^\dagger \right). \quad (6.19)$$

On the other hand, tuning the cavity to the first blue sideband,  $E_h = E_\sigma + E_c$ , we similarly obtain  $\hat{H}_{\text{node}} \approx \hat{H}_{\text{blue}}$ , with

$$\hat{H}_{\text{blue}} = g_0 \eta \left( \hat{a}_c^\dagger \hat{\sigma}^\dagger \hat{a}_h + \hat{a}_c \hat{\sigma} \hat{a}_h^\dagger \right). \quad (6.20)$$

Meanwhile, at the anti-node, to lowest order in  $\eta$  we find  $\hat{H}_{\text{anti}} \approx \hat{H}_{\text{JC}}$ , with the Jaynes-Cummings Hamiltonian [41, 42]

$$\hat{H}_{\text{JC}} = g_0 \left( \hat{\sigma}^\dagger \hat{a}_h + \hat{\sigma} \hat{a}_h^\dagger \right). \quad (6.21)$$

Thus, the type of optomechanical interaction can be selected by shifting the trap potential and the cavity frequency. Note, however, that shifting the trap potential directly would create motional excitations unless done very slowly, i.e., adiabatically. A simple dimensional estimate yields an upper velocity bound  $\partial x_0 / \partial t \ll x_{\text{zp}} E_c / 2\pi \sim 10 \mu\text{m/ms}$ . On the other hand, shifting the cavity itself could be done much faster without creating excitations, due to the higher optical frequencies. Nevertheless, the system described in Sect. 6.3 appears to be a more promising setting in which to implement such switching of the interaction.

The red sideband Hamiltonian  $\hat{H}_{\text{red}}$  is a three-body interaction of the required form (6.4) to implement a quantum absorption refrigerator. The thermal baths could be realized by driving the cavity with thermal light at high temperature  $T_h$ , while the electronic degrees of freedom naturally couple to the external radiation field at room temperature  $T_r$ . The cooling mechanism can be understood by analogy with laser sideband cooling, but with the coherent laser field replaced by a hot cavity mode. In sideband cooling, photons on the first red sideband are resonantly absorbed, thus transferring energy from the motional to internal atomic degrees of freedom [cf. Eq. (6.19)]. The excess energy is then lost to the environment by spontaneous

emission, which resets the electronic state so that it is ready to absorb another photon-phonon pair. This drives population down the ladder of motional states, as illustrated in Fig. 6.3b.

Unfortunately, this picture in terms of distinct sideband transitions is spoiled by the large natural linewidth of a typical electronic transition associated with a fast spontaneous emission rate  $\Gamma \gg E_c$ . The resulting energy uncertainty means that the motional sidebands are not “resolved”, i.e., they cannot be efficiently and selectively addressed by tuning the cavity frequency. Therefore, the rotating-wave approximation leading to Eq. (6.19) breaks down. As a result, Eq. (6.20) also contributes significantly to the dynamics by driving blue sideband transitions, which increase the number of phonons and therefore lead to motional heating (see Fig. 6.3). The momentum recoil associated with spontaneous emission leads to further heating and thus represents an additional drawback of this setup.

In the context of laser sideband cooling, these issues can be circumvented by introducing a second laser field and driving red-sideband transitions by a two-photon Raman process [38], which entirely avoids populating the excited electronic state. A similar strategy can be adopted here by introducing a second optical cavity, as explained in the following section.

### 6.2.2 Crossed-Cavity Absorption Refrigerator

In order to suppress spontaneous emission, we introduce a second cavity lying perpendicular to the first one, as illustrated in Fig. 6.4. The free Hamiltonian now reads as

$$\hat{H}_0 = \sum_{j=c,r,h} E_j \hat{a}_j^\dagger \hat{a}_j + E_\sigma \hat{\sigma}^\dagger \hat{\sigma}. \quad (6.22)$$

Here, we introduced a bosonic lowering operator  $\hat{a}_r$  for the second cavity mode with frequency  $E_r = E_h + E_c$ . The minimum of the confining potential is positioned to coincide with a node of the first cavity and an anti-node of the second cavity. According to the discussion in the previous section, the interaction Hamiltonian in the Lamb-Dicke approximation reads as

$$\hat{H}_{\text{int}} = g_h \eta (\hat{a}_c + \hat{a}_c^\dagger) (\hat{\sigma} \hat{a}_h^\dagger + \hat{\sigma}^\dagger \hat{a}_h) + g_r (\hat{\sigma} \hat{a}_r^\dagger + \hat{\sigma}^\dagger \hat{a}_r), \quad (6.23)$$

where  $g_{h,r}$  are the corresponding cavity coupling constants.

Let  $\Delta = E_\sigma - E_r$  denote the detuning from electronic resonance, and  $\Gamma$  the spontaneous emission rate. So long as  $\Gamma \ll |\Delta|$  and  $g_h g_r \eta \ll \Delta^2$ , the excited electronic state is never appreciably populated and can be adiabatically eliminated from the dynamics. As shown in Ref. [21], this leads to an effective Hamiltonian of the form

$$\hat{H} = \sum_{j=c,r,h} E_j \hat{a}_j^\dagger \hat{a}_j + g (\hat{a}_c \hat{a}_r^\dagger \hat{a}_h + \hat{a}_c^\dagger \hat{a}_r \hat{a}_h^\dagger), \quad (6.24)$$

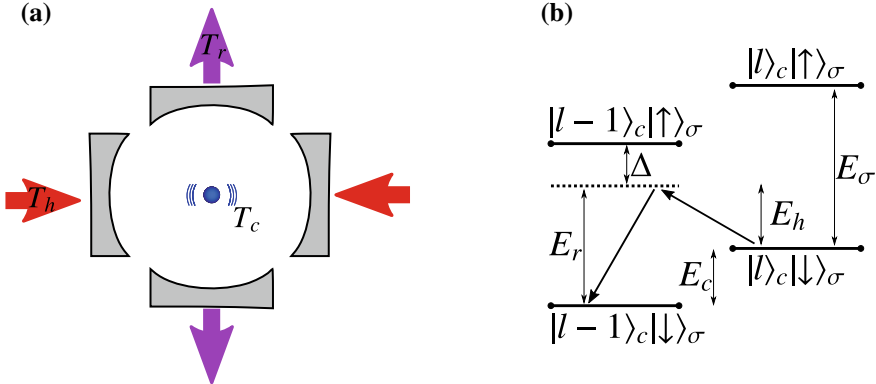


**Fig. 6.4** **a** Illustration of the crossed-cavity absorption refrigerator. An atom trapped near the node of one cavity and the anti-node of the other is cooled by driving one of the cavities with thermal light, while the other cavity couples to the room-temperature radiation field. **b** Cooling results from coherent transitions between motional states driven by the exchange of photons between the two cavities.

with  $g = -g_h g_r \eta / \Delta$  the effective coupling constant. This Hamiltonian, which has an interaction of the form (6.4), describes the coherent exchange of photons between the cavities, assisted by a change in phonon number to make up the energy mismatch  $E_c = E_r - E_h$  between the cavity modes. Therefore, when mode  $h$  is at a higher temperature than mode  $r$ , this exchange of photons drives red sideband transitions in a manner analogous to Raman sideband cooling, as illustrated in Fig. 6.4b.

In order to implement the thermal baths, we assume that cavity  $h$  couples to a thermal light field at temperature  $T_h$ , while cavity  $r$  couples to another field at temperature  $T_r$ . Meanwhile, some intrinsic motional heating of the trapped atom is unavoidable, e.g., due to fluctuations of the confining potential. The ensuing dynamics of the three harmonic modes can be described by a master equation in Lindblad form

$$\partial_t \hat{\rho} = -i[\hat{H}, \hat{\rho}] + \sum_{j=c,h,r} \mathcal{L}_j \hat{\rho}, \quad (6.25)$$

where the superoperators  $\mathcal{L}_j$  describe the coupling to the corresponding bath. We adopt a local description of dissipation, as appropriate for weak, resonant coupling between the three modes [28–30], so that

$$\mathcal{L}_j = \kappa_j (1 + n_B^j) \mathcal{D}[\hat{a}_j] + \kappa_j n_B^j \mathcal{D}[\hat{a}_j^\dagger]. \quad (6.26)$$

Here,  $\mathcal{D}[\hat{L}]\hat{\rho} = \hat{L}\hat{\rho}\hat{L}^\dagger - \frac{1}{2}\{\hat{L}^\dagger\hat{L}, \hat{\rho}\}$  denotes a Lindblad dissipator,  $\kappa_j$  are the cavity decay constants and  $n_B^j$  is the Bose-Einstein distribution

$$n_B^j = \frac{1}{e^{E_j/k_B T_j} - 1}. \quad (6.27)$$

The heat current entering the system from bath  $j$  is then defined as

$$J_j = \text{Tr} \left\{ \hat{H}_j \mathcal{L}_j \hat{\rho} \right\} = \kappa_j E_j \left( n_B^j - \text{Tr} \left\{ \hat{a}_j^\dagger \hat{a}_j \hat{\rho} \right\} \right). \quad (6.28)$$

In order for the effective Hamiltonian (6.24) to remain valid in the presence of dissipation, we require that  $\kappa_j \ll E_c, \Delta$ , i.e., the cavity linewidths must be much smaller than the sideband frequency and the detuning from electronic resonance. Using Eq. (6.25), it is straightforward to verify that Eq. (6.13), i.e.,  $\varepsilon = E_c/E_h$ , holds in the steady state when  $\partial_t \hat{\rho} = 0$ .

In Fig. 6.5 we plot the steady-state occupation of the phonon mode  $n_c^S = \lim_{t \rightarrow \infty} \text{Tr}[\hat{a}_c^\dagger \hat{a}_c \hat{\rho}(t)]$  for fixed temperatures and several different cavity parameters (see the caption of Fig. 6.5 and Table 6.1). Our calculation accounts for several experimental imperfections that we have not included in Eq. (6.25) for the sake of brevity. These include a small, identical misalignment  $\delta$  of the trap potential minimum from the node of cavity  $h$ , and an equal displacement  $\delta$  from the anti-node of

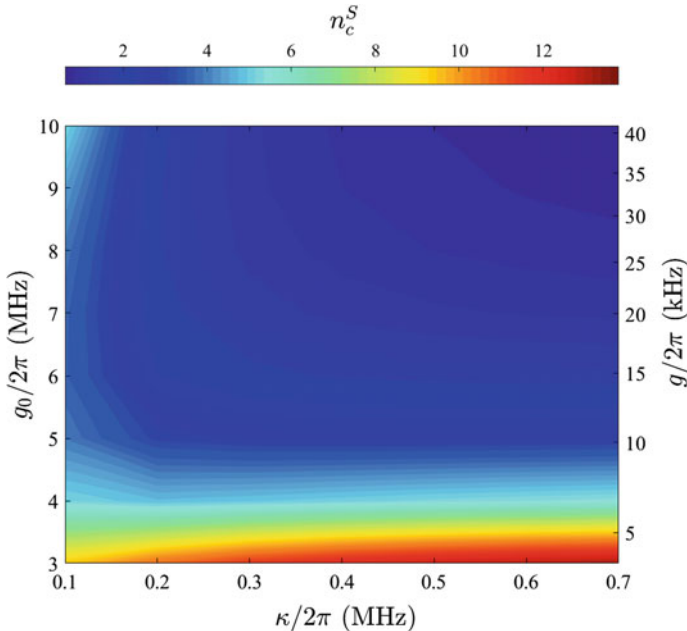


**Fig. 6.5** Steady-state phonon occupation for the atom-cavity absorption refrigerator, as a function of the (identical) cavity coupling constants  $g_h = g_r = g_0$  and decay rates  $\kappa_h = \kappa_r = \kappa$ . The effective three-body interaction strength  $g = -g_0^2 \eta / \Delta$  is also shown for comparison. Parameters:  $\Delta/2\pi = -100$  MHz,  $\Gamma/2\pi = 20$  MHz,  $\eta = 0.041$ ,  $\delta = 10$  nm,  $\kappa_c n_B^c = 10$  s $^{-1}$ , with the remaining parameters given in Table 6.1. Reproduced from Ref. [21] with modified axis scale and labels.

the cavity  $r$ . In addition, we assume that hot thermal light impinges on cavity  $h$  from only one side, with the other side coupling to the ambient field at temperature  $T_r$ . Furthermore, we account for dissipative effects due to spontaneous emission, which are suppressed by a factor  $\Gamma/\Delta$  relative to the other terms in Eq.(6.25). Note that these effects represent heat leaks that degrade performance. See Ref.[21] for full details of the calculation.

We choose  $T_c = T_r = 300$  K, corresponding to room temperature, while  $T_h = 5800$  K, the temperature of sunlight. Despite this seemingly high temperature, the mean number of photons in the cavity is very small,  $n_B^h \approx 10^{-3}$ , due to the high frequency of the optical mode. Nevertheless, the presence of the cavity greatly enhances the effect of each photon by confining it to a small volume around the atom, and we find that cooling the atomic motion close to its ground state ( $n_c^S \sim 1$ ) is possible so long as the cavity coupling constant is sufficiently large. Note that to actually achieve such temperatures with direct sunlight at the Earth's surface would require optical concentration in order to compensate for the attenuation of intensity with distance from the Sun [43, 44]. Alternatively, one could simulate thermal light using phase-randomized laser light [45, 46] for which very high values  $n_B^h \gg 1$  can be obtained, leading to an even larger cooling effect. We also mention that the effective coupling constant  $g$  can be enhanced by trapping  $N$  atoms simultaneously inside the cavity and cooling their collective center-of-mass motion [21]. This leads to an  $N$ -fold increase in  $g$ , where values  $N \sim 500$  are experimentally feasible [47].

Converting the steady-state phonon occupation  $n_c^S$  to a temperature  $T_c^S$  via the relation (6.27), we find  $T_c^S \lesssim 1$  mK. (Note that this effective temperature serves only to illustrate the mean energy since the mode is not necessarily in a thermal state.) On the other hand, the cooling power and the COP are exceedingly small (see Table 6.1). Both of these facts can be understood from the very large frequency mismatch between vibrational and optical degrees of freedom. The achievable temperature can be estimated from the virtual temperature, which for  $T_h \gg T_r$  reduces to

$$T_v \approx \frac{E_c}{E_r} T_r. \quad (6.29)$$

Since  $E_c/E_r \sim 10^{-8}$  for typical vibrational and optical frequencies, this leads to a very small virtual temperature. On the other hand, since the ideal COP (6.13) is given by  $\varepsilon = E_c/(E_r - E_c)$ , it is clear that  $\varepsilon$  is very small when  $E_c \ll E_r$ . This is quite intuitive, since a large quantity of heat  $E_h = E_r - E_c$  must be absorbed from the hot bath for every quantum of energy  $E_c$  extracted from the cold subsystem.

We finally address a very important question that we have neglected thus far. Can it really be possible to select the cavity frequencies to differ by such a relatively small amount,  $E_r - E_h = E_c \approx 10^{-8} E_r$ ? Remarkably, the answer is yes, because the cavity frequencies can be controlled to very high precision using methods such as the Pound-Drever-Hall technique [48], which requires an auxiliary laser. Importantly, this stabilization can be performed without disrupting the operation of the refrigerator, by using other frequency or polarization modes of each cavity. This indicates that cooling of very low-frequency degrees of freedom is facilitated by a stable frequency reference (the coherent laser field) or, equivalently, an accurate clock.

### 6.3 Inelastic Cooper Pair Tunneling in Circuit QED

An alternative platform for implementing the quantum absorption refrigerator is provided by superconducting circuits [50, 51], as sketched in Fig. 6.6. Within such circuits,  $LC$ -resonators (where  $L$  stands for an inductance and  $C$  for a capacitance) with a high quality factor (i.e., with low dissipation) can be designed. These  $LC$ -circuits can be modeled as standard quantum harmonic oscillators with frequencies in the microwave regime and will provide the subsystems of the refrigerator. A Josephson junction in series with the resonators results in a highly nonlinear coupling between the resonators. The circuit can then be described by the Hamiltonian [52–54]

$$\hat{H}(t) = \sum_j E_j \hat{a}_j^\dagger \hat{a}_j - \mathcal{E}_J \cos \left( \sum_j \hat{\varphi}_j + 2eVt + \phi \right), \quad (6.30)$$

where the resonators are labeled by  $j$ ,  $E_j$  denote their frequencies, and  $\hat{a}_j$  are the corresponding annihilation operators. The Josephson energy of the junction is given by  $\mathcal{E}_J$ ,  $V$  denotes an external voltage and  $\phi$  is a phase offset that is possibly due to a magnetic field (see below). The flux operators associated with the resonators read

$$\hat{\varphi}_j = \lambda_j (\hat{a}_j^\dagger + \hat{a}_j), \quad (6.31)$$

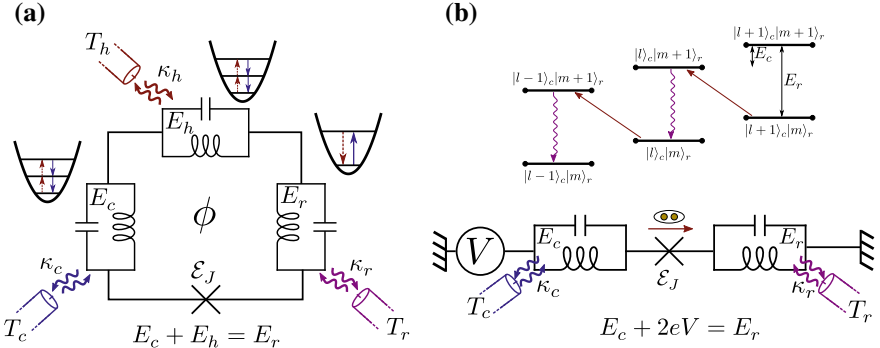


**Fig. 6.6** **a** Quantum absorption refrigerator implemented in a superconducting circuit. The subsystems are provided by three  $LC$ -resonators (with frequency  $E_j$ ) coupled to a thermal bath each (with coupling strength  $\kappa_j$ ). The Josephson junction (with Josephson energy  $\mathcal{E}_J$ ) provides a highly nonlinear interaction between the subsystems. The resonance condition [cf. Eq. (6.7)] is key to obtaining an effective three-body interaction [cf. Eq. (6.4)]. A magnetic flux  $\phi$  which pierces the structure can act as an on-off switch. This allows for observing coherence-enhanced cooling in the transient regime. Figure taken from Ref. [22]. **b** Implementation using an external voltage source instead of the hot bath as the energy source. The energy quanta of the resonator coupled to the hot bath are replaced by Cooper pairs tunneling across the Josephson junction, gaining or losing the energy  $2\text{ eV}$ . The voltage source thereby acts as a coherent external field, providing energy in the form of work. In this implementation, the refrigerator is sideband-cooling a microwave mode. Lower panel taken from Ref. [49].

with  $\lambda_j$  being a coupling constant that grows with the impedance of the resonator.

The Hamiltonian in Eq. (6.30) is just the sum of the noninteracting resonators, which define the Hamiltonians of the subsystems as  $\hat{H}_j = E_j \hat{a}_j^\dagger \hat{a}_j$ , plus the Josephson Hamiltonian which is determined by the cosine of the phase difference across the junction [51, 55]. Here the phase difference includes the fluxes of the resonators as well as the external voltage. Physically, the Cooper pairs that tunnel across the junction can exchange photons with the resonators to make up for the difference in chemical potential across the junction [55–59]. This results in the highly nonlinear interaction between the resonators.

Writing the cosine as a power series, it is clear that the Hamiltonian includes terms of all orders of  $\hat{a}_j$ . The versatility of the system stems from the fact that the external voltage can be used to tune different terms in and out of resonance. This versatility has not gone unnoticed, resulting in a number of theoretical proposals based on Eq. (6.30). In addition to the thermal machines that are discussed below, these proposals include the stabilization of a Fock state [60], the creation of a single-photon source [61], the creation of nonclassical photon pairs [62–64], the generation of bi- and multipartite entanglement [65], and the detection of Majorana fermions [66].

On the experimental side, tremendous progress has been made in recent years. The latest achievements include the observation of nonclassical radiation [67], paving the way to applications based on entangled microwave photons, and the implementation of a maser [68] as well as a parametric amplifier [69], demonstrating a high level of control in these systems.

In order to implement the quantum absorption refrigerator, the resonators have to be coupled to thermal baths. This can in principle be done via transmission lines, allowing the heat baths to be far away from each other and thus facilitating the task of maintaining a temperature gradient. As in the previous section, we model the coupling to the heat baths using a standard local Lindblad approach resulting in the master equation

$$\partial_t \hat{\rho} = -i[\hat{H}, \hat{\rho}] + \sum_j \mathcal{L}_j \hat{\rho}, \quad (6.32)$$

where the dissipative terms are given in Eq. (6.26).

### 6.3.1 Absorption Refrigerator

The quantum absorption refrigerator is implemented with three  $LC$ -resonators, i.e.,  $j = c, r, h$  in Eq. (6.30). Furthermore, since no work is involved, the external voltage is set to  $V = 0$ , resulting in a time-independent Hamiltonian. It can be shown that this Hamiltonian is well approximated by

$$\hat{H} = \sum_{j=c,r,h} \hat{H}_j + \sin(\phi) \hat{H}_{\text{on}} + \cos(\phi) \hat{H}_{\text{off}}, \quad (6.33)$$

where  $\hat{H}_{\text{on}}$  describes a three-body interaction of the form of Eq. (6.4), with

$$\hat{L}_j = \hat{A}_j \hat{a}_j, \quad g = -8\lambda_c \lambda_r \lambda_h \mathcal{E}_J. \quad (6.34)$$

Here we introduced the Hermitian operators

$$\hat{A}_j = e^{-2\lambda_j^2} \sum_{n=0}^{\infty} \frac{L_n^{(1)}(4\lambda_j^2)}{n+1} |n\rangle_j \langle n|, \quad (6.35)$$

with  $L_n^{(1)}(x)$  denoting the generalized Laguerre polynomial of degree  $n$ . Since  $[\hat{A}_j, \hat{H}_j] = 0$ , Eq. (6.5) can easily be verified. The approximative Hamiltonian in Eq. (6.33) is derived under a rotating-wave approximation, where all terms that do not commute with  $\sum_j \hat{H}_j$ , as well as terms that are higher order in  $\lambda_j$ , are dropped. For a detailed derivation, we refer the reader to Ref. [22], where Eq. (6.33) was compared to the full Josephson Hamiltonian and good agreement was found.

A particularly useful property of this implementation is the fact that the Hamiltonian can be modified by an external magnetic field. This provides the refrigerator with an on-off switch, allowing for the investigation of the transient regime, where coherence-enhanced cooling can be observed. Before exploring the transient regime, we focus on refrigeration in the steady state for  $\phi = \pi/2$ , i.e., while the fridge is switched on. Figure 6.7 (a) shows the steady-state temperature of the resonator coupled to the cold bath. As expected, we find a better cooling, the stronger the interaction between the resonators is. As shown in the inset, a higher temperature of the hot bath also increases the cooling. This is due to the fact that the hot bath is the resource of the refrigerator. The hotter it is, the stronger the resource we have at our disposal. Additional parameters which characterize the performance of the refrigerator are given in Table 6.1 and will be compared to the atom-cavity implementation below. Note that resonator  $c$  is strictly speaking not in (although close to) a thermal state. The temperature given here is the temperature of the thermal state with the mean energy of resonator  $c$ . As in the previous section, the figure of merit is thus the mean energy of resonator  $c$ . See Ref. [22] for a more detailed discussion on this.

Thanks to the magnetic flux dependence of the Hamiltonian in Eq. (6.33), the refrigerator can be turned on and off. For  $\phi = \pi/2$ , the refrigerator is on, for  $\phi = 0$ , it is off. The Hamiltonian  $\hat{H}_{\text{off}}$  also describes a refrigerator, but with a coupling strength that goes as  $(\lambda_c \lambda_r \lambda_h)^2$ , substantially suppressing any cooling. Due to the coherent nature of the three-body interaction, the temperature in resonator  $c$  will exhibit a damped oscillatory behavior upon switching on the refrigerator. These oscillations in temperature go well below the steady-state temperature. The on-off switch can be used to cool the resonator below the steady-state temperature by employing the following protocol: The refrigerator is switched on at  $t = 0$ . When the temperature in resonator  $c$  reaches its first minimum, the refrigerator is switched off again. Resonator  $c$  will then thermalize with the cold bath on a time scale given by  $1/\kappa_c$ . For a sufficiently small coupling between the resonator and the cold bath, resonator  $c$  will remain at a temperature below the steady-state temperature of the refrigerator for a

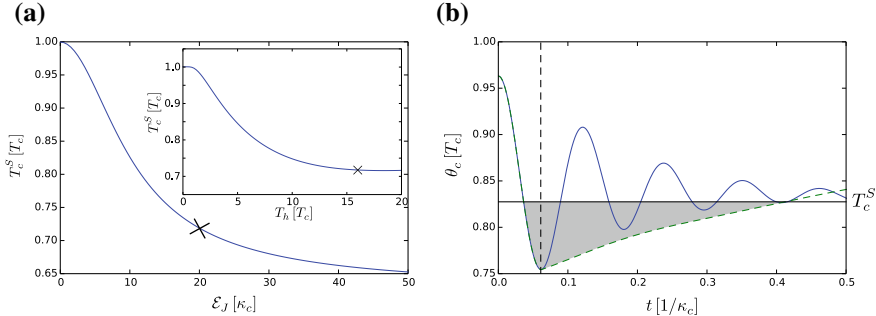


**Fig. 6.7** Performance of the refrigerator implemented in a superconducting circuit. **a** Steady-state cooling. The steady-state temperature in resonator  $c$ ,  $T_c^S$ , is shown as a function of the Josephson energy. The stronger the interaction between the resonators, the better the cooling. The inset shows the steady-state temperature as a function of the hot bath's temperature. The hotter the hot bath, the stronger the energy source which drives the refrigerator. For large temperatures  $T_h$ , cooling is reduced by the nonlinear terms in Eq. (6.34). The cross denotes the point of operation discussed in Table 6.1. Parameters:  $\kappa_c = \kappa_h = 2\pi \cdot 0.01$  GHz,  $\kappa_r = 2\pi \cdot 0.025$  GHz,  $\lambda_c = \lambda_r = \lambda_h = 0.3$ ,  $\mathcal{E}_J = 2\pi \cdot 0.2$  GHz (inset). Other parameters are given in Table 6.1. **b** Coherence-enhanced cooling. The temperature in resonator  $c$ ,  $\theta_c$ , is shown as a function of time. At  $t = 0$ , the refrigerator is switched on. The temperature then oscillates before it reaches  $T_c^S$  (blue, solid line). Switching the refrigerator off at the time the temperature is at its first minimum (dashed vertical line) allows for  $\theta_c$  to remain below  $T_c^S$  for a substantial amount of time (green, dashed line) as illustrated by the grey shading. At  $t = 0$ ,  $\theta_c$  is below the bath temperature because the system also works as a (poor) refrigerator in the off state (i.e., when  $\phi = 0$ ). Parameters are as in **a** except for  $\kappa_c = \kappa_r = \kappa_h = 2\pi \cdot 0.001$  GHz and  $T_h = 384$  mK. Figure taken from Ref. [22].

substantial amount of time. This is illustrated in Fig. 6.7b. We note that this transient cooling effect crucially relies on the coherent nature of the interaction. While for certain (in particular, finite-dimensional) systems, such a coherent interaction can be seen as a genuine quantum effect [33, 34], it was recently shown that in the case of harmonic oscillators, a classical theory can capture the coherence-enhanced cooling effect [70]. We note that coherence-enhanced cooling in the transient regime was recently observed experimentally in a trapped-ion system [23].

### 6.3.2 Sideband Cooling of Microwaves

As sketched in Fig. 6.6b, the hot bath can be replaced by an external voltage as the energy source for refrigeration. In this case, only two resonators are needed and the Hamiltonian is given by Eq. (6.30), with  $j = c, r$  and a finite voltage  $V$ . This Hamiltonian describes Cooper pairs tunneling across a voltage-biased Josephson junction. Due to the voltage, a Cooper pair needs to change its energy by  $2eV$  in order to tunnel, which can be achieved by exchanging photons with the resonators. Fixing the voltage to

$$2eV = E_r - E_c, \quad (6.36)$$

a Cooper pair can tunnel by converting photons from resonator  $c$  into photons in resonator  $r$ . In this way an electrical current, powered by the voltage, drives a heat current from the cold bath to the room-temperature bath. Using the resonance condition in Eq. (6.36) and making a rotating-wave approximation results in the approximative Hamiltonian

$$\hat{H}(t) = \sum_{j=c,r,h} \hat{H}_j + 2\lambda_c \lambda_r \mathcal{E}_J \left( \hat{L}_c^\dagger \hat{L}_r e^{i2eVt} + e^{-i2eVt} \hat{L}_r^\dagger \hat{L}_c \right), \quad (6.37)$$

where  $\hat{L}_j$  are given in Eq. (6.34). For a detailed discussion on the derivation of the last Hamiltonian, we refer the reader to Ref. [49]. As before, the coupling to the baths is described by the local Lindblad master equation given in Eq. (6.32). We note that although the last Hamiltonian includes a time-dependent field, no external time-dependent control is required. The ac Josephson effect converts a time-independent voltage bias into a field oscillating at frequency  $2eV$ . The performance of the power-driven refrigerator is illustrated in Fig. 6.8. While sideband cooling results in a qualitatively similar performance to the absorption refrigerator, a lower steady-state temperature and a higher cooling power can be obtained by using power as the resource (using the same experimental parameters, see also Table 6.1). Note however that the COP is the same for the two implementations and given by  $\varepsilon = E_c/(E_r - E_c)$  [cf. Eq. (6.13)], since both implementations rely on the lossless frequency conversion of photons from  $E_c$  to  $E_r$ .

As for the absorption refrigerator, the cooling process can be switched on and off. In the present case, the refrigerator can be switched off by setting the voltage equal to zero. In this case, tunneling Cooper pairs can not induce photon exchanges and the system is described by the Hamiltonian

$$\hat{H} = \sum_{j=c,r,h} \hat{H}_j + \mathcal{E}_J e^{-2(\lambda_c^2 + \lambda_r^2)} \sum_{n,m=0}^{\infty} L_n(4\lambda_c^2) L_m(4\lambda_r^2) |n\rangle_c \langle n| \otimes |m\rangle_r \langle m|, \quad (6.38)$$

with the Laguerre polynomials  $L_n(x) = L_n^{(0)}(x)$ . For the parameters used throughout this section, the second term in the last Hamiltonian has hardly any influence on the resonators. As for the previous implementation, coherence-enhanced cooling can thus be observed in the transient regime. Just like in the steady state, using power as a resource results in better cooling for the same system parameters.

### 6.3.3 Quantum Thermal Machines Based on Inelastic Cooper Pair Tunneling

As discussed above, a number of different effective Hamiltonians can be realized with a Josephson junction coupled to resonators. The ability to tune the desired terms into

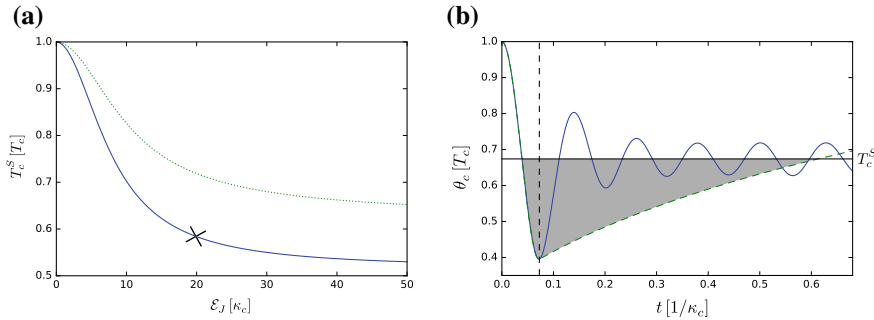


**Fig. 6.8** Sideband cooling of microwaves. **a** Steady-state cooling. The steady-state temperature in resonator  $c$ ,  $T_c^S$ , is shown as a function of the Josephson energy. For comparison, the result for the absorption refrigerator [cf. Fig. 6.7a] is shown as a green (dotted) line. The cross denotes the point of operation discussed in Table 6.1. **b** Coherence-enhanced cooling. The temperature in resonator  $c$ ,  $\theta_c$ , is shown as a function of time. Switching the refrigerator off at the time the temperature is at its first minimum (dashed vertical line) allows for  $\theta_c$  to remain below  $T_c^S$  for a substantial amount of time. Parameters are the same as in Fig. 6.7.

resonance using externally controlled parameters, such as a voltage and a magnetic field, make this system a promising candidate for implementing different types of thermal machines. In addition to the absorption refrigerator, a heat engine [49], a thermometer [8], as well as a machine that extracts work from quantum states [71] were investigated.

A heat engine is provided by operating the refrigerator based on sideband cooling in reverse. A temperature bias is then used to drive an electrical current against the voltage bias. Particularly appealing features of this machine are: 1. Work is unambiguously useful and measurable since it comes in the form of an electrical current. 2. Because Cooper pairs do not carry any heat, work and heat are carried by different particles (Cooper pairs and photons respectively). These two features make this heat engine a promising candidate to study the intricate interplay of heat and work, as well as their fluctuations, in quantum systems.

The same system can also act as a thermometer. By design, the efficiency of these small thermal machines is uniquely determined by the resonator frequencies. Furthermore, they can reach Carnot efficiency, which is uniquely determined by the bath temperatures. At the Carnot point, the bath temperatures are thus related to the resonator frequencies. Knowing the resonator frequencies as well as all but the smallest bath temperatures allows for a precise estimation of the coldest temperature. This way, an imprecise measurement of a hot temperature can be turned into a precise measurement of a cold temperature. For the system discussed above, the temperature of a microwave resonator can be determined in this way with a precision of  $\sim 2$  mK down to temperatures of  $\sim 15$  mK.

A single resonator coupled to a Josephson junction can be used to investigate work extraction from quantum states. In this scheme, the state in the resonator is the quantum state of interest and the Cooper pairs are used to extract work from it in

**Table 6.1** Realistic parameters for the different implementations of the quantum absorption refrigerator. For the superconducting implementation, numbers in brackets are for sideband cooling (i.e., using a power source instead of a hot bath as the resource for cooling).

Implementation	$E_h/2\pi$	$E_c/2\pi$	$g/2\pi$	$T_h$	$T_c/r$	$T_c^S$	$J_c$	$\varepsilon$
Atom-cavity	810THz	5MHz	20kHz	5800K	300K	1mK	<0.1yW	$<10^{-8}$
Superconductor	4.5GHz	1GHz	43.2MHz	768mK	48mK	36(28)mK	0.01(0.015)fW	22.2%

the form of an electrical current. Notably, this machine can extract the theoretical maximum of work from all Gaussian and Fock states. The phase difference across the Josephson junction thereby acts as the necessary phase reference for extracting energy stored in the coherences between energy eigenstates. The same system can also be used to investigate the conversion of work stored in a laser field to electrical work. Interestingly, there is a similar efficiency vs. power trade-off as for heat engines. This implies that work can only change its medium with unit efficiency if it does so infinitely slowly.

## 6.4 Comparison & Outlook

In the previous two sections, we discussed two different physical implementations of quantum absorption refrigerators in detail. We have seen that two very distinct physical architectures are well captured by a single framework as they essentially realize the same physics. In particular, the frequency-matching condition in Eq. (6.7) is crucial for obtaining the correct three-body interaction in both architectures. Furthermore, both architectures feature an on-off switch for the interaction. In the superconducting (circuit QED) architecture, this switch is provided by a magnetic field. In the atom-cavity architecture (cavity QED), the atom can be moved from a node to an anti-node (and back). However, in the latter case, the local Hamiltonians of the subsystems are also altered by this process, which can lead to heating unless the switching is performed slowly.

While the underlying cooling mechanism is the same in the two architectures, there are also important differences resulting in a very different performance. In Table 6.1, we compare the figures of merit as well as the important system parameters of the two implementations. The most notable difference between the architectures manifests itself in the very different frequency scales. In particular, for the atom-cavity implementation, where the subsystems are provided by different types of physical degrees of freedom, the ratio between the frequencies  $E_c/E_h \sim 10^{-8}$  is extremely small. While this results in a vanishing efficiency (and requires active stabilization of the cavity frequency), it allows for applying large temperature biases. Together with the small coupling between the cold bath and the system, this allows for cooling a quantum system that is coupled to a room temperature bath down to temperatures of the order of milli-Kelvins. This corresponds to reducing temperature by five orders of

magnitude. The superconductor implementation relies on subsystems that are identical in nature, resulting in ratios  $E_c/E_h \sim 0.22$  relatively close to unity. While this results in large efficiencies, it restricts the amount by which the quantum degree of freedom can be cooled down (here, about a factor of two).

We thus conclude that the superconducting architecture is superior if the aim is to efficiently use resources for cooling and/or if we are interested in cooling down the macroscopic bath. Should we aim at cooling down the quantum degree of freedom coupled to the cold bath, the atom-cavity implementation is the superior one.

Since the implementations discussed here were put forward as proposals, there has been an experimental implementation of a quantum absorption refrigerator based on the motional degrees of freedom of trapped ions [23]. In contrast to the standard absorption refrigerator, there are no thermal baths involved in this experiment. Instead, the three harmonic oscillators that provide the subsystems of the refrigerator are initiated in thermal states at different temperatures. The system then evolves under unitary dynamics governed by a Hamiltonian including a three-body interaction term. Interestingly, even with so few degrees of freedom, the system shows equilibration in the sense that local observables take on steady-state values at most times. We note that the recurrence time is much larger than any other time scale in this system [70]. This opens up opportunities for studying equilibration in closed systems [72]. Furthermore, temperature oscillations dipping below the steady-state value were observed in the experiment in Ref. [23], demonstrating the advantage of a coherent interaction over an incoherent one.

While the quantum absorption refrigerator is based on a quantum mechanical model which includes a coherent interaction, a clear advantage over a classical analogue is not always straightforward to establish (see Chap. 4). If the subsystems of the refrigerator are qubits, a reasonable classical analogue is obtained by replacing the coherent interaction with an incoherent one [34]. In this case, coherence-enhanced cooling in the transient regime provides a clear quantum advantage, where the quantum model outperforms the classical analogue. Furthermore, in a refrigerator based on qubits, entanglement between the subsystems has been connected to an enhanced performance of the refrigerator [73]. For refrigerators based on harmonic oscillators, such as the ones discussed here, it is more difficult to determine a genuine nonclassical signature. First, no entanglement between the subsystems has been observed so far. Second, since the classical theory of electrodynamics entails coherence, a classical model for the absorption refrigerator that includes coherence can be constructed. This model captures the coherence-enhanced cooling effect in the transient regime [70]. Similarly, one might be able to construct an alternative classical model of the qubit refrigerator in terms of precessing magnetic moments (a qubit can be realized by a spin-half magnetic moment, see also Chap. 9), whose oscillatory dynamics could potentially capture the coherence-enhanced cooling effect. This illustrates a general difficulty of demonstrating quantum enhancements in thermodynamics: there exists no universally agreed-upon notion of the “classical limit” for a quantum thermal machine. This is in stark contrast to other fields displaying quantum advantages such as computation, where the difference between a quantum and a classical computer is physically and mathematically well defined.

One possibility for determining an unambiguous quantum signature in absorption refrigerators is provided by considering energy quantization. In classical theories, single degrees of freedom usually exhibit particle-like behavior (which can result in quantization of energy) or wave-like behavior (which can result in coherence) but not both at the same time. With the coherence-enhanced cooling mechanism, we already encountered an observable effect which requires coherence. Most reasonable classical analogues of the absorption refrigerator could be ruled out if energy quantization can be shown to play a crucial role as well. On the surface, the working principle of the quantum absorption refrigerator seems to rely heavily on energy quanta [24, 74]. Indeed, it is the fact that a single photon from the hot bath is able to extract a single photon (or phonon) from the cold bath which results in the simple, universal COP. However, in order to certify that the energy passes the refrigerator in quanta, one presumably has to go beyond mean values and investigate fluctuations. In addition to possibly certifying nonclassicality, the study of fluctuations in thermal machines will lead to a deeper understanding of the underlying physics and might lead to novel mechanisms for harvesting energy from fluctuations.

Other avenues to pursue include investigating the role of measurements and possibly feedback on the refrigerator (see, for instance, Refs. [75–77] as well as Chaps. 39 and 40). Even in autonomous thermal machines, a measurement arguably needs to occur at some time (otherwise, how would one know that something beneficial happened?). This line of research could connect autonomous machines with the thermodynamics of information [78]. We have also seen that an external frequency reference or clock is useful, both in order to achieve very low steady-state temperatures in the atom-cavity system and in order to take advantage of transient temperature oscillations in the superconducting-circuit fridge. An intriguing question thus arises regarding the energetic and entropic cost of maintaining and using such a clock. Ideally, one would like to analyze the clock within a fully autonomous model in order to ensure fair bookkeeping of resources. While the first steps have been taken in this direction [9, 11, 79, 80], much work remains to be done in order to fully understand the thermodynamics of time measurements and time-dependent control of quantum systems.

We conclude this chapter by emphasizing that the quantum absorption refrigerator is an extremely versatile tool: It has already helped to deepen our understanding of thermodynamic processes in the quantum regime and promises to continue doing so in the future. Additionally, the refrigerator actually performs a useful task. Experimental implementations therefore promise to be beneficial on a fundamental as well as a practical level.

**Acknowledgements** MTM acknowledges funding from the ERC Synergy grant BioQ and the EU project QUCHIP. PPP acknowledges support from the Swiss National Science foundation, the NCCR Quantum Science and Technology (QSIT), the Swedish Research Council, and from the European Union’s Horizon 2020 research and innovation programme under the Marie Skłodowska-Curie Grant Agreement No. 796700. We also acknowledge the COST MP1209 network “Thermodynamics in the quantum regime” which fostered the research described in this chapter.

## References

1. R. Kosloff, A. Levy, Quantum heat engines and refrigerators: continuous devices. *Annu. Rev. Phys. Chem.* **65**(1), 365 (2014). <https://doi.org/10.1146/annurev-physchem-040513-103724>
2. D. Gelbwaser-Klimovsky, W. Niedenzu, G. Kurizki, Thermodynamics of quantum systems under dynamical control. *Adv. At. Mol. Opt. Phys.* **64**, 329 (2015). <https://doi.org/10.1016/bs.aamop.2015.07.002>
3. J. Goold, M. Huber, A. Riera, L. del Rio, P. Skrzypczyk, The role of quantum information in thermodynamics—a topical review. *J. Phys. A: Math. Theor.* **49**(14), 143001 (2016). <https://doi.org/10.1088/1751-8113/49/14/143001>
4. S. Vinjanampathy, J. Anders, Quantum thermodynamics. *Contemp. Phys.* **57**(4), 545 (2016). <https://doi.org/10.1080/00107514.2016.1201896>
5. G. Benenti, G. Casati, K. Saito, R.S. Whitney, Fundamental aspects of steady-state conversion of heat to work at the nanoscale. *Phys. Rep.* **694**(1), (2017). <https://doi.org/10.1016/j.physrep.2017.05.008>
6. R. Kosloff, Quantum thermodynamics: A dynamical viewpoint. *Entropy* **15**(6), 2100 (2013). <https://doi.org/10.3390/e15062100>
7. J.B. Brask, G. Haack, N. Brunner, M. Huber, Autonomous quantum thermal machine for generating steady-state entanglement. *New J. Phys.* **17**(11), 113029 (2015). <https://doi.org/10.1088/1367-2630/17/11/113029>
8. P.P. Hofer, J.B. Brask, M. Perarnau-Llobet, N. Brunner, Quantum thermal machine as a thermometer. *Phys. Rev. Lett.* **119**(9), 090603 (2017). <https://doi.org/10.1103/PhysRevLett.119.090603>
9. P. Erker, M.T. Mitchison, R. Silva, M.P. Woods, N. Brunner, M. Huber, Autonomous quantum clocks: does thermodynamics limit our ability to measure time? *Phys. Rev. X* **7**(3), 031022 (2017). <https://doi.org/10.1103/PhysRevX.7.031022>
10. F. Clivaz, R. Silva, G. Haack, J.B. Brask, N. Brunner, M. Huber, Unifying paradigms of quantum refrigeration: how resource-control determines fundamental limits [arXiv:1710.11624](https://arxiv.org/abs/1710.11624), [quant-ph] (2017)
11. M.P. Woods, R. Silva, J. Oppenheim, Autonomous quantum machines and finite sized clocks. *Ann. Henri Poincaré* **20**(1), 125–128 (2019). <https://doi.org/10.1007/s00023-018-0736-9>
12. K.E. Dorfman, D.V. Voronine, S. Mukamel, M.O. Scully, Photosynthetic reaction center as a quantum heat engine. *Proc. Natl. Acad. Sci. U. S. A.* **110**(8), 2746–2751 (2013). <https://doi.org/10.1073/pnas.1212666110>
13. C. Creatore, M.A. Parker, S. Emmott, A.W. Chin, Efficient biologically inspired photocell enhanced by delocalized quantum states. *Phys. Rev. Lett.* **111**(25), 253601 (2013). <https://doi.org/10.1103/PhysRevLett.111.253601>
14. N. Killoran, S.F. Huelga, M.B. Plenio, Enhancing light-harvesting power with coherent vibrational interactions: A quantum heat engine picture. *J. Chem. Phys.* **143**(15), 155102 (2015). <https://doi.org/10.1063/1.4932307>
15. J.P. Palao, R. Kosloff, J.M. Gordon, Quantum thermodynamic cooling cycle. *Phys. Rev. E* **64**(5), 056130 (2001). <https://doi.org/10.1103/PhysRevE.64.056130>
16. N. Linden, S. Popescu, P. Skrzypczyk, How small can thermal machines be? The smallest possible refrigerator. *Phys. Rev. Lett.* **105**(13), 130401 (2010). <https://doi.org/10.1103/PhysRevLett.105.130401>
17. A. Levy, R. Kosloff, Quantum Absorption Refrigerator. *Phys. Rev. Lett.* **108**(7), 070604 (2012). <https://doi.org/10.1103/PhysRevLett.108.070604>
18. Y.-X. Chen, S.-W. Li, Quantum refrigerator driven by current noise. *EPL (Europhys. Lett.)* **97**(4), 40003 (2012). <https://doi.org/10.1209/0295-5075/97/40003>
19. A. Mari, J. Eisert, Cooling by heating: Very hot thermal light can significantly cool quantum systems. *Phys. Rev. Lett.* **108**(12), 120602 (2012). <https://doi.org/10.1103/PhysRevLett.108.120602>

20. D. Venturelli, R. Fazio, V. Giovannetti, Minimal self-contained quantum refrigeration machine based on four quantum dots. *Phys. Rev. Lett.* **110**(25), 256801 (2013). <https://doi.org/10.1103/PhysRevLett.110.256801>
21. M.T. Mitchison, M. Huber, J. Prior, M.P. Woods, M.B. Plenio, Realising a quantum absorption refrigerator with an atom-cavity system. *Quantum Sci. Technol.* **1**(1), 015001 (2016). <https://doi.org/10.1088/2058-9565/1/1/015001>
22. P.P. Hofer, M. Perarnau-Llobet, J.B. Brask, R. Silva, M. Huber, N. Brunner, Autonomous quantum refrigerator in a circuit QED architecture based on a Josephson junction. *Phys. Rev. B* **94**(23), 235420 (2016). <https://doi.org/10.1103/PhysRevB.94.235420>
23. G. Maslennikov, S. Ding, R. Hablitzel, J. Gan, A. Roulet, S. Nimmrichter, J. Dai, V. Scarani, D. Matsukevich, Quantum absorption refrigerator with trapped ions. *Nat. Comm.* **10**, 202 (2019). <https://doi.org/10.1038/s41467-018-08090-0>
24. N. Brunner, N. Linden, S. Popescu, P. Skrzypczyk, Virtual qubits, virtual temperatures, and the foundations of thermodynamics. *Phys. Rev. E* **85**(5), 051117 (2012). <https://doi.org/10.1103/PhysRevE.85.051117>
25. P. Skrzypczyk, R. Silva, N. Brunner, Passivity, complete passivity, and virtual temperatures. *Phys. Rev. E* **91**(5), 052133 (2015). <https://doi.org/10.1103/PhysRevE.91.052133>
26. L.A. Correa, J.P. Palao, D. Alonso, Internal dissipation and heat leaks in quantum thermodynamic cycles. *Phys. Rev. E* **92**(3), 032136 (2015). <https://doi.org/10.1103/PhysRevE.92.032136>
27. L.A. Correa, J.P. Palao, G. Adesso, D. Alonso, Performance bound for quantum absorption refrigerators. *Phys. Rev. E* **87**(4), 042131 (2013). <https://doi.org/10.1103/PhysRevE.87.042131>
28. P.P. Hofer, M. Perarnau-Llobet, L.D.M. Miranda, G. Haack, R. Silva, J.B. Brask, N. Brunner, Markovian master equations for quantum thermal machines: local versus global approach. *New J. Phys.* **19**(12), 123037 (2017). <https://doi.org/10.1088/1367-2630/aa964f>
29. J.O. González, L.A. Correa, G. Nocerino, J.P. Palao, D. Alonso, G. Adesso, Testing the validity of the ‘local’ and ‘global’ GKLS master equations on an exactly solvable model. *Open Syst. Inf. Dyn.* **24**(04), 1740010 (2017). <https://doi.org/10.1142/s1230161217400108>
30. S. Seah, S. Nimmrichter, V. Scarani, Refrigeration beyond weak internal coupling. *Phys. Rev. E* **98**(1), 012131 (2018). <https://doi.org/10.1103/PhysRevE.98.012131>
31. H.E.D. Scovil, E.O. Schulz-DuBois, Three-level masers as heat engines. *Phys. Rev. Lett.* **2**(6), 262–263 (1959). <https://doi.org/10.1103/PhysRevLett.2.262>
32. P. Skrzypczyk, N. Brunner, N. Linden, S. Popescu, The smallest refrigerators can reach maximal efficiency. *J. Phys. A: Math. Theor.* **44**(49), 492002 (2011). <https://doi.org/10.1088/1751-8113/44/49/492002>
33. J.B. Brask, N. Brunner, Small quantum absorption refrigerator in the transient regime: Time scales, enhanced cooling, and entanglement. *Phys. Rev. E* **92**(6), 062101 (2015). <https://doi.org/10.1103/PhysRevE.92.062101>
34. M.T. Mitchison, M.P. Woods, J. Prior, M. Huber, Coherence-assisted single-shot cooling by quantum absorption refrigerators. *New J. Phys.* **17**(11), 115013 (2015). <https://doi.org/10.1088/1367-2630/17/11/115013>
35. R. Miller, T.E. Northup, K.M. Birnbaum, A. Boca, A.D. Boozer, H.J. Kimble, Trapped atoms in cavity QED: coupling quantized light and matter. *J. Phys. B* **38**(9), S551 (2005). <https://doi.org/10.1088/0953-4075/38/9/007>
36. H. Walther, B.T.H. Varcoe, B.-G. Englert, T. Becker, Cavity quantum electrodynamics. *Rep. Prog. Phys.* **69**(5), 1325–1382 (2006). <https://doi.org/10.1088/0034-4885/69/5/r02>
37. S. Haroche, Nobel Lecture: Controlling photons in a box and exploring the quantum to classical boundary. *Rev. Mod. Phys.* **85**(3), 1083–1102 (2013). <https://doi.org/10.1103/revmodphys.85.1083>
38. D. Leibfried, R. Blatt, C. Monroe, D. Wineland, Quantum dynamics of single trapped ions. *Rev. Mod. Phys.* **75**(1), 281–324 (2003). <https://doi.org/10.1103/RevModPhys.75.281>
39. C.A. Blockley, D.F. Walls, H. Risken, Quantum collapses and revivals in a quantized trap. *EPL (Europhys. Lett.)* **17**(6), 509–514 (1992). <https://doi.org/10.1209/0295-5075/17/6/006>

40. V. Bužek, G. Drobny, M.S. Kim, G. Adam, P.L. Knight, Cavity QED with cold trapped ions. *Phys. Rev. A* **56**(3), 2352–2360 (1997). <https://doi.org/10.1103/physreva.56.2352>
41. E.T. Jaynes, F.W. Cummings, Comparison of quantum and semiclassical radiation theories with application to the beam maser. *Proc. IEEE* **51**(1), 89–109 (1963). <https://doi.org/10.1109/proc.1963.1664>
42. B.W. Shore, P.L. Knight, The jaynes-cummings model. *J. Mod. Opt.* **40**(7), 1195–1238 (1993). <https://doi.org/10.1080/09500349314551321>
43. R. Winston, Light collection within the framework of geometrical optics. *J. Opt. Soc. Am.* **60**(2), 245 (1970). <https://doi.org/10.1364/josa.60.000245>
44. R. Alicki, D. Gelbwaser-Klimovsky, Non-equilibrium quantum heat machines. *New J. Phys.* **17**(11), 115012 (2015). <https://doi.org/10.1088/1367-2630/17/11/115012>
45. W. Martienssen, E. Spiller, Coherence and fluctuations in light beams. *Am. J. Phys.* **32**(12), 919–926 (1964). <https://doi.org/10.1119/1.1970023>
46. F.T. Arecchi, Measurement of the statistical distribution of Gaussian and laser sources. *Phys. Rev. Lett.* **15**(24), 912–916 (1965). <https://doi.org/10.1103/physrevlett.15.912>
47. P.F. Herskind, A. Dantan, J.P. Marler, M. Albert, M. Drewsen, Realization of collective strong coupling with ion Coulomb crystals in an optical cavity. *Nat. Phys.* **5**(7), 494–498 (2009). <https://doi.org/10.1038/nphys1302>
48. E.D. Black, An introduction to Pound-Drever-Hall laser frequency stabilization. *Am. J. Phys.* **69**(1), 79–87 (2001). <https://doi.org/10.1119/1.1286663>
49. P.P. Hofer, J.-R. Souquet, A.A. Clerk, Quantum heat engine based on photon-assisted Cooper pair tunneling. *Phys. Rev. B* **93**(4), 041418(R) (2016). <https://doi.org/10.1103/PhysRevB.93.041418>
50. R.J. Schoelkopf, S.M. Girvin, Wiring up quantum systems. *Nature* **451**(7179), 664 (2008). <https://doi.org/10.1038/451664a>
51. U. Vool, M. Devoret, Introduction to quantum electromagnetic circuits. *Int. J. Theor. Appl.* **45**(7), 897 (2017). <https://doi.org/10.1002/cta.2359>
52. A.D. Armour, M.P. Blencowe, E. Brahimi, A.J. Rimberg, Universal quantum fluctuations of a cavity mode driven by a Josephson junction. *Phys. Rev. Lett.* **111**(24), 247001 (2013). <https://doi.org/10.1103/PhysRevLett.111.247001>
53. V. Gramich, B. Kubala, S. Rohrer, J. Ankerhold, From Coulomb-Blockade to Nonlinear Quantum Dynamics in a Superconducting Circuit with a Resonator. *Phys. Rev. Lett.* **111**(24), 247002 (2013). <https://doi.org/10.1103/PhysRevLett.111.247002>
54. W.A. Al-Saidi, D. Stroud, Eigenstates of a small Josephson junction coupled to a resonant cavity. *Phys. Rev. B* **65**(1), 014512 (2001). <https://doi.org/10.1103/PhysRevB.65.014512>
55. G.-L. Ingold, Y.V. Nazarov, Charge tunneling rates in ultrasmall junctions, in *Single Charge Tunneling*, ed. by H. Grabert, M.H. Devoret (Springer, Berlin, 1992). <https://doi.org/10.1007/978-1-4757-2166-9>
56. D.V. Averin, Y.V. Nazarov, A.A. Odintsov, Incoherent tunneling of the Cooper pairs and magnetic flux quanta in ultrasmall Josephson junctions. *Phys. B* **165**, 945 (1990). [https://doi.org/10.1016/S0921-4526\(09\)80058-6](https://doi.org/10.1016/S0921-4526(09)80058-6)
57. T. Holst, D. Esteve, C. Urbina, M.H. Devoret, Effect of a transmission line resonator on a small capacitance tunnel junction. *Phys. Rev. Lett.* **73**(25), 3455 (1994). <https://doi.org/10.1103/PhysRevLett.73.3455>
58. J. Basset, H. Bouchiat, R. Deblock, Emission and absorption quantum noise measurement with an on-chip resonant circuit. *Phys. Rev. Lett.* **105**(16), 166801 (2010). <https://doi.org/10.1103/PhysRevLett.105.166801>
59. M. Hofheinz, F. Portier, Q. Baudouin, P. Joyez, D. Vion, P. Bertet, P. Roche, D. Esteve, Bright side of the Coulomb Blockade. *Phys. Rev. Lett.* **106**(21), 217005 (2011). <https://doi.org/10.1103/PhysRevLett.106.217005>
60. J.-R. Souquet, A.A. Clerk, Fock-state stabilization and emission in superconducting circuits using dc-biased Josephson junctions. *Phys. Rev. A* **93**(6), 060301 (2016). <https://doi.org/10.1103/PhysRevA.93.060301>

61. S. Dambach, B. Kubala, V. Gramich, J. Ankerhold, Time-resolved statistics of nonclassical light in Josephson photonics. *Phys. Rev. B* **92**(5), 054508 (2015). <https://doi.org/10.1103/PhysRevB.92.054508>
62. J. Leppäkangas, G. Johansson, M. Marthaler, M. Fogelström, Nonclassical photon pair production in a voltage-biased Josephson junction. *Phys. Rev. Lett.* **110**(26), 267004 (2013). <https://doi.org/10.1103/PhysRevLett.110.267004>
63. A.D. Armour, B. Kubala, J. Ankerhold, Josephson photonics with a two-mode superconducting circuit. *Phys. Rev. B* **91**(18), 184508 (2015). <https://doi.org/10.1103/PhysRevB.91.184508>
64. M. Trif, P. Simon, Photon cross-correlations emitted by a Josephson junction in two microwave cavities. *Phys. Rev. B* **92**(1), 014503 (2015). <https://doi.org/10.1103/PhysRevB.92.014503>
65. S. Dambach, B. Kubala, J. Ankerhold, Generating entangled quantum microwaves in a Josephson-photonics device. *New J. Phys.* **19**(2), 023027 (2017). <https://doi.org/10.1088/1367-2630/aa5bb6>
66. O. Dmytruk, M. Trif, P. Simon, Josephson effect in topological superconducting rings coupled to a microwave cavity. *Phys. Rev. B* **94**(11), 115423 (2016). <https://doi.org/10.1103/PhysRevB.94.115423>
67. M. Westig, B. Kubala, O. Parlavecchio, Y. Mukharsky, C. Altimiras, P. Joyez, D. Vion, P. Roche, D. Esteve, M. Hofheinz, M. Trif, P. Simon, J. Ankerhold, F. Portier, Emission of nonclassical radiation by inelastic Cooper pair tunneling. *Phys. Rev. Lett.* **119**(13), 137001 (2017). <https://doi.org/10.1103/PhysRevLett.119.137001>
68. F. Chen, J. Li, A.D. Armour, E. Brahim, J. Stettenheim, A.J. Sirois, R.W. Simmonds, M.P. Blencowe, A.J. Rimberg, Realization of a single-Cooper-pair Josephson laser. *Phys. Rev. B* **90**(2), 020506 (2014). <https://doi.org/10.1103/PhysRevB.90.020506>
69. S. Jebari, F. Blanchet, A. Grimm, D. Hazra, R. Albert, P. Joyez, D. Vion, D. Estève, F. Portier, M. Hofheinz, Near-quantum-limited amplification from inelastic Cooper-pair tunnelling. *Nat. Electron* **1**(4), 223 (2018). <https://doi.org/10.1038/s41928-018-0055-7>
70. S. Nimmrichter, J. Dai, A. Roulet, V. Scarani, Quantum and classical dynamics of a three-mode absorption refrigerator. *Quantum* **1**, 37 (2017). <https://doi.org/10.22331/q-2017-12-11-37>
71. N. Lörch, C. Bruder, N. Brunner, P.P. Hofer, Optimal work extraction from quantum states by photo-assisted Cooper pair tunneling. *Quantum Sci. Technol.* **3**, 035014 (2018). <https://doi.org/10.1088/2058-9565/aacbf3>
72. C. Gogolin, J. Eisert, Equilibration, thermalisation, and the emergence of statistical mechanics in closed quantum systems. *Rep. Prog. Phys.* **79**(5), 056001 (2016). <https://doi.org/10.1088/0034-4885/79/5/056001>
73. N. Brunner, M. Huber, N. Linden, S. Popescu, R. Silva, P. Skrzypczyk, Entanglement enhances cooling in microscopic quantum refrigerators. *Phys. Rev. E* **89**(3), 032115 (2014). <https://doi.org/10.1103/PhysRevE.89.032115>
74. L.A. Correa, J.P. Palao, G. Adesso, D. Alonso, Optimal performance of endoreversible quantum refrigerators. *Phys. Rev. E* **90**(6), 062124 (2014). <https://doi.org/10.1103/PhysRevE.90.062124>
75. A. Levy, L. Diósi, R. Kosloff, Quantum flywheel. *Phys. Rev. A* **93**(5), 052119 (2016). <https://doi.org/10.1103/PhysRevA.93.052119>
76. C. Elouard, D. Herrera-Martí, B. Huard, A. Auffèves, Extracting Work from quantum measurement in Maxwell's Demon engines. *Phys. Rev. Lett.* **118**(26), 260603 (2017). <https://doi.org/10.1103/PhysRevLett.118.260603>
77. M.H. Mohammady, J. Anders, A quantum Szilard engine without heat from a thermal reservoir. *New J. Phys.* **19**(11), 113026 (2017). <https://doi.org/10.1088/1367-2630/aa8ba1>
78. J.M.R. Parrondo, J.M. Horowitz, T. Sagawa, Thermodynamics of information. *Nat. Phys.* **11**(2), 131–139 (2015). <https://doi.org/10.1038/nphys3230>
79. A.S.L. Malabarba, A.J. Short, P. Kammerlander, Clock-driven quantum thermal engines. *New J. Phys.* **17**(4), 045027 (2015). <https://doi.org/10.1088/1367-2630/17/4/045027>
80. A.C. Barato, U. Seifert, Cost and precision of Brownian clocks. *Phys. Rev. X* **6**(4), 041053 (2016). <https://doi.org/10.1103/physrevx.6.041053>

# Chapter 7

# Quantum Thermodynamics of Nanoscale Thermoelectrics and Electronic Devices



Robert S. Whitney, Rafael Sánchez and Janine Splettstoesser

## 7.1 Objectives of this Chapter

This chapter is intended as a short introduction to electron flow in nanostructures. Its aim is to provide a brief overview of this topic for people who are interested in the thermodynamics of quantum systems, but know little about nanostructures. We particularly emphasize devices that work in the steady-state, such as simple thermoelectrics, but also mention cyclically driven heat engines. We do not aim to be either complete or rigorous, but use a few pages to outline some of the main ideas in the topic.

## 7.2 Introduction

*Thermoelectricity* is the name associated with any phenomena where a heat current induces an electric current, or vice versa. It was much studied in the context of

---

R. S. Whitney

Laboratoire de Physique et Modélisation des Milieux Condensés (UMR 5493),  
Université Grenoble Alpes and CNRS, Maison des Magistères, BP 166,  
38042 Grenoble, France  
e-mail: robert.whitney@grenoble.cnrs.fr

R. Sánchez

Departamento de Física Teórica de la Materia Condensada and Condensed Matter Physics Center (IFIMAC),  
Universidad Autónoma de Madrid, 28049 Madrid, Spain  
e-mail: rafael.sanchez@uam.es

J. Splettstoesser (✉)

Department of Microtechnology and Nanoscience (MC2), Chalmers University of Technology, S-412 96 Göteborg, Sweden  
e-mail: janines@chalmers.se

classical thermodynamics, with Onsager's Nobel-prize winning work on irreversible thermodynamic processes being first applied to the thermoelectric effect [1]. Thermoelectricity in *nanostructures* was first observed experimentally in the early 1990's [2], however it was little studied because the lack of good thermometry techniques at the nanoscale made quantitative experiments difficult. Now experimental progress in thermometry, see e.g. Refs. [3–11], has led to a renewed experimental interest, particularly in the use of nanoscale thermoelectrics to turn a heat flow into electrical power, or to turn electrical power into a heat flow from cold to hot (refrigeration). This raises the question of developing a quantitative understanding of thermoelectricity in nanoscale structures, where quantum effects are important.

The objective of this chapter is to briefly explain how such thermoelectric effects occur, and discuss the quantum thermodynamics of these effects. We do not intend our review to be complete. In particular, we restrict ourselves to nanostructures coupled to reservoirs of free electrons (i.e. metals or semiconductors), and will not discuss the effect of superconductors at all. Further reading is proposed at the end of this introduction.

### 7.2.1 Work Generation in Nanostructures

The main form of work produced by nanostructures is electrical; i.e. they generate electrical power through a thermoelectric effect. This work production involves moving electrons from a region of lower electro-chemical potential to a region of higher electro-chemical potential. This does work in exactly the same way as moving a mass up a hill (from lower gravitational potential to higher gravitational potential). It can be thought of as charging up a very large capacitor (turning heat into electrostatic work), charging up a battery (turning heat into chemical work) or using this potential difference to drive a motor (turning heat into mechanical work). In all cases, if the nanostructure's thermoelectric effect moves  $N$  electrons in a time  $t$  from a region of electro-chemical potential  $\mu_1$  to a region of electro-chemical potential  $\mu_2$ , then the electrical power it produces (the work it does per second) is  $(\mu_2 - \mu_1)N/t$ . In such a case, the electrical current is  $I = eN/t$ , where  $e$  is the electronic charge, and one can define the voltage difference,  $V$ , via  $eV = (\mu_1 - \mu_2)$ . Then, we recover the familiar result that the electrical power produced is<sup>1</sup>  $P = -VI$ .

---

<sup>1</sup>The negative sign in  $P$  is because we take the electric current  $I$  to be positive when it flows from the reservoir at bias  $V$  to the reservoir at zero bias. Then  $I$  has the same sign as  $V$  when it flows "downhill" (from a region of higher bias to one of lower bias) turning electrical power into Joule heating. This means that if the device is to *generate* power, then  $I$  must have the opposite sign to  $V$ , so it is pushing electrical current "uphill".

### 7.2.2 Traditional Bulk Semiconductor Thermoelectrics

It is worth mentioning that bulk semiconductor thermoelectrics have been used to turn heat into electrical power for more than 40 years. The most spectacular example being the Curiosity rover on Mars, which is a 900 kg car-sized vehicle — packed with scientific instruments — powered entirely by a thermoelectric generator (the heat source being the radioactive decay of a lump of plutonium-238). Such thermoelectrics are used in space applications because their lack of moving parts makes them incredibly durable (the radioisotope thermoelectric generator on the space-probe Voyager 1 has been working for more than 40 years, despite now being outside the solar system). Thermoelectrics can equally be used for refrigeration via the effect known as Peltier cooling. However, to-date these power sources and refrigerators are too inefficient to be competitive for everyday earth-bound applications. For example, the power source on the Curiosity rover has an efficiency of about 6%, when the Carnot efficiency for the temperature difference in question would be of order 75%.

We cannot pretend that nanoscale thermoelectrics are currently in a position to do better; the efficiencies of the current experimental nanoscale thermoelectrics are tiny. It is clear that a better understanding of nanoscale thermoelectric effects will lead to large increases in the efficiencies. Whether they will get to the point of out doing bulk semiconductor thermoelectric remains to be seen. A further expected advantage of nanoscale thermoelectric devices is however, that they provide ideas for on-chip refrigeration and waste-heat recovery for future nanoelectronic applications.

### 7.2.3 What is Different at the Nanoscale, and What is Quantum?

If we compare nanostructures with traditional bulk solid-state devices, the main difference is that shown in Fig. 7.1. In nanostructures, all the interesting dynamics happens on a scale much smaller than the typical scale over-which electrons relax to a local thermal equilibrium. Thus, the distribution of electrons in the nanostructure can be far from an equilibrium one. This means that such systems cannot be described by the usual Boltzmann transport theory, and can exhibit the rich physics associated with highly non-equilibrium distributions. At the same time, the fact that the nanostructure can be of the size of the electron's wavelength, means that it often exhibits a quantization of energy levels similar to those in an atom; such structures are thus sometimes called *artificial atoms*. A major approach to design nanostructures is by patterning semiconductor heterostructures (and thereby partially depleting a 2-dimensional electron gas forming at one of the heterostructure's interfaces), see for example Ref. [13]. Another way of building nanostructures is to grow self-assembled quantum dots, or to place molecules with interesting discrete energy levels between metallic contacts, particularly carbon nanotubes or large organic molecules.

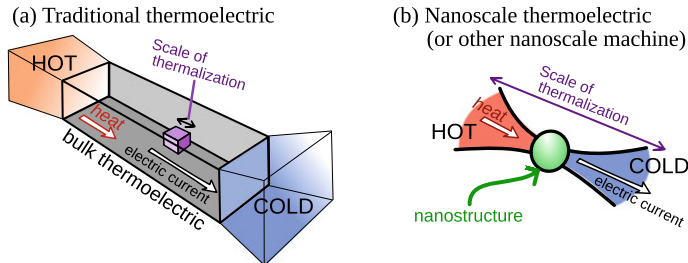


**Fig. 7.1** Figure adapted from Ref. [12]. In a traditional thermoelectric (a), the lengthscale on which the electrons relax to a local equilibrium is shorter than any lengthscale associated with the structure. As a result, the electrons at each point in the structure can be treated as being in local thermal equilibrium, and have a local temperature which varies smoothly across the structure. Then the system is well described by Boltzmann transport equations. In contrast, in nanoscale thermoelectrics (b), or other nanoscale devices, the nanoscale structure is of similar size or smaller than the lengthscale on which electrons relax to a local equilibrium. Then the physics of the system can be much richer, exhibiting highly non-equilibrium effects. The lack of local thermalization also means that the dynamics exhibit intrinsically quantum effects, which would otherwise be destroyed by the decoherence that always accompanies thermalization.

Many nanoscale structures are larger than a Fermi wavelength, and the electrons should be thought of as free particles moving around in the nanostructure, bouncing off disorder or the nanostructure's boundaries, tunnelling through barriers, etc. However, such a nanostructure is often smaller than the lengthscale over which electrons decohere; in other words, the electrons can pass through the nanostructure without losing the phase of their quantum wavefunction. This means their dynamics can exhibit interference effects analogous to those in optics (Young's interference, Fabry–Perot, Mach–Zehnder, etc.) as well as the famous Aharonov–Bohm effect, see e.g. Ref. [14]. Such effects cannot be described by the classical transport theories (such as Boltzmann transport theory) used for bulk systems.

In principle, the long coherence times of the electron wavefunctions also mean that entanglement generated between electrons (through their interactions with each other inside the nanostructure) will survive long enough to have effects on the device's operation. However, clear cut observations of entanglement has proved more difficult than observing interference effects. Some steps towards devices that involve entanglement can be seen in Refs. [15–17].

#### 7.2.4 What Else can we Learn from Thermoelectrics?

As with other systems studied in quantum thermodynamics, to find ways of generating a large power with high efficiency is not the only question. Indeed, much of the field is focused on the more fundamental issue of understanding the physics of thermoelectric nanostructures. In particular, we know that the thermoelectric response of

a system gives us access to different information from a measurement of its charge conductance. For example, in systems described by Landauer-Büttiker scattering theory<sup>2</sup> the thermoelectric response depends on the difference between the dynamics of electrons above the Fermi surface from the dynamics of electrons below the Fermi surface [21, 22] (i.e., on broken electron-hole symmetry), when the electrical conductance only depends on the sum of the two. Thus, thermoelectric effects can be used as novel probes of the physics happening within nanostructures. However, to make such a probe quantitative, one needs good quantitative models of the thermoelectric responses of all kinds of nanostructures, regardless of whether those responses are large or small.

Examples of uses of thermoelectric effects to study the physics of nanostructures include: the detection of interaction between different channels in the quantum Hall regime [23], the presence of odd superconducting states [24], the scale on which energy relaxation occurs [25, 26], signatures of exotic or topological states [27, 28], the existence of neutral modes in fractional quantum Hall states [29, 30], and anyonic currents [31].

### 7.2.5 *Further Reading*

For readers interested in more details on thermoelectric effects in nanostructures, we can suggest the review in Ref. [12]. The thermoelectricity of structures containing superconductors is discussed in Refs. [5, 32], while the quantum thermodynamics of other superconducting circuits are discussed elsewhere in this book. Reviews of quantum dots and their potential for thermoelectric effects are given in Refs. [33, 34]. Thermoelectric effects in atomic and molecular junctions are reviewed in Refs. [35–37]. Reference [38] gives a taste of a variety of topics related to mesoscopic thermoelectrics. Reference [39] is a textbook that overviews a number of theories of transport in nano-systems; those discussed here and others.

It is also worthwhile having a basic overview of thermoelectricity in bulk systems, such as provided in the textbooks [40–42]. Useful reviews on bulk thermoelectrics include Refs. [43–46], with perspectives for nano-structured bulk materials in Refs. [47, 48]. Thermal transport at the nanoscale is reviewed in Refs. [49, 50].

---

<sup>2</sup>In Landauer-Büttiker scattering theory, the mesoscopic electronic device is viewed as a scatterer onto which electronic wavefunctions, incoming from the leads, impinge and are transmitted or reflected. This well-known powerful approach is particularly useful for systems with weak Coulomb interaction and underlies the reasoning of various sections of this chapter. Details can be found in various text books, see for example [18–20].

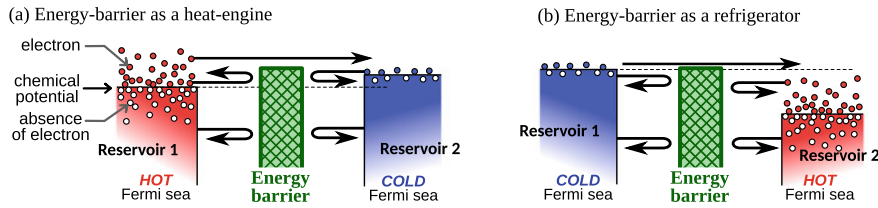


**Fig. 7.2** A sketch, adapted from Ref. [12], which shows energy selection via an energy barrier, which induces a thermoelectric effect. At zero temperature, electronic states in the reservoirs would be filled up to the Fermi energy, which is indicated by the upper limits of the red and blue regions. Non-vanishing temperatures lead to thermal electron-hole excitations modifying the occupation in the reservoirs. This simple set-up is used as a heat engine in (a); it generates power because the temperature difference means that electrons flow from a hot region of lower electrochemical potential to a cold region of higher electrochemical potential. It is used as a refrigerator in (b); it uses the potential bias to ensure that electrons above the Fermi sea can flow out of the cold reservoir, cooling it further.

### 7.3 Energy Selection for Heat to Work Conversion

The simplest solid-state device to convert heat into work (or to use work to move heat from cold to hot) is one that selects energies, by only allowing certain energies to flow through it (thereby acting as an energy filter). An energy-barrier is the simplest such energy selective system, an example is sketched in Fig. 7.2. All particles with energies above the top of the barrier can flow freely between hot and cold, while all those with energies below cannot, so the barrier is a *high-pass* energy filter.<sup>3</sup> This energy filter acts as a *thermoelectric*, because a heat current induces a charge current and vice-versa.

While bulk semiconductor thermoelectrics are not the subject here, we do note that they function in a similar manner. Their energy selection is induced by their band-structure, with charge carrier flowing at energies in a band, and not flowing at energies in a band gap. The physics is a little different because thermalization occurs inside the structure (with the local temperature dropping uniformly from hot to cold), but is well captured by Boltzmann transport theory [41, 51].

A crucial question when exploiting the exotic features of nanostructures for thermoelectrics, is how the well-known laws of thermodynamics apply. On a practical level, it is generally assumed that physical systems will not violate these laws, which raises the question of verifying that theoretical models do not violate them either. On a more philosophical level, it is believed that the laws of thermodynamics (particularly the second law) are an emergent property of more fundamental laws of physics. Thus, one can ask if they can be derived from a suitable quantum theory. This can be done relatively easily in the context of quantum thermoelectrics with weak enough

<sup>3</sup>We know from the textbook problem of a quantum particle hitting a barrier, that the transmission probability will be a smooth function of energy (going from zero at low energies to one at high energies), because the solution of the wave equation allows for tunnelling through the barrier.

electron-electron interactions that such interactions can be ignored (both in the reservoirs and in the nanostructure), see Box 1. Then, the steady-state flow through the nanostructure can be modelled with Landauer-Büttiker scattering theory. It is not hard to show, within this theory, that the dynamics will not violate the laws of thermodynamics. The detailed proofs are given elsewhere, such as in Ref. [12] and we just briefly outline them here,

- **First law of thermodynamics.** An electron with energy  $E$  passing from reservoir 1 to reservoir 2 through the nanostructure conserves its energy. In contrast, this process generates a work of  $\mu_2 - \mu_1$ , where  $\mu_1$  and  $\mu_2$  are the electro-chemical potentials of the two reservoirs. However, this process removes a heat equal to  $E - \mu_1$  from reservoir 1 and adds a heat  $E - \mu_2$  to reservoir 2. Thus, the sum of the heat and work generated by the process is zero, and we have the first law of thermodynamics.
- **Second law of thermodynamics.** Following the Clausius definition, the entropy change in reservoir  $j$  equals the change in that reservoir's heat multiplied by its inverse temperature  $\beta_j$  (for simplicity we measure entropy in units of  $k_B$ ). In Landauer scattering theory, the flow of electrons at energy  $E$  from reservoir 1 to reservoir 2 is  $\mathcal{T}(E)[(f(x_1) - f(x_2))]$ , where  $\mathcal{T}(E)$  is the transmission probability at energy  $E$ , and  $f(x_j)$  is the Fermi distribution function for electrons in the reservoir  $j$  with  $x_j = \beta_j(E - \mu_j)$ . The total entropy change (change in reservoir 1 and 2) due to electron flow at energy  $E$  is thus proportional to  $(x_2 - x_1)[f(x_1) - f(x_2)]$ . As  $f(x)$  is a monotonically decaying function of  $x$ , this is never negative, and the second law is guaranteed.

Given the proof of the second law, it is not hard to guess that the only way to make the system reversible in the thermodynamic sense (i.e. to ensure it generates no entropy) is to only allow transmission between reservoir 1 and 2 at the one energy where the Fermi distribution functions in reservoir 1 and 2 are equal. We call this reversibility energy  $E^{\rightleftharpoons}$  and it equals  $\mu_1 + \beta_2(\mu_2 - \mu_1)/(\beta_2 - \beta_1)$ . The fact that the occupation function for reservoir states is the same in the two reservoirs at this energy, means that the same number of particles flow from 1 to 2 and from 2 to 1, and so there is no heat current or electrical current. However, if one allows particles to flow in a vanishingly narrow energy window just above  $E^{\rightleftharpoons}$  then there will be an infinitesimal current, which converts heat to work with infinitesimal entropy production, so the efficiency of the conversion is arbitrarily close to Carnot efficiency [52, 53]. Such an ideal energy-selection can be constructed with a quantum dot or molecule with a single-level at an energy tuned to be at  $E^{\rightleftharpoons}$ . Systems similar to this have been made experimentally, for a recent review of quantum dots see [54], and for a discussion of molecules see [6, 10, 55]. There are various practical reasons why these systems do not reach Carnot efficiency, the most difficult one to resolve is the flow of heat from hot to cold through phonons and photons, which parasite the efficiency. Note that designs to improved bulk thermoelectrics (for example by nanostructuring them), by giving them peaked spectra have been proposed and heavily exploited [51, 56–59].

### 7.3.1 Quantum Bounds on Efficiency at Finite Power Output

The fact that electrons are quantum objects places bounds on a thermoelectric's power output and efficiency [60–62], which do not appear in classical thermodynamics. These *quantum bounds* come from the wave-like nature of the electrons. The first observation of this type was due Pendry [63], derived from the Landauer scattering

#### Box 1: Interactions between electrons in nanostructures

Interactions between electrons in nanostructures are counter-intuitive; electrons interact strongly with each other when their density is *low*, but interact weakly when their density is *high!* This is a consequence of them being fermions, and is formally described by Landau-Fermi liquid theory. However, we can get a hint of why this is from a simple argument comparing the kinetic energy to the Coulomb interaction energy. If we consider  $N$  free electrons in a  $d$ -dimensional box of size  $L$ , they form a Fermi surface whose Fermi momentum  $p_F$  is given by the equation  $N \sim (p_F L / h)^d$  (we drop all factors of order one). Thus, the kinetic energy per electron at the Fermi surface goes like  $N^{2/d}$ . In contrast, the Coulomb interaction energy goes like  $1/r$ , and the typical distance between particles  $r$  goes like  $N^{-1/d}$ , hence the Coulomb energy per electron goes like  $N^{1/d}$ . Thus, for large  $N$ , the kinetic energy will dominate over the Coulomb interaction energy, and one can guess that interaction effects will be weak. Landau-Fermi liquid theory gives a quantitative theory of this, and explains that screening effects enhance this suppression of the Coulomb interaction energy at high-density.

In the context of nanostructures, this means that we can often treat the reservoirs (which typically have a high density of electrons) as containing non-interacting electrons. However, the nanostructure itself can have a low density of electrons confined in a manner that reduces their screening. Thus, Coulomb interaction effects between the electrons in the nanostructure can be significant, and can lead to various effects, such as *Coulomb blockade* or *Luttinger liquid* physics. Alternatively, the nanostructure could consist of multiple regions with high electron densities, separated by barriers (where the electron density is low or even zero) which block the free flow of electrons. Then electrons are approximately non-interacting within each region, but there are strong interactions between the electrons in the different regions, just like the well-known interaction between capacitor plates.

The exact value of the Coulomb interaction in a given nanostructure can often be hard to predict, because it depends a lot on the screening due to the electron gases in the vicinity of the nanostructures (for example the electron gases in the reservoirs). It is thus typically quantified in terms of phenomenological capacitances, which must be measured in the nanostructure in question.

theory by observing that heat flow is maximized by having all electrons in each mode being transmitted at all energies. Then the upper bound on the heat current out of a reservoir at temperature  $T$  [63],

$$J_m = \frac{\pi^2}{6h} N (k_B T)^2. \quad (7.1)$$

Here,  $N$  is the number of modes in the cross-section through which that heat current is flowing, which is given by the cross-section measured in units of the Fermi wavelength. This is much like the Stefan-Boltzmann law for heat carried by the photons emitted from a black-body. This upper bound is due to the wave-like nature of the electrons, because if one takes the electron wavelength to zero, the number of modes  $N$  in a given cross-section diverges, and the above limit becomes irrelevant. Pendry's work [63] also used this to point out that the rate of reduction of entropy in a reservoir,  $-(dS/dt)$ , cannot exceed  $J_m/T$ , and made the connection to the amount of information that can flow in an  $N$  mode channel, but we do not discuss that further here.

As there is also an upper bound on a heat-engine's efficiency (given by Carnot efficiency), the above upper-bound on heat current directly implies an upper-bound on the heat engine's power output. A more detailed look at the Landauer scattering theory makes one realize there is a contradiction between maximizing the heat flow (which occurs when electrons flow from hot to cold at all energies) and maximizing the efficiency of a heat-engine (which requires only letting electrons flow at one specific energy). References [60–62] found the compromise between these two limits which maximizes the power output of a thermoelectric. That maximum, which depends only on temperature and universal constants, is

$$P_{\text{output}}^{\max} = \frac{A_0 \pi^2}{h} N k_B^2 (T_{\text{hot}}^2 - T_{\text{cold}}^2) \quad (7.2)$$

where  $A_0 \simeq 0.032$ . This was recently probed experimentally in a InAs nanowire [64], however to get a feeling its implications, it is easier to apply it to a more macroscopic situation. We can consider the case of recovering energy from the waste heat in car exhaust ( $T_{\text{hot}} \sim 700\text{ K}$  and  $T_{\text{cold}} \sim 300\text{ K}$ ) and a Fermi wavelength of order  $10\text{ nm}$  (such as in a typical semiconductor). This equation means that a millimetre-square cross-section (which thus carries  $N \sim 10^{10}$  modes) cannot generate more than about  $300\text{ W}$  of power. Remarkably, it is quantum mechanics which gives this bound (since it would be infinite if one sets the electron wavelength to zero), even though the cross-section and power outputs in question are macroscopic. A power output of  $300\text{ W}$  per  $\text{mm}^2$  seems fairly large, until one realizes that a filament lamp has a filament whose cross-section is ten thousand times smaller at  $10^{-4}\text{ mm}^2$  yet it can easily carry  $100\text{ W}$ .

References [60–62] show that there is a more stringent bound on efficiency than Carnot's bound at any finite power output. A device can only get to an efficiency as large as Carnot efficiency if the power output is much less than  $P_{\text{output}}^{\max}$ . The efficiency

bound deviates from Carnot efficiency by a factor which goes like  $(P_{\text{output}} / P_{\text{output}}^{\max})^{1/2}$  for  $P_{\text{output}} \ll P_{\text{output}}^{\max}$ , so Carnot efficiency is only strictly achievable when  $P_{\text{output}} \rightarrow 0$ . A more recent work [65], considered the effect of a large amount of relaxation inside the scatterer, and suggested that the deviation from Carnot efficiency might be smaller (going like  $P_{\text{output}} / P_{\text{output}}^{\max}$  for  $P_{\text{output}} \ll P_{\text{output}}^{\max}$ ). However, this still means that Carnot efficiency is only strictly achievable when  $P_{\text{output}} \rightarrow 0$ . This observation is due to the quantum nature of electrons, if one took the classical limit by taking their wavelength to zero,  $P_{\text{output}}^{\max}$  would go to infinity, and Carnot efficiency would be achievable at any  $P_{\text{output}}$ . It is not yet clear if these bounds apply beyond scattering theory, such as when there are significant Coulomb blockade effects.

### 7.3.2 Linear Response, the Seebeck Coefficient and the Figure of Merit

In the context of bulk thermoelectrics, it is common to talk about the Seebeck coefficient  $S$ , and the dimensionless figure of merit,  $ZT$ . The Seebeck coefficient is a measure of the strength of the thermoelectric effect.<sup>4</sup> The dimensionless figure of merit is a quantity that identifies the maximal thermodynamic efficiency of the thermoelectric. Both these quantities only have a sense in the so-called *linear response regime*, which occurs when the bias,  $V$ , and temperature difference  $\Delta T$ , across the sample are small enough that the electrical current is linear in  $V$  and  $\Delta T$ . This is typically the case when the temperature drop on the scale of the distance over which thermalization occurs is small compared with the temperature. In bulk thermoelectrics, this is almost always the case, see Fig. 7.1a, and so most of the literature discusses how to optimize  $S$  and  $ZT$ . In contrast, nanostructures leave the standard linear response regime as soon as the ratios  $\Delta T/T$  or  $eV/k_B T$  cease to be small.<sup>5</sup> Let us again refer to the commonly cited example of an application to generate electricity from the heat in the exhaust gases of a car at 600–700K when the surrounding temperature is at 270–300K; clearly a nanostructure that could do this would be operating far from the linear response regime, since  $\Delta T/T$  is obviously not small. Thus, this review mainly discusses modelling that goes beyond linear-response.

However, in many cases the first attempts to model a nanostructure's thermoelectric effect are in the linear-response regime, because it is simpler. So everyone interested in thermoelectrics should have a basic understanding of this regime, and the specific results one can derive there. This section briefly summarizes the most important ones, such as explaining the Seebeck coefficient  $S$ , and the dimensionless figure of merit,  $ZT$ .

<sup>4</sup>The Seebeck coefficient  $S$  is often called the thermopower, even though it does not have either the meaning or the units of power.

<sup>5</sup>In some special cases, one can construct a more exotic linear response theory when  $k_B \Delta T$  or  $eV$  are small compared to an energy scale which is not temperature.

In the thermodynamics of systems in the linear response regime, one can write the electrical current  $I$  and heat current  $J$  in terms of the thermodynamic forces,  $V/T$  and  $\Delta T/T^2$ , as follows

$$\begin{pmatrix} I \\ J \end{pmatrix} = \begin{pmatrix} L_{11} & L_{12} \\ L_{21} & L_{22} \end{pmatrix} \begin{pmatrix} V/T \\ \Delta T/T^2 \end{pmatrix} \quad (7.3)$$

where the matrix is the Onsager matrix [1]. In the context of thermoelectric systems one tends to write this matrix in terms of parameters commonly measured in experiments. Then it takes the form of the pair of coupled equations

$$I = G V + GS \Delta T, \quad (7.4)$$

$$J = G\Pi V + (K + GS\Pi) \Delta T. \quad (7.5)$$

These two equations contain four parameters with the following experimental meanings. The electrical conductance,  $G$ , is defined as the ratio  $I/V$  when there is no temperature difference,  $\Delta T = 0$ . The Seebeck coefficient,  $S$ , is a measure of the voltage generated across a thermoelectric by a temperature difference, when that thermoelectric is not connected to an electrical circuit, so  $V$  takes the value that ensures that  $I = 0$ . Hence,  $S$  defines the thermovoltage  $V_s = -S\Delta T$ <sup>6</sup> at which no charge current flows ( $V_s$  is also known as the stopping voltage). The Peltier coefficient,  $\Pi$ , is a measure of the directional heat flow induced by an electric current, when  $\Delta T = 0$ . Hence,  $\Pi$  equals the ratio  $J/I$  when  $\Delta T = 0$ . Onsager showed that  $\Pi = TS$  in the absence of an external magnetic field (or more generally, for systems with time-reversal symmetry) [1]. Finally,  $K$  is the thermal conductance, defined as the Fourier heat flow divided by  $\Delta T$ , where the Fourier heat flow is the heat flow when the thermoelectric is not connected to an electrical circuit, so  $V$  takes the value that ensures that  $I = 0$ ; hence  $K = J/\Delta T$  under the assumption that  $V = V_s$ .

If one can find  $G$ ,  $S$ ,  $\Pi$  and  $K$  for a given nanostructure, either through experimental measurement or by theoretical modelling, one has a complete description of the system's thermoelectric response, for any  $V$  and  $\Delta T$  small enough to remain in the linear response regime. One can calculate the power output  $P = -VI$  and the efficiency  $\eta = P/J$  for any given (small enough)  $\Delta T$  as a function of  $V$ . If one tunes  $V$  to maximize the heat-engine's power output  $P$  instead of  $\eta$ , one finds that the maximum power is

$$P_{\max} = \frac{1}{4}GS^2 \Delta T^2. \quad (7.6)$$

With a bit more algebra, one can find the voltage  $V$  at which the efficiency  $\eta$  is maximal, and prove that this maximal value of efficiency for a heat engine is

---

<sup>6</sup>There is ambiguity in the literature about the sign of  $S$ . One can choose either sign, as long as one is consistent.

$$\eta_{\max} = \eta_{\text{Carnot}} \frac{\sqrt{ZT + 1} - 1}{\sqrt{ZT + 1} + 1}, \quad (7.7)$$

where the Carnot efficiency in the linear response regime is given by  $\eta_{\text{Carnot}} = \Delta T / T$ , and we define the dimensionless figure of merit

$$ZT = \frac{GS^2T}{K}. \quad (7.8)$$

This dimensionless figure of merit is a simple measure of the quality of a thermoelectric; it is zero in the absence of thermoelectricity, and we see from Eq. (7.7) that Carnot efficiency requires that  $ZT \rightarrow \infty$ . Current bulk semiconductor thermoelectrics have  $ZT \sim 1$  (i.e. maximum efficiency of about  $\eta_{\text{Carnot}}/6$ ), while it is commonly stated that they will become useful for everyday applications if one could get  $ZT \sim 3$  (i.e. maximum efficiency of about  $\eta_{\text{Carnot}}/3$ ). One sees immediately why the conduction of heat by phonons and photons is always bad in pure thermoelectric applications (see the next section); they contribute to  $K$  in the denominator of  $ZT$  without making any contribution to the numerator.

As mentioned above, this linear response theory works well for bulk thermoelectrics, and the literature principally discusses maximizing  $S$  and  $ZT$ . However, in nanostructures it fails as soon as  $\Delta T/T$  (or  $eV/k_B T$ ) ceases to be small. When these are not small,  $I$  and  $J$  become highly non-linear functions of  $V$  and  $\Delta T$ , which cannot be described in terms of  $G$ ,  $S$ , etc. As a result  $ZT$  ceases to have any meaning, and instead the literature discusses power outputs and efficiencies. Thus, while modelling nanostructures in the linear response regime is extremely important for our understanding because it is often simpler than the non-linear regime, we believe that it is crucial to go beyond. We here mention an approach making use of symmetry relations of the time-evolution operator of open fermionic systems [66] that has recently been exploited to straightforwardly determine linear as well as nonlinear response-coefficients of weakly coupled quantum dots acting as thermoelectrics [67]. The rest of this review considers non-linear systems for which one must directly calculate the power outputs and efficiencies, and rarely mentions the linear-response quantities  $S$  or  $ZT$ .

## 7.4 Parasitic Heat Flows: Phonons and Photons

A problem that is not to be overlooked in any quantum thermodynamic device, but which is particularly important for nanostructures, is the problem of uncontrolled heat flows. These are nearly always parasitic for the operation of the device. Any device carries heat in the flow of electrons and also in the flow of photons and phonons. The heat carried by the electrons can be controlled, e.g., by electric fields, and can be made to produce electricity at relatively high efficiency. However, the flow of photons and phonons is hard to control, and their flow from hot to cold does

not generate any electric power. Thus, a device which efficiently converts the heat flow from hot to cold *carried by electrons* into electricity, will still have a very low thermodynamic efficiency if there is a larger heat flow from hot to cold carried by *photons or phonons*.

The problem with phonons and photons is that they are hard to control. As an example of this, it is intriguing to note (see Fig. 7.3 of Ref. [12]) that the materials which are the best thermal conductors (such as diamond or copper) have a thermal conductivity which is only about 4 orders of magnitude higher than the worst heat conductors (glasses). Indeed, even the vacuum conducts heat through the exchange of photons in the form of black-body radiation. One can compare this with electrical conductors, where the best (such as copper) have an electrical conductance which is 24 orders of magnitude higher than the worst electrical conductors (such as diamond).

Many nanostructures are studied in dilution refrigerators that cool them down to a fraction of a Kelvin (the lowest achievable temperatures are of the order of 10 milli-Kelvins). At such low temperatures, the situation is less bad than at room temperature. In particular, thermal photons in vacuum at less than a Kelvin have a wavelength of about a millimetre. So two regions of smaller than millimetre size at different temperatures will have difficulty exchanging heat by thermal photons through vacuum, because they are smaller than a wavelength. The situation is more complicated in nanostructured circuits, because the wires act as wave-guides that can carry a much shorter wavelength thermal photon from hot to cold [68, 69]. However, in general, phonons are a much more significant source of heat flow from hot to cold, since thermal phonon wavelengths are typically tens of nanometres. Most standard nanostructures are deposited on an electrically insulating substrate, which is a volume through which phonons can flow from the hot part of the nanostructure to the cold part. To avoid this, people are starting to develop suspended nanostructures, where the substrate is replaced by a vacuum [4, 55, 70, 71]. This is a huge extra technical difficulty, but it may be essential to reduce phonon flows to acceptable levels.

Currently, the field of quantum thermodynamics has two big domains of interest. One domain is the subject of this review, and is to understand the transformation of heat into work in quantum systems (with the associated question of what is heat, work and entropy in such situations). The second domain is to understand if and how isolated many-body quantum systems relax to a thermal state through internal interactions (with the associated question of how such a relaxation can be irreversible). The above discussion of the difficulties of isolating a nanostructure from its environment should make it clear that it is hard to address the second domain experimentally with such nanostructures. Trapped atomic gases are better because it is easier to isolate the many-body system in question, than in nanostructures.

### 7.4.1 Peltier Cooling — Using the Weakness of Electron-Phonon Coupling at Sub-Kelvin Temperatures

An unusual feature of sub-Kelvin systems is that the electrons and phonons are much more weakly coupled to each other than at room temperature. The strength of the electron-phonon coupling goes like the 5th power of temperature, so the coupling is  $10^{-12}$  times smaller at 1K than at 300K. Hence at low enough temperatures, one should think of the system as one containing two gases (one being the electrons and the other being the phonons) which both thermalize within themselves relatively fast, but which are so weakly interacting that they may be at different temperatures. The dilution refrigerator cools the phonons (i.e. it cools the lattice), and the temperatures given for the temperature in the refrigerator are typically those of the phonons. Experimentalists know that the electrons are often hotter, because the nanoscale circuit inside the refrigerator is coupled through wires and amplifiers to the electronics at room-temperature, used to control and probe the nanostructure. To ensure that the electrons in the nanostructure are as cold as the dilution refrigerator, one must make their coupling to room-temperature electrons much smaller than their coupling to the cold phonons in the dilution refrigerator. Despite experimental progress in isolating the nanostructure from the room-temperature electronics, this becomes increasingly challenging as one goes to lower temperatures, because of the weakness of the electron-phonon coupling.

One idea of great interest is to use thermoelectric effects to cool the electrons directly, thereby avoiding the electron-phonon coupling. One could imagine a small gas of electrons in the dilution refrigerator (at some temperature close to the refrigerator temperature) being cooled to a much lower temperature through a thermoelectric effect. Then the electrons would be colder than the phonons, but the weakness of the electron-phonon coupling would mean that electrons would stay cold, because the phonons would be rather inefficient at heating them up. Furthermore, one can also define non-invasive refrigerators, in the sense that they do not need to inject an electric current into the system to be cooled down [72, 73], which can hence be further isolated from the rest of the circuit. In the long term it is hoped that such thermoelectric cooling could enable us to study the properties of electrons (new phases of matter, quantum phase transitions, etc.) at unprecedented low temperatures. Most current experimental sub-Kelvin thermoelectric refrigerators rely on superconductors which are discussed in Refs. [5, 32, 74], although the refrigeration of microscopic semiconductor electron gases with quantum dots was also achieved some time ago [75].

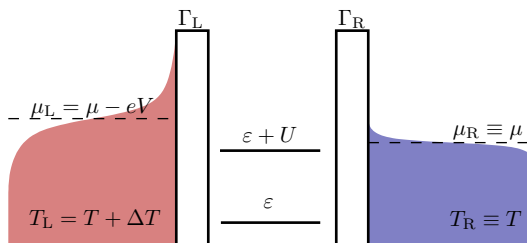
### 7.4.2 Intrinsic Leakage in Electronic Devices

In addition to the major problems of leakage heat currents carried by phonons and photons in otherwise electronic devices — as described in the sections above — the electronic heat current itself can give rise to leakage. This is also known from

### Box 2: Quantum dots

Quantum dots can be experimentally realized in a large variety of ways, including the patterning of semiconductor heterostructures, etching graphene, contacting carbon nanotubes or other types of molecules, etc. See e.g. [77, 78] or text books in which these devices are treated [13, 79]. In a quantum dot, electrons are confined and occupy discrete energy levels, similar to the situation in an atom. Furthermore, due to the smallness of the device, electrons are subject to strong Coulomb interaction. One of the important features of a quantum dot is that it can be contacted to electronic reservoirs (allowing for electronic transport through it) and controlled by external gates to which voltages can be applied. While there is possibly a large number of electrons in the quantum dot, the physics of the device is typically governed by tunnelling processes of single electrons. When describing the dot physics, we therefore set the reference occupation number to '0' and from here on talk about occupation states '0,1,2' referring to *extra-electrons* that enter the dot due to the application of bias or gate voltages.

The figure shows a sketch of the energy landscape of a quantum dot in contact with two electronic reservoirs. In this simplified (however experimentally relevant example!) we assume that a single electronic level is energetically accessible; it has the energy  $\varepsilon$ , additional term proportional to  $-eV_g$ . Such a discrete energy level is an optimal realization of the peaked energy spectrum useful to improve thermoelectric operation [51].



In order to add a second electron on the dot, the Coulomb interaction energy  $U$  has to be paid. The coupling to the left and right reservoirs is characterized by the coupling strengths  $\Gamma_L$  and  $\Gamma_R$ . In contrast to the quantum dot, the electronic reservoirs have a continuous spectrum and their occupations are given by equilibrium Fermi-functions with respect to a well-defined temperature and electrochemical potential, which can be different in each reservoir. In this example, we show Fermi distributions of a cold and a hot reservoir, relevant in the context of thermoelectrics. Note that the temperature *in the dot* is typically not a well-defined quantity!

bulk systems, where electrons can transfer heat by Coulomb interaction and electron-electron scattering, leading to electronic Fourier heat transfer in the absence of charge currents, see e.g. standard books like [76]. Its impact in nanoelectronic devices can easily be understood through the example of the quantum dot, shown in Box 2. When an electron tunnels into (or out of) the quantum dot in a single tunnelling process (sequential tunnelling), it takes along the energy determined by the single-electron energy level of the quantized spectrum. However, when the quantum dot is strongly coupled to the reservoirs, higher-order tunnelling processes through energetically forbidden states (such as elastic and inelastic cotunnelling) can occur. These processes thereby allow for energy transfer through the dot in the absence of charge transfer. Furthermore, the possibly strong on-site Coulomb interaction between electrons on the dot means that the energy to be paid in the transition  $1 \leftrightarrow 2$  is bigger by  $U$  with respect to the energy to be paid at the transition  $0 \leftrightarrow 1$ . A sequence of tunnelling processes through the dot therefore allows for the transfer of the interaction energy  $U$ , while no charge current is flowing.

## 7.5 Multi-terminal Steady-State Machines with Quantum Dots

In this section, we discuss examples for implementations of heat engines using quantum dots embedded in a multi-terminal electronic set-up. A quantum dot, see Box 2, is characterized by a discrete energy-level spectrum (similar to an atom) and possibly strong on-site Coulomb interaction. Quantum dots can be tunnel-coupled to electronic reservoirs allowing for electronic transport through them and their properties, such as the level spectrum, can be tuned via the application of external gates. These and other properties make electronic devices with quantum dots interesting for thermoelectrics or for nanoscale heat engines: first of all, their discrete spectrum provides a means for *energy-selective transport*, which is of high relevance for the efficiency of thermoelectric applications [51, 56–58]. Strong Coulomb interaction between electrons on different, *purely capacitively* coupled quantum dots can serve for the transfer of a well-defined amount of energy from a heat bath to a thermoelectrically active region. Finally, the idea of using a quantum dot — characterized by a small number of electronic states — as a working substance of a thermodynamic heat engine, requires a completely new understanding of these devices. The reason for this is that, historically, heat engines are made of large systems to which a statistical description applies. This however obviously breaks down in few-level devices such as quantum dots. Indeed, we will see at the end of this section that the resulting *absence of thermalization* in quantum dots in a non-equilibrium set-up can lead to counter-intuitive effects. All this makes quantum dot heat engines interesting from a fundamental point of view; however, as mentioned before, this research is also guided by a strong need for finding new ways of on-chip refrigeration and waste-heat recovery for future nanoelectronic applications, where quantum dot devices constitute fundamental building blocks.

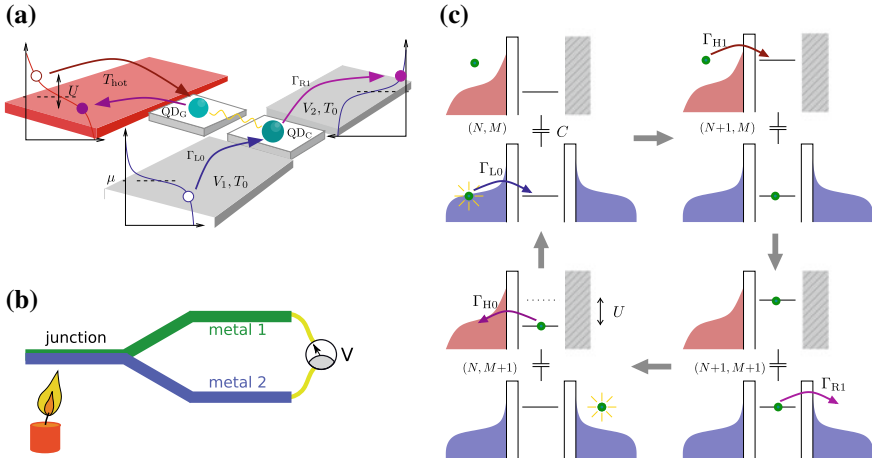


**Fig. 7.3** **a** Sketch of the three-terminal double-dot set-up acting as a nanoscale thermocouple. Heat is transferred from the electronic heat bath (in red) to the working substance (consisting in the quantum dot  $\text{QD}_C$  tunnel coupled to source and drain reservoir) via capacitive coupling between the two dots  $\text{QD}_G$  and  $\text{QD}_C$ . Coloured arrows, together with indicated states on the reservoirs Fermi distribution indicate the process shown in detail in **c**. **b** Sketch of a classical thermocouple. **c** The working principle of the nanoscale thermocouple, shown as a thermodynamic cycle. The red and blue distributions are the Fermi functions of the hot and cold reservoirs respectively. The vertical axis is energy, while the horizontal axis in the distributions is the probability, with which each energy state is occupied. (i.e. it shows a more quantitative representation of the electron distributions than sketched in Fig. 7.2). Grey, hatched regions indicate a boundary of the quantum dot without tunnel coupling.

Here we present a quantum-dot equivalent of a thermocouple (or energy harvester), proposed and analysed in Ref. [80], and recently realized experimentally in different groups [81–83], see Fig. 7.3a for a sketch of the set-up. One of the advantages of the multi-terminal design is that the heat bath is spatially separated from the working device. This might for example result in advantages with respect to the leakage effects due to phonons or tunnelling as discussed before. The set-up basically consists of two parts: the active thermoelectric region, shown in the lower, right part of the sketch is made of the central quantum dot,  $\text{QD}_C$ , tunnel-coupled to two electronic contacts at the same temperature  $T_0 < T_{\text{hot}}$ . The upper, left part of the sketch shows the heat bath in contact with a second dot  $\text{QD}_G$ . The occupation of this second dot strongly fluctuates due to the large temperature,  $T_{\text{hot}}$ , of the hot electrode, constituting the heat bath. This dot  $\text{QD}_G$  is *purely capacitively* coupled to the working substance, depicted in the lower half of the sketch. It is via this capacitive coupling between quantum dots (namely due to Coulomb interaction) that heat transfer between the heat bath and the thermoelectrically active region takes place. For simplicity, we now assume that each of the two dots can at most accept one extra-electron due to strong on-site Coulomb interaction. The two dots - forming a purely capacitively coupled double dot - can however each be singly occupied at the same time (such that the double dot

is doubly occupied); in this case the Coulomb interaction  $U$  needs to be provided. The working principle of this quantum-dot thermocouple can be understood by following the processes depicted in the sketch in Fig. 7.3c and also alluded to by the arrows in Fig. 7.3a. Assume that the two dots are initially empty and that - due to fluctuations - the lower dot gets occupied by an electron from the left reservoir. This electron has to be at the required single-particle energy for the transition from an empty to a single-occupied dot. If now a further electron enters the double dot from the hot reservoir by tunnelling into  $QD_G$ , an additional energy  $U$  has to be paid due to the capacitive coupling to the *occupied* lower dot. This extra energy  $U$  can be transferred to the working substance, when in the next process the electron of the lower dot  $QD_C$  tunnels out again, for example to the right reservoir. The described process is one of many possible tunnelling sequences that can in general occur in such a set-up. However, if  $T_{\text{hot}} > T_0$ , such that heat is on average transferred from the upper to the lower part of the device and if at the same time the asymmetry condition  $\Lambda \neq 0$  is fulfilled for

$$\Lambda = \frac{\Gamma_{L0}\Gamma_{R1} - \Gamma_{L1}\Gamma_{R0}}{(\Gamma_{L0} + \Gamma_{R0})(\Gamma_{L1} + \Gamma_{R1})}, \quad (7.9)$$

the described type of process can actually be used in order to do electrical work. The feasibility of this scheme has been proven in experiments [81–83]. Here, work is done by creating a *directed current against a bias voltage* in the lower part of the set-up - the working substance. The condition  $\Lambda \neq 0$  requires an asymmetry both in real space (the tunnel-coupling strength to the left reservoir,  $\Gamma_L$  has to be different from the tunnel coupling strength to the right reservoir,  $\Gamma_R$ ) but also an asymmetry in the energy-dependence of these couplings has to occur. The subscripts 0 and 1 indicate the tunnel couplings for the case that the upper dot is empty (0) or filled (1). Physically, such an asymmetry would make the process of Fig. 7.3c more probable than the ones with reversed directions or reversed order of tunnelling events. For the specific example, it would mean that it is more probable to fill the empty dot  $QD_C$  from the left reservoir when the upper dot  $QD_G$  is empty ( $\Gamma_{L0} > \Gamma_{R0}$ ), while it is more probable to empty the dot  $QD_C$  by an electron tunnelling to the right reservoir, when the upper dot  $QD_G$  is filled ( $\Gamma_{R1} > \Gamma_{L1}$ ).

The resulting charge current,  $I$ , between the left and the right contact is proportional to the heat current,  $J$ , transferred from the heat bath into the working substance *via the Coulomb interaction energy*. In the absence of a bias voltage between left and right reservoir, the charge current takes the simple form

$$I = \frac{-e\Lambda}{U} J_G. \quad (7.10)$$

If the asymmetry factor takes its maximal value, namely if it is equal to 1, then exactly one electron is transferred from left to right with each transfer of energy  $U$  from the heat bath to the working substance. Note that the asymmetry given in Eq. (7.9) constitutes the analogue of the two *dissimilar* metals of a classical thermocouple, as sketched in Fig. 7.3b.

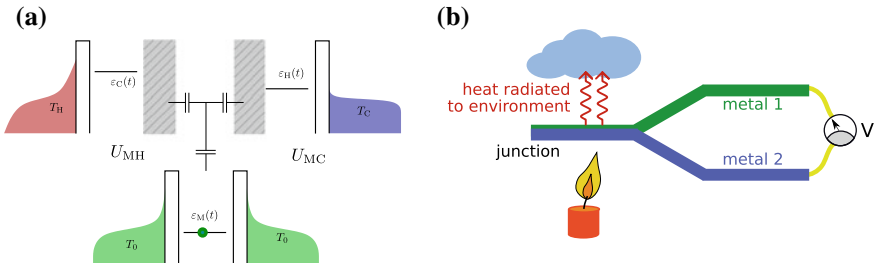


**Fig. 7.4** **a** Sketch of the four-terminal triple-dot set-up acting as a nanoscale thermocouple with two heat baths. Compared to the set-up shown in Fig. 7.3, the working substance is now additionally coupled to a cold bath. Also in this case the heat transfer between cold bath and working substance takes place via capacitive coupling between two dots. Note that in general, also capacitive coupling between the two upper dots can occur, which is detrimental for the operation of this device, but does not hinder the observed effects to occur. **b** Classical analogue, where the cold heat bath could be given by the environment to which the thermocouple can radiate heat.

As discussed previously, a big difference between classical heat engines and their quantum dot analogues lies in their dimensions with respect to the thermalization length. While a well-defined temperature can be associated to the bimetallic part of the classical thermocouple, this is in general not the case for a quantum dot when it takes the role of the working substance of a thermocouple as described above. This becomes particularly clear when one pushes the analogy to the classical thermocouple even further and assumes that in addition to the heat bath (indicated by the candle in the sketch in Figs. 7.3c and 7.4b) the thermocouple is in thermal contact also with a colder heat bath, e.g. the environment (indicated by the cloud in Fig. 7.4b). Also this set-up can be mimicked by quantum dots as shown in Fig. 7.4a, see Ref. [84].

Since now there is a capacitive coupling,  $U_{\text{MH}}$  and  $U_{\text{MC}}$ , between the working substance (dot with reservoirs) and *both* the additional quantum dots in contact with a hot and a cold reservoir, the total induced charge current (in the absence of voltage differences),<sup>7</sup>

$$I = -\frac{e\Lambda_C}{U_{\text{MC}}} J_C - \frac{e\Lambda_H}{U_{\text{MH}}} J_H. \quad (7.11)$$

has a contribution proportional to the heat current from the hot reservoir  $J_H$  to the working substance and the heat current from the cold reservoir,  $J_C$ , to the working substance. Here,  $\Lambda_C$  and  $\Lambda_H$  are the asymmetry factors in analogy with Eq. (7.9) with respect to the occupation of the dot in contact with the cold or the hot reservoir. This simple extension of the previous results, Eqs. (7.9) and (7.10), leads to an interesting twist: Even when the total heat current flowing from the heat baths *into* the working device,  $J_{\text{in}} = J_H + J_C$ , vanishes, a charge current can still be induced

<sup>7</sup>This simple relation is valid only if the direct capacitive coupling between the upper dots (which tunnel-couple to the hot and cold reservoirs) is so strong that they cannot be occupied simultaneously. Note however, that the effects described here continue to exist also in the presence of a smaller capacitive coupling,  $U_{\text{HC}} \sim U_{\text{MH}}, U_{\text{MC}}$ .

by the heat current flowing *through* the device from the hot into the cold reservoir,  $J_{\text{trans}} = J_H - J_C$ . This statement even holds when the induced current is transported against a voltage gradient between the left and right reservoir, thereby doing work. This observation leads to a number of seemingly paradoxical observations. The first direct consequence of this is obviously the possibility of doing work without absorbing heat from a heat bath! This means in particular that, in order to maintain energy conservation when doing work, heat has to be extracted from the reservoirs of the working substance, thereby cooling it down! Note that these observations - even though highly counter-intuitive - do however, as required, not violate any of the laws of thermodynamics. Not only is the total energy conserved in the process. Also the entropy of the total system does indeed increase while work is done. This is because the heat flow from the hot to the cold reservoir, which *drags* the induced current without any energy transfer, leads to an entropy production.

These effects result from the inability of the quantum dot to reach a thermal equilibrium. Importantly, when forcing the quantum dot to thermalize (for example via an additional probe contact attached to the central dot), the counter-intuitive power production without heat absorption is suppressed and the behaviour expected from a classical thermocouple is restored.

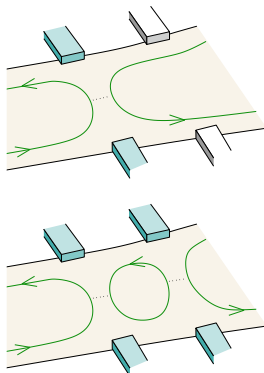
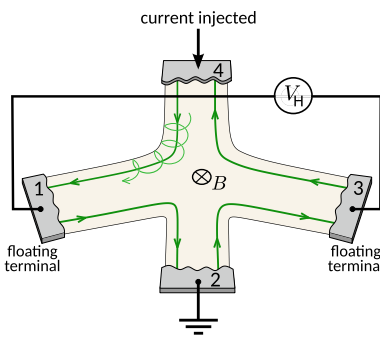
## 7.6 Quantum Hall Thermoelectrics

Quantum Hall systems, in which electron transport takes place along chiral edges, have several advantages from the thermoelectric point of view. Firstly, in quantum Hall devices, simple quantum point contacts are particularly easy to make, and allow for the implementation of thermoelectric effects. A quantum point contact forms a narrow constriction whose width controls the number of channels that can be transmitted, see also Box 3. Different channels can be totally transmitted, totally reflected, or partially transmitting. The partially transmitting ones are of interest for thermoelectrics, because the transmission probability is energy-dependent [89] (rapidly switching from low to high transmission with the magnitude of the electron's energy). This upper-pass filter is enough to break electron-hole symmetry and to give a finite thermoelectric response [60, 61]. Quantum point contacts were used for the first thermoelectric experiments in mesoscopic systems [90–92]. It has recently even permitted to infer the quantum of thermal conductance of a single *electronic* conduction channel [9], related to Eq. (7.1).

Secondly, transport through the sample is phase coherent up to device dimensions of the order of  $\mu\text{m}$ . This yields the possibility to have the heat source at a relatively large distance from the system of interest acting as the working substance. Thereby, the latter can be kept cold enough to perform operations. In this way, larger temperature gradients can be applied without overheating the system. Due to the long phase coherence length, it is furthermore possible to construct different types of interferometers (in analogy to optics) using quantum point contacts as beam splitters.

### Box 3: Quantum hall effect

A paradigmatic case of quantum electronic transport is the quantum Hall effect [85]. The occurrence of quantized conductance plateaux in this regime is a striking evidence for the fact that precise quantum measurements are not restricted to atomic scales but can also be performed in massive, disordered materials. This is ultimately due the quantization of cyclotron orbits (Landau levels) that lie below the Fermi energy in the centre of the sample but overcome it close to its borders, thereby forming chiral edge states [86]. Electron propagation in edge states occurs in analogy to photon propagation in a waveguide. However, electronic propagation in edge states is protected from backscattering by the chirality of the sample [87], even in the presence of (moderate) impurities and disorder (unlike for photons in waveguides). The figure on the right shows a typical Hall set-up, where a current is injected between terminals 4 and 2 and the transverse voltage is measured between probe terminals 1 and 3. Since electrons flow chirally along the edges of the sample, with its direction determined by the applied magnetic field, all electrons injected from terminal 4 are hence absorbed by terminal 1.



Since, furthermore, probes do not inject a net current, its potential must adapt to re-emit the same amount of charge into terminal 2. The same can be said of terminal 3, leading to a finite Hall voltage  $V_H = V_1 - V_3 = (h/e^2)I$ . The associated resistance (the von Klitzing resistance) is quantized and determined by fundamental constants (the charge of the electron,  $e$ , and Planck's constant,  $h$ ), and eventually by the number of channels,  $N$ :  $R_K = h/(Ne^2)$ .

The application of lateral gate voltages to the Hall bar can bring the two edges close enough to

each other, such that electrons can be backscattered by being transferred from one channel to the opposite. This means that a point contact is formed (in analogy to beam splitters in optics), see left figure for one (respectively two) pairs of gates to which a voltage is applied. This permits to perform scattering experiments on quantum point contacts [88], or even on different types of interferometers, like the Fabry-Perot interferometer shown in the bottom panel.

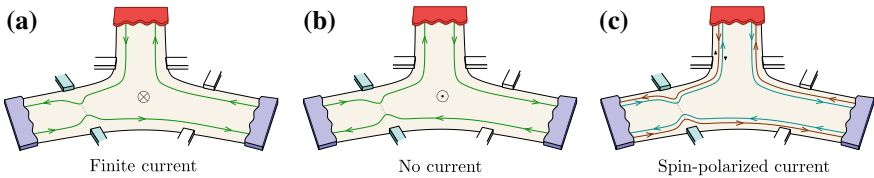


**Fig. 7.5** Chiral thermoelectrics in the quantum Hall regime. We show a three-terminal set-up, in which the upper terminal acts as a heat bath injecting a heat current into the lower part of the set-up. Only a single quantum point contact is required to produce a thermoelectric response by conversion of a heat current injected from terminal 3 into a charge current between terminals 1 and 2. In **a** electron-hole pairs injected from the hot reservoir impinge on the quantum point contact. In **b** the propagation direction of the edge channels is inverted by the inversion of the magnetic field. The result is that electron-hole pairs thermalize without having passed through the quantum point contact. **c** Modified set-up based on a topological insulator, in which spin-polarized edge states arise in the absence of a magnetic field. In all three panels, gate electrodes coloured in green are assumed to form a quantum point contact by application of a gate voltage, while we assume that no voltage is applied to gate electrodes coloured in white.

The thermoelectric response in these interferometers is then possible uniquely due to quantum interference occurring thanks to the energy dependence of the phase of the electronic wave function, which is gained in the propagation between beam splitters [93–95].

In this section, we will go further into a third reason making quantum Hall devices interesting for thermoelectrics. This is the straightforward possibility to design non-trivial multi-terminal devices — the quantum Hall effect being a multi-terminal effect by its own nature. This makes it possible to introduce quantum analogues of the Nernst effect [96, 97], where the injection of a heat current leads to a *transverse* electric response.<sup>8</sup> A minimal configuration with three terminals, as shown in Fig. 7.5, exhibits a peculiar behaviour as compared with a *trivial* three-terminal thermocouple. Let us consider a central probe terminal (indicated in red in all three figure panels) which injects heat into a system which is otherwise at the same lower temperature [62, 98, 99] (indicated by the two reservoirs at the bottom of the set-up depicted in blue). We now assume that there is a constriction realized by a quantum point contact on one side of the system only, see again Fig. 7.5. Electron-hole excitations created at the hot terminal and impinging on the lower part of the device are separated at the quantum point contact, when the latter is placed in the direction of their propagation, as realized in the sketch in panel Fig. 7.5a. This separation of electron and hole excitations results in a thermoelectric effect, namely a charge current is induced between the two lower contacts (respectively a thermovoltage builds up if the contacts are floating).

However, as soon as the magnetic field is inverted, the propagation direction along the edges is inverted, see panel (b) of Fig. 7.5. In that case, non-equilibrium electron-hole excitations propagate in the opposite direction and are all absorbed

<sup>8</sup>The thermoelectric response measured in a series of terminals has been used to probe how energy relaxation takes place along the edge, involving an elegant demonstration of chirality [25, 26].

and thermalized at the opposite terminal [100, 101]. As hot electrons and holes are never separated at the junction, no thermovoltage is generated. The chirality of the quantum Hall edge states thus manifests in the absence of a thermoelectric effect if one reverses the magnetic field. In this way, thermoelectrics can be used to probe the presence of chiral states. Interestingly, this absence of a Seebeck response (a thermovoltage) in the configuration of Fig. 7.5b comes with a finite Peltier response (namely, the application of a voltage can be used for cooling). This is a remarkable situation. As discussed in Sect. 7.3.2, the Seebeck and Peltier coefficients are directly proportional to each other whenever the system is time-reversal invariant [102]. A magnetic field obviously breaks this symmetry [22, 103], however in general both the Seebeck and the Peltier coefficient vanish simultaneously. To the best of our knowledge, only in the fully chiral system, realized in the quantum Hall regime, one of them can be zero while the other one is finite. What is remarkable, is that by changing the sign of the magnetic field, one can simply choose which of the two coefficients is zero and which one leads to a nonvanishing thermoelectric effect.

We finally want to mention two interesting extensions of this simple set-up. First, such an analogue of the Nernst effect can be used to probe the presence of edge states in two-dimensional topological insulators. In topological insulators, electrons with opposite spin flow in opposite directions due to a strong spin-orbit coupling. Transport is then said to be helical. In the geometry shown in Fig. 7.5c, one can see that spin up and down electrons propagate in opposite directions along the same edge. This picture can be immediately seen as a combination of the situation in Fig. 7.5a, b but for opposite spins. Namely, only one of the channels (the spin-up one, in this case) will lead to a thermoelectric effect, when a temperature gradient is applied between the upper contact and the lower contacts, as discussed above. Hence, the generated current is fully spin-polarized [100]. By optionally applying a gate voltage to the quantum point contacts on the two sides, the spin-polarization of the current induced by the temperature gradient can be controlled. Such effects are of interest in the context of spintronics [104].

As a second extension of the set-up discussed above, the broken time-reversal symmetry induced by the magnetic field has been suggested as a means to increase the thermoelectric efficiency at the point of maximum power generation [105]. In general, the upper bounds for the thermoelectric efficiency can be obtained from symmetry arguments [106]. A recently studied example is an engine based on the (four-terminal) Nernst effect, where the efficiency bounds can be reached only in the quantum regime [97], thereby outperforming the classical version [96]. The use of fractionally-charged carriers in fractional quantum Hall states (states induced by the interplay of electron-electron interactions and strong magnetic fields) has also been suggested in order to improve the efficiency [107].

## 7.7 Beyond Steady State: Heat Engines with a Time-Dependent Cycle

The tunability of the properties of small electronic structures, for example by applying voltages to gate electrodes, makes them interesting for the realization of heat engines with a cyclic operation. Various examples have been studied in recent years, see e.g. Refs. [108–111], some of them relying on quantum interference [112]. Also in experiments, nanoelectronic cyclic heat engines have been realized [113, 114].

Here, we explain the working principle of one simple example system, where the analogue of a Carnot engine can be implemented using time-dependently driven quantum dots [115]. The sketch in Fig. 7.6a shows the set-up with two quantum dots *tunnel-coupled* to electronic reservoirs *and* to each other (in contrast to the dots studied in the section about the quantum-dot analogue of a thermal couple presented above, which were *purely capacitively* coupled to each other). These electronic reservoirs can possibly be at different temperatures and/or electrochemical potentials and act as particle and heat baths. Depending on the gate voltage applied to the two quantum dots, this subsystem — representing the heat engine — is found in different (stable) charge configurations, see Fig. 7.6b. Some of these charge configurations are indicated in the figure; note that the degeneracy of each of these states depends on the electronic *spin*. For example, while the state  $(0, 0)$  is non-degenerate, the state  $(0, 1)$  is doubly degenerate, since the electron occupying the right dot can have either spin up or spin down. It therefore has a Shannon entropy given by  $\ln 2$ . Only at the boundaries of the stable regions, the occupation of the dot can change, and only at the so-called triple points where three stable regions touch, electron transport through the double dot can occur in a close-to-equilibrium situation. Importantly - in the weak coupling regime - electron-tunnelling at the *lines* between two stable configurations, leading to a change of the double-dot's charge state, always occurs with *one* of the reservoirs only.

We now consider a cyclic modulation of the gate voltages, which is typically used for the double dot operation as a quantized charge pump [116–118]. Such a double-dot pump can transfer charges even against an applied bias voltage and it can hence be viewed as a kind of “battery charger”; its efficiency depends on leakage currents and on the amount of heating occurring during the cycle. Interestingly, this pump can also be operated as a refrigerator or as a heat engine doing work on the AC fields, see Ref. [115] for details on the example discussed here. We now briefly explain the operational cycle of these machines, where we assume the driving to be infinitely slow. If the gate voltages,  $V_{g,L}(t)$  and  $V_{g,R}(t)$ , are driven in time in such a way that one of the triple points is enclosed by the driving cycle — see the example of the cycle around the upper triple point — exactly one electron is pumped through the device per period. Interestingly, this goes along with the transfer of a *quantized* amount of energy as well. This result can be understood following the processes occurring along the driving cycle. Let us assume that we start the driving cycle in the stable region  $(0, 0)$ . When crossing the line to the  $(1, 0)$  region, one electron is transferred from the left reservoir to the double dot, while also increasing its entropy from 0 to  $\ln 2$ .

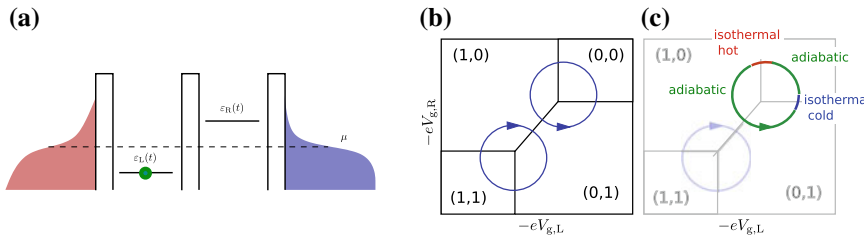


**Fig. 7.6** **a** Energy landscape of a double quantum dot, weakly coupled to a left and right reservoir which can be at different temperatures and electrochemical potentials. The single-particle levels of the two dots can be modulated by time-dependently driven gate voltages. The on-site Coulomb interaction on each dot is assumed to be infinitely strong, while the intra-dot Coulomb interaction is finite (it determines the distance between the stable regions  $(0, 0)$  and  $(1, 1)$  in the stability diagrams in **b**.) **b** Stability diagram for the weakly coupled double dot as function of the gate voltage applied to the two dots. Two possible driving cycles leading to the transfer of single electrons are indicated by blue lines. Generally, all gate voltage cycles enclosing a triple point lead to quantized charge in the slow driving regime and can even result in plateaux in the heat transport. **c** Analogy of the driving cycle with the thermodynamic cycle of a Carnot engine.

Even though the total system might be in nonequilibrium (either due to a temperature or a potential gradient or both) nonetheless the Clausius relation applies here: this is due to the fact that coupling occurs to a *single* reservoir at a time, leading to the occurrence of an *isothermal* process! The heat transferred between the reservoir and the double dot is hence given by  $k_B T_L \ln 2$ , with  $T_L$  being the temperature of the left reservoir. The following part of the cycle where an electron is transferred from the left to the right dot takes place while the double dot is effectively decoupled from both reservoirs. This part of the cycle is hence *adiabatic* in the thermodynamic sense. Finally a second isothermal transition occurs when the tunnelling process from  $(0, 1)$  to  $(0, 0)$  occurs due to coupling to the right reservoir only, leading to the transferred heat  $k_B T_R \ln 2$ . This sequence of processes leads to the transfer of quantized charge and heat and constitutes a close analogy to the Carnot cycle.

Note that the transfer of heat proportional to  $\ln 2$  directly links to the well-known Landauer principle, stating that the erasure of a bit of information (here implemented in the electron spin) goes along with the energy cost of  $k_B T \ln 2$ . The consequences of this principle are further treated in Part V of this book. Since the transfer of heat is directly linked to the spin degeneracy of the quantum dot spin, switching on a magnetic field would lead to the complete suppression of the effect.

In this infinitely slow driving regime — neglecting electronic leakage (heat or charge) currents which are strongly suppressed here — a heat engine extracting heat from the hot reservoir and doing work on the AC fields, can be operated in the Carnot limit (and similarly a refrigerator would have an optimal coefficient of performance). Note however, that a nonvanishing driving frequency drastically reduces the efficiency [115]. In contrast, the “battery charger” could operate at efficiencies of about 70% of the optimal value even when the driving frequency is increased.

## 7.8 Future Directions

This chapter shows a few examples of thermoelectric effects and heat engines proposed and/or realized in different types of nanoelectronic systems. However, the thermodynamics of nanoelectronic devices is an active research field and numerous open questions are currently being addressed, or will be of interest in the future.

On one hand, there is the ongoing quest for improving efficiencies of nanothermoelectrics, which to date are very small, with the exception of a very recent experiment [119]. The aim of such research is to improve device designs by increasing the desired electronic response and at the same time decreasing leakage (for example by introducing long photonic cavities [120] or using suspended structures [4, 55, 70, 71]).

On the other hand there are many fundamental questions (that could on the long term also lead to improved applications). For example, the nanostructures presented in this chapter involved either strong electron-electron interactions (Coloumb blockade) with weak coupling to the reservoirs, or negligibly small electron-electron interactions with arbitrarily strong coupling to the reservoirs. However, the regime of strong electron-electron interactions with strong coupling to the reservoirs is of great interest in quantum thermodynamics. In order to go to higher power outputs one is forced to consider stronger coupling. But the strong-coupling regime of nanoelectronic devices presents a challenge for theorists, see e.g., Refs. [121–125] and Chap. 23 in this book for recent developments.

Furthermore, as we mentioned previously, the potential of quantum interference and entanglement for new types of heat engine has been little exploited so far, and constitutes an intriguing direction to explore. Also, the possibility of engineering the state of the bath, using entanglement or correlations as a resource for engines, is currently investigated and addressed in other chapters of this book.

**Acknowledgements** We acknowledge the support of the COST Action MP1209 “Thermodynamics in the quantum regime” (2013–2017), which enabled us to meet regularly to learn about and discuss much of the physics presented in this chapter. RW acknowledges the financial support of the French National Research Agency’s “Investissement d’avenir” program (ANR-15-IDEX-02) via the Université Grenoble Alpes QuEnG project. RS is supported by the Spanish Ministerio de Economía y Competitividad via the Ramón y Cajal program RYC-2016-20778. JS acknowledges support from the Knut and Alice Wallenberg foundation and from the Swedish VR.

## References

1. H.B. Callen, *Thermodynamics and an Introduction to Thermostatistics* (Wiley, New York, 1985)
2. H. van Houten, L.W. Molenkamp, C.W.J. Beenakker, C.T. Foxon, Thermo-electric properties of quantum point contacts. *Semicond. Sci. Technol.* **7**(3B), B215 (1992). <https://doi.org/10.1088/0268-1242/7/3B/052>
3. J. Pekola, Trends in thermometry. *J. Low Temp. Phys.* **135**(5), 723–744 (2004). <https://doi.org/10.1023/B:JOLT.0000029516.18146.42>

4. O. Bourgeois, S.E. Skipetrov, F. Ong, J. Chaussy, Attojoule calorimetry of mesoscopic superconducting loops. Phys. Rev. Lett. **94**(5), 057007 (2005). <https://doi.org/10.1103/PhysRevLett.94.057007>
5. F. Giazotto, T.T. Heikkilä, A. Luukanen, A.M. Savin, J.P. Pekola, Opportunities for mesoscopics in thermometry and refrigeration: Physics and applications. Rev. Mod. Phys. **78**(1), 217–274 (2006). <https://doi.org/10.1103/RevModPhys.78.217>
6. P. Reddy, S.-Y. Jang, R.A. Segelman, A. Majumdar, Thermoelectricity in molecular junctions. Science **315**(5818), 1568–1571 (2007). <https://doi.org/10.1126/science.1137149>
7. J.S. Heron, T. Fournier, N. Mingo, O. Bourgeois, Mesoscopic size effects on the thermal conductance of silicon nanowire. Nano Lett. **9**(5), 601–604 (2009). <https://doi.org/10.1021/nl803844j>
8. A. Mavalankar, S.J. Chorley, J. Griffiths, G.A.C. Jones, I. Farrer, D.A. Ritchie, C.G. Smith, A non-invasive electron thermometer based on charge sensing of a quantum dot. Appl. Phys. Lett. **103**(13), 133116 (2013). <https://doi.org/10.1063/1.4823703>
9. S. Jezouin, F.D. Parmentier, A. Anthore, U. Gennser, A. Cavanna, Y. Jin, F. Pierre, Quantum limit of heat flow across a single electronic channel. Science **342**(6158), 601–604 (2013). <https://doi.org/10.1126/science.1241912>
10. Y. Kim, W. Jeong, K. Kim, W. Lee, P. Reddy, Electrostatic control of thermoelectricity in molecular junctions. Nat. Nanotechnol. **9**(11), 881–885 (2014). <https://doi.org/10.1038/nnano.2014.209>
11. L.B. Wang, O.-P. Saira, J.P. Pekola, Fast thermometry with a proximity Josephson junction. Appl. Phys. Lett. **112**(1), 013105 (2018). <https://doi.org/10.1063/1.5010236>
12. G. Benenti, G. Casati, K. Saito, R.S. Whitney, Fundamental aspects of steady-state conversion of heat to work at the nanoscale. Phys. Rep. **694**, 1–124 (2017). <https://doi.org/10.1016/j.physrep.2017.05.008>
13. T. Ihn, *Semiconductor Nanostructures* (Oxford University Press, Oxford, 2009). <https://doi.org/10.1093/acprof:oso/9780199534425.001.0001>
14. Y.V. Nazarov, Y.M. Blanter, *Quantum Transport: Introduction to Nanoscience* (Cambridge University Press, Cambridge, 2009). <https://doi.org/10.1017/CBO9780511626906>
15. B. Karimi, J.P. Pekola, M. Campisi, R. Fazio, Coupled qubits as a quantum heat switch. Quantum Sci. Tech. **2**(4), 044007 (2017). <https://doi.org/10.1088/2058-9565/aa8330>
16. N. Brunner, N. Linden, S. Popescu, P. Skrzypczyk, Virtual qubits, virtual temperatures, and the foundations of thermodynamics. Phys. Rev. E **85**(5), 051117 (2012). <https://doi.org/10.1103/PhysRevE.85.051117>
17. P.P. Hofer, M. Perarnau-Llobet, J.B. Brask, R. Silva, M. Huber, N. Brunner, Autonomous quantum refrigerator in a circuit QED architecture based on a Josephson junction. Phys. Rev. B **94**(23), 235420 (2016). <https://doi.org/10.1103/PhysRevB.94.235420>
18. M.V. Moskalets, Scattering Matrix Approach to Non-Stationary Quantum Transport (World Scientific Publishing Company. Singapore (2011). <https://doi.org/10.1142/p822>
19. S. Datta, *Electronic Transport in Mesoscopic Systems*, (Cambridge University Press, Cambridge, 1997)
20. T.T. Heikkilä, *The Physics of Nanoelectronics*, (Oxford University Press, Oxford, 2013)
21. U. Sivan, Y. Imry, Multichannel Landauer formula for thermoelectric transport with application to thermopower near the mobility edge. Phys. Rev. B **33**(1), 551–558 (1986). <https://doi.org/10.1103/PhysRevB.33.551>
22. P.N. Butcher, Thermal and electrical transport formalism for electronic microstructures with many terminals. J. Phys. Condens. Matter **2**(22), 4869 (1990). <https://doi.org/10.1088/0953-8984/2/22/008>
23. F. Ronetti, L. Vannucci, G. Dolcetto, M. Carrega, M. Sassetti, Spin-thermoelectric transport induced by interactions and spin-flip processes in two-dimensional topological insulators. Phys. Rev. B **93**(16), 165414 (2016). <https://doi.org/10.1103/PhysRevB.93.165414>
24. S.-Y. Hwang, P. Burset, B. Sothmann, Odd-frequency superconductivity revealed by thermopower. Phys. Rev. B **98**(16), 161408 (2018). <https://doi.org/10.1103/PhysRevB.98.161408>

25. G. Granger, J.P. Eisenstein, J.L. Reno, Observation of chiral heat transport in the quantum Hall regime. *Phys. Rev. Lett.* **102**(8), 086803 (2009). <https://doi.org/10.1103/PhysRevLett.102.086803>
26. S.-G. Nam, E.H. Hwang, H.-J. Lee, Thermoelectric detection of chiral heat transport in graphene in the quantum Hall regime. *Phys. Rev. Lett.* **110**(22), 226801 (2013). <https://doi.org/10.1103/PhysRevLett.110.226801>
27. B. Sothmann, E.M. Hankiewicz, Fingerprint of topological Andreev bound states in phase-dependent heat transport. *Phys. Rev. B* **94**(8), 081407 (2016). <https://doi.org/10.1103/PhysRevB.94.081407>
28. S.J. Erlingsson, A. Manolescu, G.A. Nemnes, J.H. Bardarson, D. Sánchez, Reversal of thermoelectric current in tubular nanowires. *Phys. Rev. Lett.* **119**(3), 036804 (2017). <https://doi.org/10.1103/PhysRevLett.119.036804>
29. Y. Gross, M. Dolev, M. Heiblum, V. Umansky, D. Mahalu, Upstream neutral modes in the fractional quantum Hall effect regime: heat waves or coherent dipoles. *Phys. Rev. Lett.* **108**(22), 226801 (2012). <https://doi.org/10.1103/PhysRevLett.108.226801>
30. C. Altimiras, H. le Sueur, U. Gennser, A. Anthore, A. Cavanna, D. Mailly, F. Pierre, Chargeless heat transport in the fractional quantum Hall regime. *Phys. Rev. Lett.* **109**(2), 026803 (2012). <https://doi.org/10.1103/PhysRevLett.109.026803>
31. M. Banerjee, M. Heiblum, A. Rosenblatt, Y. Oreg, D.E. Feldman, A. Stern, V. Umansky, Observed quantization of anyonic heat flow. *Nature* **545**(7652), 75–79 (2017). <https://doi.org/10.1038/nature22052>
32. J.T. Muhonen, M. Meschke, J.P. Pekola, Micrometre-scale refrigerators. *Rep. Prog. Phys.* **75**(4), 046501 (2012). <https://doi.org/10.1088/0034-4885/75/4/046501>
33. B. Sothmann, R. Sánchez, A.N. Jordan, Thermoelectric energy harvesting with quantum dots. *Nanotechnology* **26**(3), 032001 (2015). <https://doi.org/10.1088/0957-4484/26/3/032001>
34. F. Haupt, M. Leijnse, H.L. Calvo, L. Classen, J. Splettstoesser, M.R. Wegewijs, Heat, molecular vibrations, and adiabatic driving in non-equilibrium transport through interacting quantum dots. *Phys. Status. Solidi B* **250**(11), 2315–2329 (2013). <https://doi.org/10.1002/pssb.201349219>
35. Y. Dubi, M. Di Ventra, Colloquium: heat flow and thermoelectricity in atomic and molecular junctions. *Rev. Mod. Phys.* **83**(1), 131–155 (2011). <https://doi.org/10.1103/RevModPhys.83.131>
36. M. Ratner, A brief history of molecular electronics. *Nat. Nanotechnol.* **8**, 378–381 (2013). <https://doi.org/10.1038/nnano.2013.110>
37. J.P. Bergfield, M.A. Ratner, Forty years of molecular electronics: non-equilibrium heat and charge transport at the nanoscale. *Phys. Status Solidi B* **250**(11), 2249 (2013). <https://doi.org/10.1002/pssb.201370573>
38. J.-L. Pichard, R.S. Whitney (ed.), Special issue : mesoscopic thermoelectric phenomena. *C. R. Phys.* **17**(10), 1039–1174 (2016). <https://doi.org/10.1016/j.crhy.2016.08.006>
39. M. Di Ventra, *Electrical Transport in Nanoscale Systems*, (Cambridge University Press, Cambridge, 2008). <https://doi.org/10.1017/CBO9780511755606.002>
40. A.E. Ioffe, *Semiconductor Thermoelements and Thermoelectric Cooling* (Pion Ltd, London, 1958)
41. H.J. Goldsmid, *Introduction to Thermoelectricity*, Springer Series in Materials Science, (Springer, Berlin, 2009). <https://doi.org/10.1007/978-3-642-00716-3>
42. D.M. Rowe, *CRC Handbook of Thermoelectrics* (CRC Press, Boca, Raton, 1995). <https://doi.org/10.1201/9781420049718>
43. F.J. DiSalvo, Thermoelectric cooling and power generation. *Science* **285**(5428), 703–706 (1999). <https://doi.org/10.1126/science.285.5428.703>
44. A. Shakouri, M. Zebarjadi, Nanoengineered materials for thermoelectric energy conversion, in *Thermal Nanosystems and Nanomaterials*, vol. 225, ed. by S. Volz S (2009). [https://doi.org/10.1007/978-3-642-04258-4\\_9](https://doi.org/10.1007/978-3-642-04258-4_9)
45. A. Shakouri, Recent developments in semiconductor thermoelectric physics and materials. *Ann. Rev. Mater. Res.* **41**(1), 399–431 (2011). <https://doi.org/10.1146/annurev-matsci-062910-100445>

46. E. Pop, S. Sinha, K.E. Goodson, Heat generation and transport in nanometer-scale transistors. Proc. IEEE **94**(8), 1587–1601 (2006). <https://doi.org/10.1109/JPROC.2006.879794>
47. K. Koumoto, T. Mori, *Thermoelectric Nanomaterials: Materials Design and Applications, Springer Series in Materials Science*, Band 182 (Springer, Berlin, 2013). <https://doi.org/10.1007/978-3-642-37537-8>
48. E. Maciá, *Thermoelectric Materials: Advances and Applications* (Pan Stanford, The Netherlands, 2015)
49. D.G. Cahill, W.K. Ford, K.E. Goodson, G.D. Mahan, A. Majumdar, H.J. Maris, R. Merlin, S.R. Phillpot, Nanoscale thermal transport. J. Appl. Phys. **93**(2), 793–818 (2003). <https://doi.org/10.1063/1.1524305>
50. D.G. Cahill, P.V. Braun, G. Chen, D.R. Clarke, S. Fan, K.E. Goodson, P. Keblinski, W.P. King, G.D. Mahan, A. Majumdar, H.J. Maris, S.R. Phillpot, E. Pop, L. Shi, Nanoscale thermal transport. II. 2003–2012. Appl. Phys. Rev. **1**(1), 011305 (2014). <https://doi.org/10.1063/1.4832615>
51. G.D. Mahan, J.O. Sofo, The best thermoelectric. Proc. Natl. Acad. Sci. U.S.A **93**(15), 7436–7439 (1996). <https://doi.org/10.1073/pnas.93.15.7436>
52. T.E. Humphrey, R. Newbury, R.P. Taylor, H. Linke, Reversible quantum brownian heat engines for electrons. Phys. Rev. Lett. **89**(11), 116801 (2002). <https://doi.org/10.1103/PhysRevLett.89.116801>
53. N. Nakpathomkun, H.Q. Xu, H. Linke, Thermoelectric efficiency at maximum power in low-dimensional systems. Phys. Rev. B **82**(23), 235428 (2010). <https://doi.org/10.1103/PhysRevB.82.235428>
54. A. Svilans, M. Leijnse, H. Linke, Experiments on the thermoelectric properties of quantum dots. C.R. Phys. **17**(10), 1096–1108 (2016). <https://doi.org/10.1016/j.crhy.2016.08.002>
55. L. Cui, R. Miao, K. Wang, D. Thompson, L.A. Zotti, J.C. Cuevas, E. Meyhofer, P. Reddy, Peltier cooling in molecular junctions. Nat. Nanotechnol. **13**(2), 122–127 (2017). <https://doi.org/10.1038/s41565-017-0020-z>
56. L.D. Hicks, M.S. Dresselhaus, Effect of quantum-well structures on the thermoelectric figure of merit. Phys. Rev. B **47**(19), 12727–12731 (1993a). <https://doi.org/10.1103/PhysRevB.47.12727>
57. L.D. Hicks, M.S. Dresselhaus, Thermoelectric figure of merit of a one-dimensional conductor. Phys. Rev. B **47**(24), 16631–16634 (1993b). <https://doi.org/10.1103/PhysRevB.47.16631>
58. T.E. Humphrey, H. Linke, Reversible thermoelectric nanomaterials. Phys. Rev. Lett. **94**(9), 096601 (2005). <https://doi.org/10.1103/PhysRevLett.94.096601>
59. J.P. Heremans, M.S. Dresselhaus, L.E. Bell, D.T. Morelli, When thermoelectrics reached the nanoscale. Nat. Nanotechnol. **8**(7), 471 (2013). <https://doi.org/10.1038/nnano.2013.129>
60. R.S. Whitney, Most efficient quantum thermoelectric at finite power output. Phys. Rev. Lett. **112**(13), 130601 (2014). <https://doi.org/10.1103/PhysRevLett.112.130601>
61. R.S. Whitney, Finding the quantum thermoelectric with maximal efficiency and minimal entropy production at given power output. Phys. Rev. B **91**(11), 115425 (2015). <https://doi.org/10.1103/PhysRevB.91.115425>
62. R.S. Whitney, Quantum coherent three-terminal thermoelectrics: maximum efficiency at given power output. Entropy **18**(6), 208 (2016). <https://doi.org/10.3390/e18060208>
63. J.B. Pendry, Quantum limits to the flow of information and entropy. J. Phys. A Math. Gen. **16**(10), 2161 (1983). <https://doi.org/10.1088/0305-4470/16/10/012>
64. I.-J. Chen, A. Burke, A. Svilans, H. Linke, C. Thelander, Thermoelectric power factor limit of a 1D nanowire. Phys. Rev. Lett. **120**(17), 177703 (2018). <https://doi.org/10.1103/PhysRevLett.120.177703>
65. K. Brandner, U. Seifert, Bound on thermoelectric power in a magnetic field within linear response. Phys. Rev. E **91**(1), 012121 (2015). <https://doi.org/10.1103/PhysRevE.91.012121>
66. J. Schulenborg, R.B. Saptsov, F. Haupt, J. Splettstoesser, M.R. Wegewijs, Fermion-parity duality and energy relaxation in interacting open systems. Phys. Rev. B **93**(8), 081411 (2016). <https://doi.org/10.1103/PhysRevB.93.081411>

67. J. Schulenborg, A. Di Marco, J. Vanherck, M.R. Wegewijs, J. Splettstoesser, Thermoelectrics of interacting nanosystems-exploiting superselection instead of time-reversal symmetry. *Entropy* **19**(12), 668 (2017). <https://doi.org/10.3390/e19120668>
68. D.R. Schmidt, R.J. Schoelkopf, A.N. Cleland, Photon-mediated thermal relaxation of electrons in nanostructures. *Phys. Rev. Lett.* **93**(4), 045901 (2004). <https://doi.org/10.1103/PhysRevLett.93.045901>
69. L.M.A. Pascal, H. Courtois, F.W.J. Hekking, Circuit approach to photonic heat transport. *Phys. Rev. B* **83**(12), 125113 (2011). <https://doi.org/10.1103/PhysRevB.83.125113>
70. B.L. Zink, A.D. Avery, R. Sultan, D. Bassett, M.R. Pufall, Exploring thermoelectric effects and Wiedemann-Franz violation in magnetic nanostructures via micromachined thermal platforms. *Solid State Commun.* **150**(11), 514–518 (2010). <https://doi.org/10.1016/j.ssc.2009.11.003>
71. S. Poran, T. Nguyen-Duc, A. Auerbach, N. Dupuis, A. Frydman, O. Bourgeois, Quantum criticality at the superconductor to insulator transition revealed by specific heat measurements. *Nat. Commun.* **8**, 14464 (2017). <https://doi.org/10.1038/ncomms14464>
72. M. Partanen, K.Y. Tan, J. Govenius, R.E. Lake, M.K. Mäkelä, T. Tanttu, M. Möttönen, Quantum-limited heat conduction over macroscopic distances. *Nat. Phys.* **12**(5), 460–464 (2016). <https://doi.org/10.1038/nphys3642>
73. R. Sánchez, Correlation-induced refrigeration with superconducting single-electron transistors. *Appl. Phys. Lett.* **111**(22), 223103 (2017). <https://doi.org/10.1063/1.5008481>
74. H. Courtois, H.O. Nguyen, C.B. Winkelmann, J.P. Pekola, High-performance electronic cooling with superconducting tunnel junctions. *C.R. Phys.* **17**(10), 1139–1145 (2016). <https://doi.org/10.1016/j.crhy.2016.08.010>
75. J.R. Prance, C.G. Smith, J.P. Griffiths, S.J. Chorley, D. Anderson, G.A.C. Jones, I. Farrer, D.A. Ritchie, Electronic refrigeration of a two-dimensional electron gas. *Phys. Rev. Lett.* **102**(14), 146602 (2009). <https://doi.org/10.1103/PhysRevLett.102.146602>
76. N.W. Ashcroft, N.D. Mermin, *Solid State Physics* (Brooks Cole, Boston, 1976)
77. L.P. Kouwenhoven, D.G. Austing, S. Tarucha, Few-electron quantum dots. *Rep. Prog. Phys.* **64**(64), 701 (2001). <https://doi.org/10.1088/0034-4885/64/6/201>
78. R. Hanson, L.P. Kouwenhoven, J.R. Petta, S. Tarucha, L.M.K. Vandersypen, Spins in few-electron quantum dots. *Rev. Mod. Phys.* **79**(4), 1217–1265 (2007). <https://doi.org/10.1103/RevModPhys.79.1217>
79. J.P. Bird, *Electron Transport in Quantum Dots* (Springer, New York, 2003). <https://doi.org/10.1007/978-1-4615-0437-5>
80. R. Sánchez, M. Büttiker, Optimal energy quanta to current conversion. *Phys. Rev. B* **83**(8), 085428 (2011). <https://doi.org/10.1103/PhysRevB.83.085428>
81. H. Thierschmann, R. Sánchez, B. Sothmann, F. Arnold, C. Heyn, W. Hansen, H. Buhmann, L.W. Molenkamp, Three-terminal energy harvester with coupled quantum dots. *Nat. Nanotechnol.* **10**(10), 854–858 (2015). <https://doi.org/10.1038/nnano.2015.176>
82. B. Roche, P. Roulleau, T. Jullien, Y. Jompol, I. Farrer, D.A. Ritchie, D.C. Glattli, Harvesting dissipated energy with a mesoscopic ratchet. *Nat. Commun.* **6**, 6738 (2015). <https://doi.org/10.1038/ncomms7738>
83. F. Hartmann, P. Pfeffer, S. Höfling, M. Kamp, L. Worschech, Voltage fluctuation to current converter with coulomb-coupled quantum dots. *Phys. Rev. Lett.* **114**(14), 146805 (2015). <https://doi.org/10.1103/PhysRevLett.114.146805>
84. R.S. Whitney, R. Sánchez, F. Haupt, J. Splettstoesser, Thermoelectricity without absorbing energy from the heat sources. *Phys. E* **75**, 257–265 (2016). <https://doi.org/10.1016/j.physe.2015.09.025>
85. K.V. Klitzing, G. Dorda, M. Pepper, New method for high-accuracy determination of the fine-structure constant based on quantized Hall resistance. *Phys. Rev. Lett.* **45**(6), 494–497 (1980). <https://doi.org/10.1103/PhysRevLett.45.494>
86. B.I. Halperin, Quantized Hall conductance, current-carrying edge states, and the existence of extended states in a two-dimensional disordered potential. *Phys. Rev. B* **25**(4), 2185–2190 (1982). <https://doi.org/10.1103/PhysRevB.25.2185>

87. M. Büttiker, Absence of backscattering in the quantum Hall effect in multiprobe conductors. *Phys. Rev. B* **38**(14), 9375–9389 (1988a). <https://doi.org/10.1103/PhysRevB.38.9375>
88. B.J. van Wees, H. van Houten, C.W.J. Beenakker, J.G. Williamson, L.P. Kouwenhoven, D. van der Marel, C.T. Foxon, Quantized conductance of point contacts in a two-dimensional electron gas. *Rev. Lett.* **60**(9), 848–850 (1988). <https://doi.org/10.1103/PhysRevLett.60.848>
89. M. Büttiker, Quantized transmission of a saddle-point constriction. *Phys. Rev. B* **41**(11), 7906–7909 (Apr 1990). <https://doi.org/10.1103/PhysRevB.41.7906>
90. P. Streda, Quantised thermopower of a channel in the ballistic regime. *J. Phys. Condens. Matter* **1**(5), 1025 (1989). <https://doi.org/10.1088/0953-8984/1/5/021>
91. L.W. Molenkamp, H. van Houten, C.W.J. Beenakker, R. Eppenga, C.T. Foxon, Quantum oscillations in the transverse voltage of a channel in the nonlinear transport regime. *Phys. Rev. Lett.* **65**(8), 1052–1055 (1990). <https://doi.org/10.1103/PhysRevLett.65.1052>
92. L.W. Molenkamp, Th. Gravier, H. van Houten, O.J.A. Buijk, M.A.A. Mabesoone, C.T. Foxon, Peltier coefficient and thermal conductance of a quantum point contact. *Phys. Rev. Lett.* **68**(25), 3765–3768 (1992). <https://doi.org/10.1103/PhysRevLett.68.3765>
93. P.P. Hofer, B. Sothmann, Quantum heat engines based on electronic Mach-Zehnder interferometers. *Phys. Rev. B* **91**(19), 195406 (2015). <https://doi.org/10.1103/PhysRevB.91.195406>
94. L. Vannucci, F. Ronetti, G. Dolcetto, M. Carrega, M. Sassetti, Interference-induced thermoelectric switching and heat rectification in quantum Hall junctions. *Phys. Rev. B* **92**(7), 075446 (2015). <https://doi.org/10.1103/PhysRevB.92.075446>
95. P. Samuelsson, S. Kheradsoud, B. Sothmann, Optimal quantum interference thermoelectric heat engine with edge states. *Phys. Rev. Lett.* **118**(25), 256801 (2017). <https://doi.org/10.1103/PhysRevLett.118.256801>
96. J. Stark, K. Brandner, K. Saito, U. Seifert, Classical Nernst engine. *Phys. Rev. Lett.* **112**(14), 140601 (2014). <https://doi.org/10.1103/PhysRevLett.112.140601>
97. B. Sothmann, R. Sánchez, A.N. Jordan, Quantum Nernst engines. *EPL* **107**(4), 47003 (2014). <https://doi.org/10.1209/0295-5075/107/47003>
98. A.N. Jordan, B. Sothmann, R. Sánchez, M. Büttiker, Powerful and efficient energy harvester with resonant-tunneling quantum dots. *Phys. Rev. B* **87**(7), 075312 (2013). <https://doi.org/10.1103/PhysRevB.87.075312>
99. S. Donsa, S. Andergassen, K. Held, Double quantum dot as a minimal thermoelectric generator. *Phys. Rev. B* **89**(12), 125103 (2014). <https://doi.org/10.1103/PhysRevB.89.125103>
100. R. Sánchez, B. Sothmann, A.N. Jordan, Chiral thermoelectrics with quantum Hall edge states. *Phys. Rev. Lett.* **114**(14), 146801 (2015a). <https://doi.org/10.1103/PhysRevLett.114.146801>
101. R. Sánchez, B. Sothmann, A.N. Jordan, Heat diode and engine based on quantum Hall edge states. *New J. Phys.* **17**(7), 075006 (2015b). <https://doi.org/10.1088/1367-2630/17/7/075006>
102. L. Onsager, Reciprocal relations in irreversible processes. I. *Phys. Rev.* **37**(4), 405–426 (1931). <https://doi.org/10.1103/PhysRev.37.405>
103. M. Büttiker, Symmetry of electrical conduction. *IBM J. Res. Dev.* **32**(3), 317–334 (1988b). <https://doi.org/10.1147/rd.323.0317>
104. A. Mani, C. Benjamin, Helical thermoelectrics and refrigeration. *Phys. Rev. E* **97**(2), 022114 (2018). <https://doi.org/10.1103/PhysRevE.97.022114>
105. G. Benenti, K. Saito, G. Casati, Thermodynamic bounds on efficiency for systems with broken time-reversal symmetry. *Phys. Rev. Lett.* **106**(23), 230602 (2011). <https://doi.org/10.1103/PhysRevLett.106.230602>
106. K. Brandner, K. Saito, U. Seifert, Strong bounds on onsager coefficients and efficiency for three-terminal thermoelectric transport in a magnetic field. *Phys. Rev. Lett.* **110**(7), 070603 (2013). <https://doi.org/10.1103/PhysRevLett.110.070603>
107. P. Roura-Bas, L. Arrachea, E. Fradkin, Enhanced thermoelectric response in the fractional quantum Hall effect. *Phys. Rev. B* **97**(8), 081104 (2018). <https://doi.org/10.1103/PhysRevB.97.081104>
108. L. Arrachea, M. Moskalets, L. Martin-Moreno, Heat production and energy balance in nanoscale engines driven by time-dependent fields. *Phys. Rev. B* **75**(24), 245420 (2007). <https://doi.org/10.1103/PhysRevB.75.245420>

109. M.F. Ludovico, F. Battista, F. von Oppen, L. Arrachea, Adiabatic response and quantum thermoelectrics for ac-driven quantum systems. *Phys. Rev. B* **93**(7), 075136 (2016). <https://doi.org/10.1103/PhysRevB.93.075136>
110. A. Bruch, S.V. Kusminskiy, G. Refael, F. von Oppen, An interacting adiabatic quantum motor. *Phys. Rev. B* **97**(19), 195411 (2018). <https://doi.org/10.1103/PhysRevB.97.195411>
111. H.L. Calvo, F.D. Ribetto, R.A. Bustos-Marín, Real-time diagrammatic approach to current-induced forces: application to quantum-dot based nanomotors. *Phys. Rev. B* **96**(16), 165309 (2017). <https://doi.org/10.1103/PhysRevB.96.165309>
112. B. Karimi, J.P. Pekola, Otto refrigerator based on a superconducting qubit: classical and quantum performance. *Phys. Rev. B* **94**(18), 184503 (2016). <https://doi.org/10.1103/PhysRevB.94.184503>
113. J.V. Koski, V.F. Maisi, J.P. Pekola, D.V. Averin, Experimental realization of a Szilard engine with a single electron. *Proc. Natl. Acad. Sci. U.S.A.* **111**(38), 13786–13789 (2014). <https://doi.org/10.1073/pnas.1406966111>
114. J.V. Koski, A. Kutvonen, I.M. Khaymovich, T. Ala-Nissila, J.P. Pekola, On-chip Maxwell's demon as an information-powered refrigerator. *Phys. Rev. Lett.* **115**(26), 260602 (2015). <https://doi.org/10.1103/PhysRevLett.115.260602>
115. S. Juergens, F. Haupt, M. Moskalets, J. Splettstoesser, Thermoelectric performance of a driven double quantum dot. *Phys. Rev. B* **87**(24), 245423 (2013). <https://doi.org/10.1103/PhysRevB.87.245423>
116. H. Pothier, P. Lafarge, C. Urbina, D. Esteve, M.H. Devoret, Single-electron pump based on charging effects. *EPL* **17**(3), 249 (1992). <https://doi.org/10.1209/0295-5075/17/3/011>
117. S.J. Chorley, J. Frake, C.G. Smith, G.A.C. Jones, M.R. Buitelaar, Quantized charge pumping through a carbon nanotube double quantum dot. *Appl. Phys. Lett.* **100**(14), 143104 (2012). <https://doi.org/10.1063/1.3700967>
118. B. Roche, R.-P. Riwar, B. Voisin, E. Dupont-Ferrier, R. Wacquez, M. Vinet, M. Sanquer, J. Splettstoesser, X. Jehl, A two-atom electron pump. *Nat. Commun.* **4**, 1581 (2013). <https://doi.org/10.1038/ncomms2544>
119. M. Josefsson, A. Svilans, A.M. Burke, E.A. Hoffmann, S. Fahlvik, C. Thelander, M. Leijnse, H. Linke, A quantum-dot heat engine operated close to thermodynamic efficiency limits. *Nat. Nanotechnol.* (2017). <https://doi.org/10.1038/s41565-018-0200-5>
120. C. Bergenfeldt, P. Samuelsson, B.J. Sothmann, C. Flindt, M. Büttiker, Hybrid microwave-cavity heat engine. *Phys. Rev. Lett.* **112**(7), 076803 (2014). <https://doi.org/10.1103/PhysRevLett.112.076803>
121. R. Žitko, J. Mravlje, A. Ramšak, T. Rejec, Spin thermopower in the overscreened Kondo model. *New J. Phys.* **15**(10), 105023 (2013). <https://doi.org/10.1088/1367-2630/15/10/105023>
122. D.M. Kennes, D. Schuricht, V. Meden, Efficiency and power of a thermoelectric quantum dot device. *EPL* **102**(5), 57003 (2013). <https://doi.org/10.1209/0295-5075/102/57003>
123. T.A. Costi, V. Zlatić, Thermoelectric transport through strongly correlated quantum dots. *Phys. Rev. B* **81**(23), 235127 (2010). <https://doi.org/10.1103/PhysRevB.81.235127>
124. P. Strasberg, G. Schaller, N. Lambert, T. Brandes, Nonequilibrium thermodynamics in the strong coupling and non-Markovian regime based on a reaction. *New J. Phys.* **18**(7), 073007 (2016). <https://doi.org/10.1088/1367-2630/18/7/073007>
125. R.S. Whitney, Non-Markovian quantum thermodynamics: laws and fluctuation theorems. *Phys. Rev. B* **98**, 085415 (2016). <https://doi.org/10.1103/PhysRevB.98.085415>

# Chapter 8

## Quantum Batteries



Francesco Campaioli, Felix A. Pollock and Sai Vinjanampathy

### 8.1 Introduction

The thermodynamic role of batteries is that of work reservoir: In practice, classical batteries are electrochemical devices that store energy supplied by external sources and provide power to other machines, allowing for their remote usage. Their pervasive presence in our daily life has turned them into indispensable components, whose size and storage capability range from large 500kWh vehicle traction batteries to tiny 100mWh miniature cells used for implanted medical devices and calculators [1]. Along with the constant miniaturization of such user devices, batteries are also required to be smaller and smaller, thus, as their unit cells approach the size of molecules and atoms, their description has to account for quantum mechanical effects [2–4].

This premise leads to the study of *quantum batteries* (QBs), which have been introduced by R. Alicki and M. Fannes in 2013 as small quantum mechanical systems that are used to temporarily store energy, in order for it to be transferred from production to consumption centers [5]. Further works have used the same formal definition, describing QBs as  $d$ -dimensional quantum systems with non-degenerate energy levels from which work can be reversibly extracted – and on which energy can be reversibly deposited – by means of cyclic unitary operations. It is thus easy

---

F. Campaioli (✉) · F. A. Pollock

School of Physics and Astronomy, Monash University, Melbourne, Victoria 3800, Australia  
e-mail: francesco.campaioli@monash.edu

S. Vinjanampathy

Department of Physics, Indian Institute of Technology Bombay, Mumbai 400076, India  
e-mail: sai@phy.iitb.ac.in

S. Vinjanampathy

Centre for Quantum Technologies, National University of Singapore, 3 Science Drive 2,  
Singapore 117543, Singapore

to see the relationship of the battery charging problem with the emerging area of quantum thermodynamics [6].

An immediate consequence of the quantum thermodynamic context is the use of notions and techniques of quantum information, which has brought interesting conclusions and insights. For instance, entanglement and other quantum correlations (see Chap. 30) have been addressed in Refs. [5, 6] as possible resources to improve work extraction tasks. The limits to charging power have been set in [4, 7] recalling the quantum speed limit of unitary evolution [8], and using other tools of quantum optimal control theory [9–11]. However, this blossoming research field has to address many other questions, such as the stabilization of stored energy and the practical implementation of quantum batteries, offering a vast research panorama on both theoretical and experimental ends [4, 12–14].

This chapter will review the main results in this area with simple examples. We will assume the reader is familiar with standard techniques in quantum thermodynamics. The first section is dedicated to the task of work extraction, introducing the concept of passive states – from which energy can no longer be reversibly extracted via unitary cycles – and exploring the limits of classical and quantum extraction protocols. The second section treats the charging of quantum batteries, demonstrating the advantage that entangling operations have over their classical counterparts, while considering the limits of physically realizable charging schemes. In the third section we review some possible implementations of quantum batteries, concluding with a general discussion.

## 8.2 Work Extraction

The study of work extraction from small quantum systems – regarded as batteries – via reversible cyclic operations starts with the aim of defining the thermodynamical bounds and principles that are valid at those scales where a quantum mechanical description becomes necessary [5]. The intention is to look at the limits of extractable work allowed by quantum mechanics and compare them to their classical counterpart, while looking for possible advantages.

Let us start from a single *closed*<sup>1</sup> quantum battery, the fundamental unit of this discussion. It consists of a  $d$ -dimensional system with associated internal Hamiltonian  $H_0$

$$H_0 = \sum_{j=1}^d \varepsilon_j |j\rangle\langle j|, \quad (8.1)$$

with non-degenerate energy levels  $\varepsilon_j < \varepsilon_{j+1}$ . An example of a 2-level quantum battery is given in Fig. 8.1.

---

<sup>1</sup>In thermodynamics a *closed* system is only allowed to exchange either work or heat, in contrast with an *isolated* system which is not allowed to exchange either of them. Here, by closed, we mean isolated quantum system undergoing Schrödinger evolution, but whose initial state can be mixed.

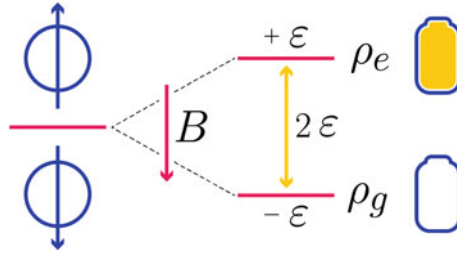


**Fig. 8.1** A simple quantum battery could consist of a spin- $\frac{1}{2}$  system immersed in a uniform magnetic field  $B$ , whose internal Hamiltonian has energy levels  $\mp\epsilon$ , associated with the eigenstates  $|\mp 1\rangle$ , respectively. A pure state  $\rho_e = |1\rangle\langle 1|$  ( $\rho_g = |-1\rangle\langle -1|$ ) is considered a charged (empty) battery, since no work can be deposited onto (extracted from) it, with respect to the internal Hamiltonian  $H_0$ .

A time-dependent field  $V(t)$  is used to reversibly extract energy from such a battery via unitary evolution generated by  $H_0 + V(t)$ . Given that the battery is found in some initial state described by the density operator  $\rho$ , the time evolution of the system is obtained from the von Neumann equation ( $\hbar = 1$ )

$$\dot{\rho}(t) = -i[H_0 + V(t), \rho(t)], \quad (8.2)$$

with  $\rho(0) = \rho$ , and where the left-hand side represents the time derivative of  $\rho(t)$ . A solution of Eq. (8.2) is given by  $\rho(t) = U(t)\rho U^\dagger(t)$ , where the unitary operator  $U(t)$  is obtained as the time-ordered exponential of the generator  $H_0 + V(t)$ , which can, in principle, correspond to any unitary transformation on the battery's Hilbert space  $\mathcal{H}$ ,

$$U(t) = \mathcal{T}\left\{\exp\left[-i\int_0^t ds(H_0 + V(s))\right]\right\}. \quad (8.3)$$

### 8.2.1 Ergotropy

The work extracted after some time  $\tau$  by such a procedure is equal to

$$W = \text{tr}[\rho H_0] - \text{tr}[\rho(\tau) H_0] \quad (8.4)$$

$$= \text{tr}[\rho H_0] - \text{tr}[U(\tau)\rho U^\dagger(\tau) H_0]. \quad (8.5)$$

Since we are interested in reversible work extraction, we look for the maximal amount of extractable work, known as *ergotropy* [15, 16], optimizing  $W$  over all unitary operations,

$$W_{\max} := \text{tr}[\rho H_0] - \min_{U \in SU(d)} \{\text{tr}[U \rho U^\dagger H_0]\}. \quad (8.6)$$

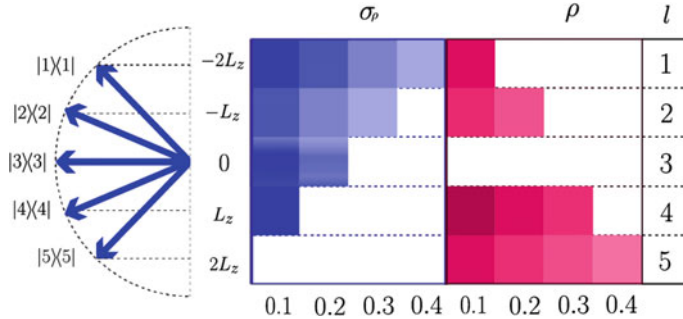


**Fig. 8.2** A 5-level system with internal Hamiltonian  $H_0(L_z) = L_z \sum_{l=1}^5 (l-3)|l\rangle\langle l|$  in state  $\rho = 0.1|1\rangle\langle 1| + 0.2|2\rangle\langle 2| + 0.3|4\rangle\langle 4| + 0.4|5\rangle\langle 5|$  has an associated passive state  $\sigma_\rho = 0.4|1\rangle\langle 1| + 0.3|2\rangle\langle 2| + 0.2|3\rangle\langle 3| + 0.1|4\rangle\langle 4|$ , from which one can extract the ergotropy  $W_{\max} = 1.8L_z$  by means of some unitary operation, such as  $U = |1\rangle\langle 5| + |2\rangle\langle 4| + |5\rangle\langle 3| + |3\rangle\langle 2| + |4\rangle\langle 1|$ . Such unitary operation is not unique, since an arbitrary relative phase can be introduced for each term  $|i\rangle\langle j|$ .

When no work can be extracted from a state  $\sigma$ , such state is said to be *passive* [5, 17, 18]. Accordingly, a state  $\sigma$  is passive if  $\text{tr}[\sigma H_0] \leq \text{tr}[U\sigma U^\dagger H_0]$  for all unitaries  $U$ , or, equivalently, if and only if  $\sigma = \sum_{j=1}^d s_j |j\rangle\langle j|$  for  $s_{j+1} \leq s_j$ , i.e. it commutes with the internal Hamiltonian  $H_0$  and has non-increasing eigenvalues, as shown in Ref. [5]. From such a definition it is easy to see that for any given state  $\rho$  there is a unique passive state  $\sigma_\rho$  that maximizes the extractable work

$$W_{\max} = \text{tr}[\rho H_0] - \text{tr}[\sigma_\rho H_0], \quad (8.7)$$

obtained via some unitary operation that rearranges the eigenvalues of  $\rho$  in non-increasing order, as can be seen in the example given in Fig. 8.2.

### 8.2.2 Bound on Extractable Work

A practical and intuitive way to bound the extractable work of Eq. (8.6) is to consider a thermal state with the same entropy as the passive state  $\sigma_\rho$ , which also minimizes the energy with respect to  $H_0$ . Indeed, it has been shown that a lower bound to the ergotropy for some state  $\rho$  is given by

$$W_{\max} \leq \text{tr}[\rho H_0] - \text{tr}[\omega_{\bar{\beta}} H_0], \quad (8.8)$$

where  $\omega_{\bar{\beta}} = \exp[-\bar{\beta}H_0]/\mathcal{Z}$  is the canonical Gibbs state with inverse temperature  $\bar{\beta}$ , and  $\bar{\beta}$  is chosen such that the von Neumann entropy  $S(\rho) = -\text{tr}[\rho \log \rho]$  of  $\rho$  is equal to that of  $\omega_{\bar{\beta}}$  [5].

Interestingly, all thermal states are passive, and, for the case of two-level systems, all passive states are thermal, since one can always define a (positive or negative)

temperature using the equation  $(1 - p)/p = \exp(-\beta\Delta E)$ . However, for systems with dimension greater than two, the Gibbs state  $\omega_{\tilde{\beta}}$  is in general different from the passive state  $\sigma_\rho$  associated to  $\rho$ . Even more interestingly, the product of two or more copies of a passive state  $\sigma_\rho$  is not necessarily the passive state of the copies of  $\rho$ , *i.e.*  $\otimes^n \sigma_\rho \neq \sigma_{\otimes^n \rho}$  [5], which leads to the definition of completely passive states, as those whose  $n$ -copy ensemble are still passive for any  $n$ . It has been shown that a state is completely passive if and only if it is a thermal state [17, 18], an observation that can be used to beat the bound given in Eq.(8.7) for many copies of the same battery by means of entangling operations [5]

### 8.2.3 Optimal Work Extraction from an Ensemble of Batteries

Consider a battery given by an ensemble of  $n$  copies of the same  $d$ -dimensional unit cell defined by Eq. (8.1). This new battery has an associated Hamiltonian  $H_0^{(n)}$  given by the sum of the local internal Hamiltonians  $H_{0,l} \otimes_{j \neq l} \mathbb{1}_j$  of the subsystems that form the global system

$$H_0^{(n)} = \sum_{l=1}^n H_{0,l}, \quad (8.9)$$

where we omit the identities to simplify the notation. Recalling that  $\otimes^n \sigma_\rho \neq \sigma_{\otimes^n \rho}$  our goal is to extract some additional work from  $\otimes^n \sigma_\rho$  until a completely passive state is reached. In the limit of large  $n$ , the maximal amount of available work per copy of battery  $w_{\max}(n)$  in a state  $\rho$  is tightly bounded as in Eq.(8.8),

$$\lim_{n \rightarrow \infty} w_{\max}(n) = \text{tr}[\rho H_0^{(1)}] - \text{tr}[\omega_{\tilde{\beta}} H_0^{(1)}], \quad (8.10)$$

where

$$w_{\max}(n) := \frac{1}{n} \left( \text{tr}[(\otimes^n \rho - \sigma_{\otimes^n \rho}) H_0^{(n)}] \right). \quad (8.11)$$

The proof relies on the idea that for a large ensemble, the energy of the passive state  $\sigma_{\otimes^n \rho}$  differs from that of  $\otimes^n \omega_{\tilde{\beta}}$  only by a small amount that tends to vanish as  $n$  increases (see Fig. 8.3 for an example).

### 8.2.4 Entanglement Generation & Power of Extracted Work

The passive state  $\sigma_{\otimes^n \rho}$  associated with any  $\otimes^n \rho$  is diagonal in the eigenbasis of the local Hamiltonian of Eq.(8.9), thus it is separable. However, as we will see later in this section, in order to unitarily connect  $\otimes^n \rho$  to its passive state, at least 2-body operations are required. This remark led Alicki and Fannes to conclude that, in order

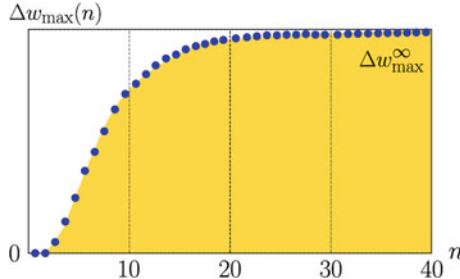


**Fig. 8.3** Let us consider an ensemble of  $n$  copies of the same passive state  $\sigma$ . As discussed in this section, there is a non-trivial amount of work per copy  $\Delta w_{\max}(n)$  that we can extract from such an ensemble by means of entangling operations (at least 2-body operations), given by  $\frac{1}{n}\{\text{tr}[(\otimes^n \sigma - \tilde{\sigma}) H_0^{(n)}]\}$ , where  $\tilde{\sigma}$  is the passive state for  $\otimes^n \sigma$ . This figure represents this additional available energy per copy for a three-level system with energy levels  $\{0, 0.579, 1\}$  and passive state  $\sigma$  with eigenvalues  $\{0.538, 0.237, 0.224\}$  [5]. In particular, the maximal amount of extractable energy  $\Delta w_{\max}^\infty$  is obtained in the limit of  $n \rightarrow \infty$ .

to reach optimal work extraction, the unit cells of such an  $n$ -fold battery have to be dynamically entangled. Their deduction turns out to be wrong, as proven in Ref. [6]: If it is true that non-local operations (at least two-body operations) are required to beat the classical limit of Eq. (8.7), then it is always possible to reach optimal work extraction without creating any entanglement (see [19] for quantum discord), at the expense of requiring more operations, and thus additional time.

### 8.2.5 Work Extraction and Indirect Path: Avoiding Entanglement

Let us consider a simple example that illustrates how to perform optimal work extraction from multiple copies of the same state without generating entanglement: A three-level system with (increasing) energy levels given by  $\{E_1, E_2, E_3\}$ , and two copies of some initial state  $\rho = p|2\rangle\langle 2| + (1-p)|3\rangle\langle 3|$ , with  $p \in (0, 1/2)$ . The objective is to transform the initial state  $\rho \otimes \rho = p^2|22\rangle\langle 22| + p(1-p)(|23\rangle\langle 23| + |32\rangle\langle 32|) + (1-p)^2|33\rangle\langle 33|$  into a passive state  $\sigma = (1-p)^2|11\rangle\langle 11| + p(1-p)(|12\rangle\langle 12| + 0.21|21\rangle\langle 21|) + p^2|13\rangle\langle 13|$  by means of the permutation that maps  $|33\rangle \rightarrow |11\rangle, \dots, |22\rangle \rightarrow |13\rangle$ . In order to avoid entanglement one can perform each swap in several steps, such as  $|33\rangle \rightarrow |13\rangle$  followed  $|13\rangle \rightarrow |11\rangle$ , each of which keeps the state in a separable form at all times, if performed by means of controlled permutations and unitaries.

This idea can be generalized to the case of arbitrary dimension  $d$  and for any number  $n$  of copies of the initial state: An  $n$ -body battery in an initial non-passive state  $\rho = \text{diag}(p_1, \dots, p_{d^n})$ , where  $p_\alpha \geq 0$  and  $\sum_\alpha p_\alpha = 1$ . To perform optimal work extraction we need to evolve  $\rho$  to the passive state  $\sigma = \text{diag}(s_1, \dots, s_{d^n})$ , where

$s_{\alpha+1} \leq s_\alpha$  and  $\langle \alpha | \sigma | \alpha \rangle = s_\alpha = \Pi_{\alpha\beta} p_\beta$ , for some permutation  $\Pi_{\alpha\beta}$ . To do so, each transposition  $\alpha \leftrightarrow \beta$  that swaps  $p_\alpha$  with  $p_\beta$  is addressed separately by transforming  $|\alpha\rangle$  to  $|\beta\rangle$  (and vice versa) with a sequence of steps: First,  $|\alpha\rangle = |i_1^\alpha i_2^\alpha \dots i_n^\alpha\rangle$  is mapped to  $|\alpha'\rangle = |i_1^\beta i_2^\alpha \dots i_n^\alpha\rangle$ , then to  $|\alpha''\rangle = |i_1^\beta i_2^\beta \dots i_n^\alpha\rangle$ , and so on until it reaches  $|\beta\rangle = |i_1^\beta i_2^\beta \dots i_n^\beta\rangle$ , after  $n$  steps. Each of these steps is obtained by a unitary operator

$$U_{\alpha\alpha'}(t) = \sum_{\mu \neq \alpha\alpha'} |\mu\rangle\langle\mu| + u_{\alpha\alpha'}(t), \quad (8.12)$$

generated by some 2-body control interaction  $V_{\alpha\alpha'}(t)$ , that has, in principle, the power to generate bipartite entanglement. The state  $\rho(t)$  of the system at time  $t$  obtained via such unitary is

$$\begin{aligned} \rho(t) &= U_{\alpha\alpha'}(t) \rho U_{\alpha\alpha'}^\dagger \\ &= (p_\alpha + p_{\alpha'}) \rho_1(t) \otimes |i_2^\alpha \dots i_n^\alpha\rangle\langle i_2^\alpha \dots i_n^\alpha| \\ &\quad + \sum_{\mu \neq \alpha\alpha'} p_\mu |\mu\rangle\langle\mu|, \end{aligned} \quad (8.13)$$

with  $\rho_1$  being itself a state. The overall state  $\rho(t)$  is thus separable at every step of the procedure, and after  $2n - 1$  total steps the target final state  $\sigma$  is reached.

Of all the possible unitary cycles that connect the state  $\otimes^n \rho$  to its passive state  $\sigma_{\otimes^n \rho}$ , those that preserve the system in a separable state are inevitably slower than those that generate entanglement. Accordingly, the authors of Ref. [6] indicate a relation between the rate of entanglement generation and the power of work extraction – defined as the ratio between extracted work and time required for the extraction – leaving the open problem of quantifying such a relation to successive work. This question paves the way for the study of charging and extracting power, as described in the next section.

## 8.3 Powerful Charging

We now consider the task of charging quantum batteries via unitary operations. The deposited energy is then simply the opposite of the work extracted, and as long as we consider closed systems, the two tasks are essentially equivalent.

### 8.3.1 Bounds on Minimal Time of Evolution

In the previous section, we saw how optimal work extraction can be performed with a sequence of unitary operations, and how the ensemble of batteries can be kept in a separable state at the expense of adding extra steps to such a sequence. If each of

those operations could be performed instantly, the total number of steps would not influence the power of work extraction. However, in practice, each of those unitary operations requires a finite amount of time to be performed, which follows from the fact that Hamiltonians have finite magnitude (*i.e.* they are bounded operators). There holds a fundamental bound on the minimum time necessary to perform a unitary evolution, known as the quantum speed limit<sup>2</sup> (QSL), which provides an operational interpretation of the time-energy uncertainty relation  $\Delta t \Delta E \geq \hbar$  [8].

The minimum time required to evolve some pure state  $|\psi\rangle$  to another pure state  $|\phi\rangle$  by means of a unitary operator  $U(t)$  generated by time-dependent Hamiltonian  $H(t) = H_0 + V(t)$  is bounded by

$$T(|\psi\rangle, |\phi\rangle) = \hbar \frac{\arccos |\langle \psi | \phi \rangle|}{\min\{E, \Delta E\}}, \quad (8.14)$$

where the numerator measures the distance<sup>3</sup> between the states, while  $E$  and  $\Delta E$  correspond to the time-averaged energy (relative to the ground state) and standard deviation of the Hamiltonian  $H(t)$  [20].

### 8.3.2 Average and Instantaneous Power

When we address the problem of charging quantum batteries, an interesting task is to understand how to deposit energy as quickly as possible, *i.e.* how to maximize average or instantaneous power. The average power  $P$  of some unitary charging between  $\rho$  and  $\rho(T) = U(T)\rho U^\dagger(T)$  is simply given by the ratio between the energy deposited on the battery during the procedure and the time required to perform the unitary operation,

$$\langle P \rangle = \frac{W}{T}, \quad (8.15)$$

remembering that from now on  $W$  has the opposite sign with respect to that of Eq. (8.4). Similarly, the instantaneous power  $P(t)$  at some time  $t$  is given by the time derivative of the energy deposited at time  $t$  along the unitary charging,

$$P(t) = \frac{d}{dt} W = \frac{d}{dt} \left\{ \text{tr}[\rho(t)H_0] - \text{tr}[\rho H_0] \right\}, \quad (8.16)$$

which becomes  $P(t) = -i \text{tr}\{[H_0 + V(t), \rho(t)]H_0\}$ , using the von Neumann equation.

<sup>2</sup>See Ref. [20] for an extended review on quantum speed limits and their applications.

<sup>3</sup>The unique distance on the space of pure states that is invariant under unitary operations is the Fubini-Study distance, given by the angle between the two considered states [21].

In order to address this optimization problem a constraint on the driving Hamiltonian  $H + V(t)$  has to be considered, to prevent one from increasing the average power by investing more energy into the driving Hamiltonian, as to allow for fair comparison between different charging procedures. The constraint can be of the form

$$\|H + V(t)\| \leq E_{\max}, \quad (8.17)$$

for some norm such as trace or operator norms, and some energy  $E_{\max} > 0$ . This constraint is operationally equivalent to limiting the energy at our disposal in order to perform the charging procedure. Starting from those considerations, it is possible to show that entangling operations are more powerful than local ones, yielding an advantage that scales up to linearly with the number  $n$  of unit cells [4, 7].

*Maybe RP quantifies the charging advantage?*

### 8.3.3 Optimal Charging of an Array of Batteries

We now consider a battery given by  $n$  copies of a  $d$ -dimensional unit cell, whose internal Hamiltonian is given by Eq. (8.9). Assuming that the energetic structure of the individual Hamiltonians  $H_l$  is the same for each copy, the highest and lowest energy states are now  $|G\rangle := \otimes^n |1\rangle$  and  $|E\rangle := \otimes^n |d\rangle$ , respectively. The energy deposited onto the battery after an evolution from  $|G\rangle$  to  $|E\rangle$  is equal to  $W(n) = n(\varepsilon_d - \varepsilon_1)$ . We are going to compare the charging power of

$$H_{\parallel}^{(n)} = \alpha_{\parallel} \sum_{l=1}^n (|1\rangle\langle d|_l + h.c.) \otimes_{j \neq l} \mathbb{1}_j, \quad (8.18)$$

$$H_{\sharp}^{(n)} = \alpha_{\sharp} (|E\rangle\langle G| + h.c.), \quad (8.19)$$

which provide the optimal local (parallel) and global (collective) driving, respectively, when we require any Hamiltonian  $H$  to satisfy the constraint<sup>4</sup>  $\|H\|_{\text{op}} = E_{\max}$ , for some energy  $E_{\max} > 0$  [7]. We thus obtain  $\alpha_{\parallel} = E_{\max}/n$  and  $\alpha_{\sharp} = E_{\max}$ , which allows us to express the time required to perform the two different procedures as

$$T_{\parallel} = n \frac{\pi}{2} \frac{1}{E_{\max}}, \quad T_{\sharp} = \frac{\pi}{2} \frac{1}{E_{\max}}. \quad (8.20)$$

If we calculate the average power according to Eq. (8.15) we obtain  $P_{\sharp} = n P_{\parallel}$ ; the power of the entangling operation is  $n$  times larger than that of local ones. These two charging procedures are schematically represented in Fig. 8.4. Such advantage can be interpreted geometrically: While the collective Hamiltonian of Eq. (8.19) drives

<sup>4</sup>The operator norm  $\|\cdot\|_{\text{op}}$  of an operator  $H$  is equal to its largest singular value; if the operator  $H$  is Hermitian (and any Hamiltonian is) then the operator norm is equal to the largest eigenvalue.

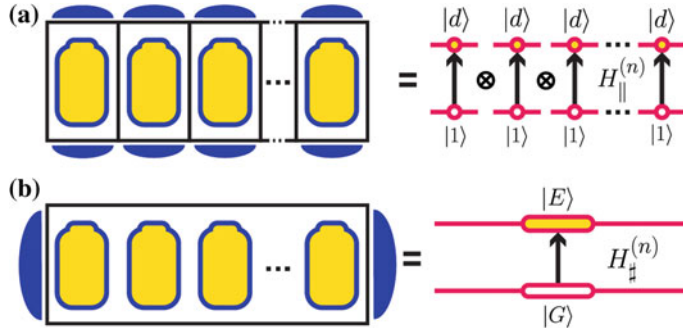


**Fig. 8.4** Local (a) and global (b) charging procedure are here schematically represented. The optimal local driving couples each individual ground state  $|1\rangle_i$  to its respective excited state  $|d\rangle_i$ , while the optimal global driving couples the collective ground state  $|G\rangle = \otimes^n|1\rangle$  to the collective excited one  $|E\rangle = \otimes^n|d\rangle$ .

the initial state along the shortest path, through the space of entangled states, the local Hamiltonian generates a longer orbit, that in return keeps the state separable for all times [7].

### 8.3.4 Quantum Advantage

Consider the task of charging an  $n$ -body battery between some product state  $\otimes^n\rho$ , to some other product state  $\otimes^n\sigma$  by means of cyclic unitary operations. We can introduce a simple parameter to quantify the advantage of using entangling operations over local ones, given by the power ratio

$$\Gamma := \frac{\langle P \rangle}{\langle P_{\parallel} \rangle} = \frac{T_{\parallel}}{T}, \quad (8.21)$$

where  $\langle P \rangle$  is the power of the considered charging procedure, while  $\langle P_{\parallel} \rangle$  is the charging power obtained with the best local driving [22]. Since the energy  $W(n)$  deposited onto the battery depends only on the choice of initial and final states,  $\Gamma$  can be simply expressed as the ratio between the optimal parallel time  $T_{\parallel}$  and the time  $T$  required to perform the charging.

The parameter  $\Gamma$ , called the quantum advantage, can be greater than unity only when entangling operations are considered [4]. Upper bounds for  $\Gamma$  are obtained using the quantum speed limit, as shown in Ref. [4], and depend on the chosen constraint on the driving Hamiltonian  $H$ . In particular, imposing a constraint on the standard deviation of the driving Hamiltonian yields an advantage that scales with  $\sqrt{n}$ , whereas a linear scaling results from constraining the average energy of  $H$  or its operator norm.

### 8.3.5 Correlations and Optimal Power

An interesting result obtained by Campaioli et al. [4] sheds light on the nature of the quantum advantage and its dependence on quantum correlations, such as entanglement. The authors provide an example where an initial, highly mixed state  $\otimes^n \rho$  of  $n$ -copies of a 2-level system evolves to some final state  $\otimes^n \sigma$ , where  $\rho = \exp[-\epsilon H_0]/\text{tr}\{\exp[-\epsilon H_0]\}$ , and  $\sigma = \exp[\epsilon H_0]/\text{tr}\{\exp[\epsilon H_0]\}$  are thermal states with inverse temperature  $\pm\epsilon$ , and where  $H_0 \propto \sigma_z$ . This system can be driven with the collective Hamiltonian in Eq. (8.19) in order to achieve a quantum advantage  $\Gamma = n$  over the optimal local charging, for any value of  $\epsilon > 0$ .

However, as  $\epsilon$  decreases the collective state  $\otimes^n \rho$  gets closer and closer to the separable ball, a spherically symmetric region of the space of states, centered around the maximally mixed state, that contains only separable states. Since the distance from the maximally mixed state is invariant under unitary evolution, the final state  $\otimes^n \sigma$ , along with every other state through which the evolution proceeds, will also be in the separable ball if the initial state  $\otimes^n \rho$  is (see Fig. 8.5). The authors show that for any  $n$  there is an  $\epsilon > 0$  small enough that the evolution can be performed entirely within the separable ball, yet still with a linear advantage in  $n$  with respect to the optimal local procedure. This leads to the conclusion that entanglement per se is not required for a quantum advantage in the charging power of quantum batteries.

The role of other forms of quantum correlations, such as quantum discord [23], has not been investigated yet; however, as we show in the next section, this example hints that a possible resource is given by the order  $k$  of non-local  $k$ -body interactions that are available for the charging task.

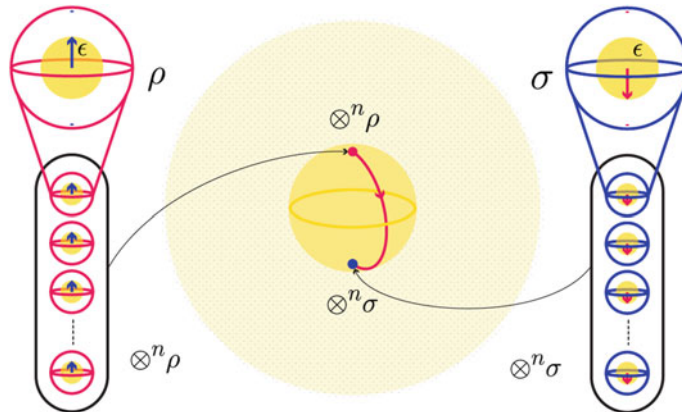


**Fig. 8.5** In the example described by Campaioli et al. a product state  $\otimes^n \rho$  of  $n$  copies of the same highly mixed state  $\rho$  of a 2-level system is unitarily evolved into  $\otimes^n \sigma$ , where  $\rho = \exp[-\epsilon \sigma_z]/Z$ , and  $\sigma = \exp[\epsilon \sigma_z]/Z$ . For large  $n$ , if the inverse temperature  $\epsilon$  is chosen to be small enough, the state of the copies lies in a region of the space of states that contains only separable states, called separable ball. Since unitary evolution cannot change the purity of a state, any driving that maps such  $\otimes^n \rho$  to  $\otimes^n \sigma$  preserves the system in a separable state at all times. The authors of Ref. [22] show that the global Hamiltonian given in Eq. (8.19) can lead to a quantum advantage  $\Gamma = n$ .

### 8.3.6 Feasible Charging Scenarios

The advantage that can be obtained using entangling operations such as that in Eq.(8.19) might be practically hard to obtain. The reason is that such collective interactions are given by highly non-local terms.<sup>5</sup> As these interactions are naturally rare or hard to engineer, it is useful to understand how to maximize the quantum advantage when we are limited to  $k$ -body interactions, with  $2 \leq k < n$ .

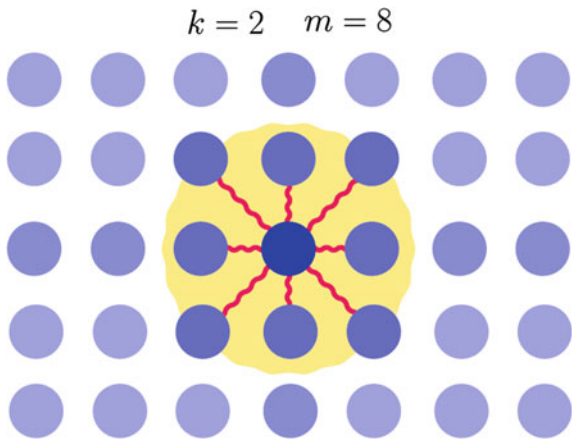
It is possible to derive a bound on  $\Gamma$  under the assumption that the operator norm of any driving Hamiltonian is bounded by some positive quantity  $E_{\max}$ , the interaction order is at most  $2 \leq k < n$ , and the participation number, *i.e.* the maximum number of interactions that each unit cell can take part in, is at most  $m > 1$ , obtaining

$$\Gamma < \gamma[k^2(m-1) + k], \quad (8.22)$$

where  $\gamma$  is a constant factor that does scale with the number  $n$  of cells (see Fig. 8.6 for an example) [4]. Such a result is obtained by performing a Trotterization of the unitary evolution, decomposed in terms of a set of  $k(m-1) + 1$  circuits, each of which is given by piece-wise time-independent Hamiltonians that have up to  $k$ -body interactions.

On one hand, this result rules out the possibility of increasing the number of cells in the battery in order to enhance its charging power. On the other, it clearly shows the importance of the order  $k$  of the interactions as an effective resource in these charging schemes.

**Fig. 8.6** Let us consider a battery given by  $n$  unit cells arranged in a 2-d lattice, where each unit cell is coupled with its neighbours via 2-body interactions ( $k = 2$ ). If the reach of these interactions is limited to the nearest neighbours, each unit cell interacts with up to 8 others ( $m = 8$ ). Under these conditions the achievable quantum advantage  $\Gamma$  is bounded as in Eq. (8.22).



<sup>5</sup>For example, in the case of 2-level systems such interactions have non-trivial components proportional to products of  $n$  Pauli operators  $\sigma_i^{(1)} \otimes \cdots \otimes \sigma_j^{(n)}$ , with  $i = 1, 2, 3$ .

### 8.3.7 Cycle Precision

Earlier in this section we discussed the importance of time-energy uncertainty relations, and how they set a bound on the minimum time required to perform the unitary cycles that we considered to charge quantum batteries. As large power corresponds to short times, short times lead to large work fluctuations, which, in turn, lead to inaccuracy. Such trade-offs between a cycle's precision and power have to be carefully addressed, in order to avoid the likely scenario of depositing a hazardous amount of energy [13]. Charging precision can be explored minimizing either the standard deviation of the final energy, or the fluctuations during the charging process [13].

This problem has been addressed by Friis and Huber who considered a model given by a number of harmonic oscillators in the canonical Gibbs state  $\omega_\beta$ , where  $\beta$  is the inverse temperature of the battery, which are then charged by means of unitary operations. The authors suggest the use of Gaussian unitary operations, *i.e.* those unitary operations that preserve the system in the space of Gaussian states, motivated by the fact that such operations are of accessible experimental realization. Gaussian operation also represent a trade-off between performance and feasibility. The authors are able to identify pure single-mode squeezing as the least-favourable operations, when one wishes to obtain precise charging of single-mode batteries, while they indicate combinations of squeezing and displacements as the most accurate and accessible operations [13].

## 8.4 Possible Implementations

The study of quantum batteries is fundamentally driven by the ambition of realizing devices of atomic and molecular size, which could gain a considerable advantage over their macroscopic counterparts for some particular tasks, so, as theoretical advancements lead the way, we must also consider experimental realizations: Fundamental milestones, such as the implementation of optimal extraction protocols, or that of an extensive quantum advantage, would be of exceptional impact.

Here we summarize some of the possible experimental scenarios that authors have indicated, such as spin-chains [14], nanofabricated quantum dots coupled to cavities, and superconducting qubits [12].

### 8.4.1 Cavity Assisted Charging

The collective terms required to maximize the charging power can be recovered by coupling the batteries to an electromagnetic field, where collective coherences lead to superradiance [4, 12]. In particular, Ferraro et al. use a Dicke model to powerfully charge an array of 2-level systems coupled with a quantized single-mode electromagnetic field [12].

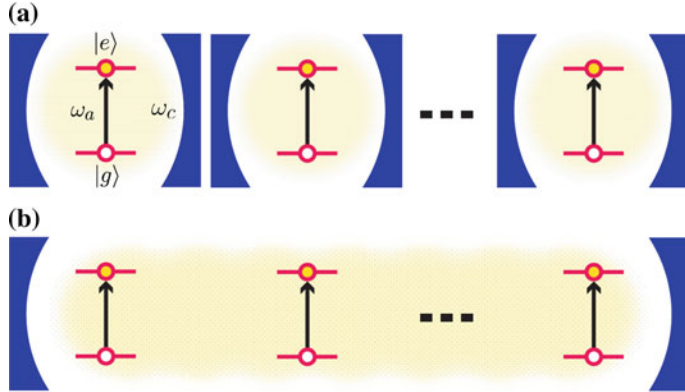


**Fig. 8.7** Ferraro et al. propose a Dicke model for a cavity-assisted quantum battery that can be charged both locally (a) and globally (b), as represented by this scheme. The cavity's single mode frequency is given by  $\omega_c$ , while the energy-splitting of each 2-level system is characterized by  $\omega_a$ . This model can be used to obtain effective  $n$ -body interactions between the  $n$  unit cells, and achieve a quantum advantage  $\Gamma \propto \sqrt{n}$ .

The model considered – schematically represented in Fig. 8.7 – is given by the time-dependent Dicke Hamiltonian

$$H^{(n)} = \hbar\omega_c \hat{a}^\dagger \hat{a} + \omega_a \hat{J}_z + 2\omega_c \lambda_t \hat{J}_x (\hat{a} + \hat{a}^\dagger), \quad (8.23)$$

where  $\hat{a}, \hat{a}^\dagger$  are the creation and annihilation operator for the single-mode cavity with frequency  $\omega_c$ , while

$$\hat{J}_i = \frac{\hbar}{2} \sum_{l=1}^n \sigma_i^{(l)}, \quad (8.24)$$

are the components of the collective spin operators expressed in terms of Pauli operators  $\sigma_i^{(l)}$  of the  $l$ th 2-level system. The energy splitting of each 2-level system is given by  $\hbar\omega_a$ , which is tuned in order to reach resonance with the cavity, *i.e.*  $\omega_a = \omega_c$ . Control is achieved by adjusting the strength of the coupling  $\lambda_t$  between cavity and array.

First, the system is initialized in state

$$|\psi^{(n)}(0)\rangle = |n\rangle \otimes |G\rangle, \quad (8.25)$$

where  $|G\rangle = \otimes^n |g\rangle$ , and where  $|n\rangle$  is the Fock state of the cavity with  $n$  photons in its single mode, and where  $|g\rangle$  is the ground state of the 2-level system. Charging is performed by turning on the coupling  $\lambda_t$  to some fixed value  $\bar{\lambda}$ , before switching it off at a later time  $\tau_c$ . Note that, in this case, while battery and cavity undergo the unitary evolution the battery alone evolves according to a non-unitary map. In particular, the energy  $W(\tau_c)$  stored at time  $\tau_c$  is calculated with respect to the array

of two-level systems (*i.e.* the battery), and thus associated with  $\omega_c \hat{J}_z$ , rather than the whole internal Hamiltonian  $H_0^{(n)} = \omega_c \hat{J}_z + \hbar\omega_c \hat{a}^\dagger \hat{a}$ .

The authors compare the maximum charging power that can be obtained in the collective case with the one that can be obtained via parallel charging, where the latter corresponds to a collection of  $n$  independent Hamiltonians  $H^{(1)}$ . They show that, in the limit of large  $n$ , the best charging power of the collective approach is up to  $\sqrt{n}$  times larger than that of the parallel approach

$$\frac{\max[\langle P_\sharp \rangle]}{\max[\langle P_\parallel \rangle]} \leq \sqrt{n}, \quad (8.26)$$

modulo some constant factor that does not depend on the number  $n$  of 2-level system considered in the protocol [12].

In the same work, Ferraro and colleagues discuss the tasks of storage and discharging, and the feasibility of the solid-state Dicke model described in their work, which can be realized by means of superconducting qubits or nanofabricated semiconductor quantum dots [12]. We now review another possible implementation of quantum batteries, proposed by Le et al., which consists in a spin-chain model characterized by many-body interactions [14].

### 8.4.2 Spin-Chain Battery

The common denominator of the batteries described so far in this chapter is the local nature of the internal Hamiltonian given by Eq.(8.9). As an alternative to such models one can consider a system composed of  $n$  unit cells whose internal Hamiltonian contains  $k$ -body interactions.

Le et al. specifically consider a one-dimensional Heisenberg spin-chain (2-level systems) characterized by 2-body interactions ( $k = 2$ ) with arbitrarily long range, which can lead to large values  $m$  of the participation number. Their internal Hamiltonian  $H_0^{(n)} = H_B + H_g$  is given by two terms,

$$H_B = B \sum_{i=1}^n \sigma_z^{(i)}, \quad (8.27)$$

$$H_g = - \sum_{i < j} g_{ij} [\sigma_z^{(i)} \otimes \sigma_z^{(j)} + \alpha (\sigma_x^{(i)} \otimes \sigma_x^{(j)} + \sigma_y^{(i)} \otimes \sigma_y^{(j)})], \quad (8.28)$$

where  $g_{ij}$  is the interaction strength between different spins, while  $\alpha$  can be tuned to recover Ising ( $\alpha = 0$ ), XXZ ( $0 < \alpha < 1$ ), and XXX ( $\alpha = 1$ ) Heisenberg models, respectively [14]. The system is then charged using an external field  $V = \omega \sum_i \sigma_x^{(i)}$ , while turning off  $H_B$ , in order to obtain the driving Hamiltonian  $H^{(n)} = H_g + V$ , which generates a time-independent unitary evolution  $U_t = \exp[-i H t]$ .

The remarkable difference between this model and the others reviewed so far is that the eigenstates of the internal Hamiltonian  $H_0^{(n)}$  can be entangled, if the coupling strength  $g_{ij}$  is non-vanishing, due to the presence of 2-body interactions between the spins. For this reason, rather than following a path from an initial to a final separable state, the authors study a quantum advantage  $\Gamma = \langle P \rangle / \langle P_{\text{ind}} \rangle$  that is given by the ratio between the power  $\langle P \rangle$  of some charging strategy and that  $\langle P_{\text{ind}} \rangle$  of the best independent driving ( $g_{ij} = 0$ ). In particular, in this case the energy can be *stored* in the interactions between the different spins.

The findings of Le and coauthors shed some light on the importance of correlations and many-body interaction for the charging power: first of all, they show that the isotropic coupling of the XXX Heisenberg model, *i.e.*  $\alpha = 1$ , leads to completely independent charging of each spin, thus to no advantage. Conversely, the full anisotropy of the XXZ model, *i.e.*  $\alpha = -1$ , leads to much higher power compared to the independent case.

Another important result is obtained when authors study the case of strong coupling  $g \gg \omega$  in order to recover effective  $n$ -body interactions. They find that the strength of such effective interactions in their model necessarily decreases with their ability to produce them, since they are only valid in a perturbative regime. As a result, the charging power of the battery is actually worse than that of the independent charging, and vanishes in the limit of large  $n$ .

An interesting quantum advantage for the charging power becomes evident in the weak interaction case, *i.e.* when  $\sum_{i < j} g_{ij} \ll n\omega$ . In particular, if the spin-spin interactions have finite range (or if the coupling strength decays more rapidly as their distance increase), such as for nearest neighbour interactions (see Fig. 8.8a), the power is enhanced only by a factor that is constant in  $n$ . When the coupling strength decays as  $1/|i - j|$ , where  $i$  and  $j$  are ordered spins  $i$  and  $j$  along the chain, the power grows super-extensively, and an advantage proportional to  $\log n$  can be achieved (see Fig. 8.8b). Finally, for uniform interaction strength the authors recover the extensive power advantage described by Eq. (8.20) (see Fig. 8.8c). These results are in full agreement with Eq. (8.22), when the interaction is  $k = 2$ , and when the participation number  $m$  is limited by the specific range of the coupling ( $m$  can be arbitrarily large in the last case), which reflect the symmetry between the roles of internal ( $H_0$ ) and driving ( $H$ ) Hamiltonians: Here, the driving Hamiltonian is local and does not increase the correlations between different spins, while the power advantage is given by the *extra* energy stored in the 2-body interactions provided by the internal Hamiltonian.

Le's results also reinforce one of the results by Campaioli et al. about the role of correlations: The infinite-ranged interacting spin chain behaves like a global classical spin in the limit of large  $n$ , while providing the largest power enhancement, supporting the conclusion that quantum correlations are unnecessary for the efficient operation of such a many-body battery [4, 14].

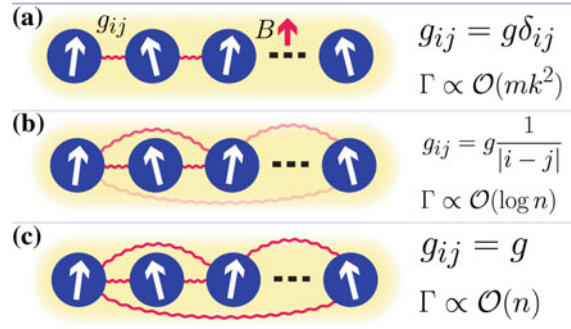


**Fig. 8.8** Le et al. consider a many-body spin-chain model to obtain a quantum battery in Ref. [14], as described in Eqs. (8.27) and (8.28). They study the dependence of the achievable quantum advantage on the interaction range in the weak coupling regime ( $\sum_{i < j} g_{ij} \ll n\omega$ ), showing that nearest-neighbour interactions (a) lead to an advantage that does not depend on the number  $n$  of unit cells, long-range interactions (b)  $g_{ij} \propto 1/|i - j|$  lead to  $\Gamma \propto \mathcal{O}(\log n)$ , while uniform interactions (c)  $g_{ij} = g$  lead to an extensive advantage. Their findings are in agreement with Eq. (8.22), when order of the interaction  $k$  and participation number  $m$  are considered.

#### 8.4.3 Coupled Cooper Pair Boxes

As mentioned earlier in this section, another implementation could be obtained by means of cooper pair boxes (CPBs) charged via gate pulses [12]. The motivation of using such systems comes from the fact that they have well defined charging energies, they are scalable and can be produced in large numbers, they are relatively easy to fabricate and allow for the design of local and two-body interactions.

A CPB comprises a small conducting island, typically made of aluminum, coupled to a conducting reservoir via a small Josephson junction. The junction allows for the tunneling of a Cooper pair, *i.e.* a pair of electrons bonded by lattice deformation, between reservoir and island. Restricted to a pair of adjacent energy levels, such a device provides a 2-level system with logical states  $|0\rangle$  and  $|1\rangle$ , associated to the absence/presence of an extra Cooper pair on the island, that can be used to implement 1-body and 2-body quantum gates [24], such as NOT and SWAPS. Due to the small capacitance of the island, the tunneling of a pair requires a significant amount of energy, which can also be adjusted by a gate voltage. Since CPBs are characterized by a well-defined charging energy they are also called *charge qubits*,<sup>6</sup> and could be thought of as elementary 2-level batteries, such as the one described in Fig. 8.1.

Since pairs of CPBs can be coupled to each other by means of junctions between their islands [24], engineering two-body interactions that could be used to obtain an advantage for the charging power becomes a promising, as well as challenging task.

<sup>6</sup>More precisely, CPBs are referred to as charge qubits in the large charging energy regime; when the charging energy is small, they are referred to as flux qubits.

As mentioned earlier in this chapter, such advantage would benefit of the order of the interactions  $k$  (here  $k = 2$ ), resulting in a charging time that could be up to two times shorter than that of any local charging procedure, when fairly compared to the case of independent CPBs.

Along with the practical implementations that we have discussed, there are many other problems that have to be addressed in order to bring quantum batteries to their first realizations, which we discuss in the next section.

## 8.5 Discussion

Until now we have considered reversible charging and extraction procedures performed via cyclic unitary operations, where initial and final states of the battery are invariant under the action of the internal Hamiltonian  $H_0$ : In such a case, once the driving field  $V(t)$  is turned off the battery remains in the desired charged state for arbitrarily long times. However, it is sensible to think that such small and sensitive systems would interact, albeit weakly, with the surrounding environment, which could dissipate the energy stored.

In order to preserve the energy stored for reasonably long times it is fundamental to understand how to counteract the action of the environment. The latter could manifest itself by inducing decoherence, amplitude damping, and energy dissipation. Such a task could be approached with tools of quantum optimal control [25–27], but nobody has addressed this problem for the specific case of quantum batteries yet. On one hand it is easy to identify the most interesting tasks, such as energy stabilization, powerful charging and optimal work extraction. Instead, modelling system-environment dynamics requires more attention, since it is not clear how quantum batteries would be realized in practice. For this reason, looking for experimental realization is just as important as optimizing charging, extraction and stability under the effect of the environment.

## References

1. C.A. Vincent, B. Scrosati, *Modern Batteries : An Introduction to Electrochemical Power Sources* (Arnold, 1997), p. 351. <https://doi.org/10.1016/B978-0-340-66278-6.X5000-1>
2. J. Goold, M. Huber, A. Riera, L. del Rio, P. Skrzypczyk, *J. Phys. A: Math. Theor.* **49**, 143001 (2016). <https://doi.org/10.1088/1751-8113/49/14/143001>
3. S. Vinjanampathy, J. Anders, *Contemp. Phys.* **57**, 545 (2016). <https://doi.org/10.1080/00107514.2016.1201896>
4. F. Campaioli, F.A. Pollock, F.C. Binder, L. Céleri, J. Goold, S. Vinjanampathy, K. Modi, *Phys. Rev. Lett.* **118**, 150601 (2017). <https://doi.org/10.1103/PhysRevLett.118.150601>
5. R. Alicki, M. Fannes, *Phys. Rev. E* **87**, 042123 (2013). <https://doi.org/10.1103/PhysRevE.87.042123>
6. K.V. Hovhannisan, M. Perarnau-Llobet, M. Huber, A. Acín, *Phys. Rev. Lett.* **111**, 240401 (2013). <https://doi.org/10.1103/PhysRevLett.111.240401>

7. F.C. Binder, S. Vinjanampathy, K. Modi, J. Goold, New J. Phys. **17**, 075015 (2015). <https://doi.org/10.1088/1367-2630/17/7/075015>
8. S. Deffner, S. Campbell, J. Phys. A: Math. Theor. **50**, 453001 (2017). <https://doi.org/10.1088/1751-8121/aa86c6>
9. J. Werschnik, E.K.U. Gross, J. Phys. B: At. Mol. Opt. Phys. **40**, R175 (2007). <https://doi.org/10.1088/0953-4075/40/18/R01>
10. T. Caneva, M. Murphy, T. Calarco, R. Fazio, S. Montangero, V. Giovannetti, G.E. Santoro, Phys. Rev. Lett. **103**, 240501 (2009), <https://doi.org/10.1103/PhysRevLett.103.240501>
11. I. Brouzos, A.I. Streltsov, A. Negretti, R.S. Said, T. Caneva, S. Montangero, T. Calarco, Phys. Rev. A **92**, 062110 (2015). <https://doi.org/10.1103/PhysRevA.92.062110>
12. D. Ferraro, M. Campisi, G.M. Andolina, V. Pellegrini, M. Polini, Phys. Rev. Lett. **120**, 117702 (2018). <https://doi.org/10.1103/PhysRevLett.120.117702>
13. N. Friis, M. Huber, Quantum **2**, 61 (2017). <https://doi.org/10.22331/q-2018-04-23-61>
14. T.P. Le, J. Levinse, K. Modi, M.M. Parish, F.A. Pollock, Phys. Rev. A **97**, 022106 (2018). <https://doi.org/10.1103/PhysRevA.97.022106>
15. A.E. Allahverdyan, R. Balian, T.M. Nieuwenhuizen, Europhys. Lett. **67**, 565 (2004). <https://doi.org/10.1209/epl/i2004-10101-2>
16. G. Francica, J. Goold, F. Plastina, M. Paternostro, npj Quantum Inf. **3**, 12 (2017). <https://doi.org/10.1038/s41534-017-0012-8>
17. W. Pusz, S.L. Woronowicz, Commun. Math. Phys. **58**, 273 (1978). <https://doi.org/10.1007/BF01614224>
18. A. Lenard, J. Stat. Phys. **19**, 575 (1978). <https://doi.org/10.1007/BF01011769>
19. G.L. Giorgi, S. Campbell, J. Phys. B: At. Mol. Opt. Phys. **48**, 035501 (2015). <https://doi.org/10.1088/0953-4075/48/3/035501>
20. S. Deffner, E. Lutz, J. Phys. A: Math. Theor. **46**, 335302 (2013). <https://doi.org/10.1088/1751-8113/46/33/335302>
21. I. Bengtsson, K. Zyczkowski, *Geometry of Quantum States : An Introduction to Quantum Entanglement* (Cambridge University Press, Cambridge, 2008), p. 419. <https://doi.org/10.1142/S1230161208000080>
22. S. Campbell, S. Deffner, Phys. Rev. Lett. **118**, 100601 (2017). <https://doi.org/10.1103/PhysRevLett.118.100601>
23. H. Ollivier, W.H. Zurek, Phys. Rev. Lett. **88**, 017901 (2001). <https://doi.org/10.1103/PhysRevLett.88.017901>
24. Y.A. Pashkin, O. Astafiev, T. Yamamoto, Y. Nakamura, J.S. Tsai, Quantum Inf. Process. **8**, 55 (2009). <https://doi.org/10.1007/s11128-009-0101-5>
25. X. Wang, S. Vinjanampathy, F.W. Strauch, K. Jacobs, Phys. Rev. Lett. **110**, 157207 (2013). <https://doi.org/10.1103/PhysRevLett.110.157207>
26. S.J. Glaser, U. Boscain, T. Calarco, C.P. Koch, W. Köckenberger, R. Kosloff, I. Kuprov, B. Luy, S. Schirmer, T. Schulte-Herbrüggen, D. Sugny, F.K. Wilhelm, Eur. Phys. J. D **69**, 279 (2015). <https://doi.org/10.1140/epjd/e2015-60464-1>
27. N. Suri, F.C. Binder, B. Muralidharan, S. Vinjanampathy (2017). <https://doi.org/10.1140/epjst/e2018-00125-6>

# Chapter 9

## Quantum Rotor Engines



Stella Seah, Stefan Nimmrichter, Alexandre Roulet and Valerio Scarani

### 9.1 Introduction

It is not easy to guess whether the performance of a thermal machine would improve or deteriorate, were the machine operated in the quantum regime. Intrinsic noise will certainly be a nuisance, while coherence and entanglement may prove additional resources if properly harnessed. Designing a thermal machine with “quantum supremacy” would be a major breakthrough in quantum thermodynamics. This chapter focuses on rotor engines, a promising testbed for identifying genuine quantum features in thermal machines.

By *engine*, we understand a thermal machine that operates between two thermal reservoirs, the hot and the cold bath, transforming heat from the hot bath into *useful energy*. In fact, the paradigmatic use of an engine is to generate *directed motion*. With this in mind, we consider engines in which the *working medium* is coupled to a *rotor* [1–3]. Its rotation leads to an unambiguous definition of mechanical output (work) in terms of directed motion.

The rotor engine will be *autonomous*, like the engine of a car: once started, the cycle is self-sustained by interplay of gears and shafts (the driver’s pedal controls

---

S. Seah (✉) · V. Scarani

Department of Physics, National University of Singapore, 2 Science Drive 3,  
Singapore 117542, Singapore  
e-mail: stellaseah@u.nus.edu

V. Scarani

e-mail: physv@nus.edu.sg

S. Nimmrichter · V. Scarani

Centre for Quantum Technologies, National University of Singapore, 3 Science Drive 2,  
Singapore 117543, Singapore  
e-mail: cqtsn@nus.edu.sg

A. Roulet

Department of Physics, University of Basel, Klingelbergstrasse 82, 4056 Basel, Switzerland  
e-mail: alexandre.roulet@unibas.ch

the effective temperature of the hot bath). An autonomous engine keeps accelerating in the absence of friction or load [1–11]; when these are present, they determine the timing of the cycle in the steady state. By contrast, textbook studies of engine cycles (see Chap. 3) tend to consider *driven* engines [2, 12–17]. Their dynamics is simpler, since the timing of the cycle is fixed, determined by an external clock. However, claims on the efficiency of such engines are to be made with care, as the energy needed to operate the driving system must be taken into account.

That being said, a rotor and a clock are very similar. We use this similarity in Sect. 9.2 to introduce rotor engines. We start off with a textbook example of a time-dependent driven system and demonstrate how its time dependence can be mapped to a rotor degree of freedom. This clarifies also the dual role of the rotor in the autonomous engine: it can be seen both as an internal engine clock and as a work repository. We then discuss various definitions of work, notably comparing intuitive ones based on the rotor’s motion with axiomatic ones like the ergotropy. In Sect. 9.3, we compare the dynamics of the quantum model with the corresponding classical dynamics. Since throughout the paper our working mode will be a qubit, this comparison will introduce two classical spin models: (i) a coin-flip toy model, based on biased thermal coin flipping rate equations; and (ii) a classical magnetic moment with linear coupling to harmonic oscillator baths.

## 9.2 From Clock-Driven Engines to Rotor Engines

Consider a generic finite-time heat engine scheme comprised of a working medium and an external clock with characteristic frequency  $\omega$  [Fig. 9.1a]. Its autonomous counterpart is obtained by replacing the clock with an embedded quantum rotor [Fig. 9.1b]. For the mathematical formulation in terms of a dynamical open quantum system model we will follow Alicki’s derivation [18].

### 9.2.1 Mathematical Model of a Clock-Driven Engine

As working medium, we choose a simple quantum system: a single or a few qubits, or harmonic modes with bare Hamiltonian  $\hat{H}_0$ . The role of this medium is to perform and receive work  $W$  and to mediate a heat transfer between a hot and a cold reservoir,  $Q = Q_h + Q_c$ . These reservoirs can be conventional thermal baths at different temperatures  $T_h > T_c$ , but we may also consider non-standard resources such as squeezed baths [19–24] or continuous measurement processes that effectively inject entropy like a heat bath. Here, the coupling to the reservoirs shall be described by time-modulated Lindblad dissipators  $\mathcal{L}_{h,c}^{tot}$  acting on the state  $\rho$  of the working medium. Assuming the clock is sufficiently slow and the time modulations weak, one derives the master equation [18]

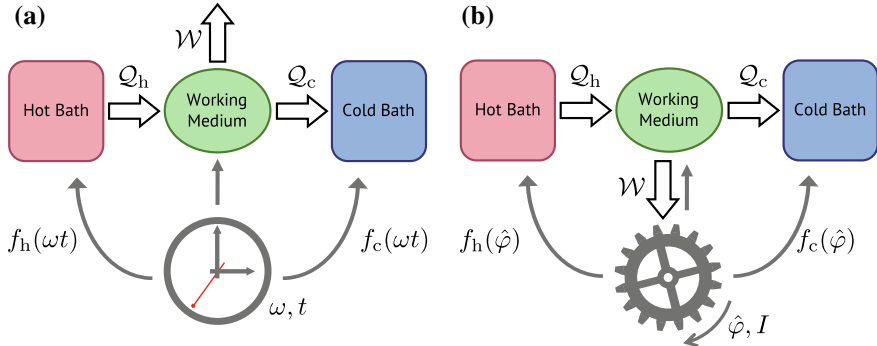


**Fig. 9.1** **a** Sketch of a clock-driven quantum engine with fixed cycle frequency  $\omega$ . The heat exchange between the engine's working medium and a hot and a cold reservoir is synchronized to the ticking clock pointer by virtue of periodic coupling functions  $f_{h,c}(\omega t)$ , while a time-periodic modulation of the medium's energy provides the interface for work in- and output. **b** Autonomous engine version, where the clock is replaced by a quantum rotor with angle  $\hat{\varphi}$  and moment of inertia  $I$ . The fluctuating angular motion determines the cycle frequency, modulates the working medium energy and serves as a flywheel energy storage.

$$\partial_t \rho = -\frac{i}{\hbar} [\hat{H}_0 + \hat{H}_{\text{int}}(\omega t), \rho] + \mathcal{L}_h^{\text{tot}} \rho + \mathcal{L}_c^{\text{tot}} \rho. \quad (9.1)$$

What dissipators are used to model the reservoir interaction for a given working medium determines whether the master equation is valid and thermodynamically consistent. In the case of weak coupling to thermal baths, for example, consistency with the second law is achieved if each dissipator would by itself describe thermalization of the whole system, i.e. drive the state  $\rho$  towards thermal equilibrium with the respective bath. However, when the working medium is a composite system, one often resorts to simpler dissipators that describe local thermalization of individual subsystems instead. Such an approximate treatment is only justified in the limit of weak intrinsic coupling between the subsystems [25–28].

The function of the clock in (9.1) is three-fold. First, it determines the duration  $\tau = 2\pi/\omega$  of an engine cycle. Second, it describes a modulation of the system energy by means of a periodic interaction Hamiltonian,  $\hat{H}_{\text{int}}(\omega t) = \hat{H}_{\text{int}}(\omega t + 2\pi)$ , and thereby provides the interface for work insertion and extraction. Third, it synchronizes the dissipative coupling between the working medium and the reservoirs in such a way that a net amount  $W$  of work is generated over each cycle. Note that, instead of idealized sequences of clearly separate heat and work strokes, we consider here continuous engine cycles with harmonic modulations of the working medium and the thermal coupling strengths,  $\hat{H}_{\text{int}}(\omega t)$  and real-valued  $f_{h,c}(\omega t)$  to be specified below.

### 9.2.1.1 Work Output and Energy Input

For the clock-driven engine, the work output is defined by separating the time-dependent modulation of the system Hamiltonian from the energy exchange with the reservoirs through the dissipators. The rate at which work is performed by the system at some time  $t$  is then given by the *output* power

$$\dot{W}(t) = -\text{tr} \left\{ \rho(t) \partial_t \hat{H}_{\text{int}}(\omega t) \right\}. \quad (9.2)$$

The energy *input* from the reservoirs, on the other hand, can be expressed in terms of the rates

$$\begin{aligned} \dot{Q}(t) &= \dot{Q}_h(t) + \dot{Q}_c(t), \\ \dot{Q}_{h,c}(t) &= \text{tr} \left\{ [\hat{H}_0 + \hat{H}_{\text{int}}(\omega t)] \mathcal{L}_{h,c}^{\omega t} \rho(t) \right\} \approx \text{tr} \left\{ \hat{H}_0 \mathcal{L}_{h,c}^{\omega t} \rho(t) \right\}, \end{aligned} \quad (9.3)$$

where the approximation holds if we are in the weak-coupling limit where the modulations of the bare system energies due to the interaction is small. For thermal reservoirs, the input will be in the form of passive, disordered energy, i.e. pure heat. But care must be taken in general, as the energy input of non-standard reservoirs could already contain a certain amount of useful work (see Chap. 2).

The total energy change in the working medium over an engine cycle is

$$\Delta E(t) = \int_t^{t+\tau} dt' [\dot{Q}(t') - \dot{W}(t')] = \text{tr} \left\{ [\hat{H}_0 + \hat{H}_{\text{int}}(\omega t)][\rho(t+\tau) - \rho(t)] \right\}, \quad (9.4)$$

which vanishes only in the quasi-static idealization where the system returns to its initial state after each cycle. For finite-time engines with finite-dimensional working media, the energy will typically grow over a number of periods before the engine reaches a steady limit cycle.

### 9.2.1.2 Driven Single-Qubit Piston Engine

As an instructive example that we will employ throughout the chapter, we consider a single qubit as working medium and the following model:

$$\begin{aligned} \hat{H}_0 &= \hbar\omega_0 |e\rangle\langle e|, \quad \hat{H}_{\text{int}}(\varphi) = \hbar g \cos \varphi |e\rangle\langle e|, \\ f_h(\varphi) &= \frac{1 + \sin \varphi}{2}, \quad f_c(\varphi) = 1, \\ \mathcal{L}_j^\varphi \rho &= \kappa f_j^2(\varphi) \{ (\bar{n}_j + 1) \mathcal{D}[\hat{\sigma}_-] \rho + \bar{n}_j \mathcal{D}[\hat{\sigma}_+] \rho \}, \end{aligned} \quad (9.5)$$

with  $\mathcal{D}[\hat{A}] \rho = \hat{A} \rho \hat{A}^\dagger - \{\hat{A}^\dagger \hat{A}, \rho\}/2$ , and with  $\hat{\sigma}_+ = |e\rangle\langle g|$  and  $\hat{\sigma}_- = |g\rangle\langle e|$  the qubit raising and lowering operators. Here we introduced the pointer coordinate  $\varphi = \omega t$  of the clock which we shall assume to point upwards to twelve o'clock at

$\varphi = 0$  and describing a clockwise rotation. The modulation  $g \cos \varphi$  of the qubit frequency  $\omega_0$  is then tied to the vertical position of the pointer (“piston”): the higher the piston, the higher the energy. Alternatively, it can be viewed as a constant pressure pushing down the piston when the qubit is excited, which corresponds to a time-dependent torque of magnitude  $\hbar g$  responsible for the work exchange.

The thermal coupling to harmonic oscillator baths of temperatures  $T_h > T_c$  and occupation numbers  $\bar{n}_{h,c} = 1/[\exp(\hbar\omega_0/k_B T_{h,c}) - 1]$  is synchronized with the horizontal pointer position. Both baths are characterized by the same thermalization rate  $\kappa$ , but while the cold one is in permanent contact to the qubit, the hot bath only couples appreciably if the clock points towards three o’clock ( $\varphi = \pi/2$ ) or around. This exact model was not studied previously but is similar to those studied in Refs. [1, 2]. To ensure validity of the weak coupling master equation (9.1), we must further assume  $g, \kappa, \omega \ll \omega_0, 1/\tau_{h,c}$  with  $\tau_{h,c}$  the bath correlation times.

It is now intuitively clear how this piston engine generates net work as the clock performs one round trip. Starting from the upper-most position, the clockwise downward motion increases the hot bath coupling, which leads to a high average qubit excitation and downward pressure. Work is generated until the lower turning point at  $\varphi = \pi$  is reached. The qubit is now predominantly coupled to the cold bath and therefore less excited on average, which results in less work being consumed in the subsequent upward motion of the pointer-piston.

Let us first analyse the quasi-static regime of slow rotation and fast thermalization,  $\omega \ll \kappa$ , where the qubit is approximately kept in thermal equilibrium. In the textbook case where the hot and the cold bath coupling occur in separate engine strokes ( $f_h(\varphi) f_c(\varphi) = 0$ ), the working qubit would dissipate to either mean excitations  $p_{h,c} = \bar{n}_{h,c}/(2\bar{n}_{h,c} + 1)$ , depending on the bath to which it is coupled. In the case of overlapping baths as we are considering here, at each time the qubit is in equilibrium at a  $\varphi$ -dependent effective temperature, with excitation probability

$$p_e(\varphi) = \frac{\bar{n}_h f_h^2(\varphi) + \bar{n}_c f_c^2(\varphi)}{(2\bar{n}_h + 1)f_h^2(\varphi) + (2\bar{n}_c + 1)f_c^2(\varphi)}. \quad (9.6)$$

If we associate a vertical piston position  $x = x_0 \cos \varphi$  to the clock angle, then the downward pressure of the excited qubit translates into an average force  $F = \hbar g p_e(\varphi)/x_0$ . This allows us to visualize the engine cycle in a phase diagram (Fig. 9.2). For finite values of  $\omega/\kappa$ , when (9.6) is not valid,  $p_e(\varphi)$  is obtained from a numerical simulation of the dynamics, for which we used the QuTiP package [29].

The enclosed area gives the *net work output per cycle*. In the ideal quasi-static limit  $\omega \ll \kappa$ , this is given by

$$W_{\text{qst}}^{\text{cyc}} = \hbar g \int_0^{2\pi} d\varphi p_e(\varphi) \sin \varphi. \quad (9.7)$$

With growing  $\omega$ , the area of the limit cycles shrinks, as the thermalization lags behind the rotation of the clock pointer.

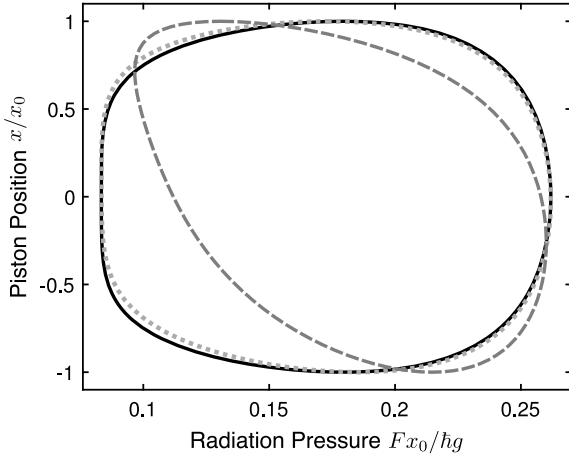


**Fig. 9.2** Phase diagrams of driven single-qubit piston engine cycles. The horizontal and the vertical axis represent the average force by the qubit (pressure) and the vertical piston position (volume), respectively. We plot the ideal quasi-static cycle  $\omega \ll \kappa$  (solid) and the finite-time limit cycles for  $\omega/\kappa = 0.1$  (dotted) and 1 (dashed). The parameters of the plot are  $(\bar{n}_h, \bar{n}_c) = (1, 0.1)$  and  $g = 10\kappa$ . For this example, the integral in (9.7) gives 0.31, the one in (9.8) gives 0.23.

It is also instructive to look at the *heat input per cycle* given by

$$Q_{h,qst}^{\text{cyc}} = \hbar\omega_0 \frac{(2\bar{n}_h + 1)\kappa}{\omega} \int_0^{2\pi} d\varphi f_h^2(\varphi) [p_h - p_e(\varphi)] \quad (9.8)$$

for  $\omega \ll \kappa$ . In the case of separate strokes, this would be  $\hbar\omega_0(p_h - p_c)$  independent of  $\omega$ . Since the cold bath is always coupled, a slower cycle leads to an excess of heat input by a factor  $\sim \kappa/\omega$ .

Finally we turn to the *efficiency per cycle*  $\eta = W_{qst}^{\text{cyc}}/Q_{h,qst}^{\text{cyc}}$ . In Fig. 9.3a, we plot it for varying engine frequencies  $\omega$  at otherwise fixed rates  $g, \kappa$  as before. The engine attains its maximum efficiency at  $\omega \sim \kappa$  (i.e. away from the quasi-static limit).

Panels (b) and (c) show the behavior of the cycle-averaged *powers* of work output and heat input, respectively. The efficiency is mainly determined by the behavior of the work output power, which deteriorates once the engine rotates faster than the qubit can thermalize. In this regime where  $\omega \gg \kappa$ , the per-cycle work output fails to reach the quasi-static optimal value (9.7).

As for the heat input power, it assumes its quasi-static minimum (9.8) at low frequencies and increases slightly with  $\omega/\kappa$ , indicating that the heat leak from the hot to the cold bath worsens when thermalization lags behind.

A velocity-dependent efficiency and output power with a sweet spot of optimal performance is typical for classical piston engines and motors. In the driven engine just discussed, it depends entirely on the intrinsic reaction time  $1/\kappa$  of the working medium. The dependence will be different once we replace the external time depen-

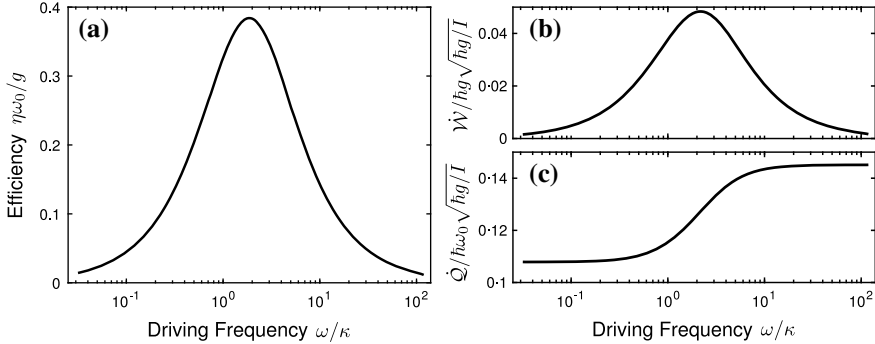


**Fig. 9.3** Performance of engine as a function of the driving frequency  $\omega$  for the same settings as Fig. 9.2. **a** Efficiency  $\eta$  in units of  $g/\omega_0$ , where  $g \ll \omega_0$ . **b** and **c** Cycle-averaged work output  $\dot{W}$  and heat input power  $\dot{Q}$  respectively. We notice that the efficiency is mostly determined by  $\dot{W}$ , while  $\dot{Q}$  is almost constant.

dence that drives the engine by an autonomous rotor clock and introduce an actual load for steady-state work extraction.

### 9.2.2 Reformulation as an Autonomous Rotor Engine

Now we replace the external clock with a built-in engine clock. To this end, we replace the regular ticks at a fixed frequency  $\omega$  with a planar rotor degree of freedom characterized by its moment of inertia  $I$  and its canonical variables  $(\hat{\phi}, \hat{L})$ , as sketched in Fig. 9.1b. The dynamical variable  $\hat{\phi}$  of the rotor now serves as an internal clock that sets the engine cycle.<sup>1</sup> Concurrently, the rotor would act as an integrated “flywheel” that captures the work injected by the thermally driven working medium in the form of kinetic energy,  $\hat{L}^2/2I$ . The master equation for the autonomous engine, replacing the previous (9.1), is now given by

$$\begin{aligned}\partial_t \rho = -\frac{i}{\hbar} & \left[ \hat{H}_0 + \hat{H}_{\text{int}}(\hat{\phi}) + \frac{\hat{L}^2}{2I}, \rho \right] + \mathcal{L}_h^\phi \rho + \mathcal{L}_c^\phi \rho, \\ \mathcal{L}_j^\phi \rho = \kappa (\bar{n}_j + 1) & \mathcal{D}[f_j(\hat{\phi}) \hat{\sigma}_-] \rho + \kappa \bar{n}_j \mathcal{D}[f_j(\hat{\phi}) \hat{\sigma}_+] \rho\end{aligned}\quad (9.9)$$

This master equation is valid only in the weak-coupling limit of  $\hbar/I$ ,  $g$ ,  $\langle \hat{L} \rangle/I$ ,  $\kappa \ll \omega_0$ , where the bare qubit frequency  $\omega_0$  can be removed by switching into the rotating frame [25–28].

<sup>1</sup>To ensure a consistent quantum description of the rotor angle, the operator  $\hat{\phi}$  will appear only in the form of strictly  $2\pi$ -periodic functions.

Here, we see two key differences between autonomous and externally-driven engines. Firstly, (9.9) describes the evolution of a composite system that comprises both the working medium and the rotor. This means that the cycle period is no longer fixed since the frequency is now a dynamical variable with mean  $\langle \hat{L} \rangle / I$ . Second, the Lindblad operators in the dissipators depend on  $\hat{\phi}$  and are thus operators acting on the rotor Hilbert space as well. Hence, they will not only describe the energy exchange of the working medium with the hot and cold reservoirs, but also an effective measurement backaction in the form of angular momentum diffusion. This results in an accumulation of passive, disordered energy in the rotor, with its heating rate given by

$$\dot{Q}_{BA} = \text{tr} \left\{ \frac{\hat{L}^2}{2I} (\mathcal{L}_h^{\hat{\phi}} + \mathcal{L}_c^{\hat{\phi}}) \rho \right\} = \frac{\hbar^2 \kappa}{4I} \sum_j \text{tr} \{ (\bar{n}_j + |e\rangle\langle e|) [f'_j(\hat{\phi})]^2 \rho \} \geq 0 \quad (9.10)$$

Concerning the engine's energy balance, we note once again that while  $\dot{Q}_{BA}$  contributes to the total heat flow, it can be omitted in the overall energy balance in the weak-coupling limit where  $g, \hbar/I, \kappa \ll \omega_0$ , see (9.3). Also,  $\dot{Q}_{BA}$  should be distinguished from the amount of *useful* work that accumulates in the form of net directed rotation. One should thus be cautious in choosing how to measure the amount of useful energy generated under autonomous operation with no load attached.

### 9.2.2.1 Autonomous Work Production

A main advantage of rotor engines is their unambiguous notion of useful energy output: the working medium generates extractable work by producing a gain in net *directed* rotation. This is intuitively clear from the viewpoint of classical motors and piston engines, but does it translate to the quantum regime?

We first look at the direct translation of the conventional work notion based on (9.2) to autonomous engines. The time derivative of the coupling Hamiltonian now turns into the (symmetrized) product of angular velocity and torque acting on the rotor. This leads to a classically inspired, intrinsic work rate definition,

$$\dot{W}_{int}(t) = -\text{tr} \left\{ \rho(t) \frac{\{\hat{L}, \partial_{\phi} \hat{H}_{int}(\hat{\phi})\}}{2I} \right\}. \quad (9.11)$$

It describes the rate of change in kinetic energy of the rotor caused solely by the interaction Hamiltonian, i.e. the force exerted by the working medium. The overall rate of change in kinetic energy is given by [2]

$$\dot{W}_{kin}(t) = \dot{W}_{int}(t) + \dot{Q}_{BA}(t). \quad (9.12)$$

For backaction-free engine designs, these two powers are equivalent, which matches a classical setting. However, as  $\langle \hat{L}^2 \rangle$  does not encode any directionality, such a gain could also be obtained from pure heating of the rotor, and it is in general not a reliable measure for the production of useful work.

Heuristically, we can alleviate this problem if we measure the kinetic energy associated only to the net directed motion,  $W_{\text{net}}(t) = \langle \hat{L} \rangle^2 / 2I$ , and its time derivative<sup>2</sup>

$$\dot{W}_{\text{net}}(t) = \frac{d}{dt} \frac{\langle \hat{L} \rangle^2}{2I} = -\text{tr} \left\{ \rho(t) \frac{\hat{L}}{I} \right\} \text{tr} \left\{ \rho(t) \partial_\varphi \hat{H}_{\text{int}}(\hat{\varphi}) \right\}. \quad (9.13)$$

This will always be smaller than the gain in kinetic energy, but it may exceed the intrinsic estimate (9.11) in the presence of backaction, as we shall see later in Fig. 9.4.

Alternatively, we can employ a formal upper bound on the amount of work that an external agent could ideally obtain from the engine motion at a given point in time, *ergotropy* [30, 31]. In this case, an agent accessing the kinetic energy stored in the engine rotor could extract at most

$$W_{\text{erg}}(t) = \max_{\hat{U}} \text{tr} \left\{ \frac{\hat{L}^2}{2I} \left[ \rho_r(t) - \hat{U} \rho_r(t) \hat{U}^\dagger \right] \right\}, \quad (9.14)$$

by means of a unitary that brings the reduced rotor state  $\rho_r(t)$  to a *passive* state.<sup>3</sup> Obviously, we can only speak of work *output* from the qubit-rotor system given an actual physical interface or load through which energy is extracted from the engine to perform a task. Hence,  $W_{\text{erg}}$  here describes an axiomatic theoretical upper bound on the extractable work at a given point in time, rather than a real-time work extraction process. For that, we refer the reader to Sect. 9.2.2.3, where we add a dissipative load to “put the wheels on the ground”.

### 9.2.2.2 Autonomous Single-Qubit Piston Engine

We will now revisit the single-qubit piston engine of Sect. 9.2.1.2 in this autonomous framework. Once again, the simulations are performed on QuTiP, with the rotor Hilbert space truncated to angular momentum eigenstates  $|\ell\rangle$  with quantum numbers  $-60 \leq \ell \leq 200$ . The simulated dynamics are well within this window. We initialize the engine at its ground state  $\rho(0) = |g\rangle\langle g| \otimes |\ell=0\rangle\langle\ell=0|$  such that  $\langle \hat{L} \rangle = \langle \hat{L}^2 \rangle = 0$ , i.e. there is no kinetic energy to start with. A different, localized initial state will be considered in Sect. 9.3 when we compare the engine to its classical counterpart. The

<sup>2</sup>We assume that the hot and cold dissipators do not themselves contribute to a net boost of angular momentum through their angular dependence. In the present case of thermal dissipators (9.10), this is ensured for real-valued modulation functions  $f_{\text{h.c.}}$ .

<sup>3</sup>A passive state is a state whose energy content cannot be reduced further by means of another unitary. This implies that this state must be diagonal in the energy eigenbasis and its eigenvalues must decrease with growing energy.

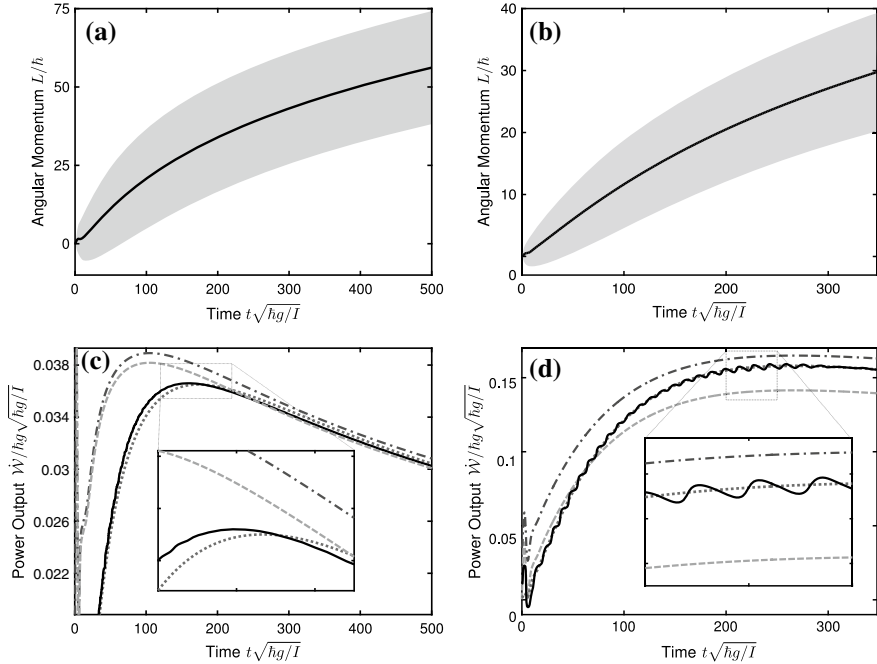
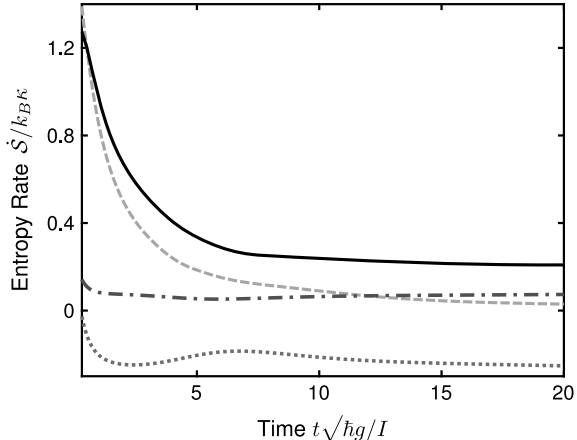


**Fig. 9.4** Simulation of the engine dynamics for different coupling strengths,  $g = 10\kappa$  in panels **(a)** and **(c)** and  $g = \kappa$  in **(b)** and **(d)**. Panels **a** and **b** depict the time evolution of angular momentum (solid), with the shaded region covering two standard deviations. Panels **c** and **d** compare the different power output definitions: rate of change in ergotropy (solid), kinetic energy (dash-dotted) and net kinetic energy (dotted) with the power associated to the intrinsic torque (dashed). The bath temperatures are  $(\bar{n}_h, \bar{n}_c) = (1, 0.1)$  and we set  $I\kappa = 10\hbar$ .

transient behavior of an autonomous engine typically depends on the initial state, and we do observe differences at short times, while the subsequent long-time trend of angular momentum gain is the same. In fact, the particular angle-dependent bath coupling ensures the rotor will eventually spin clockwise, regardless of its initial configuration.

Figures 9.4a, b compare the time evolution of angular momentum for different coupling strengths (a)  $g = 10\kappa$  and (b)  $g = \kappa$ , with  $(\bar{n}_h, \bar{n}_c) = (1, 0.1)$  and  $I\kappa = 10\hbar$ . One could show that in the regime where  $\langle \hat{L} \rangle / I \ll \kappa$ , i.e. when the rotor is just accelerating, there is a linear gain both in the mean angular momentum  $\langle \hat{L} \rangle$  of the rotor (solid line) as well as in its variance (standard deviation shaded) [1]. This means that the initial signal-to-noise ratio (the ratio between the mean and the standard deviation) increases linearly with  $\sqrt{t}$ . Once the rotor gets into the regime  $\langle \hat{L} \rangle / I \sim \kappa$ , the acceleration becomes smaller since the qubit could no longer thermalize effectively in this limit, which is similar to having a high driving frequency where  $\omega \sim \kappa$  for the externally-driven engine in Sect. 9.2.1.2. In the plots, this happens at  $\langle \hat{L} \rangle \approx 20\hbar$  where the gain is no longer linear.

**Fig. 9.5** Rate of entropy change for the same parameter settings as Figure 9.4. The net entropy production rate (solid) is obtained by subtracting the entropy rates from the cold (dotted) and hot (dash-dotted) baths from the rate of change in von Neumann entropy of the engine state (dashed).



Figures 9.4c, d compare the work production rates for the engine motion in (a) and (b) according to the different definitions introduced in Sect. 9.2.2.1. We attribute the points of maximum powers to the critical cycle duration that is determined by the finite reaction time, reached when  $\langle \hat{L} \rangle / I \sim \kappa$ . Here, the heating due to backaction  $\dot{Q}_{BA}$ , given by the offset between  $\dot{W}_{kin}$  (dash-dotted) and  $\dot{W}_{int}$  (dashed), is greater when  $g = \kappa$  (d) as compared to  $g = 10\kappa$  (c). This is apparent from (9.10) since  $\dot{W}_{int}$  scales linearly with  $g$  while  $\dot{Q}_{BA}$  scales linearly with  $\kappa$ .

The solid line depicts the time derivative of ergotropy  $\dot{W}_{erg}$  and is best matched by the rate of change in net kinetic energy  $\dot{W}_{net}$  (dotted) in both plots, vindicating the intuition derived from using a rotor. For the case of  $g = \kappa$  (d),  $\dot{W}_{erg}$  exhibits an oscillatory pattern around  $\dot{W}_{net}$ . The two curves meet when the mean angular momentum  $\langle \hat{L} \rangle$  assumes an integer multiple of  $\hbar$ : this is the consequence of momentum quantization and represents the only genuine quantum signature in the otherwise incoherent rotor dynamics [2].

Leaving the ambiguity of intrinsic work notions aside, the use of *composite* open quantum systems as autonomous engine models also raises the question of thermodynamic consistency. Specifically, the second law may or may not hold, depending on whether and how the master equation describes thermalization of the engine system with each of the reservoirs [18, 26] (see also Chap. 2). Here, as a consistency check, we show the relevant entropy rates for  $g = 10\kappa$  in Fig. 9.5. The net entropy production rate (solid) is obtained by subtracting the contributions due to the cold (dotted) and hot (dash-dotted) baths, given by  $\dot{S}_j = Q_j/k_B T_j$ , from the time derivative of the von Neumann entropy  $S_{sys} = -\text{tr}(\rho \ln \rho)$  of the engine state (dashed). In this case, we see that the net entropy production would always remain positive as it decays to a steady value of approximately  $0.21k_B\kappa$ .

### 9.2.2.3 Work Extraction by a Dissipative Load

So far, we discussed the transient work output under autonomous operation and illustrated that the kinetic energy associated to the net directed motion of the rotor follows closely with the maximum amount of work that can be extracted (ergotropy). However, we see also the drop in transient powers once the rotor gets into a critical regime  $\langle \hat{L} \rangle / I \sim \kappa$ . Hence, in most practical scenarios, work extraction would instead take place real-time via the attachment of an external load such that the engine operates at a steady state. Here, we introduce a dissipative load by means of an additional Lindblad term  $\mathcal{L}_r$  to the master equation (9.9)

$$\mathcal{L}_r \rho = \frac{2k_B T_r I \gamma}{\hbar^2} \left( \mathcal{D} \left[ \cos \hat{\phi} - \frac{i\hbar \sin \hat{\phi} \hat{L}}{4k_B T_r I} \right] \rho + \mathcal{D} \left[ \sin \hat{\phi} + \frac{i\hbar \cos \hat{\phi} \hat{L}}{4k_B T_r I} \right] \rho \right), \quad (9.15)$$

which describes angular momentum decay at a rate  $\gamma$  and effective thermalisation to a Gibbs-like state at temperature  $T_r$  [32]. This is analogous to the Caldeira–Leggett model of linear Brownian motion [33, 34], except that it consists of *two* dissipators expressed in terms of trigonometric functions to maintain  $\hat{\phi}$ -periodicity and rotor symmetry.

At steady-state operation, the output power  $\dot{W}_{\text{load}}$  is given by the energy that flows into the load per unit time,

$$\dot{W}_{\text{load}} = -\text{tr} \left\{ \left[ \frac{\hat{L}^2}{2I} + \hat{H}_{\text{int}}(\hat{\phi}) \right] \mathcal{L}_r \rho \right\} \approx \dot{W}_{\text{int}} + \dot{Q}_{\text{BA}}, \quad (9.16)$$

and we expect that this balances the net heat flow from the thermal baths. Figure 9.6 shows the steady-state  $\dot{W}_{\text{int}}$  (solid) and  $\dot{W}_{\text{load}}$  (dotted) for different coupling strengths  $g$  where (a)  $g = 10\kappa$  and (b)  $g = \kappa$ , with the same parameter settings as Fig. 9.4. We see that the maximum steady-state power to the load (dotted) exceeds the maximum for the ergotropy rate without load (dashed line). This is because in contrast with ergotropy, a dissipative load would not be able to distinguish between the energy associated to useful directed motion and passive energy, and it can extract both. Notice also that the two output powers deviate more for small coupling  $g$  (b) as a result of a greater heating due to backaction, seen also in the transient case (Fig. 9.4). In the limit where  $\gamma \rightarrow \infty$ ,  $\dot{W}_{\text{int}}$  decays to zero, that is the rotor is eventually stopped by the large dissipation rate. In the same limit,  $\dot{W}_{\text{load}} > 0$  as a result of backaction-induced momentum diffusion due to continuous exchange of excitations between the baths and the working medium, which enters the rotor via the coupling functions  $f(\phi)$ .

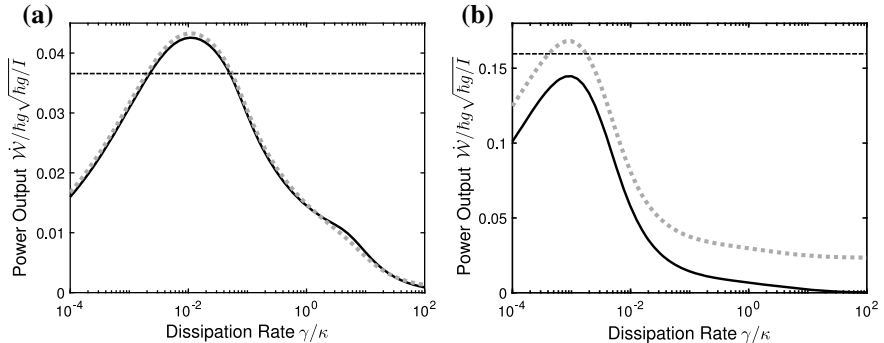


**Fig. 9.6** Steady-state power associated to the intrinsic torque  $\dot{W}_{int}$  (solid) and output power to load  $\dot{W}_{load}$  (dotted) as a function of the dissipation rate  $\gamma$  for the same parameters as Figure 9.4, with **a**  $g = 10\kappa$  and **b**  $g = \kappa$ . The horizontal dashed lines mark the greatest ergotropy rate as depicted in Figure 9.4. Here, we set  $k_B T_r = 10\hbar^2/I$ .

### 9.3 Classical Versus Quantum

Having introduced the model of the engine, we can go back to the main motivation stated in the introduction: look for genuine quantum features that may either enhance or deteriorate the performance of thermal machines, compared to a classical implementation.

One systematic approach to this problem, which is discussed in detail in Chap. 4, is to identify the effects of quantum coherence in a given quantum system by comparing it to an incoherent stochastic process with equivalent energy balance. This approach is at risk of wiping out any notion of coherence, including the coherence between modes that is allowed in classical physics.

Here, we rather look for a classical description of the degrees of freedom and their dynamics. The two approaches are known to give different results [35]. Building such a classical analog requires some choices. For instance, in a dissipator like (9.10), one has to decide how to deal with the contribution of spontaneous emission. Here, in order to translate the single-qubit piston engine into a classical framework, we need to define a classical system that mimics a qubit. We explore two possibilities: a heuristic coin flip model where the qubit is replaced by a bit, much in the spirit of the coherent-versus-incoherent method; and a more physical spin precession model, where the qubit is turned into a classical magnetic moment.

Further, in the comparison, the initial condition of the quantum evolution of the rotor should no longer be its delocalized ground state of motion  $|\ell = 0\rangle$ , because it has no classical analogue. Instead, we employ a localized wave packet at rest for the initial rotor state, described by the periodic von Mises wavefunction [36]

$$\langle \varphi | \psi \rangle = \frac{e^{\cos(\varphi - \mu)/2\sigma_\varphi^2}}{\sqrt{2\pi I_0(\sigma_\varphi^{-2})}}, \quad (9.17)$$

with  $I_0(\sigma_\varphi^{-2})$  a modified Bessel function. This choice approximates a Gaussian wave packet on the circle, localized at rotor position  $\mu_\varphi$  with standard deviation  $\sigma_\varphi$  in the limit where  $\sigma_\varphi \ll 1$ . It follows that the momentum distribution is also approximately Gaussian with standard deviation satisfying  $\sigma_\ell^2 \sigma_\varphi^2 = 1/2$ . In classical simulations, where the angle can always be unwrapped to an unbounded coordinate, we can emulate this quantum state easily by considering Gaussian distributions for both the rotor's position and momentum. In all subsequent comparisons, we consider an initial rotor state defined by  $(\mu_\varphi, \sigma_\varphi^2) = (\pi/2, 0.1)$  and  $(\mu_\ell, \sigma_\ell^2) = (0, 10)$ .

### 9.3.1 Coin Model

Heuristically, we can recast the autonomous single-qubit engine model introduced in Sect. 9.2.2 into a classical system comprised of one bit and a rotor, driven by telegraphic noise with an angle-dependent bias. For this, we note that the quantum engine dynamics in (9.9) depends solely on whether the qubit is excited, but not on its coherence between ground and excited state. Hence, we can simply read off the angle-dependent excitation rate from the master equation and introduce discrete noise that flips a classical “coin” bit between its states 0 and 1 at the rate<sup>4</sup>

$$\dot{p}_0(\varphi) = -\dot{p}_1(\varphi) = \kappa \sum_{j=h,c} f_j^2(\varphi) [(\bar{n}_j + 1)p_1(\varphi) - \bar{n}_j p_0(\varphi)]. \quad (9.18)$$

When excited, the coin shall exert a torque on the classical rotor, which can be represented by a set of stochastic differential equations for the coin state  $C_t \in \{0, 1\}$  and the rotor variables,

$$\begin{aligned} dC_t &= [1 - C_t]dN_0 - C_t dN_1, \\ d\varphi_t &= \frac{L_t}{I} dt, \quad dL_t = \hbar g C_t \sin \varphi_t dt. \end{aligned} \quad (9.19)$$

The  $dN_{0,1} \in \{0, 1\}$  are two independent random increments with expectation values

$$E[dN_m]_t = \kappa [(\bar{n}_h + m)f_h^2(\varphi_t) + (\bar{n}_c + m)f_c^2(\varphi_t)] dt. \quad (9.20)$$

We remark that the flipping noise in the coin model is simply a one-to-one translation of the quantum noise using the same parameters, i.e. it is not derived from a physical model of energy exchange with a classical thermal bath. This highlights the possibility of using alternative entropy sources apart from standard thermal baths to drive quantum or classical engines.

Figure 9.7 compares the engine dynamics for different coupling strengths  $g$ , similar to the settings used in Fig. 9.6 where (a)  $g = 10\kappa$  and (b)  $g = \kappa$ . For both param-

---

<sup>4</sup>Notice that we choose to keep the contribution of spontaneous emission.

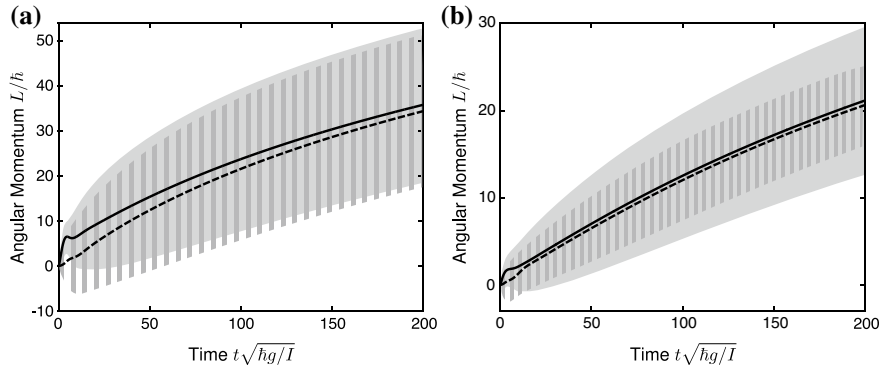


**Fig. 9.7** Comparison between engine dynamics of quantum (solid) and classical coin flip model (dashed), obtained from averaging over  $3.2 \times 10^7$  trajectories. The lines represent the mean angular momentum while the shaded regions cover two standard deviations.

eter settings, the coin flip model (dashed) predicts similar average behavior but the difference in terms of momentum noise is apparent for small  $g$ . This is because contrary to the quantum case, the coin model is backaction-free, i.e. the noise input that flips the coin does not affect the increment of the angular momentum variable. On the other hand, the Lindblad dissipators (9.10) in the quantum model describe momentum diffusion or, complementarily, *decoherence* in the angle representation and we see earlier from Fig. 9.6 that backaction noise is more prominent for small  $g$ .

### 9.3.2 Magnetic Moment Model

We have shown that the coin flip model, while reproducing the average behavior of the quantum engine, is unable to capture the effects of backaction noise. To include this aspect of the quantum dynamics in a classical setting, we consider a physical model describing a precessing magnetic moment [37], which now replaces the qubit as the working medium.

In this case, a classical magnetic moment vector  $\mu_0\mathbf{m}$  precesses about an external magnetic field  $\mathbf{B} = B_{\text{ext}}\hat{\mathbf{z}}$ , where  $\mathbf{m} = m_x\hat{\mathbf{x}} + m_y\hat{\mathbf{y}} + m_z\hat{\mathbf{z}}$  can be interpreted as the analogue of a quantum spin vector. The free Hamiltonian of the working medium is then given by  $H_s = \hbar\omega_0 m_z$ , where  $\omega_0 = \mu_0 B_{\text{ext}}/\hbar$ . The interaction between the rotor and the spin is determined by the magnitude of magnetic moment along  $+\hat{\mathbf{z}}$ , and is described by  $H_{\text{int}} = \hbar g(m + m_z)\cos\varphi$ . This system is then coupled linearly to a set of classical harmonic oscillators that serves as the thermal baths via the coupling functions  $f_j(\varphi)$  introduced earlier. The Langevin equations governing the dynamics of the engine are given by

$$\begin{aligned} dm_z &= -\kappa [f_h^2(\varphi) + f_c^2(\varphi)] \frac{m^2 - m_z^2}{m} dt - 2\kappa [\varepsilon_h f_h^2(\varphi) + \varepsilon_c f_c^2(\varphi)] \frac{m_z}{m} dt \\ &\quad + \sqrt{2\kappa (\varepsilon_h f_h^2(\varphi) + \varepsilon_c f_c^2(\varphi)) \frac{m^2 - m_z^2}{m}} dW_1, \\ dL &= \hbar g(m + m_z) \sin \varphi dt + \hbar \sqrt{2\kappa (\varepsilon_h f_h'^2(\varphi) + \varepsilon_c f_c'^2(\varphi)) \frac{m^2 - m_z^2}{m}} dW_2 \quad (9.21) \end{aligned}$$

where  $dW_{1,2}$  denote two independent real-valued Wiener increments of variance  $dt$ .

Note that backaction enters this model in the noise term present in the equation of motion for the angular momentum. For a physical comparison between the two models, we assume the same bath temperatures, where the classical excitation numbers are now determined by  $\varepsilon_{h,c} = k_B T_{h,c}/\hbar\omega_0$ . We also set the magnitude of the spin vector to  $m = 1/2$ .

Similar to previous settings, Fig. 9.8 compares the quantum and classical engine dynamics at two different coupling strengths. As expected, the classical spin model (dashed) predicts greater momentum noise as a result of the backaction term, which is now comparable to the quantum prediction (solid) both in the case of large (a) and small (b) coupling strengths. However, the average behavior differs significantly, which we attribute to the different thermal statistics. When considering a spin-1/2 of frequency  $\omega_0$  coupled to a bath of temperature  $T$ , we get

$$\langle m_z \rangle = \frac{k_B T}{\hbar\omega_0} - \frac{1}{2} \coth \left( \frac{\hbar\omega_0}{2k_B T} \right), \quad \langle \hat{\sigma}_z \rangle = -\frac{1}{2} \tanh \left( \frac{\hbar\omega_0}{2k_B T} \right), \quad (9.22)$$

since the classical spin assumes a continuous  $m_z$  value ranging from  $[-1/2, 1/2]$  while the quantum one only takes discrete values  $\pm 1/2$ . In principle, one could align the average behaviors by matching the mean spin values, but that would imply different bath temperatures for the quantum and the classical case.

## 9.4 Conclusion

Drawing analogy from classical engines capable of generating directed motion, we introduced the use of rotors in quantum engines. We first started off with a textbook example of a driven engine cycle, and demonstrated how the use of a rotor facilitates the mapping of the time-dependence  $\omega t$  to an autonomous setting characterized by  $(I, \dot{\phi})$  and see explicitly the role of the rotor as an internal clock that sets the engine cycle as well as a work storage. In particular, there is an intuitive notion of the *useful* work stored, in that the energy associated to the net motion actually matches the axiomatic maximum work extraction (ergotropy). We then looked at real-time work extraction by subjecting the rotor to an external dissipative load, and showed that the steady-state power can exceed the maximum ergotropy rate in the transient operation.

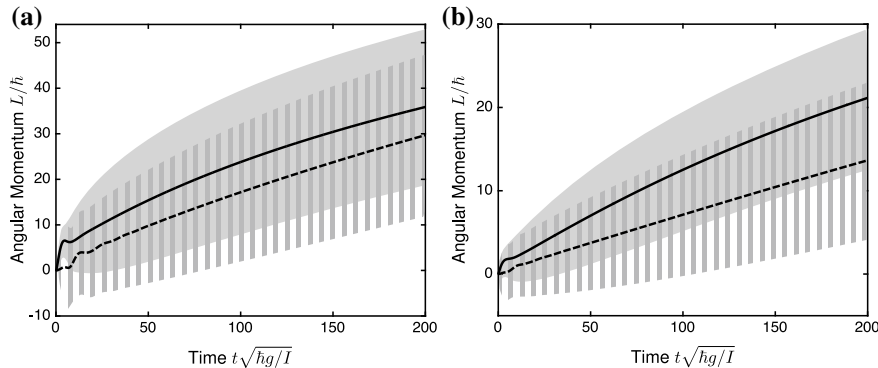


**Fig. 9.8** Comparison between engine dynamics of quantum (solid) and classical magnetic moment model (dashed), obtained from averaging over  $3.2 \times 10^7$  trajectories. The lines represent the mean angular momentum while the shaded regions cover two standard deviations.

Finally, we compared the dynamics of the engine in entirely classical frameworks. If the qubit is replaced with a coin-flip model driven by telegraphic noise, the predicted dynamics is less noisy because it does not incorporate backaction. If the qubit is replaced by a classical magnetic moment driven by linearly coupled harmonic oscillators, the average behavior is somewhat worse for a given choice of the temperatures of the baths. While these differences, at first glance, may point to quantum effects (a detrimental one in the first case and an advantageous one in the second), the general behaviors are similar to the quantum one: in particular, we do not find any evidence of “quantum supremacy”. However, rotor-based engines with classical counterparts provide a testbed for future studies of genuine quantum effects in quantum heat engines.

**Acknowledgements** This research is supported by the Singapore Ministry of Education through the Academic Research Fund Tier 3 (Grant No. MOE2012-T3-1-009); and by the same MoE and the National Research Foundation, Prime Minister’s Office, Singapore, under the Research Centres of Excellence programme. In addition, this work was financially supported by the Swiss SNF and the NCCR Quantum Science and Technology.

## References

1. A. Roulet, S. Nimmrichter, J.M. Arrazola, S. Seah, V. Scarani, Phys. Rev. E **95**, 062131 (2017). <https://doi.org/10.1103/PhysRevE.95.062131>
2. S. Seah, S. Nimmrichter, V. Scarani, New J. Phys. **20**(4), 043045 (2018). <https://doi.org/10.1088/1367-2630/aab704>
3. A. Roulet, S. Nimmrichter, J.M. Taylor, Quantum Sci. Technol. **3**, 035008 (2018). <https://doi.org/10.1088/2058-9565/aac40d>
4. F. Tonner, G. Mahler, Phys. Rev. E **72**, 066118 (2005). <https://doi.org/10.1103/PhysRevE.72.066118>

5. M. Youssef, G. Mahler, A.S. Obada, Phys. E **42**(3), 454 (2010). <https://doi.org/10.1016/j.physe.2009.06.032>
6. N. Brunner, N. Linden, S. Popescu, P. Skrzypczyk, Phys. Rev. E **85**, 051117 (2012). <https://doi.org/10.1103/PhysRevE.85.051117>
7. L. Gilz, E.P. Thesing, J.R. Anglin (2013), arXiv:1304.3222
8. A. Mari, A. Farace, V. Giovannetti, J. Phys. B **48**(17), 175501 (2015). <https://doi.org/10.1088/0953-4075/48/17/175501>
9. A. Levy, L. Diósi, R. Kosloff, Phys. Rev. A **93**, 052119 (2016). <https://doi.org/10.1103/PhysRevA.93.052119>
10. A.U.C. Hardal, N. Aslan, C.M. Wilson, Ö.E. Müstecaplıoğlu, Phys. Rev. E **96**, 062120 (2017). <https://doi.org/10.1103/PhysRevE.96.062120>
11. R. Alicki, D. Gelbwaser-Klimovsky, A. Jenkins, Ann. Phys. **378**, 71 (2017). <https://doi.org/10.1016/j.aop.2017.01.003>
12. R. Kosloff, J. Chem. Phys. **80**(4), 1625 (1984). <https://doi.org/10.1063/1.446862>
13. M.O. Scully, M.S. Zubairy, G.S. Agarwal, H. Walther, Science **299**(5608), 862 (2003). <https://doi.org/10.1126/science.1078955>
14. Y. Rezek, R. Kosloff, New J. Phys. **8**(5), 83 (2006). <https://doi.org/10.1088/1367-2630/8/5/083>
15. R. Alicki, Open Syst. Inf. Dyn. **21**(01n02), 1440002 (2014). <https://doi.org/10.1142/S1230161214400022>
16. K. Zhang, F. Bariani, P. Meystre, Phys. Rev. Lett. **112**, 150602 (2014). <https://doi.org/10.1103/PhysRevLett.112.150602>
17. R. Uzdin, A. Levy, R. Kosloff, Entropy **18**(4) (2016). <https://doi.org/10.3390/e18040124>
18. R. Alicki, J. Phys. A Math. Gen. **12**(5), L103 (1979). <https://doi.org/10.1088/0305-4470/12/5/007>
19. X.L. Huang, T. Wang, X.X. Yi, Phys. Rev. E **86**, 051105 (2012). <https://doi.org/10.1103/PhysRevE.86.051105>
20. O. Abah, E. Lutz, EPL (Europhys. Lett.) **106**(2), 20001 (2014). <https://doi.org/10.1209/0295-5075/106/20001>
21. J. Roßnagel, O. Abah, F. Schmidt-Kaler, K. Singer, E. Lutz, Phys. Rev. Lett. **112**, 030602 (2014). <https://doi.org/10.1103/PhysRevLett.112.030602>
22. W. Niedenzu, D. Gelbwaser-Klimovsky, A.G. Kofman, G. Kurizki, New J. Phys. **18**(8), 083012 (2016). <https://doi.org/10.1088/1367-2630/18/8/083012>
23. J. Klaers, S. Faelt, A. Imamoglu, E. Togan, Phys. Rev. X **7**, 031044 (2017). <https://doi.org/10.1103/PhysRevX.7.031044>
24. R. Wulfert, M. Oechsle, T. Speck, U. Seifert, Phys. Rev. E **95**, 050103 (2017). <https://doi.org/10.1103/PhysRevE.95.050103>
25. A. Rivas, A.D.K. Plato, S.F. Huelga, M.B. Plenio, New J. Phys. **12**(11), 113032 (2010). <https://doi.org/10.1088/1367-2630/12/11/113032>
26. A. Levy, R. Kosloff, Europhys. Lett. **107**(2), 20004 (2014). <https://doi.org/10.1209/0295-5075/107/20004>
27. P.P. Hofer, M. Perarnau-Llobet, L.D.M. Miranda, G. Haack, R. Silva, J.B. Brask, N. Brunner, New J. Phys. **19**, 123037 (2017). <https://doi.org/10.1088/1367-2630/aa964f>
28. J.O. González, L.A. Correa, G. Nocerino, J.P. Palao, D. Alonso, G. Adesso, Open Syst. Inf. Dyn. **24**, 1740010 (2017). <https://doi.org/10.1142/S1230161217400108>
29. J. Johansson, P. Nation, F. Nori, Comput. Phys. Commun. **184**(4), 1234 (2013). <https://doi.org/10.1016/j.cpc.2012.11.019>
30. A.E. Allahverdyan, R. Balian, T.M. Nieuwenhuizen, Europhys. Lett. **67**(4), 565 (2004). <https://doi.org/10.1209/epl/i2004-10101-2>
31. J. Goold, M. Huber, A. Riera, L. del Rio, P. Skrzypczyk, J. Phys. A **49**(14), 143001 (2016). <https://doi.org/10.1088/1751-8113/49/14/143001>
32. B.A. Stickler, B. Schrinski, K. Hornberger, Phys. Rev. Lett. **121**, 040401 (2018). <https://doi.org/10.1103/PhysRevLett.121.040401>

33. A. Caldeira, A. Leggett, Phys. A **121**(3), 587 (1983). [https://doi.org/10.1016/0378-4371\(83\)90013-4](https://doi.org/10.1016/0378-4371(83)90013-4)
34. H.P. Breuer, F. Petruccione, *The Theory of Open Quantum Systems* (Oxford University Press, Oxford, 2002). <https://doi.org/10.1093/acprof:oso/9780199213900.001.0001>
35. S. Nimmrichter, J. Dai, A. Roulet, V. Scarani, Quantum **1**, 37 (2017). <https://doi.org/10.22331/q-2017-12-11-37>
36. N.I. Fisher, *Statistical Analysis of Circular Data* (Cambridge University Press, Cambridge, 1995). <https://doi.org/10.1002/bimj.4710380307>
37. J.L. García-Palacios, *On the Statics and Dynamics of Magnetoanisotropic Nanoparticles* (Wiley-Blackwell, New Jersey, 2007), pp. 1–210. <https://doi.org/10.1002/9780470141717.ch1>

**Part II**

**Fluctuating Work and Irreversibility**

**in the Quantum Regime**

# Chapter 10

## Quantum Fluctuation Theorems



Ken Funo, Masahito Ueda and Takahiro Sagawa

Recent advances in experimental techniques allow one to measure and control systems at the level of single molecules and atoms. Here gaining information about fluctuating thermodynamic quantities is crucial for understanding nonequilibrium thermodynamic behavior of small systems. To achieve this aim, stochastic thermodynamics offers a theoretical framework, and nonequilibrium equalities such as the Jarzynski equality and fluctuation theorems provide key information about the fluctuating thermodynamic quantities. We review the recent progress in quantum fluctuation theorems, including the studies of Maxwell's demon which plays a pivotal role in connecting thermodynamics with information.

---

K. Funo

School of Physics, Peking University, Beijing 100871, China  
e-mail: kenfuno@pku.edu.cn

*Present address:*

K. Funo

RIKEN Cluster for Pioneering Research, 2-1 Hirosawa, Wako, Saitama 351-0198, Japan  
e-mail: ken.funo@riken.jp

M. Ueda

Department of Physics, The University of Tokyo, 7-3-1 Hongo, Bunkyo-ku,  
Tokyo 113-0033, Japan  
e-mail: ueda@cat.phys.s.u-tokyo.ac.jp

M. Ueda

RIKEN Center for Emergent Matter Science (CEMS), 2-1 Hirosawa, Wako,  
Saitama 351-0198, Japan

T. Sagawa (✉)

Department of Applied Physics, The University of Tokyo, 7-3-1 Hongo,  
Bunkyo-ku, Tokyo 113-8656, Japan  
e-mail: sagawa@ap.t.u-tokyo.ac.jp

## 10.1 Introduction

The fluctuation theorem (FT) may be regarded as a modern clue to the problem raised by Loschmidt, who posed a serious question about irreversible processes in time-reversal-symmetric dynamics [1]. In accordance with time-reversal symmetry, the entropy production can be negative albeit with an exponentially small probability [2, 3], which provides a new insight into our understanding about the arrow of time [2, 4]. The averaged entropy production is, however, always nonnegative, consistent with the second law of thermodynamics.

The FT reveals fundamental properties of the entropy production under nonequilibrium dynamics, which has opened up the field of stochastic thermodynamics [2, 3, 5, 6]. Various types of FT have been discussed in literature [7–15], and they can be obtained in a unified way by starting from the detailed FT [3]. In particular, the Jarzynski equality [9] and the Crooks FT [10] allow one to determine the equilibrium free energy through measurements of nonequilibrium work [16, 17]. Experimentally, the classical FT is relevant to classical small systems such as biomolecules, molecular motors, and colloidal particles, while its quantum counterpart is relevant to quantum devices such as NMR systems [18], trapped ions [19], and superconducting qubits [20].

In this article, we first review the quantum FT by focusing on the Jarzynski equality and the Crooks FT [21, 22]. These relations are applicable to externally driven quantum systems far from equilibrium, and are thus relevant to quantum devices with rapid external control. The quantum FT has been formulated for isolated systems described by unitary dynamics [23–26]. Further studies have been carried out, including the quantum FT for open quantum systems [27–32], monitored quantum systems [33–35], and quantum field theories [36–38]. In particular, the quantum jump method allows one to assign quantum work and heat along individual quantum trajectories, as in the case for classical Markov jump processes [31, 32]. For simplicity, in this article we only consider the case with a single heat bath, though the extension to the case with multiple heat baths is straightforward. This setup includes applications to quantum heat engines and quantum heat transport [39–42].

If we can access thermal fluctuations of the system via measurement and feedback control, we can establish the fundamental connections between the thermodynamic properties and the information-theoretic quantities. This setup is a modern incarnation of Maxwell’s demon [43, 44], opening an interdisciplinary field of information thermodynamics [45–47]. The fundamental bound on the capability of Maxwell’s demon has been revealed in the form of the generalized second law by including the information content [48, 49]. A generalized FT under measurement and feedback control has been derived in both classical [50, 51] and quantum [52–54] regimes.

This article is organized as follows. In Sect. 10.2, we review the second law and the FT in the quantum regime, for both isolated and open systems. In Sect. 10.3, we review the case of measurement and feedback control by Maxwell’s demon. In Sect. 10.4, we comment on related experimental studies. In Sect. 10.5, we make concluding remarks.

## 10.2 Second Law and Fluctuation Theorems

In this section, we utilize techniques in quantum information theory to derive the second law of thermodynamics, which sets a fundamental bound on the entropy production. We then discuss a stochastic version of the entropy production along individual quantum trajectories, and use it to derive the quantum FT. In Sects. 10.2.1 and 10.2.2, we consider a unitary time evolution of the composite system of a driven system and the heat bath. In Sect. 10.2.3, we consider Gibbs preserving maps and open quantum systems and discuss the quantum jump method to derive the quantum FT. See also Sects. 28.3 and 28.5 of Chap. 28 for the derivations of the second law in setups similar to those of Sects. 10.2.1 and 10.2.3 of this chapter.

### 10.2.1 Derivation of the Second Law of Thermodynamics

#### 10.2.1.1 Setup

We consider a system S interacting with a heat bath B at inverse temperature  $\beta$ , described by the Hamiltonian

$$H_{\text{tot}}(t) = H_S(t) + H_B + V_{SB}(t). \quad (10.1)$$

The system is assumed to be externally driven out of equilibrium with work being performed, as schematically illustrated in Fig. 10.1. We note that in our setup the external drive is represented by classical parameters through the time dependence of the Hamiltonian, while there is an alternative formulation that includes the driving system as a part of the quantum system [55, 56] (see also Sect. 26.5.2 of Chap. 26 for a potential problem of this formulation).

The initial state of the system and the bath is given by the product state

$$\rho_{SB}(0) = \rho_S(0) \otimes \rho_B^G, \quad (10.2)$$

where  $\rho_B^G = e^{-\beta H_B} / \text{Tr}[e^{-\beta H_B}]$  is assumed to be the Gibbs distribution of the bath. This is a crucial assumption in deriving the second law and the FT, because the Gibbs distribution is a special state that gives the maximum entropy for a given energy. The composite system evolves in time according to the Schrödinger equation, and the unitary time-evolution operator is given by  $U_{SB} = T \exp(-\frac{i}{\hbar} \int_0^\tau dt H_{\text{tot}}(t))$ , where T is the time-ordering operator. The final state is then given by  $\rho_{SB}(\tau) = U_{SB} \rho_{SB}(0) U_{SB}^\dagger$ . The following argument is applicable to an arbitrary time-dependent control, as long as the time evolution of the composite system SB is unitary. We also note that we do not make any assumption on the size of the bath; it is not necessary to take the thermodynamic limit in the following discussions.

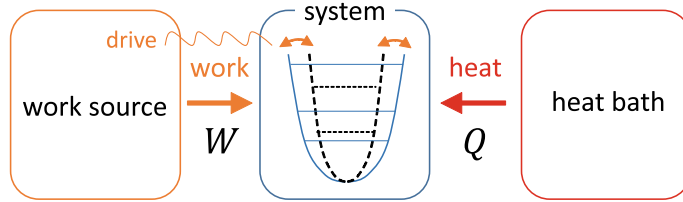


**Fig. 10.1** Setup of the quantum fluctuation theorem. The Hamiltonian of the system is modulated by an external drive, which performs work  $W$  on the system, and the system absorbs heat  $Q$  from the heat bath.

### 10.2.1.2 Second Law and Relative Entropy

We next discuss the derivation of the second law, which is shown to be fundamentally related to the non-negativity of the quantum relative entropy. First of all, the total entropy production is defined as

$$\Sigma := \Delta S - \beta Q, \quad (10.3)$$

which is a key quantity for quantifying irreversibility in nonequilibrium processes. Here,  $\Delta S := S(\rho_S(\tau)) - S(\rho_S(0))$  is the change in the von Neumann entropy  $S(\rho) := -\text{Tr}[\rho \ln \rho]$  of the system, and

$$Q := \text{Tr}[H_B \rho_B^G] - \text{Tr}[H_B \rho_B(\tau)] \quad (10.4)$$

is the heat absorbed by the system. Since  $-\beta Q$  is interpreted as the entropy change in the bath [57], Eq. (10.3) quantifies the total entropy produced in the composite system SB during nonequilibrium dynamics.

By using the unitary invariance of the von Neumann entropy, we can relate the total entropy production  $\Sigma$  to the quantum relative entropy  $S(\rho || \sigma) := \text{Tr}[\rho \ln \rho] - \text{Tr}[\rho \ln \sigma]$  [58] as

$$\Sigma = S(\rho_{SB}(\tau) || \rho_S(\tau) \otimes \rho_B^G). \quad (10.5)$$

The right-hand side is the relative entropy between the final state  $\rho_{SB}(\tau)$  of the composite system SB and a reference state  $\rho_S(\tau) \otimes \rho_B^G$  where only the bath state is replaced by a new Gibbs state, which implies that entropy production is related to the relaxation of the bath. The second law can now be obtained as a direct consequence of the nonnegativity of the quantum relative entropy [21, 46]:

$$\Sigma = \Delta S - \beta Q \geq 0. \quad (10.6)$$

Here, the equality is achieved if and only if  $\rho_{SB}(\tau) = \rho_S(\tau) \otimes \rho_B^G$ . The second law (10.6) takes the same form as the conventional Clausius inequality, while it is applicable to arbitrary nonequilibrium initial and final states and includes the von

Neumann entropy, instead of the Boltzmann entropy that is defined only for equilibrium states. Inequality (10.6) may also be regarded as a generalized Landauer principle as will be discussed in Sect. 10.2.1.3. If we have multiple heat baths,  $\beta Q$  in (10.6) should be replaced by  $\sum_i \beta_i Q_i$ , where  $\beta_i$  is the inverse temperature of the  $i$ -th bath and  $Q_i$  is the heat transfer from the  $i$ -th bath to the system.

We next define the work performed on the system through the first law of thermodynamics:

$$W := \Delta E - Q, \quad (10.7)$$

where  $\Delta E := \text{Tr}[H_S(\tau)\rho_S(\tau)] - \text{Tr}[H_S(0)\rho_S(0)]$  is the energy change of the system. Here, we assume that either (i) a weak coupling between the system and the bath or (ii)  $V_{\text{SB}}(0) = V_{\text{SB}}(\tau) = 0$ , so that the change in the interaction energy is negligible. In Eq. (10.7),  $W$  quantifies the energy that is injected into the composite system through the time-dependent Hamiltonian of the system via an external control. We note that in the strong-coupling regime the definition of the work is given by the energy difference of the composite system including the interaction energy [30, 59], and that an extension of (classical) stochastic thermodynamics has been studied in Refs. [60–62].

Now let us relate the entropy production to the work, and derive a bound on the work. For that purpose, we introduce the nonequilibrium free energy  $\mathcal{F}_S(t)$  of the system, which is motivated by the thermodynamic relation  $F = E - TS$  in macroscopic thermodynamics [63, 64]:

$$\mathcal{F}_S(t) := \text{Tr}[H_S(t)\rho_S(t)] - \beta^{-1} S(\rho_S(t)). \quad (10.8)$$

This reduces to the equilibrium free energy  $F_S^{\text{eq}}(t) := -\beta^{-1} \ln \text{Tr}[e^{-\beta H_S(t)}]$  if  $\rho_S(t) = \rho_S^G(t)$ , where  $\rho_S^G(t) := e^{-\beta(H_S(t) - F_S^{\text{eq}}(t))}$  is the Gibbs distribution of the system at time  $t$ . In general, (10.8) is bounded from below as

$$\mathcal{F}_S(t) = \beta^{-1} S(\rho_S(t) || \rho_S^G(t)) + F_S^{\text{eq}}(t) \geq F_S^{\text{eq}}(t). \quad (10.9)$$

From (10.9), we see that  $\mathcal{F}_S(t)$  quantifies the (asymmetric) distance between  $\rho_S(t)$  and  $\rho_S^G(t)$ . Using the nonequilibrium free-energy difference  $\Delta\mathcal{F}_S := \mathcal{F}_S(\tau) - \mathcal{F}_S(0)$ , the total entropy production is related to the work as

$$\Sigma = \beta W - \beta \Delta\mathcal{F}_S \geq 0. \quad (10.10)$$

Therefore, the second law (10.10) gives the fundamental lower bound on the work for arbitrary initial and final states of the system.

If the initial distribution is the Gibbs distribution, i.e.,  $\rho_S(0) = \rho_S^G(0)$ , inequality (10.10) reproduces the conventional second law of thermodynamics:

$$W - \Delta F_S^{\text{eq}} \geq 0, \quad (10.11)$$

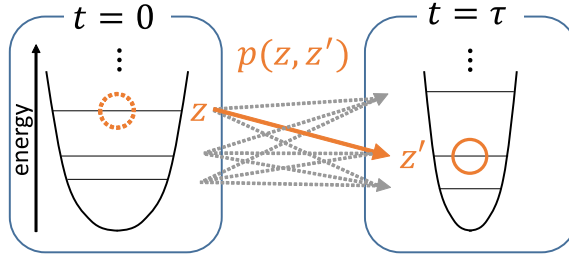


**Fig. 10.2** Energy levels of the system in the initial state (left) and the final state (right). The quantum Jarzynski equality (10.25) assumes projective measurements at  $t = 0$  and  $t = \tau$  to specify the initial and final energies. The stochastic entropy production (10.13) is associated with an individual transition  $z \rightarrow z'$ , where  $p(z, z')$  denotes the joint probability distribution.

by noting that  $F_S^{\text{eq}}(0) = \mathcal{F}_S(0)$ ,  $-F_S^{\text{eq}}(\tau) \geq -\mathcal{F}_S(\tau)$ , and  $\Delta F_S^{\text{eq}} := F_S^{\text{eq}}(\tau) - F_S^{\text{eq}}(0)$ . We remark that inequality (10.10) is tighter than (10.11), because (10.11) is valid for any final state, but (10.10) has an explicit dependence on the final state  $\rho_S(\tau)$ .

### 10.2.1.3 Landauer Principle

The Landauer principle [65–68] gives the fundamental lower bound on the heat emission during the erasure of information. The second law (10.6) is regarded as a general form of the Landauer principle, if we rewrite it as

$$-Q \geq -k_B T \Delta S, \quad (10.12)$$

where the left-hand side represents the heat emission to the bath, and  $-\Delta S$  represents the amount of the erased information. As a simple example, we consider a qubit system and a state transformation from the maximally mixed state  $\rho_S(0) = \frac{1}{2}(|0\rangle\langle 0| + |1\rangle\langle 1|)$  to a pure state  $\rho_S(\tau) = |0\rangle\langle 0|$ . Then, the von Neumann entropy of the system changes from  $\ln 2$  to 0, which is interpreted to be the erasure of one bit of information. From (10.12), we find that at least  $|Q| = k_B T \ln 2$  of heat should be emitted to the bath, which is nothing but the original Landauer bound [65].

## 10.2.2 Quantum Fluctuation Theorems

### 10.2.2.1 Stochastic Thermodynamic Quantities

The basic setup of quantum fluctuation theorems is the same as that discussed in Sect. 10.2.1.1. In addition, we introduce the two-point measurement scheme for the composite system SB and define the stochastic entropy production for individual trajectories of transitions (see also Fig. 10.2).

The two-point measurement scheme is implemented by two projective measurements at  $t = 0$  and  $t = \tau$  with the bases  $\{|\psi_S(x)\rangle \otimes |E_B(y)\rangle\}$  and  $\{|\psi'_S(x')\rangle \otimes |E_B(y')\rangle\}$ , respectively. Here,  $\{|E_B(y)\rangle\}$  is the energy eigenbasis of  $H_B$ , and  $\{|\psi_S(x)\rangle\}$  is the eigenbasis that diagonalizes the initial density operator of S:  $\rho_S(0) = \sum_x p_S(x) |\psi_S(x)\rangle \langle \psi_S(x)|$ . Similarly,  $\{|\psi'_S(x')\rangle\}$  diagonalizes  $\rho_S(\tau)$  such that  $\rho_S(\tau) = \sum_{x'} p'_S(x') |\psi'_S(x')\rangle \langle \psi'_S(x')|$ . Then, the initial measurement gives the stochastic entropy  $-\ln p_S(x)$  of S and the energy  $E_B(y)$  of B. The final measurement gives the same quantities at  $t = \tau$ . We then define the stochastic entropy production associated with the transition from  $z := \{x, y\}$  to  $z' := \{x', y'\}$  as [26, 46]

$$\sigma(z, z') := \ln p_S(x) - \ln p'_S(x') - \beta (E_B(y) - E_B(y')), \quad (10.13)$$

where the first two terms represent the stochastic entropy change of the system and the last two terms give the stochastic heat.

The joint probability of the measurement outcomes  $z$  and  $z'$  being observed is given by

$$p(z, z') = p(z' \leftarrow z) p_S(x) p_B^G(y), \quad (10.14)$$

where  $p(z' \leftarrow z) := |\langle \psi'_S(x') | \otimes \langle E_B(y') | U_{SB} | \psi_S(x) \rangle \otimes |E_B(y)\rangle|^2$  is the transition probability from  $z$  to  $z'$ , and  $p_B^G(y) = e^{-\beta E_B(y)} / Z_B$  is the Gibbs distribution of the bath. By taking the average of  $\sigma(z, z')$  with  $p(z, z')$ , we reproduce the total entropy production defined in (10.3):  $\Sigma = \sum_{z, z'} p(z, z') \sigma(z, z')$ . In addition, the probability density that  $\sigma(z, z')$  takes a particular value  $\sigma$  is given by

$$P(\sigma) = \sum_{z, z'} \delta(\sigma - \sigma(z, z')) p(z, z'), \quad (10.15)$$

where  $\delta(\cdot)$  is the delta function.

### 10.2.2.2 Quantum Fluctuation Theorem

We now discuss the notion of time-reversal symmetry, which directly leads to the quantum FT. We first introduce the backward (time-reversed) protocol and the corresponding backward probability distribution  $\tilde{p}(z, z')$  as follows:

1. We start from a state labeled by  $z' = \{x', y'\}$  with a given probability  $p'_S(x') \rho_B^G(y')$ .
2. The time evolution of the backward protocol is given by  $\tilde{U}_{SB}$ , which connects the initial state of the backward process  $|\tilde{\psi}'_S(x')\rangle \otimes |\tilde{E}_B(y')\rangle$  to its final state  $|\tilde{\psi}_S(x)\rangle \otimes |\tilde{E}_B(y)\rangle$ . Here,  $|\tilde{\phi}\rangle := \hat{\Theta}|\phi\rangle$  with  $\hat{\Theta}$  being the anti-unitary time-reversal operator, and  $\tilde{U}_{SB} := T \exp(-\frac{i}{\hbar} \int_0^\tau \tilde{H}_{\text{tot}}(t) dt)$  with  $\tilde{H}_{\text{tot}}(t) := \hat{\Theta} H_{\text{tot}}(t) \hat{\Theta}$  being the time-reversed Hamiltonian.

The backward probability distribution is then given by

$$\tilde{p}(z, z') = \tilde{p}(z \leftarrow z') p'_S(x') \rho_B^G(y'), \quad (10.16)$$

where  $\tilde{p}(z \leftarrow z') := |\langle \tilde{\psi}_S(x) | \otimes \langle \tilde{E}_B(y) | \tilde{U}_{SB} | \tilde{\psi}'_S(x') \rangle \otimes |\tilde{E}_B(y')\rangle|^2$  is the backward transition probability from  $z'$  to  $z$ .

From the unitarity of the time evolution of SB and the relation  $\hat{\Theta} \tilde{U}_{SB} \hat{\Theta} = U_{SB}^\dagger$ , the time-reversal symmetry between the forward and the backward transition probabilities holds:

$$p(z' \leftarrow z) = \tilde{p}(z \leftarrow z'). \quad (10.17)$$

As a consequence, we obtain the detailed FT [46, 69]:

$$\frac{\tilde{p}(z, z')}{p(z, z')} = e^{-\sigma(z, z')}. \quad (10.18)$$

We note that essentially the same argument as above has been discussed in Ref. [11] for classical Liouvillian dynamics. From Eq. (10.18), we derive other types of FTs as follows.

First, we directly obtain from  $P(\sigma)$  in Eq. (10.15) the Kurchan–Tasaki–Crooks FT:

$$\frac{\tilde{P}(-\sigma)}{P(\sigma)} = e^{-\sigma}. \quad (10.19)$$

Here,  $\tilde{P}(-\sigma) := \sum_{z,z'} \delta(\tilde{\sigma}(z, z') + \sigma) \tilde{p}(z, z')$  is the probability distribution of entropy production  $-\sigma$  in the backward process, where  $\tilde{\sigma}(z, z') = \ln \tilde{p}(z, z') - \ln p(z, z')$  is the backward stochastic entropy production. Equality (10.19) shows that the probability of negative entropy production is exponentially small.

We can further derive the integral quantum FT [26]:

$$\langle e^{-\sigma} \rangle = 1. \quad (10.20)$$

In fact, from Eq. (10.18), we have  $\langle e^{-\sigma} \rangle = \sum_{z,z'} p(z, z') e^{-\sigma(z, z')} = \sum_{z,z'} \tilde{p}(z, z') = 1$ , where we use the normalization condition of the backward probability distribution to obtain the last equality. By applying the Jensen inequality  $\langle e^x \rangle \geq e^{\langle x \rangle}$ , Eq. (10.20) reproduces the second law (10.6):  $\Sigma \geq 0$ . By examining the foregoing argument, one can see that the derivation of the second law based on the quantum FT is essentially the same as that based on the non-negativity of the quantum relative entropy [46]. We also note from Eq. (10.18) that  $\Sigma$  can be expressed in terms of the classical relative entropy [70] between the forward and backward probabilities:  $\Sigma = D(p || \tilde{p}) := \sum_{z,z'} p(z, z') (\ln p(z, z') - \ln \tilde{p}(z, z'))$ .

We next express the FT as a property of the characteristic function  $\chi(\nu)$  of the entropy production, which is defined by the Fourier transform of  $P(\sigma)$ :

$$\chi(\nu) := \int d\sigma e^{i\nu\sigma} P(\sigma) = \text{Tr}[V_\nu^\dagger(\tau) U_{SB} V_\nu(0) (\rho_S(0) \otimes \rho_B^G) V_\nu(0) U_{SB}^\dagger V_\nu^\dagger(\tau)]. \quad (10.21)$$

Here,  $V_\nu(t) = \exp[i\nu(\ln \rho_S(t) - \beta H_B)/2]$  is a unitary operator that includes the counting field for the full-counting statistics of the entropy production [21]. Similarly, let us introduce  $\tilde{\chi}(\nu)$  as the Fourier transform of  $\tilde{P}(\sigma)$ . Then, Eq. (10.19) is expressed in terms of the following symmetry of the characteristic function:

$$\chi(\nu) = \tilde{\chi}(-\nu + i). \quad (10.22)$$

By taking  $\nu = i$ , we also find that  $\chi(i) = \int d\sigma e^{-\sigma} P(\sigma) = \tilde{\chi}(0) = 1$ , which is nothing but the integral FT (10.20) [22]. We note that the  $n$ -th cumulant of  $\sigma$ , written as  $\langle \sigma^n \rangle_c$ , can be calculated through the cumulant generating function  $K(\nu) := \ln \chi(\nu)$ , i.e.,  $\langle \sigma^n \rangle_c = (-i\partial_\nu)^n K(\nu)|_{\nu=i}$ .

By expanding the cumulant generating function  $K(\nu)$  in terms of  $\sigma$  up to the second cumulant and by applying Eq. (10.20), we obtain the fluctuation-dissipation relation

$$\langle (\sigma - \Sigma)^2 \rangle = 2\Sigma + O(\sigma^3), \quad (10.23)$$

where the left-hand side represents the fluctuation of the entropy production and  $\Sigma$  on the right-hand side quantifies dissipation. We note that Eq. (10.23) becomes exact when  $P(\sigma)$  is the Gaussian distribution. The Onsager reciprocity relation can also be obtained from Eq. (10.18) [40]. Furthermore, the higher-order extension of these linear relations can systematically be derived from the FT [39, 41], and has experimentally been demonstrated in a quantum coherent conductor [42].

We finally consider a special case in which the initial state of the system is given by the Gibbs distribution  $\rho_S(0) = \rho_S^G(0)$  and derive the quantum Jarzynski equality. We first define the stochastic work

$$w(z, z') = (E'_S(x') + E_B(y')) - (E_S(x) + E_B(y)), \quad (10.24)$$

where  $E_S(x)$  and  $E'_S(x')$  are the initial and final energies of the system, respectively. The work probability distribution is defined as  $P(w) = \sum_{z,z'} \delta(w - w(z, z')) p(z, z')$ , where  $p(z, z')$  is given in Eq. (10.14). We note that the stochastic work  $w$  cannot be obtained from a projection measurement of a single observable [25]. We also note that analytical expressions of the work probability distribution have been obtained for a dragged harmonic oscillator in isolated systems [71], open systems [72], and a parametrically driven oscillator in isolated systems [73].

When the initial and final states of the system are given by the Gibbs distributions, the entropy production is given by the difference between the work and the equilibrium free energy:  $\sigma(z, z') = \beta(w(z, z') - \Delta F_S^{\text{eq}})$ . The integral FT (10.20) then reduces to

$$\langle e^{-\beta(w - \Delta F_S^{\text{eq}})} \rangle = 1, \quad (10.25)$$

which is called the quantum Jarzynski equality [23, 24]. We note that Eq. (10.25) is still valid when the final state of the system deviates from the Gibbs distribution [46].

### 10.2.3 Gibbs-Preserving Maps and Beyond

#### 10.2.3.1 Second Law

In Sect. 10.2.1.2, we explicitly assumed that the composite system SB obeys unitary dynamics. In this section, we adopt a slightly different approach, where the bath degrees of freedom are traced out and thermodynamic quantities are defined in terms of the degrees of freedom of the system.

In this situation, we can derive the second law from the monotonicity of the quantum relative entropy [74, 75], which states that

$$S(\rho||\sigma) \geq S(\mathcal{E}(\rho)||\mathcal{E}(\sigma)) \quad (10.26)$$

for any completely-positive and trace-preserving (CPTP) map  $\mathcal{E}(\bullet)$ . This implies that the CPTP map independently acting on the density operators  $\rho$  and  $\sigma$  does not increase their distinguishability, and therefore the (asymmetric) distance between  $\rho$  and  $\sigma$  becomes smaller. In what follows, we use (10.26) to show the second law for time-independent Hamiltonians as well as time-dependent ones.

**Time-independent control.**— We first suppose that the Hamiltonian of the system is time-independent, i.e.,  $H_S(t) = H_S$ . In this case, the time evolution describes a thermal relaxation process. Correspondingly, we assume that the CPTP map on the system is a Gibbs-preserving map whose steady state is the Gibbs distribution, i.e.,

$$\mathcal{E}(\rho_S^G) = \rho_S^G. \quad (10.27)$$

The time evolution of the system is given by  $\rho'_S = \mathcal{E}(\rho_S)$ , and the heat is defined as the increase in the energy of the system:

$$Q' := \text{Tr}[H_S \rho'_S] - \text{Tr}[H_S \rho_S]. \quad (10.28)$$

From the monotonicity of the relative entropy (10.26), we have  $S(\rho_S||\rho_S^G) \geq S(\mathcal{E}(\rho_S)||\mathcal{E}(\rho_S^G)) = S(\rho'_S||\rho_S^G)$ , which gives the second law [76]

$$\Sigma' = \Delta S - \beta Q' \geq 0. \quad (10.29)$$

In general,  $Q'$  in Eq. (10.28) is different from  $Q$  in Eq. (10.4) because of the interaction energy, and thus the second law (10.29) is different from (10.6). However, if  $\mathcal{E}$  is given by the form of  $\mathcal{E}(\rho) = \text{Tr}_B[U_{SB}(\rho_S \otimes \rho_B^G)U_{SB}^\dagger]$  with a special condition

$$[H_S + H_B, U_{SB}] = 0, \quad (10.30)$$

we can show that  $Q = Q'$  holds and thus the second laws (10.6) and (10.29) become equivalent to each other. The condition (10.30) means that the sum of the energies

of the system and the bath without the interaction energy is preserved under  $\mathcal{E}$ , and thus any transition in the system is accompanied by a transition in the bath, where their energy changes have the same absolute value. In this case,  $\mathcal{E}$  is called a thermal operation, which is an extensively used concept in the thermodynamic resource theory [55, 77]. A thermal operation is always a Gibbs-preserving map, but the converse is not necessarily true [78].

**Time-dependent control.**— We next consider the case in which the Hamiltonian of the system is time-dependent. We here assume that the dynamics of the system is described by the Markov quantum master equation, which means that we should take the weak-coupling limit between the system and the bath [79]. The CPTP map  $\mathcal{E}$  describes the solution of the master equation from  $t = 0$  to  $\tau$ , i.e.,  $\rho_S(\tau) = \mathcal{E}(\rho_S(0))$ . A crucial feature of the Markovian dynamics is that we can split  $\mathcal{E}$  into the product of infinitesimal translations:  $\mathcal{E} = \mathcal{E}_{N\Delta t} \circ \dots \circ \mathcal{E}_{2\Delta t} \circ \mathcal{E}_{\Delta t}$ , where  $\mathcal{E}_{n\Delta t}$  is a CPTP map and describes an infinitesimal evolution from  $t = (n-1)\Delta t$  to  $t = n\Delta t$  with  $N\Delta t = \tau$  and  $\Delta t \rightarrow 0$ . We assume that the system is driven slowly so that the quantum adiabatic theorem is approximately satisfied [80] and that  $\mathcal{E}_{n\Delta t}$  becomes the Gibbs-preserving map for the instantaneous Hamiltonian of the system at time  $t = (n-1)\Delta t$ .

The quantum master equation is given by the Lindblad form

$$\partial_t \rho_S(t) = \mathcal{L}_t[\rho_S(t)] = -\frac{i}{\hbar}[H_S(t), \rho_S(t)] + \sum_{k,l} \mathcal{D}[L_{kl}(t)]\rho_S(t), \quad (10.31)$$

where  $\mathcal{D}[L_{kl}(t)]\rho_S(t) = L_{kl}(t)\rho_S(t)L_{kl}^\dagger(t) - \{L_{kl}^\dagger(t)L_{kl}(t), \rho_S(t)\}/2$  describes dissipation and the Lindblad operator  $L_{kl}(t)$  describes a quantum jump from the  $k$ -th eigenstate to the  $l$ -th eigenstate of the system:  $[L_{kl}(t), H_S(t)] = \Delta_{kl}(t)L_{kl}(t)$  with  $\Delta_{kl}(t) = E_t^S(k) - E_t^S(l)$ . We further assume the detailed balance condition  $L_{lk}^\dagger(t) = L_{kl}(t)e^{-\beta\Delta_{kl}(t)/2}$ , which is a sufficient condition to make  $\mathcal{E}_t$  Gibbs-preserving, i.e.,  $\mathcal{E}_t(\rho_S^G(t)) = \rho_S^G(t)$  or equivalently  $\mathcal{L}_t[\rho_S^G(t)] = 0$ . We again note that  $\mathcal{E}_t$  is the solution to Eq. (10.31) from  $t$  to  $t + \Delta t$  such that  $\rho_S(t + \Delta t) = \mathcal{E}_t(\rho_S(t))$ .

The energy of the system is given by  $E_S(t) := \text{Tr}[\rho_S(t)H_S(t)]$ , whose time derivative gives  $\partial_t E_S(t) = \text{Tr}[\rho_S(t)\partial_t H_S(t)] + \text{Tr}[(\partial_t \rho_S(t))H_S(t)]$ . From the first law of thermodynamics, we associate these two terms with the work flux and the heat flux:

$$\dot{W} := \text{Tr}[\rho_S(t)\partial_t H_S(t)], \quad (10.32)$$

$$\dot{Q}' := \text{Tr}[(\partial_t \rho_S(t))H_S(t)] = -\sum_{k,l} \text{Tr}[L_{kl}(t)\rho_S(t)L_{kl}^\dagger(t)]\Delta_{kl}(t). \quad (10.33)$$

Here, Eq. (10.32) describes the energy change of the system via the time-dependent control of the Hamiltonian, and Eq. (10.33) describes that induced by the effect of the bath. Also, the entropy flux is given by  $\dot{S} = -\text{Tr}[\partial_t \rho_S(t) \ln \rho_S(t)]$ .

The entropy production rate is then defined as  $\dot{\Sigma}' := \dot{S} - \beta \dot{Q}'$ . Since  $\mathcal{E}_t$  is CPTP and Gibbs-preserving, we can use the monotonicity of the relative entropy (10.26)

to obtain the second law in the following form [76, 81]:

$$\dot{\Sigma}' = \lim_{\Delta t \rightarrow 0} \frac{S(\rho_S(t) || \rho_S^G(t)) - S(\rho_S(t + \Delta t) || \rho_S^G(t))}{\Delta t} \geq 0. \quad (10.34)$$

This is a generalization of (10.29) for time-dependent driving of the Hamiltonian. We note that  $\dot{\Sigma}'$  may take negative values for non-Markovian processes [82].

### 10.2.3.2 Quantum Jump Method

In Sect. 10.2.3.1, we only considered the ensemble-averaged quantities of the system described by the quantum master equation (10.31). We next consider the quantum jump method to define the stochastic version of  $\Sigma'$ , which leads to the quantum FT for open Markovian dynamics.

We start by unraveling the Lindblad master equation (10.31) to individual quantum trajectories by the following stochastic Schrödinger equation [79]:

$$d|\psi_t\rangle = \left[ -\frac{i}{\hbar} H_S^{\text{eff}}(t) + \frac{1}{2} \sum_{k,l} ||L_{kl}(t)|\psi_t\rangle||^2 \right] |\psi_t\rangle dt + \sum_{k,l} \left[ \frac{L_{kl}(t)}{||L_{kl}(t)|\psi_t\rangle||} - I \right] |\psi_t\rangle dN_{kl}(t). \quad (10.35)$$

Here,  $dN_{kl}(t)$  is a Poisson increment, which takes on 1 when the quantum jump described by  $L_{kl}(t)$  occurs, and 0 otherwise. We note that the product of  $dN_{kl}(t)$  and other terms is defined by the Itô form. Its ensemble average is given by  $\mathbb{E}[dN_{kl}(t)] = ||L_{kl}(t)|\psi_t\rangle||^2 dt$ . The second term on the right-hand side of Eq. (10.35) describes such a jump process  $|\psi_t\rangle \mapsto L_{kl}(t)|\psi_t\rangle$  up to a normalization factor. The no-jump process is described by the first term on the right-hand side, where the system evolves continuously in time via the non-Hermitian effective Hamiltonian  $H_S^{\text{eff}}(t) := H_S(t) - \frac{i\hbar}{2} \sum_{k,l} L_{kl}^\dagger(t)L_{kl}(t)$ . Since  $[H_S(t), \sum_{k,l} L_{kl}^\dagger(t)L_{kl}(t)] = 0$ , the non-unitary part of the time evolution generated by  $H_S^{\text{eff}}(t)$  has the effect of reducing the norm of the state vector  $|\psi_t\rangle$ . The density operator of the system is reproduced by taking the ensemble average:  $\mathbb{E}[|\psi_t\rangle\langle\psi_t|] = \rho_S(t)$ . Thus, the ensemble average of Eq. (10.35) reproduces the quantum master equation (10.31).

We denote the history of a jump process as  $\psi_0^\tau := \{(k_1, l_1, t_1), (k_2, l_2, t_2), \dots, (k_N, l_N, t_N)\}$  with  $0 \leq t_1 \leq t_2 \leq \dots \leq t_N \leq \tau$ , where  $t_i$  is the time at which the  $i$ -th jump process described by  $L_{k_i l_i}(t_i)$  occurs. From the record of the jump process  $\psi_0^\tau$ , we define the stochastic heat flux by

$$q'[\psi_0^\tau] := - \sum_{k,l} \int_0^\tau dN_{kl}(t) \Delta_{kl}(t), \quad (10.36)$$

which gives  $\mathbb{E}[q'] = \dot{Q}'$  in the ensemble average. As is the case for Sect. 10.2.2, let  $p_S(x)$  and  $p_S'(x')$  be the diagonal elements of the initial and final density operators, respectively. We then define the stochastic entropy production in a manner similar to Eq. (10.13):

$$\sigma'[\psi_0^\tau, x', x] := \ln p_S(x) - \ln p'_S(x') - \beta q'[\psi_0^\tau]. \quad (10.37)$$

We note that the forward path probability distribution of the trajectory  $(\psi_0^\tau, x', x)$  is given by

$$P[\psi_0^\tau, x', x] = \left| \langle \psi'_S(x') | \mathcal{U}_{\tau, t_N} L_{k_N l_N}(t_N) \mathcal{U}_{t_N, t_{N-1}} \dots \mathcal{U}_{t_2, t_1} L_{k_1 l_1}(t_1) \mathcal{U}_{t_1, 0} | \psi_S(x) \rangle \right|^2, \quad (10.38)$$

where  $\{|\psi_S(x)\rangle\}$  and  $\{|\psi'_S(x')\rangle\}$  are the eigenbases that diagonalize the initial and final density matrices of the system, respectively, and  $\mathcal{U}_{t_{i+1}, t_i} := T \exp[-\frac{i}{\hbar} \int_{t_i}^{t_{i+1}} H_S^{\text{eff}}(t) dt]$  is the non-unitary time evolution generated by the effective Hamiltonian for the no-jump process.

Using Eqs. (10.37) and (10.38), we can derive the integral FT for  $\sigma'$  [31, 83]:

$$\langle e^{-\sigma'} \rangle = 1. \quad (10.39)$$

It follows from this that, the second law (10.34) is reproduced by the Jensen inequality. Moreover, by defining the backward probability distribution in the same manner as in Eq. (10.38), we can show the detailed FT for  $\sigma'$  [31, 83]. We note that Eq. (10.39) has also been derived in Ref. [32] for a slightly different setup.

In the standard derivation of the quantum master equation (10.31) and its unravelling (10.35) from unitary dynamics of the system and the bath, the weak-coupling limit and the rotating wave approximation are assumed [79]. As a consequence, Eq. (10.30) is approximately satisfied for any infinitesimal step, and thus each infinitesimal evolution is regarded as an approximate thermal operation. Therefore, the transition in the bath for each step, represented as  $y \rightarrow y'$  in Eq. (10.14), is equivalent to a jump in the system. Indeed, the work statistics defined via the two-point measurement scheme for the composite system is found to be equivalent to that defined via the quantum jump method [84–86].

We have assumed that the instantaneous steady state at time  $t$  is given by  $\rho_S^G(t)$ . On the other hand, if the steady state is not the Gibbs distribution,  $\Sigma$  should be interpreted as a “nonadiabatic” entropy production, which satisfies the Hatano-Sasa-type fluctuation theorem [12, 15]. A quantum analogue of the Hatano-Sasa type relation has been derived and discussed in Refs. [83, 87–89]. We also note that extensions of Eq. (10.39) to the case of general CPTP maps have been discussed in Refs. [88, 89].

The derivation of Eq. (10.39) is based on the quantum jump method, which is a quantum counterpart of the Markov jump processes. The quantum Brownian motion described by the Caldeira–Leggett model [90] is a quantum counterpart of the Brownian motion described by the Langevin equation. This model is used in Refs. [72, 91] to study the quantum FT by the path integral method.

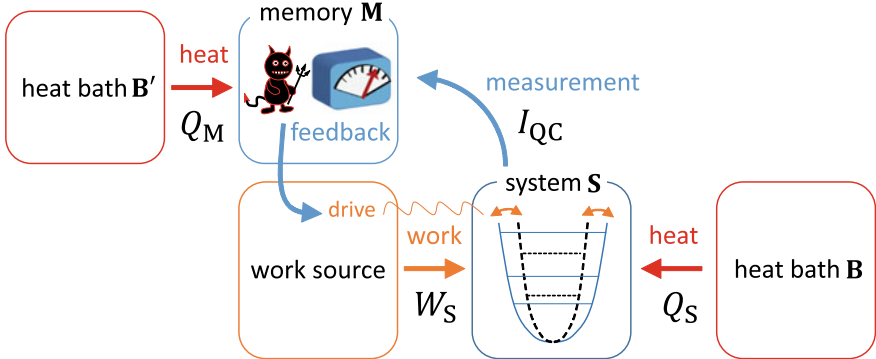


**Fig. 10.3** Schematic of the measurement and feedback processes by Maxwell's demon. Depending on the measurement outcome, the demon performs feedback control through the time-dependent control of the system's Hamiltonian.

### 10.3 Fluctuation Theorems with Measurement and Feedback Control

In this section, we generalize the second law and the FT to the case with measurement and feedback control, which is a typical setup of information thermodynamics and can be regarded as a modern formulation of Maxwell's demon. The demon is the key ingredient of information heat engines, extracting work from the system by utilizing information about fluctuations [43–47, 92–95]. The Szilard engine [92] is the quintessential model of Maxwell's demon, where the feedback controller can extract work  $|W| = k_B T \ln 2$  from the system by utilizing one bit of information. We note that a quantum extension of the Szilard engine has been studied in Refs. [93, 96, 97].

#### 10.3.1 Setup

Let us first explain our setup (see Fig. 10.3), which is an extension of the unitary setup of Sect. 10.2.1.1. We assume that the initial state is given by  $\rho_S \otimes \rho_M \otimes \rho_B^G \otimes \rho_{B'}^G$ , where  $S$  is the controlled system,  $M$  is the memory that records the measurement outcome, and  $B$  ( $B'$ ) is the heat bath which interacts with  $S$  ( $M$ ). Here,  $\rho_B^G$  and  $\rho_{B'}^G$  are the Gibbs distributions of  $B$  and  $B'$  at the same inverse temperature  $\beta$ . Note that  $M$  plays the role of Maxwell's demon. For simplicity, we assume that the initial state of  $M$  is a pure state:  $\rho_M = |\psi_M\rangle\langle\psi_M|$ , while the extension to a mixed state is straightforward. Then, the composite system  $SMBB'$  obeys the following time evolution.

*Measurement process.*— For simplicity, we assume that B is uncoupled to the system during the measurement. A general quantum measurement on S is realized by entangling S and M through a unitary transformation  $U_{\text{SMB}'}$ , where the interaction with B' is also included. Then, a projection  $P_M(k) = |\varphi_M(k)\rangle\langle\varphi_M(k)|$  on M follows. The density operator of SMB' after the measurement with a measurement outcome  $k$  takes the form

$$\rho'_{\text{SMB}'}(k) = \frac{1}{p_k} P_M(k) U_{\text{SMB}'} (\rho_S \otimes \rho_M \otimes \rho_{B'}^G) U_{\text{SMB}'}^\dagger P_M(k), \quad (10.40)$$

where  $p_k := \text{Tr}[P_M(k) U_{\text{SMB}'} (\rho_S \otimes \rho_M \otimes \rho_{B'}^G) U_{\text{SMB}'}^\dagger]$  is the probability of the outcome  $k$ . For simplicity, we assume that the effect of the measurement is described by

$$\rho'_S(k) := \text{Tr}_{\text{MB}'}[\rho'_{\text{SMB}'}(k)] = \frac{1}{p_k} M_k \rho_S M_k^\dagger, \quad (10.41)$$

where  $M_k$  is the Kraus operator satisfying  $\sum_k M_k^\dagger M_k = I$ . We note that  $p_k = \text{Tr}[M_k^\dagger M_k \rho_S]$ , where  $\{M_k^\dagger M_k\}$  is called the POVM [58].

*Feedback control.*— We suppose that the unitary time evolution operator  $U_{\text{SB}}(k)$  of SB depends on the obtained measurement outcome  $k$ . The density operator after the feedback control is given by  $\rho''_{\text{SB}}(k) = U_{\text{SB}}(k) (\rho'_S(k) \otimes \rho_{B'}^G) U_{\text{SB}}^\dagger(k)$ .

We now introduce the quantum-classical (QC) mutual information [48] (or the information gain [98, 99]) which quantifies the obtained information about the system through the measurement process. The QC-mutual information is defined by

$$I_{\text{QC}} = S(\rho_S) - \sum_k p_k S(\rho'_S(k)), \quad (10.42)$$

which quantifies how the measurement process reduces the randomness of the system quantified by the von Neumann entropy. The QC mutual information satisfies  $0 \leq I_{\text{QC}} \leq S(p)$ , where  $S(p) := -\sum_k p_k \ln p_k$  is the Shannon entropy of the measurement outcome. The upper bound  $I_{\text{QC}} = S(p)$  is achieved if every Kraus operator is a projection that commutes with  $\rho_S$ , i.e., the measurement is error-free and classical [48, 99].

We remark on the operational meaning of the QC-mutual information. Suppose that the information about a classical probability variable  $m$  is encoded in the density operator as  $\rho_S = \sum_m q(m) \sigma_S(m)$ , where  $\sigma_S(m)$ 's are not necessarily orthogonal to each other. To extract this information, we perform a measurement described by  $\{M_k\}$  on  $\rho_S$ . The joint probability of  $m$  and  $k$  is then given by  $p(k, m) := q(m) \text{Tr}[M_k^\dagger M_k \sigma_S(m)]$ . In this setup, the following inequality holds [100]:

$$0 \leq I_{\text{CL}} \leq I_{\text{QC}}, \quad (10.43)$$

where  $I_{\text{CL}} = \sum_{k,m} p(k, m) (\ln p(k, m) - \ln[q(m)p(k)])$  is the classical mutual information between  $m$  and  $k$ . Inequality (10.43) implies that the QC-mutual information

gives an upper bound on the accessible classical information that is encoded in the density operator.

We note that in general Eq. (10.41) becomes  $\rho'_S(k) = p_k^{-1} \sum_l M_{k,l} \rho_S M_{k,l}^\dagger$ , where  $l$  labels the transition of  $B'$ . This describes an inefficient measurement, where the randomness of  $M$  caused by  $B'$  is transferred to  $S$  as a measurement backaction. As a result, Eq. (10.42) can take on negative values [53, 101, 102].

### 10.3.2 Second Law of Information Thermodynamics

We now discuss several generalizations of the second law that are applicable to the measurement and feedback processes. We define the entropy production-like quantities  $\Sigma_S$  for the system and  $\Sigma_M$  for the memory by adopting a similar definition as in Eq. (10.3). The entropy change in  $SB$  for a given measurement outcome  $k$  is quantified by  $\Sigma_S := \sum_k p_k S(\rho''_S(k)) - S(\rho_S) - \beta Q_S$ , and  $Q_S := \text{Tr}[H_B \rho_B^G] - \sum_k p_k \text{Tr}[H_B \rho''_B(k)]$  is the heat transfer from  $B$  to  $S$ . Similarly, the entropy change in  $MB'$  for the measurement process is quantified by  $\Sigma_M := S(\rho'_M) - S(\rho_M) - \beta Q_M$ , where  $Q_M := \text{Tr}[H_{B'} \rho_{B'}^G] - \text{Tr}[H_{B'} \rho'_{B'}]$  is the heat transfer from  $B'$  to  $M$ , and  $\rho'_{SMB'} := \sum_k p_k \rho'_{SMB'(k)}$ .

Note that the definitions of  $\Sigma_S$  and  $\Sigma_M$  are not symmetric, because the roles of  $S$  and  $M$  are different in the measurement and feedback processes (see Fig. 10.3).

A special feature of feedback control lies in the fact that  $\Sigma_S$  can become negative down to  $-I_{QC}$ , which corresponds to the additional work extraction by Maxwell's demon as in the Szilard engine. In contrast, in the measurement process,  $\Sigma_M$  is bounded from below by  $+I_{QC}$ , and thus cannot reach zero if the memory acquires nonzero information. These are represented by the generalized second laws which incorporate the QC-mutual information [48, 49]

$$\Sigma_S \geq -I_{QC}, \quad (10.44)$$

$$\Sigma_M \geq +I_{QC}. \quad (10.45)$$

Here, we notice that  $I_{QC}$  appears with different signs on the right-hand sides of (10.44) and (10.45). Therefore, if we consider the total entropy production of  $SM$ , the QC-mutual information terms are canceled out:  $\Sigma_S + \Sigma_M \geq 0$ . This implies that Maxwell's demon is indeed consistent with the conventional second law for the total system. From the generalized second laws (10.44) and (10.45), we find that the combination of  $\Sigma_S + I_{QC}$  represents the irreversibility in the feedback control process, and  $\Sigma_M - I_{QC}$  represents the irreversibility in the measurement process. In this sense, inequalities (10.44) and (10.45) give stronger restrictions on the entropy production than the ordinary second law for the total system. The equality in (10.44) is achieved by the classical Szilard engine, where  $I_{QC} = I_{CL} = \ln 2$  and  $\Sigma_S = \beta W_S = -\ln 2$ . A more general protocol to achieve the equality in (10.44) has been discussed in Ref. [101].

We note that the role of purely quantum correlation (i.e., quantum discord) in the setup of Maxwell's demon has been studied in Refs. [103–105]. We also note that there is another formulation of Maxwell's demon, often referred to as an autonomous demon, which has been studied in both the classical [106] and the quantum [107] regimes. Such autonomous demons and the measurement-feedback setup has been studied in a unified way [108].

### 10.3.3 Quantum Fluctuation Theorem

We next consider the quantum FT for measurement and feedback control processes. The stochastic versions of  $\Sigma_S$  and  $\Sigma_M$  respectively are written as  $\sigma_S$  and  $\sigma_M$ , which are defined in a manner similar to that for a non-feedback case (10.13) (see Refs. [53, 54] for the explicit definitions). We also introduce the stochastic QC-mutual information as [53]

$$i_{QC}(x, k, x') := \ln p'_S(x'|k) - \ln p_S(x), \quad (10.46)$$

where  $p_S(x)$  and  $p'_S(x'|k)$  are the diagonal elements of  $\rho_S$  and  $\rho'_S(k)$ , respectively. We can easily show that  $\langle i_{QC} \rangle = I_{QC}$ . The right-hand side of (10.46) quantifies the stochastic entropy difference between the pre-measurement state and the post-measurement state for a given  $k$ . It is worth comparing Eq. (10.46) with the classical stochastic mutual information  $i_{CL} := \ln p_S(x|k) - \ln p_S(x)$  [50, 51], where  $p_S(x|k)$  is the initial probability distribution of the system for a given measurement outcome  $k$ . By comparing  $i_{CL}$  with  $i_{QC}$ , we find that  $i_{QC}$  contains the effect of the change in the state of the system from  $x$  to  $x'$  due to the backaction of the quantum measurement.

In terms of  $i_{QC}$  in Eq. (10.46), the integral FTs for the measurement and feedback processes are shown to be [53, 54]

$$\langle e^{-\sigma_S - i_{QC}} \rangle = 1, \quad (10.47)$$

$$\langle e^{-\sigma_M + i_{QC}} \rangle = 1. \quad (10.48)$$

The detailed FT has also been derived in Ref. [54]. Using the Jensen inequality, Eqs. (10.47) and (10.48) reproduce the generalized second laws (10.44) and (10.45), respectively. We note that the entropy production of SM also satisfies the FT:  $\langle e^{-(\sigma_S + \sigma_M)} \rangle = 1$ . Now equalities (10.47) and (10.48) include the decomposition of the entropy production of SM into  $\sigma_S - i_{QC}$  and  $\sigma_M + i_{QC}$  at the level of individual trajectories, which is consistent with the decomposition in (10.44) and (10.45) at the level of the ensemble average.

We note that Eqs. (10.47) and (10.48) were first derived in classical systems [50, 51]. In Refs. [109, 110], Eq. (10.47) has been derived on the basis of the quantum jump methods discussed in Sect. 10.2.3.2. The experimental verification of Eq. (10.47) has been done in Ref. [111] for a classical system and in Refs. [102, 112] for quantum systems.

## 10.4 Comparison with Experiments

In this section, we make a brief overview of the experimental studies on quantum thermodynamics, with a special focus on the quantum FT, the Landauer principle, and Maxwell's demon.

**Quantum FT.**— It has been discussed in Refs. [113, 114] that work statistics can be measured by adopting a Ramsey-type interferometric scheme. This technique has been utilized in an NMR experiment to obtain the work distribution [18]. A theoretical proposal to extend this technique to the case with feedback control has been discussed in Ref. [115]. Using a trapped ion system, the two-point measurement scheme has been implemented and the quantum Jarzynski equality for an isolated system has been experimentally verified [19]. Using a circuit-QED system, the authors of Ref. [20] have performed continuous measurements to extract work and heat along quantum trajectories of a qubit.

Many of the systems used in quantum thermodynamic experiments can be regarded as isolated. In such a case, the two-point energy measurement on the system, as performed in Refs. [19, 112], is essential for obtaining the quantum work distribution. If the effect of the bath cannot be ignored, it is experimentally challenging to verify the quantum FT, since one has to measure the heat exchange between the system and the bath. A possible way to overcome this difficulty is to use single-photon detectors and observe photons emitted from the quantum jump processes, which enables us to measure the stochastic heat as discussed in Sect. 10.2.3.2.

**Landauer principle.**— The Landauer principle discussed in Sect. 10.2.1.3 has been experimentally demonstrated in the classical regime by using a colloidal particle [116–121], nanomagnets [122] and a micro-electromechanical cantilever [123]. In the quantum regime, the verification of the Landauer principle has been demonstrated in an NMR experiment through measurements of the heat distribution for elementary quantum logic gates [124].

**Maxwell's demon.**— Experimental implementations of the Maxwell's demon in the classical regime have been achieved with colloidal particles [125] (see also Chaps. 39 and 40), single-electron devices [111, 126, 127], and photonic systems [128]. Maxwell's demon has also been experimentally studied in the quantum regime. Using an NMR system, the authors of Ref. [129] implemented Maxwell's demon and measured the average entropy production and the information gain. Maxwell's demon based on circuit-QED systems has been experimentally demonstrated in Refs. [102, 112, 130]. In Ref. [130], the authors studied the output power with coherent interaction between the demon and the system. In Ref. [112], a quantum non-demolition (QND) projective measurement technique was utilized to measure the stochastic work and the stochastic QC-mutual information. In Ref. [102], a weak continuous measurement was performed to acquire information about the system. Maxwell's demon has also been implemented with the NV-center by combining C-NOT gates [131]. A multi-photon optical system has been used for work extraction from entangled bipartite and tripartite states [132].

## 10.5 Concluding Remarks

In this article, we have discussed some key concepts of the second law of thermodynamics and the FT in the quantum regime. There are a number of subjects that we cannot cover in this article for lack of space. Let us finally make a few remarks about them.

**Jarzynski equality for general dynamics.**— It is interesting to know to what extent the Jarzynski equality is still valid if the dynamics is not unitary. It has been shown that if the dynamics of the system is described by a unital map (i.e., if the CPTP map does not change the identity operator), the Jarzynski equality is unchanged [133, 134]. This includes a situation where the system is subject to phase decoherence but not to energy dissipation [135], and also a situation where an isolated system is continuously monitored by a sequence of projective measurements [33].

For a general CPTP map that is not necessarily unital, the right-hand side of the Jarzynski equality can deviate from unity [133, 134, 136, 137], i.e.,

$$\langle e^{-\beta(w - \Delta F_S^{\text{sq}})} \rangle = \gamma. \quad (10.49)$$

A connection between Eq. (10.49) and the Holevo bound has been discussed in Ref. [136]. In the context of information thermodynamics, the deviation of  $\gamma$  from unity also occurs as a consequence of feedback control [50, 52, 125].

It is worth noting that the quantum Jarzynski equality has been generalized to  $\mathcal{PT}$ -symmetric non-Hermitian quantum mechanics [138].

**Quantum-classical correspondence.**— It is natural to consider connections between classical and quantum stochastic thermodynamics. Along this line, the quantum-classical correspondence for the work distributions has been shown in isolated [139, 140] and open [72] systems.

**Initial coherence between energy eigenstates.**— The role of quantum coherence in the context of FT has been explored quite recently [141–146]. For initial states with coherence between energy eigenstates, an extension of the two-point measurement scheme to define the work distribution is not unique [143, 144]. If we naively apply the two-point measurement scheme, the initial coherence is destroyed during the first energy measurement. On the other hand, we can utilize the full counting statistics [141, 142] without destroying the initial coherence, although the interference effect may lead to negative values of the work distribution. Also, a variant of the FT that fully includes the effect of coherence has been derived [146].

**Fluctuation theorems for pure thermal bath.**— In Sect. 10.2, we make a crucial assumption that the initial state of the heat bath is given by the Gibbs distribution as in Eq. (10.2). However, motivated by the recent studies of thermalization in isolated quantum systems, especially the eigenstate thermalization hypothesis [147], the authors of Refs. [148, 149] have considered a situation in which the initial state of the bath is a pure state and shown that the second law and the FT can still hold at least in a short-time regime.

In summary, the quantum FT is one of the most fundamental relations in nonequilibrium statistical mechanics and applicable to a wide range of dynamics, including quantum information processing. In view of the recent progress in quantum thermodynamics, we expect that it will further contribute to the developments of quantum technologies and to the design of microscopic devices with low dissipation that would reach the limit set by the second law of thermodynamics.

**Acknowledgements** The authors thank Y. Masuyama for providing a cartoon of Maxwell's demon in Fig. 10.3. K. F. acknowledges supports from the National Science Foundation of China under Grants No. 11375012 and 11534002, and The Recruitment Program of Global Youth Experts of China. M. U. acknowledges support by a Grant-in-Aid for Scientific Research on Innovative Areas Topological Materials Science (KAKENHI Grant No. JP15H05855). T. S. acknowledges supports from JSPS KAKENHI Grant No. JP16H02211 and No. JP25103003. Part of the research reviewed in this chapter was made possible by the COST MP1209 network "Thermodynamics in the quantum regime".

## References

1. J. Loschmidt, *Sitzungsber. Kais. Akad. Wiss. Wien, Math. Naturwiss. Classe* **73**, 128 (1876)
2. C. Jarzynski, *Annu. Rev. Condens. Matter. Phys.* **2**, 329 (2011). <https://doi.org/10.1146/annurev-conmatphys-062910-140506>
3. U. Seifert, *Rep. Prog. Phys.* **75**, 126001 (2012). <https://doi.org/10.1088/0034-4885/75/12/126001>
4. M. Campisi, P. Hanggi, *Entropy* **13**, 2024 (2011). <https://doi.org/10.3390/e13122024>
5. U. Seifert, *Eur. Phys. J. B* **64**, 423 (2008). <https://doi.org/10.1140/epjb/e2008-00001-9>
6. K. Sekimoto, *Stochastic Energetics*, Lecture Notes in Physics, vol. 799 (Springer, Berlin, 2010). <https://doi.org/10.1007/978-3-642-05411-2>
7. D.J. Evans, E.G.D. Cohen, G.P. Morriss, *Phys. Rev. Lett.* **71**, 2401 (1993). <https://doi.org/10.1103/PhysRevLett.71.2401>
8. G. Gallavotti, E.G.D. Cohen, *Phys. Rev. Lett.* **74**, 2694 (1995). <https://doi.org/10.1103/PhysRevLett.74.2694>
9. C. Jarzynski, *Phys. Rev. Lett.* **78**, 2690 (1997). <https://doi.org/10.1103/PhysRevLett.78.2690>
10. G.E. Crooks, *Phys. Rev. E* **60**, 2721–2726 (1999). <https://doi.org/10.1103/PhysRevE.60.2721>
11. C. Jarzynski, *J. Stat. Phys.* **98**, 77 (2000). <https://doi.org/10.1023/A:1018670721277>
12. T. Hatano, S.I. Sasa, *Phys. Rev. Lett.* **86**, 3463 (2001). <https://doi.org/10.1103/PhysRevLett.86.3463>
13. U. Seifert, *Phys. Rev. Lett.* **95**, 040602 (2005). <https://doi.org/10.1103/PhysRevLett.95.040602>
14. R. Kawai, J.M.R. Parrondo, C. Van den Broeck, *Phys. Rev. Lett.* **98**, 080602 (2007). <https://doi.org/10.1103/PhysRevLett.98.080602>
15. M. Esposito, C. Van den Broeck, *Phys. Rev. Lett.* **104**, 090601 (2010). <https://doi.org/10.1103/PhysRevLett.104.090601>
16. J. Liphardt, S. Dumont, S.B. Smith, I. Tinoco Jr., C. Bustamante, *Science* **296**, 1832 (2002). <https://doi.org/10.1126/science.1071152>
17. D. Collin, F. Ritort, C. Jarzynski, S.B. Smith, I. Tinoco Jr., C. Bustamante, *Nature* **437**, 231 (2005). <https://doi.org/10.1038/nature04061>
18. T.B. Batalhão, A.M. Souza, L. Mazzola, R. Auccaise, R.S. Sarthour, I.S. Oliveira, J. Goold, G. De Chiara, M. Paternostro, R.M. Serra, *Phys. Rev. Lett.* **113**, 140601 (2014). <https://doi.org/10.1103/PhysRevLett.113.140601>

19. S. An, J.-N. Zhang, M. Um, D. Lv, Y. Lu, J. Zhang, Z.-Q. Yin, H.T. Quan, K. Kim, *Nature Phys.* **11**, 193 (2015). <https://doi.org/10.1038/nphys3197>
20. M. Naghiloo, D. Tan, P.M. Harrington, J.J. Alonso, E. Lutz, A. Romito, K.W. Murch, [arXiv:1703.05885](https://arxiv.org/abs/1703.05885)
21. M. Esposito, U. Harbola, S. Mukamel, *Rev. Mod. Phys.* **81**, 1665 (2009). <https://doi.org/10.1103/RevModPhys.81.1665>
22. M. Campisi, P. Hänggi, P. Talkner, *Rev. Mod. Phys.* **83**, 771 (2011). <https://doi.org/10.1103/RevModPhys.83.771>
23. J. Kurchan, [arXiv:cond-mat/0007360](https://arxiv.org/abs/cond-mat/0007360)
24. H. Tasaki, [arXiv:cond-mat/0009244](https://arxiv.org/abs/cond-mat/0009244)
25. P. Talkner, E. Lutz, P. Hanggi, *Phys. Rev. E* **75**, 050102. <https://doi.org/10.1103/PhysRevE.75.050102>
26. S. Deffner, E. Lutz, *Phys. Rev. Lett.* **107**, 140404 (2011). <https://doi.org/10.1103/PhysRevLett.107.140404>
27. C. Jarzynski, D.K. Wójcik, *Phys. Rev. Lett.* **92**, 230602 (2004). <https://doi.org/10.1103/PhysRevLett.92.230602>
28. T. Monnai, *Phys. Rev. E* **72**, 027102 (2005). <https://doi.org/10.1103/PhysRevE.72.027102>
29. G.E. Crooks, *J. Stat. Mech.* P10023 (2008). <https://doi.org/10.1088/1742-5468/2008/10/P10023>
30. M. Campisi, P. Talkner, P. Hänggi, *Phys. Rev. Lett.* **102**, 210401 (2009). <https://doi.org/10.1103/PhysRevLett.102.210401>
31. J.M. Horowitz, *Phys. Rev. E* **85**, 031110 (2012). <https://doi.org/10.1103/PhysRevE.85.031110>
32. F.W.J. Hekking, J.P. Pekola, *Phys. Rev. Lett.* **111**, 093602 (2013). <https://doi.org/10.1103/PhysRevLett.111.093602>
33. M. Campisi, P. Talkner, P. Hanggi, *Phys. Rev. Lett.* **105**, 140601 (2010). <https://doi.org/10.1103/PhysRevLett.105.140601>
34. J.J. Alonso, E. Lutz, A. Romito, *Phys. Rev. Lett.* **116**, 080403 (2016). <https://doi.org/10.1103/PhysRevLett.116.080403>
35. C. Elouard, D.A. Herrera-Martí, M. Clusel, A. Auffeves, *npj Quantum Information* **3**, 9 (2017). <https://doi.org/10.1038/s41534-017-0008-4>
36. M. Caselle, G. Costagliola, A. Nada, M. Panero, A. Toniato, *Phys. Rev. D* **94**, 034503 (2016). <https://doi.org/10.1103/PhysRevD.94.034503>
37. M. Caselle, A. Nada, M. Panero, [arXiv:1801.03110](https://arxiv.org/abs/1801.03110)
38. A. Bartolotta, S. Deffner, *Phys. Rev. X* **8**, 011033 (2018). <https://doi.org/10.1103/PhysRevX.8.011033>
39. D. Andrieux, P. Gaspard, *J. Stat. Mech.* P0, 2007 (2006). <https://doi.org/10.1088/1742-5468/2007/02/P02006>
40. K. Saito, A. Dhar, *Phys. Rev. Lett.* **99**, 180601 (2008). <https://doi.org/10.1103/PhysRevLett.99.180601>
41. K. Saito, Y. Utsumi, *Phys. Rev. B* **78**, 115429 (2008). <https://doi.org/10.1103/PhysRevB.78.115429>
42. S. Nakamura, Y. Yamauchi, M. Hashisaka, K. Chida, K. Kobayashi, T. Ono, R. Leturcq, K. Ensslin, K. Saito, Y. Utsumi, A.C. Gossard, *Phys. Rev. Lett.* **104**, 080602 (2010). <https://doi.org/10.1103/PhysRevLett.104.080602>
43. J.C. Maxwell, *Theory of Heat* (Appleton, London, 1871)
44. K. Maruyama, F. Nori, V. Vedral, *Rev. Mod. Phys.* **81**, 1 (2009). <https://doi.org/10.1103/RevModPhys.81.1>
45. T. Sagawa, *Prog. Theo. Phys.* **127**, 1 (2012). <https://doi.org/10.1143/PTP.127.1>
46. T. Sagawa, in *Lectures on Quantum Computing, Thermodynamics, and Statistical Physics*, ed. by M. Nakahara, S. Tanaka (World Scientific, Singapore, 2012). [https://doi.org/10.1142/9789814425193\\_0003](https://doi.org/10.1142/9789814425193_0003)

47. J.M.R. Parrondo, J.M. Horowitz, T. Sagawa, Nat. Phys. **11**, 131 (2015). <https://doi.org/10.1038/nphys3230>
48. T. Sagawa, M. Ueda, Phys. Rev. Lett. **100**, 080403 (2008). <https://doi.org/10.1103/PhysRevLett.100.080403>
49. T. Sagawa, M. Ueda, Phys. Rev. Lett. **102**, 250602 (2009). <https://doi.org/10.1103/PhysRevLett.102.250602>
50. T. Sagawa, M. Ueda, Phys. Rev. Lett. **104**, 090602 (2010). <https://doi.org/10.1103/PhysRevLett.104.090602>
51. T. Sagawa, M. Ueda, Phys. Rev. Lett. **109**, 180602 (2012). <https://doi.org/10.1103/PhysRevLett.109.180602>
52. M. Morikuni, H. Tasaki, J. Stat. Phys. **143**, 1 (2011). <https://doi.org/10.1007/s10955-011-0153-7>
53. K. Funo, Y. Watanabe, M. Ueda, Phys. Rev. E **88**, 052121 (2013). <https://doi.org/10.1103/PhysRevE.88.052121>
54. K. Funo, Y. Murashita, M. Ueda, New J. Phys. **17**, 075005 (2015). <https://doi.org/10.1088/1367-2630/17/7/075005>
55. M. Horodecki, J. Oppenheim, Nat. Commun. **4**, 2059 (2013). <https://doi.org/10.1038/ncomms3059>
56. A.S.L. Malabarba, A.J. Short, P. Kammerlander, New J. Phys. **17**, 045027 (2015). <https://doi.org/10.1088/1367-2630/17/4/045027>
57. D. Kondepudi, I. Prigogine, *From Heat Engines to Dissipative Structures* (Wiley, New York, 1998). <https://doi.org/10.1002/9781118698723>
58. M.A. Nielsen, I.L. Chuang, *Quantum Computation and Quantum Information* (Cambridge University Press, Cambridge, 2000). <https://doi.org/10.2277/0521635039>
59. C. Jarzynski, J. Stat. Mech. P09006 (2004). <https://doi.org/10.1088/1742-5468/2004/09/P09005>
60. U. Seifert, Phys. Rev. Lett. **116**, 020601 (2016). <https://doi.org/10.1103/PhysRevLett.116.020601>
61. P. Talkner, P. Hänggi, Phys. Rev. E **94**, 022143 (2016). <https://doi.org/10.1103/PhysRevE.94.022143>
62. C. Jarzynski, Phys. Rev. X **7**, 011008 (2017). <https://doi.org/10.1103/PhysRevX.7.011008>
63. M. Esposito, C. Van den Broeck, Euro. Phys. Lett. **95**, 40004 (2011). <https://doi.org/10.1209/0295-5075/95/40004>
64. S. Deffner, E. Lutz, [arXiv:1201.3888](https://arxiv.org/abs/1201.3888)
65. R. Landauer, IBM, J. Res. Dev. **5**, 183–191 (1961). <https://doi.org/10.1147/rd.53.0183>
66. L. del Rio, J. Aberg, R. Renner, O. Dahlsten, V. Vedral, Nature **474**, 61–63 (2011). <https://doi.org/10.1038/nature10123>
67. D. Reeb, M.M. Wolf, New J. Phys. **16**, 103011 (2014). <https://doi.org/10.1088/1367-2630/16/10/103011>
68. T. Sagawa, As a chapter of: G. Snider et al. (eds.), Energy Limits in Computation: A Review of Landauer’s Principle, Theory and Experiments. <https://doi.org/10.1007/978-3-319-93458-7>
69. À.M. Alhambra, L. Masanes, J. Oppenheim, C. Perry, Phys. Rev. X **6**, 041017 (2016). <https://doi.org/10.1103/PhysRevX.6.041017>
70. T.M. Cover, J.A. Thomas, *Elements of Information Theory* (Wiley, 2012). <https://doi.org/10.1002/047174882X>
71. P. Talkner, P.S. Burada, P. Hänggi, Phys. Rev. E **78**, 011115 (2008). <https://doi.org/10.1103/PhysRevE.78.011115>
72. K. Funo, H.T. Quan, Phys. Rev. Lett. **121**, 040602 (2018). <https://doi.org/10.1103/PhysRevLett.121.040602>
73. S. Deffner, O. Abah, E. Lutz, Chem. Phys. **375**, 200 (2010). <https://doi.org/10.1016/j.chemphys.2010.04.042>
74. E.H. Lieb, M.B. Ruskai, Phys. Rev. Lett. **30**, 434 (1973). <https://doi.org/10.1103/PhysRevLett.30.434>
75. D. Petz, Rev. Math. Phys. **15**, 79 (2003). <https://doi.org/10.1142/S0129055X03001576>

76. H. Spohn, J.L. Lebowitz, *Adv. Chem. Phys.* **38**, 109 (1978). <https://doi.org/10.1002/9780470142578>
77. F.G.S.L. Brandão, M. Horodecki, N.H.Y. Ng, J. Oppenheim, S. Wehner, *Proc. Natl. Acad. Sci. USA* **112**, 3275 (2015). <https://doi.org/10.1073/pnas.1411728112>
78. P. Faist, J. Oppenheim, R. Renner, *New J. Phys.* **17**, 045027 (2015). <https://doi.org/10.1088/1367-2630/17/4/043003>
79. H.-P. Breuer, F. Petruccione, *The Theory of Open Quantum Systems* (Oxford University Press, Oxford, 2002). <https://doi.org/10.1093/acprof:oso/9780199213900.001.0001>
80. T. Albash, S. Boixo, D.A. Lidar, P. Zanardi, *New J. Phys.* **14**, 123016 (2012). <https://doi.org/10.1088/1367-2630/14/12/123016>
81. S. Yukawa, [arXiv:cond-mat/0108421](https://arxiv.org/abs/cond-mat/0108421)
82. M. Esposito, K. Lndenberg, C. Van den Broeck, *New J. Phys.* **12**, 013013 (2010). <https://doi.org/10.1088/1367-2630/12/1/013013>
83. J.M. Horowitz, J.M.R. Parrondo, *New J. Phys.* **15**, 085028 (2013). <https://doi.org/10.1088/1367-2630/15/8/085028>
84. M. Silaev, T.T. Heikkila, P. Virtanen, *Phys. Rev. E* **90**, 022103 (2014). <https://doi.org/10.1103/PhysRevE.90.022103>
85. F. Liu, *Phys. Rev. E* **89**, 042122 (2014). <https://doi.org/10.1103/PhysRevE.89.042122>
86. F. Liu, *Phys. Rev. E* **93**, 012127 (2016). <https://doi.org/10.1103/PhysRevE.93.012127>
87. J.M. Horowitz, T. Sagawa, *J. Stat. Phys.* **156**, 55 (2014). <https://doi.org/10.1007/s10955-014-0991-1>
88. G. Manzano, J.M. Horowitz, J.M.R. Parrondo, *Phys. Rev. E* **92**, 032129 (2015). <https://doi.org/10.1103/PhysRevE.92.032129>
89. G. Manzano, J.M. Horowitz, J.M.R. Parrondo, *Phys. Rev. X* **8**, 031037 (2018). <https://doi.org/10.1103/PhysRevX.8.031037>
90. A.O. Caldeira, *An Introduction to Macroscopic Quantum Phenomena and Quantum Dissipation* (Cambridge University Press, Cambridge, 2014). <https://doi.org/10.1017/CBO9781139035439>
91. Y. Subasi, B.L. Hu, *Phys. Rev. E* **85**, 011112 (2012). <https://doi.org/10.1103/PhysRevE.85.011112>
92. L. Szilard, *Z. Phys.* **53**, 840 (1929). <https://doi.org/10.1007/BF01341281>
93. W.H. Zurek, in *Frontiers of Nonequilibrium Statistical Physics. NATO ASI Series (Series B: Physics)*, vol. 135, ed. by G.T. Moore, M.O. Scully (Springer, Boston, 1986). [arXiv:quant-ph/0301076](https://arxiv.org/abs/quant-ph/0301076)
94. S. Lloyd, *Phys. Rev. A* **39**, 5378 (1989). <https://doi.org/10.1103/PhysRevA.39.5378>
95. M.A. Nielsen, C.M. Caves, B. Schumacher, H. Barnum, *Proc. R. Soc. London A* **454**, 277 (1998). <https://doi.org/10.1098/rspa.1998.0160>
96. S.W. Kim, T. Sagawa, S. De Liberato, M. Ueda, *Phys. Rev. Lett.* **106**, 070401 (2011). <https://doi.org/10.1103/PhysRevLett.106.070401>
97. J. Bengtsson, M. Nilsson Tengstrand, A. Wacker, P. Samuelsson, M. Ueda, H. Linke, S.M. Reimann, *Phys. Rev. Lett.* **120**, 100601 (2018). <https://doi.org/10.1103/PhysRevLett.120.100601>
98. H.J. Groenewold, *Int. J. Theor. Phys.* **4**, 327 (1971). <https://doi.org/10.1007/BF00815357>
99. M. Ozawa, *J. Math. Phys.* **27**, 759 (1986). <https://doi.org/10.1063/1.527179>
100. F. Buscemi, M. Hayashi, M. Horodecki, *Phys. Rev. Lett.* **100**, 210504 (2008). <https://doi.org/10.1103/PhysRevLett.100.210504>
101. K. Jacobs, *Phys. Rev. A* **80**, 012322 (2009). <https://doi.org/10.1103/PhysRevA.80.012322>
102. M. Naghiloo, J.J. Alonso, A. Romito, E. Lutz, K.W. Murch, *Phys. Rev. Lett.* **121**, 030604 (2018). <https://doi.org/10.1103/PhysRevLett.121.030604>
103. W.H. Zurek, *Phys. Rev. A* **67**, 012320 (2003). <https://doi.org/10.1103/PhysRevA.67.012320>
104. K. Funo, Y. Watanabe, M. Ueda, *Phys. Rev. A* **88**, 052319 (2013). <https://doi.org/10.1103/PhysRevA.88.052319>
105. J.J. Park, K.-H. Kim, T. Sagawa, S.W. Kim, *Phys. Rev. Lett.* **111**, 230402 (2013). <https://doi.org/10.1103/PhysRevLett.111.230402>

106. D. Mandal, C. Jarzynski, Proc. Natl. Acad. Sci. USA **109**, 11641 (2012). <https://doi.org/10.1073/pnas.1204263109>
107. A. Chapman, A. Miyake, Phys. Rev. E **92**, 062125 (2015). <https://doi.org/10.1103/PhysRevE.92.062125>
108. P. Strasberg, G. Schaller, T. Brandes, M. Esposito, Phys. Rev. X **7**, 021003 (2017). <https://doi.org/10.1103/PhysRevX.7.021003>
109. Z. Gong, Y. Ashida, M. Ueda, PRA **94**, 012107 (2016). <https://doi.org/10.1103/PhysRevA.94.012107>
110. Y. Murashita, Z. Gong, Y. Ashida, M. Ueda, Phys. Rev. A **96**, 043840 (2017). <https://doi.org/10.1103/PhysRevA.96.043840>
111. J.V. Koski, V.F. Maisi, T. Sagawa, J.P. Pekola, Phys. Rev. Lett. **113**, 030601 (2014). <https://doi.org/10.1103/PhysRevLett.113.030601>
112. Y. Masuyama, K. Funo, Y. Murashita, A. Noguchi, S. Kono, Y. Tabuchi, R. Yamazaki, M. Ueda, Y. Nakamura, Nat. Commun. **9**, 1291 (2018). <https://doi.org/10.1038/s41467-018-03686-y>
113. R. Dorner, S.R. Clark, L. Heaney, R. Fazio, J. Goold, V. Vedral, Phys. Rev. Lett. **110**, 230601 (2013). <https://doi.org/10.1103/PhysRevLett.110.230601>
114. L. Mazzola, G. De Chiara, M. Paternostro, Phys. Rev. Lett. **110**, 230602 (2013). <https://doi.org/10.1103/PhysRevLett.110.230602>
115. P.A. Camati, R.M. Serra, Phys. Rev. A **97**, 042127 (2018). <https://doi.org/10.1103/PhysRevA.97.042127>
116. A. Bérut, A. Arakelyan, A. Petrosyan, S. Ciliberto, R. Dillenschneider, E. Lutz, Nature **483**, 187–189 (2012). <https://doi.org/10.1038/nature10872>
117. A. Bérut, A. Petrosyan, S. Ciliberto, Europhys. Lett. **103**, 60002 (2013). <https://doi.org/10.1209/0295-5075/103/60002>
118. E. Roldán, I.A. Martínez, J.M.R. Parrondo, D. Petrov, Nat. Phys. **10**, 457–461 (2014). <https://doi.org/10.1038/nphys2940>
119. Y. Jun, M. Gavrilov, J. Bechhoefer, Phys. Rev. Lett. **113**, 190601 (2014). <https://doi.org/10.1103/PhysRevLett.113.190601>
120. M. Gavrilov, J. Bechhoefer, Phys. Rev. Lett. **117**, 200601 (2016). <https://doi.org/10.1103/PhysRevLett.117.200601>
121. M. Gavrilov, R. Chétrite, J. Bechhoefer, Proc. Natl. Acad. Sci. USA **114**, 11097–11102 (2017). <https://doi.org/10.1073/pnas.1708689114>
122. J. Hong, B. Lambson, S. Dhuey, J. Bokor, Sci. Adv. **11**, e1501492 (2016). <https://doi.org/10.1126/sciadv.1501492>
123. M. López-Suárez, I. Neri, L. Gammaitoni, Nat. Commun. **7**, 12068 (2016). <https://doi.org/10.1038/ncomms12068>
124. J.P.S. Peterson, R.S. Sarthour, A.M. Souza, I.S. Oliveira, J. Goold, K. Modi, D.O. Soares-Pinto, L.C. Céleri, Proc. R. Soc. A **472**, 20150813 (2016). <https://doi.org/10.1098/rspa.2015.0813>
125. S. Toyabe, T. Sagawa, M. Ueda, E. Muneyuki, M. Sano, Nat. Phys. **6**, 988 (2010). <https://doi.org/10.1038/nphys1821>
126. J.V. Koski, A. Kutvonen, I.M. Khaymovich, T. Ala-Nissila, J.P. Pekola, Phys. Rev. Lett. **115**, 260602 (2015). <https://doi.org/10.1103/PhysRevLett.115.260602>
127. K. Chida, S. Desai, K. Nishiguchi, A. Fujiwara, Nat. Commun. **8**, 15310 (2017). <https://doi.org/10.1038/ncomms15301>
128. M.D. Vidrighin, O. Dahlsten, M. Barbieri, M.S. Kim, V. Vedral, I.A. Walmsley, Phys. Rev. Lett. **116**, 050401 (2016). <https://doi.org/10.1103/PhysRevLett.116.050401>
129. P.A. Camati, J.P.S. Peterson, T.B. Batalhão, K. Micadei, A.M. Souza, R.S. Sarthour, I.S. Oliveira, R.M. Serra, Phys. Rev. Lett. **117**, 240502 (2016). <https://doi.org/10.1103/PhysRevLett.117.240502>
130. N. Cottet, S. Jezouin, L. Bretheau, P.C. Ibarcq, Q. Ficheux, J. Anders, A. Auffèves, R. Azouit, P. Rouchon, Proc. Natl. Acad. Sci. **114**, 7561 (2017). <https://doi.org/10.1073/pnas.1704827114>

131. W.-B. Wang, X.-Y. Chang, F. Wang, P.-Y. Hou, Y.-Y. Huang, W.-G. Zhang, X.-L. Ouyang, X.-Z. Huang, Z.-Y. Zhang, L. He, L.-M. Duan, Chinese Phys. Lett. **35**, 040301 (2018). <https://doi.org/10.1088/0256-307X/35/4/040301>
132. M.A. Ciampini, L. Mancino, A. Orioux, C. Vigliar, P. Mataloni, M. Paternostro, M. Barbieri, npj Quantum Information **3**, 10 (2017). <https://doi.org/10.1038/s41534-017-0011-9>
133. T. Albash, D.A. Lidar, M. Marvian, P. Zanardi, Phys. Rev. E **88**, 032146 (2013). <https://doi.org/10.1103/PhysRevE.88.032146>
134. A.E. Rastegin, J. Stat. Mech. P06016 (2013). <https://doi.org/10.1088/1742-5468/2013/06/P06016>
135. A. Smith, Y. Lu, S. An, X. Zhang, J.-N. Zhang, Z. Gong, H.T. Quan, C. Jarzynski, K. Kim, New J. Phys. **20**, 013008 (2018). <https://doi.org/10.1088/1367-2630/aa9cd6>
136. D. Kafri, S. Deffner, Phys. Rev. A **86**, 044302 (2012). <https://doi.org/10.1103/PhysRevA.86.044302>
137. J. Goold, M. Paternostro, K. Modi, Phys. Rev. Lett. **114**, 060602 (2015). <https://doi.org/10.1103/PhysRevLett.114.060602>
138. S. Deffner, A. Saxena, Phys. Rev. Lett. **114**, 150601 (2015). <https://doi.org/10.1103/PhysRevLett.114.150601>
139. C. Jarzynski, H.T. Quan, S. Rahav, Phys. Rev. X **5**, 031038 (2015). <https://doi.org/10.1103/PhysRevX.5.031038>
140. L. Zhu, Z. Gong, B. Wu, H.T. Quan, Phys. Rev. E **93**, 062108 (2016). <https://doi.org/10.1103/PhysRevE.93.062108>
141. P. Solinas, S. Gasparinetti, Phys. Rev. E **92**, 042150 (2015). <https://doi.org/10.1103/PhysRevE.92.042150>
142. P.P. Hofer, A.A. Clerk, Phys. Rev. Lett. **116**, 013603 (2016). <https://doi.org/10.1103/PhysRevLett.116.013603>
143. M. Hayashi, H. Tajima, Phys. Rev. A **95**, 032132 (2017). <https://doi.org/10.1103/PhysRevA.95.032132>
144. M.P. Llobet, E. Bäumer, K.V. Hovhannisyan, M. Huber, A. Acin, Phys. Rev. Lett. **118**, 070601 (2017). <https://doi.org/10.1103/PhysRevLett.118.070601>
145. M. Lostaglio, Phys. Rev. Lett. **120**, 040602 (2018). <https://doi.org/10.1103/PhysRevLett.120.040602>
146. J. Åberg, Phys. Rev. X **8**, 011019 (2018). <https://doi.org/10.1103/PhysRevX.8.011019>
147. M. Rigol, V. Dunjko, M. Olshanii, Nature **452**, 854 (2008). <https://doi.org/10.1038/nature06838>
148. E. Iyoda, K. Kaneko, T. Sagawa, Phys. Rev. Lett. **119**, 100601 (2017). <https://doi.org/10.1103/PhysRevLett.119.100601>
149. K. Kaneko, E. Iyoda, T. Sagawa, Phys. Rev. E **96**, 062148 (2017). <https://doi.org/10.1103/PhysRevE.96.062148>

# Chapter 11

## Fluctuating Work in Coherent Quantum Systems: Proposals and Limitations



Elisa Bäumer, Matteo Lostaglio, Martí Perarnau-Llobet and Rui Sampaio

The aim of this short review is to discuss different proposals and definitions of fluctuating work in quantum systems, particularly in the presence of a superposition of energies in the initial state. This is an exciting topic that has recently received a lot of attention in the community of quantum thermodynamics [1, 2]. One can identify different motivations behind this research line:

1. Fluctuations are of the same order of magnitude as average quantities in microscopic systems [3]. As a consequence, the standard laws of thermodynamics, which are formulated for average quantities, are not enough to characterise the thermodynamics of nano-scale systems [4–7].
2. Fluctuations can be of an intrinsic nature in quantum systems, since due to quantum coherence there are states of maximal knowledge (pure states) for which our ability to predict the outcome of an energy measurement is very limited. As we are mostly concerned with energy considerations, we use the term “quantum

---

E. Bäumer (✉)

Institute for Theoretical Physics, ETH Zurich, Wolfgang-Pauli-Str. 27,  
8093 Zürich, Switzerland

e-mail: ebaeumer@itp.phys.ethz.ch

M. Lostaglio

ICFO-Institut de Ciències Fotoniques, The Barcelona Institute of Science and Technology,  
08860 Castelldefels (Barcelona), Spain  
e-mail: lostaglio@gmail.com

M. Perarnau-Llobet

Max-Planck-Institut für Quantenoptik, Hans-Kopfermann-Str. 1, 85748 Garching, Germany  
e-mail: marti.perarnau@mpq.mpg.de

R. Sampaio

QTF Center of Excellence, Department of Applied Physics, Aalto University, P.O. Box 11000,  
00076 Aalto, Finland  
e-mail: rui.ferreira.sampaio@aalto.fi

coherence” to express that a quantum state is in a superposition of different energy eigenstates (a “coherent state”, not to be confused with the standard notion from quantum optics).

3. Recent results suggest that quantum coherence and entanglement play a role in several thermodynamic tasks, such as heat engines [8–17] and work extraction [18–23], in some cases leading to potential enhancements [23–29] (see also Chap. 4)

It turns out, however, that even the definition of fluctuating work (and similarly heat) in the presence of quantum coherence is a challenging task. Roughly speaking, this is because thermodynamic quantities, such as heat and work, are associated to a process, rather than to a single time event. Hence, in order to deal with fluctuations, one wishes to build a stochastic theory for processes. In classical physics, this can be naturally done by identifying trajectories in phase space. However, given a quantum evolution in time, there is no unique notion of a quantum trajectory. A quantum trajectory can be built by measuring the system at different times. Nevertheless, the measurement of an observable affects the statistics of non-commuting observables one may need to access later [30].

The goal of this short review is to elaborate more on these subtle points, and to discuss some proposals that give different insights into the notion of quantum work. We are concerned with questions like: What is work in the quantum regime? Can we define and measure fluctuations in processes with quantum interference? Can the quantum measurement back-action be reduced? Let us start by giving a bit of context to these questions.

In classical systems, fluctuations of thermodynamic quantities have been studied extensively, leading to seminal results in the form of *Fluctuation Theorems* (FTs) (see e.g. [31] for a review). First attempts to extend FTs to the quantum regime were based on the identification of work as an observable (i.e. a Hermitian operator) [32–39], leading to corrections to the standard FTs. It was later recognized that the standard FTs could be obtained by defining fluctuating work as the difference between the outcomes of two projective energy measurements (TPM) [4, 5, 40–45]. The TPM scheme gives a clear operational and physical meaning to work, is applicable to both closed and open systems [46], has been implemented in different experimental set-ups [47–50], and one can define a natural correspondence with the classical definition of work [51, 52]. This makes the TPM scheme a standard definition of fluctuating work in quantum systems nowadays.

Despite its great success, recently several authors have pointed out limitations of the TPM scheme, especially when applied to initial coherent states [53–57]. Some of the most relevant ones are:

1. Projective energy measurements are difficult to implement in certain experimental set-ups. This has motivated alternative measurements of work based on noisy energy measurements [58, 59].
2. The quantum non-equilibrium free energy [60] can be additively decomposed into an incoherent and a coherent contribution [61, 62]. An energy measurement sets

the coherent contribution to zero, hence changing the non-equilibrium properties, e.g. decreasing the maximal average amount of extractable work (see Appendix).

3. More generally, the TPM scheme is invasive and can perturb the state it acts upon. In particular, the first energy measurement projects the initial state onto the energy eigenbasis, thus destroying possible off-diagonal terms. This prevents the possibility of capturing purely coherent evolutions, i.e., interference effects due to the initial coherence in the state.

It is important to note that these limitations affect only states with coherence, and that similar limitations appear in other measurement schemes; after all, all quantum measurements are invasive in some way, have a thermodynamic cost, and quantum systems are challenging to prepare, control and measure. At the same time, one hopes that complementary proposals for measuring work can capture new aspects and provide new insights in out-of-equilibrium situations. For example, recent proposals study the possibility of using weak measurements to define quantum trajectories [59, 63, 64].

In this review we focus on point 3, and discuss alternative proposals for defining and measuring work associated with purely coherent evolutions. These include Gaussian measurements [65–67], weak measurements and quasiprobabilities [53, 54, 68, 69], collective measurements [57] and Bohmian work [70]. We discuss specific proposals in the light of a recent no-go theorem that sets fundamental limitations on the possibility to design (non-invasive) work measurements [57], as well as connections between work distributions and quantum contextuality [71]. We use these no-go results as classification tools. Finally, we briefly discuss the possibility of defining (fluctuating) work by the state of an external system that acts as a work repository, which has been put forward in resource-theoretic approaches to thermodynamics [72–74] (see also Chap. 26 and Ref. [29] for an implementation of a heat engine with a work repository).

## 11.1 Classical Work

We start by briefly discussing the notion of fluctuating work in classical systems. Given the microscopic state of the system  $z = (q, p)$ , i.e., its position and momentum, the energy is defined to be the value that the Hamiltonian  $\mathcal{H}(z, t)$  takes for this state at time  $t$ . The work done on a system evolving under Hamilton's equations can then be defined<sup>1</sup> as the power integrated along the trajectory  $z_t$  followed by the system from time  $t = 0$  to  $t = \tau$ , i.e.,

$$w = \int_0^\tau dt \partial_t \mathcal{H}(z_t) = \mathcal{H}(z_\tau, \tau) - \mathcal{H}(z_0, 0), \quad (11.1)$$

---

<sup>1</sup>Depending on the system and quantity being measured one may use other work definitions. For a concise review see, e.g., Ref. [44]. For our considerations, however, this choice is inconsequential.

where  $z_\tau$  and  $z_0$  are the system's final and initial state, respectively. Hence, under closed (Hamiltonian) dynamics, the work is just the total change in the energy. The work distribution is then defined to be

$$p_{\text{clas.}}(w) := \int dz_0 p(z_0) \delta(w - (\mathcal{H}(z_\tau, \tau) - \mathcal{H}(z_0, 0))), \quad (11.2)$$

where  $p(z_0)$  is the initial distribution of position and momentum. This distribution is well-defined at all intermediate times of the evolution.

## 11.2 Quantum Work: Setting the Stage

When dealing with quantum systems, we extend the classical picture by considering a thermally isolated system, initially prepared in a quantum state  $\rho$  and with an internal Hamiltonian  $H(0)$ . The Hamiltonian can be externally driven leading to a time-dependent Hamiltonian  $H(t)$  between time 0 and  $\tau$ . We set

$$H(0) =: H = \sum_i E_i |E_i\rangle\langle E_i|, \quad H(\tau) =: H' = \sum_j E'_j |E'_j\rangle\langle E'_j|. \quad (11.3)$$

This leads to a unitary evolution of the system  $\rho(t) = U(t)\rho U^\dagger(t)$  with  $U(t) = \mathcal{T} \exp\left(-i \int_0^t ds H(s)\right)$  and  $\mathcal{T}$  the time-ordering operator. We are interested in the energy fluctuations between 0 and  $\tau$ , induced by the unitary evolution  $U := U(\tau)$ . Given a protocol  $\mathcal{P}$  (including the specification of  $\rho$  and  $U$ ) we will define by  $p(w|\mathcal{P})$  the corresponding work distribution. The choice  $\mathcal{P} = \mathcal{P}_{\text{TPM}}$  of the TPM scheme corresponds to the following steps:

1. Projective measurement of  $H$  on  $\rho$ , returning outcome  $E_i$  and post-measurement state  $|E_i\rangle\langle E_i|$ .
2. Unitary evolution  $|E_i\rangle\langle E_i| \mapsto U|E_i\rangle\langle E_i|U^\dagger$ .
3. Projective measurement of  $H'$  on  $U|E_i\rangle\langle E_i|U^\dagger$ , returning outcome  $E'_j$ .

The values of work  $w^{(ij)}$  and the associated probabilities  $p^{(ij)}$  are then given by

$$w^{(ij)} = E'_j - E_i, \quad p_{\text{TPM}}^{(ij)} = \langle E_i | \rho | E_i \rangle \left| \langle E'_j | U | E_i \rangle \right|^2. \quad (11.4)$$

Finally, in order to account for possible degeneracies in the work values  $w^{(ij)}$ , the work probability distribution is constructed as

$$p(w|\mathcal{P}_{\text{TPM}}) = \sum_{ij} p^{(ij)} \delta(w - w^{(ij)}). \quad (11.5)$$

Note the close analogy with the classical definitions (11.1) and (11.2). Note also that this scheme becomes invasive when  $[\rho, H] \neq 0$  and  $[H, U^\dagger H' U] \neq 0$ . In this case,

the statistics collected from the measurement of  $H'$  at time  $t = \tau$  does not return the same statistics one would have obtained if  $H$  was not measured at time  $t = 0$ . In particular,  $\sum_w w p(w|\mathcal{P}_{\text{TPM}})$  in general is not equal to the average energy change induced by  $U$  on  $\rho$ .

### 11.3 Limitations, No-Go Theorems, and Contextuality

In this section, we describe a no-go result from Ref. [57] which sets fundamental limitations on the possibility to design (non-invasive) work measurements. Rather than focusing on a particular approach, the idea is to consider an arbitrary measurement scheme  $\mathcal{P}$  to measure the amount of work necessary to perform  $U$ , and then show that three general requirements cannot be simultaneously satisfied. Later, this result will serve as a basis to classify different approaches to measure quantum work.

The three requirements put forward in Ref. [57] read:

1. The first requirement can be imposed in two equivalent ways (see Appendix A of Ref. [57]):
  - (a)  $p(w|\mathcal{P})$  is a linear probability distribution. This corresponds to the assumption that  $p(w|\mathcal{P})$  is a probability distribution  $p(w|\mathcal{P}) > 0$ ,  $\sum p(w|\mathcal{P}) = 1$ , linear under mixtures of  $\rho$ . Linearity is defined as: Let  $\mathcal{P}^i$ , with  $i = 0, 1, 2$ , be protocols differing only by the initial state  $\rho_i$ . Then, if  $\rho_0 = \lambda\rho_1 + (1 - \lambda)\rho_2$  with  $\lambda \in [0, 1]$ , we demand that  $p(w|\mathcal{P}^0) = \lambda p(w|\mathcal{P}^1) + (1 - \lambda)p(w|\mathcal{P}^2)$ . This corresponds to the natural requirement that, if we condition the choice of the protocol on a coin toss, the measured fluctuations are simply the convex combination of those observed in the individual protocols.
  - (b) There exists a Positive-Operator-Valued Measure (POVM), i.e., a set of positive operators  $\{\Pi_w\}$ , dependent on  $H$ ,  $H'$  and  $U$  but *not*  $\rho$ , that satisfy  $p(w|\mathcal{P}) = \text{Tr}(\rho\Pi_w)$  and  $\sum_w \Pi_w = \mathbb{I}$ .

To understand the relation between (a) and (b), note that if (b) is not satisfied, then one can apply different measurements to  $\rho_1$ ,  $\rho_2$  and  $\lambda\rho_1 + (1 - \lambda)\rho_2$ ; so that the corresponding work distribution will not in general be convex. For a formal proof of their equivalence, we refer the reader to the first section of the Supplemental Material of Ref. [57].

2. *Agreement with the TPM scheme for non-coherent initial states.* The second requirement is based on the assumption that the TPM scheme yields the correct statistics for diagonal states, i.e.

$$p(w|\mathcal{P}) = p(w|\mathcal{P}_{\text{TPM}}) \quad \forall \rho \text{ such that } [\rho, H] = 0. \quad (11.6)$$

This condition is motivated by the success of the TPM scheme in describing work fluctuations for diagonal states, in particular in fluctuation theorems, and by results concerning the recovery of the classical limit [51].

3. *Average energy changes are respected by the measurement process.* Finally, we demand that the average energy change predicted by  $\mathcal{P}$  equals the average energy change induced by  $U$  on  $\rho$ :

$$\sum_w w p(w|\mathcal{P}) = \text{Tr}(U\rho U^\dagger H') - \text{Tr}(\rho H) \quad \forall \rho. \quad (11.7)$$

Note that this is imposed for all states, including coherent states. With this requirement, we are essentially demanding that the measurement back action is small, so that average work is not modified by the measurement scheme used to build the work probability distribution. Equation (11.7) can be understood as the first law of thermodynamics, when applied to an isolated system undergoing the evolution  $U$ .

Note that in a general protocol  $\mathcal{P}$  the values of work  $w$  in  $p(w|\mathcal{P})$  do not need to correspond to  $w^{(ij)}$  of Eq. (11.4) and can be possibly continuous. We have

**Theorem 1** ([57] No-go for  $\mathcal{P}$ ) *There exists no protocol  $\mathcal{P}$  satisfying 1, 2 and 3 for all  $\rho$ ,  $U$ ,  $H$ ,  $H'$ .*

This result shows the inherent difficulty to construct a universal scheme to measure work applicable to all processes and states, including coherent ones. The TPM scheme, for example, satisfies assumptions 1 and 2, but 3 is satisfied only if  $[\rho, H] = 0$  and/or  $[H, UH'U^\dagger] = 0$ . It also suggests that the subtleties of quantum work fluctuations cannot be captured by a single measurement scheme (or definition), but rather different measurement schemes reveal different aspects of quantum work. In the next section, we discuss different approaches to the measurement of work fluctuations from the perspective of this no-go result, but before we discuss its relation with quantum contextuality.

### 11.3.1 Relation to Contextuality

A different angle from which we can investigate general protocols  $\mathcal{P}$  is in terms of the measurement statistics they can generate. The core question is the following: can the statistics collected by the thermodynamic experiment at hand be reproduced through a classical mechanism?

There are different ways of defining what we mean by *classical mechanism*. Clearly, the more liberal this notion, the higher the bar that we are setting to call a phenomenon *non-classical*. For example, one may call non-classical any system whose state is in a superposition of some preferred eigenstates (e.g., position or energy) or any entangled state – notions, however, not independent of quantum theory. Another choice would be to call non-classical any phenomenon that is not explained by classical mechanics and the classical theory of radiation. Here, we take a much more liberal approach and define non-classical any phenomenology that cannot be explained within a *non-contextual* model.

Non-contextuality is a notion of classically dating back to the famous no-go theorem of Kochen and Specker [75, 76], and used in recent years to identify the origin of quantum advantages in certain models of computation [77–79]. Here we use a rather broad notion of contextuality due to Spekkens [80]. Before we give a precise claim, this is in summary the relation between contextuality and Theorem 1 [71]:

- A protocol  $\mathcal{P}$  that reproduces the TPM scheme for diagonal states (assumption 2 holds) can probe non-contextuality *only if*  $p(w|\mathcal{P})$  is a quasi-probability or lacks convexity (assumption 1 is violated).
- There exists a weak measurement protocol satisfying assumptions 2 and 3, with  $p(w|\mathcal{P})$  linear in  $\rho$ , such that  $p(w|\mathcal{P}) < 0$  for some  $w$  is *sufficient* to prove contextuality.

The first point is a rephrasing of Theorem 1, and clarifies the role quasi-probabilities play within fluctuation theorems. The second point will be discussed together with alternative proposals later in the text.

### 11.3.1.1 An Alternative Formulation of the No-Go Theorem

Schematically, an experiment boils down to a set of instructions telling us how to set up the system, i.e. a *preparation procedure*  $P$ , and a set of instructions telling us how to implement a measurement on the system, i.e. a *measurement procedure*  $M$ . The measurement procedure  $M$  returns outcomes  $k$  when performed after the preparation procedure  $P$ , so that the experiment collects the statistics  $p(k|P, M)$ .

Two preparation procedures  $P$  and  $P'$  may be indistinguishable in terms of the statistics they produce, in the sense that  $p(k|P, M) = p(k|P', M)$  for every  $M$  and  $k$ . We denote this fact by  $P \sim P'$ . Similarly, two measurement procedures  $M$  and  $M'$  are indistinguishable when  $p(k|P, M) = p(k|P, M')$  for every  $k$  and every preparation procedure  $P$ , a fact that we denote by  $M \sim M'$ .

The observed statistics  $p(k|P, M)$  is explained by positing the existence of an underlying set of physical states  $\lambda$ , drawn from a set  $\Lambda$  and such that

- Every time we follow the instructions  $P$ , we sample  $\Lambda$  according to a distribution  $p(\lambda|P)$ ;
- Every time we measure according to  $M$ , the device returns outcome  $k$  with probability  $p(k|M, \lambda)$  if the physical state is  $\lambda$ .

The observed statistics is explained as  $p(k|P, M) = \sum_{\lambda \in \Lambda} p(\lambda|P)p(k|M, \lambda)$ . Such a model is called an *ontological model* or a *hidden variable model*. Most famously, certain statistics are incompatible with the assumption that  $\lambda$  behaves locally [81]. Non-contextuality, instead, is defined as follows:

**Definition 1** ([80]) An ontological model is called *non-contextual* if for any  $P, P'$  with  $P \sim P'$  one has  $p(\lambda|P) \equiv p(\lambda|P')$  and for any  $M, M'$  with  $M \sim M'$  one has  $p(k|M, \lambda) \equiv p(k|M', \lambda)$ .

In other words, non-contextuality posits that the reason why certain preparations and measurements cannot be operationally distinguished is that they are the same at the ontological level. While both locality and non-contextuality hold in any classical theory, it is known that they are violated by quantum experiments. Given these definitions, Theorem 1 gives:

**Corollary 2** ([71]) *Assume no degeneracies. Any protocol  $\mathcal{P}$  satisfying 1 and 2 admits a non-contextual ontological model for the preparation of  $\rho$  and the measurement of  $p(w|\mathcal{P})$ .*

This can be seen as a corollary of Theorem 1; in fact, Theorem 1 is proven by showing that assumptions 1 and 2 imply that the POVM  $\{\Pi_w\}$  must be the TPM POVM, and the latter is easily seen to admit a non-contextual model. This result leads us naturally to review alternative proposals in which  $p(w|\mathcal{P})$  is a work quasi-probability distribution or lacks linearity.

## 11.4 Definitions and Measurements of Quantum Work Fluctuations

In this section, we discuss several proposals for definitions of fluctuating work (some of them based on explicit measurement schemes) beyond the standard TPM scheme. There are protocols that define work probabilities (condition 1 is satisfied). As imposed by Theorem 1, either the average work does not match the average energy change of the unperturbed process, or the distribution disagrees with the TPM one for diagonal states. Some protocols provide nice tradeoffs between these two extremes. Another class of protocols does not satisfy assumption 1, either because they lead to a probability distribution that is non-linear or because they yield quasi-probabilities. These can satisfy both conditions 2 and 3, and Corollary 2 suggests some of them may be linked to contextuality. To give an overview, the different approaches described below are summarized in Table 11.1, where one can see which of the conditions are satisfied in each case.

### 11.4.1 Operator of Work

The operator of work was one of the first ways proposed to define quantum work fluctuations [32–39]. The basic idea is to take as a starting point Eq. (11.7), write the right hand side as  $\text{Tr}(\rho(U^\dagger H' U - H))$ , and define the work operator as

$$\hat{W} = U^\dagger H' U - H. \quad (11.8)$$

This operator is Hermitian, and hence can be diagonalised as  $\hat{W} = \sum_i \tilde{w}_i \Pi_i$ . The eigenvalues  $\tilde{w}_i$  are then identified with work values, and the corresponding probability reads  $\text{Tr}(\rho \Pi_i)$ . One then defines  $p_{\text{ow}}(w) = \sum_i \text{Tr}[\rho \Pi_i] \delta(w - \tilde{w}_i)$ .

**Table 11.1** This table summarizes the different approaches described in the following section except for the collective measurement, where the no-go result needs to be adapted. 😊 corresponds to “satisfied” and 😞 to “not satisfied”. The list also includes families of protocols in which either one of two conditions is satisfied in a specific limit, with the family interpolating between the two (  →  ). We denote this situation simply with two 😊. We can see that there is no approach satisfying all three conditions, as anticipated by Theorem 1.

Approach	Linear positive probability distribution (Condition 1)	TPM results for non-coherent initial states (Condition 2)	Mean work equals energy change (Condition 3)
TPM [4, 5, 40–45]	😊	😊	😊
Operator of work [32–39]	😊	😞	😊
Gaussian measurements [65–67]	😊	😊	😊
Full-Counting statistics [54, 82, 83]	😊	😊	😊
Post-selection schemes [71, 84]	😊	😊	😊
Weak values quasi-probability [53, 84–87]	😊	😊	😊
Consistent Histories [86, 88, 89]	😊	😞	😊
Quantum Hamilton-Jacobi [70]	😊	😞	😊
POVM depending on the initial state [90]	😊	😊	😊

By definition, the operator of work satisfies both conditions 1 and 3. However, it fails to satisfy condition 2. This is easy to see, e.g., just note that the work values  $\tilde{w}_i$  do not correspond to energy differences of the form  $E'_j - E_i$ , where  $E_i$ ,  $E'_j$  are eigenvalues of  $H$  and  $H'$ , respectively. In fact, while the operator of work is formally and operationally well defined, the interpretation of its fluctuations as work fluctuations is problematic. To illustrate this, suppose that  $\hat{W}$  has a zero eigenvalue and consider the corresponding eigenstate  $|\psi\rangle$  with  $\hat{W}|\psi\rangle = 0$  as an initial state  $\rho = |\psi\rangle\langle\psi|$ . One can still have  $\text{Tr}[U\rho U^\dagger H^m] \neq \text{Tr}[\rho H^m]$  for some  $m > 2$  and  $U$ . In other words, the energy distribution of the state can vary (implying some energy exchange) even if  $p_{\text{ow}}(w) = 0$  for  $w \neq 0$ , i.e. even if there are no fluctuations according to the operator of work [53].

### 11.4.2 Gaussian Measurement

To explore other schemes, it is important to investigate more carefully the role of the measurement apparatus. Many proposals interpolate between a regime in which the system interacts strongly with the measurement device, recovering the TPM distribution, and one in which the interaction is minimally invasive [65–67].

In Refs. [65–67], the projective measurements of the TPM scheme are replaced by a von Neumann measurement scheme in which the Hamiltonian is coupled to the position of a pointer state, also called a “work meter” (see Chap. 14 for more details).

The pointer is taken to be a one-dimensional continuous system with conjugate variables  $X$  and  $P$ , in the simplest case a pure Gaussian state initially prepared with  $\langle X \rangle = \langle P \rangle = 0$  and trivial covariance between  $X$  and  $P$ . A measurement is described by the interaction  $V = e^{igH \otimes P}$  (with  $g$  the effective interaction strength), followed by a projective measurement of the position  $X$  of the pointer. Each outcome  $x$  defines a corresponding POVM element  $M_x$  on the system, corresponding to a more or less invasive measurement depending on  $g$  and the initial spread of the pointer. Since  $V$  shifts the pointer position by  $gE_i$ , upon observing outcome  $M_x$  one can make the unbiased estimate of the system energy  $E = x/g$ . The scheme then consists of: von Neumann interaction  $V = e^{igH \otimes P}$ ; unitary evolution  $U$  on the system; von Neumann interaction  $V' = e^{-igH' \otimes P}$  with the same pointer; measurement of  $X$  on the pointer, which defines a work probability distribution  $p(w) = p(gx)$  (an alternative scheme adds a position measurement after the first system-pointer interaction [67]).

This protocol satisfies condition 2 only in the strong-measurement limit, when  $g$  is large/the pointer distribution is sharp; in this limit, the final measurement destroys all information about the coherences in the initial state (which can be seen by direct calculation of the distribution in Ref. [65]) and, in fact,  $p(w)$  coincides with the TPM distribution (see Chap. 14 for a similar discussion). For general coupling strength and a diagonal input, the work distribution  $p(w)$  is a convolution of a Gaussian (whose width depends on the width of the pointer) and the TPM distribution (Eq. 37 of Ref. [67]), i.e., essentially a “smeared” version of the TPM distribution. Conversely, in the weak-measurement limit (where  $g$  is small/the pointer distribution is broad), the back action is suppressed and condition 3 is satisfied (Eq. 47 of Ref. [67]); however, condition 2 is not. Furthermore, in this regime work fluctuations diverge as the measurement is completely imprecise [67]. We see Theorem 1 in action in the mutual incompatibility between 3 and 2, given 1.

### 11.4.3 Full Counting Statistics

The above considerations lead to a different class of proposals. For general states and in the weak measurement limit,  $p(w)$  is a convolution of a Gaussian and a function  $q(w)$ , i.e. a “smeared” version of  $q(w)$  (Eq. 55 of Ref. [67]):

$$q(w) = \sum_{n,n',m} \langle E_n | \rho | E_{n'} \rangle \text{Tr}[|E_n\rangle\langle E_{n'}| U^\dagger |E'_m\rangle\langle E'_m| U] \delta\left(w - \left(E'_m - \frac{E_n + E_{n'}}{2}\right)\right), \quad (11.9)$$

where  $\delta(x - y) = 0$  unless  $x = y$ , in which case it equals 1. The characteristic function of  $q(w)$  can be accessed by the same scheme described for  $p(w)$ , with the difference one measures the relative phase accumulated by momentum eigenstates of the pointer rather than its position (an approach known as Full Counting Statistics, see Ref. [54, 82, 83]). This approach is rooted in the Keldysh formalism and, ultimately, in the idea of assigning a joint distribution to non-commuting observables [69].

$q(w)$  has several interesting properties, and in Ref. [82] it was proposed as a work quasi-probability. In general,  $q(w)$  equals the TPM distribution plus corrections that depend on the coherence of the initial state and are zero otherwise (Eq. 57 of Ref. [67]). Hence, for diagonal states  $q(w)$  equals the TPM distribution and condition 2 is satisfied. Furthermore,  $q(w)$  satisfies condition 3. As we know from Theorem 1, condition 1 cannot hold. Hence, since  $q(w)$  is linear, it must be a work quasi-probability. Further considerations on this scheme can be found in Ref. [68], and see also Ref. [83] for discussions on the role of coherence.

#### 11.4.4 Post-selection and Weak Values

Another proposal to assign a joint distribution to  $H$  and  $U^\dagger H' U$  can be obtained from a modification of the scheme described for  $p(w)$ . Specifically, one can define a work quasi-probability as the weak value of  $|E_k\rangle\langle E_k|$  with pre-selection  $\rho$  and post-selection  $|E'_m\rangle$ , where  $w = E'_m - E_k$  [84]. Given a pure Gaussian pointer state with spread  $s$ , the scheme is as follows: (1) the first pointer interaction is  $V_k = e^{is|E_k\rangle\langle E_k| \otimes P}$ ; (2) Measurement of  $X$  on the pointer, which defines a POVM  $M_x^{(k)}$  on the system; (3) unitary evolution  $U$  on the system; (4) Projective measurement of  $H'$  on the system. For more details see Ref. [71], Supplemental Material Sect. B. Consider now the probability  $p(E'_m)$  of observing outcome  $E'_m$  in the final measurement, independently of the observed pointer position. Multiply this by the average position of the pointer given that  $m$  is observed, denoted by  $\langle X \rangle_{|E'_m}$ . On the one hand, if step (1) is a strong measurement,  $p(E'_m)\langle X \rangle_{|E'_m}$  gives the TPM probability  $p_{\text{TPM}}^{(km)}$  of Eq. (11.4) (note in this limit the intuition of the quantity  $\langle X \rangle_{|E'_m}$  as a conditional probability for the initial energy being  $k$  given that the final energy is  $m$ :  $\langle X \rangle_{|E'_m} \rightarrow |\langle E'_m | U | E_k \rangle|^2 \langle E_k | \rho | E_k \rangle / p(E'_m)$  [71]). On the other hand, if step (1) is a weak measurement,  $p(E'_m)\langle X \rangle_{|E'_m}$  returns the Margenau-Hill work quasi-probability  $p_{MH}(k, m)$ :

$$p_{MH}(k, m) := \text{ReTr}[\rho |E_k\rangle\langle E_k| U^\dagger |E'_m\rangle\langle E'_m| U]. \quad (11.10)$$

where  $\text{Re}(x)$  takes the real part of  $x$ . One then defines  $p_{MH}(w) := \sum_{k,m} p_{MH}(k, m) \delta(w - (E'_m - E_k))$ . This was first put forward as a work quasi-probability by Allahverdyan [53], and from the above scheme one can recognize it as the (generalized) weak value [84, 85] of  $|E_k\rangle\langle E_k|$  with post-selection  $U^\dagger |E'_m\rangle\langle E'_m| U$ .  $p_{MH}(w)$  can also be derived from a consistent histories approach [86] and can be understood as an “optimal” estimate of the initial energy given the observation of the final energy and the knowledge of the initial state [87]. The marginals of  $p_{MH}$  correspond to the energy distributions of  $H$  and  $U^\dagger H' U$  on  $\rho$ , so condition 3 is satisfied.  $p_{MH}$  also coincides with the TPM distribution for diagonal states, hence it satisfies condition 2. By Theorem 1, condition 1 cannot hold, and indeed  $p_{MH}$  can become negative [53]. Finally, note that since the variance of  $X$  diverges in the weak measurement limit, this scheme requires repeated measurements on a large number of copies of  $\rho$ . Furthermore, the interaction unitary  $V_k$  has to be changed to access  $p_{MH}(w)$  for various values of  $w$ .

#### 11.4.4.1 Contextualy Proofs from Weak Values Work Quasi-probability

Corollary 2 tells us that among the family of distributions satisfying condition 2, negativity or more precisely the failure of condition 1 is a prerequisite to witness contextuality. Is it also sufficient? For the work quasi-probability  $p_{MH}(w)$ , the following theorem gives a positive answer to this question:

**Theorem 3** ([71]) *If  $p_{MH}(k, m) < 0$  for some  $E'_m$ ,  $E_k$ , if the pointer has spread s large enough there exists no non-contextual ontological model for preparation of  $\rho$ , measurement of  $M_x^{(k)}$ , unitary evolution  $U$  and post-selection of  $|E'_m\rangle\langle E'_m|$ .*

The theorem clarifies that negative values of the work quasi-probability  $p_{MH}$  are proofs of contextuality and hence witness non-classicality. This is due to the fact that these negative values are a generalisation of the so-called anomalous weak values, and the latter are known to be proofs of contextuality [91]. It is an open question if other work quasi-probabilities are associated to proofs of contextuality. Finally, we note that anomalous weak values have also been connected to violations of Leggett-Garg inequalities [54, 92–94].

#### 11.4.5 Consistent Histories

Recently, Miller and Anders [86] proposed a time-reversal symmetric work distribution based on the Consistent Histories (CH) interpretation of quantum mechanics [88, 89]. In this approach, work is associated with the histories of the power operator in Heisenberg picture  $X_H(t) \equiv U^\dagger(t)\partial_t H(t)U(t)$ , where recall that  $H(t)$  is the Hamiltonian of the system at time  $t$  and  $U(t)$  is the evolution operator from time 0 to  $t$ . The Hilbert space is taken to be finite of dimension  $d$ . Time is discretized into a grid of  $K + 1$  equally spaced points  $\{0, t_1, \dots, t_j, \dots, t_K\}$  and at each time point the spectral decomposition of  $X_H(t_j) = \sum_{n=1}^d x_n^{(j)} P_n^{(j)}$  is used to build a trajectory  $\mathbf{n} = (x_{n_0}, \dots, x_{n_j}, \dots, x_{n_K})$ . Here,  $\{P_n^{(j)}\}_{n=1}^d$  is a complete set of orthonormal projectors decomposing  $X_H(t_j)$ , with the corresponding eigenvalues  $\{x_n^{(j)}\}_{n=1}^d$ . Each trajectory  $\mathbf{n}$  is associated with a class operator  $C_{\mathbf{n}} = \overleftarrow{\mathcal{T}} \prod_{j=0}^K P_{n_j}^j$  which defines the trajectory quasi-probability  $p_{\mathbf{n}} \equiv \text{Tr}\{(C_{\mathbf{n}}^\dagger + C_{\mathbf{n}})\rho\}/2$ , where  $\rho$  is the initial state and  $\overleftarrow{\mathcal{T}}$  is the time-ordering operator, arranging the terms from right to left with increasing time. The work for a given trajectory  $\mathbf{n}$  is then defined to be  $w_{\mathbf{n}} = \sum_{j=1}^{K-1} x_{n_j}^{(j)} \Delta t$ , where  $\Delta t$  is the time step of the grid. Finally, the work quasi-probability  $p_{CH}(w)$  is given by grouping the trajectories into *histories*, such that,  $p_{CH}(w) = \text{Tr}\{(C_w^\dagger + C_w)\rho\}/2$ , where  $C_w = \sum_{\mathbf{n}} C_{\mathbf{n}} \delta(w - w_{\mathbf{n}})$  and  $\delta(x - y)$  is equal to one if  $x = y$  and zero otherwise.

The distribution respects the average energy change of the unperturbed process (requirement 3) but, in general, does not agree with the TPM scheme for initial diagonal states. In addition, the work distribution admits a notion of time-reversal symmetry, namely it respects  $\tilde{p}_{CH}(w) = p_{CH}(-w)$ , where  $\tilde{p}_{CH}(w)$  is the “time-reversed

work distribution”, constructed from the time-reversed process. Unitary processes are time-symmetric and it may be argued that the work distribution should reflect this symmetry [86]. In the present case,  $\tilde{p}_{\text{CH}}(w)$  is described by reversing the trajectory  $\mathbf{n}$ , which leads to the time-reversed class operator  $\tilde{C}_w = C_{-w}^\dagger$ . It then follows that  $\tilde{p}_{\text{CH}}(-w) = p_{\text{CH}}(w)$ . As a final remark, in the continuous limit  $K \rightarrow +\infty$ , we have that  $\sum_w w^k p_{\text{CH}}(w) = \text{Tr}(\rho \hat{W}^k)$  where  $\hat{W}$  is the work operator. However, note that  $p_{\text{CH}}(w)$  and  $p_{\text{OW}}(w)$  can be very different, as  $p_{\text{CH}}(w)$  is in general a quasi-probability distribution and it is non-zero over a different set of  $w$  [86].

### 11.4.6 Hamilton-Jacobi Equation

Consider a pure state  $\psi(q, t) = R^{(\psi)}(q, t)e^{iS^{(\psi)}(q, t)/\hbar}$ . Another alternative [70] is based on the Hamilton-Jacobi formulation of the Schrödinger equation, namely,

$$-\partial_t S^{(\psi)}(q, t) = \frac{p^{(\psi)}(q, t)^2}{2m} + V(q, t) + \mathcal{Q}^{(\psi)}(q, t); \quad (11.11)$$

$$\partial_t \rho^{(\psi)}(q, t) = -\nabla j^{(\psi)}(q, t), \quad (11.12)$$

where  $S^{(\psi)}(q, t)/\hbar \in \mathbb{R}$  is the overall phase of the state  $\psi$ ,  $p^{(\psi)}(q, t) \equiv \nabla S^{(\psi)}(q, t)$ ,  $\rho^{(\psi)}(q, t) \equiv R^{(\psi)}(q, t)^2$  is the probability density,  $j^{(\psi)}(q, t) \equiv \rho^{(\psi)}\nabla S^{(\psi)}/m$  is the probability current density and  $\mathcal{Q}^{(\psi)} \equiv -\hbar^2 \nabla^2 R^{(\psi)}/2m R^{(\psi)}$  is the so-called quantum potential. Since Eq. (11.11) is an Hamilton-Jacobi equation, one identifies the energy as  $E^{(\psi)}(q, t) \equiv -\partial_t S^{(\psi)}(q, t)$ . One can formally construct a Hamiltonian function  $\mathcal{H}^{(\psi)}(q, p, t) = p^2/2m + V(q, t) + \mathcal{Q}^{(\psi)}(q, t)$  that generates the flow lines in phase space  $\dot{q} = \partial_p \mathcal{H}$  and  $\dot{p} = -\partial_q \mathcal{H}$ . Thus, Eqs. (11.11) and (11.12) describe the evolution of a statistical ensemble of point particles in phase, which is closely connected to the Bohmian [95, 96] or Pilot-Wave [97] interpretations of quantum mechanics. A notable difference from the classical case is the single-valuedness of the  $S$  function and that all quantities are fully determined in configuration space, since the momentum of a particle at position  $q$  in a state  $\psi(q, t)$  is fixed to be  $p^{(\psi)}(q, t)$ . In other words, while in classical mechanics the state is completely determined by specifying position and momentum, in Bohmian mechanics, the state is specified by the position and wave function. A detailed description can be found in textbooks, e.g., Refs. [98, 99].

For unitary evolution, work can then be defined in a manner fully analogous to the classical case (see Introduction), namely,  $W^{(\psi)}[q_\tau] = \mathcal{H}^{(\psi)}(q_\tau, \tau) - \mathcal{H}^{(\psi)}(q_0, 0)$ . If the system is initially prepared in a state  $\psi$ , the work distribution is simply  $P(W; \psi) = \int dq |\psi(q, 0)|^2 \delta(W - W^{(\psi)}[q_\tau])$ . If the system is explicitly prepared in a statistical mixture of pure states<sup>2</sup>  $\{\psi_j\}_{j=1}^N$  with distribution  $\{p_j\}_{j=1}^N$ ,  $p_j > 0$ ,  $\sum_{j=1}^N p_j = 1$ , the

---

<sup>2</sup>We take the distribution to be discrete for simplicity sake.

work distribution is just the convex sum of the individual distribution, i.e.,  $P(W) = \sum_{j=1}^N p_j P(W; \psi_j)$ .

The work distribution is positive and respects the average energy change of the unperturbed process (requirement 3). Agreement with the TPM scheme is verified when the measurement steps do not affect the state significantly, see Ref. [70] for details. The main conceptual difference from the previous approaches, apart from the phase-space description, is that it is defined for wave functions rather than density operators. As a consequence, the work is explicitly dependent on the way the system is physically prepared or measured, that is, on the experimental details of the implementation of the protocol. In Ref. [70] an example is given for which different statistical mixtures of pure states corresponding to the same density operator give rise to different work distributions. These are experimentally accessible via weak measurement schemes [100–104] if a decomposition is explicitly selected, e.g. by a corresponding measurement that separates  $\rho$  into pure state components, as also discussed in Ref. [37]. If the system is initially entangled with other degrees of freedom, then the work distribution can be experimentally accessed only through measurements on the overall pure state, which might not be known if all the empirically accessible information is that of the reduced density operator. Nonetheless, one may still define a coarse-grained work based on the available information, but this falls outside the scope of this review. Similarly to other approaches not satisfying condition 2, it is an interesting open question how and if one can recover the appropriate classical limit.

Although quantitatively different, this approach shares many qualitative similarities to a “sub-ensemble” approach, as proposed in Ref. [37]. There, the initial state described by a density operator  $\rho$  is first split into pure states ensembles  $\{|\psi_\alpha\rangle\langle\psi_\alpha|\}_{\alpha=1}^N$ , with probabilities  $\{\lambda_\alpha\}_{\alpha=1}^N$ , such that  $\rho = \sum_{\alpha=1}^N \lambda_\alpha |\psi_\alpha\rangle\langle\psi_\alpha|$ . The fluctuating work is taken to be the change in the energy expectation value for each element of the sub-ensemble. Similar properties include, e.g., positive work distribution, average work equal to unperturbed average energy change (condition 3), ensemble dependence and non-convexity under mixtures of  $\rho$ . The main difference is that from the Hamilton-Jacobi perspective the individual states  $|\psi_\alpha\rangle\langle\psi_\alpha|$  are treated as representing another sub-ensemble of point-particles trajectories. From this perspective, the sub-ensemble approach can be viewed as a coarse-graining of the Hamilton-Jacobi approach.

### 11.4.7 POVM Depending on the Initial State

Another logical possibility is to look at measurement schemes that depend on the initial state. We have seen before that the two-projective-measurement scheme (TPM) does not satisfy condition 3 on non-diagonal states. This is because the TPM scheme projects onto the basis of the Hamiltonian and thereby destroys all coherence, so that the state to which the unitary is applied is not the initial one. However, if the initial state is known, one can always determine the basis in which it is diagonal and conduct

a projective measurement onto that basis. Then, no coherence is destroyed during the first measurement and a probability distribution that satisfies both conditions 2 and 3 can be obtained. However, the dependence on the initial state directly violates condition 1, in accordance to Theorem 1. In particular, the resulting probability distribution is not convex. We note that this kind of measurement schemes have been formally considered to obtain general fluctuation theorems [90]; however, when the initial  $\rho$  does not commute with the Hamiltonian the physical meaning of the statistics becomes unclear [90]. In particular, there is no clear recipe to assign an energy or work cost to a transition between two pure states that are in coherent superpositions of energies.

### 11.4.8 Collective Measurements

Another approach, aiming at reducing the measurement back-action of the TPM scheme, is to apply a collective measurement on  $N$  copies of the state, each of them undergoing the same unitary evolution. This possibility has been considered in Ref. [57]. Since the measurement acts on  $N$  copies, it is convex on the whole state  $\rho^{\otimes N}$ , but it is not anymore convex at the local level of  $\rho$ . For global measurements, one can naturally adapt the conditions of the no-go theorem as [57]:

1. *POVM.* There exists a Positive-Operator-Valued Measure (POVM), i.e., a set of positive operators  $\Pi_w$ , dependent on  $H$ ,  $H'$  and  $U$  but *not*  $\rho$ , that satisfies  $p(w|\mathcal{P}) = \text{Tr}(\rho^{\otimes N} \Pi_w)$  and  $\sum_w \Pi_w = \mathbb{I}$ . Note that the  $\Pi_w$  in this case are matrices with dimension  $d^N \times d^N$ , where  $d$  is the local dimension of  $\rho$ . This gives a much bigger freedom to the measurement scheme.
2. *Agreement with the TPM scheme for non-coherent states.* The  $N$ -copies protocol recovers the single-copy TPM scheme for diagonal states, i.e.,  $\text{Tr}(\rho_{\text{diag}}^{\otimes N} \Pi^{(i)}) = \text{Tr}(\rho_{\text{diag}} \Pi_{\text{TPM}}^{(i)}) \quad \forall \rho_{\text{diag}}$  such that  $[\rho_{\text{diag}}, H] = 0$ .
3. *Average energy changes are respected by the measurement process.* The  $N$ -copies average energy change equals the single-copy average energy change induced by  $U$  on  $\rho$ :

$$\sum_w w \text{Tr}(\rho^{\otimes N} \Pi_w) = \text{Tr}(U \rho U^\dagger H) - \text{Tr}(\rho H) \quad \forall \rho. \quad (11.13)$$

It was shown in Ref. [57] that it is still impossible to satisfy these weaker requirements simultaneously. That is, even when considering global measurements, there is an intrinsic back-action in measurements of quantum work. Nevertheless, global measurements allow for improvements, in the sense that one can design measurements on  $\rho^{\otimes N}$  that satisfy 1. and 2. exactly, and lead to an average energy that is closer to satisfying Eq. (11.13) as compared to the single-copy case. In particular, the following collective measurement scheme on two copies of the state has been suggested in [57]:

$$M_{\lambda}^{(ij)} = |i\rangle\langle i| \otimes \left( \langle i|T_j|i\rangle \mathbb{I} + \lambda T_j^{\text{off-diag}} \right), \quad (11.14)$$

where  $T_j = U^\dagger |j'\rangle\langle j'|U$ ,  $T_j^{\text{off-diag}}$  is the off-diagonal part of  $T_j$  in the basis of  $H$ , and  $\lambda \in [0, 1]$  is a parameter that can depend on the specific  $U$  [57]. The  $M_{\lambda}^{(ij)}$  are POVM elements acting on two copies of the state, so that  $P_{\lambda}^{(ij)} = \text{Tr}(M_{\lambda}^{(ij)} \rho^{\otimes 2})$  is the probability assigned to the work cost  $w^{(ij)}$  as given in (11.4). This collective measurement scheme has some appealing properties:

- It satisfies conditions 1. and 2. exactly. The first condition is satisfied by noting that (11.14) are POVM elements, and the second one follows from  $\text{Tr}(\rho^{\text{diag}} T_j^{\text{off-diag}}) = 0$ .
- The second term of (11.14) brings information about the purely coherent part of the evolution, hence extending the standard TPM scheme to partly describe coherent evolutions.
- The global measurement (11.14) can be expressed as two independent measurements on each copy of  $\rho$ , specifically a projective energy measurement on the first copy, and a non-projective measurement on the second copy that depends on  $U$ . By measuring each copy separately, one before and one after the evolution, the measurement back-action can be reduced.

These properties make collective measurements an interesting possibility to extend the TPM scheme to capture some of the subtle effects of coherent evolutions. Notably, the collective measurement (11.14) has been recently implemented experimentally in a photonic set-up.

In the classical limit  $N \rightarrow \infty$  one can get arbitrarily close to satisfying all requirements; in fact, taking  $H_N = \sum_i H^{(i)}/N$  ( $X^{(i)}$  denotes  $X$  in the Hilbert space of particle  $i$  and identity elsewhere) and  $\tilde{H}'_N = \sum_i U^{\dagger(i)} H'^{(i)} U^{(i)}/N$ , one gets  $[H_N, \tilde{H}'_N] \propto 1/N$ ; in other words, since all average observables commute in the asymptotic limit, and since  $\text{Tr}(U\rho U^\dagger H) - \text{Tr}(\rho H) = \text{Tr}(\rho^{\otimes N} \tilde{H}'_N) - \text{Tr}(\rho^{\otimes N} H_N)$ , non-commutativity becomes increasingly irrelevant: the TPM scheme satisfies all three assumptions arbitrarily well in the limit. However, this does not solve the issue for the thermodynamics of a small number of quantum systems.

### 11.4.9 Beyond Work Distributions

A new promising approach developed a fully quantised version of the protocols described above [72, 74]. Specifically, one can treat the work reservoir as a quantum system, rather than assume a classical external system. Furthermore, one can explicitly model a switch responsible for the change in the system Hamiltonian from  $H$  to  $H'$  (the overall Hamiltonian is time independent, but the switch induces an effective time-dependent Hamiltonian on the system). One can then impose that the overall dynamics is unitary and conserves energy. In this way the work reservoir, as well as

providing the energy necessary for the transformation, also behaves as a quantum probe for the system dynamics.

For states that are initially thermal, fluctuation-like theorems can then be written for the quantum channel induced on the work source, a quantum version of the standard theorems for  $p(w|\mathcal{P})$ . These can be tested by process tomography. The standard fluctuation theorems are recovered by looking at the evolution of the diagonal part of the work reservoir, under an additional assumption, i.e. energy translation invariance of the dynamics of the work reservoir. This assumption captures the idea that only displacements in energy of the work reservoir should matter for the definition of work. A Jarzynski equality can be verified by a TPM scheme on the work reservoir, thanks to the decoupling of diagonal and off-diagonal dynamics of the work reservoir (which follows from overall energy conservation and the assumption that the initial state of the system is thermal). Further relations hold for the evolution of the off-diagonal elements of the work reservoir. These results, and an extension to arbitrary initial states described through conditional fluctuation theorems [74], may provide a new avenue to the study of work fluctuations for coherent initial states. For further information, see also Chap. 12.

## 11.5 Outlook

The standard approach to measure work fluctuations, consisting of two projective energy measurements (TPM) before and after the evolution, becomes invasive when the initial state is coherent. This prevents the possibility of capturing interference effects arising due to the coherence in the initial state. This observation has motivated several proposals for measurements (or definitions) of work beyond the standard TPM scheme [53, 54, 57, 67–72, 74, 86]. The goal of this short review has been to put together these works in order to gain a global perspective of the topic.

As discussed in Ref. [57], the three desiderata (1) Convexity and existence of a work probability distribution, (2) Recovery of the TPM work distribution for non coherent input states, (3) Respecting the identification of average work as average energy change in the unitary process, are mutually incompatible. Furthermore, (1) and (2) alone are incompatible with the possibility of witnessing contextuality [71], a distinctive property of quantum phenomena that has been connected to quantum advantages in the realm of computation [77, 78]. Here, we have used these impossibility results to understand and classify the different definitions of work fluctuations in coherent evolutions, even though we also mentioned some notable proposals that are not captured within this framework [72, 74].

The first conclusion one can draw is that while classically there is a single definition of work for closed system evolutions, there are multiple relevant definitions of work for quantum systems (as also discussed in Chap. 14). Rather than focusing on the question of what is *the* quantum work, our view is that the relevant questions should be more pragmatic. For a given scheme, what information is encoded in the corresponding work (quasi) probability distribution? What results exist connecting

the features of such quantum work distribution to the underlying properties of the quantum process? Can the obtained statistics be simulated in classical systems (see Refs. [71, 93, 105])? If they cannot, can this lead to any genuine quantum advantage in thermodynamic tasks? Finally, can one construct fluctuation theorems for out-of-equilibrium coherent states (see [53, 68, 74] for first attempts) and, more importantly, what is their physical meaning? We hope the results discussed here provide a solid starting point to address these questions, and motivate further research in this direction.

While many partial results appeared in the literature pointing at potential quantum advantages [23–29, 106], proving a clear-cut departure from the classical world view is a necessary condition to identify any truly quantum advantage. What do we mean here by “truly”? We mean an advantage proved under very weak modelling assumptions, such as locality in Bell inequalities [107] or certain operational equivalences for contextuality [108]. This allows to pinpoint genuine quantum phenomena through a rigorous no-go theorem, as apparently quantum behaviours can often be reproduced by classical models, also in thermodynamic contexts [15].

While showing that a phenomenon defies classical explanations in a broad sense is a necessary condition for any truly quantum advantage, it is by no means sufficient. Here, quantum work distributions could provide a useful bridge, since on the one hand they may be related to thermodynamically relevant quantities, while on the other hand they may be associated to non-classicality proofs [54, 71, 93, 94]. It is in this role of probes of the behaviour of quantum systems that quantum work distributions may be most useful in helping us to identify a provable advantage of a thermodynamic protocol over its classical counterparts. Ultimately, this remains one of the most important questions posed by quantum thermodynamics.

**Acknowledgements** We thank Johan Åberg, Armen Allahverdyan, Janet Anders, Peter Hänggi, Simone Gasparinetti, Paolo Solinas and Peter Talkner for useful feedback on the manuscript. E.B. acknowledges contributions from the Swiss National Science Foundation via the NCCR QSIT as well as project No. 200020\_165843. M.P.-L. acknowledges support from the Alexander von Humboldt Foundation. M.L. acknowledges financial support from the European Union’s Marie Skłodowska-Curie individual Fellowships (H2020-MSCA-IF-2017, GA794842), Spanish MINECO (Severo OchoaSEV-2015-0522 and project QIBEQI FIS2016-80773-P), Fundacio Cellex and Generalitat de Catalunya (CERCAProgramme and SGR 875). R. S. acknowledges the Magnus Ehrnrooth Foundation and the Academy of Finland through its CoE grants 284621 and 287750. All authors are grateful for support from the EU COST Action MP1209 on Thermodynamics in the Quantum Regime.

## Appendix: Loss in Maximal Amount of Average Extractable Work Due to Energy Measurement

The maximal average amount of work that can be extracted from a quantum system in state  $\rho$  with internal Hamiltonian  $H_S$  and unitary operations on systems and a thermal bath at temperature  $T$  is

$$\langle W \rangle_{max}(\rho) = F(\rho, H_S) - F(\tau, H_S) \equiv kTS(\rho||\tau), \quad (11.15)$$

where  $\tau = \frac{e^{-\beta H_S}}{Z}$ ,  $Z = \text{Tr}[e^{-\beta H_S}]$ ,  $\beta = 1/(kT)$  with  $k$  Boltzmann constant,  $F(X, H) = \text{Tr}[HX] - kTS(X)$  with  $S(X) := -\text{Tr}[X \log X]$  the von Neumann entropy,  $S(X||Y) := \text{Tr}[X(\log X - \log Y)]$  the quantum relative entropy.

The result (11.15) can be inferred from, e.g., the derivations in [60, 109–111]. However, for clarity of the exposition, we present here a simple proof. Consider a bipartite system  $SB$  with an initial non-interacting Hamiltonian

$$H = H_S + H_B, \quad (11.16)$$

prepared in a product state

$$\rho_{SB} = \rho_S \otimes \rho_B, \quad (11.17)$$

with  $B$  a Gibbs state at inverse temperature  $\beta = (kT)^{-1}$ :

$$\rho_B = \tau_B = \frac{e^{-\beta H_B}}{\mathcal{Z}}. \quad (11.18)$$

Hence we can think of  $B$  as an auxiliary thermal state. Note that  $B$  is not necessarily a thermal bath, in the sense that it may not be macroscopic. We now consider a generic closed evolution in  $SB$ , which can always be described as a unitary operation  $U$ :

$$\rho'_{SB} = U\rho_S \otimes \rho_B U^\dagger, \quad (11.19)$$

The average extracted work is given by the energy change on  $SB$ ,

$$W = \text{Tr}[H\rho_{SB}] - \text{Tr}[H\rho'_{SB}] = F(\rho_{SB}, H) - F(\rho'_{SB}, H), \quad (11.20)$$

where we assumed that at the end of the interaction the final Hamiltonian is again  $H$ , and for the second equality we used  $S(\rho'_{SB}) = S(\rho_{SB})$ .

For any bipartite system  $X_{SB}$  with Hamiltonian  $H$ , denoting by  $X_{S/B} = \text{Tr}_{B/S}X_{SB}$ , one has that the non-equilibrium free energy decomposes into local parts plus correlations:

$$F(X_{SB}, H) = F(X_S, H_S) + F(X_B, H_B) + kTI(X_{SB}), \quad (11.21)$$

where  $I(X_{SB}) = S(X_S) + S(X_B) - S(X_{SB})$  is the mutual information (this can be verified by summing and subtracting the local entropies to the expression for  $F(X_{SB}, H)$ ).

Denoting now  $\rho'_{S/B} = \text{Tr}_{B/S}[\rho'_{SB}]$  and using the formula above, together with the fact that  $I(\rho_{SB}) = 0$ , we obtain

$$\begin{aligned} W &= F(\rho_S, H_S) - F(\rho'_S, H_S) + F(\rho_B, H_B) - F(\rho'_B, H_B) - kT I(\rho'_{SB}) \\ &= F(\rho_S, H_S) - F(\rho'_S, H_S) - kT(S(\rho'_B || \tau_B) + I(\rho'_{SB})), \end{aligned} \quad (11.22)$$

where we used  $F(\rho'_B, H_B) - F(\tau_B, H_B) = kT S(\gamma_B || \tau_B)$ . As both  $I(\cdot)$  and  $S(\cdot || \cdot)$  are non-negative quantities, we immediately obtain

$$W \leq F(\rho_S, H_S) - F(\rho'_S, H_S). \quad (11.23)$$

Note that this expression only depends on the (initial and final) state of  $S$  and the temperature of  $B$ . We can obtain a bound that is independent of the final state by adding and subtracting  $F(\tau_S, H_S)$  in Eq. (11.22) (where  $\tau_S = e^{-\beta H_S} / \text{Tr}(e^{-\beta H_S})$ ), which gives

$$W = F(\rho_S, H_S) - F(\tau_S, H_S) - T [S(\rho'_S || \tau_S) + I(\rho'_{SB}) + S(\rho'_B || \tau_B)], \quad (11.24)$$

Note again that all terms in the square parenthesis are non-negative, and each of them has an intuitive physical meaning: in order of appearance, the athermality of the final state of  $S$  (when  $\rho'_S \neq \tau_S$ ), the correlations created between  $S$  and  $B$ , and the athermality of final state of  $B$  (when  $\rho'_B \neq \tau_B$ ). With the above equality we finally obtain

$$W \leq F(\rho_S, H_S) - F(\tau_S, H_S) = \langle W \rangle_{\max}(\rho). \quad (11.25)$$

The remaining interesting question is whether these bounds can be saturated: protocols that achieve (11.15) are constructed in [109–111] which, interestingly, require  $B$  to be of macroscopic size.

We now move to the question of how energy measurements change Eq. (11.15), by making it unattainable. For simplicity of exposition, we will assume that  $H_S$  is not degenerate. If one performs an energy measurement, one obtains a pure energy state  $|E_i\rangle$  with probability  $p_i = \langle E_i | \rho | E_i \rangle$ . Using Eq. (11.15), one can see that from state  $|E_i\rangle$  one can extract a maximum amount of work equal to  $F(|E_i\rangle) - F(\tau) = E_i + kT \log Z$  (this can be understood as the conjunction of the unitary process that maps  $|E_i\rangle$  into the ground state, extracting energy  $E_i$ , followed by a protocol that extracts work  $kT \log Z$  from the purity of the ground state). To complete the process one needs to reset the memory, implicitly used in the measurement, to its “blank state”; in the presence of a bath at temperature  $T$ , this requires an investment of  $kT H(\mathbf{p})$ , where  $\mathbf{p}$  is the distribution  $p_i$  and  $H(\mathbf{p}) = -\sum_i p_i \log p_i$  is the Shannon entropy (this is known as Landauer erasure). Overall the protocol that extracts work after an energy measurement optimally achieves the average  $\langle W \rangle_{\text{meas}}(\rho) = \sum_i p_i E_i - kT H(\mathbf{p}) + kT \log Z$ . A direct calculation shows  $\langle W \rangle_{\text{meas}} = F(\mathcal{D}(\rho)) - F(\tau)$ , with  $\mathcal{D}$  the dephasing operation  $\mathcal{D}(\rho) = \sum_i p_i |E_i\rangle\langle E_i|$ . This implies

$$\langle W \rangle_{\text{meas}}(\rho) = \langle W \rangle_{\max}(\mathcal{D}(\rho)), \quad (11.26)$$

i.e. the energy measurement protocol optimally extracts an average amount of work equal to the maximum that can be extracted by first dephasing the state and then performing work extraction. This implies a loss

$$\langle W \rangle_{max}(\rho) - \langle W \rangle_{max}(\mathcal{D}(\rho)) = kTS(\mathcal{D}(\rho)) - kTS(\rho) \equiv kTS(\rho||\mathcal{D}(\rho)) := kTA(\rho), \quad (11.27)$$

proportional to a quantity  $A(\rho)$  called *asymmetry* or *relative entropy of coherence*, which is a measure of quantum coherence in the eigenbasis of  $H_S$ . Note that  $A(\rho) > 0$  if and only if  $\rho \neq \mathcal{D}(\rho)$ .

The above reasoning shows that protocols based on energy measurements cannot reach the optimal average work extraction, since they lose the possibility of extracting work from the coherence of the quantum state. This intuition can also be grounded in the non equilibrium free energy. As we discussed above,  $\langle W \rangle_{max}(\rho) = \Delta F(\rho) := F(\rho) - F(\tau)$ . Summing and subtracting  $\Delta F(\mathcal{D}(\rho)) = F(\mathcal{D}(\rho)) - F(\tau)$  one obtains, using the definition of  $A(\rho)$ ,

$$\Delta F(\rho) = \Delta F(\mathcal{D}(\rho)) + kTA(\rho), \quad (11.28)$$

i.e. the non-equilibrium free energy neatly decomposes into a contribution coming from the diagonal part of the state and a contribution coming from coherence [61, 62]. As discussed above,  $\langle W \rangle_{meas} = \Delta F(\mathcal{D}(\rho))$ , i.e. the diagonal non-equilibrium free energy captures the component that can be converted into work by the energy measurement protocol, whereas the coherent contribution is lost. One has  $\Delta F(\rho) > \Delta F(\mathcal{D}(\rho))$  whenever  $[\rho, H_S] \neq 0$ .

## References

1. J. Goold, M. Huber, A. Riera, L. d. Rio, P. Skrzypczyk, The role of quantum information in thermodynamics a topical review. *J. Phys. A*, **49**(14):143001, 2016. <https://doi.org/10.1088/1751-8113/49/14/143001>
2. S. Vinjanampathy, J. Anders, Quantum thermodynamics. *Contemp. Phys.* **57**(4), 545–579 (2016). <https://doi.org/10.1080/00107514.2016.1201896>
3. J. Åberg, Truly work-like work extraction via a single-shot analysis. *Nat. Commun.* **4**, 1925 (2013). <https://doi.org/10.1038/ncomms2712>
4. M. Campisi, P. Hägggi, P. Talkner, Colloquium. *Rev. Mod. Phys.* **83**(3), 771–791 (2011). <https://doi.org/10.1103/RevModPhys.83.771>
5. M. Esposito, U. Harbola, S. Mukamel, Nonequilibrium fluctuations, fluctuation theorems, and counting statistics in quantum systems. *Rev. Mod. Phys.* **81**(4), 1665–1702 (2009). <https://doi.org/10.1103/RevModPhys.81.1665>
6. M. Esposito, U. Harbola, S. Mukamel, Erratum: Nonequilibrium fluctuations, fluctuation theorems, and counting statistics in quantum systems [rev. mod. phys. 81, 1665 (2009)]. *Rev. Mod. Phys.*, **86**(3):1125–1125, Sep 2014. <https://doi.org/10.1103/RevModPhys.86.1125>
7. C. Jarzynski, Equalities and inequalities: Irreversibility and the second law of thermodynamics at the nanoscale. *Ann. Rev. Condens. Matter Phys.* **2**(1), 329–351 (2011). <https://doi.org/10.1146/annurev-conmatphys-062910-140506>

8. J. Roßnagel, O. Abah, F. Schmidt-Kaler, K. Singer, E. Lutz, Nanoscale heat engine beyond the carnot limit. *Phys. Rev. Lett.* **112**(3), 030602 (2014). <https://doi.org/10.1103/PhysRevLett.112.030602>
9. L.A. Correa, J.e.P. Palao, D. Alonso, G. Adesso, Quantum-enhanced absorption refrigerators. *Sci. Rep.* **4**, 3949 (2014). <https://doi.org/10.1038/srep03949>
10. R. Alicki, D. Gelbwaser-Klimovsky, Non-equilibrium quantum heat machines. *New J. Phys.* **17**(11), 115012 (2015). <https://doi.org/10.1088/1367-2630/17/11/115012>
11. J.B. Brask, N. Brunner, Small quantum absorption refrigerator in the transient regime: Time scales, enhanced cooling, and entanglement. *Phys. Rev. E* **92**(6), 062101 (2015). <https://doi.org/10.1103/PhysRevE.92.062101>
12. R. Uzdin, A. Levy, R. Kosloff (2015), Equivalence of Quantum Heat Machines, and Quantum-Thermodynamic Signatures. *Phys. Rev. X* **5**(3), 031044. <https://doi.org/10.1103/PhysRevX.5.031044>
13. M.T. Mitchison, M.P. Woods, J. Prior, M. Huber, Coherence-assisted single-shot cooling by quantum absorption refrigerators. *New J. Phys.* **17**(11), 115013 (2015). <https://doi.org/10.1088/1367-2630/17/11/115013>
14. P.P. Hofer, M. Perarnau-Llobet, J.B. Brask, R. Silva, M. Huber, N. Brunner, Autonomous quantum refrigerator in a circuit qed architecture based on a josephson junction. *Phys. Rev. B* **94**(23), 235420 (2016). <https://doi.org/10.1103/PhysRevB.94.235420>
15. S. Nimmrichter, J. Dai, A. Roulet, V. Scarani, Quantum and classical dynamics of a three-mode absorption refrigerator. *Quantum* **1**, 37 (2017). <https://doi.org/10.22331/q-2017-12-11-37>
16. K. Brandner, M. Bauer, U. Seifert, Universal coherence-induced power losses of quantum heat engines in linear response. *Phys. Rev. Lett.* **119**(17), 170602 (2017). <https://doi.org/10.1103/PhysRevLett.119.170602>
17. J. Klatzow, C. Weinzel, P.M. Ledingham, J.N. Becker, D.J. Saunders, J. Nunn, I.A. Walmsley, R. Uzdin, E. Poem, Experimental demonstration of quantum effects in the operation of microscopic heat engines (2017). [arXiv:1710.08716](https://arxiv.org/abs/1710.08716)
18. A.E. Allahverdyan, R. Balian, T.M. Nieuwenhuizen, Maximal work extraction from finite quantum systems. *EPL (Europhysics Letters)* **67**(4), 565 (2004). <https://doi.org/10.1209/epl/i2004-10101-2>
19. K. Funo, Y. Watanabe, M. Ueda, Thermodynamic work gain from entanglement. *Phys. Rev. A* **88**(5), 052319 (2013). <https://doi.org/10.1103/PhysRevA.88.052319>
20. M. Perarnau-Llobet, K.V. Hovhannisyan, M. Huber, P. Skrzypczyk, N. Brunner, A. Acín, Extractable work from correlations. *Phys. Rev. X* **5**(4), 041011 (2015). <https://doi.org/10.1103/PhysRevX.5.041011>
21. K. Korzekwa, M. Lostaglio, J. Oppenheim, D. Jennings, The extraction of work from quantum coherence. *New J. Phys.* **18**(2), 023045 (2016). <https://doi.org/10.1088/1367-2630/18/2/023045>
22. A. Misra, U. Singh, S. Bhattacharya, A.K. Pati, Energy cost of creating quantum coherence. *Phys. Rev. A* **93**(5), 052335 (2016). <https://doi.org/10.1103/PhysRevA.93.052335>
23. N. Lörch, C. Bruder, N. Brunner, P.P. Hofer, Optimal work extraction from quantum states by photo-assisted cooper pair tunneling. *Quantum Science and Technology* **3**(3), 035014 (2018). <https://doi.org/10.1088/2058-9565/aacbfb>
24. K.V. Hovhannisyan, M. Perarnau-Llobet, M. Huber, A. Acín, Entanglement generation is not necessary for optimal work extraction. *Phys. Rev. Lett.* **111**(24), 240401 (2013). <https://doi.org/10.1103/PhysRevLett.111.240401>
25. N. Brunner, M. Huber, N. Linden, S. Popescu, R. Silva, P. Skrzypczyk, Entanglement enhances cooling in microscopic quantum refrigerators. *Phys. Rev. E* **89**(3), 032115 (2014). <https://doi.org/10.1103/PhysRevE.89.032115>
26. R. Uzdin, A. Levy, R. Kosloff, Equivalence of quantum heat machines, and quantum-thermodynamic signatures. *Phys. Rev. X* **5**(3), 031044 (2015). <https://doi.org/10.1103/PhysRevX.5.031044>

27. F. Campaioli, F.A. Pollock, F.C. Binder, L. Céleri, J. Goold, S. Vinjanampathy, K. Modi, Enhancing the charging power of quantum batteries. *Phys. Rev. Lett.* **118**(15), 150601 (2017). <https://doi.org/10.1103/PhysRevLett.118.150601>
28. D. Ferraro, M. Campisi, G.M. Andolina, V. Pellegrini, M. Polini, High-power collective charging of a solid-state quantum battery. *Phys. Rev. Lett.* **120**(11), 117702 (2018). <https://doi.org/10.1103/PhysRevLett.120.117702>
29. G. Watanabe, B.P. Venkatesh, P. Talkner, A. del Campo, Quantum performance of thermal machines over many cycles. *Phys. Rev. Lett.* **118**(5), 050601 (2017). <https://doi.org/10.1103/PhysRevLett.118.050601>
30. P. Busch, P. Lahti, R.F. Werner, Colloquium: Quantum root-mean-square error and measurement uncertainty relations. *Rev. Mod. Phys.* **86**(4), 1261–1281 (2014). <https://doi.org/10.1103/RevModPhys.86.1261>
31. C. Jarzynski, Nonequilibrium work relations: foundations and applications. *J. Euro. Phys. B* **64**(3), 331–340 (2008). <https://doi.org/10.1140/epjb/e2008-00254-2>
32. G.N. Bochkov, I.E. Kuzovlev, General theory of thermal fluctuations in nonlinear systems. *Zhurnal Eksperimentalnoi i Teoreticheskoi Fiziki* **72**, 238–247 (1977)
33. G. Bochkov, Y. Kuzovlev, Nonlinear fluctuation-dissipation relations and stochastic models in nonequilibrium thermodynamics: I. generalized fluctuation-dissipation theorem. *Physica A: Statistical Mechanics and its Applications*, **106**(3):443 – 479, 1981. [https://doi.org/10.1016/0378-4371\(81\)90122-9](https://doi.org/10.1016/0378-4371(81)90122-9)
34. S. Yukawa, A quantum analogue of the jarzynski equality. *J. Phys. Soc. Japan.* **69**(8), 2367–2370 (2000). <https://doi.org/10.1143/JPSJ.69.2367>
35. T. Monnai, S. Tasaki, Quantum correction of fluctuation theorem (2003). [arXiv:1707.04930](https://arxiv.org/abs/1707.04930)
36. V. Chernyak, S. Mukamel, Effect of quantum collapse on the distribution of work in driven single molecules. *Phys. Rev. Lett.* **93**(4), 048302 (2004). <https://doi.org/10.1103/PhysRevLett.93.048302>
37. A.E. Allahverdyan, T.M. Nieuwenhuizen, Fluctuations of work from quantum subensembles: The case against quantum work-fluctuation theorems. *Phys. Rev. E* **71**(6), 066102 (2005). <https://doi.org/10.1103/PhysRevE.71.066102>
38. A. Engel, R. Nolte, Jarzynski equation for a simple quantum system: Comparing two definitions of work. *EPL (Europhysics Letters)* **79**(1), 10003 (2007). <https://doi.org/10.1209/0295-5075/79/10003>
39. M.F. Gelin, D.S. Kosov, Unified approach to the derivation of work theorems for equilibrium and steady-state, classical and quantum hamiltonian systems. *Phys. Rev. E* **78**(1), 011116 (2008). <https://doi.org/10.1103/PhysRevE.78.011116>
40. J. Kurchan, A quantum fluctuation theorem (2000). [arXiv:cond-mat/0007360](https://arxiv.org/abs/cond-mat/0007360)
41. H. Tasaki, Jarzynski relations for quantum systems and some applications (2000). [arXiv:cond-mat/0009244](https://arxiv.org/abs/cond-mat/0009244)
42. P. Talkner, E. Lutz, P. Hänggi, Fluctuation theorems: Work is not an observable. *Phys. Rev. E* **75**(5), 050102 (2007). <https://doi.org/10.1103/PhysRevE.75.050102>
43. P. Hänggi, P. Talkner, The other qft. *Nature Physics* **11**(2), 108 (2017). <https://doi.org/10.1038/nphys3167>
44. M. Campisi, P. Hänggi, P. Talkner, Colloquium: Quantum fluctuation relations: Foundations and applications. *Rev. Mod. Phys.* **83**(3), 771–791 (2011). <https://doi.org/10.1103/RevModPhys.83.771>
45. M. Campisi, P. Hänggi, P. Talkner, Erratum: Colloquium: Quantum fluctuation relations: Foundations and applications. *Rev. Mod. Phys.*, **83**(4):1653–1653, (2011). <https://doi.org/10.1103/RevModPhys.83.1653>
46. M. Campisi, P. Talkner, P. Hänggi, Fluctuation theorem for arbitrary open quantum systems. *Phys. Rev. Lett.* **102**(21), 210401 (2009). <https://doi.org/10.1103/PhysRevLett.102.210401>
47. G. Huber, F. Schmidt-Kaler, S. Deffner, E. Lutz, Employing trapped cold ions to verify the quantum jarzynski equality. *Phys. Rev. Lett.* **101**(7), 070403 (2008). <https://doi.org/10.1103/PhysRevLett.101.070403>

48. T.B. Batalhão, A.M. Souza, L. Mazzola, R. Auccaise, R.S. Sarthour, I.S. Oliveira, J. Goold, G. De Chiara, M. Paternostro, R.M. Serra, Experimental reconstruction of work distribution and study of fluctuation relations in a closed quantum system. *Phys. Rev. Lett.* **113**(14), 140601 (2014). <https://doi.org/10.1103/PhysRevLett.113.140601>
49. S. An, J.-N. Zhang, M. Um, D. Lv, Y. Lu, J. Zhang, Z.-Q. Yin, H.T. Quan, K. Kim, Experimental test of the quantum jarzynski equality with a trapped-ion system. *Nature Physics* **11**(2), 193 (2014). <https://doi.org/10.1038/nphys3197>
50. F. Cerisola, Y. Margalit, S. Machluf, A.J. Roncaglia, J.P. Paz, R. Folman, Using a quantum work meter to test non-equilibrium fluctuation theorems. *Nat. Commun.* **8**(1), 1241 (2017). <https://doi.org/10.1038/s41467-017-01308-7>
51. C. Jarzynski, H.T. Quan, S. Rahav, Quantum-classical correspondence principle for work distributions. *Phys. Rev. X* **5**(3), 031038 (2015). <https://doi.org/10.1103/PhysRevX.5.031038>
52. L. Zhu, Z. Gong, B. Wu, H.T. Quan, Quantum-classical correspondence principle for work distributions in a chaotic system. *Phys. Rev. E* **93**(6), 062108 (2016). <https://doi.org/10.1103/PhysRevE.93.062108>
53. A.E. Allahverdyan, Nonequilibrium quantum fluctuations of work. *Phys. Rev. E* **90**(3), 032137 (2014). <https://doi.org/10.1103/PhysRevE.90.032137>
54. P. Solinas, S. Gasparinetti, Full distribution of work done on a quantum system for arbitrary initial states. *Phys. Rev. E* **92**(4), 042150 (2015). <https://doi.org/10.1103/PhysRevE.92.042150>
55. P. Kammerlander, J. Anders, Coherence and measurement in quantum thermodynamics. *Scientific reports* **6**, 22174 (2016). <https://doi.org/10.1038/srep22174>
56. S. Deffner, J.P. Paz, W.H. Zurek, Quantum work and the thermodynamic cost of quantum measurements. *Phys. Rev. E* **94**(1), 010103 (2016). <https://doi.org/10.1103/PhysRevE.94.010103>
57. M. Perarnau-Llobet, E. Bäumer, K.V. Hovhannissyan, M. Huber, A. Acín, No-go theorem for the characterization of work fluctuations in coherent quantum systems. *Phys. Rev. Lett.* **118**(7), 070601 (2017). <https://doi.org/10.1103/PhysRevLett.118.070601>
58. G. Watanabe, B.P. Venkatesh, P. Talkner, Generalized energy measurements and modified transient quantum fluctuation theorems. *Phys. Rev. E* **89**(5), 052116 (2014). <https://doi.org/10.1103/PhysRevE.89.052116>
59. B.P. Venkatesh, G. Watanabe, P. Talkner, Quantum fluctuation theorems and power measurements. *New J. Phys.* **17**(7), 075018 (2015). <https://doi.org/10.1088/1367-2630/17/7/075018>
60. M. Esposito, C.V. den Broeck, Second law and landauer principle far from equilibrium. *EPL (Europhysics Letters)* **95**(4), 40004 (2011). <https://doi.org/10.1209/0295-5075/95/40004>
61. D. Janzing, Quantum thermodynamics with missing reference frames: Decompositions of free energy into non-increasing components. *J. Stat. Phys.* **125**(3), 761–776 (2006). <https://doi.org/10.1007/s10955-006-9220-x>
62. M. Lostaglio, D. Jennings, T. Rudolph, Description of quantum coherence in thermodynamic processes requires constraints beyond free energy. *Nat. Commun.* **6**, 6383 (2015). <https://doi.org/10.1038/ncomms7383>
63. J.J. Alonso, E. Lutz, A. Romito, Thermodynamics of weakly measured quantum systems. *Phys. Rev. Lett.* **116**(8), 080403 (2016). <https://doi.org/10.1103/PhysRevLett.116.080403>
64. C. Elouard, D.A. Herrera-Martí, M. Clusel, A. Auffeves, The role of quantum measurement in stochastic thermodynamics. *npj Quantum Information*, **3**(1), 9 (2017). <https://doi.org/10.1038/s41534-017-0008-4>
65. A.J. Roncaglia, F. Cerisola, J.P. Paz, Work measurement as a generalized quantum measurement. *Phys. Rev. Lett.* **113**(25), 250601 (2014) <https://doi.org/10.1103/PhysRevLett.113.250601>
66. G.D. Chiara, A.J. Roncaglia, J.P. Paz, Measuring work and heat in ultracold quantum gases. *New J. Phys.* **17**(3), 035004 (2015). <https://doi.org/10.1088/1367-2630/17/3/035004>
67. P. Talkner, P. Hänggi, Aspects of quantum work. *Phys. Rev. E* **93**(2), 022131 (2016). <https://doi.org/10.1103/PhysRevE.93.022131>

68. P. Solinas, H.J.D. Miller, J. Anders, Measurement-dependent corrections to work distributions arising from quantum coherences. *Phys. Rev. A* **96**(5), 052115 (2017). <https://doi.org/10.1103/PhysRevA.96.052115>
69. P.P. Hofer, Quasi-probability distributions for observables in dynamic systems. *Quantum* **1**, 32 (2017). <https://doi.org/10.1103/PhysRevA.96.052115>
70. R. Sampaio, S. Suomela, T. Ala-Nissila, J. Anders, T.G. Philbin, Quantum work in the bohmian framework. *Phys. Rev. A* **97**(1), 012131 (2018). <https://doi.org/10.1103/PhysRevA.97.012131>
71. M. Lostaglio, Quantum fluctuation theorems, contextuality, and work quasiprobabilities. *Phys. Rev. Lett.* **120**(4), 040602 (2018). <https://doi.org/10.1103/PhysRevLett.120.040602>
72. A.M. Alhambra, L. Masanes, J. Oppenheim, C. Perry, Fluctuating work: From quantum thermodynamical identities to a second law equality. *Phys. Rev. X* **6**(4), 041017 (2016). <https://doi.org/10.1103/PhysRevX.6.041017>
73. J.G. Richens, L. Masanes, Work extraction from quantum systems with bounded fluctuations in work. *Nat. Commun.* **7**, 13511 (2016) <https://doi.org/10.1038/ncomms13511>
74. J. Åberg, Fully quantum fluctuation theorems. *Phys. Rev. X* **8**(1), 011019 (2018). <https://doi.org/10.1103/PhysRevX.8.011019>
75. J.S. Bell, On the problem of hidden variables in quantum mechanics. *Rev. Mod. Phys.* **38**(3), 447 (1966). <https://doi.org/10.1103/RevModPhys.38.447>
76. S. Kochen, E.P. Specker, The problem of hidden variables in quantum mechanics. In *The Logico-Algebraic Approach to Quantum Mechanics*, p. 293–328. Springer, 1975. [https://doi.org/10.1007/978-94-010-1795-4\\_17](https://doi.org/10.1007/978-94-010-1795-4_17)
77. M. Howard, J. Wallman, V. Veitch, J. Emerson, Contextuality supplies the/magic/ for quantum computation. *Nature* **510**(7505), 351–355 (2014). <https://doi.org/10.1038/nature13460>
78. N. Delfosse, P.A. Guerin, J. Bian, R. Raussendorf, Wigner function negativity and contextuality in quantum computation on rebits. *Phys. Rev. X* **5**(2), 021003 (2015). <https://doi.org/10.1103/PhysRevX.5.021003>
79. J. Bermejo-Vega, N. Delfosse, D.E. Browne, C. Okay, R. Raussendorf, Contextuality as a resource for models of quantum computation with qubits. *Phys. Rev. Lett.* **119**(12), 120505 (2017). <https://doi.org/10.1103/PhysRevLett.119.120505>
80. R.W. Spekkens, Contextuality for preparations, transformations, and unsharp measurements. *Phys. Rev. A* **71**(5), 052108 (2005). <https://doi.org/10.1103/PhysRevA.71.052108>
81. N. Brunner, D. Cavalcanti, S. Pironio, V. Scarani, S. Wehner, Bell nonlocality. *Rev. Mod. Phys.* **86**(2), 419 (2014). <https://doi.org/10.1103/RevModPhys.86.419>
82. P. Solinas, S. Gasparinetti, Probing quantum interference effects in the work distribution. *Phys. Rev. A* **94**(5), 052103 (2016). <https://doi.org/10.1103/PhysRevA.94.052103>
83. B.-M. Xu, J. Zou, L.-S. Guo, X.-M. Kong, Effects of quantum coherence on work statistics. *Phys. Rev. A* **97**(5), 052122 (2018). <https://doi.org/10.1103/PhysRevA.97.052122>
84. Y. Aharonov, D.Z. Albert, L. Vaidman, How the result of a measurement of a component of the spin of a spin-1/2 particle can turn out to be 100. *Phys. Rev. Lett.* **60**(14), 1351 (1988). <https://doi.org/10.1103/PhysRevLett.60.1351>
85. H.M. Wiseman, Weak values, quantum trajectories, and the cavity-qed experiment on wave-particle correlation. *Phys. Rev. A* **65**(3), 032111 (2002). <https://doi.org/10.1103/PhysRevA.65.032111>
86. H.J.D. Miller, J. Anders, Time-reversal symmetric work distributions for closed quantum dynamics in the histories framework. *New J. Phys.* **19**(6), 062001 (2017). <https://doi.org/10.1088/1367-2630/aa703f>
87. J.W. Hall, Prior information: How to circumvent the standard joint-measurement uncertainty relation. *Phys. Rev. A* **69**(5), 052113 (2004). <https://doi.org/10.1103/PhysRevA.69.052113>
88. R.B. Griffiths, Consistent histories and the interpretation of quantum mechanics. *J. Stat. Phys.* **36**(1–2), 219–272 (1984). <https://doi.org/10.1007/BF01015734>
89. S. Goldstein, D.N. Page, Linearly positive histories: probabilities for a robust family of sequences of quantum events. *Phys. Rev. Lett.* **74**(19):3715, 1995. <https://doi.org/10.1103/PhysRevLett.74.3715>

90. T. Sagawa, *Second law-like inequalities with quantum, relative entropy: An introduction*, pages 125–190. World Scientific, 2012. [https://doi.org/10.1142/9789814425193\\_0003](https://doi.org/10.1142/9789814425193_0003)
91. M.F. Pusey, Anomalous weak values are proofs of contextuality. *Phys. Rev. Lett.* **113**(20), 200401 (2014). <https://doi.org/10.1103/PhysRevLett.113.200401>
92. N.S. Williams, A.N. Jordan, Weak values and the leggett-garg inequality in solid-state qubits. *Phys. Rev. Lett.* **100**(2), 026804 (2008). <https://doi.org/10.1103/PhysRevLett.100.026804>
93. R. Blattmann, K. Mølmer, Macroscopic realism of quantum work fluctuations. *Physical Review A* **96**(1), 012115 (2017). <https://doi.org/10.1103/PhysRevA.96.012115>
94. H.J.D. Miller, J. Anders, Leggett-garg inequalities for quantum fluctuating work. *Entropy*, **20**(3), 2018. <https://doi.org/10.3390/e20030200>
95. D. Bohm, A suggested interpretation of the quantum theory in terms of "hidden" variables. *Phys. Rev. I* **85**(2), 166–179 (1952). <https://doi.org/10.1103/PhysRev.85.166>
96. D. Bohm, A suggested interpretation of the quantum theory in terms of "hidden" variables. *Phys. Rev. II* **85**(2), 180–193 (1952). <https://doi.org/10.1103/PhysRev.85.180>
97. L. De Broglie, L'interprétation de la mécanique ondulatoire. *J. Phys. Radium.* **20**(12), 963–979 (1959). <https://doi.org/10.1051/jphysrad:019590020012096300>
98. P.R. Holland, *The quantum theory of motion: an account of the de Broglie-Bohm causal interpretation of quantum mechanics*. Cambridge university press, 1995
99. D. Dürr, S. Goldstein, N. Zanghì, *Quantum physics without quantum philosophy*. Springer Science & Business Media, 2013. <https://doi.org/10.1007/978-3-642-30690-7>
100. Y. Aharonov, D.Z. Albert, L. Vaidman, How the result of a measurement of a component of the spin of a spin-1/2 particle can turn out to be 100. *Phys. Rev. Lett.* **60**(14), 1351–1354 (1988). <https://doi.org/10.1103/PhysRevLett.60.1351>
101. I.M. Duck, P.M. Stevenson, E.C.G. Sudarshan, The sense in which a "weak measurement" of a spin particle's spin component yields a value 100. *Phys. Rev. D* **40**(6), 2112–2117 (1989). <https://doi.org/10.1103/PhysRevD.40.2112>
102. S. Kocsis, B. Braverman, S. Ravets, M.J. Stevens, R.P. Mirin, L.K. Shalm, A.M. Steinberg, Observing the average trajectories of single photons in a two-slit interferometer. *Science*, 332(6034):1170–1173, (2011). <https://doi.org/10.1126/science.1202218>
103. D.H. Mahler, L. Rozema, K. Fisher, L. Vermeyden, K.J. Resch, H.M. Wiseman, A. Steinberg, Experimental nonlocal and surreal bohmian trajectories. *Science Advances* **2**(2), e1501466 (2016). <https://doi.org/10.1126/sciadv.1501466>
104. Y. Xiao, Y. Kedem, J.-S. Xu, C.-F. Li, G.-C. Guo, Experimental nonlocal steering of bohmian trajectories. *Opt. Express* **25**(13), 14463–14472 (2017). <https://doi.org/10.1364/OE.25.014463>
105. H. Pashayan, J.J. Wallman, S.D. Bartlett, Estimating outcome probabilities of quantum circuits using quasiprobabilities. *Physical review letters* **115**(7), 070501 (2015). <https://doi.org/10.1103/PhysRevLett.115.070501>
106. H. Pashayan, J.J. Wallman, S.D. Bartlett, Quantum features and signatures of quantum-thermal machines (2018). [arXiv:1803.05586](https://arxiv.org/abs/1803.05586)
107. S. Pironio, A. Acín, S. Massar, A.B. de La Giroday, D.N. Matsukevich, P. Maunz, S. Olmschenk, D. Hayes, L. Luo, T.A. Manning et al., Random numbers certified by bell theorem. *Nature* **464**(7291), 1021 (2010). <https://doi.org/10.1038/nature09008>
108. M.D. Mazurek, M.F. Pusey, R. Kunjwal, K.J. Resch, R.W. Spekkens, An experimental test of noncontextuality without unphysical idealizations. *Nat. Commun.* **7**:ncomms11780, (2016). <https://doi.org/10.1038/ncomms11780>
109. P. Skrzypczyk, A.J. Short, S. Popescu, Work extraction and thermodynamics for individual quantum systems. *Nat. Commun.* **5**, 4185 (2014). <https://doi.org/10.1038/ncomms5185>
110. J. Åberg, Catalytic coherence. *Phys. Rev. Lett.* **113**, 150402 (2014). <https://doi.org/10.1103/PhysRevLett.113.150402>
111. D. Reeb, M.M. Wolf, An improved landauer principle with finite-size corrections. *New J. Phys.* **16**(10), 103011 (2014). <https://doi.org/10.1088/1367-2630/16/10/103011>

# Chapter 12

## The Coherent Crooks Equality



Zoe Holmes

### 12.1 Introduction

Fluctuation theorems are a pillar of contemporary thermodynamics: they are generalisations of the second law of thermodynamics that probe the irreversibility of non-equilibrium processes. Specifically, they consider systems driven from equilibrium and establish exact relations between the resultant thermal fluctuations. The emergent field of quantum fluctuation theorems aims to generalise classical fluctuation relations to the regime in which quantum phenomena such as coherence and entanglement become relevant. For a general introduction to both classical and quantum fluctuation relations, see Chap. 10 and Refs. [1–4].

Fluctuation theorems can broadly be classified as ‘detailed’ or ‘integral’ theorems, by the fluctuating quantity considered and by the nature of the non-equilibrium processes involved. ‘Detailed’ fluctuation theorems consider pairs of non-equilibrium processes (a ‘forwards’ one and its time-reversed equivalent) and quantify the relative probability of thermal fluctuations in the two processes. ‘Integral’ theorems consider a single non-equilibrium process and quantify averages, or statistical moments, of such fluctuating quantities. The classical Crooks equality [5] is a *detailed* fluctuation theorem quantifying the *fluctuating work* done on a system that is *isothermally driven by a change in Hamiltonian*. The Jarzynki equality [6] emerges as the integral variant of the Crooks equality.

A plethora of quantum Crooks and Jarzynski equalities have been proposed over the last decade. The simplest approach defines the work done on a closed system as the change in energy found by performing projective measurements at the start and end of the non-equilibrium process [7–9]. In this case, the classical Crooks equality holds unaltered. Generalisations of this simple quantum Crooks equality have largely focused on extensions to open quantum systems [10, 11], protocols

---

Z. Holmes (✉)

Department of Physics, Imperial College London, London SW7 2BW, UK  
e-mail: z.holmes15@imperial.ac.uk

represented by generic quantum channels [12–14] and alternative quantum work definitions [15–17]. The latter includes definitions utilising quasi-probabilities [18, 19], the consistent histories framework [20] and the quantum jump approach [21, 22] (see also Chap. 15). Such extensions lead to deviations from the classical equality.

The information theoretic approach (Part V) has proven an effective means of incorporating quantum mechanical phenomena into thermodynamics. The field rose to prominence with a series of papers probing the impact of entanglement on the second law of thermodynamics [23], Landauer erasure [24], the thermodynamic arrow of time [25] and thermalisation [26]. These were followed by results investigating work extraction [27–29], generalisations of the second laws [30, 31], and general criteria for state conversion [32, 33] in quantum systems. Much of this research [27–33] used insights from the thermal operations framework [34–36] (see also Chap. 26), a resource theory for quantum states out of thermal equilibrium.

The purpose of this chapter is to explicate an information theoretic approach that uses insights from the thermal operations framework to incorporate quantum coherence into fluctuation theorems. In particular, we seek to explain the coherent Crooks equality, Eq. (12.6) in Sect. 12.2, which was derived by Johan Åberg in [37]. This is a Crooks-like equality for a system with an energy supply that is in a superposition of energy eigenstates. While our focus is on this result, Álvaro Alhambra et al. independently used a similar methodology in [38] to generalise the Jarzynski equality and to investigate the consequences of introducing fluctuating work into the thermal operations framework.

## 12.2 Sketch of Framework and Equality

The key feature that distinguishes the framework of [37, 38] from other quantum fluctuation theorems is the manner in which energy conservation is explicitly accounted for. Firstly, the global Hamiltonian  $H$  is assumed to be time independent. This is in marked contrast to the classical setup, as well as most previous quantum fluctuation theorems [7–11, 18–22], which utilise explicitly time dependent Hamiltonians. Secondly, the non-equilibrium process is driven by a unitary  $V$  that is ‘strictly’ energy conserving [29] in the sense that it commutes with the global Hamiltonian,  $[H, V] = 0$ . These two restrictions are used within the resource theoretic approach to quantum thermodynamics [34–36] where they have proven an effective means of carefully tracking the evolution of the energy and coherence<sup>1</sup> of a quantum system. Moreover, as expanded upon in Sect. 12.4, these restrictions are central to the resulting form of the coherent Crooks equality.

In the standard fluctuation theorem setting a system is driven by a change in Hamiltonian resulting in exchanges of heat and work. This can be captured, using only time independent Hamiltonians and energy conserving processes, by explicitly

---

<sup>1</sup>We use the term ‘coherence’ in the sense of a ‘superposition of states belonging to different energy eigenspaces’.

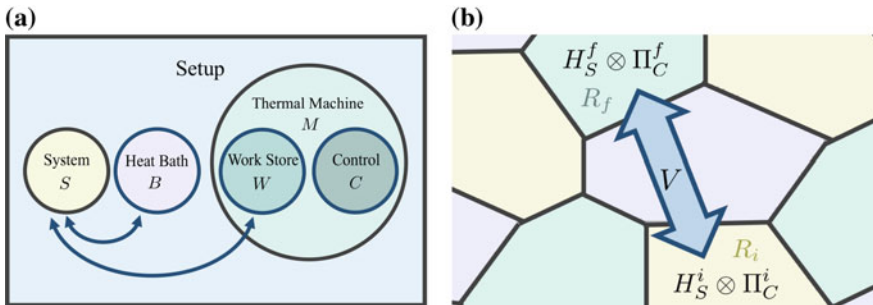


**Fig. 12.1** **a.** A sketch of the setup consisting of a system ( $S$ ), heat bath ( $B$ ), work store ( $W$ ), and control ( $C$ ). This can be reduced to a bipartite system by using a single system that we call a 'thermal machine' ( $M$ ) to act as both the work store and the control and by disregarding the heat bath and thinking of it as an implicit means of preparing the system in a thermal state. The arrows indicate the systems that exchange energy. **b.** A sketch of a Hilbert space with a Hamiltonian that varies from region to region. An effectively time dependent Hamiltonian is induced if the support of the control evolves, under some unitary operation  $V$ , from one region to the next. In the forwards process the control evolves from region  $i$  to  $f$ . In the reverse, it evolves from region  $f$  to  $i$ .

modeling the subsystems that are implicitly involved. Specifically, the total setup is taken to consist of the:

- System of interest  $S$ : this is the system that is driven by a change in Hamiltonian.
- Control system  $C$ : this enables the Hamiltonian of the system to be changed,  $H_S^i \leftrightarrow H_S^f$ .
- Work store  $W$ : this provides the energy required to change the Hamiltonian of the system.
- Thermal bath  $B$ : this enables the system to relax in response to the change in its Hamiltonian.

Crucially, the work store is assumed to be a quantum mechanical system and thus acts as a source of coherence. As the system in the standard Crooks equality starts in a thermal state which is diagonal in the energy eigenbasis, a means of introducing coherence, be it implicit or explicit, is required for any genuinely quantum mechanical Crooks equality.

Having decided to explicitly model the work store, it is then additionally used in [37] to sidestep the challenges associated with how to define fluctuating quantum work (for a review see [15] or Chap. 11). The classical definition of fluctuating work [4–6] does not follow directly over to the quantum regime as quantum particles do not have well defined trajectories. Moreover, a recent no go theorem [16] suggests there can be no definition of quantum fluctuating work that corresponds to the change in average internal energy in a closed quantum system *and* that recovers the results of classical stochastic thermodynamics for states with no coherence.

Rather than relying on one of the definitions of 'quantum work', the coherent Crooks equality is stated in terms of transition probabilities between work store

states. This is a generalisation that is consistent with the classical approach. When the work store is prepared in an energy eigenstate, the transition probabilities agree with the standard two point measurement scheme [7–9]. However, in the general case the work store can be prepared and found in a superposition of energy eigenstates.

For the purpose of this chapter we will simplify the setup and present the coherent Crooks equality for a bipartite system. This is done by first treating the control system and work store as a single system, which we will call the thermal machine  $M$ , that has the dual role of driving the change in system Hamiltonian and providing or absorbing the energy required to do so. The equality is formulated in terms of transition probabilities of the thermal machine. Secondly, we set the bath aside and think of it only as an implicit means of defining the temperature of the isothermal process and of preparing the system in a thermal state. The bipartite setup has the time-independent Hamiltonian,

$$H_{MS} = H_M \otimes \mathbb{1}_S + \mathbb{1}_M \otimes H_S + H_{MS}^{int} \quad (12.1)$$

comprised of the Hamiltonians  $H_S$  and  $H_M$  for the system and thermal machine, and their interaction  $H_{MS}^{int}$ . The full setup and this bipartite variant are sketched in Fig. 12.1a.

For concreteness, we can picture the bipartite setup using the example of a two level system and a motional thermal machine that interact via,

$$H_{MS}^{int} = E(x_M) \otimes \sigma_S^z . \quad (12.2)$$

$E(x_M)$  is an energetic level-shift that depends on the position,  $x_M$ , of the machine.  $\sigma_S^z = |es\rangle\langle es| - |gs\rangle\langle gs|$  with  $|es\rangle$  and  $|gs\rangle$  the excited and ground states of the two level system respectively. This setup could be physically implemented by a spin in a position dependent magnetic field. As sketched in Fig. 12.2, by choosing the function  $E(x)$  to be constant for  $x \leq x_i$  and for  $x \geq x_f$ , two distinct effective Hamiltonians,  $H_S^i$  and  $H_S^f$ , can be realised for the two level system. Similarly to the classical Crooks equality, the coherent Crooks equality is independent of precisely how the Hamiltonian changes from  $H_S^i$  to  $H_S^f$  and as such the choice of the form of  $E(x)$  in the region  $x_i < x < x_f$  is arbitrary. The position of the machine controls the Hamiltonian of the two level system and its energy provides the work store.

The aim now is to use this framework to probe the energy fluctuations that result from driving a system with a coherent energy supply away from equilibrium. This is done by broadly replicating the standard classical Crooks protocol but now allowing the thermal machine to exist in a superposition of energy states. The new protocol, as sketched in Fig. 12.2, consists of the following three stages:

**Preparation:** The machine is prepared in some state  $|\phi_M^i\rangle$  such that the initial effective Hamiltonian of the system is  $H_S^i$  (i.e. for our example localised such that  $\langle\phi_M^i|x_M|\phi_M^i\rangle < x_i$ ). This is the only constraint on  $|\phi_M^i\rangle$  which in general can be in a superposition of energy states. As in the classical case, the system is

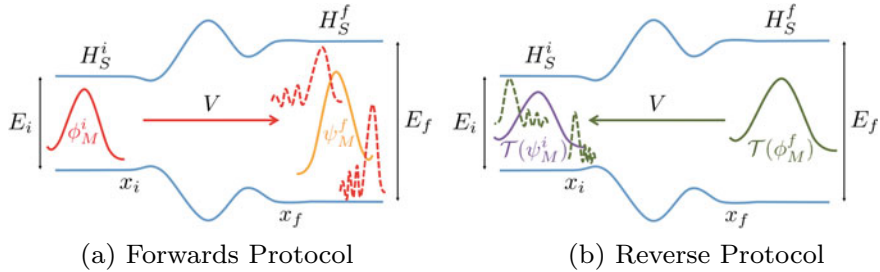


**Fig. 12.2** This is a sketch of the forwards and reverse protocols respectively for the two level system and motional machine example. The blue lines represent the ground and excited state of the two-level system as a function of position. The solid lines represent the state wave packets of the machine that are prepared at the start of the protocols (red/green) and the measurements (yellow/purple) that are performed at the end of the protocols. The dashed lines represent the evolved thermal machine states.

prepared in a thermal state, at temperature  $T$ , with respect to its initial Hamiltonian,  $\gamma(H_S^i) \propto \exp\left(-\frac{H_S^i}{k_B T}\right)$ .

**Evolution:** The system and machine then evolve under an energy conserving unitary  $V_{MS}$  that induces a change in the effective system Hamiltonian from  $H_S^i$  to  $H_S^f$ . This drives the system from equilibrium with the energy required to do so supplied by the machine.

**Measurement:** To quantify the energy changes of the driven system, a binary projective measurement is performed on the machine,  $\{|\psi_M^f\rangle\langle\psi_M^f|, \mathbb{1}_M - |\psi_M^f\rangle\langle\psi_M^f|\}$ . The only restriction on the state  $|\psi_M^f\rangle$  is that it must correspond to the final system Hamiltonian  $H_S^f$  (i.e. for our example be localised such that  $\langle\psi_M^f|x_M|\psi_M^f\rangle > x_f$ ). In general  $|\psi_M^f\rangle$  is a superposition of energy states and so this measurement probes the coherent properties of the evolved system and machine.

The transition probability for the forwards protocol,

$$\mathcal{P}_{H_S^i \rightarrow H_S^f}(|\phi_M^i\rangle \rightarrow |\psi_M^f\rangle) := \text{Tr} \left[ (|\psi_M^f\rangle\langle\psi_M^f| \otimes \mathbb{1}_S) V_{MS} (|\phi_M^i\rangle\langle\phi_M^i| \otimes \gamma(H_S^i)) V_{MS}^\dagger \right], \quad (12.3)$$

is the probability for the machine to collapse onto  $|\psi_M^f\rangle$  having been prepared in  $|\phi_M^i\rangle$ .

Similarly to the classical Crooks equality, the coherent Crooks equality purports to quantify the irreversibility of non-equilibrium processes. As such, the transition probability for the forwards process, Eq. (12.3), is compared to one for its time-reversed variant. The time reversal operation,  $\mathcal{T}$ , is introduced to characterise this reverse process. Specifically,  $\mathcal{T}$  is defined such that if we now assume that the setup and its evolution are time reversal invariant, i.e.  $\mathcal{T}(H_{MS}) = H_{MS}$  and  $\mathcal{T}(V_{MS}) = V_{MS}$ , we have that when the machine is prepared in some state  $\mathcal{T}(|\phi_M^f\rangle)$  its evolution under  $V$  drives a change in Hamiltonian from  $H_S^f$  back to  $H_S^i$ . We formally define

$\mathcal{T}$  in Sect. 12.3. The transition probability for the reverse process<sup>2</sup>,

$$\mathcal{P}_{H_S^f \rightarrow H_S^i}(\mathcal{T}(|\phi_M^f\rangle) \rightarrow \mathcal{T}(|\psi_M^i\rangle)) := \text{Tr} \left[ (\mathcal{T}(|\psi_M^i\rangle\langle\psi_M^i|) \otimes \mathbb{1}_S) V_{MS} (\mathcal{T}(|\phi_M^f\rangle\langle\phi_M^f|) \otimes \gamma(H_S^f)) V_{MS}^\dagger \right], \quad (12.4)$$

is otherwise entirely analogous to the forwards case and quantifies the probability to find the machine in  $\mathcal{T}(|\psi_M^i\rangle)$  having prepared it in  $\mathcal{T}(|\phi_M^f\rangle)$ .

In the coherent Crooks equality, the pair of machine states quantified in the reverse process,  $\mathcal{T}(|\psi_M^i\rangle)$  and  $\mathcal{T}(|\phi_M^f\rangle)$ , are constrained by the choice in states for the forwards process,  $|\psi_M^f\rangle$  and  $|\phi_M^i\rangle$ . The equality is derived by considering the ratio of the forwards, Eq. (12.3), and reverse, Eq. (12.4), transition probabilities and exploiting the fact that  $H_{MS}$  and  $V_{MS}$  commute and are time reversal invariant. It is found that the comparison of these probabilities is only possible for pairs of states related by a temperature dependent operation,

$$\begin{aligned} |\phi_M^i\rangle &\propto \exp\left(-\frac{H_M}{2k_B T}\right) |\psi_M^i\rangle \quad \text{and} \\ |\phi_M^f\rangle &\propto \exp\left(-\frac{H_M}{2k_B T}\right) |\psi_M^f\rangle. \end{aligned} \quad (12.5)$$

For energy eigenstates this operation is trivial; we have that  $|\phi_M^{i,f}\rangle = |\psi_M^{i,f}\rangle$  and the pairs of states in the forwards and reverse processes are simply the time reverse of one another. In general, the operation is non-trivial but can be seen as emerging from a seemingly natural map, called the Gibbs map, that we discuss in Sect. 12.4.

Having parameterised the relevant machine states in this way, the ratio of the transition probabilities is calculable and the coherent Crooks equality is found,

$$\frac{\mathcal{P}_{H_S^i \rightarrow H_S^f}(|\phi_M^i\rangle \rightarrow |\psi_M^f\rangle)}{\mathcal{P}_{H_S^f \rightarrow H_S^i}(\mathcal{T}(|\phi_M^f\rangle) \rightarrow \mathcal{T}(|\psi_M^i\rangle))} = \exp\left(\frac{1}{k_B T} (\Delta \tilde{E} - \Delta F)\right). \quad (12.6)$$

(This equality is Eq. 28 of [37] but written for a bipartite setup and assuming that the machine is prepared in a pure state.) The dependence on the change in equilibrium free energy  $\Delta F$  carries over from the classical Crooks equality [5]. As usual  $\Delta F := F(H_S^f, T) - F(H_S^i, T)$  with the free energy for any Hamiltonian  $H$  and temperature  $T$  given by

$$F(H, T) := -k_B T \ln \left( \text{Tr} \left[ \exp \left( -\frac{H}{k_B T} \right) \right] \right). \quad (12.7)$$

However, the classical work term is replaced with a quantum generalisation of the energy supplied to, or absorbed from, the system,  $\Delta \tilde{E} := \tilde{E}_{|\psi_M^i\rangle\langle\psi_M^i|}(H_M, T) - \tilde{E}_{|\psi_M^f\rangle\langle\psi_M^f|}(H_M, T)$ . The function  $\tilde{E}_\rho$  is a state dependent mathematical generalisation

---

<sup>2</sup>To avoid a proliferation of notation we here use the symbol  $\mathcal{T}$  to denote both a mapping on the level of Hilbert spaces and a map on the space of operators on the Hilbert space.

of the equilibrium free energy defined as

$$\tilde{E}_\rho(H, T) := -k_B T \ln \left( \text{Tr} \left[ \exp \left( -\frac{H}{k_B T} \right) \rho \right] \right). \quad (12.8)$$

As required to regain the classical limit, when the thermal machine is prepared in an energy eigenstate,  $\Delta \tilde{E}$  corresponds to the energy exchanged between the system and the thermal machine. More generally, as we discuss in Sect. 12.4,  $\tilde{E}$  appears to be a natural, temperature dependent, quantum energy measure.

The deviations from the classical Crooks equality are encapsulated in these two new concepts: the temperature dependent operation that parameterises the initial states and the substitution of the classical work term for  $\Delta \tilde{E}$ . For energy eigenstates,  $\{|E_M^k\rangle\}$ , the coherent Crooks equality reduces to

$$\frac{\mathcal{P}_{H_S^i \rightarrow H_S^f}(|E_M^i\rangle \rightarrow |E_M^f\rangle)}{\mathcal{P}_{H_S^f \rightarrow H_S^i}(|E_M^f\rangle \rightarrow |E_M^i\rangle)} = \exp \left( \frac{1}{k_B T} ((E_i - E_f) - \Delta F) \right). \quad (12.9)$$

If we then additionally assume that the evolution of the setup does not depend on the initial energy of the machine, the usual classical Crooks equality is regained by identifying its change in energy with the work done on the system. It is primarily in virtue of this that the coherent Crooks equality can be seen as a genuine quantum generalisation. However, in general the temperature dependent operation and the generalised energy flow term are essential to capture the impact of coherence.

### 12.3 Conceptual Ingredients

*Control System.* The example of the two level system that experiences a position dependent splitting is intended to provide an intuition as to the role of the control. More generally, the system Hamiltonian is changed by moving the state of the control between two regions of the total Hilbert space corresponding to different effective system Hamiltonians. This is sketched in Fig. 12.1b. Consider a system coupled to the control by a Hamiltonian of the form

$$H_{CS} = \Pi_C^i \otimes H_S^i + \Pi_C^f \otimes H_S^f + H_{CS}^\perp \quad (12.10)$$

where  $\Pi_C^i$  and  $\Pi_C^f$  are projectors onto different subregions,  $R_i$  and  $R_f$  respectively, of the control.  $H_{CS}^\perp$  has support only outside those two subspaces, i.e.  $(\Pi_C^i \otimes X_S)H_{CS}^\perp = (\Pi_C^f \otimes X_S)H_{CS}^\perp = 0$  for any system operator  $X_S$ . When the control is prepared in a state with support in region  $R_i$  only, the initial effective system Hamiltonian is  $H_S^i$ . The evolution of the control system is induced by a unitary operation that is chosen to switch the control system from a state with support in region  $R_i$  to one in  $R_f$ . This changes the effective system Hamiltonian to  $H_S^f$ .

*Time reversal.* As the classical Crooks equality relates a forwards process to its time reversed variant, any quantum generalisation of it requires a means of defining this reversed process. For this reason, the quantum time reversal operation  $\mathcal{T}$  is introduced.

The time reversal operation can be enacted by complex conjugation or the transpose operation. While complex conjugation is the ‘textbook’ [39] quantum time reversal operation, its anti-linearity can make it mathematically arduous and so in [37] the transpose is used. The two are equivalent on Hermitian operators and as such we have that for any state or observable,  $\sigma$ , that  $\mathcal{T}(\sigma) := \sigma^T \equiv \sigma^*$  where  $*$  and  $T$  are the complex conjugation and transpose operations respectively. The basis that the transpose is taken with respect to is dictated by the physical implementation considered. Specifically, it is chosen such that the time reversed control states drive the change in Hamiltonian from  $H_S^f$  back to  $H_S^i$  and such that the global Hamiltonian and evolution operator are time reversal invariant.

A sense of how  $\mathcal{T}$  operates can be gained by looking at its effect on the evolution of a state. Suppose an initial state  $\rho_i$  evolves under a time reversal invariant unitary,  $U = \mathcal{T}(U) = U^T$ , to some state  $\rho_f$ , i.e.  $\rho_f = U\rho_iU^\dagger$ . Then the time reversed version of the final state  $\mathcal{T}(\rho_f)$  evolves back under  $U$  to the time reversed version of the initial state  $\mathcal{T}(\rho_i)$ , i.e.  $\mathcal{T}(\rho_i) = U\mathcal{T}(\rho_f)U^\dagger$ . This follows from rearranging  $\rho_f^T = U^{\dagger T}\rho_i^T U^T = U^\dagger\rho_i^T U$ .

In terms of our bipartite example, it is natural to take  $\mathcal{T}()$  to be the transpose operation in the  $x_M$  and  $\sigma_S^z$  bases. This ensures the thermal states of the two level system are invariant, but that the momentum of the motional states are reversed, under  $\mathcal{T}$ . Suppose, for example, that in the forwards process the motional state is prepared and measured in optical coherent states [40]  $|\alpha_i\rangle\langle\alpha_i|_M$  and  $|\alpha_f\rangle\langle\alpha_f|_M$ , centered in the regions  $x < x_i$  and  $x > x_f$  respectively and with momentum in the positive  $x$  direction. Then the states for the reverse process, leaving aside the additional impact of the temperature dependent operator in Eq. (12.5), are  $|\alpha_i^*\rangle\langle\alpha_i^*|_M$  and  $|\alpha_f^*\rangle\langle\alpha_f^*|_M$ . As the position and momentum of a coherent state  $|\alpha\rangle$  are proportional to the real and imaginary parts of  $\alpha$  respectively, this reverses the momentum of the machine while leaving its position unchanged. As such, preparing the machine in  $|\alpha_f^*\rangle\langle\alpha_f^*|_M$  drives the required reverse change in effective system Hamiltonian.

*Derivation.* The cleanest derivation of the coherent Crooks equality makes use of two properties: ‘global invariance’ and ‘factorisability’.

Global invariance is a property of a pair of states,  $\rho_i$  and  $\rho_f$ , of a single system with a time reversal invariant Hamiltonian  $H$  and a strictly energy conserving and time reversal invariant unitary evolution  $V$ . By exploiting the fact that  $H$  and  $V$  are time reversal invariant and commute it is found that the quantity

$$\mathrm{Tr} \left[ \rho_f V \exp \left( -\frac{H}{2k_B T} \right) \rho_i \exp \left( -\frac{H}{2k_B T} \right) V^\dagger \right] \quad (12.11)$$

is invariant under the transformation  $\rho_i \rightarrow \mathcal{T}(\rho_f)$  and  $\rho_f \rightarrow \mathcal{T}(\rho_i)$ . This property is the starting point to derive a large family of quantum fluctuation theorems and plays an analogous role to detailed balance for classical fluctuation theorems.

Factorisability characterises the extent to which multiple interacting systems can be considered independent subsystems and enables a Crooks-like equality to be derived from global invariance. This condition holds when the system, thermal bath, control and work store are effectively non-interacting at the start and end of the forwards and reverse protocols. Specifically, the bipartite setup is factorisable if the exponential of  $H_{MS}$  factorises into a  $H_M$  term and a  $H_S^i$  or  $H_S^f$  term when acting on the machine states  $|\psi_M^i\rangle$  and  $|\psi_M^f\rangle$  respectively, i.e. if

$$\begin{aligned} & \exp\left(-\frac{H_{MS}}{2k_B T}\right) (|\psi_M^k\rangle\langle\psi_M^k| \otimes \mathbb{1}_S) \exp\left(-\frac{H_{MS}}{2k_B T}\right) \\ &= \exp\left(-\frac{H_M}{2k_B T}\right) |\psi_M^k\rangle\langle\psi_M^k| \exp\left(-\frac{H_M}{2k_B T}\right) \otimes \exp\left(-\frac{H_S^k}{k_B T}\right) \end{aligned} \quad (12.12)$$

for  $k = i$  and  $k = f$ .

For a complete derivation, see Appendix I of [37] or [41].

*Externally controlled and autonomous variants.* There are two variants of the coherent Crooks equality corresponding to different ways in which the evolution is induced. The equalities take the same general form; however, they are derived from different assumptions about the setup Hamiltonian.

In the externally controlled variant, the evolution is induced by the *application* of some energy conserving unitary operation. It is more natural to picture this variant when the control and work store are independent systems. The system and work store Hamiltonians are then simply assumed to be non-interacting, i.e.

$$H_{WCS} = \mathbb{1}_W \otimes H_{CS} + H_W \otimes \mathbb{1}_{CS}, \quad (12.13)$$

where  $H_{CS}$  is defined in Eq. (12.10). In the bipartite case the thermal machine and system Hamiltonians must interact for the machine to act as the control. Instead their Hamiltonian is required to not induce evolution between the initial and final subregions, i.e.  $(\mathbb{1}_M - \Pi_M^i)H_M\Pi_M^i = 0$  and  $(\mathbb{1}_M - \Pi_M^f)H_M\Pi_M^f = 0$ . These restrictions to the setup Hamiltonian ensure that the coherent Crooks equality holds exactly.

However, there is an apparent tension here. The time evolution of the setup will be determined by some Hamiltonian  $H_{WCS}^{\text{evol}}$  where  $V_{WCS} = \exp(-iH_{WCS}^{\text{evol}}t)$ . This Hamiltonian must contain interaction terms to enable the exchange of energy between the system and work store. As such,  $H_{WCS}^{\text{evol}} \neq H_{WCS}$  and we have two distinct Hamiltonians for the setup. This can be reconciled by thinking of  $H_{WCS}$  as parameterising the states at the start and end of the protocols and  $H_{WCS}^{\text{evol}}$  as the ‘true’ Hamiltonian that completely describes the energy of the setup.

The second variant avoids the tension entirely; however, at the cost of not being exact. In this case the setup Hamiltonian includes a term to drive the evolution of the control and to transfer energy between the system and work store. The setup then

evolves *autonomously* under this Hamiltonian. This case is inexact because in order for the autonomous evolution of the setup to induce the required change in system Hamiltonian, the system must be interacting with the work store and control at all times. As a result the factorisability condition does not hold exactly. The approximate nature of the autonomous coherent Crooks equality is formally quantified by an error bound in [37]. Numerical simulations [37, 41] indicate that for a wide parameter range, the errors fall below plausible experimental error margins. Hence, in such regimes the equality can nonetheless essentially be treated as exact.

The two level system with a motional machine example is most naturally understood in the autonomous variant. In this example, the Hamiltonian  $H_{MS}$  would simply contain kinetic, and possibly potential, energy terms. For example,  $H_M$  in Eq. (12.1) could be a harmonic oscillator Hamiltonian centered halfway between  $x_i$  and  $x_f$ . When the system and thermal machine evolve under  $V_{MS} = \exp(-iH_{MS}t)$  this then drives the required translation process. The coherent Crooks equality holds to a high degree of accuracy when the machine is prepared far from interaction region, i.e. outside of the region  $x_i < x < x_f$  in Fig. 12.2. This is intuitive because when prepared far from the interaction region, the interaction between the machine and the two level system is effectively negligible and consequently they can be seen as approximately independent.

The control in the autonomous variant plays a role similar to that of the quantum clocks that have been studied elsewhere in quantum thermodynamics [42] and quantum information theory [43, 44]. As with quantum clocks, this variant is partially motivated by the desire to avoid the implicit dependence on an additional, potentially classical, system (the experimentalist and their apparatus) that is required to apply a unitary operation.

## 12.4 Conceptual Significance

*Gibbs map and generalised energy flow.* We saw in Sect. 12.2 that two new concepts emerged from applying the standard Crooks equality approach of comparing a forwards and reverse process in the presence of a coherent energy supply: firstly, the operation that parameterises the thermal machine states, Eq. (12.5), and secondly, the function  $\Delta\tilde{E}$  that replaces the classical work term in the coherent Crooks equality, Eq. (12.6). Their precise forms, in particular their temperature dependence, are forced by the derivation of the coherent Crooks equality. While the full significance of these new concepts is very much an open research question; a study of their basic properties suggests that they are not only convenient mathematical definitions but also physically natural.

The temperature dependent operation that parameterises the thermal machine states in Eq. (12.5), emerges from the Gibbs map<sup>3</sup>,  $G_\rho$ , which given a system with

---

<sup>3</sup>The global invariance and factorisability conditions can be naturally reformulated in terms of the Gibbs map. If we define the transition probability from a state  $G_{\rho_A}(H, T)$  to a state  $\rho_B$  as  $P(\rho_B|G_{\rho_A}(H, T)) := \text{Tr}[\rho_B V G_{\rho_A}(H, T) V^\dagger]$ , then global invariance can be

Hamiltonian  $H$  at temperature  $T$ , is defined as,

$$G_\rho(H, T) := \frac{\exp\left(-\frac{H}{2k_B T}\right)\rho\exp\left(-\frac{H}{2k_B T}\right)}{\tilde{Z}_\rho(H, T)}, \quad (12.14)$$

$$\tilde{Z}_\rho(H, T) := \text{Tr} \left[ \exp\left(-\frac{H}{k_B T}\right)\rho \right].$$

An intuition as to the action of the map can be obtained through a couple of examples. When the energy is exactly known, the state is completely constrained, and the map has no effect: an energy eigenstate is left unchanged. However, when the energy of the state is completely uncertain, as in a maximally mixed state,  $\propto \mathbb{1}$ , or in an equal superposition,  $\propto \sum_k^N |E_k\rangle$ , a thermal rescaling is applied such that the maximally mixed state is mapped to the thermal state and the equal superposition to the coherent thermal state, a pure state with the same energy populations as the thermal state i.e.  $\propto \sum_k \exp(-E_k/2k_B T) |E_k\rangle$ . Note, the map is non-dephasing and affects the energy populations in the same way irrespective of the coherent properties and phase of the state. In this way, the map makes a state crudely ‘as thermal as possible’ subject to the constraints imposed by the input state and the temperature of the bath. However, this loose claim is not intended to be taken literally but rather as a signpost towards the map’s deeper physical significance.

The energies of the machine states are parameterised by  $\tilde{E}$  as defined in Eq. (12.8). This function is a state dependent mathematical generalisation of the equilibrium free energy, Eq. (12.7), in which the standard partition function,  $Z(H, T) := \text{Tr} \left[ \exp\left(-\frac{H}{k_B T}\right) \right]$ , is replaced by the Gibbs map normalisation term  $\tilde{Z}_\rho(H, T)$ .

A study of the properties of  $\tilde{E}$  hints at its naturalness as a statistical, temperature dependent, energy scale for quantum states. For an energy eigenstate,  $\tilde{E}$  is simply the associated eigenstate energy. This is intuitive because when the energy of a state is well-defined there is no need to statistically estimate it. Moreover, it is required to regain the classical limit. More generally,  $\tilde{E}$  is upper bounded by the average energy  $\langle H \rangle$ , and tends towards it in the high temperature limit. In the general finite temperature quantum case, where  $\tilde{E}$  does not coincide with the average energy, the function nonetheless obeys several physically desirable properties for an statistical energy scale. Firstly,  $\tilde{E}$  scales with a constant offset or multiplicative factor to  $H$  as one would expect an energy measure to scale; i.e.  $\tilde{E}_\rho(H + \delta, T) = \tilde{E}_\rho(H, T) + \delta$  and  $\tilde{E}_\rho(\lambda H, T) = \lambda \tilde{E}_\rho(H, \lambda T)$ . Secondly,  $\tilde{E}$  depends on the energy populations of a state only. This means that (i) it is independent of the phase of the state and as such in the absence of interactions remains constant in time and (ii) it takes the same value for a pure state and its completely dephased variant. Again, these properties imply that  $\tilde{E}$  has deeper physical significance that is worth further investigation [45].

---

rewritten as  $P(\rho_f|G_{\rho_i}(H, T))/P(\mathcal{T}(\rho_i)|G_{\mathcal{T}(\rho_f)}(H, T)) = \tilde{Z}_{\mathcal{T}(\rho_f)}(H, T)/\tilde{Z}_{\rho_i}(H, T)$ . The bipartite setup is factorisable if  $G_{\rho_M \otimes \rho_S}(H_M S, T) = G_{\rho_M}(H_M, T) \otimes G_{\rho_S}(H_S, T)$  and  $\tilde{Z}_{\rho_M \otimes \rho_S}(H_M S, T) = \tilde{Z}_{\rho_M}(H_M, T) \otimes \tilde{Z}_{\rho_S}(H_S, T)$ .

*Thermal operations link.* Resource theories take properties that are in some sense useful, but usually scarce, and attempt to precisely characterise them. They do this by specifying a restricted set of operations, known as ‘free operations’, and defining the states that cannot be generated using solely free operations as ‘resources’. Of particular relevance to quantum thermodynamics are the resource theories of entanglement [46], coherence [47], noise [48] and the thermal operations framework [34–36] (see also Chap. 26).

The quantum channel induced on the machine in the coherent Crooks equality is a thermal operation and as such previous results within the thermal operations framework [27–31, 33–36] are applicable. Thermal operations, consist of the following three operations: firstly, performing a global unitary,  $U$ , that strictly conserves total energy,  $H$ , in the sense that  $[H, U] = 0$ ; secondly, adding a system at thermal equilibrium; thirdly, disregarding (tracing out) any system. The quantum channel on the machine is precisely of this form. For the forwards process we have,

$$\mathcal{E}(\rho_M) = \text{Tr}_S \left[ V_{MS} (\rho_M \otimes \gamma(H_S^i)) V_{MS}^\dagger \right], \quad (12.15)$$

and the reverse process channel is identical except the system is prepared in a thermal state with respect to its final Hamiltonian. The resource states of the thermal operations framework are states with coherence with respect to the energy eigenbasis or non-thermally distributed populations. Correspondingly, the machine states are resources in virtue of being prepared in a pure state. For further discussion on incorporating fluctuating work into the thermal operations framework, see [38].

*Off-diagonal equality.* The form of the coherent Crooks equality can be better understood via a closely related equality also derived in [37]: the off-diagonal Crooks equality. This equality states that the evolution of the energy coherences of the thermal machine (the off-diagonal elements of thermal machine density operator with respect to the energy eigenbasis), evolve in the same way as the populations (the diagonal elements). The evolution of the off-diagonal elements of the machine in the energy basis are quantified by the transition amplitudes  $q_+^\delta(f|i) := \langle E_M^f | \text{Tr}_S[V(|E_M^i\rangle\langle E_M^{i+\delta}| \otimes \gamma(H_S^f))V^\dagger]|E_M^{f+\delta}\rangle$  and  $q_-^\delta(i|f) := \langle E_M^{i+\delta} | \text{Tr}_S[V(|E_M^{f+\delta}\rangle\langle E_M^f| \otimes \gamma(H_S^f))V^\dagger]|E_M^f\rangle$ . Similarly to the diagonal elements in Eq. (12.9), they are constrained to obey

$$\frac{q_+^\delta(f|i)}{q_-^\delta(i|f)} = \exp \left( \frac{1}{k_B T} ((E_i - E_f) - \Delta F) \right). \quad (12.16)$$

The off-diagonal Crooks equality can be seen as emerging from the non-trivial constraints imposed by thermal operations. That the coherences are constrained to evolve in the same way as the populations is a result of strict energy conservation and the fact the system is initially thermally distributed. Pictorially, as sketched in Fig. 12.3, energy conservation enforces a see-saw operation that maps changes in the system energy onto that of the machine. The strict conservation of energy then further ensures that a superposition of machine states is raised or lowered ‘as one’

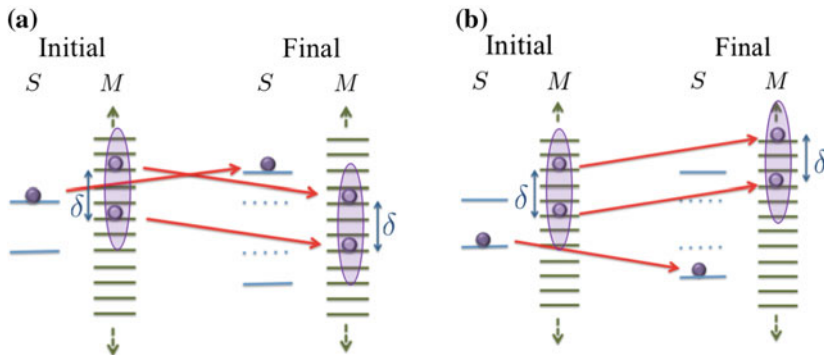


**Fig. 12.3** The process of increasing the splitting of a two level system in the presence of a harmonic oscillator machine. The left and right figures cover the cases when the qubit system starts in the excited (a) and ground (b) states respectively. The see-saw like mechanism, highlighted by the red arrows, ensures energy conservation and maps changes in the system energy onto that of the machine. A superposition of machine states is raised or lowered ‘as one’ and as such the coherences evolve in the same manner as the populations.

and as such the coherences evolve in the same manner as the populations. These constraints imposed by energy conservation can also be seen as resulting from time translation symmetry.

## 12.5 Conclusions

We have given a brief summary of a framework introduced in [37, 38] which endeavours to extend work fluctuations to the quantum regime using ideas from the information theoretic approach to quantum thermodynamics. This approach is distinguished by its use of time independent Hamiltonians and its decision to explicitly model not only a driven system and its thermal bath but also the control system and work store that enable the system to be driven. Specifically, we have presented one of the key results of this framework: a Crooks-like equality for a system with a coherent energy supply, Eq. (12.6).

The equalities that we have presented in this chapter are not the most general. There are variants of Eq. (12.6) in which (to name just a few): (i) the control and work store are separate systems; (ii) the work store is prepared in a mixed state and correspondingly a non-projective POVM is performed at the end of the protocol. (iii) the system is prepared in a non thermal state. (iv) entanglement between the subsystems is incorporated. For these more general cases and others, see [37].

The thermal bath can play a more active role than it does in the version we have discussed. The simplest way of doing so is to reinterpret the system  $S$  that we have been discussing as an enlarged system that incorporates the thermal bath. This amounts to effectively dealing with some large system that starts at equilibrium and considering changing the Hamiltonian of a small part of it. Alternatively, a quantum fluctuation relation for Markovian master equations is included in [37] to provide a link to the open quantum systems approach to quantum thermodynamics.

Moreover, in [37] the quantum Crooks equality is initially formulated in terms of the forwards and reverse quantum channels induced on the work store. This is more in the spirit of a fully quantum, information theoretic, Crooks equality. For the purpose of a pedagogical introduction, we chose to present its reformulation in terms of transition probabilities in order to maintain a closer resemblance to the classical Crooks equality.

An advantage of this transition probability formalism is that it is clearer how one might go about experimentally testing the coherent Crooks equality. This is especially true of its autonomous variant. The example of the two level system that experiences a position dependent splitting is not just a pedagogical example but the basis of an experimental proposal utilising trapped ions and the AC Stark shift that is presented in [41]. As such while the equality might appear rather abstract, it is nonetheless physically implementable.

The coherent Crooks equality is conceptually new and there remain numerous open research questions. As already discussed, the physical significance of the Gibbs map and the generalised energy flow have yet to be pinned down. In [37], links are touched on between the coherent Crooks equality and other key concepts in quantum information theory including the Petz recovery map [49], quantum reference frames [50] and quantum clocks [42–44]; these warrant further investigation. There is also the question of whether the equality could be converted from its current form in terms of transition probabilities of the energy supply, to an equality that is stated in terms of probability distributions of the energy changes of the system. More fundamentally, while it is clear that quantum coherence generates non-trivial quantum corrections to these fluctuation theorems, questions remain as to the implications for our understanding of irreversibility in quantum mechanics and as to whether they could provide any practical quantum advantage.

**Acknowledgements** The author thanks Johan Åberg, Álvaro Alhambra, Janet Anders, Florian Mintert, Erick Hinds Mingo, Tom Hebdige and Jake Lishman for commenting on drafts and David Jennings for numerous indispensable discussions. The author is supported by the Engineering and Physical Sciences Research Council Centre for Doctoral Training in Controlled Quantum Dynamics.

## References

1. M. Esposito, U. Harbola, S. Mukamel, Nonequilibrium fluctuations, fluctuation theorems, and counting statistics in quantum systems. *Rev. Mod. Phys.* **81**(4), 1665–1702 (2009). <https://doi.org/10.1103/RevModPhys.81.1665>
2. M. Campisi, P. Hänggi, P. Talkner, Colloquium: Quantum fluctuation relations: Foundations and applications. *Rev. Mod. Phys.* **83**(3), 771–791 (2011). <https://doi.org/10.1103/RevModPhys.83.771>
3. P. Hänggi, P. Talkner, The other QFT. *Nat. Phys.* **11**(2), 108–110 (2015). <https://doi.org/10.1038/nphys3167>
4. S. Vinjanampathy, J. Anders, Quantum thermodynamics. *Contemp. Phys.* **57**(4), 545–579 (2016). <https://doi.org/10.1080/00107514.2016.1201896>

5. G.E. Crooks, Entropy production fluctuation theorem and the nonequilibrium work relation for free energy differences. *Phys. Rev. E* **60**(3), 2721–2726 (1999). <https://doi.org/10.1103/PhysRevE.60.2721>
6. C. Jarzynski, How does a system respond when driven away from thermal equilibrium? *Proc. Natl. Acad. Sci.* **98**(7), 3636–3638 (2001). <https://doi.org/10.1073/pnas.081074598>
7. H. Tasaki, Jarzynski relations for quantum systems and some applications (2000). [arXiv:cond-mat/0009244](https://arxiv.org/abs/cond-mat/0009244)
8. J. Kurchan, A quantum fluctuation theorem. (2000). [arXiv:cond-mat/0007360](https://arxiv.org/abs/cond-mat/0007360)
9. P. Talkner, P. Hägggi, The Tasaki Crooks quantum fluctuation theorem. *J. Phys. A: Math. Theor.* **40**(26), F569 (2007). <https://doi.org/10.1088/1751-8113/40/26/F08>
10. M. Campisi, P. Talkner, P. Hägggi, Fluctuation theorem for arbitrary open quantum systems. *Phys. Rev. Lett.* **102**(21), 210401 (2009). <https://doi.org/10.1103/PhysRevLett.102.210401>
11. C.J. Jarzynski, Nonequilibrium work theorem for a system strongly coupled to a thermal environment. *Stat. Mech.* **2004**(9), P09005 (2004). <https://doi.org/10.1088/1742-5468/2004/09/P09005>
12. G. Manzano, J.M. Horowitz, J.M.R. Parrondo, Nonequilibrium potential and fluctuation theorems for quantum maps. *Phys. Rev. E* **92**(3), 032129 (2015). <https://doi.org/10.1103/PhysRevE.92.032129>
13. T. Albash, D.A. Lidar, M. Marvian, P. Zanardi, Fluctuation theorems for quantum processes. *Phys. Rev. E* **88**(3), 032146 (2013). <https://doi.org/10.1103/PhysRevE.88.032146>
14. A.E. Rastegin, Non-equilibrium equalities with unital quantum channels. *J. Stat. Mech.* **2013**(06), P06016 (2013). <https://doi.org/10.1088/1742-5468/2013/06/P06016>
15. P. Talkner, P. Hägggi, Aspects of quantum work. *Phys. Rev. E* **93**(2), 022131 (2016). <https://doi.org/10.1103/PhysRevE.93.022131>
16. M. Perarnau-Llobet, E. Bäumer, K.V. Hovhannisyan, M. Huber, A. Acin, No-Go Tteorem for the characterization of work fluctuations in coherent quantum systems. *Phys. Rev. Lett.* **118**(7), 070601 (2017). <https://doi.org/10.1103/PhysRevLett.118.070601>
17. M. Lostaglio, Quantum fluctuation theorems, contextuality, and work quasiprobabilities. *Phys. Rev. Lett.* **120**(4), 040602 (2018). <https://doi.org/10.1103/PhysRevLett.120.040602>
18. A. E. Allahverdyan, Nonequilibrium quantum fluctuations of work. *Phys. Rev. E* **90**(3), 032137 (2014). <https://doi.org/10.1103/PhysRevE.90.032137>
19. P. Solinas, H.J.D. Miller, J. Anders, Measurement-dependent corrections to work distributions arising from quantum coherences. *Phys. Rev. A* **96**(5), 052115 (2017). <https://doi.org/10.1103/PhysRevA.96.052115>
20. H.J.D. Miller, J. Anders, Time-reversal symmetric work distributions for closed quantum dynamics in the histories framework. *New J. Phys.* **19**(6), 062001 (2017). <https://doi.org/10.1088/1367-2630/aa703f>
21. J.M. Horowitz, Quantum-trajectory approach to the stochastic thermodynamics of a forced harmonic oscillator. *Phys. Rev. E* **85**(3), 031110 (2012). <https://doi.org/10.1103/PhysRevE.85.031110>
22. C. Elouard, D.A. Herrera-Martí, M. Clusel, A. Auffeves, The role of quantum measurement in stochastic thermodynamics. *NPJ Quantum Inf.* **3**(1), 9 (2017). <https://doi.org/10.1038/s41534-017-0008-4>
23. F.G.S.L. Brandao, M.B. Plenio, Entanglement theory and the second law of thermodynamics. *Nat. Phys.* **4**(11), 873 (2008). <https://doi.org/10.1038/nphys1100>
24. L. Del Rio, J. Åberg, R. Renner, O. Dahlsten, V. Vedral, The thermodynamic meaning of negative entropy. *Nature* **474**(7349), 61 (2011). <https://doi.org/10.1038/nature10123>
25. D. Jennings, T. Rudolph, Entanglement and the thermodynamic arrow of time. *Phys. Rev. E* **81**(6), 061130 (2010). <https://doi.org/10.1103/PhysRevE.81.061130>
26. S. Popescu, A.J. Short, A. Winter, Entanglement and the foundations of statistical mechanics. *Nat. Phys.* **2**(11), 754–758 (2006). <https://doi.org/10.1038/nphys444>
27. J. Åberg, Truly work-like work extraction via a single-shot analysis. *Nat. Commun.* **4**, 1925 (2013). <https://doi.org/10.1038/ncomms2712>

28. J. Åberg, Catalytic coherence. Phys. Rev. Lett. **113**(15), 150402 (2014). <https://doi.org/10.1103/PhysRevLett.113.150402>
29. K. Korzekwa, M. Lostaglio, J. Oppenheim, D. Jennings, The extraction of work from quantum coherence. New J. Phys. **18**(2), 023045 (2016). <https://doi.org/10.1088/1367-2630/18/2/023045>
30. F.G.S.L. Brandao, M. Horodecki, N. Ng, J. Oppenheim, S. Wehner, The second laws of quantum thermodynamics. PNAS **112**(11), 3275–3279 (2015). <https://doi.org/10.1073/pnas.1411728112>
31. M. Lostaglio, D. Jennings, T. Rudolph, Description of quantum coherence in thermodynamic processes requires constraints beyond free energy. Nat. Commun. **6**, 6383 (2015). <https://doi.org/10.1038/ncomms7383>
32. M. Horodecki, J. Oppenheim, Fundamental limitations for quantum and nanoscale thermodynamics. Nat. Commun. **4**, 2059 (2013), <http://doi.org/10.1038/ncomms3059>
33. G. Gour, D. Jennings, F. Buscemi, R. Duan, I. Marvian, Quantum majorization and a complete set of entropic conditions for quantum thermodynamics (2017). <https://doi.org/10.1038/s41467-018-06261-7>
34. D. Janzing, P. Wocjan, R. Zeier, R. Geiss, T. Beth, Thermodynamic cost of reliability and low temperatures: Tightening Landauer's principle and the Second law. Int. J. Theor. Phys. **39**(12), 2717–2753 (2000). <https://doi.org/10.1023/A:1026422630734>
35. F.G.S.L. Brandao, M. Horodecki, J. Oppenheim, J.M. Renes, R.W. Spekkens, Resource theory of quantum states out of thermal equilibrium. Phys. Rev. Lett. **111**(25), 250404 (2013). <https://doi.org/10.1103/PhysRevLett.111.250404>
36. M. Horodecki, Fundamental limitations for quantum and nanoscale thermodynamics. J. Oppenheim, Nat. Commun. **4**, 2059 (2013). <https://doi.org/10.1038/ncomms3059>
37. J. Åberg, Fully quantum fluctuation theorems. Phys. Rev. X **8**, 011019 (2018). <https://doi.org/10.1103/PhysRevX.8.011019>
38. Á.M. Alhambra, L. Masanes, Fluctuating work: From quantum thermodynamical identities to a second law equality. J. Oppenheim, C. Perry, Phys. Rev. X **6**(4), 041017 (2016). <https://doi.org/10.1103/PhysRevX.6.041017>
39. L.E. Ballentine, *Quantum Mechanics: A Modern Development* (World scientific, 1998). <https://doi.org/10.1142/3142>
40. C. Gerry, P. Knight, *Introductory Quantum Optics* (Cambridge University Press, Cambridge, 2005)
41. Z. Holmes, S. Weidt, D. Jennings, J. Anders, F. Mintert, Coherent fluctuation relations: from the abstract to the concrete (2018), <arXiv:1806.11256>
42. M. Frenzel, D. Jennings, T. Rudolph, Quasi-autonomous quantum thermal machines and quantum to classical energy flow. New J. Phys. **18**(2), 023037 (2016). <https://doi.org/10.1088/1367-2630/18/2/023037>
43. M.P. Woods, R. Silva, Autonomous quantum machines and finite sized clocks. J. Oppenheim (2016). <https://doi.org/10.1007/s00023-018-0736-9>
44. A.S.L. Malabarba, A.J. Short, P. Kammerlander, Clock-driven quantum thermal engines. New J. Phys. **17**(4), 045027 (2015). <https://doi.org/10.1088/1367-2630/17/4/045027>
45. E. Hinds Mingo, D. Jennings, Superpositions of mechanical processes, decomposable coherence and fluctuation relations (2018). <arXiv:1812.08159>
46. R. Horodecki, P. Horodecki, M. Horodecki, K. Horodecki, Quantum entanglement. Rev. Mod. Phys. **81**(2), 865–942 (2009). <https://doi.org/10.1103/RevModPhys.81.865>
47. A. Streltsov, G. Adesso, M.B. Plenio, Colloquium: Quantum coherence as a resource. Rev. Mod. Phys. **89**(4), 041003 (2017). <https://doi.org/10.1103/RevModPhys.89.041003>
48. G. Gour, M.P. Müller, V. Narasimhachar, R.W. Spekkens, N.Y. Halpern, The resource theory of informational nonequilibrium in thermodynamics. Phys. Rep. **583**, 1–58 (2015). <https://doi.org/10.1016/j.physrep.2015.04.003>
49. D. Petz, Sufficient subalgebras and the relative entropy of states of a von Neumann algebra. Commun. Math. Phys. **105**(1), 123–131 (1986). <https://doi.org/10.1007/BF01212345>
50. S.D. Bartlett, T. Rudolph, R.W. Spekkens, Reference frames, superselection rules, and quantum information. Rev. Mod. Phys. **79**(2), 555–609 (2007). <https://doi.org/10.1103/RevModPhys.79.555>

# Chapter 13

## The Role of Quantum Work Statistics in Many-Body Physics



John Goold, Francesco Plastina, Andrea Gambassi and Alessandro Silva

In this contribution, we aim to illustrate how quantum work statistics can be used as a tool in order to gain insight on the universal features of non-equilibrium many-body systems. Focusing on the two-point measurement approach to work, we first outline the formalism and show how the related irreversible entropy production may be defined for a unitary process. We then explore the physics of sudden quenches from the point of view of work statistics and show how the characteristic function of work can be expressed as the partition function of a corresponding classical statistical physics problem in a film geometry. Connections to the concept of fidelity susceptibility are explored along with the corresponding universal critical scaling. We also review how large deviation theory applied to quantum work statistics gives further insight to universal properties. The quantum-to-classical mapping turns out to have close connections with the historical problem of orthogonality catastrophe: we therefore discuss how this relationship may be exploited in order to experimentally extract quantum work statistics in many-body systems.

---

J. Goold (✉)

School of Physics, Trinity College Dublin, Dublin 2, Ireland  
e-mail: gooldj@tcd.ie

F. Plastina

Dip. Fisica, Università della Calabria, Arcavacata di Rende (CS) 87036, Italy  
and  
INFN - Gruppo collegato di Cosenza, Cosenza, Italy

A. Gambassi

SISSA — International School for Advanced Studies, via Bonomea 265, 34136 Trieste, Italy  
and  
INFN, sezione di Trieste, via Bonomea 265, 34136 Trieste, Italy

A. Silva

SISSA — International School for Advanced Studies, via Bonomea 265, 34136 Trieste, Italy

### 13.1 Introduction

Over the past decade or so, there has been a surge of interest in the non-equilibrium dynamics of closed quantum systems following a switch of a Hamiltonian parameter. This is primarily due to a series of spectacular experiments in ultra-cold atoms, whereby the high degree of isolation permits the study of coherent dynamics over timescales typically inaccessible in conventional condensed matter physics [1–3]. These experiments not only have raised new fundamental questions in the realm of non-equilibrium statistical mechanics, but have also revived a number of important theoretical issues such as the relationship between thermalisation and integrability [2, 4–7] and the universality of defect generation following evolution across a critical point [8].

Over the same period of time, there has also been a great deal of activity in the statistical mechanics community surrounding the development of stochastic thermodynamics [9] and the study of non-equilibrium fluctuation relations in both the classical [10, 11] and quantum domain [12–14]. Loosely speaking, the name of the game is to study the thermodynamics of both classical and quantum systems beyond the linear response and to describe and understand the usual thermodynamic quantities such as work, heat and entropy as stochastic variables described by probability distributions. The fluctuation relations, then, encode the full non-linear response of a system to a time-dependent change of a Hamiltonian parameter. One particular feature is that the formalism permits the definition of irreversible entropy production of a unitary evolving system following a thermodynamic transformation; and, as such, it allows us to understand the emergence of thermodynamic behaviour in systems where the microscopic laws are inherently reversible [15]. These ideas have been cross-fertilized by the emergence of another community studying what has become known as quantum thermodynamics [16] aiming at understanding the relationship between quantum mechanics and thermodynamics from first principles.

Given the current experimental interest in the non-equilibrium dynamics of quantum many-body systems, and the recent developments in statistical mechanics, along with the emergence of a flourishing community in quantum thermodynamics, it is natural to study the dynamics of quantum many-body systems in this far-from-equilibrium thermodynamical formulation. In fact, this endeavour has been initiated a decade ago by Silva, who focused on explicit calculations of work statistics in a quantum critical many-body system [17]; the universal features that can be uncovered in this way were further elucidated in a series of subsequent works [18–24]. In fact, throughout this decade, there has been quite a remarkable amount of activity uncovering the features of work statistics in a range of physical models including spin chains [15, 25–35], Fermionic systems [36–44], Bosonic systems and Luttinger liquids [45–53], periodically driven quantum systems [54–57] among many others [58–67]. Work statistics have also proved to be useful in the analysis of dynamical quantum criticality [68, 69] and more recently to shed light on the phenomenon of information scrambling [70, 71]. The purpose of this brief review is to motivate and pontificate on the view that such non-equilibrium manipulations of quantum

many-body systems can be seen, primordially, as thermodynamic transformations. In particular, we would like to focus our efforts on singling out what we consider to be the advantages of this line of reasoning and to highlight some interesting features of work statistics in many-body physics, which may not be apparent or appreciated across different communities. For the purposes of this contribution, we will primarily focus on the paradigm of sudden quenches.

We shall begin with an overview of work statistics and associated quantities such as the irreversible entropy production. We then move on to the issue of sudden quenches and show how the characteristic function is related to the partition function of a higher-dimensional statistical model. From here, we show how it is possible to understand universal features of quench problems through connections with the well-known concepts of fidelity, fidelity susceptibility and large deviation theory [72]. Furthermore, we highlight the connection with the historically important problem of Anderson orthogonality catastrophe [73] and the closely related Fermi edge singularity [74, 75] and explain how ongoing experiments in ultra-cold atoms are, in fact, linked to this problem and in principle can and should be used as a platform in order to extract work statistics in the many-body domain.

## 13.2 Quantum Work Statistics and Thermodynamics

Consider a quantum system described by a Hamiltonian  $H(\lambda)$  that depends on an external work parameter  $\lambda$ , i.e., an externally controlled parameter whose value determines the equilibrium configuration of the system. The system is prepared at time  $t \leq 0$  by allowing it to equilibrate with a heat reservoir at inverse temperature  $\beta$  for a fixed value of the time-dependent work parameter  $\lambda(t \leq 0) = \lambda_0$ . The initial state of the system is, thus, the Gibbs state  $\rho_G(\lambda_0)$ , where

$$\rho_G(\lambda) := \frac{e^{-\beta H(\lambda)}}{\mathcal{Z}(\lambda)}, \quad (13.1)$$

and the partition function  $\mathcal{Z}(\lambda) := \text{Tr}[e^{-\beta H(\lambda)}]$ . At time  $t = 0$  the system-reservoir coupling is removed and a protocol is performed on the system taking the work parameter  $\lambda(t)$  from its initial value  $\lambda_0$  to a final value  $\lambda_\tau$  at a later time  $t = \tau$ . The initial and final Hamiltonians connected by the protocol  $\lambda_0 \rightarrow \lambda_\tau$  have the spectral decompositions  $H(\lambda_0) = \sum_n \epsilon_n(\lambda_0) |\epsilon_n\rangle \langle \epsilon_n|$  and  $H(\lambda_\tau) = \sum_m \epsilon'_m(\lambda_\tau) |\epsilon'_m\rangle \langle \epsilon'_m|$ , respectively, where  $|\epsilon_n\rangle$  ( $|\epsilon'_m\rangle$ ) is the  $n$ -th ( $m$ -th) eigenstate of the initial (final) Hamiltonian with eigenvalue  $\epsilon_n$  ( $\epsilon'_m$ ). Work in the quantum domain results from a process and is not an observable in the sense that one cannot ascribe a Hermitian operator to it [76].

The definition of the work  $W$  done on the system as a consequence of the protocol requires two projective measurements; the first projects onto the eigenbasis of the initial Hamiltonian  $H(\lambda_0)$  at  $t = 0$ , with the system in thermal equilibrium and renders a certain value  $\epsilon_n$  with probability  $p_n^0 = e^{-\beta \epsilon_n} / \mathcal{Z}(\lambda_0)$ . The system, then, evolves

under the unitary dynamics  $U(\tau; 0)$  generated by the protocol  $\lambda_0 \rightarrow \lambda_\tau$  before the second measurement projects onto the eigenbasis  $\{|\epsilon'_m\rangle\}$  of the final Hamiltonian  $H(\lambda_\tau)$  and yields the values  $\{\epsilon'_m\}$  with probability  $p_{m|n}^\tau = |\langle \epsilon'_m | U(\tau, 0) | \epsilon_n \rangle|^2$ . The probability of obtaining  $\epsilon_n$  for the first measurement outcome followed by  $\epsilon'_m$  for the second measurement is then  $p_n^0 p_{m|n}^\tau$  and, accordingly, the work distribution is given by

$$P(W) = \sum_{n,m \geq 0} p_n^0 p_{m|n}^\tau \delta(W - (\epsilon'_m - \epsilon_n)). \quad (13.2)$$

Equation (13.2) therefore encodes the fluctuations in the work that arise from both the thermal statistics  $p_n^0$  and the quantum measurement statistics  $p_{m|n}^\tau$  over many identical realizations of the protocol. The first moment  $\langle W \rangle$  of the distribution is the average work done and can be easily shown to be  $\langle W \rangle = \text{Tr}[H(\lambda_\tau)\rho_\tau] - \text{Tr}[H(\lambda_0)\rho_G(\lambda_0)]$  where  $\rho_\tau = U(\tau, 0)\rho_G(\lambda_0)U^\dagger(\tau, 0)$ , i.e., nothing more than the energy change along the driven unitary process.

Now compare this transformation  $\lambda_0 \rightarrow \lambda_\tau$  with an ideal quasi-static isothermal one, which, unlike an adiabatic transformation, is not unitary in general, and would bring the system through a path within the manifold of equilibrium states described by Eq. (13.1). The work performed in the isothermal process is given by the free energy change  $\Delta F$ . When this is subtracted from the actual work done  $\langle W \rangle$ , one obtains back the so-called irreversible work  $\langle W_{irr} \rangle$ , which, when multiplied by the initial inverse temperature, defines the average irreversible entropy change

$$\langle S_{irr} \rangle = \beta \langle W_{irr} \rangle := \beta(\langle W \rangle - \Delta F) = D(\rho_\tau || \rho_G(\lambda_\tau)). \quad (13.3)$$

The energetic deviation  $\langle W_{irr} \rangle$  is often also called dissipated work rather than irreversible. The reason it is given the name irreversible is an assumption that somewhere in the background there is a canonical thermal bath where, after the driving, the system re-relaxes to a thermal state at the same initial temperature.

The last equality in Eq. (13.3) expresses the irreversible entropy as the quantum relative entropy between the actual final state  $\rho_\tau$  and the final reference state  $\rho_G(\lambda_\tau)$ ,  $D(\rho_\tau || \rho_G(\lambda_\tau)) = -S(\rho_\tau) - \text{Tr}\{\rho_\tau \ln \rho_G(\lambda_\tau)\}$ , with  $S(\rho)$  being the Von Neumann entropy  $S(\rho) = -\text{Tr}\{\rho \ln \rho\}$ .  $D$  is the quantum analogue of the Kullback–Leibler divergence and a very stringent measure of the distinguishability of two quantum states via a result known as quantum Stein’s lemma. While not itself a metric, it still upper bounds the trace distance via Pinsker’s inequality,

$$\langle S_{irr} \rangle = D[\rho_\tau || \rho_G(\lambda_0)] \geq \|\rho_\tau - \rho_G(\lambda_0)\|_1^2 / 2 \quad (13.4)$$

which captures the optimal distinguishability of quantum states with a single measurement. It can also be seen as a type of generalized second law for unitary processes [77]. A non zero  $\langle S_{irr} \rangle$ , thus, signals the fact that the system has been brought out-of-equilibrium though a thermodynamically irreversible process, and it also gives a quantification of how far from equilibrium it has gone, as it marks the difference between the actual final state  $\rho_\tau$  and the equilibrium state  $\rho_G(\lambda_\tau)$ . It is also directly

connected to the fact that the work has a stochastic nature. Indeed, the existence of work fluctuations implies that the cumulants  $C_n$  of the work distribution  $P(W)$  are in general non-zero. In particular, the fact that  $C_n \neq 0$  with  $n \geq 2$  means that  $W$  has not a well defined value, as it is the case, instead, in the macroscopic thermodynamic context. It is possible to show that the irreversible entropy is, in fact, related to these cumulants by

$$\langle S_{irr} \rangle = \sum_{n=2}^{+\infty} (-1)^n \frac{\beta^n}{n!} C_n, \quad (13.5)$$

which, in the linear response regime, under a gaussian approximation, reduces to  $\langle S_{irr} \rangle = \beta^2 \sigma^2 / 2$ , where  $\sigma^2 = C_2$  is the variance of the work distribution function.

Being cast in the form of a relative entropy, the strict positivity of  $\langle S_{irr} \rangle$  is guaranteed via Klein's inequality. In fact, one could also work directly with the fluctuation theorems to demonstrate this positivity - for example Jarzynski's equality simply states that  $\langle e^{-S_{irr}} \rangle = 1$  and then by application of Jensen's inequality one gets  $\langle S_{irr} \rangle \geq 0$ . Quantum fluctuation theorems and their important physical consequences are covered in many excellent and comprehensive overviews [12–14] and we direct the reader towards them for more in depth analysis. For more information on work statistics we recommend the original paper detailing the non-observable nature of work [76] and an excellent overview paper on many aspects of quantum work distributions [78].

### 13.3 Sudden Quench from the Ground State

#### 13.3.1 Quantum-Classical Correspondence and Universality

One particular type of protocol that is very popular in ultra cold atomic experiments is the so-called sudden quench, in which the change in the work parameter  $\lambda$  is performed on a vanishingly small time scale. A very appealing thermodynamics description of such processes is given in terms of the characteristic function of work.

Consider, first, the characteristic function of the work distribution as the Fourier transform of Eq. (13.2) for a general time-dependent driving process,

$$\begin{aligned} g(u, \tau) &:= \int dW e^{iuW} P(W), \\ &= \text{Tr} [U^\dagger(\tau, 0) e^{iuH(\lambda_\tau)} U(\tau, 0) e^{-iuH(\lambda_0)} \rho_G(\lambda_0)]. \end{aligned} \quad (13.6)$$

In the case of a sudden quench,  $\lambda_0 \rightarrow \lambda_f$ , the expression simplifies due to  $U(\tau = 0, 0) = \mathbb{1}$  such that  $g(u, \tau = 0) = g(u) = \text{Tr} [e^{iuH(\lambda_f)} e^{-iuH(\lambda_0)} \rho_G(\lambda_0)]$ . This expression is very similar, in particular in the case of a pure initial state, to the core hole Green's function, quantity typically studied in the context of X-ray Fermi edge singularities in condensed matter physics (see Sect. 13.4).

We now assume that the system is prepared in the ground state  $|\epsilon_0\rangle$  of  $H(\lambda_0)$ , i.e.,  $\rho_G(\lambda_0) = |\epsilon_0\rangle\langle\epsilon_0|$  and a sudden quench  $\lambda_0 \rightarrow \lambda_f$  is performed so that the characteristic function now takes the form

$$g(u) = e^{-i\epsilon_0 u} \langle\epsilon_0|e^{iH(\lambda_f)u}|\epsilon_0\rangle \quad (13.7)$$

$$= \sum_{m \geq 0} e^{i(\epsilon'_m - \epsilon_0)u} |\langle\epsilon'_m|\epsilon_0\rangle|^2. \quad (13.8)$$

If we interpret the conjugate variable  $u$  as a time scale, we see that this expression represents, up to a phase, a vacuum persistence amplitude, i.e., the probability amplitude to remain in the initial ground state at time  $t = u$ . As such, it is obviously related to the survival probability  $L(t) = |g^*(t)|^2$  which is often studied in quantum chaos [79]. Most importantly, with the characteristic function written as a matrix element of the evolution operator  $\exp[iH(\lambda_f)u]$  we can map upon analytic continuation  $u \rightarrow iR$  the sudden quantum quench problem to the problem of a classical system in a film geometry of thickness  $R$ . This was first pointed out by Silva in Ref. [17], but here we will outline the approach fleshed out in a later work [18].

Let us define the difference  $\Delta\epsilon_0 = \epsilon'_0 - \epsilon_0$  between the ground state energies of the pre- and post-quench Hamiltonians and perform the analytic continuation to the imaginary axis mentioned above, obtaining

$$\begin{aligned} g(R) &= e^{-\Delta\epsilon_0 R} \times \mathcal{Z}(R), \\ \mathcal{Z}(R) &= \langle\epsilon_0|e^{-[H(\lambda_f) - \epsilon'_0]R}|\epsilon_0\rangle. \end{aligned} \quad (13.9)$$

For a  $d$ -dimensional quantum system possessing a  $d + 1$  dimensional classical correspondent,  $\mathcal{Z}(R)$  can be seen as the partition function of the latter on a film of thickness  $R$ , with two boundary states  $|\epsilon_0\rangle$  and a transverse “area”  $L^d$  set by the extension of quantum system, assumed to be characterised by the large length  $L$ . With the partition function form now in place, we can appeal to traditional statistical mechanics and take the logarithm of the expression in order to get a free energy  $F(R) = -\ln(g(R))$  of the film and its corresponding density per transverse area, i.e.,  $f(R) = F(R)/L^d$ . For large  $R$  it is possible to separate this out into three contributions based on their dependence on decreasing powers of  $R$ , i.e.,

$$f(R) = R \times f_b + 2f_s + f_C(R), \quad (13.10)$$

where  $f_b = \Delta\epsilon_0/(R \times L^d)$  is the bulk free energy density of the classical system and  $f_s$  is the surface free energy per unit area associated with the two identical boundaries of the film. The remaining contribution  $f_C(R)$  represents an effective finite-size interaction per unit area between the two confining surfaces which generically decays to zero at large separation  $R$ . In particular, one can write

$$\mathcal{Z}(R) = e^{-L^d[2f_s + f_C(R)]}. \quad (13.11)$$

Let us now translate the information contained in the three components of the free energy density  $f(R)$  into information about the statistics of the work. As stated above, the bulk free energy determined by  $f_b$  is just related to a global phase in front of the vacuum persistence amplitude. Since  $f_C(R) \rightarrow 0$  as  $R \rightarrow +\infty$ , the surface component  $f_s$  of the free energy is, instead, connected to the limit for large  $R$  of the matrix element  $\langle \epsilon_0 | e^{-i[H(\lambda_f) - \epsilon'_0]R} | \epsilon_0 \rangle$  which defines  $\mathcal{Z}(R)$  in Eq. (13.9). It is then easy to see that

$$e^{-2L^d f_s} = |\langle \epsilon_0 | \epsilon'_0 \rangle|^2 = \mathcal{F}^2, \quad (13.12)$$

where the quantity  $\mathcal{F}$  introduced on the right-hand side is the so-called fidelity between the ground states of the post- and pre-quench Hamiltonians, a quantity which is intensively studied in quantum information and many-body physics. In particular, it is a useful tool for analysing quantum critical systems [80–82]. In the context of the work distribution for the sudden quench protocol at zero temperature, the fidelity  $\mathcal{F}$  is the probability to measure the adiabatic work  $W = \Delta\epsilon_0$  in the two-time measurement scheme. If the post-quench Hamiltonian  $H(\lambda_f)$  of the quantum many-body system in question has a critical point at  $\lambda_f = \lambda_c$ , then the generalised susceptibilities [80]  $\chi_n(\lambda_0, \lambda_f) = -L^{-d} \partial_{\lambda_f}^n \ln \mathcal{F}(\lambda_0, \lambda_f)$ , can develop a non-analytic behaviour [80]. In particular, it is known that the fidelity susceptibility  $\chi_2$  scales as

$$\chi_2 \propto |\lambda_f - \lambda_c|^{\nu d - 2}, \quad (13.13)$$

where  $\nu$  is the correlation length critical exponent.

The generalised susceptibilities  $\chi_n$  have a straightforward interpretation in terms of the analogy with boundary statistical mechanics, which is particularly suggestive when the quenched parameter  $\lambda$  of  $H(\lambda)$  can be interpreted as a “temperature” in the  $d+1$  classical correspondent of the quantum model. This is the case, for example, of the transverse field in the quantum Ising chain [83]. Since in general the generalized susceptibilities can be written as derivatives of the surface free energy, i.e.,

$$\chi_n(\lambda_0, \lambda_f) = \partial_{\lambda_f}^n f_s(\lambda_0, \lambda_f), \quad (13.14)$$

it is evident that, when  $\lambda$  is a temperature-like variable, they have a clear physical interpretation,  $\chi_1$  being the excess internal energy and  $\chi_2$  the excess specific heat of the corresponding  $d+1$  classical confined system. The excess specific heat is well-known to scale as  $\chi_2 \propto |\lambda_f - \lambda_c|^{-\alpha_s}$  close to the critical point where the exponent  $\alpha_s$  is related to the bulk critical exponents of the correlation length  $\nu$  and of the specific heat  $\alpha$  by  $\alpha_s = \alpha + \nu$  of the classical  $d+1$  dimensional system and satisfy the hyperscaling relation  $\alpha + \nu(d+1) = 2$  [84, 85].

Relating quantum quenches to the statistical physics of classical confined systems provides useful information not only on the singularities of the generalised susceptibilities, but also on the emergent universal features of the probability distribution function of the work when, as above, the post-quench Hamiltonian is close to a critical point. Before proceeding, we note that for a quench starting from the ground state

$|\epsilon_0\rangle$  of the pre-quench Hamiltonian, the quantity  $\Delta\epsilon_0$  represents the *reversible* work one would do on the system by performing the change  $\lambda_0 \rightarrow \lambda_f$  adiabatically. This also sets the minimal possible value of the stochastic variable  $W$  and, accordingly, the irreversible work  $W_{irr} = W - \Delta\epsilon_0$  can take only positive values. This means that its probability distribution  $P(W_{irr})$  displays a lower edge and, based on the correspondence highlighted above, we can finally demonstrate that

$$P(W_{irr}) \simeq \mathcal{F}^2 [\delta(W_{irr}) + \mathcal{C}(W_{irr} - qm)^{1-a} u_s(W_{irr} - qm) + \dots], \quad (13.15)$$

where  $u_s(\dots)$  is the Heaviside unit step and the parameters appearing in this expression are the fidelity  $\mathcal{F}$  (defined above), the mass  $m$  of the lightest quasi-particle in the model, and three *universal* constants  $\mathcal{C}$ ,  $q$ , and  $a$ .

This universality stems ultimately from the fact that the leading part of the finite-size free energy  $f_C(R)$  of the  $d+1$ -dimensional classical systems in finite-size geometry [86, 87] acquires a universal character whenever it — and thus the post-quench Hamiltonian  $H(\lambda_f)$  of the  $d$ -dimensional quantum system — is close to a bulk *critical point*. In particular this so-called critical Casimir effect [88] is characterised by a scaling behaviour

$$f_C(R) = R^{-d} \Theta_B(\pm R/\xi_+), \quad (13.16)$$

where + and − refer to the disordered and ordered phases, respectively.  $\xi_+ \propto |\lambda_f - \lambda_c|^{-\nu}$  is the exponential correlation length associated with the critical fluctuations of the relevant order parameter of the transition, which grows upon approaching it. Both  $\xi_+$  and  $R$  are assumed to be much larger than any microscopic length scale of the system such as, e.g., a possible lattice spacing. The scaling function  $\Theta_B$  is characterised by a certain degree of *universality* [88, 89], as many other properties close to critical points, which become independent of the microscopic features of the system. In particular,  $\Theta_B$  depends only on the universality class of the classical critical point and, because of the presence of the boundaries set by the quantum state  $|\epsilon_0\rangle$ , it depends also on their *surface universality class* [84, 85] or, equivalently, on which of the few effective boundary states  $\mathcal{B} \in \{|\phi_i^*\rangle\}_i$ , the initial/boundary state  $|\epsilon_0\rangle$  flows to as the critical point is approached. Accordingly,  $\Theta_B$  is also largely independent of the specific values assumed by  $\lambda_0$  and  $\lambda_f \simeq \lambda_c$ . In view of its numerous applications to the physics of soft matter, the critical Casimir effect has been extensively studied both theoretically and experimentally in the past few years (see, e.g., Ref. [88]) and many of its features are known, including the scaling function  $\Theta_B$  for a variety of bulk and surface universality classes.

While the large- $R$  decay of  $f_C$  is  $\propto R^{-d}$  at criticality  $\xi_+ = \infty$ , away from the critical point it is dictated by the asymptotic expansion of  $\Theta_B(x)$  for  $|x| \gg 1$ . Generically, it takes the form

$$\Theta_B(x \rightarrow \pm\infty) = \mathcal{C}_{\pm} |x|^{a_{\pm}} e^{-q_{\pm}|x|} + \dots, \quad (13.17)$$

where  $\mathcal{C}_\pm$ ,  $a_\pm$  and  $q_\pm > 0$  are universal constants (dependent only on  $\mathcal{B}$ ), which take different values within the ordered ( $-$ ) and disorderd ( $+$ ) phases. For the quantum (classical) Ising model in  $d = 1$  ( $d = 2$ ) one has  $q_+ = a_+ = 1$ , while  $q_- = 2$  and  $a_- = -1/2$ , corresponding to two possible instances of quenches; i.e., within the same phase or across the quantum phase transition. These constants directly enter Eq. (13.15), while the mass  $m$  of the lightest quasi-particle of the quantum model in the paramagnetic phase has to be identified with the inverse  $\xi_+^{-1}$  of the correlation length of the classical system. Performing the analytic continuation  $R \mapsto -iu$  the behavior of  $P(W)$  for  $W$  close to threshold is determined by the asymptotic behavior of the characteristic function  $g(u)$  for large  $u$ . Therefore, performing a large  $u$  expansion of  $g(u)$  and taking its Fourier transform we readily obtain that  $P(W)$  takes the form in Eq. (13.15).

### 13.3.2 Large Deviations

Work is an extensive quantity in thermodynamics. Standard statistical mechanics textbooks tell us that the mean of a generic extensive quantity such as the average work  $\langle W \rangle$  done on a system will grow proportionally to its number  $N$  of degrees of freedom, where  $N = L^d$  for a system of typical size  $L$  in  $d$  spatial dimensions. Accordingly, it is natural to define an associated *intensive* quantity  $w$  by dividing  $W$  by  $N$  and, assuming weak correlations among the  $N$  degrees of freedom, the central limit theorem tells us that the distribution of  $w$  will be generically Gaussian for large  $N$ , with fluctuations  $\Delta w = \sqrt{\langle (w - \bar{w})^2 \rangle}$  around the average value  $\bar{w} \equiv \langle w \rangle$  suppressed as  $1/\sqrt{N}$ . This means that, generically,  $w - \bar{w} \sim N^{-1/2}$  and that the distribution of  $w$  concentrates around its average and most probable value  $\bar{w}$ . However, rare as they may be, large deviations of  $w$  with  $w - \bar{w} \sim 1$  are well-known to be able to probe specific features of statistical systems [72]. As shown in Ref. [19], the work statistics of a sudden quantum quench can be cast in the framework of large deviation theory and it might display some *universal* features when the post-quench Hamiltonian is close to an equilibrium critical point.

Consider now as the stochastic variable the intensive work  $w = W/N$  as opposed to the extensive one  $W$ . As shown in Ref. [19], the probability  $P(w)$  that a large fluctuation will occur is expected to be exponentially small in the size  $N$ , i.e.,

$$P(w) \propto \exp[-NI(w)], \quad (13.18)$$

where  $I(w)$  is the non-negative rate function which characterises the large deviations and which vanishes for  $w = \bar{w}$ . The quadratic approximation of  $I(w)$  around  $w = \bar{w}$  describes the typical Gaussian fluctuations  $w - \bar{w} \sim N^{-1/2}$  expected on the basis of the central limit theorem. Let us consider the case of a quench from the ground state  $|\epsilon_0\rangle$  of the pre-quench Hamiltonian: as discussed in the previous section, the irreversible work  $W_{irr} = W - \Delta\epsilon_0$  can take only positive values. For convenience, we focus on the large deviations of the irreversible intensive work  $W_{irr}/N$ , which is

denoted below, for simplicity, by  $w$ , with  $P(w < 0) = 0$  and therefore  $I(w < 0) = +\infty$ . In order to compute  $I(w)$  appearing in Eq. (13.18) it is convenient first to focus on the moment generating function of  $W_{irr}$ , i.e., on  $\langle e^{-RW_{irr}} \rangle$  which is related to  $g(R)$  in Eq. (13.9). In particular, because of the shift in the definition of  $W_{irr}$  compared to  $W$ , the contribution  $NR \times f_b$  corresponding to the bulk free energy on the r.h.s. of that equation is cancelled, and only the so-called *excess free energy*  $Nf_{ex}(R)$ , with density  $f_{ex}(R) = f(R) - Rf_b$ , contributes to the moment generating function [19]:

$$\langle e^{-RW_{irr}} \rangle = \exp[-Nf_{ex}(R)]. \quad (13.19)$$

Note that the generating function on the r.h.s. is certainly defined for all possible non-negative values of  $R \in \mathbb{R}^+$  and it is actually related to the excess free energy density of the corresponding classical system in a film geometry  $L^d \times R$ , as discussed in Sect. 13.3.1, only in this case. Depending on the behaviour of  $P(W_{irr})$  for large  $W_{irr}$ , however, the domain  $\mathcal{D}$  within which the generating function is defined can also include negative values of  $R$  and therefore the equality on Eq. (13.19) is understood after an analytic continuation of  $f_{ex}(R)$  on the r.h.s. towards  $R < 0$ . With the generating function in the form (13.19) we can apply the formalism of large deviation theory that gives us the prescription to evaluate the rate function through the Legendre–Fenchel transformation of  $f_{ex}(R)$ ,

$$I(w) = -\inf_{R \in \mathcal{D}} [Rw - f_{ex}(R)], \quad (13.20)$$

i.e., via a saddle-point evaluation of  $P(w)$  in Eq. (13.18) as the inverse Laplace transform of Eq. (13.19) for  $N \rightarrow \infty$ . From the r.h.s. of Eq. (13.19) one sees that  $f_{ex}(0) = 0$ ,  $f'_{ex}(0) = \bar{w}$ , and that  $f_{ex}(R)$  is a concave function of  $R$ , being the exponential function on the l.h.s. a convex function. In addition,  $f_{ex}$  approaches  $2f_s$  as  $R \rightarrow \infty$ . We can infer some properties of the rate function  $I(w)$  on the basis of these qualitative features of  $f_{ex}$ . For  $w < 0$ , for example, the infimum on the r.h.s. of Eq. (13.20) is attained for  $R \rightarrow \infty$  and therefore  $I(w < 0) = +\infty$ , as expected because  $W_{irr} \geq 0$ . Similarly, the behaviour of  $I(w)$  close to the threshold  $w \rightarrow 0^+$  is determined by that of  $f_{ex}(R \rightarrow \infty)$  and, in particular,  $I(0) = 2f_s$ . The way this value is approached depends on the finite-size contribution  $f_C(R)$  in Eq. (13.10). As discussed in Sect. 13.3.1, this contribution acquires a universal character whenever the corresponding  $d+1$ -dimensional classical system — and therefore the post-quench Hamiltonian  $H(\lambda_f)$  of the  $d$ -dimensional quantum system — is close to a bulk critical point. In this case,  $f_C(R)$  takes the universal scaling form in Eq. (13.16), characterised by the scaling form  $\Theta_B$ , which is known in a variety of cases (see, e.g., Ref. [88]).

Based on this knowledge of  $\Theta_B$ , the rate function  $I(w)$  can be readily calculated via Eq. (13.20), finding

$$I(w) = 2f_s + \xi^{-d}\vartheta(w\xi^{d+1}), \quad (13.21)$$

where  $\vartheta(y)$  is the Legendre–Fenchel transform (see Eq. (13.20)) of  $x^{-d}\Theta_{\mathcal{B}}(x)$  and it is as universal as  $\Theta_{\mathcal{B}}$ .

Accordingly, not only the edge singularities of the extensive work  $W$  discussed in Sect. 13.3.1 above are determined by universal features of the system and of the quench, but also the large deviations of the intensive variable associated with the irreversible work  $W_{irr}$  display universal properties in their rate function  $I(w)$  close to the threshold  $w = 0$ . For larger values of  $w$ , the rate function  $I(w)$  depends on the excess free energy  $f_{ex}(R)$  of films with increasingly smaller thickness  $R$ , which even becomes negative for  $w \geq \bar{w}$ . In this case, the correspondence with the physics of classical systems in film geometry breaks down and universality is generically lost. However, concrete examples show that interesting phenomena analogous to a Bose-Einstein condensation [19] as well as non-analyticities of the rate function  $I(w)$  [67] similar to non-equilibrium phase transitions may occur.

### 13.3.3 Thermal Quenches

The previous two sub-sections, strictly speaking, describe only sudden quenches starting from the ground-state, which are characterised by the fact that the work  $W$  cannot be smaller than the value  $\Delta\epsilon_0$ . Accordingly, the probability distribution  $P(W)$  of  $W$  features an edge which acquires the universal features discussed above. Here we will demonstrate that interesting information can still be obtained from both the average work and the irreversible entropy production when an initial thermal state  $\rho_G(\lambda_0)$  is assumed and the edge is absent. The average work done  $\langle W \rangle = \int P(W)WdW$  by a sudden quench  $\lambda_0 \rightarrow \lambda_f$  of a parameter  $\lambda$  which couples linearly in  $H(\lambda)$  and starting from a thermal state can be written in the following form [26, 47]

$$\begin{aligned} \langle W \rangle &= \frac{\text{Tr} \{ e^{-\beta H(\lambda_0)} [H(\lambda_f) - H(\lambda_0)] \}}{\text{Tr} \{ e^{-\beta H(\lambda_0)} \}} \\ &= (\lambda_f - \lambda_0) F'_\beta(\lambda_0), \end{aligned} \quad (13.22)$$

which follows from the fact that  $H(\lambda_f) - H(\lambda_0) = (\lambda_f - \lambda_0)\partial H(\lambda_0)/\partial\lambda_0$  and equals the derivative of the equilibrium free energy with respect to the parameter  $\lambda_0$  times the quench amplitude. From this, we can see that, for sudden quenches, the expression of the irreversible work takes the interesting form  $\langle W_{irr} \rangle = \langle W \rangle - \Delta F = (\lambda_f - \lambda_0)F'_\beta(\lambda_0) - F_\beta(\lambda_f) + F_\beta(\lambda_0)$ . Let us restrict ourselves to small quenches, such that  $\delta\lambda = \lambda_f - \lambda_0 \ll 1$ ; in this case, the irreversible entropy production defined by Eq. (13.3) can be seen as proportional to the second derivative of the equilibrium free energy,

$$\langle S_{irr} \rangle = -(\delta\lambda)^2 \beta F''_\beta(\lambda_0)/2 + \mathcal{O}(\beta(\delta\lambda)^3). \quad (13.23)$$

Generically, a possible non-analytic behaviour in  $F''_\beta$  is characterised by the critical exponent  $\alpha$  of the specific heat  $C \propto -F''_\beta(\lambda_0) \propto |\lambda_0 - \lambda_c|^{-\alpha}$ . At finite temperature, there is no quantum phase transitions; but, as was shown in Ref. [15] for quenches of the Ising model, the irreversible entropy production starts to diverge as the temperature decreases, thus signalling the proximity to a quantum critical point. In a first-order quantum phase transition, the average work becomes discontinuous. A comparison between first and second order phase transitions has been performed in Ref. [26]. We note that we have been explicitly considering sudden quench problems in the preceeding sections and from the many-body perspective very little work has been done on more generic time-dependent processes [22]: it would be interesting to extend studies in this direction. In addition, there has been recently some interesting work in the direction of finite time charging of quantum batteries with connection to quantum correlations [90–94], given that these studies are finite-time manipulations of interacting quantum systems, it would be interesting to explore connections with the prescription outlined here.

## 13.4 Anderson Orthogonality Catastrophe and Current Experiments

### 13.4.1 Orthogonality Catastrophe

In this section, we would like to discuss how the concept of quantum work statistics in sudden quenches is actually connected to the historically important problem of orthogonality catastrophe (OC) in condensed matter physics. This phenomenon was discovered by Philip W. Anderson in 1967 [95]. Anderson was studying the seemingly innocuous problem of a single scatterer in the presence of a non-interacting Fermi gas. He considered the ground states of both  $N$  Fermions in a spherical box of radius  $R$  in the presence and absence of a single local scattering potential with only  $s$ -wave ( $l = 0$ ) contribution. In the presence of a scattering potential,  $V$ , the single-particle states in the box acquire a phase shift  $\delta(E)$ . The fermions being assumed to be non-interacting, the ground states are expressed as Slater determinants of the single-particle eigenstates. Let the ground state of the unperturbed system be  $\Psi_i(x_1, x_2, \dots, x_N)$  and the ground state of the perturbed system be  $\Psi_f(x_1, x_2, \dots, x_N)$ ; Anderson proved that the overlap (fidelity) of these two states scales as

$$\begin{aligned} F &= \int dx_1 dx_2 \dots dx_N \Psi_f^*(x_1, x_2, \dots, x_N) \Psi_i(x_1, x_2, \dots, x_N) \\ &= N^{-\alpha}, \end{aligned} \tag{13.24}$$

where  $\alpha = \delta^2/\pi^2$ . This implies that the ground states become orthogonal as the system size increases with a power-law that depends universally on the phase shift  $\delta$ . This phenomenon is known as the orthogonality catastrophe (OC). Innocuous and all

as this result may first seem, it actually has several deep implications for the physics of Fermi gases. For example, there is an immediate consequence for the situation where a local impurity is made to interact with the gas. Generically, the interaction between an impurity and a Fermi gas will lead to a dressing of the impurity by the excitations of the gas. In particular, when the mass of the impurity is finite, then one may talk about the formation of a well-defined quasi-particle: the Fermi polaron. In condensed matter physics, this effect is quantified by the quasi-particle residue, which, mathematically speaking, is equivalent to the fidelity between perturbed and un-perturbed ground states. In the limit of a heavy particle, instead, the problem may be framed in the infinite-mass approximation and the dressed particle loses its quasi-particle description as the fidelity goes to zero due to the manifestation of the OC.

At this point one might ask: what is the connection between work statistics and the previously recalled formalism? Well, going beyond ground-state physics, perhaps the most dramatic consequence of the OC is in non-equilibrium dynamics. Historically, this consequence was discovered, very soon after the original realisation by Anderson, by Nozières and de Dominicis [75] who were considering the many electron response to the sudden switching on of a core hole in a metal. Physically, this occurs after an X-ray photon has created a deep hole, with the promotion (emission) of a core electron in a metal. Nozières and de Dominicis considered the core hole Green's function, which is defined as

$$\mathcal{G}(t) = -ie^{-\omega_T} u_s(t) \langle e^{itH_i} e^{-it(H_i+V)} \rangle, \quad (13.25)$$

where  $\omega_T$  is the threshold frequency for the creation of a core hole in the valence band,  $u_s(t)$  is the Heaviside step function and  $H_i$  and  $H_i + V$  are the perturbed and unperturbed Hamiltonians, respectively. We note that for the purposes of illustration we are assuming an initial thermal state but the calculation can be performed directly in the zero-temperature limit [96]. The key quantity of this problem is the vacuum persistence amplitude,

$$\nu_\beta(t > 0) = \left\langle e^{\frac{i}{\hbar} \hat{H}_i t} e^{-\frac{i}{\hbar} (\hat{H}_i + \hat{V}) t} \right\rangle. \quad (13.26)$$

This gives the response of the gas to the switching on of the localized impurity potential, and, as pointed out previously, this coincides with the complex conjugate of the characteristic function of work defined by Eq. (13.8), thus giving an immediate connection to the work statistics formalism. We will return to this shortly. In the interaction picture, the expression for the vacuum persistence amplitude (or, equivalently, the complex conjugate of the characteristic function of work) reads:

$$\nu_\beta(t) = \left\langle T e^{-\frac{i}{\hbar} \int_0^t dt' \tilde{V}(t')} \right\rangle, \quad \tilde{V}(t) = e^{\frac{i}{\hbar} \hat{H}_0 t} \hat{V} e^{-\frac{i}{\hbar} \hat{H}_0 t}, \quad (13.27)$$

which, by virtue of the linked cluster theorem, reduces to an exponential sum of connected Feynman diagrams containing an increasing number of interaction vertices:

$$\Lambda_\beta(t) = \text{---} \circlearrowleft \Lambda_1^\beta(t) \bullet + \bullet \circlearrowright \Lambda_2^\beta(t) \bullet + \dots$$

If the reader is interested in precise details of the calculation of the linked cluster expansion we recommend the text book by Mahan [96]. It turns out that the first term in the sum is nothing but a first-order shift to the Fermi gas energy, which brings only a phase factor to  $\nu_\beta(t)$ . The second term, instead, gives the dominant (singular) contribution, which is a direct manifestation of the OC. Taking the  $\beta \rightarrow \infty$  limit, an explicit calculation gives

$$\Lambda_2^{\beta \rightarrow \infty}(t) = -g \ln(it/\tau_0 + 1), \quad (13.28)$$

where  $g$  is a rescaled impurity interaction strength parameter which is proportional to  $\alpha$  in the Anderson overlap. The mathematical consequence of this result is a power-law decay of  $\nu(t)$ . However, the real physical implication becomes apparent if we consider the absorption spectrum, which is precisely what is measured in X-ray scattering experiments and is defined as

$$A(\omega) = 2\text{Re} \int_0^{+\infty} dt e^{i\omega_T t} \nu(t). \quad (13.29)$$

The power-law decay of  $\nu(t)$  leads to a power-law threshold singularity in the absorption spectrum. This iconic non-equilibrium effect is known as the Fermi edge singularity in condensed matter physics. The physics is crucially encapsulated by the Anderson overlap and it is illuminating now to rather interpret the phenomenon from a thermodynamic perspective. Since  $\nu_{\beta \rightarrow \infty}$  is nothing more than the complex conjugate of the characteristic function, then the absorption spectrum can be interpreted as the probability to do work on the system as they are mathematically equivalent. Writing the absorption spectrum in the Lehmann representation, indeed, we have

$$A(\omega) \propto \sum_m |\langle \epsilon'_m | \epsilon_0 \rangle|^2 \delta(W - \epsilon'_m + \epsilon_0). \quad (13.30)$$

The thermodynamic implication of these considerations should be immediately obvious. Interpreting the creation of a core hole as thermodynamic work on a metal, and interpreting the absorption spectrum as the work distribution  $P(W)$ , we see that due to the OC there is no possibility that this process can be adiabatic. The probability to do adiabatic work  $W = \epsilon'_0 - \epsilon_0$  goes to zero as a power-law due to the OC between  $|\epsilon_0\rangle$  and the ground state of the system. In Ref. [97] the authors have undertaken a very careful examination of the moments of the work statistics and found that it was in fact the third moment of the work distribution, which quantifies the skew-

ness or asymmetry of the process, which scales with the universal exponent of the edge-singularity  $g$ . In summary, we would like to stress that, although the motivation is very different, from the operational perspective the mathematics of the Fermi-edge singularity problem at its core are identical to the formal framework needed to describe the quantum work statistics of a sudden *local* quench of a Fermi gas. This is, in fact, quite important and not just a mere curiosity, as it paves the way for a detailed experimental study of quantum work statistics in ultra-cold atom setups, where orthogonality catastrophe and Fermi-edge singularity physics are currently being probed. This connection is not fully appreciated in either the ultra-cold atom or the thermodynamics community. Indeed, it has been argued that trapped ultra-cold fermion atoms could constitute an almost ideal set-up to investigate this physics in a controlled fashion [36, 39, 98], and a detailed treatment of the Fermi edge singularity problem for a harmonically trapped gas has been recently performed [41, 44], which generalises the result in Eq. (13.28).

### 13.4.2 Experiments with Ultra-cold Fermions

The experimental extraction of quantum work statistics involves the rather precarious setting of not only having to prepare a well-defined initial state and perform controlled unitary operations, but also there is the apparent stringent necessity of performing two non-destructive projective measurements on the eigen-basis of the system. This is in contrast to classical work statistics and has rendered the experimental acquisition of quantum work statistics elusive up until relatively recently. The first proposal was for a clever phonon shelving technique for direct extraction of work statistics in an ion trap [99]. Actually as it turned out, two papers appearing at the same time proposed the use of Ramsey interferometry on an ancillary qubit in order to extract the characteristic function of work [100, 101] (see also Ref. [102]) avoiding the difficult projective measurements. This led to the first experimental extraction of work statistics and experimental verification of the fluctuation theorems in a quantum system in a liquid state NMR setup [103]. An experimental work confirming the first proposal for direct measurement in the energy domain appeared soon after in an ion trap setup [104]. More recently, following the realization that a work distribution can in principle be reformulated as a positive operator valued measurement (POVM) [50, 105], an experiment has been performed to reconstruct the distribution  $P(W)$  with Rubidium atoms in an atom chip [106].

More directly related to our discussion about the relations between work distribution and OC, two experiments have been performed with cold Li atoms, forming a Fermi sea to which an impurity K atom is coupled [107, 108]. After preparing the impurity in a superposition of its (two lowest) internal energy states, Feshbach resonance has been used to tune the coupling with the gas and to switch it on only in the excited state. The theoretical blue print for this idea were first outlined in Refs. [36] and [39]. Using Ramsey interferometry of the impurity internal state and monitoring the decoherence dynamics, the vacuum persistence amplitude has been

experimentally measured, both in amplitude and phase, together with the absorption spectrum, for both repulsive and attractive impurity-gas interactions.

Given the direct connection between work statistics and the OC and associated Fermi-edge singularity problem, we would like to strongly emphasise that these experimental platforms of dilute Fermi mixtures are ideal playgrounds for the controlled exploration of universal features in the quantum thermodynamics of many-body systems.

**Acknowledgements** J.G. is supported by a SFI Royal Society University Research Fellowship. This project has received funding under the European Union's Horizon 2020 research and innovation programme (great agreement no 758403-ODYSSEY).

## References

1. I. Bloch, J. Dalibard, W. Zwerger, Rev. Mod. Phys. **80**, 885 (2008). <https://doi.org/10.1103/RevModPhys.80.885>
2. A. Polkovnikov, K. Sengupta, A. Silva, M. Vengalattore, Rev. Mod. Phys. **83**, 863 (2011). <https://doi.org/10.1103/RevModPhys.83.863>
3. M. Cazalilla, R. Citro, T. Giamarchi, E. Orignac, M. Rigol, Rev. Mod. Phys. **83**, 1405 (2011). <https://doi.org/10.1103/RevModPhys.83.1405>
4. J. Eisert, M. Friesdorf, C. Gogolin, Nat. Phys. **11**, 124 (2015). <https://doi.org/10.1038/nphys3215>
5. F. Borgonovi, F. Izrailev, L. Santos, V. Zelevinsky, Phys. Rep. **626**, 1 (2016). <https://doi.org/10.1016/j.physrep.2016.02.005>
6. C. Gogolin, J. Eisert, Rep. Prog. Phys. **79**, 056001 (2016). <https://doi.org/10.1088/0034-4885/79/5/056001>
7. L. D'Alessio, Y. Kafri, A. Polkovnikov, M. Rigol, Adv. Phys. **65**, 239 (2016). <https://doi.org/10.1080/00018732.2016.1198134>
8. J. Dziarmaga, Adv. Phys. **59**, 1063 (2010). <https://doi.org/10.1080/00018732.2010.514702>
9. K. Sekimoto, *Stochastic Energetics*, vol. 799 (Springer, Berlin, 2010). <https://doi.org/10.1007/978-3-642-05411-2>
10. C. Jarzynski, Annu. Rev. Condens. Matter Phys. **2**, 329 (2011). <https://doi.org/10.1146/annurev-conmatphys-062910-140506>
11. U. Seifert, Rep. Prog. Phys. **75**, 126001 (2012). <https://doi.org/10.1088/0034-4885/75/12/126001>
12. M. Esposito, U. Harbola, S. Mukamel, Rev. Mod. Phys. **81**, 1665 (2009). <https://doi.org/10.1103/RevModPhys.81.1665>
13. M. Campisi, P. Hänggi, P. Talkner, Rev. Mod. Phys. **83**, 771 (2011). <https://doi.org/10.1103/RevModPhys.83.771>
14. P. Hänggi, P. Talkner, Nat. Phys. **11**, 108 (2015). <https://doi.org/10.1038/nphys3167>
15. R. Dorner, J. Goold, C. Cormick, M. Paternostro, V. Vedral, Phys. Rev. Lett. **109**, 160601 (2012). <https://doi.org/10.1103/PhysRevLett.109.160601>
16. J. Goold, M. Huber, A. Riera, L. del Rio, P. Skrzypczyk, J. Phys. A: Math. Theor. **49**, 143001 (2016). <https://doi.org/10.1088/1751-8113/49/14/143001>
17. A. Silva, Phys. Rev. Lett. **101**, 120603 (2008). <https://doi.org/10.1103/PhysRevLett.101.120603>
18. A. Gambassi, A. Silva, (2011). [arXiv:1106.2671](https://arxiv.org/abs/1106.2671)
19. A. Gambassi, A. Silva, Phys. Rev. Lett. **109**, 250602 (2012). <https://doi.org/10.1103/PhysRevLett.109.250602>

20. Y.E. Shchadilova, P. Ribeiro, M. Haque, Phys. Rev. Lett. **112**, 070601 (2014). <https://doi.org/10.1103/PhysRevLett.112.070601>
21. P. Smacchia, A. Silva, Phys. Rev. Lett. **109**, 037202 (2012). <https://doi.org/10.1103/PhysRevLett.109.037202>
22. P. Smacchia, A. Silva, Phys. Rev. E **88**, 042109 (2013). <https://doi.org/10.1103/PhysRevE.88.042109>
23. M. Kolodrubetz, V. Gritsev, A. Polkovnikov, Phys. Rev. B **88**, 064304 (2013). <https://doi.org/10.1103/PhysRevB.88.064304>
24. T. Palmai, Phys. Rev. B **92**, 235433 (2015). <https://doi.org/10.1103/PhysRevB.92.235433>
25. S. Dorosz, T. Platini, D. Karevski, Phys. Rev. E **77**, 051120 (2008). <https://doi.org/10.1103/PhysRevE.77.051120>
26. E. Mascarenhas, H. Bragança, R. Dorner, M.F. Santos, V. Vedral, K. Modi, J. Goold, Phys. Rev. E **89**, 062103 (2014). <https://doi.org/10.1103/PhysRevE.89.062103>
27. L. Fusco, S. Pigeon, T.J.G. Apollaro, A. Xuereb, L. Mazzola, M. Campisi, A. Ferraro, M. Paternostro, G. De Chiara, Phys. Rev. X **4**, 031029 (2014). <https://doi.org/10.1103/PhysRevX.4.031029>
28. M. Zhong, P. Tong, Phys. Rev. E **91**, 032137 (2015a). <https://doi.org/10.1103/PhysRevE.91.032137>
29. T.J. Apollaro, G. Francica, M. Paternostro, M. Campisi, Physica Scripta **2015**, 014023 (2015). <https://doi.org/10.1088/0031-8949/2015/T165/014023>
30. M. Zhong, P. Tong, Phys. Rev. E **91**, 032137 (2015b). <https://doi.org/10.1103/PhysRevE.91.032137>
31. D.-T. Hoang, B.P. Venkatesh, S. Han, J. Jo, G. Watanabe, M.-S. Choi, (2015). [arXiv:1508.02444](https://arxiv.org/abs/1508.02444)
32. S. Sharma, A. Dutta, Phys. Rev. E **92**, 022108 (2015). <https://doi.org/10.1103/PhysRevE.92.022108>
33. F.A. Bayocboc, F.N.C. Paraan, Phys. Rev. E **92**, 032142 (2015). <https://doi.org/10.1103/PhysRevE.92.032142>
34. P.P. Mazza, J.-M. Stéphan, E. Canovi, V. Alba, M. Brockmann, M. Haque, (2015). <https://doi.org/10.1088/1742-5468/2016/01/013104>
35. A. Bayat, T.J. Apollaro, S. Paganelli, G. De Chiara, H. Johannesson, S. Bose, P. Sodano, Phys. Rev. B **93**, 201106 (2016). <https://doi.org/10.1103/PhysRevB.93.201106>
36. J. Goold, T. Fogarty, N.L. Gullo, M. Paternostro, T. Busch, Phys. Rev. A **84**, 063632 (2011). <https://doi.org/10.1103/PhysRevA.84.063632>
37. M. Heyl, S. Kehrein, Phys. Rev. B **85**, 155413 (2012a). <https://doi.org/10.1103/PhysRevB.85.155413>
38. M. Heyl, S. Kehrein, Phys. Rev. Lett. **108**, 190601 (2012b). <https://doi.org/10.1103/PhysRevLett.108.190601>
39. M. Knap, A. Shashi, Y. Nishida, A. Imambekov, D.A. Abanin, E. Demler, Phys. Rev. X **2**, 041020 (2012). <https://doi.org/10.1103/PhysRevX.2.041020>
40. F. Plastina, A. Sindona, J. Goold, N. Lo Gullo, S. Lorenzo, Open Syst. Inf. ormation Dyn. **20**, 1340005 (2013). [arXiv:1311.1945](https://arxiv.org/abs/1311.1945)
41. A. Sindona, J. Goold, N.L. Gullo, S. Lorenzo, F. Plastina, Phys. Rev. Lett. **111**, 165303 (2013). <https://doi.org/10.1103/PhysRevLett.111.165303>
42. S. Campbell, M.Á. García-March, T. Fogarty, T. Busch, Phys. Rev. A **90**, 013617 (2014). <https://doi.org/10.1103/PhysRevA.90.013617>
43. M. Schiró, A. Mitra, Phys. Rev. Lett. **112**, 246401 (2014). <https://doi.org/10.1103/PhysRevLett.112.246401>
44. A. Sindona, J. Goold, N.L. Gullo, F. Plastina, New J. Phys. **16**, 045013 (2014). <https://doi.org/10.1088/1367-2630/16/4/045013>
45. G. Roux, Phys. Rev. A **79**, 021608 (2009). <https://doi.org/10.1103/PhysRevA.79.021608>
46. B. Dóra, A. Bácsi, G. Zaránd, Phys. Rev. B **86**, 161109 (2012). <https://doi.org/10.1103/PhysRevB.86.161109>

47. S. Sotiriadis, A. Gambassi, A. Silva, Phys. Rev. E **87**, 052129 (2013). <https://doi.org/10.1103/PhysRevE.87.052129>
48. B. Dóra, F. Pollmann, J. Fortágh, G. Zaránd, Phys. Rev. Lett. **111**, 046402 (2013). <https://doi.org/10.1103/PhysRevLett.111.046402>
49. A. Bácsi, B. Dóra, Phys. Rev. B **88**, 155115 (2013). <https://doi.org/10.1103/PhysRevB.88.155115>
50. G. De Chiara, A.J. Roncaglia, J.P. Paz, New J. Phys. **17**, 035004 (2015). <https://doi.org/10.1088/1367-2630/17/3/035004>
51. T. Johnson, F. Cosco, M. Mitchison, D. Jaksch, S. Clark, Phys. Rev. A **93**, 053619 (2016). <https://doi.org/10.1103/PhysRevA.93.053619>
52. R. Lena, G. Palma, G. De Chiara, Phys. Rev. A **93**, 053618 (2016). <https://doi.org/10.1103/PhysRevA.93.053618>
53. L. Villa, G. De Chiara, Quantum **2**, 42 (2018). <https://doi.org/10.22331/q-2018-01-04-42>
54. G. Bunin, L. D'Alessio, Y. Kafri, A. Polkovnikov, Nat. Phys. **7**, 913 (2011). <https://doi.org/10.1038/nphys2057>
55. A. Russomanno, S. Sharma, A. Dutta, G.E. Santoro, J. Stat. Mech. Theory Exp. **2015**, P08030 (2015). <https://doi.org/10.1088/1742-5468/2015/08/P08030>
56. A. Dutta, A. Das, K. Sengupta, Phys. Rev. E **92**, 012104 (2015). <https://doi.org/10.1103/PhysRevE.92.012104>
57. S. Lorenzo, J. Marino, F. Plastina, G.M. Palma, T.J. Apollaro, Sci. Rep. **7**, 5672 (2017). <https://doi.org/10.1038/s41598-017-06025-1>
58. F.N.C. Paraan, A. Silva, Phys. Rev. E **80**, 061130 (2009). <https://doi.org/10.1103/PhysRevE.80.061130>
59. D.A. Wisniacki, A.J. Roncaglia, Phys. Rev. E **87**, 050902 (2013). <https://doi.org/10.1103/PhysRevE.87.050902>
60. T. Pálmai, S. Sotiriadis, Phys. Rev. E **90**, 052102 (2014). <https://doi.org/10.1103/PhysRevE.90.052102>
61. Z. Gong, S. Deffner, H.T. Quan, Phys. Rev. E **90**, 062121 (2014). <https://doi.org/10.1103/PhysRevE.90.062121>
62. S. Deffner, A. Saxena, Phys. Rev. E **92**, 032137 (2015). <https://doi.org/10.1103/PhysRevE.92.032137>
63. N. Liu, J. Goold, I. Fuentes, V. Vedral, K. Modi, D.E. Bruschi, Class. Quantum Gravity **33**, 035003 (2016). <https://doi.org/10.1088/0264-9381/33/3/035003>
64. F. Jin, R. Steinigeweg, H. De Raedt, K. Michielsen, M. Campisi, J. Gemmer, Phys. Rev. E **94**, 012125 (2016). <https://doi.org/10.1103/PhysRevE.94.012125>
65. J. Mur-Petit, A. Relaño, R. Molina, D. Jaksch, (2017). <https://doi.org/10.1038/s41467-018-04407-1>
66. F. Cosco, M. Borrelli, P. Silvi, S. Maniscalco, G. De Chiara, Phys. Rev. A **95**, 063615 (2017). <https://doi.org/10.1103/PhysRevA.95.063615>
67. P. Rotondo, J. Minar, J.P. Garrahan, I. Lesanovsky, M. Marcuzzi, (2018). <https://doi.org/10.1103/PhysRevB.98.184303>
68. M. Heyl, A. Polkovnikov, S. Kehrein, Phys. Rev. Lett. **110**, 135704 (2013). <https://doi.org/10.1103/PhysRevLett.110.135704>
69. M. Heyl, Rep. Prog. Phys. (2018). <https://doi.org/10.1088/1361-6633/aaaf9a>
70. M. Campisi, J. Goold, Phys. Rev. E **95**, 062127 (2017). <https://doi.org/10.1103/PhysRevE.95.062127>
71. A. Chenu, I.L. Egusquiza, J. Molina-Vilaplana, A. del Campo, (2017). <https://doi.org/10.1038/s41598-018-30982-w>
72. H. Touchette, Phys. Rep. **478**, 1 (2009). <https://doi.org/10.1016/j.physrep.2009.05.002>
73. P.W. Anderson, Phys. Rev. Lett. **18**, 1049 (1967a). <https://doi.org/10.1103/PhysRevLett.18.1049>
74. G. Mahan, Phys. Rev. **163**, 612 (1967). <https://doi.org/10.1103/PhysRev.163.612>
75. P. Nozières, C. De Dominicis, Phys. Rev. **178**, 1097 (1969). <https://doi.org/10.1103/PhysRev.178.1097>

76. P. Talkner, E. Lutz, P. Hänggi, Phys. Rev. E **75**, 050102 (2007). <https://doi.org/10.1103/PhysRevE.75.050102>
77. S. Deffner, E. Lutz, Phys. Rev. Lett. **105**, 170402 (2010). <https://doi.org/10.1103/PhysRevLett.105.170402>
78. P. Talkner, P. Hänggi, Phys. Rev. E **93**, 022131 (2016). <https://doi.org/10.1103/PhysRevE.93.022131>
79. A. Peres, Phys. Rev. A **30**, 1610 (1984). <https://doi.org/10.1103/PhysRevA.30.1610>
80. L.C. Venuti, P. Zanardi, Phys. Rev. Lett. **99**, 095701 (2007). <https://doi.org/10.1103/PhysRevLett.99.095701>
81. P. Zanardi, P. Giorda, M. Cozzini, Phys. Rev. Lett. **99**, 100603 (2007). <https://doi.org/10.1103/PhysRevLett.99.100603>
82. S.-J. Gu, Int. J. Mod. Phys. B **24**, 4371 (2010). <https://doi.org/10.1142/S0217979210056335>
83. S. Sachdev, *Quantum Phase Transitions* (Wiley Online Library, 2007). <https://doi.org/10.1002/9780470022184.hmm108>
84. H.W. Diehl, in *Phase Transitions and Critical Phenomena*, vol. 10, ed. by C. Domb, J. Lebowitz (Academic, London, 1986). ISBN 0122203100
85. H.W. Diehl, Int. J. Mod. Phys. B **11**, 3503 (1997). <https://doi.org/10.1142/S0217979297001751>
86. M.N. Barber, in *Phase Transitions and Critical Phenomena*, vol. 8, ed. by C. Domb, J. Lebowitz (Academic London, 1983). ISBN 0122203089
87. J. Cardy, *Finite-Size Scaling*, vol. 2 (North Holland, 1988). ISBN 0444871098
88. M. Krech, *The Casimir Effect in Critical Systems* (World Scientific, 1994). <https://doi.org/10.1142/2434>
89. A. Gambassi, J. Phys. Conf. Ser. **161**, 012037 (2009). <https://doi.org/10.1088/1742-6596/161/1/012037>
90. R. Alicki, M. Fannes, Phys. Rev. E **87**, 042123 (2013). <https://doi.org/10.1103/PhysRevE.87.042123>
91. F.C. Binder, S. Vinjanampathy, K. Modi, J. Goold, New J. Phys. **17**, 075015 (2015). <https://doi.org/10.1088/1367-2630/17/7/075015>
92. M. Perarnau-Llobet, K.V. Hovhannисyan, M. Huber, P. Skrzypczyk, N. Brunner, A. Acín, Phys. Rev. X **5**, 041011 (2015). <https://doi.org/10.1103/PhysRevX.5.041011>
93. F. Campaioli, F.A. Pollock, F.C. Binder, L. Céleri, J. Goold, S. Vinjanampathy, K. Modi, Phys. Rev. Lett. **118**, 150601 (2017). <https://doi.org/10.1103/PhysRevLett.118.150601>
94. D. Ferraro, M. Campisi, G.M. Andolina, V. Pellegrini, M. Polini, Phys. Rev. Lett. **120**, 117702 (2018). <https://doi.org/10.1103/PhysRevLett.120.117702>
95. P.W. Anderson, Phys. Rev. Lett. **18**, 1049 (1967b). <https://doi.org/10.1103/PhysRevLett.18.1049>
96. G.D. Mahan, *Many-Particle Physics*, 3rd ed. (Springer Science, 2000). <https://doi.org/10.1007/978-1-4757-5714-9>
97. A. Sindona, M. Pisarra, M. Gravina, C.V. Gomez, P. Riccardi, G. Falcone, F. Plastina, Beilstein J. Nanotechnol. **6**, 755 (2015). <https://doi.org/10.3762/bjnano.6.78>
98. R. Schmidt, M. Knap, D.A. Ivanov, J.-S. You, M. Cetina, E. Demler, Rep. Prog. Phys. **81**, 024401 (2018). <https://doi.org/10.1088/1361-6633/aa9593>
99. G. Huber, F. Schmidt-Kaler, S. Deffner, E. Lutz, Phys. Rev. Lett. **101**, 070403 (2008). <https://doi.org/10.1103/PhysRevLett.101.070403>
100. R. Dorner, S.R. Clark, L. Heaney, R. Fazio, J. Goold, V. Vedral, Phys. Rev. Lett. **110**, 230601 (2013). <https://doi.org/10.1103/PhysRevLett.110.230601>
101. L. Mazzola, G. De Chiara, M. Paternostro, Phys. Rev. Lett. **110**, 230602 (2013). <https://doi.org/10.1103/PhysRevLett.110.230602>
102. S. Kohler, D. Zueco, M. Campisi, R. Blattmann, P. Hänggi, New J. Phys. **15**, 105028 (2013). <https://doi.org/10.1088/1367-2630/15/10/105028>
103. T.B. Batalhão, A.M. Souza, L. Mazzola, R. Accaise, R.S. Sarthour, I.S. Oliveira, J. Goold, G. De Chiara, M. Paternostro, R.M. Serra, Phys. Rev. Lett. **113**, 140601 (2014). <https://doi.org/10.1103/PhysRevLett.113.140601>

104. S. An, J.-N. Zhang, M. Um, D. Lv, Y. Lu, J. Zhang, Z.-Q. Yin, H. Quan, K. Kim, Nat. Phys. **11**, 193 (2015). <https://doi.org/10.1038/nphys3197>
105. A.J. Roncaglia, F. Cerisola, J.P. Paz, Phys. Rev. Lett. **113**, 250601 (2014). <https://doi.org/10.1103/PhysRevLett.113.250601>
106. F. Cerisola, Y. Margalit, S. Machluf, A.J. Roncaglia, J.P. Paz, R. Folman, Nat. Commun. **8**, 1241 (2017). <https://doi.org/10.1038/s41467-017-01308-7>
107. M. Cetina, M. Jag, R.S. Lous, J.T. Walraven, R. Grimm, R.S. Christensen, G.M. Bruun, Phys. Rev. Lett. **115**, 135302 (2015). <https://doi.org/10.1103/PhysRevLett.115.135302>
108. M. Cetina, M. Jag, R.S. Lous, I. Fritzsche, J.T. Walraven, R. Grimm, J. Levinsen, M.M. Parish, R. Schmidt, M. Knap et al., Science **354**, 96 (2016). <https://doi.org/10.1126/science.aaf5134>

# Chapter 14

## Ancilla-Assisted Measurement of Quantum Work



Gabriele De Chiara, Paolo Solinas, Federico Cerisola and  
Augusto J. Roncaglia

### 14.1 Introduction

The concept of work is one of the cornerstones of classical physics. In classical mechanics, it is defined as the integral of the force applied by an external agent times the displacement of the system. It is deeply related to the concept of heat through the principle of energy conservation. Heat is the dissipated energy due to the presence of non-conservative forces acting on the system. Work and heat allow us to answer to a fundamental and practical question: how much energy does a system need to perform a specific task? The advantages and elegance of such quantities relies on the fact that they can be calculated neglecting the details of the system and the dynamics.

Surprisingly, the discussion on how to extend the concept of work to the quantum domain has not been faced until recently and was motivated by a renewed interest in the study of non-equilibrium quantum systems, and the extension of classical fluctuation theorems [1, 2] to the quantum domain [3–6]. Classical fluctuation theorems are powerful tools that go beyond the linear response theory, relating for instance the work statistics with equilibrium quantities such as free energy differences.

The current interest in out-of-equilibrium quantum thermodynamics has been triggered by recent advances in the coherent manipulation of elementary quantum systems. However, as discussed in other chapters of this book, the definition of work in a quantum setting is rather problematic. Quantum mechanics is built around

---

G. De Chiara (✉)

School of Mathematics and Physics, Centre for Theoretical Atomic, Molecular and Optical Physics, Queen's University, Belfast BT7 1NN, UK  
e-mail: g.dechiara@qub.ac.uk

P. Solinas

SPIN-CNR, Via Dodecaneso 33, 16146 Genova, Italy  
e-mail: paolo.solinas@spin.cnr.it

F. Cerisola · A. J. Roncaglia

Departamento de Física, Facultad de Ciencias Exactas y Naturales, Universidad de Buenos Aires and IFIBA, CONICET, Ciudad Universitaria, 1428 Buenos Aires, Argentina

the operators which are associated to physical observables [7]. If we perform a *projective* measurement of an observable on a system, the latter collapses onto one of the eigenstates of the corresponding operator with a certain probability [7]. From this simple rule, we know how to calculate the statistics of the observable.

In this framework, the measurement of the system leads to two important implications. First, the measurement process is local in time, i.e. it is assumed to occur on timescales smaller than any other time scale and the wave-function collapse is supposed to be instantaneous. This also implies that the information about the observable and the associated operators are local in time. Second, the measurement destroys any superposition of eigenstates of the measured operator and, therefore, strongly perturbs the quantum system.

These two points caused some debates in the attempt to unambiguously define quantum work. To understand this point, let us consider a closed system in which all the energy injected by an external field is transformed in internal energy of the system, i.e. there is no dissipation or heat. For a classical system, if the initial and final energies are  $E_i$  and  $E_f$ , respectively, then the work performed is  $W = E_f - E_i$ . Therefore,  $W$  depends on the values of the observable energy at two different times and it is thus non-local in time.

As discussed above, observables in quantum mechanics are usually associated to Hermitian operators that are local in time. If we denote with  $H_f$  and  $H_i$  the final and initial Hamiltonian operators of the system, respectively, a plausible definition of a work operator could be  $W = H_f - H_i$  [8, 9]. Though this definition is formally possible and is sometimes useful to connect the work fluctuations with macroscopic measurable quantities [10, 11], it has no meaning in terms of quantum observables and measurements. Work is defined as the energy difference after a given process, and as such it characterises a process and not the system's state. In addition, the number of possible values of work typically exceeds the dimension of the system, thus work cannot be represented as a Hermitian operator. This point has generated confusions for a long time [8, 9] and it has been clarified in Ref. [12].

We arrive to the following important observation: Since quantum work does not meet the requirements to be associated to a standard (local in time) operator, the only way to clarify its meaning is to give an operative definition, that is, to describe the scheme we use to measure it.

The first proposal in this direction was done in some early papers [3–6] and it is described in Chap. 13 of this book. It is based on a double and sequential measurement of the system and we refer to it as the “Two Measurement Protocol” (TMP). The scheme is as follows: The system energy  $H_i$  is measured at the beginning of the evolution, then the system evolves under the effect of the driving field and the final energy  $H_f$  is measured again at the end of the evolution. The difference of the two energy measurements gives us information about the work statistics [3, 4, 12]. This approach was initially proposed in the context of quantum fluctuation theorems and quantum Jarzynski equalities [5, 6]. It was later extended to describe the dissipated heat in open quantum systems in the weak and strong coupling regime [5, 13, 14]. An advantage of this definition is that it clearly explains the meaning and the statistics of quantum work.

It is worth mentioning at this stage that, although quantum work is not a quantum observable [12], i.e. it is not the expectation value of a Hermitian operator, it can be formally described as a generalised measurement. Quantum work can in fact be described as a positive operator valued measure (POVM) [15] which is very common in quantum optics and information. This was an important conceptual result because it clarified the role of work in quantum mechanics. A POVM can always be interpreted (or realised) as a projective measurement in a larger Hilbert space.

If we consider a generic initial state, i.e. not an equilibrium thermalised state, the TMP is unsatisfactory and incomplete because of the collapse of the quantum state induced by the initial measurement. If the system is in a coherent superposition of eigenstates of  $H_i$ , the initial measurement destroys the quantum coherences and it completely changes the system dynamics. This has both fundamental and practical implications. From a fundamental point of view, we would like to understand if there are more general and less invasive measurement protocols that allow us to preserve the full quantum dynamics. From a practical point of view, the TMP shows an important limitation since it is not possible to answer to the question: what is the energy needed to run a quantum device?

To weigh properly the implications of the last point, we discuss a specific example. Suppose that we have a quantum computer that runs the Grover quantum database search [16, 17]. If the database is composed of  $N$  objects and the basis of all the possible logical states is denoted with  $\{|x\rangle\}$  ( $x = 0, 1, \dots, N - 1$ ), the algorithm is able to find a particular marked string  $|\bar{x}\rangle$ . As usual, let us suppose that the logical states are encoded in  $n$  qubits ( $N = 2^n$ ) so that they can be written as logical strings of 0 and 1, e.g.,  $|0\rangle = |00\dots0\rangle$ ,  $|1\rangle = |10\dots0\rangle$  and so on [16]. The algorithm starts from the equal superposition state  $|\psi\rangle = 1/\sqrt{N} \sum_x |x\rangle$  and, by means of a unitary evolution  $U_{\text{algo}}$ , transforms it in the solution state  $|\bar{x}\rangle$ , i.e.,  $|\psi\rangle \rightarrow U_{\text{algo}} |\psi\rangle = |\bar{x}\rangle$ . We want to know what is the work necessary to run the quantum database search algorithm.

To answer to this question, we must first describe the energy spectrum of a single qubit. Let a single qubit have energy  $\epsilon$  and  $-\epsilon$  for the eigenstates  $|0\rangle$  and  $|1\rangle$ . Being a string of  $|0\rangle$  and  $|1\rangle$ , every logical state  $|x\rangle$  has a defined energy that could be measured projectively. However, the initial state  $|\psi\rangle$  is not an eigenstate of the Hamiltonian and therefore it has no definite energy. Using the TMP to determine the work would lead to a collapse of  $|\psi\rangle$  into a random state  $|x\rangle$ . The dynamics induced by  $U_{\text{algo}}$  would not give the solution  $|\bar{x}\rangle$  and the final measurement would give another random value for the final energy. Therefore, the TMP makes it impossible to run the Grover algorithm because it changes completely the dynamics and, at the same time, is unable to determine what is the energy needed to run it. Furthermore, for an initial state with coherences in the energy eigenbasis, the mean value of work obtained from the TMP probability distribution and the difference between the mean initial energy and the mean final energy are in general different. Indeed in Ref. [18], an important result has been put forward: there is no scheme able to estimate work in closed systems that produces outputs whose mean value is given by the difference

in mean energies and coincides with the TMP for initial states without coherences (see also Ref. [19]). This result states that the statistics of work for initial states with coherences cannot be defined via a probability distribution compatible with the above conditions. However, as we shall see in this chapter, it is possible to define a quasi-probability distribution which can assume negative values, signalling initial quantum coherence.

These examples point out the need for a more general operational definition of work. One way to do this is to include an ancilla or quantum detector and to take into consideration its interaction with the quantum system under scrutiny and the perturbation the latter induces in the former.

Already several works suggested the use of ancillas for extracting the statistics of work. In Refs. [20, 21] a Ramsey scheme using an auxiliary qubit was proposed to measure the work characteristic function. Its experimental realisation with nuclear magnetic resonance was reported in Ref. [22]. In Ref. [15] a different approach was taken in which a detector, for example the position of a quantum particle or a light mode [23], is coupled to the system to extract directly the work probability distribution after a single quantum measurement. The scheme was recently realised with cold atoms [24].

These two schemes, reviewed in Sect. 14.2, can be understood in a more general framework: the interaction between the evolving system and the detector allows us to encode the information about the work performed on the system in the quantum state of the detector. We show below that there are several ways, that we call *protocols*, to extract this information. The choice between them depends on what kind of information we are interested in and if we want to preserve or not some of the quantum features of the dynamics. Therefore, in this general setting, the quantum work statistics can change depending on the measurement protocol used.

A measurement protocol similar to the one proposed in the full counting statistics approach [25–29] is able to completely preserve the coherence effect in the system. It leads to a quasi-probability of work distribution in which negative probability regions are signatures of the quantumness of the system [30–35].

Alternatively, with a measurement protocol conceptually similar to the von Neumann measurement scheme [36], we directly measure the work distribution that in the limit of a precise measurement coincides with the TMP scheme. In this case, the uncertainty in the measurement plays a fundamental role since imprecise measurements lead to a revival of quantum dynamics and coherence effects.

These protocols can be unified in a single approach where the only difference is the final measurement of two non-commuting observables, e.g. momentum and position of a particle detector. All the main protocols proposed in the literature can be revisited and framed in this more general measurement scheme that we explain in detail in Sect. 14.3. In Sect. 14.4, we discuss physical implementations and experimental realisations of the schemes. Finally, in Sect. 14.5, we summarise and conclude.

## 14.2 Measuring the Work Distribution with Ancillas

### 14.2.1 Preliminaries on the Work Probability Distribution in Quantum Mechanics

One of the most common definitions of work is the TMP scheme. We assume a quantum system to be initially prepared in the state  $\rho_S(0)$  and subject to the Hamiltonian  $H_S(0)$ . The initial energy of the system is measured yielding the energy eigenvalue  $\epsilon_i^0$  while the system collapses to the state  $|\epsilon_i^0\rangle$ . The system's Hamiltonian is then changed in time inducing an evolution until the final time  $T$  described by the operator  $U_S(T)$ . The final energy, described by the final Hamiltonian  $H_S(T)$ , is measured again yielding the result  $\epsilon_j^T$ . For this particular quantum trajectory the work performed on or extracted from the system is  $W = \epsilon_j^T - \epsilon_i^0$ , i.e. the difference of the final and initial energy. As the results of the measurements are stochastic with probabilities dictated by quantum theory, we find the probability distribution of work by summing over all possible measurement outcomes:

$$\mathcal{P}(W) = \sum_i P_i \sum_j P_{i \rightarrow j} \delta(W - \epsilon_j^T + \epsilon_i^0) \quad (14.1)$$

where  $P_i = \langle \epsilon_i^0 | \rho_S(0) | \epsilon_i^0 \rangle$  is the probability that the first energy measurement results in  $\epsilon_i^0$  and  $P_{i \rightarrow j} = |\langle \epsilon_j^T | U(T) | \epsilon_i^0 \rangle|^2$  is the conditional probability of obtaining  $\epsilon_j^T$  in the last measurement given that the result of the first measurement was  $\epsilon_i^0$ .

An equivalent description of the work statistics is to consider the Fourier transform of the work probability distribution known as the characteristic function of work:

$$\chi_\lambda = \int dW e^{i\lambda W} \mathcal{P}(W) \quad (14.2)$$

which can be cast in the form of two-time correlation function [5, 12]:

$$\chi_\lambda = \text{Tr}_S \left[ U_S^\dagger(T) e^{i\lambda H_S(T)} U_S(T) e^{-i\lambda H_S(0)} \tilde{\rho}_S(0) \right]. \quad (14.3)$$

where  $\tilde{\rho}_S(0) = \sum_i P_i |\epsilon_i^0\rangle \langle \epsilon_i^0|$  is the projection of the initial density matrix onto the eigenstates of  $H_S(0)$ .

Below we describe two paradigmatic schemes that allow to experimentally obtain the work probability distribution with ancillas. The first one shows how to measure the characteristic function and the second one shows how to asses directly the work probability distribution while solely performing a measurement at the end of the transformation. Interestingly, both methods have been recently verified experimentally.

### 14.2.2 Measuring the Characteristic Function: The Ramsey Scheme

In this section we review the first scheme, a Ramsey-inspired technique, to measure the work statistics. The method was originally proposed in Refs. [20, 21], and gives access to the characteristic function by coupling the system to a two-level system (qubit). The general idea of the scheme could be understood by noticing that the characteristic function for each  $\lambda$  is given by the mean value of a unitary operator, as it is shown in Eq. (14.3), and this mean value can be measured via an interferometric scheme.

The scheme starts with the system and the qubit in the product state  $\rho_S(0) \otimes |0\rangle\langle 0|$  and we assume that  $\rho_S(0)$  is diagonal in the initial energy basis, e.g. it is in a thermal state (we will discuss this assumption later). The Ramsey scheme consists of three steps:

1. The Hadamard gate [16]  $H = (\sigma_z + \sigma_x)/\sqrt{2}$  is applied to the qubit.
2. The qubit and the system evolve according to the coupled evolution:

$$M_\lambda = U_S(\mathcal{T})e^{-i\lambda H_S(0)} \otimes |0\rangle\langle 0| + e^{-i\lambda H_S(\mathcal{T})}U_S(\mathcal{T}) \otimes |1\rangle\langle 1|. \quad (14.4)$$

3. The Hadamard gate  $H$  is applied again to the qubit.

At the end of the protocol the reduced density operator of the qubit is

$$\rho_D(\lambda) = \frac{1}{2} [I_Q + (\text{Re}\chi_\lambda)\sigma_z + (\text{Im}\chi_\lambda)\sigma_y], \quad (14.5)$$

where  $I_Q$  is the identity on the auxiliary qubit. Therefore, by repeating the experiments many times for a fixed value of  $\lambda$ , corresponding to the time of interaction between system and auxiliary qubit [20, 21], one can reconstruct the value of  $\chi_\lambda$  through quantum state tomography of the qubit. Given the simple form of the density matrix (14.5), only two measurements are needed: the mean values  $\langle\sigma_z\rangle$ , related to the qubit population imbalance, and  $\langle\sigma_y\rangle$ , related to the qubit coherence. To reconstruct the whole probability distribution  $\mathcal{P}(W)$  one has to repeat the experiment many times for different values of  $\lambda$  and then Fourier transform the characteristic function  $\chi_\lambda$ .

The quantum circuit realising such a protocol is shown in Fig. 14.1a while a Mach-Zehnder interpretation of the scheme is presented in Fig. 14.1b.

The advantage of the Ramsey scheme is that it bypasses the measurement of the initial and final energy of the system. The price to pay, however, is the need of implementing the conditional evolution operator  $M_\lambda$ . We will discuss the implementation of the Ramsey scheme in Sect. 14.4.

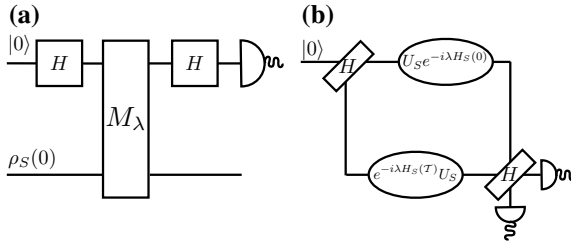


**Fig. 14.1** **a** Quantum circuit realising the Ramsey scheme. The system is prepared in an initial state  $\rho_S(0)$  which we assume diagonal in the initial energy basis. The qubit is initially in the state  $|0\rangle$ . At the end of the evolution the reduced density matrix of the qubit is reconstructed through state tomography. **b** Mach–Zehnder interpretation of the scheme. In the interferometer the state of the qubit is initially “split” by a beam-splitter (corresponding to the Hadamard gate) in a superposition of  $|0\rangle$  and  $|1\rangle$  (corresponding to the two arms of the interferometer). In the upper arm of the interferometer the system is subject to the evolution  $U_S(\mathcal{T})e^{-i\lambda H_S(0)}$  while in the lower arm  $e^{-i\lambda H_S(\mathcal{T})}U_S(\mathcal{T})$ . In the diagram for brevity we have written  $U_S = U_S(\mathcal{T})$ . At the end, the two arms pass through another beam-splitter (the second Hadamard gate) and the state of the qubit is reconstructed.

### 14.2.3 Work Measurement with a Single POVM

In this section we review the ideas developed in Ref. [15] where it is shown that work, defined by the TMP, can be measured using a single projective measurement over an ancillary system. Thus, work can be defined by a POVM, the most general possible quantum measurement that can be defined [37] and very common in quantum metrology and quantum information. A POVM can be expressed in terms of a set of operators  $A_k$ , where  $k$  labels all possible different outcomes of the measurement, such that  $A_k \geq 0$ ,  $\sum_k A_k = I$ , and the probability of obtaining outcome  $k$  of a quantum state  $\rho$  is given by  $P(k) = \text{Tr}(\rho A_k)$ . Notice that the number of outcomes could in principle be larger than the dimension of the system.

A physical interpretation of such a generalised measurement is given by Neumark’s theorem [37] which establishes that any POVM can be realised as a projective measurement on an enlarged system that evolves unitarily. In terms of the work measurement, this means that the work probability distribution can be obtained by coupling the system to an ancillary system (or measuring apparatus), letting them to evolve unitarily and then performing a projective measurement at the end of the evolution. Indeed, there is no need to perform two projective measurements at different times over the system, as the operational definition of work suggests, instead a single measurement at the very end of the protocol over an ancillary system can reveal the value of work.

It is worth noting that such an implementation is not unique, in fact there are infinitely many combinations of ancillas, unitary evolutions and projective measurements that are capable of realising the same POVM. In Ref. [15] two such implementations were proposed which we now briefly discuss.

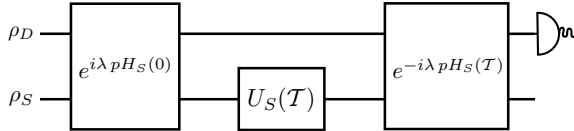


**Fig. 14.2** Quantum circuit that measures work using a single POVM. This is a possible realisation where the detector ( $D$ ) is a continuous variable system. The two entangling operations apply a conditional translation to the state of the detector. These translations at two different times depend on the value of the energy, thus the detector keeps a coherent record of the value of work before the measurement.

The POVM is implemented by introducing an auxiliary system or detector  $D$  that interacts with the system  $S$  keeping a *coherent record* of its energy at two different times. The simplest strategy would be to consider  $D$  as a continuous variable system (such that the operator  $p$  is the generator of translations) following these steps [15]:

1. Initially  $S$  and  $D$  are in a product state, and  $D$  could be, for instance, in a position eigenstate or a localized Gaussian state [23, 24].
2.  $S$  and  $D$  interact via an entangling evolution during time  $\tau$  given by the Hamiltonian:  $H_{SD} = -(\lambda/\tau) p H_S(0)$ .
3.  $S$  evolves according to a given process characterized by a unitary  $U_S(\mathcal{T})$ .
4.  $S$  and  $D$  interact via an entangling evolution during time  $\tau$  given by the Hamiltonian:  $H_{SD} = (\lambda/\tau) p H_S(\mathcal{T})$ .
5. Projective measurement over  $D$ .

In the protocol,  $\lambda$  is some constant characterizing the strength of the interaction. In summary, the unitary sequence  $U_\lambda = U_\lambda(\mathcal{T})U_S(\mathcal{T})U_\lambda^\dagger(0)$  is applied before the measurement, with

$$U_\lambda(t) = e^{-i\lambda p H_S(t)}. \quad (14.6)$$

In Fig. 14.2 it is shown the quantum circuit representing the procedure. As an example, let us consider an initial pure state of system and detector:  $|\psi_i\rangle = |0\rangle_D |\xi\rangle_S$  after the application of  $U_\lambda$  the systems will become correlated before the measurement in this way:

$$|\psi_f\rangle = \sum_{ij} |\lambda \epsilon_{ji}\rangle_D (\Pi_j^T U_S(\mathcal{T}) \Pi_i^0) |\xi\rangle_S, \quad (14.7)$$

where  $\epsilon_{ji} = \epsilon_j^T - \epsilon_i^0$  denotes a given value of work,  $|0\rangle_D$  is an initial localised state,  $|\lambda \epsilon_{ji}\rangle_D$  is the translated one, and  $\Pi_j^t$  is the projector over the energy eigenspace of the Hamiltonian  $H_S(t)$  with energy  $\epsilon_j^t$ . Notably, the detector keeps a coherent record of the value of work. Thus, all the information about the work distribution is encoded in this correlated final state. In fact, a measurement that discriminates between the different states  $|\lambda \epsilon_{ji}\rangle_D$  will reveal the value of work  $\epsilon_{ji}$  with a probability given by Eq. (14.1). After many runs of the experiment it would be possible to reconstruct the work probability distribution over this process.

The scheme allows different initial states for the system and detector, and also the measurement should be specified. In fact, if one considers initial Gaussian states for the detector and a measurement in position, one could set the interaction strength  $\lambda$  and the initial delocalisation of the state in order to obtain the work probability distribution [23, 24, 38]. Additionally, one can show that initial coherences in the energy eigenbasis could affect the resulting work distribution, if the interaction strength  $\lambda$  and the delocalisation are not adjusted properly (see Sup. Mat. [24]). On the other hand, the POVM can also be performed if one considers a discrete ancillary system. The strategy is a variation of the phase estimation algorithm and was studied in [15]. In this case, the measured distribution is a coarse grained version of the real one that can be written as the convolution of  $P(W)$  with a windowing function whose precision depends on the dimension of the ancilla.

As mentioned before, the advantage of the POVM approach is that it does not require the two time projective measurements and it furthermore allows one to directly sample the work probability distribution. This is however done at the cost of having to implement appropriate interactions between the system and the ancilla at different times. In Sect. 14.4 we review an experiment where this POVM was successfully implemented.

### 14.3 General Framework to Measure Quantum Work Distributions

In this section, we discuss a more general measurement framework to unify the two schemes discussed in the previous section. The key point is to explicitly take into account the presence and the interaction between the system and the quantum detector used to store the information about work. This analysis thus provides a strong connection between energy fluctuations and the coherence of the initial system. As mentioned in the introduction we cannot always obtain a probability distribution of work when the initial state is endowed with quantum coherences [18]. We will show that for the protocols described in this section, we either obtain a quasi probability distribution or a coarse-grained one.

#### 14.3.1 Dynamics of the System and the Detector

As discussed in the Introduction, the only clear way to define the work distribution of a quantum system is to give an operative implementation of the way we extract the information or, in other words, how we measure the energy invested or extracted in a quantum process. If we want to preserve quantum effects yet be able to assess the energetic balance of a system, one way is to use a quantum detector or measurement apparatus. We thus consider the set-up in which a system  $S$  is coupled to a detector  $D$ . This set-up is general enough to include most of the proposals in the literature and allows us to point out the differences and advantages of different measurement protocols.

As an illustrative detector we use a free quantum particle. The detector Hamiltonian is  $H_D = p^2/(2m)$  where  $p$  and  $m$  are the momentum and the detector mass, respectively. The coupling between  $S$  and  $D$  is obtained by turning on and off the interaction Hamiltonian  $H_{SD}(t) = -\beta(t)pH_S(t)$ . This choice of the detector and the system-detector coupling are not limiting since, as discussed below, they account for all the relevant features and the schemes proposed in the literature. At the same time, they allow us to simplify the discussion. We will discuss also the changes needed in case other quantum detectors are used.

To determine the system internal energy variation, the time-dependent coupling strength  $\beta(t)$  is chosen so that the detector “records” the energy of the system at the beginning and at the end of the evolution:  $\beta(t) = \lambda/p_0[\delta(t-T) - \delta(t)]$ , where the constant parameters  $\lambda$  and  $p_0$  have the dimension of time and momentum, respectively.

The delta-like behaviour of  $\beta(t)$  must be considered as a limiting case in which coupling takes place over a time scale that is fast compared to the dynamics induced by  $H_S(t)$  and  $H_D$ , so that the dynamics of the system and the detector are effectively “frozen” during the coupling. More specifically, if the interaction occurs in a time  $\Delta t$ , e.g., for  $t \leq t' \leq t + \Delta t$ , if  $H_S(t)$  changes slowly in  $\Delta t$ , we can consider  $H_S(t') \approx H_S(t)$ . Since  $[H_S(t), H_{SD}(t)] = [H_D, H_{SD}(t)] = 0$ , the full unitary operator can be easily calculated (setting  $\hbar = 1$ )

$$\begin{aligned} U(\Delta t) &= e^{-i \int_t^{t+\Delta t} dt' [H_S(t) - \lambda \beta(t)pH_S(t) + \frac{p^2}{2m}]} \\ &= e^{-i H_S(t)\Delta t} e^{i \lambda B p H_S(t)} e^{-i \frac{p^2}{2m} \Delta t} \\ &\approx e^{i \lambda B p H_S(t)} \end{aligned} \quad (14.8)$$

where  $B = \int_t^{t+\Delta t} dt' \beta(t)$  and the last step is obtained for small enough  $\Delta t$ . We can assume that the coupling function  $\beta(t)$  is normalised such that  $B = 1$ . Then the dynamics during the system-detector coupling is given by  $\exp[i\lambda p H_S(t)]$ , that is the one expected for a delta coupling.

The sequence of operations is the following: (i) at  $t = 0$ , we turn on the system-detector coupling that generates the dynamics described by  $e^{-i \frac{p\lambda}{p_0} H_S(0)}$  as in Eq. (14.8), (ii) for  $0 \leq t \leq T$ , we let the system and the detector evolve uncoupled with an external drive acting on the system. The corresponding unitary evolution is  $U_S(T)U_D(T) = \overrightarrow{T} e^{-i \int_0^T dt H_S(t)} e^{-i \frac{p^2}{2m} T}$  where we indicated with  $\overrightarrow{T}$  the temporal ordering. (iii) at  $t = T$ , we couple the system and the detector again to generate the dynamics  $e^{i \frac{p\lambda}{p_0} H_S(T)}$  analogously to Eq. (14.8). The full evolution is described by the operator  $U_\lambda(T) = e^{i \frac{p\lambda}{p_0} H_S(T)} U_S(T)U_D(T) e^{-i \frac{p\lambda}{p_0} H_S(0)}$  [30].

Notice that neither the system nor the detector is projectively measured between times 0 and  $T$ . The specific choice of  $H_{SD}$  ensures that the coupling to the detector does not induce any transition between the instantaneous system eigenstates. In other words, system and detector do not exchange energy during the coupling.

We reasonably assume that system and detector are initially prepared in a separable and pure state (the assumption on initial purity can be relaxed for the system [30]). Denoting with  $\{|\epsilon_i^0\rangle\}$  and  $\{|p\rangle\}$  the instantaneous eigenbasis of  $H_S(t)$  and the detector momentum basis, respectively, the more general initial state reads  $|\phi_0\rangle = \sum_i \int dp \psi_i^0 G(p) |\epsilon_i^0, p\rangle$ .

By applying the evolution operator  $U_\lambda(\mathcal{T})$  to  $|\phi_0\rangle$  following the steps (i) – (iii), we obtain

$$\begin{aligned} |\phi_0\rangle &\rightarrow \sum_i \int dp \psi_i^0 G(p) e^{-i\frac{p\lambda\epsilon_i^0}{p_0}} |\epsilon_i^0, p\rangle \rightarrow \sum_{ij} \int dp \psi_i^0 G(p) e^{-i[\frac{p\lambda\epsilon_i^0}{p_0} + \frac{p^2}{2m}\mathcal{T}]} U_{S,ji} |\epsilon_j^\mathcal{T}, p\rangle \\ &\rightarrow \sum_{ij} \int dp \psi_i^0 G(p) e^{i[\frac{p\lambda\epsilon_{ji}}{p_0} - \frac{p^2}{2m}\mathcal{T}]} U_{S,ji} |\epsilon_j^\mathcal{T}, p\rangle \end{aligned} \quad (14.9)$$

where  $U_{S,ji} = \langle \epsilon_j^\mathcal{T} | U_S | \epsilon_i^0 \rangle$  is the probability amplitude to go from  $|\epsilon_i^0\rangle$  to  $|\epsilon_j^\mathcal{T}\rangle$  and, as before,  $\epsilon_{ji} = \epsilon_j^\mathcal{T} - \epsilon_i^0$ .

The corresponding final density matrix reads

$$\begin{aligned} \rho_\mathcal{T} &= \sum_{ijkl} \int dp dp' \rho_{ik}^0 G(p) G^*(p') U_{S,ji} U_{S,kl}^\dagger \\ &\quad \times e^{i[\frac{p\lambda\epsilon_{ji}}{p_0} - \frac{p^2}{2m}\mathcal{T}]} e^{-i[\frac{p'\lambda\epsilon_{jk}}{p_0} - \frac{p'^2}{2m}\mathcal{T}]} |\epsilon_j^\mathcal{T}, p\rangle \langle \epsilon_l^\mathcal{T}, p'| \end{aligned} \quad (14.10)$$

where  $U_{S,kl}^\dagger = \langle \epsilon_k^0 | U_S^\dagger | \epsilon_l^\mathcal{T} \rangle$ . In writing the above equation, we have also implicitly defined the matrix elements of the initial density operator:  $\rho_{ik}^0 = \langle \epsilon_i^0 | \rho_S(0) | \epsilon_k^0 \rangle = \psi_i^0 (\psi_k^0)^*$ .

The work done, i.e., the internal energy variation  $\epsilon_{ji}$ , is now encoded in the detector degrees of freedom. Therefore, we focus on the detector and trace out the system degrees of freedom. The detector density operator  $\rho_D(\mathcal{T}) = \text{Tr}_S[\rho_\mathcal{T}] = \sum_j \langle \epsilon_j^\mathcal{T} | \rho_\mathcal{T} | \epsilon_j^\mathcal{T} \rangle$  reads

$$\begin{aligned} \rho_D(\mathcal{T}) &= \sum_{ikj} \int dp dp' \rho_{ik}^0 G(p) G^*(p') U_{S,ji} U_{S,kj}^\dagger \\ &\quad \times e^{i[\frac{p\lambda\epsilon_{ji}}{p_0} - \frac{p^2}{2m}\mathcal{T}]} e^{-i[\frac{p'\lambda\epsilon_{jk}}{p_0} - \frac{p'^2}{2m}\mathcal{T}]} |p\rangle \langle p'|. \end{aligned} \quad (14.11)$$

As we can see, the contribution  $\epsilon_{ji}$  appears in the phase accumulated between momentum eigenstates. There is also an additional term  $\exp\{-ip^2\mathcal{T}/(2m)\}$  due to the internal dynamics of the detector. Since its value is known, we could subtract its contribution from the measured work distribution by data analysis. However, in many cases, it is convenient to cancel it during the protocol. This step allows us also to keep the following discussion simple.

For a free particle detector we need to make a few additional assumptions. We suppose that there are no degenerate states in the systems, i.e.,  $\epsilon_{ji} \neq 0$  for  $i = j$ , and that the initial detector state is a Gaussian function centered in  $p = 0$ :

$G(p) = [\sigma^2/(2\pi)]^{1/4} \exp(-\sigma^2 p^2/4)$  (the reason for the choice of the variance is discussed below). In this case, only states with momentum smaller than  $p_{max} = 3/(2\sigma)$  are important in the dynamics since the others are exponentially suppressed. Therefore, if we select  $\lambda$ ,  $m$ , and  $\mathcal{T}$  in order to have  $p_{max}^2 \mathcal{T}/(2m) = 9\mathcal{T}/(8m\sigma^2) \ll 1$ , in Eq. (14.10) we can approximate  $\exp[i(\frac{p\lambda\epsilon_{ji}}{p_0} - \frac{p^2}{2m}\mathcal{T})] \approx \exp(ip\lambda\epsilon_{ji}/p_0)$  (see also Refs. [24, 38]).

Notice that, in general, the procedure to eliminate the dynamical contribution depends on the properties of both the detector and the initial state chosen. For example, for a two-level quantum detector, the dynamical phase can be eliminated by additional operations as done in optics and nuclear magnetic resonance experiments [39, 40]. In this case, the dynamical phase accumulated by the two detector states  $|0\rangle$  and  $|1\rangle$  can be eliminated by swapping the states, i.e.,  $|0\rangle \leftrightarrow |1\rangle$  and let the detector evolve for a time  $\mathcal{T}$ . At the end of this additional evolution the two states accumulate the same global phase that can be disregarded [39, 40]. This phase elimination scheme can be applied also to the particle detector when it is initially in a superposition of two momentum eigenstates  $|p\rangle$  and  $|p'\rangle$ . At the end of the evolution we can apply a unitary operator that switches the momentum states, i.e.,  $|p\rangle \leftrightarrow |p'\rangle$ , let the detector evolve for time  $\mathcal{T}$  and neglect the overall dynamical phase. In the following, we assume that the dynamical phase is cancelled or is negligible.

Under this approximation, the detector density matrix reads

$$\rho_D(\mathcal{T}) = \sum_{ikj} \int dp dp' \rho_{ik}^0 G(p) G^*(p') U_{S,ji} U_{S,kj}^\dagger e^{i\frac{p\lambda\epsilon_{ji}}{p_0}} e^{-i\frac{p'\lambda\epsilon_{jk}}{p_0}} |p\rangle\langle p'|. \quad (14.12)$$

We can rewrite it in terms of the eigenstates  $|x\rangle$  of the position operator  $x$ . This can be done inserting the completeness operator  $\int dx|x\rangle\langle x| = I$  and using the relation  $\langle x|p\rangle = e^{ixp}/\sqrt{2\pi}$ . We obtain

$$\begin{aligned} \rho_D(\mathcal{T}) &= \sum_{ikj} \int dx dx' \rho_{ik}^0 g\left(x + \frac{\lambda\epsilon_{ji}}{p_0}\right) \\ &\quad \times g^*\left(x' + \frac{\lambda\epsilon_{jk}}{p_0}\right) U_{S,ji} U_{S,kj}^\dagger |x\rangle\langle x'| \end{aligned} \quad (14.13)$$

where  $g(x) = \frac{1}{\sqrt{2\pi}} \int dp \exp\{ipx\} G(p)$  is the Fourier transform of  $G(p)$ .

With Eqs. (14.12) and (14.13) in mind we can discuss different measurement schemes while maintaining the coupled system-detector evolution. Since the detector momentum  $p$  is a conserved quantity during the evolution, the coupling between the system and the detector cannot induce transitions between different eigenstates of the momentum; instead, it changes their relative phase. This picture is obviously reversed when considering eigenstates of the position, as the system-detector coupling  $H_{SD}(t)$  induces transition between eigenstates of the position operator  $x$ . This immediately

suggests that there are two ways to extract the information about  $\epsilon_{ji}$ : we can either measure the momentum  $\{|p\rangle\}$  or the position  $\{|x\rangle\}$  of the detector. Based on these considerations, we have the following two protocols to measure the work distribution. In **Protocol 1** we prepare the detector in a superposition of momentum eigenstates and measure their relative phase at the end of the evolution. In **Protocol 2** we prepare the detector in a position eigenstate and make a position measurement at the end of the evolution. These protocols resemble the full-counting statistics formalism [18, 27, 33, 34] and the standard von Neumann measurement scheme [36], respectively. We now discuss in details their implications.

### 14.3.2 Protocol 1

We first consider Protocol 1 and focus on the phase accumulated between the momentum eigenstates  $|p_0/2\rangle$  and  $| -p_0/2\rangle$ . The accumulated phase is given by  $\langle p_0/2|\rho_D(t)| -p_0/2\rangle$ . Rescaling for the initial phase  $\langle p_0/2|\rho_D^0| -p_0/2\rangle$ , we obtain the characteristic function of work [30]  $\mathcal{G}_\lambda = \langle p_0/2|\rho_D(t)| -p_0/2\rangle / \langle p_0/2|\rho_D^0| -p_0/2\rangle$  where the  $\lambda$  dependence is implicit in the dynamics of  $\rho_D(t)$  [see Eqs. (14.12) and (14.13)].

Notice that, with the choice of the initial states with  $\pm p_0/2$ , the detector dynamical phase does not contribute to  $\langle p_0/2|\rho_D^0| -p_0/2\rangle$  as it can be seen directly from Eq. (14.12). Since this results holds at all the orders, the constraint on the variance of the initial detector states is not needed for the implementation of Protocol 1.

The  $\mathcal{G}_\lambda$  function of the work reads [30, 31]

$$\mathcal{G}_\lambda = \text{Tr}_S \left[ U_\lambda(\mathcal{T}) \rho_S(0) U_{-\lambda}^\dagger(\mathcal{T}) \right] = \text{Tr}_S \left[ e^{i \frac{p\lambda}{p_0} H_S(\mathcal{T})} U_S(\mathcal{T}) e^{-i \frac{p\lambda}{p_0} H_S(0)} \rho_S(0) e^{-i \frac{p\lambda}{p_0} H_S(0)} U_S^\dagger(\mathcal{T}) e^{i \frac{p\lambda}{p_0} H_S(\mathcal{T})} \right]. \quad (14.14)$$

and it is similar to the ones used in literature [27, 30–32, 34]. However, we must stress that we have not made any assumption about the initial state of the system. If the system is initially in a thermal equilibrium state, i.e.  $\rho_S(0) = \exp\{-\beta H_S(0)\}/Z(0)$  where  $Z(0)$  and  $\beta$  are the partition function and the inverse temperature, respectively,  $\exp\{-i \frac{p\lambda}{p_0} H_S(0)\}$  and  $\rho_S(0)$  commute. This allows us to simplify  $\mathcal{G}_\lambda$  and obtain the results of Ref. [12]. Despite the similarities in the approaches and in the expressions, this characteristic function differs from the one in Eq. (14.3). This is due to the fact that the two system-detector coupling schemes are different. In any case the derivatives of  $\mathcal{G}_\lambda$  still gives information about energy fluctuations which do not necessarily coincide with the statistical moments of work.

A connection indeed exists for the first two moments. By direct calculation we obtain for the first two derivatives

$$(-i) \left. \frac{d\mathcal{G}_\lambda(p)}{dp} \right|_{\lambda=0} = \text{Tr}_S \left[ H_S(\mathcal{T}) \rho_S(\mathcal{T}) - H_S(0) \rho_S(0) \right]. \quad (14.15)$$

and, using the property of the trace,

$$(-i)^2 \frac{d^2 \mathcal{G}_\lambda(p)}{d \lambda^2} \Big|_{\lambda=0} = \text{Tr}_S \left\{ [U_S^\dagger(\mathcal{T}) H_S(\mathcal{T}) U_S(\mathcal{T}) - H_S(0)]^2 \rho_S(0) \right\}. \quad (14.16)$$

These can be interpreted as the average work  $\langle W \rangle = \langle H_S(\mathcal{T}) \rangle - \langle H_S(0) \rangle$  and its second moment [5, 8].

Physically,  $\mathcal{G}_\lambda$  is associated to the accumulated phase in the detector and it can be measured by quantum tomography [41]. The characteristic function is therefore the primary measurement outcome in Protocol 1. From an operational point of view, the dependence of  $\mathcal{G}_\lambda$  on  $\lambda$  can be retrieved by varying either the time or the strength of the system-detector coupling.

There is an important difference between Eqs. (14.14) and (14.15) and the corresponding ones obtained with the TMP and usually discussed in literature [5, 6, 15, 20–22]. To highlight the differences, let us explicitly write  $\langle W \rangle$  as obtained from Eq. (14.15) (see also [30]):

$$\langle W \rangle = \sum_i P_i \sum_j P_{i \rightarrow j} (\epsilon_j^\mathcal{T} - \epsilon_i^0) + \sum_{j,i \neq k} \epsilon_j^\mathcal{T} \rho_{ik}^0 U_{S,ji} U_{S,kj}^\dagger, \quad (14.17)$$

where  $P_i = \rho_{ii}^0$ .

The first term in (14.17) is the same as in TMP [5, 6, 8] and can be straightforwardly interpreted in terms of classical conditional probabilities. In absence of initial coherences or when the first projective measurement in the TMP destroys them, the system can be treated as a classical ensemble with probability  $P_i$  to start from the state  $|\epsilon_i^0\rangle$  and end up in the state  $|\epsilon_j^\mathcal{T}\rangle$  with conditional probability  $P_{i \rightarrow j}$ . In this framework, the energy of the initial state is always well defined as it is the trajectory associated to the work  $\epsilon_j^\mathcal{T} - \epsilon_i^0$ .

However, this is not the full story since the remaining terms, which depend on the initial coherences  $\rho_{ik}^0$ , are of a purely quantum nature. These coherences are destroyed by the initial measurement of  $H_S(0)$  performed in TMP. This changes the dynamics as discussed in the introduction and, using Feynman's words [42], this destroys all the interference alternative of the dynamics.

To fully understand the impact of the initial coherences on the quantum work, we must answer to a much more subtle question: can the Fourier transform of the observable function  $\mathcal{G}_\lambda$  be interpreted as a probability distribution of the work? Classically, we can obtain the work probability distribution as the Fourier transform of the corresponding characteristic function. However for initial coherent states the function:  $\mathcal{P}_{\text{quasi}}(W) = 1/(2\pi) \int d\lambda \exp\{-i\lambda W\} \mathcal{G}_\lambda$  is a quasi-probability distribution, i.e. it is real but not positive definite. We can write (14.14) explicitly using the  $\{|\epsilon_j^\mathcal{T}\rangle\}$  and then calculate the Fourier transform. The details of the calculations can be found in Refs. [30, 31]; we obtain

$$\mathcal{P}_{\text{quasi}}(W) = \sum_{ikj} \rho_{ik}^0 U_{S,ji} U_{S,kj}^\dagger \delta \left[ W - \left( \epsilon_j^\mathcal{T} - \frac{\epsilon_i^0 + \epsilon_k^0}{2} \right) \right]. \quad (14.18)$$

If the density operator has no initial coherences, i.e.,  $\rho_{ik}^0 = 0$  for  $i \neq k$ , we obtain the work probability distribution Eq. (14.1) of the TMP. Following this reasoning, we refer to the terms with  $i = k$  in Eq. (14.18) as “classical contributions”.

In general, however,  $\mathcal{P}_{\text{quasi}}(W)$  depends on the additional off-diagonal density matrix terms which are the fingerprints of coherent quantum processes. To strengthen this view, we notice that the contributions  $\rho_{ik}^0 U_{S,ji} U_{S,kj}^\dagger$  are always real [31] but they are not constrained to be positive. Therefore, due to the presence of these terms,  $\mathcal{P}_{\text{quasi}}(W)$  is not positive definite and can only be referred to as a quasi-probability distribution [9, 18, 30, 34, 35].

This can be surprising, but it is not contradictory. We stress once again that the measured quantity in Protocol 1 is the characteristic function  $\mathcal{G}_\lambda$ , i.e., the accumulated phase. Being an experimentally measurable quantity, it is free of ambiguous interpretations. The work quasi-probability distribution  $\mathcal{P}_{\text{quasi}}(W)$  obtained from Fourier transforming the accumulated detector phase  $\mathcal{G}_\lambda$  is instead a *derived* quantity that we would normally *associate* to a probability distribution. The above discussion points out that this last step is not allowed if the system has initial coherences.

This situation is not new in quantum mechanics, in fact, it turns out to be associated to the violation of the Leggett–Garg inequality [18, 30, 33, 43–46]. In the Leggett–Garg model the negativity of the probability distribution occurs when we try to interpret the results of a quantum measurements in purely classical terms. In our case, the macrorealism hypothesis [43, 44] is violated since the system is initially in a coherent superposition of energy eigenstates and, thus, it does not have a well-defined energy. Similar results and interpretations have been discussed for the full counting statistics as arising from quantum interference effects [33, 34, 45, 46]. By reversing this argument, we can consider the negative regions of  $\mathcal{P}_{\text{quasi}}(W)$  as signatures of pure quantum effects.

The important question is whether Protocol 1 has any advantage over the TMP. The positive or negative answer depends on whether we have and want to preserve the quantum effects and dynamics. Recalling the example discussed in the Introduction, with Protocol 1 we can measure the work moments and, thus, the energy needed to run the database search algorithm without affecting the algorithm performance.

It is worth noticing that the idea behind Protocol 1 can be extended to measure the dissipated heat of an open quantum system [30].

### 14.3.3 Protocol 2

The second protocol is based on the position measurement of the detector at the end of the dynamical evolution. The system-detector interaction proportional to  $pH_S$  generates a shift in the position  $x$  that is proportional to the energy of the system. The coupling at the beginning and at the end gives us information about the work done on the systems during the two couplings. The relevant equation is (14.13) where we have explicitly written the detector position and its shifts.

To clarify the physical picture, let us discuss first the idealised case in which the detector is strongly localised in  $x_0$ :  $g(x) = \delta(x - x_0)$ . Formally, this limit is not

correct because of the assumption we have made to neglect the dynamical phase of the free particle detector. Despite this, it allows us to point out an important feature of the protocol. In addition, this situation can be realistic for other kinds of detectors, where we can have both localised initial states and can remove the dynamical phase (see above discussion on qubit detector and bosonic mode as in Ref. [31]).

In this case, the density matrix of the detector in Eq. (14.13) reads

$$\rho_D(\mathcal{T}) = \sum_{ikl} \int dx dx' \rho_{ik}^0 \delta\left(x - x_0 - \frac{\lambda \epsilon_{ji}}{p_0}\right) \times \delta\left(x' - x_0 - \frac{\lambda \epsilon_{jk}}{p_0}\right) U_{S,ji} U_{S,kj}^\dagger |x\rangle\langle x'|.$$

The probability to measure  $\bar{x}$  and, thus, to have a shift in the detector of  $\Delta x = \bar{x} - x_0$  is  $\mathcal{P}(\Delta x) = \langle \bar{x} | \rho_D | \bar{x} \rangle$ . Using Eq. (14.19) and performing the integration, we find that the probability distribution is non-zero only if  $\epsilon_i^0 = \epsilon_k^0$ . For non-degenerate cases, this imposes the additional constraint  $k = i$  and the probability distribution reads

$$\mathcal{P}(\Delta x) = \sum_{ij} P_i P_{i \rightarrow j} \delta\left[\Delta x - \frac{\lambda}{p_0} (\epsilon_j^T - \epsilon_i^0)\right].$$

The latter result coincides with the classical contribution in Eq. (14.18) and the one obtained with the the TMP [3–6]. For a localised initial detector state, we obtain the classical work distribution.

A more realistic situation is the one in which the detector is not perfectly localised [38, 47–50]. This uncertainty in the initial position affects the measurement of the work distribution. Following the above discussion we consider an initial state in the momentum basis as  $G(p) = [\sigma^2/(2\pi)]^{1/4} \exp(-\sigma^2 p^2/4 + ipx_0)$  so that for  $\mathcal{T}/(m\sigma^2) \gg 1$  and we can neglect the detector dynamical phase. The corresponding initial state in the coordinate representation is  $g(x) = \exp\{-\frac{(x-x_0)^2}{4\sigma^2}\}/\sqrt[4]{2\pi\sigma^2}$ . The probability to measure  $\Delta x$  gives us the wok distribution as [31]

$$\mathcal{P}(\Delta x) = \sum_{ikj} \rho_{ik}^0 U_{S,ji} U_{S,kj}^\dagger \times \frac{e^{-\frac{(\Delta x - \frac{\lambda \epsilon_{ji}}{p_0})^2 + (\Delta x - \frac{\lambda \epsilon_{jk}}{p_0})^2}{4\sigma^2}}}{\sqrt{2\pi\sigma^2}}. \quad (14.19)$$

If the system has no initial coherences, i.e.,  $\rho_{ik}^0 = 0$  for  $i \neq k$ , the work distribution can be interpreted as a classical one with uncertainty [31]. An analogous situation is obtained when in presence of initial coherences the Gaussian functions in Eq. (14.19) do not overlap. This situation occurs when  $\epsilon_j^T - \epsilon_i^0 \ll \sigma p_0/\lambda$  (for any  $j$  and  $i$ ) and the off-diagonal contributions do not contribute to Eq. (14.19). This corresponds to the physical case in which the uncertainty in the initial state is small with respect to energy variation that we want to measure. This allows us to perform a “precise” measurement of the work and to distinguish the classical trajectories and evolution associated to the energy exchanges.

At the opposite limit we have an “imprecise” measurement when  $\epsilon_k^0 - \epsilon_i^0 \approx \sigma p_0 / \lambda$ . In this case, the Gaussian functions in Eq.(14.19) overlaps and the off-diagonal contributions  $\rho_{ik}^0$  become important again. Notice that in this case  $\mathcal{P}(\Delta x)$  is still a true probability distribution, i.e., it is definite positive [31], since it is a direct measurement output. In presence of a considerable uncertainty, the classical and quantum distribution (with and without initial coherence  $\rho_{ik}^0$ ) deviate one from each other. Therefore, the uncertainty reveals the presence of an underlying coherent quantum dynamics that manifests itself as a modification of the work distribution [31, 38].

## 14.4 Physical Implementations of the Measurement Schemes

### 14.4.1 *Implementations of the Ramsey Scheme*

In Sect. 14.2.2 we discussed the use of an auxiliary qubit coupled to the system to measure its work characteristic function during a dynamical process. In Sect. 14.3.2 the Protocol 1 was introduced as a generalisation of the Ramsey scheme. Although the scheme eliminates the need for the initial and final measurement of the system energy, which in some physical systems can be challenging, the requirement is to couple the qubit and the system through the operator  $M_\lambda$  (see Eq. (14.4)). In Ref. [21] it has been shown that the gate  $M_\lambda$  can be decomposed as a series of local unitary transformations and proper controlled operations, i.e. gates that apply an operator to the system only if the qubit is in the state  $|1\rangle$ . Indeed we have:

$$\begin{aligned} M_\lambda &= (I_S \otimes \sigma_x) M_2(\lambda) (I_S \otimes \sigma_x) M_1(\lambda) \\ M_1(\lambda) &= I_S \otimes |0\rangle \langle 0| + e^{-i\lambda H_S(\mathcal{T})} U_S(\mathcal{T}) \otimes |1\rangle \langle 1| \\ M_2(\lambda) &= I_S \otimes |0\rangle \langle 0| + U_S(\mathcal{T}) e^{-i\lambda H_S(0)} \otimes |1\rangle \langle 1|. \end{aligned}$$

Moreover, Ref. [20] employs a protocol equivalent to the Ramsey scheme and shows that it only requires a conditional qubit-system interaction of the form  $V \otimes |1\rangle \langle 1|$  where  $V$  is the operator that is varied in time during the work protocol.

Reference [20] describes an ion trap experiment to measure the work done in displacing spatially the ion trap. The displacement can be described by the operator  $V = g(t)x$ , where  $x$  is the ion position. The auxiliary qubit is represented by two internal electronic levels of the ion. The required interaction between the qubit and the ion position is provided by illuminating the ion with a far-detuned elliptically polarised standing-wave laser field. In the Lamb-Dicke regime the interaction induced is of the form:

$$H_I(t) = x \otimes [g_0(t)|0\rangle \langle 0| + g_1(t)|1\rangle \langle 1|] \quad (14.20)$$

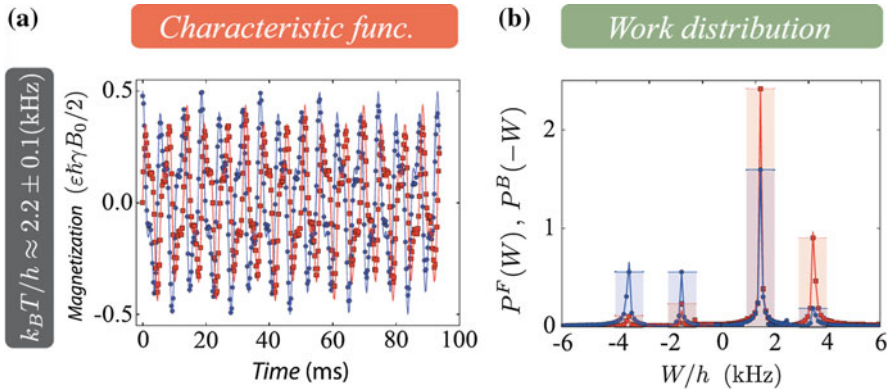


**Fig. 14.3** **a** Experimental data for the magnetisation  $\sigma_x$  and  $\sigma_y$  of the  ${}^1\text{H}$  spin (blue circles and red squares, respectively), plotted against the time length  $\lambda\pi\nu_2/J$ . The solid lines show Fourier fittings, which are in agreement with the theoretical simulation of the protocol. **b** The experimental points for the work probability distribution corresponding to the forward (backward) protocol are shown as red squares (blue circles) and obtained from the Fourier transform of the data in panel (a). Figure adapted with permission from Ref. [22].

where the couplings  $g_i(t)$  can be easily controlled by the relative intensities of two orthogonal laser polarisations.

Reference [21] instead proposes two possible implementations of the Ramsey scheme with mechanical oscillators. In the first version, an optical cavity is realised with two mirrors, one of them vibrating and playing the role of the system. The cavity also contains a two-level atom realising the auxiliary qubit which modifies the cavity field which ultimately drives the vibrating mirror. The work done on or extracted from the latter is thus conditional on the state of the qubit which acts as a switch. Conversely, one can measure the state of the qubit to estimate the work done on the vibrating mirror. In the second scenario, the system is embodied by a suspended nanomechanical beam which is coupled capacitively to a Cooper-pair box realising the auxiliary qubit. Again the position of the vibrating beam is coupled to an operator of the qubit and allows one to measure the work done on the beam by an external driving.

After the original proposals, other similar variations of the protocol have been put forward. In particular Ref. [51] extends the scheme to a circuit quantum electrodynamics setup for measuring the work done in a open driven system including a strongly dissipative regime. In Ref. [52], the authors propose a Ramsey scheme to assess the heat distribution in a quantum process and the connection to the Landauer principle. The authors of Ref. [53] employ the Ramsey scheme to measure work done on a gas of ultracold atoms. This ultimately allows them to connect work fluctuations with fluctuation theorems, e.g. the Jarzynski equality, and estimate the temperature of the gas with a precision below one nanokelvin.

The Ramsey scheme was experimentally realised in 2014 in the nuclear magnetic resonance (NMR) experiment reported in Ref. [22], only a year after the original proposals. The experiment employs a liquid sample of chloroform molecules and

involves an NMR-spectroscopy of the  $^1\text{H}$  and  $^{13}\text{C}$  nuclear spins of the molecule. The  $^{13}\text{C}$  spin plays the role of the driven system while the  $^1\text{H}$  spin acts as the auxiliary qubit. The goal is to measure the work performed on the carbon spin subject to a rotating magnetic field described by the Hamiltonian:

$$H(t) = 2\pi\hbar\nu(t) \left( \sigma_x^C \sin \frac{\pi t}{2\tau} + \sigma_y^C \cos \frac{\pi t}{2\tau} \right) \quad (14.21)$$

When the magnetic field intensity  $\nu(t)$  is changed in a time  $\tau$  with a linear ramp:  $\nu(t) = \nu_1 + (\nu_2 - \nu_1)t/\tau$ . In the above Hamiltonian  $\sigma_i^C$  is the  $i$ -th Pauli operator acting on the C nuclear spin while the ones acting on the H nuclear spin are denoted with  $\sigma_i^H$ . The process is performed both in the forward direction, increasing  $\nu(t)$  from  $\nu_1$  to  $\nu_2 > \nu_1$ , and in the backward direction, by exchanging  $\nu_1$  and  $\nu_2$ . The Ramsey protocol is implemented by taking advantage of the natural interaction between the carbon and hydrogen spins:  $H_I = 2\pi J \sigma_z^H \sigma_z^C$  where  $J$  is their coupling rate. The controlled gates  $M_1$  and  $M_2$  are realised using the free evolution induced by  $H_I$  and correcting with single-qubit gates.

At the end of the process the magnetisation of the hydrogen spin is measured to reveal the work characteristic function. The state of the carbon qubit (the system) was initialised in a thermal state with different temperatures. The results for the work characteristic function and the work probability distribution obtained by a Fourier transform are presented in Fig. 14.3 with diagrams from Ref. [22]. The real and imaginary parts of the characteristic function  $\chi_\lambda$  exhibit well defined oscillations as a function of the coupling time  $\lambda$  (measured in ms in the diagram) with a weak decay due to thermal relaxation which could potentially alter the work distribution. However the sampling time of the characteristic function has been kept much smaller than the relaxation time so that the effects of relaxation and dephasing are minimal.

The Fourier transform of the characteristic function reveals a work probability distribution, shown in Fig. 14.3b with four well defined peaks corresponding to the four allowed transitions between the two initial carbon spin states and the two final ones.

From the reconstructed  $\mathcal{P}(W)$ , the authors of Ref. [22] verified for the first time the Tasaki-Crooks relation in a fully quantum regime. To this end in Fig. 14.4, the ratio of the forward to the backward work probability distributions  $\mathcal{P}^F(W)/\mathcal{P}^B(-W)$  is shown for four different initial temperatures. The logarithm of this ratio is a linear function of the work  $W$  thus verifying the Tasaki-Crooks relation:

$$\ln \frac{\mathcal{P}^F(W)}{\mathcal{P}^B(-W)} = \beta(W - \Delta F) \quad (14.22)$$

where  $\beta$  is the initial inverse temperature of the carbon spin and  $\Delta F$  is the free energy difference between the final and the initial thermal equilibrium states. By fitting the numerical data for  $\mathcal{P}^F(W)/\mathcal{P}^B(-W)$ , the authors of Ref. [22], verified that the free energy difference obtained from the Tasaki-Crooks relation coincides, within experimental errors, with the theoretical value:

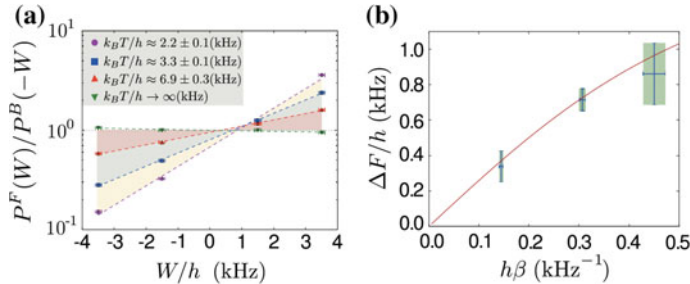


**Fig. 14.4** **a** The ratio  $\mathcal{P}^F(W)/\mathcal{P}^B(-W)$  is plotted in logarithmic scale for four values of the carbon spin initial temperature. The data are obtained from the values in Fig. 14.3. **b** Mean values for the free energy difference  $\Delta F$  and the initial inverse temperature  $\beta$  obtained using a linear fit of the data corresponding to panel (a). The full red line represents the theoretical expectation, Eq. (14.23). Figure adapted with permission from Ref. [22].

$$\Delta F = \frac{1}{\beta} \ln \frac{\cosh(\beta\nu_1)}{\cosh(\beta\nu_2)} \quad (14.23)$$

They also verified the Jarzynski equality by experimentally computing  $\ln\langle e^{-\beta W}\rangle$  and comparing it to the free energy difference obtained from the fitting of the Tasaki-Crooks relation or from the theoretical value (14.23) finding excellent agreement for different initial temperatures.

Before ending this section, it is worth commenting that the Ramsey scheme does not impose a restriction on the initial state of the system being thermal or diagonal in the initial energy eigenbasis. The Ramsey scheme allows one to measure the following quantity:

$$\text{Tr}_S \left[ U_S^\dagger(\mathcal{T}) e^{i\lambda H_S(\mathcal{T})} U_S(\mathcal{T}) e^{-i\lambda H_S(0)} \rho_S(0) \right]. \quad (14.24)$$

where the initial state  $\rho_S(0)$  can have coherences in the initial energy basis. In this case however this measured quantity does not correspond to a characteristic function of a probability distribution since its Fourier transform is in general complex. This is once more an indication of the presence of coherences in the initial state.

#### 14.4.2 Measuring Work using Light as an Ancilla

In Sect. 14.2.3 we review the method proposed in [15] that directly measures work with a single POVM. This strategy removes the need to make two measurements of the energy at different times, at the cost of implementing two entangling operations. An implementation with cold atomic ensembles was proposed in Ref. [23] which we here discuss briefly.

The scheme allows one to reconstruct the work done on an atomic ensemble subject to a rotating magnetic field of constant amplitude  $B$  and described by the Hamiltonian:

$$H(t) = -\gamma B [\cos \alpha(t) J_z + \sin \alpha(t) J_y] \quad (14.25)$$

where  $\gamma$  is the gyromagnetic ratio and we introduced the collective atomic angular momentum  $\mathbf{J} = (J_x, J_y, J_z)$ . To measure work, the authors of Ref. [23] propose the use of a continuous variable light mode embodied by the fluctuations of the polarisation along two orthogonal directions of a travelling laser mode and described by two conjugate position  $X$  and momentum  $P$  quadratures. The conditional shift needed to imprint the energy of the atomic system onto the light mode is provided by the Faraday rotation which couples the atomic angular momentum  $\mathbf{J}$  with the light polarisation through the coupled transformation  $U_I = \exp[-i\kappa P(\cos \phi J_z + \sin \phi J_y)]$  where the coupling constant  $\kappa$  depends on the intensity of the beam light, on the atom-photon interaction and the angle  $\phi$  depends on the direction of propagation of the light beam with the quantisation axis of the atomic ensemble. Notice that  $U_I$  is spatial translation operator of the light mode analogous to the transformation generated by the system-detector Hamiltonian  $H_{SD}$  of Eq. (14.6).

The protocol to extract the work distribution consists in *i.* shining the laser at an angle  $\phi = \pi + \alpha(0)$ ; *ii.* while the light beam is stored in a quantum memory, performing the rotation of the magnetic field from an angle  $\alpha(0)$  to an angle  $\alpha(T)$ ; *iii.* finally, letting the light beam to pass again through the atomic sample at an angle  $\phi = \alpha(T)$ . At the end of the process, the light beam is analysed through standard homodyne detection to reconstruct its polarisation distribution. The scheme of the protocol is sketched in Fig. 14.5. In this case, the light acts as the ancillary system ( $D$ ) which initially is a squeezed state with variance  $\sigma^2$ .

The resulting light mode distribution faithfully reproduces the work probability distribution provided that the ratio  $\sigma/\kappa$  is sufficiently smaller than the energy differences. Finding the first moments of this distribution we obtain:

$$\langle X \rangle = \kappa \langle W \rangle \quad (14.26)$$

$$\langle X^2 \rangle = \sigma^2 + \kappa^2 \langle W^2 \rangle \quad (14.27)$$

which clearly shows how to obtain the first moment of the work by analysing the fluctuations of the light mode quadrature. However it is clear from the expression of the second moment, that the initial zero-point fluctuations of the light mode will contribute with additional noise and may render difficult the estimate of  $\langle W^2 \rangle$  if the condition  $\sigma/\kappa \ll 1$  is not satisfied. The situation is dramatically worse if one wants to reconstruct the Jarzynski equality since the noise originating from the light mode will contribute to all orders and exponentially increasing. Indeed:

$$\langle e^{-\beta X/\kappa} \rangle = \langle e^{-\beta W} \rangle \exp \left( \frac{\beta^2 \sigma^2}{2\kappa^2} \right) \quad (14.28)$$

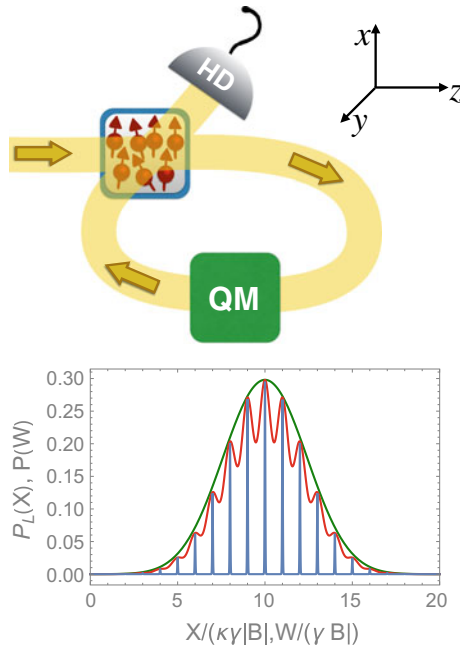


**Fig. 14.5** Top: Setup to measure the probability distribution of the work done on an atomic ensemble. A polarised beam is sent along the  $z$  ( $\phi = 0$ ) direction to interact with the atomic ensemble. The beam is then stored in a quantum memory (QM) while the magnetic field applied to the atoms is rotated from  $z$  to  $y$ . Finally the beam is redirected to the atoms at an angle  $\phi = -\pi/2$  and eventually measured. Figure reproduced with permission from Ref. [23]. Bottom: for an instantaneous rotation of the magnetic field, comparison of the work probability distribution (blue) with the rescaled light polarisation distributions for  $N = 20$  atoms,  $\sigma^2 = 1/2$ ,  $\kappa = 2$  (red) and  $\kappa = 1$  (green).

showing that the Jarzynski equality is affected by an exponential correction that diverges with  $\sigma/\kappa$  and in the limit of small temperatures [23, 32, 38].

#### 14.4.3 Experimental Realization of a Quantum Work Meter with Cold Atoms

The POVM proposed in Ref. [15] was recently realised experimentally with cold atoms in Ref. [24]. In this experimental setup, a Bose-Einstein condensate (BEC) of  $^{87}\text{Rb}$  atoms with two internal Zeeman sublevels  $|1\rangle \equiv |F = 2, m_F = 1\rangle$  and  $|2\rangle \equiv |F = 2, m_F = 2\rangle$  is trapped by an atom chip. The BEC is then released from the trap and, during the free fall, a spatially inhomogeneous magnetic field created by the atom chip is capable of realising a Stern-Gerlach type of interaction [54]. Such a process entangles the spin degree of freedom (the system of which the work injected

will be measured) with the motional degree of freedom of the atoms. This is exactly the type of interaction of Eq. (14.6) that was proposed in Ref. [15, 23].

Thus, the key element of the experiment is the atom chip, which efficiently entangles the internal and motional degrees of freedom of an atom through Stern–Gerlach type magnetic gradient pulses. These pulses are generated using a 3-current-carrying-wire setup on the chip surface. A gradient pulse along the vertical direction  $z$  direction with amplitude  $B'$  and duration  $\tau$ , induces a momentum kick  $m_F \delta p$  on an atom in the  $m_F$  state ( $\delta p \sim \mu_B g_F B' \tau$ , where  $\mu_B$  and  $g_F$  are, respectively, the Bohr magneton and the Landé factor [54]). The evolution of the state of the atom induced by such a pulse is described by the unitary operator

$$U_p = e^{i \delta p z_D \sigma_S}, \quad (14.29)$$

where the operator  $z_D$  is the generator of translations in the momentum degree of freedom, and  $\sigma_S = |1\rangle\langle 1| + 2|2\rangle\langle 2|$ . If the Hamiltonian of the atom is proportional to the operator  $\sigma_S$  this operation effectively implements the evolution of Eq. (14.6). In this case the motional degree of freedom of the atoms is the ancillary system or detector. The momentum kicks induced by both pulses are controlled in the experiment, and it is also possible to apply an RF field before the entangling operation. Thus, with these tools it is possible to simulate an arbitrary system with initial and final Hamiltonians  $H_S(0)$  and  $H_S(\mathcal{T})$  [15]. Finally, let us note that the first pulse  $B'$  and the second pulse  $\tilde{B}'$  are applied with opposite signs to ensure that the sequence creates a coherent record of the value of work.

The initial state of the spins is a pure superposition of states  $|1\rangle$  and  $|2\rangle$  in such a way that the populations correspond to a thermal state with temperature  $T$ . Since in the experiment, one is interested in the realisation of the TMP by a single POVM, one can adjust the value of  $\delta p$  such that coherences do not affect the experiment (see Ref. [24] and its Supplementary Material). The experiment proceeds as described before: (i) the atoms are released from the atom chip and while falling, (ii) internal and motional degrees of freedom are entangled with a magnetic gradient pulse, (iii) a unitary driving  $U_S(\mathcal{T})$  of the spin state is applies through a RF field. (iv) Another magnetic gradient field couples internal and motional degrees of freedom, (v) after a free fall evolution an image of the atoms is taken.

The above sequence and an example of the atomic image are shown in Fig. 14.6. The 4 peaks correspond to the 4 processes corresponding to all the transitions from the initial to the final states (similar to the Ramsey experiment in NMR). The position of the peak can be connected to the value of the work while the corresponding population is proportional to the probability for that value. It is interesting to notice that in a single run of the experiment the full probability distribution is obtained. The authors of Ref. [24] were also able to verify the Jarzynski equality for different initial temperatures of the sample and different processes  $U_S(\mathcal{T})$ .

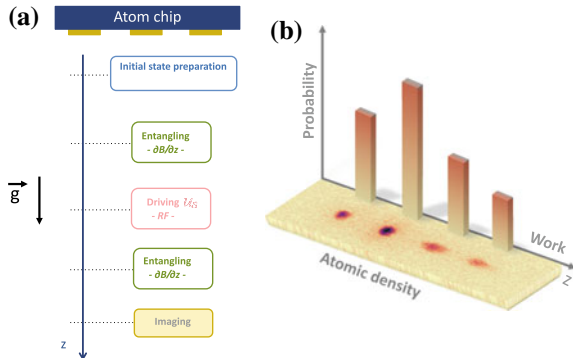


**Fig. 14.6** **a** Physical operations that allow to measure work on the spin state of a BEC under RF driving (see text). The ancillary system consists of the motional degrees of freedom of the atoms. **b** Probability distribution of work. The image shows the BEC split in 4 clouds at the end of a single run of the experiment. The  $z$  axis measures the position of the cloud and can be put in correspondence with the work done on the spins. The vertical bars correspond to the number of atoms in each of the 4 clouds and represent the probability for the corresponding work values. Figure reproduced from Ref. [24] under the CC BY licence.

## 14.5 Conclusions

In summary, we have considered protocols that allow the reconstruction of the probability distribution of work done on a quantum system using an auxiliary quantum detector. We described two paradigmatic schemes giving directly access to the characteristic function and the distribution of work, and their recent physical implementations using different setups. The necessary ingredient for these schemes is a system-detector interaction that couples the system energy operator with an observable of the detector. Then, we described a framework that provides a unified view of these ideas. In this framework fall most of the proposals and experimental measurements of heat and work that appeared in the literature in recent years. The resulting work statistics and the degree of perturbation induced in the system dynamics depend on the system-detector coupling and on the measurement done on the detector. Therefore, the protocol used to measure the work statistics must be chosen keeping in mind which quantum features we want to preserve in the dynamics.

We believe that there are many unanswered questions on the role of quantum energy coherences in thermodynamic processes. The schemes described in this chapter are important tools for such future investigations.

**Acknowledgements** We thank R. Fazio, J. Goold, L. Mazzola, K. Modi, M. Paternostro and J. P. Paz for illuminating discussions. P.S. has received funding from the European Union FP7/2007-2013 under REA Grant Agreement No. 630925, COHEAT, and from MIUR-FIRB2013, Project Coca (Grant No. RBFR1379UX). FC and AJR acknowledge financial support from ANPCyT (PICT 2013-0621 and PICT 2014-3711), CONICET and UBACyT.

## References

1. C. Jarzynski, Phys. Rev. Lett. **78**, 2690 (1997). <https://doi.org/10.1103/PhysRevLett.78.2690>
2. G.E. Crooks, Phys. Rev. E **60**, 2721 (1999). <https://doi.org/10.1103/PhysRevE.60.2721>
3. J. Kurchan (2000), arXiv:cond-mat/0007360
4. H. Tasaki (2000), arXiv:cond-mat/0009244
5. M. Campisi, P. Hänggi, P. Talkner, Rev. Mod. Phys. **83**, 771 (2011). <https://doi.org/10.1103/RevModPhys.83.771>
6. M. Esposito, U. Harbola, S. Mukamel, Rev. Mod. Phys. **81**, 1665 (2009). <https://doi.org/10.1103/RevModPhys.81.1665>
7. P.A.M. Dirac, *The Principles of Quantum Mechanics*. The International Series of Monographs on Physics, vol. 27, 4th edn. (Clarendon Press, Oxford, 1967)
8. A. Engel, R. Nolte, EPL (Europhys. Lett.) **79**, 10003 (2007). <https://doi.org/10.1209/0295-5075/79/10003>
9. A.E. Allahverdyan, Phys. Rev. E **90**, 032137 (2014). <https://doi.org/10.1103/PhysRevE.90.032137>
10. L. Fusco, S. Pigeon, T.J.G. Apollaro, A. Xuereb, L. Mazzola, M. Campisi, A. Ferraro, M. Paternostro, G. De Chiara, Phys. Rev. X **4**, 031029 (2014). <https://doi.org/10.1103/PhysRevX.4.031029>
11. L. Villa, G. De Chiara, Quantum **2**, 42 (2018). <https://doi.org/10.22331/q-2018-01-04-42>
12. P. Talkner, E. Lutz, P. Hänggi, Phys. Rev. E **75**, 050102 (2007). <https://doi.org/10.1103/PhysRevE.75.050102>
13. M. Campisi, P. Talkner, P. Hänggi, Phys. Rev. Lett. **102**, 210401 (2009). <https://doi.org/10.1103/PhysRevLett.102.210401>
14. M. Carrega, P. Solinas, M. Sassetti, U. Weiss, Phys. Rev. Lett. **116**, 240403 (2016). <https://doi.org/10.1103/PhysRevLett.116.240403>
15. A.J. Roncaglia, F. Cerisola, J.P. Paz, Phys. Rev. Lett. **113**, 250601 (2014). <https://doi.org/10.1103/PhysRevLett.113.250601>
16. M.A. Nielsen, I.L. Chuang, *Quantum Computation and Quantum Information* (Cambridge University Press, Cambridge, 2010). <https://doi.org/10.1017/CBO9780511976667>
17. L.K. Grover, in *Proceedings of the Twenty-Eighth Annual ACM Symposium on Theory of Computing*, STOC '96 (ACM, New York, NY, USA, 1996), pp. 212–219. <https://doi.org/10.1145/237814.237866>
18. M. Perarnau-Llobet, E. Bäumer, K.V. Hovhannisyan, M. Huber, A. Acin, Phys. Rev. Lett. **118**, 070601 (2017). <https://doi.org/10.1103/PhysRevLett.118.070601>
19. M. Hayashi, H. Tajima, Phys. Rev. A **95**, 032132 (2017). <https://doi.org/10.1103/PhysRevA.95.032132>
20. R. Dorner, S.R. Clark, L. Heaney, R. Fazio, J. Goold, V. Vedral, Phys. Rev. Lett. **110**, 230601 (2013). <https://doi.org/10.1103/PhysRevLett.110.230601>
21. L. Mazzola, G. De Chiara, M. Paternostro, Phys. Rev. Lett. **110**, 230602 (2013). <https://doi.org/10.1103/PhysRevLett.110.230602>
22. T.B. Batalhão, A.M. Souza, L. Mazzola, R. Aucaise, R.S. Sarthour, I.S. Oliveira, J. Goold, G. De Chiara, M. Paternostro, R.M. Serra, Phys. Rev. Lett. **113**, 140601 (2014). <https://doi.org/10.1103/PhysRevLett.113.140601>
23. G. De Chiara, A.J. Roncaglia, J.P. Paz, New J. Phys. **17**, 035004 (2015). <https://doi.org/10.1088/1367-2630/17/3/035004>
24. F. Cerisola, Y. Margalit, S. Machluf, A.J. Roncaglia, J.P. Paz, R. Folman, Nat. Commun. **8**, 1241 (2017). <https://doi.org/10.1038/s41467-017-01308-7>
25. L. Levitov, G. Lesovik, Pis'ma Zh. Eksp. Teor. Fiz. [JETP Lett.] **58**, 230 (1993)
26. L.S. Levitov, H. Lee, G.B. Lesovik, J. Math. Phys. **37**, 4845 (1996). <https://doi.org/10.1063/1.531672>
27. Y.V. Nazarov, M. Kindermann, Eur. Phys. J. B **35**, 413 (2003). <https://doi.org/10.1140/epjb/e2003-00293-1>

28. W. Belzig, Y.V. Nazarov, Phys. Rev. Lett. **87**, 197006 (2001). <https://doi.org/10.1103/PhysRevLett.87.197006>
29. W. Belzig, in *Quantum Noise in Mesoscopic Physics*, ed. by Y.V. Nazarov (Kluwer, Dordrecht, 2003). <https://doi.org/10.1007/978-94-010-0089-5>
30. P. Solinas, S. Gasparinetti, Phys. Rev. E **92**, 042150 (2015). <https://doi.org/10.1103/PhysRevE.92.042150>
31. P. Solinas, S. Gasparinetti, Phys. Rev. A **94**, 052103 (2016). <https://doi.org/10.1103/PhysRevA.94.052103>
32. P. Solinas, H.J.D. Miller, J. Anders, Phys. Rev. A **96**, 052115 (2017). <https://doi.org/10.1103/PhysRevA.96.052115>
33. A.A. Clerk, Phys. Rev. A **84**, 043824 (2011). <https://doi.org/10.1103/PhysRevA.84.043824>
34. P.P. Hofer, A.A. Clerk, Phys. Rev. Lett. **116**, 013603 (2016). <https://doi.org/10.1103/PhysRevLett.116.013603>
35. P.P. Hofer, Quantum **1**, 32 (2017). <https://doi.org/10.22331/q-2017-10-12-32>
36. J. von Neumann, *Mathematical Foundations of Quantum Mechanics*, vol. 2 (Princeton University Press, Princeton, 1955). <https://doi.org/10.23943/princeton/9780691178561.001.0001>
37. A. Peres, *Quantum Theory: Concepts and Methods*, vol. 57 (Springer Science & Business Media, Berlin, 2006). <https://doi.org/10.1007/0-306-47120-5>
38. P. Talkner, P. Hänggi, Phys. Rev. E **93**, 022131 (2016). <https://doi.org/10.1103/PhysRevE.93.022131>
39. J.A. Jones, V. Vedral, A. Ekert, G. Castagnoli, Nature **403**, 869 EP (2000). <https://doi.org/10.1038/35002528>
40. A. Ekert, M. Ericsson, P. Hayden, H. Inamori, J.A. Jones, D.K.L. Oi, V. Vedral, J. Mod. Opt. **47**, 2501 (2000). <https://doi.org/10.1080/09500340008232177>
41. M. Paris, J. Rehacek, *Quantum State Estimation*, 1st edn. (Springer Publishing Company, Incorporated, 2010). <https://doi.org/10.1007/b98673>
42. R.P. Feynman, A.R. Hibbs, *Quantum Mechanics and Path Integrals* (McGraw-Hill, New York, 1965)
43. A.J. Leggett, A. Garg, Phys. Rev. Lett. **54**, 857 (1985). <https://doi.org/10.1103/PhysRevLett.54.857>
44. C. Emary, N. Lambert, F. Nori, Rep. Prog. Phys. **77**, 016001 (2014). <https://doi.org/10.1088/0034-4885/77/1/016001>
45. A. Bednorz, W. Belzig, Phys. Rev. Lett. **105**, 106803 (2010). <https://doi.org/10.1103/PhysRevLett.105.106803>
46. A. Bednorz, W. Belzig, A. Nitzan, New J. Phys. **14**, 013009 (2012). <https://doi.org/10.1088/1367-2630/14/1/013009>
47. B.P. Venkatesh, G. Watanabe, P. Talkner, New J. Phys. **16**, 015032 (2014). <https://doi.org/10.1088/1367-2630/16/1/015032>
48. G. Watanabe, B.P. Venkatesh, P. Talkner, M. Campisi, P. Hänggi, Phys. Rev. E **89**, 032114 (2014). <https://doi.org/10.1103/PhysRevE.89.032114>
49. G. Watanabe, B.P. Venkatesh, P. Talkner, Phys. Rev. E **89**, 052116 (2014). <https://doi.org/10.1103/PhysRevE.89.052116>
50. D. Sokolovski, Phys. Lett. A **379**, 1097 (2015). <https://doi.org/10.1016/j.physleta.2015.02.018>
51. M. Campisi, R. Blattmann, S. Kohler, D. Zueco, P. Hänggi, New J. Phys. **15**, 105028 (2013). <https://doi.org/10.1088/1367-2630/15/10/105028>
52. J. Goold, U. Poschinger, K. Modi, Phys. Rev. E **90**, 020101 (2014). <https://doi.org/10.1103/PhysRevE.90.020101>
53. T.H. Johnson, F. Cosco, M.T. Mitchison, D. Jaksch, S.R. Clark, Phys. Rev. A **93**, 053619 (2016). <https://doi.org/10.1103/PhysRevA.93.053619>
54. S. Machluf, Y. Japha, R. Folman, Nat. Commun. **4**, 2424 (2013). <https://doi.org/10.1038/ncomms3424>

# Chapter 15

## Work, Heat and Entropy Production Along Quantum Trajectories



Cyril Elouard and M. Hamed Mohammady

### 15.1 Introduction

The concept of quantum trajectories was first introduced as a numerical tool to simulate non-unitary quantum evolution [1]. The underlying idea was to replace the deterministic evolution of a density matrix in a space of dimension  $d_S^2$  with a stochastic dynamics for a wave function of dimension  $d_S$ , leading to a potentially huge memory gain when simulating large quantum systems. Later on, it was understood that such trajectories actually correspond to the sequences of pure states followed by an open quantum system when its environment is continuously monitored [2, 3] (see Fig. 15.1) and the measurement record is accessible. Since then, such a situation has been implemented experimentally in various setups of quantum optics [4–7] or superconducting circuits [8–10].

Besides, it has long been noticed that an open quantum system (Fig. 15.1a) can be interpreted as the usual thermodynamic situation: a working substance (the system  $\mathcal{S}$ ) on the one hand driven by an external agent who varies a parameter  $\lambda$  in its Hamiltonian (this induces work exchanges), and on the other hand coupled to a heat bath (this causes heat dissipation) [11]. This canonical situation was extensively studied in the classical case, first restricting the working substance to near-equilibrium states and more recently, owing to the statistical thermodynamics paradigm [12, 13], for any transformation potentially bringing the system  $\mathcal{S}$  far from equilibrium.

In the formalism of classical stochastic thermodynamics, the classical system follows a stochastic trajectory in its phase space at each single realization of the studied thermodynamic transformation. The randomness in this picture originates from the

---

C. Elouard (✉)

University of Rochester, Rochester, NY, USA  
e-mail: cyril.elouard@gmail.com

M. H. Mohammady

Lancaster University, Lancaster, United Kingdom  
e-mail: m.hamed.mohammady@gmail.com

nature of the actions of the environment on the system  $\mathcal{S}$  that appear in practice to be uncontrollable and unpredictable. Thermodynamic quantities like work, dissipated heat, and entropy production become random variables defined for a single trajectory. These quantities satisfy fluctuation theorems [14–16] which constrain their out-of-equilibrium fluctuations beyond the second law of thermodynamics.

When the environment is monitored, the quantum trajectories can be seen as quantum analogues of the stochastic trajectories in phase space, enabling us to build a quantum version of the stochastic thermodynamics formalism [17–21]. However, these quantum trajectories feature two crucial differences with respect to the trajectories of classical stochastic thermodynamics: First, they correspond to sequences of states on the system's Hilbert's space  $\mathcal{H}_\mathcal{S}$  instead of in phase space. They therefore allow us to study the thermodynamic consequences of quantum specificities such as coherences and entanglement. Second, the stochasticity of the system's dynamics is a direct consequence of the randomness of quantum measurements, and is not predicated on the observer's ignorance as to the thermal environment's precise evolution. As a consequence, the framework for quantum stochastic thermodynamics presented here can also describe situations where there is no thermal reservoir, but the system is coupled to a measuring apparatus which introduces randomness and, therefore, irreversibility in the system's dynamics [20, 22, 23]. Such formalism therefore opens an avenue to describe the thermodynamics of quantum measurements.

In this chapter, we review the formalism of quantum stochastic thermodynamics and highlight some of the genuinely quantum features it opens to study owing to fundamental examples. The chapter is divided as follows: in Sect. 15.2, we introduce the concept of quantum trajectories and unraveling, first for any quantum channel, and then in the special case of a quantum open system obeying a Lindblad equation. In Sect. 15.3, we define the entropy production at the level of a quantum trajectory and show that it obeys an Integral fluctuation theorem as in the classical case. In Sect. 15.4, we analyze the energetics along a single trajectory and stress the contribution of coherence erasure induced by the quantum measurements. In Sects. 15.5–15.7 we analyze three fundamental examples: the thermalization of a quantum system, the photo-counting of a qubit's fluorescence and the continuous measurement of a qubit's observable.

## 15.2 Quantum Trajectories

### 15.2.1 Two-Point Quantum Trajectories of Open Systems

Consider a quantum system  $\mathcal{S}$ , with a Hilbert space  $\mathcal{H}_\mathcal{S} \simeq \mathbb{C}^{d_\mathcal{S}}$ , that is initially prepared in the state  $\rho_\mathcal{S} = \sum_{l=1}^{d_\mathcal{S}} p_l \Pi_\mathcal{S}[\psi_l]$ . Here  $\Pi_\mathcal{S}[\psi] \equiv |\psi\rangle\langle\psi|$  is a projection on the vector  $|\psi\rangle \in \mathcal{H}_\mathcal{S}$  and  $\{|\psi_l\rangle\}_l$  is an orthonormal basis that spans  $\mathcal{H}_\mathcal{S}$ . If the system is closed, its time evolution will be described by the unitary quantum channel  $\mathcal{V}(\rho_\mathcal{S}) := V \rho_\mathcal{S} V^\dagger = \sum_{m=1}^{d_\mathcal{S}} p_m \Pi_\mathcal{S}[\xi_m]$ , with  $\{|\xi_m\rangle\}_m$  another orthonormal basis

that spans  $\mathcal{H}_S$ . Now consider we projectively measure the system with respect to the observables  $\{\Pi_S[\psi_l]\}_{l=1}^{d_S}$  and  $\{\Pi_S[\xi_m]\}_{m=1}^{d_S}$  prior and posterior to the time evolution, respectively. The evolution of the average (unconditioned) state will still be given by  $\rho_S \mapsto V\rho_S V^\dagger$ ; this is because the observables commute with these states. Consequently, we can decompose the total evolution of the system into a collection of measurement sequences, or “two-point pure-state trajectories”,  $\Gamma := (l, m) \equiv |\psi_l\rangle \mapsto |\xi_m\rangle$ . Each trajectory  $\Gamma$  corresponds to a possible evolution of the system during a single realization of the process consisting of the first measurement, the evolution and the second measurement, the one characterized by the sequence of measurement outcomes  $(l, m)$ . The probability of the trajectory  $\Gamma$  will be given by the Born rule as

$$\begin{aligned} P(\Gamma) &= \text{tr}[\Pi_S[\xi_m]V(\Pi_S[\psi_l]\rho_S\Pi_S[\psi_l])], \\ &= \text{tr}[\Pi_S[\xi_m]V(\Pi_S[\psi_l])] \text{tr}[\Pi_S[\psi_l]\rho_S] \\ &= \text{tr}[\Pi_S[\xi_m]V(\Pi_S[\psi_l])] p_l. \end{aligned} \quad (15.1)$$

Now consider the case where  $S$  is an open system [24], such that it interacts with an environment  $E$  with Hilbert space  $\mathcal{H}_E$ . If the compound system  $S + E$  is initially prepared in the product state  $\rho_S \otimes \rho_E$ , and then evolves by a joint unitary channel  $V : \rho_S \otimes \rho_E \mapsto V(\rho_S \otimes \rho_E)V^\dagger$ , the evolution of  $S$  alone will be described by the quantum channel  $\Phi$  [25], defined as

$$\Phi(\rho_S) := \text{tr}_E[V(\rho_S \otimes \rho_E)V^\dagger]. \quad (15.2)$$

Here  $\text{tr}_E$  is the partial trace over  $\mathcal{H}_E$ . The triple  $(\mathcal{H}_E, \rho_E, V)$  is referred to as the Stinespring dilation of  $\Phi$  [26]. Whilst a quantum channel can arise from infinitely many such dilations, a given choice of environment and joint evolution describes a unique channel.

We now wish to determine the two-point measurement scheme that is compatible with the *reduced* dynamics of  $S$  as defined by the quantum channel  $\Phi$ . To this end, we must projectively measure  $S$ , at the start and end of its evolution, with observables that do not disturb its average state. The initial observable is, as before,  $\{\Pi_S[\psi_l]\}_l$ , and given that the final state of  $S$  is written as  $\Phi(\rho_S) = \sum_m p'_m \Pi_S[\xi_m]$ , the final observable is  $\{\Pi_S[\xi_m]\}_m$ . The resulting sequence of measurement outcomes will therefore define a trajectory of  $S$ , denoted  $\Gamma_S := (l, m) \equiv |\psi_l\rangle \mapsto |\xi_m\rangle$ , which will occur with the probability

$$P(\Gamma_S) = \text{tr}[\Pi_S[\xi_m]\Phi(\Pi_S[\psi_l])] p_l. \quad (15.3)$$

Let us assume that we are also capable of independently measuring the environment. Given that the initial and final state of the environment is  $\rho_E = \sum_\mu q_\mu \Pi_E[\phi_\mu]$  and  $\rho'_E = \sum_\nu q'_\nu \Pi_E[\varphi_\nu]$ , respectively, by measuring  $E$  with the observable  $\{\Pi_E[\phi_\mu]\}_\mu$ , respectively  $\{\Pi_E[\varphi_\nu]\}_\nu$ , at the start and end of the evolution, we may construct the trajectories  $\Gamma_E := (\mu, \nu) \equiv |\phi_\mu\rangle \mapsto |\varphi_\nu\rangle$ . The *joint trajectory* for both system and

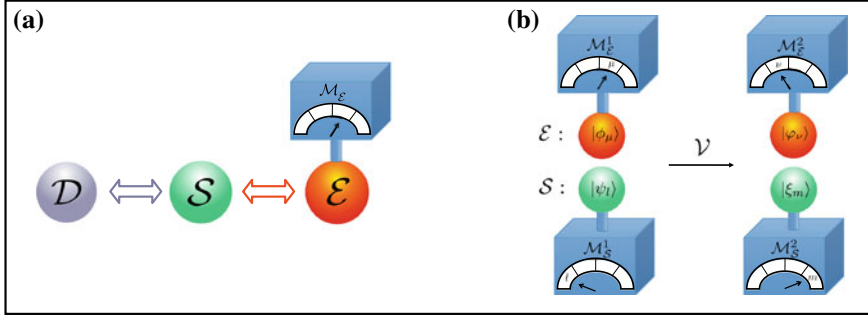


**Fig. 15.1** **a** Typical scenario of quantum open systems formalism: a system  $\mathcal{S}$  is coupled to an environment  $\mathcal{E}$  and potentially driven by an external agent  $\mathcal{D}$ . In the quantum trajectory paradigm,  $\mathcal{E}$  is monitored by a measuring apparatus  $\mathcal{M}_{\mathcal{E}}$ . **b** The joint quantum trajectory  $\Gamma := ((l, m), (\mu, \nu))$  observed when the system  $\mathcal{S}$  and environment  $\mathcal{E}$  are first measured by the detectors  $\mathcal{M}_{\mathcal{S}}^1$  and  $\mathcal{M}_{\mathcal{E}}^1$ , respectively, after which they evolve by the unitary channel  $\mathcal{V}$ . Finally, they are measured by the detectors  $\mathcal{M}_{\mathcal{S}}^2$  and  $\mathcal{M}_{\mathcal{E}}^2$  (this time measuring a different observable).

environment, therefore, is  $\Gamma := (\Gamma_{\mathcal{S}}, \Gamma_{\mathcal{E}}) = ((l, m), (\mu, \nu))$ , which occurs with the probability

$$\begin{aligned} P(\Gamma) &= \text{tr}[(\Pi_{\mathcal{S}}[\xi_m] \otimes \Pi_{\mathcal{E}}[\varphi_{\nu}])V(\Pi_{\mathcal{S}}[\psi_l] \otimes \Pi_{\mathcal{E}}[\phi_{\mu}])V^{\dagger}] \text{tr}[\Pi_{\mathcal{S}}[\psi_l]\rho_{\mathcal{S}}]\text{tr}[\Pi_{\mathcal{E}}[\phi_{\mu}]\rho_{\mathcal{E}}], \\ &= \text{tr}[(\Pi_{\mathcal{S}}[\xi_m] \otimes \Pi_{\mathcal{E}}[\varphi_{\nu}])V(\Pi_{\mathcal{S}}[\psi_l] \otimes \Pi_{\mathcal{E}}[\phi_{\mu}])V^{\dagger}] p_l q_{\mu}. \end{aligned} \quad (15.4)$$

This scheme is illustrated in Fig. 15.1. Note that while the evolution of  $\mathcal{S}$ , respectively  $\mathcal{E}$ , can be seen as a stochastic sampling from the trajectories  $\Gamma_{\mathcal{S}}$  and  $\Gamma_{\mathcal{E}}$ , the evolution of the compound system  $\mathcal{S} + \mathcal{E}$  is not given by a stochastic sampling from the joint trajectories  $\Gamma$ . This is because, generally, the compound system will be correlated at the end of the evolution, and the measurements will disturb the state.

In order to express Eq. (15.4) analogously to Eq. (15.3), i.e., in terms of dynamical processes on the system alone, we must first obtain the “Kraus” decomposition of the channel  $\Phi$  as  $\Phi(\rho_{\mathcal{S}}) = \sum_{\mu, \nu} \Phi_{\mu, \nu}(\rho_{\mathcal{S}})$ , where

$$\Phi_{\mu, \nu}(\rho_{\mathcal{S}}) = M_{\mu, \nu}\rho_{\mathcal{S}}M_{\mu, \nu}^{\dagger}, \quad (15.5)$$

such that

$$M_{\mu, \nu} := \sqrt{q_{\mu}}\langle\varphi_{\nu}|V|\phi_{\mu}\rangle \quad (15.6)$$

are the Kraus operators [27] determined by the environment trajectory  $\Gamma_{\mathcal{E}}$ . Consequently, Eq. (15.4) can be expressed as

$$P(\Gamma) = \text{tr}[\Pi_{\mathcal{S}}[\xi_m]\Phi_{\mu, \nu}(\Pi_{\mathcal{S}}[\psi_l])] p_l. \quad (15.7)$$

We note that  $\{E(\nu) := \sum_{\mu} M_{\mu,\nu}^\dagger M_{\mu,\nu}\}_{\nu}$  constitutes a generalized positive operator valued measure (POVM) on the system, with  $\nu$  denoting the measurement outcomes [28–30]. The effect operators  $E(\nu)$  will in general not be projection operators.

### 15.2.2 Quantum Trajectories and Continuous Measurement

In this section we generalize the preceding considerations to the case where the environment is subject to an arbitrarily long sequence of measurements, rather than just at the beginning and end of the transformation under study. To be sure, measuring the environment at the middle of the joint evolution will in general destroy the quantum correlations between the system and the environment built by the unitary evolution. Consequently, unlike the two-point measurement scheme discussed above, we will not be able to claim that our measurements merely track the evolution of the subsystems in general. However, if the correlations between the environment and system vanish on a time-scale much shorter than the time between two measurements on the environment, as it is the case for a Markovian environment, the repeated measurements will as before preserve the average evolution of the system.

To model this situation, we discretize the evolution time, introducing the times  $t_k = t_i + k \Delta t$  ( $t_i \equiv t_0$ ,  $t_f \equiv t_K$ ) at which the measurements are performed on the environment. More precisely, we assume that at the start  $t_{k-1}$  of each time interval  $[t_{k-1}, t_k]$ , the system and environment are in a product state  $\rho_S(t) \otimes \rho_E$ . A first measurement is performed on the environment at time  $t_{k-1}^+$ , yielding outcome  $\mu_k$ . Then the system and environment evolve unitarily during  $\Delta t$  until time  $t_k^-$  where a second measurement is performed, yielding outcome  $\mu_k$ . This in turn induces the quantum channel  $\Phi(t_{k-1}, t_k)$  on the system. Consistently with the Markovian assumption, the system and environment are assumed to be in a product state  $\rho_S(t_k) \otimes \rho_E$  at the beginning of the next evolution interval, i.e. time  $t_k$ . One often models such processes by allowing the system to interact with a new copy of the environment every  $\Delta t$ , enforcing the Markovian character of the evolution.

The full evolution between  $t_i$  and  $t_f$  is given by the composition of these channels, i.e.,  $\Phi(t_i, t_f) = \Phi(t_{K-1}, t_K) \circ \dots \circ \Phi(t_1, t_2) \circ \Phi(t_0, t_1)$ . A single realization of the process is now determined by a measurement record  $\{\alpha_k\}_{k=1}^K$ , where for each  $k$ ,  $\alpha_k = (\mu_k, \nu_k)$  compiles the outcomes obtained at the beginning and at the end of the interval  $(t_{k-1}, t_k)$ . The Kraus decomposition of each map  $\Phi(t_{k-1}, t_k)$  associated with the measurement outcomes  $\alpha_k$  obtained between  $t_{k-1}$  and  $t_k$  can be introduced similarly as in Eq. (15.5):  $\Phi(t_{k-1}, t_k) = \sum_{\alpha_k} \Phi_{\alpha_k}(t_{k-1}, t_k)$ . Let the average state of the system at time  $t_0$  and  $t_K$  be  $\rho_S(t_0) = \sum_l p_l \Pi_S[\psi_l]$  and  $\rho_S(t_K) = \sum_m p'_m \Pi_S[\xi_m]$ , respectively. As such, we obtain the trajectories  $\Gamma := ((l, m), \{\alpha_k\}_{k=1}^K)$ , with probabilities

$$P(\Gamma) = \text{tr}[\Pi_S[\xi_m](\Phi_{\alpha_K}(t_{K-1}, t_K) \circ \dots \circ \Phi_{\alpha_1}(t_0, t_1))(\Pi_S[\psi_l])] p_l. \quad (15.8)$$

Since each  $\Phi_{\alpha_k}(t_{k-1}, t_k)$  is described by a single Kraus operator  $M_{\alpha_k}$ , we may view the evolution of the system along the time sequence  $\{t_k\}_{k=0}^K$  as a trajectory of pure states

$$|\Psi_\Gamma(t_0)\rangle \mapsto |\Psi_\Gamma(t_1)\rangle \mapsto \cdots \mapsto |\Psi_\Gamma(t_K)\rangle, \quad (15.9)$$

such that

$$|\Psi_\Gamma(t_k)\rangle = \frac{M_{\alpha_k}|\Psi_\Gamma(t_{k-1})\rangle}{\|M_{\alpha_k}|\Psi_\Gamma(t_{k-1})\rangle\|^2}, \quad (15.10)$$

where  $|\Psi_\Gamma(t_0)\rangle = |\psi_l\rangle$  and  $|\Psi_\Gamma(t_K)\rangle = |\xi_m\rangle$ . Generally, the time  $\Delta t$  is chosen to be much shorter than the characteristic evolution time of the system, meaning that each  $M_{\alpha_k}$  is very close to the identity operator. As such, the states  $|\Psi_\Gamma(t_k)\rangle$  along this trajectory vary slowly, and can be in a superposition of states from the basis in which the environment induces decoherence.

A great interest of such a time-resolved measurement scheme is that it generally involves the monitoring of the environment subspace interacting with the system during the interval  $\Delta t$ , rather than the complete environment, which is amenable to experimental implementation. Conversely, performing projective measurements on the total Hilbert space of the environment – which is generally large – is usually impractical. Examples of such continuous measurement schemes include monitoring of the fluorescence emitted by a superconducting qubit in a transmission line [8], and the readout of Rydberg atoms after they interact sequentially with a cavity field [7]. In these setups, it is only required that we measure the field in the transmission line and a single atom every  $\Delta t$ , respectively, to have enough information to reconstruct the system's trajectory.

We finally note that we have considered rather ideal measurements. The present formalism can be extended to account for various practical limitations. An extension to measurements associated with non rank-1 projectors on  $\mathcal{H}_S$  is presented in Appendix A to this chapter. Other common limitations includes imperfect detection, which can be modeled by an average over a subset of the measurement record (see e.g. [30], section 4.8 and [31], section VII).

### 15.2.3 Quantum Trajectories from a Lindblad Equation

#### 15.2.3.1 Kraus Decomposition of the Lindblad Equation

For a quantum system in contact with a Markovian environment at equilibrium, the dynamics may often be described by a Lindblad equation [24]  $\partial_t \rho_S = \mathcal{L}_\lambda(\rho_S(t))$  where the Liouvillian  $\mathcal{L}_\lambda$  fulfills:

$$\mathcal{L}_\lambda(\rho_s) = i[\rho_s, H_s(\lambda)]_- + \sum_{j=1}^J \mathcal{D}_j^\lambda(\rho_s). \quad (15.11)$$

Here  $H_s(\lambda)$  is the system's Hamiltonian which depends on a parameter  $\lambda$  controlled by an external agent. This parameter is in general varied during a thermodynamical transformation, and takes the values  $\{\lambda_t\}_{t_i \leq t \leq t_f}$ .  $\mathcal{D}_j^\lambda$  is a superoperator satisfying:

$$\mathcal{D}_j^\lambda(\rho_s) := L_j(\lambda)\rho_s L_j^\dagger(\lambda) - \frac{1}{2}[\rho_s, L_j^\dagger(\lambda)L_j(\lambda)]_+. \quad (15.12)$$

Here  $[\cdot, \cdot]_-$  and  $[\cdot, \cdot]_+$  are respectively the commutator and anti-commutator and  $L_j(\lambda)$  are the so-called Lindblad (or jump) operators. The Liouville super-operator given in Eq. (15.11) generates the quantum channel  $\Phi(t_i, t_f) : \rho_s \mapsto \mathbb{T} e^{\int_{t_i}^{t_f} dt \mathcal{L}_\lambda(t)} (\rho_s)$ , with  $\mathbb{T}$  the time-ordering operator.  $\Phi(t_i, t_f)$  is a composition of infinitesimal quantum channels  $\Phi^{\lambda_k}(t_{k-1}, t_k) = \mathbb{1}_s + dt \mathcal{L}_{\lambda_k}$ , with  $\lambda_k \equiv \lambda_{t_k}$ .

The exact form of the Liouvillian in Eq. (15.11) can be derived from a given microscopic model of the system and the environment by averaging the exact unitary dynamics of the joint system over a time that is large with respect to the correlation time of the environment, but short with respect to the relaxation time of the system, and tracing over the environment [24, 32]. Alternatively, when the microscopic description of the environment is unknown, the Lindblad equation associated with a set of  $A = d_s^2 - 1$  Lindblad operators,  $d_s$  being the dimension of  $\mathcal{H}_s$ , can be used phenomenologically as the most general infinitesimal quantum channel capturing the dynamics of a system in contact with a Markovian environment [33].

The quantum trajectories are obtained from a Kraus decomposition of  $\sum_{\alpha_k} \Phi_{\alpha_k}^{\lambda_k}(t_{k-1}, t_k)$  associated with measurement outcomes  $\{\alpha_k\}$ . The environment, if Markovian, is assumed to be respectively in the states  $\rho_\varepsilon = \sum_\mu q_\mu \Pi_\varepsilon[\phi_\mu]$  and  $\rho'_\varepsilon = \sum_\mu q'_\mu \Pi_\varepsilon[\phi_\mu]$  at the infinitesimal time-steps  $t_{k-1}$  and  $t_k$ . The Markovian environment is affected very slightly by its interaction with the system, quantified by the fact that the relative entropy  $D[\rho'_\varepsilon \| \rho_\varepsilon] := \text{tr}[\rho'_\varepsilon (\ln(\rho'_\varepsilon) - \ln(\rho_\varepsilon))]$  is vanishingly small. As such, if the environment were projectively measured with respect to the same observable  $\{\Pi_\varepsilon[\phi_\mu]\}_\mu$  before and after the infinitesimal interaction time, we would have  $\alpha_k = (\mu_k, \nu_k)$ , analogously to our earlier discussion in Sect. 15.2.1. However, owing to the Markovian character of the environment, one can measure the environment in many different ways without affecting the system's master equation. The choice of a particular measurement scheme on the environment determines the so-called “unravelling” of the Lindblad master equation. As there are infinitely many ways of measuring the environment, there are infinitely many such unravellings. In the following sections, we will focus on two measurement schemes that are particularly relevant for situations of interest in thermodynamics, and have been implemented experimentally: (i) the Quantum Jump (QJ) and (ii) the Quantum State Diffusion (QSD) unravellings.

### 15.2.3.2 Quantum Jumps Unraveling

The QJ unraveling corresponds to measurement of the environment with  $J + 1$  possible outcomes. The first  $J$  outcomes  $\{\alpha_j\}_{j=1}^J$  have an infinitesimal probability of occurrence, of order  $dt$ , and are associated with a strong effect on the system called a “quantum jump” [1, 30, 34–36]. Such quantum jumps are captured by the Kraus operators:

$$M_{\alpha_j}(\lambda) = \sqrt{dt} L_j(\lambda). \quad (15.13)$$

The last outcome  $\alpha_0$ , called the “no-jump” outcome, has a probability of order 1 and is associated with an infinitesimal evolution characterized by the Kraus operator:

$$M_{\alpha_0}(\lambda) = \mathbb{1}_S - dt \left( i H_S(\lambda) + \frac{1}{2} \sum_{j=1}^J L_j^\dagger(\lambda) L_j(\lambda) \right). \quad (15.14)$$

The “no-jump” evolution can also be seen as induced by the non-Hermitian effective Hamiltonian:

$$H_{\text{eff}}(\lambda_t) := H_S(\lambda_t) - \frac{i}{2} \sum_{j=1}^J L_j^\dagger(\lambda_t) L_j(\lambda_t). \quad (15.15)$$

Such an unraveling typically arises when the measurement on the environment corresponds to counting of the excitations exchanged between the environment and the system, e.g. photon-counting. The  $L_j$  operators are then annihilation and creation operators for these excitations. Note that in most cases, only the variation of the environment’s excitation number can be accessed (rather than the absolute initial and final number of excitations in the environment), so that a proper derivation of the Kraus operators of the QJ unraveling requires us to slightly extend the paradigm introduced in Sect. 15.2.1 (see Appendix A).

### 15.2.3.3 Quantum State Diffusion Unraveling

A QSD unraveling is obtained when there is a continuous set of possible outcomes  $\alpha_k$  for the measurement performed on the environment, at time  $t_k$  [2, 30, 31, 37]. As a result the system’s evolution is determined by an infinite number of Kraus operators. The evolution of the system takes the form of a stochastic differential equation in terms of the record  $\alpha_k$ . When using Ito’s convention for stochastic calculus, one can in general cast the Kraus operators under the form:

$$M_{\alpha_k}(\lambda_k) = \left( \prod_{j=1}^J p_0(dw_j) \right)^{1/2} \left( \mathbb{1}_s - dt \left( iH_s(\lambda_k) + \frac{1}{2} \sum_{j=1}^J L_j^\dagger(\lambda_k) L_j(\lambda_k) \right) \right. \\ \left. + \sum_{j=1}^J dw_j(\alpha_k) L_j(\lambda_k) \right), \quad (15.16)$$

where the  $dw_j(\alpha_k)$ ,  $j \in \llbracket 1, J \rrbracket$  are Wiener increments, i.e. potentially complex Gaussian stochastic variables of zero expectation value and fulfilling Ito's rule  $|dw_j(\alpha_k)|^2 = dt$ . We denote  $p_0(u) = \exp(-|u|^2/2dt)/N_0$  the probability density fulfilled by the Wiener increments, where  $N_0 = 2\pi dt$  in the complex case and  $N_0 = \sqrt{2\pi dt}$  in the real case.

A typical situation leading to a QSD unraveling is when the environment of the system is actually a meter such that the measurement outcome at time  $t_k$  corresponds to a weak measurement of an observable  $X$  on the system. In such situations, there is only one Lindblad operator  $\sqrt{\gamma_{\text{mes}}}X$  associated with the Wiener increment  $dw(\alpha_k) = 2\sqrt{\gamma_{\text{mes}}}dt(\alpha_k - \langle X \rangle)$  [31]. Other common situations leading to QSD unraveling are the homodyning and heterodyning measurements of the fluorescence of an atom [2].

## 15.3 Entropy Production and Integral Fluctuation Theorem

### 15.3.1 Time-Reversed Trajectories, Stochastic Entropy Production, and the Second Law

Each trajectory  $\Gamma$  has associated with it a stochastic entropy production  $\Delta_{is}[\Gamma]$ , which quantifies the degree of irreversibility in the transformation. In concordance with the formalism of classical stochastic thermodynamics [13, 16], this quantity is obtained by comparing the probability of a trajectory  $\Gamma$  to that of its time-reversed counterpart  $\tilde{\Gamma}$ , seen as a trajectory generated by the time-reversed thermodynamic transformation. Namely, we define:

$$\Delta_{is}[\Gamma] := \ln \left( \frac{P(\Gamma)}{\tilde{P}(\tilde{\Gamma})} \right). \quad (15.17)$$

Consequently, the more probable the forward trajectory occurs, in comparison with the time-reversed trajectory, the more entropy is produced. We show below that this definition is consistent with the definition of average entropy production as the total increase in the von Neumann entropy of system and environment, evaluated with respect to their reduced states. For further justification of using Eq. (15.17) as the definition of stochastic entropy production, we refer to Chap. 16.

Several approaches have been explored to define the time-reversed trajectories and their probabilities. The approach introduced in [38] and used in [20, 21, 39] exploits a fixed point of the quantum map to define the reversed Kraus operators,

ensuring that no entropy is produced on average when the system is in the fixed point. This approach has lead to pioneering analyses of the entropy production at the level of single quantum trajectories. However, this approach may break down when the system is driven, in particular for quantum maps that do not have a fixed point [40]. The approach introduced in [22, 23] exploits the inverse of the Kraus operator, and is therefore well suited for weak measurements, while it cannot handle Kraus operators obtained by performing rank-1 projective measurements, such as those involved in the QJ unraveling. Here, in line with [40–42], we exploit the fact that when both the system and environment are measured with rank-1 projective measurements, the Kraus operator generating the time-reversed sequence of states for the system is uniquely defined. This allows us to evaluate the entropy production associated to a large variety of quantum processes as shown by the examples considered in this chapter.

Recall that a general trajectory  $\Gamma = ((l, m), \vec{\alpha})$ , where  $\vec{\alpha} := (\alpha_1, \dots, \alpha_K)$ , is defined by two measurements at the start and end of the process on the system, and a sequence of quantum maps  $\{\Phi_{\alpha_k}(t_{k-1}, t_k)\}_{k=1}^K$  that describe the stochastic transformation of the system as time moves forward from  $t_{k-1}$  to  $t_k$ . The time-reversed trajectory  $\tilde{\Gamma} = ((m, l), \overleftarrow{\alpha})$ , where  $\overleftarrow{\alpha} := (\alpha_K, \dots, \alpha_1)$ , is similarly defined with respect to a sequence of time-reversed quantum maps  $\{\tilde{\Phi}_{\alpha_k}(t_k, t_{k-1})\}_{k=K}^1$  that describe the stochastic transformation of the system as time moves backwards from  $t_k$  to  $t_{k-1}$ . Given that the initial state of the system during the time-reversed process is the average state it occupies at the end of the forward process, namely  $\rho_S(t_K) := \Phi(\rho_S) = \sum_m p'_m \Pi_S[\xi_m]$ , the probability for the time-reversed trajectory is obtained analogously to Eq. (15.8) as

$$\tilde{P}(\tilde{\Gamma}) = \text{tr}[\Pi_S[\psi_l](\tilde{\Phi}_{\alpha_1}(t_1, t_0) \circ \dots \circ \tilde{\Phi}_{\alpha_K}(t_K, t_{K-1}))(\Pi_S[\xi_m])]p'_m. \quad (15.18)$$

Let us assume for simplicity that each quantum channel  $\Phi(t_{k-1}, t_k)$  is described by the same unitary  $V$ , and initial environment state  $\rho_\varepsilon = \sum_\mu q_\mu \Pi_\varepsilon[\phi_\mu]$ . This would describe the case where the environment is Markovian. As such, Eq. (15.8) can be written as

$$P(\Gamma) = \text{tr}[\Pi_S[\xi_m]M_{\alpha_K} \dots M_{\alpha_1}\Pi_S[\psi_l]M_{\alpha_1}^\dagger \dots M_{\alpha_K}^\dagger]p_l, \quad (15.19)$$

where  $M_{\alpha_k} = \sqrt{q_{\mu_k}}\langle\varphi_{\nu_k}|V|\phi_{\mu_k}\rangle$ . Here we recall that  $q_{\mu_k}$  is the probability that the environment at time  $t_{k-1}$  occupies the state  $|\phi_{\mu_k}\rangle$ .

We now introduce the time-reversal paradigm applied in this chapter. To construct the infinitesimal maps generating the time-reversed trajectory, we assume that the initial state of the environment, at time  $t_k$ , is the average state it occupies, during the forward process at the end of interval  $(t_{k-1}, t_k)$ , i.e.,  $\rho_\varepsilon(t_k) = \text{tr}_S[V(\rho_S(t_{k-1}) \otimes \rho_\varepsilon)V^\dagger] = \sum_{\nu_k} q'_{\nu_k} \Pi_\varepsilon[\varphi_{\nu_k}]$ . Consequently, we may define the  $k$ th time reversed quantum channel as

$$\begin{aligned}\tilde{\Phi}(t_k, t_{k-1})(\sigma_s) &:= \text{tr}_\varepsilon[V^\dagger(\sigma_s \otimes \rho_\varepsilon(t_k))V], \\ &= \sum_{\alpha_k} \tilde{\Phi}_{\alpha_k}(t_k, t_{k-1})(\sigma_s),\end{aligned}\quad (15.20)$$

where we note that the unitary interaction  $V$  has been subjected to the time-reversal operation, thus transforming it to  $V^\dagger$  [42]. Each  $\tilde{\Phi}_{\alpha_k}(t_k, t_{k-1})$  is described by the Kraus operator

$$\tilde{M}_{\alpha_k} := \sqrt{q'_{\nu_k}} \langle \phi_{\mu_k} | V^\dagger | \varphi_{\nu_k} \rangle \equiv \sqrt{\frac{q'_{\nu_k}}{q_{\mu_k}}} M_{\alpha_k}^\dagger. \quad (15.21)$$

Therefore, we may write Eq. (15.18) as

$$\begin{aligned}\tilde{P}(\tilde{\Gamma}) &= \text{tr}[\Pi_s[\psi_l] \tilde{M}_{\alpha_1} \dots \tilde{M}_{\alpha_K} \Pi_s[\xi_m] \tilde{M}_{\alpha_K}^\dagger \dots \tilde{M}_{\alpha_1}^\dagger] p'_m, \\ &= \frac{q'_{\nu_1} \dots q'_{\nu_K}}{q_{\mu_1} \dots q_{\mu_K}} \text{tr}[\Pi_s[\xi_m] M_{\alpha_K} \dots M_{\alpha_1} \Pi_s[\psi_l] M_{\alpha_1}^\dagger \dots M_{\alpha_K}^\dagger] p'_m.\end{aligned}\quad (15.22)$$

Consequently, by combining Eqs. (15.17), (15.19), and (15.22), we obtain the following expression for the stochastic entropy production along each trajectory:

$$\begin{aligned}\Delta_i s[\Gamma] &= \ln \left( \frac{P(\Gamma)}{\tilde{P}(\tilde{\Gamma})} \right), \\ &= \ln \left( \frac{p_l}{p'_m} \right) + \sum_{k=1}^K \ln \left( \frac{q_{\mu_k}}{q'_{\nu_k}} \right).\end{aligned}\quad (15.23)$$

In other words, the stochastic entropy production is purely a function of the probability distributions for the system and bath, at the beginning and end of the joint dynamics during the time intervals  $(t_{k-1}, t_k)$ .

Finally, we note that the entropy production, averaged with respect to the probability distribution for the forward trajectories, gives

$$\begin{aligned}\langle \Delta_i s[\Gamma] \rangle &:= \sum_{\Gamma} P(\Gamma) \Delta_i s[\Gamma], \\ &= \Delta S_s + \sum_{k=1}^K \Delta S_\varepsilon^k \geq 0,\end{aligned}\quad (15.24)$$

where  $\Delta S_s := S(\rho_s(t_K)) - S(\rho_s)$ ,  $\Delta S_\varepsilon^k := S(\rho_\varepsilon(t_k)) - S(\rho_\varepsilon)$ , and  $S(\rho) := -\text{tr}[\rho \ln(\rho)]$  is the von-Neumann entropy of state  $\rho$ . The inequality in the final line, which can be interpreted as an expression of the second law of thermodynamics, is due to: (i) lack of initial correlations between system and environment at the start of each joint evolution; (ii) sub-additivity of the von-Neumann entropy [43]; and

(iii) the fact that unitary evolution is unital, i.e., does not decrease the von-Neumann entropy [44, 45]. In other words, the second law is always satisfied for open system dynamics. A more detailed discussion about the second law for quantum systems can be found in Chap. 28.

The entropy production  $\Delta_s[\Gamma]$  also fulfills a fluctuation Theorem:

$$\begin{aligned} \langle e^{-\Delta_s[\Gamma]} \rangle &:= \sum_{\Gamma: P(\Gamma) > 0} P(\Gamma) \frac{\tilde{P}(\tilde{\Gamma})}{P(\Gamma)} \\ &= 1 - \lambda. \end{aligned} \quad (15.25)$$

Here the sum is restricted to the trajectories  $\Gamma$  for which  $P(\Gamma) \neq 0$ , and  $\lambda \in [0, 1)$  corresponds to the cumulated probabilities of the reverse trajectories  $\tilde{\Gamma}$  for which the probability of the corresponding forward trajectory,  $P(\Gamma)$ , is zero. A situation in which  $\lambda > 0$  is referred to as “absolute irreversibility” as it is associated with a strictly positive entropy production [46, 47]. This typically arises for a system initially restricted to a subpart of its Hilbert space and then allowed to relax in the whole space.  $\lambda$  vanishes when the initial state of the system,  $\rho_s$ , has full rank, i.e., when  $\rho_s$  has  $d_s$  positive eigenvalues. An example of a full-rank state is a thermal state at finite temperature. Equation (15.25) is known as the “Integral Fluctuation Theorem” [16] (IFT) as it generates other famous fluctuation theorems when applied to specific situations. For instance, when the system and the reservoir are initialized in thermal states at the beginning of the forward and backward processes, one obtains the quantum version of the celebrated Jarzynski equality [48, 49].

We stress here that the time reversed transformation is a virtual reference with which the forward process is compared, rather than an actual physical process that needs to be implemented. Indeed, the fluctuation theorem and the second law can be tested without having to implement such reverse processes as the averages appearing in Eqs.(15.24) and (15.25) are over the forward trajectories.

Finally, we emphasize that the discussion can be extended to more general kinds of measurements performed on the system and the environment (see Appendix B).

## 15.4 First Law of Thermodynamics

### 15.4.1 Internal Energy

In this section, we focus on the energy exchanges occurring during the quantum trajectories defined above. In this chapter, we define the internal energy of system  $S$  when it is in the pure state  $|\psi_s\rangle$  following [20] by:

$$U(\lambda) := \langle \psi_s | H_s(\lambda) | \psi_s \rangle. \quad (15.26)$$

We stress that here  $|\psi_s\rangle$  can be any state of  $\mathcal{H}_s$  and in particular does not have to be an energy eigenstate of  $H_s(\lambda)$ .  $U(\lambda)$  can be interpreted as the average of results of projective energy measurement performed on many copies of the system. However, if the system is in an energy eigenstate,  $U(\lambda)$  corresponds to an eigenvalue of  $H_s(\lambda)$ . As a consequence, if one includes projective measurements of the system's energy in the thermodynamic transformation under study, one finds that  $U(\lambda)$  is given by the outputs of such measurements. This is the Two-Point Measurement (TPM) approach of quantum thermodynamics which led to pioneering results such as the first quantum fluctuation theorems [49–52] (see also Chap. 10). However, definition (15.26) can be seen as an extension of this conception of internal energy as it allows us to follow the variation in internal energy of the system even when no projective measurement is performed, provided the system's state is known. This definition is extremely useful in the context of quantum trajectories experiments which precisely lead to the knowledge of the system's quantum state at any time. Note that this definition (15.26) can be extended in the case of a mixed state  $\rho_s$  to  $U(\lambda) := \text{tr}[\rho_s H_s(\lambda)]$ . This definition of the internal energy was used in seminal studies of open quantum system thermodynamics [11] (see also Chap. 1).

### 15.4.2 Work and Heat: Two Historic Approaches

Just like in classical thermodynamics, we are now interested in splitting the variations of  $U(\lambda)$  into work, a deterministic form of energy that can be readily used for many purposes in a controllable way, and heat – a stochastic/uncontrollable form of energy exchange. The definitions of heat and work for quantum systems has a long history of attempts, mainly based on two strategies for which we briefly sum up the arguments in the following two subsections, in order to introduce the unifying paradigm we will use in this chapter.

#### 15.4.2.1 “Heat First”

Studies focusing on the cases where the environment is a thermal reservoir have generally defined heat from the outcomes of energy measurements performed on the thermal reservoir. In the context of quantum trajectories, this corresponds to an unraveling in which the bases  $\{|\varphi_n\rangle\}$  and  $\{|\phi_m\rangle\}$  are both the reservoir's energy eigenbasis.

The QJ unraveling presented above is generally the best suited to monitor this heat exchange, that we denote  $Q_{\text{cl}}$  in the following: indeed, the outcomes are directly linked to a change of the number of excitations in the environment, and therefore to a variation of the reservoir's energy [17]. Obtaining outcome  $\alpha_0$  at time  $t_k$  corresponds to a zero heat,  $\delta Q_{\text{cl}}(t_k, \alpha_0) = 0$ , while each outcome  $\alpha_j$  with  $j \geq 1$  is associated with an amount of heat  $\delta Q_{\text{cl}}(t_k, \alpha_j)$  given by the quantum of energy carried by the exchanged excitation. In the example of photon-counting, this can be summed up by saying that the heat exchanged with the reservoir is the energy carried by the

counted photons. In the case of a reservoir at thermal equilibrium, the probabilities of picking each energy eigenstates in the forward and reverse processes,  $q_\nu$  and  $q'_\mu$ , are identified with Boltzmann's distributions, such that  $\langle \delta Q_{\text{cl}}(t_k, \alpha_k) \rangle$  is linked to the variation of the thermal reservoir's Von Neumann entropy according to  $\Delta S_{\mathcal{E}} = -\langle \delta Q_{\text{cl}}(t_k, \alpha_k) \rangle / T$  (see Chap. 10).

This approach has been first used in the context of the TPM approach to quantum statistical mechanics, in which the change of the environment internal energy is assumed to be inferred from two projective measurements performed at the beginning and at the end of the trajectory [52]. Another formulation can be found in the so-called “full counting statistics” method [53], which consists of recording in a generating function the outputs of (fictitious) projective energy measurements performed on the environment at every time step. The heat statistics given by such a method is actually the same as obtained from the QJ unraveling [54]. In such studies, the rest of the internal energy variations  $\Delta U - Q_{\text{cl}}$  was identified as the work.

#### 15.4.2.2 “Work first”

Another approach, in its spirit closer to the initial formulation of thermodynamics, consists in identifying the energy deterministically exchanged with the system as the work. In the case where the dynamics is described by a Lindblad master equation, the work should then appear in the unitary part of the dynamics, while heat, which is uncontrollable, should come from the non-unitary terms. It turns out that non-zero contributions of the unitary terms in Eq.(15.11) to the variations of  $U(\lambda)$  solely appears when the parameter  $\lambda$  is varied along the transformation.<sup>1</sup> This variation can be interpreted as originating from an external driving field whose dynamics generates a sequence  $\{\lambda_t\}_{t_i \leq t \leq t_f}$ . One can then identify the elementary amount of work provided by this driving field to the system at time  $t_k$  with (see [11] and Chap. 1)

$$\delta W(\alpha_k, \lambda_{t_k}) = dt \frac{d\lambda_t(t_k)}{dt} \langle \Psi_\Gamma(t_k) | \frac{d}{d\lambda} H_{\mathcal{S}}(\lambda_{t_k}) | \Psi_\Gamma(t_k) \rangle. \quad (15.27)$$

Note that the increment of work does not depend on the measurement outcome  $\alpha_k$  obtained at time  $t_k$ , which confirms the deterministic nature of the energy exchange. Then, the remaining terms in the variation of  $U(\lambda)$  are classified as heat, acknowledging their uncontrollable nature. This approach has the great advantage to be compatible with any Lindblad equation (even for non-thermal dissipation) and any unraveling.

---

<sup>1</sup>Note that we consider here the work performed on the total system  $\mathcal{S}$ . If  $\mathcal{S}$  is composed of several subsystems, one can find deterministic energy exchanges within this subsystems, even when the total Hamiltonian of  $\mathcal{S}$  is time-independent.

### 15.4.3 The Notion of Quantum Heat

Recent studies exploring the impact of definition (15.26) to states which are not energy eigenstates [20] have evidenced that these two approaches do not agree in general. Focusing on the case of the environment being a thermal reservoir, it turns out that the heat computed as the change of the reservoir's energy and the work provided by the external drive computed from Eq.(15.27) do not in general add up to the total variations of  $U(\lambda)$ . This mismatch solely appears when coherences are built by the external drive, or are initially present in the system's state, in the basis in which the reservoir induces jumps (in the case of a QJ unraveling) or more generally in the basis in which the measurement scheme induces decoherence.

This mismatch does not mean that energy conservation fails, but simply that there is a flow of energy that is uncontrolled (non-unitary) while not provided by the thermal reservoir. This flow of energy can either be provided by the driving field (and in contrast to work  $W$  occurs in a stochastic way because it is triggered by the interaction with the reservoir) or by other sources not explicitly included in the quantum description, such as the measuring apparatus involved in the unraveling of the Lindblad equation. We stress that the precise origin of this energy flow can always be determined for a given problem from a careful microscopic model of the driving fields and measuring apparatuses involved in all steps of the studied protocol (including preparation steps) [55].

A dramatic example is the case in which the Lindblad equation is generated by the continuous monitoring of some observable (the environment is then a meter coupled to the system and periodically measured, see Sect. 15.7). In this situation, there is no thermal reservoir, but still some non-unitary energy flow exchanged with the system, which is not of thermal origin (there is no temperature involved) but which should not be called work because of its uncontrolled nature. In Refs. [56–59], this measurement-induced heat flow is exploited to build engines solely fueled by the observation process, a remarkable specificity of the quantum world.

In the end of this chapter, we shall follow [20, 54, 58, 60, 61] and call this quantity of purely quantum origin “quantum heat”. We will denote  $\delta Q_q(t_k, \alpha_k)$  the quantum heat increment at time  $t_k$ .

The expression of the quantum heat (just as the expression of the classical, thermal heat  $Q_{cl}$ ) depends on the unraveling, and it may not always be possible to split the total incoherent energy exchange into thermal and quantum heat. We analyze in Sects. 15.5–15.7 examples in which this splitting is possible

Finally the first law at the single trajectory level reads as

$$\Delta U(\Gamma) = W(\Gamma) + Q_{cl}(\Gamma) + Q_q(\Gamma), \quad (15.28)$$

where the trajectory dependent quantities  $X(\Gamma)$ , for  $X = W, Q_{cl}, Q_q$  are computed by summing all the elementary increments  $\delta X(t_k, \alpha_k)$  along trajectory  $\Gamma$ .

## 15.5 Example 1: Quantum and Classical Entropy Production Due to Thermalization

Here we shall study the simplest example of interest where a system is allowed to relax to thermal equilibrium by interacting with a thermal bath at temperature  $T$  (this discussion is based on the manuscript [62], which is currently in preparation). When the system possesses initial coherences with respect to its energy eigenbasis, the resulting entropy production can be decomposed into a quantum and classical component, with concomitant fluctuations in classical and quantum heat, respectively.

Let the system  $\mathcal{S}$ , with the Hamiltonian  $H_{\mathcal{S}} = \sum_i e_i \Pi_{\mathcal{S}}[e_i]$ , be prepared in the state  $\rho_{\mathcal{S}} = \sum_l p_l \Pi_{\mathcal{S}}[\psi_l]$ . The bath, on the other hand, has the Hamiltonian  $H_{\mathcal{E}} = \sum_i \epsilon_i \Pi_{\mathcal{E}}[i]$ , and is initially in the canonical state  $\tau_{\mathcal{E}} := e^{-H_{\mathcal{E}}/k_B T} / Z_{\mathcal{E}}$ , where  $Z_{\mathcal{E}} := \text{tr}[e^{-H_{\mathcal{E}}/k_B T}]$  is its partition function. The thermalization process is effected by a joint unitary evolution  $V$ , which commutes with the total Hamiltonian  $H_{\mathcal{S}} + H_{\mathcal{E}}$ , such that  $\text{tr}_{\mathcal{E}}[V(\rho_{\mathcal{S}} \otimes \tau_{\mathcal{E}})V^\dagger] = \tau_{\mathcal{S}} := e^{-H_{\mathcal{S}}/k_B T} / Z_{\mathcal{S}}$  and  $\text{tr}_{\mathcal{S}}[V(\rho_{\mathcal{S}} \otimes \tau_{\mathcal{E}})V^\dagger] = \tau'_{\mathcal{E}}$ . We shall assume that the bath is sufficiently large so that  $\tau'_{\mathcal{E}}$  will be “almost” thermal. This is quantified by the relative entropy  $D[\tau'_{\mathcal{E}} \parallel \tau_{\mathcal{E}}] := \text{tr}[\tau'_{\mathcal{E}}(\ln(\tau'_{\mathcal{E}}) - \ln(\tau_{\mathcal{E}}))]$  being vanishingly small.

As in the general example discussed in Sec. 15.2.1, we may construct the quantum trajectories by measuring the system and environment, before and after the joint unitary evolution, with observables that do not disturb the subsystems. However, we may “augment” these trajectories by also performing energy measurements on the system prior to its interaction with the thermal reservoir. This is valid as the resulting average entropy production, and average internal energy change of the system, will stay the same. The augmented trajectories correspond to the TPM protocol introduced above which has been historically used to derive the first versions of the quantum fluctuation theorems [49–51]. The present analysis allows us to quantify the thermodynamic consequences of the initial energy measurement.

The trajectories of the system, containing the energy measurement prior to thermalization, are defined as  $\Gamma_{\mathcal{S}} := (l, m, n) \equiv |\psi_l\rangle \mapsto |e_m\rangle \mapsto |e_n\rangle$ . The trajectories of the bath, meanwhile, are  $\Gamma_{\mathcal{E}} := (\mu, \nu) \equiv |\mu\rangle \mapsto |\nu\rangle$ . The joint trajectory  $\Gamma := ((l, m, n), (\mu, \nu))$  can therefore be decomposed into a “decoherence” trajectory  $\Gamma_q := (l, m) \equiv |\psi_l\rangle \mapsto |e_m\rangle$ , which only pertains to the system, followed by a “classical thermalization” trajectory  $\Gamma_{\text{cl}} := ((m, n), (\mu, \nu))$  which is the joint trajectory of system and bath during thermalization. As the system Hamiltonian is time-independent, the variation of its internal energy is only heat. The change in internal energy of the system during the decoherence trajectories is quantum heat as defined in Sect. 15.4.3:

$$Q_q(\Gamma) := \text{tr}[H_{\mathcal{S}}(\Pi_{\mathcal{S}}[e_m] - \Pi_{\mathcal{S}}[\psi_l])]. \quad (15.29)$$

The change in internal energy of the system during the classical thermalization trajectories is classical heat which, due to the energy conservation of the joint unitary

evolution, together with the fact that both system and bath start and end in energy eigenstates, equals the heat emitted by the bath:

$$Q_{\text{cl}}(\Gamma) := \text{tr}[H_S(\Pi_S[e_n] - \Pi_S[e_m])] = \text{tr}[H_\varepsilon(\Pi_\varepsilon[\mu] - \Pi_\varepsilon[\nu])]. \quad (15.30)$$

It is evident that the total change in the system's internal energy along a trajectory is  $Q(\Gamma) = Q_q(\Gamma) + Q_{\text{cl}}(\Gamma)$ .

Using the methods delineated in Sects. 15.2.1 and 15.3.1, we may evaluate the probabilities for each sub-trajectory, as well as their time-reversed counterparts, to be

$$\begin{aligned} P(\Gamma_q) &= \text{tr}[\Pi_S[e_m]\Pi_S[\psi_l]]\text{tr}[\Pi_S[\psi_l]\rho_S], & \tilde{P}(\tilde{\Gamma}_q) &= \text{tr}[\Pi_S[e_m]\Pi_S[\psi_l]]\text{tr}[\Pi_S[e_m]\eta_S], \\ P(\Gamma_{\text{cl}}) &= \text{tr}[\Pi_S[e_n]\Phi_{\mu,\nu}(\Pi_S[e_m])]\text{tr}[\Pi_S[e_m]\eta_S], & \tilde{P}(\tilde{\Gamma}_{\text{cl}}) &= \text{tr}[\Pi_S[e_m]\tilde{\Phi}_{\mu,\nu}(\Pi_S[e_n])]\text{tr}[\Pi_S[e_n]\tau_S], \end{aligned} \quad (15.31)$$

where

$$\eta_S := \sum_m \Pi_S[e_m]\rho_S\Pi_S[e_m] \quad (15.32)$$

is the same as the initial state  $\rho_S$ , except that its coherences with respect to the Hamiltonian eigenbasis have been removed.

The average quantum entropy production, therefore, is

$$\begin{aligned} \langle \Delta_i s[\Gamma_q] \rangle &:= \sum_{\Gamma_q} P(\Gamma_q) \ln \left( \frac{P(\Gamma_q)}{\tilde{P}(\tilde{\Gamma}_q)} \right), \\ &= \sum_{l,m} \text{tr}[\Pi_S[e_m]\Pi_S[\psi_l]]\text{tr}[\Pi_S[\psi_l]\rho_S] \ln \left( \frac{\text{tr}[\Pi_S[\psi_l]\rho_S]}{\text{tr}[\Pi_S[e_m]\eta_S]} \right), \\ &= S(\eta_S) - S(\rho_S) \equiv D[\rho_S \parallel \eta_S]. \end{aligned} \quad (15.33)$$

Moreover, noting that  $\tilde{\Phi}_{\mu,\nu}(\rho) = (q'_\nu/q_\mu)\Phi^\dagger(\rho)$ , where  $q_\mu := \langle \mu | \tau_\varepsilon | \mu \rangle$  and  $q'_\nu := \langle \nu | \tau'_\varepsilon | \nu \rangle$ , while  $\sum_\nu \text{tr}[\Phi_{\mu,\nu}(\rho)] = q_\mu$  and  $\sum_\mu \text{tr}[\tilde{\Phi}_{\mu,\nu}(\rho)] = q'_\nu$ , it follows that the average classical entropy production is given as

$$\begin{aligned} \langle \Delta_i s[\Gamma_{\text{cl}}] \rangle &:= \sum_{\Gamma_{\text{cl}}} P(\Gamma_{\text{cl}}) \ln \left( \frac{P(\Gamma_{\text{cl}})}{\tilde{P}(\tilde{\Gamma}_{\text{cl}})} \right), \\ &= \sum_{m,n,\mu,\nu} \text{tr}[\Pi_S[e_n]\Phi_{\mu,\nu}(\Pi_S[e_m])]\text{tr}[\Pi_S[e_m]\eta_S] \left( \ln \left( \frac{q_\mu}{q'_\nu} \right) \right. \\ &\quad \left. + \ln \left( \frac{\text{tr}[\Pi_S[e_m]\eta_S]}{\text{tr}[\Pi_S[e_n]\tau_S]} \right) \right), \\ &= S(\tau_S) - S(\eta_S) + S(\tau'_\varepsilon) - S(\tau_\varepsilon). \end{aligned} \quad (15.34)$$

Note that, given a thermal state  $\tau := e^{-H/k_B T}/Z$ , the following relation holds for all states  $\rho$ :

$$S(\rho) - S(\tau) = \frac{1}{k_B T} \text{tr}[H(\rho - \tau)] - D[\rho\|\tau]. \quad (15.35)$$

Using Eq. (15.35), together with the fact that  $\text{tr}[H_S(\rho_S - \eta_S)] = 0$ , and that the thermalization unitary interaction  $V$  conserves energy, it follows that the average classical entropy production is

$$\begin{aligned} \langle \Delta_i s[\Gamma_{\text{cl}}] \rangle &= S(\tau_S) - S(\eta_S) + S(\tau'_\varepsilon) - S(\tau_\varepsilon), \\ &= \frac{1}{k_B T} (\text{tr}[H_S(\tau_S - \eta_S)] + \text{tr}[H_\varepsilon(\tau'_\varepsilon - \tau_\varepsilon)]) + D[\eta_S\|\tau_S] - D[\tau'_\varepsilon\|\tau_\varepsilon], \\ &= D[\eta_S\|\tau_S] - D[\tau'_\varepsilon\|\tau_\varepsilon], \\ &\approx D[\eta_S\|\tau_S]. \end{aligned} \quad (15.36)$$

Finally, we note that the entropy production is additive along sub-trajectories, so that the average entropy production for the full process is  $\langle \Delta_i s[\Gamma] \rangle = \langle \Delta_i s[\Gamma_q] \rangle + \langle \Delta_i s[\Gamma_{\text{cl}}] \rangle = D[\rho_S\|\tau_S]$  [63, 64].

As the relative entropy is a non-negative quantity that vanishes if and only if both arguments are identical, it follows that quantum entropy production vanishes only when the initial state has no coherences with respect to the Hamiltonian eigenbasis, i.e., when  $\rho_S = \eta_S$ . Note that while the average quantum heat  $\langle Q_q(\Gamma) \rangle$  is always zero, the existence of its “fluctuations” witnesses the presence of quantum entropy production.

## 15.6 Example 2: Photo-Counting of Fluorescence

We now analyze the example of the canonical situation of quantum optics: a two-level atom (qubit) coherently driven and coupled to its electromagnetic environment (a thermal reservoir at temperature  $T$ ). We consider a photon-counting measurement, i.e. that the photons emitted and absorbed by the qubit are counted at intervals of  $\Delta t$ , with  $\gamma\Delta t \ll 1$  where  $\gamma$  is the spontaneous emission rate of the qubit. While implementing this measurement scheme at zero temperature only requires a photon-counter (absorptions impossible), its extension at non-zero temperature requires some tricks like reservoir engineering [41, 60] or a finite-size reservoir [65]. The present analysis follows from [54, 60]. Other analyses of the fluorescence thermodynamics focusing on the Floquet master equation, i.e. describing the dynamics of the atom coarse-grained over a time-scale much larger than a Rabi oscillation, can be found in [66–68]. Note that a similar situation has been experimentally implemented and analyzed with a QSD unraveling [69].

The driven qubit is described by Hamiltonian  $H_S(t) = H_0 + H_d(t) = \hbar\omega_0/2\sigma_z + \hbar g(\sigma_-e^{i\omega_L t} + \sigma_+e^{-i\omega_L t})$ , with  $\omega_0$  the bare energy of the qubit,  $\omega_L$  the frequency of

the drive and  $g$  the Rabi frequency (fixed by the drive intensity). We have introduced the Pauli matrix  $\sigma_z = |e\rangle\langle e| - |g\rangle\langle g|$  and the qubit ladder operators  $\sigma_- = |g\rangle\langle e| = \sigma_+^\dagger$ . The thermal reservoir is modeled as a collection of harmonic oscillators of Hamiltonian  $H_{\mathcal{E}} = \sum_l \hbar\omega_l a_l^\dagger a_l$ ,  $a_l$  being the annihilation operator in mode  $l$ . The coupling between the qubit and the reservoir is captured by Hamiltonian  $H_{\text{int}} = \sum_l g_l (\sigma_- a_l^\dagger + \sigma_+ a_l)$ , where the coupling strengths  $g_l$  are taken as real without loss of generality.

As soon as  $g \ll \omega_0$  and the reservoir has a correlation-time  $\tau_c$  much shorter than the inverses of  $\gamma \equiv \sum_l g_l^2 \delta(\omega_l - \omega_0)$  and  $g$ , one can coarse-grain the unitary qubit-reservoir dynamics on a time-scale  $\Delta t$  fulfilling  $\tau_c \ll \Delta t \ll \gamma^{-1}, g^{-1}$ , and trace over the reservoir degrees of freedom to obtain a Lindblad equation for the qubit density operator [32], which has the form (15.11)–(15.12) with the Lindblad operators  $\{L_j\}_{j=\pm}$ :

$$L_- = \sqrt{\gamma(\bar{n} + 1)}\sigma_- \quad (15.37)$$

$$L_+ = \sqrt{\gamma\bar{n}}\sigma_+, \quad (15.38)$$

where  $\bar{n} = (e^{\hbar\omega_0/k_B T} - 1)^{-1}$ . Alternatively, when the variation of the number of photons in the bath is monitored every  $\Delta t$ , the dynamics of the qubit is captured by a QJ unraveling as described in Sect. 15.2.3.2, with three Kraus operators labeled by  $\alpha \in \{+, -, 0\}$ .  $M_\pm = \sqrt{\Delta t} L_\pm$  are associated with the absorption and the emission of a photon, while  $M_0 = 1 - iH\Delta t - \frac{\Delta t}{2}(L_+^\dagger L_+ + L_-^\dagger L_-)$  is associated with the detection of no variation of the photon number in the environment between  $t_k$  and  $t_{k+1}$ . We denote  $|\Psi_\Gamma(t_k)\rangle$  the state of the qubit at time  $t_k$  along trajectory  $\Gamma = ((l, m), \vec{\alpha})$ .

## First law

We first analyze the energy exchanges along such QJ trajectories applying the results of Sect. 15.4. The time-dependence of  $H_s$  due to the interaction with the classical external drive can be understood as a thermodynamical transformation in which the parameter  $\lambda_t = \omega_L t$  is varied. For the sake of simplicity, we consider the TPM protocol which is associated with quantum Jarzynski equality [50, 70]: The qubit is initially at thermal equilibrium while the drive is off ( $g = 0$ ), and measured at time  $t_i$  in its energy eigenbasis, yielding state  $|\psi_i\rangle \in \{|e\rangle, |g\rangle\}$  with respective probability  $p_e^{(\text{th})} = e^{-\hbar\omega_0/k_B T}/(1 + e^{-\hbar\omega_0/k_B T})$  and  $p_g^{(\text{th})} = 1/(1 + e^{-\hbar\omega_0/k_B T})$ . Then, the drive is switched on up to time  $t_f$ , where another energy measurement is performed on the qubit yielding  $|\psi_m\rangle \in \{|e\rangle, |g\rangle\}$ .

The elementary work performed on the qubit via the drive between times  $t_{k-1}$  and  $t_k$  can be deduced from Eq. (15.27):

$$\begin{aligned} \delta W(\alpha_k, t_k) &= \Delta t \langle \Psi_\Gamma(t_k) | \partial_t H_d(t) | \Psi_\Gamma(t_k) \rangle \\ &= -g \Delta t \text{Im}(s_\Gamma(t_k)), \end{aligned} \quad (15.39)$$

where  $s_\Gamma(t_k) = \langle \Psi_\Gamma(t_k) | \sigma_- | \Psi_\Gamma(t_k) \rangle e^{i\omega_L t_k}$  is the atomic dipole in the frame rotating at the drive frequency, and  $|\Psi_\Gamma(t_k)\rangle$  is the qubit's state at time  $t_k$  along trajectory

Γ. Meanwhile, one can identify the elementary heat exchanged with the thermal reservoir between time  $t_{k-1}$  and  $t_k$  as the energy carried by the exchanged photons:

$$\delta Q_{\text{cl}}(\alpha_k, t_k) = \alpha_k \hbar \omega_0, \quad \alpha_k \in \{+, -, 0\}. \quad (15.40)$$

Finally, as the drive induces coherences in the bare atomic basis, that are erased when a photon is emitted or absorbed, there is a non-zero quantum heat contribution. This energy is provided by the same source as the work, i.e. the light driving the qubit, but in an uncontrolled/incoherent manner due to the interaction with the reservoir:

$$\delta Q_{\text{q}}(\alpha_k, t_k) = \begin{cases} -\hbar \omega_0 \frac{1 + z_\Gamma(t_k)}{2}, & \alpha_k = + \\ \hbar \omega_0 \frac{1 - z_\Gamma(t_k)}{2}, & \alpha_k = - \\ -\bar{g} \frac{\gamma(\bar{n} + 1)}{2} \Delta t \operatorname{Re}(s_\Gamma(t_k)) - \hbar \omega_0 \gamma \Delta t |s_\Gamma(t_k)|^2, & \alpha_k = 0. \end{cases}$$

Here  $z_\Gamma(t_k) = \langle \Psi_\Gamma(t_k) | \sigma_z | \Psi_\Gamma(t_k) \rangle$  is the qubit population at time  $t_k$  along trajectory Γ.

One can evaluate the mean energy exchanges using the probability of each outcome  $\alpha_k$  at time  $t_k$ :  $p_{\alpha_k} = \langle \Psi_\Gamma(t_k) | M_{\alpha_k}^\dagger M_{\alpha_k} | \Psi_\Gamma(t_k) \rangle$ . It is interesting to look at the steady state value of the energy fluxes (denoted by the subscript ∞) obtained for  $\gamma t \gg 1$ , when the atom has relaxed in the steady state of the optical Bloch equations [32]:

$$\langle \dot{W} \rangle_\infty = \gamma \hbar \omega_L \frac{g^2}{2g^2 + 4\delta^2 + \gamma^2(2\bar{n} + 1)^2} \quad (15.41)$$

$$\langle \dot{Q}_{\text{cl}} \rangle_\infty = -\gamma \hbar \omega_0 \frac{g^2}{2g^2 + 4\delta^2 + \gamma^2(2\bar{n} + 1)^2} \quad (15.42)$$

$$\langle \dot{Q}_{\text{q}} \rangle_\infty = \gamma \hbar \delta \frac{g^2}{2g^2 + 4\delta^2 + \gamma^2(2\bar{n} + 1)^2}, \quad (15.43)$$

with  $\delta = \omega_0 - \omega_L$  the detuning between the qubit and the driving frequencies. All three quantities vanish for  $g = 0$  or for a very large detuning  $|\delta| \gg \gamma, g$  such that the qubit is effectively decoupled from the driving field. The average quantum heat vanishes at resonance ( $\delta = 0$ ) while it still features non-zero fluctuations [60]. The steady state first law reads  $\langle \dot{W} \rangle_\infty + \langle \dot{Q}_{\text{cl}} \rangle_\infty + \langle \dot{Q}_{\text{q}} \rangle_\infty = 0$ .

### Second law and Jarzynski equality

The time-reversal rules of Sect. 15.3.1 lead to the following set of time-reversed Kraus operators:

$$\begin{aligned} \tilde{M}_+ &= M_- + \mathcal{O}(\gamma \Delta t)^2 \\ \tilde{M}_- &= M_+ + \mathcal{O}(\gamma \Delta t)^2 \\ \tilde{M}_0 &= M_0^\dagger + \mathcal{O}(\gamma \Delta t)^2. \end{aligned} \quad (15.44)$$

As these Kraus operators fulfill the relation  $\tilde{M}_{\alpha_k} = e^{\delta Q_{\text{cl}}(\alpha_k, t_k)/2k_B T} M_{\alpha_k}^\dagger$ , the probabilities of the forward and time-reversed trajectories are simply related by the following relation:

$$\tilde{P}(\tilde{\Gamma}) = \frac{p'_m}{p_l} e^{Q_{\text{cl}}(\Gamma)/k_B T} P(\Gamma). \quad (15.45)$$

This in turn entails the following form for the stochastic entropy production:

$$\Delta_{\text{i}} s[\Gamma] = \ln(p_l) - \ln(p'_m) - \frac{Q_{\text{cl}}(\Gamma)}{k_B T}. \quad (15.46)$$

This entropy production fulfills the IFT Eq. (15.25) and the second law:

$$\langle \Delta_{\text{i}} s[\Gamma] \rangle = \Delta S_s - \frac{\langle Q_{\text{cl}}(\Gamma) \rangle}{k_B T} \geq 0. \quad (15.47)$$

Under the assumption that both the initial and final distribution of qubit states  $p_l$  and  $p'_m$  are drawn from thermal equilibrium populations  $\{p_e^{(\text{th})}, p_g^{(\text{th})}\}$ , the entropy production takes the form

$$\begin{aligned} \Delta_{\text{i}} s[\Gamma] &= \frac{1}{k_B T} (\Delta U_s(\Gamma) - Q_{\text{cl}}(\Gamma) - \Delta F) \\ &= \frac{1}{k_B T} (W(\Gamma) + Q_q(\Gamma) - \Delta F), \end{aligned} \quad (15.48)$$

such that the IFT becomes the quantum version of the well-known Jarzynski equality. In the present example  $\Delta F = k_B T (\log Z(t_f) - \log Z(t_i)) = 0$  as the initial and final state are drawn from the same thermal distribution. Note the presence of the quantum heat term in the entropy production, which is a witness of a genuinely quantum contribution to the entropy production in this transformation: the continuous erasure by the qubit's environment of the coherences induced by the drive in the bare qubit basis. The results of Ref. [17] are retrieved by identifying the total energy provided by the drive with the sum of the work  $W$  and quantum heat  $Q_q$ .

## 15.7 Example 3: Continuous Measurement of a Qubit's Observable

### Kraus operators

We consider a setup implementing the continuous measurement of the observable  $\sigma_z$  of a qubit whose Hamiltonian is  $H_S = \hbar\omega_0\sigma_z$ . This can be done by coupling the qubit to a cavity of Hamiltonian  $H_E = \hbar\omega_c b^\dagger b$ , where  $b$  is the annihilation operator in the cavity mode. It was recently demonstrated that a very efficient technique consists in exploiting the longitudinal coupling [71] which can be modeled by Hamiltonian

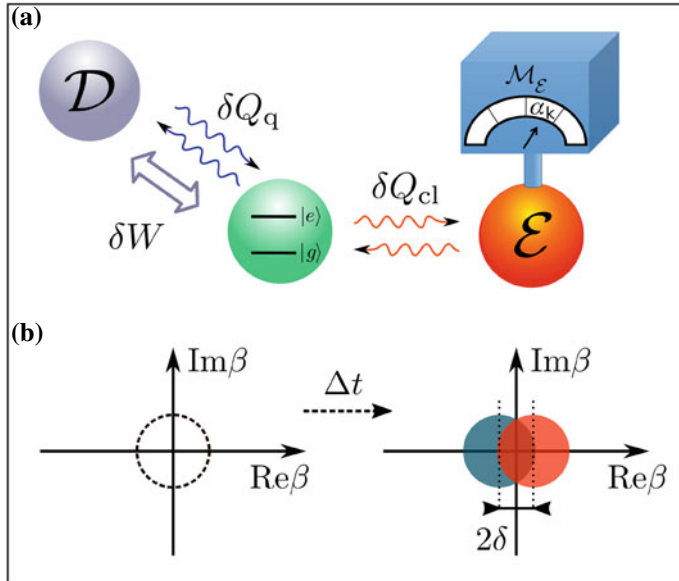


**Fig. 15.2** **a** Situation studied in Example 2. A qubit of state  $\{|e\rangle, |g\rangle\}$  is driven by an external drive  $\mathcal{D}$  modeled via the time-dependent Hamiltonian  $H_d(t)$ , and coupled to a thermal bath  $\mathcal{E}$ . A measuring apparatus monitors the variations of the number of photons in  $\mathcal{E}$  such that the systems follows trajectories corresponding to the quantum jump unraveling. Between  $t$  and  $t + \Delta t$ , the drive exchanges energy with the qubit in two forms: the work  $\delta W$  (coherent energy exchange) and the quantum heat  $\delta Q_q$  (incoherent/stochastic). Besides, the thermal bath exchanges classical heat  $\delta Q_{cl}$  with the qubit. **b** Measurement scheme of Example 3: The cavity mode used as a meter is initially in the vacuum. It is then coupled to the qubit during  $\Delta t$ , which induces a positive (resp. negative) coherent displacement when the qubit is in the excited (resp. ground) state.

$H_{int} = -i\sqrt{\gamma_m/\Delta t}(b^\dagger + b)\sigma_z$ , where  $\gamma_m$  is the measurement strength. For the sake of simplicity, we consider a transient measurement corresponding to a finite-time qubit-cavity interaction rather than the readout of the steady-state cavity proposed in [71] which implies a non-unitary evolution of the cavity. The cavity field is initially in the vacuum state  $|0\rangle$ . After interacting during  $\Delta t$  with the qubit, the field is displaced on the real axis by an amplitude proportional to the expectation value of  $\sigma_z$ . This value can then be deduced from a homodyne measurement of the real quadrature of the field. In this example, we consider the weak measurement limit, i.e.  $\gamma_m\Delta t \ll 1$  so that the two possible final coherent states of the cavity mode are strongly overlapping (see Fig. 15.2b). Note that a very similar situation exploiting a dispersive coupling between the qubit and the cavity has recently been implemented to experimentally demonstrate fluctuation theorems in presence of quantum measurement and feedback [72].

The Kraus operator associated with finding the cavity field in state  $|\beta\rangle$  after the interaction during  $\Delta t$  is (in the interaction picture):

$$M(\beta) = \frac{1}{\sqrt{\pi}} \langle \beta | e^{-i\Delta t H_{\text{int}}} | 0 \rangle. \quad (15.49)$$

Here we have taken the probability for the initial state of the cavity to be  $q_0 = 1$ . We stress that despite the fact that  $\{|\beta\rangle\}$  is an over-complete basis of  $\mathcal{H}_{\mathcal{E}}$ , it still defines a proper Kraus decomposition of the quantum map under study, provided the factor  $\frac{1}{\sqrt{\pi}}$  is included in the definition of  $M(\beta)$ , so as to ensure the normalization of the trajectory probabilities [73]. This Kraus operator can be rewritten introducing the measurement outcome  $I = -\text{Re}(\beta)/\sqrt{\gamma_m \Delta t}$ , and  $y = \text{Im}(\beta)$ , and noting the interaction induces a displacement of the cavity's state by an amplitude of  $\sqrt{\gamma_m \Delta t} \sigma_z$ :

$$M(y, I) = \frac{(\gamma_m \Delta t)^{1/4}}{\sqrt{\pi}} e^{-y^2/2 - iy\sqrt{\gamma_m \Delta t} \sigma_z} e^{-\frac{\gamma_m \Delta t}{2}(I - \sigma_z)^2} e^{-i\omega_0 \Delta t \sigma_z / 2} \quad (15.50)$$

The probability law for outcome  $(y, I)$  when the qubit is in state  $|\psi(t)\rangle = c_e|e\rangle + c_g|g\rangle$  reads

$$P(y, I) = \frac{(\gamma_m \Delta t)^{1/2}}{\pi} e^{-y^2} \left( e^{-\gamma_m \Delta t (I-1)^2} |c_e|^2 + e^{-\gamma_m \Delta t (I+1)^2} |c_g|^2 \right), \quad (15.51)$$

and is composed of two Gaussian functions centered around  $I = \pm 1$ . In the weak measurement regime under study, the two Gaussian functions strongly overlap. We can check from (15.51) that  $I$  follows a Gaussian law. It is therefore relevant to introduce a Wiener increment to describe the fluctuations of  $I$  around its mean value  $z = \langle \psi | \sigma_z | \psi \rangle$ :

$$I = z + \frac{dw(t)}{2\sqrt{\gamma_m \Delta t}}. \quad (15.52)$$

This allows us to express  $M(y, I)$  under a form similar to Eq. (15.16), highlighting that the present measurement scheme corresponds to a QSD unraveling:

$$M(y, I) = \frac{e^{-y^2/2 - iy\sqrt{\gamma_m \Delta t} \sigma_z}}{\pi^{1/4}} \left( \frac{e^{-dw(t)^2/2\Delta t}}{2\pi\Delta t} \right)^{1/2} \left( 1 - \frac{\Delta t}{2} (\gamma_m + i\omega_0) + \sqrt{\gamma_m} dw(t) \sigma_z \right). \quad (15.53)$$

The corresponding Lindblad equation can be retrieved by averaging the conditioned density operator  $M(y, I)\rho(t)M(y, I)^\dagger$  over the measurement outcomes:

$$\partial_t \rho = -i[H_s, \rho] + 2\gamma_m(\sigma_z \rho \sigma_z - \rho). \quad (15.54)$$

This master equation captures the pure dephasing in the free energy eigenbasis of the qubit induced by the measurement. Note that the uncertainty on the imaginary part of the field (responsible for the dependence on  $y$  of the probability distribution  $P(y, I)$ ) cause the effective pure dephasing rate to be equal to twice the measurement rate.

The pure dephasing can be decreased using a squeezed vacuum state [71], but will remain larger than or equal to the measurement rate.

### First law

As is clear from Eq. (15.54), the qubit does not receive any work from an external agent, solely heat due to the non-unitary term proportional to  $\gamma_m$ . This heat is quantum heat as no thermal reservoir is involved in the problem. The quantum heat increment between  $t_k$  and  $t_{k+1}$  amounts to:

$$\begin{aligned}\delta Q_q(y_k, I_k, t_k) &= \frac{\langle M(y_k, I_k)^\dagger H_S M(y_k, I_k) \rangle}{\langle M(y_k, I_k)^\dagger M(y_k, I_k) \rangle} - \langle H_S \rangle \\ &= \hbar\omega_0 (\sqrt{\gamma_m} dw(t) - 4\gamma\Delta t z_\Gamma(t)) (1 - z_\Gamma(t)^2),\end{aligned}\quad (15.55)$$

with  $z_\Gamma(t) = \langle \psi_\Gamma(t) | \sigma_z | \psi_\Gamma(t) \rangle$  the expectation value of  $\sigma_z$  in the qubit's state at time  $t$  along trajectory  $\Gamma$ . It is clear that the quantum heat is zero when the qubit is in state  $|e\rangle$  ( $z_\Gamma(t) = 1$ ) or  $|g\rangle$  ( $z_\Gamma(t) = -1$ ). As the qubit is always in a pure state along trajectory  $\Gamma$ ,  $1 - z_\Gamma(t)^2 = |\langle \psi_\Gamma(t) | e \rangle \langle g | \psi_\Gamma(t) \rangle|^2$  is directly related to the amplitude of the coherences between the energy eigenstates. Therefore, the quantum heat is non-zero solely if the qubit's state carries coherences in the  $\{|e\rangle, |g\rangle\}$  basis, i.e. solely when the measurement has an effect on the qubit's state. The quantum heat increment averaged over the measurement records (using probability  $P(y_k, I_k)$  given by Eq. (15.51) of getting outcome  $(y_k, I_k)$ ) is zero in this example. This result can also be deduced from the master equation noting that  $\text{tr}[H_S \partial_t \rho_S] = 0$  which implies that the average internal energy of the qubit is unchanged during the process. This is expected as the measured observable commutes with the Hamiltonian. Note however that, as it can be seen from Eq. (15.55), the quantum heat takes non-zero values along single trajectories such that there are fluctuations around the average. Moreover, the average would be non-zero in the case of a measurement of an observable which does not commute with the Hamiltonian, allowing e.g. to fuel an engine [56, 58].

### Second law

The time-reversed operator can be deduced from Eq. (15.21):

$$\tilde{M}(\beta) = \sqrt{P(\beta)} M(\beta)^\dagger,\quad (15.56)$$

using the fact that the probability  $P(\beta)$  for the cavity to start in state  $\beta$  in the reversed trajectory is simply the probability of getting outcome  $\beta$  in the direct trajectory. We deduce the entropy produced between  $t_{k-1}$  and  $t_k$ :

$$\begin{aligned}\delta_{IS}(y_k, I_k, t_k) &:= -\ln(P(y_k, I_k)) \\ &= \ln\left(\frac{\pi}{\sqrt{\gamma_m \Delta t}}\right) + y^2 + \ln\left(e^{-\gamma\Delta t(I_k-1)^2} |c_e(t_k)|^2 + e^{-\gamma(\Delta t+1)^2} |c_g(t_k)|^2\right).\end{aligned}\quad (15.57)$$

The entropy production contains a constant term scaling as  $\ln(\sqrt{\gamma_m \Delta t})$ , which is in general very large, but finite.<sup>2</sup> This term can be interpreted by noting that the measurement generates a set of outcomes with typical resolution  $\sqrt{\gamma_m \Delta t}$ , such that one cavity state (the vacuum) is mapped onto a number of states scaling as  $1/\sqrt{\gamma_m \Delta t}$  (see also Sect. 27.1.2 of Chap. 27).

## 15.8 Conclusion

In this chapter, we have presented a formalism based on quantum trajectories to describe the stochastic thermodynamics of quantum open systems. We have introduced the notion of time-reversed quantum trajectories to compute the entropy production at the single trajectory level. This quantity fulfills the Integral Fluctuation Theorem and the second law. We have then analyzed the energy exchanges occurring during a single realization of a thermodynamic transformation to identify work and heat contributions to the variation of the internal energy of a quantum system. In particular, we have highlighted a quantum contribution to the heat received by the system which is related to the decoherence induced by the environment. Finally, we have illustrated this framework with three examples: the thermalization of a quantum system; the fluorescence of a driven qubit; and the continuous measurement of a qubit's observable.

We have introduced the formalism of quantum stochastic thermodynamics focusing on an ideal situation involving a Markovian environment, monitored with perfect efficiency. However, the quantum trajectory framework is very flexible and can be extended to account for more complex situations. For instance, detection inefficiency can be introduced [30] to study its influence on quantum thermodynamics [60, 74]. Besides, quantum trajectories can also encompass non-Markovianity [75–78], opening avenues towards characterization of non-Markovian quantum thermodynamics. Finally, feedback mechanisms exploiting the measurement record can be analyzed in the quantum trajectory framework, allowing e.g. to check generalizations of the quantum fluctuation theorems [69, 72] (see also Sect. 10.3 of Chap. 10).

**Acknowledgements** C.E. acknowledges support by the US Department of Energy grant No. DE-SC0017890 and thanks Chapman University and the Institute for Quantum Studies for hospitality during this project. M.H.M. acknowledges support from EPSRC (Grant No. EP/P030815/1).

---

<sup>2</sup> $\Delta t$  is fixed by the time-resolution of the cavity readout.

## Appendices

### A. Trajectories in Presence of Non Rank-1 Measurements

In Sect. 15.2, we have restricted our discussion to the case where both system and environment are measured with rank-1 projective measurements, which allowed us to obtain pure-state trajectories for both system and environment. While this describes very well certain measurement schemes like a heterodyne setup [73], such measurements are unfeasible in many physical situations which still allow to track quantum trajectories. Especially, this is the case when the environment is a thermal bath with infinite degrees of freedom. To model such cases, we have to admit the possibility that not all the different pairs of outcomes  $(\mu, \nu)$  can be distinguished by the measurement. We define a set of “macroscopic” outcomes  $\{\alpha\}$  that can indeed be deduced from the measurement, where each  $\alpha$  contains several pairs  $(\mu, \nu)$ . This leads to the decomposition of the quantum map  $\Phi$  as  $\Phi(\rho_s) = \sum_{\alpha} \Phi_{\alpha}(\rho_s)$ , where

$$\Phi_{\alpha}(\rho_s) = \sum_{(\mu, \nu) \in \alpha} \Phi_{\mu, \nu}(\rho_s). \quad (15.58)$$

Such “coarse-graining” prevents us in general to write  $\Phi_{\alpha}$  under the form (15.5). Indeed,  $\Phi_{\alpha}$  will in general be described by a set of non-identical Kraus operators. As such, even if the system is initially in a pure state  $\Pi_s[\psi]$ ,  $\Phi_{\alpha}(\Pi_s[\psi])$  will in general be mixed. Remarkably however, some practical measurement schemes (e.g. the quantum jump unraveling) still allow us to define Kraus operators  $M_{\alpha}$  fulfilling  $\Phi_{\alpha}(\rho_s) = M_{\alpha}\rho_s M_{\alpha}^{\dagger}$ . Of particular interest are measurement schemes such that for every  $(\mu, \nu)$  and  $(\mu', \nu')$  in  $\alpha$ ,  $M_{\mu', \nu'} = \sqrt{\text{tr}[M_{\mu', \nu'}^{\dagger} M_{\mu', \nu'}]} / \text{tr}[M_{\mu', \nu'}^{\dagger} M_{\mu', \nu'}] M_{\mu', \nu'}$ , allowing us to define

$$M_{\alpha} := \frac{\sqrt{q_{\alpha}} M_{\mu, \nu}}{\sqrt{\text{tr}[M_{\mu, \nu}^{\dagger} M_{\mu, \nu}]}} \quad (15.59)$$

for any  $(\mu, \nu)$  in  $\alpha$ , where  $q_{\alpha} := \sum_{(\mu, \nu) \in \alpha} \text{tr}[M_{\mu, \nu}^{\dagger} M_{\mu, \nu}]$ . It is then easy to verify that  $M_{\alpha}\rho_s M_{\alpha}^{\dagger} = \sum_{(\mu, \nu) \in \alpha} M_{\mu, \nu}\rho_s M_{\mu, \nu}^{\dagger}$ . This ensures that such a coarse-graining of the environment trajectories will not alter the average evolution of the system, which will still be described by the quantum channel  $\Phi$ .

The case of a quantum jump unraveling of the Lindblad equation can be modeled by considering the macroscopic outcomes as the variations of the number of excitations in the environment between  $\Delta t$ . One only needs to know the variation  $\alpha$  and not the absolute number of excitations, neither at the beginning nor at the end of the time step to characterize the system’s evolution. Consequently, the Kraus operators  $M_{\alpha}$  are composed of several of the operators  $M_{\mu, \nu}$  that would be obtained by taking  $\{\phi_{\mu}\}$  and  $\{\varphi_{\nu}\}$  to be the number of excitations basis. With such a definition of  $M_{\mu, \nu}$ , the

QJ Kraus operators obey Eq. (15.59). As every  $M_{\mu,\nu}$  for  $(\mu, \nu) \in \alpha$  is proportional to the same jump operator  $L_j$ , we may still view the system's evolution as a trajectory of pure states.

### B. Entropy Production in Presence of Non Rank-1 Measurements

The results of Sect. 15.3.1 can be extended to the case discussed in Appendix A, wherein the measurement outcomes are coarse-grained so that  $\tilde{\Phi}_{\alpha_k} = \sum_{(\mu_k, \nu_k) \in \alpha_k} \tilde{\Phi}_{\mu_k, \nu_k}$ . In the case where the Kraus operators  $M_{\alpha_k}$  can be defined by Eq. (15.59) (e.g. the QJ unraveling), the Kraus operator for the reverse transformation will be

$$\tilde{M}_{\alpha_k} = \sqrt{\tilde{q}_{\alpha_k}} \frac{M_{\mu_k, \nu_k}^\dagger}{\sqrt{\text{tr}[M_{\mu_k, \nu_k}^\dagger M_{\mu_k, \nu_k}]}} \quad (15.60)$$

for any  $(\mu_k, \nu_k) \in \alpha_k$ , where we have introduced

$$\begin{aligned} \tilde{q}_{\alpha_k} &:= \sum_{(\mu_k, \nu_k) \in \alpha_k} \text{tr}[\tilde{M}_{\mu_k, \nu_k}^\dagger \tilde{M}_{\mu_k, \nu_k}], \\ &= \sum_{(\mu_k, \nu_k) \in \alpha_k} \frac{q'_{\nu_k}}{q_{\mu_k}} \text{tr}[M_{\mu_k, \nu_k}^\dagger M_{\mu_k, \nu_k}]. \end{aligned} \quad (15.61)$$

Consequently, the expression for stochastic entropy production along the trajectories  $\Gamma = ((l, m), \vec{\alpha})$  will be

$$\Delta_i s[\Gamma] = \ln \left( \frac{p_l}{p'_m} \right) + \sum_{k=1}^K \ln \left( \frac{q_{\alpha_k}}{\tilde{q}_{\alpha_k}} \right). \quad (15.62)$$

Note that while the entropy production contribution from the system depends on its probability distribution  $p_l$  and  $p'_m$ , at the start and end of the transformation, this is not so for the bath contributions. Notwithstanding, the IFT Eq. (15.25) is still valid, while the average entropy production now reads:

$$\langle \Delta_i s[\Gamma] \rangle = \Delta S_S + \sum_{k=1}^K \sum_{\alpha_k} \frac{\text{tr}[M_{\mu,\nu}^\dagger M_{\mu,\nu} \rho_S^{(k)}]}{\text{tr}[M_{\mu,\nu}^\dagger M_{\mu,\nu}]} q_{\alpha_k} (\ln(q_{\alpha_k}) - \ln(\tilde{q}_{\alpha_k})), \quad (15.63)$$

where  $\rho_S^{(k)} := (\Phi(t_{k-1}, t_k) \circ \dots \circ \Phi(t_0, t_1))(\rho_S)$  is the average state of the system before it interacts with the  $k^{\text{th}}$  environment. In contrast with Eq. (15.24), the second term in the right-hand side of Eq. (15.63) is not equal in general to the variation

of the environment's von-Neumann entropy. This is a consequence of the uncertainty introduced by the "coarse-graining" present in the measurement scheme, i.e. the fact that not all the couples  $(\mu, \nu)$  of outcomes can be discriminated. However, certain measurement schemes like the QJ unraveling for a qubit presented in Sect. 15.6 actually gather enough information so that the second term in (15.63) reduces to  $\Delta S_{\mathcal{E}}$ .

## References

1. K. Mølmer, Y. Castin, J. Dalibard, Monte carlo wave-function method in quantum optics. *J. Optical Soc. Am. B* **10**(3), 524–538 (1993). ISSN 0740-3224, <https://doi.org/10.1364/josab.10.000524>
2. H.M. Wiseman, Quantum trajectories and quantum measurement theory. *Q Semiclassical Opt.: J. Eur. Opt. Soc. Part B* **8**(1), 205–222 (1996). ISSN 1355-5111, <https://doi.org/10.1088/1355-5111/8/1/015>
3. T.A. Brun, A simple model of quantum trajectories. *Am. J. Phys.* **70**(7), 719–737 (2002). ISSN 0002-9505, <https://doi.org/10.1119/1.1475328>
4. W. Nagourney, J. Sandberg, H. Dehmelt, Shelved optical electron amplifier: observation of quantum jumps. *Phys. Rev. Lett.* **56**(26), 2797–2799 (1986). ISSN 0031-9007, <https://doi.org/10.1103/physrevlett.56.2797>
5. Th. Sauter, W. Neuhauser, R. Blatt, P.E. Toschek, Observation of quantum jumps. *Phys. Rev. Lett.* **57**(14), 1696–1698 (1986). ISSN 0031-9007, <https://doi.org/10.1103/physrevlett.57.1696>
6. R.G. Hulet, D.J. Wineland, J.C. Bergquist, W.M. Itano, Precise test of quantum jump theory. *Phys. Rev. A* **37**(11), 4544–4547 (1988). ISSN 0556-2791, <https://doi.org/10.1103/physreva.37.4544>
7. S. Gleyzes, S. Kuhr, C. Guerlin, J. Bernu, S. Deléglise, U.B. Hoff, M. Brune, J.-M. Raimond, S. Haroche, Quantum jumps of light recording the birth and death of a photon in a cavity. *Nature* **446**(7133), 297–300 (2007). ISSN 0028-0836, <https://doi.org/10.1038/nature05589>
8. K.W. Murch, S.J. Weber, C. Macklin, I. Siddiqi, Observing single quantum trajectories of a superconducting quantum bit. *Nature* **502**(7470), 211–214 (2013). ISSN 0028-0836, <https://doi.org/10.1038/nature12539>
9. P. Campagne-Ibarcq, E. Flurin, N. Roch, D. Darson, P. Morfin, M. Mirrahimi, M.H. Devoret, F. Mallet, B. Huard, Persistent control of a superconducting qubit by stroboscopic measurement feedback. *Phys. Rev. X* **3**(2), 021008+ (2013). ISSN 2160-3308 <https://doi.org/10.1103/physrevx.3.021008>
10. G. de Lange, D. Ristè, M.J. Tiggelman, C. Eichler, L. Tornberg, G. Johansson, A. Wallraff, R.N. Schouten, L. DiCarlo, Reversing quantum trajectories with analog feedback. *Phys. Rev. Lett.* **112**(8) (2014). ISSN 0031-9007, <https://doi.org/10.1103/physrevlett.112.080501>
11. R. Alicki, The quantum open system as a model of the heat engine. *J. Phys. A: Math. General* **12**(5), L103–L107 (1979). ISSN 0305-4470, <https://doi.org/10.1088/0305-4470/12/5/007>
12. U. Seifert, Stochastic thermodynamics: principles and perspectives. *Eur. Phys. J. B* **64**(3–4), 423–431 (2008). <https://doi.org/10.1140/epjb/e2008-00001-9>
13. K. Sekimoto, *Stochastic Energetics* (Springer, Berlin, 2010). <https://doi.org/10.1007/978-3-642-05411-2>, ISBN 9783642054112
14. C. Jarzynski, Nonequilibrium equality for free energy differences. *Phys. Rev. Lett.* **78**(14), 2690–2693 (1997). ISSN 0031-9007, <https://doi.org/10.1103/physrevlett.78.2690>
15. G.E. Crooks, Entropy production fluctuation theorem and the nonequilibrium work relation for free energy differences. *Phys. Rev. E* **60**(3), 2721–2726 (1999). ISSN 1063-651X, <https://doi.org/10.1103/physreve.60.2721>
16. U. Seifert, Entropy production along a stochastic trajectory and an integral fluctuation theorem. *Phys. Rev. Lett.* **95**(4), 040602+ (2005). <https://doi.org/10.1103/physrevlett.95.040602>

17. F.W.J. Hekking, J.P. Pekola, Quantum jump approach for work and dissipation in a two-level system. *Phys. Rev. Lett.* **111**, 093602+ (2013). <https://doi.org/10.1103/physrevlett.111.093602>
18. J.J. Alonso, E. Lutz, A. Romito, Thermodynamics of weakly measured quantum systems. *Phys. Rev. Lett.* **116**, 080403+ (2016). <https://doi.org/10.1103/physrevlett.116.080403>
19. G. Manzano, J.M. Horowitz, J.M.R. Parrondo, Nonequilibrium potential and fluctuation theorems for quantum maps. *Phys. Rev. E* **92**(3), 032129 (2015). ISSN 1539-3755, <https://doi.org/10.1103/PhysRevE.92.032129>
20. C. Elouard, D.A. Herrera-Martí, M. Clusel, A. Auffèves, The role of quantum measurement in stochastic thermodynamics. *npj Quantum Inf.* **3**(1), 9 (2017). ISSN 2056-6387, <https://doi.org/10.1038/s41534-017-0008-4>
21. S. Gherardini et al., Reconstructing quantum entropy production to probe irreversibility and correlations, *Quantum Sci. Technol.* **3**(3), 035013 (2018). <https://doi.org/10.1088/2058-9561/aac7e1>
22. J. Dressel, A. Chantasri, A.N. Jordan, A.N. Korotkov, Arrow of time for continuous quantum measurement. *Phys. Rev. Lett.* **119**(22) (2017). <https://doi.org/10.1103/physrevlett.119.220507>
23. S.K. Manikandan, A.N. Jordan, Time reversal symmetry of generalized quantum measurements with past and future boundary conditions (2018), [arXiv:1801.04364](https://arxiv.org/abs/1801.04364)
24. H.-P. Breuer, F. Petruccione, *The Theory of Open Quantum Systems* (Oxford University Press, Oxford, 2007). <https://doi.org/10.1093/acprof:oso/9780199213900.001.0001>
25. T. Heinosaari, M. Ziman, *The Mathematical Language of Quantum Theory* (Cambridge University Press, Cambridge, 2011). <https://doi.org/10.1017/CBO9781139031103.001>
26. W.F. Stinespring, Positive functions on  $c^*$ -algebras. *Proc. Am. Math. Soc.* **6**(2), 211–216 (1955). <https://doi.org/10.2307/2032342>
27. K. Kraus, *States, Effects and Operations: Fundamental Notions of Quantum Theory* (Springer, Berlin, 1983). <https://doi.org/10.1007/3-540-12732-1>
28. P. Busch, M. Grabowski, P.J. Lahti, *Operational Quantum Physics* (Springer, Berlin, 1995). <https://doi.org/10.1007/978-3-540-49239-9>
29. P. Busch, P.J. Lahti, J.-P. Pellonpää, K. Ylinen, *Quantum Measurement* (Springer, Berlin, 2016). <https://doi.org/10.1007/978-3-319-43389-9>
30. H.M. Wiseman, G.J. Milburn, *Quantum Measurement and Control* (Cambridge University Press, Cambridge, 2010). <http://www.worldcat.org/isbn/9780521804424>, ISBN 9781107424159
31. K. Jacobs, D.A. Steck, A straightforward introduction to continuous quantum measurement. *Contemp. Phys.* **47**(5), 279–303 (2006). <https://doi.org/10.1080/00107510601101934>
32. C. Cohen-Tannoudji, J. Dupont-Roc, G. Grynberg, *Atom-Photon Interactions : Basic Process and Applications* (Wiley-VCH Verlag GmbH, Weinheim, Germany, 1998). <https://doi.org/10.1002/9783527617197>
33. G. Lindblad, On the generators of quantum dynamical semigroups. *Commun. Math. Phys.* **48**(2), 119–130 (1976). <https://doi.org/10.1007/bf01608499>. ISSN 0010-3616
34. S. Haroche, J.M. Raimond, *Exploring the Quantum: Atoms, Cavities and Photons* (Oxford University Press, Oxford, 2006). <https://doi.org/10.1093/acprof:oso/9780198509141.001.0001>
35. T.B.L. Kist, M. Orszag, T.A. Brun, L. Davidovich, Stochastic schrödinger equations in cavity qed: physical interpretation and localization. *J. Opt. B: Quantum Semiclassical Opt.* **1**(2), 251–263 (1999). <https://doi.org/10.1088/1464-4266/1/2/009>, ISSN 1464-4266
36. T.A. Brun, Continuous measurements, quantum trajectories, and decoherent histories. *Phys. Rev. A* **61**(4) (2000). <https://doi.org/10.1103/physreva.61.042107>, ISSN 1050-2947
37. C.W. Gardiner, P. Zoller, *Quantum Noise* (Springer, Berlin, 2004). <https://doi.org/10.1007/978-3-662-04103-1>, ISBN 978-3-662-04105-5
38. G.E. Crooks, Quantum operation time reversal. *Phys. Rev. A* **77**, 034101+ (2008). <https://doi.org/10.1103/physreva.77.034101>
39. G. Manzano, J.M. Horowitz, J.M.R. Parrondo, Nonequilibrium potential and fluctuation theorems for quantum maps. *Phys. Rev. E* **92**(3) (2015). <https://doi.org/10.1103/physreve.92.032129>, ISSN 1539-3755

40. F. Barra, C. Lledó, Stochastic thermodynamics of quantum maps with and without equilibrium. *Phys. Rev. E* **96**(5) (2017). <https://doi.org/10.1103/physreve.96.052114>, ISSN 2470-0045
41. J.M. Horowitz, Quantum-trajectory approach to the stochastic thermodynamics of a forced harmonic oscillator. *Phys. Rev. E* **85**, 031110+ (2012). <https://doi.org/10.1103/physreve.85.031110>
42. G. Manzano, J.M. Horowitz, J.M.R. Parrondo, Quantum fluctuation theorems for arbitrary environments: adiabatic and non-adiabatic entropy production. *Phys. Rev. X* **8**, 031037 (2018). <https://doi.org/10.1103/PhysRevX.8.031037>
43. D. Petz, *Quantum Information Theory and Quantum Statistics* (Springer, Berlin, 2008). <https://doi.org/10.1007/978-3-540-74636-2>
44. P.M. Alberti, A. Uhlmann, *Stochasticity and Partial Order: Doubly Stochastic Maps and Unitary Mixing* (Springer, Berlin, 1982)
45. M. Nakahara, R. Rahimi, A. Saitoh, *Decoherence Suppression in Quantum Systems* (World Scientific, Singapore, 2008). <https://doi.org/10.1142/7653>
46. Y. Murashita, Absolute irreversibility in information thermodynamics. Master's thesis (2015). [arXiv:1506.04470](https://arxiv.org/abs/1506.04470)
47. K. Funo, Y. Murashita, M. Ueda, Quantum nonequilibrium equalities with absolute irreversibility. *New J. Phys.* **17**(7), 075005+ (2015). <https://doi.org/10.1088/1367-2630/17/7/075005>, ISSN 1367-2630
48. Jarzynski relations for quantum systems and some applications (2000). [arXiv:cond-mat/0009244.pdf](https://arxiv.org/abs/cond-mat/0009244.pdf)
49. J. Kurchan, A quantum fluctuation theorem (2001). [arXiv:cond-mat/0007360](https://arxiv.org/abs/cond-mat/0007360)
50. S. Mukamel, Quantum extension of the jarzynski relation: analogy with stochastic dephasing. *Phys. Rev. Lett.* **90**(17) (2003). <https://doi.org/10.1103/physrevlett.90.170604>
51. P. Talkner, E. Lutz, P. Hänggi, Fluctuation theorems: work is not an observable. *Phys. Rev. E* **75**(5), 050102+ (2007). <https://doi.org/10.1103/physreve.75.050102>, ISSN 1539-3755
52. M. Campisi, P. Hänggi, P. Talkner, Colloquium : Quantum fluctuation relations: foundations and applications. *tRev. Mod. Phys.* **83**(3), 771–791 (2011). <https://doi.org/10.1103/revmodphys.83.771>, ISSN 0034-6861
53. M. Esposito, U. Harbola, S. Mukamel, Nonequilibrium fluctuations, fluctuation theorems, and counting statistics in quantum systems. *Rev. Mod. Phys.* **81**(4), 1665–1702 (2009). <https://doi.org/10.1103/revmodphys.81.1665>
54. C. Elouard, D. Herrera-Martí, M. Esposito, A. Auffèves, Thermodynamics of Resonance Fluorescence, in preparation (2018)
55. C. Elouard, Thermodynamics of quantum open systems: applications in quantum optics and optomechanics (2017), [arXiv:1709.02744](https://arxiv.org/abs/1709.02744)
56. C. Elouard, D. Herrera-Martí, B. Huard, A. Auffèves, Extracting work from quantum measurement in Maxwell's Demon engines. *Phys. Rev. Lett.* **118**(26), 260603 (2017). <https://doi.org/10.1103/PhysRevLett.118.260603>, ISSN 0031-9007
57. J. Yi, P. Talkner, Y.W. Kim, Single-temperature quantum engine without feedback control. *Phys. Rev. E* **96**(2) (2017). <https://doi.org/10.1103/physreve.96.022108>, ISSN 2470-0045
58. C. Elouard, A.N. Jordan, Efficient quantum measurement engine. *Phys. Rev. Lett.* **120**, 260601 (2018). <https://doi.org/10.1103/PhysRevLett.120.260601>
59. M.H. Mohammady, J. Anders, *New J. Phys.* **19**, 113026 (2017). <https://doi.org/10.1088/1367-2630/aa8ba1>
60. C. Elouard, N.K. Bernardes, A.R.R. Carvalho, M.F. Santos, A. Auffèves, Probing quantum fluctuation theorems in engineered reservoirs. *New J. Phys.* **19**(10), 103011 (2017). <https://doi.org/10.1088/1367-2630/aa7fa2>, ISSN 1367-2630
61. S. Gherardini et al., Non-equilibrium quantum-heat statistics under stochastic projective measurements. *Phys. Rev. E* **98**(3), 032108 (2018). <https://doi.org/10.1103/PhysRevE.98.032108>
62. M.H. Mohammady, A. Auffèves, J. Anders, The two energetic facets of entropy production in the quantum regime, in preparation
63. G. Francica, J. Goold, F. Plastina, (2017). [arXiv: 1707.06950](https://arxiv.org/abs/1707.06950)
64. J.P. Santos, L.C. Céleri, G.T. Landi, M. Paternostro, (2017). [arXiv:1707.08946](https://arxiv.org/abs/1707.08946)

65. J.P. Pekola, P. Solinas, A. Shnirman, D.V. Averin, Calorimetric measurement of work in a quantum system. *New J. Phys.* **15**(11), 115006+ (2013). <https://doi.org/10.1088/1367-2630/15/11/115006>, ISSN 1367-2630
66. K. Szczygielski, D.G. Klimovsky, R. Alicki, Markovian master equation and thermodynamics of a two-level system in a strong laser field. *Phys. Rev. E* **87**, 012120+ (2013). <https://doi.org/10.1103/physreve.87.012120>
67. G.B. Cuetara, A. Engel, M. Esposito, Stochastic thermodynamics of rapidly driven systems. *New J. Phys.* **17**(5), 055002+ (2015). <https://doi.org/10.1088/1367-2630/17/5/055002>, ISSN 1367-2630
68. B. Donvil, Thermodynamics of a periodically driven qubit. *J. Stat. Mech.: Theory Exp.* (4), 043104+ (2018). <http://doi.org/10.1088/1742-5468/aab857>, ISSN 1742-5468
69. M. Naghiloo, D. Tan, P.M. Harrington, J.J. Alonso, E. Lutz, A. Romito, K.W. Murch, Thermodynamics along individual trajectories of a quantum bit (2017) [arXiv:1703.05885](https://arxiv.org/abs/1703.05885)
70. M. Campisi, P. Talkner, P. Hänggi, Fluctuation theorem for arbitrary open quantum systems. *Phys. Rev. Lett.* **102**(21), 210401+ (2009). <https://doi.org/10.1103/physrevlett.102.210401>, ISSN 0031-9007
71. N. Didier, J. Bourassa, A. Blais, Fast quantum nondemolition readout by parametric modulation of longitudinal qubit-oscillator interaction. *Phys. Rev. Lett.* **115**(20), 203601+ (2015). <https://doi.org/10.1103/physrevlett.115.203601>, ISSN 0031-9007
72. M. Naghiloo, J.J. Alonso, A. Romito, E. Lutz, K.W. Murch, Information gain and loss for a quantum Maxwell's demon (2018). <https://doi.org/10.1103/PhysRevLett.121.030604>
73. A.N. Jordan, A. Chantasri, P. Rouchon, B. Huard, Anatomy of fluorescence: quantum trajectory statistics from continuously measuring spontaneous emission. *3*(3), 237–263 (2016). <https://doi.org/10.1007/s40509-016-0075-9>
74. C.W. Wächtler, P. Strasberg, T. Brandes, Stochastic thermodynamics based on incomplete information: generalized jarzynski equality with measurement errors with or without feedback. *New J. Phys.* **18**(11), 113042+ (2016). <https://doi.org/10.1088/1367-2630/18/11/113042>, ISSN 1367-2630
75. L. Diósi, W.T. Strunz, The non-markovian stochastic schrödinger equation for open systems. *Phys. Lett. A* **235**(6), 569–573 (1997). [https://doi.org/10.1016/s0375-9601\(97\)00717-2](https://doi.org/10.1016/s0375-9601(97)00717-2), ISSN 03759601
76. W.T. Strunz, L. Diósi, N. Gisin, Open system dynamics with non-markovian quantum trajectories. *Phys. Rev. Lett.* **82**(9), 1801–1805 (1999) <https://doi.org/10.1103/physrevlett.82.1801>, ISSN 0031-9007
77. M.W. Jack, M.J. Collett, Continuous measurement and non-markovian quantum trajectories. *Phys. Rev. A* **61**(6) (2000). <https://doi.org/10.1103/physreva.61.062106>, ISSN 1050-2947
78. J. Jing, X. Zhao, J.Q. You, W.T. Strunz, T. Yu, Many-body quantum trajectories of non-markovian open systems. *Phys. Rev. A* **88**(5) (2013). <https://doi.org/10.1103/physreva.88.052122>, ISSN 1050-2947

# Chapter 16

## Characterizing Irreversibility in Open Quantum Systems



**Tiago B. Batalhão, Stefano Gherardini, Jader P. Santos, Gabriel T. Landi and Mauro Paternostro**

When watching a movie, a question that can be made is whether the movie was recorded in that way, or if we are watching a time-reversed version of the actual recording. In our everyday experience, this question is often easy to answer, because watching broken pieces of glass moving from the floor to the top of a table and assembling themselves in the shape of a cup just feels weird. It is much more likely that the movie-makers recorded a glass cup falling down and breaking. Even though we are able to reach this conclusion quickly, none of the fundamental laws of physics (e.g., Newtonian equations of motion) forbid the broken pieces to reassemble the cup. Only the second law of thermodynamics makes the argument that, as the broken pieces represent a system of larger entropy, the reassembling process is impossible or at least very unlikely.

---

T. B. Batalhão  
Singapore University of Technology and Design, 8 Somapah Road,  
Singapore 487372, Singapore

T. B. Batalhão  
Centre for Quantum Technologies, National University of Singapore, 3 Science Drive 2,  
Singapore 117543, Singapore

S. Gherardini  
Department of Physics and Astronomy, LENS and QSTAR, University of Florence,  
via G. Sansone 1, 50019 Sesto Fiorentino, Italy

J. P. Santos · G. T. Landi  
Instituto de Física da Universidade de São Paulo, 05314-970 São Paulo, Brazil

M. Paternostro (✉)  
School of Mathematics and Physics, Centre for Theoretical Atomic, Molecular, Queen's  
University Belfast, BT7 1NN Belfast, UK  
e-mail: m.paternostro@qub.ac.uk

The above is only a simple example, taken from everyday life, of a much deeper concept, namely that *the fundamental, microscopic equations of motion are symmetric under time-reversal, but the thermodynamical laws are not and establish a fundamental difference between past and future*. This apparent paradox has been known under the name of the “arrow of time”, given by Eddington in 1927 [1]. The understanding of the emergence of the arrow of time from underlying quantum dynamics, and the formalisation of a self-consistent framework for its characterisation have been the focus of much interest. On one hand, we are in great need of tools able to reveal, experimentally, the implications that non-equilibrium dynamics has on the degree of reversibility for a given quantum process. On the other hand, the tools that are currently available for the (even only theoretical) investigation of thermodynamic irreversibility lack the widespread applicability and logical self-contained nature that is required from a complete theory. Let us elaborate more on this aspect.

The entropy of an open system, unlike the energy, does not satisfy a continuity equation: in addition to entropic fluxes exchanged between a system and its environment, some entropy may also be produced within the system. This contribution is called *entropy production* and, according to the second law of thermodynamics, it is always non-negative, being zero only when the system and the environment are in thermal equilibrium. On the other hand, for closed systems that are dynamically brought out of equilibrium, the energy changes induced on a quantum system by a driving potential are not necessarily all translated into useful work that can be extracted from or performed on the system itself. Part of such energy is *lost* and gives rise to an entropic contribution akin to the entropy production above.

Entropy production thus serves as *the* measure of the irreversibility of a physical process and may be used to characterize non-equilibrium systems in a broad range of situations and across all scales. So far, several theories of entropy production have been developed in different contexts. Among the most significant examples in the classical domain are the theories formulated by Onsager [2–6] and Schnakenberg [7, 8], which have been expanded upon towards their generalization to a wide range of classical stochastic processes [9–12].

The extensions of these approaches to small-scale (mesoscopic) systems made by Gallavotti, Cohen and collaborators [13–15], Jarzynski [16, 17], and Crooks [18, 19], and the more recent attempts at formulations that are fully within the quantum domain, have shown that quantum fluctuations may play a prominent role in determining the degree of irreversibility of non-equilibrium processes.

This chapter aims at addressing core questions in the formulation of entropy production and irreversibility in quantum systems and processes, both in the closed and open-system scenario [20]. First, in Sect. 16.1 we set the context and make founding statements on the relation between entropy production and irreversibility. We then move to Sect. 16.2, where we sketch a stochastic framework for entropy production. Finally, Sect. 16.3 is dedicated to the highlighting of conceptual shortcomings in the current formulation of entropy production, and the brief discussion of a potential alternative based on the use of a Rényi-2 entropy.

## 16.1 The Foundations of Entropy Production: Closed-System Dynamics

The goal of this section is to address how the production of thermodynamic entropy is closely linked to a measure of distinguishability of past and future that can be cast as a guessing game and analysed with the tools of information theory and Bayesian reasonings. We will show that, by combining Bayes theorem from statistics with the Crooks fluctuation relation from non-equilibrium thermodynamics [19], it is possible to find an expression to quantify the level of certainty about the direction of the arrow of time [21, 22].

We consider the Bayesian view of a guessing game, where the goal is to determine the direction of the arrow of time of a given physical event (is a movie displayed in forward or time-reversed mode?), conditionally to a sequence of observations of the event itself. Let us call  $F$  ( $B$ ) the forward (backward) direction of the process. We assume that the a priori probability for both directions is  $1/2$ . Bayes' theorem provides us with the posterior probability  $P^F$  ( $P^B$ ) that the event runs in the forward (backward) direction, on the basis of the results of the observations, i.e. an explicit sequence of measurements. Explicitly

$$P^F = 1 - P^B = \frac{1}{1 + e^{-\Sigma}}, \quad (16.1)$$

where  $\Sigma$  is the (adimensional) entropy production associated with the system trajectories. When  $\Sigma \gg 1$ , then  $P^F \approx 1$ , and similarly  $P^F \approx 0$  when  $\Sigma \ll -1$ . Moreover, if  $\Sigma = 0$  (no entropy production), then  $P^F = P^B = 1/2$ . The ratio between  $P^F$  and  $P^B$  is thus given by the ratio of the corresponding likelihood functions, which is expressed by the Crooks fluctuation theorem. Accordingly, the ability to distinguish between the two directions of the arrow of time is directly linked to the entropy production along the observed trajectories.

Let us now assume that the event to witness is embodied by a process where the Hamiltonian of a quantum system experiences a change from time  $t = 0$  to  $t = \tau$ , thus generating an evolution of its initial state towards the state  $\rho_t^F$ . In doing so, an amount of thermodynamic work  $W$  is done on or by the system, and the free energy of the system changes by  $\Delta F$ . The reverse process, then, would correspond to the driving of the state of the system towards the state  $\rho_{\tau-t}^B$ . Moreover, we assume that the initial state of the system is a thermal one at inverse temperature  $\beta$ . For quantum systems, both thermal and quantum fluctuations conjure to determine the values taken by thermodynamically relevant quantities, including  $W$ , and the entropy production is written as  $\Sigma = \beta(W - \Delta F)$ . Its mean value can be shown to be given by the Kullback–Leibler relative entropy between the trajectories of time-opposite processes [23–25]

$$\langle \Sigma \rangle = \beta \langle W \rangle - \beta \Delta F = S(\rho_t^F \| \rho_{\tau-t}^B), \quad (16.2)$$

where  $S(\rho_a || \rho_b) \equiv \text{Tr}[\rho_a (\ln \rho_a - \ln \rho_b)]$  for any pair of density matrices  $\rho_{a,b}$ . In contrast with the macroscopic notion of distinguishability given by the guessing

game, Eq. (16.2) provides a microscopic measure of distinguishability of the dynamics between two processes in terms of their quantum representations in the Hilbert space, and is a nice link between the phenomenology of stochastic thermodynamics induced by a general quantum process and an information theoretical figure of merit for the difference between the states of the system in the forward and backward directions.

Equations (16.1) and (16.2) were derived with some key assumptions, common to the Crooks's theorem, i.e. that the Hamiltonian depends explicitly on time and that the initial state of the system (in both forward and backward processes) corresponds to a Gibbs equilibrium. The first hypothesis breaks time homogeneity, and leads to the emergence of an arrow of time, while the second does not come from the microscopic equations of motion, as the dynamical equations that propagate the state of the system in time are not applied for  $t < 0$ . Instead, the state at  $t = 0$  is given and the dynamics is calculated only for  $t > 0$ . This distinct treatment of past and future enforces the direction of the arrow of time.

It is worth observing that blurriness of the arrow of time does not depend explicitly on the size of system but occurs when the scale of energy changes in the system are comparable to the thermal energy  $1/\beta$ . In a truly macroscopic system, the usual energy and entropy scales are much larger than such threshold. This justifies the assumption that the arrow of time has a well-defined direction, which in turn implies that processes that lower entropy are extremely unlikely.

The measurement of entropy production, or even its theoretical calculation, are tricky propositions [26, 27], as it depends non-linearly on the density matrix and thus cannot be directly associated with a quantum mechanical observable. Some expressions have been derived in the case of relaxation [28], transport [29], and general processes in open and closed quantum systems [30–32]. Experiments have been performed in systems like biomolecules [33, 34], colloidal particles [35], levitated nanoparticles [36], nuclear magnetic resonance [37], optomechanical systems and cavity Bose-Einstein condensates [27]. Some more examples of experiments up to 2013 can be found in [12, 38]. In many of these experiments, the thermal energy is much higher than the separation of quantum energy levels, thus indicating that these experiments probed classical non-equilibrium thermodynamics. In the case of the NMR experiment reported in Ref. [37], instead, it was possible to observe quantum coherences between the energy eigenstates that were not wiped out by any decoherence process. Combined with the fact that the energy level separation was of the same order as the thermal energy, one can say that this is one example of an experiment in quantum thermodynamics.

## 16.2 Stochastic Quantum Entropy Production

The definition of stochastic quantum entropy production  $\sigma$  for an arbitrary open quantum system  $\mathcal{S}$ , and the characterization of its statistics, pass through the evaluation of the quantum fluctuation theorem for such system. As discussed in the preceding

section, the latter relies on establishing forward and backward protocols for a given non-equilibrium process, which define the difference between performing such a transformation in a direction or in its time-reversed version along the arrow of time.

In small systems, negative entropy productions can occur during individual processes. Fluctuation theorems from stochastic thermodynamics can quantify the occurrence of such events, and, thus, the characterization of the statistics of  $\sigma$  is crucial for determining irreversibility [32, 39]. If we want to measure the statistics of the entropy production of an arbitrary quantum system for each input and output measurement result, we can adopt the two-time quantum measurement scheme discussed in previous chapters, that has to be in agreement with the fluctuation theorem [19, 21, 22].

To this aim, let us consider an open quantum system that undergoes a forward transformation in the interval  $[0, \tau]$  consisting of measurement, dynamical evolution and second measurement. At time  $t = 0^-$  the system is prepared in a state  $\rho_0$  and then subjected to a measurement of the observable  $\mathcal{O}_{\text{in}}$ , which is defined by the set  $\{\Pi_m^{\text{in}}\}$  of projector operators given in terms of the  $m$ th possible outcomes of the first measurement of the protocol. After the first measurement at  $t = 0^+$ , the system undergoes a time evolution, which we assume to be described by a *unital* completely positive, trace-preserving (CPTP) map  $\Phi : L(\mathcal{H}) \rightarrow L(\mathcal{H})$ , with  $L(\mathcal{H})$  denoting the sets of density operators defined on the Hilbert space  $\mathcal{H}$ . A CPTP map is unital if it preserves the identity operator  $\mathbb{1}$  on  $\mathcal{H}$ , i.e.  $\Phi(\mathbb{1}) = \mathbb{1}$ . The request of unitality covers a large family of quantum physical transformations not increasing the purity of the initial states, including, among others, unitary evolutions and decoherence processes. Such assumption, moreover, does not limit the generality of the approach, if the open quantum system  $\mathcal{S}$  is considered to be a multipartite system [32, 39].

The time-evolved dynamics of the system is then denoted as  $\rho_{\text{fin}} \equiv \Phi(\rho_{\text{in}})$ ; in case of unitary evolution with Hamiltonian  $H(t)$ , the final quantum state at  $t = \tau^-$  is  $\rho_{\text{fin}} = \Phi(\rho_{\text{in}}) = \mathcal{U}\rho_{\text{in}}\mathcal{U}^\dagger$ , where  $\mathcal{U} = \mathbb{T} \exp(-\frac{i}{\hbar} \int_0^\tau H(t)dt)$  is the unitary time evolution operator ( $\mathbb{T}$  is the time-ordering operator). After the evolution at time  $t = \tau^+$ , the second measurement of the protocol is performed on the quantum system and the observable  $\mathcal{O}_{\text{fin}}$  is measured, where  $\Pi_k^{\text{fin}}$  is the projector operator related to the  $k$ th outcome  $a_k^{\text{fin}}$ . We denote with  $\rho_\tau$  the resulting density operator, describing the ensemble average of the post-measurement state after the second measurement. For the forward process, in order to characterize the stochastic quantum entropy production we have to record only the joint probability  $p(a_k^{\text{fin}}, a_m^{\text{in}})$  that the events “measurement of  $a_m^{\text{in}}$ ” and “measurement of  $a_k^{\text{fin}}$ ” both occur in a single realization, i.e.

$$p(a_k^{\text{fin}}, a_m^{\text{in}}) = \text{Tr} [\Pi_k^{\text{fin}} \Phi(\Pi_m^{\text{in}} \rho_0 \Pi_m^{\text{in}})]. \quad (16.3)$$

To derive the backward process  $B$ , it is essential to introduce the concept of time-reversal, which relies on the time reversal symmetry (or T-symmetry). A time reversal transformation  $T_R$  overturns the time axis, i.e.  $T_R : t \mapsto -t$ . Let us stress again that time-symmetry is broken, in general, unless the system is in an equilibrium state. Time-reversal is achieved by a time-reversal operator  $\Theta$ , which acts on the system Hilbert space and has to be an antiunitary operator, since a symmetry operation on

a quantum-mechanical system can be performed only by a unitary or antiunitary operator. An operator is antiunitary if

- (i) It is anti-linear, i.e.  $\Theta(x_1|\varphi_1\rangle + x_2|\varphi_2\rangle) = x_1^* \Theta|\varphi_1\rangle + x_2^* \Theta|\varphi_2\rangle$  for arbitrary complex coefficients  $x_1, x_2$  and  $|\varphi_1\rangle, |\varphi_2\rangle \in \mathcal{H}$ ;
- (ii) It transforms the inner product as  $\langle \tilde{\varphi}_1 | \tilde{\varphi}_2 \rangle = \langle \varphi_2 | \varphi_1 \rangle$  for  $|\tilde{\varphi}_1\rangle = \Theta|\varphi_1\rangle$  and  $|\tilde{\varphi}_2\rangle = \Theta|\varphi_2\rangle$ ,
- (iii) It satisfies the relations  $\Theta^\dagger \Theta = \Theta \Theta^\dagger = \mathbb{1}$ .

The fulfilment of each of these features ensures that  $\Theta$  obeys the T-symmetry [40]. Accordingly, we define the time-reversed density operator as  $\tilde{\rho} \equiv \Theta \rho \Theta^\dagger$ . Then, in order to obtain the backward process  $B$ , we also need to introduce the time-reversal version of the quantum evolution of the system. A significant result, first shown in Ref. [41] and recently generalized in [42], states that the time-reversed quantum map  $\tilde{\Phi}$  of the CPTP map  $\Phi$  is equally CPTP and admits an operator-sum (or Kraus) representation, obeying the relation  $\sum_u \tilde{E}_u^\dagger \tilde{E}_u = \mathbb{1}$ . Accordingly, it shall be written as  $\tilde{\Phi}(\rho) = \sum_u \tilde{E}_u \rho \tilde{E}_u^\dagger$ , where  $\tilde{E}_u$  is generally expressed as a function of  $E_u^\dagger$  and the invertible fixed point of the quantum map (notice that this might not necessarily be unique). In particular, for a unital CPTP quantum map  $\tilde{E}_u = \Theta E_u^\dagger \Theta^\dagger$ . Now, we are in the position to define the backward process. At  $t = \tau^+$  the system is prepared in the state  $\tilde{\rho}_\tau = \Theta \rho_\tau \Theta^\dagger$ , and we measure the observable  $\tilde{\mathcal{O}}_{\text{ref}}$ , that is defined by the projectors  $\tilde{\Pi}_k^{\text{ref}} = |\tilde{\phi}_{a_k}\rangle \langle \tilde{\phi}_{a_k}|$ , with  $|\tilde{\phi}_{a_k}\rangle \equiv \Theta|\phi_{a_k}\rangle$ . The first measurement of the backward process is chosen equal to the time-reversed version of the second measurement of the forward process, where the state after the first measurement of the backward process is usually called *reference state*. In this regard, it is worth noting that although the quantum fluctuation theorem can be derived without imposing a specific operator for the reference state [43], we have chosen that the reference state is identically equal to the final density operator after the second measurement of the forward process. This choice appears to be the most natural among the possible ones to design a suitable scheme for the measurement of the stochastic entropy production, consistently with the quantum fluctuation theorem and the asymmetry of the second law of thermodynamics. Afterwards, in the reversal direction of the arrow of time, the reference state undergoes the time-reversal dynamical evolution, mapping it onto the initial state of the backward process  $\tilde{\rho}_{\text{in}'} = \tilde{\Phi}(\tilde{\rho}_{\text{ref}})$ , and at  $t = 0^+$  the density operator  $\tilde{\rho}_{\text{in}'}$  is subject to the second projective measurement of the backward process, whose observable is given by  $\tilde{\mathcal{O}}_{\text{in}}$  and is defined by the projectors  $\tilde{\Pi}_m^{\text{in}} = |\tilde{\psi}_{a_m}\rangle \langle \tilde{\psi}_{a_m}|$  with  $|\tilde{\psi}_{a_m}\rangle \equiv \Theta|\psi_{a_m}\rangle$ . As for the forward process, we compute the joint probability  $p(a_m^{\text{in}}, a_k^{\text{ref}})$  to simultaneously measure the outcomes  $a_m^{\text{in}}$  and  $a_k^{\text{ref}}$  in a single realization of the backward process

$$p(a_m^{\text{in}}, a_k^{\text{ref}}) = \text{Tr}[\tilde{\Pi}_m^{\text{in}} \tilde{\Phi}(\tilde{\Pi}_k^{\text{ref}} \tilde{\rho}_\tau \tilde{\Pi}_k^{\text{ref}})]. \quad (16.4)$$

As shown in Ref. [32], the combination of the two-time quantum measurement scheme with the quantum fluctuation theorem requires to perform the 2nd and 1st measurement of the backward protocol, respectively, on the same basis of the 1st and 2nd measurement of the forward process after the time-reversal transformation.

The following scheme well summarizes the forward and backward processes of the quantum fluctuation theorem:

$$\begin{array}{c} \text{FORWARD : } \rho_0 \xrightarrow[\{\Pi_m^{\text{in}}\}]{} \rho_{\text{in}} \xrightarrow[\Phi]{} \rho_{\text{fin}} \xrightarrow[\{\Pi_k^{\text{fin}}\}]{} \rho_\tau \\ \text{BACKWARD : } \tilde{\rho}_\tau \xrightarrow[\{\tilde{\Pi}_k^{\text{ref}}\}]{} \tilde{\rho}_{\text{ref}} \xrightarrow[\tilde{\Phi}]{} \tilde{\rho}_{\text{in}'} \xrightarrow[\{\tilde{\Pi}_m^{\text{in}}\}]{} \tilde{\rho}_0' \end{array}$$

Now, we can define the stochastic quantum entropy production  $\sigma$

$$\sigma(a_k^{\text{fin}}, a_m^{\text{in}}) \equiv \ln \left[ \frac{p(a_k^{\text{fin}}, a_m^{\text{in}})}{p(a_m^{\text{in}}, a_k^{\text{ref}})} \right] = \ln \left[ \frac{p(a_k^{\text{fin}}|a_m^{\text{in}})p(a_m^{\text{in}})}{p(a_m^{\text{in}}|a_k^{\text{ref}})p(a_k^{\text{ref}})} \right], \quad (16.5)$$

thus providing a general expression of the quantum fluctuation theorem for the considered open quantum system subject to a two-time quantum measurement scheme. In Eq. (16.5)  $p(a_k^{\text{fin}}|a_m^{\text{in}})$  and  $p(a_m^{\text{in}}|a_k^{\text{ref}})$  are the conditional probabilities of measuring, respectively, the outcomes  $a_k^{\text{fin}}$  and  $a_m^{\text{in}}$ , conditioned on having first measured  $a_m^{\text{in}}$  and  $a_k^{\text{ref}}$ . Its mean value

$$\langle \sigma \rangle = \sum_{k,m} p(a_k^{\text{fin}}, a_m^{\text{in}}) \ln \left[ \frac{p(a_k^{\text{fin}}, a_m^{\text{in}})}{p(a_k^{\text{in}}, a_m^{\text{ref}})} \right] \quad (16.6)$$

corresponds to the classical relative entropy (or Kullback–Leibler divergence) between the joint probabilities  $p(a^{\text{fin}}, a^{\text{in}})$  and  $p(a^{\text{in}}, a^{\text{ref}})$  of the forward and backward processes, respectively. The Kullback–Leibler divergence is always non-negative [44], and, thus,  $\langle \sigma \rangle \geq 0$ . Here, it is worth noting how these relations are strongly connected to the results highlighted in the previous section of this chapter. In particular,  $\langle \sigma \rangle$  is effectively the amount of additional information that is required to achieve the backward process, once the quantum system has reached the final state  $\rho_\tau$ , and  $\langle \sigma \rangle = 0$  if and only if  $p(a_k^{\text{fin}}, a_m^{\text{in}}) = p(a_m^{\text{in}}, a_k^{\text{ref}})$ , i.e. if and only if  $\sigma = 0$ . Thus, the transformation from  $t = 0^-$  to  $t = \tau^+$  can be defined to be thermodynamically irreversible if  $\langle \sigma \rangle > 0$ . When, instead, all the fluctuations of  $\sigma$  shrink around  $\langle \sigma \rangle \simeq 0$  the system comes closer and closer to be reversible. We observe that a system transformation may be thermodynamically irreversible also if the system undergoes unitary evolutions with the corresponding irreversibility contributions due to applied quantum measurements. Also the measurements back-actions, indeed, lead to energy fluctuations of the quantum system. In case there is no evolution (identity map) and the two measurement operators are the same, then the transformation becomes reversible. Finally, we note that if the CPTP quantum map  $\Phi$  is unital, then  $p(a_k^{\text{fin}}|a_m^{\text{in}}) = p(a_m^{\text{in}}|a_k^{\text{ref}})$ , and the stochastic quantum entropy production  $\sigma$  turns out to be equal to

$$\sigma(a_k^{\text{fin}}, a_m^{\text{in}}) = \ln \left[ \frac{p(a_m^{\text{in}})}{p(a_k^{\text{ref}})} \right] = \ln \left[ \frac{\langle \psi_{a_m} | \rho_0 | \psi_{a_m} \rangle}{\langle \tilde{\phi}_{a_k} | \tilde{\rho}_\tau | \tilde{\phi}_{a_k} \rangle} \right]. \quad (16.7)$$

### 16.2.1 Connection with the Quantum Relative Entropy

The irreversibility of an arbitrary system transformation within a two-time measurement scheme for an open quantum system in interaction with the environment is encoded in the mean stochastic entropy production  $\langle \sigma \rangle$ . In Ref.[32], it has been proved the relation between  $\langle \sigma \rangle$  and the quantum relative entropy of the system density matrix in correspondence of the final time of the system transformation for unital CPTP quantum maps. Accordingly, under the hypotheses that (i) the reference state of the quantum fluctuation theorem is identically equal to the final density operator after the second measurement of the forward process and (ii) the first measurement of the backward process is chosen equal to the time-reversed version of the second measurement of the forward process (both hypotheses originate from the introduction of the two-time measurement scheme for the measure of  $\sigma$ ), the quantum relative entropy  $S(\rho_{\text{fin}} \parallel \rho_\tau)$  fulfills the following inequality:

$$0 \leq S(\rho_{\text{fin}} \parallel \rho_\tau) \leq \langle \sigma \rangle, \quad (16.8)$$

where the equality  $S(\rho_{\text{fin}} \parallel \rho_\tau) = 0$  holds if and only if  $\rho_{\text{fin}} = \rho_\tau$ . Moreover, for  $[\mathcal{O}_{\text{fin}}, \rho_{\text{fin}}] = 0$  one has  $\langle \sigma \rangle = S(\rho_\tau) - S(\rho_{\text{in}})$ , so that

$$0 = S(\rho_{\text{fin}} \parallel \rho_\tau) \leq \langle \sigma \rangle = S(\rho_{\text{fin}}) - S(\rho_{\text{in}}), \quad (16.9)$$

where  $S(\rho) = -\text{tr}(\rho \ln \rho)$  is the von Neumann entropy. For a closed quantum system following a unitary evolution,  $S(\rho_{\text{fin}} \parallel \rho_\tau) = \langle \sigma \rangle$ . This result is in agreement with Eq.(16.2) [24, 25, 45], which provides a microscopic measure (in terms of the Kullback–Leibler relative entropy) of the distinguishability between the system trajectories, respectively, in the forward and backward process, when the initial state of the quantum system in both processes corresponds to a Gibbs equilibrium induced by an external thermal bath. While Eq.(16.8) is more general and includes the irreversibility contributions of both the map  $\Phi$  and the final measurement, in Eq.(16.9) due to a special choice of the observable of the second measurement we obtain  $\rho_{\text{fin}} = \rho_\tau$  and, thus, the quantum relative entropy vanishes while the stochastic quantum entropy production contains the irreversibility contribution only from the map, which is given by the difference between the von Neumann entropy of the final state  $S(\rho_{\text{fin}})$  and the initial one  $S(\rho_{\text{in}})$ .

### 16.2.2 Statistics of Quantum Entropy Production

The statistics of the stochastic quantum entropy production  $\sigma$  can be computed by evaluating the corresponding probability distribution  $\text{Prob}(\sigma)$ . Indeed, depending on the values assumed by the measurement outcomes  $\{a^{\text{in}}\}$  and  $\{a^{\text{fin}}\}$ ,  $\sigma$  is a fluctuating variable. Thus, each time we repeat the experiment described above for the measure

of the stochastic quantum entropy production, we shall have a different realization for  $\sigma$ , within a set of discrete values in case  $\mathcal{S}$  is finite dimensional. The probability distribution of  $\sigma$  is thus fully determined by the knowledge of the measurement outcomes and the respective probabilities (relative frequencies). In particular, let us consider again  $p(a_k^{\text{fin}}, a_m^{\text{in}})$ , which denotes the joint probability to obtain the measurement outcomes  $a_m^{\text{in}}$  and  $a_k^{\text{fin}}$ . We have

$$p(a_k^{\text{fin}}, a_m^{\text{in}}) = \text{Tr} [\Pi_k^{\text{fin}} \Phi(\Pi_m^{\text{in}})] p(a_m^{\text{in}}), \quad (16.10)$$

where  $p(a_m^{\text{in}})$  is the probability to obtain the measurement outcome  $a_m^{\text{in}}$  after the first measurement of the forward process. Accordingly, the probability distribution  $\text{Prob}(\sigma)$  turns out to be

$$\begin{aligned} \text{Prob}(\sigma) &= \langle \delta [\sigma - \sigma(a_m^{\text{in}}, a_k^{\text{fin}})] \rangle \\ &= \sum_{k,m} \delta [\sigma - \sigma(a_m^{\text{in}}, a_k^{\text{fin}})] p(a_k^{\text{fin}}, a_m^{\text{in}}), \end{aligned} \quad (16.11)$$

where  $\delta[\cdot]$  is the Dirac-delta distribution.

In the frequency domain, the properties of the corresponding probability distribution  $\text{Prob}(\sigma)$  are completely defined by its Fourier transform, i.e. its characteristic function. The latter, similarly to the what is commonly done for the work and heat distribution [46], is a key quantity to be indirectly measured for the inference of the statistics of  $\sigma$ , and, thus, of the irreversibility for an open quantum system. The characteristic function  $G(u)$  of the probability distribution  $\text{Prob}(\sigma)$ , with  $u \in \mathbb{C}$  complex number, is defined as

$$G(u) = \int \text{Prob}(\sigma) e^{iu\sigma} d\sigma. \quad (16.12)$$

By substituting in Eq. (16.12) the expression of the probability distribution  $\text{Prob}(\sigma)$  and exploiting the linearity of the CPTP quantum maps and of the trace (with  $\Phi$  unital), the characteristic functions can be written in the following form:

$$G(u) = \text{Tr} [\rho_{\tau}^{-iu} \Phi(\rho_{\text{in}}^{1+iu})], \quad (16.13)$$

that will be used to effectively measure the thermodynamic irreversibility of  $\mathcal{S}$ . Moreover, by choosing  $u = i$ , we recover the Jarzynski identity  $\langle e^{-\sigma} \rangle \equiv G(i) = \text{Tr} \{ \rho_{\tau} \Phi [\mathbb{1}] \} = 1$  for the stochastic quantum entropy production  $\sigma$ , also called *integral quantum fluctuation theorem* [43].

### 16.2.3 Measuring Irreversibility

Until now experiments for the measurement of the quantum entropy production statistics of an open quantum system have not been performed, even if in [32] a

procedure has recently been proposed. The latter is based on quantum estimation methods, and relies on the indirect measurement of the characteristic function  $G(u = i\gamma) \equiv \langle e^{-\gamma o} \rangle$  for a set of values of  $\gamma \in \mathbb{R}$ . In particular, the characteristic function  $G(u = i\gamma)$  depends exclusively on suitable powers of the initial and final density operators of the quantum system  $\mathcal{S}$ , and these density operators are diagonal in the basis of the observable eigenvectors. Thus, they can be measured by means of standard state population measurements for each value of  $\gamma$ . This result can lead to a significant reduction of the number of measurements that is required to reconstruct the probability distribution  $\text{Prob}(\sigma)$ , beyond the direct application of the definition of Eq. (16.11).

Here, we will show in a nutshell the procedure for the indirect measurement of the characteristic function  $G(u = i\gamma)$ , leading then to the statistics of  $\sigma$ : (i) Prepare the initial product state  $\rho_{\text{in}} = \sum_m \Pi_m^{\text{fin}} p(a_m^{\text{in}})$ , which is diagonal in the basis composed by the eigenvectors of the first measurement observable  $\mathcal{O}_{\text{in}}$  and, thus, defined by the probabilities  $p(a_m^{\text{in}})$ . Then, after the quantum system is evolved within the time interval  $[0, \tau]$ , measure the occupation probabilities  $p(a_k^{\text{fin}})$  and compute the stochastic quantum entropy production  $\sigma$  as given in Eq. (16.6). (ii) For every chosen value of  $\gamma$  (one possible choice for the optimal values of the set of real parameters  $\{\gamma\}$  has been discussed in Ref. [32, 39]), prepare the quantum system in the states  $\hat{\rho}_{\text{in}}(\gamma) \equiv \rho_{\text{in}}^{1-\gamma} / \text{Tr}[\rho_{\text{in}}^{1-\gamma}]$ , and let it evolve. (iii) As we have that

$$\begin{aligned} G(i\gamma) &= \sum_k \sum_m \langle k | p(a_k^{\text{fin}})^\gamma | m \rangle \langle m | \Phi(\hat{\rho}_{\text{in}}(\gamma)) | k \rangle \\ &= \sum_k p(a_k^{\text{fin}})^\gamma \langle k | \Phi(\hat{\rho}_{\text{in}}(\gamma)) | k \rangle, \end{aligned} \quad (16.14)$$

after performing a trace operation with respect to the orthonormal basis which spans the Hilbert space of  $\mathcal{S}$ , measure the occupation probabilities  $\langle k | \Phi(\hat{\rho}_{\text{in}}(\gamma)) | k \rangle$ , so as to finally obtain  $G(i\gamma)$ .

It is worth observing that the evaluation of the characteristic functions  $G(i\gamma)$  relies only on the measure of occupation probabilities, and, thus, the proposed procedure does not require full tomography. Moreover, quite remarkably, for the three steps of the procedure the required number of measurements scales linearly with the number of possible measurement outcomes (coming from the system at the initial and final stages of the transformation), or equivalently with the number of values that can be assumed by the stochastic quantum entropy production  $\sigma$ . In conclusion, the described procedure is able to reconstruct the statistics of the stochastic quantum entropy production without directly measuring the joint probabilities  $p(a_k^{\text{fin}}, a_m^{\text{in}})$ , which instead to realize all the combinatorics concerning the measurement outcomes would require a greater number of measurements, scaling with the square of the values assumed by  $\sigma$ .

As a final remark, note that this stochastic approach for the quantification of irreversibility can also be applied to systems composed of more than a single particle. Indeed, in such a case the method would rely on considering as effective dimension

of the composite system the one that would allow for a unital dynamics. Then, the entropy production of each subsystem would be characterised as a function of the entropy generated by the whole system.

### 16.3 An Alternative Formulation to Entropy Production

This section aims at pointing out a relevant shortcoming of the formulation of entropy production in terms of the relative entropy, as discussed above. In doing so, we shall highlight a potential resolution of such issues based on the use of generalised entropy functions. The focus of our analysis is that of open quantum systems and, in order to fix the ideas, we shall assume that the dynamics of the system may be modeled by a Lindblad master equation of the form

$$\frac{d\rho_t}{dt} = -i[H, \rho_t] + \mathcal{D}(\rho_t), \quad (16.15)$$

where, as before,  $\rho_t$  is the density matrix of the system,  $H$  is its Hamiltonian, while  $\mathcal{D}(\rho_t)$  describes the dissipative process arising from its coupling to the external reservoir. In these conditions, it is often convenient to identify the formal contributions to the change of total entropy  $\Sigma(t)$  of the state of the system in terms of the equation

$$\frac{d\Sigma(t)}{dt} = \Pi(t) - \Phi(t), \quad (16.16)$$

where  $\Pi \geq 0$  is the entropy production rate and  $\Phi$  is the entropy flux rate, from the system to the environment. The entropy production rate  $\Pi$  is expected to be non-zero as long as the system is out of equilibrium. This includes transient states and non-equilibrium steady-states (NESSs), where  $d\Sigma(t)/dt = 0$  and therefore  $\Pi = \Phi > 0$ . The quantities  $\Pi$  and  $\Phi$  are not direct observables and must therefore be related to experimentally accessible quantities via a theoretical framework.

Let  $\rho^*$  denote the target state of  $\mathcal{D}(\rho_t)$  (for thermal baths  $\rho^* = \rho_{\text{eq}} = e^{-\beta H}/Z$ ). The formulation highlighted in the previous section of this chapter in terms of the relative entropy would lead us to the following expression for the entropy production rate [31, 47, 48]

$$\Pi = -\frac{d}{dt} S(\rho_t || \rho^*). \quad (16.17)$$

While we have already commented on the fact that this formulation satisfies several expected properties for an entropy production, it is worth pointing out that, for a thermal bath, Eq. (16.17) may be factored in the form of Eq. (16.16), with  $\Sigma(t)$  being equal to the von Neumann entropy, so that

$$\Phi(t) = -\frac{1}{T} \text{tr} \left[ H \mathcal{D}(\rho) \right] \equiv \frac{\Phi_E}{T}, \quad (16.18)$$

where  $\Phi_E$  denotes the energy flux from the system to the environment. This is the well known Clausius equality of classical thermodynamics.

Despite their clear physical interpretation, a unified approach for the formulation of entropy production beyond the limitations of such educated cases is still lacking: quantum systems open up the possibility for exploring environmental systems that go beyond the paradigm of equilibrium baths. Striking instances of this are dephasing noises and squeezed baths, whose description extends beyond the usual paradigms of equilibrium baths. Moreover, and quite remarkably, although  $d\Sigma/dt$  remains finite, Eqs. (16.17) and (16.18) diverge in the limit of zero temperature of the reservoir, owing to the divergence of the relative entropy when the reference state tends to a pure state [49, 50]. This divergence is clearly an inconsistency of the theory.

Fortunately, a theory of entropy production that is applicable to systems exposed to non-equilibrium reservoirs and that cures the divergence at zero temperature is possible [51]. The key to such alternative theory is the replacement of the von Neumann entropy, which is the pillar upon which the formulations illustrated in the previous sections have been built, with the Rényi-2 entropy. The latter has a similar behaviour to von Neumann's, but is much more convenient to manipulate, and is not pathological when pure reference states are considered.

In order to provide a framework where analytic expressions are possible, which will serve the purpose of illustration, we focus on bosonic systems characterized by Gaussian states. In this case the Rényi-2 entropy coincides (up to a constant) with the Wigner entropy [52]

$$S_{\mathcal{W}} = - \int d^2\alpha \mathcal{W}(\alpha^*, \alpha) \ln \mathcal{W}(\alpha^*, \alpha), \quad (16.19)$$

where  $\mathcal{W}(\alpha^*, \alpha)$  is the Wigner function and the integral is over the entire complex plane. Gaussian states have a positive Wigner function, which ensures that  $S_{\mathcal{W}}$  is real. This link between the Rényi-2 entropy and the Wigner entropy allows for a fundamental simplification of the problem, since one may map the open system dynamics into a Fokker–Planck equation for  $\mathcal{W}$  and hence employ tools of classical stochastic processes to obtain simple expressions for  $\Pi$  and  $\Phi$ . This idea was already used in Refs. [27, 53] via a quantum-to-classical correspondence to treat the case of simple heat baths. Ref. [51] has instead demonstrated the possibility to successfully address squeezed and dephasing reservoirs, while keeping the entropy flux and entropy production rate finite for a system in contact with a thermal reservoir at zero temperature. Remarkably, for an harmonic oscillator, compact and physically clear expressions are possible for such quantities. Following Ref. [51], we have

$$\begin{aligned} \Pi &= \frac{4}{\gamma(\bar{n} + 1/2)} \int d^2\alpha \frac{|J(\mathcal{W})|^2}{\mathcal{W}}, \\ \Phi &= \frac{\gamma}{\bar{n} + 1/2} (\langle N \rangle - \bar{n}), \end{aligned} \quad (16.20)$$

where  $\gamma$  is the damping rate of the oscillator,  $\langle N \rangle$  is the mean excitation number for the harmonic oscillator,  $\bar{n}$  is the analogous quantity for the bath, and

$$J(\mathcal{W}) = \frac{\gamma}{2} \left[ \alpha \mathcal{W} + (\bar{n} + 1/2) \partial_{\alpha^*} \mathcal{W} \right], \quad (16.21)$$

with  $\alpha$  the complex phase-space variable of the Wigner function. It can be shown that  $J$  is in a relation with the phase-space version of the dissipator  $\mathcal{D}$  akin to a continuity equation. Specifically [51]

$$\mathcal{D}(\mathcal{W}) = \partial_\alpha J(\mathcal{W}) + \partial_{\alpha^*} J^*(\mathcal{W}), \quad (16.22)$$

which leads to the interpretation of  $J(\mathcal{W})$  as an *irreversible* component of the probability current that is null only when the target state is a thermal one (stating the nullity of all probability currents, in this case). The inspection of Eq. (16.20) shows that, even for zero-temperature baths,  $\Phi$  remains finite. In light of the relation between total entropy rate,  $\Phi$  and  $\Pi$ , we deduce that also  $\Pi$  does not diverge in such a limit, therefore providing a much more satisfactory result than the one arising from an approach based on the von Neumann entropy. The generalization to other types of baths is straightforward [51].

## 16.4 Conclusions

We have illustrated the current formulation of entropy production in both closed and open systems, highlighting its features and issues, and proposing suitable modifications aimed at defining a full-fledged framework for the characterisation of irreversibility.

**Acknowledgements** TBB acknowledges support from National Research Foundation (Singapore), Ministry of Education (Singapore), and United States Air Force Office of Scientific Research (FA2386-15-1-4082). He acknowledges helpful discussions with R. M. Serra and his group at Universidade Federal do ABC, while developing some of the work reported in this chapter as part of his Ph.D. thesis. SG gratefully thanks Filippo Caruso, Stefano Ruffo, Andrea Trombettoni, and Matthias M. Mueller for useful discussions and their support, especially during the last period of his PhD thesis. GTL would like to acknowledge the São Paulo Research Foundation, under grant number 2016/08721-7. JPS would like to acknowledge the financial support from the CAPES (PNPD program) for the postdoctoral grant. MP thanks the DfE-SFI Investigator Programme (grant 15/IA/2864), the Royal Society Newton Mobility Grant NI160057, and the H2020 collaborative Project TEQ (grant no. 766900).

## References

1. A.S. Eddington, *The Nature of the Physical World* (Folcroft Library Editions, Delaware, 1935)
2. L. Onsager, Reciprocal relations in irreversible processes. I. Phys. Rev. **37**, 405 (1931). <https://doi.org/10.1103/PhysRev.37.405>
3. L. Onsager, Reciprocal relations in irreversible processes. II. Phys. Rev. **38**, 2265 (1931). <https://doi.org/10.1103/PhysRev.38.2265>
4. S. Machlup, L. Onsager, Fluctuations and irreversible process. II. Systems with kinetic energy. Phys. Rev. **91**, 1512 (1953). <https://doi.org/10.1103/PhysRev.91.1512>
5. S.R. de Groot, P. Mazur, *Non-Equilibrium Thermodynamics*, 1st edn. (North-Holland Physics Publishing, Amsterdam, 1961)
6. L. Tisza, I. Manning, Fluctuations and irreversible thermodynamics. Phys. Rev. **105**, 1695 (1957). <https://doi.org/10.1103/PhysRev.105.1695>
7. J. Schnakenberg, Network theory of microscopic and macroscopic behavior of master equation systems. Rev. Mod. Phys. **48**, 571 (1976). <https://doi.org/10.1103/RevModPhys.48.571>
8. T. Tomé, M.J. de Oliveira, Entropy production in nonequilibrium systems at stationary states. Phys. Rev. Lett. **108**, 020601 (2012). <https://doi.org/10.1103/PhysRevLett.108.020601>
9. T. Tomé, M.J. de Oliveira, Entropy production in irreversible systems described by a Fokker-Planck equation. Phys. Rev. E **82**, 021120 (2010). <https://doi.org/10.1103/PhysRevE.82.021120>
10. R.E. Spinney, I.J. Ford, Entropy production in full phase space for continuous stochastic dynamics. Phys. Rev. E **85**, 051113 (2012). <https://doi.org/10.1103/PhysRevE.85.051113>
11. G.T. Landi, T. Tomé, M.J. de Oliveira, Entropy production in linear Langevin systems. J. Phys. A **46**, 395001 (2013). <https://doi.org/10.1088/1751-8113/46/39/395001>
12. U. Seifert, Stochastic thermodynamics, fluctuation theorems and molecular machines. Rep. Prog. Phys. **75**, 126001 (2012). <https://doi.org/10.1088/0034-4885/75/12/126001>
13. D.J. Evans, E.G.D. Cohen, G.P. Morriss, Probability of second law violations in shearing steady states. Phys. Rev. Lett. **71**, 2401 (1993). <https://doi.org/10.1103/PhysRevLett.71.2401>
14. D.J. Evans, D.J. Searles, Equilibrium microstates which generate second law violating steady states. Phys. Rev. E **50**, 1645 (1994). <https://doi.org/10.1103/PhysRevE.50.1645>
15. G. Gallavotti, E.G.D. Cohen, Dynamical ensembles in nonequilibrium statistical mechanics. Phys. Rev. Lett. **74**, 2694 (1995). <https://doi.org/10.1103/PhysRevLett.74.2694>
16. C. Jarzynski, Nonequilibrium equality for free energy differences. Phys. Rev. Lett. **78**, 2690 (1997). <https://doi.org/10.1103/PhysRevLett.78.2690>
17. C. Jarzynski, Equilibrium free-energy differences from nonequilibrium measurements: a master-equation approach. Phys. Rev. E **56**, 5018 (1997). <https://doi.org/10.1103/PhysRevE.56.5018>
18. G.E. Crooks, Nonequilibrium measurements of free energy differences for microscopically reversible Markovian systems. J. Stat. Phys. **90**, 1481 (1998). <https://doi.org/10.1023/A:102308217925>
19. G.E. Crooks, Path-ensemble averages in systems driven far from equilibrium. Phys. Rev. E **61**, 2361 (2000). <https://doi.org/10.1103/PhysRevE.61.2361>
20. J. Goold, F. Plastina, A. Gambassi, A. Silva, The role of quantum work statistics in many-body physics (2018). [arXiv:1804.02805](https://arxiv.org/abs/1804.02805)
21. M. Campisi, P. Hänggi, Fluctuation, dissipation and the arrow of time. Entropy **13**, 2024–2035 (2011). <https://doi.org/10.3390/e13122024>
22. C. Jarzynski, Equalities and inequalities: irreversibility and the second law of thermodynamics at the nanoscale. Ann. Rev. Condens. Mat. Phys. **2**, 329 (2011). <https://doi.org/10.1146/annurev-commatphys-062910-140506>
23. R. Kawai, J.M.R. Parrondo, C. Van den Broeck, Dissipation: the phase-space perspective. Phys. Rev. Lett. **98**, 080602 (2007). <https://doi.org/10.1103/PhysRevLett.98.080602>
24. S. Vaikuntanathan, C. Jarzynski, Dissipation and lag in irreversible processes. Europhys. Lett. **87**, 60005 (2009). <https://doi.org/10.1209/0295-5075/87/60005>

25. J.M.R. Parrondo, C. Van den Broeck, R. Kawai, Entropy production and the arrow of time. *New J. Phys.* **11**, 073008 (2009). <https://doi.org/10.1088/1367-2630/11/7/073008>
26. G.T. Landi, T. Tomé, M.J. de Oliveira, Entropy production in linear Langevin systems. *J. Phys. A Math. Theor.* **46**, 395001 (2013). <https://doi.org/10.1088/1751-8113/46/39/395001>
27. M. Brunelli, L. Fusco, R. Landig, W. Wieczorek, J. Hoelscher-Obermaier, G. Landi, F.L. Semião, A. Ferraro, N. Kiesel, T. Donner, G. De Chiara, M. Paternostro, Experimental determination of irreversible entropy production in out-of-equilibrium mesoscopic quantum systems. *Phys. Rev. Lett.* **121**, 160604 (2018). <https://doi.org/10.1103/PhysRevLett.121.160604>
28. F. Schloegl, Stochastic measures in nonequilibrium thermodynamics. *Phys. Rep.* **62**, 267 (1980). [https://doi.org/10.1016/0370-1573\(80\)90019-8](https://doi.org/10.1016/0370-1573(80)90019-8)
29. H. Spohn, J.L. Lebowitz, Irreversible thermodynamics for quantum systems weakly coupled to thermal reservoirs, *Advances in Chemical Physics: For Ilya Prigogine* (Wiley, New Jersey, 2007). <https://doi.org/10.1002/9780470142578.ch2>
30. S. Deffner, E. Lutz, Generalized clausius inequality for nonequilibrium quantum processes. *Phys. Rev. Lett.* **105**, 170402 (2010). <https://doi.org/10.1103/PhysRevLett.105.170402>
31. S. Deffner, E. Lutz, Nonequilibrium Entropy production for open quantum systems. *Phys. Rev. Lett.* **107**, 140404 (2011). <https://doi.org/10.1103/PhysRevLett.107.140404>
32. S. Gherardini, M.M. Mueller, A. Trombettoni, S. Ruffo, F. Caruso, Reconstructing quantum entropy production to probe irreversibility and correlations. *Quantum Sci. Technol.* **3**(3), 035013 (2018). <https://doi.org/10.1088/2058-9565/aac7e1>
33. J. Liphardt, S. Dumont, S.B. Smith, I. Tinoco, C. Bustamante, Equilibrium information from nonequilibrium measurements in an experimental test of Jarzynski's equality. *Science* **296**, 1832 (2002). <https://doi.org/10.1126/science.1071152>
34. D. Collin, F. Ritort, C. Jarzynski, S.B. Smith, I. Tinoco, C. Bustamante, Verification of the Crooks fluctuation theorem and recovery of RNA folding free energies. *Nature* **437**, 231 (2005). <https://doi.org/10.1038/nature04061>
35. V. Blickle, T. Speck, L. Helden, U. Seifert, C. Bechinger, Thermodynamics of a colloidal particle in a time-dependent nonharmonic potential. *Phys. Rev. Lett.* **96**, 070603 (2006). <https://doi.org/10.1103/PhysRevLett.96.070603>
36. J. Gieseler, R. Quidant, C. Dellago, L. Novotny, Dynamic relaxation of a levitated nanoparticle from a non-equilibrium steady state. *Nature Nanotech.* **9**, 358 (2014). <https://doi.org/10.1038/nnano.2014.40>
37. T.B. Batalhão, A.M. Souza, R.S. Sarthour, I.S. Oliveira, M. Paternostro, E. Lutz, R.M. Serra, Irreversibility and the arrow of time in a quenched quantum system. *Phys. Rev. Lett.* **115**, 190601 (2015). <https://doi.org/10.1103/PhysRevLett.115.190601>
38. S. Ciliberto, R. Gomez-Solano, A. Petrosyan, Fluctuations, linear response, and currents in out-of-equilibrium systems. *Ann. Rev. Condens. Matter Phys.* **4**, 235 (2013). <https://doi.org/10.1146/annurev-conmatphys-030212-184240>
39. S. Gherardini, Noise as a Resource. Ph.D. thesis, University of Florence (Italy, 2018). [arXiv:1805.01800](https://arxiv.org/abs/1805.01800)
40. M. Sozzi, *Discrete Symmetries and CP Violation* (Oxford University Press, Oxford, 2008)
41. G. Crooks, Quantum operation time reversal. *Phys. Rev. A* **77**, 034101 (2008). <https://doi.org/10.1103/PhysRevA.77.034101>
42. G. Manzano, J.M. Horowitz, J.M.R. Parrondo, Nonequilibrium potential and fluctuation theorems for quantum maps. *Phys. Rev. E* **92**, 032129 (2015). <https://doi.org/10.1103/PhysRevE.92.032129>
43. T. Sagawa, in *Lectures on Quantum Computing, Thermodynamics and Statistical Physics*, ed. by N. Mikio, et al. (World Scientific Publishing Co. Pte. Ltd, Singapore, 2013)
44. T. Cover, J. Thomas, *Elements of Information Theory* (Wiley-Interscience, New Jersey, 2006)
45. R. Kawai, J.M.R. Parrondo, C. Van der Broeck, Dissipation: the phase-space perspective. *Phys. Rev. Lett.* **98**, 080602 (2007). <https://doi.org/10.1103/PhysRevLett.98.080602>

46. S. Gherardini, et al. Nonequilibrium quantum-heat statistics under stochastic projective measurements. *Phys. Rev. E* **98**(3), 032108 (2018). <https://doi.org/10.1103/PhysRevE.98.032108>
47. H.-P. Breuer, Quantum jumps and entropy production. *Phys. Rev. A* **68**, 032105 (2003). <https://doi.org/10.1103/PhysRevA.68.032105>
48. H.-P. Breuer, F. Petruccione, *The Theory of Open Quantum Systems* (Oxford University Press, Oxford, 2007). <https://doi.org/10.1093/acprof:oso/9780199213900.001.0001>
49. S. Abe, Nonadditive generalization of the quantum Kullback-Leibler divergence for measuring the degree of purification. *Phys. Rev. A* **68**, 032302 (2003). <https://doi.org/10.1103/PhysRevA.68.032302>
50. K.M.R. Audenaert, Quantum skew divergence. *J. Math. Phys.* **55**, 112202 (2014). <https://doi.org/10.1063/1.4901039>
51. J.P. Santos, G. Landi, M. Paternostro, Wigner entropy production rate. *Phys. Rev. Lett.* **118**, 220601 (2017). <https://doi.org/10.1103/PhysRevLett.118.220601>
52. G. Adesso, D. Girolami, A. Serafini, Measuring Gaussian quantum information and correlations using the Rényi entropy of order 2. *Phys. Rev. Lett.* **109**, 190502 (2012). <https://doi.org/10.1103/PhysRevLett.109.190502>
53. M. Brunelli, M. Paternostro, Irreversibility and correlations in coupled quantum oscillators (2016). [arXiv:1610.01172v1](https://arxiv.org/abs/1610.01172v1)

## **Part III**

# **Equilibration and Thermalization**

# Chapter 17

## Dynamical Typicality for Initial States with a Preset Measurement Statistics of Several Commuting Observables



**Ben N. Balz, Jonas Richter, Jochen Gemmer, Robin Steinigeweg  
and Peter Reimann**

### 17.1 Introduction and Overview

Why are macroscopic experiments reproducible, although the molecular details in each repetition of the experiment are largely unknown and not reproducible? A first path breaking step towards answering this question was established by Bartsch and Gemmer [1], putting forward the following so-called dynamical typicality property: The overwhelming majority of all pure states, which exhibit very similar expectation values of a generic observable at some initial time, will yield very similar expectation values for this observable also at any later time point, provided the relevant Hilbert space is of large (but finite) dimension. In proving this statement, a technical assumption is needed, which can strictly speaking only be taken for granted if the given initial expectation value differs sufficiently little from the expectation value in the corresponding microcanonical equilibrium state [1].

Here, we work out a significant extension of the original dynamical typicality scenario from Ref. [1]. Namely, we consider the set of all initial states, which now may be either pure or mixed, and for which all possible measurement outcomes for several commuting observables exhibit certain preset expectation values (projection probabilities). Similarly as in [1], we then show that upon evolving those initial states according to the pertinent Schrödinger or von Neumann equation up to some later time point, the vast majority of them still gives rise to very similar expectation values for any given observable. But unlike in [1], the latter observable may now be different from those which determine the initial conditions, and the dynamics may be governed by an arbitrary, possibly even explicitly time dependent Hamiltonian.

---

B. N. Balz (✉) · P. Reimann

Fakultät für Physik, Universität Bielefeld, 33615 Bielefeld, Germany  
e-mail: bbalz@physik.uni-bielefeld.de

J. Richter · J. Gemmer · R. Steinigeweg

Department of Physics, University of Osnabrück, 49069 Osnabrück, Germany

With respect to our analytical explorations, certain partial aspects are also related to numerous previous works, for instance Refs. [2–7]. Yet the main physical conclusions as well as the technical methods are quite different. Concerning the numerical applications, the basic concepts together with the relevant previous literature will be reviewed in the last section.

Our present topic of dynamical typicality also exhibits certain similarities with non-dynamical typicality phenomena, originally due to Lloyd [8], and independently rediscovered under the labels “canonical typicality” and “concentration of measure effects” in Refs. [9, 10], see also [4, 11–15]. In those non-dynamical typicality explorations, the focus is on *all* quantum states of a high dimensional Hilbert space, without any further restriction regarding the expectation value of some observable, and without considering the temporal evolution of those states. The key result in this context is that the expectation value of any given observable is for the overwhelming majority of those states extremely close to the pertinent microcanonical (thermal equilibrium) expectation value of the high dimensional Hilbert space under consideration. A first main virtue of the present dynamical typicality approach is to pick out a small subsets of states with distinct non-thermal features, and then to prove typicality properties of their further evolution in time.

Another main virtue of such an approach is to admit statements about the time evolution without actually solving the dynamics. As exemplified by Chaps. 18 and 19, the latter is a very challenging task in itself and is outside the conceptual framework of our present chapter. On the other hand, our approach goes beyond the scope of Chaps. 18, 19 and 20 in that our systems are in general not even required to exhibit equilibration or thermalization in the long time limit. Moreover, our dynamical typicality based numerical scheme can deal with considerably larger systems than many other methods, such as exact diagonalization.

## 17.2 General Framework

We consider quantum mechanical model systems, which can be described by a Hilbert space  $\mathcal{H}$  of large but finite dimension  $D$ . The initial state of the system will be specified in terms of a set of commuting observables,<sup>1</sup> whose common eigenspaces are denoted as  $\mathcal{H}_n$  with  $n = 1, \dots, N$ . Hence the projectors  $P_n$  onto those subspaces  $\mathcal{H}_n$  satisfy  $P_m P_n = \delta_{mn} P_n$  and  $\sum_{n=1}^N P_n = \mathbb{1}_{\mathcal{H}}$  (identity on  $\mathcal{H}$ ), and the dimensions of the  $\mathcal{H}_n$  are given by

$$d_n = \text{Tr}\{P_n\} , \quad (17.1)$$

with  $D = \sum_{n=1}^N d_n$ .

---

<sup>1</sup>The set of commuting observables is not required to be complete, and even a single observable is admissible.

Denoting by  $\rho(0)$  any density operator (pure or mixed system state) at the initial time  $t = 0$ , and considering the  $P_n$ 's as observables, the corresponding expectation values (projection probabilities) are given by

$$p_n = \text{Tr}\{\rho(0) P_n\} \quad (17.2)$$

with  $p_n \geq 0$  and  $\sum_{n=1}^N p_n = 1$ . At the focus of our present investigation will be the set of all initial states  $\rho(0)$  which satisfy the  $N$  constraints (17.2) for arbitrary but fixed values of the projection probabilities  $\{p_n\}_{n=1}^N$ .

Physically speaking, we have mainly quantum many-body systems in mind where, following von Neumann [16], it seems reasonable to expect that a simultaneous measurement of two or more (almost) commuting observables is indeed feasible. In many cases, some or all of those observables will correspond to macroscopic (coarse grained) quantities and one of them will usually be the energy (coarse grained Hamiltonian). Although such an (approximate) commutation of those coarse grained observables is usually rather difficult to justify more rigorously, it is commonly considered as a plausible working hypothesis [15, 17–22]. For example, we may be dealing with multiple macroscopic observables, that can be measured simultaneously, or with a single microscopic observable together with the coarse grained Hamiltonian: Indeed, it appears as a decent working hypothesis to assume that the measurement, e.g., of a single particle velocity leaves the (coarse grained) energy distribution of the many-body system practically unaffected. On the other hand multiple microscopic observables are not expected to commute even approximately. It should be emphasized that within this mindest not the exact Hamiltonian, which governs the dynamics, but only its coarse grained counterpart is imagined to (approximately) commute with the coarse grained macroscopic observables. In particular, the observables are not required to be conserved quantities. We also emphasize that this physical interpretation of the considered mathematical setup will never be actually used in our subsequent calculations.

Our next observation is that any real measurement device can only exhibit a limited number of different possible outcomes. For instance, a digital instrument with  $K$  digits can only display  $10^K$  different measurement values. Hence, we can and will assume that the number  $N$  of common eigenspaces of all the commuting observables at hand respects some reasonable bound, say

$$N \leq 10^{20}. \quad (17.3)$$

Differently speaking, the number of commuting observables as well as their resolution limits are assumed to remain experimentally realistic. In principle, also very low  $N$  values are conceivable and admitted in what follows. In the extreme case, there may be just one observable with two different possible measurement outcomes, implying  $N = 2$ .

On the other hand, for generic macroscopic systems with typically  $f \approx 10^{23}$  degrees of freedom, the dimension  $D$  of the relevant Hilbert space is exponentially large in  $f$ . For instance,  $\mathcal{H}$  may be an energy shell, spanned by the eigenvalues of the system Hamiltonian with eigenenergies within an energy interval, which is macroscopically small (well defined macroscopic system energy) but microscopically large (exponentially large  $D$ ). As a consequence, at least one of the subspaces  $\mathcal{H}_n$  must be extremely high dimensional. More generally, it appears reasonable to assume that many or even all the  $\mathcal{H}_n$  will exhibit a very large dimensionality  $d_n$ , at least as long as peculiarities such as experimentally resolvable gaps in the measurement spectra are absent. Note that even if all  $d_n$ 's are large, some of them may still be very much larger than others.

Compared to the above mentioned previous works (see Introduction), we thus admit the possibility of a relatively detailed knowledge about the initial system state: Not only one single expectation value, but rather the full statistics of all possible measurement outcomes of all the commuting observables is considered to be (approximately) fixed via the preset values of the projection probabilities  $p_n$  in (17.2). Yet, this information is obviously still far from being sufficient to uniquely determine the actual microscopic initial state  $\rho(0)$  of the system.

The time evolution of any given initial state  $\rho(0)$  in (17.2) is governed by the usual Schrödinger or von Neumann equation. For our present purposes it is particularly convenient to adopt the Heisenberg picture of quantum mechanics to express the time-dependent expectation value of any given observable, described by some Hermitian operator  $A$ , as

$$\langle A \rangle_{\rho(t)} := \text{Tr}\{\rho(0)A_t\} , \quad (17.4)$$

$$A_t := \mathcal{U}_t^\dagger A \mathcal{U}_t , \quad (17.5)$$

where  $\mathcal{U}_t$  is the quantum-mechanical time evolution operator. For a time-independent Hamiltonian  $H$ , the propagator  $\mathcal{U}_t$  takes the simple form  $\exp\{-iHt/\hbar\}$ , but in full generality, also any explicitly time dependent Hamiltonian  $H(t)$  is admitted in (17.4), (17.5). In particular, the system is not required to exhibit equilibration or thermalization in the long time limit (see Chap. 18).

Finally, largely arbitrary observables  $A$  are admitted in (17.5), except for the weak and physically reasonable restriction that the measurement range

$$\Delta_A := a_{\max} - a_{\min} , \quad (17.6)$$

i.e., the difference between the largest and smallest possible eigenvalues (or measurement outcomes) of  $A$  must be finite, and that the maximal resolution  $\delta A$  of the considered measurement device must not be unrealistically small compared to  $\Delta_A$ . For instance, if the measurement device yields at most  $K$  relevant digits, then we know that  $\Delta_A/\delta A \leq 10^K$ . Alternatively,  $\delta A$  may also account for the finite precision when solving the considered quantum system by numerical means, or simply for the accuracy with which we actually want or need to know the expectation value in

(17.4). In any case, the natural reference scale for  $\delta A$  is the measurement range from (17.6), i.e., the appropriate quantity to consider is the ratio between resolution and range,

$$R := \delta A / \Delta_A . \quad (17.7)$$

### 17.3 Main Idea and Result

In essence, our main idea will be as follows: We start by distributing all initial states  $\rho(0)$  compatible with (17.2) into different subsets. Next, we show that the vast majority of all  $\rho(0)$ 's within any given subset exhibits very similar expectation values in (17.4) for an arbitrary but fixed  $A_t$ . Finally, we will see that the average of the expectation values in (17.4) over all  $\rho(0)$ 's from one subset is actually equal for all subsets. As a consequence, the expectation values in (17.4) must be very similar for the vast majority of *all*  $\rho(0)$ 's which satisfy (17.2), independently of the subset to which each of them belongs. In order to show the similarity of (17.4) for most  $\rho(0)$ 's within one subset, certain (quite weak) assumptions will be required. Once again, these requirements will turn out to be the same for all subsets and thus for all  $\rho(0)$  which satisfy (17.2).

To begin with, we denote by  $U_n$  any unitary transformation within the subspace  $\mathcal{H}_n$  introduced above Eq. (17.1), i.e.,  $U_n : \mathcal{H}_n \rightarrow \mathcal{H}_n$  and  $U_n^\dagger U_n = \mathbb{1}_{\mathcal{H}_n}$  (identity on  $\mathcal{H}_n$ ). As usual, this operator on  $\mathcal{H}_n$  can be readily “lifted” to the full space  $\mathcal{H}$ , i.e., the same symbol  $U_n$  now denotes an operator on  $\mathcal{H}$  with the key properties that  $U_n^\dagger U_n = P_n$  and  $U_n P_m = P_m U_n = \delta_{mn} U_n$  for all  $m, n \in \{1, \dots, N\}$ . One thus can infer that

$$U := \sum_{n=1}^N U_n \quad (17.8)$$

is a unitary transformation on  $\mathcal{H}$ , i.e.,  $U^\dagger U = \mathbb{1}_{\mathcal{H}}$ . The set of unitaries  $U$  which can be generated via all possible choices the  $U_n$ 's in (17.8) is denoted as  $S_U$ . One readily confirms that any  $U \in S_U$  commutes with all the  $P_n$ 's. Furthermore, if  $\rho(0)$  satisfies the  $N$  constraints (17.2), then also

$$\rho_U(0) := U^\dagger \rho(0) U \quad (17.9)$$

will do so for all  $U \in S_U$ .

Any given  $\rho(0)$  which satisfies (17.2) thus generates one of the above announced subsets, namely  $S_{\rho(0)} := \{\rho_U(0) \mid U \in S_U\}$ . Obviously, many different  $\rho(0)$ 's which satisfy (17.2) generate identical subsets  $S_{\rho(0)}$ . On the other hand, the union of all subsets contains all  $\rho(0)$ 's which satisfy (17.2). As an aside we note that all  $\rho(0)$ 's

from the same subset exhibit the same spectrum, but not all  $\rho(0)$ 's with same spectrum belong to the same subset.

Finally, we assign a probability to the  $U \in S_U$  as follows: For any given  $n$ , the  $U_n$ 's are assumed to be uniformly distributed (Haar measure with respect to the subspace  $\mathcal{H}_n$ ), i.e., all of them are equally probable and statistically independent of each other for different indices  $n$ . Accordingly, the probability of  $U$  in (17.8) is defined as the joint probability of all the  $U_n$ 's appearing on the right hand side, i.e., each combination of  $U_n$ 's in (17.8) is realized with equal probability. Averaging any  $U$ -dependent quantity  $X(U)$  over all  $U$ 's according to this probability measure is henceforth indicated by the symbol  $[X(U)]_U$ .

Intuitively, this choice is extremely natural. Indeed, if it is understood that the probability of any  $\rho_U(0)$  within a given set  $S_{\rho(0)}$  equals the probability of  $U$ , then our above choice is the only one which is consistent, i.e., each  $\rho(0)$  which generates the same set  $S_{\rho(0)}$  also generates the same probability measure on it.

Next we consider  $A$  and  $t$  in (17.5) and thus  $A_t$  in (17.4) as arbitrary but fixed. In general, different  $\rho(0)$ 's which satisfy (17.2) are expected to entail different expectation values in (17.4). Focusing on all  $\rho(0)$ 's which belong to the same, arbitrary but fixed subset  $S_{\rho(0)}$ , one finds for the average and the variance of the expectations values in (17.4) the following results

$$\mu_t := [\text{Tr}\{\rho_U(0)A_t\}]_U = \sum_{n=1}^N \frac{p_n}{d_n} \text{Tr}\{A_t P_n\}, \quad (17.10)$$

$$\sigma_t^2 := [(\text{Tr}\{\rho_U(0)A_t\} - \mu_t)^2]_U \leq \lambda \Delta_A^2, \quad (17.11)$$

$$\lambda := 5 \max_n \left( \frac{p_n}{d_n} \right). \quad (17.12)$$

These relations (17.10)–(17.12) represent the main result of our present work. However, their detailed derivation is tedious, not very insightful, and hence postponed to the Appendix.

## 17.4 Discussion

As announced at the beginning of the previous section, the right hand side of (17.10) is independent of the actual subset  $S_{\rho(0)}$ , over which the average on the left hand side is performed, and likewise for (17.11). Hence, the following conclusion, which a priori implicitly assumes that the  $\rho(0)$ 's are randomly sampled from one single subset  $S_{\rho(0)}$ , de facto also remains true when randomly sampling  $\rho(0)$ 's from *any* of those subsets, i.e., for *all*  $\rho(0)$ 's which satisfy (17.2). Taking into account this fact and (17.11), it follows either obviously or by exploiting the so-called Chebyshev (or Markov) inequality that

$$\text{Prob}(|\text{Tr}\{\rho(0)A_t\} - \mu_t| > \epsilon) \leq \lambda (\Delta_A/\epsilon)^2 \quad (17.13)$$

for any  $\epsilon > 0$ , where the probability on the left hand side is understood as the fraction of all  $\rho(0)$ 's compatible with (17.2), for which  $\text{Tr}\{\rho(0)A_t\}$  differs by more than  $\epsilon$  from the mean value  $\mu_t$ . If we choose for  $\epsilon$  the pertinent experimental, numerical, or theoretically required resolution  $\delta A$  in (17.7), then

$$\lambda \ll R^2 \quad (17.14)$$

implies that  $\text{Tr}\{\rho(0)A_t\}$  can be considered as indistinguishable<sup>2</sup> from  $\mu_t$  for the vast majority of all  $\rho(0)$ 's which satisfy (17.2). In view of (17.4) and (17.10) this means that all those  $\rho(0)$ 's satisfy the approximation

$$\langle A \rangle_{\rho(t)} = \text{Tr}\{\rho_{\text{gmc}} A_t\} \quad (17.15)$$

for our purposes practically perfectly well, where

$$\rho_{\text{gmc}} := \sum_{n=1}^N p_n \rho_{\text{mc}}^{(n)}, \quad (17.16)$$

$$\rho_{\text{mc}}^{(n)} := \frac{1}{d_n} P_n. \quad (17.17)$$

With (17.1) one readily sees that  $\rho_{\text{mc}}^{(n)}$  in (17.17) amounts to a microcanonical density operator on the subspace  $\mathcal{H}_n$ , hence  $\rho_{\text{gmc}}$  in (17.16) may be viewed as a “generalized microcanonical ensemble”, properly accounting for the preset weight  $p_n$  of each subspace in (17.2).

According to the definitions (17.1) and (17.2), the ratio  $p_n/d_n$  may be viewed as the (mean) population per eigenstate within any given eigenspace  $\mathcal{H}_n$ . Recalling that  $p_n \geq 0$ ,  $\sum_{n=1}^N p_n = 1$ , and that the total number of eigenstates  $D$  is unimaginably large, it is obvious that (17.14) with (17.7) and (17.12) will be satisfied under many very common circumstances. For instance, one often expects (see below (17.3)) that the dimension  $d_n$  of every eigenspace  $\mathcal{H}_n$  is so large that (17.14) is automatically fulfilled without any further restriction regarding the  $p_n$ 's in (17.12). Moreover, even if certain subspaces  $\mathcal{H}_n$  should happen to be relatively low dimensional, it will be sufficient that their “weights”  $p_n$  are not unreasonably large (compared to their relatively low dimensions) in order to still guarantee (17.14). Note that this argument even admits that  $d_n = 1$  for all  $n$ , though such cases seem physically unrealistic according to the considerations below (17.3).

Finally, it is possible to further generalize our so far results in the following two ways:

---

<sup>2</sup>More sophisticated distinguishability measures between quantum states than expectation values could in principle be taken into account along similar lines as in Ref. [23].

First, there may be one exceptional subspace  $\mathcal{H}_n$  of dimension  $d_n = 1$ , for which  $p_n$  is not restricted at all. In other words, one  $n$  with  $d_n = 1$  may be disregarded when taking the maximum on the right hand side of (17.12). For instance, this case may be of interest for a system with a non-degenerate ground state, which is energetically separated by a gap from the first excited state and thus may exhibit an exceptionally large (macroscopic) population  $p_n$  compared to all the other level populations  $p_m/d_m$  with  $m \neq n$ . The derivation of this generalization amounts to a straightforward combination of the approach in Refs. [23, 24] and in the Appendix below, and is therefore omitted.

Second, not all weights  $p_n$  may be known, but, say, only those with indices  $n \in \{1, \dots, N'\}$ , where  $N' < N$ . Accordingly, there are only  $N'$  constraints of the form (17.2) with  $p_n \geq 0$  and  $\sum_{n=1}^{N'} p_n \leq 1$ . It follows that the union (direct sum) of all the remaining subspaces  $\tilde{\mathcal{H}} := \mathcal{H}_{N'+1} \oplus \dots \oplus \mathcal{H}_N$  will be populated with probability  $\tilde{p} := 1 - \sum_{n=1}^{N'} p_n$  and that the projector onto this subspace  $\tilde{\mathcal{H}}$  is given by  $\tilde{P} := P_{N'+1} + \dots + P_N$ . Altogether the case at hand can thus be reduced to the original situation with a new “effective”  $N$  value, namely  $N = N' + 1$ , complemented by  $P_N := \tilde{P}$  and  $p_N := \tilde{p}$ .

Taking for granted that condition (17.14) is satisfied, it follows that the expectation values of  $A$  at time  $t$  on the left hand side of (17.15) are practically indistinguishable from each other for the vast majority of all initial states  $\rho(0)$  which satisfy the  $N$  constraints (17.2), i.e., we recover our main dynamical typicality result announced in the first section.

Note that there may still be a small set of “untypical”  $\rho(0)$ ’s which satisfy (17.2) but notably violate the approximation (17.15). Recalling that  $A$  and  $t$  in (17.5) and thus  $A_t$  in (17.4) are still considered as arbitrary but fixed (see above (17.10)), this set of “untypical”  $\rho(0)$ ’s will usually be different for different time points  $t$  and/or different observables  $A$ . In this context, it is worth noting that the upper bound in (17.11) does not depend on  $t$ . Since averaging over  $U$  and integrating over  $t$  are commuting operations, we thus can conclude from (17.11) that

$$Q := [q_U]_U \leq \lambda \Delta_A^2, \quad (17.18)$$

where

$$q_U := \frac{1}{t_2 - t_1} \int_{t_1}^{t_2} \xi_U^2(t) dt \quad (17.19)$$

and

$$\xi_U(t) := \text{Tr}\{\rho_U(0)A_t\} - \mu_t \quad (17.20)$$

for arbitrary  $t_2 > t_1 \geq 0$ . Since  $q_U \geq 0$ , one can conclude as before from (17.14) and (17.18) that the quantity  $q_U$  must be very small for the vast majority of all  $\rho(0)$ ’s. For any given such  $\rho(0)$ , also the integrand  $\xi_U^2(t)$  in (17.19) must be very

small *simultaneously* for all  $t \in [t_1, t_2]$ , apart from a negligible small fraction of exceptional times  $t$ 's. For sufficiently small  $\lambda$  in (17.14), those exceptional  $t$ 's become unobservably rare and can be ignored. We thus can conclude that for any given time interval and any given observable  $A$ , most  $\rho(0)$ 's which satisfy (17.2) exhibit very similar expectation values of  $A$  over the entire time interval.

Formally, this typical time evolution is given by the right hand side of (17.15), but its explicit quantitative evaluation is usually very difficult (see Chaps. 18 and 19) and goes beyond the scope of our present work. In fact, it is exactly one of the main conceptual virtues of such a dynamical typicality approach that interesting predictions can be obtained without actually solving the dynamics. In particular, our present finding helps us to better understand and explain the well established fact that a few macroscopic features are sufficient to ensure the reproducibility of experimental measurements despite many unknown and uncontrollable microscopic details of the system.

## 17.5 Typicality as Numerical Technique

As already mentioned at the end of the previous section, the typical time evolution is given by the expression for the ensemble average on the right hand side of (17.15). The precise quantitative evaluation of this expression can be a challenging task for a specific observable and many-body quantum model and therefore it very often has to be done numerically (see Chap. 19). In this context, the left hand side of (17.15) turns out to be very useful in order to establish a powerful numerical technique [6, 25–32]. This technique employs the fact that, for a fixed initial value (17.2), the ensemble average is accurately imitated by a single pure state. This section describes such a dynamical typicality based numerical method and its central advantages.

To start with, it is convenient to discuss existing numerical approaches. Within the large variety of different approaches, a straightforward and widely used procedure is the direct evaluation of the ensemble average via

$$\text{Tr}\{\rho_{\text{gmc}} A_t\} = \sum_{\mu, \nu=1}^D \langle \mu | \rho_{\text{gmc}} | \nu \rangle \langle \nu | A | \mu \rangle e^{i(E_\nu - E_\mu)t/\hbar}, \quad (17.21)$$

where  $|\mu\rangle$ ,  $|\nu\rangle$  and  $E_\mu$ ,  $E_\nu$  are the eigenstates and corresponding eigenenergies of a given many-body Hamiltonian  $H$ . In principle, these eigenstates and eigenenergies can be calculated numerically by the exact diagonalization of systems of finite size. However, because the Hilbert-space dimension  $D$  grows exponentially fast in the number of degrees of freedom, exact diagonalization is only feasible for rather small system sizes and finite-size effects can be huge. For a Heisenberg spin-1/2 chain of length  $L$ , for example,  $D = 2^L$  and  $L_{\max} \sim 20$  is the maximum length treatable [27–30]. For a Fermi–Hubbard chain with  $L$  sites, as another important example,  $D = 4^L$  and  $L_{\max} \sim 10$  is even much less. Clearly, if the Hamiltonian  $H$  and the observable  $A$  have common and mutually commuting symmetries, such as total

magnetization/particle number or translation invariance, it is also possible to exploit these symmetries via

$$\text{Tr}\{\rho_{\text{gmc}} A_t\} = \sum_{m=1}^M \sum_{\mu, \nu=1}^{d_m} \langle m, \mu | \rho_{\text{gmc}} | m, \nu \rangle \langle m, \nu | A | m, \mu \rangle e^{i(E_{m,\nu} - E_{m,\mu})t/\hbar}. \quad (17.22)$$

However, using these symmetries for the above examples yields a largest subspace with the dimension  $d_m$  being  $d_m \approx (L, L/2)/L$  for the Heisenberg spin-1/2 chain and  $d_m \approx (2L, L)/L$  for the Fermi–Hubbard chain [33], where the bracket  $(n, k) := n!/[k! \cdot (n-k)!]$  denotes the binomial coefficient. In fact, symmetries are already exploited to reach the aforementioned system sizes  $L_{\max}$ .

As compared to exact diagonalization (see Chap. 19), a dynamical typicality based scheme can treat much larger Hilbert spaces and thus allows for significant progress in the context of real-time dynamics of expectation values. This scheme is based on (17.15) with a randomly sampled initial state of the form

$$\rho(0) := \frac{1}{2 \langle \psi | \rho_{\text{gmc}} | \psi \rangle} (\rho_{\text{gmc}} | \psi \rangle \langle \psi | + \text{h.c.}), \quad (17.23)$$

with the (unnormalized) pure state

$$| \psi \rangle := \sum_{k=1}^D (a_k + i b_k) | k \rangle, \quad (17.24)$$

where  $| k \rangle$  is an arbitrary but fixed orthonormal basis, and where the  $a_k$  and  $b_k$  are independent, normally distributed random variables (i.e. Gaussian distributed with zero mean and unit variance). One readily confirms that all statistical properties of the random ensemble of pure states in (17.23) are independent of the choice of the basis  $| k \rangle$  in (17.24). In particular, this basis needs not to be the eigenbasis of  $H$ . Rather, any numerically convenient basis will do the job. In particular, the basis can be but does not need to be adapted to the symmetries of the specific system under consideration.

It readily follows that  $\rho(0)^\dagger = \rho(0)$  and  $\text{Tr}\{\rho(0)\} = 1$ . Moreover, by means of similar calculations as in the section “Main idea and results” one finds that

$$\langle \psi | P_n \rho_{\text{gmc}} | \psi \rangle = \frac{p_n}{d_n} \langle \psi | P_n | \psi \rangle \approx 2 p_n, \quad \langle \psi | \rho_{\text{gmc}} | \psi \rangle = \sum_{n=1}^N \frac{p_n}{d_n} \langle \psi | P_n | \psi \rangle \approx 2 \quad (17.25)$$

for sufficiently large subspace dimensions  $d_n$ . For the initial state  $\rho(0)$  in (17.23), these two equations lead to the expectation value  $\text{Tr}\{P_n \rho(0)\} \approx p_n$ , i.e., the condition in (17.2). Therefore, (17.15) applies to this initial state and yields

$$\text{Tr}\{\rho_{\text{gmc}} A_t\} \approx \frac{\langle\psi|(\rho_{\text{gmc}} A_t + \text{h.c.})|\psi\rangle}{2\langle\psi|\rho_{\text{gmc}}|\psi\rangle} = \frac{\text{Re}\langle\psi|\rho_{\text{gmc}} A_t|\psi\rangle}{\langle\psi|\rho_{\text{gmc}}|\psi\rangle} \quad (17.26)$$

and, using  $\langle\psi|\rho_{\text{gmc}}|\psi\rangle \approx 2$  again, as well as  $\langle\psi|\psi\rangle \approx 2D$ , one obtains the relation

$$\text{Tr}\{\rho_{\text{gmc}} A_t\} \approx D \frac{\text{Re}\langle\psi|\rho_{\text{gmc}} A_t|\psi\rangle}{\langle\psi|\psi\rangle}. \quad (17.27)$$

Thus, the trace  $\text{Tr}\{\bullet\}$  is essentially replaced by a scalar product  $\langle\psi|\bullet|\psi\rangle$  involving a single pure state drawn at random from a Hilbert space of finite but high dimension  $D$ . This relation can be also written in the form

$$\text{Tr}\{\rho_{\text{gmc}} A_t\} \approx D \frac{\text{Re}\langle\Phi(t)|A|\varphi(t)\rangle}{\langle\varphi(0)|\varphi(0)\rangle} \quad (17.28)$$

with the two auxiliary pure states

$$|\varphi(t)\rangle := e^{-iHt/\hbar}|\psi\rangle, \quad |\Phi(t)\rangle := e^{-iHt/\hbar}\rho_{\text{gmc}}|\psi\rangle. \quad (17.29)$$

Note that these pure states look similar but differ from each other because of the additional operator  $\rho_{\text{gmc}}$  in the definition of  $|\Phi(t)\rangle$ .

A central advantage of the relation in (17.28) is that no time dependence of operators occurs. Instead, the full time dependence appears as a property of pure states only. As a consequence, one does no need to (i) employ exact diagonalization and (ii) store full matrices in computer memory. To see that exact diagonalization can be circumvented, consider the Schrödinger equation

$$\frac{d}{dt}|\varphi(t)\rangle = -\frac{i}{\hbar}H|\varphi(t)\rangle \quad (17.30)$$

for  $|\varphi(t)\rangle$ . This differential equation and the corresponding equation for  $|\Phi(t)\rangle$  can be solved numerically by straightforward iterator schemes like fourth-order Runge–Kutta [27–29] or more sophisticated schemes like Trotter decompositions or Chebyshev polynomials [34, 35]. Still, one has to implement the action of the Hamiltonian on pure states. Since it is possible to carry out these matrix-vector multiplications without storing matrices in computer memory, the memory requirement of the algorithm is set only by the size of vectors, i.e.,  $\mathcal{O}(D)$  or, in case of symmetry reduction,  $\mathcal{O}(d_m)$ . Nevertheless, to reduce the run time of the algorithm, it is convenient to store at least parts of matrices in computer memory. In this respect, one can profit from the fact that the Hamiltonian is usually a few-body operator with a sparse-matrix representation. Thus, the memory requirement essentially remains linear in the relevant Hilbert-space dimension. In this way, for the above example of a Heisenberg spin-1/2 chain,  $L_{\max} = 34$  [28] has been reached using medium-sized

clusters while  $L_{\max} > 34$  is feasible using massive parallelization and supercomputers [30, 36]. As compared to exact diagonalization, the corresponding Hilbert space dimension is larger by several orders of magnitude, e.g., by a factor  $2^{34}/2^{20} = \mathcal{O}(10^4)$ . For such finite but already huge Hilbert spaces, the typicality-related approximation error has been demonstrated to be negligibly small, by a detailed comparison with other state-of-the-art numerical methods including time-dependent density-matrix renormalization group [28] and Lanczos diagonalization [29].

To illustrate the accuracy of the numerical method and the validity of the analytical considerations of the last sections in detail, let us consider the Heisenberg spin-1/2 chain and the specific operators  $n_r = S_r^z + 1/2$ , where  $S_r^z$  is the  $z$ -component of a spin at site  $r$ . These  $L$  local operators are mutually commuting and can be adjusted independently between 0 and 1. We choose initial conditions  $\rho(0)$  with  $\langle n_r \rangle_{\rho(0)} = 1$  at a single site  $r$  and  $\langle n_{r'} \rangle_{\rho(0)} = 1/2$  at all other sites  $r' \neq r$ . This choice corresponds to  $\rho_{\text{gmc}} = n_r/2^{L-1}$  and, for the observable  $A = n_r$ , the ensemble average is then given by the two-point correlation function  $\text{Tr}\{\rho_{\text{gmc}} A_t\} = \text{Tr}\{n_r n_r(t)\}/2^{L-1}$  at formally infinite temperature, see (17.31) below or Ref. [30]. In Fig. 17.1a we show this ensemble average, as obtained from exact diagonalization for a finite lattice with  $L = 14$  sites. We further depict the approximation in Eq. (17.28), as obtained from the Runge–Kutta propagation of a random pure state. Clearly, both curves are very close to each other, especially in view of the small  $L = 14$ . Moreover, an agreement of the same quality is found for another random pure state. In Fig. 17.1c we compare the approximation in Eq. (17.28) for two different pure states drawn at random and a substantially larger lattice with  $L = 28$  sites. Apparently, the corresponding curves are much closer to each other. This closeness demonstrates the fact that the approximation in Eq. (17.28) becomes exact in the thermodynamic limit  $L \rightarrow \infty$ .

Remarkably, typicality also provides the basis of a numerical approach to auto-correlation functions at finite temperatures. This approach is based on the relation [27–29]

$$\frac{\text{Re } \text{Tr}\{e^{-\beta H} AA_t\}}{\text{Tr}\{e^{-\beta H}\}} \approx \frac{\text{Re } \langle \psi | e^{-\beta H} AA_t | \psi \rangle}{\langle \psi | e^{-\beta H} | \psi \rangle}, \quad (17.31)$$

where  $\beta = 1/k_B T$  denotes the inverse temperature and  $|\psi\rangle$  is a randomly sampled pure state as defined before. Thus, once again, the trace  $\text{Tr}\{\bullet\}$  is replaced by the scalar product  $\langle \psi | \bullet | \psi \rangle$ . Similar to (17.28), this relation can be rewritten as

$$\frac{\text{Re } \text{Tr}\{e^{-\beta H} AA_t\}}{\text{Tr}\{e^{-\beta H}\}} \approx \frac{\text{Re } \langle \Phi_\beta(t) | A | \varphi_\beta(t) \rangle}{\langle \varphi_\beta(0) | \varphi_\beta(0) \rangle} \quad (17.32)$$

with the two modified auxiliary pure states

$$|\varphi_\beta(t)\rangle := e^{-iHt/\hbar} e^{-\beta H/2} |\psi\rangle, \quad |\Phi(t)\rangle := e^{-iHt/\hbar} A e^{-\beta H/2} |\psi\rangle. \quad (17.33)$$

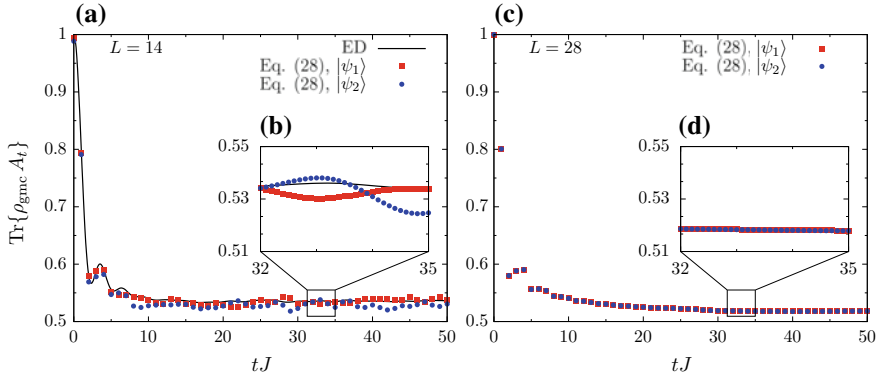


**Fig. 17.1** **a** Time-dependent expectation value  $\text{Tr}\{\rho_{\text{gmc}} A_t\}$  for  $\rho_{\text{gmc}} = n_r$ ,  $A = n_r$ , and a Heisenberg spin-1/2 chain of length  $L = 14$ . Exact diagonalization (ED) is compared to the approximation in Eq. (17.28) and two states  $|\psi_1\rangle$  and  $|\psi_2\rangle$  drawn at random. **c** Approximation in Eq. (17.28) for two random states  $|\psi_1\rangle$  and  $|\psi_2\rangle$  in a lattice with  $L = 28$  sites. **b, d** zoom of **a, c**.

An important difference between these pure states and the ones in (17.29) is the additional occurrence of the imaginary time  $\beta$ . As the dependence on real time  $t$ , this dependence can be obtained from iteratively solving an imaginary-time Schrödinger equation,

$$\frac{d}{d\beta} |\varphi_\beta(0)\rangle = -\frac{1}{2} H |\varphi_\beta(0)\rangle \quad (17.34)$$

for  $|\varphi_\beta(0)\rangle$  and analogously for  $|\Phi_\beta(0)\rangle$ . Certainly, typicality arguments justify the relation in (17.32) only, if the dimensions of the relevant energy subspaces are sufficiently large. If the inverse temperature  $\beta$  is small, the dominant contribution stems from energy subspaces far from the borders of the spectrum. However, if the inverse temperature  $\beta$  is large, the dominant contribution stems from small energy subspaces close to the lower border of the spectrum and typicality arguments cannot be employed any further [31].

Interestingly, however, this relation does not break down in the limit  $\beta \rightarrow \infty$  and even becomes exact in this limit. This fact follows from the definition of the two pure states in (17.33) and whenever the random pure state  $|\psi\rangle$  has a finite overlap with the ground state  $|\mu_0\rangle$ ,

$$|\langle \mu_0 | \psi \rangle| > 0, \quad (17.35)$$

even if this overlap is tiny. Then,

$$\lim_{\beta \rightarrow \infty} \frac{|\varphi_\beta(t)\rangle}{\sqrt{\langle \varphi_\beta(0) | \varphi_\beta(0) \rangle}} = e^{-iHt/\hbar} |\mu_0\rangle, \quad \lim_{\beta \rightarrow \infty} \frac{|\Phi_\beta(t)\rangle}{\sqrt{\langle \varphi_\beta(0) | \varphi_\beta(0) \rangle}} = e^{-iHt/\hbar} A |\mu_0\rangle \quad (17.36)$$

and, as a consequence,

$$\lim_{\beta \rightarrow \infty} \frac{\text{Re} \langle \Phi_\beta(t) | A | \varphi_\beta(t) \rangle}{\langle \varphi_\beta(0) | \varphi_\beta(0) \rangle} = \text{Re} \langle \mu_0 | A A_t | \mu_0 \rangle. \quad (17.37)$$

Thus, in conclusion, Eq. (17.32) also provides a reasonable numerical approach to low temperatures.

**Acknowledgements** This work was supported by the Deutsche Forschungsgemeinschaft (DFG) under Grants No. RE 1344/10-1, RE 1344/12-1, GE 1657/3-1, STE 2243/3-1 within the Research Unit FOR 2692, Grant No. 355031190, and by the Studienstiftung des Deutschen Volkes.

## Appendix

This appendix provides the detailed derivation of the main result (17.10)–(17.12) of our present work. For notational simplicity, we adopt the abbreviations

$$\rho := \rho(0) \quad (17.38)$$

$$B := A_t, \quad (17.39)$$

where  $A_t$  is defined in (17.5). It follows that the eigenvalues of  $B$  are identical to those of  $A$ . In particular, the measurement range  $\Delta_B$  of  $B$  will agree with the measurement range  $\Delta_A$  of  $A$  from (17.6), i.e.,

$$\Delta_A = \Delta_B. \quad (17.40)$$

### Derivation of (17.10)

For any given  $n \in \{1, \dots, N\}$ , we denote by  $\{|n, a\rangle\}_{a=1}^{d_n}$  an arbitrary but fixed orthonormal basis of  $\mathcal{H}_n$ . The union of all those bases thus amounts to an orthonormal basis of  $\mathcal{H}$ , i.e.,

$$\langle n, a | m, b \rangle = \delta_{mn} \delta_{ab} \quad (17.41)$$

$$\sum_{n=1}^N \sum_{a=1}^{d_n} |n, a\rangle \langle n, a| = \mathbb{1}_{\mathcal{H}}. \quad (17.42)$$

Inserting  $\mathbb{1}_{\mathcal{H}}$  from (17.42) three times into the definition of  $\mu_t$  in (17.10) and observing (17.9) yields

$$\begin{aligned} \mu_t &= \left[ \sum_{l,j,m,n} \sum_{\alpha,\beta,a,b} \langle l, \alpha | U^\dagger | m, a \rangle \langle m, a | \rho | n, b \rangle \langle n, b | U | j, \beta \rangle \langle j, \beta | B | l, \alpha \rangle \right]_U \\ &= \left[ \sum_{m,n} \sum_{\alpha,\beta,a,b} \langle m, \alpha | U^\dagger | m, a \rangle \langle m, a | \rho | n, b \rangle \langle n, b | U | n, \beta \rangle \langle n, \beta | B | m, \alpha \rangle \right]_U \end{aligned} \quad (17.43)$$

In the last step above we used  $\langle n, b | U | m, \beta \rangle = \delta_{mn} \langle n, b | U | n, \beta \rangle$  since any  $U \in S_U$  commutes with all the  $P_n$ 's as mentioned below (17.8). Now, we define the abbreviation for the basis representation of the  $U_n$  introduced above (17.8) as

$$U_{n,b\beta} := \langle n, b | U_n | n, \beta \rangle = \langle n, b | U | n, \beta \rangle. \quad (17.44)$$

This enables us to rewrite Eq.(17.43) as

$$\mu_t = \sum_{m,n} \sum_{\alpha,\beta,a,b} \langle m, a | \rho | n, b \rangle \langle n, \beta | B | m, \alpha \rangle [U_{m,a\alpha}^* U_{n,b\beta}]_U. \quad (17.45)$$

To continue evaluating this expression we revert to [37]. There, the following is stated for the average over uniformly (Haar) distributed unitaries<sup>3</sup>:

$$[U_{l,a_1b_1} \dots U_{l,a_m b_m} U_{l,\alpha_1\beta_1}^* \dots U_{l,\alpha_n\beta_n}^*]_{U_l} = \delta_{mn} \sum_{\Pi,\Pi'} V_{\Pi,\Pi'} \prod_{j=1}^n \delta_{a_j \alpha_{\Pi(j)}} \delta_{b_j \beta_{\Pi'(j)}}. \quad (17.46)$$

Quoting verbatim from [37]: “the summation is over all permutations  $\Pi$  and  $\Pi'$  of the numbers  $1, \dots, n$ . The coefficients  $V_{\Pi,\Pi'}$  depend only on the cycle structure of the permutation  $\Pi^{-1}\Pi'$ . Recall that each permutation of  $1, \dots, n$  has a unique factorization in disjoint cyclic permutations (“cycles”) of lengths  $c_1, \dots, c_k$  (where  $n = \sum_{j=1}^k c_j$ ). The statement that  $V_{\Pi,\Pi'}$  depends only on the cycle structure of  $\Pi^{-1}\Pi'$  means that  $V_{\Pi,\Pi'}$  depends only on the lengths  $c_1, \dots, c_k$  of the cycles in the factorization of  $\Pi^{-1}\Pi'$ . One may therefore write  $V_{c_1, \dots, c_k}$  instead of  $V_{\Pi,\Pi'}$ . The factors  $V_{c_1, \dots, c_k}$  are given by the columns “CUE” of Tables II and IV in [37].

As said below (17.9), the symbol  $[...]_U$  indicates an average over all  $U_n$  within each  $\mathcal{H}_n$  according to the Haar measure. Averages over Haar measures in distinct eigenspaces are statistically independent (see below (17.9)). Thus, by applying (17.46)–(17.45) we see that  $m$  has to equal  $n$  or the average vanishes

$$\mu_t = \sum_{n=1}^N \sum_{\alpha,\beta,a,b} \langle n, a | \rho | n, b \rangle \langle n, \beta | B | n, \alpha \rangle [U_{n,a\alpha}^* U_{n,b\beta}]_{U_n} \quad (17.47)$$

$$= \sum_{n=1}^N \sum_{\alpha,\beta,a,b} \langle n, a | \rho | n, b \rangle \langle n, \beta | B | n, \alpha \rangle V_{\Pi_1,\Pi_1} \delta_{a\alpha} \delta_{b\beta}. \quad (17.48)$$

Here, there is only one permutation: namely the identity, denoted by  $\Pi_1$ . In this case  $\Pi_1^{-1}\Pi_1 = \Pi_1$  yields only one cycle of length  $c_1 = 1$ . The corresponding  $V_{\Pi_1} = V_1$  can be found, in the Tables II and IV in [37] (column “CUE”, row  $n = 1$ ) as  $V_{\Pi_1} = \frac{1}{d_n}$ . Plugging this back into the above equation we obtain

<sup>3</sup>Averages of this type were analyzed by many authors [11, 38–42], often independently. We refer to [37], since only there cases up to  $n \leq 5$  are provided, although in the following  $n \leq 2$ .

$$\mu_t = \sum_{n=1}^N \frac{1}{d_n} \text{Tr} \{ \rho P_n \} \text{Tr} \{ B P_n \}. \quad (17.49)$$

Observing (17.2) and (17.39), we finally recover (17.10).

### ***Derivation of (17.11) and (17.12)***

The variance in (17.11) can be rewritten as

$$\sigma_t^2 = [\text{Tr} \{ \rho_U B \}^2]_U - \mu_t^2. \quad (17.50)$$

On the right hand side, the last term  $\mu_t^2$  follows from (17.49) above. Turning to the first term, one finds similarly as in (17.43) and (17.45) that

$$[\text{Tr} \{ \rho_U B \}^2]_U = \left[ \sum_{l,j} \sum_{\alpha,\beta,a,b} U_{l,a\alpha}^* U_{j,b\beta} \langle l, a | \rho | j, b \rangle \langle j, \beta | B | l, \alpha \rangle \right. \\ \left. \cdot \sum_{m,n} \sum_{\gamma,\omega,c,d} U_{m,c\gamma}^* U_{n,d\omega} \langle m, c | \rho | n, d \rangle \langle n, \omega | B | m, \gamma \rangle \right]_U. \quad (17.51)$$

For the summation indices  $l, j, m, n$  we define the set of quadruples

$$S := \{(l, j, m, n) | l, j, m, n \in \{1, \dots, N\}\}. \quad (17.52)$$

If one reverts back to Eq.(17.46), one finds the necessity to study three cases for which the average in (17.51) does not vanish, which amount to the following index subsets of  $S$ :  $S_1 : l = j \neq m = n$ ,  $S_2 : l = j = m = n$  and  $S_3 : l = n \neq m = j$ . From now on, the  $S_i$  refer not only to the corresponding index sets but to the associated terms in (17.51). Thus the following holds

$$[\text{Tr} \{ \rho_U B \}^2]_U = [S_1]_U + [S_2]_U + [S_3]_U. \quad (17.53)$$

In the first case,  $S_1$ , the average over  $U$  factorizes into two averages over the eigenspaces labeled by  $l$  and  $m$ . Hence, the calculation reduces to the derivation of (17.10) and we find

$$\begin{aligned}
[S_1]_U &= \sum_{l \neq m} \sum_{\alpha, \beta, a, b} \langle l, a | \rho | l, b \rangle \langle l, \beta | B | l, \alpha \rangle [U_{l,a\alpha}^* U_{l,b\beta}]_{U_l} \\
&\quad \cdot \sum_{\gamma, \omega, c, d} \langle m, c | \rho | m, d \rangle \langle m, \omega | B | m, \gamma \rangle [U_{m,c\gamma}^* U_{m,d\omega}]_{U_m} \\
&= \sum_{l \neq m} \frac{1}{d_l} \text{Tr} \{ \rho P_l \} \text{Tr} \{ B P_l \} \frac{1}{d_m} \text{Tr} \{ \rho P_m \} \text{Tr} \{ B P_m \}
\end{aligned} \tag{17.54}$$

In the second case,  $S_2$ , the unitary average is not the same as performed before, but instead:

$$[S_2]_U = \sum_{l=1}^N \sum_{\alpha, \beta, a, b} \langle l, a | \rho | l, b \rangle \langle l, \beta | B | l, \alpha \rangle \sum_{\gamma, \omega, c, d} \langle l, c | \rho | l, d \rangle \langle l, \omega | B | l, \gamma \rangle [U_{l,a\alpha}^* U_{l,b\beta} U_{l,c\gamma}^* U_{l,d\omega}]_{U_l} \tag{17.55}$$

To further evaluate this expression we make again use of (17.46), arriving at

$$\begin{aligned}
[U_{l,b\beta} U_{l,d\omega} U_{l,a\alpha}^* U_{l,c\gamma}]_{U_l} &= \underbrace{V_{\Pi_1, \Pi_1}}_{1/(d_l^2 - 1)} \delta_{ba} \delta_{dc} \delta_{\beta\alpha} \delta_{\omega\gamma} + \underbrace{V_{\Pi_1, \Pi_2}}_{-1/(d_l(d_l^2 - 1))} \delta_{ba} \delta_{dc} \delta_{\beta\gamma} \delta_{\omega\alpha} \\
&\quad + \underbrace{V_{\Pi_2, \Pi_1}}_{-1/(d_l(d_l^2 - 1))} \delta_{bc} \delta_{da} \delta_{\beta\alpha} \delta_{\omega\gamma} + \underbrace{V_{\Pi_2, \Pi_2}}_{1/(d_l^2 - 1)} \delta_{bc} \delta_{da} \delta_{\beta\gamma} \delta_{\omega\alpha}.
\end{aligned} \tag{17.56}$$

Here,  $\Pi_1$  still equates to the identity, but now  $\Pi_2$  denotes the permutation exchanging the numbers 1 and 2. Therefore,  $\Pi_1^{-1} \Pi_1 = \Pi_2^{-1} \Pi_2 = \Pi_1$  decomposes in two cycles of lengths  $c_1 = c_2 = 1$ , while  $\Pi_2^{-1} \Pi_1 = \Pi_1^{-1} \Pi_2 = \Pi_2$  exhibits one cycle with  $c_2 = 2$ . The corresponding  $V_{\Pi_1, \Pi_1} = V_{\Pi_2, \Pi_2} = V_{1,1}$  and  $V_{\Pi_2, \Pi_1} = V_{\Pi_1, \Pi_2} = V_2$  can again be found, in the Tables II and IV in [37] (column ‘‘CUE’’, row  $n = 2$ ) with the above cited results. Plugging (17.56) back into (17.55) and additionally using  $1/(d_l^2 - 1) = 1/d_l^2 + 1/(d_l^2(d_l^2 - 1))$ , we obtain

$$[S_2]_U = \sum_{l=1}^N \frac{1}{d_l^2} \text{Tr} \{ \rho P_l \}^2 \text{Tr} \{ B P_l \}^2 + S'_2, \tag{17.57}$$

$$\begin{aligned}
S'_2 &:= \sum_{l=1}^N \left[ \frac{1}{d_l^2 (d_l^2 - 1)} \text{Tr} \{ \rho P_l \}^2 \text{Tr} \{ B P_l \}^2 \right. \\
&\quad - \frac{1}{d_l (d_l^2 - 1)} \text{Tr} \{ \rho P_l \}^2 \text{Tr} \{ B P_l B P_l \} \\
&\quad - \frac{1}{d_l (d_l^2 - 1)} \sum_{a,b} |\langle l, a | \rho | l, b \rangle|^2 \text{Tr} \{ B P_l \}^2 \\
&\quad \left. + \frac{1}{d_l^2 - 1} \sum_{a,b} |\langle l, a | \rho | l, b \rangle|^2 \text{Tr} \{ B P_l B P_l \} \right].
\end{aligned} \tag{17.58}$$

The very first summand of the above expression,  $[S_2]_U$ , can be used, combined with the first case,  $[S_1]_U$ , to eliminate the second part of the variance,  $\mu_t^2$ :

$$\sigma_t^2 = |[S_1]_U + [S_2]_U - \mu_t^2 + [S_3]_U| \leq |S'_2| + |[S_3]_U|. \quad (17.59)$$

To start estimating an upper bound we notice that there exists a self-adjoint and non-negative operator  $\rho^{1/2}$  which fulfills  $\rho^{1/2}\rho^{1/2} = \rho$ . This enables us to use the Cauchy–Schwarz inequality on

$$\sum_{a,b} |\langle l, a | \rho | l, b \rangle|^2 \leq \sum_{a,b} \langle l, a | \rho | l, a \rangle \langle l, b | \rho | l, b \rangle = \text{Tr} \{ \rho P_l \}^2. \quad (17.60)$$

Also, we state that the variance is invariant under a shift  $B \rightarrow B + 1_{\mathcal{H}c}$ , where  $c$  is an arbitrary real number. We perform this shift such that  $B$  will be positive definite. Then we observe that

$$\text{Tr} \{ CD \} \leq |D| \text{Tr} \{ C \}, \quad (17.61)$$

with  $|D|$  denoting the operator norm and with  $C$  as well as  $D$  being self-adjoint and non-negative operators. One readily verifies that  $P_l$  and  $B P_l B$  are self adjoint and non-negative as well. Applying all this we can bound

$$|S'_2| \leq \sum_{l=1}^N \left( \frac{p_l^2 |B|^2 d_l^2}{d_l^2 (d_l^2 - 1)} + \frac{p_l^2 |B|^2 (d_l + d_l^2)}{d_l (d_l^2 - 1)} + \frac{p_l^2 |B|^2 d_l}{d_l^2 - 1} \right) \quad (17.62)$$

For  $d \geq 2$  and the correct choice of  $c$ , such that  $|B| = \Delta_B$ , we find

$$|S'_2| \leq 4 (\Delta_B)^2 \max_n \left( \frac{p_n}{d_n} \right). \quad (17.63)$$

This leaves us to evaluate the third case, namely  $S_3$ ,

$$[S_3]_U = \sum_{l \neq j} \sum_{\alpha, \beta, a, b} \langle l, a | \rho | j, b \rangle \langle j, \beta | B | l, \alpha \rangle \sum_{\gamma, \omega, c, d} \langle j, c | \rho | l, d \rangle \langle l, \omega | B | j, \gamma \rangle \cdot [U_{j,b\beta} U_{l,d\omega} U_{l,a\alpha}^* U_{j,c\gamma}^*]_U \quad (17.64)$$

The unitary average here amounts to the same calculation as in Eqs.(17.48) and (17.54):

$$[U_{j,b\beta} U_{l,d\omega} U_{l,a\alpha}^* U_{j,c\gamma}^*]_U = [U_{j,b\beta} U_{j,c\gamma}^*]_{U_j} [U_{l,d\omega} U_{l,a\alpha}^*]_{U_l} = \frac{1}{d_j} \delta_{bc} \delta_{\beta\gamma} \frac{1}{d_l} \delta_{da} \delta_{\omega\alpha}, \quad (17.65)$$

implying that

$$|[S_3]_U| = \left| \sum_{l \neq j} \sum_{\alpha, \beta, a, b} \frac{1}{d_l d_j} \langle l, a | \rho | j, b \rangle \langle j, \beta | B | l, \alpha \rangle \langle j, b | \rho | l, a \rangle \langle l, \alpha | B | j, \beta \rangle \right| \quad (17.66)$$

Now we invoke the Cauchy–Schwarz inequality from (17.60) again to arrive at

$$|[S_3]_U| \leq \sum_{l=j} \frac{1}{d_l d_j} \text{Tr} \{ \rho P_l \} \text{Tr} \{ \rho P_j \} |\text{Tr} \{ B P_l B P_j \}| \quad (17.67)$$

$$\leq \max_n \left( \frac{p_n}{d_n} \right) \sum_j \frac{1}{d_j} \text{Tr} \{ \rho P_j \} \text{Tr} \left\{ B \sum_l P_l B P_j \right\} \quad (17.68)$$

$$\leq \max_n \left( \frac{p_n}{d_n} \right) (\Delta_B)^2. \quad (17.69)$$

In (17.68) we noticed that  $\text{Tr} \{ B P_l B P_j \}$  has to be non-negative since  $B P_l B$  as well as  $P_j$  are non-negative operators. To achieve Eq.(17.69) we made use of (17.61),  $|B^2| = |B|^2$  and  $|B| = \Delta_B$ .

Recalling (17.59) and making use of (17.63) as well as (17.69) we obtain the following bound for the variance

$$\sigma_t^2 \leq 5 (\Delta_B)^2 \max_n \left( \frac{p_n}{d_n} \right). \quad (17.70)$$

Finally, using (17.40) we reach (17.11), (17.12).

## References

1. C. Bartsch, J. Gemmer, Phys. Rev. Lett. **102**, 110403 (2009). <https://doi.org/10.1103/PhysRevLett.102.110403>
2. M.P. Müller, D. Gross, J. Eisert, Commun. Math. Phys. **303**, 785 (2011). <https://doi.org/10.1007/s00220-011-1205-1>
3. B.V. Fine, Phys. Rev. E **80**, 051130 (2009). <https://doi.org/10.1103/PhysRevE.80.051130>
4. P. Reimann, Phys. Rev. Lett. **99**, 160404 (2007). <https://doi.org/10.1103/PhysRevLett.99.160404>
5. G.A. Alvarez, E.P. Danieli, P.R. Levstein, H.M. Pastawski, Phys. Rev. Lett. **101**, 120503 (2008). <https://doi.org/10.1103/PhysRevLett.101.120503>
6. S. Sugiura, A. Shimizu, Phys. Rev. Lett. **108**, 240401 (2012). <https://doi.org/10.1103/PhysRevLett.108.240401>
7. P. Reimann, Phys. Rev. Lett. **120**, 230601 (2018). <https://doi.org/10.1103/PhysRevLett.120.230601>
8. S. Lloyd, Ph.D. Thesis, The Rockefeller University (1988), Chapter 3. [arXiv:1307.0378](https://arxiv.org/abs/1307.0378)
9. S. Goldstein, J.L. Lebowitz, R. Tumulka, N. Zanghi, Phys. Rev. Lett. **96**, 050403 (2006). <https://doi.org/10.1103/PhysRevLett.96.050403>

10. S. Popescu, A.J. Short, A. Winter, Nat. Phys. **2**, 754 (2006). <https://doi.org/10.1038/nphys444>
11. J. Gemmer, M. Michel, G. Mahler, *Quantum Thermodynamics*, 1st edn. (Springer, Berlin, 2004). Appendix A. <https://doi.org/10.1007/978-3-540-70510-9>
12. S. Lloyd, Nat. Phys. **2**, 727 (2006). <https://doi.org/10.1038/nphys456>
13. A. Sugita, Nonlinear Phenom. Complex Syst. **10**, 192 (2007)
14. V. Balasubramanian, B. Czech, V.E. Hubeny, K. Lario, M. Rangamani, J. Simon, Gen. Relat. Gravit. **40**, 1863 (2008). <https://doi.org/10.1007/s10714-008-0606-8>
15. H. Tasaki, J. Stat. Phys. **163**, 937 (2016). <https://doi.org/10.1007/s10955-016-1511-2>
16. J. von Neumann, Z. Phys. **57**, 30 (1929). [English translation by R. Tumulka, Eur. Phys. J. H **35**, 201 (2010)]. <https://doi.org/10.1140/epjh/e2010-00008-5>
17. S. Goldstein, J.L. Lebowitz, C. Mastrodonato, R. Tumulka, N. Zanghi, Phys. Rev. E **81**, 011109 (2010). <https://doi.org/10.1103/PhysRevE.81.011109>
18. S. Goldstein, D.A. Huse, J.L. Lebowitz, R. Tumulka, Phys. Rev. Lett. **115**, 100402 (2015). <https://doi.org/10.1103/PhysRevLett.115.100402>
19. K.R. Davidson, Math. Scand. **56**, 222 (1985). <https://doi.org/10.7146/math.scand.a-12098>
20. H. Lin, In: Fillmore, P. A., Mingo, J. A. (eds.) Operator Algebras and their Applications (Fields Institute Communications 13), pp. 193– 233. American Mathematical Society (1997). <https://doi.org/10.1090/fic/013>
21. M.B. Hastings, Commun. Math. Phys. **291**, 321 (2009). <https://doi.org/10.1007/s00220-009-0877-2>
22. Y. Ogata, J. Funct. Anal. **264**, 2005 (2013). <https://doi.org/10.1016/j.jfa.2013.01.021>
23. B.N. Balz, P. Reimann, Phys. Rev. E **93**, 062107 (2016). <https://doi.org/10.1103/PhysRevE.93.062107>
24. P. Reimann, M. Kastner, New J. Phys. **14**, 043020 (2012). <https://doi.org/10.1088/1367-2630/14/4/043020>
25. S. Sugiura, A. Shimizu, Phys. Rev. Lett. **111**, 010401 (2013). <https://doi.org/10.1103/PhysRevLett.111.010401>
26. T. Itaka, T. Ebisuzaki, Phys. Rev. Lett. **90**, 047203 (2003). <https://doi.org/10.1103/PhysRevLett.90.047203>
27. T.A. Elsayed, B.V. Fine, Phys. Rev. Lett. **110**, 070404 (2013). <https://doi.org/10.1103/PhysRevLett.110.070404>
28. R. Steinigeweg, J. Gemmer, W. Brenig, Phys. Rev. Lett. **112**, 120601 (2014); Phys. Rev. B **91**, 104404 (2015). <https://doi.org/10.1103/PhysRevLett.112.120601>
29. R. Steinigeweg, J. Herbrych, X. Zotos, W. Brenig, Phys. Rev. Lett. **116**, 017202 (2016). <https://doi.org/10.1103/PhysRevLett.116.017202>
30. R. Steinigeweg, F. Jin, D. Schmidtke, H. De Raedt, K. Michielsen, J. Gemmer, Phys. Rev. B **95**, 035155 (2017). <https://doi.org/10.1103/PhysRevB.95.035155>
31. R. Steinigeweg, A. Khodja, H. Niemeyer, C. Gogolin, J. Gemmer, Phys. Rev. Lett. **112**, 130403 (2014). <https://doi.org/10.1103/PhysRevLett.112.130403>
32. D.J. Luitz, Y. Bar Lev, Phys. Rev. B **96**, 020406(R) (2017). <https://doi.org/10.1103/PhysRevB.96.020406>
33. A.W. Sandvik, AIP Conf. Proc. **1297**, 135 (2010). <https://doi.org/10.1063/1.3518900>
34. A. Weiße, G. Wellein, A. Alvermann, H. Fehske, Rev. Mod. Phys. **78**, 275 (2006). <https://doi.org/10.1103/RevModPhys.78.275>
35. H. De Raedt, K. Michielsen, *Computational Methods for Simulating Quantum Computers in Handbook of Theoretical and Computational Nanotechnology* (American Scientific Publishers, Los Angeles, 2006)
36. *World record: quantum computer with 46 qubits simulated* (Press release, Forschungszentrum Jülich, 2017)
37. P.W. Brouwer, C.W.J. Beenakker, J. Math. Phys. **37**, 4904 (1996). <https://doi.org/10.1063/1.531667>
38. I.E. Farquhar, P.T. Landsberg, Proc. R. Soc. Lond. **239**, 134 (1957). <https://doi.org/10.1098/rspa.1957.0027>

39. P. Bocchieri, A. Loinger, Phys. Rev. **111**, 668 (1958). <https://doi.org/10.1103/PhysRev.111.668>
40. P. Bocchieri, A. Loinger, Phys. Rev. **114**, 948 (1959). <https://doi.org/10.1103/PhysRev.114.948>
41. T.A. Brody, J. Flores, J.B. French, P.A. Mello, A. Pandey, S.S.M. Wong, Rev. Mod. Phys. **53**, 385 (1981). Sect. VIII.B. <https://doi.org/10.1103/RevModPhys.53.385>
42. P. Pechukas, J. Math. Phys. **25**, 534 (1984). <https://doi.org/10.1063/1.526202>

# Chapter 18

## Equilibration Times in Closed Quantum Many-Body Systems



Henrik Wilming, Thiago R. de Oliveira, Anthony J. Short and Jens Eisert

For a quantum system to be captured by a stationary statistical ensemble, as is common in thermodynamics and statistical mechanics, it is necessary that it reaches some apparently stationary state in the first place. In this book chapter, we discuss the problem of equilibration and specifically provide insights into how long it takes to reach equilibrium in closed quantum systems. We first briefly discuss the connection of this problem with recent experiments and forthcoming quantum simulators. Then we provide a comprehensive discussion of equilibration from a heuristic point of view, with a focus on providing an intuitive understanding and connecting the problem with general properties of interacting many-body systems. Finally, we provide a concise review of the rigorous results on equilibration times that are known in the literature.

---

H. Wilming (✉) and J. Eisert

Dahlem Center for Complex Quantum Systems, Freie Universität Berlin, 14195

Berlin, Germany

e-mail: henrikw@phys.ethz.ch

J. Eisert

e-mail: jense@zedat.fu-berlin.de

H. Wilming

Institute for Theoretical Physics, ETH Zurich, 8093 Zurich, Switzerland

T. R. de Oliveira

Instituto de Física, Universidade Federal Fluminense, Niterói,

Rio de Janeiro 24 210-346, Brazil

e-mail: tro@if.uff.br

A. J. Short

H. H. Wills Physics Laboratory, University of Bristol, Tyndall Avenue,

Bristol BS8 1TL, UK

e-mail: tony.short@bristol.ac.uk

## 18.1 Introduction

The observation that closed quantum systems with many degrees of freedom generically equilibrate to a seemingly stationary state has already intrigued the forefathers of quantum mechanics [1, 2]. Indeed, such complex quantum systems seemingly relax to stationarity, despite the entire system undergoing perfectly unitary dynamics. This is not a contradiction: Unitary dynamics is compatible with many observables relaxing in their expectation values to high accuracy, such that the coherent time-evolution can only be witnessed by measuring complex, global observables to high accuracy.

Insights into equilibration of quantum many-body systems are at the heart of the foundations of quantum statistical mechanics: After all, the notion of an equilibrium ensemble naturally makes sense only if one can think of stationary properties, and if these are to be compatible with the microscopic laws of quantum mechanics, they have to emerge from quantum dynamics in one way or the other (see the reviews Refs. [3, 4] and, e.g., Refs. [5–10]). These conceptual considerations are largely backed up by a body of numerical studies (see again the reviews Refs. [4, 11] and, e.g., Refs. [12–18] for a selection of works). Indeed, much of the interest in the question of equilibration is motivated by and stems from research questions on the foundations of statistical mechanics.

More recently, and equally importantly, questions of equilibration have risen to prominence again due to the fact that they feature strongly in the analysis of quenched quantum many-body systems out of equilibrium [4, 11], in a way they can be precisely probed and explored with cold atomic systems [19] and other controlled quantum systems including trapped ions [20]. Since the time-evolution of complex many-body systems cannot be efficiently simulated using classical computers, but may be simulated in such experimental set-ups, many of the recent efforts of dynamical quantum simulation also hint at or build upon questions of equilibration. While the basic mechanism of equilibration of closed quantum systems due to dephasing is largely understood, much less is known on the time-scales at which this is expected to happen. Indeed, since much of the question of equilibration times is still open, quantum simulation allows us to assess a regime of quantum many-body physics that can not yet be backed up in all details by a theoretical underpinning.

This book chapter addresses the questions of what is known on equilibration times of closed quantum many-body systems. We aim at both providing an intuitive understanding of equilibration in terms of dephasing in connection with physically plausible assumptions on quantum many-body system as well as providing a concise review of the rigorous results available in the literature, in the hope to motivate more researchers to work on this interesting and interdisciplinary problem.

## 18.2 Quench Experiments and Non-equilibrium Dynamics

Before coming to the theoretical discussion of equilibration, let us briefly discuss how equilibration of complex many-body systems can be studied experimentally. One of the most prominent architectures for probing out of equilibrium dynamics of quantum many-body systems is constituted by cold atoms in optical lattices or in the continuum, another is that of trapped ions. In fact, some of the research questions addressed in this book chapter have been triggered by experimental findings from that context that have not yet found a satisfactory explanation.

### 18.2.1 Cold Atomic Settings

One of the earliest experiments with cold atoms in optical lattices was concerned with a sudden “quench” in which the Hamiltonian parameters were rapidly changed from a superfluid to a Mott phase and the subsequent non-equilibrium dynamics monitored [21]. Genuine equilibration was observed in a setting in which a charge density wave was initially prepared, making use of an optical superlattice, quenched to an interacting many-body Hamiltonian well captured by a Bose–Hubbard model [22]. In such a setting, several quantities can then be precisely observed as they evolve in time, prominently the imbalance [14] between odd and even sites of the lattice. This quantity exhibits a characteristic equilibration dynamics, following a power law in time in the close to integrable settings [5, 14]. Since then, several settings featuring equilibration have been studied [4, 11, 19, 23, 24]. Importantly, systems featuring many-body localisation [24] equilibrate in the sense that the state becomes locally practically indistinguishable from its time average for most times. However, they do not thermalise, in that the expectation values obtained are different from the ones of the canonical ensemble. Reference [23] observes specifically local equilibration and thermalisation, while showing the coherence of the full evolution. In continuous systems of cold atoms [25], similar features of equilibration are observed.

### 18.2.2 Trapped Ions and Hot Electrons

Complementing this development, systems of trapped ions [20] allow us to monitor equilibration dynamics in time. For example, Refs. [26, 27] observe dynamical quantum phase transitions, but along the way also notice features of equilibration. Another example is the experimental realisation of a physical system featuring many-body localisation in a system of trapped ions with programmable disorder [28], again exhibiting equilibration in time. Having said that, experimental studies of non-equilibrium dynamics in the sense discussed here is by no means confined to cold

atomic systems or settings of trapped ions: Ref. [29], e.g., shows ultra-fast relaxation of hot electrons. In all these setting, questions of equilibration times arise, further motivating the endeavors described in this chapter.

## 18.3 Heuristic Discussion of Equilibration

### 18.3.1 *What it Means for a Closed System to Equilibrate*

In this section, we aim to establish an intuitive understanding of how equilibration in closed systems happens and why it seems plausible that it happens quickly in a generic many-body system. The discussion in this section follows Refs. [30, 31], where more detailed expositions can be found. In Sect. 18.4, we then present rigorous results on equilibration, both in finite and in infinite time.

Consider a finite quantum system, described by Hamiltonian  $H$  with spectral decomposition

$$H = \sum_{k=1}^{d_E} E_k P_k. \quad (18.1)$$

Here,  $E_k$  are the eigenvalues and  $P_k$  the projectors onto its eigenspaces, which can be degenerate so that  $d_E$  may be smaller than the total Hilbert space dimension  $d_T$ . As we are interested in studying the dynamics of closed quantum systems, we will assume that the system is initially in a pure state vector, which can be written as  $|\psi_0\rangle = \sum_k c_k |E_k\rangle$  with  $c_k = \langle E_k | \psi_0 \rangle$ . We can always choose a basis in each degenerate energy-eigenspace  $P_k$  so that  $|\psi_0\rangle$  only has overlap with one basis-vector  $|E_k\rangle$  in this subspace and in the following always assume this choice of basis. As time evolves, the state vector of the system is given by<sup>1</sup>

$$|\psi(t)\rangle = \sum c_k e^{-iE_k t} |E_k\rangle. \quad (18.2)$$

Unless the initial state is an eigenstate of  $H$ , the system will never stop evolving and in this sense the system never equilibrates. But for quantum many-body systems we also do not expect to have access to the instantaneous full quantum state of the system as we would need to keep track of an astronomical number of observables. Usually, we are only interested in a small, fixed set of observables, such as local observables. Also interesting and physically plausible are often sums of local terms, such as the magnetisation in a spin-system. At this level we then may have equilibration due to the fact that we are not accessing all the information about the system.

---

<sup>1</sup>Note that we take  $\hbar = 1$  throughout.

Let us assume we are interested in some observable  $A$ , whose expectation value evolves in time as

$$\langle \psi(t) | A | \psi(t) \rangle = \sum_{i,j} c_j^* A_{j,i} c_i e^{-i(E_i - E_j)t} \quad (18.3)$$

with  $A_{i,j} = \langle E_i | A | E_j \rangle$ . The question is then if such an observable can equilibrate. A system that is equilibrating has to equilibrate to the infinite time-average

$$\lim_{T \rightarrow \infty} \frac{1}{T} \int_0^T \langle \psi(t) | A | \psi(t) \rangle dt = \sum_i |c_i|^2 A_{i,i}, \quad (18.4)$$

since the expectation value of  $A$  for an equilibrating system is close to a particular value for the vast majority of the time and hence the time-average of  $A$  is also close to this value.<sup>2</sup> The time-averaged expectation value corresponds to the expectation value of  $A$  in the quantum state  $\omega = \sum |c_i|^2 |E_i\rangle\langle E_i|$  that maximises the von Neumann entropy given all the conserved quantities of the dynamics [32]. However, in any finite system there will be recurrences, so that  $\langle \psi(t) | A | \psi(t) \rangle$  is in fact quasi-periodic and never equilibrates perfectly [33]. Nevertheless, it can happen, and indeed often does happen, that the deviation of  $\langle \psi(t) | A | \psi(t) \rangle$  from its time-average, which is given by

$$\Delta A(t) = \sum_{i \neq j} c_j^* A_{j,i} c_i e^{-i(E_i - E_j)t}, \quad (18.5)$$

is undetectably small for most of the time. To show this, one often analyses the infinite time-average of the fluctuations  $\Delta A(t)^2$  and we will later present rigorous results which show that this quantity is often extremely small in large systems. If this is the case, i.e., if the time-average of the fluctuations is very small, then the fluctuation  $\Delta A(t)^2$  is small for most times. It is in this sense, that typically the fluctuations are undetectable, that we can meaningfully speak about equilibration of closed quantum systems.

It is important to stress that this does not say much about how long it takes the system to reach equilibrium. If a system of  $N \sim 10^{23}$  particles takes a time that is exponential in  $N$  to reach equilibrium, it practically does not equilibrate. Very roughly speaking, we will thus say that a system equilibrates quickly if the time it takes to reach equilibrium does not depend strongly on the physical size of the system. To explain equilibration in many-body systems, it is thus necessary to explain both why such systems equilibrate at all and why the time it takes them to equilibrate does not increase strongly with the system size.

So far we have talked only about the equilibration of the expectation value of a given observable. A more stringent notion of equilibration requires that the whole probability distribution of measurement outcomes of a given observable equilibrates.

---

<sup>2</sup>Furthermore, it is straightforward to show that  $\lim_{T \rightarrow \infty} \frac{1}{T} \int_0^T (\langle \psi(t) | A | \psi(t) \rangle - A_{\text{eq}})^2 dt$  is minimised by setting  $A_{\text{eq}} = \lim_{T \rightarrow \infty} \frac{1}{T} \int_0^T \langle \psi(t) | A | \psi(t) \rangle dt$ .

If  $A = \sum_{\lambda=1}^{d_A} a_\lambda P_\lambda$  is the spectral decomposition of  $A$ , we thus require that all the spectral projections  $P_\lambda$  equilibrate in expectation value. In the following heuristic discussions, we do not emphasise this but simply assume that the arguments also apply for the projectors  $P_\lambda$ , but this point will be discussed more thoroughly in the section on rigorous results. For now, simply note that in many-body systems the physical relevant observables are usually local observables and the corresponding projectors  $P_\lambda$  are also local observables. Thus, any argument that shows equilibration for all local observables also shows equilibration of their measurement statistics, justifying this simplification.

### 18.3.2 Intuitive Understanding of Equilibration as Dephasing

Having explained in which sense we can say that a closed, finite, quantum system equilibrates, let us now start to develop an intuitive explanation of this process. The expression for the fluctuations away from equilibrium can be rewritten as

$$\Delta A(t) = \sum_{\alpha} v_{\alpha} e^{-iG_{\alpha}t}, \quad (18.6)$$

where  $\alpha \in \mathcal{G} = \{(i, j) : i, j \in \{1, \dots, d_E\}, i \neq j\}$  labels the energy gaps  $G_{\alpha} = (E_j - E_i)$  appearing in the system's spectrum and  $v_{\alpha} = c_j^* A_{j,i} c_i$ . The expression is similar to a Fourier series, but it is not a Fourier series as in general  $G_{\alpha}$  are not multiples of some fundamental “frequency” and we hence obtain a quasi-periodic function, whose rigorous mathematical treatment is complex in general.

Thus we will in the following first try to give intuitive and heuristic arguments about its behaviour and therefore about equilibration. One way to understand the behaviour of  $\Delta A(t)$  is to consider each term  $v_{\alpha} e^{-iG_{\alpha}t}$  as a vector or point in the complex plane evolving with time, with each point moving on a circle of radius  $|v_{\alpha}|$  with angular velocity  $G_{\alpha}$ . We can thus think about these points as a cloud of points evolving in time, see Fig. 18.1 for a numerical example using a XXZ model and Ref. [31] for further numerical examples of systems that do equilibrate and systems that do not equilibrate.

As the value of  $\Delta A(t)$  is the total vector, to have a large fluctuation we need most of the vectors pointing roughly in the same direction, i.e., the cloud of points cannot be isotropic. This suggests that in a given initial state, randomly chosen observables are typically already equilibrated (also see Sect. 18.4 and Chap. 17). Suppose now that the initial state is out of equilibrium:  $\Delta A(t)$  is large and most of the vectors  $v_{\alpha}$  point in the same direction. As time evolves each vector  $v_{\alpha}$  will start to rotate with a angular velocity  $G_{\alpha}$ . If we assume that every gap  $G_{\alpha}$  is unique, all the points move with a different velocity and therefore the vectors will start to distribute more isotropically in the complex plane and their sum will become small. In the case where we have

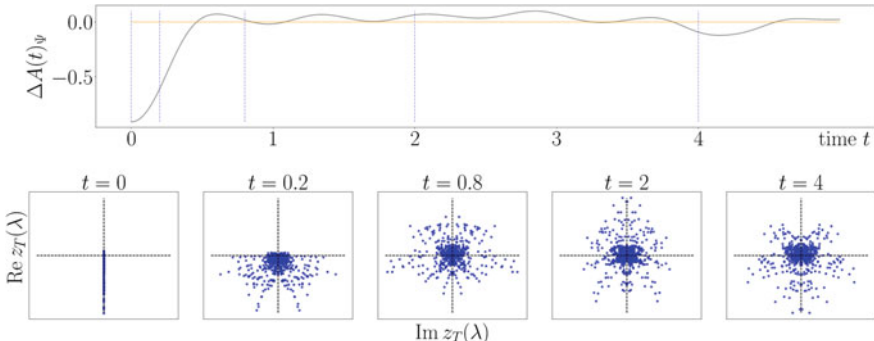


**Fig. 18.1** Time-evolution of a XXZ model with next-nearest neighbour interaction on 15 lattice sites and charge-density wave as initial state  $\Psi$  (see Ref. [31] for details). The upper panel shows the time-evolution of  $\Delta A(t)$ , where the observable is given by  $\sigma_z$  on a single spin. The lower panels show the time-evolution of the regularised  $z_G$  in the complex plane (see paragraph before (18.10)), which are here denoted by  $z_T(\lambda)$  instead of  $z_T^N(G)$ , for  $T \approx 33$ . (Figure from Ref. [31].)

$G_\alpha = G_\beta$  for  $\alpha \neq \beta$ , we can first regroup the vectors into new vectors  $z_G = \sum v_\alpha$ , where the sum is over all  $\alpha$  with  $G_\alpha = G$  and then apply the same reasoning to the representation of  $\Delta A(t)$  as

$$\Delta A(t) = \sum_{G \in \text{Gaps}} z_G e^{-iGt}, \quad (18.7)$$

where the set  $\text{Gaps} = \{G_\alpha : \alpha \in \mathcal{G}\}$  is the set of different energy gaps. This mechanism, usually called dephasing, occurs in many physical phenomena, as the spreading of a wave propagating in a dispersive media or the spreading of the wave-function of a particle in quantum mechanics. The essential difference to our case is that we have a discrete distribution of points and frequencies and not a smooth distribution of points and frequencies, which makes the analysis more complex.

There are hence two fundamental ingredients here: (i) the number and distribution of the vectors  $v_\alpha$  contributing to the sum, (ii) the distribution of the values of  $G_\alpha$ . If there are just a few vectors, or if most of them are negligible, then the vectors will align again in a short time: we will have oscillations and not equilibration. On the other hand if there are many of them it will take a long time to have a realignment; in fact this is the recurrence time which typically increases very fast with the number of vectors. Besides, it can be shown that the typical value of the fluctuation is upper bounded by  $\sum_\alpha |v_\alpha|^2$ . Therefore to have equilibration we need many  $v_\alpha$  contributing to the sum. This is typically the case for generic initial states in many-body systems, since there are roughly  $d_E^2$  energy gaps in the spectrum, which is a number exponentially large in the system size, and generic states will have small overlap with all energy eigenvectors.

Regarding the angular velocities,  $G_\alpha$ , to have equilibration in short time, they must not have a sharp distribution, since then the time for the vectors to spread will be very large since they only disperse very slowly. In sum, to have good equilibration we need

many vectors contributing and the time for it to happen depends on the distribution of the values of  $G_\alpha$  and the corresponding amplitudes  $v_\alpha$ . But how do the equilibration properties of the system depend on the distributions of these quantities?

One way to approach the problem is to assume that the distributions of  $v_\alpha$  and  $G_\alpha$  can be well approximated by a smooth distribution. By this, we mean that

$$\Delta A(t) = \sum_\alpha v_\alpha e^{-iG_\alpha t} = \int \mu(G)v(G)e^{-iGt}dG \quad (18.8)$$

$$\approx \int z(G)e^{-iGt}dG, \quad (18.9)$$

where  $v$  is the distribution of the  $v_\alpha$  and  $\mu$  is the density of energy-gaps (in a distributional sense) and we assume that  $z$  is a continuous function. The most important case where we can hope to make sense of such an approximation is that of a scaling limit of a many-body system, in which the recurrent nature of the dynamics of the finite dimensional quantum system is broken. Suppose therefore, that we have a sequence of system-sizes  $N$  and choose for every system-size a Hamiltonian, observable and initial state in a compatible manner. The prototypical example is given by a translational invariant local Hamiltonian on a square lattice with a translational invariant, pure product state as initial state (possibly with a larger periodicity in space than the Hamiltonian, such as a charge density wave) and with  $A$  being a fixed local observable around the origin of the lattice. In this case, Lieb-Robinson bounds [34, 35] imply that if the system can be shown to equilibrate in the thermodynamic limit  $N \rightarrow \infty$  in time  $\tau$ , then it will also equilibrate in time  $\tau$  and remain equilibrated for a long time for sufficiently large, but finite systems.

We can thus hope that a continuous distribution  $z$  emerges in the thermodynamic limit and use the form of this function to argue about the equilibration time. To be more precise about how such convergence may be understood we should first regularize the discrete distribution of  $z_G$  (or  $v_\alpha$ ) into a smooth distribution, for example by convolving with a Gaussian of variance  $1/T$ , yielding a smooth distribution  $z_T^N$  for every system size  $N$  of the sequence of initial states, Hamiltonians and observables that we consider. Equation (18.9) then holds in terms of  $z_T^N$  for times much smaller than  $T$ . The statement that the distribution of  $v_\alpha$  and  $G_\alpha$  converge to a continuous function then means that the limit

$$\lim_{T \rightarrow \infty} \lim_{N \rightarrow \infty} z_T^N(G) = z(G) \quad (18.10)$$

exists and yields a continuous function.

The fluctuations in time are then approximated by the Fourier transform of the function  $z$ . As a simple example, assume that  $z$  is real and given by a Gaussian with mean zero and variance  $1/\tau$ . We then have

$$\Delta A(t) \approx \Delta A(0) e^{(-t/\tau)^2}. \quad (18.11)$$

Thus  $\Delta A(t)$  is also a Gaussian with mean zero and variance  $\tau$ . Using the variance as the scale for the decay of the Gaussian we can identify  $\tau$  as an equilibration time-scale: the equilibration time is the variance of  $\Delta A(t)$ , which is proportional to the inverse of the variance of  $z$ . A similar relationship, which is a kind of uncertainty principle, can be expected to hold whenever  $z$  is a bounded, (square-)integrable function and is roughly unimodal, i.e., only has one strong peak. In particular, whenever  $z$  is square-integrable,  $\Delta A(t)$  is also square-integrable and hence has to decay to zero as  $|t| \rightarrow \infty$ . We will later provide arguments that make this form of  $z$  plausible for generic many-body systems if the observable  $A$  is a local observable. The rigorous results presented in Sect. 18.4 will further elaborate on the connection between the equilibration time and the form of the probability distribution  $p_\alpha = |v_\alpha|/Q$ , where  $Q = \sum_\alpha |v_\alpha|$ .

### 18.3.3 Connecting to General Properties of Many-Body Systems

As emphasized in the previous section, the equilibration behaviour depends on the initial state, Hamiltonian and the observable one is interested in. In this section we specialise to the case of a local many-body system and present general properties of such systems that add plausibility to the assumptions that we made in the previous section. In the following we thus consider a situation, where (i) the Hamiltonian is a local Hamiltonian  $H = \sum_{x \in \Lambda} h_x$  on some regular lattice  $\Lambda$  with  $|\Lambda| = N$  lattice sites; (ii) the observable  $A$  is a local observable, i.e., supported on some finite region independent of the system size, for example a spin in the center of the system; (iii) the initial state  $\rho$  is pure and has a finite correlation length  $\xi > 0$ ,

$$|\mathrm{tr}(\rho AB) - \mathrm{tr}(\rho A)\mathrm{tr}(\rho B)| \leq \|A\| \|B\| e^{-d(A,B)/\xi}, \quad (18.12)$$

where  $d(A, B)$  is the lattice distance between the support of the observables  $A$  and  $B$  and  $\|\cdot\|$  denotes the operator norm, so the largest singular value. The last assumption is of particular relevance for quench experiments in optical lattices, where the initial state is often given by either a well controlled product state or the ground-state of some non-critical, local Hamiltonian.

Let us begin with discussing the relevant properties of the underlying Hamiltonian. In a quench experiment, the initial state  $\rho$  can usually be expected to have a finite energy density with respect to the Hamiltonian  $H$ . It will thus be supported not on the low-energy subspace close to the groundstate, but in the bulk of the spectrum. We are hence interested in how the bulk of the energy-spectrum looks like for generic, local Hamiltonians. The first important observation to make is that the number of different eigenvalues of a local Hamiltonian is typically exponentially large in the size of the system, while their magnitude is at most linear in the size of the system. Therefore, at least in the bulk of the spectrum, the spectrum is extremely dense and typical differences between neighbouring eigenvalues are exponentially small in the system

size. Indeed, it is well known that the energy-spectrum of a generic local Hamiltonian can be well approximated by a Gaussian in the bulk of the spectrum. To understand this, observe that the energy spectrum can be seen as the probability distribution of energy in the maximally mixed state  $1/d_T$ . Since this state is a product-state and the Hamiltonian consists of a large sum of operators, with the support of each of them overlapping only with the support of finitely many other ones, we can understand the spectrum of the Hamiltonian as a large sum of weakly-correlated, bounded random variables. We can hence expect that a central-limit theorem applies, yielding a Gaussian density of states in the bulk of the spectrum. Indeed, such arguments can be made rigorous, showing that for any state with a finite correlation length, the distribution of energies  $p_i = \text{tr}(\rho|E_i\rangle\langle E_i|)$  is roughly Gaussian with a standard deviation of order  $\sqrt{N}$  [36–38]. As a consequence of these results, we can also expect that the distribution of energy gaps follows a roughly Gaussian distribution with standard deviation of order  $\sqrt{N}$ . Since energy gaps always come in pairs  $G_{(i,j)} = -G_{(j,i)}$ , this distribution has mean zero. At this point, it is worth emphasizing that we are here talking about the full distribution of energy-differences in the spectrum of the many-body Hamiltonian, and *not* about what is known as the *level-statistics* in random matrix theory (see Chap. 19), which is concerned with the expected distance in energy between the  $i$ -th energy level and the  $i + 1$ -th energy level (or, more generally, the  $i + k$ -th energy level).

The above discussion already suggests that for a pure initial state with finite correlation length and finite energy density, the expansion coefficients  $c_i$  in the energy eigenbasis can be thought of as a smooth distribution that is spread out over exponentially many energy-levels, with each  $c_i$  being exponentially small in absolute value. Indeed, there are several arguments supporting that one can expect that the *inverse participation ratio* IPR or the inverse of the *effective dimension*  $d^{\text{eff}}$  are exponentially small in the system size for generic, interacting many-body systems [6, 9, 10, 32, 39–41],

$$\sum_i |c_i|^4 = \text{IPR}(\rho, H) = \frac{1}{d^{\text{eff}}(\rho, H)} \leq e^{-kN}, \quad (18.13)$$

for some constant  $k > 0$ . This quantity will also play an important role in the following section, treating rigorous results about equilibration.

Let us now turn to the observable  $A$ . Intuitively, a local observable should only be able to connect energy eigenstates which differ by a small amount in energy, suggesting that matrix elements  $A_{i,j}$  are very small if  $|E_i - E_j|$  is large. This can indeed be made rigorous, as has been shown in Refs. [30, 42]. In a local many-body system and for any fixed local observable there exists constants  $\alpha, R > 0$  such that

$$|A_{i,j}| \leq \|A\| e^{-\alpha(|E_i - E_j| - 2R)}, \quad (18.14)$$

where  $R$  is proportional to the support of  $A$ . This implies that the coefficients  $v_\alpha$  are exponentially small in  $G_\alpha$  and the function  $z$  can be expected to fall off exponentially.

tially in  $|G|$ . Since the gaps are distributed essentially like a Gaussian with standard deviation of order  $\sqrt{N}$ , this implies that on the scale of the gaps that are relevant to the problem, the distribution of gaps can be expected to be essentially *uniform*. Thus we can, by making only a small error, replace the distribution  $\mu$  in (18.9) by  $1/2G_{\max}$ , where  $G_{\max}$  is some cut-off gap. As long as the distribution  $v$  is a well-defined bounded function, we then obtain equilibration in a time that does not diverge with the system size, since the function  $z$  will be bounded and integrable. Since we expect the coefficients  $c_i$  and hence the  $v_\alpha$  to be exponentially small in  $N$ , this seems highly plausible. However, since the number of coefficients  $v_\alpha$  is also exponentially large in  $N$ , it is in principle possible that as we increase the system size, exponentially many of them concentrate in an exponentially small region of gaps  $G$ , leading to a situation where  $v$  (and hence  $z$ ) is not given by a bounded function, but can only be understood in a distributional sense. Thus, while the above arguments make it plausible that generical many-body systems equilibrate quickly and allow us to understand in a qualitative way how this happens, they do not provide a rigorous proof. Having discussed the heuristics of equilibration in many-body systems, let us now turn to rigorous, general results about equilibration in closed quantum systems.

## 18.4 Rigorous Results

Consider an arbitrary initial state  $\rho(0)$  (which may be pure or mixed) of a finite-dimensional quantum system, evolving via a Hamiltonian  $H = \sum_{k=1}^{d_E} E_k P_k$ . Let us denote the time averaging of an arbitrary quantity  $f(\cdot)$  over a finite interval of time  $T$  by

$$\langle f(t) \rangle_T = \frac{1}{T} \int_0^T f(t) dt, \quad (18.15)$$

where  $\langle f(t) \rangle_\infty = \lim_{T \rightarrow \infty} \langle f(t) \rangle_T$ . For the state to equilibrate with respect to a given observable  $A$  it is necessary for the expectation value of  $A$  for  $\rho(t)$  to be very close to the expectation value of  $A$  for the static equilibrium state  $\omega = \langle \rho(t) \rangle_\infty$  for most times. This happens under very general conditions. Indeed, all that is required is that the state is spread over many different energies, and that the Hamiltonian does not contain any highly degenerate energy gaps in its spectrum. In particular, it can be proven that [7, 8]

$$\langle (\text{tr}(\rho(t)A) - \text{tr}(\omega A))^2 \rangle_\infty \leq g \sum_\alpha |v_\alpha|^2 \leq \frac{g \|A\|^2}{d^{\text{eff}}}, \quad (18.16)$$

where  $g$  is the degeneracy of the most degenerate energy gap,<sup>3</sup>  $v_\alpha = \rho_{i,j} A_{j,i}$  is the quantity described in Sect. 18.3.2 (generalised slightly to include initial mixed states),  $\|\cdot\|$  again denotes the operator norm, and

---

<sup>3</sup>I.e.  $g = \max_\alpha |\{\beta : G_\beta = G_\alpha\}|$ .

$$d^{\text{eff}} = \frac{1}{\sum_k \text{tr}(P_k \rho(0))^2}, \quad (18.17)$$

is the *effective dimension* of the state, describing approximately how many different energies it is spread over (e.g. if the state is spread equally over  $N$  different energy levels then  $d^{\text{eff}} = N$ ). Hence if  $g$  is not too large, as one would expect for a physically realistic interacting Hamiltonian, and  $d^{\text{eff}}$  is large, as one would expect for a realistic quantum many-body system state, then  $\langle (\text{tr}(\rho(t)A) - \text{tr}(\omega A))^2 \rangle_\infty \ll \|A\|^2$  and the expectation value of  $A$  equilibrates. One expects the effective dimension to grow with the system size, leading to less pronounced deviations from the time average. Again, there is strong numerical evidence for this expectation [15] and theoretical arguments which suggest that  $d^{\text{eff}}$  grows exponentially with  $N$  in many interacting many-body systems, see references before (18.13).

Note that although equilibration of the expectation value is a necessary condition for equilibration, it is not by itself sufficient, as one can construct very different observable distributions with the same expectation value. A stronger definition of equilibration with respect to an observable  $A$  is to show that for most times one cannot distinguish  $\rho(t)$  from  $\omega$  via a measurement of  $A$ . We define the distinguishability  $D_A(\rho(t), \omega)$  as the statistical distance between the probability distributions obtained when measuring  $A$  on  $\rho(t)$  and  $\omega$ .<sup>4</sup> The previous result can then be used to obtain a bound on the distinguishability [8, 43, 44], giving

$$\langle D_A(\rho(t), \omega) \rangle_\infty \leq \frac{1}{2} \left( \frac{g(N-1)}{d^{\text{eff}}} \right)^{1/2}, \quad (18.18)$$

where  $N$  is the number of possible outcomes in the measurement of  $A$  (i.e., the number of distinct eigenvalues of  $A$ ), which is typically much less than  $d^{\text{eff}}$  for realistic measurements on quantum many-body systems. Similar results can be obtained for finite sets of measurements [8, 43], or for all possible measurements on a small subsystem, proving that small subsystems interacting with a large bath generally equilibrate to a static reduced density operator [6, 8].

The above results apply to infinite time equilibration, but can be extended to equilibration over a finite time interval [8]. In the case of (18.16) this gives

$$\langle (\text{tr}(\rho(t)A) - \text{tr}(\omega A))^2 \rangle_T \leq \frac{g\|A\|^2}{d^{\text{eff}}} \left( 1 + \frac{8 \log_2 d_E}{\epsilon_{\min} T} \right), \quad (18.19)$$

where  $\epsilon_{\min}$  is the smallest difference between energy gaps<sup>5</sup> (i.e.,  $\epsilon_{\min} = \min_{\alpha \neq \beta} |G_\alpha - G_\beta|$ ). The  $\log_2 d_E$  term is slightly awkward, as it means that the bound does not extend

<sup>4</sup>Hence  $D_A(\rho(t), \omega) = \frac{1}{2} \sum_i |p_i(\rho(t)) - p_i(\omega)|$ , where  $p_i(\rho(t))$  is the probability for result  $i$  in a measurement of  $A$  on state  $\rho(t)$ . This can be understood operationally in terms of the maximal success probability  $p$  of guessing correctly whether the state is  $\rho(t)$  or  $\omega$  after measuring  $A$  (given that you are given either  $\rho(t)$  or  $\omega$  with equal probability) via  $D_A(\rho(t), \omega) = 2p - 1$ .

<sup>5</sup>If desired, one can replace  $\epsilon_{\min}$  with an arbitrary energy  $\epsilon > 0$ , and  $g$  by  $N(\epsilon)$ , the maximum number of energy gaps which fit within a window of size  $\epsilon > 0$ .

to infinite dimensional systems with discrete spectra. However, a different approach [45] can eliminate this term at the expense of a slightly worse infinite-time limit, giving

$$\langle (\text{tr}(\rho(t)A) - \text{tr}(\omega A))^2 \rangle_T \leq \frac{g\|A\|^2}{d^{\text{eff}}} \frac{5\pi}{2} \left( \frac{3}{2} + \frac{1}{\epsilon_{\min} T} \right). \quad (18.20)$$

Similarly to before, this result can also be used to bound the distinguishability via

$$\langle D_A(\rho(t), \omega) \rangle_T \leq \frac{1}{2} \left( \frac{g(N-1)}{d^{\text{eff}}} \frac{5\pi}{2} \left( \frac{3}{2} + \frac{1}{\epsilon_{\min} T} \right) \right)^{1/2}. \quad (18.21)$$

These results are very general, but as a consequence they generally lead to very large equilibration time bounds. In particular, consider a system whose state is prepared in an energy window of width  $\Delta E$  containing  $d$  states. Then even in the best case we would have  $d^{\text{eff}} = d$  and  $\epsilon_{\min} \approx 2\Delta E/d^2$  (as there are  $d^2$  energy gaps between  $d$  levels, and the range of gaps is twice as large as the energy range), requiring  $T \approx d/\Delta E$  for the bound to become significant. This is much shorter than the recurrence time (which is typically exponential in the dimension [46]) but is still much larger than observed equilibration times for realistic physical systems.

One might wonder whether this general bound could be tightened significantly, or whether systems could exist which really required such large equilibration times. The answer is the latter [45, 47]. Indeed for any initial pure state with high effective dimension, we can construct an observable which takes an extremely long time to equilibrate. Consider the projector onto the subspace spanned by ‘snapshots’ of the evolving state for many successive discrete time steps. By choosing an appropriate size and number of time-steps, one can show that this observable will take longer than  $d^{\text{eff}}/(1000\sigma_E)$  to equilibrate [45] (where  $\sigma_E$  is the standard deviation in energy). This has a similar scaling to the general bound considered above.

One limited situation in which fast equilibration can be proven is when the observable to be measured has only two possible outcomes, and the rank of the projector onto one of the outcomes (which we will denote by  $K$ ) is very small. In this case, one can show that [45]

$$\langle D_A(\rho(t), \omega) \rangle_T \leq c \left( K \eta_{\frac{1}{T}} \right)^{1/2}, \quad (18.22)$$

where  $c \simeq 7$  and  $\eta_{\frac{1}{T}}$  is the maximum probability of the state lying in an energy window of width  $1/T$  (i.e., the maximum over  $E$  of the probability of the energy being in the range  $(E, E + 1/T)$ ). For an initial state with a dense set of occupied energy levels, we could approximate the energy distribution via a continuous function. If this function is approximately unimodal (i.e., with ‘one hump’, such as a Gaussian or top-hat function) then the maximum probability density will be  $\sim 1/\sigma_E$ . In such a case, we would obtain  $\eta_{\frac{1}{T}} \sim 1/(\sigma_E T)$ . More generally, we can always define constants  $a$  and  $\delta$  such that

$$\eta_{\frac{1}{T}} \leq \frac{a}{\sigma_E T} + \delta, \quad (18.23)$$

where  $a > 0$  is a real parameter which captures the shape of the distribution and  $\delta > 0$  corrects for the discreteness of the spectrum. For approximately unimodal energy distributions spread over many energy levels, we would expect  $a \sim 1$  and  $\delta \ll 1$ . Inserting (18.23) into (18.22) we obtain

$$\langle D_A(\rho(t), \omega) \rangle_T \leq c \left( K \left( \frac{a}{\sigma_E T} + \delta \right) \right)^{1/2}, \quad (18.24)$$

giving good equilibration after  $T \sim 1000aK/\sigma_E$ , a typically fast time scale with no explicit dependence on  $d^{\text{eff}}$ . When the initial state is pure, a particularly interesting case of such an observable is the projection onto the initial state, for which  $K = 1$ . We will return to this example in the next subsection.

Another possibility is to calculate equilibrium times for specific systems. In Ref. [5] (see also Refs. [48, 49]) it is shown that the Bose–Hubbard model quenched from a Mott quantum phase to the free strong superfluid regime obeys local equilibration over the entire interval  $[t_{\text{Relax}}, t_{\text{Relax}} + t_{\text{Recurrence}}]$  (i.e., individual sites or small blocks are almost indistinguishable from a static state for all times in this interval). The equilibration time,  $t_{\text{Relax}}$ , is relatively fast, and is governed by the inverse of the hopping parameter (which determines the speed of sound in the system) and the desired equilibration closeness, whilst  $t_{\text{Recurrence}}$  can be made arbitrarily large by increasing the size of the system.

### 18.4.1 Bounding Equilibration Times Using Randomness

Although we have shown that in general equilibration times can be very large, most observables of interest in the real world seem to equilibrate much faster – typically in time scales which depend on the physical size of the system rather than its dimension (which for a many body system is given by  $\log d$  rather than  $d$ ). An interesting question is to consider the equilibration times of ‘typical’ situations, which might equilibrate much faster than the general bound. One way to approach this is to choose one of the components of the setup (the observable, Hamiltonian, or initial state) at random - thereby avoiding fine-tuned setups. The effect of introducing randomness in each of the three components has been considered [45, 50, 50–57], and does indeed lead to much faster equilibration times.

#### 18.4.1.1 Random Observables

Let us first consider the equilibration of a randomly chosen observable, given a fixed Hamiltonian and a fixed pure initial state with high effective dimension. Note firstly that most observables are already equilibrated (assuming they have a reasonable number of distinct outcomes  $N \ll d$ ), in the sense that they cannot distinguish the true state  $\rho(t)$  from the equilibrium state  $\omega$  over any interval. In particular

$$\langle D_A(\rho(t), \omega) \rangle_A \leq \frac{1}{2} \left( \frac{N}{d+1} \right)^{1/2}, \quad (18.25)$$

where the average is not over time but over all observables  $A$  with a fixed spectrum but a randomly chosen eigenbasis.<sup>6</sup> Hence also  $\langle\langle D_A(\rho(t), \omega) \rangle_T \rangle_A \leq \frac{1}{2}(N/(d+1))^{1/2} \ll 1$  for any  $T$ .

To make this situation more interesting, we can consider all observables for which the initial state is an eigenstate, which are typically out of equilibrium initially. For such observables, we find

$$\langle D_A(\rho(t), \omega) \rangle_A \leq D_{\rho(0)}(\rho(t), \omega) + \frac{1}{2} \left( \frac{N}{d-1} \right)^{1/2} \quad (18.26)$$

and, hence, using the result in the previous section,

$$\langle\langle D_A(\rho(t), \omega) \rangle_T \rangle_A \leq c \left( \frac{a}{\sigma_E T} + \delta \right)^{1/2} + \frac{1}{2} \left( \frac{N}{d-1} \right)^{1/2}, \quad (18.27)$$

which will generally yield a very fast equilibration time.

Similar fast equilibration is obtained in Ref. [56], which considers a projector  $P_{\text{neq}}$  onto a subspace of non-equilibrium states of dimension  $d_{\text{neq}} \ll d$ , and initial states within a narrow energy band with an exponentially increasing density of states characterized by inverse temperature  $\beta$ . When this projector is chosen at random within the energy band, any initial state leaves this space of non-equilibrium states very fast. In particular,

$$\langle \text{tr}(\rho(t) P_{\text{neq}}) \rangle_T \lesssim \frac{2\pi\beta}{T} \quad (18.28)$$

for all  $T$  less than

$$T_{\max} = 2\pi\beta \min \left\{ \left( \frac{d}{d_{\text{neq}}} \right)^{\frac{1}{4}}, d^{\frac{1}{6}} \right\}. \quad (18.29)$$

#### 18.4.1.2 Random Hamiltonians

Another place that randomness can be included, needless to say, is the Hamiltonian. In particular, consider that the initial state and observable as well as the spectrum of the Hamiltonian are fixed, but that the eigenbasis of the Hamiltonian is chosen at random<sup>7</sup> [50, 51, 54, 55, 57]. In this case, not only the equilibration time but

<sup>6</sup>Here and later in this section, by random we mean chosen with respect to the unitarily invariant Haar measure.

<sup>7</sup>Note that if the initial state is entirely contained in some energy window, then one can consider only the restricted Hilbert space in that window and consider a rotation of the eigenbasis only within that subspace, in which case the results below are relative to that subspace.

the full time-evolution can be approximated. Note that this paradigmatic situation is quite different from the physically more plausible one in which a local Hamiltonian has additional random terms, such as in models featuring many-body localisation [24]. In Ref. [54] the equilibrium of a small system interacting with a large bath is considered in this context, and it is shown that

$$\langle \text{tr}(\rho_S(t) - \omega_S)^2 \rangle_H \leq \frac{|\chi|^2}{d_S d^2} + \left( \frac{|\zeta|^2}{d^2} - \frac{\gamma}{d^2} \right)^2 + O\left(\frac{1}{d_B}\right), \quad (18.30)$$

where  $\langle \cdot \rangle_H$  denotes the average over Hamiltonians,  $d_S$  and  $d_B$  are the dimension of the system and bath respectively (with  $d = d_S d_B$ ),

$$\chi = \sum_{k=1}^{d_E} d_k e^{2iE_k t}, \quad \zeta = \sum_{k=1}^{d_E} d_k e^{iE_k t}, \quad \gamma = \sum_{k=1}^{d_E} d_k^2, \quad (18.31)$$

where  $d_k$  is the degeneracy of the  $k$ th energy level. The bound given in (18.30) can be straightforwardly extended to a bound on the trace-distance, which describes how well  $\rho_S(t)$  can be distinguished from  $\omega_S$  using any measurement,<sup>8</sup> via  $\langle \|\rho_S(t) - \omega_S\|_1 \rangle_H \leq (d_S \langle \text{tr}(\rho_S(t) - \omega_S)^2 \rangle_H)^{1/2}$ . Related results for subsystem equilibration in the presence of a random Hamiltonian are given in Refs. [50, 55, 57].

The equilibration of a particular observable with respect to a random Hamiltonian is shown in Ref. [51] to be approximately given by

$$\text{tr}(\rho(t)A) \simeq \text{tr}(\rho_{\text{av}}A) + F(t)(\text{tr}(\rho(0)A) - \text{tr}(\rho_{\text{av}}A)) \quad (18.32)$$

for the vast majority of times and choices of Hamiltonian, where  $\rho_{\text{av}}$  is the equilibrium state  $\omega$  averaged over different choices for the Hamiltonian (resulting in  $\rho_{\text{av}}$  being close to the maximally mixed state), and

$$F(t) = \frac{d}{d-1} \left( \left| \frac{1}{d} \sum_{j=1}^d e^{iE_j t} \right|^2 - \frac{1}{d} \right). \quad (18.33)$$

Note that  $F(0) = 1$ , and that  $F(t)$  tends towards zero as  $t$  increases, becoming  $O(1/d)$  in the large  $t$  limit in which the phases randomise. In the physically relevant case in which the initial state lies within a microcanonical energy window of width  $\Delta E$  with exponentially increasing density of states, corresponding to a thermal bath with inverse temperature  $\beta$  (where  $\beta \Delta E \gg 1$ ), then

$$F(t) \simeq \frac{1}{1 + (t/\beta)^2}, \quad (18.34)$$

---

<sup>8</sup>In particular  $D(\rho_S(t), \omega_S) = \frac{1}{2} \|\rho_S(t) - \omega_S\|_1$  can be understood operationally in terms of the maximal success probability  $p$  of guessing correctly whether the state is  $\rho_S(t)$  or  $\omega_S$  (given each with equal probability) using any measurement on the system, via  $D(\rho_S(t), \omega_S) = 2p - 1$ .

giving an equilibration time comparable with  $\beta$ , which is very fast. Furthermore, in this case the equilibrium state is typically very close to the microcanonical state (i.e., the state thermalises as well as equilibrates). Excitingly, this equilibration behaviour has been observed in experiments [51]. What is more, similar equilibration behaviour can be shown even when the energy eigenstates are randomly permuted rather than chosen at random [53], although in this case the system will not generally thermalise.

### 18.4.1.3 Random States

The final place to introduce randomness is the initial state, for a fixed observable and Hamiltonian. As in the case of a random observable, most initial states are already equilibrated. However, interesting results can be obtained by dividing the quantum system up into a particular small subsystem of interest, and a large bath which is in a randomly chosen, or highly mixed, initial state [52]. The key technical result is

$$\langle (\text{tr}(\rho(t)A) - \text{tr}(\omega A))^2 \rangle_T \leq 4\pi \|A\|^2 d \text{tr}(\rho(0))^2 \xi_{\frac{1}{T}}, \quad (18.35)$$

where  $\xi_{\frac{1}{T}}$  is the analogous function to  $\eta_{\frac{1}{T}}$ , but applied to the probability distribution  $p_\alpha = |v_\alpha|/Q$  where  $Q = \sum_\alpha |v_\alpha|$ . We can bound  $\xi_{\frac{1}{T}}$  analogously to (18.23) by

$$\xi_{\frac{1}{T}} \leq \left( \frac{a}{\sigma_G T} + \delta \right), \quad (18.36)$$

introducing parameters  $a, \delta > 0$  which characterise the probability distribution, and denoting by  $\sigma_G$  the standard deviation of gaps with respect to this distribution. If  $p_\alpha$  is approximately unimodal with a dense spectrum, we would expect  $a \sim 1$  and  $\delta \ll 1$  as before. If the state is highly mixed initially then this can give fast equilibration times. For example if  $\rho(0) = \rho_S \otimes I_B/d_B$  for a small system of dimension  $d_S$  (on which the observable  $A$  acts) interacting with a maximally mixed bath of dimension  $d_B$ , then

$$\langle (\text{tr}(\rho(t)A) - \text{tr}(\omega A))^2 \rangle_T \leq 4\pi \|A\|^2 d_S \left( \frac{a}{\sigma_G T} + \delta \right), \quad (18.37)$$

which leads to equilibration times comparable to  $ad_S/\sigma_G$  and independent of the bath size.

This result can be extended to bound the equilibration time for a system interacting with a bath in the microcanonical state of width  $\Delta E$  with an exponentially increasing density of states with inverse temperature  $\beta$  (where  $\beta\Delta E \gg 1$ ) to get [52]<sup>9</sup>

---

<sup>9</sup>Note that this is a slightly simplified form of the bound given in Ref. [52] neglecting minor corrections. The version given in Ref. [52] also includes the bound  $\sigma_G^2 \geq (Q\|A\|)^{-1} |\text{tr}([\rho(0), H], H]A)|$  which can be substituted in place of  $\sigma_G$  and is simpler to compute.

$$\langle (\text{tr}(\rho(t)A) - \text{tr}(\omega A))^2 \rangle_T \lesssim 4\|A\|^2 \left( \pi d s e^{\beta \|H_S\| + (1 + \sqrt{d_S}) K \beta \|H_I\|} \left( \frac{a}{\sigma_G T} + \delta \right) + \frac{18}{K^2} \right), \quad (18.38)$$

where  $H_S$  and  $H_I$  are the system and interaction Hamiltonians respectively, and  $K$  is an arbitrary constant. Note that the bath Hamiltonian and bath dimension do not feature. Although this result and (18.37) refer to mixed initial states of the bath, very similar results can be obtained for randomly chosen pure initial states of the bath.

## 18.5 Summary and Outlook

We have discussed the problem of equilibration times in closed quantum systems from a heuristic as well as a rigorous point of view. From the point of view of many-body physics, it seems highly plausible that generic, complex many-body systems equilibrate in a time that depends only weakly on the system-size. However, while quite a few results are available in the case of integrable systems [5, 12, 58–66], whose equilibration behaviour follows a power-law, very little can be said generally about this equilibration time in strongly interacting systems; in particular, it is not yet clear in which way which concrete physical properties influence how quickly a system equilibrates. Numerical studies on classical computers are out-of-reach for these questions since large systems have to be simulated for long times. Therefore this question is an ideal use-case for forthcoming quantum simulators in which Hamiltonians and initial states can be controlled reliably.

While the heuristic discussion provided significant evidence that locally interacting many-body systems indeed equilibrate, the given arguments are not mathematically rigorous. The rigorous results presented in the subsequent section, on the other hand, generally provide fairly weak general bounds on equilibration times, or extremely fast equilibration when some part of the setup is chosen at random. It is thus highly desirable to bridge the two worlds by incorporating general properties of many-body systems as assumptions to obtain stronger, yet rigorous bound on equilibration times which do not rely on randomness. We hope that this book chapter can provide a starting point and as an invitation for further researchers to study this interesting and important problem.

**Acknowledgements** We would like to thank Lea F. Santos, C. Gogolin, and P. Reimann for comments on an earlier draft. H. W. and J. E. acknowledge funding from the Studienstiftung des Deutschen Volkes, the ERC (TAQ), the DFG (EI 519/14-1, EI 519/7-1, CRC 183), and the Templeton Foundation. T. R. O. is supported by the Brazilian National Institute for Science and Technology of Quantum Information (INCT-IQ) and the National Counsel of Technological and Scientific Development (CNPq).

## References

1. E. Schrödinger, Ann. Phys. **388**, 956 (1927). <https://doi.org/10.1002/andp.19273881504>
2. J. von Neumann, Z. Phys. A **57**, 30 (1929). <https://doi.org/10.1007/BF01339852>
3. C. Gogolin, J. Eisert, Rep. Prog. Phys. **79**, 56001 (2016). <https://doi.org/10.1088/0034-4885/79/5/056001>
4. A. Polkovnikov, K. Sengupta, A. Silva, M. Vengalattore, Rev. Mod. Phys. **83**, 863 (2011). <https://doi.org/10.1103/RevModPhys.83.863>
5. M. Cramer, C.M. Dawson, J. Eisert, T.J. Osborne, Phys. Rev. Lett. **100**, 030602 (2008a). <https://doi.org/10.1103/PhysRevLett.100.030602>
6. N. Linden, S. Popescu, A.J. Short, A. Winter, Phys. Rev. E **79**, 61103 (2009). <https://doi.org/10.1103/PhysRevE.79.061103>
7. P. Reimann, Phys. Rev. Lett. **101**, 190403 (2008). <https://doi.org/10.1103/PhysRevLett.101.190403>
8. A.J. Short, T.C. Farrelly, New J. Phys. **14**, 013063 (2012). <https://doi.org/10.1088/1367-2630/14/1/013063>
9. P. Reimann, M. Kastner, New J. Phys. **14**, 43020 (2012). <https://doi.org/10.1088/1367-2630/14/4/043020>
10. T. Farrelly, F.G. Brandão, M. Cramer, Phys. Rev. Lett. **118**, 140601 (2017). <https://doi.org/10.1103/PhysRevLett.118.140601>
11. J. Eisert, M. Friesdorf, C. Gogolin, Nature Phys. **11**, 124 (2015). <https://doi.org/10.1038/nphys3215>
12. M. Rigol, V. Dunjko, V. Yurovsky, M. Olshanii, Phys. Rev. Lett. **98**, 050405 (2007). <https://doi.org/10.1103/PhysRevLett.98.050405>
13. M. Rigol, Phys. Rev. A **80**, 053607 (2009). <https://doi.org/10.1103/PhysRevA.80.053607>
14. M. Cramer, A. Flesch, I.P. McCulloch, U. Schollwoeck, J. Eisert, Phys. Rev. Lett. **101**, 063001 (2008b). <https://doi.org/10.1103/PhysRevLett.101.063001>
15. P.R. Zangara, A.D. Dente, E.J. Torres-Herrera, H.M. Pastawski, A. Iucci, L.F. Santos, Phys. Rev. E **88**, 032913 (2013). <https://doi.org/10.1103/PhysRevE.88.032913>
16. F. Goth, F.F. Assaad, Phys. Rev. B **85**, 085129 (2012). <https://doi.org/10.1103/PhysRevB.85.085129>
17. M. Eckstein, M. Kollar, P. Werner, Phys. Rev. B **81**, 115131 (2010). <https://doi.org/10.1103/PhysRevB.81.115131>
18. J.-S. Bernier, R. Citro, C. Kollath, E. Orignac, Phys. Rev. Lett. **112**, 065301 (2014). <https://doi.org/10.1103/PhysRevLett.112.065301>
19. I. Bloch, J. Dalibard, S. Nascimbene, Nature Phys. **8**, 267 (2012). <https://doi.org/10.1038/nphys2259>
20. R. Blatt, C.F. Roos, Nature Phys. **8**, 277 (2012). <https://doi.org/10.1038/nphys2252>
21. M. Greiner, O. Mandel, T.W. Haensch, I. Bloch, Nature **419**, 51 (2002). <https://doi.org/10.1038/nature00968>
22. S. Trotzky, Y.-A. Chen, A. Flesch, I.P. McCulloch, U. Schollwöck, J. Eisert, I. Bloch, Nature Phys. **8**, 325 (2012). <https://doi.org/10.1038/nphys2232>
23. A.M. Kaufman, M.E. Tai, A. Lukin, M. Rispoli, R. Schittko, P.M. Preiss, M. Greiner, Science **353**, 794 (2016). <https://doi.org/10.1126/science.aaf6725>
24. M. Schreiber, S.S. Hodgman, P. Bordia, H.P. Lüschen, M.H. Fischer, R. Vosk, E. Altman, U. Schneider, I. Bloch, Science **349**, 842 (2015). <https://doi.org/10.1126/science.aaa7432>
25. M. Gring, M. Kuhnert, T. Langen, T. Kitagawa, B. Rauer, M. Schreitl, I. Mazets, D.A. Smith, E. Demler, J. Schmiedmayer, Science **337**, 1318 (2012). <https://doi.org/10.1126/science.1224953>
26. P. Jurcevic, H. Shen, P. Hauke, C. Maier, T. Brydges, C. Hempel, B.P. Lanyon, M. Heyl, R. Blatt, C.F. Roos, Phys. Rev. Lett. **119**, 080501 (2017). <https://doi.org/10.1103/PhysRevLett.119.080501>
27. J. Zhang, G. Pagano, P.W. Hess, A. Kyprianidis, P. Becker, H. Kaplan, A.V. Gorshkov, Z.-X. Gong, C. Monroe, Nature **551**, 601 (2017). <https://doi.org/10.1038/nature24654>

28. J. Smith, A. Lee, P. Richerme, B. Neyenhuis, P.W. Hess, P. Hauke, M. Heyl, D.A. Huse, C. Monroe, *Nature Phys.* **12**, 907 (2016). <https://doi.org/10.1038/nphys3783>
29. L. Guidoni, E. Beaurepaire, J.-Y. Bigot, *Phys. Rev. Lett.* **89**, 017401 (2002). <https://doi.org/10.1103/PhysRevLett.89.017401>
30. T.R. de Oliveira, C. Charalambous, D. Jonathan, M. Lewenstein, A. Riera, *New J. Phys.* **20**, 033032 (2018). <https://doi.org/10.1088/1367-2630/aab03b>
31. H. Wilming, M. Goihl, C. Krumnow, J. Eisert, (2017). <arXiv:1704.06291>
32. C. Gogolin, M.P. Müller, J. Eisert, *Phys. Rev. Lett.* **106**, 040401 (2011). <https://doi.org/10.1103/PhysRevLett.106.040401>
33. D. Wallace, *J. Math. Phys.* **56**, 022105 (2015). <arXiv:1306.3925>
34. E.H. Lieb, D.W. Robinson, *Commun. Math. Phys.* **28**, 251 (1972). <https://doi.org/10.1007/BF01645779>
35. M. Kliesch, C. Gogolin, J. Eisert, Lieb-Robinson Bounds and the simulation of time-evolution of local observables in lattice systems, in *Many-Electron Approaches in Physics, Chemistry and Mathematics: A Multidisciplinary View*, ed. by V. Bach, L. Delle Site (Springer International Publishing, Cham, 2014), pp. 301–318. [https://doi.org/10.1007/978-3-319-06379-9\\_17](https://doi.org/10.1007/978-3-319-06379-9_17)
36. F.G.S.L. Brandao, M. Cramer, (2015). <arXiv:1502.03263>
37. J.P. Keating, N. Linden, H.J. Wells, *Commun. Math. Phys.* **338**, 81 (2015). <https://doi.org/10.1007/s00220-015-2366-0>
38. A. Anshu, *New J. Phys.* **18**, 083011 (2016). <https://doi.org/10.1088/1367-2630/18/8/083011>
39. P. Reimann, *Phys. Scr.* **86**, 58512 (2012). <arXiv:1210.5821>
40. R. Gallego, H. Wilming, J. Eisert, C. Gogolin, (2017). <https://doi.org/10.1103/PhysRevA.96.022135>
41. H. Wilming, M. Goihl, I. Roth, J. Eisert, (2018). <arXiv:1802.02052>
42. I. Arad, T. Kuwahara, Z. Landau, *J. Stat. Mech.* **2016**, 033301 (2016). <https://doi.org/10.1088/1742-5468/2016/03/033301>
43. A.J. Short, *New J. Phys.* **13**, 053009 (2011). <https://doi.org/10.1088/1367-2630/13/5/053009>
44. A.S.L. Malabarba, T. Farrelly, A.J. Short, *Phys. Rev. E* **94**, 032119 (2016). <https://doi.org/10.1103/PhysRevE.94.032119>
45. A.S.L. Malabarba, L.P. García-Pintos, N. Linden, T.C. Farrelly, A.J. Short, *Phys. Rev. E* **90**, 012121 (2014). <arXiv:1402.1093v1>
46. P.C. Hemmer, L.C. Maximon, H. Wergeland, *Phys. Rev.* **111**, 689 (1958). <https://doi.org/10.1103/PhysRev.111.689>
47. S. Goldstein, T. Hara, H. Tasaki, *Phys. Rev. Lett.* **111**, 140401 (2013). <https://doi.org/10.1103/PhysRevLett.111.140401>
48. M. Gluza, C. Krumnow, M. Friesdorf, C. Gogolin, J. Eisert, *Phys. Rev. Lett.* **117**, 190602 (2016a). <https://doi.org/10.1103/PhysRevLett.117.190602>
49. P. Calabrese, F.H.L. Essler, M. Fagotti, *J. Stat. Mech.* **2012**, P07022 (2012). <https://doi.org/10.1088/1742-5468/2012/07/P07022>
50. L. Masanes, A.J. Roncaglia, A. Acín, *Phys. Rev. E* **87**, 32137 (2013). <https://doi.org/10.1103/PhysRevE.87.032137>
51. P. Reimann, *Nature Comm.* **7**, 10821 (2016). <https://doi.org/10.1038/ncomms10821>
52. L.P. García-Pintos, N. Linden, A.S.L. Malabarba, A.J. Short, A. Winter, *Phys. Rev. X* **7**, 031027 (2017). <https://doi.org/10.1103/PhysRevX.7.031027>
53. B.N. Balz, P. Reimann, *Phys. Rev. Lett.* **118**, 190601 (2017). <https://doi.org/10.1103/PhysRevLett.118.190601>
54. F.G.S.L. Brandão, P. Ćwikliński, M. Horodecki, P. Horodecki, J.K. Korbicz, M. Mozrzymas, *Phys. Rev. E* **86**, 031101 (2012). <https://doi.org/10.1103/PhysRevE.86.031101>
55. M. Cramer, *New J. Phys.* **14**, 053051 (2012). <https://doi.org/10.1088/1367-2630/14/5/053051>
56. S. Goldstein, T. Hara, H. Tasaki, *New J. Phys.* **17**, 045002 (2015). <arXiv:1402.3380>
57. Vinayak, M. Znidaric, *J. Phys. A* **45**, 125204 (2012). <https://doi.org/10.1088/1751-8113/45/12/125204>
58. P. Calabrese, J. Cardy, *Phys. Rev. Lett.* **136** 801 (2006). <https://doi.org/10.1103/PhysRevLett.96.136801>

59. P. Calabrese, J.-S. Caux, J. Stat. Mech. P08032 (2007). <https://doi.org/10.1088/1742-5468/2007/08/P08032>
60. V. Eisler, I. Peschel, J. Stat. Mech. **2007**, P06005 (2007). <https://doi.org/10.1088/1742-5468/2007/06/P06005>
61. M. Cramer, A. Flesch, I.P. McCulloch, U. Schollwöck, J. Eisert, Phys. Rev. Lett. **101**, 063001 (2008c). <https://doi.org/10.1103/PhysRevLett.101.063001>
62. T. Barthel, U. Schollwöck, Phys. Rev. Lett. **100**, 100601 (2008). <https://doi.org/10.1103/PhysRevLett.100.100601>
63. A. Flesch, M. Cramer, I.P. McCulloch, U. Schollwoeck, J. Eisert, Phys. Rev. A **78**, 033608 (2008). <https://doi.org/10.1103/PhysRevA.78.033608>
64. P. Calabrese, F.H.L. Essler, M. Fagotti, Phys. Rev. Lett. **106**, 227203 (2011). <https://doi.org/10.1103/PhysRevLett.106.227203>
65. J.-S. Caux, F.H.L. Essler, Phys. Rev. Lett. **110**, 257203 (2013). <https://doi.org/10.1103/PhysRevLett.110.257203>
66. M. Gluza, C. Krumnow, M. Friesdorf, C. Gogolin, J. Eisert, Phys. Rev. Lett. **117**, 190602 (2016b). <https://doi.org/10.1103/PhysRevLett.117.190602>

# Chapter 19

# Nonequilibrium Many-Body Quantum Dynamics: From Full Random Matrices to Real Systems



Lea F. Santos and Eduardo Jonathan Torres-Herrera

## 19.1 Introduction

More than 90 years after the derivation of the Schrödinger equation, studies of the evolution of isolated quantum systems still receive much theoretical and experimental attention. This may be surprising, since we are simply dealing with linear dynamics. However, the complexity of these quantum systems lies in the effects of the interactions between their many particles, which in most cases prevent analytical results and limits numerical studies to small system sizes. Several open questions permeate the field, including the description of the relaxation to equilibrium and the viability of thermalization [1–3], the existence of a localized phase in the presence of disorder [4], the possibility of saturating bounds for the quantum speed limit [5], and the quantum-classical correspondence [6].

For one-body chaos, the quantum-classical correspondence is well understood. There are conjectures [7] and numerical studies [8] connecting classical chaos with specific properties of the spectrum of quantum systems and also semiclassical methods that bridge the classical and quantum domains [9, 10]. Specifically, quantum systems whose classical counterparts are chaotic have correlated eigenvalues which repel each other resulting in a rigid spectrum. This is to be contrasted with integrable quantum systems whose classical counterparts show regular dynamics. In this case, the eigenvalues are uncorrelated. In chaotic systems, the distribution of the spacings of neighboring levels follows the Wigner-Dyson distribution [11, 12] instead of the Poissonian distribution that is usually found in regular systems.

---

L. F. Santos (✉)

Department of Physics, Yeshiva University, New York, NY 10016, USA  
e-mail: lsantos2@yu.edu

E. J. Torres-Herrera

Instituto de Física, Benemérita Universidad Autónoma de Puebla,  
Apartado Postal J-48, 72570 Puebla, Puebla, México  
e-mail: etorresh@ifuap.buap.mx

When it comes to interacting many-body quantum systems, the quantum-classical correspondence is still missing. This is ironic, because the field of quantum chaos has in fact been strongly influenced by Wigner's studies of many-body nuclear systems [13, 14]. One often extends the findings from one-body chaos and refers to many-body quantum systems with Wigner-Dyson distributions as chaotic systems, as we do in this chapter, but this link has not been proved yet. The subject has recently received much attention [15–18], leading to significant progress in the development of semiclassical analysis for interacting many-body systems [6, 19].

Along the years, there have also been several attempts to connect exponential behaviors in the quantum domain with classical chaos [20, 21]. This topic has been revived once again, now in the context of the so-called out-of-time-ordered four-point correlator (OTOC). While exponential behaviors for the OTOC have been confirmed in some cases of one-body chaos [22–24] and for the Dicke model, which has two degrees of freedom [25], there is no consensus on what we might expect for many-body systems [26].

In a new study [18], it has been shown that the number of states participating in the evolution of realistic interacting many-body quantum systems perturbed far from equilibrium grows exponentially fast in time. This number, known as participation ratio or number of principal components, is a four-point correlation function and thus an example of an OTOC. This result indicates that exponential instability is not exclusive to classical chaos, but emerges also in quantum chaotic systems. The quantum-classical correspondence suggested in Ref. [18] comes from the analogy between the growth of the volume filled by the states participating in the evolution and the growth of the volume of the classical phase-space visited by the classical trajectories. For both, the growth is exponential and the rate should be given by the Kolmogorov-Sinai entropy.

In this chapter, we focus on the survival probability, which is a two-point correlation function, and study its entire evolution after a quench. We show that the dynamics at short times cannot distinguish between many-body quantum systems with and without level repulsion [27–33]. The fast initial decay of the survival probability, Gaussian or exponential, emerges in systems with and without correlated eigenvalues. As a matter of fact, the same is true for the linear increase in time of entropies [33–35] and, equivalently, for the exponential growth of the participation ratio. Therefore, if exponential behaviors at the quantum level are to be linked with classical chaos, then either level repulsion ceases to be essential for many-body quantum chaos, which contrasts with one-body quantum chaos, or there is something missing in the discussions of these exponential behaviors.

We show that unambiguous signatures of level repulsion emerge only at long times [36–38], after the initial fast dynamics. Long times are required for the dynamics to be able to resolve the discreteness of the spectrum and detect whether the eigenvalues are or not correlated. We stress, however, that this chapter does not answer the question of whether there is indeed a one-to-one correspondence between level repulsion and many-body quantum chaos.

The survival probability presents different behaviors at different time scales [36–45]. To better understand the causes of these behaviors in realistic many-body

quantum systems, we analyze the survival probability evolving under full random matrices (FRM). These matrices are not realistic, since they imply the interaction of all particles at the same time, but they allow us to extract analytical expressions, which guide our studies of realistic systems [38].

The systems considered are finite, so the dynamics for both FRM and realistic chaotic many-body quantum models eventually saturates to a value determined by the level of delocalization of the initial state written in the energy eigenbasis. Before reaching this point, we witness the following behaviors in this order: (i) a universal initial quadratic decay that later remains Gaussian or switches into an exponential; (ii) a slower power-law evolution caused by the bounds in the spectrum, (iii) a dip below the saturation point caused by the presence of correlated eigenvalues. This dip, known as correlation hole [46–50], is nonexistent in systems that have uncorrelated eigenvalues or continuous spectrum, being an unequivocal manifestation of level repulsion.

## 19.2 Models

We consider systems described by the Hamiltonian

$$H = H_0 + \lambda V, \quad (19.1)$$

where  $H_0$  is an integrable Hamiltonian corresponding to the unperturbed part of the total Hamiltonian  $H$ , and  $V$  is a perturbation of strength  $\lambda$ . We set  $\hbar = 1$  and  $\lambda = 1$ , unless said otherwise.

We denote the eigenvalues and eigenstates of  $H$  as  $E_\alpha$  and  $|\alpha\rangle$ , respectively, and those of  $H_0$  as  $\varepsilon_n$  and  $|n\rangle$ . Two models are studied, a FRM model and a realistic spin model.

### 19.2.1 Full Random Matrix Model

We study the evolution under FRM from a Gaussian orthogonal ensemble (GOE) [11, 12, 51]. The matrix is constructed as follows. We fill a  $\mathcal{D} \times \mathcal{D}$  matrix with  $\mathcal{D}^2$  real random numbers from a Gaussian distribution with mean zero and standard deviation 1. We then sum the matrix to its transpose, which results in a real and symmetric matrix that belongs to the GOE. The diagonal elements, which constitute  $H_0$ , have variance

$$\langle H_{ii}^2 \rangle = 4$$

and the off-diagonal elements, which compose  $V$ , have variance

$$\langle H_{ij}^2 \rangle = 2 \quad \text{for} \quad i \neq j$$

### 19.2.1.1 Density of States: Semicircle

The density of states (i.e., the histogram of all eigenvalues) of FRM follows the standard semicircle distribution [52],

$$\text{DOS}(E) = \frac{2}{\pi\mathcal{E}} \sqrt{1 - \left(\frac{E}{\mathcal{E}}\right)^2}, \quad (19.2)$$

where  $2\mathcal{E}$  is the length of the spectrum, that is  $-\mathcal{E} \leq E \leq \mathcal{E}$ . We show  $\text{DOS}(E)$  for one realization of a GOE FRM in Fig. 19.1a. Notice that in this chapter we are interested in all eigenvalues and eigenstates, so the numerical method used is full exact diagonalization.

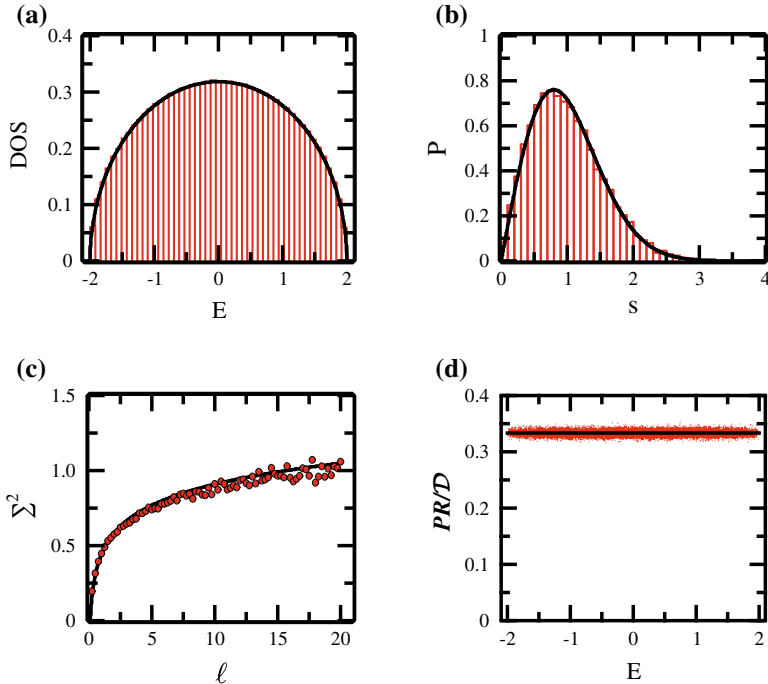


**Fig. 19.1** Results for a single GOE random matrix. **a** Numerical DOS (shade area) compared with Eq. (19.2) (solid curve). **b** Numerical  $P(s)$  (shaded area) and Eq. (19.3) (solid curve). **c** Level number variance: circles are numerical results and solid curve is Eq. (19.4). **d** Normalized PR versus  $E$ : dots are numerical results obtained with exact diagonalization and the solid line is the analytical result  $1/3$ . We divide the eigenvalues by the width of the DOS for a better comparison with the results for the disordered spin model. The dimension of the matrix is  $\mathcal{D} = 12\,870$ , in anticipation of the dimension used for the spin model (see Sect. 19.2.2).

### 19.2.1.2 Correlatated Eigenvalues

The eigenvalues of FRM are correlated. They are prohibited from crossing, so there are no degenerate levels. Such level repulsion is evident in the distribution  $P(s)$  of the spacings  $s$  between neighboring levels. To obtain  $P(s)$ , we first need to rescale the energies (unfold the spectrum), so that the specific mean level density of the system is removed from the data [53]. This allows us to compare spectra from different systems and in different energy regions. After unfolding the spectrum [53], one finds for GOE FRM the following Wigner-Dyson distribution [12],

$$P(s) = \frac{\pi}{2} s \exp\left(-\frac{\pi}{4}s^2\right). \quad (19.3)$$

We show  $P(s)$  for one realization of a GOE FRM in Fig. 19.1b.

The level spacing distribution  $P(s)$  detects short-range correlations between the eigenvalues. There are quantities that capture also long-range correlations, such as the level number variance  $\Sigma^2(\ell)$ . Studying different quantities, we get a more complete picture of the spectrum. The level number variance is the variance of the number of unfolded eigenvalues in a given interval of length  $\ell$ . For FRM,  $\Sigma^2(\ell)$  grows logarithmically with  $\ell$ . For the specific case of GOE FRM [12], the dependence on  $\ell$  is

$$\Sigma^2(\ell) = \frac{2}{\pi^2} \left[ \ln(2\pi\ell) + \gamma_e + 1 - \frac{\pi^2}{8} \right], \quad (19.4)$$

where  $\gamma_e = 0.5772\dots$  is Euler's constant. We show  $\Sigma^2(\ell)$  for one realization of a GOE FRM in Fig. 19.1c.

### 19.2.1.3 Delocalized Eigenstates

The eigenstates  $|\alpha\rangle = \sum_n C_n^\alpha |n\rangle$  of FRM are random vectors, that is the components  $C_n^\alpha$  are random numbers constrained by the normalization condition,  $\sum_n |C_n^\alpha|^2 = 1$ . For GOE FRM, the components are real random numbers from a Gaussian distribution.

To quantify how much delocalized a state is in a certain basis  $|n\rangle$ , we use measures such as the participation ratio, defined as

$$PR^\alpha = \frac{1}{\sum_{n=1}^D |C_n^\alpha|^4}. \quad (19.5)$$

This quantity has been used for many decades in the context of localization and chaos [54]. More recently, in studies of relaxation, it is also sometimes referred to as effective dimension (see Chap. 18 in this book). For GOE FRM, one can show that

$PR \simeq \mathcal{D}/3$  [44]. In Fig. 19.1d, we show  $PR$  for all eigenstates of one realization of a GOE FRM. As one sees, all eigenstates are equally delocalized, apart from small fluctuations.

### 19.2.2 Disordered Spin-1/2 Model

The physical many-body system that we analyze is a one-dimensional (1D) system of interacting spins-1/2. It has  $L$  sites, periodic boundary conditions, and onsite disorder. The unperturbed part of  $H$  is

$$H_0 = \sum_{k=1}^L h_k S_k^z + \sum_{k=1}^L S_k^z S_{k+1}^z, \quad (19.6)$$

where  $S_k$  are the spin operators on site  $k$ . The Zeeman splittings  $h_k$  are random numbers from a uniform distribution  $[-h, h]$  and  $h$  is the disorder strength. We refer to the eigenstates of  $H_0$  as site-basis vectors, also known as computational basis vectors. They correspond to states that on each site has either a spin pointing up in the  $z$ -direction or pointing down. The perturbation is given by

$$V = \sum_{k=1}^L (S_k^x S_{k+1}^x + S_k^y S_{k+1}^y). \quad (19.7)$$

In the site-basis,  $V$  constitutes the off-diagonal part of  $H$ .

The total spin Hamiltonian  $H$  conserves the total spin in the  $z$ -direction,  $\mathcal{S}^z = \sum_k S_k^z$ . We study the largest subspace,  $\mathcal{S}^z = 0$ , which has dimension  $\mathcal{D} = L!/(L/2)!^2$ .

The disordered spin Hamiltonian has been considered in studies of spatial localization since 2004 [55–58] (for more recent works see [4, 59]). An advantage of using this model for studies of dynamics is that we deal with averages over disorder realizations, which is a way to reduce finite size effects and smoothen the curves [36, 39]. This is particularly important in studies of long-time evolution, as done here.

#### 19.2.2.1 Density of States: Gaussian

The density of states of delocalized many-body quantum systems with few-body (in our case, two-body) interactions is Gaussian [60]. This can be shown analytically in the case of integrable models [61]. In Fig. 19.2a, we show  $DOS(E)$  for one realization of the disordered spin model with  $h = 0.5$ .

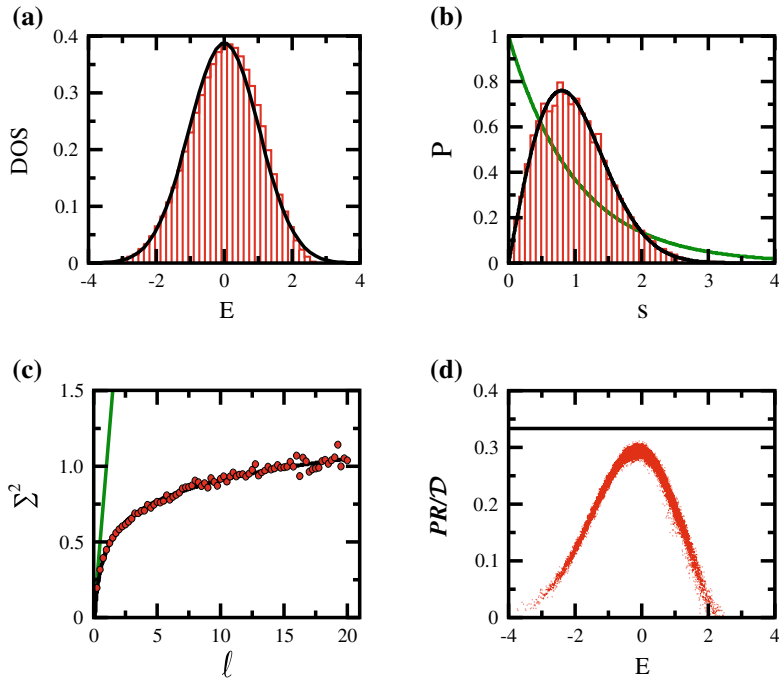


**Fig. 19.2** Results for a single realization of the realistic disordered spin model with  $h = 0.5$ . **a** Numerical DOS (shaded area) compared with a Gaussian distribution (solid curve). **b** Numerical  $P(s)$  (shaded area), Wigner-Dyson distribution Eq. (19.3) (black solid curve), and Poissonian distribution  $P(s) = \exp(-s)$  (green solid curve). **c** Level number variance: circles are numerical results and solid curves are Eq. (19.4) (black) and  $\Sigma^2(\ell) = \ell$  (green). **d** Normalized PR versus  $E$ : dots are numerical results and the solid line is the analytical result  $1/3$  for GOE FRM. The eigenvalues are rescaled as in Fig. 19.1, by dividing them by the width of the DOS;  $\mathcal{D} = 12\,870$ .

### 19.2.2.2 Eigenvalues

The properties of the spectrum of the spin model depend on the strength of the disorder. When  $h$  is of the order of  $J$ , the eigenvalues are correlated and show a Wigner-Dyson distribution. For the system size considered here ( $L = 16$ ,  $\mathcal{D} = 12870$ ), strong level repulsion occurs for  $h = 0.5$  [36], as depicted in Fig. 19.2b.

In integrable models, the eigenvalues are uncorrelated and the levels are not prohibited from crossing. Usually, the level spacing distribution is Poissonian,  $P(s) = \exp(-s)$ , but different shapes are observed when the spectrum has an excessive number of degeneracies [62] or the spacings between the levels are nearly equal [63]. Our disordered model has two integrable points, one when  $h = 0$  and the other when  $h > h_c$ , where  $h_c$  is a critical point above which the system becomes localized in space. Away from the integrable and chaotic points, the level spacing distribution is intermediate between Poissonian and Wigner-Dyson [36].

When it comes to the level number variance, we find that deep in the chaotic regime ( $h = 0.5$ ),  $\Sigma^2(\ell)$  agrees well with the results for the GOE FRM for the values of  $\ell$  shown in Fig. 19.2c. For uncorrelated eigenvalues, the level number variance grows linearly with  $\ell$ , that is  $\Sigma^2(\ell) = \ell$ . In the case of our spin model, as the disorder strength moves away from the chaotic region and approaches the integrable limits ( $h > h_c$  or  $h \rightarrow 0$ ), the points for the level number variance get out of the logarithmic curve for smaller values of  $\ell$  and after that, they follow a curve that is closer to linear than logarithmic [64].

### 19.2.2.3 Eigenstates

The components of the eigenstates of realistic systems are never completely uncorrelated as in FRM, so we do not have  $PR \simeq D/3$ . However, in the chaotic domain, we do find  $PR \propto D$  [36, 39], with pre-factors smaller than 1/3.

Contrary to FRM, where the basis is ill defined, the values of the  $PR$  for realistic systems depend on the chosen basis. The appropriate basis to analyze the transition to chaos is the mean-field basis, as discussed in Refs. [1, 33–35]. In contrast, to study localization in space, the site-basis is the natural choice.

The level of delocalization of the eigenstates of realistic systems also depends on their energy. Eigenstates closer to the middle of the spectrum tend to be more delocalized than those closer to the edges. In Fig. 19.2d we show  $PR$  for all eigenstates of one realization of the disordered spin model in the chaotic limit,  $h = 0.5$ .

## 19.3 Survival Probability

We prepare the system in an eigenstate  $|n_0\rangle \equiv |\Psi(0)\rangle$  of  $H_0$  and let it evolve according to the total Hamiltonian  $H$ , that is

$$|\Psi(t)\rangle = e^{-iHt}|\Psi(0)\rangle = \sum_{\alpha} C_{n_0}^{\alpha} e^{-iE_{\alpha}t}|\alpha\rangle,$$

where  $C_{n_0}^{\alpha} = \langle \alpha | \Psi(0) \rangle$  is the overlap between the initial state and the energy eigenbasis.

We study the survival probability, which is one of the simplest observables and allows us to obtain detailed information about the entire evolution of the system. Mathematically, it is given by

$$W_{n_0}(t) = |\langle \Psi(0) | \Psi(t) \rangle|^2 = \left| \sum_{\alpha} |C_{n_0}^{\alpha}|^2 e^{-iE_{\alpha}t} \right|^2. \quad (19.8)$$

Physically, it is the probability of finding the initial state at time  $t$ . The sum in Eq. (19.8) can be written in terms of an integral as

$$W_{n_0}(t) = \left| \int dE e^{-iEt} \rho_{n_0}(E) \right|^2, \quad (19.9)$$

where

$$\rho_{n_0}(E) \equiv \sum_{\alpha} |C_{n_0}^{\alpha}|^2 \delta(E - E_{\alpha}) \quad (19.10)$$

is the energy distribution weighted by the components  $|C_{n_0}^{\alpha}|^2$  of the initial state. It is called local density of states (LDOS). The survival probability is the absolute square of the Fourier transform of the LDOS.

The energy of the initial state is the mean of the LDOS,

$$E_{n_0} = \langle \Psi(0) | H | \Psi(0) \rangle = \sum_{\alpha} |C_{n_0}^{\alpha}|^2 E_{\alpha}, \quad (19.11)$$

and the variance of the LDOS is

$$\sigma_{n_0}^2 = \sum_{\alpha} |C_{n_0}^{\alpha}|^2 (E_{\alpha} - E_{n_0})^2. \quad (19.12)$$

At very short times,  $t \ll \sigma_{n_0}^{-1}$ , independently of the model or of the initial state, the survival probability shows a universal quadratic behavior in  $t$ ,

$$W_{n_0}(t) \approx 1 - \sigma_{n_0}^2 t^2. \quad (19.13)$$

This is obtained by expanding Eq. (19.8) [28, 42]. At later times, the behavior of the survival probability depends on the time scale.

## 19.4 Dynamics of Chaotic Systems

To better understand the different behaviors of the survival probability at different time scales, we compare the results obtained for the evolution under FRM with those for the disordered spin-1/2 model in the chaotic limit,  $h = 0.5$ .

### 19.4.1 Fast Initial Decay

Beyond the universal quadratic decay, the evolution of the survival probability is initially controlled by the shape of the envelope of the LDOS.

### 19.4.1.1 Full Random Matrices

The shape of the LDOS of an arbitrary initial state extracted from  $H_0$  and projected into the eigenstates of a FRM coincides with the shape of the DOS, that is, the envelope is semicircular [27, 28, 30], just as in Eq. (19.2). The width of the LDOS can be obtained from

$$\sigma_{n_0} = \sqrt{\int_{-\mathcal{E}}^{\mathcal{E}} \rho_{n_0}(E) E^2 dE} = \frac{\mathcal{E}}{2}. \quad (19.14)$$

The LDOS is shown in Fig. 19.3a.

The Fourier transform of a semicircle gives [27, 28, 30]

$$W_{n_0}(t) = \frac{\mathcal{J}_1^2(2\sigma_{n_0} t)}{(\sigma_{n_0} t)^2}, \quad (19.15)$$

where  $\mathcal{J}_1(t)$  is the Bessel function of first kind. This leads to a very fast initial decay, as shown in Fig. 19.3b. This is the fastest decay that we can have for lattice many-

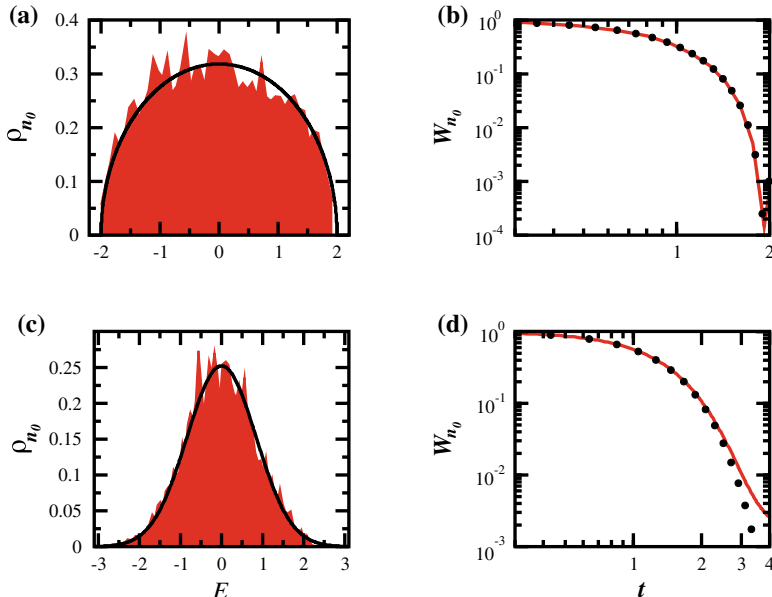


**Fig. 19.3** Local density of states (**a**, **c**) and survival probability (**b**, **d**) for the GOE FRM (top) and the disordered spin model with  $h = 0.5$  (bottom). For both, the initial state  $|\Psi(0)\rangle$  has energy  $E_{n_0}$  close to zero. In (**a**, **c**) the red shaded areas are numerical results for one realization and the black solid lines are the semicircle (**a**) and the Gaussian function (**c**). In (**b**, **d**) the red solid curves are numerical results and the dots correspond to Eq. (19.15) in (**b**) and Eq. (19.16) in (**d**). In (**b**) an average over  $10^4$  data was carried out, while in (**d**) the average is over 77 random realizations and 1 287 initial states ( $10^5$  data). For all panels  $\mathcal{D} = 12\,870$ .

body quantum systems where the LDOS has a single peak. In quench dynamics, where the LDOS becomes bimodal, the dynamics can be even faster [30].

### 19.4.1.2 Chaotic Spin-1/2 Model

For the chaotic spin model, we select as initial states, eigenstates from  $H_0$  (19.6) with energy  $E_{n_0}$  very close to the middle of the spectrum. The strength of the perturbation that takes  $H_0$  into  $H$  is strong. In this case, the LDOS, just as the DOS, has a Gaussian shape, as shown in Fig. 19.3c.

The Fourier transform of a Gaussian gives a Gaussian decay,

$$W_{n_0}(t) = \exp(-\sigma_{n_0}^2 t^2), \quad (19.16)$$

as indeed seen in Fig. 19.3d. The curve is an average over several initial states and disorder realizations that total  $10^5$  data. We stress that the decay is truly Gaussian and not only the quadratic behavior at short times.

The decay functions for FRM and realistic models are, of course, different, but the cause of the behaviors is the same, namely the shape of the envelope of the LDOS. We note that the shape depends on the model, on the energy of the initial state, and on the strength of the perturbation, but not on the existence of level repulsion [27–30]. Integrable models can also lead to Gaussian or exponential decays. To illustrate this fact, we show in Fig. 19.4, the survival probability for the integrable XXZ model described by

$$H_{XXZ} = \sum_{k=1}^{L-1} (S_k^x S_{k+1}^x + S_k^y S_{k+1}^y + \lambda S_k^z S_{k+1}^z). \quad (19.17)$$

We assume that the unperturbed and perturbed parts of the Hamiltonian are:

$$H_0 = \sum_{k=1}^{L-1} (S_k^x S_{k+1}^x + S_k^y S_{k+1}^y), \quad V = \sum_{k=1}^{L-1} S_k^z S_{k+1}^z, \quad (19.18)$$

and  $\lambda$  is the strength of the perturbation. We take as initial state an eigenstate of  $H_0$  with  $E_{n_0} \sim 0$ .

When  $\lambda$  is very small, the initial state is not so different from one of the energy eigenbasis and the LDOS is very narrow [Fig. 19.4a], resulting in a very slow evolution [Fig. 19.4b]. As  $\lambda$  increases, the LDOS broadens and becomes Lorentzian [Fig. 19.4c], which leads to the exponential behavior of the survival probability [Fig. 19.4d]. If we increase  $\lambda$  even further, the LDOS broadens even more, eventually approaching the Gaussian shape of the DOS [Fig. 19.4e]. This is the limit of very strong perturbation, which causes the Gaussian decay [Fig. 19.4f].

Note that the clean system described by Eq. (19.17) has symmetries that do not exist in the disordered model. To avoid degeneracies emerging from translational

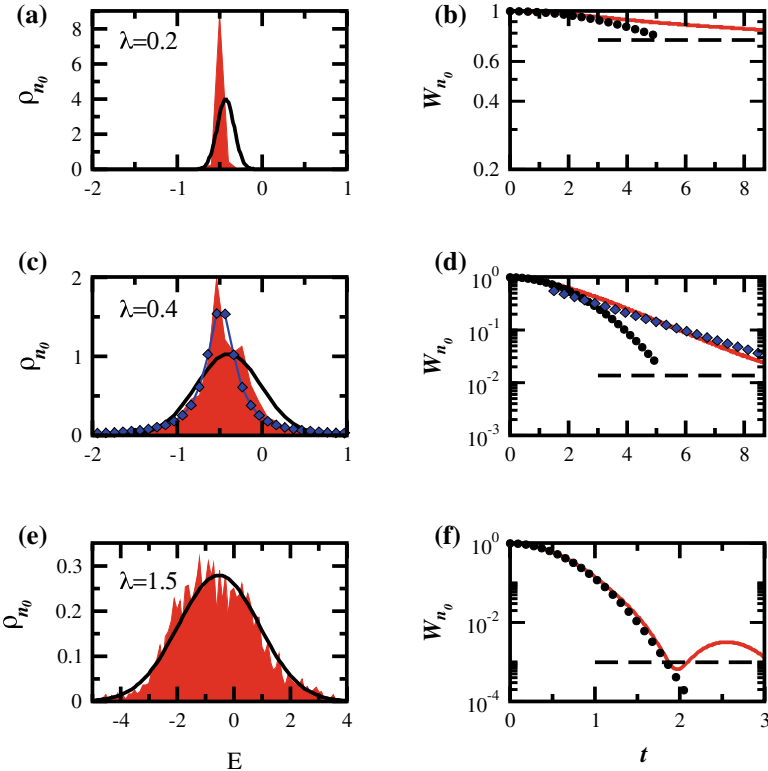


**Fig. 19.4** Local density of states (left column) and survival probability (right column) for the XXZ model [Eq. (19.17)]. The values of  $\lambda$  are indicated in the figure. The initial state  $|\Psi(0)\rangle$  has energy far from the edges of the spectrum. Black solid line (left) and black circles (right): Gaussian LDOS and Gaussian decay, respectively, with  $\sigma_0$  from Eq. (19.12). Red shaded area (left) and red solid lines (right): numerical results. Blue diamonds in (c) and (d): Lorentzian fit and exponential decay, respectively.  $L = 18$ , 6 up-spins,  $\mathcal{D} = 18\,564$ , open chain. Horizontal dashed lines indicate the saturation value [Eq. (19.22)].

symmetry, we consider open boundary conditions. In addition, in Fig. 19.4, we choose  $L = 18$  and 6 up-spins, that is 1/3 filling instead of 1/2, as used previously. This choice avoids spin reversal symmetry.

#### 19.4.2 Power-Law Decays at Intermediate Times

Any quantum system has at least one energy bound in the spectrum corresponding to the ground state. In the case of finite systems, there are two energy bounds. The presence of these bounds cause the eventual partial reconstruction of the initial

state [65], which slows down the evolution of the survival probability. We then find power-law decays even in the most chaotic scenario of FRM [31, 41, 42]. The value of the power-law exponent depends on how the LDOS approaches the energy bounds.

If the LDOS goes to zero at the bound  $E_{low}$  as

$$\rho_{n_0}(E) = (E - E_{low})^\xi \eta(E), \quad (19.19)$$

with

$$\lim_{E \rightarrow E_{low}} \eta(E) > 0,$$

then the decay of the survival probability at long times is given by

$$W_{n_0}(t) \propto t^{-2(\xi+1)}. \quad (19.20)$$

More details can be found in [41, 42, 66, 67].

#### 19.4.2.1 Full Random Matrices

The tails of the LDOS of FRM falls with the square root of the energy,  $E^{1/2}$ , so one has  $\xi = 1/2$ . Following Eq.(19.20), the decay should be  $t^{-3}$ , as indeed confirmed by Fig. 19.5a. The power-law decay is the envelope of the decay of the oscillations caused by the Bessel function in Eq.(19.15).

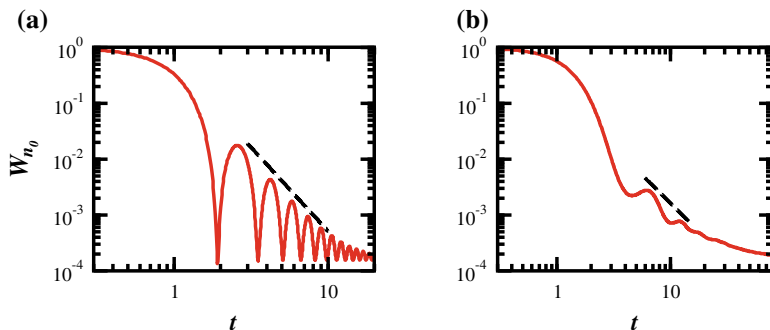


**Fig. 19.5** Power-law decay of the survival probability. In **a** the GOE FRM: numerical results (solid line) and  $t^{-3}$  decay (dashed line). In **b** the disordered spin model with  $h = 0.5$ : numerical results (solid line) and  $t^{-2}$  decay (dashed line). The spectrum is rescaled as described in Fig.(19.1) and Fig.(19.2). In **(a)** the average is over  $10^4$  data and in **(b)** the average is over  $10^5$  data. For both models  $\mathcal{D} = 12\,870$ .

The  $t^{-3}$  behavior can also be directly derived by studying Eq.(19.15) asymptotically,  $t \gg \sigma_{n_0}^{-1}$ , as shown in [41, 42]. In this case, we find that

$$W_{n_0}(t) \rightarrow \frac{1 - \sin(4\sigma_{n_0} t)}{2\pi\sigma_{n_0}^3 t^3}, \quad (19.21)$$

which makes evident the power-law decay.

#### 19.4.2.2 Chaotic Spin-1/2 Model

The corroboration of the power-law decay for the FRM suggests that we should expect the same for our realistic chaotic spin model. In chaotic systems perturbed far from equilibrium, the LDOS is ergodically filled, so the dynamics should have enough time to detect the bounds in the spectrum, before resolving the discreteness of the spectrum.

The LDOS of the chaotic spin model is Gaussian, so the tails become approximately constant in energy. Following Eq. (19.20), one has  $\xi = 0$ , so  $W_{n_0}(t) \propto t^{-2}$ . This power-law exponent can also be obtained from the direct Fourier transform of the Gaussian LDOS taking the bounds into account when doing the integral (see Refs. [41, 42]).

In Fig. 19.5b, we show with a dashed line the  $t^{-2}$  decay. Larger system sizes are needed to make this behavior more evident. Longer time intervals where the  $t^{-2}$  decay is indeed observed are shown in Fig. 1 of Ref. [68], where we have  $L$  up to 24. We note that also for FRM, the duration of the power-law behavior shrinks as the system size decreases [69].

#### 19.4.3 Correlation Hole

We deal with finite systems, so the evolution of the survival probability eventually saturates to its infinite-time average,

$$\overline{W}_{n_0} = \sum_{\alpha} |C_{n_0}^{\alpha}|^4, \quad (19.22)$$

which is the inverse of the participation ratio for the initial state written in the energy eigenbasis. For FRM,  $\overline{W}_{n_0} \simeq 3/\mathcal{D}$  and larger values are reached for realistic models.

The dynamics can resolve the discreteness of the spectrum before saturation. In chaotic systems, this happens when the evolution perceives the correlations between the eigenvalues. For the survival probability, these correlations are manifested in the form of a dip below the saturation point, known as correlation hole [46–49, 70–79]. The correlation hole was studied in the context of FRM, billiards, and molecules. We have extended these studies to realistic lattice many-body models [36–38, 43–45].

### 19.4.3.1 Full Random Matrices

To understand the origins of the correlation hole, one needs to write Eq. (19.8) as

$$W_{n_0}(t) = \sum_{\alpha_1, \alpha_2} |C_{n_0}^{\alpha_1}|^2 |C_{n_0}^{\alpha_2}|^2 e^{iE_{\alpha_1}t} e^{-iE_{\alpha_2}t} = \int G(E) e^{-iEt} dE + \overline{W}_{n_0}, \quad (19.23)$$

where

$$G(E) = \sum_{\alpha_1 \neq \alpha_2} |C_{n_0}^{\alpha_1}|^2 |C_{n_0}^{\alpha_2}|^2 \delta(E - E_{\alpha_1} + E_{\alpha_2}) \quad (19.24)$$

is the spectral autocorrelation function.

When dealing with FRM, we usually perform averages  $\langle \cdot \rangle_{\text{FRM}}$  over ensembles of random matrices. Since the eigenvalues and eigenstates of FRM are statistically independent, we can write  $G(E)$  as

$$\langle G(E) \rangle_{\text{FRM}} = \left\langle \sum_{\alpha_1 \neq \alpha_2} |C_{n_0}^{\alpha_1}|^2 |C_{n_0}^{\alpha_2}|^2 \right\rangle_{\text{FRM}} \langle \delta(E - E_{\alpha_1} + E_{\alpha_2}) \rangle_{\text{FRM}}. \quad (19.25)$$

The first factor on the right hand side depends only on the random real components of the initial state,

$$\left\langle \sum_{\alpha_1 \neq \alpha_2} |C_{n_0}^{\alpha_1}|^2 |C_{n_0}^{\alpha_2}|^2 \right\rangle_{\text{FRM}} = 1 - \left\langle \sum_{\alpha} |C_{n_0}^{\alpha}|^4 \right\rangle_{\text{FRM}} = 1 - \langle \overline{W}_{n_0} \rangle_{\text{FRM}}. \quad (19.26)$$

The second factor in Eq. (19.25) is the one that captures the correlations between the eigenvalues. It can be written as

$$\langle \delta(E - E_{\alpha_1} + E_{\alpha_2}) \rangle_{\text{FRM}} = \frac{\mathcal{D}!}{(\mathcal{D}-2)!} \int \int \delta(E - E_{\alpha_1} + E_{\alpha_2}) R_2(E_{\alpha_1}, E_{\alpha_2}) dE_{\alpha_1} dE_{\alpha_2}, \quad (19.27)$$

where  $R_2(E_{\alpha_1}, E_{\alpha_2})$  is the Dyson two-point correlation function.  $R_2$  gives the probability density of finding an energy level around each of the energies  $E_{\alpha_1}, E_{\alpha_2}$ . The two-point correlation function can be divided as

$$R_2(E_{\alpha_1}, E_{\alpha_2}) = R_1(E_{\alpha_1}) R_1(E_{\alpha_2}) - T_2(E_{\alpha_1}, E_{\alpha_2}), \quad (19.28)$$

where  $R_1$  is the DOS and  $T_2(E_{\alpha_1}, E_{\alpha_2})$  is the two-level cluster function [11].

The Fourier transform of  $R_1$  leads to the behavior described by Eq. (19.15). The Fourier transform of  $T_2$  gives the two-level form factor, which for GOE matrices reads [11]

$$b_2(\bar{t}) = [1 - 2\bar{t} + \bar{t} \ln(1 + 2\bar{t})] \Theta(1 - \bar{t}) + \{-1 + \bar{t} \ln[(2\bar{t} + 1)/(2\bar{t} - 1)]\} \Theta(\bar{t} - 1), \quad (19.29)$$

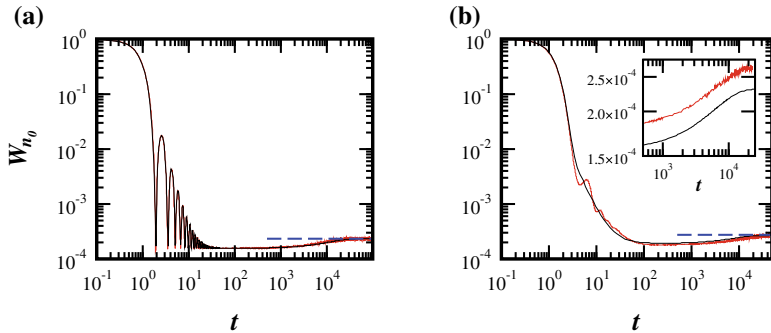


**Fig. 19.6** Survival probability. **a** Numerical results for GOE FRM (red) and Eq. (19.30) (black) are superposed. **b** Numerical results for the disordered model with  $h = 0.5$  (red) and the fitting curve in Eq. (19.31) (black). In both panels the blue dashed lines are the corresponding saturation values. The spectrum is rescaled as described in Figs. (19.1) and (19.2). Inset of (b) shows the growth of  $W_{n_0}(t)$  from the bottom of the correlation hole to saturation: Eq. (19.30) (bottom black curve) and numerical results for  $h = 0.5$  averaged over small time windows (top red curve). In (a) average over  $10^4$  disorder realizations. In (b) the average is over 1 287 different initial states and 77 different disorder realizations, adding up to  $10^5$  data. For both panels  $\mathcal{D} = 12\,870$ .

where  $\Theta$  is the Heaviside step function (see details of the derivation in [11, 43, 49]). The  $b_2$  function, which is related to the level number variance [12], is responsible for the correlation hole. The Bessel decay in Eq. (19.15) is interrupted by  $b_2$ , which, after the hole, brings the survival probability to the saturation point.

The  $b_2$  function differs from zero only if the eigenvalues have some degree of correlation. It is therefore an unambiguous signature of the presence of level repulsion found by studying the time evolution of the system [37]. If the eigenvalues are uncorrelated,  $b_2(\bar{t}) = 0$ .

The complete analytical expression for the survival probability evolving under GOE FRM of large dimensions was obtained in Ref. [38]. It is given by

$$\langle W_{n_0}(t) \rangle_{\text{FRM}} = \frac{1 - \langle \bar{W}_{n_0} \rangle_{\text{FRM}}}{\mathcal{D} - 1} \left[ 4\mathcal{D} \frac{\mathcal{J}_1^2(\mathcal{E}t)}{(\mathcal{E}t)^2} - b_2 \left( \frac{\mathcal{E}t}{4\mathcal{D}} \right) \right] + \langle \bar{W}_{n_0} \rangle_{\text{FRM}}. \quad (19.30)$$

This expression matches the numerical result extremely well, as seen in Fig. 19.6a.

### 19.4.3.2 Chaotic Spin-1/2 Model

The correlation hole is also evident in the chaotic spin model. As seen in the inset of Fig. 19.6b, the curve for the hole for the spin model is nearly parallel to the analytical one for FRM in Eq. (19.30).<sup>1</sup> This implies that the same  $b_2$  function can be used

<sup>1</sup>Notice that here and in all other figures, apart from Fig. 19.4, the spectra of the FRM and of the spin model are rescaled by the width of their DOS for a better comparison.

to describe the long-time behavior of the survival probability of realistic chaotic models. At such long times, the dynamics no longer depends on details, such as the shape of the DOS and LDOS and the structure of the eigenstates, but cares only about the correlations between the eigenvalues.

Motivated by the comparisons between our results for the FRM and for the chaotic spin model, we proposed in Ref. [38] an expression to describe the entire evolution of the survival probability for the spin model. It is written as

$$\langle W_{n_0}(t) \rangle = \frac{1 - \langle \bar{W}_{n_0} \rangle}{\mathcal{D} - 1} \left[ \mathcal{D} \frac{g(t)}{g(0)} - b_2 \left( \frac{\sigma_{n_0} t}{2\mathcal{D}} \right) \right] + \langle \bar{W}_{n_0} \rangle, \quad (19.31)$$

where

$$g(t) = e^{-\sigma_{n_0}^2 t^2} + A \frac{1 - e^{-\sigma_{n_0}^2 t^2}}{\sigma_{n_0}^2 t^2} \quad (19.32)$$

and  $A$  is a fitting constant. The function  $g(t)$  is used to capture the initial Gaussian decay and the subsequent power-law behavior  $\propto t^{-2}$ . The curve from Eq. (19.31) is shown in Fig. 19.6b together with the numerical result. It is quite impressive that we can match the entire evolution so well using a single fitting constant.

## 19.5 Dynamics: From Chaos to Localization

As we increase  $h$  above 0.5 and the system approaches a localized phase in space, the evolution of the survival probability slows down and saturates at a higher plateau, as shown in Fig. 19.7a.

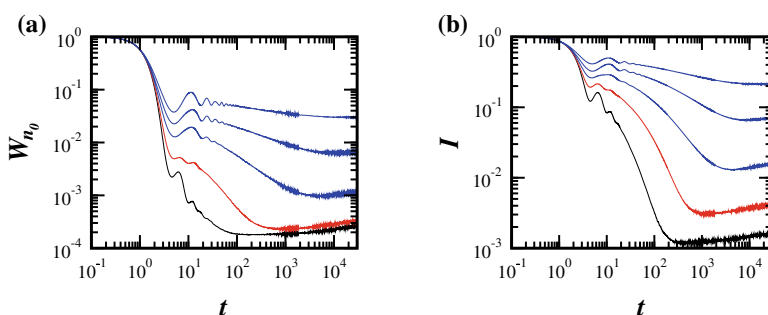


**Fig. 19.7** Full decay of the survival probability (a) and of the spin density imbalance (b) for the disordered spin model. The numerical results from bottom to top have  $h = 0.5, 1, 1.5, 2, 2.5$ . In (a), the average is over  $10^5$  data as in Fig. (19.6)b. In (b) the average is over  $10^4$  data. For both panels  $\mathcal{D} = 12\,870$ .

For  $0.5 \leq h \leq 1$ , where the system is chaotic, the power-law exponent  $\gamma$  of  $W_{n_0}(t) \propto t^{-\gamma}$  is  $2 \leq \gamma \leq 1$ . As we said above,  $\gamma = 2$  is caused by the energy bounds. The values  $2 < \gamma \leq 1$  must be caused by a combination of bound effects and possible small correlations between the eigenstates [41, 42].

When  $h > 1$ , the LDOS becomes sparse and the initial states are no longer fully delocalized in the energy eigenbasis, that is  $PR_{n_0} = \overline{W}_{n_0}^{-1} \propto \mathcal{D}^{D_2}$ , where  $D_2 < 1$ . The exponent  $D_2$  is the fractal dimension. As shown in Ref. [39],  $D_2$  coincides with  $\gamma$ . This implies that the components  $|C_{n_0}^\alpha|^2$  are correlated and the spectral autocorrelation function in Eq. (19.24) becomes

$$G(E) \propto E^{D_2-1}. \quad (19.33)$$

The power-law exponent  $\gamma = D_2 < 1$  is caused by the fractality of the eigenstates.

As we mentioned when describing Fig. 19.2, as  $h$  increases above 0.5, the level number variance escapes the logarithmic behavior for smaller values of  $\ell$  and the level spacing distribution changes gradually from Wigner-Dyson to Poissonian. This happens because the eigenvalues become less correlated. This is reflected also in the correlation hole. It gets less deep as the system moves away from the chaotic region and the minimum point of the hole takes place later in time. The gradual shift of the correlation hole to later times is directly related with the earlier point where  $\Sigma^2(\ell)$  leaves the logarithmic curve and is related with the Thouless energy [45].

We note that the correlation hole is not exclusive to the survival probability [38]. It is found also in other observables, such as the imbalance of the spin density for all sites [80, 81],

$$I(t) = \frac{4}{L} \sum_{k=1}^L \langle \Psi(0) | S_k^z(0) S_k^z(t) | \Psi(0) \rangle. \quad (19.34)$$

We show results for  $I(t)$  in Fig. 19.7b for different values of  $h$ . The curves are comparable to those seen for the survival probability in Fig. 19.7a. The correlation hole is deep and broad in the chaotic limit,  $h = 0.5$ . It shrinks and becomes shallower as  $h$  increases [38]. We should expect similar behaviors for other observables, such as the OTOC [38]. In Ref. [37] we also saw a sign of the correlation hole in the evolution of the Shannon (information) entropy. There, it appeared as a bulge above the saturation point. It was, however, very small.

Direct manifestations of level repulsion, such as the correlation hole, happen at exceedingly long times. To observe the correlation hole experimentally, the dynamics would need to remain coherent for very long times. Furthermore, averages over disorder realizations or, in the case of clean systems [37], over initial states are needed to reveal the hole.

## 19.6 Conclusion

We have developed a detailed picture of the entire evolution of the survival probability for realistic lattice many-body quantum systems. We are now extending this understanding to other observables and hope to be able to suggest equations similar to Eq.(19.31) for generic observables. We believe that comparisons with results for FRM and banded random matrices will be helpful in this pursuit. Despite being unrealistic, FRM allows for analytical results, which can guide us when studying realistic models.

We stress that signatures of level repulsion show up at long times, when the dynamics resolves the discreteness of the spectrum. It remains to be understood whether level repulsion is essential for many-body quantum chaos, as it is for one-body quantum chaos. This is an important question for studies of thermalization, since for many years, chaos has been seen as the main mechanism for the relaxation of isolated many-body quantum systems to thermal equilibrium.

**Acknowledgements** L.F.S. was supported by the NSF grant No. DMR-1603418. E.J.T.-H. acknowledges funding from CONACyT and VIEP-BUAP, Mexico. He is also grateful to LNS-BUAP for allowing use of their supercomputing facility.

## References

1. F. Borgonovi, F.M. Izrailev, L.F. Santos, V.G. Zelevinsky, Quantum chaos and thermalization in isolated systems of interacting particles. *Phys. Rep.* **626**(1), 00 (2016). <https://doi.org/10.1016/j.physrep.2016.02.005>
2. C. Gogolin, J. Eisert, Equilibration, thermalisation, and the emergence of statistical mechanics in closed quantum systems. *Rep. Prog. Phys.* **79**, 056001 (2016). <https://doi.org/10.1088/0034-4885/79/5/056001>
3. L. D'Alessio, Y. Kafri, A. Polkovnikov, M. Rigol, From quantum chaos and eigenstate thermalization to statistical mechanics and thermodynamics. *Adv. Phys.* **65**, 239 (2016). <https://doi.org/10.1080/00018732.2016.1198134>
4. D.J. Luitz, Y.B. Lev, The ergodic side of the many-body localization transition. *Ann. Phys.* **529**, 1600350 (2017). Berlin. <https://doi.org/10.1002/andp.201600350>
5. V. Giovannetti, S. Lloyd, L. Maccone, Quantum limits to dynamical evolution. *Phys. Rev. A* **67**, 052109 (2003). <https://doi.org/10.1103/PhysRevA.67.052109>
6. M. Akila, D. Waltner, B. Gutkin, P. Braun, T. Guhr, Semiclassical identification of periodic orbits in a quantum many-body system. *Phys. Rev. Lett.* **118**, 164101 (2017). <https://doi.org/10.1103/PhysRevLett.118.164101>
7. O. Bohigas, M.J. Giannoni, C. Schmit, Characterization of chaotic quantum spectra and universality of level fluctuation laws. *Phys. Rev. Lett.* **52**, 1 (1984). <https://doi.org/10.1103/PhysRevLett.52.1>
8. G. Casati, F. Valz-Gris, I. Guarneri, On the connection between quantization of nonintegrable systems and statistical theory of spectra. *Lett. Nuovo Cimento* **28**, 279 (1980). 1971–1985. <https://doi.org/10.1007/BF02798790>
9. M.C. Gutzwiller, Periodic orbits and classical quantization conditions. *J. Math. Phys.* **12**, 343 (1971). <https://doi.org/10.1063/1.1665596>
10. V. Strutinskii, A. Magner, Quasiclassical theory of nuclear shell structure (Classical motion). *Sov. J. Part. Nucl.* **7**, 138 (1976). <http://pepan.jinr.ru/pepan/eng/archive/1/1970s/1976/2>

11. M.L. Mehta, *Random Matrices* (Academic Press, Boston, 2004). <https://www.elsevier.com/books/random-matrices/lal-mehta/978-0-12-088409-4>, ISBN 9780120884094
12. T. Guhr, A. Mueller-Gröeling, H.A. Weidenmüller, Random matrix theories in quantum physics: common concepts. *Phys. Rep.* **299**, 189 (1998). [https://doi.org/10.1016/S0370-1573\(97\)00088-4](https://doi.org/10.1016/S0370-1573(97)00088-4)
13. E.P. Wigner, On the statistical distribution of the widths and spacings of nuclear resonance levels. *Proc. Cambridge Phil. Soc.* **47**, 790 (1951). <https://doi.org/10.1017/S0305004100027237>
14. E.P. Wigner, On the distribution of the roots of certain symmetric matrices. *Ann. Math.* **67**, 325 (1958). <https://doi.org/10.2307/1970008>
15. T. Sccaffidi, E. Altman, Semiclassical theory of many-body quantum chaos and its bound. [arXiv:1711.04768](https://arxiv.org/abs/1711.04768)
16. E. Bianchi, L. Hackl, N. Yokomizo, Linear growth of the entanglement entropy and the Kolmogorov-Sinai rate. *J. High Energy Phys.* **2018**, 25 (2018). [https://doi.org/10.1007/JHEP03\(2018\)025](https://doi.org/10.1007/JHEP03(2018)025)
17. M. Schmitt, D. Sels, S. Kehrein, A. Polkovnikov, Semiclassical echo dynamics in the Sachdev-Ye-Kitaev model. [arXiv:1802.06796](https://arxiv.org/abs/1802.06796)
18. F. Borgonovi, F.M. Izrailev, L.F. Santos, Exponentially fast dynamics in the Fock space of chaotic many-body systems. <https://doi.org/10.1103/PhysRevE.99.010101>
19. C. Khrapkov, A. Vardi, D. Cohen, Semiclassical theory of strong localization for quantum thermalization. *Phys. Rev. E* **97**, 022127 (2018). <https://doi.org/10.1103/PhysRevE.97.022127>
20. R.A. Jalabert, H.M. Pastawski, Environment-independent decoherence rate in classically chaotic systems. *Phys. Rev. Lett.* **86**, 2490 (2001). <https://doi.org/10.1103/PhysRevLett.86.2490>
21. T. Gorin, T. Prosen, T.H. Seligman, M. Žnidarič, Dynamics of loschmidt echoes and fidelity decay. *Phys. Rep.* **435**, 33 (2006). <https://doi.org/10.1016/j.physrep.2006.09.003>
22. E.B. Rozenbaum, S. Ganeshan, V. Galitski, Lyapunov exponent and out-of-time-ordered correlator's growth rate in a chaotic system. *Phys. Rev. Lett.* **118**, 086801 (2017). <https://doi.org/10.1103/PhysRevLett.118.086801>
23. K. Hashimoto, K. Murata, R. Yoshii, Out-of-time-order correlators in quantum mechanics. *J. High Energy Phys.* **2017**, 138 (2017). [https://doi.org/10.1007/JHEP10\(2017\)138](https://doi.org/10.1007/JHEP10(2017)138)
24. E.B. Rozenbaum, S. Ganeshan, V. Galitski, Universal level statistics of the out-of-time-ordered operator. [arXiv:1801.10591](https://arxiv.org/abs/1801.10591)
25. J. Chávez-Carlos, B.L. del Carpio, M.A. Bastarrachea-Magnani, P. Stránský, S. Lerma-Hernández, L.F. Santos, J.G. Hirsch, Quantum and classical Lyapunov exponents in atom-field interaction systems. *Phys. Rev. Lett.* **122**, 024101 (2019). <https://doi.org/10.1103/PhysRevLett.122.024101>
26. D.J. Luitz, Y. Bar Lev, Information propagation in isolated quantum systems. *Phys. Rev. B* **96**, 020406 (2017). <https://doi.org/10.1103/PhysRevB.96.020406>
27. E.J. Torres-Herrera, L.F. Santos, Quench dynamics of isolated many-body quantum systems. *Phys. Rev. A* **89**, 043620 (2014). <https://doi.org/10.1103/PhysRevA.89.043620>
28. E.J. Torres-Herrera, M. Vyas, L.F. Santos, General features of the relaxation dynamics of interacting quantum systems. *New J. Phys.* **16**, 063010 (2014). <https://doi.org/10.1088/1367-2630/16/6/063010>
29. E.J. Torres-Herrera, L.F. Santos, Local quenches with global effects in interacting quantum systems. *Phys. Rev. E* **89**, 062110 (2014). <https://doi.org/10.1103/PhysRevE.89.062110>
30. E.J. Torres-Herrera, L.F. Santos, Nonexponential fidelity decay in isolated interacting quantum systems. *Phys. Rev. A* **90**, 033623 (2014). <https://doi.org/10.1103/PhysRevA.90.033623>
31. E.J. Torres-Herrera, D. Kollmar, L.F. Santos, Relaxation and thermalization of isolated many-body quantum systems. *Phys. Scr. T* **165**, 014018 (2015). <https://doi.org/10.1088/0031-8949/2015/T165/014018>
32. E.J. Torres-Herrera, L.F. Santos, Isolated many-body quantum systems far from equilibrium: Relaxation process and thermalization, in *AIP Conference Proceedings*, vol. 1619, ed. by P. Danieliewicz, V. Zelevinsky (APS, East Lansing, Michigan, 2014), pp.171–180. <https://doi.org/10.1063/1.4899233>

33. E.J. Torres-Herrera, J. Karp, M. Távora, L.F. Santos, Realistic many-body quantum systems versus full random matrices: Static and dynamical properties. *Entropy* **18**, 359 (2016). <https://doi.org/10.3390/e18100359>
34. L.F. Santos, F. Borgonovi, F.M. Izrailev, Chaos and statistical relaxation in quantum systems of interacting particles. *Phys. Rev. Lett.* **108**, 094102 (2012). <https://doi.org/10.1103/PhysRevLett.108.094102>
35. L.F. Santos, F. Borgonovi, F.M. Izrailev, Onset of chaos and relaxation in isolated systems of interacting spins-1/2: energy shell approach. *Phys. Rev. E* **85**, 036209 (2012). <https://doi.org/10.1103/PhysRevE.85.036209>
36. E.J. Torres-Herrera, L.F. Santos, Extended nonergodic states in disordered many-body quantum systems. *Ann. Phys.* **1600284** (2017). Berlin. <https://doi.org/10.1002/andp.201600284>
37. E.J. Torres-Herrera, L.F. Santos, Dynamical manifestations of quantum chaos: correlation hole and bulge. *Philos. Trans. Royal Soc. A* **375** (2017). <https://doi.org/10.1098/rsta.2016.0434>
38. E.J. Torres-Herrera, A.M. García-García, L.F. Santos, Generic dynamical features of quenched interacting quantum systems: Survival probability, density imbalance, and out-of-time-ordered correlator. *Phys. Rev. B* **97**, 060303(R) (2018). <https://doi.org/10.1103/PhysRevB.97.060303>
39. E.J. Torres-Herrera, L.F. Santos, *Dynamics at the many-body localization transition*, *Phys. Rev. B* **92**, 014208 (2015). <https://doi.org/10.1103/PhysRevB.92.014208>
40. E.J. Torres-Herrera, M. Távora, L.F. Santos, Survival probability of the néel state in clean and disordered systems: an overview. *Braz. J. Phys.* **46**, 239 (2016). <https://doi.org/10.1007/s13538-015-0366-3>
41. M. Távora, E.J. Torres-Herrera, L.F. Santos, Inevitable power-law behavior of isolated many-body quantum systems and how it anticipates thermalization. *Phys. Rev. A* **94**, 041603 (2016). <https://doi.org/10.1103/PhysRevA.94.041603>
42. M. Távora, E.J. Torres-Herrera, L.F. Santos, Power-law decay exponents: A dynamical criterion for predicting thermalization. *Phys. Rev. A* **95**, 013604 (2017). <https://doi.org/10.1103/PhysRevA.95.013604>
43. L.F. Santos, E.J. Torres-Herrera, Analytical expressions for the evolution of many-body quantum systems quenched far from equilibrium, in *AIP Conference Proceedings*, vol. 1912 (2017), p. 020015. <https://doi.org/10.1063/1.5016140>
44. L.F. Santos, E.J. Torres-Herrera, in *Chaotic, Fractional, and Complex Dynamics: New Insights and Perspectives*, ed. by M. Edelman, E.E.N. Macau, M.A.F. Sanjuán (Springer International Publishing, Cham, 2018), pp. 231–260. <https://doi.org/10.1007/978-3-319-68109-2>
45. M. Schiulaz, E.J. Torres-Herrera, L.F. Santos, Thouless and relaxation time scales in many-body quantum systems. [arXiv:1807.07577](https://arxiv.org/abs/1807.07577)
46. L. Leviandier, M. Lombardi, R. Jost, J.P. Pique, Fourier transform: a tool to measure statistical level properties in very complex spectra. *Phys. Rev. Lett.* **56**, 2449 (1986). <https://doi.org/10.1103/PhysRevLett.56.2449>
47. T. Guhr, H. Weidenmüller, Correlations in anticrossing spectra and scattering theory. analytical aspects. *Chem. Phys.* **146**, 21 (1990). [https://doi.org/10.1016/0301-0104\(90\)90003-R](https://doi.org/10.1016/0301-0104(90)90003-R)
48. J. Wilkie, P. Brumer, Time-dependent manifestations of quantum chaos. *Phys. Rev. Lett.* **67**, 1185 (1991). <https://doi.org/10.1103/PhysRevLett.67.1185>
49. Y. Alhassid, R.D. Levine, Spectral autocorrelation function in the statistical theory of energy levels. *Phys. Rev. A* **46**, 4650 (1992). <https://doi.org/10.1103/PhysRevA.46.4650>
50. T. Gorin, T.H. Seligman, Signatures of the correlation hole in total and partial cross sections. *Phys. Rev. E* **65**, 026214 (2002). <https://doi.org/10.1103/PhysRevE.65.026214>
51. F.J. Dyson, The threefold way. algebraic structure of symmetry groups and ensembles in quantum mechanics. *J. Math. Phys.* **3**, 1199 (1962). <https://doi.org/10.1063/1.1703863>
52. E.P. Wigner, Characteristic vectors of bordered matrices with infinite dimensions. *Ann. Math.* **62**, 548 (1955). <https://doi.org/10.2307/1970079>
53. A. Gubin, L.F. Santos, Quantum chaos: An introduction via chains of interacting spins 1/2. *Am. J. Phys.* **80**, 246 (2012). <https://doi.org/10.1119/1.3671068>
54. F. Wegner, Inverse participation ratio in  $2 + \varepsilon$  dimensions. *Z. Phys. B* **36**, 209 (1980). <https://doi.org/10.1007/BF01325284>

55. L.F. Santos, Integrability of a disordered Heisenberg spin-1/2 chain. *J. Phys. A* **37**, 4723 (2004). <https://doi.org/10.1088/0305-4470/37/17/004>
56. L.F. Santos, G. Rigolin, C.O. Escobar, Entanglement versus chaos in disordered spin systems. *Phys. Rev. A* **69**, 042304 (2004). <https://doi.org/10.1103/PhysRevA.69.042304>
57. L.F. Santos, M.I. Dykman, M. Shapiro, F.M. Izrailev, Strong many-particle localization and quantum computing with perpetually coupled qubits. *Phys. Rev. A* **71**, 012317 (2005). <https://doi.org/10.1103/PhysRevA.71.012317>
58. F. Dukesz, M. Zilbergerts, L.F. Santos, Interplay between interaction and (un)correlated disorder in one-dimensional many-particle systems: delocalization and global entanglement. *New J. Phys.* **11**, 043026 (2009). <https://doi.org/10.1088/1367-2630/11/4/043026>
59. A. Kartiek, A. Ehud, D. Eugene, G. Sarang, A.H. Huse, K. Michael, Rare-region effects and dynamics near the many-body localization transition. *Ann. Phys.* **529**, 1600326 (2017). Berlin. <https://doi.org/10.1002/andp.201600326>
60. T.A. Brody, J. Flores, J.B. French, P.A. Mello, A. Pandey, S.S.M. Wong, Random-matrix physics – spectrum and strength fluctuations. *Rev. Mod. Phys.* **53**, 385 (1981). <https://doi.org/10.1103/RevModPhys.53.385>
61. M. Schiulaz, M. Távora, L.F. Santos, From few- to many-body quantum systems. <https://doi.org/10.1088/2058-9565/aad913>
62. P.R. Zangara, A.D. Dente, E.J. Torres-Herrera, H.M. Pastawski, A. Iucci, L.F. Santos, Time fluctuations in isolated quantum systems of interacting particles. *Phys. Rev. E* **88**, 032913 (2013). <https://doi.org/10.1103/PhysRevE.88.032913>
63. M.V. Berry, M. Tabor, *Proc. R. Soc. Lond. A* **356**, 375 (1977). <https://doi.org/10.1098/rspa.1977.0140>
64. C.L. Bertrand, A.M. García-García, Anomalous Thouless energy and critical statistics on the metallic side of the many-body localization transition. *Phys. Rev. B* **94**, 144201 (2016). <https://doi.org/10.1103/PhysRevB.94.144201>
65. J.G. Muga, A. Ruschhaupt, A. del Campo, *Time in Quantum Mechanics*, vol. 2 (Springer, London, 2009). <https://doi.org/10.1007/978-3-642-03174-8>
66. A. Erdélyi, Asymptotic expansions of fourier integrals involving logarithmic singularities. *J. Soc. Indust. Appl. Math.* **4**, 38 (1956). <https://doi.org/10.1137/0104003>
67. K. Urbanowski, General properties of the evolution of unstable states at long times. *Eur. Phys. J. D* **54**, 25 (2009). <https://doi.org/10.1140/epjd/e2009-00165-x>
68. E.J. Torres-Herrera, L.F. Santos, *Signatures of chaos and thermalization in the dynamics of many-body quantum systems*. [arXiv:1804.06401](https://arxiv.org/abs/1804.06401)
69. A. del Campo, J. Molina Vilaplana, L.F. Santos, J. Sonner, Decay of a thermofield-double state in chaotic quantum systems. <https://doi.org/10.1140/epjst/e2018-00083-5>
70. J.P. Pique, Y. Chen, R.W. Field, J.L. Kinsey, Chaos and dynamics on 0.5–300 ps time scales in vibrationally excited acetylene: Fourier transform of stimulated-emission pumping spectrum. *Phys. Rev. Lett.* **58**, 475 (1987). <https://doi.org/10.1103/PhysRevLett.58.475>
71. U. Hartmann, H. Weidenmüller, T. Guhr, Correlations in anticrossing spectra and scattering theory: Numerical simulations. *Chem. Phys.* **150**, 311 (1991). [https://doi.org/10.1016/0301-0104\(91\)87105-5](https://doi.org/10.1016/0301-0104(91)87105-5)
72. A. Delon, R. Jost, M. Lombardi, NO<sub>2</sub> jet cooled visible excitation spectrum: Vibronic chaos induced by the X<sup>2</sup>A<sub>1</sub>–A<sup>2</sup>B<sub>2</sub> interaction. *J. Chem. Phys.* **95**, 5701 (1991). <https://doi.org/10.1063/1.461620>
73. M. Lombardi, T.H. Seligman, Universal and nonuniversal statistical properties of levels and intensities for chaotic rydberg molecules. *Phys. Rev. A* **47**, 3571 (1993). <https://doi.org/10.1103/PhysRevA.47.3571>
74. A. Kudrolli, S. Sridhar, A. Pandey, R. Ramaswamy, Signatures of chaos in quantum billiards: Microwave experiments. *Phys. Rev. E* **49**, R11 (1994). <https://doi.org/10.1103/PhysRevE.49.R11>
75. H. Alt, H.-D. Gräf, T. Guhr, H.L. Harney, R. Hofferbert, H. Rehfeld, A. Richter, P. Schardt, Correlation-hole method for the spectra of superconducting microwave billiards. *Phys. Rev. E* **55**, 6674 (1997). <https://doi.org/10.1103/PhysRevE.55.6674>

76. L. Michaille, J.-P. Pique, Influence of experimental resolution on the spectral statistics used to show quantum chaos: the case of molecular vibrational chaos. *Phys. Rev. Lett.* **82**, 2083 (1999). <https://doi.org/10.1103/PhysRevLett.82.2083>
77. T. Gorin, T. Prosen, T.H. Seligman, A random matrix formulation of fidelity decay. *New J. Phys.* **6**, 20 (2004). <https://doi.org/10.1088/1367-2630/6/1/020>
78. Y. Alhassid, Y.V. Fyodorov, T. Gorin, W. Ihra, B. Mehlig, Fano interference and cross-section fluctuations in molecular photodissociation. *Phys. Rev. A* **73**, 042711 (2006). <https://doi.org/10.1103/PhysRevA.73.042711>
79. F. Leyvraz, A. García, H. Kohler, T.H. Seligman, Fidelity under isospectral perturbations: a random matrix study. *J. Phys. A* **46**, 275303 (2013). <https://doi.org/10.1088/1751-8113/46/27/275303>
80. D.J. Luitz, N. Laflorencie, F. Alet, Extended slow dynamical regime close to the many-body localization transition. *Phys. Rev. B* **93**, 060201 (2016). <https://doi.org/10.1103/PhysRevB.93.060201>
81. M. Lee, T.R. Look, S.P. Lim, D.N. Sheng, Many-body localization in spin chain systems with quasiperiodic fields. *Phys. Rev. B* **96**, 075146 (2017). <https://doi.org/10.1103/PhysRevB.96.075146>

# Chapter 20

# Properties of Thermal Quantum States: Locality of Temperature, Decay of Correlations, and More



Martin Kliesch and Arnau Riera

## 20.1 Introduction

Thermal or Gibbs states are arguably the most relevant class of states in nature. They appear to have many very different unique properties. On one hand, they provide an efficient description of the equilibrium state for most systems (see Chap. 17 and Ref. [1] for a detailed review). Jaynes gave a justification of this observation by means of the principle of maximum entropy [2, 3]. For a given energy, the thermal state is the one that maximizes the von Neumann entropy. This is in fact the reason why they minimize the free energy potential.

At the same time, in the context of extracting work from closed systems by means of unitary transformations, thermal states appear as the only ones that are completely passive states [4]. That is, for any other passive state [5], i.e. a state whose (average) energy cannot be lowered by applying a unitary transformation, it is always possible to form an active state by joining sufficiently many copies. Note that this property is crucial for establishing both a resource theory of thermodynamics and a consistent zero-th law (see Chaps. 25 and 33).

---

M. Kliesch

Institute of Theoretical Physics and Astrophysics, National Quantum Information Centre,  
University of Gdańsk, ul. Gen. Wł. Andersa 27, 81-824 Sopot, Poland

M. Kliesch (✉)

Institute for Theoretical Physics, Heinrich Heine University Düsseldorf, Universitätsstraße 1,  
40225 Düsseldorf, Germany  
e-mail: science@mkliesch.eu

A. Riera

ICFO – Institut de Ciències Fotoniques, The Barcelona Institute of Science and Technology,  
08860 Castelldefels, Spain

A. Riera

Max-Planck-Institut für Quantenoptik, 85748 Garching, Germany  
e-mail: arnauriera@gmail.com

Last but not least, if one accepts that the equilibrium population of a configuration should only be a function of its energy, the canonical ensemble becomes the single probability distribution that allows for a free choice of the energy origin, or in other words, that is invariant under energy shifts. More explicitly, any other relation between populations and energy would imply that observers with different energy origins would observe different equilibrium states. The proof of that statement is a good exercise.

In this chapter, we study the properties of thermal states for a class of Hamiltonians highly relevant in condensed matter physics: spin lattice Hamiltonians with short range interactions. We particularly focus on results where the application of tools coming from quantum information theory has been particularly successful in recent years.

A first issue where quantum information tools have been helpful is in the rigorous proof of long-standing conjectures concerning the correlations of many-body systems. The most paradigmatic example is the proof that unique ground states of gapped Hamiltonians have an exponential decay of correlations [6, 7]. In Sect. 20.3 we overview the main results on the scaling of the correlations for both thermal states and absolute zero temperature states. The understanding of the correlations of many-body systems is particularly relevant since they are a signature of phase transitions and critical phenomena [8, 9]. Furthermore, they are also related to the stability of thermal states, that is, to the robustness of thermal states against distant and/or weak Hamiltonian perturbations [10].

The stability of thermal states is actually crucial for understanding to what extent temperature can be assigned locally in a system [10–13]. For weakly interacting systems temperature is an intensive quantity, in the sense that every subsystem is in a thermal state with the temperature identical to the global one. However, when interactions between subsystems are not negligible, this property does no longer hold, as can be the case for quantum systems [14, 15]. A first step to circumvent the problem of assigning temperature locally to a subsystem was made in Refs. [16, 17], where it was shown that it is sufficient to extend the subsystem by a boundary region that, when traced out, disregards the correlations and the boundary effects. If the size of such a boundary region is independent of the total system size, temperature can still be said to be *local*. In Ref. [10] it is shown that the thickness of the boundary region is determined by the decay of a *generalized covariance*, which captures the response in a local operator of perturbing a thermal state and ultimately at what length scales temperature can be defined. In other words, the clustering of the generalized covariance allows for a local definition of temperature. This issue is particularly relevant in Chap. 21, where the problem of local thermometry is considered.

Another feature of the thermal states that exhibit a clustering of correlations is that they can be efficiently classically represented by so-called tensor network states [18]. The simulation of quantum many body systems by classical means, and more specifically by using tensor network states, has been one of the most fruitful topics in the interplay between condensed-matter physics and quantum information. Tensor networks have been shown to satisfactorily describe locally entangled states in one and two spatial dimensions and even systems at criticality [19]. Applications

of thermal states with exponentially decaying correlations are presented in Sect. 20.3.5.

In Sect. 20.4, we focus on the study of the energy distribution of states not necessarily thermal but with a finite correlation length. In particular, it can be shown that for large system sizes the energy distribution of a state with a finite correlation length has an energy distribution that tends to a Gaussian whose standard deviation scales with the square root of the system size [20].

The last part of the chapter in Sect. 20.5 is dedicated to present a rigorous formulation of the equivalence between the canonical and the microcanonical ensembles [20, 21].

We finally conclude with a brief summary and a discussion on what might be the most relevant open questions of the field.

## 20.2 Setting

Throughout the chapter we set  $\hbar = 1 = k_{\text{Boltzmann}}$  and assume all Hilbert space dimensions to be finite. For a positive integer  $n$  we set  $[n] := \{1, 2, \dots, n\}$ . The *spectral norm* and *trace norm* on operators are denoted by  $\|\cdot\|$  and  $\|\cdot\|_1$ . They are given by the largest and the sum of the operator's singular values, respectively.

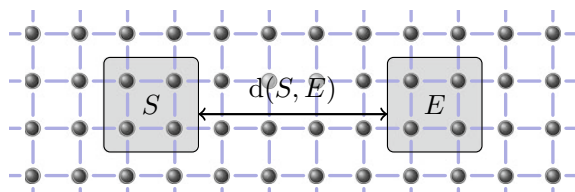
We consider quantum spin-lattice systems: the Hilbert space is given by  $\mathcal{H} = \bigotimes_{x \in \mathcal{V}} \mathcal{H}_x$ , where  $\mathcal{V}$  is a finite set, called the *vertex set*.  $\mathcal{H}_x$  are the *local* Hilbert spaces. Usually, they have all the same dimension, i.e.,  $\mathcal{H}_x \cong \mathbb{C}^d$  and  $d$  is called the *local Hilbert space dimension*.

The *partial trace* over a subsystem  $S \subset \mathcal{V}$  of an operator  $\rho$  is denoted by  $\text{Tr}_S[\rho]$ . Complementary, we set the reduction of  $\rho$  to  $S$  to be  $\rho^S := \text{Tr}_{\mathcal{V} \setminus S}[\rho]$ . The *support*  $\text{supp}(A) \subseteq \mathcal{V}$  of an observable  $A$  on  $\mathcal{H}$  is the set of vertices where  $A$  does not act as the identity operator. For two observables  $A, B$  we set their *distance*  $\text{dist}(A, B)$  to be the graph distance between their supports; see Fig. 20.1 for an illustration with  $S = \text{supp}(A)$  and  $E = \text{supp}(B)$ .

Let us consider a graph  $(\mathcal{V}, \mathcal{E})$ , where  $\mathcal{E}$  is the *edges set* containing two-element subsets of  $\mathcal{V}$ . For a subset  $S \subset \mathcal{V}$  we denote the set of boundary vertices of  $S$  by  $\partial S := \{v \in S : \text{dist}(v, \mathcal{V} \setminus S) = 1\}$  and, for an observable  $A$  we set  $\partial A := \partial \text{supp}(A)$ .

We say that a Hamiltonian  $H$  has *interaction graph*  $(\mathcal{V}, \mathcal{E})$  and *interaction strength* (bounded by)  $J$  if it can be written as

**Fig. 20.1** Two spatially separated regions  $S$  and  $E$  in a lattice.



$$H = \sum_{e \in \mathcal{E}} h_e \quad (20.1)$$

with  $h_e$  being supported on  $e$  and  $\|h_e\| \leq J$  for all  $e \in \mathcal{E}$ .

To give an example, for the simple one-dimensional Ising model the introduced quantities are  $\mathcal{V} = [n]$ ,  $\mathcal{E} = \{\{1, 2\}, \{2, 3\}, \dots, \{n-1, n\}\}$ , and  $h_{\{j, j+1\}} = \mathbb{1}^{\otimes(j-1)} \otimes \sigma^{(z)} \otimes \sigma^{(z)} \otimes \mathbb{1}^{\otimes(n-j-1)}$ , where  $\mathbb{1}^{\otimes k} := \mathbb{1} \otimes \mathbb{1} \otimes \dots \otimes \mathbb{1}$  denotes  $k$  tensor copies of the local identity operator  $\mathbb{1}$ . The support of  $h_{\{j, j+1\}}$  is  $\{j, j+1\}$ . As an example for a boundary we have  $\partial\{2, 3, 4\} = \{2, 4\}$ . Moreover,  $\text{dist}(h_{\{1, 2\}}, h_{\{6, 7\}}) = 6 - 2 = 4$ .

We denote the *thermal state*, or Gibbs state, of a Hamiltonian  $H$  at *inverse temperature*  $\beta$  by

$$g(\beta) := \frac{e^{-\beta H}}{Z(\beta)}, \quad (20.2)$$

with  $Z(\beta) := \text{Tr}(e^{-\beta H})$  being the *partition function*. If we mean the thermal state or partition function of a different Hamiltonian  $H'$ , we write  $g[H'](\beta)$  or  $Z[H'](\beta)$ .

We measure correlations by the (*generalized*) *covariance* that we define for any two operators  $A$  and  $A'$ , full-rank quantum state  $\rho$ , and parameter  $\tau \in [0, 1]$  as

$$\text{cov}_\rho^\tau(A, A') := \text{Tr}(\rho^\tau A \rho^{1-\tau} A') - \text{Tr}(\rho A) \text{Tr}(\rho A'). \quad (20.3)$$

This quantity is closely related to the Duhamel two-point function, which is defined as the average  $\int_0^1 d\tau \text{Tr}(\rho^\tau A \rho^{1-\tau} A')$  (see, e.g., [22, Sect. 2]). The usual *covariance*, denoted by  $\text{cov}_\rho(A, A')$ , is obtained by setting  $\rho^\tau = \rho$  and  $\rho^{1-\tau} = \mathbb{1}$ , see also [10, Sect. IV.A].

It is interesting to point out that the clustering of the standard covariance implies the clustering of the Duhamel two-point function [22, Theorem 2.1]. In this case, we mean by clustering that the covariance tends to zero in the limit of the spatial distance between the non-trivial support of the operators  $A$  and  $A'$  tends to infinity. However, given a state  $\rho$  and two observables  $A$  and  $A'$ , the generalized covariance as a function of  $\tau$  is not monotonic and can have zeros and saddle points.

Let us finally introduce the *relative entropy* between two quantum states  $\rho$  and  $\sigma$ , which is defined as

$$S(\rho \|\sigma) := -\text{Tr}[\rho \log_2(\sigma)] - S(\rho), \quad (20.4)$$

where  $S(\rho) := -\text{Tr}[\rho \log_2(\rho)]$  is the von Neumann entropy. The relative entropy provides a notion of non-symmetric distance between states, and can be operationally interpreted as the physical distinguishability from many copies [23]. The relative entropy is closely related to the *free energy* when its second argument  $\sigma$  is a thermal state,

$$F(\rho) - F(g(\beta)) = \frac{1}{\beta} S(\rho \| g(\beta)), \quad (20.5)$$

where  $F(\rho, H) := \text{Tr}(\rho H) - \beta^{-1} S(\rho)$  is the out of equilibrium *free energy*. In a similar way, the *mutual information* of a bipartite state  $\rho$  can also be written in terms of the relative entropy

$$I(A : B)_\rho = S(\rho \| \rho_A \otimes \rho_B). \quad (20.6)$$

Recall that the mutual information, defined as  $I(A : B)_\rho := S(\rho_A) + S(\rho_B) - S(\rho)$ , is a measure of the total correlations between the parties  $A$  and  $B$  [24].

## 20.3 Clustering of Correlations

In quantum lattice models with local Hamiltonians, a relevant class of observables are the local ones, that is, operators that only have non-trivial support on a few connected sites. However, local operators cannot witness global properties of the state such as entanglement, correlations or long range order. The simplest observables that can reveal this type of features are the two-point correlation functions or, as they have been introduced in the former section, the covariance. In condensed-matter physics, the scaling of the covariance with the distance between the two “points” is an important measure of correlations. In this section, we review the current understanding on the sorts of scalings that the covariance of thermal states and zero temperature states can exhibit.

### 20.3.1 High Temperature States

Bounding correlations in thermal spin systems has a long tradition in theoretical and mathematical physics; see e.g. Ref. [25] classical systems, [26] for quantum gases (translation-invariant Hamiltonians in the continuum), and Refs. [27–29] cubic lattices. Here, we review a general result for finite dimensional systems.

Any graph that is a regular lattice has an associated (cell or lattice animal) *growth constant*  $\alpha \in \mathbb{R}_+$ , which captures the local connectivity of a lattice [30, 31]. For instance, for lattices in  $D$  spatial dimensions,  $\alpha \leq 2 D \exp(1)$  [31, Lemma 2].

The following theorem provides a universal upper bound to all critical temperatures that only depends on the growth constant  $\alpha$ .

**Theorem 1** (High temperatures [10, Theorem 2]). *For a graph  $(V, \mathcal{E})$  with growth constant  $\alpha$  define the constant (critical inverse temperature)*

$$\beta^* := \ln[(1 + \sqrt{1 + 4/\alpha})/2]/(2 J) \quad (20.7)$$

and function  $\xi$  (correlation length) by

$$\xi(\beta) := |\ln[\alpha e^{2|\beta|J}(e^{2|\beta|J} - 1)]|^{-1}. \quad (20.8)$$

Then, a thermal state  $g$  of any Hamiltonian with interaction graph  $(\mathcal{V}, \mathcal{E})$  and local interaction strength  $J$  satisfies the following: for every  $|\beta| < \beta^*$ , parameter  $\tau \in [0, 1]$ , and every two operators  $A$  and  $B$

$$|\text{cov}_{g(\beta)}^\tau(A, B)| \leq \frac{4a}{\ln(3)(1 - e^{-1/\xi(\beta)})} e^{-\text{dist}(A, B)/\xi(\beta)} \quad (20.9)$$

whenever  $\text{dist}(A, B)$  exceeds some minimal distance  $L_0$  (given in [10, Eq. (50)]) and with parameter  $a := \|A\| \|B\| \min\{|\partial A|, |\partial B|\}$ .

This theorem guarantees that below an inverse universal critical temperature  $\beta^*$  correlations always decay with a correlation length at most  $\xi(\beta)$ . The inverse critical temperature  $\beta^*$  and correlation length  $\xi$  are universal bounds to the corresponding actual physical quantities.

For the proof of Theorem 1, four weighted copies of the system  $\mathcal{V}$  are considered and a cluster expansion analysis from Hastings [32] is tightened for this particular case. Originally, Hastings used this cluster expansion to show that high temperature thermal states on spin lattices can be approximated by so-called MPOs; see also Sect. 20.3.5.3 on classical simulability below.

### 20.3.2 Ground States of Gapped Hamiltonians

The following theorem, first proved by Hastings, Koma, Nachtergael, and Sims [6, 7], confirmed a long-standing conjecture in condensed-matter physics, that gapped Hamiltonian systems have exponentially clustering correlations in the ground state. A *gapped Hamiltonian* is a Hamiltonian whose gap, that is, the energy difference between the ground and the first excited states (or eigenspaces), is lower bounded by a constant in the thermodynamic limit. The proof of the theorem is based on Lieb-Robinson bounds which provide a bound on the speed of propagation of correlation under Hamiltonian evolution. There is a constant speed limit that only depends on the maximum number of lattice nearest neighbors and the interaction strength and is called *Lieb-Robinson speed*, see Ref. [33] for a review on that topic.

**Theorem 2** (Unique ground states [34, Theorem 4.1]). *Let  $H$  be a local Hamiltonian with interaction graph  $(\mathcal{V}, \mathcal{E})$ , a unique ground state  $\psi$ , and a spectral gap  $\Delta E > 0$ . Then, for all observables  $A$  and  $B$ ,*

$$|\text{cov}_\psi(A, B)| \leq C a e^{-\mu \text{dist}(A, B)}, \quad (20.10)$$

where  $a := \|A\| \|B\|_\infty \min\{|\partial A|, |\partial B|\}$ , the constant  $C$  depends on  $\Delta E$  and the local lattice geometry, and the constant  $\mu$  on  $\Delta E$  and the Lieb-Robinson speed.

This theorem tells us that correlations in ground states of gapped Hamiltonians decay with a correlation length that is bounded in terms of the spectral energy gap above the ground state.

It is interesting to point out that one dimensional systems in a pure state with exponentially decaying correlations obey an area law for the entanglement entropy [35], that is, the entropy of the reduced state of a subregion grows like its boundary and not like its volume [36]. The same statement remains open in higher dimensions. Theorem 2 together with Ref. [35] is an alternative way to see that ground-states of gapped Hamiltonians obey an area law for the entanglement entropy [37].

For the case of non-zero temperature, by inserting in Eq. (20.5) the thermal states of an interacting Hamiltonian  $H = H_S \otimes \mathbb{1} + \mathbb{1} \otimes H_E + H_I$  and a non-interacting one  $H_S \otimes \mathbb{1} + \mathbb{1} \otimes H_E$  of a composite system with parties  $S$  and  $E$ , one obtains

$$I(S : E)_{g(\beta)} \leq 2\beta \|H_I\| - S[g^S(\beta) \otimes g^E(\beta)] \|g(\beta)\] \quad (20.11)$$

for the mutual information of  $S$  and  $E$ . This equation implies an area law for the mutual information when applied on local Hamiltonians since  $\|H_I\|$  scales as the boundary between  $S$  and  $E$  [38] and the relative entropy is non-negative.

The area law for the mutual information does not contradict the fact that most energy eigenstates of non-integrable/chaotic systems away from the edges of the spectrum exhibit a volume law for the entanglement entropy [36, 39, 40]. At relatively large temperatures, when these excited states start to have non-negligible populations, their contribution to the entropy due to exhibiting a volume law is compensated by the entropy of the global state, which also exhibits a volume law for the entanglement.

### 20.3.3 Critical Points at Zero and Finite Temperature

We have seen that in the regime of high temperatures and for gapped Hamiltonians at absolute zero temperature, the covariance decays exponentially with the distance. In the following, we review the behavior of correlations for gapless Hamiltonians at zero temperature and for arbitrary local Hamiltonians below the critical temperature (20.7).

#### 20.3.3.1 Gappless Hamiltonians at Zero Temperature

If the system is gapless and no other assumption is made on the Hamiltonian, then, roughly speaking, any correlation behavior is possible. For instance, by a proper fine-tuning of the coupling constants of a nearest neighbor interacting spin-1/2 Hamiltonian, it is possible to maximally entangle spins arbitrarily far away [41]. It is also remarkable that even ground-states of one dimensional translation invariant Hamiltonians with nearest neighbor interactions can exhibit a volume law for the entanglement entropy [42, 43].

However, in practice, the relevant gapless models in condensed-matter physics have ground states satisfying an area-law for the entanglement entropy with only logarithmic corrections. These logarithmic corrections are a manifestation of a power-

law decay in the two-body correlations. It is useful to introduce the notion of critical system and the critical exponents. A system at zero temperature is said to be critical when the spectral gap  $\Delta$  between the energy ground state (space) and the first excited state closes in the thermodynamic limit. More explicitly, we say the system to be critical when the gap scales as

$$\Delta \propto N^{-z\nu}, \quad (20.12)$$

where  $N = |\mathcal{V}|$  is the system size, and  $z$  and  $\nu$  are the critical exponents that control how fast the gap  $\Delta$  tends to zero. Actually,  $\nu$  is the critical exponent that controls the divergence of the correlation length in the vicinity of the critical point

$$\xi \propto N^\nu, \quad (20.13)$$

and  $z$  the one that determines the dynamic scaling (see [8, Chap. 10]). The previous divergences are a signature of the *scale invariance* that the system experiences at criticality [8]. If the critical exponent  $z = 1$ , the time and space correlations scale identically. This implies a further symmetry enhancement and the system becomes *conformal invariant*. The group of conformal transformations includes, in addition to scale transformations, translations and rotations. Such group is particularly powerful in  $1 + 1$  dimensions when we address the problem of the locality of temperature. The conformal symmetry completely determines the difference between a local expectation value of the infinite Hamiltonian and the truncated one.

### 20.3.3.2 Arbitrary Systems at Finite Temperature

In a similar way to the ground state case, it is an open question what kind of scalings the correlation functions of thermal states at finite temperature can exhibit in general. The most common picture is that there exists at least a renormalization group fixed point in the space of couplings of the Hamiltonian ([8, Chap. 3]). Away from the fixed point, the correlations decay exponentially. In contrast, in its vicinity, the renormalization group transformations can be linearized and some scaling laws for both the free energy and the correlation functions are obtained. In particular, the correlation length is shown to diverge as Eq. (20.13).

### 20.3.4 Correlations and Stability

Let us again assume that a quantum system is in a thermal state  $g(\beta)$  w.r.t. an arbitrary Hamiltonian  $H$ . If we assume that a subsystem  $S$  is little correlated with a disjoint subsystem  $E$ , say due spatial separation as sketched in Fig. 20.1, then it is expected that a “perturbation” of the Hamiltonian on  $E$  has only little effect on the state on  $S$ . This expectation can be rigorously confirmed and is implied by the following statement, which holds in more generality (no spin-lattice setup required).

**Theorem 3** (Perturbation formula [10, Theorem 1]). *Let  $H_0$  and  $H$  be Hamiltonians acting on the same Hilbert space. For  $s \in [0, 1]$ , define an interpolating Hamiltonian by  $H(s) := H_0 + s(H - H_0)$  and denote its thermal state by  $g_s := g[H(s)]$ . Then,*

$$\mathrm{Tr}[A g_0(\beta)] - \mathrm{Tr}[A g(\beta)] = \beta \int_0^1 d\tau \int_0^1 ds \, \mathrm{cov}_{g_s(\beta)}^\tau(H - H_0, A) \quad (20.14)$$

for any operator  $A$ .

The theorem holds, in particular, for all observables  $A$  supported on  $S$  and a perturbation  $H - H_0$  only supported on  $E$ . As

$$\|(\Delta\rho)^S\|_1 = \sup_{\substack{\|A\|=1 \\ \mathrm{supp}(A)=S}} \mathrm{Tr}[A \Delta\rho] \quad (20.15)$$

for any operator  $\Delta\rho$ , the theorem indeed confirms the expectation developed before the theorem statement.

Note that due to the factor  $\beta$  on the RHS, the perturbation formula (20.14) does not directly apply to ground states, as it is unclear how one can calculate the limit  $\beta \rightarrow \infty$ .

The proof of Theorem 3 is essentially a consequence of Duhamel's formula, where the key was to find the right correlation measure, the averaged generalized covariance.

### 20.3.5 Applications

The understanding of the correlations of thermal states and, in particular, the exponential clustering in some regimes has several applications. We review the main ones in this section.

#### 20.3.5.1 Thermal Lieb-Robinson Bound

Whenever one has an explicit bound on the correlation decay in a thermal quantum system, the perturbation formula Theorem 3 yields an explicit local stability statement. Now we discuss this idea explicitly for small inverse temperature  $\beta < \beta^*$ , where an exponential correlation decay is guaranteed by Theorem 1. Specifically, we get back to the geometric setup sketched before Theorem 3 of a Hamiltonian  $H_0$  that is perturbed on region  $E$ , which is spatially separated from a subsystem of interest  $S$ , e.g., such as sketched in Fig. 20.1.

**Corollary 4** (Thermal Lieb-Robinson bound). *Let  $S, E \subset \mathcal{V}$  be subsystems that are separated by the minimal distance,  $\text{dist}(S, E) \geq L_0$ . Moreover, let  $H$  and  $H_0$  be a Hamiltonians with  $\text{supp}(H - H_0) \subseteq E$  and that have the same interaction graph satisfying the conditions of Theorem 1. Then, for any  $|\beta| < \beta^*$ ,*

$$\|g^S(\beta) - g_0^S(\beta)\|_1 \leq \frac{w |\beta| J}{1 - e^{-1/\xi(\beta)}} e^{-\text{dist}(S, E)/\xi(\beta)}, \quad (20.16)$$

where  $g$  and  $g_0$  are the thermal states of  $H$  and  $H_0$ , respectively,  $w := 4 \min\{|\partial S|, |\partial E|\} |E| / \ln(3)$ , and  $J$  bounds the interaction strengths of  $H$ ,  $H_0$ , and  $H - H_0$ .

This result says that, at high temperatures, the effect on  $S$  of the perturbation of  $H_0$  on  $E$  is exponentially suppressed in the distance between  $S$  and  $E$ . In particular, this statement can be used to bound the error made when locally (on  $S$ ) approximating a thermal state by the thermal state of a truncated Hamiltonian (see [10, Corollary 2] for an explicit discussion).

This bound is reminiscent of Lieb-Robinson bounds, which can be used, e.g., to rigorously bound the error made when locally (on  $S$ ) approximating the time evolution operator of the full Hamiltonian by a truncated one.

The Thermal Lieb-Robinson bound (20.16) motivates the following definition [20].

**Definition 5** We say that a state  $\rho$  on a spin lattice with graph  $(\mathcal{V}, \mathcal{E})$  has  $(\xi, z)$ -exponentially decaying correlations if for any two observables  $A, B$  that are normalized ( $\|A\| = 1 = \|B\|$ ) and have disjoint support

$$\text{cov}_\rho(A, B) \leq |\mathcal{V}|^z e^{-\text{dist}(A, B)/\xi}. \quad (20.17)$$

Then Corollary 4 can be summarized as follows. Below the critical inverse temperature  $\beta^*$  thermal states have  $(\xi, z)$ -exponentially decaying correlations.

### 20.3.5.2 Locality of Temperature

Basic statistical mechanics teaches us that *temperature* is intensive, i.e., it is a physical quantity that can be measured locally and is the same throughout the system. This statement holds for non-interacting systems where the global thermal state is a tensor product of the local ones. However, in the presence of interactions the intensiveness of temperature can break down [14] and an extension of this concept is required. For this purpose, the idea of a *buffer region* was introduced [15, 16]. Here, one can take a “ring”  $E = \{v \in \mathcal{V} : \text{dist}(v, S) = r\}$  around  $S$ , which yields a partition of the total system  $\mathcal{V} = B \cup E \cup F$  (disjoint union) where  $S \subset B$  is the buffer region of  $S$  and does not interact with  $F$ , see Fig. 20.2. Next, we choose  $H_0 := H_B + H_F$ , where  $H_B$  is the Hamiltonian only containing those interactions fully contained in  $B$  and similarly for  $H_F$ . We consider  $H - H_0$  as a perturbation and note that  $\text{supp}(H - H_0) = E$ . As  $g_{H_0} = g_{H_F} g_{H_B}$ , Corollary 4 implies that the Hamiltonians  $H$  and  $H_B$  have approximately the same states on  $S$ ,

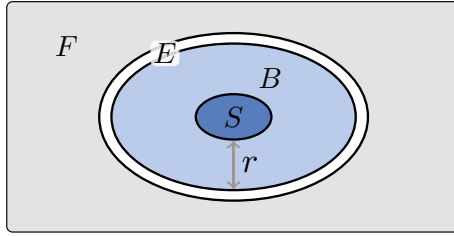


**Fig. 20.2** Partition of the system  $\mathcal{V} = B \cup E \cup F$  with  $S \subset B$ .

$$g_H^S(\beta) \approx g_{H_B}^S(\beta) \quad \forall \beta < \beta^*, \quad (20.18)$$

up to an error exponentially small in the distance  $r$ .

As the physical application, the approximation (20.18) can be used to assign a temperature to  $S$  by just knowing the state of  $B$ . This idea extends the intensiveness of temperature to non-critical interacting quantum systems.

With respect to the critical case, in 1+1 dimensions, conformal symmetry completely dictates how correlation functions behave and how local expectation values of local observables of infinite systems differ from those taken for finite ones. Hence, conformal field theory establishes that

$$\text{Tr}[O g(\beta)] - \text{Tr}[O g(\beta, H_0)] \simeq \frac{1}{r^y} \quad (20.19)$$

up to higher order terms, where  $y$  is the *scaling dimension* of the operator  $H_E$  [44, 45]. If  $H_E$  is a standard Hamiltonian term, in the sense that the system is homogeneous, its leading scaling dimension is  $y = 2$ .

In what follows, the same idea leads to a computational application: The state on  $S$  can be simulated by only calculating the state on  $B$ . If one wants to simulate the global thermal state then one can resort to certain tensor network approximations discussed in the next section.

### 20.3.5.3 Classical Simulability of Many-Body Quantum Systems

A naive approach for the classical simulation of many-body quantum systems requires an amount of resources (memory and time) that scales exponentially in the system size. However, in many cases, smart classical methods allow for the simulation of quantum systems by only employing polynomial resources. A powerful family of these classical simulation methods for interacting quantum systems relies on so-called *tensor networks*, see [19] for an introduction. A key to the success of these methods is to find computation friendly parametrizations of quantum many-body states that have limited correlations. The most prominent class of states are *matrix product states* (MPS), which usually represent state vectors in the Hilbert space of

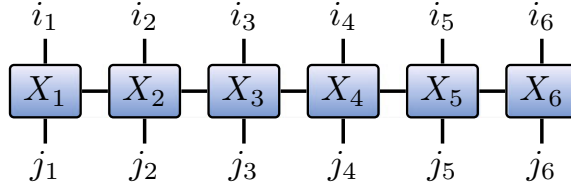


**Fig. 20.3** Graphical MPO representation of an operator  $\rho$  on a six site spin-chain. Each site  $v \in \mathcal{V} = [6]$  is associated with a tensor  $X_v \in \mathbb{C}^{D(v-1)} \otimes L(\mathcal{H}_v) \otimes \mathbb{C}^{D(v)}$  with bond dimensions  $D(v)$ , where  $D(0) = D(6) = 1$ . The components  $\rho_{(i_1, i_2, \dots, i_6), (j_1, j_2, \dots, j_6)}$  are given by the displayed tensor network, which is given by contracting the  $X(v)$  over each pair of bond indices in  $\{1, 2, \dots, D(v)\}$ .

$n$  spins. The operator analogue of MPS are *matrix product operators* (MPOs), see Fig. 20.3 for a rough definition. Practically, they can be used to (approximately) represent density matrices [46, 47].

Hastings has used a certain cluster expansion method to show that thermal spin lattice states can also be approximated by MPOs [32, Sect. V], see also [10, Sect. III.C]. After this cluster expansion method has been formalized [10] the MPO approximation was improved and made efficient by Molnár et al. [18].

For the cluster expansion one starts by expanding the exponential series of  $e^{-\beta H}$  and the Hamiltonian sum (20.1) as

$$e^{-\beta H} = \sum_{j=0}^{\infty} \sum_{w \in \mathcal{E}^j} \frac{(-\beta)^j}{j!} h(w), \quad (20.20)$$

where  $h(w) := h_{w_1} h_{w_2} \dots h_{w_j}$ . It can be made rigorous that correlations of range  $L$  in the thermal state are due to those terms  $h(w)$  where  $w \in \mathcal{E}^j$  contains long connected regions in the graph  $(\mathcal{V}, \mathcal{E})$  of size at least  $L$  [10, 32]. The idea underlying the MPO approximation of the thermal state is to drop those terms in the series (20.20). Then one can show that the resulting operator approximates the thermal state for small inverse temperatures  $\beta < 2\beta^*$  with  $\beta^*$  from Eq. (20.7)<sup>1</sup> and is an MPO, where the size of the single tensors is determined by  $L$  [10, Theorem 3]. By an improved smart choice of selecting the terms in the series (20.20) one can algorithmically obtain an improved MPO approximation to thermal states where the size of the MPO tensors scales polynomially in the system size [18].

The efficient MPO approximation of thermal states [18] naturally has implications on the simulability of thermal states. Tensor network methods work best for spin-chains, i.e., in one spatial dimension. Here, the MPO approximation allows for efficient classical simulation including, e.g., the efficient approximation of MPO observables.

<sup>1</sup>The discrepancy of the factor of 2 in the inverse temperature bound is due to considering two copies of the system in the proof of Theorem 1.

As a last remark we comment on the positivity of MPOs. In general, one cannot practically check whether or not an MPO is positive-semidefinite and, hence, can be a density operator [48]. However, for the thermal state MPO approximations one can easily circumvent this issue by first approximating  $e^{-\beta H/2}$  and then squaring the MPO at the cost of squaring the bond dimension [32].

#### 20.3.5.4 Phase Transitions

Expectation values and thermodynamic potentials of thermal states of finite systems are differentiable with respect to the Hamiltonian couplings and do not have non-analyticities. In contrast, in nature, we observe abrupt changes and discontinuities of the thermodynamic potentials and their derivatives. The solution to this apparent contradiction relies in the fact that these discontinuities only appear in the limit of infinitely large system sizes, usually denoted as the thermodynamic limit. This is actually one of the reasons why it is so difficult to prove the existence of phase transitions.

Hence, showing some behaviour for the scaling of the covariance for any system size can help to discard the existence of phase transitions. This is the case of the clustering of correlations proven in Theorem 1. It discards the possibility of a phase transition above the critical temperature, i. e. where  $\beta < \beta^*$  [10].

In this context, it is interesting to mention the existence of spontaneous magnetization at sufficiently low temperatures  $\beta > \beta_{\text{FSS}}$  in a relevant family of spin systems in 3 or more spatial dimensions [22]. This family of models includes Hamiltonians as the XX model and the antiferromagnetic Heisenberg model with spin 1, 3/2, ... The threshold temperature  $\beta_{\text{FSS}}$  has a non-trivial expression given in Ref. [22]. Note that the above statement simultaneously discards the existence of phase transitions at the very low temperature regime,  $\beta < \beta_{\text{FSS}}$ , for this type of models, and ensures the existence of a critical point below the disordered phase such that its Curie inverse temperature fulfills  $\beta_{\text{FSS}} > \beta_c > \beta^*$ .

## 20.4 Energy Distribution of Thermal States

Another important property of thermal states is their energy distribution. The mean energy of a thermal state is given by

$$U(T) := \text{Tr} (H g(T^{-1})) . \quad (20.21)$$

For short ranged Hamiltonians this quantity scales as the volume  $N = |\mathcal{V}|$ . It is then common to use the energy density, which is defined as the energy per site,

$$u(T) := U(T)/N. \quad (20.22)$$

A first question is what the qualitative relation between energy and temperature is. The *heat capacity* and *specific heat capacity* of the system at temperature  $T$  are the quantities that tell us how much energy is necessary to increase the temperature of the system by one unit and are defined as

$$C(T) := \frac{dU(T')}{dT'} \Big|_{T'=T}, \quad c(T) := \frac{du(T')}{dT'} \Big|_{T'=T}. \quad (20.23)$$

A straightforward calculation leads to the identity

$$C(T) = \frac{\Delta E(T)^2}{T^2} \geq 0, \quad (20.24)$$

where  $\Delta E^2(T) = \text{Tr}[H^2 g(\beta)] - (\text{Tr}[Hg(\beta)])^2$  is the variance of the energy. Two salient comments regarding Eq. (20.24) are in order. First, the positivity of the heat capacity shows that energy is a monotonically increasing function of temperature for any system, matching with our daily life intuition. This is in fact the reason why the energy-entropy diagrams presented in Chap. 33 are convex, which is a crucial property to have a non-trivial theory of thermodynamics.

Second, we can see in Eq. (20.24) that the energy fluctuations of a thermal state do not scale with the energy of the system but with its square root. In other words, the energy distribution of thermal states become relatively thinner and thinner as the system size increases, and this happens irrespective of the Hamiltonian of the system. Note that this property is necessary in order for an equivalence of ensembles to be possible. This issue is discussed in Sect. 20.5.

It is interesting to point out that systems that are out of equilibrium and have a wide energy distribution cannot thermalize, that is, cannot equilibrate towards a Gibbs state. This is a consequence of the fact that the energy distribution of a system does not vary during the evolution and thermal states have relatively small energy fluctuations.

If we now focus on the relevant family of states that have a finite correlation length, it is even possible to show that the energy distribution converges to a Gaussian with increasing system size [20, 49].

Below, we state the latest result [20] applied to 2-local Hamiltonians, i.e., to Hamiltonians on cubic lattices. A *cubic* interaction graph has a vertex set  $\mathcal{V} = [n]^D$  and two sites  $v, w \in [n]^D$  are connected if  $\sum_{i=1}^D |v_i - w_i| = 1$ ; see Fig. 20.1 for  $D = 2$ .

**Theorem 6** (Berry-Esseen bound [20, Lemma 8]). *Let  $H$  be a Hamiltonian (20.1) with cubic interaction graph  $[n]^D$  with  $N := n^D$  sites and  $\rho$  a state with  $(\xi, z)$ -exponentially decaying correlations (20.17). Moreover, let*

$$F(x) := \sum_{k: E_k \leq x} \langle k | \rho | k \rangle, \quad (20.25)$$

$$\mu := \text{Tr}(\rho H), \quad (20.26)$$

$$\sigma^2 := \text{Tr}(\rho(H - \mu)^2) \quad (20.27)$$

and define the Gaussian cumulative distribution function with mean  $\mu$  and variance  $\sigma^2$  by

$$G(x) = \frac{1}{\sqrt{2\pi\sigma^2}} \int_{-\infty}^x dy e^{-\frac{(y-\mu)^2}{2\sigma^2}}. \quad (20.28)$$

Then

$$\sup_x |F(x) - G(x)| \leq C \frac{\ln^{2d}(N)}{\sqrt{N}}, \quad (20.29)$$

where  $C$  is a constant that depends only on  $\xi$ ,  $z$  and the local Hilbert-space dimension.

Hence, the distance between the cumulative distributions  $F$  and  $G$  can be made arbitrarily small in  $L_\infty$ -norm for sufficiently large system sizes  $N$ . Note that the theorem applies to all states with clustering of correlations, irrespective of being thermal.

The Gaussian distribution has an exponential decay outside an energy windows of a width scaling as  $\sigma \sim \sqrt{N}$ . Hence, the theorem also suggests such a decay for states with  $(\xi, z)$ -exponentially decaying correlations. However, the error term in Eq. (20.29) scales like  $\tilde{O}(1/\sqrt{N})$  and, hence, such a decay is not implied. However, a (sub)exponential decay can be guaranteed using a version of a non-commutative Chernoff-Hoeffding inequality [50–52].

Let us now insert in Eq. (20.25) the maximally mixed state  $\rho = \mathbb{1}/d$ , with  $d$  being the dimension of the Hilbert space. Then,  $F(x)$  becomes

$$F(x) = \frac{1}{d} \int_{-\infty}^x \sum_k \delta(E - E_k) dE \quad (20.30)$$

which is nothing but the cumulative distribution of the density of states. As the maximally mixed state is a product state, a corollary of Theorem 6 is that short-ranged Hamiltonians have a density of states that tends to a Gaussian in the thermodynamic limit.

## 20.5 Equivalence of Ensembles

The question of equivalence of ensembles (EoE) has a long tradition in statistical physics. Gibbs stated that, in the thermodynamic limit, an observable has the same average value in both the canonical and the microcanonical ensemble [53, Chap. 10]; see also Ref. [54] for recent rigorous treatment of classical systems. The argument given by Gibbs is that the energy fluctuations of the canonical ensemble (relatively) vanish in the limit of infinitely large systems.

In classical systems, the microcanonical ensemble describes systems at equilibrium with a well defined energy  $E$ . It assigns the same probability to all the configurations of the system (points in phase space) compatible with that energy.

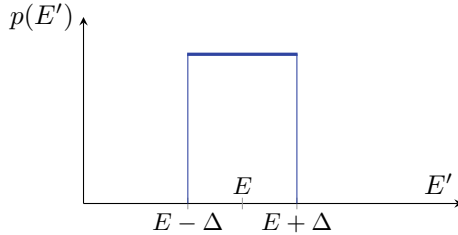


**Fig. 20.4** The microcanonical energy distribution. The microcanonical state  $\square_{E,\Delta}$  is the corresponding maximally mixed state on energy subspace given by energies  $E'$  with  $|E - E'| \leq \Delta$ , i.e., given by the density matrix diagonal in the energy eigenbasis and with eigenvalues given by the microcanonical energy distribution.

In quantum theory, however, for systems with a discrete energy spectrum, the classical definition of microcanonical ensemble breaks down, since there often is, if any, only a single physical configuration for a given energy. Hence, in quantum systems the notion of microcanonical states needs to be slightly changed and the system is not considered to have a well defined energy but a uniform distribution within a narrow energy window of width  $2\Delta$ . More specifically, the microcanonical ensemble or *microcanonical state*  $\square_{E,\Delta}$  of a quantum systems is defined as the completely mixed state within the energy subspace spanned by all the eigenvectors with energy  $|E_k - E| \leq \Delta$  (see Fig. 20.4).

Let us mention that the microcanonical ensemble is equivalent to the principle of equal a priori probabilities, which states that, once at equilibrium, the system is equally likely to be found in any of its accessible states. This assumption lies at the heart of statistical mechanics since it allows for the computation of equilibrium expectation values by performing averages on the phase space. However, there is no reason in the laws of mechanics (and quantum mechanics) to suggest that the system explores its set of accessible states uniformly. Therefore, the equal a priori probabilities principle has to be put in by hand.

One of the main insights from the field of quantum information theory to statistical mechanics is the substitution of the equal-a-priori-probabilities-postulate by the use of typicality arguments [55, 56]. This issue is discussed in detail in Chap. 16.

An *equivalence of ensembles* statement says that a certain state is locally indistinguishable from a thermal state with the right temperature. Such statements are often shown for the microcanonical state  $\square_{E,\Delta}$ , see Refs. [20, 57, 58] investigations of quantum lattice systems.

**Theorem 7** (EoE [20, Theorem 1, special case]). *Let  $g(1/T)$  be the thermal state of a Hamiltonian (20.1) with cubic interaction graph  $[n]^D$  and with energy density  $u(T)$  (20.22) and specific heat capacity  $c(T)$  (20.23) with  $(\xi, z)$ -exponentially decaying correlations (20.17).*

Let  $\sqcap_{eN,\delta\sqrt{N}}$  be the microcanonical state with mean energy density  $e$  specified by

$$|e - u(T)| \leq \frac{\sqrt{c(T)T^2}}{\sqrt{N}} \quad (20.31)$$

and energy spread  $\delta\sqrt{N}$  specified by

$$C_1 \frac{\ln(N)^{2D}}{\sqrt{N}} \leq \frac{\delta}{\sqrt{c(T)T^2}} \leq 1, \quad (20.32)$$

where  $N := n^D$  denotes the volume and  $C_1$  a constant. Then, for a linear system size scaling as  $n \in \tilde{\Omega}(l^{D+1}/\epsilon^2)$ ,

$$\left\| \tau_{e,\delta}^{S_l} - g(1/T)^{S_l} \right\|_1 \leq \epsilon \quad (20.33)$$

for any cube  $S_l$  of edge length  $l$ .

All implicit constants and  $C_1$  depend on the temperature  $T$ , the correlation decay  $(\xi, z)$ , and the spatial and Hilbert space dimension  $D$  and  $d$  (explicitly given in [20]).

This theorem tells us that for an energy window that needs to have a width scaling roughly as  $\Delta = \delta\sqrt{N} \sim \sqrt{N}$  and matching median energy  $E = eN \approx U(T)$  the microcanonical state is locally indistinguishable from the thermal state whenever the total system is large enough.

The original statement [20, Theorem 1] is more general (but also more technical): (i) it also holds for  $k$ -local Hamiltonians ( $k$ -body interactions) and (ii) for systems that are not translation-invariant. In the case of (ii) the trace distance (20.33) needs to be replaced with a trace distance averaged over all translates of the cube  $S_l = [l]^D$ . This means that the EoE statement holds in most regions of the non-translation invariant lattice.

The proof [20] of Theorem 7 is based on an information theoretic result for quantum many-body systems: If a state  $\rho$  has  $(\xi, z)$ -exponentially decaying correlations and  $\tau$  is another state such that the relative entropy  $S(\tau\|\rho)$  has a certain sub-volume scaling then  $\tau^{S_l} \approx \rho^{S_l}$  on average over all cubes of edge length  $l$ . The approximation error depends on the explicit scaling of  $S(\tau\|\rho)$ . Then a bound on  $S(\sqcap_{E,\Delta}\|g(\beta))$  is proven. For this proof the Berry-Esseen bound Theorem 6 is derived.

## 20.6 Conclusions and Outlook

In this chapter we have reviewed several properties of thermal states of spin lattice Hamiltonians. We have seen that, in a regime of high temperatures and for gapped Hamiltonians at zero temperature, equilibrium states exhibit an exponential cluster-

ing of correlations. This fast decay of the correlations can be exploited in several ways. It allows for locally assigning temperature to a subsystem even in the presence of interactions, as well as for approximating expectation values of local operators in infinite systems by means of finite ones. Furthermore, clustering of correlations in the high temperature regime discards the existence of phase transitions within that regime and implies that thermal states can be efficiently represented by means of matrix product operators. We have finally seen that states with a finite correlation length have a Gaussian energy distribution and, in the case that they are thermal, cannot be distinguished by local observables from the microcanonical ensemble, fleshing out in such a way the equivalence of ensembles.

Let us conclude the chapter by mentioning the problems that we consider relevant in the field and still remain open. One of the issues where progress seems to be very difficult is the extension of the well established theorems that logically connect area-law for the entanglement entropy, gapped Hamiltonian, and exponential clustering of correlations to a number of spatial dimensions higher than one. We also noticed a lack of results in the direction of understanding how much correlated thermal states of local Hamiltonians can be. More explicitly, how far concrete models are from saturating the area law for the mutual information. While there has been an important effort to contrive local Hamiltonians with highly entangled ground states, little is known for thermal states.

Completely new physics is expected to appear if one goes beyond the assumption of short ranged interactions. In this respect, a class of relevant models that both appears frequently in nature and can be easily engineered, e.g. in ion traps, are systems with long range interactions. For those, most of the questions discussed above are unexplored. As it already happened for the Lieb-Robinson bounds [59–61], some of the above properties, e.g. some type of clustering of correlations, could, at least in spirit, be reproduced. Indeed, for fermionic spin lattices an algebraic correlation decay can be shown for power-law interactions at non-zero temperature [62].

An interesting feature of systems with long range interactions is that they do not have a finite correlation length and thereby the results on equivalence of ensembles presented above cannot be applied. This opens fundamental questions in the field of equilibration of closed quantum systems, since it is not obvious that the canonical ensemble will be an appropriate description of the equilibrium state [63]. The challenge of the equivalence of ensembles for states with a power law decay of the correlations yields another relevant question in the field.

Other than extending EoE statements to long range interactions it is also important to extend them to larger classes of states. Often, states in quantum experiments arise from quenched dynamics and is a largely open and challenging problem to characterize the thermalization behaviour. Part of the problem is the equivalence of the equilibrium state (given by an infinite time average [55]) and the thermal state. For non-critical systems such a statement can indeed be proven [64].

Thermal states have been introduced at the beginning of this book chapter as states that maximize the Von Neumann entropy given the energy as conserved quantity. However, in many relevant situations, in particular for integrable models evolving completely isolated from their environments (closed system dynamics), it is well

known that the thermal state is not a good description of the equilibrium state. These type of systems require to consider additional conserved quantities and their equilibrium state is given by the so called Generalized Gibbs Ensemble (GGE), which is the state maximizing the entropy given a set of conserved quantities. In the recent years, several studies on the laws of thermodynamics when GGE states are taken as heat baths have been realized (see Chap. 30). However, their intrinsic properties are in general completely unknown: scaling of the correlations, the shape of the energy distribution, or the locality of the Lagrange multipliers (e.g. temperature and chemical potential). Characterizing these properties constitutes an extensive research endeavor.

**Acknowledgements** We would like to thank C. Gogolin for helpful comments. The work of MK was funded by the National Science Centre, Poland within the project Polonez (2015/19/P/ST2/03001) which has received funding from the European Union's Horizon 2020 research and innovation programme under the Marie Skłodowska-Curie grant agreement No 665778. AR acknowledges Generalitat de Catalunya (AGAUR Grant No. 2017 SGR 1341, SGR 875 and CERCA/Program), the Spanish Ministry MINECO (National Plan 15 Grant:FISICATEAMO No. FIS2016-79508-P, SEVERO OCHOA No. SEV-2015-0522), Fundació Cellex, ERC AdG OSYRIS, EU FETPRO QUIC, and the CELLEX-ICFO-MPQ fellowship.

## References

1. C. Gogolin, J. Eisert, Equilibration, thermalisation, and the emergence of statistical mechanics in closed quantum systems. *Rep. Prog. Phys.* **79**, 056001 (2016). <https://doi.org/10.1088/0034-4885/79/5/056001>
2. E. Jaynes, Information theory and statistical mechanics. *Phys. Rev.* **106**, 620 (1957a). <https://doi.org/10.1103/PhysRev.106.620>
3. E. Jaynes, Information theory and statistical mechanics. II. *Phys. Rev.* **108**, 171 (1957b). <https://doi.org/10.1103/PhysRev.108.171>
4. R. Alicki, M. Fannes, Entanglement boost for extractable work from ensembles of quantum batteries. *Phys. Rev. E* **87**, 042123 (2013). <https://doi.org/10.1103/PhysRevE.87.042123>
5. W. Pusz, S.L. Woronowicz, Passive states and KMS states for general quantum systems. *Commun. Math. Phys.* **58**, 273 (1978). <https://doi.org/10.1007/BF01614224>
6. M.B. Hastings, T. Koma, Spectral gap and exponential decay of correlations. *Commun. Math. Phys.* **265**, 781 (2006). <https://doi.org/10.1007/s00220-006-0030-4>
7. B. Nachtergaele, R. Sims, Lieb-Robinson bounds and the exponential clustering theorem. *Commun. Math. Phys.* **265**, 119 (2006). <https://doi.org/10.1007/s00220-006-1556-1>
8. J. Cardy, *Scaling and Renormalization in Statistical Physics*, Lecture notes in physics (Cambridge University Press, Cambridge, 1996). <https://doi.org/10.1017/CBO9781316036440>
9. C. Domb, J. Lebowitz, *Phase Transitions and Critical Phenomena*, Phase transitions and critical phenomena series (Academic Press, New York, 2000). <https://books.google.es/books?id=FYvFm4xF7CgC>
10. M. Kliesch, C. Gogolin, M.J. Kastoryano, A. Riera, J. Eisert, Locality of temperature. *Phys. Rev. X* **4**, 031019 (2014a). <https://doi.org/10.1103/PhysRevX.4.031019>
11. S. Hernández-Santana, A. Riera, K.V. Hovhannисyan, M. Perarnau-Llobet, L. Tagliacozzo, A. Acin, Locality of temperature in spin chains. *New. J. Phys.* **17**, 085007 (2015). <https://doi.org/10.1088/1367-2630/17/8/085007>
12. A. De Pasquale, D. Rossini, R. Fazio, V. Giovannetti, Local quantum thermal susceptibility. *Nat. Commun.* **7** (2016). <https://doi.org/10.1038/ncomms12782>

13. G. De Palma, A. De Pasquale, V. Giovannetti, Universal locality of quantum thermal susceptibility. *Phys. Rev. A* **95**, 052115 (2017). <https://doi.org/10.1103/PhysRevA.95.052115>
14. M. Hartmann, G. Mahler, Measurable consequences of the local breakdown of the concept of temperature. *Europhys. Lett.* **70**, 579 (2005). <https://doi.org/10.1209/epl/i2004-10518-5>
15. M. Hartmann, Minimal length scales for the existence of local temperature. *Contemporary Physics* **47**, 89 (2006). <https://doi.org/10.1080/00107510600581136>
16. A. Ferraro, A. Garca-Saez, A. Acin, Intensive temperature and quantum correlations for refined quantum measurements. *Europhys. Lett.* **98**, 10009 (2012). <https://doi.org/10.1209/0295-5075/98/10009>
17. A. Garca-Saez, A. Ferraro, A. Acin, Local temperature in quantum thermal states. *Phys. Rev. A* **79**, 052340 (2009). <https://doi.org/10.1103/PhysRevA.79.052340>
18. A. Molnár, N. Schuch, F. Verstraete, J.I. Cirac, Approximating gibbs states of local hamiltonians efficiently with PEPS. *Phys. Rev. B* **91**, 045138 (2015). <https://doi.org/10.1103/PhysRevB.91.045138>
19. U. Schollwöck, The density-matrix renormalization group in the age of matrix product states. *Ann. Phys.* **326**, 96 (2011). <https://doi.org/10.1016/j.aop.2010.09.012>
20. F.G.S.L. Brandao, M. Cramer, Equivalence of statistical mechanical ensembles for non-critical quantum systems, [arXiv:1502.03263](https://arxiv.org/abs/1502.03263) [quant-ph]
21. M.P. Mueller, E. Adlam, L. Masanes, N. Wiebe, Thermalization and canonical typicality in translation-invariant quantum lattice systems. *Commun. Math. Phys.* **340**, 499 (2015). <https://doi.org/10.1007/s00220-015-2473-y>
22. F. Dyson, E. Lieb, B. Simon, Phase transitions in quantum spin systems with isotropic and nonisotropic interactions. *J. Stat. Phys.* **18**, 335 (1978). <https://doi.org/10.1007/BF01106729>
23. K.M.R. Audenaert, M. Mosonyi, F. Verstraete, Quantum state discrimination bounds for finite sample size. *J. Math. Phys.* **53**, 122205 (2012). <https://doi.org/10.1063/1.4768252>
24. M.A. Nielsen, I.L. Chuang, *Quantum Computation and Quantum Information* (Cambridge university press, Cambridge, 2010). <https://doi.org/10.1017/CBO9780511976667>
25. D. Ruelle, *Statistical Mechanics: Rigorous Results* (W. A. Benjamin, New York, 1969)
26. J. Ginibre, Reduced density matrices of quantum gases. II. cluster property. *J. Math. Phys.* **6**, 252 (1965). <https://doi.org/10.1063/1.1704276>
27. O. Bratteli, D.W. Robinson, *Operator Algebras and Quantum Statistical Mechanics: Equilibrium States. Models in Quantum Statistical Mechanics*, 2nd edn. (Springer, Berlin, 1997). <https://doi.org/10.1007/978-3-662-09089-3>
28. W. Greenberg, Critical temperature bounds of quantum lattice gases. *Commun. Math. Phys.* **13**, 335 (1969). <https://doi.org/10.1007/BF01645417>
29. Y. Park, H. Yoo, Uniqueness and clustering properties of Gibbs states for classical and quantum unbounded spin systems. *J. Stat. Phys.* **80**, 223 (1995). <https://doi.org/10.1007/BF02178359>
30. D.A. Klarner, Cell growth problems. *Canad. J. Math* **19**, 23 (1967)
31. Y.M. Miranda, G. Slade, The growth constants of lattice trees and lattice animals in high dimensions. *Elect. Comm. Probab.* **16**, 129 (2011), [arXiv:1102.3682](https://arxiv.org/abs/1102.3682) [math.PR]
32. M.B. Hastings, Solving gapped Hamiltonians locally, *Phys. Rev. B* **73**, 085115 (2006). <https://doi.org/10.1103/PhysRevB.73.085115>
33. M. Kliesch, C. Gogolin, J. Eisert, in *Many-Electron Approaches in Physics, Chemistry and Mathematics*, Mathematical physics studies, ed. by V. Bach, L. Delle Site (Springer International Publishing, 2014), pp. 301–318. [https://doi.org/10.1007/978-3-319-06379-9\\_17](https://doi.org/10.1007/978-3-319-06379-9_17)
34. B. Nachtergaelie, R. Sims, Contemporary mathematics, in *Entropy and the Quantum*, ed. by R. Sims, D. Ueltschi (American Mathematical Society, 2010), pp. 141–176, [arXiv:1004.2086](https://arxiv.org/abs/1004.2086) [math-ph]
35. F.G.S.L. Brandão, M. Horodecki, Exponential decay of correlations implies area law. *Comm. Math. Phys.* **333**, 761 (2015). <https://doi.org/10.1007/s00220-014-2213-8>
36. J. Eisert, M. Cramer, M.B. Plenio, Colloquium: area laws for the entanglement entropy. *Rev. Mod. Phys.* **82**, 277 (2010). <https://doi.org/10.1103/RevModPhys.82.277>
37. M.B. Hastings, An area law for one-dimensional quantum systems. *J. Stat. Mech. Theory Exp.* **2007**, P08024 (2007). <https://doi.org/10.1088/1742-5468/2007/08/P08024>

38. M.M. Wolf, F. Verstraete, M.B. Hastings, J.I. Cirac, Area laws in quantum systems: mutual information and correlations. *Phys. Rev. Lett.* **100**, 070502 (2008). <https://doi.org/10.1103/PhysRevLett.100.070502>
39. S. Das, S. Shankaranarayanan, How robust is the entanglement entropy-area relation? *Phys. Rev. D* **73**, 121701 (2006). <https://doi.org/10.1103/PhysRevD.73.121701>
40. L. Masanes, Area law for the entropy of low-energy states. *Phys. Rev. A* **80**, 052104 (2009). <https://doi.org/10.1103/PhysRevA.80.052104>
41. G. Vitagliano, A. Riera, J.I. Latorre, Volume-law scaling for the entanglement entropy in spin-1/2 chains. *New. J. Phys.* **12**, 113049 (2010). <https://doi.org/10.1088/1367-2630/12/11/113049>
42. D. Aharonov, D. Gottesman, S. Irani, J. Kempe, The power of quantum systems on a line. *Commun. Math. Phys.* **287**, 41 (2009). <https://doi.org/10.1007/s00220-008-0710-3>
43. D. Gottesma, S. Irani, The quantum and classical complexity of translationally invariant tiling and hamiltonian problems, in *Proceedings of the 2009 50th Annual IEEE Symposium on Foundations of Computer Science FOCS '09* (IEEE Computer Society, USA, 2009), pp. 95–104. <https://doi.org/10.1109/FOCS.2009.22>
44. J.L. Cardy, Conformal invariance and surface critical behavior. *Nucl. Phys. B* **240**, 514 (1984). [https://doi.org/10.1016/0550-3213\(84\)90241-4](https://doi.org/10.1016/0550-3213(84)90241-4)
45. J.L. Cardy, Effect of boundary conditions on the operator content of two-dimensional conformally invariant theories. *Nucl. Phys. B* **275**, 200 (1986). [https://doi.org/10.1016/0550-3213\(86\)90596-1](https://doi.org/10.1016/0550-3213(86)90596-1)
46. M. Zwolak, G. Vidal, Mixed-state dynamics in one-dimensional quantum lattice systems: a time-dependent superoperator renormalization algorithm. *Phys. Rev. Lett.* **93**, 207205 (2004). <https://doi.org/10.1103/PhysRevLett.93.207205>
47. F. Verstraete, J.J. Garcia-Ripoll, J.I. Cirac, Matrix product density operators: simulation of finite-temperature and dissipative systems. *Phys. Rev. Lett.* **93**, 207204 (2004). <https://doi.org/10.1103/PhysRevLett.93.207204>
48. M. Kliesch, D. Gross, J. Eisert, Matrix-product operators and states: NP-hardness and undecidability. *Phys. Rev. Lett.* **113**, 160503 (2014c). <https://doi.org/10.1103/PhysRevLett.113.160503>
49. J.P. Keating, N. Linden, H.J. Wells, Spectra and eigenstates of spin chain hamiltonians. *Commun. Math. Phys.* **338**, 81 (2015). <https://doi.org/10.1007/s00220-015-2366-0>
50. I. Arad, T. Kuwahara, Z. Landau, Connecting global and local energy distributions in quantum spin models on a lattice. *J. Stat. Mech. Theory Exp.* **3**, 033301 (2016). <https://doi.org/10.1088/1742-5468/2016/03/033301>
51. A. Anshu, Concentration bounds for quantum states with finite correlation length on quantum spin lattice systems. *New J. Phys.* **18**, 083011 (2016). <https://doi.org/10.1088/1367-2630/18/8/083011>
52. T. Kuwahara, Connecting the probability distributions of different operators and generalization of the Chernoff-Hoeffding inequality. *J. Stat. Mech. Theory Exp.* **11**, 113103 (2016). <https://doi.org/10.1088/1742-5468/2016/11/113103>
53. J.W. Gibbs, *Elementary Principles in Statistical Mechanics with Especial Reference to the Rational Foundation of Thermodynamics* (Yale University Press, 1902)
54. H. Touchette, Equivalence and nonequivalence of ensembles: thermodynamic, macrostate, and measure levels. *J. Stat. Phys.* **159**, 987 (2015). <https://doi.org/10.1007/s10955-015-1212-2>
55. S. Popescu, A.J. Short, A. Winter, Entanglement and the foundations of statistical mechanics. *Nat. Phys.* **2**, 754 (2006). <https://doi.org/10.1038/nphys444>
56. S. Goldstein, J.L. Lebowitz, R. Tumulka, N. Zanghi, Canonical typicality. *Phys. Rev. Lett.* **96**, 050403 (2006). <https://doi.org/10.1103/PhysRevLett.96.050403>
57. R. Lima, Equivalence of ensembles in quantum lattice systems: states. *Commun. Math. Phys.* **24**, 180 (1972). <https://doi.org/10.1007/BF01877711>
58. M.P. Müller, E. Adlam, L. Masanes, N. Wiebe, Thermalization and canonical typicality in translation-invariant quantum lattice systems. *Commun. Math. Phys.* **340**, 499 (2015). <https://doi.org/10.1007/s00220-015-2473-y>

59. Z.-X. Gong, M. Foss-Feig, S. Michalakis, A.V. Gorshkov, Persistence of locality in systems with power-law interactions. *Phys. Rev. Lett.* **113**, 030602 (2014). <https://doi.org/10.1103/PhysRevLett.113.030602>
60. P. Hauke, L. Tagliacozzo, Spread of correlations in long-range interacting quantum systems. *Phys. Rev. Lett.* **111**, 207202 (2013). <https://doi.org/10.1103/PhysRevLett.111.207202>
61. T. Matsuta, T. Koma, S. Nakamura, Improving the Lieb–Robinson bound for long-range interactions. *Ann. Henri Poincaré* **18**, 519 (2017). <https://doi.org/10.1007/s00023-016-0526-1>
62. S. Hernández-Santana, C. Gogolin, J.I. Cirac, A. Acín, Correlation decay in fermionic lattice systems with power-law interactions at nonzero temperature. *Phys. Rev. Lett.* **119**, 110601 (2017). <https://doi.org/10.1103/PhysRevLett.119.110601>
63. L. Casetti, M. Kastner, Partial equivalence of statistical ensembles and kinetic energy. *Phys. A* **384**, 318 (2007). <https://doi.org/10.1016/j.physa.2007.05.043>
64. T. Farrelly, F.G.S.L. Brandão, M. Cramer, Thermalization and return to equilibrium on finite quantum lattice systems. *Phys. Rev. Lett.* **118**, 140601 (2017). <https://doi.org/10.1103/PhysRevLett.118.140601>

# Chapter 21

## Quantum Thermometry



Antonella De Pasquale and Thomas M. Stace

### 21.1 Introduction

When studying a physical system, there are physically important quantities that cannot be directly measured, either in principle or due to some technical obstructions. Temperature represents a paradigmatic example: it is a non-linear function of the density matrix, so it is not a (quantum) observable of the system. Instead, to infer its value, we need to measure another physical quantity, such as the mean kinetic energy, which is related to the quantity of interest. The theory of estimation provides the formal framework in order to tackle these kinds of indirect measurements.

This situation is precisely the one faced in modern primary and secondary thermometry standards. For instance, current primary thermometers are based on the resonant frequency of a precisely machined microwave resonator filled with a noble gas [1]. The temperature dependence of the refractive index of the gas is theoretically calculable to high accuracy, and so the resonant frequency of the system provides an indirect measurement of the temperature, via the geometry and the refractive index of the gas-filled resonator. In the case of ultra-high precision secondary thermometers [2], the same operational principle applies: the resonant frequency of a toroidal micro-resonator depends on the refractive index of the glass medium, which

---

A. De Pasquale (✉)

Department of Physics and Astronomy,  
University of Florence, Via G. Sansone 1, I-50019 Sesto Fiorentino (FI), Italy  
e-mail: adepasquale83@gmail.com

A. De Pasquale

INFN Sezione di Firenze, via G. Sansone 1, I-50019 Sesto Fiorentino (FI), Italy

A. De Pasquale

NEST, Scuola Normale Superiore and Istituto Nanoscienze-CNR, I-56126 Pisa, Italy

T. M. Stace

ARC Centre for Engineered Quantum System, Department of Physics,  
University of Queensland, Brisbane, QLD 4072, Australia

is itself a thermodynamic (and thus temperature-dependent) quantity, albeit in practice too complicated to calculate at sufficiently high accuracy from first principles. Moreover, within the plethora of recent theoretical efforts aiming at a self-consistent generalization of the classical thermodynamics to small-scale physics, where quantum effects become predominant [3–6], precision nanothermometry proved to be quite successful in exploiting quantum effects [7–10].

Throughout this chapter, after introducing some general tools both of classical and quantum estimation theory, we focus on different thermometric tasks, also discussing the role played by quantum correlations and coherence in order to enhance the accuracy level achievable when measuring the temperature. We start by considering systems of arbitrary dimensions with no restrictions on the structure of the corresponding Hamiltonian. Then we focus on the case of single qubit thermometry.

## 21.2 Quantum Estimation Theory and Quantum Metrology

To begin the discussion of the formalism, we start by considering the reconstruction of an unknown parameter  $\lambda$ , which we suppose is not directly observable, but which we can connect via theoretical considerations to a  $\lambda$ -dependent quantity  $\Theta$ , which can be directly measured. Once a large sequence of independent identically distributed measurements of  $\Theta$ ,  $\vec{\theta} = \{\theta_1, \theta_2, \dots, \theta_N\}$  ( $N \gg 1$ ), are collected, the value of  $\lambda$  is recovered in the form of a random variable  $\lambda^{(\text{est})}$ , representing the estimation of  $\lambda$  retrieved from  $\vec{\theta}$ .

The ultimate precision limit on the estimation of  $\lambda$  is given by the Cramér–Rao bound [11–13] on the Root Mean Square Error (RMSE)  $\Delta\lambda = \sqrt{\mathbb{E}[(\lambda^{(\text{est})} - \lambda)^2]}$ :

$$\Delta\lambda \geq \frac{1}{\sqrt{N\mathcal{F}(\lambda)}} \quad (21.1)$$

with

$$\mathcal{F}(\lambda) = \int d\theta \frac{1}{p(\theta|\lambda)} \left( \frac{\partial p(\theta|\lambda)}{\partial \lambda} \right)^2. \quad (21.2)$$

Here  $\mathbb{E}[x]$  indicates the expectation value of the random variable  $x$ , and  $p(\theta|\lambda)$  is the conditional probability of measuring  $\theta$  (here assumed continuous for simplicity) if the value of the parameter under consideration is  $\lambda$ . The quantity  $\mathcal{F}$  is the *Fisher Information* (FI), and derives from the Fisher–Rao distance between probability distributions differing by an infinitesimal increment in  $\lambda$ , namely  $p(\theta|\lambda)$  and  $p(\theta|\lambda + \delta\lambda)$ .

The Cramér–Rao bound basically sets the rules for recognizing whether the procedure followed in order to retrieve  $\lambda$  is optimal or not. On the one hand, the probability distribution  $p(\theta|\lambda)$  (and thus its sensitivity to small variations of the parameter of interest  $\lambda$ ) depends on the chosen measurement: optimal measurements are those with

conditional probability maximizing the Fisher Information. On the other hand, for any fixed measurement, an efficient estimator is the one that saturates the Cramér–Rao inequality. If the data sample is sufficiently large, it results that an efficient estimator is provided by the maximum-likelihood principle, based on the intuition that the observed data  $\vec{\theta}$  have been measured since they hold the highest probability to be obtained.<sup>1</sup> This is a typical example of an asymptotically efficient estimator. There also exist special families of probability distributions allowing for the construction of an estimator with only a finite number of measurements.

The pre-factor  $1/\sqrt{N}$  in the Cramér–Rao bound (21.1) is due to the additivity of the Fisher Information for the case of independent measures, and is a direct consequence of the central limit theorem according to which the average of a large number  $N$  of independent measurements (each having a standard deviation  $\Delta\sigma$ ) converges to a Gaussian distribution with standard deviation  $\Delta\sigma/\sqrt{N}$ , thus yielding the scaling  $1/\sqrt{N}$  on the error on the average. We will return to this point when, in the context of single qubit thermometers, we will compare the estimation strategy hinging upon independent measurements, with a protocol based on measurements of multi-particle correlated states, see Eqs. (21.33)–(21.35).

In high-precision measurements, and in the quantum regime, it is important to include a proper accounting of the measurement process and the apparatus. We introduce an ancillary physical system, the probe, over which we assume a high degree of control. As the system of interest interacts with the probe, the information about the system quantity  $\lambda$  is encoded into the state of the probe. We then make a measurement on the probe, in order to make an inference about  $\lambda$ . This protocol is summarised as follows:

- (i) Probe initialization: the probing system is prepared in an assigned state  $\rho_0$ .
- (ii) Probe evolution: the probe interacts with the system, and evolves according to a  $\lambda$ -dependent process described by a superoperator  $\mathcal{E}_\lambda$ , so as to imprint  $\lambda$  onto the probe state, via  $\rho_\lambda = \mathcal{E}_\lambda(\rho_0)$ .
- (iii) Probe readout: a (quantum) measurement is performed on  $\rho_\lambda$ , followed by classical data processing on the outcomes. This is what is properly defined as the ‘estimation step’.

This sequence is repeated for  $N$  independent probes, all initialized in the same initial state  $\rho_0$ . Figure 21.1a illustrates this protocol schematically.

<sup>1</sup>The maximum-likelihood principle selects the parameter values that make the data most probable. It stems from the definition of the likelihood function  $\mathcal{L}(\lambda)$  as the joint conditional probability of the observed data, that for the case of independent measurements reduces to the product of the probabilities of the single outcomes  $\theta_i$ ,

$$\mathcal{L}(\lambda) = \mathcal{L}(\vec{\theta}|\lambda) = \prod_i^N p(\theta_i|\lambda). \quad (21.3)$$

The maximum-likelihood estimate is the value of  $\lambda$  that maximizes  $\mathcal{L}(\lambda)$  or equivalently its logarithm. This procedure selects the parameter values that make the data most probable. It results that the variance on the maximum-likelihood estimate of  $\lambda$ , in the limit of large  $N$ , saturates the Cramér–Rao bound (21.1).

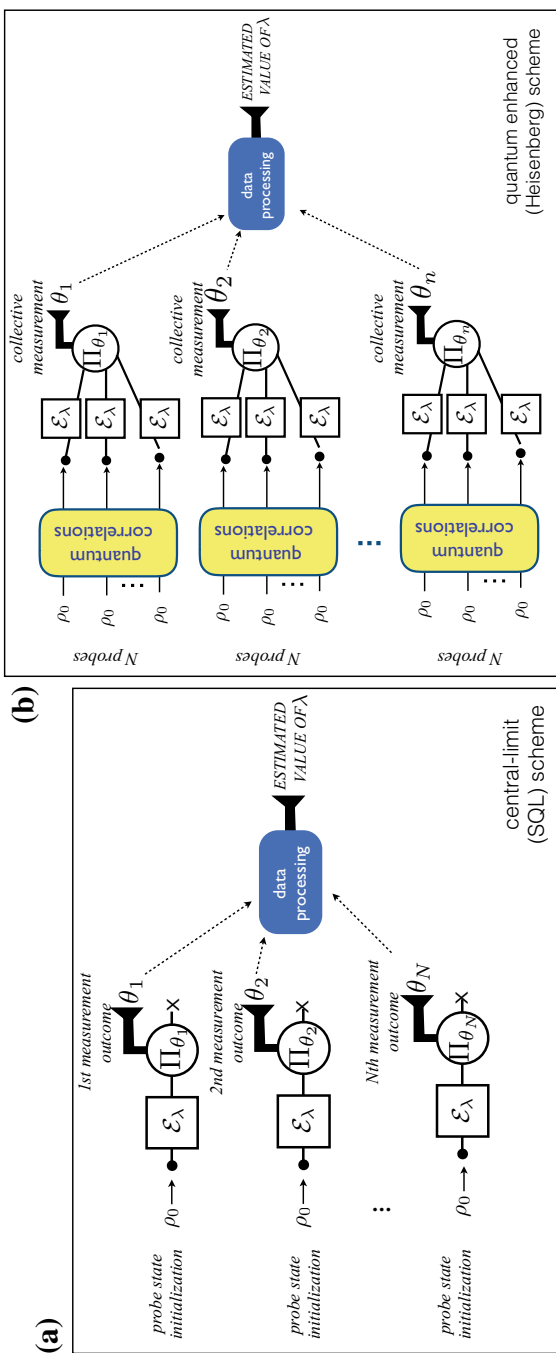


**Fig. 21.1** Schematic representation of typical estimation schemes. The central-limit scheme, in panel **(a)**, refers to the preparation of  $N$  independent probes prepared in the same state and separately measured, yielding a precision in the estimation of  $\lambda$  scaling as  $1/\sqrt{N}$ . In panel **b** is shown a schematic representation of an estimation protocol based on the introduction of quantum correlations in the probe preparation stage and eventually on nonlocal measurements, leading to the Heisenberg bound  $1/(N\sqrt{n})$  in the estimation of  $\lambda$ , where  $N$  is the number of probes in each entangled block, and  $n$  is the number of repeated measurements.

By reference to the practical primary and secondary thermometry examples introduced at the start of this chapter, the ‘system’ consists of the thermodynamic medium (gas or glass), with a temperature dependent refractive index. The ‘probe’ consists of the electromagnetic modes that couple to the medium. The measurement step consists of measuring the resonant frequency of the probe, which is both an observable and is practically accessible.

Formally, the general connection between the final state of the probe and the desired measurement result is achieved by expressing the measurement in terms of a set of positive operators  $\Pi_\theta$ , realizing a partition of unity  $\int d\theta \Pi_\theta = \mathbb{I}$ , that form a Positive Operator Valued Measure (POVM). The conditional probability of obtaining the outcome  $\theta$  if the probe state is  $\rho_\lambda$  is given by  $p(\theta|\lambda) = \text{Tr}[\Pi_\theta \rho_\lambda]$ . We note that  $\theta$  does not necessarily represent the eigenvalue of a quantum observable: POVMs are more general than projective measurements, including for instance the possibility of measurement imperfections.

Classically, a probe could be designed in principle to encode  $\lambda$  with arbitrary precision, in which case measurements of  $\lambda$  would be correspondingly precise. However, the Heisenberg uncertainty relations constrain the capability of quantum systems. Furthermore, the finite size of the probe also limits the amount of information it can encode. The main objective of quantum estimation theory is to optimize the measurement protocol, to obtain the best estimate of  $\lambda$  given the resources (probe size, number of probes, interaction time, etc) available. More precisely, it has been shown that the bound in Eq. (21.1) can be further boosted by maximizing the FI with respect to all possible POVMs, yielding

$$\Delta\lambda \geq \frac{1}{\sqrt{N \max_{\{\Pi_\theta\}} \mathcal{F}(\lambda)}} \geq \frac{1}{\sqrt{N \mathcal{Q}(\lambda)}}. \quad (21.4)$$

The term on the right is known as the quantum Cramér–Rao bound and is written in terms of the so-called Quantum Fisher Information (QFI)  $\mathcal{Q}(\lambda)$  [14]. The physical meaning of this functional is rooted in the geometrical structure of the statistical model used to parametrize the Hilbert space of the probe. Indeed  $\mathcal{Q}(\lambda)$  can be expressed as the infinitesimal variation of the probing system quantified by the Bures distance  $\mathcal{D}_B$  [24], i.e.

$$\mathcal{Q}(\lambda) = 4 \lim_{\delta\lambda \rightarrow 0} \frac{\mathcal{D}_B^2(\rho_\lambda, \rho_{\lambda+\delta\lambda})}{\delta\lambda^2} = 8 \lim_{\delta\lambda \rightarrow 0} \frac{1 - F(\rho_\lambda, \rho_{\lambda+\delta\lambda})}{\delta\lambda^2}, \quad (21.5)$$

where  $F(\rho, \rho') = \text{Tr}[\sqrt{\sqrt{\rho}\rho'\sqrt{\rho}}]$  is the Uhlmann fidelity between the states  $\rho$  and  $\rho'$  [15, 16]. The quantum Cramér–Rao bound holds for all possible POVMs on the  $N$  probes, including joint measurements that might exploit quantum resources like entanglement [17]. It is known that the bound in Eq. (21.4) is achievable through estimation strategies exploiting only local operations and classical communication [18, 19]. More precisely, a sufficient condition [20, 21] for saturating the quantum Cramér–Rao bound is given by the use of a POVM given by one-

dimensional projection operators onto the eigenstates of the so-called Symmetric Logarithmic Derivative (SLD)  $L_\lambda$ , a selfadjoint operator satisfying the equation

$$\frac{\partial \rho_\lambda}{\partial \lambda} = \frac{L_\lambda \rho_\lambda + \rho_\lambda L_\lambda}{2}. \quad (21.6)$$

Indeed it results that the QFI can be also computed as  $\mathcal{Q}(\lambda) = \text{Tr}[\rho_\lambda L_\lambda^2]$ . It is important to notice that although the use of this optimal POVM is sufficient to saturate the bound (21.4), such optimal measure depends, in general, on the true value of the parameter one wants to estimate, therefore asking for adaptive estimation strategies [22, 23].

The paradigmatic quantum estimation problem in the literature is to estimate the phase  $\lambda$  parametrizing a unitary transformation on  $\rho_0$ ,  $\mathcal{E}_\lambda(\rho_0) = e^{-i\lambda H} \rho_0 e^{i\lambda H}$  generated by the ‘Hamiltonian’  $H$ , which we assume to be independent of  $\lambda$ . In this simple scenario, also the QFI is independent of  $\lambda$ , and is given by [50]

$$\mathcal{Q} = 4 \sum_{i < j} \frac{(\phi_i - \phi_j)^2}{\phi_i + \phi_j} |\langle \phi_i | H | \phi_j \rangle|^2, \quad (21.7)$$

where  $\phi_i$  and  $|\phi_i\rangle$  are the eigenvalues and the eigenvectors of  $\rho_0$ , respectively, i.e.  $\rho_0 = \sum_j \phi_j |\phi_j\rangle \langle \phi_j|$ . From the property of strong concavity for the fidelity<sup>2</sup>  $\mathcal{Q}$  is maximised for pure states  $\rho_0 = |\phi_0\rangle \langle \phi_0|$ , and it is proportional to the variance of  $H$ ,

$$\mathcal{Q}(\lambda) = 4 (\langle \phi_0 | H^2 | \phi_0 \rangle - \langle \phi_0 | H | \phi_0 \rangle)^2. \quad (21.8)$$

It follows that the optimal state maximizing the value of  $\mathcal{Q}$  is the equally weighted superposition of the eigenvectors corresponding to the maximum,  $h_{\max}$ , and minimum,  $h_{\min}$ , eigenvalues of  $H$ , i.e.  $|\phi_0^{(\text{opt})}\rangle = \frac{1}{\sqrt{2}}(|h_{\max}\rangle + |h_{\min}\rangle)$ , yielding  $\mathcal{Q}(\lambda) = (h_{\max} - h_{\min})^2$ .

Returning to the quantum Cramér–Rao bound in Eq. (21.4), the central-limit scaling  $1/\sqrt{N}$ , known colloquially (and somewhat misleadingly) in the literature as the Standard Quantum Limit (SQL), is the benchmark of estimation strategies based on independent identically distributed (i.i.d.) variables. In optical experiments, the SQL manifests as a significant technical noise floor (e.g. in homodyne or heterodyne field measurements), and is a consequence of quantum shot noise, associated to the Poissonian arrival times of quantised photons in a coherent state. From a mathematical point of view, it is a direct consequence of the additivity of the Quantum Fisher Information when applied to the tensor states  $(\rho_\lambda)^{\otimes N}$ , describing the global state of the  $N$  independent probes.

<sup>2</sup>Given  $p_i$  and  $p'_i$  two probability density distributions, and  $\{\rho_i\}$  and  $\{\rho'_i\}$  two sets of density matrices, it results that  $\mathcal{F}(\sum_i p_i \rho_i, \sum_i p'_i \rho'_i) \geq \sum_i \sqrt{p_i p'_i} \mathcal{F}(\rho_i, \rho'_i)$ . This property is dubbed strong concavity property for the fidelity.

Despite its evocative name, the SQL is not a fundamental limit, and can be broken. In particular it has been shown [25] that in absence of external noise, (e.g. for unitary phase estimation), the quantum Cramér–Rao bound implies that the use of entanglement between the  $N$  probe systems, together with joint measurements on the probes, leads to an improvement in precision by a factor of  $\sqrt{N}$ . In other words, if we change the measurement protocol to use a total of  $\nu = nN$  probes, in which we entangle blocks of  $N$  probes, and repeat  $n$  times (as shown in Fig. 21.1b) we get a measurement precision of

$$\Delta\lambda \geq \frac{1}{N\sqrt{n\mathcal{Q}(\lambda)}}. \quad (21.9)$$

The improved scaling  $\sim 1/N$ , known as the “Heisenberg bound”, stems only from the employment of quantum resources in the preparation stage. The bound in Eq. (21.9) may be achievable with adaptive strategies based on a POVM that acts locally on each probe [26].

When the number  $n$  of repetitions is small, special instances of phase estimation have been found in which a scaling of the order of  $\nu^{-1} \log(\nu)$  can be achieved [27, 28]. Of practical significance is to characterize optimal performances in presence of external disturbance: many discouraging results attest to the fragility of entanglement which, in a noisy environment, limits any precision improvement at most to a constant factor independent of  $N$  [29], or to a super-classical precision scaling  $N^{5/6}$ , achieved when the perturbation involves a preferential direction perpendicular to the unitary evolution governed by the parameter to be estimated [30]. As yet, an exhaustive answer, providing a systematic method for taking into account the presence of noise, is still missing.

One of the challenges of quantum metrology is to design protocols that achieve Heisenberg-like scaling for various estimation purposes [17, 31–33]. The paradigm of phase estimation in quantum optical systems has been an influential motivator [34–37], and has specific applications in gravitational wave detection and biological microscopy [38].

### 21.3 Quantum Thermometry

Let us now apply the tools of quantum estimation theory to a measuring temperature. Temperature is not a quantum observable, unlike the phase in an interferometer, so it necessarily must be inferred from an intermediate quantity.<sup>3</sup> This subtlety makes the problem paradigmatic for quantum measurement of more general non-Hamiltonian quantities.

---

<sup>3</sup>Although we note that the ‘phase operator’ of a harmonic oscillator is itself only properly defined in a limiting sense, much like the position operator of a free particle: one can write a limit of hermitian operators that localise the quantity, but they are accompanied by a divergence in the conjugate variable (number or position), which leads to unphysical energetic divergences. However, this is different from temperature, which cannot be defined as the limit of a sequence of hermitian operators.

In the examples of high-precision thermometers given above, and in almost all other practical thermometers, the measurement device comes into thermal equilibrium with the bath that is being measured. We call such a device a ‘thermalising’ thermometer.

Consider a quantum system  $\mathcal{S}$  at thermal equilibrium with an external bath at temperature  $T$ . The state of  $\mathcal{S}$  is described by the canonical Gibbs ensemble  $\rho_\beta = e^{-\beta H} / \mathcal{Z}_\beta$ , where  $H$  is the system Hamiltonian,  $\beta = 1/(k_B T)$  the inverse temperature of the system with  $k_B$  the Boltzmann constant, and  $\mathcal{Z}_\beta = \text{Tr}[e^{-\beta H}]$  the associated partition function. Notice that with respect to the three-step scheme of typical quantum estimation protocols discussed earlier, we are assuming to have already carried out the first two duties,  $\rho_\beta$  being the state of  $\mathcal{S}$  already holding a dependence on  $T$ . Here we will focus on the so-called ‘estimation step’.

In [39], a very simple argument is given establishing that if we assume that a thermalising thermometer has an extensive thermodynamic energy, i.e.  $\bar{E} \equiv -\frac{\partial \ln \mathcal{Z}_\beta}{\partial \beta} = N\bar{\varepsilon}(\beta)$ , where  $\bar{\varepsilon}$  is the average internal energy per particle, then the uncertainty (measured by the root-mean-square error) in the measurement of  $\beta$  is

$$\Delta\beta \geq \frac{1}{\sqrt{N}} \frac{1}{\sqrt{\bar{\varepsilon}'}}, \quad (21.10)$$

where  $\bar{\varepsilon}' = |d\bar{\varepsilon}/d\beta|$ . We review the argument in [39] briefly. Consider a thermometer in the thermal state  $\rho_\beta$ . Assuming that the average internal energy of the thermometer is extensive, it is given by  $\bar{E} = N\bar{\varepsilon}(\beta)$ . Since  $\bar{\varepsilon}(\beta)$  is a monotonically increasing function of temperature, the sample standard deviation of  $\bar{\varepsilon}$  and  $\beta$  are related by the identity  $\Delta\beta = \Delta\varepsilon/\bar{\varepsilon}'$ . To calculate  $\Delta\varepsilon$ , note that the sample variance in the total internal energy is given by

$$\Delta^2 E = \frac{\partial^2 \ln \mathcal{Z}_\beta}{\partial \beta^2} = -\frac{\partial \bar{E}}{\partial \beta} = N\bar{\varepsilon}', \quad (21.11)$$

which demonstrates that the variance in the total internal energy of the thermometer is extensive. The relative uncertainty in the energy per particle is thus

$$\frac{\Delta\varepsilon}{\bar{\varepsilon}} = \frac{\Delta E}{\bar{E}} = \frac{1}{\sqrt{N}} \frac{\sqrt{\bar{\varepsilon}'}}{\bar{\varepsilon}}. \quad (21.12)$$

Equation (21.12) and the identity  $\Delta\beta = \Delta\varepsilon/\bar{\varepsilon}'$  together imply (21.10), thus establishing the shot noise limit on extensive, thermalising thermometers.

This accords with the quantum Cramér–Rao bound in Eq. (21.4) on temperature estimation, which depends on the system heat capacity  $c_v$  [40, 41]

$$\Delta T \geq \frac{1}{\sqrt{N}\mathcal{Q}(T)}, \quad \mathcal{Q}(T) = \frac{1}{k_B^2 T^4} (\text{Tr}[\rho_\beta H^2] - \text{Tr}[\rho_\beta H]^2) = \frac{c_v}{k_B T^2}, \quad (21.13)$$

where  $\mathcal{Q}(T)$  is the QFI (21.5) for the temperature  $T$  and  $1/\sqrt{N}$  is the SQL-scaling in the number  $N$  of independent probes. In other words, the ultimate limit to the precision at which the temperature of a thermal state can be determined is set by an energy measure on  $\rho_\beta$ .<sup>4</sup> The above inequality builds a first significant bridge between two apparently independent theoretical frameworks: quantum thermodynamics and quantum estimation theory.

This scaling is a potentially significant issue for high precision thermometry. For instance, in Doppler gas thermometry, high precision spectroscopy of a gas in thermal equilibrium with a heat bath reveals the Maxwell-Boltzmann distribution of velocities [43–45], whose width is a direct measure of  $k_B T$  of the gas. In recent Doppler thermometry experiments in alkali vapours the atomic flux through a beam of  $\sim 10$  cm length and 2 mm diameter is  $\dot{N} \sim 10^{15}$  atoms/s [46]. The limit to the precision of such a thermometer is then  $\Delta\beta \sim (\dot{N}\tau)^{-1/2} \approx 10^{-7.5}\tau^{1/2}$ , where  $\tau$  is the integration time and  $\Delta\beta \geq 1/\sqrt{N\mathcal{Q}(\beta)}$ . At 1 s this sets a maximum precision in measurements of  $k_B$  of 1 part in  $10^{7.5}$ , which is about 1.5 orders of magnitude better than the current CODATA estimates for  $k_B$ .

### 21.3.1 Heisenberg Limited Thermometry

The SQL-like  $1/\sqrt{N}$  scaling in Eq. (21.10) is evocative of similar scaling in shot-noise limited phase estimation. It is therefore interesting to question whether there is a way to improve this scaling in thermometry to the Heisenberg scaling limit,  $\sim 1/N$ . This question was answered in the affirmative way in [39], based on a constructive toy model which demonstrates this possibility.

The thermometer in the toy model does not come to thermal equilibrium with the bath, and therefore is not subject to the argument that yields Eq. (21.10). Instead, the toy model takes advantage of several key observations:

1. Thermometry (like all physical measurements) can be cast as a counting problem.
2. Any counting measurement can be turned into a phase estimation problem.
3. Phase estimation can be performed with Heisenberg-limited scaling.

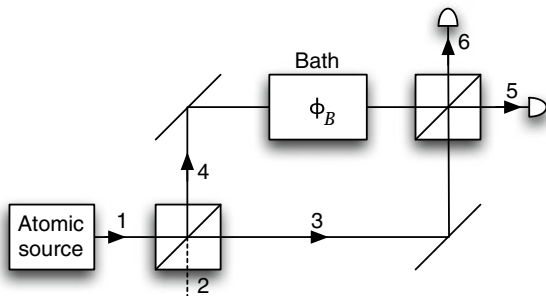
It follows that the thermometry can be done with an accuracy that improves as  $1/N$ .

To see how thermometry can be described as a counting problem, consider a bath of  $M$  identical two-level atoms, each with energy splitting  $\epsilon$  between the ground and excited state. If the atoms are at some temperature  $T$ , the populations of the energy eigenstate will be given by  $\rho_\beta$ . This is plainly a thermodynamic quantity, so counting the number of excited atoms,  $m$ , is a proxy observable from which we can estimate the temperature via  $\langle m \rangle = M \frac{e^{-\beta\epsilon}}{1+e^{-\beta\epsilon}}$ .

---

<sup>4</sup>It results that in this case the SLD commutes with the system Hamiltonian, implying that energy measurements are optimal. Moreover, thermal states represent a special case as they belong to the so-called exponential class [42].

**Fig. 21.2** An atomic interferometer with the bath in one branch. Atoms from the thermometer are input into mode 1 and detected in modes 5 and 6. Mode 2 is the vacuum port. The figure is reprinted from T.M. Stace, *Phys. Rev. A* **82**, 011611 (2010).



To see how to turn a counting problem into a phase estimation problem, consider the following specially designed interaction Hamiltonian describing a dispersive coupling between the  $M$  atoms in the thermal bath, and  $N$  atoms which are part of a thermometric probe

$$H^{(\text{int})} = \alpha \sum_{j=1}^N \sum_{k=1}^M |\epsilon_j\rangle\langle\epsilon| \otimes |\epsilon_k\rangle\langle\epsilon|. \quad (21.14)$$

If the interaction between a given probe atom, prepared in its excited state  $|\epsilon\rangle$  and the  $M$  thermalised atoms lasts for a time  $\tau$ , a phase  $\phi_B = \alpha m \tau$  will accumulate on the probe atom. Thus, counting  $m$  can be turned into the problem of measuring the phase  $\phi_B$ .

This phase can be made observable if the probe atom can be introduced to an interferometer, with the interaction region in one branch of the interferometer, as shown in Fig. 21.2. Finally, as described earlier, if the atoms in the interferometer are prepared in a highly mode-entangled state (such as the well-known ‘NOON’ state), it is possible to perform phase estimation with Heisenberg-limited scaling.

### 21.3.2 Global Versus Local Measurements

What happens when technical or practical limitations restrict our capabilities to local probing? In such a case, the lower bound on the root-mean-square error on  $T$  must be computed optimizing the Fisher Information over all possible local measurements on an accessible subsystem of  $\mathcal{S}$ . Without loss of generality, let us assume  $\mathcal{S}$  to be composed of two subsystems  $\mathcal{A}$  and  $\mathcal{B}$ , and to have access only to subsystem  $\mathcal{A}$ . In general, the global Hamiltonian shows local terms (acting on  $\mathcal{A}$  or  $\mathcal{B}$  separately) to be summed to interactions terms between the subsystems, i.e.  $H = H_{\mathcal{A}} + H_{\mathcal{B}} + H_{\mathcal{AB}}^{(\text{int})}$ . By definition, if we assume to perform a POVM on  $\mathcal{A}$ , the quantum Cramér–Rao bound (21.13) reads

$$\Delta T^{\mathcal{A}} \geq 1/\sqrt{N \mathcal{Q}_{\mathcal{A}}(T)} = k_B T^2 / \sqrt{N \mathfrak{S}_{\mathcal{A}}[\rho_{\beta}]}, \quad (21.15)$$

where  $\mathfrak{S}_{\mathcal{A}}$  is the so-called Local Quantum Thermal Susceptibility (LQTS) introduced with this name in [47], and corresponding to the QFI for the estimation of the inverse temperature  $\beta$  computed on the reduced state  $\rho_{\beta}^{\mathcal{A}} = \text{Tr}_{\mathcal{B}}[\rho_{\beta}]$ ,

$$\mathfrak{S}_{\mathcal{A}}[\rho_{\beta}] := 8 \lim_{\delta\beta \rightarrow 0} \frac{1 - F(\rho_{\beta}^{\mathcal{A}}, \rho_{\beta+\delta\beta}^{\mathcal{A}})}{\delta\beta^2}. \quad (21.16)$$

This functional quantifies the ultimate precision limit to estimate the temperature  $T$  by means of a local (quantum) measurement on subsystem  $\mathcal{A}$ , and by definition gauges how modifications on the global system temperature affect the local state  $\rho_{\beta}^{\mathcal{A}}$ : the larger is  $\mathfrak{S}_{\mathcal{A}}[\rho_{\beta}]$  the more sensitive is the subsystem response. Notice that  $H_{\mathcal{AB}}^{(\text{int})}$  can be arbitrarily strong. A closed expression for LQTS can be determined by applying Uhlmann's theorem for the fidelity [48], according to which the fidelity between the mixed states  $\rho_{\beta}^{\mathcal{A}}$  and  $\rho_{\beta+\delta\beta}^{\mathcal{A}}$  can be computed by means of a maximization over all possible purifications  $|\rho_{\beta}\rangle$  and  $|\rho_{\beta+\delta\beta}\rangle$  of such density matrices, through an ancillary system  $a$ <sup>5</sup>

$$F(\rho_{\beta}^{\mathcal{A}}, \rho_{\beta+\delta\beta}^{\mathcal{A}}) = \max_{|\rho_{\beta}\rangle, |\rho_{\beta+\delta\beta}\rangle} |\langle \rho_{\beta} | \rho_{\beta+\delta\beta} \rangle|. \quad (21.17)$$

A convenient choice is to set the ancilla as  $a = \mathcal{B}\mathcal{A}'\mathcal{B}'$ , with  $\mathcal{S}' = \mathcal{A}'\mathcal{B}'$  isomorphic to  $\mathcal{S} = \mathcal{A}\mathcal{B}$ , and  $|\rho_{\beta}\rangle = \sum_i (e^{-\beta E_i/2}) / \sqrt{Z_{\beta}} |E_i\rangle_{\mathcal{AB}} \otimes |E_i\rangle_{\mathcal{A}'\mathcal{B}'}$ , being  $H = \sum_i E_i |E_i\rangle_{\mathcal{AB}} \langle E_i|$  the spectral decomposition of the system Hamiltonian. By exploiting the freedom in the purifications, it can be shown that the LQTS can be expressed as

$$\mathfrak{S}_{\mathcal{A}}[\rho_{\beta}] = (\text{Tr}[\rho_{\beta} H^2] - \text{Tr}[\rho_{\beta} H]^2) - s_a = \frac{c_v}{k_B \beta^2} - s_a \quad (21.18)$$

with

$$s_a = \sum_{i < j} \frac{(e_i - e_j)^2}{e_i + e_j} |\langle e_i | H' | e_j \rangle|^2. \quad (21.19)$$

Here  $H'$  is the copy of  $H$  acting on the isomorphic space, and  $e_k$  and  $|e_k\rangle$  are the eigenvalues and eigenvectors, respectively, of the ancilla density matrix  $\rho_{\beta}^a = \text{Tr}_{\mathcal{A}}[|\rho_{\beta}\rangle\langle\rho_{\beta}|]$  sharing the same spectrum with  $\rho_{\beta}^{\mathcal{A}} = \text{Tr}_{\mathcal{B}}[|\rho_{\beta}\rangle\langle\rho_{\beta}|]$ . It follows

$$\mathcal{Q}_{\mathcal{A}}(T) = \mathcal{Q}(T) - \frac{s_a}{k_B^2 T^4}. \quad (21.20)$$

---

<sup>5</sup>Let  $\rho^{\Gamma}$  be the state of a given system  $\Gamma$ . It is always possible to introduce another system  $a$  (the so-called reference or ancillary system) and define a pure state  $|\rho^{\Gamma}\rangle$  on  $\Gamma a$  such that  $\rho^{\Gamma} = \text{Tr}_a[|\rho^{\Gamma}\rangle\langle\rho^{\Gamma}|]$ . Furthermore, if  $|\rho^{\Gamma}\rangle$  and  $|\rho'^{\Gamma}\rangle$  are two purifications of  $\rho^{\Gamma}$  on  $\Gamma a$  there exists a unitary transformation  $U$  on  $a$  such that  $|\rho'^{\Gamma}\rangle = (\mathbb{I}_{\Gamma} \otimes U)|\rho^{\Gamma}\rangle$ , being  $\mathbb{I}_{\Gamma}$  the identity operator on  $\Gamma$ . The last property is known as “freedom in purifications” [49].

Notice that  $s_a$  is always greater than zero, thus there is an ordering between the ultimate precision accuracy achievable via global and local measurements,  $\mathcal{Q}_{\mathcal{A}}(T) \leq \mathcal{Q}(T)$ , the inequality being saturated when  $\mathcal{A}$  coincides with the whole system  $\mathcal{S}$ . The same ordering holds at local level, since by construction,  $\mathcal{Q}_{\mathcal{A}}(T) = \mathfrak{S}_{\mathcal{A}}[\rho_{\beta}]/(k_B T^4)$  is a positive quantity which diminishes as the size of  $\mathcal{A}$  is reduced, the smaller being the portion of the system we have access to, the worse being the accuracy we can achieve.<sup>6</sup>

What is the role played by the interactions between the probed subsystem  $\mathcal{A}$  and the remaining part  $\mathcal{B}$  of the global system  $\mathcal{S}$ , the latter being prepared in the thermal state  $\rho_{\beta}$ ? In absence of interactions (i.e.,  $H_{\mathcal{AB}}^{(\text{int})} = 0$ ), the local state of  $\mathcal{A}$  reads

$$\rho_{\beta}^{\mathcal{A}} = e^{-\beta H_{\mathcal{A}}}/Z_{\beta}^{\mathcal{A}} \quad (21.23)$$

with  $Z_{\beta}^{\mathcal{A}} = \text{Tr}[e^{-\beta H_{\mathcal{A}}}]$ , yielding

$$\mathcal{Q}_{\mathcal{A}}(T) = c_v^{\mathcal{A}}/(k_B T^2), \quad (21.24)$$

where  $c_v^{\mathcal{A}} = (\text{Tr}[\rho_{\beta}^{\mathcal{A}} H_{\mathcal{A}}^2] - \text{Tr}[\rho_{\beta}^{\mathcal{A}} H_{\mathcal{A}}]^2)/(k_B T^2)$  is the local heat-capacity of subsystem  $\mathcal{A}$ . Up to which limit does such local description hold in presence of interactions? This problem has been explicitly tackled in the framework of locally interacting quantum systems [51], a very general class of models encompassing most of the fundamental spin models, such as the Ising model [52], the Heisenberg model [53], the Potts model [54], the Hubbard model [55], etc (see Chap. 20 for an extended review). A crucial property characterizing these Hamiltonians is that they admit a critical temperature  $T^*$  above which the correlation between any two observables  $O_{\mathcal{A}}, O'_{\mathcal{A}'}$  acting two subsystems  $\mathcal{A}$  and  $\mathcal{A}'$  of global system  $\mathcal{S}$ , the latter described by

<sup>6</sup>The same conclusions can be driven by noticing an interesting connection between the LQTS, related to the reconstruction of  $T$ , and the more studied case of phase estimation mentioned in the former section. Indeed by comparing relations (21.7)–(21.8) with (21.19)–(21.20) we have

$$\mathfrak{S}_{\mathcal{A}}[\rho_{\beta}] + \mathcal{Q}_a(\lambda) = \mathcal{Q}_{SS'}(\lambda) \quad (21.21)$$

where  $\mathcal{Q}_a(\lambda)$  and  $\mathcal{Q}_{SS'}(\lambda)$  are the QFI associated to the estimation of  $\lambda$  encoded on  $|\rho_{\beta}\rangle$  via the unitary superoperator  $\mathcal{E}_{\lambda/2}$  such that  $\mathcal{E}_{\lambda/2}(|\rho_{\beta}\rangle\langle\rho_{\beta}|) = e^{-iH'\lambda/2}|\rho_{\beta}\rangle\langle\rho_{\beta}|e^{iH'\lambda/2} = |\rho_{\beta}^{(\lambda)}\rangle\langle\rho_{\beta}^{(\lambda)}|$ , assuming to have access at the measurement stage to subsystem  $a = \mathcal{B}\mathcal{A}'\mathcal{B}'$  and  $SS' = \mathcal{A}\mathcal{A}'$ , respectively:

$$\mathcal{Q}_a(\lambda) = \sum_{i < j} \frac{(e_i - e_j)^2}{e_i + e_j} |\langle e_i | H' | e_j \rangle|^2, \quad \mathcal{Q}_{SS'}(\lambda) = \langle \rho_{\beta} | H'^2 | \rho_{\beta} \rangle - \langle \rho_{\beta} | H' | \rho_{\beta} \rangle^2 = \langle \rho_{\beta} | H^2 | \rho_{\beta} \rangle - \langle \rho_{\beta} | H | \rho_{\beta} \rangle^2. \quad (21.22)$$

In other words the accuracies corresponding to the temperature estimation on  $\mathcal{A}$  and the phase estimation on its complementary counterpart  $a$ , which are both positive quantities, are forced to sum up to the energy variance of the global system, thus establishing a sort of complementarity relation. Indeed, as already mentioned, the LQTS  $\mathfrak{S}_{\mathcal{A}}[\rho_{\beta}]$  and similarly  $\mathcal{Q}_a(\lambda)$  are increasing functions of the dimension of  $\mathcal{A}$  and  $a$ , respectively.

the thermal state  $\rho_\beta$ , decays exponentially with the distance  $d(\mathcal{A}, \mathcal{A}')$  between their supports [56], i.e

$$\left| \text{Tr}[\rho_\beta O_{\mathcal{A}} O'_{\mathcal{A}'}] - \text{Tr}[\rho_\beta O_{\mathcal{A}}] \text{Tr}[\rho_\beta O'_{\mathcal{A}'}] \right| \leq C_{\mathcal{A}\mathcal{A}'} (\xi(T) + 1) e^{-\frac{d(\mathcal{A}, \mathcal{A}')}{\xi(T)}}, \quad (21.25)$$

where  $C_{\mathcal{A}\mathcal{A}'}$  is a constant fixed by  $O_{\mathcal{A}}$  and  $O'_{\mathcal{A}'}$  and  $\xi(T)$  is the so-called correlation length of the system. It has been rigorously proved [57] that if the correlation length is much smaller than the volume to surface ratio of a given subsystem  $\mathcal{A}$ , the  $\mathcal{Q}_{\mathcal{A}}(T)$  is a local quantity proportional to  $c_v^{\mathcal{A}}$ . Therefore, under this condition, local interactions between  $\mathcal{A}$  and the remaining part of  $\mathcal{S}$  (i.e.  $\mathcal{B}$ ) do not significantly affect the precision of local measurements of the temperature. This condition is typically violated in the proximity of a critical point when the correlation length diverges, or for subsystems made by only few sites.

Let us conclude this section by considering the thermal response at low temperature of two prototypical many-body systems featuring quantum phase transitions. In the specific, here we analyze the behavior of the quantum spin-1/2 Ising and Heisenberg chains, in a transverse magnetic field  $h$  and with a  $z$ -axis anisotropy  $\Delta$  respectively, both with periodic boundary conditions:

$$H_{\text{Ising}} = - \sum_i [\sigma_i^x \sigma_{i+1}^x + h \sigma_i^z], \quad (21.26)$$

$$H_{\text{XXZ}} = \sum_i [(\sigma_i^x \sigma_{i+1}^x + \sigma_i^y \sigma_{i+1}^y) + \Delta \sigma_i^z \sigma_{i+1}^z] \quad (21.27)$$

(we have set to 1 the system energy scale). Here  $\sigma_i^\alpha$  denotes the Pauli matrices on the  $i$ th site, ( $\alpha = x, y, z$ ). At zero temperature, the Ising model presents a  $\mathbb{Z}_2$ -symmetry breaking phase transition at  $|h_c| = 1$ , belonging to the Ising universality class. On the other hand, the XXZ-Hamiltonian shows a critical behaviour for  $-1 \leq \Delta \leq 1$  and presents a ferromagnetic or antiferromagnetic ordering elsewhere, exhibiting in correspondence to the ferromagnetic point  $\Delta = -1$  a first-order quantum phase transition, and a continuous one of the Kosterlitz–Thouless type at the antiferromagnetic point  $\Delta = 1$ . Figure 21.3 displays the small-temperature limit of the LQTS  $\mathfrak{S}_{\mathcal{A}}[\rho_\beta] = k_B^2 T^4 \mathcal{Q}_{\mathcal{A}}(T) = \mathcal{Q}_{\mathcal{A}}(T)/(k_B^2 \beta^4)$  for these two Hamiltonians. Observe that as expected the LQTS is a monotonically increasing function of the number  $n_{\mathcal{A}}$  of contiguous spins belonging to the tested subsystem  $\mathcal{A}$ . An interesting fact is that, even at finite temperatures and for systems composed of twelve sites, the LQTS seems to be sensitive to the presence of critical regions. This effect can be naively understood by observing that at low temperatures the Hamiltonian energy levels which play a significant role in the system dynamics are the ground state and the first excited levels, whose interplay underpins the emergence of quantum phase transitions. The sensitivity of LQTS to critical points can be understood by noticing that by definition it basically addresses the degree of distinguishability among such energy levels.

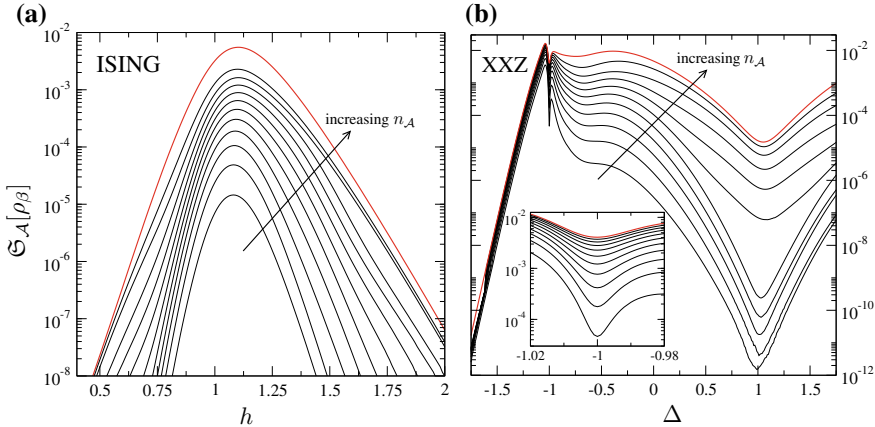


**Fig. 21.3** Numerical curves representing the behavior of the LQTS in the low-temperature regime ( $\beta = 9$ ) for the Ising (panel **a**) and the Heisenberg XXZ chains (panel **b**) with twelve sites. The uppermost curve corresponds to the global quantum thermal susceptibility proportional to the heat capacity. The other curves have been computed for different sizes  $n_A$  of the measured subsystem  $\mathcal{A}$ . In the XXZ model, the LQTS for  $n_A = 1$  vanishes. The figure is reprinted from A. De Pasquale, et al. *Nat. Commun.* **7**, 12782 (2016), CC - by - 4.0 license.

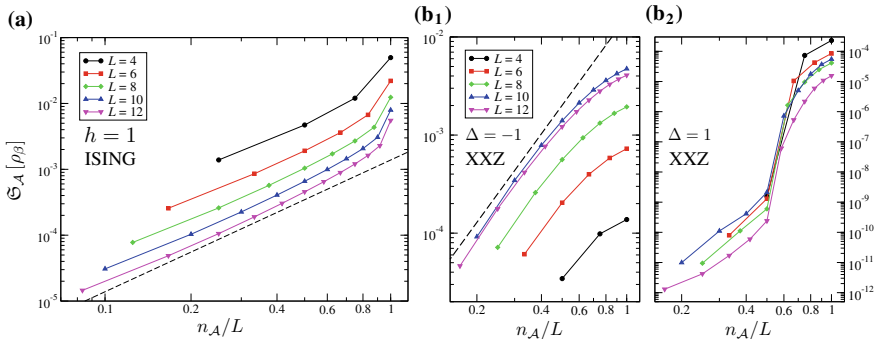


**Fig. 21.4** Analysis of the peak values of the LQTS for the Ising and the XXZ models, as a function of the dimension of the measured subsystem  $n_A$  and for different system lengths  $L$ . For the Ising model (panel **a**) the dashed line denotes a power-law behaviour  $\mathfrak{S}_A \sim (n_A/L)^2$ , and is plotted as a guideline. For the XXZ chain (panels **b**<sub>1</sub> and **b**<sub>2</sub>) the data refer to the minima close to the critical points  $\Delta = \pm 1$ . The dashed line for  $\Delta = -1$  (panel **b**<sub>1</sub>) denotes the behaviour  $\mathfrak{S}_A \sim (n_A/L)^3$ . In all panels we have set  $h = 1$  and  $\beta = 3L/4$ . The figure is reprinted from A. De Pasquale, et al. *Nat. Commun.* **7**, 12782 (2016), CC - by - 4.0 license.

A fulfilling quantum-metrology approach to quantum phase transitions at finite temperatures can be found in [58, 59]. The numerical analysis reported in Fig. 21.4 of the scaling of the LQTS close to quantum phase transition points shows significant deviations from a linear growth with  $n_A$ , indicating that, as expected, in these points the correlations cannot be neglected already for the sizes considered here.

## 21.4 Single Qubit Thermometry

The recent technological progress in manipulating individual quantum systems, has enabled their employment as temperature probes. Indeed, accurate temperature readings at nanoscopic level can find applications in many research areas, ranging from materials science [60, 61] to medicine and biology [62, 63], and in most of the situations addressed by the all field of quantum thermodynamics [64–68] requiring the control of quantum thermal devices. In this section we will tackle different aspects of a quite typical quantum estimation problem: the reconstruction of the unknown temperature of a sample by putting it in thermal contact with an individual quantum probe, acting as a thermometer.

### 21.4.1 Temperature Discrimination Using a Single Qubit

Given a probe, plainly measuring the temperature is sufficient to discriminate between two temperatures. However, the more elementary thermometric task of discriminating between whether a bath (a sample characterized by a large number of subcomponents) is ‘hot’ or ‘cold’ does not require a numerical temperature scale. In the context of quantum thermometry, it was shown in [69] that a quantum two-level system can perform this task. We suppose the bath is at either  $T_h$  or  $T_c$ , and we wish to optimally discriminate between these two. A single qubit may be brought into thermal contact with the bath, and after interacting with it for some time  $t$ , the state of the qubit is measured.

In this scenario, the Fisher Information is not the relevant measure: we are not attempting to discriminate between a continuum of states, but between two distinct states of the qubit. As such, the trace distance, which is given by the Euclidean distance  $\Delta(\vec{r}_h(t), \vec{r}_c(t))$  between the Bloch vectors  $\vec{r}_h(t)$  and  $\vec{r}_c(t)$  of the possible states of the qubit, determines our ability to discriminate between the two states.

Jevtic et al. [69] studied this model as a function of the relative temperatures, the interaction time, and the initial state of the probe qubit. Assuming a Markovian interaction between the qubit and the bath (characterised by a thermalisation rate  $\tilde{\gamma}$ ) they find that  $\Delta(\vec{r}_h(t), \vec{r}_c(t))$  is maximised at a finite interaction time, and with the qubit initialised in the ground state. This is shown in the red curve in Fig. 21.5, where time is measured in units of  $\tilde{\gamma}^{-1}$ : up until the cusp around  $t \approx 0.1/\tilde{\gamma}$ , the optimal initial state of the qubit is  $|g\rangle$ . Clearly, the maximum value of that curve occurs in this interval, indicating that the globally optimal strategy is to initialise the qubit in the ground state, and run the interaction for  $t \approx 0.06/\tilde{\gamma}$ . If the interaction time is longer than  $t \approx 0.1/\tilde{\gamma}$ , the locally optimal initial state is no longer the ground state, but some coherent superposition of ground and excited. Thus quantum coherence provides some enhancement in a limited sense in this temperature discrimination problem.

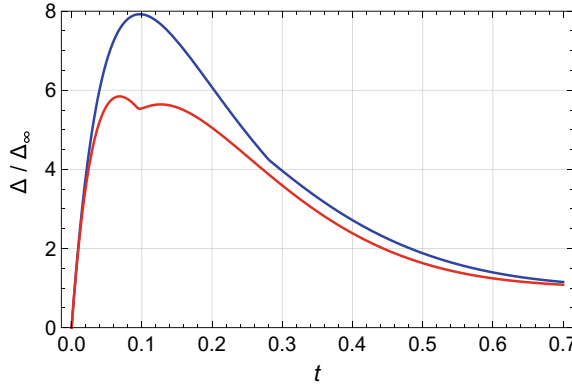


**Fig. 21.5** Trace distance between the state of a probe qubit after thermalising with either a hot bath at temperature  $T_h$ , or a cold bath at temperature  $T_c$ . The distance measure  $\Delta(\vec{r}_h(t), \vec{r}_c(t))$  is the distance between the Bloch vectors  $\vec{r}_h(t)$  and  $\vec{r}_c(t)$  of the corresponding qubit states,  $\rho_h$  or  $\rho_c$ , after thermalisation for  $t$  units of time. The normalisation  $\Delta_\infty$  is the distance at thermal equilibrium, i.e. at  $t \rightarrow \infty$ . The figure is reprinted from S. Jevtic, et al. *Phys. Rev. A* **91**, 012331 (2015).

In [69], it was also shown that including an ancilla qubit, which is initialised in a maximally entangled state with the probe qubit yields better performance, as indicated by the blue curve in Fig. 21.5. Clearly it is higher than the red curve at all interaction times, indicating that quantum entanglement is a potentially useful resource in this state discrimination task.

#### 21.4.2 Fundamental Limitations on Temperature Estimation with Individual Quantum Probes

We now discuss temperature reconstruction of a reservoir at thermal equilibrium. In standard thermometry, the thermometer is put in contact with the bath and then it is allowed to equilibrate, so that it finally ends up to be in a thermal state  $\rho_\beta = e^{-\beta H} / \mathcal{Z}_\beta$ . Therefore, as seen in the former section the highest achievable accuracy on temperature estimation through optimal measurements on the probe (21.13) is proportional to the its heat capacity, that is to the variance of  $H$ :

$$\Delta T \geq \frac{1}{\sqrt{N \mathcal{Q}(T)}}, \quad \mathcal{Q}(T) = \frac{c_v}{k_B T^2} = \frac{1}{k_B^2 T^4} (\text{Tr}[\rho_\beta H^2] - \text{Tr}[\rho_\beta H]^2), \quad (21.28)$$

where  $N \gg 1$  is the number of probes at disposal, or the repetition of same the estimation procedure. It follows that the optimal choice of the probing system allowing for maximal thermal sensitivity, consists in finding the energy spectrum with the largest possible energy variance at thermal equilibrium. If, without loss of generality, the probing system is assumed to be  $M$ -dimensional, the solution to this problem

amounts to solve  $M$ -coupled transcendental equations

$$\frac{\partial}{\partial E_m} \left[ \frac{1}{Z_\beta} \sum_i E_i^2 e^{-E_i/(k_B T)} - \frac{1}{Z_\beta^2} \left( \sum_i E_i e^{-E_i/(k_B T)} \right)^2 \right] = 0, \quad (21.29)$$

where  $H = \sum_i E_i |E_i\rangle\langle E_i|$  is the Hamiltonian spectral decomposition. It can be shown [10, 70] that the optimal quantum probes, acting as thermometers of maximal thermal sensitivity, are given by effective two-level atoms with maximally degenerate excited state and with a temperature dependent energy gap (this is equivalent to saying that for a fixed energy gap of the qubit thermometer there exists a temperature which can be retrieved with optimal accuracy).

### 21.4.3 Single-Qubit Thermometry Through Sequential Measurements

The analysis outlined above hinges upon two hypothesis:

- (i) The interaction time is sufficiently long to let the probe thermalize with the bath.
- (ii) A certain number  $N$  of probes prepared in the same input state, say  $\rho_0$ , interact with the bath and are measured independently, or equivalently if one has at disposal a single probe it is reinitialized in the same state after each of the  $N$  measurement stages. In other words, the whole experiment requires  $N$  independent and identically distributed (i.i.d.) measurements leading to the Cramér–Rao bound (21.1).

However, in practice (i) and (ii) can find some limitations. On the one hand, one may need to read the temperature of the outgoing probe before the latter attains full thermalization. This for instance happens if it is not possible to arrange the interaction time with the reservoir to be long enough, or if the bath itself is unstable (e.g. in the low temperature regime when too strong correlations are established between the probe and the sample [71], and fundamental limits emerge in temperature reconstruction [72]). In general if (i) is violated, but it is still possible to fulfill (ii), it has been observed [10] that a convenient choice for  $\rho_0$  is represented by the Hamiltonian ground state. On the other hand, also the arbitrary initialization of  $N$  independent probing systems, or of the single probe at disposal after each measurement readout, might encounter some obstructions, thus violating condition (ii). In order to attack this limitation, one possibility is relying on sequential measurement schemes [73, 74], where repeated consecutive measurements are performed on a single probe without reinitializing it. For the sake of clarity let us indicate as  $\mathcal{E}_T^\tau$  the superoperator defining the process that the probe undergoes when interacting with the sample, thus explicitly labelling it with the temperature  $T$  of the sample, and with the interaction time  $\tau$  between the probe and the bath. Furthermore, in order to provide a simple, but mathematically rigorous, description of the sequential mea-

surement protocol, it is useful to introduce a description also of the measurement process in terms of superoperators. In general, once a POVM,  $\{\Pi_\theta\}$ ,  $\int d\theta \Pi_\theta = \mathbb{I}$ , has been selected, we can associate to it a family of superoperators  $\{\mathcal{M}_\theta\}$  fulfilling the normalization condition  $\int d\theta \mathcal{M}_\theta = \mathcal{I}$ , with  $\mathcal{I}$  being the identity superoperator (i.e.  $\mathcal{I}(\rho_0) = \rho_0$ ). When applied to an arbitrary state  $\rho$ , these superoperators give the outcome  $\theta$  with probability  $p(\theta|\rho) = \text{Tr}[\mathcal{M}_\theta(\rho)] = \text{Tr}[\Pi_\theta \rho]$ , and transform  $\rho$  as  $\mathcal{M}_\theta(\rho)/\text{Tr}[\mathcal{M}_\theta(\rho)]$ .<sup>7</sup>

In Fig. 21.6 we have provided a pictorial representation of the two temperature estimation protocols we aim to compare.

Let us stress that while in the standard approach the collected data  $\vec{\theta} = \{\theta_1, \theta_2, \dots, \theta_N\}$  are independent identically distributed (i.i.d.), this is no more true for the sequential measurement scheme. Therefore, in the first case the global probability distribution of a  $N$ -long sequence  $\vec{\theta}$  reads

$$p_{\text{i.i.d.}}^{(N)}(\vec{\theta}|T) = \prod_{i=1}^N p(\theta_i|T), \quad (21.30)$$

with  $p(\theta_i|T) = \text{Tr}[\mathcal{M}_{\theta_i} \circ \mathcal{E}_T^\tau(\rho_0)]$  all independent from each other, and the symbol “ $\circ$ ” representing the composition of superoperators. On the contrary, in the second scenario we have

$$p_{\text{s.m.s.}}^{(N)}(\vec{\theta}|T) = \prod_{i=1}^N p(\theta_i|T; \theta_1, \dots, \theta_{i-1}) \quad (21.31)$$

with  $p(\theta_i|T; \theta_1, \dots, \theta_{i-1}) = \text{Tr}[(\mathcal{M}_{\theta_i} \circ \mathcal{E}_T^\tau)(\rho^{[\theta_1, \dots, \theta_{i-1}]})]$ , and  $\rho_0, \rho_1^{[\theta_1]}, \rho_2^{[\theta_1, \theta_2]}, \dots, \rho_N^{[\theta_1, \dots, \theta_N]}$  the density matrices generated by the measurement stochastic process

$$\begin{aligned} \rho_1^{[\theta_1]} &= \frac{(\mathcal{M}_{\theta_1} \circ \mathcal{E}_T^\tau)(\rho_0)}{\text{Tr}[(\mathcal{M}_{\theta_1} \circ \mathcal{E}_T^\tau)(\rho_0)]} && (t = \tau), \\ \rho_2^{[\theta_1, \theta_2]} &= \frac{(\mathcal{M}_{\theta_2} \circ \mathcal{E}_T^\tau)(\rho_1^{[\theta_1]})}{\text{Tr}[(\mathcal{M}_{\theta_2} \circ \mathcal{E}_T^\tau)(\rho_1^{[\theta_1]})]} && (t = 2\tau), \\ &\vdots \\ \rho_N^{[\theta_1, \dots, \theta_N]} &= \frac{(\mathcal{M}_{\theta_N} \circ \mathcal{E}_T^\tau)(\rho_{N-1}^{[\theta_1, \dots, \theta_{N-1}]})}{\text{Tr}[(\mathcal{M}_{\theta_N} \circ \mathcal{E}_T^\tau)(\rho_{N-1}^{[\theta_1, \dots, \theta_{N-1}]})]} && (t = N\tau). \end{aligned} \quad (21.32)$$

---

<sup>7</sup>By definition the elements  $\Pi_\theta$  of a POVM are positive operators. This implies that for each  $\Pi_\theta$  there exists an other positive operator  $M_\theta$ , determined up to a unitary transformation, such that  $\Pi_\theta = M_\theta^\dagger M_\theta$  and  $\int d\theta M_\theta^\dagger M_\theta = \mathbb{I}$ . Therefore the probability of measuring  $\theta$  on a state  $\rho$  is given by  $p(\theta|\rho) = \text{Tr}[\Pi_\theta \rho] = \text{Tr}[M_\theta \rho M_\theta^\dagger]$ , and the normalized state of the system after the measurement reads  $\rho_\theta = M_\theta \rho M_\theta^\dagger / p(\theta|\rho)$ . Finally, to each operator  $M_\theta$  we can associate a superoperator  $\mathcal{M}_\theta$  such that  $\mathcal{M}_\theta(\rho) = M_\theta \rho M_\theta^\dagger$  and  $\int d\theta \mathcal{M}_\theta = \mathcal{I}$ , with  $\mathcal{I}$  being the identity superoperator.

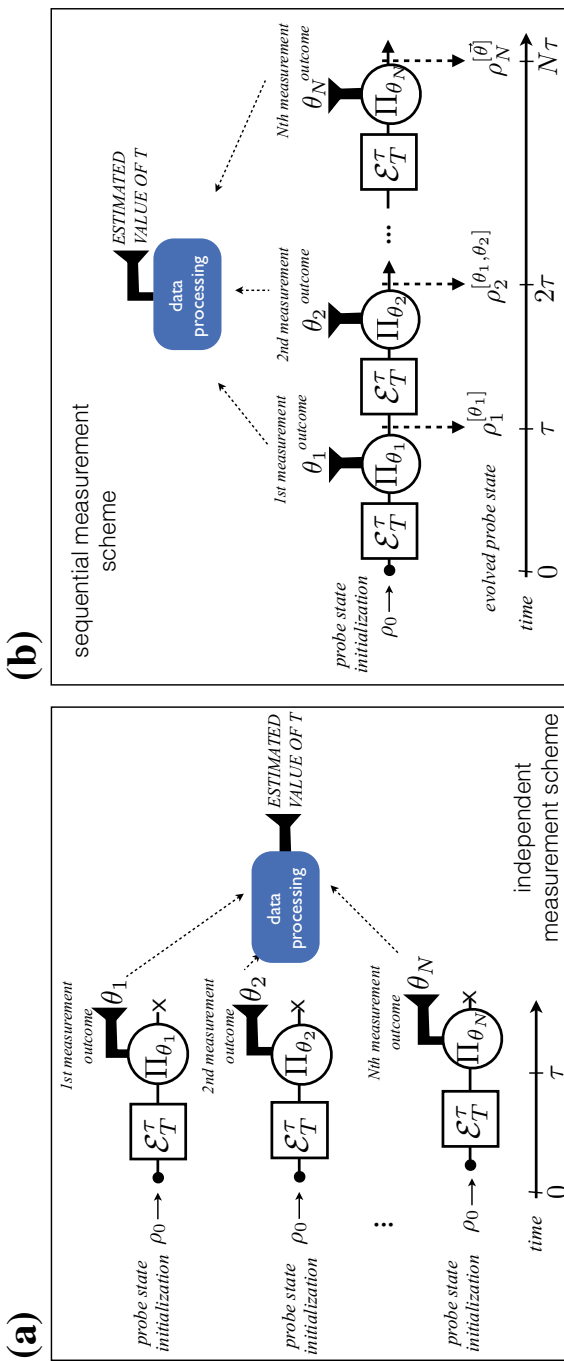


**Fig. 21.6** Schematic representation of two estimation temperature schemes realized by letting a probe (behaving as a thermometer) interact with a sample for a time interval  $\tau$ . Panel **a** represents the standard scheme relying on  $N$  i.i.d. measurements performed on  $N$  distinct probes (as in panel **a** of Fig. 21.1). Panel **b** refers to  $N$  sequential measurements on the same probe which is initialized only once.

Here, we have also assumed to neglect the measurement time. Notice that  $p_{\text{s.m.s.}}^{(N)}(\vec{\theta}|T)$  can be equivalently written as  $p_{\text{s.m.s.}}^{(N)}(\vec{\theta}|T) = \text{Tr}[(\mathcal{M}_{\theta_N} \circ \mathcal{E}_T^\tau \circ \mathcal{M}_{\theta_{N-1}} \circ \mathcal{E}_T^\tau \circ \cdots \circ \mathcal{M}_{\theta_1} \circ \mathcal{E}_T^\tau)(\rho_0)]$ .

The difference between the two approaches clearly emerges in the computation of the Cramér–Rao bound. For the case of i.i.d. readouts, we get the scaling in (21.1) given by  $1/\sqrt{N}$

$$\Delta T_{\text{i.i.d.}}^{(N)} \geq \frac{1}{\sqrt{\mathcal{F}_{\text{i.i.d.}}^{(N)}(T)}} = \frac{1}{\sqrt{N\mathcal{F}(T)}}, \quad (21.33)$$

where  $\mathcal{F}(T)$  is the Fisher Information associated to the selected POVM, i.e.

$$\begin{aligned} \mathcal{F}_{\text{i.i.d.}}^{(N)} &= \int d\vec{\theta} \frac{1}{p_{\text{i.i.d.}}^{(N)}(\vec{\theta}|T)} \left( \frac{\partial p_{\text{i.i.d.}}^{(N)}(\vec{\theta}|T)}{\partial T} \right)^2 = N\mathcal{F}(T), \\ \mathcal{F}(T) &= \int d\theta \frac{1}{p(\theta|T)} \left( \frac{\partial p(\theta|T)}{\partial T} \right)^2. \end{aligned} \quad (21.34)$$

The same scaling does not hold for sequential measurements since the integral over  $d\vec{\theta}$  does not factorise, yielding

$$\Delta T_{\text{s.m.s.}}^{(N)} \geq \frac{1}{\sqrt{\mathcal{F}_{\text{s.m.s.}}^{(N)}(T)}}, \quad \mathcal{F}_{\text{s.m.s.}}^{(N)}(T) = \int d\vec{\theta} \frac{1}{p_{\text{s.m.s.}}^{(N)}(\vec{\theta}|T)} \left( \frac{\partial p_{\text{s.m.s.}}^{(N)}(\vec{\theta}|T)}{\partial T} \right)^2. \quad (21.35)$$

Finally, the quantum Cramér–Rao bound can be determined via a maximization over all possible POVMs.

Actually, in what follows we will assume a more practical perspective and present some results [75] dealing with a quite standard model for the reservoir and for the probe-sample interaction, and referring to a specific choice for the readout measurements. In the specific we consider a qubit system initialised in the state  $\rho_0$  and put in contact, at time  $t = 0$ , with a Bosonic thermal reservoir of unknown temperature  $T$ . At  $t > 0$  the state of probe reads  $\rho_T(t) = \mathcal{E}_T^t(\rho_0) = e^{t\mathcal{L}_T}(\rho_0)$ , where  $\mathcal{L}_T$  is the Lindblad superoperator defined as

$$\mathcal{L}_T(\dots) = -\frac{i}{2}\Omega[\sigma_z, (\dots)]_- + \sum_{s=\pm 1} \gamma_s \left( \sigma_{-s}(\dots)\sigma_s - \frac{1}{2}[\sigma_s\sigma_{-s}, (\dots)]_+ \right), \quad (21.36)$$

with  $[(\dots), (\dots)]_\pm$  being the commutator ( $-$ ) and anti-commutator ( $+$ ) brackets, and  $\sigma_\pm = (\sigma_x \pm i\sigma_y)/2$  being the spin-flip operators. In this expression, the two relaxation constants  $\gamma_-$  (for excitation) and  $\gamma_+$  (for decay) are related to the temperature  $T$  of the reservoir through the detailed balance condition and are given by

$$\gamma_+ = (1 + N_{\text{th}})\gamma, \quad \gamma_- = N_{\text{th}}\gamma, \quad (21.37)$$

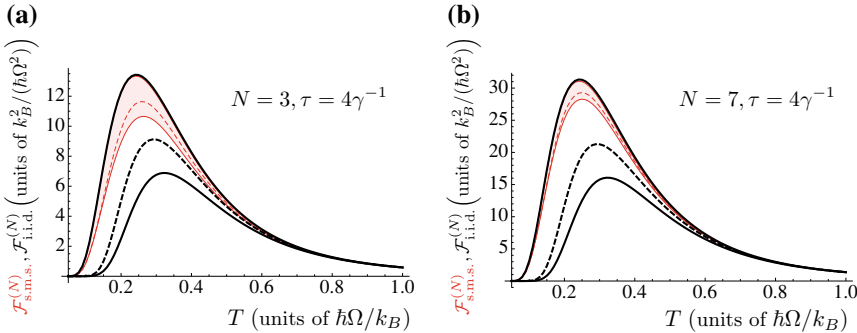


**Fig. 21.7** Fisher Information for projective measurements on the probe. The panels refer to different values of the number of repetitions  $N$  and to an interaction time  $\tau = 4\gamma^{-1}$ . Thick (black) lines refer to the standard protocol based on i.i.d. measurements while the thin (red) ones refer to sequential measurements (for the latter case the region between the optimal and worst performance ruled by the choice of the initial state of probe is shaded). The figure is reprinted from A. De Pasquale, et al. *Phys. Rev. A* **96**, 012316 (2017).

where  $N_{\text{th}} = 1/(e^{\beta\hbar\Omega} - 1)$  is the average thermal number of Bosonic bath excitations, and  $\gamma$  is a temperature-independent parameter gauging the strength of the probe-sample interactions. The qubit acts a thermometer, and  $T$  is recovered by monitoring the populations of its two energy levels at time intervals  $\tau$ . The simplest POVM which can be realized to this end is given by the rank-one projectors  $\Pi_{\pm} = (\mathbb{I} \pm \sigma_z)/2$  on the energy levels of the probe Hamiltonian  $\frac{1}{2}\hbar\Omega\sigma_z$ . In Fig. 21.7 the FI associated to the two above mentioned estimation schemes, (21.34) and (21.35), is plotted by setting the number measurements to be equal to 3 and 7, and the probe-sample interaction time as  $\tau = 4\gamma^{-1}$  (the full thermalization time of the probes can be considered reached already for  $\tau \gtrsim 9.5\gamma^{-1}$ ). The uppermost and lowest solid lines correspond to the optimal and worst choices of the input state  $\rho_0$  (which coincide with the ground state and with the first excited level, respectively) while the dashed lines refer to the average of the FI over uniformly sampled input probe states  $\rho_0$  (physically the latter curves correspond to the practical situation in which the experimenter is not able to completely control the probe preparation stage). It results that for the optimal choice of the probe input state the standard protocol based on i.i.d. measurements slightly outperforms the sequential measurement scheme. However a more interesting phenomenon is observed for non-optimal input states: for all temperatures of the bath, the sequential measurement protocol outperforms the standard one, at least on average and for the worst choice of the probe input state. Furthermore, also the gap between the optimal and the worst choice of the probe is smaller for sequential measurements than for i.i.d. ones, thus yielding a higher degree of versatility with respect to the choice of the initial state of the probe. This effect can be explained by observing that in this estimation approach the probe gradually loses the memory of the initial condition, moving towards a fixed-point configuration depending on the bath temperature. It results that even a non-optimal initialization of the probe

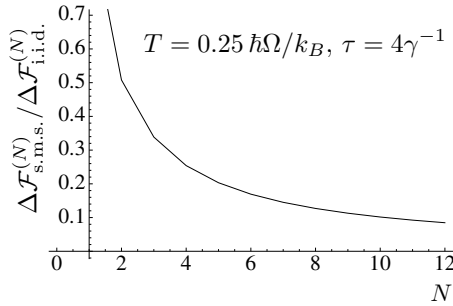


**Fig. 21.8** Plot of the ratio between  $\Delta\mathcal{F}_{\text{s.m.s.}}^{(N)}$  and  $\Delta\mathcal{F}_{\text{i.i.d.}}^{(N)}$ , the max-min gap of the FI due to the choice of the initial state for the probe. It results that  $\Delta\mathcal{F}_{\text{s.m.s.}}^{(N)}$  shrinks more rapidly than  $\Delta\mathcal{F}_{\text{i.i.d.}}^{(N)}$ . The figure is reprinted from A. De Pasquale, et al. *Phys. Rev. A* **96**, 012316 (2017).

can in the end provide a relatively good estimation of the temperature. Figure 21.8 shows that the gap between optimal and worst performances in case of sequential measurements  $\Delta\mathcal{F}_{\text{s.m.s.}}^{(N)}$  is lower and closes faster than that yielded in standard case indicated as  $\Delta\mathcal{F}_{\text{i.i.d.}}^{(N)}$ . Finally, when the probe thermalization with the bath has taken place, it can be shown that all the above mentioned curves collapse.

## 21.5 Conclusions

We have discussed the application of techniques from quantum estimation theory and quantum metrology to thermometry.

It results that the Quantum Fisher Information plays an important role, and we have presented a toy model which demonstrates the possibility of Heisenberg-like scaling for thermometry. Then, we have introduced a theoretical approach to temperature locality, aiming at avoiding any restrictive hypothesis on the dimension of the system or on its Hamiltonian ruling the interactions between its subcomponents. This has led to the definition of the so-called Local Quantum Thermal Susceptibility, a functional which operationally highlights the degree at which the thermal equilibrium of the global system is perceived locally, and reduces to the system heat capacity when the global system is probed. Finally, moving from the observation that two-level quantum systems can be exploited as efficient thermometers to establish the temperature of a thermal bath, we have discussed different techniques of single qubit thermometry.

**Acknowledgements** ADP acknowledges financial support from the University of Florence in the framework of the University Strategic Project Program 2015 (project BRS00215).

## References

1. P.J. Mohr, B.N. Taylor, Rev. Mod. Phys. **77**, 1 (2005). <https://doi.org/10.1103/RevModPhys.77.1>
2. W. Weng, J.D. Anstie, T.M. Stace, G. Campbell, F.N. Baynes, A.N. Luiten, Phys. Rev. Lett. **112**, 160801 (2014). <https://doi.org/10.1103/PhysRevLett.112.160801>
3. K.V. Hovhannyan, L.A. Correa, Phys. Rev. B **98**, 045101(2018). <https://doi.org/10.1103/PhysRevB.98.045101>
4. A.E. Allahverdyan, Th.M. Nieuwenhuizen, Phys. Rev. B **66**, 115309 (2002). <https://doi.org/10.1103/PhysRevB.66.115309>
5. S. Hilt, E. Lutz, Phys. Rev. A **79**, 010101 (R) (2009). <https://doi.org/10.1103/PhysRevA.79.010101>
6. N.S. Williams, K. Le Hur, A.N. Jordan, J. Phys. A Math. Theor. **44**, 385003 (2011). <https://doi.org/10.1088/1751-8113/44/38/385003>
7. M. Brunelli, S. Olivares, M.G.A. Paris, Phys. Rev. A **84**, 032105 (2011). <https://doi.org/10.1103/PhysRevA.84.032105>
8. U. Marzolini, D. Braun, Phys. Rev. A **88**, 063609 (2013). <https://doi.org/10.1103/PhysRevA.88.063609>
9. G. Salvatori, A. Mandarino, M.G.A. Paris, Phys. Rev. A **90**, 022111 (2014). <https://doi.org/10.1103/PhysRevA.90.022111>
10. L.A. Correa, M. Mehboudi, G. Adesso, A. Sanpera, Phys. Rev. Lett. **114**, 220405 (2015). <https://doi.org/10.1103/PhysRevLett.114.220405>
11. M.G.A. Paris, J. Řeháček, *Quantum State Estimation*. Lecture Notes in Physics, vol. 649 (Springer, Berlin, 2004). <https://doi.org/10.1007/b98673>
12. M.G.A. Paris, Int. J. Quantum Inf. **7**, 125 (2009). [arXiv:0804.2981](https://arxiv.org/abs/0804.2981)
13. H. Cramér, *Mathematical Methods of Statistics* (Princeton University Press, Princeton, 1946)
14. S.L. Braunstein, C.M. Caves, G.J. Milburn, Ann. Phys. (N.Y.) **247**, 135 (1996). <https://doi.org/10.1006/aphy.1996.0040>
15. A. Peres, Phys. Rev. A **30**, 1610 (1984). <https://doi.org/10.1103/PhysRevA.30.1610>
16. R. Jozsa, J. Mod. Opt. **41**, 2315 (1994). <https://doi.org/10.1080/09500349414552171>
17. V. Giovannetti, S. Lloyd, L. Maccone, Nat. Photon. **5**, 222 (2011). <https://doi.org/10.1038/nphoton.2011.35>
18. M. Hayashi, *Asymptotic Theory of Quantum Statistical Inference: Selected Papers* (World Scientific, Singapore, 2005). <https://doi.org/10.1142/5630>
19. M. Hayashi, *Quantum Information*, Ch. 6–7 (Springer, Berlin, 2006). <https://doi.org/10.1007/3-540-30266-2>
20. C.W. Helstrom, Phys. Lett. A **25** (1967). [https://doi.org/10.1016/0375-9601\(67\)90366-0](https://doi.org/10.1016/0375-9601(67)90366-0)
21. A.S. Holevo, *Probabilistic and Statistical Aspects of Quantum Theory* (North-Holland, Amsterdam, 1982). <https://doi.org/10.1007/978-88-7642-378-9>
22. D.G. Fischer, M. Freyberger, Phys. Lett. A **273**, 293 (2000). [https://doi.org/10.1016/S0375-9601\(00\)00513-2](https://doi.org/10.1016/S0375-9601(00)00513-2)
23. A. Fujiwara, J. Phys. A Math. Gen. **39**, 12489 (2006). <https://doi.org/10.1088/0305-4470/39/40/014>
24. D.J.C. Bures, Trans. Am. Math. Soc. **135**, 199 (1969). <https://doi.org/10.1090/S0002-9947-1969-0236719-2>
25. V. Giovannetti, S. Lloyd, L. Maccone, Science **306**, 1330 (2004). <https://doi.org/10.1126/science.1104149>
26. V. Giovannetti, S. Lloyd, L. Maccone, Phys. Rev. Lett. **96**, 010401 (2006). <https://doi.org/10.1103/PhysRevLett.96.010401>
27. M. de Burgh, S.D. Bartlett, Phys. Rev. A **72**, 042301 (2005). <https://doi.org/10.1103/PhysRevA.72.042301>
28. Z. Ji, G. Wang, R. Duan, Y. Feng, M. Ying, IEEE Trans. Inf. Theory **54**, 5172 (2008). <https://doi.org/10.1109/TIT.2008.929940>

29. S.F. Huelga, C. Macchiavello, T. Pellizzari, A.K. Ekert, M.B. Plenio, J.I. Cirac, Phys. Rev. Lett. **79**, 3865 (1997). <https://doi.org/10.1103/PhysRevLett.79.3865>
30. R. Chaves, J.B. Brask, M. Markiewicz, J. Kołodyński, A. Acín, Phys. Rev. Lett. **111**, 120401 (2013). <https://doi.org/10.1103/PhysRevLett.111.120401>
31. J. Kołodyński, R. Demkowicz-Dobrzański, Phys. Rev. A **82**, 053804 (2010). <https://doi.org/10.1103/PhysRevA.82.053804>
32. B.M. Escher, R.L. de Matos Filho, L. Davidovich, Nat. Phys. **7**, 406 (2011). <https://doi.org/10.1038/nphys1958>
33. A. De Pasquale, D. Rossini, P. Facchi, V. Giovannetti, Phys. Rev. A **88**, 052117 (2013). <https://doi.org/10.1103/PhysRevA.88.052117>
34. C.M. Caves, Phys. Rev. D **23**, 1693 (1981). <https://doi.org/10.1103/PhysRevD.23.1693>
35. B. Yurke, S.L. McCall, J.R. Klauder, Phys. Rev. A **33**, 4033 (1986). <https://doi.org/10.1103/PhysRevA.33.4033>
36. J.P. Dowling, Phys. Rev. A **57**, 4736 (1998). <https://doi.org/10.1103/PhysRevA.57.4736>
37. S.M. Barnett, C. Fabre, A. Maître, Eur. Phys. J. D **22**, 513 (2003). <https://doi.org/10.1140/epjd/e2003-00003-3>
38. M.A. Taylor, J. Janousek, V. Daria, J. Knittel, B. Hage, H.-A. Bachor, W.P. Bowen, Nat. Photon. **7**, 229 (2013). <https://doi.org/10.1038/nphoton.2012.346>
39. T.M. Stace, Phys. Rev. A **82**, 011611 (2010). <https://doi.org/10.1103/PhysRevA.82.011611>
40. P. Zanardi, P. Giorda, M. Cozzini, Phys. Rev. Lett. **99**, 100603 (2007). <https://doi.org/10.1103/PhysRevLett.99.100603>
41. P. Zanardi, M.G.A. Paris, L.C. Venuti, Phys. Rev. A **78**, 042105 (2008). <https://doi.org/10.1103/PhysRevA.78.042105>
42. H.J.D. Miller<sup>1</sup>, J. Anders. <https://doi.org/10.1038/s41467-018-04536-7>
43. T.M. Stace, A.N. Luiten, Phys. Rev. A **81**, 033848 (2010). <https://doi.org/10.1103/PhysRevA.81.033848>
44. C. Daussy, M. Guinet, A. Amy-Klein, K. Djerroud, Y. Hermier, S. Briaudeau, Ch.J. Bordé, C. Chardonnet, Phys. Rev. Lett. **98**, 250801 (2007). <https://doi.org/10.1103/PhysRevLett.98.250801>
45. G. Casa, A. Castrillo, G. Galzerano, R. Wehr, A. Merlone, D. Di Serafino, P. Laporta, L. Gianfrani, Phys. Rev. Lett. **100**, 200801 (2008). <https://doi.org/10.1103/PhysRevLett.100.200801>
46. G.-W. Truong, J.D. Anstie, E.F. May, T.M. Stace, A.N. Luiten, Nat. Commun. **6**, 8345 (2015). <https://doi.org/10.1038/ncomms9345>
47. A. De Pasquale, D. Rossini, R. Fazio, V. Giovannetti, Nat. Commun. **7**, 12782 (2016). <https://doi.org/10.1038/ncomms12782>
48. A. Uhlmann, Rep. Math. Phys. **9**, 273–279 (1976). [https://doi.org/10.1016/0034-4877\(76\)90060-4](https://doi.org/10.1016/0034-4877(76)90060-4)
49. M.A. Nielsen, I.L. Chuang, *Quantum Computation and Quantum Information* (Cambridge University Press, Cambridge, 2000). <https://doi.org/10.1017/CBO9780511976667>
50. S.L. Braunstein, C.M. Caves, Phys. Rev. Lett. **72**, 3439 (1994). <https://doi.org/10.1103/PhysRevLett.72.3439>
51. C. Gogolin, J. Eisert, Rep. Prog. Phys. **79**, 056001 (2016). <https://doi.org/10.1088/0034-4885/79/5/056001>
52. E. Ising, Zeitschrift für Physik A Hadrons and Nuclei **31**, 253 (1925). <https://doi.org/10.1007/BF02980577>
53. H. Bethe, Zeitschrift für Physik **71**, 205 (1931). <https://doi.org/10.1007/BF01341708>
54. F.-Y. Wu, Rev. Mod. Phys. **54**, 235 (1982). <https://doi.org/10.1103/RevModPhys.54.235>
55. J. Hubbard, Proc. R. Soc. Lond. A Math. Phys. Eng. Sci. **276**, 238 (1963). <https://doi.org/10.1098/rspa.1963.0204>
56. M. Kliesch, C. Gogolin, M. Kastoryano, A. Riera, J. Eisert, Phys. Rev. X **4**, 031019 (2014). <https://doi.org/10.1103/PhysRevX.4.031019>
57. G. De Palma, A. De Pasquale, V. Giovannetti, Phys. Rev. A **95**, 052115 (2017). <https://doi.org/10.1103/PhysRevA.95.052115>

58. P. Zanardi, L. Campos Venuti, P. Giorda, Phys. Rev. A **76**, 062318 (2007). <https://doi.org/10.1103/PhysRevA.76.062318>
59. M. Mehboudi, M. Moreno-Cardoner, G. De Chiara, A. Sanpera, New J. Phys. **17**, 055020 (2015). <https://doi.org/10.1088/1367-2630/17/5/055020>
60. K. Schwab, E.A. Henriksen, J.M. Worlock, M.L. Roukes, Nature (London) **404**, 974 (2000). <https://doi.org/10.1038/35010065>
61. N. Linden, S. Popescu, P. Skrzypczyk, Phys. Rev. Lett. **105**, 130401 (2010). <https://doi.org/10.1103/PhysRevLett.105.130401>
62. B. Klinkert, F. Narberhaus, Cell. Mol. Life Sci. **66**, 2661 (2009). <https://doi.org/10.1007/s00018-009-0041-3>
63. R. Schirhagl, K. Chang, M. Loretz, C.L. Degen, Annu. Rev. Phys. Chem. **65**, 83 (2014). <https://doi.org/10.1146/annurev-physchem-040513-103659>
64. J. Gemmer, M. Michel, G. Mahler, *Quantum Thermodynamics* (Springer, Berlin, 2004). <https://doi.org/10.1007/b98082>
65. M. Campisi, P. Hänggi, P. Talkner, Rev. Mod. Phys. **83**, 771 (2011). Erratum: Rev. Mod. Phys. **83**, 1653 (2011). <https://doi.org/10.1103/RevModPhys.83.771>
66. M. Horodecki, J. Oppenheim, Nat. Commun. **4**, 2059 (2013). <https://doi.org/10.1038/ncomms3059>
67. M. Carrega, P. Solinas, A. Braggio, M. Sassetti, U. Weiss, New J. Phys. **17**, 045030 (2015). <https://doi.org/10.1088/1367-2630/17/4/045030>
68. M. Carrega, P. Solinas, A. Braggio, M. Sassetti, U. Weiss, Phys. Rev. Lett. **116**, 240403 (2016). <https://doi.org/10.1103/PhysRevLett.116.240403>
69. S. Jevtic, D. Newman, T. Rudolph, T.M. Stace, Phys. Rev. A **91**, 012331 (2015). <https://doi.org/10.1103/PhysRevA.91.012331>
70. D. Reeb, M.M. Wolf, IEEE Trans. Inf. Theory **61**, 1458 (2015). <https://doi.org/10.1109/TIT.2014.2387822>
71. L.A. Correa, M. Perarnau-Llobet, K.V. Hovhannisyan, S. Hernández-Santana, M. Mehboudi, A. Sanpera, Phys. Rev. A **96**, 062103 (2017). <https://doi.org/10.1103/PhysRevA.96.062103>
72. P.P. Hofer, J.B. Brask, N. Brunner, [arXiv:1711.09827v2](https://arxiv.org/abs/1711.09827v2)
73. M. Guță, Phys. Rev. A **83**, 062324 (2011). <https://doi.org/10.1103/PhysRevA.83.062324>
74. D. Burgarth, V. Giovannetti, A.N. Kato, K. Yuasa, New J. Phys. **17**, 113055 (2015). <https://doi.org/10.1088/1367-2630/17/11/113055>
75. A. De Pasquale, K. Yuasa, V. Giovannetti, Phys. Rev. A **96**, 012316 (2017). <https://doi.org/10.1103/PhysRevA.96.012316>

**Part IV**

**Thermodynamics of Strongly-Coupled  
Open Systems**

# Chapter 22

## Hamiltonian of Mean Force for Strongly-Coupled Systems



Harry J. D. Miller

### 22.1 Introduction

Despite the many paradigm shifts in physics over the last 150 years, thermodynamics has proved to be one of the most robust physical theories in modern science. While it initially grew out of a necessity to design efficient heat engines in the early 18th century, pioneering work by Boltzmann and Gibbs developed thermodynamics into a fundamental theory which has become crucial to our understanding of irreversibility in nature and the flow of time. As Einstein famously remarked, “Thermodynamics is the only physical theory which I am convinced will never be overthrown, within the framework of applicability of its basic concepts.” [1].

One of those basic concepts is the notion of weak coupling. If we consider a macroscopic three-dimensional body interacting with its environment, then simple intuition suggests that the energy contained in this interaction should be sufficiently negligible. This is because interactions will typically only occur along the body’s surface boundary, involving only a small fraction of the atoms making up the system. Compared with the energy contained in the bulk material this is negligible, and the energetics of the system and environment can be partitioned separately. In the standard formulation of thermodynamics this weak-coupling assumption is crucial for a consistent description of heat flow, as any energy lost by the system during a process can simply be equated to energy dissipated into the environment in the form of heat. In addition to energy, this assumption is directly related to fundamental properties of the thermodynamic entropy and heat capacity, as both quantities become extensive with respect to the volume of the system [2].

While traditionally thermodynamics has always been concerned with describing macroscopic systems consisting of a large number of particles, advancements in nano- and meso-scoptic physics demonstrate that small systems, such as biopolymers

---

H. J. D. Miller (✉)

Department of Physics and Astronomy, University of Exeter, Exeter EX4 4QL, UK  
e-mail: hm419@exeter.ac.uk

and colloidal particles, may exhibit non-trivial thermal behaviour even at sub-micron scales. For example, individual protein molecules can function as tiny motors that convert chemical energy into mechanical work [3], and single strands of RNA that are manipulated using optical tweezers exhibit dissipation and lag much like any macroscopic system governed by the laws of thermodynamics [4]. One may even conceive of quantum thermal machines constructed from individual few-level systems [5], and the analysis regarding the transport of heat and energy at the quantum scale suggests that thermodynamics can be consistently extended beyond the classical, macroscopic setting [6]. At these length scales both stochastic and quantum fluctuations begin to dominate, and current research is now devoted to investigating the potential modifications to thermodynamics that occur at or below the nanoscale.

One major modification is the break-down of the weak coupling approximation. It becomes clear that the heuristic argument used to justify this assumption fails to apply to systems with smaller volumes. If the surface area of the system becomes comparable to its volume then the energetic contributions to the interaction with the environment also become comparable to its own internal energy. When this occurs the thermodynamic properties of the system become dependent on the nature of the interaction, both in and out of equilibrium [7]. One clear example of this behaviour occurs in the collapse transition of a polymer immersed in a solvent, which can become significantly dependent on the structure of the solvent itself rather than just the surrounding temperature [8]. Another example concerns a quantum harmonic oscillator in a black-body radiation field, whereby the free energy of the oscillator shifts by a temperature and coupling-dependent term due to a non-vanishing dipole interaction with the field [9].

In such situations special care needs to be taken when defining notions of heat, work and entropy, as the thermal properties of these small systems cannot generally be determined simply by their respective internal Hamiltonians. It will be shown that this issue stems from the fact that the equilibrium configuration of the system can deviate from the familiar Gibbs distribution when interactions are non-negligible. This invalidates the usual formulas used to compute the associated thermodynamic potentials, such as the free energy, as these are derived from the assumption that the equilibrium state of the system is of Gibbs form. This of course does not mean that thermodynamics breaks down. Instead, one can construct alternative thermodynamic potentials via an effective operator or function known as the *Hamiltonian of mean force* (HMF). Much like standard methods in statistical mechanics, this mathematical object can be used to compute an effective partition function for the system, which provides the basis for defining the system's free energy and all resulting equilibrium properties. This effective description of the system in terms of the modified partition function dates back to the early work of Kirkwood in his analysis of the statistical properties of fluid mixtures [10]. Here we will discuss the role played by the HMF in extending thermodynamics beyond the weak-coupling regime in both quantum and classical settings. We will see that the HMF provides a consistent generalisation of the laws of thermodynamics and fluctuation relations, and can be used to define entropy production for out-of-equilibrium processes.

## 22.2 The Equilibrium State at Strong Coupling

In standard thermodynamics it is customary to describe the equilibrium state of a system  $\mathcal{S}$  in contact with a large reservoir  $\mathcal{R}$  at inverse temperature  $\beta = T^{-1}$  by the canonical Gibbs state,  $\hat{\pi}_\mathcal{S}^{(c)} = e^{-\beta \hat{H}_\mathcal{S}} / Z_\mathcal{S}$ . Here  $\hat{H}_\mathcal{S}$  is the internal Hamiltonian,  $Z_\mathcal{S} = \text{tr}_\mathcal{S}[e^{-\beta \hat{H}_\mathcal{S}}]$  is the partition function and we have set the Boltzmann constant to unity [2]. However, this description of the system and its associated thermodynamic potentials can only be justified if one neglects the interactions between the system and its surroundings. This issue becomes apparent when we consider the structure of the global equilibrium state of the system and reservoir, which we denote by  $\hat{\pi}_{\mathcal{S}\cup\mathcal{R}}$ . Without loss of generality the total Hamiltonian of  $\mathcal{S} \cup \mathcal{R}$  can be expressed in the form

$$\hat{H}_{\mathcal{S}\cup\mathcal{R}} := \hat{H}_\mathcal{S} \otimes \hat{\mathbb{I}}_\mathcal{R} + \hat{\mathbb{I}}_\mathcal{S} \otimes \hat{H}_\mathcal{R} + \gamma \hat{V}_{\mathcal{S}\cup\mathcal{R}}, \quad (22.1)$$

where  $\hat{H}_\mathcal{R}$  is the Hamiltonian of the reservoir  $\mathcal{R}$ ,  $\hat{V}_{\mathcal{S}\cup\mathcal{R}}$  is an arbitrary interaction term shared between  $\mathcal{S}$  and  $\mathcal{R}$  and  $\gamma$  is a scalar parameter quantifying the relative strength of the interaction. Formally if one considers  $\mathcal{S} \cup \mathcal{R}$  to be isolated with a fixed total energy  $U_{\mathcal{S}\cup\mathcal{R}}$  then the composite state is best described by the micro-canonical ensemble  $\hat{\pi}_{\mathcal{S}\cup\mathcal{R}} \propto \delta(U_{\mathcal{S}\cup\mathcal{R}} - \hat{H}_{\mathcal{S}\cup\mathcal{R}})$ , with inverse temperature  $\beta = \partial S_{\mathcal{S}\cup\mathcal{R}} / \partial U_{\mathcal{S}\cup\mathcal{R}}$  and  $S_{\mathcal{S}\cup\mathcal{R}}$  the thermodynamic entropy [11]. However, by imposing reasonable macroscopic conditions on the reservoir and taking the thermodynamic limit, we can safely replace the micro-canonical ensemble with the canonical one due to ensemble equivalence, so that  $\hat{\pi}_{\mathcal{S}\cup\mathcal{R}} = e^{-\beta \hat{H}_{\mathcal{S}\cup\mathcal{R}}} / Z_{\mathcal{S}\cup\mathcal{R}}$  with  $Z_{\mathcal{S}\cup\mathcal{R}} = \text{tr}_{\mathcal{S}\cup\mathcal{R}}[e^{-\beta \hat{H}_{\mathcal{S}\cup\mathcal{R}}}]$  [12]. By taking the partial trace over  $\mathcal{R}$ , the state of the system at equilibrium is given by  $\hat{\pi}_\mathcal{S} = \text{tr}_\mathcal{R}[\hat{\pi}_{\mathcal{S}\cup\mathcal{R}}]$ , which can be expressed in the following form:

$$\hat{\pi}_\mathcal{S} = \frac{e^{-\beta \hat{H}_\mathcal{S}^*}}{Z_\mathcal{S}^*}; \quad Z_\mathcal{S}^* := \text{tr}_\mathcal{S}[e^{-\beta \hat{H}_\mathcal{S}^*}], \quad (22.2)$$

where

$$\hat{H}_\mathcal{S}^* := -\frac{1}{\beta} \ln \left( \frac{\text{tr}_\mathcal{R}[e^{-\beta \hat{H}_{\mathcal{S}\cup\mathcal{R}}}]}{\text{tr}_\mathcal{R}[e^{-\beta \hat{H}_\mathcal{R}}]} \right), \quad (22.3)$$

is known as the *Hamiltonian of mean force* [13–15]. This operator can be interpreted as an effective Hamiltonian describing  $\mathcal{S}$ , and unlike the bare Hamiltonian  $\hat{H}_\mathcal{S}$ , it implicitly depends on both the temperature  $T$  and interaction  $\hat{V}_{\mathcal{S}\cup\mathcal{R}}$ .

Before we discuss the thermodynamic role played by the HMF, it is worth analysing the dynamical models in which the state (22.2) emerges. The clearest example occurs in the paradigmatic model of Quantum Brownian Motion (QBM) [16–18]. In such a situation one wishes to construct a microscopic model for  $\mathcal{S} \cup \mathcal{R}$  that reproduces a quantum Langevin equation, which is an equation that describes the motion of a damped oscillator in contact with a thermal environment. One particular

model describing QBM, attributed to Caldeira and Leggett [16], consists of a single oscillator  $\mathcal{S}$  linearly coupled to a collection of  $N$  harmonic oscillators that make up the reservoir  $\mathcal{R}$ , and the respective Hamiltonians in (22.1) are given by

$$\hat{H}_{\mathcal{S}} := \frac{\hat{P}_0^2}{2m_0} + \frac{m_0\omega_0^2}{2}\hat{X}_0^2, \quad \hat{H}_{\mathcal{R}} := \sum_{i=1}^N \left[ \frac{\hat{P}_i^2}{2m_i} + \frac{m_i\omega_i^2}{2}\hat{X}_i^2 \right], \quad (22.4)$$

The interaction term is generically expressed in the linear form

$$\hat{V}_{\mathcal{S} \cup \mathcal{R}} := \sum_{i=1}^N \left[ \left( \frac{\gamma_i^2}{2m_i\omega_i^2} \right) \hat{X}_0 - \gamma_i \hat{X}_0 \otimes \hat{X}_i \right]. \quad (22.5)$$

Here the position and momentum operators are given by  $(\hat{X}_0, \hat{P}_0)$  for  $\mathcal{S}$  and  $(\hat{X}_i, \hat{P}_i)$  for the  $i$ 'th oscillator in  $\mathcal{R}$ , while  $\gamma_i = \gamma C_i$  denotes the coupling constant between the system and each oscillator in the reservoir. Similarly  $(m_0, \omega_0)$  and  $(m_i, \omega_i)$  denote the mass and frequencies of the respective oscillators in  $\mathcal{S}$  and  $\mathcal{R}$ . To accurately model the reservoir one takes the thermodynamic limit  $N \rightarrow \infty$ , and  $\mathcal{R}$  becomes characterised by an Ohmic spectral density function. Examples of open quantum systems that can be modelled by (22.4) are nanoscale resonators, such as those manipulated in recent quantum control experiments [19]. We remark here that one may construct alternative Hamiltonians that describe QBM, such as the continuum approach adopted in the Huttner–Barnett model, whose thermodynamic properties are explored in [20].

Let us now suppose that prior to interactions the system and reservoir are uncoupled, so that the initial state at time  $t = 0$  is of the form  $\hat{\rho}_{\mathcal{S} \cup \mathcal{R}}(0) := \hat{\rho}_{\mathcal{S}}(0) \otimes \hat{\pi}_{\mathcal{R}}^{(c)}$ , where  $\hat{\rho}_{\mathcal{S}}(0)$  is an arbitrary state of  $\mathcal{S}$  and the reservoir is assumed to be in canonical equilibrium with respect to  $\hat{H}_{\mathcal{R}}$  at inverse temperature  $\beta$ . The benefit of the QBM model is that it is linear, and so the dynamics can be solved through an exact master equation governing the Wigner function of the system, regardless of the strength of the coupling  $\gamma$  [18]. Note that in the high temperature limit the model is equivalent to the classical Fokker-Planck process for a damped harmonic oscillator [17]. Solving the master equation and taking the asymptotic time limit one finds that the steady state of the system is indeed given by the reduced canonical state, so that  $\lim_{t \rightarrow \infty} \hat{\rho}_{\mathcal{S}}(t) = \text{tr}_{\mathcal{R}}[\hat{\pi}_{\mathcal{S} \cup \mathcal{R}}]$  [17]. The corresponding stationary Wigner function turns out to be of Gaussian form, and thus the resulting HMF for  $\mathcal{S}$  takes the form of an effective harmonic oscillator:

$$\hat{H}_{\mathcal{S}}^* = \frac{\hat{P}_0^2}{2m_*} + \frac{m_*\omega_*^2}{2}\hat{X}_0^2, \quad (22.6)$$

where  $m_* = m_*(\beta, \gamma)$  and  $\omega_* = \omega_*(\beta, \gamma)$  represent an effective mass and frequency of the oscillator that explicitly depend on both the temperature of  $\mathcal{R}$  and the strength of the interaction. In turn these terms can be computed from the equilibrium averages of the squared position and momentum of  $\mathcal{S}$ , since

$$\omega_*(\beta, \gamma) = \frac{2}{\beta \hbar} \operatorname{arccoth} \left( \frac{2}{\hbar} \langle \hat{P}_0^2 \rangle \langle \hat{X}_0^2 \rangle \right), \quad m_*(\beta, \gamma) = \omega_*^{-1} \sqrt{\frac{\langle \hat{P}_0^2 \rangle}{\langle \hat{X}_0^2 \rangle}}. \quad (22.7)$$

Though not explicitly stated here, the quadratures  $\langle \hat{X}_0^2 \rangle$  and  $\langle \hat{P}_0^2 \rangle$  have a complicated dependence of  $\gamma$  and  $\beta$ , and it may be shown that one only recovers the bare mass and frequency  $m_*(\beta, \gamma) = m_0$  and  $\omega_*(\beta, \gamma) = \omega_0$  if  $\gamma \ll 1$  [17]. This clearly demonstrates that the presence of the finite coupling modifies the equilibrium properties of the system, as its mass and frequency become explicitly dependent on the interaction with the reservoir.

For a generic system-reservoir interaction model satisfying the weak-coupling approximation  $\gamma \ll 1$ , a standard textbook calculation shows that  $\hat{H}_S^* \simeq \hat{H}_S$  and the state of the system reduces to the familiar canonical ensemble,  $\hat{\pi}_S \simeq \hat{\pi}_S^{(c)}$  [2]. Furthermore, in this regime correlations between  $S$  and  $R$  can be neglected and the total state factorises into  $\hat{\pi}_{S \cup R} \simeq \hat{\pi}_S^{(c)} \otimes \hat{\pi}_R^{(c)}$ , where  $\hat{\pi}_R^{(c)} = e^{-\beta \hat{H}_R} / Z_R$  and  $Z_R = \operatorname{tr}_R[e^{-\beta \hat{H}_R}]$  is the partition function for the reservoir in the absence of any coupling to  $S$  [21]. It is in this limit at which standard thermodynamics is formulated, and we can identify the energies of  $S$  and  $R$  with their bare Hamiltonians. This leads to a consistent notion of heat; any energy gained by  $R$  is the energy lost by  $S$  [21]. There are also notable cases where we can recover the usual Gibbs distribution even when  $\gamma$  is non-negligible. One example is if the interaction Hamiltonian is constructed from a random-matrix ensemble, in which case it can be rigorously proven that  $\hat{H}_S^* \simeq \hat{H}_S$  regardless of the strength of interaction [22]. Heuristically, due to the random nature of the interaction its influence on  $S$  effectively averages out to zero. For spin and fermionic lattice systems, one can recover the local Gibbs state above a certain critical temperature, at which point correlations between the system and its surroundings decay exponentially [23].

However, in the general case where  $\gamma$  is non-negligible the system remains correlated with  $R$  and its thermodynamic properties are modified through the additional dependence on the coupling. It has been shown that the reduced Gibbs state (22.2) becomes the steady-state solution in more general non-linear system-reservoir interaction models, assuming an initial thermal reservoir uncorrelated with  $S$  [24]. In addition to QBM models, results based on typicality also demonstrate that the equilibrium state (22.2) emerges dynamically out of global pure state evolution for arbitrary interaction strengths [25]. Overall these results clearly motivate the need to generalise thermodynamics beyond weak coupling and canonical equilibrium, and we will see that the HMF provides the theoretic tool to achieve this.

## 22.3 Effective Thermodynamic Potentials

In statistical mechanics the partition function encodes information about how the occupation probabilities are distributed between the different micro-states of  $S$ , and it can be used to calculate the relevant thermodynamic potentials such as the free

energy, internal energy and entropy. For a state in canonical equilibrium  $\hat{\pi}_S^{(c)}$ , the free energy of  $S$  is given by  $F_S^{(c)} = U_S^{(c)} - TS_S^{(c)}$ , with  $U_S^{(c)} = \text{tr}_S[\hat{\pi}_S^{(c)} \hat{H}_S]$  the average internal energy and  $S_S^{(c)} = -\text{tr}_S[\hat{\pi}_S^{(c)} \ln \hat{\pi}_S^{(c)}]$  the von–Neumann entropy. From an information-theoretic perspective the canonical state represents the best possible guess for the configuration of  $S$  given prior knowledge of the system’s energy, as it maximises the the information entropy given a fixed average energy according to the Maximum Entropy principle [26]. We can compute the free energy through knowledge of  $Z_S$  since  $F_S^{(c)} := -\frac{1}{\beta} \ln Z_S$ , and similar expressions follow for  $U_S^{(c)}$  and  $S_S^{(c)}$ .

On the other hand, in the strong-coupling regime we obtain the alternative partition function  $\mathcal{Z}_S^*$ . This motivates the following definition for the generalised free energy of the system for finite  $\gamma$ :

$$F_S := -\frac{1}{\beta} \ln \mathcal{Z}_S^*. \quad (22.8)$$

Of course this definition of free energy requires further justification. Jarzynski has shown that the reversible work required to drive a system quasi-statically through a series of equilibrium states at strong-coupling is exactly given by the change in the free energy function (22.8) [13]. To see this let us parameterise the bare Hamiltonian of the system in (22.1) with some control parameter  $\lambda$ , so that  $\hat{H}_S = \hat{H}_S(\lambda)$ . For example, if our system is composed of a collection of spins then  $\lambda$  could denote the strength of an applied magnetic field. Now we assume that the parameter is smoothly varied in time between two values  $\lambda_A \rightarrow \lambda_B$ , such that the system always remains in the state (22.2) throughout the process whilst strongly interacting with  $\mathcal{R}$ . Then the free energy change, denoted  $\Delta F_S := F_S(\lambda_B) - F_S(\lambda_A)$ , can be expressed as

$$\Delta F_S = \int_A^B d\lambda \left\langle \frac{\partial \hat{H}_S(\lambda)}{\partial \lambda} \right\rangle_{\lambda}^{\text{eq}}, \quad (22.9)$$

where  $\langle \dots \rangle_{\lambda}^{\text{eq}}$  denotes the expectation value with respect to the state (22.2) at some fixed value of  $\lambda$ . As the process is quasi-static and only the system degrees of freedom are controlled, (22.9) is nothing but the integrated power over time, or equivalently the integrated rate of change of total energy. This means we can equate  $\Delta F_S = \langle W \rangle$ , where  $\langle W \rangle$  is the work done on the system. Crucially this remains consistent with the usual thermodynamic definition of free energy, which quantifies the system’s ability to perform work. We will later see that this notion of free energy can also be applied to more general non-equilibrium processes, in which case one can derive a statement about the second law of thermodynamics at strong coupling.

With the definition of free energy established we can also obtain the respective thermodynamic entropy and internal energy of the strongly-coupled system, which are each related to the free energy according to

$$S_S := \beta^2 \frac{\partial F_S}{\partial \beta}, \quad U_S := \frac{\partial (\beta F_S)}{\partial \beta}. \quad (22.10)$$

We remark that these definitions satisfy the usual relation  $F_s = U_s - TS_s$  which means the thermodynamic potentials are related via the Legendre transform in the usual way. It can be shown that the partition function for  $\mathcal{S}$  can be expressed as the ratio  $\mathcal{Z}_s^* = \mathcal{Z}_{s\cup\mathcal{R}}/\mathcal{Z}_{\mathcal{R}}$ , which implies the following additive relation for the thermodynamic potentials [27]:

$$\chi_s = \chi_{s\cup\mathcal{R}}^{(c)} - \chi_{\mathcal{R}}^{(c)}, \quad (22.11)$$

where  $\chi = F, S, U$ . In other words, each potential for the system is equivalent to the difference between the potential for the total canonical state of  $\mathcal{S} \cup \mathcal{R}$  and the isolated canonical state of  $\mathcal{R}$ . This additivity offers an intuitive interpretation of the expressions for  $F_s, S_s, U_s$ . For example, the free energy  $F_s$  represents the reversible work required to immerse  $\mathcal{S}$  into the composite state in  $\mathcal{S} \cup \mathcal{R}$ , which of course is given by the change in total free energy  $F_{s\cup\mathcal{R}}^{(c)} - F_{\mathcal{R}}^{(c)}$  expressed in (22.11) [7]. We remark here that this definition of internal energy leads to a consistent derivation of the Casimir effect in quantum electrodynamics, where the energy of the electromagnetic field is obtained by subtracting the contributions of the decoupled reservoir fields from the total energy [28].

Since the free energy, entropy and internal energies are defined through the partition function, they are essentially average quantities associated to the thermodynamic ensemble. However, one can also consider the corresponding operator expressions. Let us first note that the derivative of the exponential operator  $e^{-\beta\hat{H}_s^*}$  can be expanded as [29]

$$\partial_\beta e^{-\beta\hat{H}_s^*} := - \int_0^1 ds e^{-(1-s)\beta\hat{H}_s^*} [\partial_\beta(\beta\hat{H}_s^*)] e^{-s\beta\hat{H}_s^*}. \quad (22.12)$$

Denoting expectation values by  $\langle (\dots) \rangle^{\text{eq}} = \text{tr}[(\dots)\hat{\pi}_s]$  and using (22.12), the internal energy  $U_s = -\partial_\beta \ln \mathcal{Z}_s^*$  can thus be rewritten as [27, 30]:

$$U_s = \langle \hat{E}_s^* \rangle^{\text{eq}}; \quad \hat{E}_s^* := \partial_\beta(\beta\hat{H}_s^*). \quad (22.13)$$

Thus we can interpret  $\hat{E}_s^*$  as the internal energy operator for the strongly-coupled system. As discussed in [30], this operator is not equivalent to  $\hat{H}_s^*$  due to the additional term  $\partial_\beta\hat{H}_s^*$  in (22.13). It is only in exceptional cases where the HMF becomes temperature-independent, such as in the bilinear coupling model for Brownian motion formulated in [31], that one has  $\hat{E}_s^* \simeq \hat{H}_s^*$ . In general this in-equivalence has interesting quantum-mechanical consequences, as it implies that the temperature-dependence of the HMF is responsible for the presence of energy coherences in the equilibrium state [30]. This follows from the fact that in general, one has  $[\hat{E}_s^*, \hat{\pi}_s] \neq 0$  outside of the weak-coupling limit, leading to additional quantum uncertainty in the energy. One notable consequence of this is that the fluctuations in internal energy are generally not accessible via projective measurements of the operator  $\hat{E}_s^*$ , as these measurements remove coherences with respect to this observable and disturb the

evolution of the system. The thermodynamic implications of this fact remain to be explored.

Turning to the entropy, it can be similarly shown that

$$S_s = -\langle \ln \hat{\pi}_s \rangle^{\text{eq}} + \beta^2 \langle \partial_\beta \hat{H}_s^* \rangle^{\text{eq}}. \quad (22.14)$$

We recognise the first contribution as the von-Neumann entropy for the system, while the second term again stems from the temperature-dependence of the HMF. This implies that the thermodynamic entropy is not generally equivalent to the information contained in the equilibrium state when interactions are present. However, we can obtain a connection to information theory by looking at the expression for the free energy. This is determined by simply combining (22.13) and (22.14) to give  $F_s = \langle \hat{H}_s^* \rangle^{\text{eq}} + \beta^{-1} \langle \ln \hat{\pi}_s \rangle^{\text{eq}}$ . We can use this to introduce the non-equilibrium free energy of an arbitrary quantum state. Let us denote  $\langle \dots \rangle = \text{tr}[(\dots) \hat{\rho}_s]$  as the expectation value with respect to some state  $\hat{\rho}_s$ . Then the non-equilibrium free energy  $\tilde{F}_s$  with respect to inverse temperature  $\beta$  is defined as

$$\tilde{F}_s := \langle \hat{H}_s^* \rangle + \beta^{-1} \langle \ln \hat{\rho}_s \rangle. \quad (22.15)$$

A simple calculation then shows that the equilibrium and non-equilibrium free energies are related to each other via the following expression:

$$\tilde{F}_s = F_s + S(\hat{\rho}_s || \hat{\pi}_s), \quad (22.16)$$

where

$$S(\hat{\rho}_s || \hat{\pi}_s) := \text{tr}[\hat{\rho}_s \ln \hat{\rho}_s] - \text{tr}[\hat{\rho}_s \ln \hat{\pi}_s], \quad (22.17)$$

is the *quantum relative entropy*. The relative entropy is a state distinguishability measure and here quantifies the additional information needed to specify the non-equilibrium state. Note from the positivity of the relative entropy one has  $\tilde{F}_s \geq F_s$  for any state  $\hat{\rho}_s$ . From (22.16) we conclude that the equilibrium state  $\hat{\pi}_s$  minimises the free energy function  $\tilde{F}_s$ , much like the standard definition of the non-equilibrium free energy in the thermodynamics of weakly-coupled systems [32].

## 22.4 Specific Heat Capacity

The specific heat capacity  $C_s$  of a thermal system at constant volume quantifies the susceptibility of the system to change its energy with respect to variations in temperature, and is formally defined as

$$C_s := \frac{\partial U_s}{\partial T}. \quad (22.18)$$

In the weak-coupling limit it is well known that  $C_s$  is proportional to the variance in internal energy, i.e.,  $C_s = \beta^2 \Delta U_s^2$  [2]. This standard result is a form of fluctuation-dissipation relation; the rate of change of the system's energy with temperature is directly linked to the resulting energy fluctuations at equilibrium. Notably since the variance of a random variable is strictly non-negative, this implies  $C_s \geq 0$ . This result tells us a basic fact about systems in thermal equilibrium, namely that heating up the system will increase its energy.

On the other hand, for finite coupling  $\gamma$  there are open quantum systems that may exhibit a negative specific heat at low temperatures, meaning that the fluctuation-dissipation relation cannot generally hold in this regime. Examples of such systems are the one-dimensional isotropic XY spin chain [33], a damped free particle [34], and a qubit coupled to a single bath resonator [35]. While perhaps unintuitive, the fact that  $C_s < 0$  is permissible implies that there are regions of temperature for which the system's energy actually increases as it is cooled down. The reason that one may obtain a negative heat capacity is because coupling the system to the reservoir may actually decrease the overall heat capacity due to the presence of non-vanishing interactions [34]. Analogously to (22.11), the heat capacity also satisfies the following additive relation:

$$C_s = C_{S\cup R}^{(c)} - C_R^{(c)}, \quad (22.19)$$

which clearly shows that  $C_s$  can be negative if the total heat capacity decreases when the system is immersed in the reservoir.

While the standard fluctuation-dissipation relation is not generally fulfilled for finite  $\gamma$ , one can still derive a relation between the heat capacity and fluctuations in energy [30]. Let us denote the variance in the internal energy by  $\Delta U_s^2 = \langle (\delta \hat{E}_s^*)^2 \rangle^{\text{eq}}$  with  $\delta \hat{E}_s^* = \hat{E}_s^* - \langle \hat{E}_s^* \rangle^{\text{eq}}$ . It can be proven that the following modified fluctuation-dissipation relation holds [30]:

$$C_s = \beta^2 \Delta U_s^2 - \beta^2 Q_s[\hat{E}_s^*, \hat{\pi}_s] + \langle \partial_\tau \hat{E}_s^* \rangle^{\text{eq}}, \quad (22.20)$$

where

$$Q_s[\hat{E}_s^*, \hat{\pi}_s] := -\frac{1}{2} \int_0^1 d\alpha \text{tr}_s[[\hat{E}_s^*, \hat{\pi}_s^\alpha][\hat{E}_s^*, \hat{\pi}_s^{1-\alpha}]], \quad (22.21)$$

is known as the *average Wigner-Yanase-Dyson skew information* with respect to the observable  $\hat{E}_s^*$  [36]. This function quantifies the quantum fluctuations in energy, which are separated from contributions to the total variance due to classical mixing. In other words, the first correction term  $Q_s[\hat{E}_s^*, \hat{\pi}_s]$  stems from the non-commutativity between the energy operator  $\hat{E}_s^*$  and the system's equilibrium state  $\hat{\pi}_s$ . In addition to this, the second correction term  $\langle \partial_\tau \hat{E}_s^* \rangle^{\text{eq}}$  quantifies the temperature dependence of  $\hat{E}_s^*$ , and clearly remains in the classical limit. Note that in the weak coupling limit one has  $\hat{E}_s^* \simeq \hat{H}_s$ , and thus the correction terms vanish, meaning the heat capacity simply becomes proportional to the energy variance as expected [30].

## 22.5 Work Fluctuation Relations at Strong-Coupling

Thus far we have only considered the properties of static equilibrium states of the form (22.2). However, the HMF also plays an important role in the description of processes operating away from equilibrium. The celebrated work fluctuation relations refine the standard laws of thermodynamics for states driven out of equilibrium [37]. It will be shown in this section that the HMF and its associated free energy function (22.8) can be used to generalise both the Crooks relation [38] and the Jarzynski equality [39] in the strong-coupling regime, and in turn arrive at an expression for the second law of thermodynamics valid at all coupling strengths.

To see this suppose that the Hamiltonian of  $\mathcal{S}$  is varied in time according to  $\hat{H}_\mathcal{S}(t)$  over the interval  $t \in [t_i, t_f]$ , and assume that the initial state of  $\mathcal{S} \cup \mathcal{R}$  is in a global canonical equilibrium state. We also denote  $\hat{H}_{\mathcal{S} \cup \mathcal{R}} = \hat{H}_{\mathcal{S} \cup \mathcal{R}}(t)$ ,  $\mathcal{Z}_\mathcal{S}^* = \mathcal{Z}_\mathcal{S}^*(t)$  and  $\hat{\pi}_{\mathcal{S} \cup \mathcal{R}}(t)$  with the variable  $t$  due to the fact that  $\hat{H}_\mathcal{S}(t)$  depends on time. It is assumed that  $\mathcal{S}$  remains strongly coupled to  $\mathcal{R}$  throughout the evolution, with the interaction  $\hat{V}_{\mathcal{S} \cup \mathcal{R}}$  held fixed. Due to the change in the total Hamiltonian, work is done on the system and it is driven away from equilibrium. The resulting unitary for driving of the Hamiltonian is given by

$$\hat{U}_{t_i \rightarrow t_f} := \exp \left[ -\frac{i}{\hbar} \int_{t_i}^{t_f} dt \hat{H}_{\mathcal{S} \cup \mathcal{R}}(t) \right] \quad (22.22)$$

Furthermore let us denote the instantaneous spectral decomposition of the total Hamiltonian by

$$\hat{H}_{\mathcal{S} \cup \mathcal{R}}(t) = \sum_n \epsilon_n(t) |\epsilon_n(t)\rangle \langle \epsilon_n(t)|. \quad (22.23)$$

For a single run of the process, the work done on the system is a fluctuating variable and is given by the change in total energy after projecting onto the energy basis of the joint system and reservoir at times  $t_i$  and  $t_f$  [40]. The resulting work probability distribution is thus given by the following:

$$\vec{P}(W) := \sum_{n,m} \delta[W - \epsilon_m(t_f) + \epsilon_n(t_i)] P[\epsilon_m(t_f)|\epsilon_n(t_i)] P[\epsilon_n(t_i)], \quad (22.24)$$

where

$$P[\epsilon_n(t_i)] := \langle \epsilon_n(t_i) | \hat{\pi}_{\mathcal{S} \cup \mathcal{R}}(t_i) | \epsilon_n(t_i) \rangle; \quad P[\epsilon_m(t_f)|\epsilon_n(t_i)] := |\langle \epsilon_m(t_f) | \hat{U}_{t_i \rightarrow t_f} | \epsilon_n(t_i) \rangle|^2. \quad (22.25)$$

It is assumed that after time  $t_f$  the total system is allowed to reach equilibrium with respect to Hamiltonian  $\hat{H}_{\mathcal{S} \cup \mathcal{R}}(t_f)$ . During this thermalisation process no work is done as the Hamiltonian is kept constant. Let us now compare these statistics

with a hypothetical process moving backwards in time. In this case the Hamiltonian is driven back to its original configuration, and assuming time-reversal invariance this generates the unitary  $\hat{U}_{t_f \rightarrow t_i} = \hat{U}_{t_i \rightarrow t_f}^\dagger$ . The work distribution for the backwards process is given by

$$\overleftarrow{P}(W) := \sum_{n,m} \delta[W + \epsilon_m(t_f) - \epsilon_n(t_i)] P[\epsilon_m(t_f)|\epsilon_n(t_i)] P[\epsilon_n(t_f)], \quad (22.26)$$

where  $P[\epsilon_n(t_f)] = \langle \epsilon_n(t_f) | \hat{\pi}_{S \cup R}(t_f) | \epsilon_n(t_f) \rangle$  and we note that the conditional probability to observe an energy transition along the backwards process is equal to the forward probability due to the unitarity of the evolution. Campisi et al. [15] prove that the Crooks relation and Jarzynski equality remain valid regardless of the coupling strength:

$$\frac{\overrightarrow{P}(+W)}{\overleftarrow{P}(-W)} = e^{\beta(W - \Delta F_S)}; \quad \langle e^{-\beta W} \rangle = e^{-\beta \Delta F_S}, \quad (22.27)$$

where  $\Delta F_S = -\beta^{-1} \ln \mathcal{Z}_S^*(t_f)/\mathcal{Z}_S^*(t_i)$  is the change in equilibrium free energy. As expected these relations also hold true in the classical limit [13].

Through the use of the Jensen inequality, the Jarzynski equality (22.27) leads to the bound  $\langle W \rangle \geq \Delta F_S$ . This can be interpreted as a statement of the second law of thermodynamics; *one cannot extract more work from a system than the associated decrease in free energy*. The crucial point here is that this form of the second law and fluctuation relation are directly expressed in terms of the chosen free energy definition (22.8), which was defined through the effective partition function  $\mathcal{Z}_S^*$  that depends on the coupling to the reservoir.

## 22.6 Entropy Production and Effective Potentials Away from Equilibrium

In the previous section we considered states that are driven away from initial global canonical equilibrium. However, one may go a step further and derive fluctuation relations for more general processes involving transitions between different non-equilibrium states [27, 41]. The caveat here is that we will restrict our attention to classical systems, which are described in terms of phase space rather than operators on a Hilbert space. We begin by considering the following global Hamiltonian *function* analogous to (22.1), that depends on some external time-dependent parameter  $\lambda_t$ :

$$H_{S \cup R}(z_t; \lambda_t) := H_S(x_t; \lambda_t) + H_R(y_t) + \gamma V_{S \cup R}(z_t), \quad (22.28)$$

where  $z_t = (x_t, y_t)$  denotes the collective phase-space coordinate of  $\mathcal{S}$  and  $\mathcal{R}$  respectively at time  $t$ . Denote the global canonical state with respect to a fixed value of  $\lambda_t$  by

$$\pi_{\mathcal{S} \cup \mathcal{R}}^{(c)}(z_t; \lambda_t) = \frac{1}{Z_{\mathcal{S} \cup \mathcal{R}}(\lambda_t)} e^{-\beta H_{\mathcal{S} \cup \mathcal{R}}(z_t; \lambda_t)}. \quad (22.29)$$

Analogous to the quantum HMF (22.3), the corresponding *classical* HMF for  $\mathcal{S}$  can be expressed as

$$H_{\mathcal{S}}^*(x_t; \lambda_t) := H_{\mathcal{S}}(x_t; \lambda_t) - \frac{1}{\beta} \ln \langle e^{-\beta \gamma V_{\mathcal{S} \cup \mathcal{R}}(z_t)} \rangle_{\mathcal{R}}^{\text{eq}}, \quad (22.30)$$

where  $\langle [..] \rangle_{\mathcal{R}}^{\text{eq}} = \int dy_t \pi_{\mathcal{R}}^{(c)}(y_t)[..]$  represents an average with respect to the canonical state of the reservoir in the absence of any coupling. Here in the classical case we can interpret the additional contribution to the Hamiltonian in (22.30) as the work required to turn on the interaction for a fixed configuration of  $\mathcal{S}$  [7].

We will now restrict our attention to a class of non-equilibrium states in  $\mathcal{S} \cup \mathcal{R}$ , denoted  $\sigma_{\mathcal{S} \cup \mathcal{R}}(z_t) \in \mathcal{N}_{\beta}$ , referred to as the *stationary preparation class* with respect to inverse temperature  $\beta$  [42]. These states take the following form:

$$\sigma_{\mathcal{S} \cup \mathcal{R}}(z_t; t) := \rho_{\mathcal{S}}(x_t; t) \pi_{\mathcal{R}}(y_t|x_t); \quad \pi_{\mathcal{R}}(y_t|x_t) := \frac{\pi_{\mathcal{S} \cup \mathcal{R}}^{(c)}(z_t; \lambda_t)}{\int dx_t \pi_{\mathcal{S} \cup \mathcal{R}}^{(c)}(z_t; \lambda_t)}. \quad (22.31)$$

Here the state of  $\mathcal{S}$  is arbitrary, whilst the reservoir behaves as if the whole configuration is in canonical equilibrium conditioned on some micro-state of  $\mathcal{S}$ , which simply follows from Bayes' theorem. Note that this conditional probability is independent of  $\lambda_t$ . From a dynamical perspective, it can be shown that the set of states (22.31) naturally emerge if the thermalisation time-scale of  $\mathcal{R}$  is much faster than that of  $\mathcal{S}$ , as shown by Strassberg and Esposito in [43]. In the weak coupling limit, (22.31) reduces to the uncorrelated state  $\rho_{\mathcal{S}}(x_t; t)\pi_{\mathcal{R}}^{(c)}(y_t)$  whilst for finite coupling  $\gamma$  the system and reservoir remain correlated.

Suppose now that  $\mathcal{S} \cup \mathcal{R}$  is initialised in some state  $\sigma_{\mathcal{S} \cup \mathcal{R}}(z_{t_i}; t_i) \in \mathcal{N}_{\beta}$  at time  $t_i$ , and is subsequently driven via changing the parameter  $\lambda_t$  to some final configuration  $\rho_{\mathcal{S} \cup \mathcal{R}}(z_{t_f}; t_f)$  at later time  $t_f > t_i$ . As before it is assumed the global evolution is closed and governed by  $\partial_t \rho_{\mathcal{S} \cup \mathcal{R}}(z_t; t) = \mathcal{L}[\rho_{\mathcal{S} \cup \mathcal{R}}(z_t; t)]$ , where  $\mathcal{L}[(..)]$  is the Liouvillean determined by Hamilton's classical equations of motion. For a generic process operating away from equilibrium, with  $\mathcal{S}$  coupled to  $\mathcal{R}$  at inverse temperature  $\beta$ , the entropy and internal energy of  $\mathcal{S}$  undergo stochastic fluctuations. These fluctuating non-equilibrium potentials can be defined via the HMF in analogy to the operator expressions given in (22.13) and (22.14) [27], so that

$$\tilde{u}_{\mathcal{S}}(x_t; \lambda_t) := \partial_{\beta}[\beta H_{\mathcal{S}}^*(x_t; \lambda_t)], \quad (22.32)$$

$$\tilde{s}_{\mathcal{S}}(x_t; \lambda_t) := -\ln \rho_{\mathcal{S}}(x_t; t) + \beta^2 \partial_{\beta} H_{\mathcal{S}}^*(x_t; \lambda_t). \quad (22.33)$$

Here the equilibrium averages of the internal energy,  $\langle \tilde{u}(x_t; \lambda_t) \rangle^{\text{eq}}$ , and entropy  $\langle \tilde{s}(x_t; \lambda_t) \rangle^{\text{eq}}$ , reduce to the expressions (22.10) as expected. It should be stressed here that the average fluctuating entropy  $\langle \tilde{s}_S(x_t; \lambda_t) \rangle$  is not equivalent to the Shannon information entropy due to the temperature dependence of the mean force Hamiltonian. According to the first law of thermodynamics heat dissipated into  $\mathcal{R}$  is given by the work done on  $\mathcal{S}$  minus the change in internal energy. Using (22.32), the fluctuating heat up to time  $t_f$  can be expressed as follows:

$$\tilde{q}_S(z_{t_f}, t_f) := \tilde{u}_S(x_{t_i}; \lambda_{t_i}) - \tilde{u}_S(x_{t_f}; \lambda_{t_f}) + \int_{t_i}^{t_f} dt \partial_t \tilde{u}_S(x_t; \lambda_t), \quad (22.34)$$

where the second term represents the integrated power over time, which equates to the work done on  $\mathcal{S}$ .

In standard stochastic thermodynamics, where the weak-coupling limit applies, the entropy production is a quantity used to quantify the irreversibility of a process, and is necessarily non-negative on average [44, 45]. One can also define a fluctuating entropy production for the situation considered here, formally given by the sum of dissipated heat and entropy change [27]:

$$\tilde{\Sigma}_S(z_t; t) := \tilde{s}_S(x_{t_f}; \lambda_{t_f}) - \tilde{s}_S(x_{t_i}; \lambda_{t_i}) + \beta \tilde{q}_S(z_t, t), \quad (22.35)$$

The statistics of entropy production up to time  $t_f$  are then given by the following distribution:

$$\overrightarrow{P}(\tilde{\Sigma}_S) := \int dz_{t_i} \sigma_{S \cup \mathcal{R}}(z_{t_i}; t_i) \delta[\tilde{\Sigma}_S - \tilde{\Sigma}_S(z_{t_f}; t_f)], \quad (22.36)$$

where we note that  $\tilde{\Sigma}_S(z_{t_f}; t_f)$  implicitly depends on the sampling of the initial phase space point  $z_{t_i}$ . Computing the average of (22.35) leads to the following equality [41]:

$$\langle \tilde{\Sigma}_S \rangle = S(\rho_{S \cup \mathcal{R}}(z_{t_f}; t_f) || \sigma_{S \cup \mathcal{R}}(z_{t_f}; t_f)) \geq 0, \quad (22.37)$$

where  $S(\rho(z_{t_f}; t_f) || \sigma_{S \cup \mathcal{R}}(z_{t_f}; t_f))$  is the Kullback–Lieber divergence, the classical analogue to the quantum relative entropy. From an information theoretic perspective we can interpret  $\langle \tilde{\Sigma}_S \rangle$  as a measure of distinguishability between the final configuration and the corresponding state  $\sigma_{S \cup \mathcal{R}}(z_{t_f}; t_f) \in \mathcal{N}_\beta$  for a given temperature. The fact that entropy production is non-negative if and only if  $\mathcal{S} \cup \mathcal{R}$  is driven away from the class of states in  $\mathcal{N}_\beta$  can be taken as a generalised statement of the second law of thermodynamics for non-equilibrium processes, taking into account strong-interactions and correlations between  $\mathcal{S}$  and  $\mathcal{R}$ . In other words, (22.37) is equivalent to the Clausius inequality; *dissipated heat is always greater than the corresponding decrease in entropy multiplied by the temperature*. We remark that if one maintains the standard canonical definitions of heat and entropy, then the above process can result in supposed violations of the Clausius inequality if correlations exist between  $\mathcal{S}$  and  $\mathcal{R}$  due to strong interactions [46]. However, adopting the HMF and its ther-

modynamic potentials as the true description of thermodynamics at strong coupling indeed resolves these apparent paradoxes. Indeed, (22.37) can be rewritten as a strong-coupling extension of the Clausius inequality:

$$\langle \tilde{q}_S \rangle \geq -T \Delta \langle \tilde{s}_S \rangle, \quad (22.38)$$

so that the heat dissipated in  $\mathcal{R}$  is always greater than the corresponding *decrease* in the entropy of  $\mathcal{S}$ , multiplied by the temperature.

It is also possible to derive fluctuation relations for this process. Firstly, computing the exponentiated entropy production along the forward trajectory leads to the following fluctuation relation [27]:

$$\langle e^{-\tilde{\Sigma}_S(z_f; t)} \rangle = 1, \quad (22.39)$$

which is the strong-coupling analogue to the integral fluctuation relation [47]. To obtain a generalised form of the Crooks relation, one can consider a conjugate process moving backwards in time in which the total configuration is prepared in the state  $\sigma_{S \cup R}(z_f^*; t_f)$ , where the superscript denotes the fact that the time-reversal operation has been applied to each phase space point. By using the time-reversed form of the Liouville equation governing the forward process, one obtains the following Crooks-like relation between the forward and backward statistics for entropy production [41]:

$$\frac{\overrightarrow{P}(+\tilde{\Sigma}_S)}{\overleftarrow{P}(-\tilde{\Sigma}_S)} = e^{\tilde{\Sigma}_S}. \quad (22.40)$$

The reason that (22.40) holds is because the entropy production given by (22.35) can alternatively be represented as the log-ratio of the initial phase space configurations of  $\mathcal{S} \cup \mathcal{R}$  for the process and its time-reverse [48]. The relation (22.40) can be interpreted as a stronger statement of the second law, as it implies that positive entropy production along the forwards process is exponentially favoured against the equivalent decrease in entropy production along the backwards process. This highlights the connection between entropy production and time-asymmetry in the strong-coupling regime [41].

## 22.7 Volume, Pressure and Alternative Approaches

In the formalism presented thus far, the volume of the system has been assumed to be fixed. However, by taking into account fluctuations in the volume, one can obtain an alternative interpretation of the mean force Hamiltonian in terms of enthalpy [7]. Let us first suppose that the state of  $\mathcal{S} \cup \mathcal{R}$  is given by the isothermal-isobaric ensemble:

$$\varrho_{S \cup R}(x, y; \lambda) := \frac{1}{Z_{S \cup R}} e^{-\beta[H_{S \cup R}(x, y; \lambda) + P \mathcal{V}_{\mathcal{R}}(y)]}. \quad (22.41)$$

Here we assume the Hamiltonian of  $\mathcal{S} \cup \mathcal{R}$  is given as before by (22.28) and again denote  $z = (x, y)$  as the collective phase space points of  $\mathcal{S}$  and  $\mathcal{R}$  respectively. In this situation one assumes that the volume of  $\mathcal{R}$ , denoted  $\mathcal{V}_{\mathcal{R}}(y)$ , fluctuates around equilibrium at fixed pressure  $P$ . This contrasts with the canonical ensemble (22.29), which has a *fixed* volume. As shown in [7], in the thermodynamic limit the canonical and isothermal–isobaric ensembles become indistinguishable due to ensemble equivalence, which removes any ambiguity in the particular choice of ensemble for  $\mathcal{S} \cup \mathcal{R}$ . After integrating over the reservoir degrees of freedom, the reduced state of  $\mathcal{S}$  can be expressed as follows:

$$\varrho_{\mathcal{S}}(x; \lambda) = \frac{1}{Z_{\mathcal{S}}^*(\lambda)} e^{-\beta[H_{\mathcal{S}}(x, \lambda) + \phi_{\mathcal{S}}(x)]}, \quad (22.42)$$

where

$$\phi_{\mathcal{S}}(x) := -\frac{1}{\beta} \ln \langle e^{-\beta \gamma V_{\mathcal{S} \cup \mathcal{R}}(z)} \rangle_{\mathcal{R}}^{\text{eq}}, \quad (22.43)$$

is referred to as the *solvation* Hamiltonian of mean force [7]. Here  $\langle \dots \rangle_{\mathcal{R}}^{\text{eq}} = \int dy \varrho_{\mathcal{R}}(y) \dots$  is now an average with respect to the *bare* isothermal–isobaric reservoir. Note that  $\phi_{\mathcal{S}}(x)$  is independent of the external parameter  $\lambda$ , but implicitly depends on the pressure  $P$  of the surrounding reservoir.

Of course the volume of  $\mathcal{S}$  also fluctuates at pressure  $P$ , and one can use  $\phi_{\mathcal{S}}(x)$  to obtain a thermodynamic definition of its volume. However, the interesting point here is that there are two separate approaches to defining the volume, and this further leads to ambiguity in the definition of both the entropy and internal energy of  $\mathcal{S}$ . One approach, referred to in [7] as the *partial molar representation*, follows the same framework that has been presented so far. In this case, the volume of  $\mathcal{S}$  is defined from the solvation HMF according to

$$\tilde{v}_{\mathcal{S}}(x) := \frac{\partial \phi_{\mathcal{S}}(x)}{\partial P}. \quad (22.44)$$

In this representation it can be shown that the average volume of  $\mathcal{S}$  is equivalent to the difference between the total volume of  $\mathcal{S} \cup \mathcal{R}$  minus the volume of the bare reservoir in the absence of any coupling to  $\mathcal{S}$ . This follows the same form for the internal energy, entropy and free energy expressed in the additive relation (22.11) for the canonical ensemble. To be more specific, the average volume of  $\mathcal{S} \cup \mathcal{R}$  is given by  $\mathcal{V}_{\mathcal{S} \cup \mathcal{R}} = \int dz \varrho_{\mathcal{S} \cup \mathcal{R}}(x, y; \lambda) \mathcal{V}_{\mathcal{R}}(y)$ , while the average volume of  $\mathcal{S}$  is given by  $\mathcal{V}_{\mathcal{S}} = \int dx \varrho_{\mathcal{S}}(x; \lambda) \tilde{v}_{\mathcal{S}}(x)$ . It can then be shown that

$$\mathcal{V}_{\mathcal{S}} = \mathcal{V}_{\mathcal{S} \cup \mathcal{R}} - \langle \mathcal{V}_{\mathcal{R}}(y) \rangle_{\mathcal{R}}^{\text{eq}}. \quad (22.45)$$

As with (22.32), the fluctuating internal energy and entropy of  $\mathcal{S}$  are defined by

$$\tilde{u}_{\mathcal{S}}(x, \lambda) := H_{\mathcal{S}}(x, \lambda) + \beta \frac{\partial \phi_{\mathcal{S}}(x)}{\partial \beta} - P \tilde{v}_{\mathcal{S}}(x), \quad (22.46)$$

$$\tilde{s}_S(x, \lambda) := -\ln \varrho_S(x; \lambda) + \beta^2 \partial_\beta \phi_S(x), \quad (22.47)$$

where we note that the internal energy now contains an additional pressure term. The fluctuating *enthalpy*, which is used to quantify the work done on  $S$  due to variations in both the parameter  $\lambda$  and changes in the volume, is subsequently given by

$$\tilde{h}_S(x, \lambda) := \tilde{u}_S(x, \lambda) + P \tilde{v}_S(x). \quad (22.48)$$

If one consider variations in the parameter  $\lambda_t$  as a function of time  $t \in [t_i, t_f]$ , then the first law of thermodynamics at the stochastic level can be expressed as

$$\tilde{q}_S(z_{t_f}, t_f) := \tilde{h}_S(x_{t_i}; \lambda_{t_i}) - \tilde{h}_S(x_{t_f}; \lambda_{t_f}) + \int_{t_i}^{t_f} dt \partial_t \tilde{h}_S(x_t; \lambda_t). \quad (22.49)$$

Here  $\tilde{q}_S(z_{t_f}, t_f)$  is the fluctuating heat dissipated into  $\mathcal{R}$  up to time  $t_f$ , which consists of the total decrease in enthalpy of  $S$  plus the work done along the process. The second term in (22.49) is the work done on  $S$ , and is given by the integrated rate of change of enthalpy. If the system is initially in equilibrium, then it can be shown that the average dissipated heat resulting from changes in parameter  $\lambda_t$  leads to the second law of thermodynamics;  $\langle \tilde{q}_S \rangle \geq -T \Delta \langle \tilde{s}_S \rangle$  [7]. Similar consistency with the Jarzynski and Crooks fluctuation relations can also be proven.

If one neglects the pressure term and sets  $P = 0$  then the above formalism reduces to that presented in the previous section, with the enthalpy equivalent to the internal energy. However, an alternative *bare* representation can also be conceived that also remains consistent with the first and second law of thermodynamics. Contrasting with the previous approach, one can instead use the solvation HMF to define the volume of  $S$  according to

$$\tilde{v}'_S(x) := \frac{\phi_S(x)}{P}, \quad (22.50)$$

which is not equivalent to the volume (22.44) unless the interaction can be neglected. Furthermore, the internal energy can be equated to the bare Hamiltonian:

$$\tilde{u}'_S(x, \lambda) := H_S(x, \lambda), \quad (22.51)$$

and the entropy is simply the log-likelihood of the system's configuration:

$$\tilde{s}'_S(x, \lambda) := -\ln \varrho_S(x; \lambda), \quad (22.52)$$

which is equal to the Shannon information entropy on average. Taking these definitions together, the enthalpy of  $S$  in the bare representation becomes  $\tilde{h}'_S(x, \lambda) := \tilde{u}'_S(x, \lambda) + P \tilde{v}'_S(x)$ . Finally, an alternative definition of heat, denoted  $\tilde{q}'_S(z_{t_f}, t_f)$ , follows from replacement  $\tilde{h}_S(x_t, \lambda_t) \rightarrow \tilde{h}'_S(x_t, \lambda_t)$  in (22.49). Surprisingly, it is shown in [7] that these definitions of heat and entropy are also consistent with the second law

of thermodynamics, namely  $\langle \tilde{q}'_{\mathcal{S}} \rangle \geq -T \Delta \langle \tilde{s}'_{\mathcal{S}} \rangle$ , and the Jarzynski and Crooks fluctuation relations continue to hold. The reason that these work fluctuation relations remain valid is because the rate of change of enthalpy in both the partial molar and bare representations are the same, thus the total work done on  $\mathcal{S}$  remains unchanged in both frameworks.

It is important to note that both the partial-molar and bare representations become equivalent in the weak-coupling limit  $\gamma \ll 1$ . Thus this apparent ambiguity in the thermodynamic formalism stems from the presence of non-negligible interactions between  $\mathcal{S}$  and  $\mathcal{R}$ . As there is no clear energetic division between the system and reservoir, this leaves the definition of the system's volume somewhat ambiguous. While both representations lead to a consistent thermodynamic framework, there is currently no physical principle to discriminate between the two. It is further argued in [42] that while the notion of work is clearly well-defined regardless of the coupling  $\gamma$ , as work is always given by the total change in energy of  $\mathcal{S} \cup \mathcal{R}$ , the dissipated heat is an ambiguous quantity at both the ensemble and stochastic level. This again stems from the non-unique definition of the system's internal energy. It remains an open question as to whether or not a more solid definition of heat can be formulated in the strong-coupling regime.

## 22.8 Conclusion

In this chapter we have presented an overview of the thermodynamics of strongly-coupled quantum and classical systems. We have seen that the presence of a finite interaction between the system and its reservoir, which can occur when the system's volume is significantly small, imposes significant modifications to the equilibrium properties of the system. In order to account for the coupling between  $\mathcal{S}$  and  $\mathcal{R}$ , the Hamiltonian of mean force can be introduced in order to describe the *effective* thermodynamics of  $\mathcal{S}$  through a modified partition function. This allows one to define effective forms of entropy, internal and free energy that remain consistent with the laws of thermodynamics, and this unified approach is able to successfully interpolate between the weak and strong-coupling regimes. Furthermore, while the HMF is derived from standard equilibrium thermodynamics, we have also seen that it can even be applied to non-equilibrium processes in both quantum and classical settings. In particular, the HMF not only generalises the standard second law, but also the Jarzynski and Crooks fluctuation relations. Overall, the HMF proves to be a fundamental tool that can be used to describe thermodynamic processes in which the weak-coupling approximation breaks down.

## References

1. A. Einstein, in *Autobiographical Notes*, ed. by P.A. Schilpp (Open Court Publishing, La Salle, 1979)

2. L. Landau, E. Lifshitz, *Course of Theoretical Physics: Statistical Physics*, vol. 5 (Pergamon, Oxford, 1958), p. 76
3. A.B. Kolomeisky, M.E. Fisher, Ann. Rev. Phys. Chem. **58**, 675 (2007). <https://doi.org/10.1146/annurev.physchem.58.032806.104532>
4. D. Collin, F. Ritort, C. Jarzynski, S.B. Smith, I. Tinoco, C. Bustamante, Nature **437**, 231 (2005). <https://doi.org/10.1038/nature04061>
5. R. Kosloff, A. Levy, Ann. Rev. Phys. Chem. **65**, 365 (2013). <https://doi.org/10.1146/annurev-physics-040513-103724>
6. P. Hänggi, P. Talkner, Nat. Phys. **11**, 108 (2015). <https://doi.org/10.1038/nphys3167>
7. C. Jarzynski, Phys. Rev. X **7**, 011008 (2017). <https://doi.org/10.1103/PhysRevX.7.011008>
8. K. Huang, *Lectures on Statistical Physics and Protein Folding* (World Scientific Publishing, Singapore, 2005)
9. G.W. Ford, J.T. Lewis, R.F. O'Connell, Phys. Rev. Lett. **55**, 2273 (1985). <https://doi.org/10.1103/PhysRevLett.55.2273>
10. J.G. Kirkwood, J. Chem. Phys. **3**, 300 (1935). <https://doi.org/10.1063/1.1749657>
11. S. Hilbert, P. Hänggi, J. Dunkel, Phys. Rev. E **90**, 062116 (2014). <https://doi.org/10.1103/PhysRevE.90.062116>
12. H. Touchette, J. Stat. Phys. **159**, 987 (2015). <https://doi.org/10.1007/s10955-015-1212-2>
13. C. Jarzynski, J. Stat. Mech. **2004**, P09005 (2004). <https://doi.org/10.1088/1742-5468/2004/09/P09005>
14. M.F. Gelin, M. Thoss, Phys. Rev. E **79**, 051121 (2009). <https://doi.org/10.1103/PhysRevE.79.051121>
15. M. Campisi, P. Talkner, P. Hänggi, Phys. Rev. Lett. **102**, 210401 (2009a). <https://doi.org/10.1103/PhysRevLett.102.210401>
16. A. Caldeira, A. Leggett, Phys. A **121**, 587 (1983). [https://doi.org/10.1016/0378-4371\(83\)90013-4](https://doi.org/10.1016/0378-4371(83)90013-4)
17. H. Grabert, U. Weiss, P. Talkner, Z. Phys. B **55**, 87 (1984). <https://doi.org/10.1007/BF01307505>
18. B.L. Hu, J.P. Paz, Phys. Rev. D **45**, 2843 (1992). <https://doi.org/10.1103/PhysRevD.45.2843>
19. A.D.O. Connell, M. Hofheinz, M. Ansmann, R.C. Bialczak, M. Lenander, E. Lucero, M. Neeley, D. Sank, H. Wang, M. Weides, J. Wenner, J.M. Martinis, A.N. Cleland, Nature **464**, 697 (2010). <https://doi.org/10.1038/nature08967>
20. T.G. Philbin, J. Anders, J. Phys. A Math. Theor. **49**, 215303 (2016). <https://doi.org/10.1088/1751-8113/49/21/215303>
21. P. Talkner, M. Campisi, P. Hänggi, J. Stat. Mech. **2009**, P02025 (2009). <https://doi.org/10.1088/1742-5468/2009/02/P02025>
22. J.L. Lebowitz, L. Pastur, J. Phys. A **48**, 265201 (2015). <https://doi.org/10.1088/1751-8113/48/26/265201>
23. M. Kliesch, C. Gogolin, M.J. Kastoryano, A. Riera, J. Eisert, Phys. Rev. X **4**, 031019 (2014). <https://doi.org/10.1103/PhysRevX.4.031019>
24. Y. Subasi, C.H. Fleming, J.M. Taylor, B.L. Hu, Phys. Rev. E **061132**, 061132 (2012). <https://doi.org/10.1103/PhysRevE.86.061132>
25. C. Gogolin, J. Eisert, Rep. Prog. Phys. **79**, 056001 (2016). <https://doi.org/10.1088/0034-4885/79/5/056001>
26. E.T. Jaynes, Phys. Rev. **106**, 620 (1957). <https://doi.org/10.1103/PhysRev.106.620>
27. U. Seifert, Phys. Rev. Lett. **116**, 020601 (2016). <https://doi.org/10.1103/PhysRevLett.116.020601>
28. T.G. Philbin, N. J. Phys. **13**, 063026 (2011). <https://doi.org/10.1088/1367-2630/13/6/063026>
29. R.M. Wilcox, J. Math. Phys. **8**, 962 (1967). <https://doi.org/10.1063/1.1705306>
30. H.J.D. Miller, J. Anders, Nat. Comm. **9**, 2203 (2018). <https://doi.org/10.1038/s41467-018-04536-7>
31. P. Ullersma, Physica **32**, 27 (1966). [https://doi.org/10.1016/0031-8914\(66\)90102-9](https://doi.org/10.1016/0031-8914(66)90102-9)
32. M.J. Donald, J. Stat. Phys. **49**, 81 (1987). <https://doi.org/10.1007/BF01009955>
33. M. Campisi, D. Zueco, P. Talkner, Chem. Phys. **375**, 187 (2010). <https://doi.org/10.1016/j.chemphys.2010.04.026>

34. G. Ingold, P. Hänggi, P. Talkner, Phys. Rev. E **79**, 061105 (2008). <https://doi.org/10.1103/PhysRevE.79.061105>
35. M. Campisi, P. Talkner, P. Hänggi, J. Phys. A Math. Theor. **42**, 392002 (2009b). <https://doi.org/10.1088/1751-8113/42/39/392002>
36. I. Frérot, T. Roscilde, Phys. Rev. B **94**, 075121 (2016). <https://doi.org/10.1103/PhysRevB.94.075121>
37. C. Jarzynski, Ann. Rev. Condens. Matter Phys. **2**, 329 (2011). <https://doi.org/10.1146/annurev-conmatphys-062910-140506>
38. G. Crooks, Phys. Rev. E **60**, 2721 (1999). <https://doi.org/10.1103/PhysRevE.60.2721>
39. C. Jarzynski, Phys. Rev. Lett. **78**, 2690 (1997). <https://doi.org/10.1103/PhysRevLett.78.2690>
40. P. Talkner, E. Lutz, P. Hänggi, Phys. Rev. E **75**, 050102 (2007). <https://doi.org/10.1103/PhysRevE.75.050102>
41. H.J. Miller, J. Anders, Phys. Rev. E **95**, 062123 (2017). <https://doi.org/10.1103/PhysRevE.95.062123>
42. P. Talkner, P. Hanggi, Phys. Rev. E **94**, 022143 (2016). <https://doi.org/10.1103/PhysRevE.94.022143>
43. P. Strasberg, M. Esposito, Phys. Rev. E **95**, 062101 (2017). <https://doi.org/10.1103/PhysRevE.95.062101>
44. U. Seifert, Eur. Phys. J. B **64**, 423 (2008). <https://doi.org/10.1140/epjb/e2008-00001-9>
45. U. Seifert, Rep. Prog. Phys. **75**, 126001 (2012). <https://doi.org/10.1088/0034-4885/75/12/126001>
46. A.E. Allahverdyan, T.M. Nieuwenhuizen, Phys. Rev. Lett. **85**, 1799 (2000). <https://doi.org/10.1103/PhysRevLett.85.1799>
47. U. Seifert, Phys. Rev. Lett. **95**, 040602 (2005). <https://doi.org/10.1103/PhysRevLett.95.040602>
48. E. Aurell, Phys. Rev. E **97**, 042112 (2018). <https://doi.org/10.1103/PhysRevE.97.042112>

# Chapter 23

## The Reaction Coordinate Mapping in Quantum Thermodynamics



Ahsan Nazir and Gernot Schaller

### 23.1 Introduction

The standard formulation of thermodynamics is based around the assumption of vanishingly weak interactions between the system of interest and any thermal reservoirs to which it is attached. Under these conditions, a system that is put into contact with a single heat reservoir will customarily thermalise to a canonical Gibbs state, with the reservoir itself assumed to remain in thermal equilibrium at a given temperature. A weak coupling approximation is generally very well justified on macroscopic scales, whereby only a small fraction of the system and reservoir constituent degrees of freedom are usually in contact. On nanoscales, however, such a simplification becomes much more questionable, perhaps particularly so when the system and reservoir are quantum mechanical in nature and the generation of non-classical correlations between the two may then play a prominent role.

Several attempts have therefore been made to move beyond weak coupling in this context [1–28]. Examples include consideration of the Hamiltonian of mean force, which was reviewed in the previous chapter, the hierarchical equations of motion technique to be reviewed in the following chapter, and unitary transform methods [13, 16]. Here we consider another established but powerful approach [29–32] that was recently put forward in a thermodynamic context [11, 18, 22, 33–35], namely the reaction coordinate mapping. This technique aims to explicitly account for the most prominent reservoir influences by defining a collective degree of freedom of the reservoir (the reaction coordinate) that is then absorbed into an enlarged supersystem.

---

A. Nazir (✉)

School of Physics and Astronomy, The University of Manchester,  
Manchester M13 9PL, UK  
e-mail: ahsan.nazir@manchester.ac.uk

G. Schaller

Institut für Theoretische Physik, Technische Universität Berlin,  
10623 Berlin, Germany  
e-mail: gernot.schaller@tu-berlin.de

The remaining reservoir degrees of freedom are then treated in the usual manner as being weakly coupled to the supersystem. As we shall see, one advantage of such a formalism is that it allows us to apply much of the intuition of standard weak-coupling thermodynamics, though now without the restriction to vanishingly weak system-reservoir interactions. Furthermore, dynamical and steady-state benchmarking of the reaction coordinate technique has demonstrated that it is extremely accurate in a number of situations of practical interest, in particular when non-Markovian and strong system-reservoir correlation effects become important [11, 36].

The chapter is organised as follows. In the next section we summarise the main ideas behind the reaction coordinate mapping and give the essential details pertaining to both bosonic and fermionic reservoirs. We then analyse the stationary state of the mapped system, explain how it differs from a Gibbs state of the original unmapped system, and outline its connection to the Hamiltonian of mean force. Subsequently, we discuss applications of the reaction coordinate formalism to discrete stroke heat engines such as the Otto cycle, and then continuously operating thermo-machines through the example of a single-electron transistor. Finally, we present an outlook on potential future applications of the reaction coordinate technique to related problems where accounting for strong system-reservoir coupling is of crucial importance. For completeness, mathematical details are presented in appendices.

## 23.2 The Reaction Coordinate Mapping

Many typical system-reservoir setups employ simple non-interacting Hamiltonians for the reservoirs and assume that they are coupled linearly to the system. This means that the reservoir Hamiltonian is generally quadratic in bosonic or fermionic creation and annihilation operators, whereas these operators enter the interaction Hamiltonian only linearly, e.g. as absorption/emission or tunneling terms. Such systems can be treated with the approach that we shall now discuss.

A schematic of the reaction coordinate mapping is shown in Fig. 23.1. Formally, such mappings can be realized as Bogoliubov transforms, whereby bosonic (or

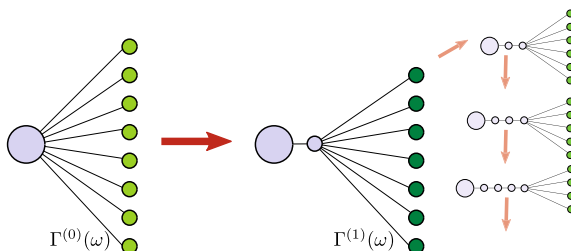


**Fig. 23.1** Sketch of the reaction coordinate mapping. A collective degree of freedom of the reservoir is joined with the system to form the supersystem. This transforms the spectral density  $\Gamma^{(0)}(\omega)$  to  $\Gamma^{(1)}(\omega)$ . The mapping can be applied recursively, converting a star configuration into a chain, but also other mappings are conceivable [37].

fermionic) annihilation operators  $a_k$  are linearly transformed to new bosonic (or fermionic) modes  $b_q$ . The *reaction coordinate* is then selected as one of these new modes  $b = b_1$ :

$$a_k = u_{k1}b + \sum_{q>1} u_{kq}b_q + v_{k1}b^\dagger + \sum_{q>1} v_{kq}b_q^\dagger. \quad (23.1)$$

To preserve the bosonic (fermionic anti-) commutation relations, the Bogoliubov transform needs to be symplectic, i.e., the matrices formed by the complex-valued coefficients  $U = (u_{kq})$  and  $V = (v_{kq})$  have to obey the relations  $UU^\dagger \pm VV^\dagger = \mathbf{1}$  and  $UV^T \pm VU^T = \mathbf{0}$ , where the  $-$  sign accounts for bosons and the  $+$  sign for fermions, respectively. For example, when the transform does not mix creation and annihilation operators ( $V = \mathbf{0}$ ),  $U$  just needs to be a unitary matrix. As another example, one can construct a bosonic symplectic transform which mixes between annihilation and creation operators from a given orthogonal transform via  $u_{kq} = \frac{1}{2} \left( \frac{\bar{a}_k}{b_q} + \frac{\bar{b}_q}{\bar{a}_k} \right) \Lambda_{kq}$  and  $v_{kq} = \frac{1}{2} \left( \frac{\bar{a}_k}{b_q} - \frac{\bar{b}_q}{\bar{a}_k} \right) \Lambda_{kq}$  where  $\bar{a}_k$  and  $\bar{b}_q$  are real parameters and the orthogonality relation just imposes the constraint  $\sum_q \Lambda_{kq} \Lambda_{k'q} = \delta_{kk'}$ . In general, there is an infinite number of such transformations, and we are interested in the ones giving rise to special mappings between Hamiltonians as considered below.

### 23.2.1 Spectral Bounds

Many generic bosonic Hamiltonians are specifically designed for the weak-coupling limit. When these are naively extrapolated towards strong couplings, it may happen that the spectrum of the complete system is no longer bounded from below, leading to unphysical artifacts. This problem can be circumvented by writing the initial Hamiltonian as a sum of positive definite terms, which upon expansion leads to a renormalized system Hamiltonian. In our considerations below, we will assume that a decomposition of the total Hamiltonian into completed squares has initially been performed, such that the spectrum is always bounded from below for any value of the coupling strength.

### 23.2.2 Mappings for Continuous Bosonic Reservoirs

#### 23.2.2.1 Phonon Mapping

We would like to obtain a map satisfying

$$\begin{aligned}
H &= H_S + S \sum_k \left( h_k a_k + h_k^* a_k^\dagger \right) + \sum_k \omega_k a_k^\dagger a_k \\
&= H_S + \lambda S(b + b^\dagger) + \Omega b^\dagger b + (b + b^\dagger) \tilde{\sum}_k \left( H_k b_k + H_k^* b_k^\dagger \right) + \tilde{\sum}_k \Omega_k b_k^\dagger b_k,
\end{aligned} \tag{23.2}$$

where  $S$  denotes a dimensionless operator acting in the system Hilbert space only, which need not necessarily be bosonic. We term this the phonon mapping due to the position-like couplings both before and after the transformation [32]. In the second line the symbol  $\tilde{\sum}$  indicates that the mapped reservoir terms contain one mode less (we may not consistently use this in the following, as the number of modes should become clear from the context). We further note that we have chosen  $\lambda > 0$ , as a possible phase can be absorbed into the  $b$  and  $b_k$  operators, eventually only leading to a phase in the  $H_k$  coefficients. With the same argument, we can choose the  $h_k$  coefficients to be real-valued from the beginning. We follow the conventions of defining the corresponding spectral (coupling) densities as

$$\Gamma^{(0)}(\omega) = 2\pi \sum_k |h_k|^2 \delta(\omega - \omega_k), \quad \Gamma^{(1)}(\omega) = 2\pi \tilde{\sum}_k |H_k|^2 \delta(\omega - \Omega_k). \tag{23.3}$$

In our units, these have dimensions of energy.

In terms of Bogoliubov transforms, the mapping (23.2) can be realized with a normal-mode transformation, where

$$u_{kq} = \frac{1}{2} \left( \sqrt{\frac{\omega_k}{\Omega_q}} + \sqrt{\frac{\Omega_q}{\omega_k}} \right) \Lambda_{kq}, \quad v_{kq} = \frac{1}{2} \left( \sqrt{\frac{\omega_k}{\Omega_q}} - \sqrt{\frac{\Omega_q}{\omega_k}} \right) \Lambda_{kq}, \tag{23.4}$$

with real-valued orthogonal matrix  $\Lambda_{kq}$ , and where the  $\omega_k$  are the natural frequencies of the original modes  $a_k$  and the  $\Omega_q$  the energies of the transformed modes; specifically  $\Omega_1 = \Omega$  is the reaction coordinate energy. Some algebra shows that the first column of the orthogonal matrix is fixed by the original system-reservoir coupling  $\Lambda_{k1} = \frac{h_k}{\lambda} \sqrt{\frac{\omega_k}{\Omega}}$ . With this, one obtains the new coupling strength from the old spectral density via

$$\lambda^2 = \frac{1}{2\pi\Omega} \int_0^\infty \omega \Gamma^{(0)}(\omega) d\omega, \tag{23.5}$$

where the energy of the reaction coordinate is determined by

$$\Omega^2 = \frac{\int_0^\infty \omega^3 \Gamma^{(0)}(\omega) d\omega}{\int_0^\infty \omega \Gamma^{(0)}(\omega) d\omega}, \tag{23.6}$$

such that both  $\lambda$  and  $\Omega$  have dimensions of energy, see Refs. [18, 31] (note the different factor of two in the definition of the spectral densities).

With the mapping (23.2), manipulations on the Heisenberg equations of motion (see Appendix A) tell us that under appropriate conditions the transformed spectral density can be obtained from the old one by the following transformation:

$$\Gamma^{(1)}(\omega) = \frac{4\lambda^2\Gamma^{(0)}(\omega)}{\left[\frac{1}{\pi}\mathcal{P} \int \frac{\Gamma^{(0)}(\omega')}{\omega' - \omega} d\omega'\right]^2 + [\Gamma^{(0)}(\omega)]^2}, \quad (23.7)$$

where  $\mathcal{P}$  denotes the Cauchy principal value, and we see that  $\Gamma^{(1)}(\omega)$  also has units of energy. In this relation, the analytic continuation of the spectral density to the complete real axis  $\Gamma(-\omega) = -\Gamma(+\omega)$  is understood. This is again compatible with previous discussions [31] when the factor of two in the definition of the spectral densities and the correct dimensionality of coupling coefficients in each representation are taken into account. Further, the mapping can be applied recursively, e.g. in the next step we have  $S = b + b^\dagger$ , and its convergence properties have been thoroughly investigated [31, 32]. It is straightforward to see that when rescaling  $\Gamma^{(0)}(\omega) \rightarrow \alpha\Gamma^{(0)}(\omega)$  with some dimensionless constant  $\alpha > 0$ , we will just modify the transformed system-reaction coordinate coupling  $\lambda \rightarrow \sqrt{\alpha}\lambda$ , but the residual spectral density  $\Gamma^{(1)}(\omega)$  will remain unaffected. This already tells us that the method can be used to explore the strong-coupling limit of extremely large  $\alpha$  whenever the residual coupling is small. We furthermore see that the spectrum of the supersystem Hamiltonian is bounded from below for any value of  $\lambda$  when one can decompose  $H_S = H_S^0 + \frac{\lambda^2}{\Omega} S^2$ , where  $H_S^0$  is bounded from below.

In Table 23.1 we summarize a few spectral densities for which an analytic computation of the mapping relations according to Eqs. (23.5)–(23.7) is possible. One can see that without a rigid cutoff, one may soon obtain spectral densities that do not decay fast enough to allow for another recursive mapping. With a rigid cutoff, we can however observe convergence towards a stationary Rubin-type spectral density as in the bottom right of Table 23.1, see also Fig. 23.2 (left panel).

### 23.2.2.2 Particle Mapping

In analogy with the phonon mapping case, we let the particle mapping be given by

$$\begin{aligned} H &= H_S + S \sum_k h_k^* a_k^\dagger + S^\dagger \sum_k h_k a_k + \sum_k \omega_k a_k^\dagger a_k \\ &= H_S + \lambda S b^\dagger + \lambda S^\dagger b + \Omega b^\dagger b + b \sum_k H_k^* b_k^\dagger + b^\dagger \sum_k H_k b_k + \sum_k \Omega_k b_k^\dagger b_k. \end{aligned} \quad (23.8)$$

**Table 23.1** Phonon-type mappings for selected spectral densities according to Eqs. (23.5), (23.6), and (23.7) with either a soft or a rigid ultraviolet cutoff. All spectral densities are – when analytically continued to the complete real axis – odd functions of  $\omega$ . All parameters have dimension of energy.

$\Gamma^{(0)}(\omega)$	$\lambda^2$	$\Omega$	$\Gamma^{(1)}(\omega)$
$\frac{8\Gamma\delta^4\epsilon\omega(\omega^2+\delta^2+\epsilon^2)}{[\delta^2+(\omega-\epsilon)^2]^2[\delta^2+(\omega+\epsilon)^2]^2}$	$\frac{\Gamma\delta\epsilon}{4\sqrt{3\delta^2+\epsilon^2}}$	$\sqrt{3\delta^2+\epsilon^2}$	$\frac{8\delta^3\omega(\delta^2+\omega^2+\epsilon^2)}{\sqrt{3\delta^2+\epsilon^2}\left[2\omega^2\left(5\delta^2-\epsilon^2\right)+\left(3\delta^2+\epsilon^2\right)^2+\omega^4\right]}$
$\frac{4\Gamma\delta^5\omega^3}{[\delta^2+(\omega-\epsilon)^2]^2[\delta^2+(\omega+\epsilon)^2]^2}$	$\frac{\Gamma\delta^2}{16\sqrt{3\delta^2+\epsilon^2}}$	$\sqrt{5\delta^2+\epsilon^2}$	$\frac{16\delta^3\omega^3}{\sqrt{5\delta^2+\epsilon^2}\left[\delta^4+2\delta^2\left(7\omega^2+\epsilon^2\right)+\left(\omega^2-\epsilon^2\right)^2\right]}$
$\Gamma\frac{\omega}{\omega_m}\Theta(\omega_m - \omega)$	$\frac{1}{6\pi}\sqrt{\frac{3}{5}}\Gamma\omega_m$	$\sqrt{\frac{3}{5}}\omega_m$	$\frac{2\sqrt{\frac{3}{5}}\pi\omega\omega_m^2}{3\left[\pi^2\omega^2+4\omega\text{arctanh}\left(\frac{\omega}{\omega_m}\right)\left(\omega\text{arctanh}\left(\frac{\omega}{\omega_m}\right)-2\omega_m\right)+4\omega_m^2\right]}\Theta(\omega_m - \omega)$
$\Gamma\frac{\omega}{\omega_m}\sqrt{1 - \frac{\omega^2}{\omega_m^2}}\Theta(\omega_m - \omega)$	$\frac{\Gamma\omega_m}{16\sqrt{2}}$	$\frac{\omega_m}{\sqrt{2}}$	$\frac{\omega}{\sqrt{2}}\sqrt{1 - \frac{\omega^2}{\omega_m^2}}\Theta(\omega_m - \omega)$

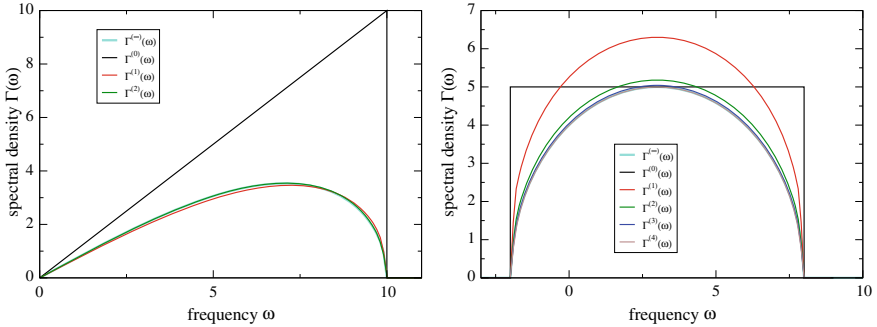


**Fig. 23.2** **Left:** Numerical bosonic phonon mapping of an initially linear spectral density with a rigid cutoff at  $\omega_{ct} = 10$ . The light blue curve in the background corresponds to the analytic Rubin spectral density in the bottom right of Table 23.1. **Right:** Numerical fermionic particle mapping of an initially box-shaped spectral density with rigid cutoffs at  $\omega_{ct,1} = -2$  and  $\omega_{ct,2} = 8$ . The light blue curve in the background corresponds to the semicircle spectral density in the bottom right of Table 23.2 ( $\delta = 5$  and  $\epsilon = 3$ ).

Here,  $S$  is again some dimensionless system operator, which need not necessarily be Hermitian, and it suffices to choose the Bogoliubov transform as unitary ( $v_{kq} = 0$ ), see also Ref. [32] for examples. Then, from identifying  $\lambda b = \sum_k h_k a_k$  and demanding bosonic commutation relations, we must have

$$\lambda^2 = \sum_k |h_k|^2 = \frac{1}{2\pi} \int_0^\infty \Gamma^{(0)}(\omega) d\omega. \quad (23.9)$$

Second, we see that the relations  $\sum_k h_k u_{k1} = \sum_k h_k^* u_{k1}^* = \lambda$  together with the unitarity relation  $\sum_k |u_{k1}|^2 = 1$  fix the first coefficients  $u_{k1} = h_k^*/\lambda$ , which when inserted into the energy of the reaction coordinate  $\Omega = \sum_k \omega_k |u_{k1}|^2$  eventually yields

$$\Omega = \frac{1}{2\pi\lambda^2} \int_0^\infty \omega \Gamma^{(0)}(\omega) d\omega , \quad (23.10)$$

such that  $\Omega$  also has dimensions of energy.

The Heisenberg equations (see Appendix B) tell us that the following spectral density mapping relation should hold

$$\Gamma^{(1)}(\omega) = \frac{4\lambda^2 \Gamma^{(0)}(\omega)}{\left[ \frac{1}{\pi} \mathcal{P} \int_0^\infty \frac{\Gamma^{(0)}(\omega')}{\omega' - \omega} d\omega' \right]^2 + [\Gamma^{(0)}(\omega)]^2} . \quad (23.11)$$

Here, the difference to the phonon mapping is that  $\Gamma^{(n)}(\omega)$  are not analytically continued to the complete real axis, as  $\omega > 0$  is assumed throughout. The convergence properties of related recursion relations have been discussed in great detail [32, 38, 39].

As with the previous treatment, the structure of the Hamiltonian (bosonic tunneling) is similar before and after the transformation, we just need to redefine the system and reservoir. Therefore, it can also be applied recursively. This way, we can understand the reaction coordinate mapping as the sequential application of multiple Bogoliubov transformations. In practise, one would truncate the resulting chain at some point, using a perturbative approach such as the master equation [11, 36].

Now, the spectrum of the supersystem Hamiltonian is bounded from below for any value of  $\lambda$  when one can decompose it as  $H_S = H_S^0 + \frac{\lambda^2}{\Omega} S^\dagger S$ , where  $H_S^0$  is bounded from below. We finally note that by choosing  $S = a + a^\dagger$  we can switch from a phonon-type representation to a particle-type representation.

### 23.2.3 Fermionic Particle Mapping

We can also investigate these problems for fermions, where the mapping reads

$$\begin{aligned} H &= H_S + c \sum_k t_k^* c_k^\dagger - c^\dagger \sum_k t_k c_k + \sum_k \epsilon_k c_k^\dagger c_k \\ &= H_S + \lambda c d^\dagger - \lambda c^\dagger d + \varepsilon d^\dagger d + d \sum_k T_k^* d_k^\dagger - d^\dagger \sum_k T_k d_k + \sum_k \varepsilon_k d_k^\dagger d_k . \end{aligned} \quad (23.12)$$

The difference is that the spectral densities can be defined also for negative frequencies, such that no analytic continuation is necessary. Now, we obtain the reaction coordinate coupling and energy from integrals over the complete energies

$$\lambda^2 = \frac{1}{2\pi} \int \Gamma^{(0)}(\omega) d\omega , \quad \varepsilon = \frac{1}{2\pi\lambda^2} \int \omega \Gamma^{(0)}(\omega) d\omega . \quad (23.13)$$

**Table 23.2** Selected mappings for spectral densities according to Eqs. (23.13) and (23.14), using  $\Theta(x, a, b) = \Theta(x - a)\Theta(b - x)$  and  $\text{erf}(z) = \frac{2}{\sqrt{\pi}} \int_0^z e^{-t^2} dt$ . For the evaluation of the first row reaction coordinate energy  $\varepsilon$ , the principal value has to be taken, as the ordinary integral does not converge. As a rule of thumb, the width of the old spectral density becomes the coupling strength of the new spectral density, and only a rigid cutoff will survive recursive transformations. When the original spectral density strictly vanishes for negative  $\omega$  (accessible with the last three rows for suitable parameters), we recover the bosonic particle mapping from Eqs. (23.9)–(23.11).

$\Gamma^{(0)}(\omega)$	$\lambda^2$	$\varepsilon$	$\Gamma^{(1)}(\omega)$
$\Gamma \frac{\delta^2}{(\omega-\epsilon)^2+\delta^2}$	$\frac{\Gamma\delta}{2}$	$\epsilon$	$2\delta$
$\Gamma \frac{\delta^4}{[(\omega-\epsilon)^2+\delta^2]^2}$	$\frac{\Gamma\delta}{4}$	$\epsilon$	$\frac{\delta(2\delta)^2}{(\omega-\epsilon)^2+(2\delta)^2}$
$\Gamma e^{-\frac{(\omega-\epsilon)^2}{\delta^2}}$	$\frac{\Gamma\delta}{2\sqrt{\pi}}$	$\epsilon$	$\frac{2\delta e + \frac{(\omega-\epsilon)^2}{\delta^2}}{\sqrt{\pi}[1-\text{erf}^2(i\frac{\omega-\epsilon}{\delta})]}$
$\Gamma \Theta(\omega, \epsilon - \delta, \epsilon + \delta)$	$\frac{\Gamma\delta}{\pi}$	$\epsilon$	$\frac{4\pi\delta}{\pi^2+4\text{arctanh}^2\left(\frac{\epsilon-\omega}{\delta}\right)} \Theta(\omega, \epsilon - \delta, \epsilon + \delta)$
$\Gamma \left[1 - \left(\frac{\omega}{\delta} - \frac{\epsilon}{\delta}\right)^2\right] \Theta(\omega, \epsilon - \delta, \epsilon + \delta)$	$\frac{2}{3} \frac{\Gamma\delta}{\pi}$	$\epsilon$	$\frac{8\delta}{3\pi} \frac{\left[1 - \frac{(\omega-\epsilon)^2}{\delta^2}\right] \Theta(\omega, \epsilon - \delta, \epsilon + \delta)}{\frac{4(\delta(\omega-\epsilon) - (\omega+\delta-\epsilon)(\omega-\delta-\epsilon))\text{arctanh}\left[\frac{\omega-\epsilon}{\delta}\right]}{\pi^2\delta^4} + \left(1 - \frac{(\omega-\epsilon)^2}{\delta^2}\right)^2}$
$\Gamma \sqrt{1 - \left(\frac{\omega}{\delta} - \frac{\epsilon}{\delta}\right)^2} \Theta(\omega, \epsilon - \delta, \epsilon + \delta)$	$\frac{\Gamma\delta}{4}$	$\epsilon$	$\delta \sqrt{1 - \left(\frac{\omega}{\delta} - \frac{\epsilon}{\delta}\right)^2} \Theta(\omega, \epsilon - \delta, \epsilon + \delta)$

The Heisenberg equations (see Appendix C) tell us that the following mapping relations should hold

$$\Gamma^{(1)}(\omega) = \frac{4\lambda^2 \Gamma^{(0)}(\omega)}{\left[\frac{1}{\pi} \mathcal{P} \int \frac{\Gamma^{(0)}(\omega')}{\omega' - \omega} d\omega'\right]^2 + [\Gamma^{(0)}(\omega)]^2}, \quad (23.14)$$

where we again stress that the spectral density is defined also for negative energies. When we consider the case that it strictly vanishes for negative energies, we recover the case of bosonic particle mappings from Eqs. (23.9)–(23.11).

Table 23.2 provides some examples of spectral densities and their mappings according to Eqs. (23.13) and (23.14). The functional form of the mapping implies that convergence of all integrals is ensured only for a hard cutoff. In particular, the limiting case for particle mappings with a rigid cutoff is a semicircle, see the bottom right entry in Table 23.2, which we also observe numerically in Fig. 23.2 (right panel).

### 23.2.4 General Properties: Stationary State of the Supersystem

In the strong-coupling limit, we no longer expect the local Gibbs state  $e^{-\beta H_S}/Z_S$  to be the stationary state of the system. Rather, one might expect it to be given by the reduced density matrix of the total Gibbs state [28, 40]

$$\bar{\rho}_S \approx \text{Tr}_B \left\{ \frac{e^{-\beta(H_S + H_B + H_I)}}{Z} \right\}, \quad (23.15)$$

which would only coincide with the system-local Gibbs state when  $H_I \rightarrow 0$  (vanishingly weak coupling). Since the reaction coordinate mappings allow for arbitrarily strong coupling between the original system and reservoir, we can test when the resulting stationary state in the supersystem is consistent with these expectations.

In particular, we assume here that the coupling between the supersystem and residual reservoir is small, such that we can apply the master equation formalism to the supersystem [11, 36]

$$H'_S = H_S + H_{RC} + H_I, \quad (23.16)$$

composed of system and reaction coordinate. For the standard quantum-optical master equation (based in general on Born–Markov and secular approximations) it is known that for a single reservoir the stationary state will approach the system-local Gibbs state [41, 42], now associated with the supersystem [11]

$$\bar{\rho}'_S = \frac{e^{-\beta H'_S}}{\text{Tr}_{S,RC} \{ e^{-\beta H'_S} \}}. \quad (23.17)$$

We define a Hamiltonian of mean force  $H^*$  – see also the previous chapter – via the relation

$$e^{-\beta H^*} = \frac{\text{Tr}_B \{ e^{-\beta(H_S + H_B + H_I)} \}}{\text{Tr}_B \{ e^{-\beta H_B} \}}. \quad (23.18)$$

It can be seen as an effective Hamiltonian for the system in the strong coupling limit. In the weak-coupling limit ( $H_I \rightarrow 0$ ) we get  $H^* \rightarrow H_S$ . By construction, the Hamiltonian of mean force obeys

$$e^{-\beta H^*} = \frac{\text{Tr}_{RC,B'} \{ e^{-\beta(H'_S + \tilde{\lambda} H'_I + H'_B)} \}}{\text{Tr}_{RC,B'} \{ e^{-\beta(H_{RC} + \tilde{\lambda} H'_I + H'_B)} \}} = \frac{\text{Tr}_{RC} \{ e^{-\beta H'_S} \}}{\text{Tr}_{RC} \{ e^{-\beta H_{RC}} \}} + \mathcal{O}\{\tilde{\lambda}\}. \quad (23.19)$$

Here,  $\tilde{\lambda}$  serves as a dimensionless bookkeeping parameter for the coupling between the reaction coordinate and the residual reservoir. With Eq. (23.17), this implies that the reduced steady state of the original system becomes

$$\begin{aligned} \bar{\rho}_S &= \text{Tr}_{RC} \{ \bar{\rho}'_S \} = \frac{\text{Tr}_{RC} \{ e^{-\beta H'_S} \}}{\text{Tr}_{S,RC} \{ e^{-\beta H'_S} \}} = \frac{e^{-\beta H^*} \text{Tr}_{RC} \{ e^{-\beta H_{RC}} \}}{\text{Tr}_{S,RC} \{ e^{-\beta H'_S} \}} + \mathcal{O}\{\tilde{\lambda}\} \\ &= \frac{e^{-\beta H^*}}{\text{Tr}_S \{ e^{-\beta H^*} \}} + \mathcal{O}\{\tilde{\lambda}\}, \end{aligned} \quad (23.20)$$

where the last equality follows directly from performing  $\text{Tr}_S \{ e^{-\beta H^*} \}$ . That is, when the coupling  $\tilde{\lambda}$  between the supersystem and the residual reservoir (i.e. the transformed spectral density) is small, the approach recovers the reduced steady state (23.15) of the global Gibbs state [11, 18].

### 23.3 Applications to Thermal Machines

Heat engines generate useful work by harnessing heat flow between hot and cold reservoirs. Usually, heat engine models are analysed under the simplifying assumption of negligibly weak interactions between the working system and the reservoirs. However, as argued earlier, for heat engines operating at the quantum scale such an approximation may not be well justified, since interaction energies potentially become comparable with system and reservoir self-energy scales. The treatment becomes even more challenging when one allows for driven heat engines, where the coupling strength between the system and reservoir is modified periodically. In such cases, even the correct partition of the time-dependent system-reservoir driving into heat and work contributions is generally a challenging task, where the reaction coordinate treatment is indeed helpful [35]. For conceptual simplicity, however, we shall put the simultaneous treatment of driving and dissipation aside and therefore review two types of heat engine model in this section – discrete stroke and continuous – that have recently been analysed beyond weak system-reservoir coupling by employing the reaction coordinate formalism outlined above.

#### 23.3.1 Discrete Stroke Engines: The Otto Cycle

Discrete stroke heat engines operate in closed cycles that are divided into individual sections (strokes) in which particular operations such as heat exchange, expansion, compression, or combinations, take place. The working system returns to its original state at the end of the cycle and in order to produce a finite power output, each stroke must be performed within a finite time. Nevertheless, the study of infinite time cycles (which produce work but zero power output) has been crucial in identifying fundamental thermodynamic bounds on heat engine performance, and indeed led to Carnot's principle. Furthermore, the identification of a closed cycle is made easier in the infinite time limit due to the knowledge of the state (whether within the weak-coupling or reaction coordinate approaches) after equilibration between the system and the hot or cold reservoir. Thus, zero power cycles provide a natural setting in which to begin exploring extensions of heat engine models beyond the weak system-reservoir coupling regime.

Here we shall review the reaction coordinate analysis of a discrete stroke quantum Otto cycle beyond weak reservoir coupling as presented in Ref. [22]. This cycle is

a quantum analogy of a four-stroke internal combustion engine model. It has the advantage of separating strokes in which energy is exchanged between the system and the reservoirs from those in which work is either extracted from or done on the system with the reservoirs uncoupled. In this way, we seek to avoid the complications of defining work and heat at strong-coupling for strokes in which both may be important, as encountered for example within the Carnot cycle.

The strokes of our quantum Otto cycle are depicted schematically in Fig. 23.3. We consider a two-level working system with ground state  $|g\rangle$  and excited state  $|e\rangle$ , split by an energy  $\mu$ . The system may be coupled to and decoupled from two reservoirs, one hot and one cold. In the standard approach assuming negligibly weak system-reservoir interactions these coupling and decoupling steps make no energetic contribution to the cycle. This can be seen, for example, if we consider the system to couple linearly to bosonic reservoirs that remain in thermal equilibrium (factorised from the system state) throughout the cycle, in which case the trace of the interaction Hamiltonian evaluates to zero. Under these conditions, the Otto cycle consists of four strokes, two isentropes in which the system Hamiltonian is varied in time in the absence of any reservoir coupling, and two isochores in which the system equilibrates with either the hot or cold reservoir without any variations in the system Hamiltonian. However, for the case of finite reservoir coupling that is of interest here, there is no reason to believe that the coupling and decoupling steps can be neglected. We must therefore enlarge the cycle to include these contributions as well, leading to the primed points in Fig. 23.3.

Let us now analyse the cycle in more detail, contrasting the reaction coordinate and weakly-interacting approaches. Starting, arbitrarily, at point  $A'$  in Fig. 23.3, the

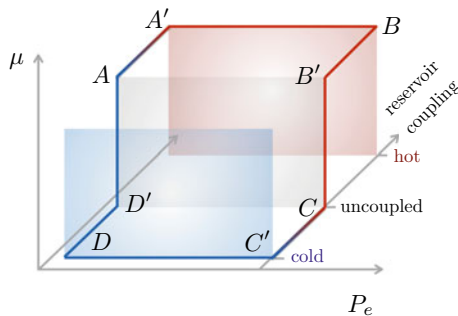


**Fig. 23.3** Schematic of a quantum Otto cycle for a two-level system with splitting  $\mu$  (vertical axis) and excited state population  $P_e$  (horizontal axis), which may be coupled to and decoupled from hot and cold reservoirs (red and blue shaded areas, respectively). The depicted cycle strokes are: isochoric equilibration  $A' \rightarrow B$ , decoupling from the hot reservoir  $B \rightarrow B'$ , isentropic expansion  $B' \rightarrow C$ , coupling to the cold reservoir  $C \rightarrow C'$ , isochoric equilibration  $C' \rightarrow D$ , decoupling from the cold reservoir  $D \rightarrow D'$ , isentropic compression  $D' \rightarrow A$ , and coupling to the hot reservoir  $A \rightarrow A'$ . Reprinted with permission from D. Newman, F. Mintert, and A. Nazir, Physical Review E 95, 032139 (2017), <https://dx.doi.org/10.1103/PhysRevE.95.032139>. Copyright (2017) by the American Physical Society.

system and hot reservoir have just been coupled. They are allowed to equilibrate along the subsequent stroke, known as the hot isochore, which means that within the weak-coupling limit the state of the system plus hot reservoir is given at point  $B$  by

$$\tilde{\rho}_S^0 \otimes \rho_h = \frac{e^{-\beta_h H_S}}{\text{Tr}_S \{ e^{-\beta_h H_S} \}} \otimes \frac{e^{-\beta_h H_B}}{\text{Tr}_S \{ e^{-\beta_h H_B} \}}. \quad (23.21)$$

Here,  $\beta_h = 1/T_h$  is the inverse temperature of the hot reservoir with internal Hamiltonian  $H_B$ . For weak coupling, the system simply thermalises along the stroke with respect to its internal Hamiltonian  $H_S$ . The system-reservoir coupling strength thus plays no role in the infinite time weak-coupling limit. In contrast, within the reaction coordinate formalism the state at the end of the stroke is given by

$$\tilde{\rho}'_S \otimes \tilde{\rho}_h = \tilde{\rho}'_S \otimes \frac{e^{-\beta_h \tilde{H}_B}}{\text{Tr}_S \{ e^{-\beta_h \tilde{H}_B} \}}, \quad (23.22)$$

where  $\tilde{\rho}'_S$  is now a Gibbs (thermal) state of the supersystem comprised of both the original two-level system and the reaction coordinate, as defined in Eq.(23.17) with  $\beta \rightarrow \beta_h$ . This encodes correlations due to finite interactions between the system and reservoir, and thus has a natural dependence on the system-reservoir coupling strength as well as the reservoir temperature. Note that the factorisation in Eq.(23.22) is made only with respect to the mapped residual bath with internal Hamiltonian  $\tilde{H}_B$ , given for example by the final terms in Eqs.(23.2) and (23.8). It is not, therefore, equivalent to a weak-coupling approximation between the system and the full reservoir as in Eq.(23.21). Accordingly, numerical benchmarking of the reaction coordinate method has shown it to be accurate over a very wide range of system-environment coupling strengths [11, 36].

The quantity of interest for analysing the cycle performance is the energy expectation value at the end of each stroke. In the weak coupling limit only changes to the two-level system energy are tracked, and so we consider

$$\langle H \rangle_{\text{weak}} = \text{Tr}\{H_S \tilde{\rho}_S^0\}. \quad (23.23)$$

In the reaction coordinate approach, on the other hand, changes to both the system and reaction coordinate are monitored, and so we have

$$\langle H \rangle = \text{Tr}\{H'_S \tilde{\rho}'_S\}, \quad (23.24)$$

which includes additional contributions from the reaction coordinate and system-reaction coordinate Hamiltonians through  $H'_S$ , as well as correlation effects through  $\tilde{\rho}'_S$ .<sup>1</sup>

---

<sup>1</sup>Note that there is a subtlety in the strong-coupling cycle. When coupled, the interaction between the system and the reservoir pushes the latter out of thermal equilibrium. We assume that once the

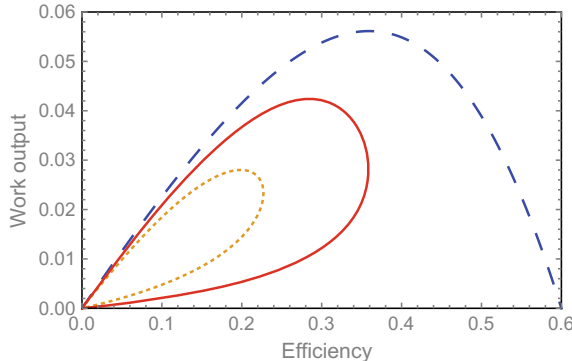


**Fig. 23.4** Example parametric plots of Otto cycle work output and efficiency. Each curve is generated by varying the difference in splittings  $\mu$  between the start and the end of the isentropic strokes. The blue dashed curve shows the weak-coupling treatment. The red solid and orange dashed curves show the reaction coordinate treatment with adiabatic and instantaneous decoupling of the reservoirs, respectively. Reprinted with permission from D. Newman, F. Mintert, and A. Nazir, Physical Review E 95, 032139 (2017), <https://dx.doi.org/10.1103/PhysRevE.95.032139>. Copyright (2017) by the American Physical Society.

At point  $B$  the interaction between the system and hot reservoir is now turned off to reach point  $B'$ , which we must explicitly account for within the reaction coordinate analysis. For simplicity we shall assume this happens suddenly, such that the full state does not change, and hence define a work cost associated with decoupling of

$$\text{Tr}\{(H_S + H_{RC} - H'_S)\bar{\rho}'_S\} = -\text{Tr}\{H_I\bar{\rho}'_S\}. \quad (23.25)$$

This cost impacts adversely on the total work output of the cycle. In Ref. [22] it is shown that part (though not all) of the work cost can be mitigated by decoupling the system and reservoir slowly (i.e. in the adiabatic limit), see also Fig. 23.4.

From point  $B'$  to  $C$  the system Hamiltonian is changed such that the splitting is reduced ( $\mu_{B'} > \mu_C$ ) in the absence of any reservoir coupling, with the stroke thus being termed isentropic expansion. For changes that are slow enough to justify use of the quantum adiabatic theorem, the average system energy along the stroke is given simply by

$$\langle H_S(t) \rangle = \frac{\mu(t)}{\mu(0)} \langle H_S(0) \rangle, \quad (23.26)$$

---

system and reservoir are decoupled at the end of the stroke, the reservoir rapidly relaxes back to equilibrium. Hence, when the system comes to be coupled to the reservoir again on the next cycle, the reservoir is thermal once more. The re-thermalisation of the reservoirs entails accounting for some extra energetic contributions around the cycle, as described in detail in [22].

where  $t = 0$  refers to the start of the stroke,  $\langle H_S(0) \rangle = \text{Tr}\{H_S(0)\tilde{\rho}_S^0(0)\}$  in the weak-coupling case, and  $\langle H_S(0) \rangle = \text{Tr}\{H_S(0)\tilde{\rho}'_S(0)\}$  in the reaction coordinate treatment. Thus, the work output of the stroke becomes

$$W_{\text{stroke}} = \left( \frac{\mu_C}{\mu_{B'}} - 1 \right) \langle H_S(0) \rangle, \quad (23.27)$$

which is negative by convention.

The coupling to the cold reservoir is now switched on ( $C \rightarrow C'$ ). We assume the reservoirs relax back to thermal equilibrium when decoupled from the system, and so there is no work contribution associated with this step in either treatment as the trace of the interaction Hamiltonian is then zero. The system and cold reservoir now equilibrate along the subsequent stroke ( $C' \rightarrow D$ ), which we may analyse in the same way as the hot isochore. They are then decoupled ( $D \rightarrow D'$ ) once more incurring a work cost in the reaction coordinate treatment. Subsequently, we do work on the system during an isentropic compression ( $D' \rightarrow A$ ). Here, the system splitting is adiabatically increased back to its earlier value, such that  $\mu_A = \mu_{B'}$ . Finally, the system and hot reservoir are coupled ( $A \rightarrow A'$ , no work cost) and the cycle is complete.

In Fig. 23.4 we show some example parametric plots of the efficiency and work output of the Otto cycle as treated within both the weak-coupling and reaction coordinate frameworks. To generate these curves the difference in splittings between the start and end of the isentropic strokes is varied. In the weak-coupling case, the net work output is simply the difference in work along the two isentropic strokes, whereas in the reaction coordinate treatment we must include the decoupling costs as well. In both cases, we define the efficiency in the standard way as

$$\eta = \frac{W}{Q_{A'B}}, \quad (23.28)$$

where  $W$  is the cycle net work output and  $Q_{A'B}$  is the energy change along the hot isochore. For the weak-coupling case this can be expressed in the simple form  $\eta_{\text{weak}} = 1 - \mu_C/\mu_{B'}$ , which depends only on the ratio of the two-level splittings. We can see from Fig. 23.4 that the weak-coupling efficiency reaches a maximum at the point at which the work output vanishes. Here, the ratio of splittings becomes equal to the ratio of cold to hot reservoir temperatures,  $T_c/T_h$ , and so the weak-coupling efficiency reaches the Carnot bound. The behaviour of the cycle is qualitatively different, and inferior, in the reaction coordinate case. The maximum efficiency occurs at finite work output, though takes values well below the Carnot bound, and the efficiency also falls to zero as the work output vanishes at larger ratios of the two-level splittings. The decoupling cost contributions are the primary cause for the reduced engine performance at strong-coupling, with a small reduction in energy absorbed along the hot isochore insufficient to overcome their detrimental effect to the efficiency [22]. Finally, we note that an adiabatic decoupling protocol can improve both efficiency and work output (though not up to the idealised weak-coupling limit),

and should thus be an important consideration in optimising the performance of nanoscale (quantum) engine cycles where the presence of non-negligible reservoir couplings is expected [43–46].

### 23.3.2 Continuously Operating Thermo-Machines

For continuously operating heat engines (or refrigerators), the system of interest is coupled to multiple reservoirs that are held at different local thermal equilibrium states throughout [47]. It is then possible to use, for example, a thermal gradient between the reservoirs to extract (chemical) work by transporting electrons against a bias (heat engine) or to cool the coldest reservoir by investing work (chemical work or the energy provided by a so-called work reservoir). In this section, we shall exemplarily benchmark the reaction coordinate treatment of an exactly-solvable two-terminal model.

The single-electron transistor (SET) with Hamiltonian

$$H = \epsilon d^\dagger d + \sum_{k\alpha} \left[ t_{k\alpha} d c_{k\alpha}^\dagger + \text{h.c.} \right] + \sum_{k\alpha} \epsilon_{k\alpha} c_{k\alpha}^\dagger c_{k\alpha} \quad (23.29)$$

describes a single quantum dot  $d$  with on-site energy  $\epsilon$  that is coupled via tunneling amplitudes  $t_{k\alpha}$  to two fermionic leads  $\alpha \in \{L, R\}$ . Letting the leads become continuous, we introduce the original lead spectral densities  $\Gamma_\alpha^{(0)}(\omega) = 2\pi \sum_k |t_{k\alpha}|^2 \delta(\omega - \epsilon_{k\alpha})$ . The model can be analyzed as a heat engine with a perturbative treatment of the  $t_{k\alpha}$  [48]. However, an exact solution can also be derived [49] and analyzed from a thermodynamic viewpoint [50]. We consider reservoirs described by inverse temperatures  $\beta_\alpha$  and chemical potentials  $\mu_\alpha$  and use conservation of energy and matter currents at steady state throughout.

One observable of interest is then the chemical work rate extracted from the system

$$P = -(\mu_L - \mu_R) I_M , \quad (23.30)$$

where  $I_M$  denotes the electronic matter current counting positive from left to right. For  $P > 0$ , this process can be interpreted as electric power used to transport electrons against a bias voltage  $V = \mu_L - \mu_R$ . Furthermore, we define the stationary heat currents entering the system as

$$\dot{Q}_L = I_E - \mu_L I_M , \quad \dot{Q}_R = -(I_E - \mu_R I_M) , \quad (23.31)$$

where  $I_E$  denotes the energy current counting positive from left to right. Without loss of generality, we consider setups where  $\mu_L > \mu_R$  and  $\beta_L > \beta_R$  (implying  $T_L < T_R$  for the temperatures). Then, the efficiency of generating electric power  $P > 0$  from the heat coming from the hot reservoir  $\dot{Q}_R > 0$  becomes

$$\eta = \frac{P\Theta(P)}{\dot{Q}_R} \leq 1 - \frac{T_L}{T_R} = \eta_{\text{Ca}}, \quad (23.32)$$

where  $\Theta(P)$  denotes the Heaviside- $\Theta$  function. Here, the upper bound by Carnot efficiency follows from the positivity of the entropy production rate, which at steady state reduces to  $\dot{S}_{\text{i}} = -\beta_L \dot{Q}_L - \beta_R \dot{Q}_R \geq 0$  [50]. With the same argument, the coefficient of performance (COP) for cooling the cold reservoir  $\dot{Q}_L > 0$  by investing chemical work  $P < 0$ ,

$$\text{COP} = \frac{\dot{Q}_L \Theta(\dot{Q}_L)}{-P} \leq \frac{T_L}{T_R - T_L} = \text{COP}_{\text{Ca}}, \quad (23.33)$$

must also obey a Carnot bound.

We can exactly evaluate energy and matter currents for the SET model using for example nonequilibrium Green's function techniques [49, 51] or other approaches [50], which eventually allows for an exact evaluation of heat engine efficiency (23.32) and COP (23.33) for arbitrary system-reservoir coupling strengths. Alternatively, we can apply the fermionic reaction coordinate mapping [34], which – when we use a separate reaction coordinate for every reservoir – transforms the SET to a triple quantum dot that is tunnel-coupled to two residual leads [33]

$$H = \epsilon d^\dagger d + \sum_{\alpha} \lambda_{\alpha} (dd_{\alpha}^\dagger + d_{\alpha} d^\dagger) + \sum_{\alpha} \epsilon_{\alpha} d_{\alpha}^\dagger d_{\alpha} + \sum_{k\alpha} \left[ T_{k\alpha} d_{\alpha} d_{k\alpha}^\dagger + \text{h.c.} \right] + \sum_{k\alpha} \tilde{\epsilon}_{k\alpha} d_{k\alpha}^\dagger d_{k\alpha}, \quad (23.34)$$

where we have reaction coordinate couplings  $\lambda_{\alpha}$  and energies  $\epsilon_{\alpha}$  as well as a new spectral density  $\Gamma^{(1)}(\omega) = 2\pi \sum_k |T_{k\alpha}|^2 \delta(\omega - \tilde{\epsilon}_{k\alpha})$ . Specifically, using the Lorentzian spectral density from the first row of Table 23.2 centred around  $\epsilon_{\alpha}$  with coupling strengths  $\Gamma_{\alpha}$  and widths  $\delta_{\alpha}$ , we see that the resulting triple quantum dot is tunnel-coupled to two residual reservoirs with a flat spectral density, to which a Markovian treatment of the supersystem (first three terms in the above equation) should apply when  $\beta_{\alpha} \delta_{\alpha}$  is small. For this supersystem, we can set up the (non-secular) master equation (compare with Ref. [33] in absence of feedback control operations) and compute energy and matter currents entering the supersystem from the residual reservoirs. At steady state, we can identify these with the original currents defined above (the reaction coordinates can only host finite charge/energy) and therefore likewise evaluate heat engine efficiency and COP within the reaction coordinate formalism. The result of this procedure is depicted in Fig. 23.5 (left panel). There we see that at vanishing coupling, where the conventional single dot master equation approach to the SET applies [48], maximal efficiencies are actually reached (albeit at zero power or cooling current, respectively), and the transition between heat engine and cooling operational modes happens directly. This can be understood since in the limit of vanishing coupling, the SET obeys the so-called *tight-coupling* condition  $I_E = \epsilon I_M$ . For finite coupling strengths  $\Gamma$ , a gap between these modes opens, which is also observed in other models beyond the weak-coupling limit [35]. When we further

increase the coupling strength, the cooling function is no longer attainable, and also the efficiency of the heat engine decreases. Most importantly, we see that the reaction coordinate treatment (dashed contours), reproduces the exact solution (colours and solid green contours) well, which is attributable to the fact that we choose initially highly peaked spectral densities, such that the residual coupling  $\beta_\alpha \delta_\alpha$  is very small and the reaction coordinate treatment is valid.

One might now be tempted to think that larger coupling strengths are always detrimental to the performance of thermoelectric devices, compare Ref. [28] or the discussion in the previous subsection. With the exact solution at hand, there is little intuitive evidence for finding other interesting parameter regimes. However, going further towards ultra-strong coupling reveals that there is a regime where the heat engine efficiency increases again, and even the cooling operational mode is revived, as is illustrated in Fig. 23.5 (right panel). From comparing the contours we can see that the reaction coordinate treatment (dashed) correctly predicts the revival of the cooling mode and the strengthening of the heat engine efficiency in this limit. We note that as the tunnel amplitudes scale only with the root of the coupling strength  $T_{k\alpha} \leq \sqrt{\Gamma_{\max} \delta / 2} \approx 32\epsilon$  for the parameters in Fig. 23.5, this regime is actually not unrealistic, as has been experimentally demonstrated in various quantum dot sys-

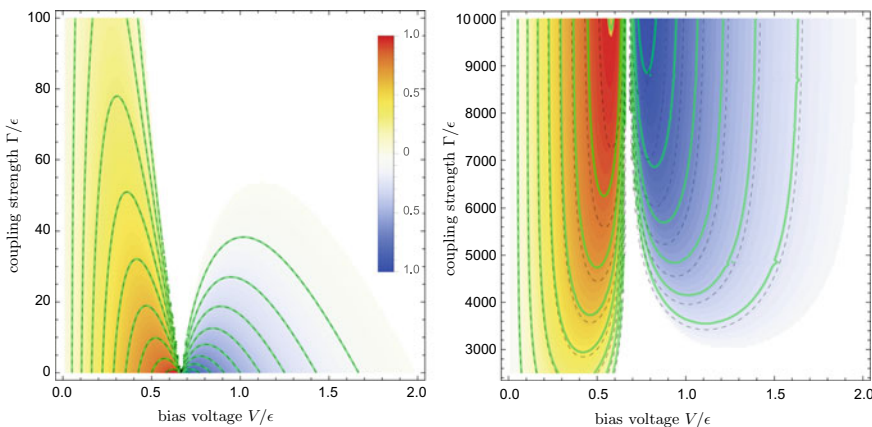


**Fig. 23.5** **Left:** Density plot of the heat engine (red colours) and cooling (blue colours) efficiencies in units of their maximum Carnot value versus dimensionless bias voltage  $V/\epsilon$  (horizontal axis) and coupling strength  $\Gamma/\epsilon$  (vertical axis). Colours and solid green contour lines (in steps of 0.1) correspond to the exact solution of the SET. They agree perfectly with the thin dashed contour lines, which have been calculated using a Born–Markov master equation treatment of the triple dot (reaction coordinate) supersystem. At vanishing coupling strength (bottom), the maximum Carnot values are reached, and we see a direct transition from heat engine to refrigerator operational modes. For stronger couplings, a gap between these modes opens, performances decrease, and while for strong couplings the cooling mode vanishes completely, the device may still act as a heat engine – albeit at reduced efficiency. Other parameters:  $\Gamma_L = \Gamma_R = \Gamma$ ,  $\delta_L = \delta_R = 0.01\epsilon$ ,  $\epsilon_L = \epsilon_R = \epsilon$ ,  $\mu_L = -\mu_R = V/2$ ,  $\beta_R \epsilon = 1$ ,  $\beta_L \epsilon = 2$ . **Right:** Continuation of the left panel towards the ultrastrong coupling regime (with otherwise identical parameters). Heat engine efficiency increases again and also cooling function is revived.

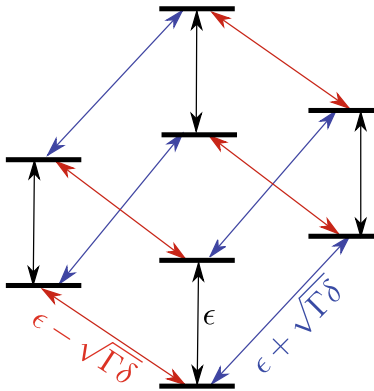


**Fig. 23.6** Sketch of the supersystem spectrum consisting of the vacuum state (bottom), three singly charged states, three doubly occupied states, and the fully charged state (top). For  $\delta_L = \delta_R = \delta$ ,  $\Gamma_L = \Gamma_R = \Gamma$ , and  $\epsilon_L = \epsilon_R = \epsilon$ , the allowed transitions (non-vanishing matrix elements of operators  $d_{L/R}^{(\dagger)}$ ) only admit three transition frequencies:  $\Delta E = \epsilon$  (black arrows),  $\Delta E = \epsilon - \sqrt{\Gamma\delta}$  (red arrows), and  $\Delta E = \epsilon + \sqrt{\Gamma\delta}$  (blue arrows).

tems [52–54]. From the experimental side, the challenge is rather the maintenance of a thermal gradient.

Within the reaction coordinate picture, this worsening and re-strengthening of performance can be understood with a simple transport spectroscopy interpretation. It is rather straightforward to diagonalize the supersystem Hamiltonian in the first three terms of Eq. (23.34). Between the 8 energy eigenstates of the supersystem, not all transitions are allowed in the sequential tunneling regime, see Fig. 23.6. Adopting equal coupling strengths  $\Gamma_L = \Gamma_R \equiv \Gamma$  and widths  $\delta_L = \delta_R \equiv \delta$  for both reservoirs, and matching the maximum tunneling rate with that of the central dot  $\epsilon_L = \epsilon_R = \epsilon$ , the allowed transition frequencies simplify to

$$\Delta E \in \left\{ \epsilon, \epsilon - \sqrt{\Gamma\delta}, \epsilon + \sqrt{\Gamma\delta} \right\}. \quad (23.35)$$

With modifying the coupling strength  $\Gamma$ , we therefore change the transition energies as well. For vanishingly small coupling strengths  $\Gamma$ , the splitting is not resolved by the rather large reservoir temperatures as  $\beta_\alpha \sqrt{\Gamma\delta} \ll 1$ , and the only visible transition frequency is  $\epsilon$ . As mentioned, in this regime the setup approximately obeys the tight-coupling property  $I_E \approx \epsilon I_M$ , and maximum efficiencies are reached (albeit at vanishing power) [55–57]. Here, even the naive (weak-coupling) SET master equation treatment is valid. When we increase the coupling strength, we leave the tight-coupling regime, i.e. energy and matter currents are no longer proportional to each other, which is known to decrease efficiencies, eventually even leading to the loss of the cooling function. However, when  $\beta_\alpha \sqrt{\Gamma\delta} \gg 1$ ,  $\epsilon + \sqrt{\Gamma\delta} \gg \mu_L$ , and  $\epsilon - \sqrt{\Gamma\delta} \ll \mu_R$ , the two shifted excitation energies will have left the transport window and will no longer participate in transport. Then, tight coupling is again restored as

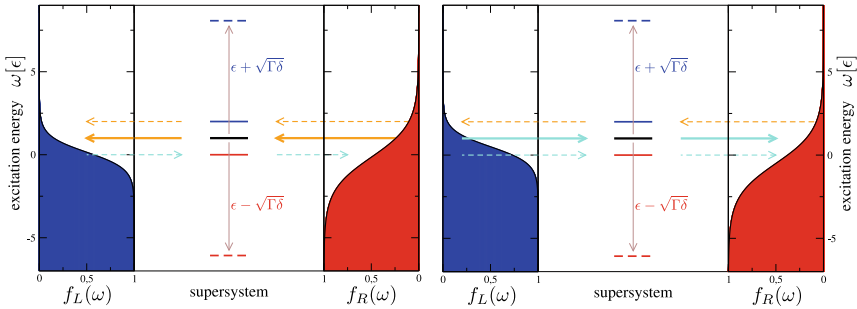


**Fig. 23.7** Illustration of the supersystem transport window in the heat engine regime  $V/\epsilon = 0.3$  (left) and in the cooling regime  $V/\epsilon = 1.0$  (right). Coloured regions left and right denote actual Fermi functions at the parameters used in the calculations. Levels in the centre represent excitation energies of the supersystem depending on the coupling strength, and the current through each transition is directed from the lead with larger Fermi function to the lead with the lower Fermi function. In the heat engine regime (left), transport of electrons against the bias is induced by a thermal gradient (solid orange arrows). In the cooling regime (right), transport is driven by the voltage gradient and cools the cold (left) reservoir (solid blue arrows). For small couplings, the three transition frequencies essentially merge into one at  $\epsilon$  (black) and the reservoirs cannot resolve between them. We then approximately have tight coupling  $I_E \approx \epsilon I_M$  and the naive (weak-coupling) single dot master equation applies. For stronger couplings, two transition energies (23.35) split (solid red and blue for  $\Gamma = 100\epsilon$ ), destroying tight coupling  $I_E \neq \epsilon I_M$ , reducing efficiencies, and even inhibiting the cooling function as one level supports a current with opposite sign (dashed arrows). For ultrastrong couplings, the two variable transition frequencies have left the transport window (dashed red and blue for  $\Gamma = 5000\epsilon$ ) and thus no longer participate in transport, such that tight coupling  $I_E \approx \epsilon I_M$  is restored. Other parameters have been chosen as in Fig. 23.5.

only one transition energy  $\Delta E = \epsilon$  remains inside the transport window. We illustrate this in Fig. 23.7.

Beyond a benchmark of the reaction coordinate treatment, this example provides a simple explanation of the observed behaviour and demonstrates that the mapping can be used as a tool to identify interesting parameter regimes, allowing for useful operational modes. Strong coupling is not always detrimental to the efficiency of continuous heat engines. However, regarding overall power output, it should be noted that we had to choose small  $\delta$  (highly structured reservoirs) to maintain the validity of the reaction coordinate treatment. This does of course bound the total power output of the device, which is not proportional to the coupling strength in this regime.

## 23.4 Outlook

The reaction coordinate mapping is typically used to explore the strong-coupling regime, and as such it has found widespread application. We stress here that it may also be extended to fermionic reservoirs. By construction, the mapping itself is exact and thus barely suffers from additional constraints. It can also be combined, for exam-

ple, with formally exact methods such as nonequilibrium Green's functions [49], to simplify the structure of the resulting equations. However, when it is combined with some perturbative technique, its applicability will be limited to a certain degree. For example, to apply a master equation to the supersystem, it is required that the residual (mapped) spectral density allows for a Markovian treatment. Thus, the master equation solution obtained via the reaction coordinate mapping will in general have a different range of validity than the master equation solution of the original system [11, 36]. We further note that with the mapping, one can transfer the time-dependence of parameters into the supersystem, thus enabling the treatment of open-loop control schemes such as periodic driving [35], or feedback control schemes such as Maxwell's demon [33], from the perspective of a driven system only.

The intuitive simplicity of the reaction coordinate technique makes it suitable to extend the range of validity of many different perturbative approaches. Indeed, beyond strong coupling, other problems can be treated with reaction coordinate mappings. For example, with the mapping one can study the effect of initial system-reservoir correlations by means of master equations. Furthermore, as the treatment of the supersystem is Markovian, but the reduced dynamics of the original need not be, one can see the reaction coordinate mapping as a Markovian embedding to study non-Markovian dynamics.

Finally, we mention that one can also use the mapping to engineer structured reservoirs. Equipping a quantum system of interest with auxiliary degrees of freedom, which are coupled to structureless reservoirs, we can interpret the auxiliary degrees of freedom as reaction coordinates and perform the inverse mapping. Eventually, this yields a system coupled to structured reservoirs, with reaction coordinates that can for example be used as frequency filters to optimize performance of heat engines or other devices.

**Acknowledgements** G.S. gratefully acknowledges discussions with J. Cerrillo, N. Martensen, S. Restrepo, and P. Strasberg and financial support by the DFG (GRK 1558, SFB 910, SCHA 1646/3-1, BR 1528/9-1).

A.N. would like to thank D. Newman, F. Mintert, J. Iles-Smith, N. Lambert, Z. Blunden-Codd and V. Jouffrey for discussions. A.N. is supported by the Engineering and Physical Sciences Research Council, grant no. EP/N008154/1.

## Appendix A: Heisenberg Equations for the Phonon Mapping

The Heisenberg equations of motion for a system observable  $A = A^\dagger$  read in the original representation

$$\begin{aligned} \dot{A} &= iS_1(t) + iS_2(t) \sum_k \left( h_k a_k + h_k^* a_k^\dagger \right), & S_1(t) &= [H_S, A], & S_2(t) &= [S, A], \\ \dot{a}_k &= -i\omega_k a_k - ih_k^* S, & \dot{a}_k^\dagger &= +i\omega_k a_k^\dagger + ih_k S. \end{aligned} \tag{A1}$$

We now Fourier-transform these equations according to  $\int[\dots]e^{+izt}dt$  with the convention  $\Im z > 0$ . In  $z$ -space, the creation and annihilation operators are no longer adjoint to each other, but we will keep the  $\dagger$ -notation. This yields the algebraic equations (convolution theorem)

$$\begin{aligned} izA(z) &= iS_1(z) + \frac{i}{2\pi} \int S_2(z') \sum_k \left[ h_k a_k(z - z') + h_k^* a_k^\dagger(z - z') \right] dz' , \\ iz a_k(z) &= -i\omega_k a_k(z) - ih_k^* S(z) , \quad iz a_k^\dagger(z) = +i\omega_k a_k^\dagger(z) + ih_k S(z) . \end{aligned} \quad (\text{A2})$$

We can solve the last two equations  $a_k(z) = -\frac{h_k^*}{z+\omega_k} S(z)$  and  $a_k^\dagger(z) = +\frac{h_k}{z-\omega_k} S(z)$ , and insert them into the first

$$\begin{aligned} zA(z) &= S_1(z) + \frac{1}{2\pi} \int S_2(z') \left[ \sum_k \frac{-|h_k|^2}{z - z' + \omega_k} + \sum_k \frac{+|h_k|^2}{z - z' - \omega_k} \right] S(z - z') dz' \\ &= S_1(z) + \frac{1}{2\pi} \int S_2(z') \left[ \frac{1}{\pi} \int_0^\infty \frac{\omega \Gamma^{(0)}(\omega)}{(z - z')^2 - \omega^2} d\omega \right] S(z - z') dz' \\ &= S_1(z) - \frac{1}{2\pi} \int S_2(z') \frac{1}{2} W^{(0)}(z - z') S(z - z') dz' . \end{aligned} \quad (\text{A3})$$

Here, we have in the first step used the fact that the harmonic oscillator frequencies  $\omega_k$  are by construction all positive and we have introduced the Cauchy transform

$$W^{(n)}(z) = \frac{2}{\pi} \int_0^\infty \frac{\omega \Gamma^{(n)}(\omega)}{\omega^2 - z^2} d\omega = \frac{1}{\pi} \int_{-\infty}^{+\infty} \frac{\Gamma^{(n)}(\omega)}{\omega - z} d\omega , \quad (\text{A4})$$

where the last equality sign holds for analytic continuation as an odd function  $\Gamma(-\omega) = -\Gamma(+\omega)$ . In particular, we note the important property

$$\Gamma^{(n)}(\omega) = \lim_{\epsilon \rightarrow 0^+} \Im W^{(n)}(\omega + i\epsilon) . \quad (\text{A5})$$

Similarly, we can derive the Heisenberg equations of motion in the mapped representation, and Fourier-transform them according to the same prescription, yielding

$$\begin{aligned} zA(z) &= S_1(z) + \frac{\lambda}{2\pi} \int S_2(z') \left[ b(z - z') + b^\dagger(z - z') \right] dz' , \\ zb(z) &= -\lambda S(z) - \Omega b(z) - \sum_k \left[ H_k b_k(z) + H_k^* b_k^\dagger(z) \right] , \\ zb^\dagger(z) &= +\lambda S(z) + \Omega b^\dagger(z) + \sum_k \left[ H_k b_k(z) + H_k^* b_k^\dagger(z) \right] , \\ zb_k(z) &= -\Omega_k b_k(z) - H_k^* \left[ b(z) + b^\dagger(z) \right] , \quad zb_k^\dagger(z) = +\Omega_k b_k^\dagger(z) + H_k \left[ b(z) + b^\dagger(z) \right] . \end{aligned} \quad (\text{A6})$$

Again, we follow the approach of successively eliminating the  $b_k(z)$ ,  $b_k^\dagger(z)$ , and then the  $b(z)$ ,  $b^\dagger(z)$  variables, yielding for the remaining equation

$$zA(z) = S_1(z) + \frac{1}{2\pi} \int S_2(z') \frac{2\lambda^2 \Omega}{(z-z')^2 - \Omega^2 + \Omega W^{(1)}(z-z')} S(z-z') dz'. \quad (\text{A7})$$

Comparing this with the original representation, we can infer a relation between  $W^{(0)}(z)$  and  $W^{(1)}(z)$ , which can be used to obtain the transformed spectral density

$$\Gamma^{(1)}(\omega) = -\lim_{\epsilon \rightarrow 0^+} \Im \frac{4\lambda^2}{W^{(0)}(\omega + i\epsilon)} = \frac{+4\lambda^2 \Gamma^{(0)}(\omega)}{\left[ \frac{1}{\pi} \mathcal{P} \int \frac{\Gamma^{(0)}(\omega')}{\omega - \omega'} d\omega' \right]^2 + [\Gamma^{(0)}(\omega)]^2}. \quad (\text{A8})$$

## Appendix B: Heisenberg Equations for the Particle Mapping

Now, the Heisenberg equations of motion for a system observable  $A = A^\dagger$  read in the original representation

$$\begin{aligned} \dot{A} &= iS_1(t) + iS_2(t) \sum_k h_k^* a_k^\dagger - iS_2^\dagger(t) \sum_k h_k a_k, \quad S_1(t) = [H_S, A], \quad S_2(t) = [S, A], \\ \dot{a}_k &= -i\omega_k a_k - ih_k^* S, \quad \dot{a}_k^\dagger = +i\omega_k a_k^\dagger + ih_k S^\dagger. \end{aligned} \quad (\text{B1})$$

Fourier-transformation yields

$$\begin{aligned} zA(z) &= S_1(z) + \frac{1}{2\pi} \int \left[ S_2(z') \sum_k h_k^* a_k^\dagger(z-z') - S_2^\dagger(z') \sum_k h_k a_k(z-z') \right] dz', \\ za_k(z) &= -\omega_k a_k(z) - h_k^* S(z), \quad za_k^\dagger(z) = +\omega_k a_k^\dagger(z) + h_k S^\dagger(z). \end{aligned} \quad (\text{B2})$$

Inserting the solutions of the last two equations into the first we get

$$zA(z) = S_1(z) + \frac{1}{2\pi} \int \left[ S_2(z') \sum_k \frac{|h_k|^2}{z-z'-\omega_k} S^\dagger(z-z') + S_2^\dagger(z') \sum_k \frac{|h_k|^2}{z-z'+\omega_k} S(z-z') \right]. \quad (\text{B3})$$

In the mapped representation, we have

$$\begin{aligned} \dot{A} &= iS_1(t) + i\lambda S_2(t)b^\dagger - i\lambda S_2^\dagger(t)b, \\ \dot{b} &= -i\lambda S - i\Omega b - i \sum_k H_k b_k, \quad \dot{b}^\dagger = +i\lambda S^\dagger + i\Omega b^\dagger + i \sum_k H_k^* b_k^\dagger, \\ \dot{b}_k &= -iH_k^* b - i\Omega_k b_k, \quad \dot{b}_k^\dagger = +iH_k b^\dagger + i\Omega_k b_k^\dagger, \end{aligned} \quad (\text{B4})$$

such that Fourier transformation yields

$$\begin{aligned} zA(z) &= S_1(z) + \frac{\lambda}{2\pi} \int [S_2(z') b^\dagger(z - z') - S_2^\dagger(z') b(z - z')] dz', \\ zb(z) &= -\lambda S(z) - \Omega b(z), \quad zb^\dagger(z) = +\lambda S^\dagger(z) + \Omega b^\dagger(z) + \sum_k H_k^* b_k^\dagger(z), \\ z b_k(z) &= -H_k^* b(z) - \Omega_k b_k(z), \quad z b_k^\dagger(z) = +H_k b^\dagger(z) + \Omega_k b_k^\dagger(z). \end{aligned} \quad (\text{B5})$$

Successive elimination of the last four equations yields for the remaining one

$$\begin{aligned} zA(z) &= S_1(z) \\ &+ \frac{\lambda}{2\pi} \int \left[ S_2(z') \frac{+\lambda}{z - z' - \Omega - \sum_k \frac{|H_k|^2}{z - z' - \Omega_k}} S^\dagger(z - z') \right. \\ &\quad \left. + S_2^\dagger(z') \frac{\lambda}{z - z' + \Omega - \sum_k \frac{|H_k|^2}{z - z' + \Omega_k}} S(z - z') \right]. \end{aligned} \quad (\text{B6})$$

From comparison with the first representation, we conclude

$$\sum_k \frac{|h_k|^2}{z - \omega_k} = \frac{\lambda^2}{z - \Omega - \sum_k \frac{|H_k|^2}{z - \Omega_k}}, \quad \sum_k \frac{|h_k|^2}{z + \omega_k} = \frac{\lambda^2}{z + \Omega - \sum_k \frac{|H_k|^2}{z + \Omega_k}}, \quad (\text{B7})$$

where the second equation just encodes the first at  $-z$  and is therefore not independent.

From realizing that

$$\lim_{\epsilon \rightarrow 0} \frac{1}{2\pi} \int_0^\infty \frac{\Gamma(\omega')}{\omega - \omega' + i\epsilon} d\omega' \stackrel{\omega \geq 0}{=} \frac{1}{2\pi} \mathcal{P} \int_0^\infty \frac{\Gamma(\omega')}{\omega - \omega'} d\omega' - \frac{i}{2} \Gamma(\omega), \quad (\text{B8})$$

we can use e.g. the first of these relations to infer a mapping relation between the spectral densities,

$$\Gamma^{(1)}(\omega) = \frac{4\lambda^2 \Gamma^{(0)}(\omega)}{\left[ \frac{1}{\pi} \mathcal{P} \int_0^\infty \frac{\Gamma^{(0)}(\omega')}{\omega - \omega'} d\omega' \right]^2 + [\Gamma^{(0)}(\omega)]^2}, \quad (\text{B9})$$

where  $\omega > 0$  is assumed throughout.

## Appendix C: Heisenberg Equations for Fermionic Reservoirs

To avoid case distinctions on whether the system operator  $A$  commutes or anti-commutes with the coupling operator, we just consider the Heisenberg equations for the creation and annihilation operators. In the original representation, they become

$$\dot{c} = i[H_S, c] + i \sum_k t_k c_k = iS(t) + i \sum_k t_k c_k, \quad \dot{c}_k = it_k^* c - i\epsilon_k c_k, \quad (C1)$$

and similarly for the creation operators. Since at this level they do not mix, we consider only the annihilation operators. Fourier-transformation yields

$$zc(z) = S(z) + \sum_k t_k c_k(z), \quad zc_k(z) = t_k^* c(z) - \epsilon_k c_k(z). \quad (C2)$$

Eliminating the second equation then gives

$$zc(z) = S_1(z) + \sum_k \frac{|t_k|^2}{z + \epsilon_k} c(z). \quad (C3)$$

In contrast, the mapped representation yields

$$\dot{c} = iS(t) + i\lambda d, \quad \dot{d} = -i\lambda c - i\epsilon d + i \sum_k T_k d_k, \quad \dot{d}_k = iT_k^* d - i\epsilon_k d_k. \quad (C4)$$

Fourier-transforming and eliminating the non-system variables then gives

$$zc(z) = S(z) - \frac{\lambda^2}{z + \epsilon - \sum_k \frac{|T_k|^2}{z + \epsilon_k}} c(z), \quad (C5)$$

and from comparison we get the relation

$$\sum_k \frac{|t_k|^2}{z + \epsilon_k} = - \frac{\lambda^2}{z + \epsilon - \sum_k \frac{|T_k|^2}{z + \epsilon_k}}. \quad (C6)$$

Converting the sums to integrals and evaluating at  $z = -\omega + i\delta$  when  $\delta \rightarrow 0^+$  we obtain a mapping relation between the fermionic spectral densities:

$$\Gamma^{(1)}(\omega) = \frac{4\lambda^2 \Gamma^{(0)}(\omega)}{\left[ \frac{1}{\pi} \mathcal{P} \int \frac{\Gamma^{(0)}(\omega')}{\omega - \omega'} d\omega' \right]^2 + [\Gamma^{(0)}(\omega)]^2}. \quad (C7)$$

## References

1. Y. Liu, Y. Zheng, W. Gong, W. Gao, T. Lü, Phys. Lett. A **365**, 495 (2007). <https://doi.org/10.1016/j.physleta.2007.02.005>
2. F. Nesi, E. Paladino, M. Thorwart, M. Grifoni, Europhys. Lett. **80**, 40005 (2007). <https://doi.org/10.1209/0295-5075/80/40005>
3. C. Hörhammer, H. Büttner, J. Stat. Phys. **133**, 1161 (2008). <https://doi.org/10.1007/s10955-008-9640-x>
4. M. Campisi, P. Talkner, P. Hänggi, Phys. Rev. Lett. **102**, 210401 (2009). <https://doi.org/10.1103/PhysRevLett.102.210401>
5. L. Nicolin, D. Segal, Phys. Rev. B **84**, 161414 (2011). <https://doi.org/10.1103/PhysRevB.84.161414>
6. S. Deffner, E. Lutz, Phys. Rev. Lett. **107**, 140404 (2011). <https://doi.org/10.1103/PhysRevLett.107.140404>
7. J. Hausinger, M. Grifoni, Phys. Rev. A **83**, 030301 (2011). <https://doi.org/10.1103/PhysRevA.83.030301>
8. L. Pucci, M. Esposito, L. Peliti, J. Stat. Mech. Theory Exp. **2013**, P04005 (2013). <https://doi.org/10.1088/1742-5468/2013/04/P04005>
9. G. Schaller, T. Krause, T. Brandes, M. Esposito, New J. Phys. **15**, 033032 (2013). <https://doi.org/10.1088/1367-2630/15/3/033032>
10. J. Ankerhold, J.P. Pekola, Phys. Rev. B **90**, 075421 (2014). <https://doi.org/10.1103/PhysRevB.90.075421>
11. J. Iles-Smith, N. Lambert, A. Nazir, Phys. Rev. A **90**, 032114 (2014). <https://doi.org/10.1103/PhysRevA.90.032114>
12. R. Gallego, A. Riera, J. Eisert, New J. Phys. **16**, 125009 (2014). <https://doi.org/10.1088/1367-2630/16/12/125009>
13. C. Wang, J. Ren, J. Cao, Sci. Rep. **5**, 11787 (2015). <https://doi.org/10.1038/srep11787>
14. M. Esposito, M.A. Ochoa, M. Galperin, Phys. Rev. Lett. **114**, 080602 (2015a). <https://doi.org/10.1103/PhysRevLett.114.080602>
15. M. Esposito, M.A. Ochoa, M. Galperin, Phys. Rev. B **92**, 235440 (2015b). <https://doi.org/10.1103/PhysRevB.92.235440>
16. D. Gelbwaser-Klimovsky, A. Aspuru-Guzik, J. Phys. Chem. Lett. **6**, 3477 (2015). <https://doi.org/10.1021/acs.jpclett.5b01404>
17. M. Carrega, P. Solinas, A. Braggio, M. Sassetto, U. Weiss, New J. Phys. **17**, 045030 (2015). <https://doi.org/10.1088/1367-2630/17/4/045030>
18. P. Strasberg, G. Schaller, N. Lambert, T. Brandes, New J. Phys. **18**, 073007 (2016). <https://doi.org/10.1088/1367-2630/18/7/073007>
19. G. Katz, R. Kosloff, Entropy **18**, 186 (2016). <https://doi.org/10.3390/e18050186>
20. J. Cerrillo, M. Buser, T. Brandes, Phys. Rev. B **94**, 214308 (2016). <https://doi.org/10.1103/PhysRevB.94.214308>
21. U. Seifert, Phys. Rev. Lett. **116**, 020601 (2016). <https://doi.org/10.1103/PhysRevLett.116.020601>
22. D. Newman, F. Mintert, A. Nazir, Phys. Rev. E **95**, 032139 (2017). <https://doi.org/10.1103/PhysRevE.95.032139>
23. P. Strasberg, M. Esposito, Phys. Rev. E **95**, 062101 (2017). <https://doi.org/10.1103/PhysRevE.95.062101>
24. H.J.D. Miller, J. Anders, Phys. Rev. E **95**, 062123 (2017). <https://doi.org/10.1103/PhysRevE.95.062123>
25. A. Mu, B.K. Agarwalla, G. Schaller, D. Segal, New J. Phys. **19**, 123034 (2017). <https://doi.org/10.1088/1367-2630/aa9b75>
26. C. Jarzynski, Phys. Rev. X **7**, 011008 (2017). <https://doi.org/10.1103/PhysRevX.7.011008>
27. N. Freitas, J.P. Paz, Phys. Rev. E **95**, 012146 (2017). <https://doi.org/10.1103/PhysRevE.95.012146>

28. M. Perarnau-Llobet, H. Wilming, A. Riera, R. Gallego, J. Eisert, Phys. Rev. Lett. **120**, 120602 (2018). <https://doi.org/10.1103/PhysRevLett.120.120602>
29. R.S. Burkey, C.D. Cantrell, J. Opt. Soc. Am. B **1**, 169 (1984). <https://doi.org/10.1364/JOSAB.1.000169>
30. A. Garg, J.N. Onuchic, V. Ambegaokar, J. Chem. Phys. **83**, 4491 (1985). <https://doi.org/10.1063/1.449017>
31. R. Martinazzo, B. Vacchini, K.H. Hughes, I. Burghardt, J. Chem. Phys. **134**, 011101 (2011). <https://doi.org/10.1063/1.3532408>
32. M.P. Woods, R. Groux, A.W. Chin, S.F. Huelga, M.B. Plenio, J. Math. Phys. **55**, 032101 (2014). <https://doi.org/10.1063/1.4866769>
33. G. Schaller, J. Cerrillo, G. Engelhardt, P. Strasberg, Phys. Rev. B **97**, 195104 (2018). <https://doi.org/10.1103/PhysRevB.97.195104>
34. P. Strasberg, G. Schaller, T.L. Schmidt, M. Esposito, Phys. Rev. B **97**, 205405 (2018). <https://doi.org/10.1103/PhysRevB.97.205405>
35. S. Restrepo, J. Cerrillo, P. Strasberg, G. Schaller, New J. Phys. (2018). <https://doi.org/10.1088/1367-2630/aac583>
36. J. Iles-Smith, A.G. Dijkstra, N. Lambert, A. Nazir, J. Chem. Phys. **144**, 044110 (2016). <https://doi.org/10.1063/1.4940218>
37. J. Huh, S. Mostame, T. Fujita, M.-H. Yung, A. Aspuru-Guzik, New J. Phys. **16**, 123008 (2014). <https://doi.org/10.1088/1367-2630/16/12/123008>
38. M.P. Woods, M. Cramer, M.B. Plenio, Phys. Rev. Lett. **115**, 130401 (2015). <https://doi.org/10.1103/PhysRevLett.115.130401>
39. M.P. Woods, M.B. Plenio, J. Math. Phys. **57**, 022105 (2016). <https://doi.org/10.1063/1.4940436>
40. C. Gogolin, J. Eisert, Rep. Prog. Phys. **79**, 056001 (2016). <https://doi.org/10.1088/0034-4885/79/5/056001>
41. R. Dümccke, H. Spohn, Z. Phys. B **34**, 419 (1979). <https://doi.org/10.1007/BF01325208>
42. H.P. Breuer, F. Petruccione, *The Theory of Open Quantum Systems* (Oxford University Press, Oxford, 2002). <https://doi.org/10.1093/acprof:oso/9780199213900.001.0001>
43. K. Le Hur, Phys. Rev. B **85**, 140506 (2012). <https://doi.org/10.1103/PhysRevB.85.140506>
44. M. Goldstein, M.H. Devoret, M. Houzet, L.I. Glazman, Phys. Rev. Lett. **110**, 017002 (2013). <https://doi.org/10.1103/PhysRevLett.110.017002>
45. B. Peropadre, D. Zueco, D. Porras, J.J. García-Ripoll, Phys. Rev. Lett. **111**, 243602 (2013). <https://doi.org/10.1103/PhysRevLett.111.243602>
46. A. Nazir, D.P.S. McCutcheon, J. Phys. Condens. Matter **28**, 103002 (2016). <https://doi.org/10.1088/0953-8984/28/10/103002>
47. R. Kosloff, A. Levy, Annu. Rev. Phys. Chem. **65**, 365 (2014). <https://doi.org/10.1146/annurev-physchem-040513-103724>
48. M. Esposito, K. Lindenberg, C.V. den Broeck, Europhys. Lett. **85**, 60010 (2009). <https://doi.org/10.1209/0295-5075/85/60010>
49. H. Haug, A.-P. Jauho, *Quantum Kinetics in Transport and Optics of Semiconductors* (Springer, Berlin, 2008). <https://doi.org/10.1007/978-3-540-73564-9>
50. G.E. Topp, T. Brandes, G. Schaller, Europhys. Lett. **110**, 67003 (2015). <https://doi.org/10.1209/0295-5075/110/67003>
51. A. Bruch, M. Thomas, S. Viola Kusminskiy, F. von Oppen, A. Nitzan, Phys. Rev. B **93**, 115318 (2016). <https://doi.org/10.1103/PhysRevB.93.115318>
52. D.Y. Baines, T. Meunier, D. Mailly, A.D. Wieck, C. Bäuerle, L. Saminadayar, P.S. Cornaglia, G. Usaj, C.A. Balseiro, D. Feinberg, Phys. Rev. B **85**, 195117 (2012). <https://doi.org/10.1103/PhysRevB.85.195117>
53. T. Hensgens, T. Fujita, L. Janssen, X. Li, C.J.V. Diepen, C. Reichl, W. Wegscheider, S.D. Sarma, L.M.K. Vandersypen, Nature **548**, 70 (2017). <https://doi.org/10.1038/nature23022>
54. J.C. Bayer, T. Wagner, E.P. Rugeramigabo, R.J. Haug, Phys. Rev. B **96**, 235305 (2017). <https://doi.org/10.1103/PhysRevB.96.235305>

55. C.V. den Broeck, Phys. Rev. Lett. **95**, 190602 (2005). <https://doi.org/10.1103/PhysRevLett.95.190602>
56. A. Gomez-Marin, J.M. Sancho, Phys. Rev. E **74**, 062102 (2006). <https://doi.org/10.1103/PhysRevE.74.062102>
57. S. Sheng, Z.C. Tu, J. Phys. Math. Theor. **46**, 402001 (2013). <https://doi.org/10.1088/1751-8113/46/40/402001>

# Chapter 24

## Hierarchical Equations of Motion

### Approach to Quantum Thermodynamics



Akihito Kato and Yoshitaka Tanimura

#### 24.1 Introduction

Recent progress in manipulating small-scale systems provides the possibility of examining the foundation of statistical mechanics in nano materials [1–3]. In particular, elucidating how such purely quantum mechanical phenomena as quantum entanglement and coherence are manifested in thermodynamics is of particular interest in the field of quantum thermodynamics [4, 5]. Such problems have been studied with approaches developed through application of open quantum dynamics theory.

Widely used approaches employ a quantum master equation (QME) that can be derived from the quantum Liouville equation with a system plus bath Hamiltonian by tracing out the heat bath degrees of freedom. To obtain time-evolution equations for the reduced density operator in a compact form, one usually employs the Markov approximation, in which the bath correlation time is very short in comparison to the characteristic time of the system dynamics. The QME with the second-order treatment of the system-bath interaction and the Redfield equation (RE) have been derived with the projection operator method, for example [6, 7]. As we will show in Fig. 24.1, however, even if the dissipation process is Markovian, the fluctuation process may not be, because the latter has to be related to the former through the fluctuation-dissipation theorem (FDT). For this reason, if we apply the QME under Markovian assumption to low temperature systems, then the positivity of the probability distributions of the reduced system cannot be maintained. As a method to preserve positivity, the rotating wave approximation (RWA), which eliminates the non-resonant interaction between

---

A. Kato

Institute for Molecular Science, National Institutes of Natural Sciences,  
Okazaki 444-8585, Japan  
e-mail: kato@ims.ac.jp

Y. Tanimura (✉)

Department of Chemistry, Graduate School of Science,  
Kyoto University, Sakyo-ku, Kyoto 606-8502, Japan  
e-mail: tanimura.yoshitaka.5w@kyoto-u.ac.jp

the system and the heat bath, has been applied in order to write the master equation in the Lindblad form. However, this approximation may modify the thermal equilibrium state as well as the dynamics of the original total Hamiltonian, because the FDT is also altered. For example, while the true thermal equilibrium state of the system at inverse temperature  $\beta$  is given by  $\text{Tr}_{\text{bath}}[\exp(-\beta \hat{H}_{\text{total}})]/\text{Tr}_{\text{total}}[\exp(-\beta \hat{H}_{\text{total}})]$ , where  $\hat{H}_{\text{total}}$  is the total system-plus-bath Hamiltonian, the thermal equilibrium state obtained from the second-order QME approach is  $\exp(-\beta \hat{H}_{\text{sys}})/\text{Tr}_{\text{sys}}[\exp(-\beta \hat{H}_{\text{sys}})]$  where  $\hat{H}_{\text{sys}}$  is the bare system Hamiltonian. This implies that the Markovian assumption even in a perturbative system-bath coupling regime is incompatible through obtaining a quantum mechanical description of dissipative dynamics at low temperature[8]. Furthermore, the consistent description of the QME with the FDT is important to investigate the non-trivial quantum thermodynamic processes, because the violation of the FDT is responsible for the heat generation [9, 10].

As explained in the above, there is a strong limitation on the basis of the conventional QME approaches for the study of quantum thermodynamics, despite their successes to predict the performance of heat machines and propose systems. For example, the inconsistency between the global and local QME, in which the bath couples to the eigenstates of the system and the eigenstates of the sub-system, respectively, have to be reconciled even in a weak system-bath coupling regime [11, 12]. While the global QME can predict the Gibbs distribution in the equilibrium situations, some unphysical behavior caused by employing the global QME in the non-equilibrium situations are reported. Moreover, the local QME may violate the second law of thermodynamics. Attempt to recover the correct thermodynamic description of the global QME was made by incorporating the non-additive dissipation [13], which was not treated in the conventional QME approaches. The interplay between the quantum coherence and environmental noise is essential to optimize the excitation energy and heat transport [14, 15] that should be clarified by using the non-perturbative and non-Markovian quantum dynamical theory [16].

To this time, the approaches used to study the strong coupling regime in the field of quantum thermodynamics include the QME employing a renormalized system-plus-bath Hamiltonian derived with the polaron transformation [17] or the reaction-coordinate mapping [18, 19], the non-equilibrium Green's function (NEGF) method [20–22], the functional integral approach [23], and the stochastic Liouville-von Neumann equation approach [24]. However, the QME with the renormalized Hamiltonians and the NEGF method are limited to a case with a slowly driving field. The stochastic Liouville-von Neumann equation approach is only applicable to the short-time region due to an enormous number of stochastic sampling.

Many of the above-mentioned limitations can be overcome with the hierarchical equations of motion (HEOM), which are derived by differentiating the reduced density matrix elements defined by path integrals [25–30]. This approach allows us to treat systems subject to external driving fields in a numerically rigorous manner under non-Markovian and non-perturbative system-bath coupling conditions and have been applied for the studies of quantum information theory [31, 32] and quantum thermodynamics [33, 34]. Moreover, non-additive dissipation can be incorporated into

the HEOM approach through the explicit non-Markovian treatment of the reduced dynamics.

This chapter presents the introduction of the HEOM for the open quantum dynamics and its application to the quantum thermodynamic processes by evaluating the heat current transferred between the system and the bath in a numerically rigorous manner. As we shown in Ref. [34], the heat current is defined so as to be consistent with the first and second laws of thermodynamics by incorporating non-trivial tripartite correlations. The exact reduced expression for the heat current and the way to numerically evaluate it through the use of the HEOM approach are presented. Then, the numerical illustrations of our approach are given for the two-level heat transfer model and the three-level autonomous heat engine model.

## 24.2 Hierachal Equations of Motion Approach

We consider a system coupled to multiple heat baths at different temperatures. With  $K$  heat baths, the total Hamiltonian is written

$$\hat{H}(t) = \hat{H}_{\text{sys}}(t) + \sum_{k=1}^K \left( \hat{H}_{\text{int}}^{(k)} + \hat{H}_{\text{bath}}^{(k)} \right), \quad (24.1)$$

where  $\hat{H}_{\text{sys}}(t)$  is the system Hamiltonian, whose explicit time dependence originates from the coupling with the external driving field. The Hamiltonian of the  $k$ th bath and the Hamiltonian representing the interaction between the system and the  $k$ th bath are given by  $\hat{H}_{\text{bath}}^{(k)} = \sum_j \hbar \omega_{k,j} \hat{b}_{k,j}^\dagger \hat{b}_{k,j}$  and  $\hat{H}_{\text{int}}^{(k)} = \hat{V}_k \sum_j g_{k,j} (\hat{b}_{k,j}^\dagger + \hat{b}_{k,j})$ , respectively, where  $\hat{V}_k$  is the system operator that describes the coupling to the  $k$ th bath. Here,  $\omega_{k,j}$ ,  $g_{k,j}$ , and  $\hat{b}_{k,j}$  and  $\hat{b}_{k,j}^\dagger$  are the frequency, coupling strength, and the annihilation and creation operators for the  $j$ th mode of the  $k$ th bath, respectively. We assume the factorized initial conditions,  $\hat{\rho}_{\text{tot}}(0) = \hat{\rho}(0) \prod_{k=1}^K e^{-\beta_k \hat{H}_{\text{bath}}^{(k)}} / \text{Tr}(e^{-\beta_k \hat{H}_{\text{bath}}^{(k)}})$ , where  $\hat{\rho}$  is the reduced density operator of the system.

Due to the Bosonic nature of the bath, all bath effects on the system are determined by the bath correlation function,  $C_k(t) \equiv \langle \hat{X}_k(t) \hat{X}_k(0) \rangle_B$ , where  $\hat{X}_k \equiv \sum_j g_{k,j} (\hat{b}_{k,j}^\dagger + \hat{b}_{k,j})$  is the collective coordinate of the  $k$ th bath and  $\langle \dots \rangle_B$  represents the average taken with respect to the canonical density operator of the baths. The bath correlation function is expressed in terms of the bath spectral density,  $J_k(\omega)$ , as

$$C_k(t) = \int_0^\infty d\omega \frac{J_k(\omega)}{\pi} \left[ \coth \left( \frac{\beta_k \hbar \omega}{2} \right) \cos(\omega t) - i \sin(\omega t) \right], \quad (24.2)$$

where  $J_k(\omega) \equiv \pi \sum_j g_{k,j}^2 \delta(\omega - \omega_{k,j})$ , and  $\beta_k$  is the inverse temperature of the  $k$ th bath. The real part of Eq. (24.2) is analogous to the classical correlation function of the bath and corresponds to the fluctuations, while the imaginary part of its corresponds to the dissipation. The fluctuation term is related to the dissipation term through the quantum version of the FDT.

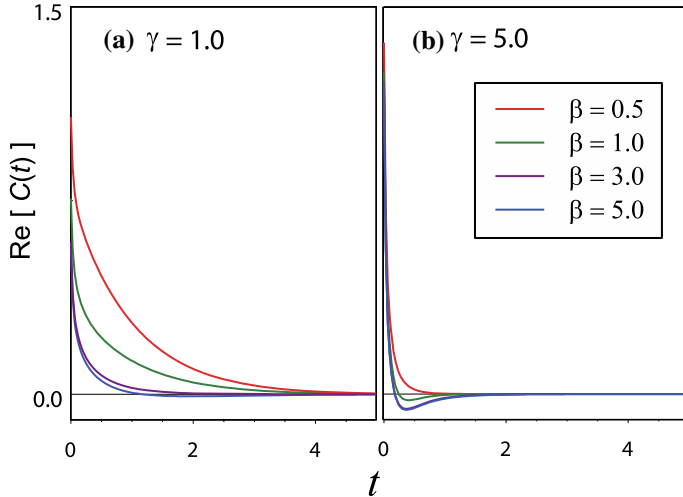


**Fig. 24.1** The real part of Eq. (24.2), depicted as a function of the dimensionless time  $t$  for the intermediate and large values of the inverse noise correlation time: **a**  $\gamma = 1$  and **b**  $\gamma = 5$  for the Drude spectrum,  $J(\omega) = \zeta\gamma^2\omega/(\omega^2 + \gamma^2)$  with  $\zeta = 1$ . Note that  $\gamma \rightarrow \infty$  corresponds to the Markovian (Ohmic) limit. The inverse temperatures are, from top to bottom,  $\beta\hbar = 0.5, 1.0, 3.0$ , and  $5$ . The bath correlation function becomes negative in **a** and **b** at low temperature [28, 30].

Here, in order to illustrate the origin of the positivity problem in the Markovian master equation and RE [28, 30], we present the profiles of fluctuation term,  $\text{Re}[C(t)]$ , for the Drude spectrum,  $J(\omega) = \zeta\gamma^2\omega/(\omega^2 + \gamma^2)$  with  $\zeta$  and  $\gamma$  being the coupling strength and cutoff frequency, respectively, which will be employed in the subsequent numerical calculations. As shown in Fig. 24.1, the fluctuation term becomes negative at low temperature in the region of small  $t$ . This behavior is characteristic of quantum noise [28, 30]. We note that the characteristic time scale that we observe  $\text{Re}[C(t)] < 0$  is not determined from the bath spectral density  $J(\omega)$ , but from the bath temperature. Thus, the validity of the Markovian (or  $\delta(t)$ -correlated) noise assumption is limited in the quantum case to the high temperature regime. Approaches employing the Markovian master equation and the RE, which are usually applied to systems possessing discretized energy states, ignore or simplify such non-Markovian contributions of the fluctuation, and this is the reason that the positivity condition of the population states is broken. As a method to resolve this problem, the RWA is often employed, but a system treated under this approximation will not satisfy the FDT, and thus the use of such an approximation may introduce significant error in the thermal equilibrium state and in the time evolution of the system toward equilibrium. Because the origin of the positivity problem lies in the unphysical Markovian assumption for the fluctuation term, the situation is better in the non-Markovian case, even within the framework of the RE without the RWA [30].

With the factorized initial conditions we can obtain the exact expression for  $\hat{\rho}(t)$ , for example, by using the cumulant expansion technique. In the following, the interaction representation of any operator,  $\hat{A}$ , with respect to the non-interacting

Hamiltonian is expressed as  $\tilde{A}(t)$ . Then, the reduced density operator is written as  $\tilde{\rho}(t) = \mathcal{T}_+[\mathcal{U}_{\text{IF}}(t, 0)\hat{\rho}(0)]$ , where  $\mathcal{U}_{\text{IF}}(t, t_0) = \prod_{k=1}^K \exp[\int_{t_0}^t d\tau W_k(\tau, t_0)]$  is the Feynman–Vernon influence functional in operator form, and  $\mathcal{T}_+[\dots]$  is the time-ordering operator, where the operators in  $[\dots]$  are arranged in a chronological order. The operators of the influence phase are defined by

$$W_k(\tau, t_0) = \int_{t_0}^{\tau} d\tau' \tilde{\Phi}_k(\tau') \left\{ \text{Re}[C_k(\tau - \tau')] \tilde{\Phi}_k(\tau') - \text{Im}[C_k(\tau - \tau')] \tilde{\Psi}_k(\tau') \right\}, \quad (24.3)$$

where  $\hat{\Phi}_k \hat{A} = (i/\hbar)[\hat{V}_k, \hat{A}]$  and  $\hat{\Psi}_k \hat{A} = (1/\hbar)\{\hat{V}_k, \hat{A}\}$ . This expression for the reduced density operator, however, does not lead to the closed time-evolution equation.

Then, Tanimura and his collaborators developed the hierarchical equations of motion (HEOM) that consist of the set of equations of motion for the auxiliary density operators (ADOs) as the closed time-evolution equations [25–30]. Here, we consider the case that the bath correlation function, Eq. (24.2), is written as a linear combination of exponential functions,  $C_k(t) = \sum_{l=0}^{L_k} c_{k,l} e^{-\gamma_{k,l}|t|}$ , which is realized for the Drude, Lorentz [35, 36], and Brownian bath spectral models [37] (and combinations thereof [38, 39]). Note that, using a set of special functions instead of the exponential functions, we can treat a system with a sub-Ohmic spectral distribution at the zero temperature, where the quantum phase transition occurs [40, 41]. We might include a delta function for better description of the bath correlation function for the HEOM formalism, for example, to approximate the contribution from the higher-order Matsubara frequency terms [27]. The ADOs introduced in the HEOM are defined by

$$\begin{aligned} \hat{\rho}_{\vec{n}}(t) &\equiv \mathcal{T}_+ \left\{ \exp \left[ -\frac{i}{\hbar} \int_0^t ds \mathcal{L}(s) \right] \right\} \\ &\times \mathcal{T}_+ \left\{ \prod_{k=1}^K \prod_{l=0}^{L_k} \left[ - \int_0^t d\tau e^{-\gamma_{k,l}(t-\tau)} \tilde{\Theta}_{k,l}(\tau) \right]^{n_{k,l}} \mathcal{U}_{\text{IF}}(t, 0) \hat{\rho}(0) \right\}. \end{aligned} \quad (24.4)$$

Here, we have  $\tilde{\Theta}_{k,l} \equiv \text{Re}(c_{k,l})\hat{\Phi}_k - \text{Im}(c_{k,l})\hat{\Psi}_k$  and  $\mathcal{L}(t)\hat{\rho} = [\hat{H}_{\text{sys}}(t), \hat{\rho}]$ . Each ADO is specified by the index  $\vec{n} = (n_{1,0}, \dots, n_{1,L_1}, n_{2,0}, \dots, n_{K,L_K})$ , where each element takes an integer value larger than zero. The ADO for which all elements are zero,  $n_{1,0} = n_{1,1} = \dots = n_{K,L_K} = 0$ , corresponds to the actual reduced density operator. Taking the time derivative of Eq. (24.4), the equations of motion for the ADOs are obtained as

$$\begin{aligned} \frac{d}{dt} \hat{\rho}_{\vec{n}}(t) &= - \left[ \frac{i}{\hbar} \mathcal{L}(t) + \sum_{k=1}^K \sum_{l=0}^{L_k} n_{k,l} \gamma_{k,l} \right] \hat{\rho}_{\vec{n}}(t) \\ &- \sum_{k=1}^K \hat{\Phi}_k \sum_{l=0}^{L_k} \hat{\rho}_{\vec{n}+\vec{e}_{k,l}}(t) - \sum_{k=1}^K \sum_{l=0}^{L_k} n_{k,l} \hat{\Theta}_{k,l} \hat{\rho}_{\vec{n}-\vec{e}_{k,l}}(t), \end{aligned} \quad (24.5)$$

where  $\vec{e}_{k,l}$  is the unit vector along the  $k \times (l+1)$ th direction. The HEOM consist of an infinite number of equations, but they can be truncated at finite order by ignoring all ADOs beyond the value at which  $\sum_{k,l} n_{k,l}$  first exceeds some appropriately large value  $N$ . In principle, the HEOM provides an asymptotic approach that allows us to calculate various physical quantities with any desired accuracy by adjusting the number of hierachal elements determined by  $N$ ; the error introduced by the truncation is negligibly small in the case that  $N$  is sufficiently large. Note that we can also derive the HEOM for the Fermionic baths [42–44]. Therefore, we can extend the present investigations for the heat transport to the electronic heat current problem.

### 24.3 Heat Currents

For this system-bath Hamiltonian, the heat current (HC) is defined as the rate of decrease of the bath energy,  $\dot{Q}_{\text{HC},k}(t) \equiv -d\langle \hat{H}_{\text{bath}}^{(k)}(t) \rangle / dt$ . Using the Heisenberg equations, the heat current can be rewritten as (see Appendix A for the derivation)

$$\dot{Q}_{\text{HC},k}(t) = \dot{Q}_{\text{SEC},k}(t) + \frac{d}{dt} \left\langle \hat{H}_{\text{int}}^{(k)}(t) \right\rangle + \sum_{k' \neq k} \dot{I}_{k,k'}, \quad (24.6)$$

where

$$\dot{Q}_{\text{SEC},k}(t) = \frac{i}{\hbar} \left\langle \left[ \hat{H}_{\text{int}}^{(k)}(t), \hat{H}_{\text{sys}}(t) \right] \right\rangle \quad (24.7)$$

and

$$\dot{I}_{k,k'}(t) = \frac{i}{\hbar} \left\langle \left[ \hat{H}_{\text{int}}^{(k)}(t), \hat{H}_{\text{int}}^{(k')}(t) \right] \right\rangle. \quad (24.8)$$

The first term on the right-hand side of Eq. (24.6),  $\dot{Q}_{\text{SEC},k}$ , describes the change of the system energy due to the coupling with the  $k$ th bath that is defined as the total  $k$ th heat current in the conventional QME approaches, which we call it the system energy current (SEC). The second term vanishes under steady-state conditions and in the limit of a weak system-bath coupling. The third term contributes to the HC even under steady-state conditions, while it vanishes in the weak coupling limit. The third term is the main difference with the SEC. This term plays a significant role in the case that the  $k$ th and  $k'$ th system-bath interactions are non-commuting and each system-bath coupling is strong. We also note that because this third term is of greater than fourth-order in the system-bath interaction, it does not appear in the second-order QME approach. Therefore only non-perturbative approaches that include higher-order QME approaches allow us to reveal the features. Here, we investigate this contribution using the HEOM theory. Hereafter, we refer to this term as the “tri-partite correlations” (TPC) because the statistical correlation among the

$k$ th bath, system, and  $k'$ th bath is at least necessary for  $I_{k,k'}$  to be present. There are two physical situations that the TPC contributions of Eq.(24.8) vanishes: One is that each  $\hat{V}_k$  acts on a different Hilbert space of the system, which is realized for a mesoscopic heat-transport system, including nanotubes and nanowires. This is because the left and right reservoirs are coupled to the left and right end degrees of freedom of the system. Another is the cases for  $\hat{V}_k \propto \hat{V}_{k'}$ , which is often assumed for a simple heat transport system. However, for a microscopic system that includes single-molecular junctions and superconducting qubits, the TPC contribution may play a significant role because of the microscopic manipulation of the system-bath interactions for  $[\hat{V}_k, \hat{V}_{k'}] \neq 0$ .

Note that, although here we focus only on the first moment of the work and the heat, we can investigate the characteristic features of quantum thermodynamics on the basis of the distribution functions of them by using the HEOM [45] and other approaches [23, 46].

### 24.3.1 The First and Second Laws of Thermodynamics

In this section, we formulate the first and second laws of quantum thermodynamics that are valid for any system-bath coupling strength, as the natural extensions of the classical thermodynamic laws. This is because we are not sure how the quantum thermodynamic effects emerge into the extension of the classical thermodynamic laws, in particular, in the strong coupling regime. Then we restrict our investigation of the second law in the steady state case, because there is an ambiguity of formulating the second law under non-steady case in a strong coupling regime [21].

We can obtain the first law of thermodynamics by summing Eq.(24.6) over all  $k$ :

$$\sum_{k=1}^K \dot{Q}_{\text{HC},k}(t) = \frac{d}{dt} \left\langle \hat{H}_{\text{sys}}(t) + \sum_{k=1}^K \hat{H}_{\text{int}}^{(k)}(t) \right\rangle - \dot{W}(t), \quad (24.9)$$

where  $\dot{W}(t) = \langle (\partial \hat{H}_{\text{sys}}(t) / \partial t) \rangle$  is the power. The quantity,  $\hat{H}_{\text{sys}}(t) + \sum_{k=1}^K \hat{H}_{\text{int}}^{(k)}(t)$ , is identified as the internal energy, because the contributions of  $I_{k,k'}$  cancel out.

In a steady state without external driving forces, the second law is expressed as [47, 48]

$$-\sum_{k=1}^K \beta_k \dot{Q}_{\text{HC},k} \geq 0, \quad (24.10)$$

while with a periodic external driving force, it is given by

$$-\sum_{k=1}^K \beta_k Q_{\text{HC},k}^{\text{cyc}} \geq 0, \quad (24.11)$$

where  $Q_{\text{HC},k}^{\text{cyc}} = \oint_{\text{cyc}} dt \dot{Q}_{\text{HC},k}(t)$  is the heat absorbed or released per cycle. When the system is coupled to the hot ( $k = h$ ) and the cold ( $k = c$ ) baths and is driven by

the periodic field, the heat to work conversion efficiency is bounded by the Carnot efficiency, which is derived by the combination of the first and second laws, as

$$\eta \equiv \frac{-W^{\text{cyc}}}{Q_{\text{HC},k}^{\text{cyc}}} \leq 1 - \frac{\beta_h}{\beta_c}. \quad (24.12)$$

The second law without a driving force can be rewritten in terms of the SEC as

$$-\sum_{k=1}^K \beta_k \dot{Q}_{\text{SEC},k} \geq \sum_{k,k'=1}^K \beta_k \dot{I}_{k,k'}. \quad (24.13)$$

When the right-hand side of Eq. (24.13) is negative, the left-hand side can also take negative values. However, this contradicts the Clausius statement of the second law, i.e., that heat never flows spontaneously from a cold body to a hot body. As we show in the following sections, it is necessary to include the TPC terms to have a thermodynamically valid description.

## 24.4 Reduced Description of Heat Currents

For the bosonic bath Hamiltonians considered here, we can trace out the bath degrees of freedom in an exact manner by using the second-order cumulant expansion and obtain the reduced expression for the HC, Eq. (24.6). The derivation is given in Appendix B and Ref. [34] in cases that the bath correlation function involves the delta function. The analytical reduced expression for the  $k$ th HC is given by

$$\dot{Q}_{\text{HC},k}(t) = \frac{2}{\hbar} \int_0^t d\tau \text{Im} \left[ \dot{C}_k(t-\tau) \langle \hat{V}_k(t) \hat{V}_k(\tau) \rangle \right] + \frac{2}{\hbar} \text{Im} [C_k(0)] \langle \hat{V}_k^2(t) \rangle. \quad (24.14)$$

Note that the second term on the right-hand side of Eq. (24.14) should vanish as can be seen from the definition of the bath correlation function. However, for the Drude bath spectrum, the contribution of second term is finite, and is found to be necessary to guarantee the first law at least numerically, because of the coarse-grained (long-time approximation) nature of the Drude model [14, 49]. The first term of Eq. (24.14) consists of non-equilibrium two-time correlation functions of the system operator in the interaction Hamiltonian, and the calculation of these terms seems to be formidable task specifically when the system is driven by the external fields. However, by employing the noise decomposition of the HEOM approach for the bath correlation functions in Eq. (24.14), and comparing the resulting expressions with the definition of the ADOs given in Eq. (24.4), we can evaluate the HC in terms of the ADOs as [34]

$$\dot{Q}_{\text{HC},k}(t) = - \sum_{l=0}^{L_k} \gamma_{k,l} \text{Tr} \left[ \hat{V}_k \hat{\rho}_{1 \times \vec{e}_{k,l}}(t) \right] + \frac{2}{\hbar} \text{Im} [C_k(0)] \text{Tr} \left[ \hat{V}_k^2 \hat{\rho}_0(t) \right]. \quad (24.15)$$

We note that the ADOs here we employed are the same as that of the conventional HEOM: Using ADOs obtained from the numerical integrating of the HEOM in Eq. (24.5), we can calculate the HC.

## 24.5 Numerical Illustration

To demonstrate a role of the TPC in the HC, we consider a two-level heat transfer model [50–53] and a three-level autonomous heat engine model [18] (Fig. 24.2). We investigate the steady-state HC and SEC obtained from Eq. (24.5) with the condition  $(d/dt)\hat{\rho}_n = 0$  using the BiCGSafe method for linear equations [54]. We assume that the spectral density of each bath takes the Drude form,  $J_k(\omega) = \zeta_k \gamma^2 \omega / (\omega^2 + \gamma^2)$ , where  $\zeta_k$  is the system-bath coupling strength, and  $\gamma$  is the cutoff frequency. A Padé spectral decomposition scheme [55–57] is employed to obtain the expansion coefficients of the bath correlation functions. The accuracy of numerical results is examined by increasing the values of  $L_1, \dots, L_K$  and  $N$  until convergence is reached.

### 24.5.1 Two-Level Heat Transfer Model

The model studied here consists of a two-level system coupled to two Bosonic baths at different temperatures. This model has been employed extensively as the simplest heat-transport model. The system Hamiltonian is given by  $\hat{H}_{\text{sys}} = (\hbar\omega_0/2)\sigma_z$ . We consider the case in which the system is coupled to the hot bath through  $\hat{V}_h = \sigma_x$  and to the cold bath through  $\sigma_x$  and  $\sigma_z$  in the form  $\hat{V}_c = (\sigma_x + \sigma_z)/\sqrt{2}$ . In order to investigate the difference in the HC with the SEC that usually calculated from the

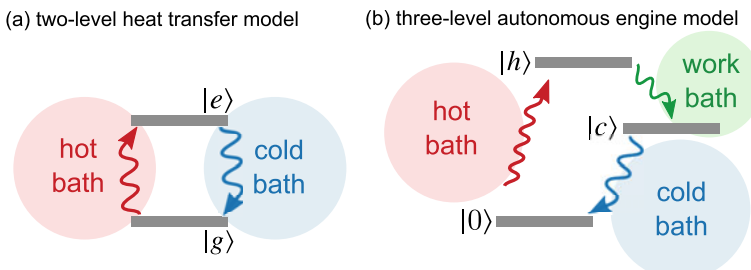
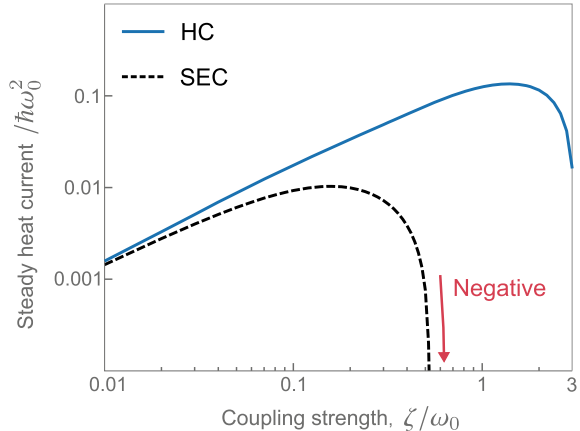


**Fig. 24.2** Schematic depiction of **a** the two-level heat transfer model and **b** the three-level autonomous heat engine model investigated in this study.

**Fig. 24.3** The heat current (HC) and system energy current (SEC) for the two-level heat transfer model as functions of the system-bath coupling. Both currents are calculated from the HEOM, Eq. (24.5).



QME approaches, we consider the case  $[\hat{V}_h, \hat{V}_c] \neq 0$ , because otherwise the TPC term vanishes. This is the case that most of previous investigations have considered. We chose  $\beta_h = 0.5 \hbar\omega_0$ ,  $\beta_c = \hbar\omega_0$ , and  $\gamma = 2\omega_0$ .

Figure 24.3 depicts the HCs in the steady state,  $\dot{Q}_{HC,h} = -\dot{Q}_{HC,c}$  or  $\dot{Q}_{SEC} \equiv \dot{Q}_{SEC,h} = -\dot{Q}_{SEC,c}$ , as functions of the system-bath coupling strength,  $\zeta \equiv \zeta_h = \zeta_c$ . In the weak system-bath coupling regime, both HC and SEC increase linearly with the coupling strength in similar manners. In this case, we found that the TPC contribution is minor. As the strength of the system-bath coupling increases, the difference between them becomes large: While  $\dot{Q}_{SEC}$  decreases after reaching a maximum value near  $\zeta = 0.2\omega_0$ , the TPC contribution,  $\dot{I}_{h,c}$ , dominates the HC, and as a result, it remains relatively large. Thus, in this regime, the SEC becomes much smaller than the HC. In the very strong coupling regime, the SEC eventually becomes negative, which indicates the violation of the second law. In order to eliminate such non-physical behavior, we have to include the  $\dot{I}_{h,c}$  term in the definition of the SEC. Note that the differences between the SEC and HC described above vanish when  $\hat{V}_c = \hat{V}_h = \sigma_x$ , and hence in this case, there is no negative current problem.

### 24.5.2 Autonomous Three-Level Engine

The autonomous three-level heat engine model considered here consists of three states, denoted by  $|0\rangle$ ,  $|h\rangle$ , and  $|c\rangle$ , coupled to three bosonic baths. The work is extracted through the work bath. The system Hamiltonian is expressed as  $\hat{H}_{sys} = \sum_{i=0,h,c} \hbar\omega_i |i\rangle\langle i|$  with  $\omega_h > \omega_c > \omega_0$ . The system-bath interactions are defined as  $\hat{V}_h = |0\rangle\langle h| + |h\rangle\langle 0|$ ,  $\hat{V}_c = |0\rangle\langle c| + |c\rangle\langle 0|$ , and  $\hat{V}_w = |h\rangle\langle c| + |c\rangle\langle h|$ . We set  $\omega_0 = 0$  without loss of generality. A mechanism for the system acting as the heat engine is as follows: First, the heat is absorbed from the hot bath. This heat is transferred from the system to the work bath in the form of the work, while the remaining heat is

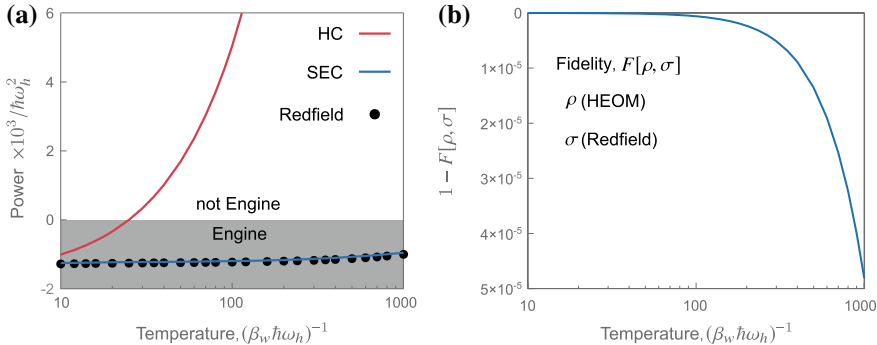


**Fig. 24.4** **a** The heat current (HC, red line) and the system energy current (SEC, blue line) calculated from the HEOM approach, and the HC from the RE approach (black circles) as functions of the temperature of the work bath. The shaded area represents the region that the system acts as the heat engine. **b** The fidelity  $F[\rho, \sigma]$  as a function of the temperature of the work bath, where  $\rho$  and  $\sigma$  are the reduced density matrix in the steady state calculated from the HEOM and RE approaches, respectively.

damped into the cold bath. Therefore, the sign conditions for the HC have to be  $\dot{Q}_{HC,h} > 0$ ,  $\dot{Q}_{HC,c} < 0$ , and  $\dot{Q}_{HC,w} < 0$ . However, in order to identify the HC to the work bath with the power, the entropy change of the work bath have to be negligibly small, which is realized when the temperature of the work bath becomes infinitely high,  $\beta_w \rightarrow 0$  [48, 58, 59]. It should be noted that the stochastic Liouville equation (SLE), in which the back action to the reservoir is ignored, corresponds to the infinite temperature limit of the HEOM [28]. Therefore the entropy calculated from the SLE does not change. When the temperature of the work bath is finite, only the part of the energy extracted from the system can be used as work. However, we show in the following calculation that the system does not act as the engine in the infinitely high temperature limit of the work bath. We set  $\omega_c = 0.5 \omega_h$ ,  $\zeta_h = \zeta_c = \zeta_w = 0.001 \omega_h$ ,  $\gamma = 10 \omega_h$ ,  $\beta_h \hbar\omega_h = 0.1$ , and  $\beta_c \hbar\omega_h = 1$ .

In Fig. 24.4a, we depict the HC evaluated from the HEOM approach, Eq. (24.15), SEC, and the HC from the RE approach, as functions of the temperature of the work bath. While the SEC and the HC from the RE approach look identical and weakly dependent on the work-bath temperature with the negative sign, the actual HC increases as the temperature of the work bath increases, and eventually its sign changes from negative to positive in the vicinity of  $(\beta_w \hbar\omega_h)^{-1} = 20 - 30$ . This indicates that the TPC determines the characteristic of the heat-engine system; the system no longer acts as the heat engine.

It should be noted that the TPC effect on the HC becomes important even in the weak system-bath coupling case, as we chose  $\zeta = 0.001 \omega_h$ . To illustrate this point, we plot the fidelity,  $F[\rho, \sigma] = \text{Tr}[\sqrt{\sqrt{\rho}\sigma\sqrt{\rho}}]$ , where  $\rho$  and  $\sigma$  are the steady state distributions calculated from the HEOM and the RE approaches, respectively, in Fig. 24.4b. For all temperature region, the deviation of the fidelity from 1 is negligibly small indicating the system-bath coupling strength is sufficiently weak to be the

RE approach valid. This implies that both the HEOM and RE give the identical steady state, while there is large discrepancy between the HEOM and RE results in the calculation of HC in Fig. 24.4a. Thus, we have to introduce autonomous heat engine models which are robust against the tri-partite correlations. The theoretical prescription for the finite temperature bath is required to divide the energy obtained from the system into work and heat. Because of the tri-partite correlations, the QME approach is not valid even in the weak-coupling regime.

## 24.6 Concluding Remarks

In this paper, we introduced an explicit analytical expression for the heat current (HC) on the basis of the energy change of the baths, which includes contributions from the tri-partite correlations (TPC) in addition to that from the system energy current (SEC). Our definition of the HC can be applied to any system with any bath spectral distribution and any strength of the system-bath coupling. Investigation on the basis of the HEOM approach indicated that the HC is physically more appropriate thermodynamics variable than the SEC; the TPC contribution in the heat-engine system is significantly large even in a weak system-bath coupling regime.

In this study, we restricted our analysis to a system described by several energy states. Using the HEOM approach it is possible to investigate a system described by coordinate and momentum (Wigner space) to treat potentials of any form with time-dependent external forces [30, 60]. This feature is ideal for studying quantum transport systems, including the self-current oscillation of a resonant tunneling diode system [61] and the tunneling effect of a ratchet system [62]. Moreover, this treatment allows identification of purely quantum mechanical effects through comparison of classical and quantum results in the Wigner distribution [60, 62, 63].

Although our analysis are limited to the harmonic heat bath, now it becomes possible to study a system with many degrees of freedom, for example, a part of which can be regarded as a spin bath, due to the advent of the computer technology. The numerical implementation of the HEOM by a message passing interface [64], graphical processing unit [65, 66], and the open computer language [67] or the HEOM combined with the stochastic Schrödinger equation [68–70] are such examples.

We leave such extensions to future studies to be carried out in the context of quantum thermodynamics.

**Acknowledgements** The authors are grateful for motivating us to write this article with Yoshi Oono. A. K. is supported by JSPS KAKENHI Grant Number 17H02946. Y. T. is supported by JSPS KAKENHI Grant Number A26248005.

## Appendix A: Derivation of Equation (24.6)

The heat current is defined as the rate of decrease of the bath energy,  $\dot{Q}_{\text{HC},k}(t) = -d\langle \hat{H}_{\text{bath}}^{(k)}(t) \rangle / dt$ , which can be rewritten by using the Heisenberg equations for  $\hat{H}_{\text{int}}^{(k)}$  and  $\hat{H}_{\text{bath}}^{(k)}$  as

$$\begin{aligned}\dot{Q}_{\text{HC},k}(t) &= \frac{i}{\hbar} \left\langle \left[ \hat{H}_{\text{bath}}^{(k)}(t), \hat{H}_{\text{int}}^{(k)}(t) \right] \right\rangle \\ &= \frac{i}{\hbar} \left\langle \left[ \hat{H}_{\text{int}}^{(k)}(t), \hat{H}_{\text{sys}}(t) \right] \right\rangle + \frac{d}{dt} \left\langle \hat{H}_{\text{int}}^{(k)}(t) \right\rangle + \sum_{k'} \frac{i}{\hbar} \left\langle \left[ \hat{H}_{\text{int}}^{(k)}(t), \hat{H}_{\text{int}}^{(k')}(t) \right] \right\rangle.\end{aligned}\quad (24.16)$$

The first term of r.h.s. of Eq. (24.16) is related to the energy flow to the  $k$ th bath via the energy conservation equation for  $\hat{H}_{\text{sys}}$  as  $\frac{d}{dt} \langle \hat{H}_{\text{sys}}(t) \rangle = \dot{W}(t) + \sum_k \dot{Q}_{\text{SEC},k}(t)$ , where  $\dot{Q}_{\text{SEC},k}(t) = (i/\hbar) \langle [\hat{H}_{\text{int}}^{(k)}(t), \hat{H}_{\text{sys}}(t)] \rangle$ . Therefore, by using the above definition for  $\dot{Q}_{\text{SEC},k}(t)$  and Eqs. (24.8), (24.6) is derived.

## Appendix B: Derivation of Equation (24.14)

To derive Eq. (24.14), we adapt a generating functional approach by adding the source term,  $f_k(t)$ , for the  $k$ th interaction Hamiltonian as

$$\hat{V}_k \hat{X}_k \rightarrow \hat{V}_{k,f}(t) \hat{X}_k \equiv \left( \hat{V}_k + f_k(t) \right) \hat{X}_k \quad (24.17)$$

Here, in order to evaluate an expectation value, we add the source term to the ket (left) side of the density operator, which does not change a role of the system-bath interaction in the time-evolution operator. This source term enables us to have a collective bath coordinate with the functional derivative as

$$\tilde{X}_k(t) \tilde{\rho}_{\text{tot}}(t) = i \hbar \frac{\delta}{\delta f_k(t)} \tilde{\rho}_{\text{tot},f}(t) \Big|_{f \equiv 0}. \quad (24.18)$$

Then, the expectation value of the operator  $\hat{Z}_k \equiv \hat{A} \hat{X}_k$  for any system operator  $\hat{A}$  reads

$$\begin{aligned}\langle \hat{Z}_k(t) \rangle &= \text{Tr}_{\text{sys}} \left[ \tilde{A}(t) i \hbar \frac{\delta}{\delta f_k(t)} \tilde{\rho}_f(t) \Big|_{f \equiv 0} \right] \\ &= \frac{2}{\hbar} \int_0^t d\tau \text{Im} \left[ C_k(t - \tau) \langle \hat{A}(t) \hat{V}_k(\tau) \rangle \right].\end{aligned}\quad (24.19)$$

Next, the  $k$ th HC, Eq.(24.6), is rewritten by using the Heisenberg equation for  $\hat{V}_k$  as  $\dot{\hat{Q}}_k(t) = \frac{d}{dt}\langle\hat{H}_{\text{int}}^{(k)}(t)\rangle - \langle(\frac{d}{dt}\hat{V}_k(t))\hat{X}_k(t)\rangle$ . The time derivatives,  $\frac{d}{dt}\langle\hat{H}_{\text{int}}^{(k)}(t)\rangle$  and  $\langle(\frac{d}{dt}\hat{V}_k(t))\hat{X}_k(t)\rangle$ , are given by the time differentiation of Eq.(24.19) for  $\hat{A} = \hat{V}_k$  and Eq.(24.19) for  $\hat{A} = \frac{d}{dt}\hat{V}_k$ , respectively. This immediately leads to the expression for the  $k$ th HC in Eq.(24.14).

## References

1. M. Campisi, P. Hänggi, P. Talkner, Colloquium: quantum fluctuation relations: foundations and applications. *Rev. Mod. Phys.* **83**(3), 771 (2011). <https://doi.org/10.1103/RevModPhys.83.771>
2. A. Polkovnikov, K. Sengupta, A. Silva, M. Vengalattore, Colloquium: nonequilibrium dynamics of closed interacting quantum systems. *Rev. Mod. Phys.* **83**(3), 863 (2011). <https://doi.org/10.1103/RevModPhys.83.863>
3. J. Eisert, M. Friesdorf, C. Gogolin, Quantum many-body systems out of equilibrium. *Nat. Phys.* **11**(2), 124 (2015). <https://doi.org/10.1038/nphys3215>
4. M. Lostaglio, K. Korzekwa, D. Jennings, T. Rudolph, Quantum coherence, time-translation symmetry, and thermodynamics. *Phys. Rev. X* **5**(2), 021001 (2015). <https://doi.org/10.1103/PhysRevX.5.021001>
5. K. Korzekwa, M. Lostaglio, J. Oppenheim, D. Jennings, The extraction of work from quantum coherence. *N. J. Phys.* **18**(2), 023045 (2016). <https://doi.org/10.1088/1367-2630/18/2/023045>
6. H.P. Breuer, F. Petruccione, *The Theory of Open Quantum Systems* (Oxford University Press, New York, 2002). <https://doi.org/10.1093/acprof:oso/9780199213900.001.0001>
7. R. Kosloff, Quantum thermodynamics: a dynamical viewpoint. *Entropy* **15**(12), 2100 (2013). <https://doi.org/10.3390/e15062100>
8. P. Häggi, G.-L. Ingold, Fundamental aspects of quantum brownian motion. *Chaos* **15**(2), 026105 (2005). <https://doi.org/10.1063/1.1853631>
9. T. Harada, S. Sasa, Equality connecting energy dissipation with a violation of the fluctuation-response relation. *Phys. Rev. Lett.* **95**(13), 130602 (2005). <https://doi.org/10.1103/PhysRevLett.95.130602>
10. K. Saito, Energy dissipation and fluctuation response in driven quantum langevin dynamics. *Europhys. Lett.* **83**(5), 50006 (2008). <https://doi.org/10.1209/0295-5075/83/50006>
11. P. Hofer, M. Perarnau-Llobet, L. Miranda, M. David, G. Haack, R. Silva, J.B. Brask, N. Brunner, Markovian master equations for quantum thermal machines: local versus global approach. *N. J. Phys.* **19**(12), 123037 (2017). <https://doi.org/10.1088/1367-2630/aa964f>
12. J.O. González, L.A. Correa, G. Nocerino, J.P. Palao, D. Alonso, G. Adesso, Testing the validity of the ‘local’ and ‘global’ GKLS master equations on an exactly solvable model. *Open System and Information Dynamics* **24**(4), 1740010 (2017). <https://doi.org/10.1142/S1230161217400108>
13. M.T. Mitchison, M.B. Plenio, Non-additive dissipation in open quantum networks out of equilibrium. *N. J. Phys.* **20**(3), 033005 (2018). <https://doi.org/10.1088/1367-2630/aa9f70>
14. A. Ishizaki, G. Fleming, Unified treatment of quantum coherent and incoherent hopping dynamics in electronic energy transfer: reduced hierarchy equation approach. *J. Chem. Phys.* **130**(23), 234111 (2009). <https://doi.org/10.1063/1.3155372>
15. S. Huelga, M. Plenio, Vibrations, quanta and biology. *Contemp. Phys.* **54**(4), 181 (2013). <https://doi.org/10.1080/00405000.2013.829687>
16. I. de Vega, D. Alonso, Dynamics of non-Markovian open quantum systems. *Rev. Mod. Phys.* **89**(1), 015001 (2017). <https://doi.org/10.1103/RevModPhys.89.015001>
17. D. Gelbwaser-Klimovsky, A. Aspuru-Guzik, Strongly coupled quantum heat machines. *J. Phys. Chem. Lett.* **6**(17), 3477 (2015). <https://doi.org/10.1021/acs.jpclett.5b01404>

18. P. Strasberg, G. Schaller, N. Lambert, T. Brandes, Nonequilibrium thermodynamics in the strong coupling and non-Markovian regime based on a reaction coordinate mapping. *N. J. Phys.* **18**(7), 073007 (2016). <https://doi.org/10.1088/1367-2630/18/7/073007>
19. D. Newman, F. Mintert, A. Nazir, Performance of a quantum heat engine at strong reservoir coupling. *Phys. Rev. E* **95**(3), 032139 (2017). <https://doi.org/10.1103/PhysRevE.95.032139>
20. M. Esposito, M.A. Ochoa, M. Galperin, Quantum thermodynamics: a nonequilibrium green's function approach. *Phys. Rev. Lett.* **114**(8), 080602 (2015). <https://doi.org/10.1103/PhysRevLett.114.080602>
21. M. Esposito, M.A. Ochoa, M. Galperin, Nature of heat in strongly coupled open quantum systems. *Phys. Rev. B* **92**(23), 235440 (2015). <https://doi.org/10.1103/PhysRevB.92.235440>
22. A. Bruch, M. Thomas, S.V. Kusminskiy, F. von Oppen, A. Nitzan, Quantum thermodynamics of the driven resonant level model. *Phys. Rev. B* **93**(11), 115318 (2016). <https://doi.org/10.1103/PhysRevB.93.115318>
23. M. Carrega, P. Solinas, M. Sassetti, U. Weiss, Energy exchange in driven open quantum systems at strong coupling. *Phys. Rev. Lett.* **116**(24), 240403 (2016). <https://doi.org/10.1103/PhysRevLett.116.240403>
24. R. Schmidt, M.F. Carusela, J.P. Pekola, S. Suomela, J. Ankerhold, Work and heat for two-level systems in dissipative environments: strong driving and non-markovian dynamics. *Phys. Rev. B* **91**(22), 224303 (2015). <https://doi.org/10.1103/PhysRevB.91.224303>
25. Y. Tanimura, R. Kubo, Time evolution of a quantum system in contact with a nearly gaussian-markoffian noise bath. *J. Phys. Soc. Jpn.* **58**(101), 101 (1989). <https://doi.org/10.1143/JPSJ.58.101>
26. Y. Tanimura, Nonperturbative expansion method for a quantum system coupled to a harmonic-oscillator bath. *Phys. Rev. A* **41**(12), 6676 (1990). <https://doi.org/10.1103/PhysRevA.41.6676>
27. A. Ishizaki, Y. Tanimura, Quantum dynamics of system strongly coupled to low-temperature colored noise bath: reduced hierarchy equations approach. *J. Phys. Soc. Jpn.* **74**(12), 3131 (2005). <https://doi.org/10.1143/JPSJ.74.3131>
28. Y. Tanimura, Stochastic liouville, langevin, fokker-planck, and master equation approaches to quantum dissipative systems. *J. Phys. Soc. Jpn.* **75**(8), 082001 (2006). <https://doi.org/10.1143/JPSJ.75.082001>
29. Y. Tanimura, Reduced hierarchical equations of motion in real and imaginary time: correlated initial states and thermodynamic quantities. *J. Chem. Phys.* **141**(4), 044114 (2014). <https://doi.org/10.1063/1.4890441>
30. Y. Tanimura, Real-time and imaginary-time quantum hierachal fokker-planck equations. *J. Chem. Phys.* **142**(14), 144110 (2015). <https://doi.org/10.1063/1.4916647>
31. A.G. Dijkstra, Y. Tanimura, Non-markovian entanglement dynamics in the presence of system-bath coherence. *Phys. Rev. Lett.* **104**(25), 250401 (2010). <https://doi.org/10.1103/PhysRevLett.104.250401>
32. A.G. Dijkstra, Y. Tanimura, System bath correlations and the nonlinear response of qubits. *J. Phys. Soc. Jpn.* **81**(6), 063301 (2012). <https://doi.org/10.1143/JPSJ.81.063301>
33. A. Kato, Y. Tanimura, Quantum heat transport of a two-qubit system: interplay between system-bath coherence and qubit-qubit coherence. *J. Chem. Phys.* **143**(6), 064107 (2015). <https://doi.org/10.1063/1.4928192>
34. A. Kato, Y. Tanimura, Quantum heat current under non-perturbative and non-markovian conditions: applications to heat machines. *J. Chem. Phys.* **145**(22), 224105 (2016). <https://doi.org/10.1063/1.4971370>
35. C. Kreisbeck, T. Kramer, Long-lived electronic coherence in dissipative exciton dynamics of light-harvesting complexes. *J. Phys. Chem. Lett.* **3**(19), 2828 (2012). <https://doi.org/10.1021/jz3012029>
36. J. Ma, Z. Sun, X. Wang, F. Nori, Entanglement dynamics of two qubits in a common bath. *Phys. Rev. A* **85**(6), 062323 (2012). <https://doi.org/10.1103/PhysRevA.85.062323>
37. M. Tanaka, Y. Tanimura, Quantum dissipative dynamics of electron transfer reaction system: nonperturbative hierarchy equations approach. *J. Phys. Soc. Jpn.* **78**(7), 073802 (2009). <https://doi.org/10.1143/JPSJ.78.073802>

38. H. Liu, L. Zhu, S. Bai, Q. Shi, Reduced quantum dynamics with arbitrary bath spectral densities: hierarchical equations of motion based on several different bath decomposition schemes. *J. Chem. Phys.* **140**(13), 134106 (2014). <https://doi.org/10.1063/1.4870035>
39. Y. Tanimura, Reduced hierarchy equations of motion approach with drude plus brownian spectral distribution: probing electron transfer processes by means of two-dimensional correlation spectroscopy. *J. Chem. Phys.* **137**(22), 22A550 (2012). <https://doi.org/10.1063/1.4766931>
40. Z. Tang, O.Z. Gong, H. Wang, J. Wu, Extended hierarchy equation of motion for the spin-boson model. *J. Chem. Phys.* **143**(22), 224112 (2015). <https://doi.org/10.1063/1.4936924>
41. C. Duan, Z. Tang, J. Cao, J. Wu, Zero-temperature localization in a sub-ohmic spin-boson model investigated by an extended hierarchy equation of motion. *Phys. Rev. B* **95**(21), 214308 (2017). <https://doi.org/10.1103/PhysRevB.95.214308>
42. J. Jin, X. Zheng, Y. Yan, Exact dynamics of dissipative electronic systems and quantum transport: hierarchical equations of motion approach. *J. Chem. Phys.* **128**(23), 234703 (2008). <https://doi.org/10.1063/1.2938087>
43. R. Härtle, G. Cohen, D.R. Reichman, A.J. Millis, Decoherence and lead-induced interdot coupling in nonequilibrium electron transport through interacting quantum dots: a hierarchical quantum master equation approach. *Phys. Rev. B* **88**(23), 235426 (2013). <https://doi.org/10.1103/PhysRevB.88.235426>
44. L. Ye, X. Wang, D. Hou, R.-X. Xu, X. Zheng, Y. Yan, HEOM-QUICK: a program for accurate, efficient, and universal characterization of strongly correlated quantum impurity systems. *WIREs Comput. Mol. Sci.* **6**(6), 608 (2016). <https://doi.org/10.1002/wcms.1269>
45. J. Cerrillo, M. Buser, T. Brandes, Nonequilibrium quantum transport coefficients and transient dynamics of full counting statistics in the strong-coupling and non-markovian regimes. *Phys. Rev. B* **94**(21), 214308 (2016). <https://doi.org/10.1103/PhysRevB.94.214308>
46. E. Aurell, The characteristic functions of quantum heat with baths at different temperatures. *Phys. Rev. E* **97**, 062117 (2018). <https://doi.org/10.1103/PhysRevE.97.062117>
47. S. Deffner, C. Jarzynski, Information processing and the second law of thermodynamics: an inclusive, hamiltonian approach. *Phys. Rev. X* **3**(4), 041003 (2013). <https://doi.org/10.1103/PhysRevX.3.041003>
48. P. Strasberg, G. Schaller, T. Brandes, M. Esposito, Quantum and information thermodynamics: a unifying framework based on repeated interactions. *Phys. Rev. X* **7**(2), 021003 (2017). <https://doi.org/10.1103/PhysRevX.7.021003>
49. R. Kubo, M. Toda, N. Hashitsume, *Statistical Physics II: Nonequilibrium Statistical Mechanics* (Springer, Berlin, 1985). <https://doi.org/10.1007/978-3-642-96701-6>
50. D. Segal, A. Nitzan, Spin-boson thermal rectifier. *Phys. Rev. Lett.* **94**(3), 034301 (2005). <https://doi.org/10.1103/PhysRevLett.94.034301>
51. K.A. Velizhanin, H. Wang, M. Thoss, Heat transport through model molecular junctions: a multilayer multiconfiguration time-dependent hartree approach. *Chem. Phys. Lett.* **460**(1–3), 325 (2008). <https://doi.org/10.1016/j.cplett.2008.05.065>
52. T. Ruokola, T. Ojanen, Thermal conductance in a spin-boson model: cotunneling and low-temperature properties. *Phys. Rev. B* **83**(4), 045417 (2011). <https://doi.org/10.1103/PhysRevB.83.045417>
53. C. Wang, J. Ren, J. Cao, Nonequilibrium energy transfer at nanoscale: a unified theory from weak to strong coupling. *Sci. Rep.* **5**(1), 11787 (2015). <https://doi.org/10.1038/srep11787>
54. S. Fujino, M. Fujiwara, M. Yoshida, BiCGSafe method based on minimization of associate residual. *Trans. JSCE* **8**, 145 (2005). [in Japanese]. [https://www.jstage.jst.go.jp/article/jscse/2005/0/2005\\_0\\_20050028/\\_article/-char/en](https://www.jstage.jst.go.jp/article/jscse/2005/0/2005_0_20050028/_article/-char/en)
55. J. Hu, R.X. Xu, Y.J. Yan, Communication: padé spectrum decomposition of fermi function and bose function. *J. Chem. Phys.* **133**(10), 101106 (2010). <https://doi.org/10.1063/1.3484491>
56. B.L. Tian, J.J. Ding, R.X. Xu, Y.J. Yan, Biexponential theory of drude dissipation via hierarchical quantum master equation. *J. Chem. Phys.* **133**(11), 114112 (2010). <https://doi.org/10.1063/1.3491270>
57. J. Hu, M. Luo, F. Jiang, R.-X. Xu, Y. Yan, Padé spectrum decompositions of quantum distribution functions and optimal hierarchical equations of motion construction for quantum open systems. *J. Chem. Phys.* **134**(24), 244106 (2011). <https://doi.org/10.1063/1.3602466>

58. J.E. Geusic, E.O. Schulz-DuBois, H.E.D. Scovil, Quantum equivalent of the carnot cycle. *Phys. Rev.* **156**(2), 343 (1967). <https://doi.org/10.1103/PhysRev.156.343>
59. M.P. Woods, N. Ng, S. Wehner, The maximum efficiency of nano heat engines depends on more than temperature. [arXiv:1506.02322](https://arxiv.org/abs/1506.02322)
60. Y. Tanimura, P.G. Wolynes, The interplay of tunneling, resonance, and dissipation in quantum barrier crossing: a numerical study. *J. Chem. Phys.* **96**(11), 8485 (1992). <https://doi.org/10.1063/1.462301>
61. A. Sakurai, Y. Tanimura, Self-excited current oscillations in a resonant tunneling diode described by a model based on the caldeira-leggett hamiltonian. *N. J. Phys.* **16**(1), 015002 (2014). <https://doi.org/10.1088/1367-2630/16/1/015002>
62. A. Kato, Y. Tanimura, Quantum suppression of ratchet rectification in a brownian system driven by a biharmonic force. *J. Phys. Chem. B* **117**(42), 13132 (2013). <https://doi.org/10.1021/jp403056h>
63. A. Sakurai, Y. Tanimura, Does  $\hbar$  play a role in multidimensional spectroscopy? Reduced hierarchy equations of motion approach to molecular vibrations. *J. Phys. Chem. A* **115**(16), 4009 (2011). <https://doi.org/10.1021/jp1095618>
64. J. Strümpfer, K. Schulten, Open quantum dynamics calculations with the hierarchy equations of motion on parallel computers. *J. Chem. Theory Comput.* **8**(8), 2808 (2012). <https://doi.org/10.1021/ct3003833>
65. M. Tsuchimoto, Y. Tanimura, Spins dynamics in a dissipative environment: hierachal equations of motion approach using a Graphics Processing Unit (GPU). *J. Chem. Theory Comput.* **11**(8), 3859 (2015). <https://doi.org/10.1021/acs.jctc.5b00488>
66. C. Kreisbeck, T. Kramer, M. Rodríguez, B. Hein, High-performance solution of hierarchical equations of motion for studying energy transfer in light-harvesting complexes. *J. Chem. Theory Comput.* **7**(7), 2166 (2011). <https://doi.org/10.1021/ct200126d>
67. C. Kreisbeck, T. Kramer, A. Aspuru-Guzik, Scalable high-performance algorithm for the simulation of exciton dynamics. Application to the light-harvesting complex II in the presence of resonant vibrational modes. *J. Chem. Theory Comput.* **10**(9), 4045 (2014). <https://doi.org/10.1021/ct500629s>
68. D. Suess, A. Eisfeld, W.T. Strunz, Hierarchy of stochastic pure states for open quantum system dynamics. *Phys. Rev. Lett.* **113**(15), 150403 (2014). <https://doi.org/10.1103/PhysRevLett.113.150403>
69. K. Song, L. Song, Q. Shi, An alternative realization of the exact non-markovian stochastic schrödinger equation. *J. Chem. Phys.* **144**(22), 224105 (2016). <https://doi.org/10.1063/1.4953244>
70. Y. Ke, Y. Zhao, Hierarchy of forward-backward stochastic schrödinger equation. *J. Chem. Phys.* **145**(2), 024101 (2016). <https://doi.org/10.1063/1.4955107>

# Chapter 25

## Cooling to Absolute Zero: The Unattainability Principle



Nahuel Freitas, Rodrigo Gallego, Lluís Masanes and Juan Pablo Paz

### 25.1 Introduction

The necessity of the third law of thermodynamics and its physical content were heatedly debated by Nernst, Planck and Einstein at the beginning of the 20th century. Several inequivalent formulations of the law [1–4] were proposed, but the one that has been mostly considered by subsequent authors is the

**Unattainability principle:** *It is impossible by any procedure, no matter how idealized, to reduce any assembly to absolute zero temperature in a finite number of operations (Nernst [5]).*

The above statement makes use of ambiguous concepts such as “procedure” and “operation” which are concomitant to formulations of thermodynamics present at the time. Within the contemporary formulation of thermodynamics, by “any procedure”

---

N. Freitas (✉)

Theoretische Physik, Universität des Saarlandes, 66123 Saarbrücken, Germany  
e-mail: nahuel.freitas@gmail.com

R. Gallego

Dahlem Center for Complex Quantum Systems,  
Freie Universität Berlin, 14195 Berlin, Germany

L. Masanes

Department of Physics and Astronomy,  
University College London, WC1E 6BT London, UK

J. P. Paz

Departamento de Física, FCEyN, UBA, Pabellón 1,  
Ciudad Universitaria, 1428 Buenos Aires, Argentina

J. P. Paz

Instituto de Física de Buenos Aires, UBA CONICET,  
Pabellón 1, Ciudad Universitaria, 1428 Buenos Aires, Argentina

it is meant any process whose underlying dynamics is unitary, and hence, it does not include measurements or preparations (unless the measurement apparatus is included in the “assembly”). Note that, otherwise, we could violate the unattainability principle (UP) simply by measuring the energy of a two level system and conditionally driving it to its ground state.

Another ambiguity is the notion of “operation”, on which, supposedly, any procedure can be decomposed. A finite number of operations translates simply in that the duration of the overall procedure is finite. This relation between finiteness of time and number of operations is reminiscent of the very specific type of thermodynamic operations (isothermal, adiabatic, etc.) considered at the time. At present, however, we would like a formulation of the UP that applies to the widest range of physical procedures —not necessarily decomposable into specific types of operations— hence, we need to generalize the constraint that *the time duration of the procedure is finite* in a setup-independent fashion. This can be done with the following

**Finiteness assumption:** *Within a finite time, a system can only interact with finitely-many other systems, each having effectively finite size. Also, within a finite time, only a finite amount of work can be injected into a system.*

The notion of “finite size” that appears in the above assumption is formalized in different ways: finite heat capacity, finite volume (Sect. 25.4), finite Hilbert space dimension (Sect. 25.3) and finite largest eigenvalue of the Hamiltonian (Sect. 25.5). The finiteness of the volume can be justified by, for example, invoking the finite speed of information propagation from Special Relativity or the Lieb-Robinson bound [6]. The finiteness of the Hilbert space dimension is more appropriate in the context of quantum computers and artificial systems. This is particularly relevant because quantum computation requires initial pure states, and as we see below, the task of distilling pure states is essentially equivalent, in relation to the UP, to that of cooling to absolute zero.

The Finiteness Assumption also puts limits on the amount of thermodynamic resources (Sect. 25.3) and work (Sects. 25.4 and 25.5) that can be consumed in a cooling process. The translation of “time” to all these mentioned physical parameters allows to go beyond the original UP, and provide quantitative versions of it. That is, relationships between the lowest achievable temperature and the value of the physical parameters associated to time.

This chapter is organized as follows: In Sect. 25.2 we lay out and discuss the assumptions and features of a general cooling protocol. In Sect. 25.3 we show recent bounds on cooling protocols with infinite heat baths and catalysts using states out of equilibrium as a resource for cooling [7]. In Sect. 25.4 we consider the case of work as a resource for cooling in the presence of a finite heat bath [8]. In Sect. 25.5 we present formulations of the UP in terms of the dimension of the heat bath. Lastly, in Sect. 25.6 we consider a less general scenario of more practical relevance by studying the cooling bounds and the UP for networks of harmonic oscillators [9].

## 25.2 General Setup for Cooling Processes

In the following we lay out a general framework that includes as particular cases the different types of cooling protocols. This general cooling process consists of a joint transformation of the following subsystems:

- **The system S** is what we want to cool down to the lowest possible temperature. The system has Hilbert space dimension  $d_S$ , and its initial and final states are denoted by  $\rho_S$  and  $\rho'_S$  respectively. The Hamiltonian  $H_S$  has ground-space projector  $P_{\text{gr}}$  with degeneracy  $g$ , and the energy gap above the ground state is  $\Delta$ . Most of the following results apply to the case where the system is initially in thermal equilibrium  $\rho_S = \omega_\beta(H_S)$ , at the same temperature than the bath  $T = 1/\beta$ , where we define the equilibrium state

$$\omega_\beta(H) := \frac{e^{-\beta H}}{\text{Tr}(e^{-\beta H})}. \quad (25.1)$$

The quality of the cooling procedure is quantified by the cooling error

$$\epsilon = 1 - \text{Tr}(\rho'_S P_{\text{gr}}), \quad (25.2)$$

or the final temperature-like quantity

$$T' \geq \frac{\Delta}{\ln(d_S/g\epsilon)}. \quad (25.3)$$

The unattainability results that are presented in what follows, constitute lower bounds for the quantities  $\epsilon$  and  $T'$ , which prevent them to be zero.

- **The bath B** can be seen as the environment of the system, and as such, it is in thermal equilibrium  $\rho_B = \omega_\beta(H_B)$  at temperature  $T = 1/\beta$ . The role of the Bath is to absorb entropy from the system S contributing to its temperature reduction. The Hilbert-space dimension of the bath can be finite  $d_B$  or infinite. Its Hamiltonian  $H_B$  has energy range  $J_B = \lambda_{\max}(H_B) - \lambda_{\min}(H_B)$ , where  $\lambda_{\max/min}(H_B)$  are its largest/lowest eigenvalue. The energy range  $J_B$  can also be finite or infinite.
- **The catalyst C** represents the machine that we use for cooling. As a tool, its initial and final states must be equal  $\rho'_C = \rho_C$ , such that, at the end of the protocol it can be re-used in the next repetition of the process (Sect. 25.3).
- **The resource R** is the fuel that will be consumed in the cooling transformation. As such, there are no constraints on the final state of the resource  $\rho'_R$ . The initial state of the resource must necessarily be not in equilibrium  $\rho_R \neq \omega_\beta(H_R)$ , and its utility increases when increasing its energy and/or decreasing its entropy. Thermodynamic work can also be seen as a type of resource with conditions on its final state, so that, dumping entropy in  $\rho'_R$  is not allowed.

Once the subsystems of the cooling protocol have been presented we state now formally some fundamental assumptions that are used in the rest of the chapter.

- **Independence Assumption.** All subsystems are initially in a product state  $\rho_S \otimes \rho_B \otimes \rho_C \otimes \rho_R$ , and the total Hamiltonian is initially non-interacting  $H = H_S + H_B + H_C + H_R$ .
- **Unitarity Assumption.** The joint transformation of all subsystems is unitary:

$$\rho'_S = \text{Tr}_{BCR} [U (\rho_S \otimes \rho_B \otimes \rho_C \otimes \rho_R) U^\dagger] \quad (25.4)$$

where  $U$  is a unitary operator.

- **Energy Conservation** is the requirement that the global unitary commutes with the total Hamiltonian  $[U, H] = 0$ . This assumption is considered in Sect. 25.3. On the other hand, in Sects. 25.4 and 25.5, the unitary operator  $U$  is unrestricted. This energetic imbalance is compensated by an expenditure or generation of work. In general, this work fluctuates, taking different values in different repetitions of the procedure, or adopting coherent super-positions. It is important to mention that any non-energy-conserving unitary  $U$  can be simulated by an energy-conserving one  $V$  acting on a larger compound

$$U \rho_S U^\dagger = \text{Tr}_R (V \rho_S \otimes \rho_R V^\dagger), \quad (25.5)$$

where  $[V, H_S + H_R] = 0$ . For this to be possible, the Hamiltonian  $H_R$  and the state of the extra system  $\rho_R$  have to be of a particular form [10].

Although giving up on the Independence Assumption might be of interest, it is ubiquitously assumed in the derivation of bounds and laws of thermodynamics and necessary to obtain usual derivations of the second law of thermodynamics [11]. However, it is important to mention that recent efforts [12] are going beyond this framework. Regarding the Unitarity Assumption it is mainly motivated by the formalism of quantum mechanics, which prescribes a unitary evolution for systems evolving under time-dependent Hamiltonians [13, 14].

The following table includes the classification of all the unattainability results explained in this chapter (first column). The “limiting factor” (second column) contains the physical parameters that need to become infinite in order to achieve absolute zero. These can be: the Hilbert-space dimension of the bath  $d_B$ , the energy range of its Hamiltonian  $J_B$ , the heat capacity of the bath  $C_B(E)$  (defined in Sect. 25.4). The smaller the value of these parameters is, the further from absolute zero the final state of the system becomes. The third column tells us which results assume energy conservation (“yes”), and which ones require fluctuating work to compensate for the energetic imbalances (“no”). The fourth column specifies which results assume that the heat bath has finite volume, and which do not. The fifth column informs us about the thermodynamical resource that fuels the transformation. This can be work, non-equilibrium resources  $\rho_R$ , or both. The sixth column tells us which setups include a catalyst and which do not.

	limiting factor	$[U, H] = 0$	finite bath	resource	catalyst
Allahverdyan (2011) [15]	finite $d_B$ and $J_B$	no	yes	work	no
Reeb (2014) [16]	finite $J_B$	no	yes	work	no
Scharlau (2016) [17]	finite $d_B$ and $J_B$	yes	yes	work	no
Masanes (2017) [8]	finite $C_B(E)$ and $W_{wc}$	no	yes	work	no
Wilming (2017) [7]	finite resources	yes	no	non-eq.	yes
Müller (2017) [18]	finite catalyst	yes	no	both	yes

### 25.3 Cooling with Finite Resources

In this section we will summarize the results of Ref. [7]. There, cooling processes are considered which involve arbitrary heat bath and catalyst. The only limiting factor is the size of the resource  $R$ , which is assumed to be finite dimensional, and, as we will see, the lowest possible temperature can be compactly expressed as a function of the initial state of the resource  $\rho_R$ .

We will use the set-up of *catalytic thermal operations* [13, 19, 20] applied to the task of cooling. For this, consider a thermal bath  $B$  described by state and Hamiltonian  $(\omega_\beta(H_B), H_B)$ , a catalyst  $(\sigma_C, H_C)$  and a finite-dimensional resource  $R$  described by  $(\rho_R, H_R)$ . We do not impose any restriction on the size or dimensionality of  $B$  and the dimension of  $C$  and allow for arbitrary  $H_B$ ,  $\sigma_C$  and  $H_C$ . These three systems are brought to interact with a system  $S$  which one aims at cooling and is initially at thermal equilibrium with the thermal bath, that is  $\rho_S = \omega_\beta(H_S)$ . By imposing the three assumptions laid out in Sect. 25.2 —namely, Independence, Unitarity and Energy Conservation— and that the catalyst is returned in the same state we obtain transitions of the form

$$\rho'_S \otimes \sigma_C = \text{Tr}_{RB} [U \rho_R \otimes \rho_S \otimes \sigma_C \otimes \omega_\beta(H_B) U^\dagger]. \quad (25.6)$$

where  $U$  commutes with the total Hamiltonian. Note that we demand that the catalyst is returned in the same state and uncorrelated with the system  $S$  that one aims at cooling, in this way, it can be re-used for arbitrary future transitions. The allowed transitions of the form (25.6) have been characterized in Ref. [20] for diagonal states, that is, with  $[\rho_R, H_R] = 0$  and  $[\rho'_S, H_S] = 0$ . It is shown that a transition is possible if and only if

$$S_\alpha(\rho_R \| \omega_\beta(H_R)) \geq S_\alpha(\rho'_S \| \omega_\beta(H_S)) \quad \forall \alpha \geq 0, \quad (25.7)$$

where  $S_\alpha$  are so-called *Renyi-divergences*. Note that it is in principle necessary to check an infinite number of conditions —one for each real value of  $\alpha$ — to certify that the cooling protocol is possible. In Ref. [7] it is shown that in the limit of very small final temperature  $T'$  the infinite set of conditions reduces essentially to the evaluation of a single function, referred to as *vacancy*, and defined by

$$\mathcal{V}_\beta(\rho, H) := S(\omega_\beta(H) \| \rho), \quad (25.8)$$

where  $S$  is the quantum relative entropy defined as  $S(\rho\|\sigma) = \text{Tr}(\rho \log \rho) - \text{Tr}(\rho \log \sigma)$ . The vacancy becomes a key quantity in relation with the UP, since it is shown that sufficient and necessary conditions for cooling to sufficiently low  $T'$  are given respectively by

$$\mathcal{V}_\beta(\rho_R, H_R) - K(\rho_R, H_R, \rho_S, H_S, \beta) \geq \mathcal{V}_\beta(\rho_S, H_S), \quad (25.9)$$

$$\mathcal{V}_\beta(\rho_R, H_R) \geq \mathcal{V}_\beta(\rho_S, H_S), \quad (25.10)$$

where  $K(\rho_R, H_R, \rho_S, H_S, \beta) \rightarrow 0$  as  $T' \rightarrow 0$ . (See [7] for a definition of  $K$ .) Hence, in the limit of very cold final states where the UP applies, both inequalities converge to a single one ruled by the vacancy. These conditions can be also re-expressed for the multi-copy case  $\rho_R = \rho^{\otimes n}$ , where each copy has a local Hamiltonian  $h$ , to obtain lower bound for the final temperature  $T' \geq k(n\mathcal{V}_\beta(\rho, h))^{-1}$  where  $k$  is a constant.

It is illustrative to compare these bounds with the actual cooling rates achieved by protocols of Algorithmic Cooling [21–24]. For example, in the seminal work of Ref. [21] it is considered a cooling protocol like the ones described in Sect. 25.2 but without heat bath nor catalyst, and simply a resource  $\mathbf{R}$  of the form  $\rho^{\otimes N}$  with trivial Hamiltonian  $h = 0$ . This protocol provides a cooling error that decreases exponentially with the size of the resource  $\epsilon \propto \exp(-kn)$  with  $k$  being a constant. In turn, the inequality (25.10) implies a bound of the form  $\epsilon \geq C \exp(-Rn)$  with  $C$  and  $R$  being constants which depend of  $\mathcal{V}_\beta(\rho, h)$ . This has as an implication that for the case of *i.i.d.* resources the simple protocol of algorithmic cooling from Ref. [21] offers an exponential scaling which is (up to factors in the exponent) optimal, even within the much larger family of protocols which employ an arbitrarily large bath and catalyst as considered here.

Lastly, let us briefly mention on the significance that the vacancy rules low temperature cooling. For this, it is illustrative to compare to formulations of the second law which bound the extractable work from a given resource  $\rho_R$ . As it is well-known, the extractable work  $W$  satisfies

$$W \leq F_\beta(\rho_R, H_R) - F_\beta(\omega(H_R), H_R) \propto S(\rho_R\|\omega_\beta(H_R)) \quad (25.11)$$

where  $F_\beta(\rho, H) = \text{Tr}(\rho H) - \beta^{-1}S(\rho)$  is simply the free energy [10, 25, 26]. Importantly, note the similarities between the vacancy (25.8) and the r.h.s. of (25.11). This gives a common interpretation for the second and third laws in terms of a common function, the relative entropy, which can be regarded as a distance, or a measure of distinguishability between quantum states. The ordering of the arguments is related with strategies of hypothesis testing to discriminate between both states [27]. In this way one arrives to the general explanation that the *value* of a given resource is determined by its distinguishability from its thermal state, this is measured with the free-energy for the task of work extraction, and measured with the vacancy for the task of cooling.

### 25.3.1 Work as a Resource for Cooling

It is also possible to incorporate in the framework of this section models of work as a particular case of a resource. As already laid out in Sect. 25.2, it is possible to simulate the action of a unitary evolution which inputs work—that is, with  $[U, H] \neq 0$ —by considering an external system,  $R$  in this case, which compensates for the energy imbalance. For this one can follow the approach of Ref. [13] considering as a resource  $R$  a qubit in state  $\rho_R = |1\rangle\langle 1|$  and with Hamiltonian  $H_R = W |1\rangle\langle 1|$ . One finds that in this case it is possible to cool down to absolute zero, since the transition

$$\omega_\beta(H_S) \otimes |1\rangle\langle 1| \mapsto |0\rangle\langle 0| \otimes |0\rangle\langle 0| \quad (25.12)$$

is possible whenever  $W > \log Z_\beta$  where  $Z_\beta$  is the partition function of  $S$  [13]. Although this seems to be in contradiction with the third law of thermodynamics, we note that this procedure only works if the initial resource  $\rho_R$  is exactly pure. If instead we consider slightly noisy work  $\rho_R = \epsilon |0\rangle\langle 0| + (1 - \epsilon) |1\rangle\langle 1|$ , then perfect cooling is impossible for any  $\epsilon > 0$ , regardless of the value of  $W$  (even if it diverges) [7]. In this sense, perfect cooling is only possible if we have already as a resource a state which is not full-rank.

### 25.3.2 Cooling by Building up Correlations

In the description of the catalytic thermal operations of Eq. (25.6) we impose that the catalyst is returned in the same state and also uncorrelated with the system being cooled  $S$ . Possible alternatives to this scenario have been recently considered [18, 28, 29], where the system  $S$  is allowed to build correlations with the catalyst. In this way, the l.h.s. of (25.6) is substituted by a possibly correlated state  $\rho'_{SC}$  so that  $\text{Tr}_S(\rho'_{SC}) = \sigma_C$ . These correlations do not prevent one from re-using the catalyst for subsequent cooling protocols. In particular, suppose that we have a series of uncorrelated systems  $S_1, \dots, S_N$  that we want to cool. One can first apply a cooling protocol using  $S_1$  and  $C$ , initially uncorrelated, and produce  $\rho'_{S_1C}$ . Afterwards, the catalyst is re-used together with  $S_2$  for another repetition of the cooling protocol, which is possible regardless of the correlations that  $C$  has established with  $S_1$ . Building up correlations in this form is advantageous for implementing cooling processes as shown in Ref. [18]. There it is shown that, if two diagonal states  $[\rho_R, H_R] = [\rho'_S, H_S] = 0$  satisfy  $F_\beta(\rho_R, H_S) \geq F_\beta(\rho'_S, H_S)$  then there always exist a catalyst and a thermal bath so that

$$\gamma_{SC} = \text{Tr}_B(U \rho_R \otimes \omega_\beta(H_S) \otimes \sigma_C \otimes \omega_\beta(H_B) U^\dagger) \quad (25.13)$$

with  $U$  commuting with the total Hamiltonian,  $\text{Tr}_S(\gamma_{SC}) = \sigma_C$  and  $\text{Tr}_C(\gamma_{SC})$  arbitrarily close to  $\rho'_S$ . This can be used to cool at arbitrarily low temperatures while

employing finite resources. For instance, take  $\rho_R$  to be a qubit so that  $F(\rho_R, H_R) > F(|0\rangle\langle 0|, H_S)$  where  $|0\rangle\langle 0|$  is the ground state of  $H_S$ . One can always find such a state  $\rho_R$  by making it sufficiently energetic. Then Eq. (25.13) implies that it is possible to cool as close to zero temperature as desired just with  $\rho_R$  as a resource. It is natural to ask now if this represents a violation of the UP. It turns out that the dimension of  $C$  and  $B$ , at least this is the case in the construction of Ref. [18], diverge as we approximate better the final zero temperature state. Hence, using the Finiteness Assumption introduced in Sect. 25.1, one would also require diverging time to implement this protocol. On the other hand it is to date unclear what is the particular scaling of the dimension of  $CB$  in the optimal construction, hence it is open in this scenario which are the actual bounds relating time and temperature.

## 25.4 Cooling with a Bath Having Finite Heat Capacity

The Finiteness Assumption (Sect. 25.1) imposes that, within a process lasting for a finite time, the volume of the effective heat bath assisting the transformation must be finite. In physical setups where this volume is not defined, one can impose, alternatively, the finiteness of the heat capacity or free energy. We stress that the finiteness of these quantities is independent to that of the Hilbert space dimension. And in particular, a finite region of a typical heat bath (radiation, air, etc) is described by an infinite-dimensional Hilbert space.

The Finiteness Assumption also imposes that, within a finite time, the amount of work injected into the system and bath must remain finite. In general, this work expenditure fluctuates, taking different values in different repetitions of the procedure, or adopting quantum super-positions. Since the UP is a bound on the worst-case cooling time (not the average time), the relevant quantity here is the *worst-case work* (not the average work). Also, the necessity of considering the worst-case work follows from the observation that, if the worst-case work is not constrained then perfect cooling is possible with a heat bath consisting of a single harmonic oscillator (Sec. V in [15]).

The physical setup considered in [8] is the following. The global unitary  $U$  characterizing the transformation

$$\rho'_S = \text{Tr}_B(U\rho_S \otimes \rho_B U^\dagger) \quad (25.14)$$

is not required to commute with the total Hamiltonian  $H = H_S + H_B$ . This violation of energy conservation must be compensated by an expenditure or generation of work. That is, energy that is injected into the system and bath without changing their entropy. There are different ways to define work in this setup, a standard definition being the average value  $\bar{W} = \text{Tr}[(H - U^\dagger H U)\rho_S \otimes \rho_B]$ . However, as mentioned above, we need to consider the *worst-case work*

$$W_{wc} = \max_{|\phi_1\rangle, |\phi_2\rangle} \{E_2 - E_1 : \langle \phi_2 | U | \phi_1 \rangle \neq 0 \text{ and } H |\phi_{1,2}\rangle = E_{1,2} |\phi_{1,2}\rangle\}. \quad (25.15)$$

That is, the largest transition between the energy levels of  $H$  generated by  $U$ . Note that this expression only makes sense when the initial state  $\rho_S \otimes \rho_B$  has full rank, which is our case. Finally, we remark that this setup does not include a catalyst, and, whether a catalyst would constitute an advantage is an open problem.

### 25.4.1 Results

For the sake of simplicity, here we consider the case where the Hilbert space of the system has finite dimension  $d_S$  and its initial state is thermal at the same temperature than the bath  $\rho_S = \omega_\beta(H_S)$ . The general case is analyzed in [8]. Next we see that, in the context of the UP, a central quantity is the density of states of the bath  $\Omega(E)$ , that is, the number of eigenvalues of  $H_B$  within an energy window around  $E$ . This allows to write Boltzman's entropy as  $\ln \Omega(E)$ .

The most general result of this section is the following. In any cooling process assisted by a bath with density of states  $\Omega(E)$ , and using worst-case work  $W_{wc}$ , the “cooling error”  $\epsilon$  satisfies, to leading order,

$$\epsilon \geq \frac{\Omega(E_0) e^{-E_0/T}}{\text{Tr}(e^{-H_B/T})}, \quad (25.16)$$

where  $E_0$  is the solution of equation

$$\frac{\partial \ln \Omega(E_0)}{\partial E_0} = \frac{\ln(2d_S/3g)}{W_{wc}}. \quad (25.17)$$

By “leading order” it is meant that the bound holds for sufficiently large  $W_{wc}$ . Equation (25.17) always has a unique solution, provided that the micro-canonical heat capacity of the bath

$$C_B(E) = - \left( \frac{\partial \ln \Omega(E)}{\partial E} \right)^2 \left( \frac{\partial^2 \ln \Omega(E)}{\partial E^2} \right)^{-1} \quad (25.18)$$

is positive and finite for all  $E$ . (An example of system with negative heat capacity is a black hole.)

It is important to mention that bound (25.16) can be applied to any thermodynamical transformation  $\rho_S \rightarrow \rho'_S$  that decreases the rank of the state. Where neither the initial nor the final states need to be thermal. In this more general case we define  $d_S = \text{rank}(\rho_S)$  and  $g = \text{rank}(\rho'_S)$ , and note that nothing in Eqs. (25.16) and (25.17) depends on  $H_S$ . (This is because we are in the regime  $W_{wc} \gg \|H_S\|_\infty$ .) In particular, setting  $H_S = 0$ ,  $d_S = 2$  and  $g = 1$ , we arrive at the scenario called Landauer's Erasure (see Sect. 25.5.1). This shows that the tasks of cooling and erasing information are essentially equivalent.

In order to understand how this result works, let us apply it to a very general family of baths with density of states  $\Omega(E, V) = \exp(aV^{1-\nu}E^\nu)$ , where  $\nu$  is a free

parameter in the ranger  $0 < \nu < 1$ . Note that the associated Boltzman entropy is extensive  $\ln \Omega(2E, 2V) = 2 \ln \Omega(E, V)$ . Substituting this in (25.16) and (25.17) we obtain the explicit bound

$$\epsilon \geq \exp \left[ -\frac{V}{T} \left( \frac{a\nu W_{\text{wc}}}{\ln(2d_{\mathbb{S}}/3g)} \right)^{\frac{1}{1-\nu}} \right]. \quad (25.19)$$

As expected, the larger  $V$  and  $W_{\text{wc}}$  are, the lower  $\epsilon$  can become. An interesting observation is that, the faster  $\Omega(E)$  grows ( $\nu$  closer to 1), the weaker is the bound. Therefore, we can obtain the most general unattainability result by applying result (25.16) to the heat bath with fastest growth of its density of states  $\Omega(E)$ . To our knowledge, the system with fastest  $\Omega(E)$  growth is electro-magnetic radiation (or any massless bosonic field), whose density of states is of the form written above with parameters  $\nu = 3/4$  and  $a = \frac{4}{3} 15^{-1/4} \sqrt{\pi} (\hbar c)^{-3/4}$ . Therefore, at this point, we can obtain a universal unattainability result if we use inequality (25.3) and substitute in our bound (25.19) with the parameters of electro-magnetic radiation, obtaining

$$T' \geq \frac{15c^3 \hbar^3}{\pi^2} \ln^4 \left( \frac{2d_{\mathbb{S}}}{3g} \right) \frac{T \Delta}{V W_{\text{wc}}^4}, \quad (25.20)$$

in the regime of large  $V$  and  $W_{\text{wc}}^4$ .

Finally, let us write an UP in terms of time  $t$ . From special relativity we have that  $V \leq (ct)^3$ , and considering, for example, the linear relation  $W_{\text{wc}} \propto t$ , we obtain

$$T' \geq \text{const} \frac{1}{t^7}. \quad (25.21)$$

Other setups will have different relations between  $V$ ,  $W_{\text{wc}}^4$  and  $t$ . But one can always substitute those in (25.20) and obtain a suitable UP in terms of time.

## 25.5 Cooling with a Finite-Dimensional Bath

### 25.5.1 Landauer's Erasure

The aim of Landauer's Erasure is to transform any given state  $\rho_{\mathbb{S}}$  to a fixed pure state  $|0\rangle\langle 0|$ , where the Hamiltonian of the system is trivial  $H_{\mathbb{S}} = 0$ . For this to be possible, all the entropy from  $\rho_{\mathbb{S}}$  has to be transferred to the bath by consuming work. Here we consider erasure protocols where any unitary acting on  $\mathbb{S}\mathbb{B}$  is allowed, without necessarily commuting with the total Hamiltonian. After tracing out the bath we obtain the final state

$$\rho'_{\mathbb{R}} = \text{Tr}_{\mathbb{B}}(U \rho_{\mathbb{S}} \otimes \omega_{\beta}(H_{\mathbb{B}}) U^\dagger). \quad (25.22)$$

Limitations on the purity of the final state  $\rho'_S$  have been investigated in Ref. [16] where it is shown that

$$\lambda_{\min}(\rho'_S) \geq e^{-\beta J_B} \lambda_{\min}(\rho_S), \quad (25.23)$$

where  $\lambda_{\min}(\rho)$  is the smallest eigenvalue of  $\rho$  and  $J_B = \lambda_{\max}(H_B) - \lambda_{\min}(H_B)$  is the energy range of  $H_B$ . If one assumes a linear scaling of  $J_B$  with the size of  $B$ , this provides bounds with a similar scaling of those for algorithmic cooling (see discussion in Sect. 25.3). Note also that the fluctuations of external work applied in the process can be at most  $J_B$ . The bound (25.23) exemplifies that for obtaining perfectly pure states  $\lambda_{\min}(\rho'_R) = 0$  the norm of the bath's Hamiltonian has to diverge, which will also affect the worst-case work, again in the spirit of the results laid out in Sect. 25.4.

### 25.5.2 Other Results

The following two results address the problem of cooling a qubit with Hamiltonian  $H_S = \Delta |1\rangle\langle 1|$ . In Scharlau's result [17] the initial state of the qubit is  $\rho_S = |1\rangle\langle 1|$ . But despite being pure, it is not trivial to map it to  $|0\rangle\langle 0|$ , because only energy-conserving unitaries are allowed in that setup. This implies that the final temperature of the system is bounded by

$$T' \geq \frac{T\Delta}{J_B + T \ln d_B}. \quad (25.24)$$

In Allahverdyan's result [15], the initial state of the qubit is thermal  $\rho_S = \omega_\beta(H_S)$  at the same temperature than the bath. This state has more entropy than the one considered in (25.24), and hence cooling requires more effort. On the other hand, arbitrary unitaries are allowed here, giving

$$T' \geq \frac{T\Delta}{J_B}. \quad (25.25)$$

## 25.6 Cooling with Linear Quantum Refrigerators

In this section we explain a rather independent development with the goal of identifying fundamental limits for cooling on a specific class of quantum refrigerators. The results presented in the previous sections are based on the assumption that one has access to arbitrary energy conserving operations over the compound of subsystems given by the system to be cooled, the thermal bath, catalyst, and work reservoirs. This is important in order to assess the ultimate limitations for achieving a particular task, which is cooling in this case. However, the operations that are actually available in

practice are much more restricted. Thus, it is also relevant to study the fundamental limitations for less general cooling schemes, that however more closely resemble experimental settings.

We consider the following family of linear and driven quantum refrigerators. A central system, an arbitrary network of harmonic oscillators, is connected to different and independent bosonic thermal reservoirs at different temperatures (see Fig. 25.1). The central network is thus open and can also be driven parametrically, by changing in time the frequency of each oscillator in the network and the interactions between them. The goal is to drive the system in order to cool a given thermal reservoir, extracting energy out of it. Many experimental cooling techniques can be viewed in this way. For example, during laser cooling of trapped ions, the internal electronic degrees of freedom are driven by a laser field and act as a ‘heat pump’ that removes energy from the motional degrees of freedom, dumping it into the electromagnetic field as emitted photons.

The proposed model has the virtue of being exactly solvable, without invoking common approximations for the description of open and driven quantum systems. Therefore, it is possible to obtain and interpret clear mathematical expressions for key thermodynamic quantities, like work and heat currents. Despite its simplicity, this general model of thermal machines displays interesting features. We will see that the fundamental limit for cooling in this kind of machines is imposed by a pair creation mechanism analogous to the Dynamical Casimir Effect (DCE). Also, it will be clear that this process cannot be captured by standard techniques based on master equations valid up to second order in the coupling between the central system and the thermal reservoirs.

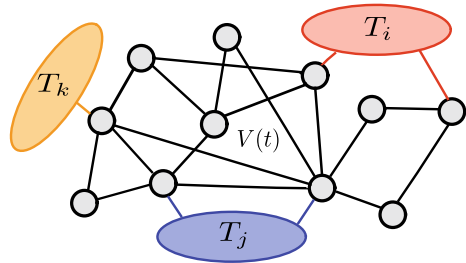
### 25.6.1 The Model

Figure 25.1 shows a scheme of the considered model. Each black circle represent one of the  $N$  quantum harmonic oscillators composing the network, and links between them represent bilinear interactions. The natural frequencies of each oscillator and the interactions between them can be changed in time. Therefore, the harmonic network is described by the following quadratic Hamiltonian:

$$H_S(t) = \frac{1}{2}P^T M^{-1}P + \frac{1}{2}X^T V(t)X, \quad (25.26)$$

where  $X$  and  $P$  are vectors whose components are the position and momentum operators of each oscillator, which satisfy the usual commutation relations,  $[X_i, X_j] = [P_i, P_j] = 0$  and  $[X_i, P_j] = i\delta_{i,j}$  ( $\hbar = 1$ ). The matrix  $M$  has the masses of each oscillator along the diagonal and zeros elsewhere, while the matrix  $V(t)$  encodes the frequencies of each oscillator and the interactions between them. The variation in time of the matrix  $V(t)$  allow us to model an external control that can be performed on the system.

**Fig. 25.1** Scheme of the model.



Some nodes of the network are also connected to independent thermal reservoirs. We will model the reservoirs as collections of harmonic modes which are initially in a thermal state. Thus, the reservoir or environment  $\mathcal{E}_\alpha$  has a Hamiltonian

$$H_{\mathcal{E}_\alpha} = \sum_{j=1}^{N_\alpha} \frac{\pi_{\alpha,j}^2}{2m} + \frac{m\omega_{\alpha,j}^2}{2} q_{\alpha,j}^2$$

where the operator  $q_{\alpha,j}$  is the position operator of the  $j$ th oscillator in the  $\alpha$ th environment, and  $\pi_{\alpha,j}$  its associate momentum. Also, we consider a bilinear interaction between system and reservoirs through the position coordinates. Thus, for each environment  $\mathcal{E}_\alpha$  we have an interaction Hamiltonian

$$H_{S,\mathcal{E}_\alpha} = \sum_{j,k} C_{\alpha,jk} X_j q_{\alpha,k}, \quad (25.27)$$

where  $C_{\alpha,jk}$  are time-independent interaction constants. Thus, the full Hamiltonian for system and reservoirs is  $H_T(t) = H_S(t) + \sum_\alpha H_{\mathcal{E}_\alpha} + \sum_\alpha H_{S,\alpha}$ . In the following we will consider cyclic thermodynamic processes for which the driving performed on the network is periodic. Thus, the function  $V(t)$  can be decomposed in terms of Fourier components  $V_k$  as  $V(t) = \sum_k V_k e^{ik\omega_d t}$ , where  $\omega_d$  is the angular frequency of the driving.

As we explain below, thermodynamic quantities like heat currents can be obtained from the state of the central system alone. Thus, if  $\rho_T(0) = \rho_S(0) \otimes \rho_E(0)$  is an initial product state for the system and the environment, our main objective is to calculate the subsequent reduced state for the system:

$$\rho_S(t) = \text{Tr}_E (U(t)\rho_T(0)U^\dagger(t)) \quad (25.28)$$

where the global unitary evolution  $U(t)$  corresponds to the Hamiltonian  $H_T(t)$ . We can do that by solving the equations of motion for the system's operators in the Heisenberg picture. The linearity of these equations (which follows from the quadratic structure of the total Hamiltonian) can be exploited to exactly integrate them in terms of the Green's function of the system. A detailed explanation of the procedure is given in [30]. Here, it is enough to note that since the Hamiltonian is

quadratic in the phase space coordinates, if the full initial state is a Gaussian state, it will remain Gaussian during the time evolution. Therefore, a complete description of the central system state  $\rho_S(t)$  is given by the first moments  $\langle X_i \rangle$  and  $\langle P_i \rangle$ , and the second moments  $\sigma_{i,j}^{xx} = \langle X_i X_j \rangle$ ,  $\sigma_{i,j}^{pp} = \langle P_i P_j \rangle$ , and  $\sigma_{i,j}^{xp} = \langle X_i P_j + X_j P_i \rangle / 2$ . Even if the initial state of the system is not Gaussian, in the regime where the interplay between the driving and the dissipation induced by the environments determines a unique asymptotic steady state, this state will also be Gaussian. Although we will assume in the following that the system is indeed in such regime, it should be pointed out that in general this will not be the case, since the driving could give place to parametric resonances, in which the dynamics is not stable and the memory of the initial state of the central system is never lost.

As said before, a central object in our treatment is the Green's function of the harmonic network, which solves its equations of motion and exactly takes into account the driving and the dissipation induced by the environment. Explicitly, the Green's function  $G(t, t')$  is the  $N \times N$  matrix which is the solution to the following integro-differential equation:

$$M \frac{\partial^2}{\partial t^2} G(t, t') + V_R(t) G(t, t') + \int_0^t \gamma(t - \tau) \frac{\partial}{\partial \tau} G(\tau, t') d\tau = 0, \quad (25.29)$$

with initial conditions  $G(t = t', t') = 0$  and  $\frac{\partial}{\partial t} G(t = t', t') = \mathbb{1}_N$ . In the previous equation the matrix function  $\gamma(t)$ , known as the ‘damping kernel’, takes into account the non-Markovian and dissipative effects induced by the environment on the network, and  $V_R(t) = V(t) - \gamma(0)$  is a renormalized potential energy matrix. Specifically, the coefficient  $G(t, t')_{j,k}$  encodes the response of the node  $j$  at time  $t$ , as a result of a delta-like impulse on node  $k$  at time  $t'$ . Under the assumptions that the driving  $V(t)$  is periodic and that the dynamics is stable, it can be shown that in the asymptotic regime this function accepts the following decomposition:

$$G(t, t') = \frac{1}{2\pi} \sum_k \int_{-\infty}^{\infty} d\omega A_k(\omega) e^{i\omega(t-t')} e^{ik\omega_d t}, \quad (25.30)$$

where the matrix coefficients  $A_k(\omega)$  can be found by solving a set of linear equations, and can be explicitly calculated in interesting limits such as the weak driving limit ( $|V_k| \ll |V_0|$ ). From Eq. (25.30), it is possible to show that for long times the system attains an asymptotic state which is periodic (with the same period as the driving) and is independent of the initial state. Also, the second moments  $\sigma_{i,j}^{xx}(t)$ ,  $\sigma_{i,j}^{xp}(t)$ , and  $\sigma_{i,j}^{pp}(t)$  in the asymptotic state can be explicitly calculated in terms of  $A_k(\omega)$  (see Eq. (25.36) below).

In addition to the Green's function of the network, that characterizes its dynamics, there are other important quantities that characterize the reservoirs to which the network is connected. They are the spectral densities  $I_\alpha(\omega)$ , one for each reservoir  $\mathcal{E}_\alpha$ , which are  $N \times N$  matrices with coefficients defined as

$$[I_\alpha(\omega)]_{j,k} = \sum_{p=1}^{N_\alpha} \frac{1}{m\omega} C_{\alpha,jp} C_{\alpha,kp} \delta(\omega - \omega_{\alpha,p}), \quad (25.31)$$

where  $C_{\alpha,jp}$  are the coupling constants appearing in Eq. (25.27).

### 25.6.2 Definition of Work and Heat Currents

We must now define the basic notions of work and heat in our setting. For this, we can inspect the different contributions to the total time variation of the energy of the central system,  $H_S$ , which satisfies

$$\frac{d\langle H_S \rangle}{dt} = \langle \partial H_S / \partial t \rangle - i \sum_\alpha \langle [H_S, H_{S,\alpha}] \rangle. \quad (25.32)$$

Thus, the variation of the energy induced by the explicit time dependence of the system's Hamiltonian is associated with work (more precisely, with power), as

$$\dot{\mathcal{W}} = \langle \partial H_S / \partial t \rangle. \quad (25.33)$$

In turn, the variation of the energy of  $\mathcal{S}$  arising from the interaction with each reservoir  $\mathcal{E}_\alpha$  is associated with the heat flowing into the system per unit time, which we denote as  $\dot{\mathcal{Q}}_\alpha$  and turns out to be

$$\dot{\mathcal{Q}}_\alpha = -i \langle [H_S, H_{S,\alpha}] \rangle. \quad (25.34)$$

Therefore, Eq. (25.32) is nothing but the first law of thermodynamics, i.e.  $d\langle H_S \rangle / dt = \dot{\mathcal{W}} + \sum_\alpha \dot{\mathcal{Q}}_\alpha$ . In what follows we will study the average values of the work and the heat currents over a driving period (in the asymptotic regime). These quantities will be respectively defined as  $\bar{\mathcal{W}}$  and  $\bar{\dot{\mathcal{Q}}}_\alpha$ . Then, the averaged version of the first law is simply the identity  $0 = \bar{\mathcal{W}} + \sum_\alpha \bar{\dot{\mathcal{Q}}}_\alpha$ . It is interesting to note that an alternative natural definition for the heat currents could have been given by the energy change of each reservoir, i.e.,  $\dot{\mathcal{Q}}_\alpha = -\langle dH_{\mathcal{E}_\alpha} / dt \rangle$ . As shown in [30], in the asymptotic regime and averaging over a driving period, these two definitions are equivalent. Thus, the energy lost by  $\mathcal{E}_\alpha$  is gained by  $\mathcal{S}$  over a driving period (equivalently, on average, no energy is stored in the interaction terms).

Introducing the explicit form of the Hamiltonians into Eq. (25.34) it is possible to arrive at the following expression for the average heat current corresponding to reservoir  $\mathcal{E}_\alpha$ :

$$\dot{\mathcal{Q}}_\alpha = \text{Tr} \left[ P_\alpha \overline{V(t)\sigma^{xp}(t)} M^{-1} \right], \quad (25.35)$$

where  $\overline{X(t)}$  represents the average value of  $X(t)$  over a period of the driving in the asymptotic state, and  $P_\alpha$  is a projector over the sites of the network connected to

reservoir  $\mathcal{E}_\alpha$ . In turn, the matrix of position-momentum correlations  $\sigma^{xp}(t)$  can be expressed as  $\sigma^{xp}(t) = \Re \left[ \sum_{j,k} S_{j,k}^{xp} e^{i\omega_d(j-k)t} \right]$  with:

$$S_{j,k}^{xp} = \frac{1}{2} \sum_\alpha \int_0^\infty (\omega + k\omega_d) A_j(\omega, \omega_d) I_\alpha(\omega) A_k^\dagger(\omega, \omega_d) \coth(\omega/2T_\alpha) d\omega \quad (25.36)$$

where  $T_\alpha$  is the temperature of the initial thermal state of reservoir  $\mathcal{E}_\alpha$ . From these exact results it is possible to derive a physically appealing expression for  $\dot{Q}_\alpha$ , which has a simple and clear interpretation, as discussed in the following.

### 25.6.3 Heat Currents in Terms of Elementary Processes

It is possible to identify different contributions to the heat current  $\dot{Q}_\alpha$ , and to interpret them in terms of elementary processes that transport or create excitations in the reservoirs. In [30] it is shown that  $\dot{Q}_\alpha$  can be decomposed as the sum of three terms:

$$\dot{Q}_\alpha = \dot{Q}_\alpha^{\text{RP}} + \dot{Q}_\alpha^{\text{RH}} + \dot{Q}_\alpha^{\text{NRH}}, \quad (25.37)$$

which, respectively, are referred as the ‘resonant pumping’ (RP), ‘resonant heating’ (RH), and ‘non-resonant heating’ (NRH) contributions. We will describe below the explicit form of each of these contributions and their physical interpretation in terms of elementary processes. The central quantity appearing in the explicit expressions for  $\dot{Q}_\alpha^{\text{RP}}$ ,  $\dot{Q}_\alpha^{\text{RH}}$  and  $\dot{Q}_\alpha^{\text{NRH}}$  is the following ‘transfer’ function:

$$p_{\alpha,\beta}^{(k)}(\omega) = \frac{\pi}{2} \text{Tr} \left[ I_\alpha(|\omega + k\omega_d|) A_k(\omega) I_\beta(\omega) A_k^\dagger(\omega) \right], \quad (25.38)$$

which combines the spectral densities  $I_\alpha(\omega)$  (characterizing the spectral content and couplings of each reservoir) and the coefficients  $A_k(\omega)$  (that determine the Green’s function  $G(t, t')$  and therefore characterize the dynamics of the network). As it will be clear from what follows, the quantity  $p_{\alpha,\beta}^{(k)}(\omega)$  can be interpreted as the probability per unit time that a quantum of energy  $\omega$  is removed from  $\mathcal{E}_\beta$  while an quantum of energy  $|\omega + k\omega_d|$  is dumped on  $\mathcal{E}_\alpha$ , via absorption (or emission, depending on the sign of  $k$ ) of an amount of energy equal to  $|k\omega_d|$  from (or to) the driving field.

The resonant pumping (RP) contribution reads:

$$\dot{Q}_\alpha^{\text{RP}} = \sum_{\beta \neq \alpha} \sum_k \int_0^\infty d\omega \left[ \omega p_{\beta,\alpha}^{(k)}(\omega) N_\alpha(\omega) - (\omega + k\omega_d) p_{\alpha,\beta}^{(k)}(\omega) N_\beta(\omega) \right], \quad (25.39)$$

where  $N_\alpha(\omega) = (e^{\omega/T_\alpha} - 1)^{-1}$  is the Planck distribution at the temperature  $T_\alpha$  corresponding to the initial state of reservoir  $\mathcal{E}_\alpha$  (the Boltzmann constant is  $k_b = 1$ ). The first term in Eq. (25.39) is positive and accounts for energy flowing out of  $\mathcal{E}_\alpha$ : a

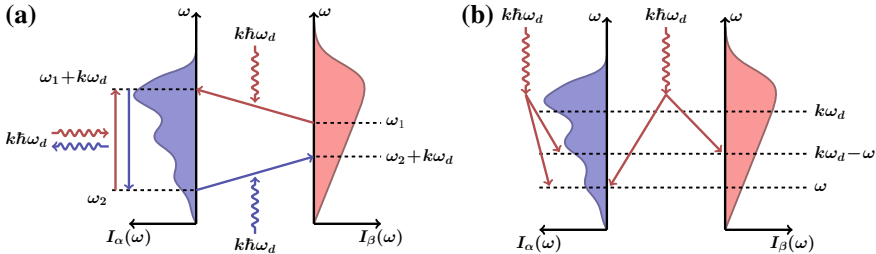


**Fig. 25.2** Illustration of the elementary processes contributing to the heat currents. Two reservoirs  $\mathcal{E}_\alpha$  and  $\mathcal{E}_\beta$  are represented by their spectral functions. In **a** only the resonant processes are depicted. They conserve the number of excitations in the environment (but not the energy) and can involve two environmental modes in different reservoirs (RP) or in the same reservoir (RH). In the last case, in overall, these processes always produce heating. In **b** the non-resonant processes are shown: energy extracted from the driving field is used to simultaneously create two excitations in the environment. Again, this can involve modes of in the same or in different reservoirs.

quantum of energy  $\omega$  is lost in  $\mathcal{E}_\alpha$  and excites a mode of frequency  $\omega + k\omega_d$  in  $\mathcal{E}_\beta$  after absorbing energy  $k\omega_d$  from the driving. The second term corresponds to the opposite effect: a quantum of energy  $\omega$  is lost from  $\mathcal{E}_\beta$  and dumped into a mode of frequency  $\omega + k\omega_d$  in  $\mathcal{E}_\alpha$  after absorbing energy  $k\omega_d$  from the driving. These processes are represented in Fig. 25.2a. In the same figure it is shown that the same processes can take place between two modes of the same reservoir, which, in overall, always results in heating of that reservoir (since initially low frequency modes are more populated than high frequency modes and therefore processes that increase the energy of the reservoir are more probable than their inversions). Thus, they are considered in the resonant heating (RH) contribution, which reads

$$\dot{Q}_\alpha^{\text{RH}} = - \sum_k \int_{0'}^\infty d\omega k\omega_d p_{\alpha,\alpha}^{(k)}(\omega) N_\alpha(\omega) \quad (25.40)$$

The lower limit in the frequency integrals of Eqs. (25.39) and (25.40) is  $0' = \max\{0, -k\omega_d\}$ , since for  $k < 0$  the mentioned processes can only take place if the frequency of the arrival mode,  $\omega + k\omega_d$ , is greater than zero.

Finally, the last contribution to the heat current is given by the non-resonant heating term  $\dot{Q}_{\text{NRH}}$ , which for a driving invariant under time reversal (i.e., such that  $V(-t) = V(t + t_0)$ ), reads:

$$\begin{aligned} \dot{Q}_\alpha^{\text{NRH}} = & - \sum_{k>0} \int_0^{k\omega_d} d\omega k\omega_d p_{\alpha,\alpha}^{(-k)}(\omega) (N_\alpha(\omega) + 1/2) \\ & - \sum_{\beta \neq \alpha} \sum_{k>0} \int_0^{k\omega_d} d\omega (k\omega_d - \omega) p_{\alpha,\beta}^{(-k)}(\omega) (N_\beta(\omega) + 1/2) \\ & - \sum_{\beta \neq \alpha} \sum_{k>0} \int_0^{k\omega_d} d\omega \omega p_{\beta,\alpha}^{(-k)}(\omega) (N_\alpha(\omega) + 1/2), \end{aligned} \quad (25.41)$$

The physical meaning of this last expression is different than in the previous contributions. In this case, excitations are not transported among different modes, but created in pairs from the driving. For example, the first line of Eq. (25.41) takes into account processes in which energy  $k\omega_d$  from the driving is used to simultaneously create two excitations in modes of reservoir  $\mathcal{E}_\alpha$  with frequencies  $\omega$  and  $k\omega_d - \omega$ , in such a way that their sum equals  $k\omega_d$  (note that only terms with  $k > 0$  enter in the previous expression). The second and third lines of Eq. (25.41) account for processes in which the excitations are created in modes of different reservoirs, as depicted in Fig. 25.2b. Thus, at variance with the RP and RH processes, the ones giving rise to the NRH contribution do not conserve the number of excitations in the environment. Consequently, they always produce heating in all reservoirs (i.e.,  $\dot{Q}_\alpha^{\text{NRH}} \leq 0$ ).

The only contribution to the heat current capable of describing cooling of reservoir  $\mathcal{E}_\alpha$  is  $\dot{Q}_\alpha^{\text{RP}}$ . The other two contributions correspond to processes that end up heating reservoir  $\mathcal{E}_\alpha$  and are always negative. Thus, to cool this reservoir it is necessary to engineer the driving  $V(t)$  or the spectral densities in order to satisfy the condition

$$\dot{Q}_\alpha^{\text{RP}} > |\dot{Q}_\alpha^{\text{RH}} + \dot{Q}_\alpha^{\text{NRH}}|. \quad (25.42)$$

Let's suppose that all the reservoirs are at the same temperature  $T$ . As discussed next, there is always a minimum value of  $T$  below which it is impossible to fulfill the previous condition. Thus, it is impossible to cool reservoir  $\mathcal{E}_\alpha$  below this minimum temperature.

### 25.6.4 Pairs Creation as a Limitation for Cooling

There are other important differences between the resonant and non-resonant contributions to the heat currents. In first place, we see from Eqs. (25.39) and (25.40) that  $\dot{Q}_\alpha^{\text{RP}}$  and  $\dot{Q}_\alpha^{\text{RH}}$  vanish in the limit of ultra-low temperatures ( $T_\alpha \rightarrow 0 \forall \alpha$ ). In contrast,  $\dot{Q}_\alpha^{\text{NRH}}$  does not vanish but (for  $\omega_d > 0$ ) remains constant and negative in the same limit. This is natural, since in the ultra-low temperature regime there are no excitations to transport around, but they can still be created by the driving. Thus, we immediately see that for sufficiently low temperatures the pair creation mechanism described above will dominate over the other contributions and will prevent any cooling.

There is an interesting analogy that might help to understand the appearance of pairs creation in the environment of an open and driven quantum system. In fact, the integrand in the first line of Eq. (25.41) is analogous to the spectrum of created photons in the Dynamical Casimir Effect (DCE). The typical explanation of this effect involves an electromagnetic cavity with periodic boundary conditions. For example, in a cavity formed by two opposing mirrors, the oscillation of the mirrors induces the creation of photon pairs inside the cavity. In our setting, we can see the driven central system as a periodically changing boundary condition for the environmental modes. Therefore, it is natural to expect the creation of excitations pairs in the same

way as in the DCE. The role of the DCE as a fundamental limitation for cooling was, to the best of our knowledge, first identified in [31].

### 25.6.4.1 Pairs Creation and the Weak Coupling Approximation

Another important difference between the contributions  $\dot{Q}_\alpha^{\text{RP}}$  or  $\dot{Q}_\alpha^{\text{RH}}$  on one hand, and  $\dot{Q}_\alpha^{\text{NRH}}$  on the other hand, is their scaling with the coupling strength between the central system and the reservoirs. This can be understood as follows. First, let's assume that the spectral densities  $I_\alpha(\omega)$  are proportional to some frequency  $\gamma$ , which typically fixes the rate of the dissipation that the environment induces on the central system, and is itself quadratic on the couplings between the system and reservoirs (see Eq. (25.31)). Also, for simplicity, let's focus in the weak driving regime ( $|V_k| \ll |V_0|$  for  $k \neq 0$ ). In this regime, up to second order in  $V_k$ , we have that the matrix coefficients  $A_k(\omega)$  in the decomposition of the Green's function (Eq. (25.30)) are given by  $A_k(\omega) = -\hat{g}(i(\omega + k\omega_d)V_k)\hat{g}(i\omega)$  for  $k \neq 0$ , where  $\hat{g}(i\omega)$  is the Laplace transform of the Green's function of the network without driving. Therefore, the functions  $p_{\alpha,\beta}^{(k)}(\omega)$  are:

$$p_{\alpha,\beta}^{(k)}(\omega) = \frac{\pi}{2} \text{Tr} [I_\alpha(|\omega + k\omega_d|)\hat{g}(i(\omega + k\omega_d)V_k)\hat{g}(i\omega)I_\beta(\omega)\hat{g}(-i\omega)V_k\hat{g}(-i(\omega + k\omega_d))]. \quad (25.43)$$

These functions are proportional to  $\gamma^2$ . However, when integrated over the full frequency range, as in Eqs. (25.39) and (25.40), the result is proportional to  $\gamma$ . The reason for this is the presence of poles, or resonance peaks, in the function  $\hat{g}(i\omega)$ , whose contribution depends on the dissipation rate and thus on  $\gamma$ . Then, the resonant parts of the heat current,  $\dot{Q}_\alpha^{\text{RP}}$  and  $\dot{Q}_\alpha^{\text{RH}}$ , are proportional to  $\gamma$ . In contrast, that is not always the case for  $\dot{Q}_\alpha^{\text{NRH}}$ , since the integration range in the terms of Eq. (25.41) is limited to  $k\omega_d$  and might not include any resonance peak of the functions  $p_{\alpha,\beta}^{(-k)}(\omega)$ . As a simple example, if we have a purely harmonic driving at frequency  $\omega_d$  (i.e., we only have Fourier coefficients  $V_{\pm 1}$  and  $V_0$ , and  $|V_{\pm 1}| \ll V_0$ ), then  $\dot{Q}_\alpha^{\text{NRH}} \propto \gamma^2$  for  $\omega_d < \Omega_0$ , where  $\Omega_0$  is the smallest resonant frequency in  $p_{\alpha,\beta}^{(-1)}(\omega)$ . Thus, in this situation, the creation of excitation pairs in the environment is a process of fourth order in the interaction Hamiltonian between system and reservoirs (recall that  $\gamma$  is second order in the interaction constants). For this reason, it is not captured by master equations that are derived under the ‘weak coupling’ approximation and are valid, as is usual, only to second order in the interaction Hamiltonian.

For high temperatures and in the weak coupling regime, the term  $\dot{Q}_\alpha^{\text{NRH}}$  can be disregarded in front of  $\dot{Q}_\alpha^{\text{R}} = \dot{Q}_\alpha^{\text{RH}} + \dot{Q}_\alpha^{\text{RP}}$ . However for any fixed value of  $\gamma$ , no matter how small, there exist a minimum temperature below which  $\dot{Q}_\alpha^{\text{NRH}}$  will dominate over  $\dot{Q}_\alpha^{\text{R}}$ . This minimum temperature will depend on  $\gamma$ , and from other details such as the driving protocol and the spectral densities of the reservoirs. An analysis of the minimum temperature for an adaptive procedure that was proposed to violate the unattainability principle [32] was presented in [30]. Also, in [9] it is shown that

the standard limits for Doppler and sideband cooling of a single quantum harmonic oscillator can be derived from this formalism as a special case. This is reviewed in the next section.

The breakdown of the weak coupling approximation for low temperatures is known and can also be deduced from the failure of this approximation to capture quantum correlations between system and environment in that regime [33]. However, our study of this exactly solvable model of driven and open quantum system allows us to understand what kind of processes are missed by that approximation. Also, it makes clear that the pair creation process is the one imposing a minimum achievable temperature for the studied family of driven refrigerators. As a final comment, we note that the if the pairs creation process is not taken into account, the validity of the unattainability principle depends on the properties of the spectral densities [34].

### 25.6.5 Cooling a Single Harmonic Oscillator

In this section we employ the formalism explained above to analyze a simple situation: the cooling of a single quantum oscillator. Analyzing the cooling limit for a single oscillator is relevant in several contexts, such as in the case of cold trapped ions [35], trapped atoms [36], or micromechanical oscillators [37]. For this we will consider that our working medium  $\mathcal{S}$  is a single parametrically driven harmonic oscillator that is in simultaneous contact with two reservoirs. One of these reservoirs,  $\mathcal{E}_A$  has a single harmonic mode that we want to cool. The other reservoir,  $\mathcal{E}_B$ , is where the energy is dumped (this reservoir typically represents the electromagnetic field). As we will see, this model is an interesting analogy to other more realistic models for laser cooling. Notably, this simple model is sufficient to derive the lowest achievable temperatures in the most relevant physical regimes (and to predict their values in other, still unexplored, regimes).

Thus, we consider the spectral density of  $\mathcal{E}_A$  to be such that

$$I_A(\omega) = \tilde{I}_A \delta(\omega - \omega_m). \quad (25.44)$$

where  $\omega_m$  is the frequency of the mode to be cooled and  $\tilde{I}_A$  is a constant measuring the strength of the coupling between  $\mathcal{E}_A$  and  $\mathcal{S}$ . In this case, the frequency integrals needed to obtain the different contributions to the heat current  $\dot{Q}_A$  are trivial. Clearly, the RH contribution is absent since  $\mathcal{E}_A$  consists only of a single mode. The lowest achievable temperature is defined as the one for which the heating and cooling terms balance each other. Using Eqs. (25.39) and (25.41) it is simple to compute their ratio as

$$\left| \frac{\dot{Q}_A^{RP}}{\dot{Q}_A^{NRH}} \right| = \frac{\bar{n}}{1 + \bar{n}} \frac{\sum_{k \geq 1} I_B(k\omega_d + \omega_m) |A_k(\omega_m)|^2}{\sum_{k \geq k_d} I_B(k\omega_d - \omega_m) |A_{-k}(\omega_m)|^2}, \quad (25.45)$$

where  $k_d$  is the smallest integer for which  $k_d\omega_d > \omega_m$  and  $\bar{n} = N_A(\omega_m)$  is the average number of excitations in the motional mode. In order to simplify our analysis, we neglected the heating term appearing in the resonant pumping current  $\dot{Q}^{RP}$  (i.e, the

transport of excitations from  $\mathcal{E}_B$  to  $\mathcal{E}_A$ ). By doing this, we study the most favorable condition for cooling, assuming that the pumping of excitations from  $\mathcal{E}_B$  into  $\mathcal{E}_A$  is negligible. This is equivalent to assuming that the temperature of  $\mathcal{E}_B$  is  $T_B \simeq 0$ . Although this is a reasonable approximation in many cases (such as the cooling of a single trapped ion) we should have in mind that by doing this, the limiting temperature we will obtain should be viewed as a lower bound to the actual one. Thus, the condition defining the lowest bound is that the ratio between the RP and NRH currents is of order unity. Using the previous expressions, it is simple to show that this implies that

$$\frac{\bar{n}}{\bar{n} + 1} = \frac{\sum_{k \geq k_d} I_B(k\omega_d - \omega_m) |A_{-k}(\omega_m)|^2}{\sum_{k \geq 1} I_B(k\omega_d + \omega_m) |A_k(\omega_m)|^2}. \quad (25.46)$$

To pursue our analysis, we need an expression for the Floquet coefficients  $A_k(\omega)$ . This can be obtained under some simplifying assumptions. In fact, if the driving is harmonic (i.e. if  $V(t) = V_0 + V(e^{i\omega_d t} + e^{-i\omega_d t})$ ) and its amplitude is small (i.e. if  $V \ll V_0$ ), we can use perturbation theory to compute the Floquet coefficients to leading order in  $V$ . In fact,

$$A_{\pm 1}(\omega_m) \approx -\hat{g}(i(\omega_m \pm \omega_d)) V \hat{g}(i\omega_m). \quad (25.47)$$

These are the dominant terms when  $\omega_d > \omega_m$  (which implies that  $k_d = 1$ ). For smaller driving frequencies, which would require longer equilibration times and involve longer temporal scales, terms of higher order in  $k$  (which are higher order in the amplitude  $V$ ) should be taken into account. Using the above results, we find that

$$\frac{\bar{n}}{\bar{n} + 1} = \frac{I_B(\omega_d - \omega_m) |\hat{g}(i(\omega_d - \omega_m))|^2}{I_B(\omega_d + \omega_m) |\hat{g}(i(\omega_d + \omega_m))|^2}. \quad (25.48)$$

It is interesting to realize that this last expression can be rewritten as a detailed balance condition. In fact, this can be done by noticing that the Planck distribution satisfies the identity  $\bar{n}/(1 + \bar{n}) = p_{n+1}/p_n$ , where  $p_n$  is the probability for the  $n$ -phonon state. Then, Eq. (25.48) can be rewritten as  $P_{heat} = P_{cool}$ , i.e. as the condition for the identity between the probability of a heating process and the one of a cooling process. The cooling probability,  $P_{cool}$ , is proportional to the product of  $p_{n+1}$  (the probability of having  $n + 1$ -phonons in the motional mode),  $|\hat{g}(i(\omega_d + \omega_m))|^2$  (the probability for propagating a perturbation with frequency  $\omega_d + \omega_m$  through the work medium) and  $I_B(\omega_d + \omega_m)$  (the density of final states in the reservoir where the energy of the propagating excitation is dumped). During this process the motional mode necessarily loses energy. This is the case because the energy propagating through  $\mathcal{S}$  is larger than the driving quantum. The extra energy propagating through  $\mathcal{S}$  is provided by  $\mathcal{E}_A$ , that is therefore cooled. On the other hand, the heating probability,  $P_{heat}$  is the product of  $p_n$  (the probability for  $n$ -phonons in  $\mathcal{S}$ ),  $|\hat{g}(i(\omega_d - \omega_m))|^2$  (the probability for propagating a perturbation with frequency  $\omega_d - \omega_m$  through the

work medium) and  $I_B(\omega_d - \omega_m)$  (the density of final states in the reservoir where the energy is dumped). In this case, the motional mode necessarily gains energy because the energy propagating through  $\mathcal{S}$  is smaller than  $\omega_d$  (the quantum of energy provided by the driving). The extra energy is absorbed by  $\mathcal{E}_A$ , which is therefore heated. It is interesting to note that this detailed balance condition is obtained from our formalism as a simple limiting case. A more general detailed balance condition can be read from Eq. (25.46) (which goes beyond the harmonic, weak driving or adiabatic approximations).

To continue the analysis it is necessary to give an expression for  $\hat{g}(s)$  (the propagator of the undriven work medium). For this we use a semi phenomenological approach by simply assuming that, in the absence of driving, the coupling with the reservoirs induces an exponential decay of the oscillations of  $\mathcal{S}$ . In this case, we can simply write  $\hat{g}(i\omega) = 1/((\omega - i\gamma)^2 - \omega_0^2)$ , where  $\gamma$  is the decay rate and  $\omega_0$  is the renormalized frequency of  $\mathcal{S}$ . The same expression is obtained if we assume that  $\mathcal{S}$  behaves as if it were coupled with a single ohmic environment (this is indeed a reasonable assumption in many cases, which is equivalent to a Markovian approximation, but it certainly requires the back action of  $\mathcal{E}_A$  on  $\mathcal{S}$  to be negligible in the long time limit). Inserting this expression for  $\hat{g}(i\omega)$  into Eq. (25.48), we can ask what is the optimal value of the driving frequency  $\omega_d$  that minimizes  $\bar{n}$ , for given parameters  $\omega_0$ ,  $\omega_m$  and  $\gamma$ . As explained in detail in [9], in this way it is possible to recover the well known limits for the regimes of Doppler and sideband cooling. For the case of Doppler cooling, in which  $\gamma \gg \omega_m$ , we obtain that the optimal driving frequency is  $\omega_d \simeq \omega_0 - \gamma$  and the corresponding minimum occupation is:

$$\bar{n}_{\text{doppler}} = \frac{\gamma}{2\omega_m} \frac{\omega_0}{\omega_0 - \gamma} \gg 1 \quad (25.49)$$

under the additional assumption that  $\omega_0 \gg \omega_m$  (that is compatible with optical settings). In the opposite limit of sideband cooling ( $\gamma \ll \omega_m$ ) we have that the minimum occupation is achieved for  $\omega_d = \omega_0 - \omega_m$  and is:

$$\bar{n}_{\text{sideband}} \simeq \frac{\gamma^2}{4\omega_m^2} \ll 1 \quad (25.50)$$

under the same assumptions. However, our treatment is not restricted to these regimes and can be employed to obtain the optimal driving frequency and minimal occupation in the general case.

### 25.6.6 The Role of Pair Creation in Laser Cooling

According to the previous results, the origin of the lowest achievable temperature for the refrigerators we analyzed is imposed by pair creation from the driving. This is certainly not the typical explanation for the reason why laser cooling stops. However,

we will see now that pair creation has a natural role in laser cooling. The relevant processes that play a role in the resonant pumping and non resonant heating currents are shown in Fig. 25.3a (for  $\omega_d > \omega_m$ ). Thus, the resonant pumping of energy out of  $\mathcal{E}_A$  (blue arrow in Fig. 25.3a) corresponds to a removal of a motional excitation (a phonon) and its transfer into the photonic environment. A phonon with frequency  $\omega_m$  disappears in  $\mathcal{E}_A$  and a photon with frequency  $\omega_0$  appears in  $\mathcal{E}_B$ . This is possible by absorbing energy  $\omega_d = \omega_0 - \omega_m$  from the driving. This process is usually visualized in a different way in the standard literature of laser cooling [38–40], as shown in Fig. 25.3b. This figure shows the energy levels of the combined system formed by  $\mathcal{E}_A$  and  $\mathcal{S}$ . In our case, both systems are oscillators and each one of them has an infinite number of energy levels. However, we only pay attention to the lowest levels of  $\mathcal{S}$ . Thus, the resonant pumping process (RP) takes the system from the lowest energy level of  $\mathcal{S}$  with  $n$  phonons into the excited level of  $\mathcal{S}$  with  $(n-1)$  phonons. Then, as  $\mathcal{S}$  is coupled to the environment  $\mathcal{E}_B$ , it decays from the excited  $|e\rangle$  to the ground state  $|g\rangle$  by emitting an excitation (a photon) in  $\mathcal{E}_B$ , whose frequency is  $\omega_0$ . This is the key process responsible for sideband resolved laser cooling. The system is cooled because resonant pumping forces the combined  $\mathcal{E}_A - \mathcal{S}$  system to move down in the staircase of energy levels.

However, if resonant pumping were the only relevant process, the above argument would induce us to conclude that laser cooling could achieve zero temperature: by going down the staircase of energy levels,  $\mathcal{S}$  would end up in its ground state and the motional mode would end up with  $n = 0$  phonons. The reason why this does not happen is the existence of non resonant heating. This process is described as NRH in Fig. 25.3a. It corresponds to the creation of a pair of excitations consisting of a phonon and a photon. The phonon has frequency  $\omega_m$  while the photon should have frequency  $\omega_d - \omega_m$ . We may choose to describe this pair creation process as a sequence of heating transitions that move the combined  $\mathcal{S}-\mathcal{E}_A$  system up along the staircase of energy levels. This can be done as follows: Suppose that we start from  $n$  phonons in the motional state and  $\mathcal{S}$  in the ground state  $|g\rangle$ . Then,  $\mathcal{S}$  can absorb energy  $\omega_d$  from

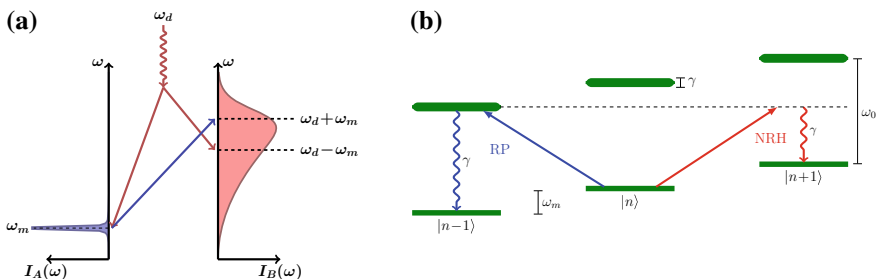


**Fig. 25.3** **a** Relevant processes contributing to the heat current of reservoir  $\mathcal{E}_A$  when  $\omega_d > \omega_m$  and  $T_B \simeq 0$ . Energy flows out of  $\mathcal{E}_A$  and into  $\mathcal{E}_B$  due to a resonant process. Also energy is dumped into both  $\mathcal{E}_A$  and  $\mathcal{E}_B$  due to non resonant pair creation. **b** Usual depiction of the staircase of energy levels and the transitions between them involved in sideband resolved laser cooling (actually, there are other non resonant processes in play, see [38]).

the driving and jump into a virtual state from which it can decay back into  $|g\rangle$  but with a motional state with  $n + 1$  phonons. This heating transition has the net effect of creating a phonon and emitting a photon. As before, laser cooling stops (in this sideband resolved limit) when the resonant cooling transitions are compensated by non resonant heating transitions where energy is absorbed from the driving and is split between two excitations: one in the motional mode (a phonon) and one in the environmental mode (a photon). As a consequence of the non resonant transitions, the motion heats up. The limiting temperature is achieved when the resonant (RP) and non resonant (NRH) processes balance each other.

Of course, the way in which we are describing the processes involved in laser cooling (both the cooling and the heating transitions) is not the standard one, but provides a new perspective that allows to draw parallels with other refrigeration schemes based on external driving.

## References

1. W. Nernst, Ueber die berechnung chemischer gleichgewichte aus thermischen messungen. Nachrichten von der Gesellschaft der Wissenschaften zu Göttingen, Mathematisch-Physikalische Klasse **1906**, 1–40 (1906), <http://eudml.org/doc/58630>
2. M. Planck, *Thermodynamik*, 3rd edn. (De Gruyter, Berlin, 1911)
3. A. Einstein, Beiträge zur quantentheorie. Deutsche Phys. Gesellschaft. Verh. **16**, 820828 (1914)
4. W. Nernst, Über die beziehungen zwischen wärmeentwicklung und maximaler arbeit bei kondensierten systemen. Sitzungsberichte der Königlich Preußischen Akademie der Wissenschaften zu Berlin, 933–940 (1906)
5. W. Nernst, Sitzberg. Kgl. Preuss. Akad. Wiss. Physik.-Math. Kl (1912)
6. E.H. Lieb, D.W. Robinson, Commun. Math. Phys. **28**, 251257 (1972). <https://doi.org/10.1007/BF01645779>
7. H. Wilming, R. Gallego, Third law of thermodynamics as a single inequality. Phys. Rev. X **7**, 041033 (2017). <https://doi.org/10.1103/PhysRevX.7.041033>
8. L. Masanes, J. Oppenheim, A general derivation and quantification of the third law of thermodynamics. Nat. Commun. **8** (2017). <https://doi.org/10.1038/ncomms14538>
9. N. Freitas, J.P. Paz, Cooling a quantum oscillator: a useful analogy to understand laser cooling as a thermodynamical process. Phys. Rev. A **97**, 032104 (2018). <https://doi.org/10.1103/PhysRevA.97.032104>
10. J. Åberg, Truly work-like work extraction via a single-shot analysis. Nat. Commun. **4**, 1925 (2013). <https://doi.org/10.1038/ncomms2712>
11. D. Jennings, T. Rudolph, Entanglement and the thermodynamic arrow of time. Phys. Rev. E **81**, 061130 (2010). <https://doi.org/10.1103/PhysRevE.81.061130>
12. M.N. Bera, A. Riera, M. Lewenstein, A. Winter, Generalized laws of thermodynamics in the presence of correlations. Nat. Commun. **8**, 2180 (2017). <https://doi.org/10.1038/s41467-017-02370-x>
13. M. Horodecki, J. Oppenheim, Fundamental limitations for quantum and nanoscale thermodynamics. Nat. Commun. **4**, 2059 (2013). <https://doi.org/10.1038/ncomms3059>
14. F.G.S.L. Brandao, M. Horodecki, J. Oppenheim, J.M. Renes, R.W. Spekkens, The resource theory of quantum states out of thermal equilibrium. Phys. Rev. Lett. **111**, 250404 (2013). <https://doi.org/10.1103/PhysRevLett.111.250404>
15. A.E. Allahverdyan, K.V. Hovhannisan, D. Janzing, G. Mahler, Thermodynamic limits of dynamic cooling. Phys. Rev. E **84** (2011). <https://doi.org/10.1103/physreve.84.041109>

16. D. Reeb, M.M. Wolf, An improved Landauer principle with finite-size corrections. *New J. Phys.* **16**, 103011 (2014). <https://doi.org/10.1088/1367-2630/16/10/103011>
17. J. Scharlau, M.P. Mueller, Quantum horn's lemma, finite heat baths, and the third law of thermodynamics. *Quantum* **2**, 54 (2018). <https://doi.org/10.22331/q-2018-02-22-54>
18. M.P. Mueller, Correlating thermal machines and the second law at the nanoscale. *Phys. Rev. X* **8**, 041051 (2018). <https://doi.org/10.1103/PhysRevX.8.041051>
19. D. Janzing, P. Wocjan, R. Zeier, R. Geiss, Th. Beth, Thermodynamic cost of reliability and low temperatures: tightening Landauer's principle and the second law. *Int. J. Theor. Phys.* **39**, 2717 (2000). [arXiv:quant-ph/0002048](https://arxiv.org/abs/quant-ph/0002048)
20. F.G.S.L. Brandao, M. Horodecki, N.H.Y. Ng, J. Oppenheim, S. Wehner, The second laws of quantum thermodynamics. *PNAS* **112**, 3275 (2015). <https://doi.org/10.1073/pnas.1411728112>
21. L.J. Schulman, U.V. Vazirani, Molecular scale heat engines and scalable quantum computation, in *Proceedings of the Thirty-First Annual ACM Symposium on Theory of Computing - STOC* 99 (1999). <https://doi.org/10.1145/301250.301332>
22. P.O. Boykin, T. Mor, V. Roychowdhury, F. Vatan, R. Vrijen, Algorithmic cooling and scalable NMR quantum computers. *PNAS* **99**, 33883393 (2002). <https://doi.org/10.1073/pnas.241641898>
23. L.J. Schulman, T. Mor, Y. Weinstein, Physical limits of heat-bath algorithmic cooling. *Phys. Rev. Lett.* **94** (2005). <https://doi.org/10.1103/physrevlett.94.120501>
24. S. Raeisi, M. Mosca, Asymptotic bound for heat-bath algorithmic cooling. *Phys. Rev. Lett.* **114** (2015). <https://doi.org/10.1103/physrevlett.114.100404>
25. R. Alicki, M. Horodecki, P. Horodecki, R. Horodecki, Thermodynamics of quantum informational systems - Hamiltonian description. *Open Syst. Inf. Dyn.* **11**, 205 (2004). [arXiv:quant-ph/0402012](https://arxiv.org/abs/quant-ph/0402012)
26. P. Skrzypczyk, A.J. Short, S. Popescu, Work extraction and thermodynamics for individual quantum systems. *Nat. Commun.* **5**, 4185 (2014). <https://doi.org/10.1038/ncomms5185>
27. M. Tomamichel, *Quantum Information Processing with Finite Resources*. SpringerBriefs in Mathematical Physics (Springer, Berlin, 2016). <https://doi.org/10.1007/978-3-319-21891-5>
28. C. Sparaciari, D. Jennings, J. Oppenheim, Energetic instability of passive states in thermodynamics. *Nat. Commun.* **8**, 1895 (2017). <https://doi.org/10.1038/s41467-017-01505-4>
29. H. Wilming, R. Gallego, J. Eisert, Axiomatic characterization of the quantum relative entropy and free energy. *Entropy* **19**, 241 (2017). <https://doi.org/10.3390/e19060241>
30. N. Freitas, J.P. Paz, Fundamental limits for cooling of linear quantum refrigerators. *Phys. Rev. E* **95**, 012146 (2017). <https://doi.org/10.1103/PhysRevE.95.012146>
31. G. Benenti, G. Strini, Dynamical Casimir effect and minimal temperature in quantum thermodynamics. *Phys. Rev. A* **91**, 020502 (2015). <https://doi.org/10.1103/PhysRevA.91.020502>
32. M. Kolar, R. Alicki, D. Gelbwaser, G. Kurizki, *Phys. Rev. Lett.* **109**, 090601 (2012). <https://doi.org/10.1103/PhysRevLett.109.090601>
33. A.E. Allahverdyan, K.V. Hovhannisyan, G. Mahler, Comment on cooling by heating: refrigeration powered by photons. *Phys. Rev. Lett.* **109** (2012). <https://doi.org/10.1103/physrevlett.109.248903>
34. A. Levy, R. Alicki, R. Kosloff, Quantum refrigerators and the third law of thermodynamics. *Phys. Rev. E* **85**, 061126 (2012). <https://doi.org/10.1103/PhysRevE.85.061126>
35. F. Diedrich, J.C. Bergquist, W.M. Itano, D.J. Wineland, Laser cooling to the zero-point energy of motion. *Phys. Rev. Lett.* **62**, 403 (1989). <https://doi.org/10.1103/PhysRevLett.62.403>
36. S.E. Hamann, D.L. Haycock, G. Klose, P.H. Pax, I.H. Deutsch, P.S. Jessen, Resolved-sideband Raman cooling to the ground state of an optical lattice. *Phys. Rev. Lett.* **80**, 4149 (1998). <https://doi.org/10.1103/PhysRevLett.80.4149>
37. J.D. Teufel, T. Donner, D. Li, J.W. Harlow, M.S. Allman, K. Cicak, A.J. Sirois, J.D. Whittaker, K.W. Lehnert, R.W. Simmonds, Sideband cooling of micromechanical motion to the quantum ground state. *Nature* **475**, 359 (2011). <https://doi.org/10.1038/nature10261>
38. J. Eschner, G. Morigi, F. Schmidt-Kaler, R. Blatt, Laser cooling of trapped ions. *JOSA B* **20**, 1003–1015 (2003). <https://doi.org/10.1364/JOSAB.20.001003>

39. F. Marquardt, J.P. Chen, A.A. Clerk, S.M. Girvin, Quantum theory of cavity-assisted sideband cooling of mechanical motion. *Phys. Rev. Lett.* **99**, 093902 (2007). <https://doi.org/10.1103/PhysRevLett.99.093902>
40. I. Wilson-Rae, N. Nooshi, W. Zwerger, T.J. Kippenberg, Theory of ground state cooling of a mechanical oscillator using dynamical backaction. *Phys. Rev. Lett.* **99**, 093901 (2007). <https://doi.org/10.1103/PhysRevLett.99.093901>

**Part V**

**Information-Theoretic Approaches to**

**Quantum Thermodynamics**

# Chapter 26

# Resource Theory of Quantum Thermodynamics: Thermal Operations and Second Laws



Nelly Huei Ying Ng and Mischa Prebin Woods

## 26.1 Introduction

The term “resource” refers to something that is useful, and most of the time, also scarce. This is because efforts are needed to create, store, and manage these things. What is useful, however, depends on the user: if one wants to send a message to a friend in a distant land, then digital communication channels are useful; if one would instead like to run a long computational code, then the computational power of his machine is the relevant resource.

Resource theories are conceptual, information-theoretic frameworks allowing one to quantify and manage resources. If an experimenter in his/her lab has a constrained ability to perform certain types of operations, then any initial state that cannot be created from such operations becomes valuable to him/her. A generic resource theory therefore is determined by two key elements:

1. a class of *free operations* that are allowed to be implemented at no cost,
2. a class of *free states* that one can generate and use at no cost.<sup>1</sup>

Given the above operations and (an arbitrarily large number of copies of) free states that are assumed to be easily created, one can ask: if the experimenter possesses a quantum state  $\rho$ , what are the set of states he/she can possibly reach by manipulation of  $\rho$ , under the usage of these free operations and states? This produces the third aspect of resource theories, namely:

---

<sup>1</sup> Any state which is not a free state is then called a resource state.

N. H. Y. Ng

Dahlem Center for Complex Quantum Systems, Freie Universität Berlin,

14195 Berlin, Germany

e-mail: nelly.hy.ng@gmail.com

M. P. Woods (✉)

Institute for Theoretical Physics, ETH Zürich, Wolfgang-Pauli-Str. 27,

8093 Zürich, Switzerland

e-mail: mischa.woods@gmail.com

3. *state conversion conditions* that determine the possibility of inter-conversion between states, via the usage of free operations and free states. These conditions, either necessary or sufficient (sometimes both), are commonly phrased as *monotones*, i.e. the transition is possible if a particular function  $f$  decreases in the transition  $\rho \rightarrow \rho'$ , i.e.  $f(\rho) \geq f(\rho')$ .

A classic example of a resource theory comes from quantum information, in identifying *entanglement* between quantum states as a resource. Specifically, suppose that Alice and Bob are two distant parties who are capable of creating any local quantum states in their own labs and manipulating them via arbitrary local quantum operations. Furthermore, since classical communication is well established today (i.e. any transfer of non-quantum information such as an email encoded in a binary string “001101...”), we may suppose that Alice and Bob can easily communicate with each other classically. Such additional classical communication allows them to create a joint, bipartite quantum state  $\rho_{AB}$  which is correlated. This set of operations is known as Local Operations and Classical Communication (LOCC) [1, 2], which defines a set of free operations and states. However, if Alice and Bob are allowed only such operations, it is then impossible for them to create any entanglement, so  $\rho_{AB}$  is separable. Therefore, any prior entangled state they share becomes a valuable resource, and it would be wise for them to manage it well, since it proves to be useful in various tasks. For example, if Alice and Bob share entanglement, they can use it together with classical communication to perform *teleportation*—the transfer of a quantum state. A challenge is that many such tasks require entanglement in a pure, maximal form, namely in pure Bell states; while it is practically much easier to create states which are not maximally entangled. Therefore, the question of how can one *distil* entanglement optimally is also frequently studied. In Ref. [2], it was shown that if Alice and Bob have  $n$  copies of a partially entangled state  $\rho_{AB}^{\otimes n}$ , one can, via LOCC, concentrate the amount of entanglement by producing  $m$  copies of Bell states (where  $m$  is smaller than  $n$ ). Since its pioneering introduction, much experimental progress has been pursued, aiming to manage entanglement resources for the use of long-distance quantum communication [3–5]. In recent years, quantum resource theories have been studied not only in the generality of its mathematical framework [6, 7], but also in particular those related to entanglement theory [8, 9], coherent operations [10, 11], or energetically in thermodynamics [12, 13]. In fact, the application of this framework in modelling thermal interactions has produced perhaps one of the most fundamental paradigms of quantum thermodynamics, inspiring the interpretation of many information-theoretic results to study thermodynamics for finite-sized quantum systems.

Before we focus on the thermodynamic resource theory framework, let us consider once again the grand scheme of resource theories: Table 26.1 summarizes and compares the main characteristics for various different quantum resource theories. Entanglement theory is the most extensively studied case; however, due to great similarities in the mathematical framework, results can often be extended to the other resource theories as well. In the paradigm of entanglement resource theory: if one considers the set of LOCC operations as free operations, and separable states as

**Table 26.1** A comparison of various resource theories. A quantum channel is a completely positive, trace preserving map.

Resource Theory	Free operations	Free states	State conversion conditions
Entanglement (bipartite) [1]	Local unitaries and classical communication	Any separable state $\sum_i p_i \rho_{A,i} \otimes \rho_{B,i}$	$ \psi\rangle\langle\psi _{AB} \rightarrow  \phi\rangle\langle\phi _{AB}$ iff majorization holds: $\text{eig}(\psi_A) \prec \text{eig}(\phi_A)$ . This condition implies that $S(\psi_A) \geq S(\phi_A)$ , i.e. the von Neumann entropy is a monotone, however the former condition is strictly stronger.
Asymmetry w.r.t. a group G [14]	Any quantum channel $\mathcal{E}$ such that for any unitary representation $U_G$ , $g \in G$ , $\mathcal{E}\left[U_g(\cdot)U_g^\dagger\right] = U_g\mathcal{E}(\cdot)U_g^\dagger$ .	Any state $\rho$ such that $\forall U_g$ , $U_g\rho U_g^\dagger = \rho$	For the symmetric group given by $\text{Sym}_G(\rho) = \{g \in G : U_g\rho U_g^\dagger = \rho\}$ , then $\rho \rightarrow \rho'$ only if $\text{Sym}_G(\rho) \subseteq \text{Sym}_G(\rho')$ .
Coherence w.r.t. a basis [10] $\{ i\rangle\}$	Incoherent operations, i.e. any quantum channel $\mathcal{E}$ such that for any $\rho \in \mathcal{I}$ , then $\mathcal{E}(\rho) \in \mathcal{I}$ ; where $\mathcal{I}$ is the set of states diagonal w.r.t. basis $\{ i\rangle\}$ .	Any $\rho \in \mathcal{I}$ diagonal in the basis $\{ i\rangle\}$	For the relative entropy of coherence given by $\mathbf{C}_{RE}(\rho) = \min_{\sigma \in \mathcal{I}} D(\rho\ \sigma)$ , then $\rho \rightarrow \rho'$ only if $\mathbf{C}_{RE}(\rho) \geq \mathbf{C}_{RE}(\rho')$ .
Purity	Unitary operations	Maximally mixed states	Majorization: $\rho \rightarrow \rho'$ iff $\text{eig}(\rho) \succ \text{eig}(\rho')$ (Eq. (26.2)).
Thermodynamics	Energy-preserving unitary operations	Gibbs states (see Eq. (26.6))	Thermo-majorization (see Theorem 2)

free states, then any state that contains entanglement is a resource. In the next few sections, we shall identify the basic elements in a thermodynamic resource theory framework.

## 26.2 Building the Thermodynamic Resource Theory (TRT)

As we have seen in the Chap. 1, thermodynamics is a theory concerning the change in energy and entropy of states in the presence of a heat bath. A special case in the theory, is when the heat bath has a fully degenerate Hamiltonian. In such cases, one cannot exchange energy with the heat bath, thus all operations consist in changes in entropy only. Before considering the full thermodynamic setting with arbitrary heat baths in Sect. 26.2.2, it is illustrative to study this toy model first in Sect. 26.2.1. We will then finalise this section with a discussion on the difficult topic of defining work in such small scale quantum systems in Sect. 26.2.4, and the relation to other operations in Sect. 26.2.3.

### 26.2.1 Noisy Operations (NO)

*Noisy operations*, which is perhaps the simplest known resource theory, is characterized by the following:

1. Free states are maximally mixed states of arbitrary (finite) dimension, with the form  $\frac{1}{d}$ ,
2. All unitary transformations and the partial trace are free operations.

Here the resource is *purity*, which we shall quantify later. One can see intuitively why this is so: free states are those which have maximum disorder (entropy); on the other hand, unitary transformations preserve entropy, while the partial trace is an act of forgetting information, so these operations can never decrease entropy. The higher the purity of a quantum state, the more valuable it would be under noisy operations.

NOs are concerned only about the information carried in systems; instead of energy. For this reason, it has also been referred to as the *resource theory of informational nonequilibrium* [15], or the *resource theory of purity*. This toy model for thermodynamics was first described in [12] and has its roots in the problem of exorcising Maxwell's demon [16, 17], building on the resource theory of entanglement manipulations [2, 18–21].

Formally, a transition  $\rho_S \xrightarrow[\text{NO}]{\quad} \rho'_S$  is possible if and only if there exists an ancilla  $R$  (with dimension  $d_R$ ) such that

$$\rho'_S := \mathcal{E}_{\text{Noisy}}(\rho_S) := \text{tr} \left[ U_{SR} \left( \rho_S \otimes \frac{\mathbb{1}_R}{d_R} \right) U_{SR}^\dagger \right]. \quad (26.1)$$

Note that also since only unitaries  $U_{SR}$  are allowed,  $\mathcal{E}_{\text{Noisy}}$  always preserves the maximally mixed state  $\rho_S = \frac{\mathbb{1}_S}{d_S}$ , i.e. it is a unital channel. Furthermore, since all unitaries can be performed for free, it is sufficient to consider only the case where  $\rho_S, \rho'_S$  are diagonal in the same basis. Otherwise, one may simply define a similar NO, namely a unitary on  $S$  that changes  $\rho_S$  to a state which commutes with  $\rho'_S$ . Now, let us denote the eigenvalues of  $\rho_S$  and  $\rho'_S$  as probability vectors  $p = \text{eig}(\rho_S)$  and  $p' = \text{eig}(\rho'_S)$  respectively. It has been shown [15] that the following statements are equivalent:

1. There exists  $\mathcal{E}_{\text{Noisy}}$  so that Eq. (26.1) holds.<sup>2</sup>
2. There exists a bistochastic matrix  $\Lambda_{\text{Noisy}}$  (namely, a matrix such that each row and each column add up to unity), such that  $\Lambda_{\text{Noisy}} p = p'$ .

This tells us that the state transition conditions for noisy operations are dependant solely in terms of the eigenvalues of initial and target quantum states. An integral concept for understanding state inter-convertibility under NO is *majorization*, which we now define.

---

<sup>2</sup>Up to an arbitrarily good approximation to the final state  $\rho'_S$  for fixed dimensional  $\mathcal{H}_S$ , in operator norm.

**Definition 1** (*Majorization*). For two vectors  $p, p'$ , we say that  $p$  majorizes  $p'$  and write  $p \succ p'$ , if

$$\sum_{i=1}^k p_i^\downarrow \geq \sum_{i=1}^k p'_i^\downarrow \quad \forall 1 \leq k \leq d, \quad (26.2)$$

where  $p^\downarrow$  and  $p'^\downarrow$  denote non-increasingly ordered permutations of  $p$  and  $p'$ .

The following theorem demonstrates the importance of majorization in resource theoretic thermodynamics:

**Theorem 1** (Birkhoff-von Neumann theorem, [22, 23]) *For all  $n$ -dimensional probability vectors  $p$  and  $p'$ , the following are equivalent:*

1.  $p$  majorizes  $p'$ , namely  $p \succ p'$ .
2.  $Ap = p'$  where  $A$  is a bistochastic matrix.

Quantum versions of the above theorem have been developed, and we refer the reader to a detailed set of notes on majorization in [24]. The condition that  $\rho_S$  can be transformed into  $\rho'_S$  via noisy operations, is therefore a simple condition about the eigenvalues [12]:

$$\rho_S \xrightarrow[\text{NO}]{\text{NO}} \rho'_S \iff p \succ p'. \quad (26.3)$$

In fact, more can be said about the dimension of the ancilla  $R$ : it only needs to be as large as  $S$ , to enable the full set of possible transitions for any initial state  $\rho_S$  [25].

It is perhaps now interesting to note also that given the von Neumann entropy

$$S(\rho) := -\text{tr } \rho \log \rho = H(\text{eig}(\rho)),$$

where  $H(p) = -\sum_i p_i \log p_i$  is the Shannon entropy, Eq. (26.3) also implies that  $S(\rho_S) \leq S(\rho'_S)$ . Such functions which invert the majorization order in Eq. (26.3) are called Schur concave functions. This tells us that noisy operations always increase the entropy of system  $S$ . However, majorization is also a much more stringent condition compared to the non-decreasing of entropy, since there exists many other Schur concave functions. Well-known examples are the  $\alpha$ -Rényi entropies, which for  $\alpha \in (-\infty, \infty) \setminus \{1\}$  are given by

$$S_\alpha(\rho_S) := \frac{\text{sgn}(\alpha)}{1-\alpha} \log \text{tr } \rho_S^\alpha = H_\alpha(p), \quad (26.4)$$

$$H_\alpha(p) := \frac{\text{sgn}(\alpha)}{1-\alpha} \log \sum_i p_i^\alpha, \quad (26.5)$$

where the function  $\text{sgn}(\alpha)$  gives 1 for  $\alpha \geq 0$  and  $-1$  for  $\alpha < 0$ . The von Neumann entropy and Shannon entropy can be viewed as special cases of Eqs. (26.4) and (26.5). Indeed, one can define  $S_1(\rho_S)$  and  $H_1(p)$  by demanding continuity in  $\alpha$ . Doing so, one finds that  $S_1(\rho_S)$  and  $H_1(p)$  give us the von Neumann and Shannon entropy

respectively. All  $\alpha$ -Rényi entropies are monotonically non-decreasing with respect to NOs.

### 26.2.2 Thermal Operations (TO)

In what sense are noisy operations similar to thermodynamical interactions?

Note that the maximally mixed state (which we allow as free states in NOs) has a few unique properties: firstly, it is the state with the maximum amount of von Neumann entropy. It is also the state which is preserved by any noisy operation. This reminds one of the perhaps shortest way to describe the second law of classical thermodynamics: in an isolated system, disorder/entropy always increases. On the other hand, one can understand the emergence of the well-known canonical, Gibbs ensemble in thermodynamics as a statistical inference that assumes full ignorance (therefore maximum entropy) about the state, under the constraints of known macroscopic variables or conserved quantities such as average total energy. In particular, if the Hamiltonian of the system is fully degenerate, i.e. all microstates have the same amount of energy, then the Gibbs state is precisely the maximally mixed state.

On the other hand, if the system has a non-trivial distribution of energy levels in its Hamiltonian  $\hat{H}$ , then under the constraint of fixed average energy, the state with maximum entropy is called the *thermal/Gibbs state*, which has the form:

$$\tau^\beta = \frac{e^{-\beta\hat{H}}}{Z^\beta}, \quad (26.6)$$

where  $\beta > 0$  is the inverse temperature and is in a one-to-one correspondence with the mean energy of the Gibbs state, while  $Z^\beta = \text{tr}(e^{-\beta\hat{H}})$  is known as the *partition function* of the system. This quantity is directly related to crucial properties such as mean energy and entropy of a thermalized system, and here one sees that it is also the normalization factor for  $\tau^\beta$ . Since the Gibbs state commutes with the Hamiltonian, it is also stationary under the evolution of the Hamiltonian.

Much work has been done to derive the emergence of Gibbs states in equilibration processes from the basic principles of quantum theory. The reader may refer to Part III for a more detailed explanation. From this, we conclude that most quantum systems (i.e. generic Hamiltonians and initial states) will eventually equilibrate and tend towards the Gibbs state. This motivates the usage of Gibbs states as free states in the resource theory framework for thermodynamics. It has been noticed also that states of the form in Eq. (26.6) have a unique structure, called *complete passivity* [26]. This implies that even when provided with arbitrarily many identical copies, one cannot increase the mean energy contained in such states via unitary operations. The fact that energy preserving operations have to preserve the thermal state has been noted as early as [27], while in [28], by considering an explicit work-storage system while allowing only unitaries that commute with the global Hamiltonian, the thermal states defined in Eq. (26.6) enjoy a unique physical significance: they are the only states which cannot be used to extract work. This also implies that they are the only

valid free states, since taking any other non-Gibbs state to be free states will allow arbitrary state transitions  $\rho \rightarrow \sigma$ , for any energy-incoherent  $\rho$  and  $\sigma$ . This further justifies the usage of such Gibbs states as free states.

With these in mind, thermal operations were first considered in [27] and further developed in [13, 29] in order to model the interaction of quantum systems with their larger immediate steady-state environment. The first restriction considered is that of *energy-conserving unitary dynamics*: since systems are described by quantum states, the evolution should be described by unitary evolutions  $U_{SR}$  across the closed system  $S$  and bath  $R$ . Furthermore, the thermodynamical process described should preserve energy over the global system. Note that the demand that energy is conserved, implies that  $U_{SR}$  commutes with the total Hamiltonian  $\hat{H}_{SR} = \hat{H}_S \otimes \mathbb{1}_R + \mathbb{1}_S \otimes \hat{H}_R$ . This still allows for energy exchange to occur between different systems, however, the interactions (governed by unitary dynamics) have to commute with the initial global Hamiltonian.

We are now ready to define thermal operations. Consider a system  $S$  governed by Hamiltonian  $\hat{H}_S$ . For any  $\beta \in \mathbb{R}_{\geq 0}$ , a quantum channel  $\mathcal{E}_{TO}$  is a  $\beta$ -thermal operation if and only if there exists:

1. (free states) a Hamiltonian  $\hat{H}_R$ , with a corresponding Gibbs state

$$\tau_R^\beta = \frac{1}{Z_R^\beta} e^{-\beta \hat{H}_R}, \quad Z_R^\beta = \text{tr} \left( e^{-\beta \hat{H}_R} \right), \quad (26.7)$$

2. (free operations) and a unitary  $U$  such that  $[U, \hat{H}_{SR}] = 0$ , with

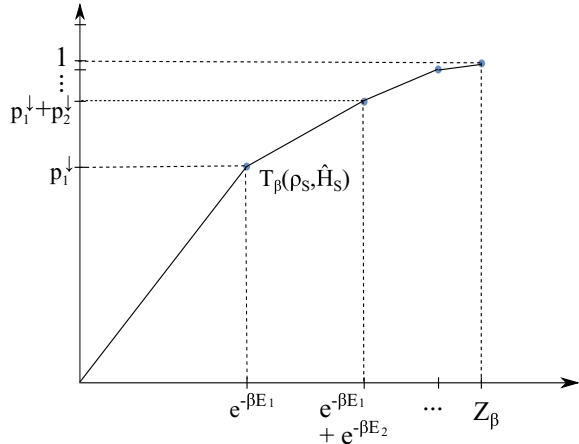
$$\mathcal{E}_{TO}(\rho_S) = \text{tr}_R \left[ U_{SR} \left( \rho_S \otimes \tau_R^\beta \right) U_{SR}^\dagger \right]. \quad (26.8)$$

In the special case where  $\hat{H}_S = \mathbb{1}_S$  and  $\hat{H}_R = \mathbb{1}_R$ , thermal operations  $\mathcal{E}_{TO}$  reduce to noisy operations.

A natural question to ask is what are the conditions on states  $\rho_S, \rho'_S$  with Hamiltonian  $\hat{H}_S$  such that they are related via a thermal operation, namely  $\rho_S \xrightarrow{\text{TO}} \rho'_S$ ? Ref. [13] first considered this question for asymptotic conversion rates, i.e. the optimal rate of conversion  $R(\rho_S \rightarrow \rho'_S) = \frac{m}{n}$  such that  $\rho_S^{\otimes n} \rightarrow \rho'^{\otimes m}_S$ , for the limit  $n \rightarrow \infty$ . Later, Ref. [29] derived a set of majorization-like conditions which determine state transition conditions for a single copy of  $\rho_S$  and  $\rho'_S$ . Such conditions are known as *thermo-majorization*, and are shown to be necessary conditions for arbitrary state transitions via TO. Furthermore, when the target state  $\rho'_S$  commutes with  $\hat{H}_S$ , these conditions become also sufficient.

To describe these conditions, first let us explain a thermo-majorization curve. Consider any state-Hamiltonian pair  $(\rho_S, \hat{H}_S)$  where  $\rho_S$  has rank  $d$  and commutes with  $\hat{H}_S$ . These states are commonly analyzed in the framework of thermodynamic resource theories, and are referred to as *energy incoherent states*, or simply states that

**Fig. 26.1** An example of a thermo-majorization curve of a state-Hamiltonian pair  $T_\beta(\rho_S, \hat{H}_S)$ .



are *block-diagonal*. Because  $\rho_S$  and  $\hat{H}_S$  commute,  $\rho_S$  is diagonalisable in a particular energy eigenbasis of  $\hat{H}_S$ , and can be written in the form

$$\rho_S = \sum_{E, g_E} p_{E, g_E} |E, g_E\rangle\langle E, g_E|_S, \quad (26.9)$$

where  $p_{E, g_E}$  are eigenvalues of  $\rho_S$  and  $\{|E, g_E\rangle\}_{g_E}$ ,  $E$  are the corresponding energy eigenvectors and values of  $\hat{H}_S$  with degeneracy  $g_E$ . A thermo-majorization curve is then defined in Definition 2 (Box 1), and Fig. 26.1 shows an example of a thermo-majorization diagram defined by coordinates in Eq. (26.11). Notice that if  $E_1 = E_2 = \dots = E_d$ , then the intervals on the  $x$ -axis are equally spaced, and  $\beta$ -ordering would be the ordering of eigenvalues  $p_i$  in a non-increasing manner. On the other hand, for such Hamiltonians, thermal operations reduce to noisy operations, and the state transition conditions to majorization. It is proven in [29], that for states commuting with their Hamiltonian, the comparison of two thermo-majorization curves also dictate the possibility of state transition via thermal operations, as detailed by the following theorem:

**Theorem 2** Consider state-Hamiltonian pairs  $(\rho_S, \hat{H}_S)$  and  $(\rho'_S, \hat{H}'_S)$ , such that  $[\rho_S, \hat{H}_S] = [\rho'_S, \hat{H}'_S] = 0$ . The state transition  $\rho_S \xrightarrow{\text{TO}} \rho'_S$  can happen if and only if  $T_\beta(\rho_S, \hat{H}_S) \geq T_\beta(\rho'_S, \hat{H}'_S)$ , i.e. the  $\beta$  thermo-majorization curve of  $(\rho_S, \hat{H}_S)$  lies above that of  $(\rho'_S, \hat{H}'_S)$ . In this case, we say that  $\rho_S$  thermo-majorizes  $\rho'_S$ .

Note that for the state  $\tau_S^\beta = (Z_S^\beta)^{-1} \cdot e^{-\beta \hat{H}_S}$ , its thermo-majorization curve  $T_\beta(\tau_S^\beta, \hat{H}_S)$  simply forms a straight line with endpoints  $(0, 0)$  and  $(Z_\beta, 1)$ . Therefore, for any other block-diagonal state  $\rho_S$ , Theorem 2 implies that  $\rho_S \xrightarrow{\text{TO}} \tau_S^\beta$  is always possible via a  $\beta$ -thermal operation, in accordance with the laws of thermodynamics and our notion of a free state.

As a closing remark, the astute reader may have noticed that we have not commented on the conditions for state conversion under TO when the initial and (or) final states are energy-coherent. For arbitrary states  $\tilde{\rho}_S$ , the corresponding thermo-majorization is defined to coincide with the dephased version of  $\tilde{\rho}_S$  in the energy eigenbasis; and this still provides necessary conditions for state transition [30]. So in conclusion, in general, for TOs it remains an open question as to what are the necessary and sufficient conditions characterizing transitions between arbitrary, energy-coherent states.

**Definition 2** (*Thermo-majorization curve*). A  $\beta$  thermo-majorization curve  $T_\beta(\rho_S, \hat{H}_S)$  is defined by first ordering the eigenvalues of  $\rho_S$  in Eq. (26.9) to have  $p^{\downarrow\beta} = (p_1^\downarrow, \dots, p_d^\downarrow)$  with the corresponding energy eigenvalues  $E_1, \dots, E_d$  such that

$$p_1^\downarrow e^{\beta E_1} \geq p_2^\downarrow e^{\beta E_2} \geq \dots \geq p_d^\downarrow e^{\beta E_d}. \quad (26.10)$$

Such an ordering is called  $\beta$ -ordering, which may be non-unique when parts of Eq. (26.10) are satisfied with inequality. However, once the eigenvalues are ordered this way, a concave, piecewise linear curve called the *thermo-majorization curve of*  $(\rho_S, \hat{H}_S)$  is uniquely defined: by joining all the points

$$\left\{ (0, 0), \left( e^{-\beta E_1}, p_1^\downarrow \right), \left( e^{-\beta E_1} + e^{-\beta E_2}, p_1^\downarrow + p_2^\downarrow \right), \dots, \left( \sum_{i=1}^d e^{-\beta E_i}, \sum_{i=1}^d p_i^\downarrow \right) \right\}. \quad (26.11)$$

### 26.2.3 Relation to Other Operations

#### 26.2.3.1 Gibbs Preserving Maps (GPs)

Within the resource theory approach to quantum thermodynamics, and arguably further afield, the most generic model for thermal interactions are *Gibbs preserving maps*. Understood literally, this means that the set of free operations is simply the set of all quantum channels that preserve the Gibbs state of some inverse temperature  $\beta$ , i.e.

$$\mathcal{E}_{GP} \left( \tau_S^\beta \right) = \tau_S^\beta. \quad (26.12)$$

One can view GPs as highlighting the “bottomline” of any model for thermodynamical interactions. For initial and final states which are block-diagonal, the set of allowed transitions via GPs coincide with thermal operations. However, for general quantum states, GPs may act on energy-incoherent initial states to create energy-coherent final states. This is not possible via thermal operations.

GPs are one of the less studied thermodynamic resource theory models, since there is no known explicit physical process that describes the full set of GPs. Nevertheless, the existence of a GP map can be phrased as a semi-definite problem, and this gives rise to straightforward necessary and sufficient conditions for such a map. In [31], it has been shown that this condition can be phrased in terms of a new entropic quantity, that acts as a parent quantity for several entropic generalizations.

### 26.2.3.2 Multiple Conserved Quantities

A quantum system may in general obey several conservation laws other than total energy, where the conserved quantities (such as spin, momentum etc) are represented by operators on the system which do not generally commute. In this case, one can also further restrict the set of free operations to conserve other constants of motion. Systems in this case tend to equilibrate to the generalized Gibbs ensemble instead of thermalizing to Eq. (26.6). The commuting case was first studied in [32, 33], while in [34–37], non-commuting scenarios have been studied. These works model not only energetic/information exchanges in thermodynamics, but also include exchanges of other non-commuting observables. For further discussion, refer to Chap. 31. In another vein, necessary and sufficient conditions for arbitrary state transitions have been derived in [38] for a set of operations called *generalized thermal processes*, which also take into account such non-commuting variables. While it is unclear if such operations reduce to the set of TOs in the case where only energy is conserved, nevertheless, when the considered states are energy-incoherent, the necessary and sufficient conditions in [38] do reduce to thermo-majorization.

### 26.2.4 Defining Work

A central focus of thermodynamics is the consumption/extraction of work, which is the output/input of ordered energy to a system. Therefore, we must ask the question: in the context of TRTs, what does it mean to extract work?

To gain some intuition for a rigorous formulation, let us recall how this is approached in classical thermodynamics. Work is often pragmatically pictured as the effect of storing potential energy on a system, for example designing a protocol involving a hanging weight, such that in the end, the weight undergoes a height difference  $\Delta x$ . It is also a long-standing observation that one cannot extract work solely from a thermal reservoir; however given two reservoirs at distinct temperatures, one can design protocols to extract work. A common approach is to consider a heat engine, where a machine interacts with two different heat baths successively, and undergoes a cyclic process [39–42]. A physical example of such a “machine” could be a cylinder of ideal gas, where the volume can be changed with a piston. By coupling the piston to the weight, and allowing the machine to go through a series of isothermal/adabatic processes while interacting with two reservoirs, one may analyze the net energy flow in and out of this machine system, and calculate the energy output on the weight, while assuming that energy lost/dissipated (for example, via friction) is negligible.

In the quantum regime, earlier approaches [43–47] have considered different sets of operations. Some popular approaches include allowing for a mixture of (1) level transformations, which is the freedom to tune energy levels in the Hamiltonian and (2) thermalization. These operations are non-energy preserving in general. Therefore, with each operation, one may refer to an amount of work done on/by the system [48]. This amount of work would be largely influenced by energy fluctuations in the system. In particular, much discussion has gone into how one should differentiate work from heat [45, 49–51]. Although both contribute to a change in energy of the system, work stored is of an *ordered* form, and therefore can be extracted and used, while heat is irreversibly dissipated/lost. Though a seemingly simple problem, there is no consensus among the community as to how work should be defined. We describe the main two different strategies in this section.

#### 26.2.4.1 Average Work

A popular way to quantify work is to model the weight as a quantum system (referred to as a battery) that undergoes a change  $\rho_W \rightarrow \rho'_W$  during a thermodynamic process [52–54]. Work is then defined as  $\Delta W = \text{tr}(\hat{H}_W \rho'_W) - \text{tr}(\hat{H}_W \rho_W)$ . Since  $\Delta W$  is the average energy change, which is subjected to random processes (ex: thermalization), work is treated as a random variable. Studies have shown that for example, an optimal amount of average work (equal to the free energy of the system) can be drawn, or that Carnot efficiency can be achieved [53].

The simplicity of this quantity makes it one of the first choices in quantifying work. However, when such a measure is used, it is crucial that the amount of entropy has to be separately analyzed, in order to show that heat contributions to the average energy increase are either negligible, or at least accounted for. This is because thermodynamic processes could, and often do produce work with fluctuations of the same order [45, 55]. Such fluctuations are undesirable for two reasons: (1) they affect the reusability of the battery, i.e. one might not be able to extract the full amount of  $\Delta W$  out again, (2) the battery could have potentially been used as an “entropy sink”, where the average work cannot capture this effect, thus leading to an apparent violation of the second law.

To solve the latter problem, a recent approach is to further restrict the allowed operations, so that they satisfy *translational invariance* on the battery [56, 57]. By this restriction, one can show that defining work as above still allows one to formulate refined versions of the second law. While this approach is conceptually a large step forward in justifying the reasonableness in using average energy as a work quantifier, several improvements await. One of the main caveats is that the current battery models in such approaches have no ground state; which is a reasonable approximation only when the initial and final states of the battery have extremely high energy. Understanding the corrections that enter this picture when using physical battery models is therefore of high importance.

### 26.2.4.2 Single-Shot and Deterministic Work

Another common approach in TRTs [28, 29] (although not restricted to resource theories), is to phrase the work extraction problem as a state transition problem on the battery. More concretely, one fixes a particular desirable, perhaps more physically motivated battery Hamiltonian  $H_W$ , along with specific battery states  $\rho_W, \rho'_W$ , and then consider the possibility of the state transition

$$\rho_S \otimes \rho_W \xrightarrow{X} \rho'_S \otimes \rho'_W, \quad (26.13)$$

for any arbitrary final state  $\rho'_S$  (one can consider  $X$  for TOs, CTOs, or other processes as well). Commonly used models of battery Hamiltonians include a two-level qubit with a tunable energy gap [28, 29], a harmonic oscillator [53], or a system with quasi-continuous energy levels [58]. For an explicit example, if we use the two-level qubit battery such that  $\hat{H}_W = W_{\text{ext}}|1\rangle\langle 1|_W$ , then a transition from the state  $\rho_W = |0\rangle\langle 0|_W$  to  $\rho'_W = |1\rangle\langle 1|_W$  corresponds to extracting an amount of work equal to  $W_{\text{ext}}$ . At the same time, we have required that we retain perfect knowledge of the final state of  $\rho'_W$ , and no entropy increase occurs.

Most often, the explicit battery model (i.e. its Hamiltonian  $\hat{H}_W$ ) does not affect the amount of work stored/used. However, it does depend on the initial and final battery states  $\rho_W, \rho'_W$ .

## 26.3 Second Laws of Quantum Thermodynamics

The framework of thermal operations, presented so far, incorporates the zeroth and first law of thermodynamics very naturally. The zeroth law is established by noting that Gibbs states are singled out as special, free states that are uniquely characterized by a parameter  $\beta$ . The first law comes in due to the requirement that only energy preserving unitaries are allowed. But where is our second law? Thermo-majorization governs state transitions, however it is very different from what we usually know as the second law, namely: when a system is brought into contact with a heat bath, its free energy

$$F(\rho, \hat{H}) := \text{tr}(\rho \hat{H}) - \beta^{-1} S(\rho), \quad (26.14)$$

never increases. While we know that if  $\rho$  thermo-majorizes  $\sigma$ , then  $F(\rho) \geq F(\sigma)$ , thermo-majorization is however much stricter than just requiring free energy to decrease. Is there hope to bridge these two statements more closely? The answer is affirmative, by two steps: (1) allowing a catalyst, and (2) looking at approximate transitions in the i.i.d. limit.

### 26.3.1 Catalytic TOs (CTOs)

CTOs are extensions of TOs, where in addition to the same free resources and operations, catalysts that remain uncorrelated and unchanged are allowed. In other words,  $\rho_S \xrightarrow{\text{CTO}} \rho'_S$  is possible via a  $\beta$ -CTO iff there exists

1. (free states) a Hamiltonian  $\hat{H}_R$ , with a corresponding Gibbs state  $\tau_R^\beta$  as in Eq. (26.7),
2. (catalysts) any additional finite-dimensional quantum state  $\omega_C$  with Hamiltonian  $\hat{H}_C$ ,
3. (free operations) a global unitary  $U_{SRC}$  such that  $[U_{SRC}, \hat{H}_{SRC}] = 0$ , and

$$\text{tr}_R \left[ U_{SRC} \left( \rho_S \otimes \tau_R^\beta \otimes \omega_C \right) U_{SRC}^\dagger \right] = \rho'_S \otimes \omega_C. \quad (26.15)$$

There are transitions that cannot occur via TOs, but are made possible by a catalyst. An example is seen in classical thermodynamics: a system going through a heat engine cycle, interacting successively with multiple heat baths and outputting some work before returning to its original state. Mathematically, non-trivial examples can already be demonstrated for systems of dimension 4, with a 2-dimensional catalyst [59]. Similarly to the case of TO, for CTO we would like to have conditions on the states  $\rho_S$ ,  $\rho'_S$  and their Hamiltonian  $\hat{H}_S$  for  $\rho_S \xrightarrow{\text{CTO}} \rho'_S$  to occur. It turns out that such conditions exist, and they show a deep connection with entropic measures used often in quantum information theory.

### 26.3.2 Necessary Conditions for Arbitrary State Transitions

As earlier mentioned, necessary and sufficient conditions for state transitions under TO remains a large open question for TRTs. This is also the case for CTO. However, we know that since TOs are quantum channels that preserve the thermal state, one can derive easily necessary conditions for CTOs. In particular, if we have any function  $f(\rho||\sigma)$  where  $\rho, \sigma$  are density matrices, and if we know that  $f$  satisfies the data processing inequality, meaning that for any quantum channel  $\mathcal{E}$ , and any  $\rho, \sigma$ , we have

$$f(\rho||\sigma) \geq f(\mathcal{E}(\rho)||\mathcal{E}(\sigma)), \quad (26.16)$$

then we can derive that  $f(\rho_S||\tau_S^\beta)$  is also monotonically decreasing under TOs, where  $\tau_S^\beta$  is simply the thermal state of the system, w.r.t. Hamiltonian  $\hat{H}_S$ . Examples of such functions are the quantum Rényi divergences:

$$\tilde{D}_\alpha(\rho||\sigma) = \begin{cases} \frac{1}{\alpha-1} \log \text{tr}(\rho^\alpha \sigma^{1-\alpha}) & \alpha \in [0, 1) \\ \log \left( (\sigma^{\frac{1-\alpha}{2\alpha}} \rho \sigma^{\frac{1-\alpha}{2\alpha}})^\alpha \right) & \alpha > 1, \end{cases} \quad (26.17)$$

where for  $\alpha = 1$ ,  $\tilde{D}_1(\rho||\sigma) = \text{tr}(\rho(\log \rho - \log \sigma))$  which follows by demanding continuity in  $\alpha$ . To apply these data processing inequalities for CTOs, note that CTOs and TOs are directly related, i.e.

$$\rho_S \xrightarrow{\text{CTO}} \rho'_S \iff \rho_S \otimes \omega_C \xrightarrow{\text{TO}} \rho'_S \otimes \omega_C \quad (26.18)$$

for some  $\omega_C$ . Let  $\mathcal{N}_{\text{TO}}$  be the quantum channel such that  $\mathcal{N}_{\text{TO}}(\rho_S \otimes \omega_C) = \rho'_S \otimes \omega_C$ . Then we also know that  $\mathcal{N}_{\text{TO}}(\tau_{SC}^\beta) = \tau_{SC}^\beta$ , i.e. the thermal state of  $\tau_{SC}^\beta = \tau_S^\beta \otimes \tau_C^\beta$  is of product form (because it is assumed that there is no interaction term in the Hamiltonian of  $\hat{H}_{SC}$ ), and is preserved by  $\mathcal{N}_{\text{TO}}$ . If we know that  $\rho_S \xrightarrow{\text{CTO}} \rho'_S$ , then for any quantity  $f$  that satisfies a data processing inequality in Eq. (26.16), there exists  $\omega_C$  such that

$$f(\rho_S \otimes \omega_C || \tau_{SC}^\beta) \geq f(\rho'_S \otimes \omega_C || \tau_{SC}^\beta). \quad (26.19)$$

Furthermore, if  $f$  is additive under tensor product, as both variants of the quantum Rényi divergences are, we have  $f(\rho_S || \tau_S) \geq f(\rho'_S || \tau_S)$ .

The fact that  $\tilde{D}_\alpha(\rho_S || \tau_S)$  decreases is insufficient to guarantee that a transition may occur via TO/CTO. For example, instead of using  $\tau_S^\beta$  in the second argument of  $f$ , one can consider the quantity  $\tilde{D}_\alpha(\rho_S || \mathcal{D}_{\hat{H}_S}(\rho_S))$ , where  $\mathcal{D}_{\hat{H}_S}$  is the operation that decoheres  $\rho_S$  in the energy eigenbasis of  $\hat{H}_S$ . Then it is also known [60] that  $\tilde{D}_\alpha(\rho_S || \mathcal{D}_{\hat{H}_S}(\rho_S)) \geq \tilde{D}_\alpha(\rho'_S || \mathcal{D}_{\hat{H}_S}(\rho'_S))$  must also be true, and one can find examples where  $\tilde{D}_\alpha(\rho_S || \tau_S)$  decreases but  $\tilde{D}_\alpha(\rho_S || \mathcal{D}_{\hat{H}_S}(\rho_S))$  does not. Intuitively, this quantifies solely the amount of coherence between distinct energy subspaces in the state  $\rho_S$ ; and such coherences can only decrease under TOs/CTOs. However, demanding that both quantities are decreasing still does not provide sufficient conditions for a transition.

### 26.3.3 Necessary and Sufficient Conditions for Energy-Incoherent States

If we consider only initial and final states  $\rho_S, \rho'_S$  which are energy-incoherent, then the necessary conditions we saw on  $\tilde{D}_\alpha(\rho_S || \tau_S^\beta)$  can be extended to become sufficient as well. First of all, note that if  $\rho_S$  and  $\rho'_S$  both commute with  $\tau_S^\beta$ , the quantum Rényi divergences simplify to their classical decompositions  $D_\alpha(p || q)$ , where  $p$  and  $q$  are simply the eigenvalues of respective states. For example, let  $\rho_S = \sum_i p_i |E_i\rangle\langle E_i|$ , and  $\tau_S^\beta = \sum_i q_i |E_i\rangle\langle E_i|$ , where  $q_i = e^{-\beta E_i} / Z_\beta$ . Then we know that  $\tilde{D}_\alpha(\rho_S || \tau_S^\beta) = D_\alpha(p || q)$ , where

$$D_\alpha(p || q) := \frac{1}{\alpha - 1} \ln \left( \sum_i p_i^\alpha q_i^{1-\alpha} \right), \quad \forall \alpha \geq 0. \quad (26.20)$$

Therefore, for two commuting states  $\rho, \sigma$ , we will also write  $D_\alpha(\rho||\sigma) = D_\alpha(\text{eig}(\rho)||\text{eig}(\sigma))$ . In order to specify the state transition conditions, one needs to extend the definition of  $D_\alpha$  for the regime of  $\alpha < 0$ , by multiplying Eq. (26.20) with  $\text{sgn}(\alpha)$ . For the regime of  $\alpha \geq 0$ , Eq. (26.20) remains unchanged; however for negative  $\alpha$ ,

$$D_\alpha(p||q) := \frac{1}{1-\alpha} \ln \left( \sum_i p_i^\alpha q_i^{1-\alpha} \right), \quad \forall \alpha < 0. \quad (26.21)$$

The Rényi divergences in Eqs. (26.20) and (26.21) now collectively determine the possibility of a state transition via CTOs. We state this in terms of the following theorem:

**Theorem 3** (Second laws for block-diagonal states) *Consider a system with Hamiltonian  $\hat{H}_S$ , and states  $\rho_S, \rho'_S$  such that  $[\rho_S, \hat{H}_S] = [\rho'_S, \hat{H}_S] = 0$ . Then for any  $\varepsilon > 0$ , the following are equivalent:*

1.  $D_\alpha(\rho_S||\tau_S^\beta) \geq D_\alpha(\rho'_S||\tau_S^\beta), \forall \alpha \in (-\infty, \infty)$ .
2. For any  $\varepsilon > 0$ , there exists a catalyst  $\omega_C$ , and a thermal operation  $\mathcal{N}_{\text{TO}}$  such that  $\mathcal{N}_{\text{TO}}(\rho_S \otimes \omega_C) = \rho'_S \otimes \omega_C$  and  $d(\rho'_S, \rho_S^\varepsilon) \leq \varepsilon$ .

In other words, the transition  $\rho_S \xrightarrow{\text{CTO}} \rho'_S$  can be performed arbitrarily well, if and only if we have  $D_\alpha(\rho_S||\tau_S^\beta) \geq D_\alpha(\rho'_S||\tau_S^\beta)$  as defined in Eqs. (26.20) and (26.21). Moreover, if one is willing to use an additional, pure qubit ancilla  $|0\rangle\langle 0|$  and return it back  $\varepsilon$ -close to its original state, then the requirement on Rényi divergences for  $\alpha < 0$  is no longer necessary, because they will be automatically determined by the fulfillment of  $D_0(\rho_S||\tau_S^\beta) \geq D_0(\rho'_S||\tau_S^\beta)$ . Thererfore, in that case, only the Rényi divergences for  $\alpha \geq 0$  matter.

For an energy-incoherent state  $\rho_S$ , one can define *generalized free energies*

$$F_\alpha(\rho_S, \hat{H}) := \beta^{-1} \left[ \ln Z_\beta + D_\alpha(\rho_S||\tau_S^\beta) \right]. \quad (26.22)$$

Since these are equivalent to  $D_\alpha$  up to an extra multiplicative and additive constant, we see that  $\rho_S \xrightarrow{\text{CTO}} \rho'_S$  iff  $F_\alpha(\rho_S, \hat{H}) \geq F_\alpha(\rho'_S, \hat{H})$ . These inequalities are known as the generalized second laws of quantum thermodynamics [61].

While this is a continuous family of second laws, there are three special instances of  $\alpha$  for Eq. (26.22) that have notable significance. The quantity  $F_1$  is defined by demanding continuity in  $\alpha$ , and is equal to the well-known non-equilibrium free energy in Eq. (26.14). Therefore, these generalized second laws contain the standard second law as a special case, but demonstrate that we have more constraints when considering small quantum systems.

On the other hand, the quantities  $F_0$  and  $F_\infty := \lim_{\alpha \rightarrow \infty} F_\alpha$  correspond to the amount of *single-shot distillable work* and *work of formation* [29] respectively. In other words, if we adapt the requirements on work as described in Sect. 26.2.4.2, then  $F_0(\rho_S, \hat{H}_S)$  gives the maximum amount of work extractable  $W_{\text{ext}}$ , when considering  $\hat{H}_W = W_{\text{ext}}|1\rangle\langle 1|_W$ , such that the transition  $\rho_S \otimes |0\rangle\langle 0|_W \xrightarrow{\text{CTO}} \rho'_S \otimes |1\rangle\langle 1|_W$  is

possible for some  $\rho'_S$ . One can easily show that  $\rho'_S = \tau_S$  obtains the maximum  $W_{\text{ext}}$ . Therefore, the maximum amount of single-shot work can always be obtained by thermalizing  $S$  to its surroundings. In fact, for such a transition, a catalyst is not needed; therefore  $W_{\text{ext}}$  when maximized over all final states, can already be achieved via TOs. However, if we would require a particular fixed  $\rho'_S \neq \tau_S$  to be achieved, then the corresponding amount of  $W_{\text{ext}}$  is given by optimizing

$$W_{\text{ext}} = \inf_{\alpha \geq 0} [F_\alpha(\rho_S, \hat{H}_S) - F_\alpha(\rho'_S, \hat{H}_S)], \quad (26.23)$$

where the infimum may happen on any  $\alpha$ , depending on the specific states  $\rho_S, \rho'_S$ . Similar to the quantity  $F_0, F_\infty(\rho_S, \hat{H}_S)$  gives the minimum amount of work  $W_{\text{form}}$  required to create  $\rho_S$  starting from the thermal state  $\tau_S$ . More precisely, it gives the minimum possible value of  $W_{\text{form}}$  where  $\hat{H}_W = W_{\text{form}}|1\rangle\langle 1|_W$ , so that the transition  $\tau_S \otimes |1\rangle\langle 1|_W \xrightarrow{\text{CTO}} \rho_S \otimes |0\rangle\langle 0|_W$  is possible. Again, one can also achieve this optimal value of  $W_{\text{form}}$  without a catalyst, since the initial state is thermalized with its environment.

### 26.3.4 Relaxing Conditions on CTOs

Given the continuous, infinite set of generalized second laws that are hard to check, the question naturally arises to whether one can further extend CTOs so that these laws simplify. In particular, one could ask: what happens if we allow for the catalyst to be returned only approximately after the process? This question is also physically motivated, since for realistic scenarios, the catalyst might undergo slight degradation due to uncertainties such as those in the initial state, or imperfections in the implementation of quantum operations. These factors can induce small, unnoticed changes in a single use of the catalyst, and cause it to gradually lose its catalytic ability. At the macroscopic scale, the fact that a process is only approximately cyclic has generally been assumed to be enough to guarantee the second law. However, this is not the case in the microscopic regime, which leads to a phenomenon known as *thermal embezzling*.

#### 26.3.4.1 Thermal Embezzling and Approximate Catalysis

At first glance, one might be tempted to demand closeness of  $\omega_C$  to  $\omega'_C$  to be quantified in terms of trace distance  $d(\omega_C, \omega'_C)$ , since this quantity tells us how well one can distinguish two quantum states, given the best possible measurement. In terms of the catalyst, one might hence ask that  $d(\omega_C, \omega'_C) \leq \varepsilon$  for some arbitrary small  $\varepsilon$ .

However, if there are no additional restrictions on what catalysts are allowed, then the generalized free energies are non-robust against errors induced in the catalyst. This can already be demonstrated in the case where all involved Hamiltonians are fully-degenerate: given a  $d_S$ -dimensional system  $S$ , for any  $\varepsilon > 0$  error one allows

on the catalyst, one can always find a corresponding  $d_C(\varepsilon)$ -dimensional catalyst  $\omega_C$ , such that any state transition  $\rho_S \otimes \omega_C \rightarrow \rho'_S \otimes \omega'_C$  is allowed for all  $\rho_S$  and  $\rho'_S$ , while  $d(\omega_C, \omega'_C) \leq \varepsilon$ . Naturally, the dimension  $d_C$  has to diverge as  $\varepsilon \rightarrow 0$ . Intuitively, one understands this by the fact that maximum entropic difference between  $\omega_C$  and  $\omega'_C$  is not only determined by  $\varepsilon$ , but also grows with  $\log d_C$  (as shown in the Fannes-Audenaert inequality [62]). Therefore, any restriction on trace distance error  $\varepsilon$  can be hidden by choosing a large enough catalyst Hilbert space, so that one extracts a small amount of resource (in terms of energy/purity) that remains relatively unnoticed, and using this resource to enable transitions on the (relatively small) system  $S$ . Thermal embezzling tells us that whenever catalysts are used, it is important to assess changes, however slight (even according to seemingly reasonable measures), on the catalyst. There are currently two known ways to further restrict approximate catalysis, in a way that the family of generalized free energies relax to the standard free energy in Eq. (26.14) being the only condition for state transitions (for energy-incoherent states):

1. Requiring that the catalyst used must be returned with error  $d(\omega_C, \omega'_C) \leq O\left(\frac{\varepsilon}{\log d_C}\right)$  for any fixed  $\varepsilon > 0$ , and  $d_C$  being the dimension of the catalyst [28]. This restriction guarantees that although the catalyst is returned with some error, embezzling is avoided since the free energy difference between  $\omega_C$  and  $\omega'_C$  is required to be arbitrarily small.
2. Allowing correlations to build up in the final reduced state of  $\rho'_{SC}$ , such that  $\rho'_C = \omega_C$  is still returned exactly [63], while allowing some error  $\varepsilon$  on the final, created state. It is important to note that as the desired  $\varepsilon \rightarrow 0$  is desired, the required catalyst dimension  $d_C \rightarrow \infty$  as well. Nevertheless, this construction has the appealing effect that the final reduced state  $\rho'_C$  is exactly preserved after enabling the transformation on system  $S$ , and therefore  $\rho'_C$  can be used in a second, fresh round of state transitions on  $S'$ , as long as  $S'$  is initially uncorrelated from  $S$ .

#### 26.3.4.2 Approximate System Transformations Recovering Standard Free Energy in the Thermodynamic Limit

While most literature on TRTs are concerned with exact state transformations, in realistic implementations, we may be satisfied as long as the transition is approximately achieved. This has been studied theoretically, for example in the context of probabilistic thermal operations [64], and in work extraction protocols when heat/entropy is inevitably produced alongside [45, 58]. Therefore, it is a natural and physical relaxation of CTOs to consider approximate state transitions: in other words, given initial and target states  $\rho_S$  and  $\rho'_S$ , and some error parameter  $\varepsilon$ , can we decide if there exists:

1. a state  $\sigma_S$  such that  $d(\rho_S, \sigma_S) \leq \varepsilon$ ,
2. a state  $\sigma'_S$  such that  $d(\rho'_S, \sigma'_S) \leq \varepsilon$ ,

such that  $\sigma_S \xrightarrow{\text{CTO}} \sigma'_S$ ? Another motivation for considering approximate CTOs is to investigate how the macroscopic law of thermodynamics emerges, in the thermodynamic limit. We know that if no approximation is allowed, then the generalized

second laws do not change at all, since these quantities are additive under tensor product. However, it has been shown that the conditions for approximate CTOs can be given by a family of *smoothed generalized free energies*, denoted as  $F_\alpha^\varepsilon(\rho_S, \hat{H})$ . Moreover, consider multiple identical systems  $\rho_S^{\otimes n}$  with respect to the joint Hamiltonian  $\hat{H}_n = \sum_{i=1}^n \hat{H}_i$ . Then, in the limit where  $n \rightarrow \infty$  and  $\varepsilon \rightarrow 0$ , all the smoothed quantities  $F_\alpha^\varepsilon(\rho_S, \hat{H}_n)$  converge to the standard free energy in Eq. (26.14), namely for all  $\alpha \geq 0$ ,

$$\lim_{\varepsilon \rightarrow 0} \lim_{n \rightarrow \infty} \frac{1}{n} F_\alpha^\varepsilon(\rho_S^{\otimes n}, \hat{H}_n) = F(\rho_S, \hat{H}). \quad (26.24)$$

## 26.4 Application of Second Laws: Fundamental Limits on Quantum Heat Engines

### 26.4.1 Introduction and Motivation

One of the initial motivations for the development of thermodynamics was to understand heat engines. Prior to the development of thermodynamics, engineers had little idea whether there were fundamental limits to the efficiency of heat engines, nor what quantities, if any, such hypothetical limit might depend on. It was Nicolas Léonard Sadi Carnot who is credited with proposing the first successful theory on maximum efficiency of heat engines in 1824 [65]. In particular, Carnot studied heat engines that extract energy by interacting with different *working fluids*, which are substances (usually gas or liquid) at different temperatures in thermal states; and as such, are defined in terms of their Hamiltonians. He concluded that the maximum efficiency attainable did not depend on the exact nature of the working fluids, but only on their inverse temperatures,  $\beta_{\text{Hot}}$ ,  $\beta_{\text{Cold}}$ . It was later demonstrated that this maximum efficiency—now known as the Carnot efficiency—is  $\eta_c = 1 - \beta_{\text{Hot}}\beta_{\text{Cold}}^{-1}$ . Carnot's results are known to hold in the realm of macroscopic systems—indeed, the form of  $\eta_c$  can be derived from the standard second law of thermodynamics.

Given that the generalized second laws of thermodynamics govern state transitions for microscopic systems, where the laws of large numbers do not apply; a natural question is: *does Carnot's famous result still hold?* The importance of this question goes beyond purely academic interests, since people are starting to build atomic scale heat engines [66, 67]. We discuss some recent progress in this direction.

### 26.4.2 Setup of a Microscopic Heat Engine

A heat engine consists of 4 parts; a hot bath, a cold bath, a working body or machine, and a battery where the extracted work can be stored. The Hamiltonians of the systems are  $\hat{H}_{\text{Hot}}$ ,  $\hat{H}_{\text{Cold}}$ ,  $\hat{H}_M$ ,  $\hat{H}_W$ , respectively, with a total Hamiltonian  $\hat{H}_{\text{tot}}$  being simply the sum of free Hamiltonians of the individual systems. A working heat engine

should not need any additional systems in order to work. Moreover, allowing for them without explicitly accounting for them, could inadvertently allow for cheating; since one could draw heat or work from them. As such, we only allow for closed dynamics. The machine can be transformed to any state as long as it is returned to its initial state after one cycle. The dynamics during one cycle can be represented by an energy preserving unitary; namely  $U(t)$ , with  $[U(t), \hat{H}_{\text{tot}}] = 0$ . Here,  $t$  is the time per cycle of the heat engine. Note that this formalism allows for an arbitrarily strong interaction term  $\hat{I}_{\text{ColdHotMW}}$  between subsystems, as long as it commutes with  $\hat{H}_{\text{tot}}$  to preserve energy. This set-up readily fits into the resource theory framework: the machine acts as a catalyst, while one of the thermal baths is explicitly accounted for in the system, for example the cold bath,  $\tau_{\text{Cold}}^0$ . In the language of CTOs, one cycle of the heat engine is possible, iff  $\tau_{\beta_{\text{Cold}}}^0 \otimes \rho_W^0 \xrightarrow{\text{CTO}} \rho_{\text{ColdW}}^1$ , where  $\rho_{\text{ColdW}}^1$  is the final state of the cold bath and battery.

As we have seen in Sect. 26.2.4, not all measures of energetic changes can act as a suitable quantifier of work. Several different characterizations of work have been proposed, and it is very important to first specify which characterization is considered, when comparing and analysing the maximum efficiency of heat engines. For example, it was shown in [68] that with a particular characterization called *imperfect* work, one can surpass the Carnot efficiency with this set-up. This is not because microscopic heat engines are superior to macroscopic ones, but because imperfect work detects only the average amount of energy change in the battery, but not the amount of entropy production. On the other hand, at the microscopic scale, one has to be careful not to go to the opposite extreme, since it was proven in [58] that there exists no final state  $\rho_{\text{ColdW}}^1$ , where the battery outputs deterministic work, namely  $\rho_W^0 = |E_j\rangle\langle E_j|_W$ ,  $\rho_W^1 = |E_k\rangle\langle E_k|_W$ ,  $E_k - E_j > 0$ , which was defined in Sect. 26.2.4.2. This motivates the following definition of work, which for all purposes, is as good as deterministic work, but without the technical caveats. Let the final battery state be  $\varepsilon$  close to  $|E_k\rangle\langle E_k|_W$  in trace distance,  $d(\rho_W^1, |E_k\rangle\langle E_k|_W) = \varepsilon$ , with  $\varepsilon$  bounded away from one. The work extracted,  $W_{\text{ext}} = E_k - E_j$ , is *near perfect* if there exists an infinite sequence of heat engines such that, for all  $p > 0$ ,

$$0 < \frac{\Delta S}{W_{\text{ext}}} \leq p \quad (26.25)$$

holds for some proper subset of the sequence, where  $\Delta S$  is the increase in von Neumann entropy of the battery.

### 26.4.3 Heat Engine Efficiency

The efficiency of a heat engine is defined as  $\eta := \frac{W_{\text{ext}}}{\Delta H}$ , where  $\Delta H$  is the amount of heat drawn from the hot bath, namely  $\Delta H = \text{tr}(\hat{H}_{\text{Hot}}\rho_{\text{Hot}}^0) - \text{tr}(\hat{H}_{\text{Hot}}\rho_{\text{Hot}}^1)$ . Since the machine's final and initial states are the same after one cycle, and the initial state of the cold bath is fixed; due to total mean energy conservation,  $\Delta H$  is a function of  $\rho_{\text{Cold}}^1$

and  $W_{\text{ext}}$ . We can then define the maximum achievable efficiency in the nanoregime  $\eta^{\text{nano}}$  as a function of the final state of the cold bath  $\rho_{\text{Cold}}^1$ . More precisely,

$$\eta^{\text{nano}}(\rho_{\text{Cold}}^1) := \sup_{W_{\text{ext}} > 0} \eta(\rho_{\text{Cold}}^1) \quad \text{subject to} \quad (26.26)$$

$$F_\alpha(\rho_W^0 \otimes \tau_{\text{Cold}}^0) \geq F_\alpha(\rho_{\text{Cold}W}^1) \quad \forall \alpha \geq 0, \quad (26.27)$$

where  $F_\alpha$  are defined in Eq. (26.22).

We are interested in answering the question: under what conditions, if any, can Carnot efficiency be achieved? It is known that in regimes where we only have the usual 2nd law, Carnot efficiency can only be achieved when the free energy remains constant during the transition. This is the special case in Eq. (26.27) corresponding to

$$F_1(\rho_W^0 \otimes \tau_{\text{Cold}}^0) = F_1(\rho_{\text{Cold}W}^1). \quad (26.28)$$

Due to sub-additivity of entropy,  $F_1(\rho_{\text{Cold}W}^1) > F_1(\rho_{\text{Cold}}^1 \otimes \rho_W^1)$  iff  $\rho_{\text{Cold}W}^1$  is correlated, so correlations in the final state cannot help one to achieve the Carnot efficiency if one assumes finite-dimensional catalysts. In addition, it can be shown that for near perfect work, that for constant  $\Delta C$ , the state of the cold bath which maximises the efficiency  $\eta$  when only  $F_1$  is required to be non-increasing, is when  $\rho_{\text{Cold}}^1$  is a Gibbs state. Furthermore, when  $\rho_{\text{Cold}}^1$  is a Gibbs state, equality in Eq. (26.28) can only be achieved in the limiting case in which the temperature of the final state of the cold bath approaches the initial cold bath temperature from above. We call this limit in which the Carnot efficiency can be reached, according to the standard second law, the *quasi-static heat engine* limit. The natural question, is whether or not a quasi-static heat engine can achieve the efficiency in the microscopic regime. For this, not only will  $F_1$  have to be non-increasing, but rather all generalised free energies in Eq. (26.27) will have to be.

To answer this question, we specialise to the case in which the cold bath Hamiltonian is comprised of  $n$  qubits, with the  $i$ -th qubit energy gap denoted  $\Delta E_i$ ; and introduce the parameter  $\Omega$

$$\Omega := \min_{i=1,2,\dots,n} (\beta_{\text{Cold}} - \beta_{\text{Hot}}) \frac{\Delta E_i}{Z_i e^{\beta_{\text{Cold}} \Delta E_i}} \quad (26.29)$$

where  $Z_i$  is the partition function of the  $i$ -th qubit.

**Theorem 4** (From [58]) *A quasi-static heat engine extracting near perfect work can achieve the Carnot efficiency, iff  $\Omega \leq 1$ , otherwise only a strictly smaller efficiency is achievable, specifically*

$$\eta^{\text{nano}} = \left( 1 + \frac{\beta_{\text{Hot}}}{\beta_{\text{Cold}} - \beta_{\text{Hot}}} \Omega \right)^{-1}. \quad (26.30)$$

To see that Eq. (26.30) is indeed less than the Carnot efficiency when  $\Omega > 1$ , observe that  $\eta^{\text{nano}}$  achieves the Carnot efficiency for  $\Omega = 1$  and that it is monotonically decreasing in  $\Omega$ .

Theorem 4 has significant consequences for Carnot's famous results about the universality of the maximum efficiency of heat engines. Namely, that it does not apply at the microscopic scale when at least one of the baths is finite, since not all Hamiltonians of the thermal baths—the working fluids, in the language of Carnot—can achieve Carnot efficiency. This said, observe how for any pair  $\beta_{\text{Hot}}, \beta_{\text{Cold}}$ ; when energy gaps of the cold bath are sufficiently small such that  $\Omega < 1$ , then Carnot efficiency is again achievable; even for this finite heat bath.

## 26.5 Developments and Open Questions in Thermodynamic Resource Theories

The simplicity of a resource theoretic approach towards quantum thermodynamics is its main appeal and power, although it may at the same time be its weakness. Given the large amount of past endeavours in modeling thermodynamical interactions, via Master/Linblad equations [69–75] (especially those involving strong coupling system-bath Hamiltonians [76–78]), time dependence in Hamiltonians (such as quenches [79, 80]) etc, the question arises as to how TRTs relate to these approaches. Since the primitive version of noisy/thermal operations, various works have endeavoured to extend and connect the usage of TRTs with other approaches. In particular, we list some important results to date.

### 26.5.1 Inclusion of Catalysts

Thanks to the understanding of CTOs, any experimental apparatus used to implement TOs can now be modelled as additional quantum systems, and be included into the framework of thermal operations. The criteria and guidelines for choosing appropriate catalyst states have been studied, including inexact catalysis, catalysts that may correlate with the system [63], and energy-coherent catalysts [81]. Despite increasing knowledge on this subject, we still lack a clear consensus on the full role of catalysts. In light of thermal embezzling, a question arises as to how one may quantify/justify errors on the catalyst. Moreover, for current results on the subject, the state of a useful catalyst still depends strongly on the desired transformation (initial and final states of the system), and it would be desirable to have generic catalysts which are not only useful for particular transformations, but at least for a subset of processes.

### 26.5.2 Implementation of TOs via Autonomous Models

A fully autonomous model of thermodynamical interactions would simply be described by a time independent Hamiltonian. Such a scenario usually depicts a naturally arising physical process, since systems simply evolve spontaneously according to a fixed Hamiltonian without any control from an observer. Since unitary operations such as those in TRTs are applied at a specific time, one can understand them to be implemented by using an additional quantum system as a clock, and a time independent Hamiltonian over the system and clock Hilbert-spaces, controlled on the clock's state. One of the initial models to attempt to address this issue [82], suffers from the flaw of having a clock with no ground state (thus infinite energy), where no physical realization is possible. This has the unphysical consequence of never suffering any back-reaction of the clock due to the implementation of unitaries regardless of how quickly they are implemented. Another approach [83], while not suffering from these issues, has so-far proven inconclusive about the true thermodynamical cost, and whether there is extra cost unaccounted for in controlling quantum systems by applying autonomously energy preserving unitaries. Despite exciting progress that has been made, this is still an important ongoing area of research.

### 26.5.3 Equivalence to Other Operations

In order to study the fundamental limits to thermodynamics, TOs consider a large set of operations: the experimenter is allowed to use an arbitrary thermal bath, and any energy-preserving unitary. This allows for the derivation of statements holding for full generality, however, one may question if there exist simple operations that would also achieve the full power of TOs. Recently it has been shown that all TOs for energy-incoherent states can be accomplished via a finite number of *coarse operations* [84], where the latter involves qubit baths, level transformations and thermalization. This partially reconciles the TRT framework with various other approaches in quantum thermodynamics [43–47]. Moreover, recent studies have further identified subsets of TOs that have clear experimental realizations [85]. These efforts pave the way to designing protocols that achieve the optimal state transitions as predicted by TOs. See [86] for a more detailed review of recent attempts to realise resource theoretic approaches to quantum thermodynamics.

### 26.5.4 Relation with Fluctuation Theorems

A distinct approach to quantum thermodynamics known as fluctuation relations has been independently progressing in parallel to the development of TRTs [87–90]. A handful of experimental verifications for these relations have been demonstrated, both in the classical [91] and quantum regime [92, 93]. However, the stark conceptual differences between fluctuation relations and TRTs have prevented them, so far, from being connected. Recently, the possibility of connecting both to form a harmonious

picture of thermodynamics has been explored [57, 94, 95]. Should this be achieved, it would provide us potential means to experimentally investigate the predictions of TRTs by making use of fluctuation relations demonstrations.

**Acknowledgements** N.N. acknowledges funding from the Alexander von Humboldt foundation. M.W. acknowledges the Swiss National Science Foundation (SNSF) via the NCCR QSIT. M.W. would like to acknowledge the COST MP1209 network “Thermodynamics in the quantum regime”, to which he was a member and from which part of the research reviewed in this chapter was made possible.

## References

1. M.A. Nielsen, I.L. Chuang, *Quantum Computation and Quantum Information* (Cambridge University Press, Cambridge, 2000)
2. C.H. Bennett, H.J. Bernstein, S. Popescu, B. Schumacher, Phys. Rev. A **53**, 2046 (1996a). <https://doi.org/10.1103/PhysRevA.53.2046>
3. P.G. Kwiat, S. Barraza-Lopez, A. Stefanov, N. Gisin, Nature **409**, 1014 (2001). <https://doi.org/10.1038/35059017>
4. H. Takahashi, J.S. Neergaard-Nielsen, M. Takeuchi, M. Takeoka, K. Hayasaka, A. Furusawa, M. Sasaki, Nat. Photonics **4**, 178 (2010). <https://doi.org/10.1038/nphoton.2010.1>
5. K.G.H. Vollbrecht, C.A. Muschik, J.I. Cirac, Phys. Rev. Lett. **107**, 120502 (2011). <https://doi.org/10.1103/PhysRevLett.107.120502>
6. F.G. Brandão, G. Gour, Phys. Rev. Lett. **115**, 070503 (2015). <https://doi.org/10.1103/PhysRevLett.115.070503>
7. G. Gour, R.W. Spekkens, New J. Phys. **10**, 033023 (2008). <https://doi.org/10.1088/1367-2630/10/3/033023>
8. M.B. Plenio, S. Virmani, Quantum Inf. Comput. **7**, 1 (2007). [arXiv:quant-ph/0504163](https://arxiv.org/abs/quant-ph/0504163)
9. R. Horodecki, P. Horodecki, M. Horodecki, K. Horodecki, Rev. Mod. Phys. **81**, 865 (2009). <https://doi.org/10.1103/RevModPhys.81.865>
10. T. Baumgratz, M. Cramer, M. Plenio, Phys. Rev. Lett. **113**, 140401 (2014). <https://doi.org/10.1103/PhysRevLett.113.140401>
11. A. Winter, D. Yang, Phys. Rev. Lett. **116**, 120404 (2016). <https://doi.org/10.1103/PhysRevLett.116.120404>
12. M. Horodecki, P. Horodecki, J. Oppenheim, Phys. Rev. A **67**, 062104 (2003). <https://doi.org/10.1103/PhysRevA.67.062104>
13. F.G.S.L. Brandão, M. Horodecki, J. Oppenheim, J.M. Renes, R.W. Spekkens, Phys. Rev. Lett. **111**, 250404 (2013). <https://doi.org/10.1103/PhysRevLett.111.250404>
14. I. Marvian, R.W. Spekkens, New J. Phys. **15**, 033001 (2013). <https://doi.org/10.1088/1367-2630/15/3/033001>
15. G. Gour, M.P. Müller, V. Narasimhachar, R.W. Spekkens, N. Yunger Halpern, Physics Reports **583**, 1 (2015). <https://doi.org/10.1016/j.physrep.2015.04.003>
16. C.H. Bennett, Int. J. Theor. Phys. **21**, 905 (1982). <https://doi.org/10.1007/BF02084158>
17. R. Landauer, IBM J. Res. Dev. **5**, 183 (1961). <https://doi.org/10.1147/rd.53.0183>
18. C.H. Bennett, G. Brassard, S. Popescu, B. Schumacher, J.A. Smolin, W.K. Wootters, Phys. Rev. Lett. **76**, 722 (1996b). <https://doi.org/10.1103/PhysRevLett.76.722>
19. M. Horodecki, J. Oppenheim, R. Horodecki, Phys. Rev. Lett. **89**, 240403 (2002). <https://doi.org/10.1103/PhysRevLett.89.240403>
20. I. Devetak, A. Harrow, A. Winter, IEEE Trans. Inf. Theory **54**, 4587 (2008). <https://doi.org/10.1109/TIT.2008.928980>
21. R. Alicki, M. Horodecki, P. Horodecki, R. Horodecki, Open Syst. Inf. Dyn. **11**, 205 (2004). [arXiv:quant-ph/0402012](https://arxiv.org/abs/quant-ph/0402012)

22. R. Bhatia, *Matrix Analysis*, Graduate texts in mathematics (Springer, Berlin, 1997). <https://doi.org/10.1007/978-1-4612-0653-8>
23. G.H. Hardy, J.E. Littlewood, G. Pólya, *Inequalities* (Cambridge University Press, Cambridge, 1952)
24. M.A. Nielsen, *Lect. Notes*, Department of physics (University of Queensland, Australia, 2002)
25. J. Scharlau, M.P. Mueller, *Quantum* **2**, 54 (2018). <https://doi.org/10.22331/q-2018-02-22-54>
26. W. Pusz, S.L. Woronowicz, *Commun. Math. Phys.* **58**, 273 (1978). <https://doi.org/10.1007/BF01614224>
27. D. Janzing, P. Wocjan, R. Zeier, R. Geiss, T. Beth, *Int. J. Theor. Phys.* **39**, 2717 (2000). [arXiv:quant-ph/0002048](https://arxiv.org/abs/quant-ph/0002048)
28. F. Brandão, M. Horodecki, N. Ng, J. Oppenheim, S. Wehner, *Proc. Natl. Acad. Sci.* **112**, 3275 (2015a). <https://doi.org/10.1073/pnas.1411728112>
29. M. Horodecki, J. Oppenheim, *Nat. Commun.* **4** (2013). <https://doi.org/10.1038/ncomms3059>
30. M. Lostaglio, K. Korzekwa, D. Jennings, T. Rudolph, *Phys. Rev. X* **5**, 021001 (2015a). <https://doi.org/10.1103/PhysRevX.5.021001>
31. P. Faist, R. Renner, *Phys. Rev. X* **8**, 021011 (2018). <https://doi.org/10.1103/PhysRevX.8.021011>
32. N. Yunger Halpern, J.M. Renes, *Phys. Rev. E* **93**, 022126 (2016). <https://doi.org/10.1103/PhysRevE.93.022126>
33. N. Yunger Halpern, *J. Phys. A: Math. Theor.* **51**, 094001 (2018). <https://doi.org/10.1088/1751-8121/aaa62f>
34. N. Yunger Halpern, P. Faist, J. Oppenheim, A. Winter, *Nat. Commun.* **7** (2016). <https://doi.org/10.1038/ncomms12051>
35. Y. Guryanova, S. Popescu, A.J. Short, R. Silva, P. Skrzypczyk, *Nat. Comm.* **7** (2016). <https://doi.org/10.1038/ncomms12049>
36. M. Lostaglio, D. Jennings, T. Rudolph, *New J. Phys.* **19**, 043008 (2017). <https://doi.org/10.1088/1367-2630/aa617f>
37. S. Popescu, A.B. Sainz, A.J. Short, A. Winter, *Phil. Trans. Roy. Soc. A* **376**(2123), 20180111 (2018). <https://doi.org/10.1098/rsta.2018.0111>
38. G. Gour, D. Jennings, F. Buscemi, R. Duan, I. Marvian, *Nat. Commun.* **9**(5352) (2018). <https://doi.org/10.1038/s41467-018-06261-7>
39. F. Reif, *Fundamentals of Statistical and Thermal Physics* (Waveland Press, 2009)
40. C. Adkins, *Equilibrium Thermodynamics* (Cambridge University Press, Cambridge, 1983)
41. D. Schroeder, *An Introduction to Thermal Physics* (Addison Wesley, USA, 2000). <https://doi.org/10.1119/1.19116>
42. K. Huang, *Statistical Mechanics* (Wiley, New York, 1987)
43. D. Egloff, O.C.O. Dahlsten, R. Renner, V. Vedral, *New J. Phys.* **17**, 073001 (2015). <https://doi.org/10.1088/1367-2630/17/7/073001>
44. L. Del Rio, J. Åberg, R. Renner, O. Dahlsten, V. Vedral, *Nature* **474**, 61 (2011). <https://doi.org/10.1038/nature10123>
45. J. Åberg, *Nat. Commun.* **4** (2013). <https://doi.org/10.1038/ncomms2712>
46. G.E. Crooks, *J. Stat. Phys.* **90**, 1481 (1998). <https://doi.org/10.1023/A:1023208217925>
47. B. Piechocinska, *Phys. Rev. A* **61**, 062314 (2000). <https://doi.org/10.1103/PhysRevA.61.062314>
48. M. Esposito, C.V. den Broeck, *EPL (Europhys. Lett.)* **95**, 40004 (2011). <https://doi.org/10.1209/0295-5075/95/40004>
49. H. Hosseini-Nejad, E.J. O'Reilly, A. Olaya-Castro, *New J. Phys.* **17**, 075014 (2015). <https://doi.org/10.1088/1367-2630/17/7/075014>
50. R. Gallego, J. Eisert, H. Wilming, *New J. Phys.* **18**, 103017 (2016). <https://doi.org/10.1088/1367-2630/18/10/103017>
51. J. Gemmer, J. Anders, *New J. Phys.* **17**, 085006 (2015). <https://doi.org/10.1088/1367-2630/17/8/085006>
52. M. Perarnau-Llobet, K.V. Hovhannyan, M. Huber, P. Skrzypczyk, N. Brunner, A. Acín, *Phys. Rev. X* **5**, 041011 (2015). <https://doi.org/10.1103/PhysRevX.5.041011>

53. P. Skrzypczyk, A.J. Short, S. Popescu, Nat. Commun. **5** (2014). <https://doi.org/10.1038/ncomms5185>
54. M.O. Scully, Phys. Rev. Lett. **88**, 050602 (2002). <https://doi.org/10.1103/PhysRevLett.88.050602>
55. J.G. Richens, L. Masanes, Nat. Commun. **7**, 13511 (2016). <https://doi.org/10.1038/ncomms13511>
56. J. Åberg, Phys. Rev. X **8**, 011019 (2018). <https://doi.org/10.1103/PhysRevX.8.011019>
57. Á. M. Alhambra, L. Masanes, J. Oppenheim, C. Perry, Phys. Rev. X **6**, 041017 (2016). <https://doi.org/10.1103/PhysRevX.6.041017>
58. M.P. Woods, N. Ng, S. Wehner (2015). [arXiv: 1506.02322](https://arxiv.org/abs/1506.02322)
59. D. Jonathan, M.B. Plenio, Phys. Rev. Lett. **83**, 3566 (1999). <https://doi.org/10.1103/PhysRevLett.83.3566>
60. M. Lostaglio, D. Jennings, T. Rudolph, Nat. Commun. **6**, 6383 (2015b). <https://doi.org/10.1038/ncomms57383>
61. F. Brandão, M. Horodecki, N. Ng, J. Oppenheim, S. Wehner, The second laws of quantum thermodynamics (2015b). <https://doi.org/10.1073/pnas.1411728112>
62. K.M. Audenaert, J. Phys. A: Math. Theor. **40**, 8127 (2007). <https://doi.org/10.1088/1751-8113/40/28/S18>
63. M.P. Mueller, Phys. Rev. X **8**, 041051 (2018). <https://doi.org/10.1103/PhysRevX.8.041051>
64. Á.M. Alhambra, J. Oppenheim, C. Perry, Phys. Rev. X **6**, 041016 (2016). <https://doi.org/10.1103/PhysRevX.6.041016>
65. S. Carnot, *Reflections on the Motive Power of Fire* (1824)
66. M. Scully, M. Zubairy, G. Agarwal, H. Walther, Science **299**, 862 (2003). <https://doi.org/10.1126/science.1078955>
67. J. Roßnagel, O. Abah, F. Schmidt-Kaler, K. Singer, E. Lutz, Phys. Rev. Lett. **112**, 030602 (2014). <https://doi.org/10.1103/PhysRevLett.112.030602>
68. N.H.Y. Ng, M.P. Woods, S. Wehner, New J. Phys. **19**, 113005 (2017). <https://doi.org/10.1088/1367-2630/aa8ced>
69. J. Gemmer, M. Michel, G. Mahler, *Quantum thermodynamics* (Springer, Berlin, 2009). <https://doi.org/10.1007/978-3-540-70510-9>
70. R. Kosloff, Entropy **15**, 2100 (2013). <https://doi.org/10.3390/e15062100>
71. R. Alicki, J. Phys. A: Math. Gen. **12**, L103 (1979). <https://doi.org/10.1088/0305-4470/12/5/007>
72. N. Brunner, M. Huber, N. Linden, S. Popescu, R. Silva, P. Skrzypczyk, Phys. Rev. E **89**, 032115 (2014). <https://doi.org/10.1103/PhysRevE.89.032115>
73. N. Linden, S. Popescu, P. Skrzypczyk, Phys. Rev. Lett. **105**, 130401 (2010). <https://doi.org/10.1103/PhysRevLett.105.130401>
74. K. Szczygielski, D. Gelbwaser-Klimovsky, R. Alicki, Phys. Rev. E **87**, 012120 (2013). <https://doi.org/10.1103/PhysRevE.87.012120>
75. R. Uzdin, A. Levy, R. Kosloff, Phys. Rev. X **5**, 031044 (2015). <https://doi.org/10.1103/PhysRevX.5.031044>
76. S. Hilt, E. Lutz, Phys. Rev. A **79**, 010101 (2009). <https://doi.org/10.1103/PhysRevA.79.010101>
77. H. Peter, G.-L. Ingold, P. Talkner et al., New J. Phys. **10**, 115008 (2008). <https://doi.org/10.1088/1367-2630/10/11/115008>
78. G.-L. Ingold, P. Hänggi, P. Talkner, Phys. Rev. E **79**, 061105 (2009). <https://doi.org/10.1103/PhysRevE.79.061105>
79. P. Calabrese, J. Cardy, Phys. Rev. Lett. **96**, 136801 (2006). <https://doi.org/10.1103/PhysRevLett.96.136801>
80. M. Cramer, C.M. Dawson, J. Eisert, T.J. Osborne, Phys. Rev. Lett. **100**, 030602 (2008). <https://doi.org/10.1103/PhysRevLett.100.030602>
81. J. Åberg, Phys. Rev. Lett. **113**, 150402 (2014). <https://doi.org/10.1103/PhysRevLett.113.150402>
82. A.S. Malabarba, A.J. Short, P. Kammerlander, New J. Phys. **17**, 045027 (2015). <https://doi.org/10.1088/1367-2630/17/4/045027>

83. M.P. Woods, R. Silva, J. Oppenheim (2016). <https://doi.org/10.1007/s00023-018-0736-9>
84. C. Perry, P. Ćwikliński, J. Anders, M. Horodecki, J. Oppenheim, Phys. Rev. X **8**, 041049 (2018). <https://doi.org/10.1103/PhysRevX.8.041049>
85. M. Lostaglio, Á.M. Alhambra, C. Perry, Quantum **2**, 52 (2018). <https://doi.org/10.22331/q-2018-02-08-52>
86. N. Yunger Halpern, Toward physical realizations of thermodynamic resource theories, in *Information and Interaction: Eddington, Wheeler, and the Limits of Knowledge*, ed. by I.T. Durham, D. Rickles (Springer International Publishing, Cham, 2017), pp. 135–166. <https://doi.org/10.1007/978-3-319-43760-6>
87. C. Jarzynski, Ann. Rev. Condens. Matter Phys. **2**, 329 (2011). <https://doi.org/10.1146/annurev-conmatphys-062910-140506>
88. M. Esposito, U. Harbola, S. Mukamel, Rev. Mod. Phys. **81**, 1665 (2009). <https://doi.org/10.1103/RevModPhys.81.1665>
89. M. Campisi, P. Hänggi, P. Talkner, Rev. Mod. Phys. **83**, 771 (2011). <https://doi.org/10.1103/RevModPhys.83.771>
90. U. Seifert, Rep. Prog. Phys. **75** (2012). <https://doi.org/10.1088/0034-4885/75/12/126001>
91. G.M. Wang, E.M. Sevick, E. Mittag, D.J. Searles, D.J. Evans, Phys. Rev. Lett. **89**, 050601 (2002). <https://doi.org/10.1103/PhysRevLett.89.050601>
92. Y. Utsumi, D.S. Golubev, M. Marthaler, K. Saito, T. Fujisawa, G. Schön, Phys. Rev. B **81**, 125331 (2010). <https://doi.org/10.1103/PhysRevB.81.125331>
93. T.B. Batalhão, A.M. Souza, L. Mazzola, R. Auccaise, R.S. Sarthour, I.S. Oliveira, J. Goold, G. De Chiara, M. Paternostro, R.M. Serra, Phys. Rev. Lett. **113**, 140601 (2014). <https://doi.org/10.1103/PhysRevLett.113.140601>
94. S. Salek, K. Wiesner, Phys. Rev. A **96**, 052114 (2017). <https://doi.org/10.1103/PhysRevA.96.052114>
95. A.M. Alhambra, S. Wehner, M.M. Wilde, M.P. Woods, Phys. Rev. A **97**(6), 062114 (2018). <https://doi.org/10.1103/PhysRevA.97.062114>

# Chapter 27

## One-Shot Information-Theoretical Approaches to Fluctuation Theorems



Andrew J. P. Garner

Modern technological developments have driven interest in the thermal properties of systems of ever-diminishing size. The build-up of dissipated heat is a limiting factor on the speed of microprocessors. Over four decades of adherence to Moore's law [1] (an exponential decrease in the size of electronics) has shrunk the size of transistors on commercial chips to 10 nm (e.g. [2]), and there are experimental demonstrations of transistors as small as just 7 atoms [3]. The advent of quantum computing [4] takes computation to an even smaller scale, where the fundamental unit of quantum information – a qubit – may be physically represented by a choice between two energy levels of a *single* atom [5, 6]. As such, there is a pressing need to understand and characterize the thermal behaviour of extremely small systems.

On the other hand, the traditional laws of thermodynamics [7] are understood to govern the behaviour of asymptotically large ensembles of independent systems. Here, by the law of large numbers, properties of the system observed in any given experimental run closely match the average value. Moreover, traditional thermodynamics applies to processes where one compares states of a system in thermodynamic equilibrium—completely characterized by a few state variables, such as temperature or free energy. Doing this implies an additional assumption on the system: namely, that it must spend a sufficiently long (theoretically, sometimes infinite) amount of time thermalizing during any process (see also Part III).

---

A. J. P. Garner (✉)

Centre for Quantum Technologies, National University of Singapore, 3 Science Drive 2,  
Singapore 117543, Singapore  
e-mail: physics@ajpgarner.co.uk

*Present address:*

A. J. P. Garner

Institute for Quantum Optics and Quantum Information, Austrian Academy of Sciences,  
Boltzmanngasse 3, 1090 Vienna, Austria

To what extent does it make sense to use thermal quantities, such as *heat* and *work*, outside of these large, slow settings? Two major fields within modern thermodynamics seek to address this. The first field, *non-equilibrium statistical mechanics* (see e.g. [8]), characterizes the behaviour of systems taken out of thermal equilibrium. A notable approach that I shall discuss in this chapter are *fluctuation relations* [9–11] (see Part II), which relate the non-equilibrium behaviour of a driven system to equilibrium values such as free energy. The second field *one-shot statistical mechanics* (see e.g. [12–19]) draws techniques from one-shot information theory [20–23] (see also Chap. 32) to tackle deviations in statistical behaviour when the mean regime no longer describes a process well.

In this chapter, I discuss a modern approach that draws from both fields: the application of one-shot information theoretic quantities to characterize processes governed by fluctuation relations. I aim here to provide a gentle introduction to the topic, rather than a comprehensive review, and as such shall spend a fair amount of time explaining the prerequisite concepts. I begin in Sect. 27.1 with a review of information-theoretic entropy. Here I will attempt to provide some intuition for one-shot entropies, relative entropies (divergences), and the quantum extensions of these quantities. In Sect. 27.2, I outline the role of information within thermodynamics, and then present a generic setting in which we can discuss both one-shot and non-equilibrium thermodynamics. In Sect. 27.3, I discuss how one-shot entropies fit with the formalism of *fluctuation theorems*, before finally in Sect. 27.4, I consider the case when those fluctuation theorems are *quantum*.

## 27.1 One-Shot Entropies and Divergences

### 27.1.1 The Shannon and Rényi Entropies

Consider a random variable  $X$  that corresponds to choice of  $x_i$  from alphabet  $\mathcal{X}$ , where  $x_i$  is selected with probability  $p_x(i)$ . The *Shannon entropy*  $H(X)$  is then defined [24]:

$$H(X) = - \sum_i p_x(i) \ln p_x(i). \quad (27.1)$$

It is common to refer to  $H(X)$  as the *information* of random variable  $X$ . Although one can take a formal axiomatic approach to deriving this quantity [20, 24, 25], let us here present a looser intuitive understanding [26, 27]: One can consider  $\ln[1/p_x(i)]$  as a measure of “surprise” on receiving some output  $x_i$ . The smaller the  $p_x(i)$ , the greater the surprise.<sup>1</sup> In this picture, the Shannon entropy is therefore the *average surprise* one experiences upon sampling  $X$ , since the various surprises of each outcome are weighted by  $p_x(i)$  in the sum Eq. (27.1).

---

<sup>1</sup>The surprise involves a logarithm rather than just the reciprocal probability to ensure additivity of surprises. For two mutually exclusive events with joint probability  $p \cdot q$ , the joint surprise  $-\ln(p \cdot q) = -\ln(p) - \ln(q)$ .

Information theory is typically concerned about asymptotic limits. We must therefore exercise caution when using its tools to describe the behaviour of small systems, or the statistics formed through limited repetitions of an experiment. Let us reflect on the physical meaning of the Shannon entropy, by considering how information is *encoded* onto a physical system. Suppose we wish to encode random variable  $X$  onto a physical system  $\mathsf{E}$ . The naïve temptation is to assign one microstate of the system for each variate  $x_i$  in  $\mathcal{X}$ . However, the behaviour of the system under this encoding will not match that predicted by equations involving the Shannon entropy, except in the special case of distributions where each variate  $x_i$  occurs with equal probability. Rather, the meaning of Shannon entropy comes from the *source coding theorem* [24]: that in the limit of large  $N$ ,  $N$  independent and identically distributed (*i.i.d.*) instances of a random variable  $X$  can be encoded onto a physical medium with  $e^{NH(X)}$  configurations.<sup>2</sup> In other words, in the limit of large  $N$ , there is always an optimal encoding that allows one to store (or to send) strings of length  $N$  in a physical system with  $e^{NH(X)}$  configurations, and to recover the exact string encoded almost perfectly (i.e. with arbitrarily small error probability). Conversely, if the physical medium has fewer than  $e^{NH(X)}$  configurations, then there will almost always be messages that cannot be recovered.

The existence of such an encoding follows from the principle of *typical sequences*, which in turn relates to the law of large numbers—valid, as implied by the name, only when  $N$  is sufficiently large. The set of typical sequences<sup>3</sup> has size  $e^{NH(X)}$ , as opposed to the much greater number  $|\mathcal{X}|^N$  of total possible strings. Moreover, every typical sequence will occur with equal probability. For large  $N$ , the probability that a randomly sampled string is a *typical sequence* approaches unity. In this asymptotic limit, the efficient encoding is then to associate each configuration of the physical system with a typical sequence.

This encoding, however, is strictly asymptotic. Consider the distribution

$$P(X) = \left[ \frac{1}{2}, \frac{1}{4}, \frac{1}{8}, \frac{1}{16}, \frac{1}{16} \right] \quad \text{over} \quad \mathcal{X} = \{x_a, x_b, x_c, x_d, x_e\}. \quad (27.2)$$

This has a Shannon entropy of  $\frac{15}{8} \ln 2$  nats, so by the source coding theorem there is an asymptotic encoding for strings of length  $N$  that requires  $e^{N \frac{15 \ln 2}{8}}$  distinct configurations. On the other hand, suppose we only have one copy of  $X$  that we wish to encode onto a single physical system. Naïvely applying the source coding theorem suggests that we only require  $\approx 3.87$  configurations, but even rounding up to 4, it is immediately obvious that a physical system with 4 configurations is insufficient to reliably encode a single message: the best (most likely to succeed) scheme is one where we allocate each of  $x_a$ ,  $x_b$  and  $x_c$ , and one of  $x_d$  or  $x_e$  to the 4 physical configurations. Here, there remains a probability  $\frac{1}{16}$  of failing to encode the

<sup>2</sup>The base here is  $e$  because we have defined  $H$  in units of *nats*. If we had defined  $H$  in *bits* using  $-\sum_i p_x(i) \log_2 p_x(i)$ , the base would be 2.

<sup>3</sup>In the context of *i.i.d.*  $X$ , a sequence will be typical if and only if each symbol  $x_i$  appears  $p_i N$  times.

message<sup>4</sup>—much worse than the certainty of success promised by the source encoding theorem. Indeed, we see that when  $N = 1$ , five distinct configurations are necessary to encode a single message  $X$  without error: one for each possible symbol in the set  $\mathcal{X}$ .

This motivates the search for additional information quantities beyond the Shannon entropy when dealing with small  $N$ . In the above example, the pertinent quantity is in fact the *max-entropy* (or *Hartley entropy*)  $H_0$ , which is defined

$$H_0 := \ln |\text{support}(X)| \quad (27.3)$$

(where the *support* is the set of elements in  $\mathcal{X}$  that occur with probability strictly greater than 0, and  $|\text{support}(X)|$  is the number of these nonzero elements). In our example,  $H_0(X) = \ln 5$ , and it is obvious that a physical system with  $e^{\ln 5} = 5$  configurations would be sufficient to reliably encode a single instance of  $X$ . One alternative intuition of  $H_0(X)$  is that it is the Shannon entropy of the most random distribution possible that has the same support as  $X$ —the uniform distribution of the same size as  $X$ . As such,  $H_0$  always upper bounds the Shannon entropy.

More generally, the Shannon entropy and the max-entropy are both part of a broader family of *Rényi entropies*, defined [20]:

$$H_\alpha(X) := \frac{1}{1-\alpha} \ln \left[ \sum_i p_X(i)^\alpha \right], \quad \alpha \geq 0. \quad (27.4)$$

We see that the special case  $\alpha = 0$  corresponds to the max-entropy<sup>5</sup>; and if we take the limit  $\alpha \rightarrow 1$ , we recover the Shannon entropy. In general, Rényi entropies are non-increasing with  $\alpha$ , such that the *max-entropy* ( $\alpha = 0$ ) is the largest entropy value. (Even broader generalizations of entropy are possible—see, for example [21] or [25].)

Let us discuss one other important Rényi entropy: the *min-entropy*, defined as  $\alpha \rightarrow \infty$ :

$$H_\infty(X) := \lim_{\alpha \rightarrow \infty} H_\alpha(X) = -\ln [\max_i p_i]. \quad (27.5)$$

Intuitively, this quantifies the *worst-case randomness* of a variable in cryptographic contexts where randomness is a resource [22] (here, “worst” means least random, as opposed to thermodynamic contexts, where states of low entropy are often more useful). This is because  $H_\infty$  quantifies the maximum amount of *uniform randomness* that we can extract from a string of  $N$  copies of  $X$ , if  $X$  is our only source of randomness. In such a context, we cannot do probabilistic post-processing, but rather the best we may do is to *coarse-grain* the various strings in  $\mathcal{X}^{\otimes N}$  such that the binned

<sup>4</sup>Or conversely, we encode both  $x_d$  and  $x_e$  to the same physical configuration. Then,  $\frac{1}{8}$  of messages have an indistinguishable  $x_d/x_e$ , and we can guess the correct symbol  $\frac{1}{2}$  of the time: resulting in a  $\frac{1}{16}$  probability that the message is incorrectly decoded.

<sup>5</sup>Sometimes the  $H_{\frac{1}{2}}$  is also referred to as the max-entropy. To avoid ambiguity, here we label the entropy explicitly by the parameter  $\alpha$ , i.e. writing  $H_0$  rather than the ambiguous “ $H_{\max}$ ”.

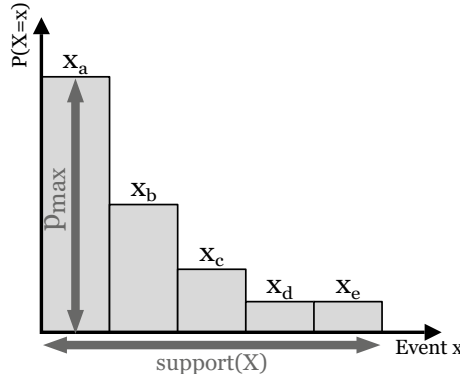


**Fig. 27.1 Example distribution.** The probability distribution  $(\frac{1}{2}, \frac{1}{4}, \frac{1}{8}, \frac{1}{16}, \frac{1}{16})$  of our example random variable  $X$  is drawn. The “width” of this distribution is the support (number of elements), 5, and determines the max-entropy  $H_0$ . The “height” of this distribution is the maximum probability  $p_{\max} = \frac{1}{2}$  and determines the min-entropy  $H_\infty$ . The Shannon entropy  $H_1$  is a weighted function of both width and height (see also [14]).

distribution  $Y$  is uniformly random (that is apply a many-to-one map of  $x^{\otimes N}$  onto  $y \in \mathcal{Y}$ ). In this setting, the *most likely* string of length  $N$  will occur with probability  $p_{\max}^N$ , where  $p_{\max} := \max_i p_x(i)$ . Since all strings from  $X^{\otimes N}$  must be included in a bin, and inclusion of additional strings in the bin can only ever increase the total probability of sampling that bin, we see that at least one variate  $y'$  of  $Y$  must have at least the probability  $p_{\max}^N$  of occurring. Since we want a uniformly random  $Y$ , *at best*  $\mathcal{Y}$  can then contain only  $p_{\max}^{-N}$  outcomes, each occurring with probability  $p_{\max}^N$ . The distribution over this binned  $Y$  has a (Shannon) entropy of  $N \log p_{\max}$ , which we normalize by  $N$  to  $\log p_{\max}$  per sample of  $X$ .

Rényi entropies are often colloquially referred to as “one-shot” quantities, but the above context shows that this does not preclude them from also having asymptotic meanings. A more directly “one-shot intuition” of  $H_\infty$  is that it is the *least surprised* we can be upon learning an outcome of  $X$ . In our above example [Eq. (27.2)]:  $H_\infty = \ln 2$  nats (i.e. 1 bit). This corresponds to a randomness-extraction scheme where we coarse-grain  $X$  into two sets  $\{\{x_a\}, \{x_b, x_c, x_d, x_e\}\}$ , each occurring with probability  $\frac{1}{2}$ . Alternatively, we are the least surprised by  $X$  when it generates outcome  $x_a$ , which happens with probability  $\frac{1}{2}$ .

Different Rényi entropies characterize different aspects of a probability distribution (see Fig. 27.1). One can interpret [14] the parameter  $\alpha$  as weighting the relative importance between the “width” (i.e. support), and the “heights” (read: probabilities) of the distribution. Finally, although it is beyond the scope of this chapter, we note that Rényi entropies can be *smoothed* [21–23] (see also Chap. 32). This amounts to a reshuffling of the probability distribution (bounded according to some distance measure) in order to extremize the entropic quantity at hand. For instance, one could smooth  $H_0(X)$  by discounting the least likely  $x_i$ , up to some total probability  $\epsilon$ . A pedagogical introduction to this may be found in Dahlsten [14].

### 27.1.2 Differential Entropies

The probabilities of continuous variables are often expressed in terms of a *probability density function*  $P(x)$ , which must be integrated over a range in order to yield the probability of observing a sample within that range. When discussing information entropies of a continuous distribution, it is often useful to use a *differential entropy*, since the usual information entropies are typically divergent when faced with a set of infinitesimal probabilities. Suppose we binned  $P(x)$  into bins of size  $\delta x$ , such that (in the limit of small  $\delta x$ ) the probability of each bin is  $P(x)\delta x$ . Then as  $\delta x \rightarrow 0$ , the Shannon entropy will contain divergent terms of the form  $-\ln [P(x)\delta x] \rightarrow \infty$ . This is not incorrect! We would indeed be infinitely surprised to see any *exact* outcome  $x$ —any countable set of real numbers is a measure zero set of a continuum.

This does not mean we have to give up on quantifying entropy for continuous distributions, though we must concede that they are, in general, infinitely more entropic than discrete ones (consider the number of bits a classical digital computer would require to perfectly store a real number to arbitrarily high accuracy [28]). However, by expanding  $\ln [P(x)\delta x] = \ln [P(x)] + \ln \delta x$ , we see it is in fact the second term that is upsetting, and this term is independent of  $P(x)$ . Thus, one takes instead a *differential entropy*, which measures how much more entropic  $P(x)$  is with respect to some implicit reference distribution. Moreover, this difference can be defined in terms of  $\delta x$ , where terms in  $\ln \delta x$  cancel *before* the limit  $\delta x \rightarrow 0$  is taken. This allows us to effectively “renormalize” the entropy.

Typically, the reference distribution is a uniform distribution of unit width and height. This is an arbitrary choice (e.g. thinner uniform distributions will have negative entropies, and this has no special physical meaning). This raises an important concern when we consider a probability density over a dimensionful quantity such as work (energy), or height (distance). If we always choose a width of 1 and a height as 1 as our reference distribution then either: (i) this makes no dimensional sense, or (ii) if we add units to fix the problem i (i.e. for a probability distribution over a quantity measured in units of  $k$ , take a reference distribution of width  $1 k$  and height  $1 k^{-1}$ ), then probability densities referring to the *same data* expressed in different units will have different differential entropies, because the implied reference distributions will be different. For example, consider a probability distribution over heights of people, measured both in feet and in meters: the implied reference distribution for the former is a uniform distribution over 1 foot, the latter over 1 meter – and hence the differential entropy for this same physical distribution expressed in two different units will be different.

To avoid this problem, we should explicitly write our choice of reference when we define the differential entropy. Let us take as such a reference a uniform distribution  $K(x)$ , and compare the difference in Shannon entropy between  $P_{\text{bin}}(x)$  and  $K_{\text{bin}}(x)$  – the distributions formed by binning  $P(x)$  and  $K(x)$  into a discrete distributions the binned alphabet  $\mathcal{B}$ , and probabilities given by  $P(x)\delta x$  and  $K(x)\delta x$  respectively (for small  $\delta x$ ):

$$\begin{aligned}
H_1[P_{\text{bin}}(x)] - H_1[K_{\text{bin}}(x)] &= - \sum_{x \in \mathcal{B}} P(x) \delta x \ln [P(x) \delta x] + \sum_{x \in \mathcal{B}} K(x) \delta x \ln [K(x) \delta x] \\
&= - \sum_{x \in \mathcal{B}} \{P(x) \delta x \ln [P(x)] + P(x) \delta x \ln [\delta x]\} \\
&\quad + \sum_{x \in \mathcal{B}} \{K(x) \delta x \ln [K(x)] + K(x) \delta x \ln [dx]\} \\
&= - \sum_{x \in \mathcal{B}} P(x) \delta x \ln [P(x)] - \ln \delta x + \sum_{x \in \mathcal{B}} K(x) \delta x \ln [K(x)] + \ln \delta x \\
&= - \sum_{x \in \mathcal{B}} P(x) \delta x \ln [P(x)] + \sum_{x \in \mathcal{B}} K(x) \delta x \ln [K(x)]
\end{aligned} \tag{27.6}$$

(We have used that  $\sum P(x) \delta x = \sum K(x) \delta x = 1$ , such that the terms in  $\ln \delta x$  exactly cancel.) In this form, it can be explicitly seen that the difference between the entropy of two distributions does not contain any terms that will diverge as we take the limit  $\delta x \rightarrow 0$ , whereby the sums convert into integrals.

Suppose we choose  $K(x)$  to be a uniform distribution over width  $k$  with probability density  $k^{-1}$ , then the right-most term of Eq. (27.6) becomes  $-\ln k$  [in the same units as the left-hand term in  $P(x)$ ], and so the differential Shannon entropy of probability density function  $P(x)$  with respect to this reference may be written

$$\begin{aligned}
H_1^k[P(x)] &:= \lim_{\delta x \rightarrow 0} \{H_1[P_{\text{bin}}(x)] - H_1[K_{\text{bin}}(x)]\} \\
&= - \int_{-\infty}^{\infty} P(x) \ln [k P(x)] dx.
\end{aligned} \tag{27.7}$$

Similar forms exist for other differential Rényi entropies, for example,  $H_0^k$  and  $H_{\infty}^k$ :

$$H_0^k[P(x)] := \ln \left[ \frac{1}{k} \text{support}[P(x)] \right] \tag{27.8}$$

$$H_{\infty}^k[P(x)] := -\ln \left[ k \max_x [P(x)] \right]. \tag{27.9}$$

The former compares the support of  $P(x)$  with the range  $k$ ; the latter compares the maximum density of  $P(x)$  with  $k^{-1}$ . One additional benefit of these definitions including  $k$  is that it avoids equations where one seemingly must take the logarithm of dimensionful quantities.

The values given by different choices of  $k$  are related by a constant offset given by the difference in the entropy between the different implied reference distributions. In thermodynamic settings, where we are commonly concerned with distributions over energies (work and heat), a natural reference is to set  $k = k_B T$ , since this is the characteristic energy scale of fluctuations at temperature  $T$  [29]. This is formally equivalent to taking probability distributions over energies expressed in units of

$k_B T$ , and then using the traditional form of differential entropies where the reference distribution is implicit.

### 27.1.3 Relative Entropies and Divergences

Conceptually related to information entropies are *relative entropies*, also known as *divergences*. While information entropies quantify the randomness intrinsic to a variable, the relative entropy quantifies deviations in statistical behaviour between two probability distributions.

Consider the random variables  $X$  and  $Y$  with probabilities of outcomes  $\{p_x(i)\}$  and  $\{p_y(i)\}$  respectively (wherein  $X$  and  $Y$  have alphabets such that the index  $i$  labels the same symbol from alphabet  $\mathcal{A}$ ). The *Kullback–Leibler divergence* (or *average relative entropy*) is defined:

$$D_1(X \parallel Y) = - \sum_i p_x(i) \log \frac{p_y(i)}{p_x(i)}. \quad (27.10)$$

We can understand this divergence as a measure of relative surprise [27]. Suppose that we had some system configured according to random variable  $X$ , but we thought it was configured according to  $Y$ . Our surprise at each outcome will be given by terms of the form  $\ln p_y(i)$ , but these surprises occur with probabilities given by the true probabilities  $p_x(i)$ . On average our misidentified system will surprise us by  $-\sum_i p_x(i) \ln p_y(i)$ . The average discrepancy between this, and the true amount ( $-\ln p_x(i)$ ) that we should have been surprised by, is then Kullback–Leibler divergence  $D_1$ .

Equivalently,  $D_1$  quantifies the average amount of information we gain when we misidentify a system  $\xi$  configured in  $X$  as one configured in  $Y$ , and then are subsequently corrected [30]. The interpretation of Kullback–Leibler divergence as *information gain* gives it a role in *machine learning* [31]. Suppose a machine is attempting to learn some the distribution of system  $\xi$  that is configured according to  $X$ . If  $Y$  is the machine's current estimate of  $\xi$ , upon receiving a new sample from the true distribution  $X$ , the average information gained is  $D_1(X \parallel Y)$ . (When the learning is eventually complete,  $Y = X$ , and  $D_1(X \parallel Y) = 0$ ; here, the machine no longer learns new information upon sampling  $\xi$ , since its model is already perfect).

Like the Shannon entropy,  $D_1$  is an asymptotic quantity, involving averages, and so might have limited meaning in a regime where the number of experimental trials are limited. Thus, as with the Shannon entropy, we can generalize this quantity to a family of Rényi divergences [32], which characterise various aspects of the discrepancy between two distributions beyond the asymptotic limit:

$$D_\alpha(X \parallel Y) := \frac{1}{\alpha - 1} \ln \left( \sum_i \frac{p_i^\alpha}{q_i^{\alpha-1}} \right), \quad \alpha \geq 0. \quad (27.11)$$

The limiting case  $\alpha \rightarrow 1$  yields the Kullback–Leibler divergence. There are two other special cases we are particularly interested in. The first,  $\alpha = 0$ , quantifies a difference in support between  $X$  and  $Y$ :

$$D_0(X \parallel Y) = -\ln \left[ \sum_{i \in \{i | p_x(i) > 0\}} p_y(i) \right]. \quad (27.12)$$

That is, we measure a function of the probability that a sample of  $Y$  is within the support of  $X$ . This can be also be interpreted in a one-shot information gain context but where we only consider if events are possible or not, and put no weighting on the probability of events distributed according to  $X$ . If the support of  $X$  and  $Y$  are the same, then no single outcome of  $X$  will challenge our belief that the system is configured according to  $Y$ —reflected by  $D_0(X \parallel Y) = 0$ . On the other hand, if some of the outcomes in  $Y$  are not in  $X$ , these outcomes will never be observed by sampling  $\xi$ , and so each sample makes us more likely to believe the system is not configured according to  $Y$ ,  $D_0(X \parallel Y) > 0$ . Finally, if there is an outcome  $j$  in  $X$  but not in  $Y$  (where  $p_x(j) > 0$  but  $p_y(j) = 0$ ) then observing this outcome will make us *certain* that we were not configured according  $X$ . Here,  $D_0(X \parallel Y)$  is infinite, since  $j$  would be infinitely surprising to us with our erroneous distribution  $Y$ .

The final special case we shall discuss is  $\alpha \rightarrow \infty$ :

$$D_\infty(X \parallel Y) = -\log \left[ \max_i \left( \frac{p_y(i)}{p_x(i)} \right) \right]. \quad (27.13)$$

This quantifies the most shocking discrepancy between  $X$  and  $Y$ , quantifying the *greatest extent* we can be surprised by an outcome if we thought we had  $Y$  but actually had  $X$ . This does not factor in that the variate that maximises this quantity may be very unlikely to occur. As before, if the  $i$ th outcome occurs with some probability in  $X$  but not in  $Y$ , then  $\frac{p_y(i)}{p_x(i)} = 0$  and Eq. (27.13) diverges: here, such an outcome would completely falsify our belief that we had distribution  $Y$  in a single-shot.

$D_\alpha$  also obeys a monotonic relationship with  $\alpha$ , but in the opposite direction to the Rényi entropies.  $D_\alpha$  is monotonically non-decreasing with  $\alpha$  such that  $D_0$  will be the lowest value, and  $D_\infty$  the highest.

Divergences readily generalize to continuous distributions. Since the divergence implicitly involves a difference in the first place, the problems of renormalization intrinsic to the differential entropy (see discussion in Sect. 27.1.2) do not appear here; no implicit reference distribution is required, since we are already directly comparing two distributions. For two probability density functions  $P(x)$  and  $Q(x)$  over  $x$ , we have:

$$D_\alpha(P(x) \parallel Q(x)) = \frac{1}{\alpha - 1} \int_{-\infty}^{\infty} dx \ln [P(x)^\alpha Q(x)^{1-\alpha}], \quad (27.14)$$

$$D_0(P(x) \parallel Q(x)) = -\ln \left( \int_{-\infty}^{\infty} dx \theta[P(x)] Q(x) \right), \quad (27.15)$$

$$D_1(P(x) \parallel Q(x)) = \int_{-\infty}^{\infty} dx \ P(x) \ln \frac{P(x)}{Q(x)}, \quad (27.16)$$

$$D_{\infty}(P(x) \parallel Q(x)) = \begin{cases} \ln(\min\{\lambda \mid P(x) \leq \lambda Q(x) \forall x\}) & \text{support } Q \subseteq \text{support } X, \\ \infty & \text{otherwise,} \end{cases} \quad (27.17)$$

where in Eq. (27.15),  $\theta(y) = 1$  if  $y > 0$  and 0 otherwise.

### 27.1.4 Entropies in Quantum Information Theory

All of the above entropic quantities have quantum equivalents. Classical probability distributions may be thought of as special cases of quantum states that are diagonal in the basis of the measurement distinguishing between the variates. Consider the set of variates  $\mathcal{X} = \{x_i\}$  that form the alphabet of some random variable. One may express the choice from this set as a Hilbert space of dimension  $|\mathcal{X}|$ . Then for a random variable  $X$  where each outcome  $x_i$  occurs with probability  $p_x(i)$ , one can construct a quantum state  $\rho_X = \sum_i p_x(i)|x_i\rangle\langle x_i|$  where  $\{|x_i\rangle\}$  are an orthonormal basis. The state  $\rho_X$  hence has eigenvalues that are the probabilities associated with  $X$ , and eigenvectors that are in one-to-one correspondence with each variate  $x_i$  of  $X$ , and hence knowing the matrix  $\rho_X$  would allow us to reconstruct random variable  $X$  if we are also given the alphabet  $\mathcal{X}$ .

It is natural therefore to seek quantum analogues of classical entropies that are functions of quantum states. The further subtlety in quantum information is that our entropic measure must also accommodate the possibility of coherences between outcomes (non-diagonal elements in the density matrix). Moreover, when extracting probabilities from a quantum state, there are many choices of measurement. Thus, to be a function of a quantum state, rather than also of an (implicit) measurement, one typically defines a quantum entropy with respect to a minimization over all choices of projective measurement [4]. If one then calculates a Rényi entropy on these probabilities (or indeed, any concave function), the Schur–Horn theorem tells us that this minimization will be achieved when we measure in the diagonal basis of the density operator – that is, when the outcome probabilities of the measurement are given by the eigenvalues of the quantum state.

For the case of the quantum generalization of the Shannon entropy, we can write this minimization directly in terms of  $\rho$  to yield the *von Neumann entropy*

$$H_1(\rho) = -\text{Tr}(\rho \ln \rho). \quad (27.18)$$

It is sometimes fashionable to introduce additional notation ( $S$  and  $H$ ) to distinguish the von Neumann entropy from the Shannon entropy. We here view that as redundant mysticism, since classical probability theory is a subset of quantum information

theory, and applying Eq. (27.18) to the appropriate quantum representation  $\rho_X$  of the classical random variable  $X$  will yield exactly the same value as calculating the Shannon entropy directly. Although some subtlety must be considered with mutual informations and conditional entropies, for unipartite systems the operational meaning of information entropy is the same between the classical and quantum cases: *Schumacher compression* [33] quantizes Shannon's source coding theorem, demonstrating that  $N$  independent copies of a quantum state  $\rho$  can be transmitted in a Hilbert space (i.e. quantum configuration space) of size  $N H_1(\rho)$ , in the asymptotic limit  $N \rightarrow \infty$ .

Likewise, one can define [34] the family of quantum Rényi entropies associated with quantum state  $\rho$ :

$$H_\alpha(\rho) := \frac{1}{1-\alpha} \ln \left[ \frac{\text{Tr } \rho^\alpha}{\text{Tr } \rho} \right], \quad \alpha \geq 0. \quad (27.19)$$

When  $\rho$  is chosen to encode a classical probability distribution, Eq. (27.4) is recovered. (The  $\text{Tr } \rho$  in the denominator accommodates the possibility of unnormalized  $\rho$ .)

Similarly, there are quantum definitions for divergences. For quantum states  $\rho, \sigma$ , the Kullback–Leibler divergence ( $\alpha = 1$ ) is defined as

$$D_1(\rho || \sigma) := \text{Tr } \rho (\ln \rho - \ln \sigma). \quad (27.20)$$

The general quantum Rényi relative entropy is expressed [34]:

$$D_\alpha(\rho || \sigma) := \frac{1}{\alpha - 1} \ln \left[ \frac{\text{Tr } \rho^\alpha \sigma^{1-\alpha}}{\text{Tr } \rho} \right]. \quad (27.21)$$

Other quantum generalizations are possible, such as the *sandwiched quantum Rényi divergence* [34–36], which coincides with the above when  $\rho$  and  $\sigma$  commute. In this form, it can be straightforwardly seen [34] by setting  $\sigma = \mathbb{1}$  that  $H_\alpha(\rho) = -D_\alpha(\rho || \mathbb{1})$ —that is, the Rényi entropy itself can be considered as a divergence of  $\rho$  from the (unnormalized) state  $\mathbb{1}$ . Alternatively if we consider the uniform random state with the same dimension  $d$  as  $\rho$ ,  $\pi := \mathbb{1}/d$ , then we also have  $H_\alpha(\rho) = \log d - D_\alpha(\rho || \pi)$ . Since  $D_\alpha \geq 0$  (with equality holding for general  $\alpha$  only when  $\rho = \pi$ ), this also tells us that for all  $\alpha$ , the maximum value  $H_\alpha$  can take is  $\log d$  and that this is saturated when the quantum state is maximally mixed. That is, the uniformly random probability distribution maximizes all Rényi entropies for a given alphabet size.

We conclude this section by giving the explicit forms [36] for the quantum Rényi relative entropies in the cases  $\alpha = 0$ :

$$D_0(\rho || \sigma) = -\ln \text{Tr} (\pi_\rho \sigma) \quad (27.22)$$

where  $\pi_\rho$  is projection onto the support of  $\rho$ ; and in the case of  $\alpha \rightarrow \infty$ :

$$D_\infty(\rho || \sigma) = \ln \max_{i,j} \left\{ \frac{\lambda_i}{\mu_j} : \langle i | \tilde{j} \rangle \neq 0 \right\}, \quad (27.23)$$

where  $\rho = \sum_i \lambda_i |i\rangle\langle i|$  and  $\sigma = \sum_j \mu_j |\tilde{j}\rangle\langle \tilde{j}|$ . In all these cases, it is left as an exercise to the reader to show that when  $\rho$  and  $\sigma$  are classical probability distributions, these quantities reduce to their respective classical versions.

## 27.2 Thermodynamic Prerequisites

### 27.2.1 Information Entropy in Thermodynamics

Having now equipped ourselves with some information-theoretic hammers, let us seek out some thermodynamic nails. Broadly, there are two different contexts where information entropy appears in modern thermodynamics. (i) The entropy of the state of (small, possibly quantum) systems, undergoing some transformation. (ii) The entropy of distributions of variables associated with thermodynamic processes, such as the total amount of work investment into a system as it undergoes some protocol.

These two contexts are conceptually very different. In the former, information entropy is akin to a thermodynamic state variable,<sup>6</sup> since it is something that can be assigned to a given system at a point in time. The second context is more statistical in nature: the entropy here is not so associated with the system itself, but instead with data built up over many trials of an experiment. In both these contexts, where Shannon entropies are used to quantify average properties, one may consider alternative statements involving Rényi entropies that allow statements to be made outside of this asymptotic limit.

In this article, we shall primarily focus on context (ii). However, let us first make a few comments about (i), since it is a lively area of active research (see Chaps. 29 and 33).

Approach (i) follows the modern information thermodynamics paradigm established by Landauer [37] and Bennett [38, 39] asserting the *inevitable physicality of information* [40]. This is particularly useful if we wish to make statements about the fundamental thermal costs of information processing. Indeed, Maxwell's daemon [41, 42] – an intelligent agent that can seemingly violate the second law of thermodynamics by converting heat to work without any other consequence – is resolved by noting that this agent must maintain some kind of *memory*, and this memory is itself a physical system that must be reset at some thermodynamic cost in order to have a complete thermodynamic cycle.

---

<sup>6</sup>A formal discussion on where the information entropy can be considered a thermodynamic entropy is presented by Weilenmann et al. [19].

The exact lower bound on the cost of reconfiguring memory may be quantified by Landauer's principle [37], which relates the *Shannon entropy* of the memory – an information-theoretical quantity – to the exchange of thermodynamic work – a physical quantity, such as the raising or lowering of a weight. Namely, consider a random variable  $X$  corresponding to a choice of  $x_i \in \mathcal{X}$ , each occurring with probability  $p_x(i)$ , and a random variable  $Y$  corresponding to  $y_i \in \mathcal{Y}$  with probabilities  $\{p_y(i)\}$ . Suppose some physical system  $\Xi$  encodes the variable  $X$ . If we wish to reconfigure  $\Xi$  so that it encodes the variable  $Y$ , if this reconfiguration is done in contact with a thermal reservoir at temperature  $T$ , then the *minimum* average work investment required is given by:

$$W \geq k_B T [H(X) - H(Y)], \quad (27.24)$$

where  $H(A)$  is the Shannon entropy of  $A$ . If  $H(X) < H(Y)$ , then the right-hand-side is negative, signifying that work can be *extracted* from the physical system, at the cost of making it more random. It follows from the first law that this work investment will be accompanied by an equal and opposite exchange of heat with the thermal reservoir.

As an example, consider *bit reset*: here,  $X$  is a  $(\frac{1}{2}, \frac{1}{2})$  distribution over two possibilities, whereas  $Y$  reflects a pure state of certainty [probabilities  $(1, 0)$ ]. Thus  $H(X) = \ln 2$ ,  $H(Y) = 0$ , and we recover the well-known “Landauer erasure” cost of  $k_B T \ln 2$ .

Various thought experiments, such as Szilard's engine [42, 43] allow the derivation of this same cost from physical considerations (e.g. applying ideal gas laws to expanding pistons). Should some previously unknown material be discovered, we would not expect that it could be used to form a perpetual motion machine: the second law of thermodynamics likely holds independently of the underlying physical mechanisms. Similarly, we can understand Landauer's principle as an *emergent physical law* that we expect to hold true no matter the specifics of the microscopic laws governing the system on which it is applied. Systems that claim to violate this bound typically also draw from another type of reservoir that is freely convertible into work, such as information reservoirs, or move the entropy onto a different physical system (or into correlations) that is unaccounted for. The work cost associated with a change of information entropy encoded on *any* physical medium will be subject to this limit.<sup>7</sup>

For any physically realisable experiment, a larger work investment than predicted from the Landauer bound will typically be required for two distinct reasons: (i) Landauer's bound assumes a quasistatic change, where the physical system is kept in thermal equilibrium throughout the reconfiguration. This requires infinitely slow adjustments, whereas conversely, real experiments proceed in a finite amount of time. (ii) The bound is derived on *asymptotic* information quantities: assuming either a large number of copies of the systems that can be compressed (i.e. such that the bound is a limit “per system on average”), or many repetitions of the experiment

<sup>7</sup>Conversely, this limit can be sharpened by restricting the set of allowed protocols (such as by bounding the effective dimension of the thermal reservoir [44]).

where the statistics are collected and averaged, and the thermal reservoir is assumed to be infinitely large (whereas in fact it could also be of limited size [44]).

Non-equilibrium statistical mechanics can help us with reason (i), wherein the difference between entropies informs the free energy difference associated with states encoded in different distributions. Conversely, *one-shot statistical mechanics* (sometimes called single-shot statistical mechanics) allows us to go beyond this average regime. There are a wealth of papers on this topic (e.g. [12–19]) that extend well beyond the scope of this chapter. For a particularly pedagogical introduction, one could consult Dahlsten [14].

### 27.2.2 Work Extraction Games

Let us now turn our attention to the second context in which entropies can appear in the discussion of thermodynamics. We begin by setting out the following very general thermodynamic scheme (Fig. 27.2): Suppose there is an experiment consisting of three components (a) a working medium, or *system*, (b) a work reservoir, or *battery* (e.g. a raising weight), (c) a heat reservoir, or *heat bath* at some temperature  $T$ . On this set-up, one composes a *protocol*: a predefined sequence of actions taken on the system involving two types of interaction: The first type is to allow some total-energy preserving interaction<sup>8</sup> with the battery, such that energy is exchanged between the battery and the system. This energy change could either be due to some joint dynamic on the working medium and the battery (a favoured approach for truly quantum thermodynamics), or could be viewed abstractly as the imposition of a time-varying Hamiltonian on the system, where the battery acts as a generic work reservoir that can supply the resulting difference in internal energy on the system, such as by raising or lowering a weight.<sup>9</sup> Energy exchanged in this manner is classified as *work*.

The second type of interaction is thermal contact between the system and the heat reservoir (though the system need not necessarily fully equilibrate). Energetic exchanges resulting from this are considered *heat*.

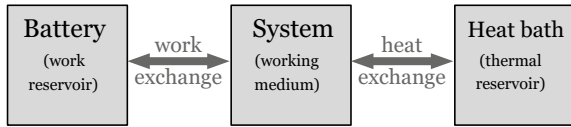
In an experiment, one can perform many *trials* of this protocol, and each trial will exchange some amount of work  $W$  with the battery, and some amount of heat  $Q$  with the heat bath. From the collated statistics of  $W$  over many trials, one can form

<sup>8</sup>The reader should take care that there are varying notions of energy conservation, and in resource-theoretic frameworks, this will alter the set of permitted “thermal operations”. In particular, one may admit any operation that conserves energy on average (as per [45]), or alternatively could place stricter restrictions, such as mandating that the unitary representation of the dynamics on the system-battery commute with the total Hamiltonian (as per [16]). Here, we present a general scheme that can be adapted to either notion.

<sup>9</sup>Furthermore, these two pictures can be seen to be equivalent: a time-varying Hamiltonian can be recast as a time-invariant Hamiltonian with the help of an ancillary “clock” system – for details, see Supplementary Material Sect. VIII of Brandão et al. [46], Appendix D2 of Unger Halpern et al. [29], or Sect. IIA in Alhambra et al. [47].

**Fig. 27.2 Generic one-bath thermodynamic scheme.** A working medium (system) exchanges work with a battery (work reservoir), and heat with a heat bath (thermal reservoir).

### B. Work extraction games



a *work distribution*  $P(W)$ . (One might also infer  $P(W)$  from the theoretical details of a given protocol).

This scheme is sufficiently general that it describes the thermodynamic behaviour of any system interacting thermally with a single heat bath and drawing upon (or depositing into) a work reservoir. We can flesh it out with some details to specialize to the microscopic quantum case where the working medium has discrete energy levels (following the lead of, say, [14, 15, 48]). Here, the working medium is characterised by its time-varying Hamiltonian  $H(t) := \sum_i E_i(t)|E_i(t)\rangle\langle E_i(t)|$ , and its *state*  $\rho(t)$ , which represents a distribution over energy levels. If the system is classical, then  $\rho = \sum_i p_i(t)|E_i(t)\rangle\langle E_i(t)|$  is diagonal with respect to the Hamiltonian basis.

The system's average internal energy is given  $\langle H \rangle = \text{Tr } \rho H = \sum_i p_i E_i$ . If the system is classical, its state remains diagonal with respect to the Hamiltonian at each timestep (e.g. by actively avoiding the build up of quantum coherence [49]), and hence may always be expressed as a classical distribution over energy levels. In this case, the total differential change to the energy may be expressed

$$d\langle H \rangle = \sum_i p_i dE_i + \sum_i E_i dp_i. \quad (27.25)$$

By analogy with the first law  $dU = dW + dQ$  we can divide these two terms into [15, 50–52]:

1. **Exchanges of work:**  $dW = \sum_i p_i dE_i$ , associated with changing the Hamiltonian at fixed occupation probability. This is motivated as work, since it corresponds to a change in energy as a consequence of some external action on the system [53] (i.e. arises due to the time-dependence of the Hamiltonian) such as adjusting an external magnetic field or raising a weight.
2. **Exchanges of heat:**  $dQ = \sum_i E_i dp_i$ , associated with changing the populations at fixed Hamiltonian. This is motivated as heat, since it corresponds to the changes in energy effected by thermalization as a system is moved towards its equilibrium state (see e.g. [16, 29]).

In general, a protocol is constructed by inducing a combination of the above two classes of operations. Physical considerations may lead us to impose further constraints, particularly to ensure that the allowed heat-like exchanges obey the second law. An obviously motivated restriction (see, e.g. [16]) is that heat-like changes should move the system towards a thermal equilibrium state (the *Gibbs*

$$Q = \sum_i E_i d\bar{p}_i \quad W = \sum_i \bar{p}_i dE_i$$

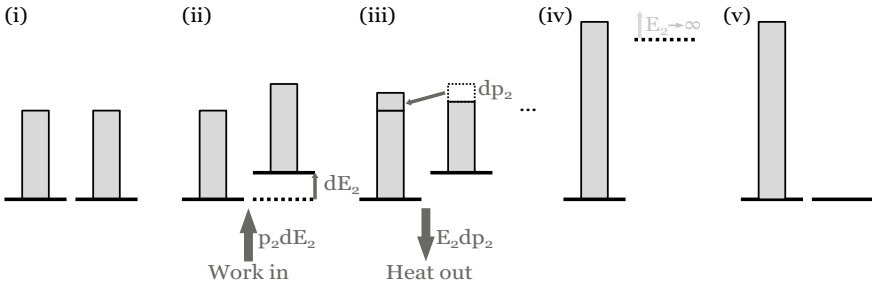


**Fig. 27.3 Landauer bit reset.** A diagrammatic representation of the bit reset protocol (following notation of Åberg [15]), representing the system’s state and Hamiltonian throughout the protocol. The two thick horizontal lines represent energy levels, with their relative vertical position representing the energy of each level. The gray bars above each level represents its occupation probability. **i** Initially the system is in an equal mix of degenerate energy levels. **ii** At each time-step, the second level is raised by  $dE_2$ , at work cost  $p_2 dE_2$ . **iii** The system is then left to thermalize such that the probability of the second level being occupied changes by  $dp_2$ . This exchanges heat  $E_2 dP_2$  with the heat reservoir. **iv** Steps ii and iii are repeated until the second level is raised to infinity, and hence totally depopulated. **v** The system is then decoupled from the thermal reservoir, such that the (empty) second level can be set back to 0 energy without any associated energy change. The total work cost over the entire protocol is  $k_B T \ln 2$ .

state  $\gamma = \text{diag} [e^{-\beta E_1}/Z, \dots, e^{-\beta E_N}/Z]$  where  $Z := \sum_i e^{-\beta E_i}$  is the partition function.) We can further restrict heat-like interactions to obey *detailed balance*<sup>10</sup> such that the ratio of transition probabilities between two configurations  $i$  and  $j$  obeys  $P(i \rightarrow j)/P(j \rightarrow i) = \exp [-\beta (E_j - E_i)]$ .

As an example, let us consider quasistatic *bit reset*: the process of taking a two-level system from state  $\rho = \text{diag} (\frac{1}{2}, \frac{1}{2})$  to  $\rho = \text{diag} (1, 0)$ , where the initial and final Hamiltonian is  $H = 0$ . This is expressed diagrammatically in Fig. 27.3. The theoretically-perfect quasistatic protocol for reset is to slowly increase the second level to  $\infty$ , allowing the system to fully equilibrate (that is, to reach the Gibbs state  $\gamma = \text{diag} [1/(1 + e^{-\beta E_2}), e^{-\beta E_2}/(1 + e^{-\beta E_2})]$ , where  $\beta = 1/k_B T$  is the inverse temperature) between each infinitesimal change in  $E_2$ . Once the second level has been fully raised, the system is decoupled from the thermal reservoir, and the (now empty) second level is lowered back to 0, completing the protocol. The latter stage has no associated work cost, since it is a change in energy of a completely depopulated level, and so the total expected work cost  $\langle W_{\text{reset}} \rangle$  of the protocol is given by the first stage:

$$\langle W_{\text{reset}} \rangle = \int_0^\infty p_2 dE_2 = \int_0^\infty \frac{e^{-\beta E_2}}{1 + e^{-\beta E_2}} dE_2 = \frac{1}{\beta} \ln 2 = k_B T \ln 2. \quad (27.26)$$

This work cost exactly matches that predicted by applying Landauer’s principle on the change between initial and final entropies [Eq. (27.24)], indicating that this protocol is optimal. A similar integration over population changes will yield

<sup>10</sup>This constraint is closely related to first, see Appendix A of [29].

$\langle Q_{\text{reset}} \rangle = -k_B T \ln 2$ , just as we would expect from the first law (since  $\Delta U = 0$ ). One can also formulate variations of this protocol outside of the quasistatic limit, by accommodating the possibility that the system does not thermalize completely between each change in the energy of the second level [49].

These quantities correspond to average behaviours. When the system is classical, it is straight-forward to generalize this to a *trajectory formalism* (as per [10] or in [14, 15]), and talk about single trials of the experiment. Here, the system is taken to occupy one particular energy level at any given time (i.e. so that the density matrix is always a rank one projector in the energy eigenbasis). In this picture, thermalization corresponds to random jumps between energy levels. A single trajectory is then a “path” through the system’s state space (i.e. a list of energy levels occupied and the times of transitions between them). Work and heat costs may then be calculated for a given trajectory, such that the mean values correspond to the average over all trajectories.

### 27.2.3 Worst-Case and $\epsilon$ -Guaranteed Work

When we use heat and work in the context of traditional thermodynamic processes, we typically refer to the mean (“average” or “expected”) work  $\langle W \rangle$  (cf. heat  $\langle Q \rangle$ ) taken over many runs of an experiment. If the thermodynamic protocol acts on a large system and is quasistatic (evolving sufficiently slowly that the system remains in internal equilibrium), the work costs of individual runs of the experiment do not deviate much from the mean values. However, when the protocol happens over a finite amount of time, the system can be driven out of thermal equilibrium, and the work cost of an individual run of the experiment can deviate quite significantly from the mean value. Here, one instead records a *work distribution*  $P(W)$ —a probability density function over the work costs of each run of the experiment. From this distribution, one can calculate the mean work  $\langle W \rangle$  in the usual way:  $\langle W \rangle = \int_{-\infty}^{\infty} dW W P(W)$ .

There are circumstances where mean properties of a distribution are misleading. Consider a game where a ball is launched upwards from the ground, with the aim that it reaches a table of height 1 m. Suppose with probability 0.99 the ball reaches only 0.1 m, but with probability 0.01 it is launched to 100 m. The mean height reached by this ball is 1.099 m, which is greater than the table height – but the ball will not reach the table in 99% of launches. As such, the mean is not a good characterisation of the process for the purposes of determining whether some threshold is met.

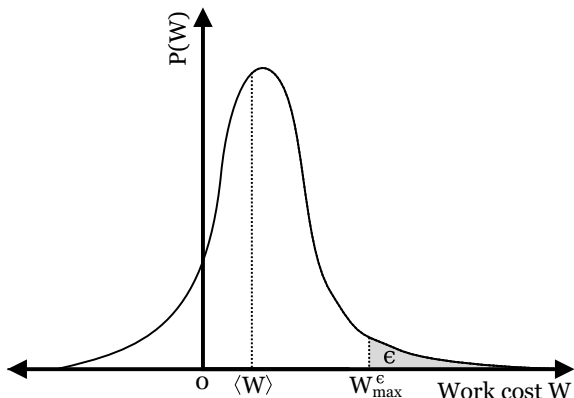
Similar circumstances arise in a thermal contexts with respect to work distributions  $P(W)$ . It could be that a single instance of the experiment is powered by a battery that can only impart so much work in one run, or the system contains some small wire (such as might be found in the filaments of microprocessor’s transistors) that can only support up to a maximum amount of heat dissipation before it overheats and breaks. In these contexts, we are less concerned by the average work  $\langle W \rangle$ , but rather wish to know the maximum work  $W_{\max} := \max_W \{W | P(W) > 0\}$ . In protocols whose net

In what situations  
worst-case  
quantities  
are bad?  
as well

We are not interested  
in the deterministic  
but we have some  
time to do it  
(i.e. we can perform it K  
times)

Interpret height  
as a thermo  
game  
↓  
interpret  $W_{\max}$

**Fig. 27.4 Example work distribution**, with the mean work ( $\langle W \rangle$ ) and the  $\epsilon$ -guaranteed worst-case work  $W_{\max}^\epsilon$  marked. Positive  $W$  indicates work must be invested from the battery into the system. The grey area shaded region has area  $\epsilon$ , such that the probability that a work sampled from this distribution exceeds  $W_{\max}^\epsilon$  is  $\epsilon$ .



work exchange is to invest work from the battery into the system, this maximum quantity is sometimes referred to as the *worst-case work cost*.

Conversely, for processes where work is typically extracted out of the system and into the battery, the “maximum” quantity will be the least negative. Here, the process could be providing the input energy to trigger another process with a minimum activation energy: an “all or nothing” threshold that must be crossed in order to start a chemical reaction (similar to the ball and table example above). In this extraction context,  $-W_{\max}$  is sometimes known as the *guaranteed work*, since each trial of the protocol is guaranteed to output at least that much work. (Here, extracting more work is desirable, so the term “worst-case” would still be an appropriate adjective).

Sometimes, we are not interested in the *absolute* worst-case scenario, but can tolerate some *failure probability*  $\epsilon$ . The  $\epsilon$ -guaranteed worst-case work cost is the lowest value  $W_{\max}^\epsilon$  that satisfies

$$\int_{W_{\max}^\epsilon}^{\infty} dW P(W) = \epsilon. \quad (27.27)$$

(This is drawn in Fig. 27.4).

One expects the work cost of a trial to exceed  $W_{\max}^\epsilon$  only with probability  $\epsilon$ . This is a generalization of the work distribution’s median value; setting  $\epsilon = \frac{1}{2}$  yields the median work. This definition also holds for processes where work is output (though we must pay attention to the signs). Should we alternatively express such a process in terms of  $-W$  (i.e. exchanging the sign), we have

$$\int_{-\infty}^{W_{\text{worst}}^\epsilon} dW P(-W) = \epsilon, \quad (27.28)$$

where  $W_{\text{worst}}^\epsilon$  is the  $\epsilon$ -guaranteed work output. Precisely what *failure* means is context-dependent: it could mean that in  $\epsilon$  of cases the protocol completes, but costs

more work than allowed; or it could mean that in  $\epsilon$  of cases a different protocol is executed (say, because the battery is drained).

In the case of quasistatic processes on large systems (particularly, on ensembles of many systems that are independent or otherwise have correlations that are limited in range), the work distribution  $P(W)$  will be (close to) a Dirac delta function  $P(W) = \delta(W - \Delta F)$  (where  $\Delta F$  is the free energy change). Here,  $\langle W \rangle \approx W_{\max}^\epsilon$  for all  $\epsilon$ , and knowing the mean work is sufficient to characterize the protocol's work cost. In the next section we shall discuss the far more interesting context wherein the system is driven out of equilibrium, and the work distribution is no longer well-characterized by the mean.

### 27.3 Work Fluctuation Theorems and One-Shot Entropies

Fluctuation theorems are powerful tools that allow us to make statements relating out of equilibrium behaviour with equilibrium properties such as free energy differences. Of particular interest is Crooks' fluctuation theorem [11], that relates the entropy production of a system driven in one direction, with that of the reversely driven system. This relation holds under the assumption that each individual microscopic trajectory the system takes is *reversible*. In this context, *microscopic reversibility* means that for each forward process trajectory there exists a corresponding reverse trajectory in the reversed process that moves through the same states but in time-reversed order, and that the ratio of probabilities that the system evolves according to these trajectories in their respective process directions is given by  $\exp(-\beta Q)$  where  $Q$  is the heat exchanged with the thermal reservoir during the forward trajectory [11]. Microscopic reversibility is satisfied if the driving of the protocol is characterized by a single parameter, and the thermalizing interactions obey detailed balance [10].

The killer application of Crooks' theorem (provided also in [11]) is to model the probabilistic work cost of out-of-equilibrium thermodynamic processes. Suppose there is a process that begins in a thermal state (with respect to initial Hamiltonian), and undergoes evolution driven by a single external parameter  $\lambda(t)$  (over range 0 to  $\tau$ ), and where all thermalizing interactions obey *detailed balance*. Such a process has a well-defined *reverse*, wherein the driving parameter  $\lambda$  is varied from  $\tau$  back to 0, and the initial state of the reverse is the thermal state of the system where the external parameter is  $\tau$  (this is not necessarily the same as the final state of the forward process, since in general the system may have been moved out of thermal equilibrium). When the evolution is not quasistatically slow, there is an element of randomness to the *work cost*  $W$  of these processes. Describing the distribution over work cost in the forward case by  $P_{\text{fwd}}$  and in the reverse as  $P_{\text{rev}}$ , Crooks' fluctuation theorem [11] implies<sup>11</sup> the *nonequilibrium work relation*:

---

<sup>11</sup>Sometimes Eq. (27.29) is referred to as Crooks' theorem itself. However, in [11], Crooks proves a more general statement about entropy production systems with microscopically reversible dynam-

$$\frac{P_{\text{fwd}}(W)}{P_{\text{rev}}(-W)} = \exp [\beta (W - \Delta F)], \quad (27.29)$$

where  $\Delta F$  is the equilibrium free-energy change<sup>12</sup> associated with the forward process.

Although we here shall not supply a full proof of the equality,<sup>13</sup> we can see intuitively why the free energy difference appears: our set-up involves two thermal states, and these effectively encode within them the partition function  $Z$  associated with their respective Hamiltonians. Elementary statistical mechanics tells us that  $F = -k_B T \ln Z$ , and so a logarithm of the ratio of partition functions (as will be generated when we sum over the probabilities associated with the two thermal states) will supply terms of the form  $\Delta F$ .

Crooks' fluctuation theorem implies other important thermodynamic statements. For instance, multiplying Eq. 27.29 by  $e^{\beta \Delta F} P_{\text{rev}}(-W)$  then integrating over  $W$  yields the famous Jarzynski equality [9]:

$$\langle e^{\beta W} \rangle = e^{\beta \Delta F}. \quad (27.30)$$

In turn, applying Jensen's inequality to Eq. (27.30) yields a statement of the second law in the form  $\langle W \rangle \geq \Delta F$ .

The energetic quantity appearing on the right hand side of Eq. (27.29) is known as the *dissipated work*  $W_{\text{diss}} := W - \Delta F$ . The *dissipated work* quantifies the excess work investment required to complete a protocol beyond the free energy difference between the initial and final states. Since  $\Delta F$  is a property of the protocol (rather than of trials), it is the same for every run of an experiment, and hence one can define the *average dissipated work*  $\langle W_{\text{diss}} \rangle = \langle W \rangle - \Delta F$ .

This dissipated work represents a wastefulness caused by taking the system out of thermodynamic equilibrium. The free energy difference of a process and its reverse are related by simple negation. However,  $\langle W_{\text{diss}} \rangle \geq 0$  in *both* directions. (If this were not true, one could close either of these processes into a cycle with the dissipation-free quasistatic variant of the reserve, and violate the second law.) This follows also from Crooks' fluctuation theorem [55, 56]. Recall the definition of the Kullback–Leibler divergence (Eq. (27.16)), and substitute in Eq. (27.29):

---

ics:  $P_{\text{fwd}}(\omega) / P_{\text{rev}}(-\omega) = \exp(\omega)$ . The equation pertaining to work exchanges is the most notable example, and was also provided by Crooks' in the same article.

<sup>12</sup>Under the assumptions that allow us to use Crooks' nonequilibrium work relation, the initial state is in thermal equilibrium and its free energy may be defined in the usual way. At time  $\tau$ , the system may not be in thermal equilibrium. However, we can consider the state that would be reached (for the same final Hamiltonian) if that system were allowed to fully thermalize (limit  $t \rightarrow \infty$ ), and take the free energy of that thermal state instead. It is the difference in free energy between the initial thermal state and the thermalized version of the final state that determines  $\Delta F$ .

<sup>13</sup>Quan and Dong [54] provide a derivation of this in a language familiar to quantum information scientists.

$$\begin{aligned}
D_1(P_{\text{fwd}}(W) \parallel P_{\text{rev}}(-W)) &= \int_{-\infty}^{\infty} dx \ P_{\text{fwd}}(W) \ln \frac{P_{\text{fwd}}(W)}{P_{\text{rev}}(-W)} \\
&= \int_{-\infty}^{\infty} dx \ P_{\text{fwd}}(W) \beta [W - \Delta F] \\
&= \beta \langle W_{\text{diss}} \rangle.
\end{aligned} \tag{27.31}$$

Thus, the Kullback–Leibler divergence between the distribution of work invested into the forward process, and the distribution of work extracted from the reversed process is directly proportional to the average dissipated work.  $\langle W_{\text{diss}} \rangle \geq 0$  then follows from the positivity of  $D_1$ . Moreover we see that  $\langle W_{\text{diss}} \rangle = 0$  if and only if  $P_{\text{fwd}}(W) = P_{\text{rev}}(-W)$  for all  $W$ , which provides us with a slightly more generic definition of thermodynamic reversibility [56].

Yunger Halpern et al. [57] show that a similar relation holds true for the *worst-case dissipated work*, defined  $W_{\text{diss}}^{\text{worst}} := W_{\text{max}} - \Delta F$ :

$$W_{\text{diss}}^{\text{worst}} = k_B T D_\infty(P_{\text{fwd}}(W) \parallel P_{\text{rev}}(-W)). \tag{27.32}$$

Similarly to  $D_1$ , one proves this by substituting Crooks' nonequilibrium work relation into the definition of  $D_\infty$ . The protocol's adherence to Eq.(27.29) guarantees that distributions  $P_{\text{fwd}}(W)$  and  $P_{\text{rev}}(-W)$  have the same support. Therefore, the largest value of  $W$  in the forward process  $W_{\text{max}}$  is exactly the one which maximizes the right-hand side of Eq.(27.29), and hence determines the minimum value of  $\lambda$  in the right-hand-side of Eq.(27.17).

A related equality is derived by Dahlsten et al. [58]. Consider a system in an initial state  $\rho_0$ , which does not need to be a thermal state of the initial Hamiltonian, but must be diagonal in that basis. Let that system evolve by some process  $\mathcal{P}_{\text{fwd}}$ , consisting of changes in energy levels, and thermalizations that respect detailed balance. Ultimately, one arrives at a bound of the form  $W < W_{\text{max}}^\varepsilon$  where

$$W_{\text{max}}^\varepsilon = k_B T \left[ D_\infty \left( \tilde{P}_{\text{fwd}}(W) \parallel \tilde{P}_{\text{rev}}(-W) \right) - \ln \left( \frac{Z_f}{\tilde{Z}} \right) \right], \tag{27.33}$$

consisting of two terms, which we shall explain. The first term is the worst case dissipated work encoded between the forward and reverse work distributions (as in [57], discussed above). The tilde above  $\tilde{P}$  indicates a smoothed work distribution (see [58] for detail) formed from the true work distribution by discounting trajectories in the following “tails”: (i) the values which are unlikely to be seen since they have very low support in the initial state  $\rho_0$  (total probability  $p_{\text{out}}$ ); (ii) the highest (i.e. worst-case) work values beyond some tunable cut-off value. This is a type of *smoothing* and is done to lessen the influence of very unlikely trajectories, and to explicitly incorporate a degree of error we are willing to tolerate in the bound.

The second term is a modification of the usual free energy difference.  $Z_f$  is the partition function of the final Hamiltonian, but  $\tilde{Z}$  is some modified function that replaces the role of the initial partition function  $Z_i$ . Particularly,  $\tilde{Z}$  omits terms

corresponding to energy levels that are in the set **OUT** of system configurations that have the least support in the initial state  $\rho_0$ . That is  $\tilde{Z} = 1/(1 - p_{\text{out}}) \sum_{i \notin \text{OUT}} \exp(-\beta E_i)$ , where  $p_{\text{out}}$  is the total support of  $\rho_0$  on these unlikely **OUT** states. Using  $\tilde{Z}$  instead of the true initial partition function will provide us a bound on the worst case work, since one can then construct a process  $\tilde{\mathcal{P}}$  whose work costs upper bound that in the true process  $\mathcal{P}$ , but that begins in the thermal state  $\tilde{\gamma}$  associated with  $\tilde{Z}$  (details in [58]).

In this context, it is unimportant that the initial state be thermal, because we concerned only with a single trajectory (namely, the non-excluded trajectory with the worst work cost) without regards to how likely it is to occur, and the support of  $\rho_0^{\text{IN}}$  ( $\rho_0$  omitting terms in **OUT** and renormalized) and that of the thermal state of  $\tilde{Z}$  are identical.

For Eq. (27.33) to be useful, we must also bound the failure probability  $\varepsilon$ . Let  $p_{\text{work-tail}}$  be the probability that a trajectory is culled for being too expensive, and recall that the probability that the system is in **OUT** is  $p_{\text{out}}$ . We then see the total error is bounded  $\varepsilon \leq p_{\text{work-tail}} + p_{\text{out}}$  (and will be strictly less if some of the worst-case work trajectories begin in an **OUT** state). However,  $p_{\text{work-tail}}$  is not quite the same as the  $\epsilon$  guarantee discussed earlier, since the former quantity relates to the smoothed  $P(W)$  arising from modified process  $\tilde{\mathcal{P}}$ , whereas the  $\epsilon$  is defined with respect to the true work distribution  $\mathcal{P}$ . However, we can bound  $p_{\text{work-tail}} \leq d(\rho_0, \tilde{\gamma}) + \epsilon$  where  $d(\cdot, \cdot)$  is the trace distance, and  $\epsilon$  the “guarantee”. As such, the total error probability is upper bounded by:

$$\varepsilon \leq p_{\text{out}} + d(\rho_0, \tilde{\gamma}) + \epsilon. \quad (27.34)$$

In another approach from Yunger Halpern et al. [29], a one-shot entropy is combined with Crooks’ nonequilibrium work relation to bound the worst-case work of a process with respect to an entropic property of the reverse process’s work distribution. Particularly, suppose there is some process  $\mathcal{P}_{\text{fwd}}$  with a distribution over work costs given  $P_{\text{fwd}}(W)$ . We can bound the  $\epsilon$ -guaranteed worst-case (i.e. lowest) work  $W_{\text{worst}}^\epsilon$  that can be extracted from the reverse process  $\mathcal{P}_{\text{rev}}$  by

$$W_{\text{worst}}^\epsilon \leq \Delta F - k_B T \left[ H_\infty^{k_B T}(P_{\text{fwd}}) + \log(1 + \epsilon) \right]. \quad (27.35)$$

where  $H_\infty^{k_B T}$  is the differential min-entropy (order- $\infty$  Rényi entropy) taken with respect to a reference probability distribution with width  $k_B T$  and height  $\beta$  (see discussion at the end of Sect. 27.1.2). The proof follows by first deriving an minor modification to Jarzynski’s equality

$$(1 - \epsilon) e^{-\beta \Delta F} = \int_{W_{\text{worst}}^\epsilon}^{\infty} P_{\text{fwd}}(W) e^{-\beta W} \quad (27.36)$$

by rearranging Eq. (27.29), and integrating over  $W_{\text{worst}}^\epsilon$  to  $\infty$  (cf. the lower limit  $-\infty$ , which would recover the standard Jarzynski equality). One can then bound the integral on the right-hand side using the largest value of  $P_{\text{fwd}}(W)$ ,  $P_{\text{fwd}}^{\max}$ :

$$\begin{aligned}
\int_{W_{\text{worst}}^{\epsilon}}^{\infty} P_{\text{fwd}}(W) e^{-\beta W} &\leq P_{\text{fwd}}^{\max} \int_{W_{\text{worst}}^{\epsilon}}^{\infty} dW e^{-\beta W} \\
&= \exp(\ln(P_{\text{fwd}}^{\max}/\beta)) \exp(-\beta W_{\text{worst}}^{\epsilon}) \\
&= \exp(-H_{\infty}^{\beta}(P_{\text{fwd}}) - \beta W_{\text{worst}}^{\epsilon}),
\end{aligned} \tag{27.37}$$

and then rearrange to arrive at Eq. (27.35).

Yunger Halpern and Jarzynski [59] apply Ineq. (27.35) to upper bound the estimate on the number of trials required to estimate the free energy difference of a process in terms of the min-entropy  $H_{\infty}^{k_B T}[P(W)]$ . From Jarzynski's equality [9], it had been established [60] that around  $N \sim \exp(\beta \langle W_{\text{diss}} \rangle)$  experimental runs are required to form a good estimate of  $\Delta F$ . In particular, averages of the exponential quantity  $\langle e^{\beta W} \rangle$  are dominated by large values of  $W$ . Thus, to get a good estimate, one hopes to sample one of these large values. Since these large values appear in the tail of the distribution, they may not be likely, and so one might need to take many samples before one appears: namely, requiring a number of trials proportional to the inverse of the tail's total probability.

Consider sampling the work cost of some reverse  $\mathcal{P}_{\text{rev}}$  of some process  $\mathcal{P}_{\text{fwd}}$ . One may wish to pick some  $\delta$ -guaranteed output work value  $W^{\delta}$  (known in this context as a  $\delta$ -dominant work value), wherein the probability of an experimental trial outputting less work than that is  $\delta$ . Then, approximately  $N_{\delta} \sim \frac{1}{\delta}$  trials will be performed before such a trial is encountered. One can rearrange Eq. (27.35) and lower bound this number:

$$N_{\delta} \geq \exp[\beta(W^{\delta} - \Delta F) + H_{\infty}^{k_B T}(P_{\text{fwd}})]. \tag{27.38}$$

If  $W^{\delta}$  is chosen such that  $W^{\delta} = \langle W \rangle_{\text{fwd}}$ , then  $N_{\delta} \geq \exp[\beta(\langle W_{\text{diss}} \rangle) + H_{\infty}^{k_B T}(P_{\text{fwd}})]$ . Furthermore, if the probability density  $P_{\text{fwd}}(W)$  is less than  $\beta$ , then  $H_{\infty}^{k_B T}(P_{\text{fwd}}) \geq 0$ , and the bound on  $N_{\delta}$  from Eq. (27.38) will be tighter than that implied by Jarzynski [60].

## 27.4 Quantum Fluctuation Theorems and One-Shot Entropies

Let us conclude this chapter by considering a few instances in which one-shot entropies have been applied to *quantum fluctuation relations* (for other discussion of quantum fluctuations, see Part II of this book).

It was shown by Kurchan [61] and Tasaki [62] that Jarzynski's equality can be applied in the quantum realm for a restricted set of protocols where a quantum system begins in a thermal state with respect to its initial Hamiltonian, and undergoes unitary evolution governed by a time-dependent Hamiltonian  $H(t) = \sum_i E_i(t)|E_i(t)\rangle\langle E_i(t)|$  from time  $t = 0$  to  $\tau$ . At the end of this evolution, the system is projectively measured in the basis of the final Hamiltonian  $\tilde{H} := H(\tau)$ . In these

protocols, since the system is decoupled from the thermal reservoir throughout its evolution, one may call the energy difference between projective energy measurements made in  $H(0)$  at the beginning and  $H(\tau)$  end of the protocol the work cost of the protocol. In this setting, if the system begins in energy level  $i$  and ends in energy level  $j$ , the work cost would be  $W = E_j(\tau) - E_i(0)$ . Following these rules, one ends up with the Jarzynski equality wherein  $\Delta F$  corresponds to the difference in the free energy between the initial (thermal) state, and the thermal state associated with the final Hamiltonian  $H(\tau)$ .

An especially brief proof that such a set-up will obey the Jarzynski equality is supplied by Vedral [63], who points out that the equality holds essentially because quantum transformations conserve total probability. Consider a system prepared initially in state  $\rho_0 = \sum_i P(i)|i\rangle\langle i|$ , and subjected to evolution by the unitary  $U$ . After this evolution, the system is measured in the basis of projective measurement  $\{|j\rangle\}$ . According to the Born rule, the joint probability of starting in  $|i\rangle$  and ending in  $|j\rangle$  is given

$$P(i, j) = \text{Tr} [|j\rangle\langle j|U|i\rangle\langle i|\rho_0|i\rangle\langle i|U^\dagger|j\rangle\langle j|] = \text{Tr} [|j\rangle\langle j|U|i\rangle\langle i|U^\dagger] \times \text{Tr} [|i\rangle\langle i|\rho_0]. \quad (27.39)$$

The factorisation on the right-hand side expresses a simple probabilistic chain rule,

$$P(i, j) = Q(j|i)P(i), \quad (27.40)$$

where  $P(i)$  is the probability of beginning in state  $i$ , and  $Q(j|i)$  is the *conditional probability* of ending in state  $j$  given we started in  $i$ . The final probability of interest,  $Q(j) = \text{Tr} [|j\rangle\langle j|U\rho_0U^\dagger]$ , is the probability that the system is measured in state  $j$ , given that it was initially prepared according to the density matrix  $\rho_0$ . One can define a (simple, classical) mutual information between the outcomes of the two measurements

$$I_{ij} = -\ln Q(j) + \ln Q(j|i), \quad (27.41)$$

and then calculate

$$\begin{aligned} \langle e^{I_{ij}} \rangle &= \sum_{ij} P(i, j) \exp(I_{ij}) = \sum_{ij} P(i, j) \frac{Q(j)}{Q(j|i)} \\ &= \sum_{ij} P(i) \times Q(j) = \sum_i P(i) \times \sum_j Q(j) = 1. \end{aligned} \quad (27.42)$$

Suppose now that one takes the initial measurement as the Hamiltonian  $H(0)$ , the initial state as the thermal state of that Hamiltonian, and the final measurement as the Hamiltonian  $H(\tau)$ . After some minor algebra, we find that  $I_{ij} = \beta [E_i(0) - E_j(\tau)] - \beta \Delta F$ , and since  $\langle e^{-I_{ij}} \rangle = 1$ , this recovers Jarzynski's equality for quantum systems.

Such a quantum process has a naturally defined *reverse process*, wherein  $\tilde{H}(t) := H(\tau - t)$ . The reverse process state is written as  $\tilde{\rho}(t)$ , and the initial state  $\tilde{\rho}(0)$  is here

the thermal state of  $\tilde{H}(0)$  (i.e. the associated thermal state with the final Hamiltonian  $H(\tau)$  of the forward process). Parrondo et al. [64] demonstrate that for such a process and its reverse, a quantum fluctuation theorem can be used to determine the mean dissipated work:

$$\langle W_{\text{diss}} \rangle = k_B T D_1(\rho(t) || \tilde{\rho}(\tau - t)). \quad (27.43)$$

The left-hand side has no time dependence (this would not make sense, since  $\langle W_{\text{diss}} \rangle$  is a property of the whole protocol rather than of one instance in time). Indeed, the choice of time in  $\rho / \tilde{\rho}$  does not matter:  $D_1(\rho(t) || \tilde{\rho}(\tau - t))$  is an entropic quantity that is invariant under unitary transformations of its arguments, and the time evolution for both the process and its reverse is unitary. An obvious choice of  $\rho$  and  $\tilde{\rho}$  is then to set  $t = 0$  so that the arguments of  $D_1$  are the thermal states of the initial and final Hamiltonians. By putting these into the definition of  $D_1$  [Eq. (27.20)], the free energy difference immediately comes out, and one arrives at Eq. (27.43).

Yunger Halpern et al. [57] show that a similar quantum equality<sup>14</sup> holds relating the worst-case work with the order- $\infty$  Rényi divergence:

$$W_{\text{diss}}^{\text{worst}} = k_B T D_\infty(\rho(t) || \tilde{\rho}(\tau - t)). \quad (27.44)$$

The proof follows a similar path to that in [64] for  $D_1$ . Noting the time-invariance of  $D_\infty$ , one plugs the thermal states corresponding to the beginning of each protocol into (27.23), to arrive at

$$D_\infty(\rho(0) || \tilde{\rho}(0)) = \ln \max_{i,j} \left\{ \exp \left[ \beta \left( \tilde{E}_j - E_i - \Delta F \right) \right] \right\}, \quad (27.45)$$

where  $\{\tilde{E}_j\}_j$  are the energies of the final Hamiltonian, and  $\{E_i\}_i$  of the initial. This quantity is clearly maximized when  $\tilde{E}_j - E_i$  takes its largest value, and so the entire right-hand side corresponds to  $\beta W_{\text{diss}}^{\text{worst}}$ .

A related equality for the case of finite- $\alpha$  Rényi relative entropies has been derived by [65]:

$$\left\langle \left( e^{-\beta W_{\text{diss}}} \right)^\alpha \right\rangle = \exp(-\alpha \beta \Delta F) \exp(D_\alpha(\rho(t) || \tilde{\rho}(\tau - t))). \quad (27.46)$$

This is a generalization of the Jarzynski equality, as seen by setting  $\alpha = 1$ . This equation opens up new experimental possibilities for determining Rényi divergences between quantum states (which is difficult to do via direct tomography). This facilitates, for instance, the experimental testing of recent advances in modern thermodynamics that involve Rényi divergences between a state and its thermal equilibrium state [18, 66–69]. Through the use of *single-qubit probes* [70–73] (a type of Ramsey interferometry – see Chap. 14), one can characterize the work-distribution, and then

<sup>14</sup>In addition to this and the work fluctuation equation discussed in Sect. 27.3, Yunger Halpern et al. [57] also demonstrate that this equality holds for classical phase space fluctuations.

use the above equalities to determine the Rényi divergences between the initial and final thermal states [74].

We conclude by noting that recent developments in field of quantum fluctuation relations extend their remit beyond the regime of assumptions made by Tasaki (e.g. [47, 75] or Chap. 12). From the success of the results presented thus far, we suspect that wherever the Kullback–Leibler divergence might appears in these general contexts, an equivalent expression that uses Rényi divergences should also be possible.

**Acknowledgements** The author is grateful for discussions, comments and suggestions from Felix Binder, Oscar Dahlsten, Jayne Thompson, Vlatko Vedral, and Nicole Yunger Halpern. The author is financially supported by the Foundational Questions Institute “Physics of the Observer” large grant FQXi-RFP-1614.

## References

1. G.E. Moore, Cramming more components onto integrated circuits (Reprinted from Electronics, pp. 114–117, April 19, 1965). Proc. IEEE **86**(1), 82–85 (1965). <https://doi.org/10.1109/N-SSC.2006.4785860>, ISSN 1098-4232
2. Intel, Intel’s 10 nm technology: delivering the highest logic transistor density in the industry through the use of hyper scaling (2017), <https://newsroom.intel.com/newsroom/wp-content/uploads/sites/11/2017/09/10-nm-icf-fact-sheet.pdf>
3. M. Ruechle, S. Mahapatra, F.A. Zwanenburg, M. Friesen, M.A. Eriksson, M.Y. Simmons, Spectroscopy of few-electron single-crystal silicon quantum dots. Nat. Nanotechnol. **5**(7), 502–505 (2010). <https://doi.org/10.1038/nnano.2010.95>
4. M.A. Nielsen, I.L. Chuang, *Quantum Computation and Quantum Information* (Cambridge University Press, Cambridge, 2000). ISBN 0521635039
5. J.I. Cirac, P. Zoller, Quantum computations with cold trapped ions. Phys. Rev. Lett. **74**(20), 4091–4094 (1995). <https://doi.org/10.1103/PhysRevLett.74.4091>, ISSN 0031-9007
6. T.D. Ladd, F. Jelezko, R. Laflamme, Y. Nakamura, C. Monroe, J.L. O’Brien, Quantum computers. Nature **464**(7285), 45–53 (2010). <https://doi.org/10.1038/nature08812>, ISSN 0028-0836
7. S.J. Blundell, K.M. Blundell, *Concepts in Thermal Physics* (Oxford University Press, Oxford, 2006). ISBN 978-0199562107
8. D.N. Zubarev, V. Morozov, G. Ropke, *Statistical Mechanics of Nonequilibrium Processes* (Akademie Verlag, 1996). ISBN 3055017080
9. C. Jarzynski, Nonequilibrium equality for free energy differences. Phys. Rev. Lett. **78**(14), 2690–2693 (1997). <https://doi.org/10.1103/PhysRevLett.78.2690>, ISSN 0031-9007
10. G.E. Crooks, Nonequilibrium measurements of free energy differences for microscopically reversible Markovian systems. J. Stat. Phys. **90**(5–6), 1481–1487 (1998). <https://doi.org/10.1023/A:1023208217925>, ISSN 1572-9613
11. G.E. Crooks, Entropy production fluctuation theorem and the nonequilibrium work relation for free energy differences. Phys. Rev. E **60**(3), 2721–2726 (1999). <https://doi.org/10.1103/PhysRevE.60.2721>, ISSN 1063-651X
12. L. del Rio, J. Åberg, R. Renner, O.C.O. Dahlsten, V. Vedral, The thermodynamic meaning of negative entropy. Nature **474**(7349), 61–63 (2011). <https://doi.org/10.1038/nature10123>, ISSN 1476-4687
13. O.C.O. Dahlsten, R. Renner, E. Rieper, V. Vedral, Inadequacy of von Neumann entropy for characterizing extractable work. New J. Phys. **13**(5), 053015 (2011). <https://doi.org/10.1088/1367-2630/13/5/053015>
14. O.C.O. Dahlsten, Non-equilibrium statistical mechanics inspired by modern information theory. Entropy **15**(12), 5346–5361 (2013). <https://doi.org/10.3390/e15125346>

15. J. Åberg, Truly work-like work extraction via a single-shot analysis. *Nat. Commun.* **4**, 1925 (2013). <https://doi.org/10.1038/ncomms2712>, ISSN 20411723
16. M. Horodecki, J. Oppenheim, Fundamental limitations for quantum and nanoscale thermodynamics. *Nat. Commun.* **4**, 2059 (2013). <https://doi.org/10.1038/ncomms3059>, ISSN 2041-1723
17. D. Egloff, O.C.O. Dahlsten, R. Renner, V. Vedral, A measure of majorization emerging from single-shot statistical mechanics. *New J. Phys.* **17**(7), 073001 (2015). <https://doi.org/10.1088/1367-2630/17/7/073001>, ISSN 1367-2630
18. F.G.S.L. Brandão, M. Horodecki, N. Ng, J. Oppenheim, S. Wehner, The second laws of quantum thermodynamics. *Proc. Natl. Acad. Sci.* **112**(11), 201411728 (2015). <https://doi.org/10.1073/pnas.1411728112>, ISSN 0027-8424
19. M. Weilenmann, L. Kraemer, P. Faist, R. Renner, Axiomatic relation between thermodynamic and information-theoretic entropies. *Phys. Rev. Lett.* **117**(26), 260601 (2016). <https://doi.org/10.1103/PhysRevLett.117.260601>, ISSN 0031-9007
20. A. Rényi, On measures of entropy and information, in *Proceedings of Fourth Berkeley Symposium on Mathematics, Statistics and Probability*, vol. 1, pp. 547–561 (University of California Press, 1961)
21. R. Renner, S. Wolf, Smooth Renyi entropy and applications, in *International Symposium on Information Theory, 2004, ISIT 2004. Proceedings*, p. 232 (IEEE, 2004)
22. R. Renner, Security of quantum key distribution, Ph.D. thesis, ETH Zürich, 2005, <http://arxiv.org/abs/quant-ph/0512258>
23. M. Tomamichel, *Quantum Information Processing with Finite Resources* (Springer, New York, 2016). [https://doi.org/10.1007/978-3-319-21890-8](https://doi.org/10.1007/978-3-319-21891-5), ISBN 978-3-319-21890-8
24. C.E. Shannon, A mathematical theory of communication. *Bell Sys. Tech. J.* **27**(3), 379–423, 623–656 (1948). <https://doi.org/10.1002/j.1538-7305.1948.tb01338.x>, ISSN 00058580
25. R. Hanel, S. Thurner, Generalized (c, d)-entropy and aging random walks. *Entropy* **15**(12), 5324–5337 (2013). <https://doi.org/10.3390/e15125324>, ISSN 1099-4300
26. D.S. Jones, *Elementary Information Theory* (Clarendon Press, Oxford, 1979). ISBN 9780198596363
27. V. Vedral, The role of relative entropy in quantum information theory. *Rev. Modern Phys.* **74**(1), 197–234 (2002), [http://rmp.aps.org/abstract/RMP/v74/i1/p197\\_1](http://rmp.aps.org/abstract/RMP/v74/i1/p197_1), ISSN 0034-6861
28. A.J.P. Garner, Q. Liu, J. Thompson, V. Vedral, M. Gu, Provably unbounded memory advantage in stochastic simulation using quantum mechanics. *New J. Phys.* (2017). <https://doi.org/10.1088/1367-2630/AA82DF>, ISSN 1367-2630
29. N. Yunger Halpern, A.J.P. Garner, O.C.O. Dahlsten, V. Vedral, Introducing one-shot work into fluctuation theorems. *New J. Phys.* **17**, 095003 (2015). <https://doi.org/10.1088/1367-2630/17/9/095003>
30. T.M. Cover, J.A. Thomas, *Elements of Information Theory* (Wiley, New York, 2006), <https://www.wiley.com/en-sg/Elements+of+Information+Theory,+2nd+Edition-p-9780471241959>. ISBN 9780471241959
31. T.M. Mitchell, *Machine Learning* (McGraw-Hill, New York, 1997). ISBN 0070428077
32. T. Van Erven, P. Harrémos, Rényi divergence and Kullback–Leibler divergence. *IEEE Trans. Inf. Theory* **60**(7), 3797–3820 (2014). <https://doi.org/10.1109/TIT.2014.2320500>, ISSN 00189448
33. B. Schumacher, Quantum coding. *Phys. Rev. A* **51**(4), 2738–2747 (1995). <https://doi.org/10.1103/PhysRevA.51.2738>, ISSN 1050-2947
34. M. Müller-Lennert, F. Dupuis, S. Szehr, S. Fehr, M. Tomamichel, On quantum Rényi entropies: a new generalization and some properties. *J. Math. Phys.* **54**(12), 122203 (2013). <https://doi.org/10.1063/1.4838856>, ISSN 0022-2488
35. M.M. Wilde, A. Winter, D. Yang, Strong converse for the classical capacity of entanglement-breaking and hadamard channels via a sandwiched Rényi relative entropy. *Commun. Math. Phys.* **331**(2), 593–622 (2014). <https://doi.org/10.1007/s00220-014-2122-x>, ISSN 0010-3616
36. M. Tomamichel, M. Berta, M. Hayashi, Relating different quantum generalizations of the conditional Rényi entropy. *J. Math. Phys.* **55**(8), 082206 (2014). <https://doi.org/10.1063/1.4892761>, ISSN 0022-2488

37. R. Landauer, Irreversibility and heat generation in the computer process. *IBM J. Res. Dev.* **5**, 183–191 (1961). <https://doi.org/10.1147/rd.53.0183>
38. C.H. Bennett, The thermodynamics of computation a review. *Int. J. Theor. Phys.* **21**(12), 905–940 (1982). <https://doi.org/10.1007/BF02084158>, ISSN 0020-7748
39. C.H. Bennett, Notes on Landauer's principle, reversible computation, and Maxwell's Demon. *Stud. Hist. Philos. Sci. Part B Stud. Hist. Philos. Modern Phys.* **34**(3), 501–510 (2003). [https://doi.org/10.1016/S1355-2198\(03\)00039-X](https://doi.org/10.1016/S1355-2198(03)00039-X), ISSN 13552198
40. R. Landauer, The physical nature of information. *Phys. Lett. A* **217**(4), 188–193 (1996), <http://www.sciencedirect.com/science/article/pii/0375960196004537>
41. J.C. Maxwell, *Theory of Heat* (Longmans, Green & Co, 1902 edition, 1870)
42. H. Leff, A.F. Rex, *Maxwell's Demon 2: Entropy, Classical and Quantum Information, Computing* (Taylor & Francis, London, 2002)
43. L. Szilard, über die Enfropieuerminderung in einem thermodynamischen System bei Eingrifen intelligenter Wesen. *Zeitschrift für Physik* **53**, 840–856 (1929)
44. D. Reeb, M.M. Wolf, An improved Landauer principle with finite-size corrections. *New J. Phys.* **16**(10), 103011 (2014). <https://doi.org/10.1088/1367-2630/16/10/103011>, ISSN 1367-2630
45. P. Skrzypczyk, A.J. Short, S. Popescu, Work extraction and thermodynamics for individual quantum systems. *Nat. Commun.* **5**, 4185 (2014). <https://doi.org/10.1038/ncomms5185>, ISSN 2041-1723
46. F.G.S.L. Brandão, M. Horodecki, J. Oppenheim, J.M. Renes, R.W. Spekkens, Resource theory of quantum states out of thermal equilibrium. *Phys. Rev. Lett.* **111**(25), 250404 (2013). <https://doi.org/10.1103/PhysRevLett.111.250404>, ISSN 0031-9007
47. A.M. Alhambra, L. Masanes, J. Oppenheim, C. Perry, Fluctuating work: from quantum thermodynamical identities to a second law equality. *Phys. Rev. X* **6**(4), 041017 (2016). <https://doi.org/10.1103/PhysRevX.6.041017>, ISSN 2160-3308
48. J. Anders, V. Giovannetti, Thermodynamics of discrete quantum processes. *New J. Phys.* **15**(3), 033022 (2013). <https://doi.org/10.1088/1367-2630/15/3/033022>, ISSN 1367-2630
49. C. Browne, A.J.P. Garner, O.C.O. Dahlsten, V. Vedral, Guaranteed energy-efficient bit reset in finite time. *Phys. Rev. Lett.* **113**(10), 100603 (2014). <https://doi.org/10.1103/PhysRevLett.113.100603>, ISSN 0031-9007
50. R. Alicki, The quantum open system as a model of the heat engine. *J. Phys. A Math. Gen.* **12**(5), L103–L107 (1979). <https://doi.org/10.1088/0305-4470/12/5/007>, ISSN 0305-4470
51. B. Piechocinska, Information erasure. *Phys. Rev. A* **61**(6), 062314 (2000). <https://doi.org/10.1103/PhysRevA.61.062314>, ISSN 1050-2947
52. R. Alicki, M. Horodecki, P. Horodecki, R. Horodecki, thermodynamics of quantum information systems Hamiltonian description. *Open Syst. Inf. Dyn. (OSID)* **11**(03), 205–217 (2004). <https://doi.org/10.1023/B:OPSY.0000047566.72717.71>, ISSN 1230-1612
53. E. Schrödinger, *Statistical Thermodynamics*, 2nd edn. (Cambridge University Press, Cambridge, 1946)
54. H.T. Quan, H. Dong, Quantum Crooks fluctuation theorem and quantum Jarzynski equality in the presence of a reservoir, 6 (2008), <http://arxiv.org/abs/0812.4955>
55. D. Wu, D.A. Kofke, Phase-space overlap measures. I. fail-safe bias detection in free energies calculated by molecular simulation. *J. Chem. Phys.* **123**(5), 054103 (2005). <https://doi.org/10.1063/1.1992483>, ISSN 0021-9606
56. A. Gomez-Marin, J.M.R. Parrondo, C. Van den Broeck, The footprints of irreversibility. *EPL (Europhys. Lett.)* **82**(5), 50002 (2008). <https://doi.org/10.1209/0295-5075/82/50002>, ISSN 0295-5075
57. N. Yunger Halpern, A.J.P. Garner, O.C.O. Dahlsten, V. Vedral, Maximum one-shot dissipated work from Rényi divergences. *Phys. Rev. E* **97**(5), 052135 (2018). <https://doi.org/10.1103/PhysRevE.97.052135>, ISSN 2470-0045
58. O.C.O. Dahlsten, M.-S. Choi, D. Braun, A.J.P. Garner, N. Yunger Halpern, V. Vedral, Entropic equality for worst-case work at any protocol speed. *New J. Phys.* **19**(4), 043013 (2017). <https://doi.org/10.1088/1367-2630/aa62ba>, ISSN 1367-2630

59. N. Yunger Halpern, C. Jarzynski, Number of trials required to estimate a free-energy difference, using fluctuation relations. *Phys. Rev. E* **93**(5), 052144 (2016). <https://doi.org/10.1103/PhysRevE.93.052144>, ISSN 2470-0045D
60. C. Jarzynski, Rare events and the convergence of exponentially averaged work values. *Phys. Rev. E* **73**(4), 046105 (2006). <https://doi.org/10.1103/PhysRevE.73.046105>, ISSN 1539-3755
61. J. Kurchan, A quantum fluctuation theorem (2000), <http://arxiv.org/abs/cond-mat/0007360>
62. H. Tasaki, Jarzynski relations for quantum systems and some applications, 11 (2000), <http://arxiv.org/abs/cond-mat/0009244>
63. V. Vedral, An information theoretic equality implying the Jarzynski relation. *J. Phys. A Math. Theor.* **45**(27), 272001 (2012). <https://doi.org/10.1088/1751-8113/45/27/272001>, ISSN 1751-8113
64. J.M.R. Parrondo, C. Van den Broeck, R. Kawai, Entropy production and the arrow of time. *New J. Phys.* **11**(7), 073008 (2009). <https://doi.org/10.1088/1367-2630/11/7/073008>, ISSN 1367-2630
65. B. Wei, M.B. Plenio, Relations between dissipated work in non-equilibrium process and the family of Rényi divergences. *New J. Phys.* **19**(2), 023002 (2017). <https://doi.org/10.1088/1367-2630/aa579e>, ISSN 1367-2630
66. G. Gour, M.P. Müller, V. Narasimhachar, R.W. Spekkens, N. Yunger Halpern, The resource theory of informational nonequilibrium in thermodynamics. *Phys. Rep.* **583**, 1–58 (2015). <https://doi.org/10.1016/j.physrep.2015.04.003>
67. M. Lostaglio, D. Jennings, T. Rudolph, Description of quantum coherence in thermodynamic processes requires constraints beyond free energy. *Nat. Commun.* **6**(1), 6383 (2015). <https://doi.org/10.1038/ncomms7383>, ISSN 2041-1723
68. M. Lostaglio, K. Korzekwa, D. Jennings, T. Rudolph, Quantum coherence, time-translation symmetry, and thermodynamics. *Phys. Rev. X* **5**(2), 021001 (2015). <https://doi.org/10.1103/PhysRevX.5.021001>, ISSN 2160-3308
69. P. Ćwikliński, M. Studziński, M. Horodecki, J. Oppenheim, Limitations on the evolution of quantum coherences: towards fully quantum second laws of thermodynamics. *Phys. Rev. Lett.* **115**(21), 210403 (2015). <https://doi.org/10.1103/PhysRevLett.115.210403>, ISSN 0031-9007
70. R. Dorner, J. Goold, C. Cormick, M. Paternostro, V. Vedral, Emergent thermodynamics in a quenched quantum many-body system. *Phys. Rev. Lett.* **109**(16), 160601 (2012). <https://doi.org/10.1103/PhysRevLett.109.160601>, ISSN 0031-9007
71. R. Dorner, S.R. Clark, L. Heaney, R. Fazio, J. Goold, V. Vedral, Extracting quantum work statistics and fluctuation theorems by single-qubit interferometry. *Phys. Rev. Lett.* **110**(23), 230601 (2013). <https://doi.org/10.1103/PhysRevLett.110.230601>, ISSN 0031-9007
72. T.B. Batalhão, A.M. Souza, R.S. Sarthour, I.S. Oliveira, M. Paternostro, E. Lutz, R.M. Serra, Irreversibility and the arrow of time in a quenched quantum system. *Phys. Rev. Lett.* **115**(19), 190601 (2015). <https://doi.org/10.1103/PhysRevLett.115.190601>, ISSN 0031-9007
73. T.P. Xiong, L.L. Yan, F. Zhou, K. Rehan, D.F. Liang, L. Chen, W.L. Yang, Z.H. Ma, M. Feng, V. Vedral, Experimental verification of a Jarzynski-related information-theoretic equality by a single trapped ion. *Phys. Rev. Lett.* **120**(1), 010601 (2018). <https://doi.org/10.1103/PhysRevLett.120.010601>, ISSN 0031-9007
74. X.-Y. Guo, Y. Peng, C. Peng, H. Deng, Y.-R. Jin, C. Tang, X. Zhu, D. Zheng, H. Fan, Demonstration of irreversibility and dissipation relation of thermodynamics with a superconducting qubit (2017), <http://arxiv.org/abs/1710.10234>
75. J. Åberg, Fully quantum fluctuation theorems. *Phys. Rev. X* **8**(1), 011019 (2018). <https://doi.org/10.1103/PhysRevX.8.011019>, ISSN 2160-3308

# Chapter 28

## The Second Law and Beyond in Microscopic Quantum Setups



Raam Uzdin

### 28.1 Introduction

Quantum thermodynamics deals with a broad spectrum of issues related to thermodynamics of small and quantum systems. In particular, this chapter examines the applicability of one of the most fundamental ideas in thermodynamics: the second law. In addition to its classical role, the second law is the main connecting thread between classical thermodynamics and thermodynamics of microscopic (possibly highly quantum) systems.

The second law has various formulations. Here we consider one of the most versatile and useful forms: the Clausius inequality

$$\Delta S - \int \frac{\delta Q}{T} \geq 0, \quad (28.1)$$

where  $S$  is the entropy of the system, and  $Q$  is the heat exchanged with a bath at temperature  $T$ . In classical thermodynamics, entropy changes are defined by the quantity  $\int \frac{\delta Q}{T}$  evaluated for a reversible process between two equilibrium states. The bath is assumed to be large with a well-defined temperature at all stages of the evolution.

The Clausius equality (CI) is quite remarkable. It provides a quantitative prediction that can easily be adapted to the quantum microscopic world. One of the important results of applying the CI to the microscopic and/or quantum world, is that the efficiency of quantum heat engines is limited by the Carnot efficiency even when the evolution exploits unique quantum properties such as entanglement. Moreover, the CI is the underlying principle behind Szilard engines, and Landauer's erasure principle [1, 2] (see also Chap. 29).

---

R. Uzdin (✉)

Fritz Haber Research Center for Molecular Dynamics, Hebrew University  
of Jerusalem, 9190401 Jerusalem, Israel  
e-mail: raam@mail.huji.ac.il

As described later in detail, under reasonable assumptions the CI is well understood, and can be obtained for microscopic systems using several different approaches. However, there are various open questions and challenges related to the CI: (1) Is the current regime of validity sufficiently large to handle important microscopic scenarios? If not, the CI should be further explored and extended. (2) In microscopic setups where the CI is valid, is it also *useful*, i.e., does it provide practical predictions? (3) Is the CI a one of a kind constraint, or is it just one member of a family of constraints on microscopic thermodynamic processes? Recent studies show that additional constraints do exist [3–6].

The importance of additional constraints or “laws” comes from the fact that in nanoscopic setups, systems are easily taken out of equilibrium. In equilibrium macroscopic systems, knowledge of a few coarse-grained properties (e.g., internal energy, volume, pressure, etc.) is sufficient for knowing almost everything about the system. In contrast, in small out of equilibrium systems, changes in the internal energy, for example, provide only a limited amount of information on how the energy distribution deviates from equilibrium. Moreover, in small systems, it is possible to experimentally probe features that are more detailed than the average energy, e.g., the energy variance. Thus, it is intriguing to ask if there are thermodynamic constraints, perhaps of the CI form, on other moments of the energy [6], or on other measurable features of the system. Furthermore, in microscopic setups, the environment itself may be very small. Thus, it is conceivable to measure various environment properties (e.g. energy variance) as the environment starts to deviate from its initial equilibrium state.

In trying to extend the regime of validity of the CI, or in the search of new thermodynamic constraints on new quantities, it is important to keep track on what properties of the CI have been retained, what features have been lost or replaced, and at what cost. In particular, it is important that the suggested extension involves measurable quantities, and that it has predictive power with respect to present and future experiments. For example, thermodynamic resource theory (see Chap. 26) predicts that there are families of mathematical constraints on a specific set of processes involving thermal baths [3, 4, 7]. This is a very interesting and important finding. However, these constraints do not deal directly with observable quantities and their operational (or informational) meaning has not been clarified yet. Nevertheless, in the asymptotic many copies limit, resource theory reduce to the free-energy (single bath) form of the second law [3, 4, 7–9]. It is not a necessary requirement that new constraints will have the same form and nature of the CI. However, it is very interesting to explore and find constraints that resemble the second law and its rock-solid, well-established logic. Thus, this chapter puts emphasis on the structure of the CI, and its various features.

In what follows, we aim to achieve the goals stated in the abstract by studying three different approaches of deriving the CI: (1) The reduced entropy approach; (2) The global passivity approach; (3) The Completely positive maps approach. Each approach shows different aspects of the CI, and can lead to new challenges related to the second law in nanoscopic setups. Before exploring each approach let us state the CI statement of the second law in microscopic setups.

## 28.2 The CI in Microscopic and Quantum Setups

Consider a setup that is composed of a system that is initially in an arbitrary mixed or pure state, and several environments that are initially in thermal equilibrium (each environment is in a Gibbs state with some temperature). All elements ('element' may refer to the system, or to one of its environments) are initially uncorrelated. Thus, at  $t_0$  the setup shown in Fig. 28.1a is described by the following total density matrix:

$$\rho_0^{tot} = \rho_0^{sys} \otimes \frac{e^{-\beta_1 H_1}}{Z_1} \otimes \frac{e^{-\beta_2 H_2}}{Z_2} \otimes \dots \quad (28.2)$$

where  $H_k$  is the Hamiltonian of environment  $k$ ,  $\beta_k = 1/T_k$  is its *initial* inverse temperature, and the  $Z_k$ 's are normalization factors. The Boltzmann constant  $k_B$  is set 1 throughout the chapter. We call an environment that is initially prepared in a thermal state a 'microbath' (later denoted in equations by  $\mu b$ ). Unlike macroscopic baths, microbaths are not assumed to be large and to remain in a thermal state while interacting with the system. The only requirement of a microbath is that its initial state is thermal. That said, the microbath is allowed to be very large. The preparation process of a microbath is outside the scope of the present discussion. We shall assume that such (possibly small) initially thermal environments are given in the beginning of the experiment. Nevertheless, in principle, they can be prepared by weakly interacting with a much larger thermal environment. Another option is to use a heat exchanger as in [10].

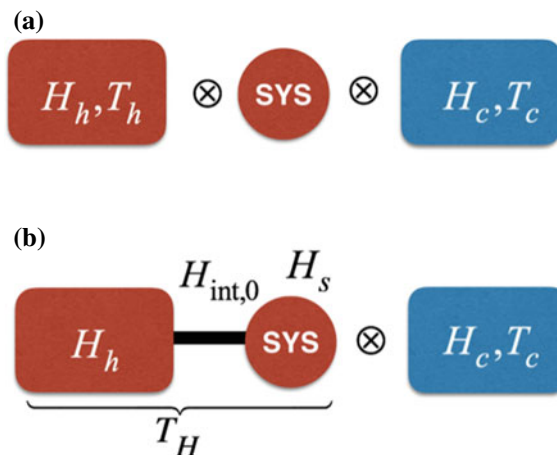


**Fig. 28.1** **a** The standard CI form of the second law assumes that all elements are initially uncorrelated (28.2). **b** In microscopic setups where a system is initially strongly coupled to one of the environments, the system starts in a *coupled* Gibbs state (28.54). Hence, in general, the system does not have a thermal form when the environment is traced out. The CI does not hold in this scenario. Nonetheless, new approaches can successfully handle this scenario (Sect. 28.4.4).

The evolution of the setup is generated by some global time-dependent Hamiltonian that describes all the interactions between the system, the microbaths, and external fields (i.e., driving). In such setups the following microscopic form of the CI [11–18] holds:

$$\Delta S_{VN}^{sys} + \sum \beta_k q_k \geq 0, \quad (28.3)$$

$$q_k = \Delta \langle H_k \rangle, \quad (28.4)$$

where  $S_{VN}^{sys} = -tr[\rho^{sys} \ln \rho^{sys}]$  is the von Neumann entropy of the system (we shall drop the VN subscript hereafter). *The  $\Delta$  always refers to changes with respect to time  $t_0$  where (28.2) holds*, e.g., at time  $t$ :  $\Delta S^{sys} = S(t) - S(t_0)$ .  $q_k$  is the heat or more accurately the energy change in the  $k$ th microbath. For  $q_k$  to represent the energy change in bath  $k$ ,  $H_k$  must satisfy  $H_k(t_f) = H_k(t_0)$  which means that at the end of the process the environment is not modified directly by an external field. A classical derivation is carried out in [19, 20]. We point out a few interesting facts on the microscopic CI result (28.3)

- As long as the initial condition (28.2) holds, the interaction between the elements and the external driving can be arbitrarily strong and lead to highly non-Markovian dynamics (i.e., there is no reduced Markovian description for the dynamics of the system).
- The microbaths and the system can be arbitrary small in size (e.g., a single spin) as long as the initial state of the setup is given by (28.2).
- The microbath can be very far from thermal equilibrium at the end and during the interaction with the system. The  $\beta_k$ 's refer only to the *initial* temperatures of the microbath.

For additional refinements of the CI (see [2, 21]). In what follows, we derive the CI (28.3) using different approaches.

### 28.3 The Reduced Entropy Approach

To keep the notation simple, let us assume we have only three elements: a system ‘ $s$ ’, and two environments ‘ $A$ ’ and ‘ $B$ ’. At this point, it is not assumed that the environments are initially thermal. However, all three elements are assumed to be initially uncorrelated to each other, and therefore the initial density matrix is given by

$$\rho_0^{tot} = \rho_0^s \otimes \rho_0^A \otimes \rho_0^B. \quad (28.5)$$

Next, we assume that the evolution is generated by some time-dependent Hamiltonian of the form:

$$H_{tot}(t) = H_s(t) + H_A(t) + H_B(t) + H_{int}(t), \quad (28.6)$$

where the first term describes possible external driving of the system (e.g. by laser light), the next two terms are the environment Hamiltonians (which may also be subjected to external fields), and the last term describes the time-dependent interactions between the three elements. This generic Hamiltonian can describe almost any thermodynamic protocol that does not involve feedback or measurements during the evolution. No other interactions or other parties are involved. Note that typically the environments ( $A$  and  $B$ ) are either not driven  $\frac{d}{dt}H_{A(B)} = 0$  by external fields, or at the very least are not modified at the end of the thermodynamic protocol

$$H_{A(B)}(t_f) = H_{A(B)}(t_0). \quad (28.7)$$

However, this assumption is not needed until Eq. (28.22).

In quantum mechanics, any  $H_{tot}(t)$  leads to a unitary evolution operator  $U$  (i.e.,  $U^\dagger U = I$ ) that relates the final density matrix to the initial one,

$$\rho_t^{tot} = U \rho_0^{tot} U^\dagger. \quad (28.8)$$

Finally, we consider a slightly more general case where there is some noise in  $H_{tot}(t)$  (this noise can be a control amplitude noise, timing noise, etc) so that with probability  $p_j$ ,  $U_j$  is executed instead of the desired  $U$ . As a result, the evolution of the setup is described by a mixture of unitaries

$$\rho_t^{tot} = \sum p_k U_k \rho_0^{tot} U_k^\dagger. \quad (28.9)$$

Next, we use the non-negativity of the quantum relative entropy [22] for any two density matrices  $\rho$  and  $\sigma$

$$D(\rho|\sigma) \doteq \text{tr}[\rho(\ln \rho - \ln \sigma)] \geq 0, \quad (28.10)$$

where equality holds if and only if  $\rho = \sigma$ . We set  $\rho$  to be the state of the setup at time  $t$   $\rho = \rho_t^{tot}$ , and  $\sigma$  to be the tensor product of the local density matrices  $\sigma = \rho_t^s \otimes \rho_t^A \otimes \rho_t^B$  where  $\rho_t^{(i)} \doteq \text{tr}_{\neq i}[\rho_t^{tot}]$ . Using the log property for *product states* ( $\sigma$ ), we get

$$D(\rho_t^{tot}|\rho_t^s \otimes \rho_t^A \otimes \rho_t^B) = \left( \sum_{j=s,A,B} S_t^j \right) - S_t^{tot} \geq 0, \quad (28.11)$$

where the inequality follows from the non-negativity of the quantum relative entropy (28.10). If the global evolution is unitary (28.8), then  $S_t^{tot} = S_0^{tot}$  since all the eigenvalues of the total density matrix are conserved quantities. If the global evolution is a mixture of unitaries (28.9) then due to the Schur concavity [23] of the von Neumann entropy it holds that,

$$S_t^{tot} \geq S_0^{tot}. \quad (28.12)$$

Note that this inequality is *not* a manifestation of the second law. Unlike the inequality (28.11) that holds also for a unitary evolution, Eq.(28.12) originates from the randomness/noise in the protocol that we have included for generality. Using (28.12) in (28.11) we get

$$\left( \sum_{j=s,A,B} S_t^j \right) - S_0^{tot} \geq 0. \quad (28.13)$$

Since the setup starts in a product state (28.5) it holds that  $S_0^{tot} = \sum_{j=s,A,B} S_0^j$  and (28.13) becomes the reduced entropy growth form of the (microscopic) second law [11–13, 18],

$$\sum_{j=s,A,B} \Delta S^j \geq 0. \quad (28.14)$$

This form is strictly entropic and has no reference to heat or energy. Moreover, (28.14) holds even if the environments are initially in highly non-thermal states. For two parties, (28.14) can be obtained from the non-negativity of the quantum mutual information [22]. When there are more parties, (28.11) should be used.

Equation (28.14) has the following informational interpretation. For any global unitary the total entropy is conserved  $\Delta S^{tot} = 0$ . However, the final density matrix contains classical and quantum correlations between the different elements. The sum of reduced entropies does not include these correlations, and therefore it grows despite the fact that the total entropy is conserved.

It is important to highlight several points. (1) This growth is only with respect to the initial values, and it is typically non-monotonic in time due to the possible non-Markovian nature of the evolution. (2) The reason that the entropy is growing and not decreasing is due to the special assumption that the elements are initially uncorrelated. (3) As mentioned earlier, no assumptions were made on the size of the elements. The microbath or the system can be as small as a single spin. These features make the entropic form of the second law useful for understanding processes involving small quantum systems (e.g., algorithmic cooling [24]).

To conclude this section, we would like to discuss the zero entropy production limit that appears in infinitesimal transformations with respect to the initial product density matrix. The relative entropy has two useful properties. (1) It is easy to verify that the following general result holds

$$D(\rho_t^{tot} | \rho_0^s \otimes \rho_0^A \otimes \rho_0^B) \geq D(\rho_t^{tot} | \rho_t^s \otimes \rho_t^A \otimes \rho_t^B), \quad (28.15)$$

(2) The relative entropy is quadratic in small perturbations

$$D(\sigma + \delta\sigma | \sigma) = O(|\delta\sigma|^2). \quad (28.16)$$

There is no linear term in  $\delta\sigma$  as it would have implied  $D(\sigma - \delta\sigma | \sigma) < 0$  and the relative entropy cannot be negative. Next we consider an infinitesimal evolution of

the whole setup  $\rho_f^{tot} = \delta\rho^{tot} + \rho_0^{tot}$  where  $|\delta\rho^{tot}| \ll 1$ . Using (28.11), (28.15) and (28.16) we get

$$O(|\delta\rho^{tot}|^2) \geq \sum_{j=s, A, B} \Delta S^j. \quad (28.17)$$

Equation (28.17) implies that  $\sum_{j=s, A, B} \Delta S^j \rightarrow 0$  as  $\delta\rho^{tot} \rightarrow 0$ . This is not a trivial statement, since the individual changes in the local entropies are  $\Delta S^j = O(|\delta\rho^{tot}|)$ . That is, entropy is moved around between the elements and not created through build up of correlations. This result will become important in studying the reversible limit of the Clausius inequality in Sect. 28.3.3.

### 28.3.1 The Clausius Inequality: The Energy-Information Form of the Second Law

The transition from the entropic form of the second law to the energy-information CI form, involves three more simple steps. The first is to apply the following identity that holds for any two density matrices  $\rho_1, \rho_2$ .

$$S(\rho_2) - S(\rho_1) \equiv \text{tr}[(\rho_2 - \rho_1)(-\ln \rho_1)] - D(\rho_2|\rho_1). \quad (28.18)$$

Applying this identity to the initial and final reduced states of the  $k$ th environment

$$\Delta S^{env,k} = \Delta \left\langle -\ln \rho_0^{env,k} \right\rangle - D(\rho_f^{ub,k}|\rho_0^{ub,k}), \quad (28.19)$$

and substituting it in (28.14) we obtain

$$\Delta S^{sys} + \sum_k \Delta \left\langle -\ln \rho_0^{env,k} \right\rangle \geq \sum_k D(\rho_f^{ub,k}|\rho_0^{ub,k}). \quad (28.20)$$

The next step is to set the environments to be microbaths, i.e.  $\rho_0^{env,k} \rightarrow \rho_0^{ub,k} = e^{-\beta_k H_k^{ub}}/Z_k$  and get

$$\Delta S^{sys} + \sum_k \beta_k q_k \geq \sum_k D(\rho_f^{ub,k}|\rho_0^{ub,k}), \quad (28.21)$$

where, as before, we denote the change in the average energy of bath  $k$  by  $q_k$

$$q_k \doteq \text{tr}[(\rho_f^{ub,k} - \rho_0^{ub,k})H_k^{ub}]. \quad (28.22)$$

To interpret  $q_k$  as the change in the energy of the bath we have used assumption (28.7). Due to the relative entropy terms in (28.21), form (28.21) is slightly stronger

than the standard CI (28.3). However, the relative entropy terms cannot be easily measured. Nevertheless, they are not void of physical meaning. They represent the work that can be extracted from the microbaths due to the fact they are not in a thermal state at the end of the process. If, for example, *an additional auxiliary large bath* at temperature  $T_h$  was available, then a  $T_h D(\rho_f^{\mu b,h} | \rho_0^{\mu b,h})$  amount of work could have been reversibly extracted from the hot microbath. However, as we consider an entropically self-contained setups (where a large external bath is not included), this work extraction scheme is irrelevant.

In the last third step, the relative entropy property  $D(\rho_f^k | \rho_0^k) \geq 0$  is used to obtain the CI inequality (28.3) from (28.21). Finally, by defining the operator

$$B^{env} = -\ln \rho_0^{env}, \quad (28.23)$$

where  $\rho_0^{baths}$  is the initial density matrix of all the microbaths in the setup, the CI can be written more compactly as

$$\Delta S^{sys} + \Delta \langle B^{env} \rangle \geq 0. \quad (28.24)$$

This form will be used in Sect. 28.4.4.

### 28.3.2 The Structure of the CI

The CI connects two very different quantities. One is an information measure, and the other is an expectation value obtained from energy measurements. These two quantities have completely different nature and properties.  $S^{sys}(\rho_{sys})$  is an information measure and as such it is nonlinear in  $\rho_{sys}$ . It is basis-independent, and invariant to level permutations and, more generally, to unitary transformations  $S^{sys}(\rho^{sys}) = S^{sys}(U \rho^{sys} U^\dagger)$ . That is, only the eigenvalues of the density matrix are important. It matters not to which orthogonal states these eigenvalues are assigned. If the system is in a known pure state  $|\psi\rangle$  then  $S^{sys}(|\psi\rangle \langle \psi|) = 0$ . If  $\rho^{sys}$  is in a fully mixed state then  $S^{sys}$  obtains a maximal value.

The second term in the CI,  $\sum \beta_k q_k = \beta \Delta \langle H_k^{\mu b} \rangle$  is completely different. First, it is linear in the density matrix. Second, it is not invariant under local permutations and more general local unitary transformations  $tr[U_k \rho^{\mu b} U_k^\dagger H_k^{\mu b}] \neq tr[\rho^{\mu b} H_k^{\mu b}]$ . Moreover,  $\langle H_k^{\mu b} \rangle$  involves only the diagonal elements of the density matrix in the energy basis. Thus, dephasing all the coherences in the energy basis will not change the energy expectation values at a given instant (it will, however, change the evolution from that point on). In contrast, information quantities such as the von Neumann entropy are very sensitive to dephasing. All types of dephasing operations increase the values of  $S^{sys}(\rho^{sys})$ . We point out that all Schur concave information measures have this property [6, 23].

This relation between a quantity that is basis-independent and a quantity that is basis-dependent can be quite powerful. For example, if we erase one bit of information from our system (no matter in which basis), then according to the CI (Landauer principle [1] Reeb and Wolf [2]) at least  $T \ln 2$  amount of heat has to be exchanged with the bath (see Chap. 29 for more general forms of erasure). Thus, although nonlinear quantities such as  $S^{\text{sys}}(\rho^{\text{sys}})$  are not directly measurable (they are not associated with a Hermitian operator), they can be quite insightful when associated with expectation values as in the CI. Note that in the CI the nonlinear quantities involve only the system, which at least in nanoscopic setups can be regarded as small. For example, it is not unreasonable to perform tomography of a two-spin system, if needed. On the other hand, it is not practical to perform a full tomography of a thirty-spin microbath in order to evaluate its entropy changes. Hence, when using nonlinear quantities in thermodynamics, we should be mindful of how they can be evaluated or used either directly or indirectly.

### 28.3.3 The Reversible Limit of the CI

A major feature of the CI is that the inequality is saturated (becomes an equality) for reversible processes. The saturation limit of the CI is highly important for two main reasons. First, inequalities that are not saturated can be completely useless. For example,  $\Delta S + \beta q + 10^{100} \geq 0$  is also a valid inequality, but it is trivially satisfied and cannot be used to state something useful on  $\Delta S$  by knowing  $q$  or vice versa. The second reason why the CI saturation is important is that it provides a special meaning to reversible processes compared to irreversible processes. All reversible processes between two endpoints (two density matrices of the systems) are equivalent in terms of heat, work, and entropy changes in the bath. On the other hand, irreversible processes are path-dependent and lead to suboptimal work extraction. Note that creating a reversible interaction with microbaths is not as straightforward as it is in macroscopic setups since, in general, the microbaths do not remain in a Gibbs state.

Equation (28.21) implies that in saturation the relative entropy terms on the right hand side must vanish. We show now that this naturally happens in infinitesimal transformations  $|\delta\rho^{\text{tot}}| \ll 1$  where (28.17) holds. It is always possible to choose  $\delta\rho^{\text{tot}}$  small enough so that  $|\delta\rho^{\text{env}}| \ll 1$  also holds. According to (28.16)  $|\delta\rho^{\text{env}}| \ll 1$  implies  $D(\rho_f^{\text{env}}|\rho_0^{\text{env}}) = O(|\delta\rho^{\text{env}}|^2)$ . To connect this to the right hand side of (28.21) we use the fact that for initially uncorrelated microbath it holds that  $D(\rho_f^{\text{env}}|\rho_0^{\text{env}}) \geq \sum_k D(\rho_f^{\mu b,k}|\rho_0^{\mu b,k})$ . Thus, the right hand side of (28.21) vanishes as  $O(|\delta\rho^{\text{env}}|^2)$  for infinitesimal transformations. Note that the entropy in the microbath changes linearly in  $\delta\rho^{\text{env}}$  via the term  $\Delta \langle B^{\text{env}} \rangle$ . Thus, in reversible transformations  $\Delta \langle B^{\text{env}} \rangle$  represent the entropy flow from the system to the environment and the total entropy production is zero. For a large environment,  $|\delta\rho^{\text{env}}|$  can be made very small as the interaction with the system involves many degrees of freedom (particles) in the environment where each one changes only a little. Therefore, finite heat exchanges

with a large environment may still involve a vanishing  $\sum_k D(\rho_f^{\mu b, k} \|\rho_0^{\mu b, k})$ . Crucially, for markovian dynamics large environments are needed in order to maintain (to a good approximation) the product state assumption  $\rho_t^{tot} = \rho_t^{sys} \otimes \rho_t^{env}$  at each instant of the evolution and not just for the initial state. For markovian dynamics in microscopic heat capacity reservoirs, see [25].

### 28.3.4 Fluctuation Theorems and Clausius-Like Inequalities

Fluctuation theorems (FT's) are intensively studied for the last few decades (see [26–29] and Chap. 10). Their main appeal is that they provide *equalities* that hold even when the system is driven far away from equilibrium. In contrast, the CI provides a potentially saturated *inequality* in non-equilibrium dynamics.

Interestingly, by applying the Jensen inequality some manifestations of the CI can be retrieved from FT's. For this reason, it is sometimes claimed that FT's are more fundamental than the CI. However, it is highly important to remember that, presently, the CI is applicable in various scenarios where FT's may not hold or become impractically to use: (1) Initial coherence in the energy eigenbasis of the systems. (2) the FT equalities may not involve the quantities of interest. For example Jarzynski equality yields a prediction on  $\langle e^{-\beta w} \rangle$  and not on the average work  $\langle w \rangle$ , or on a distinct moment of the work  $\langle w^n \rangle$ . Instead it provides information on  $\sum_{n=0}^{\infty} \frac{(-\beta)^2}{n!} \langle w^n \rangle$ . This is still useful as a tool for evaluating free energy differences but not for relating average work to heat flows.

In summary, in comparison to the CI, fluctuation theorems presently provide stronger statements (equalities) but for more limited physical scenarios. Further study is needed to understand if there is a fundamental complementarity between the strength of non-equilibrium results (FT or CI) and their regime of validity, or perhaps it is possible to hold the stick at both ends and find FT's that are both more general and stronger than the CI.

Finally, we point that energy appears in the CI in the form of “difference of averages”  $q = \langle H_{\mu b} \rangle_f - \langle H_{\mu b} \rangle_0$ , while in FT (e.g. [29, 30]) energy appears as “nonlinear average of differences”, e.g.,  $\langle e^{-\beta(E_f - E_0)} \rangle$  where  $E_f$  and  $E_0$  are initial and final energy measurements in a specific realization (trajectory) [30]. That is, the energy term in the CI has the structure  $\Delta \langle g(H) \rangle$  while in FTs the structure is  $\langle \tilde{g}(\Delta E) \rangle$  where  $g$  and  $\tilde{g}$  are some analytic functions. In FT's the evaluation of  $\Delta E$  involves measuring  $E_0$  and  $E_f$  in the same run of the experiment. In quantum mechanics  $E_0$  measurements will modify the evolution due to the loss of coherence (wavefunction “collapse”). In contrast, quantities such  $\langle g(H) \rangle_f$  and  $\langle g(H) \rangle_0$  are evaluated over multiple runs of the experiment: in one set of experimental runs  $\langle g(H) \rangle_0$  is measured and evaluated, and in another set of runs  $\langle g(H) \rangle_f$  is measured. Therefore, the structure of  $\Delta \langle g(H) \rangle$  is more compatible with quantum mechanics compared to  $\langle \tilde{g}(\Delta E) \rangle$  that appears in FTs.

### 28.3.5 Deficiencies and Limitations of the CI

Despite its great success and its internal consistency, the CI also has a few deficiencies. One deficiency concerns very cold environments and the other occurs in dephasing interactions. These deficiencies are not inconsistencies but scenarios where the CI provides trivial and useless predictions.

In the limit of a very low temperature, the predictive power of the Clausius inequality is degraded. As  $T = \frac{1}{\beta} \rightarrow 0$ , the  $\beta q$  term diverges and the changes in the entropy of the system becomes negligible (the entropy changes in the system are bounded by the logarithm of the system's Hilbert dimension). Hence, in this limit, the CI reads  $\beta q \geq 0$ , which means that heat is flowing into this initially very cold bath. This is hardly a surprise. If the initial temperature is very low the microbath will be in the ground state. Thus, it is clear that any interaction with other agents can only increase its average energy.

Another trivial, and somewhat useless prediction of the CI is obtained in dephasing interactions. Such interactions satisfy  $[H_{int}, H_{sys}] = 0$  and typically also  $[H_{int}, H_{env}] = 0$ . Consequently, dephasing interactions do not affect the energy distributions of the system and the environment. However, they degrade the coherence in the energy basis of the system. Since there is no heat flow involved, the CI predicts  $\Delta S^{sys} \geq 0$ . This is a trivial result: any dephasing process can be written as a mixture of unitaries operating on the system only, and mixture of unitaries always increases the entropy due to the concavity of the von Neumann entropy.

In addition to these two deficiencies, two more obvious deficiencies should be mentioned. The first is the restriction to initially uncorrelated system and environment. In some important microscopic scenarios, this assumption is not valid [31–34]. This is not a limitation of the derivation in Sect. 28.3.1 since in the presence of an initial correlation it is easy to find scenarios which indeed violate the CI (e.g., [37]). Another limitation of the CI is that in some cases it does not deal with the quantities of interest. For example in Sect. 28.6.3, we discuss machines whose output cannot be expressed in terms of average energy changes or entropy changes. Hence, the CI does not impose a performance limit for these machines.

### 28.3.6 The Passive CI Form: Environment Energy Versus Heat

In this chapter we refer to  $q$ , the energy exchanged with the bath, as heat. However, this terminology ignores the fact that the final non-equilibrium state of the microbath may admit work extraction by applying a local unitary on the microbath. Moreover, some studies suggested using ‘squeezed thermal bath’ as fuel for quantum heat machines [38–40]. A squeezed microbath is obtained by applying a unitary  $U_{\mu b}$  to a microbath  $\rho_{\beta,sq}^{\mu b} = U_{\mu b} \rho_{\beta}^{\mu b} U_{\mu b}^\dagger$ . Since the thermal state has the lowest average energy for a given von Neumann entropy, any squeezing operation of a thermal state

increases the energy of the bath. Thus, the preparation of squeezed baths requires the consumption of external work.

Next, we use similar arguments to those in [41] (see also Chap. 2) to show that squeezing can be fully captured in a slightly modified version of the CI. For this, we need to introduce the notion of passive states [42, 43], ergotropy [44], and passive energy [41]. A passive state (passive density matrix) with respect to a Hamiltonian is one in which lower energy states are more populated than higher energy states. In addition, the passive density matrix has no coherences in the energy basis of the Hamiltonian. These states are called passive states since no transient local unitary (acting on the system alone) can reduce the average energy of a system prepared in this state. That is, no work can be extracted from such a state if at the end of the process the system Hamiltonian returns to its initial value (transient unitary). Passive states are discussed in detail in Sects. 28.4.1 and 28.4.2.

The maximal amount of work that can be extracted using local transient unitaries is called ergotropy [44]. It is obtained by bringing a non-passive density matrix into its passive form with respect to the Hamiltonian. Let  $\mathcal{E}$  denote the ‘passive energy’ [41] that is defined as the energy that remains after extracting all the ergotropy. It is the energy of the passive state associated with some initial non-passive state. Since unitaries do not change the eigenvalues of the density matrix, the initial non-passive state dictates the eigenvalues of the passive state. Therefore, the initial state uniquely determines the passive state up to degeneracies in the Hamiltonian. These possible degeneracies are not important in the present chapter.

The entropic form of the CI (28.14) holds regardless of squeezing, since squeezing is a local operation that does not change the local entropies. Applying unitary invariance of the VN entropy to squeezed microbaths we can write

$$\Delta S^{\mu b} = S(\rho_f^{\mu b}) - S(\rho_{sq}^{\mu b}), \quad (28.25)$$

as

$$\begin{aligned} \Delta S^{\mu b} &= S(U_f \rho_{fin}^{\mu b} U_f^\dagger) - S(U_i \rho_{sq,\beta}^{\mu b} U_i^\dagger) \\ &= S(\rho_{f,pass}^{\mu b}) - S(\rho_\beta^{\mu b}), \end{aligned} \quad (28.26)$$

where  $U_f$  is the unitary that takes the final state of the microbath into a passive state, and  $U_i$  is the unitary that takes the initial state of the microbath to a thermal passive state. Using (28.26) in (28.18) we get

$$\Delta S^{\mu b} = \beta \Delta \mathcal{E}^{\mu b} - D(\rho_{f,pass}^{\mu b} | \rho_\beta^{\mu b}), \quad (28.27)$$

where  $\Delta \mathcal{E}^{\mu b} = \text{tr}[(\rho_{f,pass}^{\mu b} - \rho_\beta^{\mu b}) H^{\mu b}]$  is the change in the passive energy (defined above) of the microbath. Next, we use (28.14) and (28.27) and obtain the passive form of the CI [41]

$$\Delta S^{sys} + \sum \beta_k \Delta \mathcal{E}_k \geq 0, \quad (28.28)$$

where  $\beta_k$  is the initial temperature of the unsqueezed  $k$ th microbath, and  $\mathcal{E}_k$  is the passive energy of the  $k$ th microbath. One can argue that  $\Delta\mathcal{E}_k$  is a more accurate definition of heat compared to  $\Delta\langle H_k \rangle$  as it excludes ergotropy [41, 45]. However, another point of view is that heat is related to energy that cannot be operationally extracted *in practice*. If retrieving the ergotropy from the bath is too complicated to implement then for all practical purposes all energy dumped into the microbath can be considered as heat. For macroscopic baths, direct work on the bath is usually not considered as it may often involve keeping track of phases of many interacting degrees of freedom. However, in the microscopic world where the size of the microbath may be comparable to that of the system, work extraction from a microbath is not an unreasonable operation. In conclusion, the decision whether to use (28.3) or (28.28) may strongly depend on the experimental capabilities in a specific setup.

That said, one of the nice features of the CI (28.3) is that it does not depend on heat and work separation or interpretation. It simply puts a limit on the changes in the average energy of the microbaths. Work and heat separation and the very definition of work become very obscure, and to some extent immaterial, when trying to define higher moments of work in the presence of initial coherences in the energy basis (see, for example, [46]). On the other hand, changes in higher moments of the energy of the system are well defined even in the presence of initial coherences (see Sect. 28.3.4). This is exploited in [6]. See [41, 47] for schemes that suggest some alternative separations of heat and work.

### 28.3.7 Quantum Coherence and the Clausius Inequality

The microscopic form of the CI (28.3) is so similar to the historical macroscopic form put together by Clausius (28.1), that one may wonder if (28.3) contains any quantum features at all. The difference between stochastic dynamics of energy population and quantum dynamics manifests in ‘coherences’: the off-diagonal elements of the density matrix that quantify quantum superposition of energy states. Coherence and its quantification is actively studied in recent years [48].

Removal of the system coherence by some process increases the entropy of the system. According to the CI the growth of entropy sets a bound on how much heat can be exchanged in such a decoherence process that affects only the off diagonal elements of the density matrix of the system. Indeed, as discussed in Sect. 28.3.5, by using a specific type of system-environment dephasing interactions it is possible to decohere the system without changing the energy of the system or the microbath (no heat flow). This thermodynamically irreversible process involves significant correlation buildup between the system and the microbath [49]. However, in [50] a protocol was suggested to remove the coherence in a reversible process.

The Kammerlander-Anders protocol [50] reversibly implements  $\rho_i \rightarrow \text{diag}(\rho_i)$  in two stages. In stage *I*, a unitary transformation is applied to the system, and brings it into an energy diagonal state. This step involves work without any entropy changes  $S'_I = S_I = S(\rho_i)$ . In stage *II* a standard reversible diagonal/stochastic state

preparation protocol [6, 12, 50, 51] is employed to change  $\text{diag}(\rho')$  to  $\text{diag}(\rho_i)$ . The details of this part of the protocol are not important. Only the entropy change in this stage is needed for our analysis

$$\Delta S_{II} = S[\text{diag}(\rho_i)] - S'_I = S[\text{diag}(\rho_i)] - S(\rho_i). \quad (28.29)$$

Note that this expression is always positive as it can be written in terms of quantum relative entropy

$$\Delta S_H = S[\text{diag}(\rho_i)] - S(\rho_i) = D[\rho_i | \text{diag}(\rho_i)] \geq 0. \quad (28.30)$$

The heat required to reversibly generate this entropy difference using a single-bath is given by the CI

$$q^{rev} = -T \Delta S_{II}. \quad (28.31)$$

Since the initial and final average energy are the same (same values of the diagonal elements, and the same Hamiltonian) it follows that the work in this reversible process is

$$W^{rev} = q^{rev} = T D[\rho_i | \text{diag}(\rho_i)] \geq 0. \quad (28.32)$$

Since the CI dictates  $q \geq q^{rev}$  it follows that  $W^{rev} \geq W$ . This result means that work can always be extracted by reversibly removing the coherence in a reversible way. Moreover, reversible protocols extract the maximal amount of work from coherences. Using the CI it was not necessary to describe the protocol in full detail (see [6, 50]) to obtain the optimal work extraction.

Another way to think of the thermodynamic role of coherence in the energy basis is to define the non-equilibrium free energy [12, 51]  $\mathcal{F}$  through the Clausius inequality (28.3). Starting with the CI

$$\Delta(S + \beta \Delta \langle H^{\mu b} \rangle) \geq 0, \quad (28.33)$$

and using energy conservation  $W + \Delta \langle H^{\mu b} \rangle + \Delta \langle H^{sys} \rangle = 0$  (no initial or final interaction terms), we get the non-equilibrium free energy form of the CI

$$W \leq -\Delta \mathcal{F}, \quad (28.34)$$

where  $\mathcal{F} = \langle H^{sys} \rangle - TS(\rho^{sys})$  is the non-equilibrium free energy [6, 12, 51]. As in the CI, (28.34) becomes an equality for reversible processes. Since  $S[\text{diag}(\rho^{sys})] \geq S(\rho^{sys})$ , (28.34) predicts that in a reversible coherence removal process the extracted work is  $W = -T\{S(\rho^{sys}) - S[\text{diag}(\rho^{sys})]\} > 0$  as obtained by the Kammerlander-Anders protocol described above.

Based on the derivations in the last two sections, we can add two more items to CI properties listed in Sect. 28.2.

- The passive CI can handle squeezed thermal baths.

- System coherences are taken into account, and play an important role in the microscopic CI.

## 28.4 Global Passivity Approach

### 28.4.1 Traditional Passivity and Work Extraction

As mentioned briefly in Sect. 28.3.6, passivity was broadly used in thermodynamics in the context of work extraction [41–44]. We start with the definition of passivity, and then exploit it in new ways [49]. Consider a system subjected to a transient pulse

$$H(t) = H_0 + H_{pulse}(t).$$

The pulse satisfies  $H_{pulse}(t \leq 0; t \geq \tau_{pulse}) = 0$  so after time  $\tau_{pulse}$ , the Hamiltonian returns to its initial form. However the final density matrix is modified  $\rho_f \neq \rho_0$  due to non-adiabatic coupling the pulse induced. Since this Hamiltonian generates a unitary transformation, all eigenvalues of the initial density matrix  $\lambda(\rho_0)$  must be conserved (in particular, the entropy is conserved). To maximize the amount of average energy the pulse is extracting from the system (work) we want to minimize the quantity

$$\Delta \langle H_0 \rangle = \text{tr}[\rho_f H_0] - \text{tr}[\rho_0 H_0]. \quad (28.35)$$

The second term is fixed by the initial condition, so the first term  $\text{tr}[\rho_f H_0]$  has to be minimized. Since the eigenvalues are conserved  $\lambda(\rho_f) = \lambda(\rho_0)$ , the minimal value of  $\text{tr}[\rho_f H_0]$  is obtained by making  $\rho_f$  diagonal in the energy basis and assigning lower energies with higher eigenvalues of the density matrix (probabilities). This is called the passive distribution. Writing  $\lambda_1^\downarrow \geq \lambda_2^\downarrow \geq \lambda_3^\downarrow \dots$  the passive density matrix with respect to the Hamiltonian is

$$\rho_{pass} = \sum_k \lambda_k^\downarrow |k^\uparrow\rangle\langle k^\uparrow|$$

where  $|k^\uparrow\rangle$  are the eigenstates of  $H_0$  sorted in energy-increasing order  $E_k \leq E_{k+1} \leq E_{k+2} \dots$  Alternatively stated, for a system starting in a passive state  $\rho_{pass}$  with respect to  $H_0$  it holds that

$$\Delta \langle H_0 \rangle_{pass \rightarrow fin} = \text{tr}[\rho_f H_0] - \text{tr}[\rho_{pass} H_0] \geq 0, \quad (28.36)$$

for any transient unitary (pulse-like operation). Moreover, from linearity, (28.36) also holds for any mixture of unitaries (28.9). As mentioned earlier, the maximal amount of work that can be extracted from an initial state using a transient unitary process is called ergotropy [44] and is equal to

$$erg = -(\text{tr}[\rho_{\text{pass}} H_0] - \text{tr}[\rho_0 H_0]) \geq 0.$$

Thermal states are passive with respect to the Hamiltonian, but not all passive states are thermal. It turns out that the relationship between thermal states and passive states has a more profound aspect. For a given  $\rho_0$  and  $H_0$  the passive state is determined up to degeneracies in  $H_0$ . If  $\rho_0$  is not specified, then a given Hamiltonian  $H_0$  has many possible passive states. However, thermal states are the only *completely passive* states. That is, when taking any number  $n$  of uncorrelated copies in a thermal state  $\rho_{\text{tot}} = \rho_{\beta}^{\otimes n}$  then  $\rho_{\text{tot}}$  is always passive with respect to the total Hamiltonian  $H_0 \otimes I \otimes I \cdots + I \otimes H_0 \otimes I \cdots + \cdots$  ( $I$  is the identity operator). In particular, the thermal state is the only state that remains passive in the limit  $n \rightarrow \infty$ . This is a very important property from the point of view of the second law. If the thermal state was not completely passive then by joining many identical thermal microbaths we could have obtained a non-passive state, and extract work from it, which is in contradiction to the second law. However as discussed earlier in Sect. 28.3.6, the CI is a bit more general as it can handle squeezed microbaths as well.

### 28.4.2 Global Passivity

It is important to understand that passivity is not a property of a state  $\rho$  or of an operator  $\mathcal{A}$ , it is a joint property of the pair  $\{\rho, \mathcal{A}\}$  (we will denote in calligraphic letter operators that are passive with respect to the initial state). While passivity was traditionally used to describe work extraction of from a system, in [49] it was suggested that passivity is a much more general concept that can be used for other operators (not just Hamiltonians) and to other objects (not just the system). Based on these observation it was shown in [49] that passivity plays a much more significant role in thermodynamics compared to the way it was used thus far.

First, we point out that there is no reason to limit passivity to be with respect to the Hamiltonian of the system or the bath. The definition above is applicable to any observable described by a Hermitian operator. For example given a state  $\rho_0$  in some basis one can ask what is the passive state with respect to the angular momentum operator. In what follows, not only that we will not use passivity with respect to the Hamiltonian, we will also use observables (operators) that involve the *whole* setup.

Second, in the context of passivity,  $\mathcal{A}$  is usually given (the Hamiltonian of the system or of a microbath), and the focus is on the passive state associated with it [41–44, 52, 53]. In [49] it was suggested to look on the opposite problem. Given an initial state (which may not be passive with respect to the Hamiltonian), what are the passive operators with respect to this state? That is, *what are the  $\mathcal{A}$ 's such that  $\Delta \langle \mathcal{A} \rangle \geq 0$  for any (transient) unitary transformation (28.8) or a mixture of unitaries (28.9)?*

Let  $\rho_0^{\text{tot}}$  be the density matrix that describes the total setup (system plus microbaths). A thermodynamic protocol is a sequence of unitary operations that describe system-environment interaction and interaction with external fields (e.g. a laser field)

that act as work repositories. The accumulated effect of this protocol is given by a global unitary  $U$  or by a mixture of unitaries (28.9).

Global passivity [49] is defined as follows: An operator  $\mathcal{B}$  is globally passive (i.e. passive with respect to  $\rho_0^{tot}$ ), if it satisfies

$$\Delta \langle \mathcal{B} \rangle \geq 0, \quad (28.37)$$

for any thermodynamic protocol (for any  $p_k$ , and  $U_k$  in (28.9)).

As we shall see for any initial preparation  $\rho_0^{tot}$  there are many families of globally passive operators. To systematically find the passive operators associated with  $\rho_0^{tot}$  we can use the fact that in thermodynamic processes  $\rho_0^{tot}$  is explicitly known (in contrast to  $\rho_f^{tot}$ ) and construct operators from it. The simplest choice with the strongest kinship to the CI is

$$\mathcal{B}^{tot} = -\ln \rho_0^{tot}. \quad (28.38)$$

We emphasize that this is a *time-independent operator* and its expectation value is linear in the instantaneous density matrix  $\rho_t^{tot}$ . That is, the expectation value at time  $t$  is  $\langle \mathcal{B}^{tot} \rangle_t = \text{tr}[\rho_t^{tot}(-\ln \rho_0^{tot})]$ . It is easy to verify that this operator is globally passive. According to (28.38) the probability of observing an eigenvalue  $\lambda_{\mathcal{B}}$  is  $p_{\lambda_{\mathcal{B}}} = e^{-\lambda_{\mathcal{B}}}$ . Hence, larger eigenvalues are associated with lower probabilities and we can conclude that  $\rho_0^{tot}$  and  $\mathcal{B}^{tot}$  form a passive pair, and therefore

$$\Delta \langle \mathcal{B}^{tot} \rangle \geq 0, \quad (28.39)$$

for any mixture of unitaries (28.9). The connection of the global passivity inequality (28.39) to the standard CI will be explored in the next section. However, a major difference already stands out: in contrast to the CI (28.39) holds for any initial  $\rho_0^{tot}$  even if the system and microbaths are all initially strongly correlated. Thus, (28.39) has the potential to go beyond a mere re-derivation of the CI.

### 28.4.3 The Observable-Only Analog of the CI

To see the first connection between (28.39) and the CI we assume the standard thermodynamics assumption on the initial preparation (28.2) and get that relation (28.39) now reads

$$\Delta \langle \mathcal{B}^{sys} \rangle + \sum_k \beta_k q_k \geq 0, \quad (28.40)$$

where  $\mathcal{B}^{sys}$  is a time-independent operator

$$\mathcal{B}^{sys} \doteq -\ln \rho_0^{sys}, \quad (28.41)$$

and as in Sect. 28.3.1,  $q_k = \Delta \langle H_k \rangle$  is the change in the average energy of the ‘ $k$ ’th microbath. Form (28.40) is linear in the final density matrix and involves only expectations values. Equation (28.40) looks similar to the CI (28.3), but instead of the change in the entropy  $\Delta S^{sys}$ , there is a change in the expectation value of the operator  $\mathcal{B}^{sys}$ . Before doing the comparison it is important to point out that in setups that consist of only microbaths and no system (e.g. in absorption refrigerator tricycles [54], or in a simple bath-to-bath heat flow) then both (28.40) and the CI reduce to  $\sum_i \beta_i q_i \geq 0$ . To quantitatively compare the standard CI and (28.40) in the general case, we use (28.18) to rewrite (28.40) as

$$\Delta S^{sys} + \sum_k \beta_k q_k \geq -D(\rho_f^{sys} \mid \rho_0^{sys}). \quad (28.42)$$

The term on the right-hand side is negative, which means that (28.40) is a weaker inequality compared to the CI. Nonetheless, (28.40) has an important merit. To experimentally evaluate  $\Delta S^{sys}$  a full system tomography is needed ( $S_f^{sys}$  is calculated from  $\rho_f^{sys}$ ). In contrast, for  $\Delta \langle \mathcal{B}^{sys} \rangle$  we need to measure only the expectation value of  $\mathcal{B}^{sys}$ . Not only that this involves only  $N$  elements out of the full  $N \times N$  density matrix of the system, the elements (probability in the basis of  $\mathcal{B}^{sys}$ ) need not be known explicitly. The average  $\langle \mathcal{B}^{sys} \rangle$  converges much faster compared to evaluation/estimation of the individual probabilities via tomography.

#### 28.4.4 ICCI - Initial Correlation Clausius Inequality

To get the full energy-information form of the CI (28.3), and to *go beyond* the standard validity regime (28.2), we introduce the notion of passivity-divergence relation [49]. We start by writing the identity (28.18) for the whole setup

$$\Delta \langle \mathcal{B}^{tot} \rangle \equiv \Delta S^{tot} + D(\rho_f^{tot} \mid \rho_0^{tot}) \quad (28.43)$$

where  $\mathcal{B}^{tot}$  is defined in (28.38). When a specific protocol described by a global unitary  $U$  is applied to the setup, then  $\Delta S^{tot} = 0$  since the eigenvalues of the total density matrix do not change in a unitary evolution. What if we have some noise in our controls that implements  $U$  and the evolution is described by a mixture of unitaries? In this case it holds that

$$\Delta S^{tot} \geq 0. \quad (28.44)$$

This result can be obtained from the concavity of the von Neumann entropy:

$$\begin{aligned} S(\rho_f^{tot}) &= S\left(\sum p_k U_k \rho_0^{tot} U_k^\dagger\right) \geq \\ &\geq \sum_k p_k S(U_k \rho_0^{tot} U_k^\dagger) = S(\rho_0^{tot}). \end{aligned} \quad (28.45)$$

Property (28.44) is not unique to the von Neumann entropy, it holds for any Schur concave function [23]. A density matrix  $\rho_f^{tot}$  generated by a mixture of unitaries is majorized by the initial density matrix  $\rho_0^{tot} \prec \rho_0^{tot}$  (see, e.g., [55]). Therefore, for any Schur concave function  $\mathcal{S}$ , it holds that  $\mathcal{S}(\rho_f^{tot}) \geq \mathcal{S}(\rho_0^{tot})$  [23]. Equation (28.44) should not be confused with (28.14) that describes the increase of the sum of reduced entropies when starting from uncorrelated state. While (28.14) contains the essence of the standard CI, (28.44) describes another layer of irreversibility created by the noise in the protocol. As we shall see shortly the CI will be obtained from (28.43) even when there is no randomness in the protocol and  $\Delta S^{tot} = 0$ .

Using (28.44) in (28.43), we obtain the ‘passivity-divergence relation’

$$\Delta \langle \mathcal{B}^{tot} \rangle \geq D(\rho_f^{tot} \mid \rho_0^{tot}). \quad (28.46)$$

This inequality can be viewed as a stronger version of passivity for the following reasons: First, global passivity (28.39) immediately follows from (28.46) due to the non-negativity of the quantum relative entropy. Second, (28.46) implies that the change in the expectation value is not only non-negative, but also larger than  $D(\rho_f^{tot} \mid \rho_0^{tot}) \geq 0$ . Equations (28.43)–(28.46) constitute an alternative way of proving (28.39).

The passivity-divergence relation (28.46) is expressed in terms of the setup states without any explicit reference to the system. To obtain an energy-information form (system’s information) we use the monotonicity property of relative entropy

$$D(\rho_f^{tot} \mid \rho_0^{tot}) \geq D(\rho_f^{sys} \mid \rho_0^{sys}). \quad (28.47)$$

This property follows from joint convexity of the quantum relative entropy and it holds for any  $\rho_f^{tot}, \rho_0^{tot}$  even in the presence of quantum or classical correlations. Mathematically, the quantum relative entropy is a *divergence*. Divergence is a measure that quantifies how different two density matrices are. In general, it is not a distance in the mathematical sense as it may not satisfy the triangle inequality. Equation (28.47) states that the disparity of the reduced states is smaller than the disparity of the total states. This is plausible since some of the differences are traced out. Nevertheless, there are divergences which do not satisfy this property. Using (28.46)–(28.47) we get

$$\Delta \langle \mathcal{B}^{tot} \rangle \geq D(\rho_f^{sys} \mid \rho_0^{sys}). \quad (28.48)$$

As we show next, it is this very step that generates an extended version of the CI. By applying (28.18) to the relative entropy of the system in (28.48) we get

$$\Delta \langle \mathcal{B}^{tot} \rangle \geq -\Delta S^{sys} + \Delta \langle \mathcal{B}^{sys} \rangle. \quad (28.49)$$

where  $\mathcal{B}^{sys}$  is defined by (28.41) even if the system is initially correlated to the environment. Rearranging we obtain the *initial correlation Clausius inequality* (ICCI) [49]

$$\Delta S^{sys} + \Delta \langle \mathcal{B}^{tot} \rangle - \Delta \langle \mathcal{B}^{sys} \rangle \geq 0, \quad (28.50)$$

For initially uncorrelated system and environment  $\rho_0^{tot} = \rho_0^{sys} \otimes \rho_0^{env}$  it holds that  $\mathcal{B}^{tot} = \mathcal{B}^{sys} \otimes I^{env} + I^{sys} \otimes \mathcal{B}^{env}$  and the ICCI reduces to the CI (28.24)

$$\Delta S^{sys} + \Delta \langle \mathcal{B}^{env} \rangle \geq 0. \quad (28.51)$$

Therefore, we conclude that in the presence of initial correlations the environment operator  $\mathcal{B}^{env}$  must be replaced by  $\mathcal{B}^{tot} - \mathcal{B}^{sys}$ . This is the content of the ICCI. The local environment expectation value is replaced by a global expectation value. If the environment is composed of microbaths initially prepared in a thermal state we get the standard CI (28.3). Note that the ICCI can also be written as

$$\Delta S^{sys} + \Delta \langle \mathcal{B}^{env} \rangle + \Delta \langle \mathcal{B}^{corr} \rangle \geq 0, \quad (28.52)$$

when

$$\mathcal{B}^{corr} = \mathcal{B}^{tot} - \mathcal{B}^{sys} \otimes I^{env} - I^{sys} \otimes \mathcal{B}^{env}, \quad (28.53)$$

and  $I^{sys}, I^{env}$  are identity operators. The correlation operator  $\mathcal{B}^{corr}$  becomes identically zero when  $\rho_0^{tot} = \rho_0^{sys} \otimes \rho_0^{env}$ . Note that  $\langle \mathcal{B}^{corr} \rangle_{t_0}$  is a measurable correlation quantifier of the initial state as it contains only expectation values (in contrast to mutual information, for example).

### The ICCI for a Coupled System-Environment Initial Thermal State

Next, we consider an important case where initial correlations naturally arise. In the setup in Fig. 28.1b there is a cold microbath and a hot microbath and the system is initially coupled to the hot microbath. We assume the system was coupled to the hot microbath while the hot microbath was prepared (e.g., by weak coupling to a macroscopic bath). As a result, the hot microbath is not in a thermal state, rather, the microbath plus the system are in a thermal state. Hence, the initial density matrix is

$$\rho_0^{tot} = \frac{1}{Z_{hs} Z_c} e^{-\beta_h (H_h + H_s + H_{int,0})} e^{-\beta_c H_c}. \quad (28.54)$$

Using this in the ICCI (28.50) we get:

$$\Delta S^{sys} + \beta_c q_c + \beta_h q_h + \beta_h \Delta \langle H_{int,0} \rangle + \beta_h (H_s - H_s^{eff}) \geq 0, \quad (28.55)$$

where the effective Hamiltonian is defined via  $\rho_0^{sys} = e^{-\beta H_s^{eff}} / Z$ . The  $Z$  normalization factor yields an additive constant that can be omitted so

$$H_s^{eff} \doteq -\frac{1}{\beta_h} \ln \rho_0^{sys} = -\frac{1}{\beta_h} \ln \text{tr}_h e^{-\beta_h (H_s + H_{int,0} + H_h)}. \quad (28.56)$$

Note that all the Hamiltonians on the right hand side of (28.56) refer to their value at time zero, and not to their possibly different instantaneous values. The term  $H_s^{eff} - H_s$  is known as the potential of mean force [31] or the solvation potential [34] (see also Chap. 21). The first three terms in (28.55) are the standard “bare” Clausius terms. The fourth term represents changes in the interaction energy and the last term is a system dressing effect. The last term represents the fact that the reduced state of the system is not the thermal state of the bare Hamiltonian of the system. See [49] for an explicit calculation of  $H_{sys}^{eff}$  for a dephasing interaction and a swap interaction.

The coupled thermal ICCI (28.55) has some similarity to the classical result in [32–36]. However, our result is valid also in the presence of coherences (in the energy basis) and quantum correlations that arise from the initial system-environment coupling.

### 28.4.5 An Outlook for the Global Passivity Approach

So far, we have used global passivity to extend the validity regime of the CI to the case of initial system-environment correlation. In doing so, we maintained the CI structure described in Sect. 28.3.2. Remarkably, global passivity can generate additional thermodynamic inequalities that involve different quantities. In [49] it was pointed out that since  $(\mathcal{B}^{tot})^\alpha$  and  $\mathcal{B}^{tot}$  have the same eigenvectors and the same eigenvalue ordering for  $\alpha > 0$  ( $(\mathcal{B}^{tot})^\alpha$  is a stretched/squeezed version of  $\mathcal{B}^{tot}$ ) it follows that  $(\mathcal{B}^{tot})^\alpha$  is also globally passive (with respect to  $\rho_0^{tot}$ ) and therefore

$$\Delta \langle (\mathcal{B}^{tot})^\alpha \rangle \geq 0, \quad (28.57)$$

for any  $\alpha > 0$  and for any thermodynamic protocol (28.9). These inequalities involve higher moments of the energy. In [49] it was exploited to detect “lazy Maxwell’s demons” (subtle feedback operations) and hidden heat leaks that the CI cannot detect. In addition, it was used to put a bound the build up of system-environment correlations in quantum dephasing scenarios. Hopefully, such inequalities will significantly extend the scope of the microscopic thermodynamic framework as discussed in Sect. 28.6.

## 28.5 CPTP Maps Approach

The previous derivation is based on global arguments that take into account the whole setup including the microbaths. In this section, we adopt a system point of view where the environment is represented by its action on the system. To simplify the notations, a single bath is considered in the section.

Using the definition of the relative entropy and the von Neumann entropy it is straightforward to verify that the following identity holds for any  $\rho_1, \rho_2, \rho_{ref}$

$$S(\rho_2) - S(\rho_1) + \text{tr}[(\rho_2 - \rho_1)(\ln \rho_{ref})] \equiv D(\rho_1|\rho_{ref}) - D(\rho_2|\rho_{ref}). \quad (28.58)$$

By taking  $\rho_{ref} = \rho_1$  in (28.58), (28.18) is obtained. Alternatively, by using (28.18) once for  $\rho_2$ ,  $\rho_{ref}$  and once for  $\rho_1$ ,  $\rho_{ref}$  it is possible to get (28.58). Focusing on the left hand side we see a familiar structure, entropy difference followed by a change in the expectation value of the Hermitian operator  $\ln \rho_{ref}$ . Next we choose  $\rho_2 = \rho_t^s$ ,  $\rho_1 = \rho_0^s$ ,  $\rho_{ref} = \rho_\beta^s = e^{-\beta H_s}/Z$  and get

$$\Delta S_{sys} - \beta \Delta \langle H_s \rangle \equiv D(\rho_0^{sys}|\rho_\beta) - D(\rho_f^{sys}|\rho_\beta). \quad (28.59)$$

Despite the close similarity to the CI expression, (28.59) is an identity void of any physical content. Our first step, then, is to assign a physical scenario to the left hand side. In order to identify the change  $\beta \Delta \langle H_s \rangle$  of the energy of the system with heat as in the CI, we need a scenario with zero work. Using the standard system-based definitions of work and heat

$$W = \int^t \text{tr} \left[ \rho_s \frac{d}{dt} H_s \right], \quad (28.60)$$

$$Q = \int^t \text{tr} \left[ H_s \frac{d}{dt} \rho_s \right], \quad (28.61)$$

we see that to have zero work, the Hamiltonian of the system has to be fixed in time. Such a process is called an isochore since it is the analog of the fixed volume process in macroscopic thermodynamics. Thus, for an isochore it holds that

$$\Delta S_{sys}^{ISC} - \beta Q^{ISC} = D(\rho_0^{sys}|\rho_\beta) - D(\rho_f^{sys}|\rho_\beta). \quad (28.62)$$

The identity sign was removed as this expression holds just for isochores. Now we are in position to focus on the right hand side.

### 28.5.1 Completely Positive Maps with a Thermal Fixed Point

Completely positive trace preserving maps (CPTP) are very useful in describing measurements, feedback, dephasing, and interaction with thermal baths. One way of representing CPTP maps is by using Kraus operators. This is a local approach where the environment is not explicitly described. Another way to describe a CPTP map is by interacting with an auxiliary system (environment). Any CPTP map  $\rho_f^s = M(\rho_0^s)$  can be written as

$$M(\rho_0^s) = \rho_f^s = \text{tr}_A[U \rho_0^{env} \otimes \rho_0^s U^\dagger], \quad (28.63)$$

where  $\rho_0^{env}$  is the initial density matrix of some environment and  $U$  is a global unitary that describes the system-environment interaction. CPTP maps have the following

monotonicity property for any two density matrices  $\rho, \sigma$  [22]

$$D(\rho|\sigma) \geq D[M(\rho)|M(\sigma)]. \quad (28.64)$$

That is, a CPTP map is “contractive” with respect to the quantum relative entropy divergence. Roughly speaking, operating with  $M$  on two distinct states make them more similar to each other. If  $M$  has a fixed point  $M(\rho_{FP}) = \rho_{FP}$ , (28.64) reads

$$D(\rho|\rho_{FP}) \geq D[M(\rho)|\rho_{FP}], \quad (28.65)$$

which means that when  $M$  is applied all  $\rho$ ’s “approach” the fixed point of the map. Next, we make the physical choice that in isochores where a system is coupled to a bath, the thermal state  $\rho_s = e^{-\beta(H_s - F_s)}$  is the fixed point. If we connect an already thermal system to a bath in the same temperature, nothing will happen. This is the CPTP equivalent of the zeroth law. This non-trivial feature has to be properly justified and in what follows we discuss the emergence of thermal fixed points in CPTP maps.

### Fixed Points of CPTP Maps

Let our environment be initialized at a Gibbs state  $\rho_\beta^b = e^{-\beta(H_b - F_b)}$  where  $F_b = -\frac{1}{\beta} \ln \text{tr}(e^{-\beta H_b})$ . Next, we assume that the interaction Hamiltonian  $H_{int}$  commutes with the total system-bath bare Hamiltonians

$$[H_{int}, H_s + H_b] = 0. \quad (28.66)$$

This guarantees that  $\langle H_s \rangle + \langle H_b \rangle = \text{const}$  and that no energy is transferred to the interaction energy. This condition also assures that no work has to be invested in coupling the system to the bath. In thermodynamic resource theory this condition is often written as  $[U, H_s + H_b] = 0$ . Under this condition, it follows that the thermal state of the system is a fixed point of the CPTP map since

$$\begin{aligned} M(\rho_\beta^s) &= \text{tr}_b[U \rho_\beta^b \otimes \rho_\beta^s U^\dagger] \\ &= \text{tr}_b[U e^{-\beta(H_s + H_b - F_s - F_b)} U^\dagger] \\ &= \text{tr}_b[e^{-\beta(H_s + H_b - F_s - F_b)} U U^\dagger] \\ &= \rho_\beta^s. \end{aligned} \quad (28.67)$$

See [56] for a discussion of the difference between Gibbs preserving maps and the map considered above.

There are other scenarios where fixed points occur. For example, if two baths are coupled simultaneously to the same levels of the system, the fixed point will not be thermal, in general. We call it a ‘leaky fixed point’ since in such cases even in steady state there is a constant heat flow (heat leak) between the baths. We will return to this point at the end of the section.

### 28.5.2 From Fixed Points to the Clausius Inequality

Under condition (28.66),  $\rho_\beta^s$  is a fixed point of a CPTP map obtained by interacting with an initially thermal environment. Using the contractivity (28.65) with respect to the thermal fixed point we get that for isochores (ISC)

$$\Delta S_{ISC}^{sys} - \beta Q_{ISC} \geq 0. \quad (28.68)$$

To extend this isochoore result to general thermodynamic scenarios we need to include the possibility of doing pure work on the system without contact with the bath. For a unitary transformation on the system (this may include either changing the energy levels in time, or applying an external field to change the population and coherences), it holds that the heat flow is zero

$$\frac{dQ}{dt} = \text{tr} \left[ \frac{d\rho^s}{dt} H(t) \right] = \text{tr} \{-i[H(t), \rho]H(t)\} = 0, \quad (28.69)$$

where we used the cyclic property of the trace in the last transition. Furthermore, the system entropy does not change under local unitaries, hence for unitary evolution (UNI)  $\Delta S_{UNI}^{sys} = 0$ ,  $Q_{UNI} = 0$ . The unitary evolution is the analog of the macroscopic thermodynamic adiabat. Now, if we have a sequence of an isochoore and a unitary, the Clausius term is

$$\Delta S - \beta Q = (\Delta S_{ISC} + \Delta S_{UNI}) + \beta(Q_{ISC} + Q_{UNI}) \quad (28.70)$$

$$= \Delta S_{ISC} + \beta Q_{ISC} \geq 0. \quad (28.71)$$

Hence,

$$\Delta S - \beta Q \geq 0, \quad (28.72)$$

for any concatenation of isochoores (thermal CPTP maps) and unitaries. One can show that other processes such as isotherms can be constructed from a concatenation of isochoores and adiabats [6, 57]. A similar analysis to the one given above appears in Chap. 10.

For isotherm,  $\Delta S = \beta Q$  and the reversible saturation of the CI is obtained. This can also be shown by direct integration. For isotherms, the state is always in a thermal state even when the Hamiltonian (slowly) changes in time. Therefore  $\rho_s = e^{-\beta(t)[H(t)-F(t)]}$  and  $H(t) = F(t) + T(t) \ln \rho^s(t)$  ( $F$  is a scalar matrix). Using it in the entropy definition we get

$$\Delta S = \int^t \text{tr} \left[ - \left( \frac{d}{dt} \rho_s \right) \ln \rho_s \right] = \int^t \text{tr} \left\{ \beta(t)[H(t) - F(t)] \frac{d}{dt} \rho_s \right\} = \int^t \beta \frac{dQ}{dt}. \quad (28.73)$$

where we have used  $\frac{d}{dt} \text{tr}(\rho_s) = 0$  for the second term. Note that  $Q$  represents the change in the energy of the system due to the interaction of the bath. However, since

we assumed that condition (28.66) holds, it follows that  $-Q = q = \Delta \langle H_b \rangle$ . Thus, we have retrieved the reversible saturation in an isothermal reversible process (for unitaries it is trivially satisfied).

This derivation has two main drawbacks. The first is that condition (28.66) does not always hold. In particular, in short interaction time, before the rotating wave approximation becomes valid, there are counter-rotating terms that do not satisfy (28.66). The second drawback concerns the ability of CPTP maps to describe a general interaction with a thermal bath. As mentioned earlier, a general protocol can be decomposed into adiabats and isochores. However, the assumption that at each isochore the fixed point is the thermal state requires that the bath be large and the coupling to it is weak. Weak coupling is needed in order to ensure negligible system-bath correlation at the beginning of each isochore (see (28.63)). This is necessary for using the CPTP contractivity property (28.64) and (28.65).

Interestingly, in the presence of heat leaks, the local fixed point approach may provide different predictions from the standard global approach to the CI. There is no contradiction between the local approach described above (28.72) and the CI, but they provide predictions on different quantities. Consider the case where a two-level system is connected simultaneously to two large thermal baths with temperature  $1/\beta_1$  and  $1/\beta_2$ . The fixed point of the two-level system will be some diagonal state with some intermediate temperature  $1/\beta_{eff}$  that depends on the interaction strength (thermalization rate) with each bath. In systems with more levels, the steady state will not be thermal in general. According to the local approach (28.72) the  $\beta$  that should be used in the CI is  $\beta_{eff}$  so that  $\Delta S - \beta_{eff} Q \geq 0$ . However, according to the global approach (28.24), we have  $\Delta S + \beta_1 q_1 + \beta_2 q_2 \geq 0$ . Both expressions are correct but they contain information on different quantities.

## 28.6 Outlook and Challenges

New approaches to the second law, as well as new mathematical tools such as those discussed in the previous sections (e.g. Sect. 28.4), lead to additional thermodynamic constraints on operations that involve thermal environments. In the context of the second law in microscopic setups, there are several main challenges that deserve further research:

- Strongly correlated thermal systems
- Correlation dynamics and higher order energy moments
- Exotic heat machines ('X machines')
- Heat leaks and feedback detection
- Deviation from the standard energy-information paradigm
- Fluctuation theorems and CI extensions

### 28.6.1 Strongly Correlated Thermal Systems

Consider a system composed of several dozen interacting particles, e.g., interacting spins in a lattice. The particles are initially in a thermal state. Next, a unitary operation (e.g., lattice shaking, or interactions with external fields) is applied to the setup and takes it out of equilibrium. When the particle number exceeds three dozen or so, the dynamics cannot be carried out numerically with present computational resources. Hence, thermodynamic predictions can be quite useful. Applying the second law to the whole setup yields a very trivial result. There is no change in entropy, and there is no heat exchange with some external environment. The energy changes in the setup are purely work related.

To understand the *internal* energy flows and *local* entropy changes, we need to choose some artificial partitioning according to our zone of interest. The zone of interest constitutes the ‘system’, and everything else is the ‘environment’ (even if it is very small and comparable to the system’s size). For example, the system can be a collection of a few neighboring spins or even a single spin. The system can even be disconnected, e.g., two non-adjacent spins or a sparse lattice that includes only a subset of the total number of spins (e.g., every second spin in a chain configuration). In all these examples, it is interesting how the *reduced* entropy of the zone of interest changes (the total entropy of the setup is conserved) when energy flows in and out of it. Due to the equilibrium interaction, the spins are initially correlated to each other. Consequently, the partitions suggested above cannot be studied with the CI. In contrast, the ICCI is suitable for this scenario. It is interesting to explore what insights the ICCI, (and other yet undiscovered thermodynamics constraints), can provide to this important scenario. See Chap. 34 for studies of non-equilibrium dynamics in isolated setups.

### 28.6.2 Correlation Dynamics and Higher Order Energy Moments

The changes in the first moment of the microbath energy (heat) are constrained by the CI. What about the second or even higher moments of the energy of the microbath or the system? The CI does not deal with these quantities. Does this mean that any change is possible, or perhaps there are analogs of the CI that limit higher order moments of the energy?

In large baths that to a good approximation remain in a thermal state it is enough to know the changes in the average energy to predict their final temperature. However, the final state of microbaths is typically a non-equilibrium state. Thus, information on changes in higher order moments of the energy becomes important. In [6] it was shown that in some scenarios it is possible to write Clausius-like inequalities for higher moments of the energy. Interestingly, it is shown that changes in higher-moments of the energy are associated with information measures that differ from the

von Neumann entropy. If the new Clausius-like inequalities are tight (become equalities) for reversible processes (as in [6]), it is expected that changes in non-extensive higher moments of the energy, be associated with non-extensive information measures. The work in [6] is based on the local approach presented in Sect. 28.5.2.

Higher order moments of the energy are also very important when the correlation buildup between system and bath is studied. The CI is based on the fact that elements that start uncorrelated become correlated. However, the CI does not set a bound on how big or how small these correlations should be in terms of observable quantities. Consider for example the system-bath covariance  $\text{cov}(H_s, H_b) \doteq \langle H_s H_b \rangle - \langle H_s \rangle \langle H_b \rangle$ . When it is zero the system and bath are uncorrelated and when it is equal to  $\sqrt{\text{var}(H_s)}\sqrt{\text{var}(H_b)}$  the system and bath are maximally correlated. Unlike mutual information, the covariance is an observable measure of correlation. However, it is quadratic in energy, and therefore not constrained by the second law. In [49] it was shown that in some cases global passivity framework imposes constraints on the covariance buildup. Moreover, system-environment correlations can develop between other observables. For example, in a spin decoherence setup [49], correlation builds up between the bath Hamiltonian and the initial polarization operator of the spin. It is interesting to find thermodynamic bounds on this covariance. The bounds in [49] have not been proven optimal or unique. Thus, this topic warrants further study.

### 28.6.3 Exotic Heat Machines

Similarly to standard heat machines such as engines or refrigerators, *exotic heat machines* (X machines) [58] are machines that exploit thermodynamic resources (i.e. work repositories and microbaths) to execute a task of interest. However, the task of the X machine is not cooling (reduction of the entropy or the average energy) or work extraction. The tasks of X machines, especially in the microscopic realm, can be much more fine-grained and customized for a specific scenario. Machines for entanglement generation have been suggested and studied in [59, 60].

As a concrete example of an X machine setup, consider a qutrit system such as that shown in Fig. 28.2. The system can interact with a three-spin environment that is initially prepared in a thermal state (microbath) with inverse temperature  $\beta$ . The goal of this setup is to deplete as much as possible the second level of the qutrit. This task is of importance when trying to inhibit an undesired interaction or chemical reaction associated with the second level of the qutrit. The task is carried out by some global unitary transformation on the qutrit and spins setup. Crucially, to accomplish this goal, we allow for both the entropy and the average energy of the qutrit to grow, as long as the population of the second level reduces. Thus, this task cannot be considered as cooling, heating, or work extraction. More formally, the task of this heat machine is to minimize the expectation value of a target operator  $\mathcal{A}_{\text{target}}$  which in this case equals to  $\mathcal{A}_{\text{target}} = |2_{\text{sys}}\rangle\langle 2_{\text{sys}}|$ .

On top of their potential practical value, X machines present us with fantastic and exciting thermodynamic challenges. The minimization of  $\langle \mathcal{A}_{\text{target}} \rangle$  may be

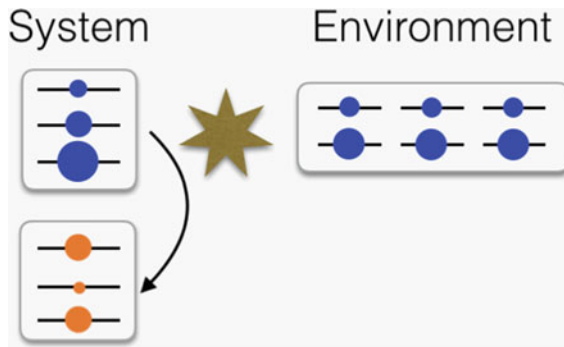


**Fig. 28.2** An example of an ‘X machine’ setup. These machines use thermal resources (a three-spin microbath in this case) to execute a non-thermodynamic task such as depleting the second level in the qutrit system. Since the goal of X machines is not to manipulate average energy or entropy, the second law does not set a performance bound for such machines.

completely unrelated to changes in the average energy or in the entropy. Thus, even in cases where the CI holds for X machines, it does not provide a performance bound. For example, how well can these machines perform as a function of the initial temperature of the environment and its size? To understand this, it is vital to find additional CI-like inequalities that will relate changes in  $\langle A_{target} \rangle$  (output), to changes in the microbath (resources). In analogy to reversible processes in conventional machines, it will be very appealing to find bounds that can be saturated by known protocols.

#### 28.6.4 Detecting Heat Leaks and Lazy Maxwell’s Demons

The CI has a clear regime of validity. If, for some reason, we find that in our setup the CI does not hold, we can conclude that the process in this setup is outside the regime of validity of the CI. The information on being outside the regime of validity can be used to deduce some conclusions on the cause of the anomaly. For example, in a Maxwell demon setup, if we see heat flowing from the cold bath to the hot bath without applying work (CI violation), we can deduce the existence of a Maxwell demon even if we do not observe the demon directly, only the outcome of its operation. Similarly, in thermodynamic setups in superconducting circuits, a violation of the CI may indicate that the intrinsic thermalization to the background temperature cannot be ignored. Thus, CI violation can provide information on the setup and on the processes that take place.

Next, we ask how far it is possible to push this notion of detection using the violation of thermodynamic inequalities. Perhaps the simplest scenario to consider is the “lazy Maxwell demon” [49]. The setup is initialized with cold molecules in one chamber and hot molecules in another. A Maxwell demon that controls a trap door between the chambers, measures the speed of the incoming molecules on both sides, and according to the results, it decides whether to open or close the door. If the demon performs properly, it can make the cold bath colder and the hot bath hotter. This violation of the CI occurs since feedback operations (the demon’s action) are

outside the regime of validity of the CI (unless the feedback mechanism is included in the setup [61]).

Consider the case where the demon is lazy, and it often dozes off while the trap door is open. In these cases, the average energy (heat) flows naturally from the hot bath to the cold bath. If the fraction of the time when the demon is awake is too small, the cold bath will get warmer, and the hot bath will get colder. Since in this case the CI is not violated, the demon cannot be detected using the CI. We ask if there are other thermodynamic inequalities that can detect the presence of feedback even when the first moment of the energies changes consistently with the CI. In [49] it was shown for a specific example that global passivity inequalities can detect lazy demons that the CI cannot detect. If, however, the feedback is too weak (a very lazy demon), even the global passivity inequalities may not be able to detect it.

Although the findings in [49] show that this kind of improved thermodynamic demon detection is possible, a big question still remains: can any feedback operation, even a very subtle one, be detected by some thermodynamic constraints on observables such as the CI? Most likely, the resolution of this question will lead to a more comprehensive thermodynamic framework.

### 28.6.5 Deviation from the Standard Energy-Information Paradigm

In this chapter, an emphasis has been put on the energy-information structure of the CI. However, in [62] a fluctuation theorem has been used to derive an elegant relation between average heat and a new type of measure  $B_Q$  that replaces the entropy change of the system. The  $B_Q$  measure is defined as

$$B_Q = -\ln \text{tr}(M\rho_0^s), \quad (28.74)$$

where

$$M = \text{tr}_E[U(\rho^{env} \otimes I^{sys})U^\dagger], \quad (28.75)$$

and  $U$  stands for the global evolution operator.  $M$  describes how a system identity state ( $I^{sys}/\text{tr}[I^{sys}]$ , super hot state), evolves under the operator  $U$ . The relation to heat found in [62] is

$$\beta q \geq B_Q. \quad (28.76)$$

It is both interesting and important to understand the advantages and disadvantages of  $B_Q$  (and similar measures) with respect to the CI.

As mentioned in Sect. 28.3.5, one of the deficiencies of the CI is its trivial prediction for extremely cold microbaths. It simply predicts that energy in this super cold bath will increase. This problem has been elegantly addressed for an harmonic oscillator system using a phase space approach [63]. For an initial Gaussian state, the authors find a CI-like relation between the purity and the heat. In the CI-like

expression in [63] the diverging  $\beta$  factor is replaced by an expression that does not diverge as  $\beta \rightarrow \infty$ .

Another interesting deviation from the standard energy-information employs catalysts and many copies of the same setup [47] (see also Chap. 33). Using the theorem described in [47] (see also [64]), it is possible to employ a global unitary and an external catalyst to change a given initial density matrix  $\rho_0$  to any isentropic state  $\rho_f$  such that  $S(\rho_f) = S(\rho_0)$ . Thus, it is possible to transform the initial state to a thermal state  $\rho_{\beta_{eff}}$ , whose temperature  $1/\beta_{eff}$  is chosen to satisfy  $S(\rho_0) = S(\rho_{\beta_{eff}})$ . Now, all initial non-equilibrium scenarios can be treated as if they are initially thermal with some effective temperature. For example, if there is a non-thermal reservoir one can write a Clausius inequality for it with  $1/\beta_{eff}$  as its initial temperature.

It is interesting to pursue these approaches and to find new approaches that can overcome the deficiencies of the CI.

### 28.6.6 Fluctuation Theorems and CI Extensions

As mentioned in Sect. 28.3.4, in their regime of validity, fluctuation theorems (FT) yield stronger statements than the CI, and they can reduce to the CI by using some mathematical inequalities such as the Jensen inequality. As described in Sect. 28.4.5 [49] and in Sect. 28.6.2 [6], non-trivial extensions of the CI can be derived. These extensions provide inequalities on new observables (e.g., higher order energy moments), and can extend the regime of validity of the CI (e.g., to initial system-environment correlations). It is fascinating to investigate if some of these new CI extensions (e.g. Eq. (28.57)) can be obtained from fluctuation theorems.

## References

1. R. Landauer, IBM J. Res. Dev. **5**, 183 (1961). <https://doi.org/10.1147/rd.53.0183>
2. D. Reeb, M.M. Wolf, New J. Phys. **16**, 103011 (2014). <https://doi.org/10.1088/1367-2630/16/10/103011>
3. F. Brandão, M. Horodecki, N. Ng, J. Oppenheim, S. Wehner, Proc. Natl. Acad. Sci. **112**, 3275 (2015). <https://doi.org/10.1073/pnas.1411728112>
4. M. Horodecki, J. Oppenheim, Nat. Commun. **4**, 2059 (2013). <https://doi.org/10.1038/ncomms3059>
5. M. Lostaglio, D. Jennings, T. Rudolph, Nat. Commun. **6**, 6383 (2015). <https://doi.org/10.1038/ncomms7383>
6. R. Uzdin, Phys. Rev. E **96**, 032128 (2017). <https://doi.org/10.1103/PhysRevE.96.032128>
7. G. Gour, M.P. Müller, V. Narasimhachar, R.W. Spekkens, N. Yunger Halpern, Phys. Rep. **583**, 1 (2015). <https://doi.org/10.1016/j.physrep.2015.04.003>
8. N. Yunger Halpern, J.M. Renes, Phys. Rev. E **93**, 022126 (2016). <https://doi.org/10.1103/PhysRevE.93.022126>
9. N. Yunger Halpern, J. Phys. A Math. Theor. **51**, Art (2018). <https://doi.org/10.1088/1751-8121/aaa62f>

10. R. Uzdin, A. Levy, R. Kosloff, Entropy **18**, 124 (2016). <https://doi.org/10.3390/e18040124>
11. A. Peres, *Quantum Theory: Concepts and Methods*, vol. 57 (Springer Science & Business Media, Berlin, 2006). <https://doi.org/10.1007/0-306-47120-5>
12. M. Esposito, C. Van den Broeck, EPL (Europhys. Lett.) **95**, 40004 (2011). <https://doi.org/10.1209/0295-5075/95/40004>
13. T. Sagawa, *Lectures on Quantum Computing, Thermodynamics and Statistical Physics*, vol. 8 (2012), p. 127
14. P. Strasberg, G. Schaller, T. Brandes, M. Esposito, Phys. Rev. X **7**, 021003 (2017). <https://doi.org/10.1103/PhysRevX.7.021003>
15. M. Lostaglio, D. Jennings, T. Rudolph, New J. Phys. **19**, 043008 (2017). <https://doi.org/10.1088/1367-2630/aa617f>
16. Y. Guryanova, S. Popescu, A.J. Short, R. Silva, P. Skrzypczyk, Nat. Commun. **7**, 12049 (2016). <https://doi.org/10.1038/ncomms12049>
17. N. Yunger Halpern, P. Faist, J. Oppenheim, A. Winter, Nat. Commun. **7**, 12051 (2016). <https://doi.org/10.1038/ncomms12051>
18. M. Esposito, K. Lindenberg, C. Van den Broeck, New J. Phys. **12**, 013013 (2010). <https://doi.org/10.1088/1367-2630/12/1/013013>
19. C. Jarzynski, J. Stat. Phys. **96**, 415 (1999). <https://doi.org/10.1023/A:1004541004050>
20. S. Deffner, C. Jarzynski, Phys. Rev. X **3**, 041003 (2013). <https://doi.org/10.1103/PhysRevX.3.041003>
21. S. Deffner, E. Lutz, Phys. Rev. Lett. **105**, 170402 (2010). <https://doi.org/10.1103/PhysRevLett.105.170402>
22. M.A. Nielsen, I. Chuang, *Quantum Computation and Quantum Information* (2002)
23. A.W. Marshall, I. Olkin, B.C. Arnold, *Inequalities: Theory of Majorization and Its Applications*, vol. 143 (Springer, Berlin, 1979). <https://doi.org/10.1007/978-0-387-68276-1>
24. P. Oscar Boykin, T. Mor, V. Roychowdhury, F. Vatan, R. Vrijen, Proc. Nat. Acad. Sci. **99**, 3388 (2002). <https://doi.org/10.1073/pnas.241641898>
25. R. Uzdin, S. Gasparinetti, R. Ozeri, R. Kosloff, New J. Phys. **20**, 063030 (2018). <https://doi.org/10.1088/1367-2630/aae932>
26. C. Jarzynski, Annu. Rev. Condens. Matter Phys. **2**, 329 (2011). <https://doi.org/10.1146/annurev-connatphys-062910-140506>
27. T. Speck, U. Seifert, J. Stat. Mech. Theory Exp. **2007**, L09002 (2007). <https://doi.org/10.1088/1742-5468/2007/09/L09002>
28. R. Harris, G. Schütz, J. Stat. Mech. Theory Exp. **2007**, P07020 (2007). <https://doi.org/10.1088/1742-5468/2007/07/P07020>
29. M. Campisi, J. Pekola, R. Fazio, New J. Phys. **17**, 035012 (2015). <https://doi.org/10.1088/1367-2630/17/3/035012>
30. C. Jarzynski, Phys. Rev. Lett. **78**, 2690 (1997). <https://doi.org/10.1103/PhysRevLett.78.2690>
31. J.G. Kirkwood, J. Chem. Phys. **3**, 300 (1935). <https://doi.org/10.1063/1.1749657>
32. U. Seifert, Phys. Rev. Lett. **116**, 020601 (2016). <https://doi.org/10.1103/PhysRevLett.116.020601>
33. H.J.D. Miller, J. Anders, Phys. Rev. E **95**, 062123 (2017). <https://doi.org/10.1103/PhysRevE.95.062123>
34. C. Jarzynski, Phys. Rev. X **7**, 011008 (2017). <https://doi.org/10.1103/PhysRevX.7.011008>
35. P. Strasberg, M. Esposito, Phys. Rev. E **95**, 062101 (2017). <https://doi.org/10.1103/PhysRevE.95.062101>
36. P. Strasberg, M. Esposito, Phys. Rev. E **99**, 012120 (2019). <https://doi.org/10.1103/PhysRevE.99.012120>
37. K. Micadei, J.P. Peterson, A.M. Souza, R.S. Sarthour, I.S. Oliveira, G.T. Landi, T.B. Batalhão, R.M. Serra, E. Lutz (2017), [arXiv:1711.03323](https://arxiv.org/abs/1711.03323)
38. J. Roßnagel, O. Abah, F. Schmidt-Kaler, K. Singer, E. Lutz, Phys. Rev. Lett. **112**, 030602 (2014). <https://doi.org/10.1103/PhysRevLett.112.030602>
39. G. Manzano, F. Galve, R. Zambrini, J.M. Parrondo, Phys. Rev. E **93**, 052120 (2016). <https://doi.org/10.1103/PhysRevE.93.052120>

40. G. Maslennikov, S. Ding, R. Hablitzel, J. Gan, A. Roulet, S. Nimmrichter, J. Dai, V. Scarani, D. Matsukevich, Nat. Commun. **10**, 202 (2019). <https://doi.org/10.1038/s41467-018-08090-0>
41. W. Niedenzu, V. Mukherjee, A. Ghosh, A.G. Kofman, G. Kurizki, Nat. Commun. **9**, 165 (2018). <https://doi.org/10.1038/s41467-017-01991-6>
42. W. Pusz, S. Wornwicz, Commun. Math. Phys. **58**, 273 (1978), <https://projecteuclid.org/euclid.cmp/1103901491>
43. A. Lenard, J. Stat. Phys. **19**, 575 (1978). <https://doi.org/10.1007/BF01011769>
44. A.E. Allahverdyan, R. Balian, Th.M. Nieuwenhuizen, Euro. Phys. Lett. **67**, 565 (2004). <https://doi.org/10.1209/epl/i2004-10101-2>
45. F. Binder, S. Vinjanampathy, K. Modi, J. Goold, Phys. Rev. E **91**, 032119 (2015). <https://doi.org/10.1103/PhysRevE.91.032119>
46. M. Perarnau-Llobet, E. Bäumer, K.V. Hovhannisyan, M. Huber, A. Acín, Phys. Rev. Lett. **118**, 070601 (2017). <https://doi.org/10.1103/PhysRevLett.118.070601>
47. M.N. Bera, A. Riera, M. Lewenstein, A. Winter (2017). [arXiv:1707.01750](https://arxiv.org/abs/1707.01750)
48. A. Streltsov, G. Adesso, M.B. Plenio, Rev. Modern Phys. **89**, 041003 (2017). <https://doi.org/10.1103/RevModPhys.89.041003>
49. R. Uzdin, S. Rahav, Phys. Rev. X **8**, 021064 (2018). <https://doi.org/10.1103/PhysRevX.8.021064>
50. P. Kammerlander, J. Anders, Sci. Rep. **6**, 22174 (2016). <https://doi.org/10.1038/srep22174>
51. S. Still, D.A. Sivak, A.J. Bell, G.E. Crooks, Phys. Rev. Lett. **109**, 120604 (2012). <https://doi.org/10.1103/PhysRevLett.109.120604>
52. M. Perarnau-Llobet, K.V. Hovhannisyan, M. Huber, P. Skrzypczyk, J. Tura, A. Acín, Phys. Rev. E **92**, 042147 (2015a). <https://doi.org/10.1103/PhysRevE.92.042147>
53. M. Perarnau-Llobet, K.V. Hovhannisyan, M. Huber, P. Skrzypczyk, N. Brunner, A. Acín, Phys. Rev. X **5**, 041011 (2015b). <https://doi.org/10.1103/PhysRevX.5.041011>
54. A. Levy, R. Kosloff, Phys. Rev. Lett. **108**, 070604 (2012). <https://doi.org/10.1103/PhysRevLett.108.070604>
55. F.C. Binder, Work, heat, and power of quantum processes. Ph.D. thesis, School University of Oxford, 2016
56. P. Faist, J. Oppenheim, R. Renner, New J. Phys. **17**, 043003 (2015). <https://doi.org/10.1088/1367-2630/17/4/043003>
57. J. Anders, V. Giovannetti, New J. Phys. **15**, 033022 (2013). <https://doi.org/10.1088/1367-2630/15/3/033022>
58. R. Uzdin, In Preparation
59. J.B. Brask, G. Haack, N. Brunner, M. Huber, New J. Phys. **17**, 113029 (2015). <https://doi.org/10.1088/1367-2630/17/11/113029>
60. F. Tacchino, A. Auffèves, M. Santos, D. Gerace, Phys. Rev. Lett. **120**, 063604 (2018). <https://doi.org/10.1103/PhysRevLett.120.063604>
61. H.S. Leff, A.F. Rex, *Maxwell's Demon: Entropy, Information, Computing* (Princeton University Press, Princeton, 2014)
62. J. Goold, M. Paternostro, K. Modi, Phys. Rev. Lett. **114**, 060602 (2015). <https://doi.org/10.1103/PhysRevLett.114.060602>
63. J.P. Santos, G.T. Landi, M. Paternostro, Phys. Rev. Lett. **118**, 220601 (2017). <https://doi.org/10.1103/PhysRevLett.118.220601>
64. C. Sparaciari, D. Jennings, J. Oppenheim, Nat. Commun. **8**, 1895 (2017). <https://doi.org/10.1038/s41467-017-01505-4>

# Chapter 29

## Information Erasure



Toshio Croucher, Jackson Wright, André R. R. Carvalho, Stephen M. Barnett  
and Joan A. Vaccaro

### 29.1 Introduction

The origin of thermodynamics is intimately related to the development of heat engines in the 18th century. Understanding the connections between macroscopic quantities such as pressure, volume and temperature, as well as the interplay between work and heat in engine cycles, led to the formulation of the fundamental laws underpinning thermodynamical transformations. The analysis of the Carnot heat engine, for example, is the root behind the second law of thermodynamics.

The thermodynamical behaviour of macroscopic systems can also be understood as emerging from microscopic dynamical laws and the intrinsic statistical uncertainty about the state of the system. This statistical approach to thermodynamics, pioneered by Maxwell, Boltzmann, and Gibbs, brought to centre stage the concept of information, which is our main concern in this chapter. Perhaps the first instance where information and thermodynamics are linked together is in the scenario of Maxwell's demon, where a hypothetical microscopic intelligent being is able to follow the state of individual molecules and act on the system to apparently violate the second law. For recent experiments on Maxwell's demon, we refer the reader to Chaps. 39 and 40.

While Maxwell himself [1] seemed to be open to the possibility that our conclusions about the behaviour of macroscopic systems may simply not be applicable to

---

T. Croucher · J. Wright · A. R. R. Carvalho · J. A. Vaccaro (✉)  
Centre for Quantum Dynamics, Griffith University, 170 Kessels Road,  
Brisbane, QLD 4111, Australia  
e-mail: J.A.Vaccaro@griffith.edu.au

S. M. Barnett  
School of Physics and Astronomy, University of Glasgow, Kelvin Building,  
University Avenue, Glasgow G12 8QQ, United Kingdom

situations where individual constituents can be observed and manipulated<sup>1</sup>, most of the subsequent work on Maxwell's demon paradox focused on trying to reconcile the second law with the underlying dynamical microscopic description of the system [2, 3].

An important contribution in this direction was made by Szilard [4], who designed a single molecule heat engine that would work in apparent violation of the second law, provided that information about the partition occupied by the molecule were measured and recorded. Szilard circumvents this violation by asserting that such acquisition of information would necessarily incur on an entropy increase not less than  $k_B \ln(2)$ , although he doesn't pinpoint when such an increase occurs in his engine cycle. Subsequently, Brillouin [5, 6] showed that the same entropy bound follows from the act of measurement itself, narrowing down the possible source of entropy cost.

A few years later, in principle in an unrelated context, Landauer [7] investigated the question of the physical cost of performing basic computation. Using the simplest irreversible logical operation of resetting an unknown bit of information, Landauer showed that this *erasure* process would require a minimum of  $k_B T \ln(2)$  of energy to be dissipated as heat into the environment surrounding the bit. But it was only twenty years later that Bennett [8, 9] established the connection between Landauer's erasure principle and the Maxwell's demon problem. Moreover, Bennett also proposed a reversible measurement scheme that wouldn't involve thermodynamical costs, proving that the real reason why the demon doesn't violate the second law is the necessity to erase the demon's memory rather than any energy costs associated with measuring and storing the information.

Formulating the problem in information-theoretical terms allows one to detach the statistical aspects of the theory from the specificities of any physical realization, a view that is at the core of Jaynes' maximum entropy principle [10, 11]. This principle states that, in order to make inferences based on partial information about a system, one must use the probability distribution that maximises the entropy subject to this information constraint. The probability distribution resulting from this maximisation procedure has exactly the same form of the distribution obtained using traditional methods in statistical mechanics but without requiring the enumeration of states, or the knowledge of the physical properties of the system and its constants of motion. An important consequence of this approach is that one is allowed to move away from a standpoint where energy plays a privileged role in the theory and treat different conserved quantities on equal footing.

But not until 2006 was the potential of Jaynes' generalisation of statistical mechanics for erasure and heat engines appreciated [12, 13]. Vaccaro and Barnett realised that under Jaynes' framework, it was natural to question the special role of energy in Landauer's erasure mechanism. In their work, for example, they propose an erasure

<sup>1</sup>Maxwell states in his book [1]: "This is only one of the instances in which conclusions which we have drawn from our experience of bodies consisting of an immense number of molecules may be found not to be applicable to the more delicate observations and experiments which we may suppose made by one who can perceive and handle the individual molecules."

that works at the cost of angular momentum rather than energy. Much in the same spirit, an extension of Landauer's principle using arbitrary degrees of freedom has been recently considered under a resource theoretical framework [14, 15]. For an overview on a resource theory approach, and the role of multiple conserved quantities in quantum thermodynamics, please refer to Chaps. 26 and 31, respectively.

This brings us back to where we started: the cornerstone of thermodynamics, the heat engine. Since Landauer's principle explains that an erasure step is required to allow Szilard's engine to work without violating the second law, the ideas put forward in [12, 13] indicate that heat engines can work with a single thermal reservoir, as long as there is another process that takes care of the erasure as, for example, a reservoir of another conserved quantity. In fact, any physical resource that could account for the increase in entropy in the reservoir as it absorbs the entropy from the erased information would be an equally valid choice. A notable resource in this context is quantum correlations. In [16], for example, Alicki *et al.* have shown that work can be extracted from an initially entangled composite quantum system with the aid of single local reservoirs, while, in [17], del Rio et al. have proposed an erasure procedure assisted by a quantum memory entangled to the system.

Here, we will focus on the analysis of information erasure using multiple conserved quantities and its impact on heat engines design. It should be noted, however, that there is a vast body of literature on other aspects of Landauer's erasure principle, including alternative derivations [18, 19] and extensions and improvements on Landauer's bound [20].

This chapter is organised as follows. In the next section, we discuss in more detail the principles of information erasure, from Landauer's energetic cost to Vaccaro-Barnett's approach in terms of multiple conserved quantities. Then, we describe how these ideas can be used to design fundamentally different heat engines. Finally, we discuss fluctuation theorems associated with erasure and end with a discussion.

## 29.2 The General Principles of Information Erasure

We should be clear from the outset what is meant by erasing information. In particular, we need to distinguish between *losing* knowledge about a system and *resetting* its state. For example, the state of an open system may evolve from a pure state to a mixed state by interacting with its environment. As the pure state represents complete knowledge of the system and the mixed state represents incomplete knowledge, our knowledge of the system is lost over time. The extreme case where the state becomes maximally mixed represents a complete loss of knowledge. However, to say that information has been erased in this case would not be following conventional terminology, although this use is occasionally found in the literature [21]. Rather, the term erasure is more-often reserved for the quite distinct task of resetting the state of a system. An example of setting a state is given by the state preparation that typically occurs at the beginning of an experiment in many branches of quantum physics. Resetting would occur if the same system is reused for a subsequent experiment.

Landauer was interested in the task of resetting the memory systems of computing machines. For each particular computation performed by the machine, the state of the memory system encodes a corresponding result and, in this context, the state represents information. However, the resetting task needs to be independent of any particular computation, and so must be capable of resetting a memory system that contains an arbitrary result. As an arbitrary result is represented by a mixed state, the objective of resetting is to replace such a state with a pure reset state. This is the conceptual framework of *erasure of information*: the arbitrary information that is encoded in the memory system is erased by physically manipulating the memory system so that it evolves from the associated mixed state into the pure reset state. In this context, it is particularly interesting to consider the memory initially in a maximally mixed state, as it represents a complete lack of knowledge on the system and, consequently, incurs in the maximum cost of erasure.

To explore how information erasure can be performed, let the memory system be a two state system whose state space is spanned by the basis  $\{|0\rangle, |1\rangle\}$  labelled according to corresponding binary values, and let the reset state be  $|0\rangle$ . The erasure process needs to replace the maximally mixed state  $\frac{1}{2}(|0\rangle\langle 0| + |1\rangle\langle 1|)$  with the pure state  $|0\rangle\langle 0|$ . This requires the two orthogonal states  $|0\rangle$  and  $|1\rangle$  to be mapped to the same state  $|0\rangle$ , which rules out a unitary operation on the memory system alone. It can, however, be represented by a unitary SWAP operation on the combination of the memory and an ancillary system that has been prepared in the reset state  $|0\rangle$ , i.e.

$$\frac{1}{2}(|0\rangle\langle 0| + |1\rangle\langle 1|)_M \otimes |0\rangle\langle 0|_A \xrightarrow{\text{SWAP}} |0\rangle\langle 0|_M \otimes \frac{1}{2}(|0\rangle\langle 0| + |1\rangle\langle 1|)_A \quad (29.1)$$

where  $M$  and  $A$  label the memory and ancilla density operators, respectively. Of course, this immediately raises the question of the preparation of the state of the ancilla. According to Jaynes' maximum entropy (MaxEnt) principle, without knowing anything about the history of the ancilla, the best state that describes it is a maximally mixed one. In other words, in the absence of prior knowledge, all the states of the ancilla should be equally probable. The situation of ancilla being freely available in the reset state  $|0\rangle$  is, therefore, an unlikely one and so using a SWAP operation merely defers the problem of erasure to the preparation of the ancilla system. To avoid this problem, we need to consider an erasure process that make use of freely available resources.

Thermal reservoirs at a fixed temperature  $T$ , such as the temperature of the local environment, are regarded as freely available [22, Chap. 25]. As such, the task of erasure needs to be cast in terms of transferring the entropy from the memory system into a thermal reservoir at finite temperature  $T$ . This is essentially the problem that Landauer considered [7].

If the erasure is to be most efficient it should be reversible and, fortunately, this makes calculating the minimal physical effort of an erasure process easy to quantify. As the total entropy of the memory and reservoir system is fixed for a reversible process, any change of  $\Delta S_M$  in the entropy of the memory is accompanied by an opposing change of  $\Delta S_R = -\Delta S_M$  in the entropy of the reservoir. If the reservoir is

sufficiently large that its temperature  $T$  remains constant throughout the erasure, it will absorb the corresponding amount  $Q_R = T \Delta S_R$  of heat in the process. The 1 bit of information that is erased from the memory represents a change in Gibbs entropy of  $\Delta S_M = -k_B \ln(2)$ , where  $k_B$  is Boltzmann's constant, and so  $Q_R = k_B T \ln(2)$ . This is Landauer's result that the minimal cost of the erasure of 1 bit of information is the dissipation of heat of  $k_B T \ln(2)$  in the surroundings [7]. Landauer did not prescribe any particular method for the erasure process, rather he asserted only that a minimum heating effect accompanies the erasure of information in general, and gave the example of heat of  $k_B T \ln(2)$  per bit being transferred to the surroundings under equilibrium conditions [7]. This general effect is now known as Landauer's erasure principle.

It is instructive to have a simple dynamical model of an erasure process, and one that serves this purpose well involves doing work on the memory system to slowly increase the gap in the energy of its states  $|0\rangle$  and  $|1\rangle$  while keeping it in thermal equilibrium with the reservoir at fixed temperature  $T$ . This is similar to one of the work extraction models in [16], but done in the erasure context. Let the energy gap  $E$  be produced by increasing the energy of the state  $|1\rangle$  by a small amount,  $dE$ , while keeping the energy of the state  $|0\rangle$  unchanged. As the memory system is maintained in thermal equilibrium with the reservoir, its state when the energy gap is  $E$  is described by the density operator

$$\hat{\rho} = \frac{|0\rangle\langle 0| + e^{-E/k_B T}|1\rangle\langle 1|}{1 + e^{-E/k_B T}}. \quad (29.2)$$

The work required to increase the gap from  $E$  to  $E + dE$  is given by the probability,  $p_1$ , of the occupation of the state  $|1\rangle$  multiplied by  $dE$ , that is  $dW = p_1 dE$ , where  $p_1 = e^{-E/k_B T} (1 + e^{-E/k_B T})^{-1}$ . The total work done in increasing the gap from zero to infinity<sup>2</sup> is  $W_M = \int dW = k_B T \ln 2$  [7]. At the same time as the gap increases from  $E$  to  $E + dE$ , heat of  $dQ = Edp_1$  is transferred between the memory and the reservoir. Writing  $E = k_B T \ln[(1 - p_1)/p_1]$  and integrating over  $p_1$  from  $\frac{1}{2}$  to 0 gives the total heat transferred as  $Q_M = -k_B T \ln(2)$  and so heat of  $Q_R = -Q_M = k_B T \ln(2)$  is transferred to the reservoir, as before. Once the work process is completed, the memory system will be in the reset state  $|0\rangle$ . It is then thermally isolated from the reservoir and the energy degeneracy of its states is restored without any further work cost or gain. The process can be described as follows:

**Erasure by increasing energy gap:** *entropy is transferred from the memory system to the reservoir, under equilibrium conditions and the conservation of energy, as the energy gap between the information-carrying states of the memory system is slowly increased.*

We now use this description to generalise Landauer's erasure principle. Landauer repeatedly justified his claim that “information is physical” on the basis that information is inevitably tied to physical degrees of freedom and thus to physical laws [23]. An implicit consequence of this is that there is a minimal *physical cost* associated

---

<sup>2</sup>In practical terms, the fact that the probability  $p_1$  reduces exponentially with  $E$ , means the work process may be halted at a finite value of the gap for a correspondingly small probability of error.

with the erasure of information. Although he regarded the transfer of entropy from the memory system to the surroundings as an essential part of erasure, he demonstrated the physical cost only in terms of *heat and energy* [7, 23]. In our description of a specific erasure process, energy appears in two important contexts: in the physical cost of increasing the energy gap, and as a conserved quantity. If the conserved quantity was something other than energy, then the cost of the erasure process might also be in terms of the different quantity and not energy. It was a rumination of this kind that led to our generalisation of Landauer's principle [12, 13, 24, 25]. Taking account of Jaynes' generalisation of Gibbs ensemble for the case where the state of the reservoir involves multiple physical observables  $\hat{V}_k$  for  $k = 1, 2, \dots$  allows us to find the general cost of erasing information as follows [25]. The role played by the  $k$ th observable  $\hat{V}_k$  is like that of energy in conventional thermodynamics and, following Jaynes [10], will be referred to as the  $k$ th type of energy. The density operator giving the best description of the reservoir when the averages  $\langle \hat{V}_k \rangle$  are known can be obtained using the MaxEnt principle, which corresponds to maximising the von Neumann entropy

$$S = -\text{Tr} [\hat{\rho} \ln \hat{\rho}] \quad (29.3)$$

given the constraints

$$\text{Tr} [\hat{\rho} \hat{V}_k] = \langle \hat{V}_k \rangle, \quad (29.4)$$

$$\text{Tr} [\hat{\rho}] = 1. \quad (29.5)$$

The solution, obtained using Lagrange multipliers, is given by [10]

$$\hat{\rho} = \exp \left( -\mu - \sum_k \lambda_k \hat{V}_k \right), \quad (29.6)$$

with the corresponding entropy and partition function being, respectively,

$$S = \mu + \sum_k \lambda_k \langle \hat{V}_k \rangle, \quad (29.7)$$

and

$$Z = \text{Tr} \left[ \exp \left( - \sum_k \lambda_k \hat{V}_k \right) \right]. \quad (29.8)$$

Here,  $\mu = \ln Z$  and  $\lambda_k = -\partial S / \partial \langle \hat{V}_k \rangle$  are the Lagrange multipliers associated with the constraints on normalisation and on the averages of the  $k$ th type of energies, respectively. Allowing changes in  $\hat{V}_k$  to be independent of those of the state of the reservoir implies that the corresponding changes  $\langle \delta \hat{V}_k \rangle$  and  $\delta \langle \hat{V}_k \rangle$  are independent,

and so [10]

$$\delta S = \sum_k \lambda_k \delta Q_k \quad (29.9)$$

where

$$\delta Q_k \equiv \delta \langle \hat{V}_k \rangle - \langle \delta \hat{V}_k \rangle \quad (29.10)$$

corresponds to the  $k$ th type of heat. Rearranging Eq. (29.10) as

$$\delta U_k = \delta W_k + \delta Q_k \quad (29.11)$$

expresses the first law for  $\hat{V}_k$  in terms of the change  $\delta U_k \equiv \delta \langle \hat{V}_k \rangle$  in the  $k$ th type of internal energy, the amount  $\delta W_k \equiv \langle \delta \hat{V}_k \rangle$  of the  $k$ th type of work done on the reservoir, and the amount  $\delta Q_k$  of the  $k$ th type of heat transferred to it.

If this more general reservoir is used for the erasure of 1 bit of information in a reversible, and thus efficient, manner then the total entropy of the reservoir and memory system will be unchanged. Allowing for irreversible processes, the information erased from the memory appears as an increase of  $\Delta S \geq \ln(2)$  nats in the entropy of the reservoirs and, from Eq. (29.9), this implies

$$\sum_k \lambda_k \Delta Q_k \geq \ln(2) \quad (29.12)$$

which was first derived in Ref. [25]. This result represents the reservoir gaining an entropy of at least  $\ln(2)$  nats by the transfer of different types of heat  $\Delta Q_k$  to the reservoir with the only restriction being that their  $\lambda_k$ -weighted sum is bounded below by  $\ln(2)$ . There are a number of comments to make about this result. The first is that if the cost is paid in only one type of heat, say for  $k = 1$ , it can be expressed as

$$\Delta Q_1 \geq \frac{\ln(2)}{\lambda_1} . \quad (29.13)$$

In the case where  $\hat{V}_1$  is the operator for energy  $\hat{H}_R$ , the Lagrange multiplier  $\lambda_1$  is the inverse temperature  $\beta = 1/k_B T$ , the change  $\Delta Q_1$  is the heat  $Q$ , and we recover Landauer's result  $Q = k_B T \ln(2)$  [7]. Alternatively, in the case where  $\hat{V}_1$  is the  $z$  component of spin angular momentum  $\hat{J}_z$ , the Lagrange multiplier  $\lambda_1$  is the corresponding inverse spin temperature  $\gamma$ . For a reservoir consisting of  $N$  spin 1/2 systems, the inverse temperature is explicitly given by  $\gamma = \ln [(1 - \alpha)/\alpha]/\hbar$ , where  $\alpha$  is the fraction of particles in the spin up state [24]. The change  $\Delta Q_1$  is the spin-equivalent of heat  $Q_s$  called *spintherm* [26], where

$$Q_s \equiv \delta \langle \hat{J}_z \rangle - \langle \delta \hat{J}_z \rangle , \quad (29.14)$$

and we recover our previous result [25, 27]

$$\mathcal{Q}_s \geq \gamma^{-1} \ln(2) . \quad (29.15)$$

Lostaglio et al. [28] have shown how the cost of erasing 1 bit of information can be paid in varying amounts of heat  $Q$  and spintherm  $\mathcal{Q}_s$  satisfying  $\ln(2) = \beta Q + \gamma \mathcal{Q}_s$ .

The description given above for a specific erasure method can easily be generalised to accommodate this versatility in the cost of erasure as follows:

**Erasure by increasing arbitrary eigenvalue gap:** *entropy is transferred from the memory system to the reservoir, under equilibrium conditions and the conservation of the set of observables  $\{\hat{V}_k : k = 1, 2, \dots\}$ , as the gap between the eigenvalues associated with the information-carrying eigenstates of an observable  $\hat{V}_j$  of the memory system is slowly increased.*

The erasure process is additive in the sense that it can be applied in a sequence of stages, each one erasing successively more information. The choice for the index  $j$  and the amount of information erased in each stage determines the proportion of the corresponding cost  $\Delta Q_j$  in Eq. (29.12) [28].

### 29.3 Erasure of Information Carried by Discrete Variables

The descriptions of the specific erasure processes in the preceding section assume that the eigenvalues corresponding to the information-carrying eigenstates of the observable  $\hat{V}_j$  can be varied continuously. In the particular case of energy, although the information-carrying states may belong to a discrete portion of the eigenvalue spectrum, the spacing of the spectrum can be adjusted, in principle, through the use of an external potential. However, observables such as angular momentum do not have this possibility for fundamental reasons and so they call for special treatment. In this section, we use the  $z$  component of spin angular momentum,  $\hat{J}_z$ , as our prototypical discrete observable to illustrate the kinds of issues that arise.

Although it is not possible to vary the eigenvalues of a spin observable, an increase in the gap between the information-carrying eigenstates can be *simulated* as follows. Consider a memory system composed of a spin- $\frac{1}{2}$  particle where  $\hat{V}_j$  corresponds to the  $z$  component of angular momentum and the information-carrying states are its eigenstates. By augmenting the memory spin with a collection of ancilla spin- $\frac{1}{2}$  particles, it is possible to select pairs of eigenstates of the  $z$  component of total angular momentum whose eigenvalues differ by  $\Delta J_z = n\hbar$  for  $n = 1, 2, \dots$ . A sequence of pairs with increasing differences, i.e.  $\Delta J_z = \hbar, 2\hbar, \dots$ , can be used as the information-carrying states as described in Refs. [24, 25]. The operation of transferring the information from one pair to the next in the sequence requires the corresponding  $k$ th type of work, i.e.

$$\mathcal{L}_s \equiv \langle \delta \hat{J}_z \rangle , \quad (29.16)$$

which has been called *spinlabor* [26]. However, as the increase in the gap is not continuous but rather in steps of  $\hbar$ , the simulation is only approximate. Nevertheless, the erasure process will be approximately quasi-static provided this step size is small compared to the spin temperature, i.e.  $\hbar \ll \gamma^{-1}$ . Being not quite reversible, the actual cost of erasure in this case would be higher than the lower bound in Eq. (29.15).

Another issue that arises when treating a spin- $\frac{1}{2}$  memory system is that the memory requires angular momentum of  $\frac{1}{2}\hbar$ , on average, to go from the initial maximally-mixed state,<sup>3</sup>

$$\frac{1}{2}(|\uparrow\rangle\langle\uparrow| + |\downarrow\rangle\langle\downarrow|)_M , \quad (29.17)$$

to the reset state  $|\uparrow\rangle\langle\uparrow|_M$ , where  $|\downarrow\rangle, |\uparrow\rangle$  are the eigenstates of  $\hat{J}_z$  corresponding to the eigenvalues  $-\frac{1}{2}\hbar, \frac{1}{2}\hbar$ , respectively. This increases the amount of spinlabor needed as follows. The first law for  $\hat{J}_z$  is given, according to Eq. (29.11) with the definitions Eqs. (29.14) and (29.16), by

$$\delta\langle\hat{J}_z\rangle_R = \mathcal{L}_{s,R} + \mathcal{Q}_{s,R} , \quad \delta\langle\hat{J}_z\rangle_{MR} = \mathcal{L}_{s,MR} + \mathcal{Q}_{s,MR} , \quad (29.18)$$

for the reservoir (labeled  $R$ ) and the memory-reservoir combined system (labeled  $MR$ ), respectively. Taking note of the facts that spin angular momentum and spinlabor are additive, i.e.  $\delta\langle\hat{J}_z\rangle_{MR} = \delta\langle\hat{J}_z\rangle_M + \delta\langle\hat{J}_z\rangle_R$  and  $\mathcal{L}_{s,MR} = \mathcal{L}_{s,M} + \mathcal{L}_{s,R}$ , respectively, no spinlabor is performed on the reservoir, i.e.  $\mathcal{L}_{s,R} = 0$ , the erasure produces the change  $\delta\langle\hat{J}_z\rangle_M = \frac{1}{2}\hbar$  in the memory, and no spintherm is exchanged between the memory-reservoir combined system and its environment, i.e.  $\mathcal{Q}_{s,MR} = 0$ , reveals [26]

$$\mathcal{Q}_{s,R} = \mathcal{L}_{s,M} - \frac{1}{2}\hbar . \quad (29.19)$$

This shows that  $\frac{1}{2}\hbar$  of the spinlabor  $\mathcal{L}_{s,M}$  is retained by memory and the remainder is dissipated as spintherm in the reservoir. If, instead, the reset state was  $|\downarrow\rangle\langle\downarrow|_M$ , the result would be

$$\mathcal{Q}_{s,R} = \mathcal{L}_{s,M} + \frac{1}{2}\hbar , \quad (29.20)$$

i.e. there would be an additional contribution of  $\frac{1}{2}\hbar$  to the spintherm of the reservoir due the change in the state of the memory. The same value of  $\mathcal{Q}_s$  occurs in Eqs. (29.19) and (29.20)—it is the spintherm associated with a transfer of  $\ln(2)$  in entropy to the reservoir and it is bounded below by Eq. (29.15). The values of the spinlabor  $\mathcal{L}_{s,M}$  in Eqs. (29.19) and (29.20) are, however, different and reflect the physical effort needed for different tasks.

<sup>3</sup>We use subscripted labels  $M$  and  $R$  to distinguish quantities associated with the memory and reservoir, respectively, when confusion might otherwise arise.

Finally, discrete observables also allow different kinds of erasure mechanisms. We briefly describe here one that arises within the framework of the central spin problem; its full details may be found in Ref. [29]. The memory is represented by the central spin, typically an electron, and the reservoir is a collection of spins, typically nuclei, that surround it. We assume the hyperfine interaction between the electron and nuclei is the dominant interaction and that other interactions can be ignored. Let the reservoir comprise spin- $\frac{1}{2}$  particles that are initially in the fully polarised spin-up state  $|0\rangle_R \equiv |\uparrow\uparrow\cdots\rangle_R$  where the 0 represents no particle is spin down. In general, we will write  $|n\rangle_R$  to represent a future-evolved state of the reservoir that is a sum of different permutations of  $n$  nuclei spin down and the remainder spin up. The memory is initially in the mixed state given by Eq. (29.17) and the hyperfine interaction induces the memory and reservoir to exchange spin angular momentum at a particular rate, flipping the spin of the memory in a way that conserves total angular momentum. Note however, that the state  $|\uparrow\rangle_M|0\rangle_R$  is a fixed point of the evolution because exchanging spin is not possible, whereas the state  $|\downarrow\rangle_M|0\rangle_R$  evolves to  $|\uparrow\rangle_M|1\rangle_R$  at half the spin flipping period. This situation is represented by the mapping<sup>4</sup>

$$|\uparrow\rangle_M|0\rangle_R \xrightarrow{\text{HF}} |\uparrow\rangle_M|0\rangle_R \quad (\text{fixed point}) \quad (29.21)$$

$$|\downarrow\rangle_M|0\rangle_R \xrightarrow{\text{HF}} |\uparrow\rangle_M|1\rangle_R . \quad (29.22)$$

Applying the mapping to the initial state of the memory and reservoir gives

$$\frac{1}{2}(|\uparrow\rangle\langle\uparrow| + |\downarrow\rangle\langle\downarrow|)_M \otimes |0\rangle\langle 0|_R \xrightarrow{\text{HF}} |\uparrow\rangle\langle\uparrow|_M \otimes \frac{1}{2}(|0\rangle\langle 0| + |1\rangle\langle 1|)_R . \quad (29.23)$$

which shows that entropy is transferred from the memory to the reservoir. The memory is therefore erased and the reservoir has lost some of its polarisation as illustrated in Fig. 29.1a. The principle underlying this kind of erasure is that the reset state of the memory, i.e.  $|\uparrow\rangle_M$ , is a fixed point of the evolution for the reservoir state  $|0\rangle_R$  whereas the other memory state  $|\downarrow\rangle_M$  is not.

Attempting to repeat the erasure a second time, however, faces the problem that the reset state  $|\uparrow\rangle_M$  is not a fixed point of the evolution for the reservoir state  $|1\rangle_R$  and so an error would result as illustrated in Fig. 29.1b. There is a 25% chance that this situation will occur. Fortunately, there is a way to circumvent this problem [29]. Applying a spatially-varying, pulsed magnetic field orientated along the  $z$  direction will induce relative phase shifts between the nuclei depending on their position and their spin state. This induces the mapping, illustrated in Fig. 29.1c,

$$|n\rangle_R \xrightarrow{\text{MP}} |n, \mathbf{t}\rangle_R \quad (29.24)$$

---

<sup>4</sup>For brevity, we ignore irrelevant phase factors when writing down states of the memory and reservoir.

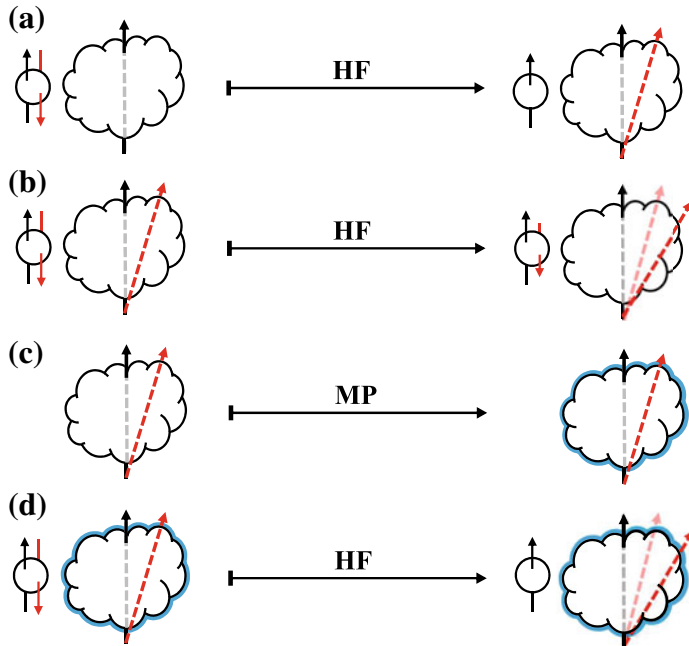


**Fig. 29.1** Sketches representing the mappings for the partial fixed-point erasure process. The circle represents the memory spin and the cloud represents the spin reservoir. Arrows represent the direction of spin angular momentum and their colours represent different states in a statistical mixture. The effect of the magnetic pulse on the reservoir is represented by a blue halo. Panel **a** represents the mapping induced by the hyperfine interaction in Eq. (29.23) for erasing the first bit of information, **b** represents the incomplete erasure when the same mapping is applied to the second bit, **c** represents the mapping induced by a spatially-varying magnetic pulse in Eq. (29.26), and **d** represents the complete erasure of the second bit following the magnetic pulse.

where the label  $\mathbf{t}$  characterises the pulse. An appropriately designed magnetic pulse will have the effect that  $|\uparrow\rangle_M|n, \mathbf{t}\rangle_R$  is essentially a fixed point of the hyperfine evolution as illustrated in Fig. 29.1d.<sup>5</sup> The combination of the hyperfine interaction and appropriate magnetic pulses gives the general mappings:

$$\frac{1}{2}(|\uparrow\rangle\langle\uparrow| + |\downarrow\rangle\langle\downarrow|)_M \otimes |n, \mathbf{t}\rangle\langle n, \mathbf{t}|_R \xrightarrow{\text{HF}} |\uparrow\rangle\langle\uparrow|_M \otimes \frac{1}{2}(|n, \mathbf{t}\rangle\langle n, \mathbf{t}| + |n+1, \mathbf{t}\rangle\langle n+1, \mathbf{t}|)_R \quad (29.25)$$

$$|n, \mathbf{t}\rangle\langle n, \mathbf{t}|_R \xrightarrow{\text{MP}} |n, \mathbf{t}'\rangle\langle n, \mathbf{t}'|_R. \quad (29.26)$$

The erasure process can, therefore, be operated multiple times in cycles involving the hyperfine interaction for an appropriate duration followed by a brief magnetic pulse. It can be described as follows:

---

<sup>5</sup>The fixed point condition is not satisfied exactly, however, it can be approached with small error, in principle.

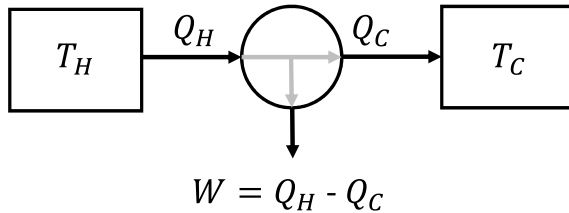


**Fig. 29.2** A Carnot engine diagram: The heat  $Q_H$  flows from a hot body of temperature  $T_H$  to the colder body  $T_C$  by the second law of thermodynamics. Not all the heat flows to the cold body, any excess is represented by mechanical or electrical work on the engine's environment.

**Erasure by partial fixed point evolution:** *entropy is transferred from the memory system to the reservoir by ensuring the reset state of the memory is a fixed point of the memory-reservoir interaction, and the unwanted state of the memory evolves into the reset state.*

In the following section we show how it can be used in a heat engine to erase information in the working fluid.

## 29.4 Connection with Heat Engines

As discussed in the previous sections, Landauer’s erasure reconciles Maxwell’s demon with the second law of thermodynamics. As a consequence, heat engines, powered by an intelligent being or any mechanical equivalent, must still work under the bounds of a Carnot cycle. This means that the heat  $Q_H$  extracted from a hot reservoir is only partially converted into the work  $W$  as shown in Fig. 29.2. Under Landauer’s principle, the difference  $Q_H - W$  represents the internal work that is needed to erase the demon’s memory and be dissipated into the cold reservoir as waste heat  $Q_C$ .

This situation is radically changed when multiple conserved quantities are considered. In this case, since one does not need to rely on energy to erase the memory [12, 13, 24, 25], it is therefore possible to design an engine where the output work amounts to *all* of the heat extracted from a single thermal reservoir, as shown in Fig. 29.3. It must be noted that there is no “free lunch” and that the cost of dumping the entropy from the system still needs to be paid. It is just that, under this new paradigm, the cost can be paid using a different “currency”, chosen from whatever other conserved quantity is available for use. Modern information-theoretical approaches to thermodynamics recognise this possibility, with a number of contributions describing the interplay between multiple conserved quantities in the cost of thermodynamical transformations [30–32].

In the situation considered in [12, 13, 24, 25], the erasure cost is given specifically in terms of angular momentum. A generalised heat engine based on this scenario is depicted in Fig. 29.3, where the cold thermal bath is replaced by a polarized spin angular momentum reservoir. Following the work of Vaccaro and Barnett, we call

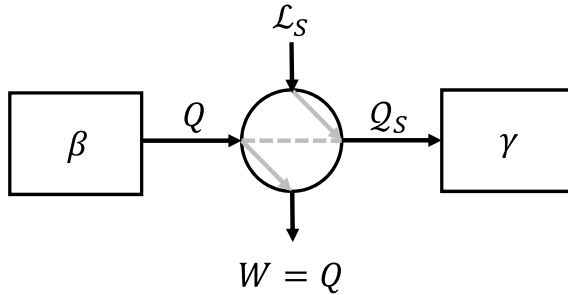


**Fig. 29.3** The conceptual diagram of the VB spin-heat engine (SHE): The work  $W$  output is equal to the heat  $Q$  extracted from the thermal reservoir at inverse temperature  $\beta$  leaving entropy in the working fluid. The entropy in the working fluid is erased at a cost of spinlabor  $L_s$  which is dissipated as spintherm  $Q_s$  in the spin reservoir. The spin reservoir has its own inverse spin temperature  $\gamma$ .

this conceptual engine the VB spin-heat engine (SHE). The thermodynamical transformations in this engine take into account not only heat and work, but also the exchange of the previously defined *spinlabor*  $L_s$  and *spintherm*  $Q_s$ . In contrast to the Carnot engine where the increase of entropy happens within the cooler thermal reservoir by heat flow, the SHE's entropy increases as a result of information erasure by dissipating an amount of spinlabor as spintherm into the spin reservoir, as shown in Fig. 29.3. Overall, the thermal reservoir cools down, and the spin reservoir experiences a reduction of polarisation to extract work.

Wright et al. [29] have recently designed an implementation of this generalised heat engine in a quantum dot system. The working fluid is represented by an electron trapped inside the quantum dot, which has an electronic level structure in a  $\Lambda$  configuration with two energy degenerate ground states. The thermal and spin reservoirs in the diagram of Fig. 29.3 are represented, respectively, by the phonons in the crystal and by the nuclear spin of the nuclei surrounding the confined electron.

This quantum dot SHE works in three distinct stages. First, the electron is initially prepared in the ground state with spin up ( $g_\uparrow$ ). Then a red-detuned Raman pulse is applied such that thermal energy  $Q$  from the phonon reservoir is required for the transition to the spin down ground state ( $g_\downarrow$ ) to occur, resulting in heat being converted into work  $W$  in the form of coherent light. Note that in this process  $W = Q$  but there is also an amount of spinlabour  $L_s = -\hbar$  provided to the dot by the laser pulse. A successful work extraction stage is marked by the transfer of electronic population from  $g_\uparrow$  to  $g_\downarrow$ . For the cycle to be complete, this information need to be erased, and the population reset to the original ground state  $g_\uparrow$ . This is achieved through the hyperfine interaction between the electron and the nuclei spins as described in Sect. 29.3. Since the two ground states are energy degenerate, the cost of information erasure in this last process is solely given in terms of spintherm,  $Q_s$ , corresponding to the decrease in nuclear spin polarisation.

## 29.5 Fluctuations

The expressions of the cost of erasure in Eqs.(29.12), (29.13) and (29.15) are in terms of average values taken over many experimental runs. Each average value has an associated probability distribution with a finite spread, and so each run can result in an outcome that differs from the average value. It is possible, therefore, that the cost of erasure in one run of an experiment can *violate* the expressions given above. Single values such as the standard deviation have long been used as measures of the extent any particular outcome may differ from the average. However, the last three decades has seen the development of methods for studying the detailed statistics of the fluctuations in the outcomes over many runs [33, 34]. Multiple chapters in this book deal with this kind of problem and we refer to Chaps. 10, 11, 12, 13, 14, 15, 35, 36, 37, 38 and 39 for more information on Fluctuation Theorems and the Jarzynski Equality.

For example, Dillenschneider and Lutz [35] found the probability that the heat  $Q$  dissipated in the reservoir in erasing 1 bit in one run of an experiment will violate Landauer's bound by the amount  $\epsilon$  is given by

$$P(Q < \beta^{-1} \ln 2 - \epsilon) < \exp(-\epsilon\beta), \quad (29.27)$$

that is, the probability of violation falls off exponentially with  $\epsilon$  and the inverse temperature  $\beta = 1/k_B T$ . Another way to say this is that large fluctuations are exponentially suppressed.

The corresponding Jarzynski equality [36] for the work  $W$  performed in the erasure is

$$\langle \exp(-\beta W - \Delta F) \rangle = 1 \quad (29.28)$$

where  $\Delta F = -\beta^{-1} \ln(Z_f/Z_i)$  is the change in free energy and  $Z_i$  and  $Z_f$  are the initial and final partition functions. Note that  $\Delta F$  has just one particular value over all experimental runs whereas the work  $W$  fluctuates from one run to the next. In the case of the erasure of 1 bit of information  $\Delta F = \beta^{-1} \ln 2$ . Using Jensen's equality [37] with (29.28) yields

$$\langle W \rangle \geq \beta^{-1} \ln 2 \quad (29.29)$$

which shows that the bound is satisfied on average, as expected. These results assume that the erasure is carried out quasi-statically, i.e. very slowly, and have been verified experimentally in an ion trap using a  $\text{Ca}^+$  ion by Xion et al. [38]. An experimental investigation of the fluctuations as the rate of the erasure process increases has also been reported by Bérut, Petrosyan and Ciliberto [39] using a silica bead in an optical trap.

In contrast to the continuous variables treated above, we have analysed the fluctuations in the spinlabor cost  $\mathcal{L}_s$  in the discrete case [26]. The problem involved

erasing of 1 bit of information stored in a spin- $\frac{1}{2}$  memory using a spin reservoir and the increasing gap erasure process described in Sect. 29.3. The variable  $\hat{V}_k$  in this case is  $\hat{J}_z$ , the  $z$  component of angular momentum, and the bound on the total angular momentum cost for the particular problem studied is

$$\Delta J_z \geq \frac{\ln 2}{\gamma} , \quad (29.30)$$

which implies

$$\mathcal{L}_s \geq \frac{\ln 2}{\gamma} - Q_s . \quad (29.31)$$

We found the fluctuations in  $\mathcal{L}_s$  are described by the Jarzynski-like equality:

$$\langle \exp(-\gamma \mathcal{L}_s + \ln 2) \rangle = \frac{1 + e^{-\gamma \hbar}}{1 + e^{-2\gamma \hbar}} = A . \quad (29.32)$$

The non-unity value on the right side reflects the fact that the initial state of the memory, being maximally mixed, corresponds to a zero inverse spin temperature and is, therefore, out of equilibrium with the spin reservoir whose inverse spin temperature,  $\gamma$ , is finite. This initial disequilibrium represents another feature that can occur when information is encoded using discrete observables. Using Eq. (29.32) and standard analytical techniques, we find the probability that the spinlabor cost will violate the bound in Eq. (29.31) by  $\epsilon$  is given by

$$P(\mathcal{L}_s \leq \gamma^{-1} \ln 2 - \epsilon) \leq A \exp(-\gamma \epsilon) \quad (29.33)$$

which, apart from the factor  $A$ , has the same form as Eq. (29.27). However, using a semi-analytic method, we also found a tighter bound for  $\hbar \gamma < 1$  given by

$$P(\mathcal{L}_s \leq \gamma^{-1} \ln 2 - \epsilon) \leq C \exp\left(-\sqrt{\frac{\gamma}{\hbar}} \epsilon\right) , \quad (29.34)$$

where  $C = P(\mathcal{L}_s \leq \gamma^{-1} \ln 2)$ . That is, in the high spin-temperature limit (i.e.  $\gamma^{-1} \gg \hbar$ ), large fluctuations are exponentially suppressed to a greater degree in comparison to the corresponding energy case in Eq. (29.27). In this regime, the spins in the reservoir approach their maximally mixed state, and evidently this constrains the fluctuations.

## 29.6 Discussion

The history of the link between information and thermodynamics is a long and interesting one. Some of the key steps were the discussion by Maxwell of his demon

[1], Szilard's observation that acquiring information could be associated with an entropy reduction [4] and, of course, Shannon's theory of communications, which definitively determined that entropy is the mathematical measure of information [40]. Our topic in this chapter has been information erasure, which Landauer famously linked with a minimum energy cost using thermodynamic principles, much as Szilard had done [7]. We have shown, however, that the energy cost is not fundamental and that the cost of erasure can be paid by expending other resources in place of energy [12, 13, 24, 25, 28]. Yet, the link between information erasure and thermodynamics raises interesting questions for the second law of thermodynamics, although we must be careful to keep in mind Eddington's warning "*But if your theory is found to be against the second law of thermodynamics I can give you no hope; there is nothing for it but to collapse in deepest humiliation.*" [41]

The strength of the link between Landauer's erasure principle and the second law was made clear by Schumacher who showed that defeating Landauer's principle would enable us to break the second law and also that if we can violate the second law then we can also erase information without incurring the energy cost demanded by Landauer's principle [42]. We have seen that it is possible to erase information without incurring the energy cost and this necessarily implies a modification of the second law of thermodynamics and, indeed, points to the necessity of modifying it by replacing the familiar thermodynamical entropy by the more general expression (29.7). Thus, logically, we may trace the origins of generalisations of the second law [22, 43] back to information erasure without an energy cost. Perhaps we might even adopt the entropic cost of information erasure as a physical principle.

**Acknowledgements** J.A.V. thanks the Australian Research Council (LP140100797) and the Lockheed Martin Corporation for financial support. S.M.B. thanks the Royal Society for support (RP150122).

## References

1. J.C. Maxwell, *Theory of Heat* (Longmans, Green and Co., 1902). <https://openlibrary.org/books/OL7243600M>
2. H. Leff, A. Rex (eds.), *Maxwell's Demon: Entropy, Information, Computing Chronological Bibliography*, p. 290 (Princeton University Press, Boston, 1990)
3. H. Leff, A. Rex, *Maxwell's demon 2: Entropy, Classical and Quantum Information, Computing* (Institute of Physics Publishing, London, 2003)
4. L. Szilard, On the decrease of entropy in a thermodynamic system by the intervention of intelligent beings. *Behavior. Sci.* **9**, 301–310 (1964) [English translation of Über die Entropieuer-minderung in einem thermodynamischen System bei Eingrifen intelligenter Wesen, *Zeitschrift für Physik*, 53, 840–856 (1929)]. <https://doi.org/10.1002/bs.3830090402>
5. L. Brillouin, *J. Appl. Phys.* **24**, 1152 (1953). <https://doi.org/10.1063/1.1721463>
6. L. Brillouin, *Science and Information Theory* (Academic Press, New York, 1965)
7. R. Landauer, *IBM J.* **183** (1961). <https://doi.org/10.1147/rd.53.0183>
8. C.H. Bennett, *Int. J. Theor. Phys.* **21**, 905 (1982). <https://doi.org/10.1007/BF02084158>
9. C.H. Bennett, *Sci. Am.* (1987). <https://doi.org/10.1038/scientificamerican1187-108>
10. E.T. Jaynes, *Phys. Rev.* **106**, 620 (1957). Generalized Statistical Mechanics. <https://doi.org/10.1103/PhysRev.106.620>

11. E.T. Jaynes, Phys. Rev. **108**, 171 (1957b). <https://doi.org/10.1103/PhysRev.108.171>
12. J.A. Vaccaro, S.M. Barnett, in *Asian Conference on Quantum Information Science*, September, Beijing, China, pp. 1–4 (2006), <http://aqis-conf.org/archives/aqis06/>
13. J.A. Vaccaro, S.M. Barnett, in *Quantum Communication, Measurement and Computing (QCMC)*, calgary, Canada, 19–24 August 2008. AIP Conference Proceedings, vol. 1110, pp. 37–40 (2008). <https://doi.org/10.1063/1.3131353>
14. N. Yunger Halpern, P. Faist, J. Oppenheim, A. Winter, Nat. Commun. **7**, 12051 (2016). <https://doi.org/10.1038/ncomms12051>
15. N. Yunger Halpern, J.M. Renes, Phys. Rev. E **93**, 022126 (2016). <https://doi.org/10.1103/physreve.93.022126>
16. R. Alicki, M. Horodecki, P. Horodecki, R. Horodecki, Open Syst. Inf. Dyn. **11**, 205 (2004). <https://doi.org/10.1023/B:OPSY.0000047566.72717.71>
17. L. del Rio, J. Åberg, R. Renner, O. Dahlsten, V. Vedral, Nature **474**, 61 (2011). <https://doi.org/10.1038/nature10123>
18. K. Shizume, Phys. Rev. E **52**, 3495 (1995). <https://doi.org/10.1103/PhysRevE.52.3495>
19. B. Piechocinska, Phys. Rev. A **61**, 062314 (2000). <https://doi.org/10.1103/PhysRevA.61.062314>
20. D. Reeb, M.M. Wolf, New J. Phys. **16**, 103011 (2014). <https://doi.org/10.1088/1367-2630/16/10/103011>
21. T.J.G. Apollaro, S. Lorenzo, C.D. Franco, F. Plastina, M. Paternostro, Phys. Rev. A **90** (2014). <https://doi.org/10.1103/physreva.90.012310>
22. F. Brandão, M. Horodecki, N. Ng, J. Oppenheim, S. Wehner, Proc. Natl. Acad. Sci. **112**, 3275 (2015). <https://doi.org/10.1073/pnas.1411728112>
23. R. Landauer, in *Proceedings of the Workshop on Physics and Computation PhysComp'92*, p. 1 (IEEE Computer Society Press, Los Alamos, 1993). <https://doi.org/10.1109/PHYCMP.1992.615478>
24. J.A. Vaccaro, S.M. Barnett, Proc. R. Soc. A Math. Phys. Eng. Sci. **467**, 1770 (2011). <https://doi.org/10.1098/rspa.2010.0577>
25. S.M. Barnett, J.A. Vaccaro, Entropy **15**, 4956 (2013). <https://doi.org/10.3390/e15114956>
26. T. Croucher, S. Bedkihal, J.A. Vaccaro, Phys. Rev. Lett. **118**, 060602 (2017). <https://doi.org/10.1103/physrevlett.118.060602>
27. J.A. Vaccaro, S.M. Barnett, AIP Conf. Proc. **1110**, 37 (2009). <https://doi.org/10.1063/1.3131353>
28. M. Lostaglio, D. Jennings, T. Rudolph, **19**, 043008. <https://doi.org/10.1088/1367-2630/aa617f>
29. J.S.S.T. Wright, T. Gould, A.R.R. Carvalho, S. Bedkihal, J.A. Vaccaro, Phys. Rev. A **97**, 052104 (2018). <https://doi.org/10.1103/PhysRevA.97.052104>
30. Y. Guryanova, S. Popescu, A. Short, R. Silva, P. Skrzypczyk, Nat. Commun. **7**, 12049 (2016). <https://doi.org/10.1038/ncomms12049>
31. K. Ito, M. Hayashi, Phys. Rev. E **97** (2018). <https://doi.org/10.1103/physreve.97.012129>
32. M.N. Bera, A. Riera, M. Lewenstein, A. Winter (2017), arXiv:1707.01750v1
33. D.J. Evans, E.G.D. Cohen, G.P. Morriss, Phys. Rev. Lett. **71**, 2401 (1993). <https://doi.org/10.1103/PhysRevLett.71.2401>
34. D.J. Evans, D.J. Searles, Phys. Rev. E **50**, 1645 (1994). <https://doi.org/10.1103/PhysRevE.50.1645>
35. R. Dillenschneider, E. Lutz, Phys. Rev. Lett. **102** (2009). <https://doi.org/10.1103/physrevlett.102.210601>
36. C. Jarzynski, Phys. Rev. E **56** (1997). <https://doi.org/10.1103/PhysRevE.56.5018>
37. J.L.W.V. Jensen, Acta Math. **30**, 175 (1906). <https://doi.org/10.1007/BF02418571>
38. T. Xiong, L. Yan, F. Zhou, K. Rehan, D. Liang, L. Chen, W. Yang, Z. Ma, M. Feng, V. Vedral, Phys. Rev. Lett. **120** (2018). <https://doi.org/10.1103/physrevlett.120.010601>
39. A. Berut, A. Petrosyan, S. Ciliberto, Europhys. Lett. **103**, 60002 (2013). <https://doi.org/10.1209/0295-5075/103/60002>
40. C.E. Shannon, W. Weaver, *The Mathematical Theory of Communication* (University of Illinois Press, Urbana Il, 1963)

41. A. Eddington, *The Nature of the Physical World* (J. M. Dent, London, 1928). <https://openlibrary.org/books/OL15026629M>
42. B. Schumacher, *Quantum Information and Foundations of Thermodynamics* (ETH Zürich, 2011), <https://www.video.ethz.ch/conferences/2011/qiftw11/f9bb6f3d-7461-4971-8213-2e3ceb48c0ba.html>. Accessed 13 Mar 2018
43. D. Song, E. Winstanley, Int. J. Theor. Phys. **47**, 1692 (2007). <https://doi.org/10.1007/s10773-007-9610-0>

# Chapter 30

## Trade-Off Between Work and Correlations in Quantum Thermodynamics



Giuseppe Vitagliano, Claude Klöckl, Marcus Huber and Nicolai Friis

### 30.1 Introduction

From its inception, classical thermodynamics has been a practically minded theory, aiming to quantify the usefulness and capabilities of machines in terms of performing work. One of the distinguishing features of quantum thermodynamics with respect to classical thermodynamics (and standard quantum statistics) is the level of control that one assumes to have over the degrees of freedom of microscopic (and mesoscopic) quantum systems. This control allows one to identify genuine quantum behaviour in thermodynamics beyond contributions via statistical deviations, e.g., due to the indistinguishability of bosons and fermions. Moreover, this control permits us to consider individual quantum systems as the figurative gears of a quantum machine—quantum “cogwheels” that can be used to extract or store work, which act as catalysts, or mediate interactions. The operating principle of such a (quantum) machine is to use the control over the system to convert one kind of resource into another, for instance, thermal energy into mechanical work. Quantum thermodynamics can hence be viewed as a resource theory [1], where energy<sup>1</sup> is a resource, while systems in thermal equilibrium with the environment are considered to be freely available.

---

<sup>1</sup>Or, more generally, out-of-equilibrium states from which energy can be extracted.

G. Vitagliano (✉) · C. Klöckl · M. Huber · N. Friis

Institute for Quantum Optics and Quantum Information - IQOQI Vienna,  
Austrian Academy of Sciences, Boltzmanngasse 3, 1090 Vienna, Austria  
e-mail: giuseppe.vitagliano@univie.ac.at

C. Klöckl  
e-mail: claude.kloeckl@oeaw.ac.at

M. Huber  
e-mail: marcus.huber@univie.ac.at

N. Friis  
e-mail: nicolai.friis@univie.ac.at

The control over the system then determines how energy can be spent to manipulate (thermal) quantum states.

At the same time, the manipulation of well-controlled quantum systems is the basic premise for quantum information processing [2]. The latter, in turn, can also be understood as a resource theory with respect to (quantum) correlations [3, 4]. However, it is clear that for any practical application, that this abstract information-theoretic construct must be embedded within a physical context, e.g., such as that provided by quantum thermodynamics. It therefore seems natural to wonder, how the resources of quantum thermodynamics and quantum information theory are related, how they can be converted into each other, and what role resources of one theory play in the other, respectively.

Here, we want to discuss these questions and review the role of (quantum) correlations in quantum thermodynamics (see Refs. [5–7] for recent reviews). In Sect. 30.2, we briefly review a few key areas within quantum thermodynamics where (quantum) correlations are of significance, starting with an overview of the basic concepts and definitions in Sects. 30.2.1.1 and 30.2.1.2. In Sects. 30.2.1.3 and 30.2.2 the consequences of the presence of correlations for the formulation of thermodynamic laws and for the task of work extraction are discussed, respectively.

In Sect. 30.3, we then focus on the specific question of converting the resource of quantum thermodynamics, i.e., energy, into the resource of quantum information, i.e., correlations. To this end, we first review previous key results [8–12] that provide bounds on the performance of this resource conversion, before turning to a, thus far, unresolved problem: the question of the existence of optimally correlating unitaries. We show that such operations do not always exist and analyse the implications of this observation. Finally, we discuss pertinent open problems in understanding the role of correlations in thermodynamics.

## 30.2 Correlations in Quantum Thermodynamics

### 30.2.1 Framework

#### 30.2.1.1 Quantum Thermodynamics in a Nutshell

In the following, we consider pairs of quantum mechanical systems that may share correlations. In the context of thermodynamics, these might be, e.g., a system (working body) and a heat bath. In quantum mechanics, these systems are encoded into a bipartite Hilbert space  $\mathcal{H}_{AB} = \mathcal{H}_A \otimes \mathcal{H}_B$ , where the tensor factors represent the two subsystems,  $A$  and  $B$ . States describing the joint system are given by density operators  $\rho_{AB} \in \mathcal{L}(\mathcal{H}_{AB})$ , i.e., positive-semidefinite ( $\rho_{AB} \geq 0$ ), linear operators over  $\mathcal{H}_{AB}$  that satisfy  $\text{Tr}(\rho_{AB}) = 1$ . The energy of the system is further determined by the Hamiltonian  $H_{AB}$ , i.e., a self-adjoint operator over  $\mathcal{H}_{AB}$  usually assumed to be bounded from below. Besides the average (internal) energy  $E(\rho_{AB}) = \text{Tr}(H\rho_{AB})$  of the joint system, other

state functions central to quantum thermodynamics are the *von Neumann entropy*  $S(\rho_{AB}) = -\text{Tr}(\rho_{AB} \ln(\rho_{AB}))$  and the *free energy*  $F(\rho_{AB}) = E(\rho_{AB}) - TS(\rho_{AB})$ , as well as the analogous quantities for the reduced states  $\rho_A = \text{Tr}_B(\rho_{AB})$  and  $\rho_B = \text{Tr}_A(\rho_{AB})$  of the subsystems.

The focus of quantum thermodynamics then lies on the study of the (possible) evolution of  $\rho_{AB}$  and the subsystem states  $\rho_A = \text{Tr}_B(\rho_{AB})$  and  $\rho_B = \text{Tr}_A(\rho_{AB})$  subject to certain constraints on the allowed transformations of the joint system, such as, for example:

- (i) Conservation of (total) energy of A and B:

$$\rho_{AB} \mapsto \sigma_{AB} : \text{Tr}(H_{AB}\rho_{AB}) = \text{Tr}(H_{AB}\sigma_{AB})$$

- (ii) Closed system dynamics:

$$\rho_{AB} \mapsto U_{AB}\rho_{AB}U_{AB}^\dagger$$

for some global unitary transformation  $U_{AB}$ .

To state its basic laws, then, a first main goal of quantum thermodynamics is to provide meaningful definitions of *heat*  $\Delta Q$  and *work*  $\Delta W$  exchanged between the subsystems. These quantities are not just functions of the state, but depend on the concrete transformations that are applied. In particular, suitable definitions are usually chosen such that the *first law of thermodynamics* holds for closed joint systems, i.e.,

$$\Delta E = \Delta Q + \Delta W, \quad (30.1)$$

with  $\Delta E = E(\rho_A(t + \Delta t)) - E(\rho_A(t))$ . For this purpose a quantifier often used for the information change within the subsystems is the *relative entropy*  $S(\rho_A(t + \Delta t) \parallel \rho_A(t))$  of  $\rho_A(t + \Delta t)$  w.r.t.  $\rho_A(t)$ . For arbitrary states  $\rho$  and  $\sigma$  it is defined as

$$S(\sigma \parallel \rho) = -S(\sigma) - \text{Tr}(\sigma \ln(\rho)). \quad (30.2)$$

The relative entropy is nonnegative,  $S(\sigma \parallel \rho) \geq 0$ , for all pairs  $\rho$  and  $\sigma$ , with equality iff  $\rho = \sigma$  (see, e.g., [13] for details), and coincides with the free energy difference  $S(\sigma \parallel \rho) = F(\sigma) - F(\rho)$ , whenever  $\rho = \tau(\beta)$  is thermal. That is, given a Hamiltonian  $H_{AB}$ , the corresponding *thermal state* is defined as

$$\tau_{AB}(\beta) = \mathcal{Z}^{-1}e^{-\beta H_{AB}}, \quad (30.3)$$

where  $\beta = 1/T$  denotes the inverse temperature<sup>2</sup> and  $\mathcal{Z} = \text{Tr}(e^{-\beta H_{AB}})$  is called the *partition function*. The above thermal state  $\tau_{AB}(\beta)$  can be considered as the state of the joint system of A and B at thermal equilibrium with an external heat bath

---

<sup>2</sup>We use units where  $\hbar = k_B = 1$  throughout.

at temperature  $T$ , and represents the maximum entropy state for fixed (internal) energy [14]. The relative entropy can hence be understood as measure of distance from thermal equilibrium of the total system.

### 30.2.1.2 Quantifying Correlations

The properties of equilibrium states strongly depend on the system Hamiltonian. For instance, the joint thermal state  $\tau_{AB}$  of systems  $A$  and  $B$  is completely uncorrelated whenever they are noninteracting, i.e., when  $H_{AB} = H_A + H_B$ , where  $H_A$  and  $H_B$  act nontrivially only on  $\mathcal{H}_A$  and  $\mathcal{H}_B$ , respectively. In this case  $\tau_{AB}$  is a product state  $\tau_{AB}(\beta) = \tau_A(\beta) \otimes \tau_B(\beta)$ , where  $\tau_A$  and  $\tau_B$  are thermal states at the same temperature  $T = 1/\beta$  w.r.t. the local Hamiltonians  $H_A$  and  $H_B$ , respectively. Conversely, in an interacting system the global state  $\rho_{AB}$  will typically be correlated, and may even be entangled, meaning that the state cannot be decomposed into a mixture of uncorrelated states (see, e.g., [11] for a discussion).

Such correlations can be quantified in terms of the *mutual information*<sup>3</sup>

$$\mathcal{I}(\rho_{AB}) = S(\rho_A) + S(\rho_B) - S(\rho_{AB}). \quad (30.4)$$

That is,  $\mathcal{I}$  quantifies the amount of information about the system that is available globally but not locally. Here, it is important to note  $\mathcal{I}$  captures both classical and genuine quantum correlations in the sense that nonzero values of  $\mathcal{I}$  may originate in either type of correlation. Nonetheless, it should be noted that any state  $\rho_{AB}$  for which  $\mathcal{I}(\rho_{AB}) > S(\rho_A)$  or  $\mathcal{I}(\rho_{AB}) > S(\rho_B)$  features a negative conditional entropy  $S(A||B) = S(\rho_A) - \mathcal{I}(\rho_{AB})$ , and is hence [15, 16] necessarily entangled to some extent<sup>4</sup>.

### 30.2.1.3 Role of Correlations for Thermodynamic Laws

Indeed, correlations are already central to the foundations of quantum thermodynamics. This manifests in the fundamental difference between describing thermodynamic systems as being composed of isolated parts, or as interacting with each other. When subsystems are considered to be completely isolated, just as in classical thermodynamics, this translates to the quantum mechanical notion of a product state  $\rho_A \otimes \rho_B$ . However, there are continuing efforts to expand and even challenge this seemingly basic assumption. This includes, e.g., approaches where subsystems (and hence potential correlations between them) are defined using thermodynamic principles

<sup>3</sup>This is one of the most widely used measures of correlations in the context of thermodynamics, which arises quite naturally, due to being a linear function of the von Neumann entropies of the subsystems, and thus directly related to thermodynamical potentials. See also the subsequent discussion.

<sup>4</sup>See, e.g., [17] for a pedagogical introduction to entanglement detection via conditional entropies and mutual information.

ples [18], or those where work and heat exchange in interacting systems is defined in terms of effective local Hamiltonians that depend on correlations [19, 20]. In other approaches, the traditional setting of a system separable from its surrounding thermal bath can be extended to a state  $\rho_{AB}$  with *correlations between system and bath* [21–28]. This leads to reformulations of the concepts of heat and work and modifications of the classical laws of thermodynamics via the introduction of correlated baths.

In particular, the second law deserves a special mention in this respect. Loosely speaking, it states that the entropy of a subsystem cannot decrease after a thermodynamical transformation, i.e.,  $\Delta S = S(\rho_A(t + \Delta t)) - S(\rho_A(t)) \geq 0$ , an observation that lies at the heart of the emergence of the so-called *thermodynamical arrow of time*. However, several authors, have observed how such a relation does not hold true anymore when system and bath are allowed to be initially correlated [21, 22]. This insight can even be traced back to Boltzmann himself [29, 30], who, while introducing the so-called *Stosszahlansatz* (i.e., the assumption of molecular chaos), noticed that in order for the second law of thermodynamics to emerge it was necessary to assume a weakly correlated (cosmological) environment.

Formally speaking, the basic argument showing the intimate connection of correlations with the thermodynamical arrow of time works as follows in its extremal version [21–24]. Consider a system and bath with local Hamiltonians  $H_A$  and  $H_B$ , such that  $H_A |n\rangle_A = E_n^A |n\rangle_A$  and  $H_B |n\rangle_B = E_n^B |n\rangle_B$ . Suppose that there exist constants  $\mu_A$  and  $\mu_B$  such that the local energy levels  $E_n^A$  and  $E_n^B$  satisfy  $\mu_A E_n^A = \mu_B E_n^B = \epsilon_n$  for all  $n$ . Let us further assume that initially system and bath are jointly very close to a (pure) *highly entangled* state<sup>5</sup>

$$|\psi\rangle_{AB} = \mathcal{Z}^{-1/2} \sum_n \exp(-\gamma\epsilon_n/2) |n, n\rangle_{AB}, \quad (30.5)$$

which can be thought of as a thermal state of a suitable interacting Hamiltonian  $H_{AB}$  for very low temperatures (i.e., in the limit  $\beta \rightarrow \infty$ ). The two marginal states  $\rho_A$  and  $\rho_B$  are thermal w.r.t.  $H_A$  and  $H_B$  at (different) inverse temperatures  $\beta_A = \mu_A \gamma$  and  $\beta_B = \mu_B \gamma$  respectively, but with the same entropy  $S(\rho_A) = S(\rho_B)$  since  $\rho_A$  and  $\rho_B$  have the same spectrum. Suppose now that the two subsystems interact through a global unitary transformation that allows some exchange of energy between the subsystems. Further, let us assume that, w.r.t. to a suitable definition of  $Q$  [see the discussion surrounding Eq. (30.1)], this exchange is interpreted simply as a heat exchange, meaning that the local changes of internal energy satisfy  $\Delta E_A = \Delta Q_A$  and  $\Delta E_B = \Delta Q_B$ , respectively. Since the marginals are initially thermal, we have  $\Delta F_A = \Delta E_A - T_A \Delta S_A \geq 0$  and  $\Delta F_B = \Delta E_B - T_B \Delta S_B \geq 0$ , which leads to  $\beta_A \Delta Q_A \geq \Delta S_A$  and  $\beta_B \Delta Q_B \geq \Delta S_B$ , while  $\Delta Q_A + \Delta Q_B = 0$ . Globally, the constraint on heat exchanges implies

$$\beta_A \Delta Q_A + \beta_B \Delta Q_B \geq \Delta \mathcal{I}_{AB}, \quad (30.6)$$

---

<sup>5</sup>For simplicity here we could consider finite-dimensional systems.

where  $\Delta\mathcal{I}_{AB} = \Delta S_A + \Delta S_B$  is the change in the mutual information after the transformation since the unitary leaves the overall entropy invariant. The crucial observation is then that for the above global state  $|\psi\rangle_{AB}$  the mutual information can be very high initially and can decrease during the transformation such that  $\Delta\mathcal{I}_{AB} < 0$ . Heat may thus be allowed to flow from the cold to the hot subsystem (e.g.,  $\Delta Q_A \geq 0$  for  $\beta_A \leq \beta_B$ ). Correlations can thus lead to an *anomalous heat flow* (see Chap. 4). Moreover, since the above global state remains pure, the marginals have the same spectra, and we have  $\Delta S_A = \Delta S_B$ . Therefore, an anomalous heat flow implies a violation of the classical second law of thermodynamics,  $\Delta\mathcal{I}_{AB} < 0 \Rightarrow \Delta S_A = \Delta S_B < 0$ , i.e., the local entropies both decrease, reversing the direction of the thermodynamical arrow of time.

Following this observation, several authors, adopting an information theoretic perspective, have investigated the possibility to generalize the thermodynamic laws in the presence of initial correlations between system and bath, see, e.g., Refs. [25–28, 31]. Furthermore, experiments are now being performed for quantum mechanical systems realized in several platforms to observe violations of classical laws of thermodynamics, especially regarding the inversion of the thermodynamic arrow of time [32].

Correlations therefore need to be carefully incorporated into the formulation of quantum thermodynamics. However, correlations are not only a source of seemingly paradoxical situations but can also have direct practical relevance for paradigmatic tasks in quantum thermodynamics, as we will discuss in Sect. 30.2.2, before we analyse what quantum thermodynamics tells us about the work cost and level of control necessary to create correlations in Sect. 30.3.

### 30.2.2 Extracting Work from Correlations

#### 30.2.2.1 Work Extraction Using Cyclic Transformations

A basic but crucial application of thermodynamics is to quantify how much work can be extracted from a given machine operating under a *cycle of transformations*. In this context, one may consider subsystem  $A$  to be a quantum machine that is controlled by the external subsystem  $B$ . As a general model of such a machine one usually considers an ensemble of, say,  $N$  quantum mechanical units, i.e., subsystem  $A$  has a Hilbert space  $\mathcal{H}_A = \mathcal{H}^{\otimes N}$  with a given (free) Hamiltonian  $H_A$ . This allows statements about the scaling of the quantum machine's efficiency and eventual gain (e.g., originating from the ability to create correlations) with  $N$  as compared to analogous classical machines.

The external control is usually modelled as a switchable time-dependent (and cyclic) Hamiltonian  $H(t)$ , such that  $H(0) = H(t_{\text{cycle}})$  where  $t_{\text{cycle}}$  is the time of a whole cycle. The following question then arises naturally: *Can correlations between the  $N$  units of the machine help in extracting work during a thermodynamical cycle?*

More specifically, if we evolve the initial state  $\rho_A$  with an externally controlled unitary transformation  $U$  and compare the resulting difference in energy we get the quantity

$$\Delta W_U = \text{Tr}(\rho_A H_A) - \text{Tr}(U \rho_A U^\dagger H_A). \quad (30.7)$$

If positive, it describes the amount of energy that is gained after  $U$  and is usually interpreted as extracted work, i.e., the process is assumed to be performed adiabatically with the external control [33]. Thus, frequently (30.7) is seen as a figure of merit that should be maximized with respect to the available resources, like the initial state  $\rho_A$ , the externally controlled evolution  $U$  and the free system Hamiltonian  $H_A$ . Fixing or optimizing over the triple  $(\rho_A, U, H_A)$  allows one to ask questions like: *Which combination of resources yields the most work?* A frequently studied special case is that of *ergotropy* [34], corresponding to a fixed Hamiltonian and a fixed state while optimizing over all unitaries on  $\mathcal{H}_A$ , i.e.,

$$\Delta W_{\text{ergotropy}} := \max_U \Delta W_U. \quad (30.8)$$

States that do not allow for work extraction with respect to a specified class of operations (typically unitary transformations) are called *passive* [35].

In other words, for any state  $\rho$  the unitary realizing the maximum in Eq. (30.8) is the one that transforms the state to a corresponding passive state  $U \rho U^\dagger = \rho_{\text{passive}}$ , and the ergotropy represents the work that is extractable from the system with the specified operations. Quantum systems in passive states thus have a simple practical interpretation as the analogues of *empty batteries*.

### 30.2.2.2 Role of Correlations for Work Extraction

An interesting distinction between the concepts of passive and thermal states that has recently been discovered [36] is the following. A state is passive if and only if it is diagonal in the energy eigenbasis and its eigenvalues are decreasing with increasing energy. While this is certainly true for thermal states, it can also be the case for many other eigenvalue distributions which are not thermal. In summary, thermality implies passivity, but the converse is not necessarily true.

The special role of thermal states comes to light when considering many copies of the system: While  $\tau(\beta)^{\otimes N}$  is still thermal (and thus passive) for any  $N$ ,  $\rho_{\text{passive}}^{\otimes N}$  is passive for all  $N$  if and only if  $\rho_{\text{passive}}$  is a thermal state [36, 37]. In other words, thermal states are the only *completely passive* states. This has interesting consequences when interpreting passive states as empty batteries. While a single battery appears empty, i.e., no work whatsoever can be extracted, it may be the case that adding a second empty battery would enable a correlating global transformation to extract work out of the two empty batteries. This interesting situation is termed *work extraction by activation*.

This fact leads to a first affirmative answer to the question of whether correlating operations can help for work extraction: Unitary transformations can extract work more efficiently if they are able to generate entanglement. More precisely, a quantitative analysis of the relation between entanglement generation and work extraction [38] shows that the trade-off is more accurately specified as occurring between entangling power and the number of required operations (in other words, time) for work extraction: The less entanglement is generated during the work extraction process<sup>6</sup>, the more time is needed to extract work.

The above example of two empty batteries showing the difference between local passivity and (true global) passivity can be employed to construct another enlightening example. In analogy to the batteries above, let us define a state  $\rho_{AB}$  that is locally thermal (thus locally passive) in each marginal, i.e.,  $\text{Tr}_B(\rho_{AB}) = \tau_A(\beta)$  and  $\text{Tr}_A(\rho_{AB}) = \tau_B(\beta)$ . Let us now imagine that, contrary to the previous example, the state  $\rho_{AB}$  is correlated. If we can extract work from this state, then it can be argued that all the work must have come from its correlations, since there can be no contributions from local operations (due to the passivity of the marginals) nor from activation, due to the fact that thermal states do not allow for work extraction by activation. An example of such a state is provided in [33]. For locally thermal states of noninteracting systems all correlations hence imply extractable work.

### 30.2.2.3 Role of Correlations for Work Storage

A problem that can be considered dual to the above is how to efficiently charge an initially empty quantum battery (see Chap. 8). Formally, the problem is to find a suitable way of transforming a state  $\rho$  to another state  $\sigma = U\rho U^\dagger$  such that the latter contains more extractable work, i.e.,  $\Delta W_U \leq 0$  as in Eq. (30.7). As previously for work extraction, one is primarily interested in charging processes based on cycles of transformations. However, in contrast to the previous problem, one is here not necessarily interested in asking how much work may be stored in principle. Instead other figures of merit become important, indicating certain desirable properties of the charging process or the final state for fixed  $\Delta W_U$ . Examples for such properties include charging power [39], fluctuations during the charging process or the variance of the final charge [40]. The key question that we wish to discuss here is: *Is it beneficial for work storage to (be able to) generate correlations during the process?*

While correlations themselves turn out not to be directly relevant in any crucial way, it appears that the control over correlating transformations can provide significant advantages, even if no actual correlations are created. Specifically, in Ref. [39] the authors show that the power of charging a battery, defined as  $P := \langle \Delta W_U \rangle / \Delta t$ , i.e., the ratio of average work  $\langle \Delta W_U \rangle$  and time  $\Delta t$ , can be enhanced by allowing entangling global unitaries  $U$  on an initially uncorrelated product state  $\rho_1 \otimes \cdots \otimes \rho_N$ . However, whether such entangling operations actually create entanglement during the cycle is irrelevant [41]. As is discussed in more detail

---

<sup>6</sup>Note that the final state need not be entangled.

Can we instead use a local unitary  $(I^A \otimes U^B)$  and get the same advantage when  $\rho^{AB}$  is entangled? This would be a dense-coding analogy for thermo.

in Chap. 8, the trade-off is rather between entanglement generated during the process and the speed of the process itself. Focussing on the practical aspects of implementing this idea, in Ref. [42] the authors study a non-unitary charging process of a quantum battery of  $N$  qubits coupled to a single photonic mode.

### 30.2.2.4 Work Extraction and Storage with Restricted Control

For understanding fundamental bounds on work extraction and storage correlations are thus of significance, or rather, the ability to create them. This highlights the fact that this ability is linked to the control one has over the system and operations thereon. In particular, maximization such as in Eq. (30.8) may yield solutions that cannot be practically implemented or whose realization comes at a high cost itself. Therefore, subsequent works have focused on understanding the limitations of work extraction and work storage in terms of more restricted sets of states/operations such as Gaussian states and unitaries [40, 43]. This has been motivated also by the easier practical implementation in CV systems such as encountered in quantum optics of Gaussian operations, as opposed to arbitrary unitaries. In particular, this is manifest when considering driven transformations, where Gaussian operations appear as the simplest type of operation according to the hierarchy of driving Hamiltonians, which are at most quadratic in the system's annihilation and creation operators for Gaussian unitaries.

As we have already emphasized, passivity is defined with respect to an underlying class of state transformations, i.e., unitaries (cyclic Hamiltonian processes). An interesting variant of the problem in Eq. (30.8) is thus given by the restricted case of Gaussian unitary transformations [43]. This leads to the notion of *Gaussian passivity* as a special case of passivity in the sense that passivity implies Gaussian passivity, but not vice versa. The role of correlations in such a scenario is particularly interesting. In particular, the authors show that it is always possible to extract work from an entangled Gaussian state via two-mode squeezing operations. For general non-Gaussian states, however, the ability to extract work via (dis)entangling Gaussian unitaries (two-mode squeezing) does not indicate entanglement, and the inability to do so does not imply separability either.

In the complementary problem of battery charging, the subset of Gaussian operations turns out to provide a trade-off between good precision (energy variance) and practical implementability of a battery charging protocol with a fixed target amount of energy  $\Delta W$  [40]. Here, correlations can provide minor advantages in some cases but do not play a conceptually important role.

To conclude this section it is also interesting to point out that, as observed in Ref. [44] the argument that entanglement (or the ability to create it) can provide an advantage in work extraction can also be turned around and exploited to design entanglement certification schemes based on extractable work. In other words, it is possible to witness entanglement by quantifying the extracted work from a thermodynamic cycle, such as the *Szilard engine* considered in [44]. Interestingly,

the entanglement criterion based on work extraction becomes necessary and sufficient for two-mode Gaussian states. However, the authors also show that the above scheme cannot be applied for the certification of genuine multipartite entanglement.

### 30.3 Energy Cost of Creating Correlations

#### 30.3.1 Trade-Off Between Work and Correlations

Now that we have an overview of the importance of correlations (and the transformations that can create them) for quantum thermodynamics and its paradigmatic tasks, let us consider the situation from a different perspective. Correlations, in particular, entanglement, are the backbone of quantum information processing. However, if an abstract information theory is to be applied in practice, it requires a physical context, such as is provided by quantum thermodynamics. There, as we have seen above, the freely available equilibrium state of two (noninteracting) systems is uncorrelated. This means that both an investment of energy and a certain level of control (the ability to perform correlating transformations) are required to create the desired correlations.

Thus, formally speaking, one is interested in determining the fundamental limits for the energy cost of creating correlations, where we choose to quantify the latter by the mutual information of Eq. (30.4) between two quantum systems  $A$  and  $B$ , since the mutual information arises quite naturally in the thermodynamic context. These subsystems are assumed to be initially in a joint thermal state  $\tau_{AB}(\beta) = \tau_A(\beta) \otimes \tau_B(\beta)$  with respect to a noninteracting Hamiltonian  $H_{AB} = H_A + H_B$  at a particular ambient temperature  $T = 1/\beta$ . To correlate  $A$  and  $B$ , it is necessary to move the joint system out of equilibrium, which comes at a nonzero work cost  $W$ . For instance, when one acts unitarily on the system, this cost can be expressed as  $W = \Delta E_A + \Delta E_B$ . The question at hand is then: *What is the maximal amount of correlation between  $A$  and  $B$  that can be reached, given a fixed amount of available energy  $W$ ?*

Clearly, the answer very much depends on the operations that are allowed, as well as on the energy level structure of the local Hamiltonians. For instance, one may consider applying only global unitary transformations  $U_{AB}$ , realized via some external control. If one wishes to optimally convert work into correlations, it is clear that the marginals of the final state must be passive. Otherwise, energy extractable by local unitaries (which leave  $\mathcal{I}_{AB}$  invariant) would be left in the system. Indeed, the marginals must be completely passive (thus thermal), such that no work can be extracted locally<sup>7</sup> from any number of copies. The optimally correlated target state  $\rho_{AB} = U_{AB}\tau_{AB}(\beta)U_{AB}^\dagger$  must hence be such that  $\rho_A = \text{Tr}_B(\rho_{AB}) = \tau_A(\beta_A)$  and  $\rho_B = \text{Tr}_A(\rho_{AB}) = \tau_B(\beta_B)$ . At the same time, one wishes to increase the correlations, i.e., to achieve the maximal

---

<sup>7</sup>Here, local refers to the collections of subsystems  $A_1, \dots, A_N$  and  $B_1, \dots, B_N$  for  $N$  copies of  $\rho_{AB}$ .

amount of mutual information increase  $\Delta\mathcal{I}_{AB} = \Delta S_A + \Delta S_B \geq 0$ . At fixed average energy input  $\Delta E = E(\tau_A(\beta_A)) + E(\tau_B(\beta_B)) - E(\tau_{AB}(\beta))$ , the mutual information is then maximized for maximal  $S(\tau_A(\beta_A)) + S(\tau_B(\beta_B)) = S(\tau_A(\beta_A) \otimes \tau_B(\beta_B))$ . The maximum entropy principle then suggests that the final state marginals should be thermal at the same temperature  $\beta_A = \beta_B$ . But do unitaries exist that can achieve this?

The above requirements are indeed already quite strong, as we can observe through the following extremal example. Let us imagine that initially the two subsystems are in a pure (ground) state (i.e., the limit  $\beta \rightarrow \infty$ )  $\tau_{AB}(\beta) = |0\rangle\langle 0|_A \otimes |0\rangle\langle 0|_B$  at zero initial energy. Then, any unitary will still output a pure state  $|\psi\rangle_{AB} = U_{AB}|00\rangle_{AB}$ , and the requirement of the marginals to be thermal states leads to a state as in Eq. (30.5), i.e.,

$$|\psi\rangle_{AB} = \mathcal{Z}^{-1/2} \sum_n \lambda_n |n, n\rangle_{AB}, \quad (30.9)$$

with  $\lambda_n^2 = \exp(-\beta_A E_n^A) = \exp(-\beta_B E_n^B)$ . The requirement of having a fixed amount of energy available further demands

$$W = \sum_n \lambda_n^2 (E_n^A + E_n^B), \quad (30.10)$$

which in general translates into a complicated relation between the two final effective inverse temperatures  $\beta_A$  and  $\beta_B$ .

Thus, further constraints, e.g., on the final temperatures of the marginal states, on the initial Hamiltonians of the two systems, or on the external control available might already lead to an impossibility of achieving such an optimal conversion between work and correlations. In the following we will make this statement more precise, discuss the relevant questions arising in this context, and give some (partial) answers.

### 30.3.2 Fundamental Cost of Correlations

With the realization that there is a finite work cost for the creation of correlations in noninteracting systems [8, 9], or for the increase of correlations in the presence of correlated thermal states for interacting systems [11], two immediate pertinent questions for the trade-off between the resources work and correlations can be formulated.

- (i) On the one hand, it is of interest to understand the fundamental limitations on achievable correlations without any restrictions on the complexity of the involved operations or the time these may take. We can thus ask: *What is the theoretical minimum work cost for any amount of correlation between two given systems?*
- (ii) On the other hand, it is of course of practical importance to learn what can be achieved under practical conditions, i.e., in finite time and with limited control over the system, that is: *What is the minimum work cost of correlations that is practically achievable?*

Let us formulate those questions more precisely following the treatment in [9]. We first observe that any physical transformation of a system  $S$  can be thought of as a unitary map  $U_{SR}$  acting on a larger Hilbert space that includes an external reservoir  $R$ . In this context one may further assume that  $S$  and  $R$  are initially not correlated, i.e., that initially we have  $\tau_{SR}(\beta) = \tau_S(\beta) \otimes \tau_R(\beta)$ . Then, the work cost to bring such a state out of equilibrium is

$$W = \text{Tr}\left(H[\rho_{SR} - \tau_{SR}(\beta)]\right) = \Delta E_S + \Delta E_R, \quad (30.11)$$

where the overall final state is  $\rho_{SR} = U_{SR}\tau_{SR}(\beta)U_{SR}^\dagger$ , and if we further assume that  $H = H_S + H_R$ , then the energy contributions split up into  $\Delta E_S = \text{Tr}(H_S[\rho_{SR} - \tau_{SR}(\beta)])$  and  $\Delta E_R = \text{Tr}(H_R[\rho_{SR} - \tau_{SR}(\beta)])$ . We note also that similar expressions in related contexts can be found, e.g., in [45–48]. One may then rewrite Eq. (30.11) by expressing the internal energy differences via the changes in free energy and entropy and obtain

$$W = \Delta F_S + \Delta F_R + T \mathcal{I}_{SR}, \quad (30.12)$$

where one makes also use of the fact that the initial thermal state is uncorrelated,  $S(\tau_{SR}) = S(\tau_S) + S(\tau_R)$  and that  $U_{SR}$  leaves the global entropy invariant, i.e.,  $S(\rho_{SR}) = S(\tau_{SR})$ .

In the above expression, one recognizes the mutual information  $\mathcal{I}_{SR}$  between the system and the reservoir. In complete analogy to the reasoning that leads to Eq. (30.12), one may further rewrite the free energy change of the system  $S$  comprising the subsystems  $A$  and  $B$  as

$$\Delta F_S = \Delta F_A + \Delta F_B + T \mathcal{I}_{AB}. \quad (30.13)$$

Combining Eqs. (30.12) and (30.13) and noting that the initial states of  $A$ ,  $B$  and  $R$  are thermal, such that the free energy differences can be expressed via the relative entropy, one thus arrives at

$$\beta W = S(\rho_R \| \tau_R) + S(\rho_A \| \tau_A) + S(\rho_B \| \tau_B) + \mathcal{I}_{SR} + \mathcal{I}_{AB}, \quad (30.14)$$

where  $\rho_A = \text{Tr}_{BR}(\rho_{SR})$ ,  $\rho_B = \text{Tr}_{AR}(\rho_{SR})$ , and  $\rho_R = \text{Tr}_{AB}(\rho_{SR})$  are the reduced states after the transformation. Since  $S(\rho \| \sigma) \geq 0$  for all  $\rho$  and  $\sigma$  and  $\mathcal{I}_{SR} \geq 0$  as well, it becomes clear that the fundamental upper bound for the correlations between  $A$  and  $B$  is

$$\mathcal{I}_{AB} \leq \beta W. \quad (30.15)$$

It is then crucial to note that tightness of this bound is only given when  $S(\rho_R \| \tau_R) = 0$  and  $\mathcal{I}_{SR} = 0$ . On the one hand, these conditions are trivially met when one performs unitary operations acting solely on the system  $S$ , but not on  $R$ . We will return to this scenario in Sect. 30.3.3. On the other hand, one could assume perfect control over an arbitrarily large reservoir  $R$ , i.e., one that is complex enough to thermalize the

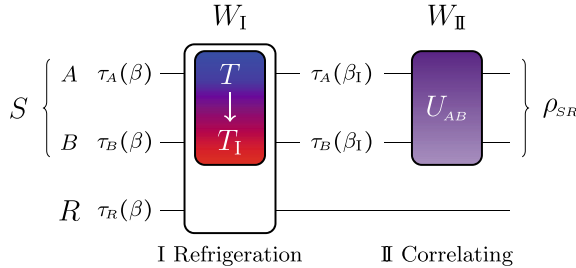


**Fig. 30.1** Two-step correlating protocol: The temperature of the initially uncorrelated subsystems \$A\$ and \$B\$ forming the system \$S\$ is first lowered from \$T\$ to \$T\_I < T\$ using the interaction with the reservoir \$R\$ at the expense of the work \$W\_I\$. In a second step, the reservoir is decoupled from the system, before \$A\$ and \$B\$ are correlated by a unitary \$U\_{AB}\$, at energy cost \$W\_{\text{II}}\$.

system whenever \$S\$ and \$R\$ come in contact [49] (see also [50] for description of the involved unitaries), such that \$R\$ can be assumed to be left in its original state with no correlations created between \$S\$ and \$R\$.

A protocol that operates based on the latter premise was presented in [9] and consists of two steps to reach the optimal trade-off between work and correlations, i.e., \$\mathcal{I}\_{AB} = \beta W\$, see Fig. 30.1. In the first step with work cost \$W\_I\$, the temperature of the system \$S\$ is lowered from \$T\$ to \$T\_I = 1/\beta\_I < T\$. Here one uses the contact to \$R\$ to refrigerate \$S\$, resorting to arbitrarily slow processes to do so, such that the cooling cost is given by the free energy difference, \$W\_I = F(\tau\_S(\beta\_I)) - F(\tau\_S(\beta))\$. In the second step, a unitary \$U\_{AB}\$ acting only on \$S\$ is used to correlate \$A\$ and \$B\$ at work cost \$W\_{\text{II}}\$. It is assumed that \$U\_{AB}\$ is of such a form that the marginals are returned to locally thermal states at the original temperature \$T\$. That is, they have to satisfy \$\rho\_A = \tau\_A(\beta)\$ and \$\rho\_B = \tau\_B(\beta)\$ in order to obtain \$S(\rho\_A \parallel \tau\_A) = S(\rho\_B \parallel \tau\_B) = 0\$ in Eq. (30.14). This last requirement determines the splitting of the work cost \$W\$ into \$W\_I\$ and \$W\_{\text{II}}\$. One thus finds that there exists a (low-energy) regime, at least in principle, with a linear trade-off between work and correlations, provided that one can exert the mentioned rigorous control over the degrees of freedom of \$R\$ and that the desired optimal unitaries \$U\_{AB}\$ exist.

However, even if this is so, there is a threshold input energy, above which the conversion can only occur sublinearly [9]. That is, when \$\beta W > S(\tau\_S(\beta))\$, the conditions above mean that the ground state is reached in the first step of the protocol, and the excess energy is invested into the second step (a situation similar to the example mentioned in the above preliminary discussion). While the protocol is still optimal, one nonetheless has the strict inequality \$\mathcal{I}\_{AB} < \beta W\$.

### 30.3.3 Optimally Correlating Unitaries

However, open questions remain associated to the protocol discussed in the previous section. First, the protocol makes use of the conjectured existence of the unitaries  $U_{AB}$ , allowing to reach a final state with  $\rho_A = \tau_A(\beta)$  and  $\rho_B = \tau_B(\beta)$  starting from  $\tau_S(\beta_1)$ , i.e., with final state marginals that are both effectively at the original temperature. Second, one may question the practicality of the assumptions about the control over  $R$  and whether  $W_1 = F(\tau_S(\beta_1)) - F(\tau_S(\beta))$ ,  $S(\rho_R \| \tau_R) = 0$  and  $\mathcal{I}_{SR} = 0$  may be achieved within reasonable (time) constraints. Both of these issues connect to the previously mentioned scenario where one operates exclusively (and unitarily) on the closed systems  $S$ . There, the control requirement on  $R$  is relaxed from assuming the ability to perform arbitrary unitaries on the overall Hilbert space, to that of isolating and unitarily acting on the significantly smaller system  $S$ .

Moreover, both situations raise the question whether the respective optimal unitaries exist. In the case of the unitaries  $U_{AB}$  for step II of the protocol described in the previous section, the special requirement to reach  $\mathcal{I}_{AB} = \beta W$  in the low-energy regime where  $\beta W \leq S(\tau_S(\beta))$ , is that the effective temperatures of the marginals of the final state are both the original temperature  $T = 1/\beta$ . Mathematically, we can phrase the question of the existence of  $U_{AB}$  like this:

**Question 1** Does there exist a unitary  $U_{AB}$  on  $\mathcal{H}_{AB}$  such that

$$\rho_A = \text{Tr}_B(U_{AB}\tau_{AB}(\beta_1)U_{AB}^\dagger) = \tau_A(\beta), \quad (30.16)$$

$$\rho_B = \text{Tr}_A(U_{AB}\tau_{AB}(\beta_1)U_{AB}^\dagger) = \tau_B(\beta), \quad (30.17)$$

for every pair of local Hamiltonians  $H_A$  and  $H_B$ , for all temperatures  $T_1 = 1/\beta_1$  (after the step I) and all initial (and thus effective final) temperatures  $T = 1/\beta \geq T_1$ ?

For some important special cases, Question 1 can be answered affirmatively. For instance, it was shown in [8] that such optimally correlating unitaries exist whenever the local Hamiltonians are identical,  $H_A = H_B$ , and either all energy levels are equally spaced, i.e., and  $E_{m+1} - E_m = E_{n+1} - E_n$  for all  $m, n$  such that  $H_A |n\rangle = E_n |n\rangle$ , or for arbitrary spacings when the difference between  $T_1$  and  $T$  is large enough (for a quantitative statement see the appendix of [8]).

In particular, for two qubits,  $\mathcal{H}_A = \mathcal{H}_B = \mathbb{C}^2$  this means that optimal generation of correlations in the low-energy regime is always possible as long as  $H_A = H_B$ , since qubits only posses a single energy gap. However, as the preliminary extremal example treated above in Sect. 30.3.1 suggests, whenever  $H_A \neq H_B$  the optimally correlating unitaries  $U_{AB}$  cannot always lead to final states with marginals at the same temperatures, in particular, not in the limiting case when  $T_1 = 0$ . To be more precise, the subadditivity of the von Neumann entropy imposes the constraint

$$|S(\tau_A(\beta)) - S(\tau_B(\beta))| \leq S(\tau_{AB}(\beta)) = S(\tau_{AB}(\beta_1)) = S(\tau_A(\beta_1)) + S(\tau_B(\beta_1)) \quad (30.18)$$

between the initial and final marginal entropies. This constraint is not automatically satisfied if the energy levels of the Hamiltonians  $H_A$  and  $H_B$  are not equal, since  $S(\tau_A(\beta)) \neq S(\tau_B(\beta))$  in that case. Let us now also work out a counterexample for  $T_I > 0$ .

Consider a bipartite system with local Hamiltonians  $H_A = \omega_A |1\rangle\langle 1|_A$  and  $H_B = \omega_B |1\rangle\langle 1|_B$  with gaps  $\omega_A$  and  $\omega_B$ , respectively, where we have set the ground state energy levels to zero without loss of generality. Let us further define  $a_I := 1/(1 + e^{-\beta_I \omega_A})$  and  $b_I := 1/(1 + e^{-\beta_I \omega_B})$ . The initial state  $\tau_S(\beta_I)$  is then of the form

$$\tau_S(\beta_I) = \text{diag}\{a_I b_I, a_I(1-b_I), (1-a_I)b_I, (1-a_I)(1-b_I)\}. \quad (30.19)$$

If a unitary  $U_{AB}$  exists satisfying the requirements of Question 1, then the local reduced states  $\rho_A$  and  $\rho_B$  must be thermal (at the same temperature  $T = 1/\beta$ ), and hence diagonal w.r.t. the respective energy eigenbases. In particular, in the limiting case  $\omega_B \rightarrow \infty$  it is easy to see that the entropies of the single-qubit initial and final marginals for subsystem  $B$  are  $S(\tau_B(\beta)) = S(\tau_B(\beta_I)) = 0$  and the subadditivity constraint above would require  $S(\tau_A(\beta)) \leq S(\tau_A(\beta_I))$ , which cannot be satisfied for  $\beta < \beta_I$  for finite and nonzero  $\omega_A$ . To illustrate this more explicitly, we consider an example for finite temperatures and energy gaps, which for simplicity of presentation assumes only a restricted class of unitaries. That is, let us assume that only unitaries can be performed such that the density operator of the two-qubit final state  $\rho_S = U\tau_S U^\dagger$  is of the form

$$\rho_S = \begin{pmatrix} \rho_{00} & 0 & 0 & d_2 \\ 0 & \rho_{01} & d_1 & 0 \\ 0 & d_1^* & \rho_{10} & 0 \\ d_2^* & 0 & 0 & \rho_{11} \end{pmatrix} \quad (30.20)$$

for some appropriate  $d_1, d_2 \in \mathbb{C}$  and probabilities  $\rho_{00} + \rho_{01} + \rho_{10} + \rho_{11} = 1$ . The corresponding marginals are thus

$$\rho_A = \begin{pmatrix} \rho_{00} + \rho_{01} & 0 \\ 0 & \rho_{10} + \rho_{11} \end{pmatrix}, \quad \rho_B = \begin{pmatrix} \rho_{00} + \rho_{10} & 0 \\ 0 & \rho_{01} + \rho_{11} \end{pmatrix}, \quad (30.21)$$

such that  $\rho_{00} + \rho_{01} = 1/(1 + e^{-\beta \omega_A}) =: a$  and  $\rho_{00} + \rho_{10} = 1/(1 + e^{-\beta \omega_B}) =: b$ . Using these two conditions along with the normalization condition, we can express the diagonal elements of  $\rho_S$  as  $\rho_{01} = a - \rho_{00}$ ,  $\rho_{10} = b - \rho_{00}$ , and  $\rho_{11} = 1 + \rho_{00} - a - b$ . We can then calculate the eigenvalues  $\lambda_i$  (for  $i = 1, 2, 3, 4$ ) of  $\rho_S$  in terms of the variables  $\rho_{00}$ ,  $a$ ,  $b$ ,  $d_1$  and  $d_2$ , obtaining

$$\lambda_{1,4} = \rho_{00} + \frac{1}{2}(1 - a - b) \pm \sqrt{\left(\frac{1-a-b}{2}\right)^2 + |d_2|^2}, \quad (30.22a)$$

$$\lambda_{2,3} = \frac{1}{2}(a + b) - \rho_{00} \pm \sqrt{\left(\frac{a-b}{2}\right)^2 + |d_1|^2}. \quad (30.22b)$$

For any fixed choice of  $\omega_A$ ,  $\omega_B$ ,  $\beta$  and  $\beta < \beta_I$ , the state  $\rho_S$  lies in the unitary orbit of  $\tau_S(\beta_I)$ , when there exist valid choices of  $\rho_{00}$ ,  $d_1$  and  $d_2$ , such that the ordered list of the  $\lambda_i$  matches the diagonal entries of  $\tau_S$  given by Eq. (30.19). Here, note that since  $\lambda_4 \leq \lambda_1$  and  $\lambda_3 \leq \lambda_2$ , there are in principle 6 possible ways in which the  $\lambda_i$  could be ordered. For each of these 6 combinations, one can express  $\rho_{00}$  by adding  $\lambda_4$  and  $\lambda_1$  (or, equivalently,  $\lambda_3$  and  $\lambda_2$ ), which eliminates dependencies on the off-diagonals  $d_j$ . For instance, when  $\omega_A = 3\omega_B = 3\sqrt{\ln 2}$  and  $\beta_I = 2\beta = 2\sqrt{\ln 2}$ , one finds

$$\tau_S(\beta_I) = \text{diag} \left\{ \frac{256}{325}, \frac{64}{325}, \frac{4}{325}, \frac{1}{325} \right\}. \quad (30.23)$$

and the six possible ways to match with the  $\lambda_i$  result in the values

$$\rho_{00} = \frac{1}{5850} \times \begin{cases} 4505 & \text{if } \lambda_4 < \lambda_1 < \lambda_3 < \lambda_2 \\ 3965 & \text{if } \lambda_4 < \lambda_3 < \lambda_1 < \lambda_2 \\ 2237 & \text{if } \lambda_4 < \lambda_3 < \lambda_2 < \lambda_1 \\ 1670 & \text{if } \lambda_3 < \lambda_2 < \lambda_4 < \lambda_1 \\ 2210 & \text{if } \lambda_3 < \lambda_4 < \lambda_2 < \lambda_1 \\ 3938 & \text{if } \lambda_3 < \lambda_4 < \lambda_1 < \lambda_2 \end{cases}. \quad (30.24)$$

At the same time, the positivity of  $\lambda_3 \geq 0$  and  $\lambda_4 \geq 0$  then demands that

$$\left( \frac{7}{9} - \rho_{00} \right)^2 - \frac{1}{81} \geq |d_1|^2 \geq 0, \quad (30.25)$$

$$\left( \rho_{00} - \frac{5}{18} \right)^2 - \left( \frac{5}{18} \right)^2 \geq |d_2|^2 \geq 0, \quad (30.26)$$

which can be turned into the inequality

$$\frac{3250}{5850} \leq \rho_{00} \leq \frac{3900}{5850}. \quad (30.27)$$

Since none of the values in Eq. (30.24) satisfy this inequality, there are some choices of  $\omega_A$ ,  $\omega_B$ ,  $\beta_I$  and  $\beta < \beta_I$  such that it is impossible to find the corresponding  $\rho_{00}$ . Together, these examples illustrate that unitaries allowing to achieve  $\mathcal{I}_{AB} = \beta W$  in the low-energy regime of the two-step protocol of [9] do not exist in general.

Although the general answer to Question 1 is thus negative, this leaves us with a number of interesting open problems, with which we conclude.

## 30.4 Open Problems and Conclusion

First, we note that a more restricted version of Question 1 for the large class of situations when the local Hamiltonians are identical but not equally spaced (beyond local dimension 2) remains unanswered. Moreover, one could ask more generally about the optimal conversion of average energy to mutual information in the unitary case and whether it is possible to find cases, where some of the invested work

necessarily gets stuck in locally passive, but not thermal states. Second, while we have seen from Eq. (30.14) that reaching  $\mathcal{I}_{AB} = \beta W$  is in general not possible for solely unitary correlating protocols (since this would require  $S(\rho_A \| \tau_A) = S(\rho_B \| \tau_B) = 0$  and hence  $\rho_A = \tau_A$  and  $\rho_B = \tau_B$ ), one may ask what the optimal trade-off between work and correlations is in such cases. This question also applies in equal manner to the high-energy regime where  $W > S(\tau_S(\beta))$ , which corresponds exactly to the example in Sect. 30.3.1.

Another interesting problem is the question whether it is possible that there is a combination of  $H_A$ ,  $H_B$ , and  $\beta$  such that for some given amount of work  $W$ , the restricted unitary  $U_{AB}$  required for the low-energy regime of the two-step protocol of Sect. 30.3.2 exists, allowing correlations to be created in the amount of  $\beta W$ , while no optimally correlating unitaries exists that could achieve  $\beta W$  directly (without cooling). This would imply that correlations could be created optimally only by using control over the reservoir  $R$  for cooling, but the corresponding work value stored in the correlations [33] could not be retrieved unitarily from the system. In this sense work would be *bound* in the system.

Let us also remark that the protocols and optimal unitaries discussed here apply for the creation of correlations as measured by the mutual information. However, when one restricts to genuine quantum correlations, i.e., entanglement, the situation becomes vastly more complicated, starting with the fact that there are many inequivalent measures and it is in general hard to even calculate how much entanglement is present w.r.t. any of these. Consequently, some simple cases of optimal protocols are known [8, 9], suggesting that, indeed, quite different protocols are required, but much is yet to be discovered. Nonetheless, a measure-independent question is of course the (partial)-separability of quantum states. There is a minimum work cost to turn a thermal product state into a (multipartite) entangled state. In [8], limiting temperatures for entanglement generation were shown to scale linearly with the number of parties, i.e.,  $T_{\max} \leq O(E \cdot (n - 1))$  for an exponentially small work cost, i.e.,  $W \leq O(E \cdot n \cdot c^{-n})$ , where  $c$  is a constant. Alternatively, one might also consider correlation quantifiers that do not distinguish between classical and quantum correlations at all, which is of relevance, e.g., when assessing the correlations between a measured system and the measurement apparatus after non-ideal measurement procedures [51].

In conclusion, the interplay of work and correlations provides a fascinating but complex interface between quantum thermodynamics and quantum information theory that reveals interesting quantum effects in thermodynamics and allows for advantages for certain paradigmatic tasks such as work extraction. While some of the questions arising from the conversion of these resources have been addressed, a number of subtle but challenging open problems remain.

**Acknowledgements** We are grateful to Faraj Bakhshinezhad, Felix Binder, and Felix Pollock for helpful comments and suggestions. We thank Rick Sanchez for moral support. We acknowledge support from the Austrian Science Fund (FWF) through the START project Y879-N27, the Lise-Meitner project M 2462-N27, the project P 31339-N27, and the joint Czech-Austrian project MultiQUEST (I 3053-N27 and GF17-33780L).

## References

1. F.G.S.L. Brandão, M. Horodecki, J. Oppenheim, J.M. Renes, R.W. Spekkens, The resource theory of quantum states out of thermal equilibrium. *Phys. Rev. Lett.* **111**, 250404 (2013). <https://doi.org/10.1103/PhysRevLett.111.250404>
2. M.A. Nielsen, I.L. Chuang, *Quantum Computation and Quantum Information* (Cambridge University Press, Cambridge). <https://doi.org/10.1017/CBO9780511976667.001>
3. M. Horodecki, J. Oppenheim, Quantumness in the context of resource theories. *Int. J. Mod. Phys. B* **27**, 1345019 (2013). <https://doi.org/10.1142/S0217979213450197>
4. C. Eltschka, J. Siewert, Quantifying entanglement resources. *J. Phys. A: Math. Theor.* **47**, 424005 (2014). <https://doi.org/10.1088/1751-8113/47/42/424005>
5. J. Goold, M. Huber, A. Riera, L. del Rio, P. Skrzypczyk, The role of quantum information in thermodynamics – a topical review. *J. Phys. A: Math. Theor.* **49**, 143001 (2016). <https://doi.org/10.1088/1751-8113/49/14/143001>
6. J. Millen, A. Xuereb, Perspective on quantum thermodynamics. *New J. Phys.* **18**, 011002 (2016). <https://doi.org/10.1088/1367-2630/18/1/011002>
7. S. Vinjanampathy, J. Anders, Quantum thermodynamics. *Contemp. Phys.* **57**, 1 (2016). <https://doi.org/10.1080/00107514.2016.1201896>
8. M. Huber, M. Perarnau-Llobet, K.V. Hovhannisyan, P. Skrzypczyk, C. Klöckl, N. Brunner, A. Acín, Thermodynamic cost of creating correlations. *New J. Phys.* **17**, 065008 (2015). <https://doi.org/10.1088/1367-2630/17/6/065008>
9. D.E. Bruschi, M. Perarnau-Llobet, N. Friis, K.V. Hovhannisyan, M. Huber, The thermodynamics of creating correlations: Limitations and optimal protocols. *Phys. Rev. E* **91**, 032118 (2015). <https://doi.org/10.1103/PhysRevE.91.032118>
10. G.L. Giorgi, S. Campbell, Correlation approach to work extraction from finite quantum systems. *J. Phys. B: At. Mol. Opt. Phys.* **48**, 035501 (2015). <https://doi.org/10.1088/0953-4075/48/3/035501>
11. N. Friis, M. Huber, M. Perarnau-Llobet, Energetics of correlations in interacting systems. *Phys. Rev. E* **93**, 042135 (2016). <https://doi.org/10.1103/PhysRevE.93.042135>
12. G. Francica, J. Goold, F. Plastina, M. Paternostro, Daemonic ergotropy: enhanced work extraction from quantum correlations. *npj Quantum Inf.* **3**, 12 (2017). <https://doi.org/10.1038/s41534-017-0012-8>
13. V. Vedral, The role of relative entropy in quantum information theory. *Rev. Mod. Phys.* **74**, 197–234 (2002). <https://doi.org/10.1103/RevModPhys.74.197>
14. E.T. Jaynes, Information theory and statistical mechanics. *Phys. Rev.* **106**, 620–630 (1957). <https://doi.org/10.1103/PhysRev.106.620>
15. N.J. Cerf, C. Adami, Quantum extension of conditional probability. *Phys. Rev. A* **60**, 893 (1999). <https://doi.org/10.1103/PhysRevA.60.893>
16. L. Del Rio, J. Åberg, R. Renner, O. Dahlsten, V. Vedral, *Nature* **474**, 61–63 (2011), <https://doi.org/10.1038/nature10123>
17. N. Friis, S. Bulusu, R.A. Bertlmann, Geometry of two-qubit states with negative conditional entropy. *J. Phys. A: Math. Theor.* **50**, 125301 (2017). <https://doi.org/10.1088/1751-8121/aa5dfd>
18. A. Stokes, P. Deb, A. Beige, Using thermodynamics to identify quantum subsystems. *J. Mod. Opt.* **64**, S7–S19 (2017). <https://doi.org/10.1080/09500340.2017.1295108>
19. H. Weimer, M.J. Henrich, F. Rempp, H. Schröder, G. Mahler, Local effective dynamics of quantum systems: a generalized approach to work and heat. *Europhys. Lett.* **83**, 30008 (2008). <https://doi.org/10.1209/0295-5075/83/30008>
20. J. Teifel, G. Mahler, Autonomous modular quantum systems: contextual Jarzynski relations. *Phys. Rev. E* **83**, 041131 (2011). <https://doi.org/10.1103/PhysRevE.83.041131>
21. M.H. Partovi, Entanglement versus Stosszahlansatz: Disappearance of the thermodynamic arrow in a high-correlation environment. *Phys. Rev. E* **77**, 021110 (2008). <https://doi.org/10.1103/PhysRevE.77.021110>

22. D. Jennings, T. Rudolph, Entanglement and the thermodynamic arrow of time. *Phys. Rev. E* **81**, 061130 (2010). <https://doi.org/10.1103/PhysRevE.81.061130>
23. S. Jevtic, D. Jennings, T. Rudolph, Maximally and minimally correlated states attainable within a closed evolving system. *Phys. Rev. Lett.* **108**, 110403 (2012a). <https://doi.org/10.1103/PhysRevLett.108.110403>
24. S. Jevtic, D. Jennings, T. Rudolph, Quantum mutual information along unitary orbits. *Phys. Rev. A* **85**, 052121 (2012b). <https://doi.org/10.1103/PhysRevA.85.052121>
25. F. Brandão, M. Horodecki, N. Ng, J. Oppenheim, S. Wehner, The second laws of quantum thermodynamics. *Proc. Natl. Acad. Sci. U.S.A.* **11**, 3275–3279 (2015). <https://doi.org/10.1073/pnas.1411728112>
26. S. Alipour, F. Benatti, F. Bakhshinezhad, M. Afsary, S. Marcantoni, A.T. Rezakhani, Correlations in quantum thermodynamics: Heat, work, and entropy production. *Sci. Rep.* **6**, 35568 (2016). <https://doi.org/10.1038/srep35568>
27. M.N. Bera, A. Riera, M. Lewenstein, A. Winter, Generalized laws of thermodynamics in the presence of correlations. *Nat. Commun.* **8**, 2180 (2017). <https://doi.org/10.1038/s41467-017-02370-x>
28. M.P. Müller, Correlating thermal machines and the second law at the nanoscale. *Phys. Rev. X* **8**, 041051 (2018). <https://doi.org/10.1103/PhysRevX.8.041051>
29. L. Boltzmann, Weitere Studien über das Wärmegleichgewicht unter Gasmolekülen, in *Kinetische Theorie II: Irreversible Prozesse Einführung und Originaltexte* (Vieweg+Teubner Verlag, Wiesbaden, 1970) pp. 115–225. [https://doi.org/10.1007/978-3-322-84986-1\\_3](https://doi.org/10.1007/978-3-322-84986-1_3)
30. L. Boltzmann, Zu Hrn. Zermelos Abhandlung über die mechanische Erklärung irreversiler Vorgänge (On the mechanical explanation of irreversible processes). *Ann. Phys.* **60**, 392–398 (1897). <https://doi.org/10.1002/andp.18972960216>
31. L. del Rio, A. Hutter, R. Renner, S. Wehner, Relative Thermalization. *Phys. Rev. E* **94**, 022104 (2016). <https://doi.org/10.1103/PhysRevE.94.022104>
32. K. Micadei, J.P.S. Peterson, A.M. Souza, R.S. Sarthour, I.S. Oliveira, G.T. Landi, T.B. Batalhão, R.M. Serra, E. Lutz, Reversing the thermodynamic arrow of time using quantum correlations (2017). [arXiv:1711.03323](https://arxiv.org/abs/1711.03323)
33. M. Perarnau-Llobet, K.V. Hovhannisyan, M. Huber, P. Skrzypczyk, N. Brunner, A. Acín, Extractable work from correlations. *Phys. Rev. X* **5**, 041011 (2015). <https://doi.org/10.1103/PhysRevX.5.041011>
34. A.E. Allahverdyan, R. Balian, T.M. Nieuwenhuizen, Maximal work extraction from finite quantum systems. *Europhys. Lett.* **67**, 565 (2004). <https://doi.org/10.1209/epl/i2004-10101-2>
35. W. Pusz, S.L. Woronowicz, Passive states and KMS states for general quantum systems. *Commun. Math. Phys.* **58**, 273–290 (1978). <https://doi.org/10.1007/BF01614224>
36. R. Alicki, M. Fannes, Entanglement boost for extractable work from ensembles of quantum batteries. *Phys. Rev. E* **87**, 042123 (2013). <https://doi.org/10.1103/PhysRevE.87.042123>
37. A. Lenard, Thermodynamical proof of the Gibbs formula for elementary quantum system. *J. Stat. Phys.* **19**, 575–586 (1978). <https://doi.org/10.1007/BF01011769>
38. K.V. Hovhannisyan, M. Perarnau-Llobet, M. Huber, A. Acín, Entanglement generation is not necessary for optimal work extraction. *Phys. Rev. Lett.* **111**, 240401 (2013). <https://doi.org/10.1103/PhysRevLett.111.240401>
39. F.C. Binder, S. Vinjanampathy, K. Modi, J. Goold, Quantacell: powerful charging of quantum batteries. *New J. Phys.* **17**, 075015 (2015). <https://doi.org/10.1088/1367-2630/17/7/075015>
40. N. Friis, M. Huber, Precision and work fluctuations in gaussian battery charging. *Quantum* **2**, 61 (2018). <https://doi.org/10.22331/q-2018-04-23-61>
41. F. Campaioli, F.A. Pollock, F.C. Binder, L.C. Céleri, J. Goold, S. Vinjanampathy, K. Modi, Enhancing the charging power of quantum batteries. *Phys. Rev. Lett.* **118**, 150601 (2017). <https://doi.org/10.1103/PhysRevLett.118.150601>
42. D. Ferraro, M. Campisi, G.M. Andolina, V. Pellegrini, M. Polini, High-power collective charging of a solid-state quantum battery. *Phys. Rev. Lett.* **120**, 117702 (2018). <https://doi.org/10.1103/PhysRevLett.120.117702>

43. E.G. Brown, N. Friis, M. Huber, Passivity and practical work extraction using Gaussian operations. *New J. Phys.* **18**, 113028 (2016). <https://doi.org/10.1088/1367-2630/18/11/113028>
44. M. Brunelli, M.G. Genoni, M. Barbieri, M. Paternostro, Detecting Gaussian entanglement via extractable work. *Phys. Rev. A* **96**, 062311 (2017). <https://doi.org/10.1103/PhysRevA.96.062311>
45. J. Oppenheim, M. Horodecki, P. Horodecki, R. Horodecki, A thermodynamical approach to quantifying quantum correlations. *Phys. Rev. Lett.* **89**, 180402 (2002). <https://doi.org/10.1103/PhysRevLett.89.180402>
46. J. Oppenheim, K. Horodecki, M. Horodecki, P. Horodecki, R. Horodecki, A new type of complementarity between quantum and classical information. *Phys. Rev. A* **68**, 022307 (2003). <https://doi.org/10.1103/PhysRevA.68.022307>
47. M. Esposito, C. Van den Broeck, Second law and landauer principle far from equilibrium. *Europhys. Lett.* **95**, 40004 (2011). <https://doi.org/10.1209/0295-5075/95/40004>
48. D. Reeb, M.M. Wolf, An improved Landauer Principle with finite-size corrections. *New J. Phys.* **16**, 103011 (2014). <https://doi.org/10.1088/1367-2630/16/10/103011>
49. J. Åberg, Truly work-like work extraction via a single-shot analysis. *Nat. Commun.* **4**, 1925 (2013). <https://doi.org/10.1038/ncomms2712>
50. P. Skrzypczyk, A.J. Short, S. Popescu, Work extraction and thermodynamics for individual quantum systems. *Nat. Commun.* **5**, 4185 (2014). <https://doi.org/10.1038/ncomms5185>
51. Y. Guryanova, N. Friis, M. Huber, Ideal projective measurements have infinite resource costs. [arXiv:1805.11899](https://arxiv.org/abs/1805.11899)

# Chapter 31

## Quantum Thermodynamics with Multiple Conserved Quantities



Erick Hinds Mingo, Yelena Guryanova, Philippe Faist and David Jennings

### 31.1 Introduction

Thermodynamics has been remarkable in its applicability to a vast array of systems. Indeed, the laws of macroscopic thermodynamics have been successfully applied to the studies of magnetization [1, 2], superconductivity [3], cosmology [4], chemical reactions [5] and biological phenomena [6, 7], to name a few fields. In thermodynamics, energy plays a key role as a thermodynamic potential, that is, as a function of the other thermodynamic variables which characterize all the thermodynamic properties of the system. In the presence of thermodynamic reservoirs, however, physical quantities which are globally conserved can be exchanged with the reservoirs, and the thermodynamic properties of the system are more conveniently expressed in terms of other potentials. For example, in the grand canonical ensemble, particle number  $N$  as well as energy  $E$  are exchanged with a reservoir. The relevant thermodynamic potential becomes,

$$F = E - \mu N - TS , \quad (31.1)$$

where  $S$  is the entropy, and where  $T$  and  $\mu$  are the *temperature* of the heat bath and the *chemical potential* of the particle reservoir, respectively. The chemical potential

---

E. Hinds Mingo

QOLS, Blackett Laboratory, Imperial College London, London SW7 2AZ, United Kingdom

Y. Guryanova

Institute for Quantum Optics and Quantum Information (IQOQI), Boltzmanngasse 3,  
1090 Vienna, Austria

P. Faist

Institute for Quantum Information and Matter, Caltech, Pasadena CA 91125, USA

E. Hinds Mingo · D. Jennings (✉)

Department of Physics, University of Oxford, Oxford OX1 3PU, United Kingdom  
e-mail: david.jennings@physics.ox.ac.uk

$\mu$  acts as an ‘exchange rate’ between particle number and energy, in the same way that temperature  $T$  acts as an exchange rate between entropy and energy. Thus,  $\mu$  describes the energetic cost of adding another particle to a gas at constant entropy. In classical equilibrium thermodynamics, for  $k$  conserved quantities, or *charges*<sup>1</sup>  $\{Q_k\}$  the function  $U(S, Q_1, \dots, Q_r)$  characterises the internal energy of the system. Each charge has an associated ‘exchange rate’  $\mu_i := \frac{\partial U}{\partial Q_i}$  that governs the response in energy when one varies the equilibrium value of  $Q_i$ .

Equivalently, one can use the entropic formulation of thermodynamics to interpret the change in a system at equilibrium. The ‘entropic response’ to any change in an extensive variable is given by the generalised temperatures  $\beta_k := \frac{\partial S}{\partial Q_k}$ , which are related to the chemical potentials by  $\beta_k = \frac{\mu_k}{T}$ .

A canonical example is provided by a macroscopic system with angular momentum observables  $(J_x, J_y, J_z) =: \mathbf{J}$ , which has a non-zero polarization in these observables along some axis when in thermodynamic equilibrium. The internal energy for this thermodynamic system is therefore a function  $U(S, \mathbf{J})$  where  $\mathbf{J} = \mathbf{J} \cdot \mathbf{n}$ , and  $\mathbf{n}$  is a unit vector along the distinguished axis. Any relaxation to equilibrium occurs through the microscopic exchange of angular momentum with the environment. Indeed, the environment must play a role of defining a thermodynamic constraints for the system, in both energy and angular momentum. Subject to these constraints, the equilibrium thermodynamics is determined by maximization of the entropy  $S$  in the usual way.

More recently, researchers have been experimenting with the idea that quantum mechanics could also present interesting and novel features in conjunction with thermodynamic systems on the microscopic scale. While a well-established framework exists for macroscopic equilibrium systems, it is less clear how to handle finite-sized systems with multiple conserved charges that may display quantum mechanical features, such as complementarity.

A straightforward approach to studying thermodynamics of systems possessing multiple conserved charges is to apply the quantum version of Jaynes’ principle [8, 9], which prescribes that one should maximize the (von Neumann) entropy subject to constraints on the average values  $\{v_j\}$  of the conserved charges  $\{Q_j\}$ :

$$\begin{aligned} & \text{maximize: } S(\tau) \\ & \text{subject to: } \text{Tr}(Q_j \tau) = v_j \quad \forall j . \end{aligned} \tag{31.2}$$

The unique solution is the so-called *generalized Gibbs state* (or *generalized Gibbs ensemble*)

$$\tau = \frac{e^{-(\beta_1 Q_1 + \dots + \beta_k Q_k)}}{\mathcal{Z}}, \tag{31.3}$$

---

<sup>1</sup>Terms we will use interchangeably.

where the  $\{\beta_j\}$  are generalized inverse temperatures or generalized chemical potentials which are determined by the  $\{v_j\}$ . The partition function  $\mathcal{Z} = \text{Tr}[e^{-(\beta_1 Q_1 + \dots + \beta_k Q_k)}]$  normalises the state.

While the generalized Gibbs state is distinguished as resulting from Jaynes' principle, it is not clear how this state may be interpreted as the thermal state of the system on a physical level.

As an illustration, we could consider a single spin-1/2 particle with degenerate Hamiltonian  $H = 0$  and spin angular momentum operators given by the Pauli operators  $(\sigma_x, \sigma_y, \sigma_z)$ . We might wish to create constraints on this system such that the expectation values are fixed  $\langle \sigma_x \rangle = s_x$  and  $\langle \sigma_y \rangle = s_y$  for constant  $s_x, s_y$ . In accordance with the maximum entropy formulation, the state we infer from these constraints admits the form

$$\tau = \frac{e^{-\beta_x \sigma_x - \beta_y \sigma_y}}{\mathcal{Z}}, \quad (31.4)$$

for  $\mathcal{Z} = \text{Tr}[e^{-\beta_x \sigma_x - \beta_y \sigma_y}]$ , and some constants  $\beta_x$  and  $\beta_y$ . In realisations of this setup, one might expect the quantum system could interact with its environment and relax under some dynamics to the generalized Gibbs state, which is addressed in Part III when dealing with dynamical equilibration.

Subtleties arise in making this assumption. The existence of a physical map that realises this state subject to the constraints turns out to be forbidden by quantum mechanics. Specifically it is known the so-called ‘pancake map’ that projects a spin-1/2 state onto the disk in  $X - Y$  plane would be allowed if quantum mechanics had no entanglement, but the presence of entanglement creates negative probabilities and is thus an unphysical transformation (technically, this map is not completely positive) [10].

Given this and other subtleties (such as even defining a micro-canonical ensemble for non-commuting charges), a basic question for contemporary quantum thermodynamics is therefore to understand whether the thermal state of a quantum system is indeed given by (31.3) in the presence of multiple, possibly non-commuting charges [11].

In the situation where the charges commute, it was already shown that Landauer erasure could be carried out by utilizing physical quantities other than energy [12, 13] (see also Chap. 29), and that the resource theory approach to quantum thermodynamics [14, 15] (see also Chap. 26) could be generalized to multiple physical quantities [11, 16, 17].

On the other hand, the generalized Gibbs ensemble was given considerable interest in the context of systems which are integrable, i.e., which do not thermalize, as further constants of motion constrain the evolution of the system [18, 19]. Such situations have been demonstrated experimentally [20, 21]. Work extraction was also studied in the context of generalized Gibbs ensembles, bridging both aspects [22].

In this chapter, we derive the form of this state through the lens of two different approaches introduced in Refs. [10, 23, 24]. In the process, we explain how these approaches fit together with the usual concepts of statistical mechanics such as the microcanonical state on one hand, and with the second law of thermodynamics and

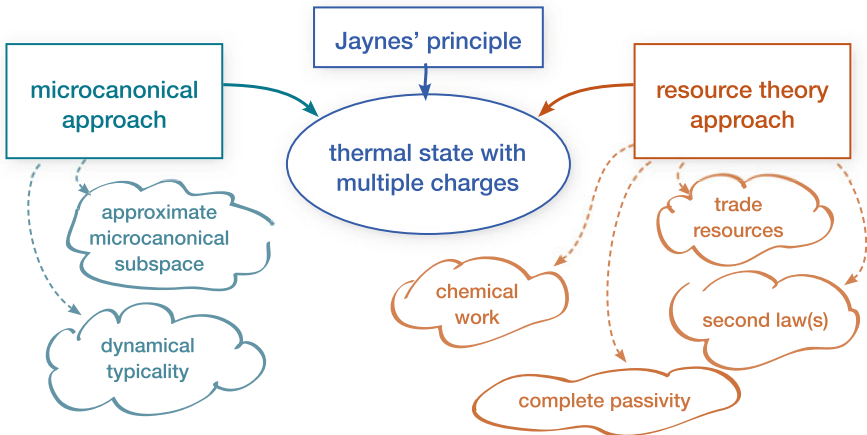


**Fig. 31.1** The thermal state in the presence of multiple reservoirs corresponding to different physical charges can be determined via several approaches. If the charges commute, the equilibrium state of a system is a corresponding grand-canonical state, which is readily derived by either considering a microcanonical ensemble over the system and the reservoirs, by Jaynes' principle, or via resource-theoretic considerations [16]. While it is straightforward to apply Jaynes' principle to the case of non-commuting charges, the other two approaches need to be adapted. This chapter reviews how to generalize these approaches to non-commuting charges, introducing along the way the notions of an approximate microcanonical subspace and how it connects with dynamical typicality, as well as the idea of trading resources using batteries, the second law and complete passivity for non-commuting charges, and chemical work.

complete passivity on the other (Fig. 31.1). We primarily address the topic using tools from quantum information theory, which provide novel approaches for dynamical typicality and equilibration theory of arbitrary charges  $\{Q_1, \dots, Q_n\}$  that may have non-trivial commutation relations among themselves. In addition, the recent resource-theoretic approach to thermodynamics has allowed a well-defined framework in which to analyse quantum thermodynamics without the need to use notions of ‘heat’ or ‘work’ as defining concepts. We also discuss how multiple conserved charges can fit into such an approach and discuss the subtleties that can arise when one attempts to do so. Finally we discuss information-theoretic aspects of quantum thermodynamics with multiple conserved charges and provide a generalized Landauer bound that shows that erasure can be carried out at no energetic cost. Lastly, we discuss the status of this topic within contemporary quantum thermodynamics and the core challenges that exist going forward.

## 31.2 Microcanonical Approach

In this section we present an approach for deriving the form of the generalized Gibbs state by generalizing the concept of a microcanonical subspace to noncommuting charges.

In the presence of reservoirs exchanging commuting charges, the thermal state of the system can be derived by considering the system together with the reservoirs as a huge system in a microcanonical state, i.e., the maximally mixed state living in the common subspace of fixed total value of each charge, and then tracing out the reservoirs. For instance, if a system  $s$  is in contact with both a heat reservoir  $R_1$  and a particle reservoir  $R_2$ , we assume that the total system has fixed values of energy  $E$  and number of particles  $N$  and we consider the common eigenspace of the Hamiltonian and the number operator on the total system, the projector on which we denote by  $\Pi^{(E,N)}$ . Due to the fundamental postulate of statistical mechanics, the corresponding microcanonical state is  $\Omega^{(E,N)} = \Pi^{(E,N)} / \text{Tr}[\Pi^{(E,N)}]$ , and under mild assumptions one can show that for large reservoirs the reduced state on the system is the grand canonical ensemble,  $\tau = \text{Tr}_{R_1 R_2} [\Omega^{(E,N)}] \approx e^{-\beta(H_s - \mu N_s)} / \mathcal{Z}(\beta, \mu)$ , where  $\beta, \mu$  are the inverse temperature and the chemical potential, respectively, and where  $H_s$  and  $N_s$  are the Hamiltonian and number operator of the system (see Part III, as well as Refs. [25, 26]).

If the charges do not commute, then there are no common eigenspaces for the different charges, and we cannot define  $\Pi^{(E,N)}$  as above. However, this approach can be adapted so that it applies to noncommuting charges. The key idea, proposed by Yunger Halpern et al. [23], is the following: If we consider many copies of the system, there may be no exact common eigenspaces, but we may define instead an *approximate microcanonical subspace*. Instead of fixing the values of the charges exactly, the approximate microcanonical subspace only fixes them approximately, by considering states which have sharply peaked statistics for each charge (Fig. 31.2). So, we may consider the maximally mixed state supported on this subspace, and it turns out that tracing out the reservoirs yields a thermal state of the required form (31.3).

The argument of Ref. [23] goes as follows. Consider a system  $s$  with multiple physical charges represented by operators  $Q_1, \dots, Q_k$ , which do not necessarily commute. We consider  $N$  copies of  $s$ ; conceptually we might, for instance, think of the first copy as being the system of interest, and the rest as parts forming a large bath. The composite average observables are defined as:

$$\bar{Q}_i := \frac{1}{N} \sum_{l=0}^{N-1} \mathbb{1}^{\otimes l} \otimes Q_i \otimes \mathbb{1}^{\otimes(N-1-l)}. \quad (31.5)$$

Because the charges do not commute, there may be no common eigenspaces to the set of operators  $\bar{Q}_i$ . However, the noncommutativity of the  $\bar{Q}_i$  “wears out” over many copies: One readily sees that  $\|[\bar{Q}_i, \bar{Q}_j]\| \sim 1/N \rightarrow 0$  as  $N \rightarrow \infty$ . Intuitively, it should be possible to find a subspace which behaves approximately like a microcanonical subspace over the  $N$  systems for large  $N$ . For commuting charges, a defining property of the usual microcanonical subspace is that it contains all states which have a fixed given value for each charge. So, for noncommuting charges, a natural

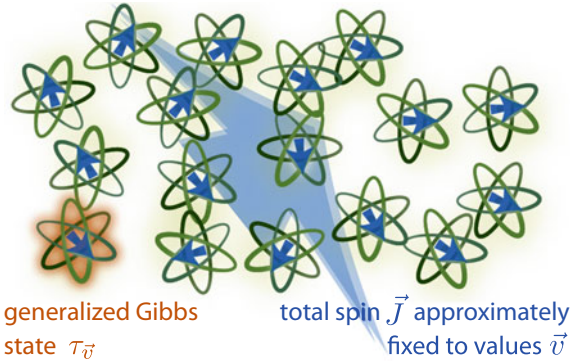


**Fig. 31.2** The thermal state of a system in the presence of multiple noncommuting conserved charges can be derived from an approximate microcanonical subspace on many copies of the system. (For instance, the charges might be components of the spin  $\mathbf{J}$ .) This subspace has the property that states within the subspace have statistics for each charge that are sharply peaked around a given set of values  $\mathbf{v}$ . If we trace out all systems except one, the reduced state is close to the generalized Gibbs state  $\tau_{\mathbf{v}} \propto \exp(-\sum \beta_i J_i)$  for appropriate generalized chemical potentials  $\{\beta_i\}$ . Figure reproduced from Ref. [23] (CC-BY) with adapted notation.

loosening of this condition is to require that any state in the subspace has sharply peaked statistics for each charge, and conversely, that any state with sharply peaked statistics for each charge has large overlap with the subspace. Such a subspace is called an *approximate microcanonical subspace*:

**Definition 1** An *approximate microcanonical subspace*  $\mathcal{M}$  associated to fixed average values  $\{v_j\}$  of the charges  $\{Q_j\}$ , is a subspace of  $\mathcal{H}_s^{\otimes N}$  obeying the two following properties:

- (i) Any state  $\rho$  with support inside  $\mathcal{M}$  produces sharp statistics for measurements of  $\bar{Q}_j$  for all  $j$ :

$$\rho \text{ in } \mathcal{M} \quad \Rightarrow \quad \Pr[(\text{outcome of } \bar{Q}_j) \approx v_j] \approx 1 \quad \forall j ; \quad (31.6)$$

- (ii) Conversely, any state  $\rho$  producing sharp statistics for all  $Q_j$  has high overlap with  $\mathcal{M}$ :

$$\Pr[(\text{outcome of } \bar{Q}_j) \approx v_j] \approx 1 \quad \forall j \quad \Rightarrow \quad \text{Tr}[P\rho] \approx 1 , \quad (31.7)$$

where  $P$  is the projector onto the subspace  $\mathcal{M}$ .

(This definition is made technically precise by introducing an additive tolerance parameter for each approximation denoted by ‘ $\approx$ ’ above [23].) It is not obvious that this “epsilonification” of the usual microcanonical ensemble still has the properties we would like—in particular, that the reduced state on a single system is close to the generalized Gibbs state (31.3). It turns out, though, that any approximate

microcanonical subspace has this property. We can quantify the distance between the reduced states on each system and the generalized Gibbs state using the relative entropy  $D(\rho\|\sigma) = \text{Tr}(\rho(\log\rho - \log\sigma))$ . The average relative entropy to the generalized Gibbs state of the reduced states on each system is small:

**Theorem 2** *Let  $\mathcal{M}$  be any approximate microcanonical subspace on  $\mathcal{H}_s^{\otimes N}$ , and define the approximate microcanonical state  $\Omega = P/\text{Tr}[P]$ , where  $P$  is the projector onto the subspace  $\mathcal{M}$ . Then, on average, the reduced state on system  $\ell$  looks like the generalized Gibbs state:*

$$\frac{1}{N} \sum_{\ell=1}^N D \left( \text{Tr}_{1,\dots,\ell-1,\ell+1,\dots,N}[\Omega] \middle\| \frac{e^{-\sum_i \beta_i Q_i}}{\mathcal{Z}(\beta_1, \dots, \beta_k)} \right) \sim \frac{1}{\sqrt{N}}, \quad (31.8)$$

for appropriate generalized inverse temperatures  $\{\beta_j\}$ .

It is left to show that it is possible to actually construct an approximate microcanonical subspace, i.e., that such a subspace actually exists for any collection of observables and for large enough  $N$ . We may construct an approximate microcanonical subspace as follows. A theorem by Ogata [27] guarantees that there exist operators  $\{\bar{Y}_j\}$  on the  $N$  systems which are close to the  $\{\bar{Q}_j\}$ , and which *do* commute exactly:  $[\bar{Y}_i, \bar{Y}_j] = 0$  for all  $i, j$  and  $\|\bar{Y}_j - \bar{Q}_j\| \rightarrow 0$  as  $N \rightarrow \infty$ . So, given a set of charge values  $\{v_j\}$ , it is possible to consider the common eigenspace  $\mathcal{M}_{\text{com}}$  of all the  $\{\bar{Y}_j\}$  corresponding to eigenvalues which are approximately equal to  $\{v_j\}$ . The subspace  $\mathcal{M}_{\text{com}}$  is an approximate microcanonical subspace for the commuting observables  $\bar{Y}_j$  and values  $\{v_j\}$ , because a usual microcanonical subspace is in particular an approximate microcanonical subspace.<sup>2</sup> Now, because  $\bar{Y}_j \approx \bar{Q}_j$ , a state with sharp statistics for  $\bar{Y}_j$  also has sharp statistics for  $\bar{Q}_j$  and *vice versa*. Hence finally, the subspace  $\mathcal{M}_{\text{com}}$  is in fact (after adapting the tolerance parameters) also an approximate microcanonical subspace for the  $\{\bar{Q}_j\}$ . The construction works for any  $N$  large enough, and the tolerance parameters of the subspace may be taken to all go to zero simultaneously as  $N \rightarrow \infty$ .

While Ogata's theorem provides an intuitive way to construct an approximate microcanonical subspace, we note that other constructions are possible. Furthermore it is possible to ensure that the subspace is manifestly permutation-invariant [28].

### 31.2.1 Dynamical Typicality and Evolution

One may ask, is there any sense in which the system can be argued to *evolve* towards the generalized Gibbs state (31.3)? A possible answer to this question is provided from the point of view of dynamical typicality, or canonical typicality (see Part III

---

<sup>2</sup>In Ref. [23], the argument considers more generally an approximate microcanonical subspace over  $m$  copies of the whole system, i.e., over a total of  $Nm$  systems.

as well as Refs. [29–31]). There, the idea is that on a system and a reservoir, any state chosen at random in a microcanonical subspace has a reduced state on the single system that looks thermal with overwhelming probability. If the evolution is sufficiently ergodic, exploring the full accessible state space, then the system will look thermal over an overwhelmingly large fraction of time.

The microcanonical approach provides a useful tool to analyze the situation of noncommuting multiple charges in the context of dynamical typicality [23]. Consider as above  $N$  copies of a system  $s$  with a collection of physical quantities  $\{\bar{Q}_j\}$ . Here we assume that all charges commute with the Hamiltonian  $H$  governing the time evolution ( $H$  may or may not be included in the collection  $\{Q_j\}$ ). Assume that the  $N$  systems are in a state  $|\psi\rangle$  which lives in an approximate microcanonical subspace  $\mathcal{M}$  corresponding to charge values  $\{v_j\}$ . Canonical typicality asserts that if  $|\psi\rangle$  is chosen uniformly at random in the subspace, then on average the reduced state on any single system  $\ell$  is well approximated by the reduced microcanonical state:

$$\left\langle \frac{1}{2} \left\| \text{Tr}_{1,\dots,\ell-1,\ell+1,\dots,N}(\psi) - \text{Tr}_{1,\dots,\ell-1,\ell+1,\dots,N}(\Omega) \right\|_1 \right\rangle_{\psi} \leq \frac{\dim(s)}{\sqrt{\dim(\mathcal{M})}} , \quad (31.9)$$

noting that  $\dim(s)/\sqrt{\dim(\mathcal{M})} \rightarrow 0$  as  $N \rightarrow \infty$  because  $\dim(\mathcal{M})$  scales exponentially in  $N$  while  $\dim(s)$  is constant. Combined with (31.8), this tells us that, with high probability, the reduced state of  $|\psi\rangle \in \mathcal{M}$  on a single system is close to the generalized Gibbs state.

Under suitable assumptions, the evolution of the system is ergodic, meaning that (31.9) holds as an average over the time evolution [31]. More precisely, for almost all initial states  $|\psi(0)\rangle$ , and denoting by  $|\psi(t)\rangle$  the corresponding time-evolved state, we have

$$\lim_{T \rightarrow \infty} \frac{1}{T} \int_0^T \frac{1}{2} \left\| \text{Tr}_{1,\dots,\ell-1,\ell+1,\dots,N}(\psi(t)) - \text{Tr}_{1,\dots,\ell-1,\ell+1,\dots,N}(\Omega) \right\|_1 dt \leq \frac{\dim(s)}{\sqrt{\dim(\mathcal{M})}} . \quad (31.10)$$

Combining this with (31.8), we see that for almost all initial states  $|\psi(0)\rangle \in \mathcal{M}$ , over time the state on a single system stays close to the generalized Gibbs state.

This treatment only scratches the surface of the question of equilibration in the presence of multiple conserved quantities, and a more detailed analysis is still an open question.

### 31.3 Resource Theory Approach

In this section we generalise the resource theoretic framework introduced in Chap. 26 to the framework of multiple conserved quantities. We focus, in particular, on single-shot thermodynamics and work extraction in this paradigm. This approach that was

first put on firm footing in [14, 15, 32, 33] (see also Chap. 26) and provided a single-shot and resource theoretic approach for one conserved quantity – energy. The motivation to extend these ideas to more quantities lies in the desire to understand the privileged status that energy has in our world. What thermodynamics can we do when energy plays no important role and all conserved quantities appear on a level playing field? Does this framework give us access to new physics and how does it deviate from what we observe?

We proceed to tell the story in the standard general framework of thermodynamics, that consists of a thermal bath  $b$ , an out-of-equilibrium system  $s$  in a state  $\rho_s$ , and a number of batteries where we can store the extracted resources. Recall that when building a resource theory one must first fix the state space and the allowed state transformations. Following this, one investigates the resulting structure on the state space and the properties arising from such assignments specifying (*i*) the class of *free operations*, that can be applied at no cost; (*ii*) the class of *free states* that can be prepared at no cost, i.e. the states that are invariant under the class of free operations.

When the resource theory concerns thermodynamics with one conserved quantity, the free operations are generated by energy-preserving unitaries,  $[U, H] = 0$ , where  $H = H_s + H_b$  is additive over the system and bath. The free states are the familiar Gibbs states  $\tau = e^{-\beta H_s} / \mathcal{Z}$ . When the system has not one, but two conserved quantities  $Q_1 = A_s$  and  $Q_2 = B_s$ , the general recipe for constructing the resource theory does not change. We take the state space to be the joint Hilbert space of the system and bath, and specify the allowed transformations to be global unitaries which preserve the additive quantities  $A$  as well as  $B$ , namely  $[U, A] = [U, B] = 0$ . The free states become the *generalised* Gibbs states  $\tau = e^{-(\beta_A A_s + \beta_B B_s)} / \mathcal{Z}$ . The relationship between  $A$  and  $B$  is important and affects the results, depending on whether they are functionally related or how they commute.

### 31.3.1 The Generalised Gibbs State

We will begin by stating the generalised thermal state – the free state of our theory – and then proceed to derive it from resource-theoretic considerations. To this end we follow Jaynes [8, 9] and take a ‘thermal bath’ to be a collection of particles each in the generalised thermal state given in (31.3). At this moment, we place no restrictions on the conserved quantities – they may or may not commute and they may or may not be functionally related, moreover energy need not even be one of these quantities. To derive this state, we return to standard thermodynamics and recall that when restricting considerations to energy, there are two ways to define the thermal state: either by maximising the von Neumann entropy subject to the average energy being given *or* by minimising the free energy given the inverse temperature

$$\tau(\beta_E) = \frac{e^{-\beta_E E}}{\mathcal{Z}} \quad \left\{ \begin{array}{ll} \text{maximises} & S(\rho) = -\text{Tr}[\rho \log \rho] \quad \text{given } \bar{E} \\ \text{minimises} & F(\rho) = \langle E \rangle_\rho - T_E S(\rho) \quad \text{given } \beta_E \end{array} \right. \quad (31.11)$$

where  $T_E = 1/\beta_E$  and the average  $\text{Tr}[\rho E] = \bar{E}$ . The thermal state is the state which simultaneously extremises two quantities – the entropy and the free energy. In similar spirit, we would like for the generalised thermal state in Eq. (31.3) to be the state that also extremises two functions. From Jaynes we know that the generalised thermal state is still the state that maximises the entropy given the expectation values. The second quantity we are looking for is then the one that is minimised by the generalised thermal state. Previously, this was the free energy where the constant multiplying the entropy was the temperature. We do not have a notion of multiple entropies to couple the temperatures in order to extend the definition, but we can couple the inverse temperatures to the conserved quantities. We define the *free entropy*

**Definition 3** (*Free entropy*) The free entropy of a system  $\rho$  is a map from density matrices to real numbers  $\tilde{F} : \mathcal{S}(\mathcal{H}) \rightarrow \mathbb{R}$ ,

$$\tilde{F}(\rho) = \sum_i \beta_i \langle Q_i \rangle_\rho - S(\rho). \quad (31.12)$$

where  $\langle Q_i \rangle_\rho = \text{Tr}[Q_i \rho]$  and  $S$  is the von Neumann entropy.

The generalised thermal state is then the state that simultaneously maximises the von Neumann entropy and minimises the free entropy.

**Theorem 4** *The generalised thermal state*

$$\tau(\beta) = \frac{e^{-\sum_i \beta_i Q_i}}{\mathcal{Z}} \quad \left\{ \begin{array}{ll} \text{maximises} & S(\rho) = -\text{Tr}[\rho \log \rho] \quad \text{given } \overline{Q_1}, \dots, \overline{Q_k} \\ \text{minimises} & \tilde{F}(\rho) = \sum_i \beta_i \langle Q_i \rangle - S(\rho) \quad \text{given } \beta_1, \dots, \beta_k \end{array} \right. \quad (31.13)$$

where we have collected the inverse temperatures into a vector  $\beta = (\beta_1, \dots, \beta_k)$  and  $\mathcal{Z} = \text{Tr}[e^{-\sum_i \beta_i Q_i}]$ .

The thermal state is diagonal in the basis of the large observable  $R = \sum_i \beta_i Q_i$ . If the eigenvalues of  $R$  are  $\{r_i\}$  then the probability of a particle being in the  $i$ -th state is  $p_i = e^{-r_i}/\mathcal{Z}$ . If the observables  $Q_i$  commute then the probabilities becomes  $p_i = e^{-(\beta_1 q_i^1 + \dots + \beta_k q_i^k)}/\mathcal{Z}$ , where  $q_i^k$  is the  $i$ -th eigenvalue of observable  $k$ . Equation (31.13) can also be viewed as a duality relation for an optimization problem. The free entropy is a dimensionless function of state and can be viewed as the dual quantity to entropy. While the entropy is a function of extensive quantities  $Q_i$  and is maximised, performing the Legendre transform yields the dual function  $\tilde{F}$  of

intensive quantities  $\beta_i$  which is minimized. The proofs of Eq. (31.13) for both commuting and non-commuting quantum observables can be found in [24]. Proofs from a Bayesian perspective were first presented by Jaynes [8] and via a different method more recently by Liu [34].

*Example 5 (Energy and angular momentum)* An example of two commuting (and functionally dependent) conserved observables are energy  $E$  (i.e. the Hamiltonian) and angular momentum  $L$ , where  $E = L^2/2I$  and  $I$  is the moment of inertia. A thermal bath characterised by energy and angular momentum is a collection of thermal states of the form  $\tau(\beta_E, \beta_L) = e^{-(\beta_E E + \beta_L L)} / \mathcal{Z}$ . One may picture a ‘sea’ of flywheels, each with different moments of inertia, rotating with different angular momenta (clockwise/anticlockwise at different rates). Picking a particular flywheel from the bath, the likelihood that it has angular momentum  $L_i$  and energy  $E_i = L_i^2/2I$  is given by the probability  $p_i = e^{-(\beta_E E_i + \beta_L L_i)} / \mathcal{Z}$ .

There are two arguments to encourage the reader to adopt the new ‘free entropy’ definition. In the standard definition in Eq. (31.11), the free energy was minimised only for positive temperature  $T_E > 0$  (and consequently positive inverse temperature  $\beta_E > 0$ ). For negative temperature,<sup>3</sup> one must reverse the argument to conclude that the thermal state  $\tau(\beta_E)$  maximises the free energy. On the other hand, the generalised thermal state in (31.13) is the state that minimises the free entropy for all inverse temperatures  $\beta_i$  regardless of whether they are positive or negative, lending a kind of universality to the new definition and standing up to arguments that the free entropy is a quantity that is purely ‘rescaled’. The second observation is that since each term  $\beta_i Q_i$  is dimensionless, they can be regarded as entropy-like quantities, not least because the difference in free entropy between any state  $\rho$  and the generalised thermal state is equal to the relative entropy difference between those two states.

$$\tilde{F}(\rho_s) - \tilde{F}(\tau(\beta)) = \Delta \tilde{F} = D(\rho_s \parallel \tau(\beta)). \quad (31.14)$$

where  $D(\rho \parallel \sigma) = -S(\rho) - \text{Tr}[\rho \log \sigma]$ . In this way, all quantities are placed on equal footing and energy (should it appear as one of the conserved quantities) plays no special role.

### 31.3.2 Second Laws

We will look to derive the second law from operational principles. For clarity, and to avoid clutter we will concentrate on two quantities  $A$  and  $B$ , since the generalisation to  $k$  quantities follows naturally. In the standard picture of thermodynamics in the

---

<sup>3</sup>In a finite quantised spectrum, a population inversion with a Gibbs profile is equivalent to a negative temperature system. Since population inversion and thus negative temperatures are accessible in experimental settings, it is preferable to have an argument that is independent of the sign of the temperature.

single-shot regime, one takes a finite number of bath states and a quantum system, initially uncorrelated and out-of-equilibrium with respect to the bath  $\rho_s \otimes \tau(\beta_E)^{\otimes N}$  and looks for energy conserving unitaries which ‘do work’, for instance to raise a weight. To this end, one effects the transformation  $U_{sb}(\rho_s \otimes \tau(\beta_E)^{\otimes N}) U_{sb}^\dagger$ . The amount of energetic work  $\Delta W_E$  that can be extracted from the system, i.e. the amount by which an arbitrary weight (in any level) can be raised, is constrained by the second law of thermodynamics

$$\Delta W_E \leq -\Delta F_s \quad (31.15)$$

where  $F$  is the free energy of the system as given in (31.11). Equality is achieved when the right unitary is executed and the system thermalises to be indistinguishable from the states of the bath  $\rho_s \rightarrow \tau(\beta_E)$ . A Kelvin-Planck type statement of the second law is that ‘there is no way to extract energy from a single thermal bath’. In the picture involving two quantities  $A$  and  $B$ , the recipe is much the same. One starts by taking a finite number of systems from a generalised thermal bath and an out-of-equilibrium quantum system, which is initially uncorrelated from the bath  $\rho_s \otimes \tau(\beta_A, \beta_B)^{\otimes N}$ . The focus is now on extracting  $A$  and  $B$  from the system and storing them in their associated batteries. As the quantities are additive, their amounts in the system and bath can be treated independently. The  $A$ - and  $B$ -type work are defined in such a way that they automatically include the *first law of thermodynamics*

$$\Delta W_A = -\Delta A_s - \Delta A_b \quad \Delta W_B = -\Delta B_s - \Delta B_b \quad (31.16)$$

where  $\Delta A_s = \text{Tr}[A_s(\rho'_s - \rho_s)]$  and  $\Delta A_b = \text{Tr}[A_b(\rho'_b - \rho_b)]$  and analogously for  $B$ . When talking about work extraction there are two ways to proceed: either by including batteries implicitly, or explicitly, in the formalism.

**Implicit battery.** The global amount of  $A$  and  $B$  in the system and bath change. These changes are defined as ‘A-type’ work  $\Delta W_A$  and ‘B-type’ work  $\Delta W_B$ , which are quantities that have been extracted from (or done on) the global system. Due to the conservation laws (31.16), when  $A$  or  $B$  of the system and bath change, this change is compensated by a corresponding change to the external environment, i.e. the implicit battery. The transformations one considers are of the form  $U_{sb}(\rho_s \otimes \tau(\beta_A, \beta_B)^{\otimes N}) U_{sb}^\dagger$ .

**Explicit battery.** An explicit battery is a mathematical model for a work storage device. It accepts only a single type of work (i.e. an ‘A-type’ battery will only accept ‘A-type’ work, and a ‘B-type’ battery only ‘B-type’ work). The transformations one considers are of the form  $U(\rho_s \otimes \tau(\beta_A, \beta_B)^{\otimes N} \otimes \rho_{w_A} \otimes \rho_{w_B}) U^\dagger$ , where  $\rho_{w_A}$  is the state of battery- $A$ , or ‘weight’- $A$  and similarly for  $\rho_{w_B}$ . The global  $U$  acts on all four systems.

**Theorem 6** (The Second Law) *Given a generalised thermal state characterised by two inverse temperatures  $\tau(\beta_A, \beta_B)$  and an out of equilibrium quantum system  $\rho_s$*

*the maximum amount of A- and B-type work which one can extract is constrained in the following way*

$$\beta_A \Delta W_A + \beta_B \Delta W_B \leq -\Delta \tilde{F}_s. \quad (31.17)$$

**Corollary 7** (The Second Law with only a bath) *Given a generalised thermal bath characterised by two inverse temperatures  $\tau(\beta_A, \beta_B)$  (and therefore a quantum system which is also thermal  $\rho_s = \tau(\beta_A, \beta_B)$ ) the maximum amount of A- and B-type work which one can extract is constrained in the following way*

$$\beta_A \Delta W_A + \beta_B \Delta W_B \leq 0. \quad (31.18)$$

*Proof of the Second Law: implicit batteries* (See Chap. 28) First, since we restrict to unitary transformations the total entropy of the global system remains unchanged,  $S(\rho'_{sb}) = S(\rho_{sb})$ , and from the fact that the system and bath are initially uncorrelated, along with sub-additivity of von Neumann entropy, we have

$$S(\rho_s) + S(\rho_b) = S(\rho_{sb}) \quad \text{and} \quad S(\rho'_s) + S(\rho'_b) \geq S(\rho'_{sb}) \quad (31.19)$$

$$\Rightarrow \Delta S_s + \Delta S_b \geq \Delta S_{sb} = 0 \quad (31.20)$$

where  $\Delta S_s = S(\rho'_s) - S(\rho_s)$ , and analogously for  $\Delta S_b$  and  $\Delta S_{sb}$ . Second, since the bath starts in the thermal state  $\tau(\beta_A, \beta_B)$ , which is in a minimum of the free entropy by definition, its free entropy can only increase, thus

$$\Delta \tilde{F}_b = \beta_A \Delta A_b + \beta_B \Delta B_b - \Delta S_b \geq 0. \quad (31.21)$$

Now, eliminating all quantities on the bath, by substituting from the first laws (31.16) and from (31.20)+, we finally arrive at

$$-\beta_A (\Delta A_s + \Delta W_A) - \beta_B (\Delta B_s + \Delta W_B) + \Delta S_s \geq 0 \quad (31.22)$$

$$\beta_A \Delta W_A + \beta_B \Delta W_B \leq -\Delta \tilde{F}_s. \quad (31.23)$$

Note that the proof does not rely on any particular properties of A and B, which need not even commute, and so in the implicit battery case, the result is trivially generalised to  $k$  conserved quantities.

*Proof sketch of the second law: explicit batteries* In order to prove the second law with explicit batteries, one must supply a model. The batteries are modelled as ‘weights’ living on ladders such that the value of observable A on the battery is proportional to the position operator  $A_{w_A} = c_a \hat{x}_a$ , where  $c_a$  is a constant of appropriate units. The corresponding translation operator  $\Gamma_{\omega_A}^\epsilon = \exp(-i\epsilon \hat{p}_a)$  effects the transformation  $\Gamma_{\omega_A}^\epsilon |x_a\rangle = |x + \epsilon\rangle$  on unnormalised position states of the pointer (where  $\hat{p}_a$  is the momentum operator, canonically conjugate to the position). The objective is to

have a reliable ‘meter’ for a system of any dimension and the fact that the ladders are unbounded allows one to avoid boundary details, which are not the primary focus of this discussion.<sup>4</sup> Work is defined as  $\Delta W_A = \Delta A_{w_A}$ , and analogously for  $B$ . In order to eliminate the possibility of cheating one must introduce conditions on the batteries. ‘Cheating’ can encompass a variety of actions, such as bringing in ancillas, which would contribute as external sources of free entropy or work by using the batteries as cold reservoirs to embezzle work. The four assumptions that are made are:

1. *Independence*: Batteries are independent of one another and only accept and store one type of conserved quantity. Each quantity is assigned its own battery system.

2. *First laws*: The set of allowed operations are global unitaries  $U$  on the bath, system and batteries that conserve  $A$  and  $B$ , in other words  $[U, A_b + A_s + A_{w_A}] = [U, B_b + B_s + B_{w_B}] = 0$ , which impose the first laws of thermodynamics.<sup>5</sup>

3. *Translational invariance*: Only displacements in the position on the ladders are important. This implies all  $U$  should commute with translation operators  $\Gamma_{\omega_A}^\epsilon, \Gamma_{\omega_B}^\epsilon, \dots$  on each battery.

4. *Initially uncorrelated*: The initial state of the systems is of the product form  $\rho_s \otimes \tau^{\otimes N} \otimes \rho_{w_A} \otimes \rho_{w_B}$ .

One then uses a theorem (see [24]) that says that unitary evolutions  $U$  which are weight-translation invariant cannot decrease the entropy of the system and bath  $\Delta S(\rho_{sb}) \geq 0$ . This then allows one to say that  $\Delta S_b \geq -\Delta S_s$  and repeat the arguments as in the implicit battery case in Eqs. (31.21)–(31.22) to arrive at the second law.

*Example 8 (Energy and angular momentum)* The battery used to store energy can be thought of as a weight and the battery storing the angular momentum a flywheel. We wish for the batteries to operate independently, as per assumption (1). The energy of the weight is simply the Hamiltonian. If we take the flywheel to be very massive, i.e. the momentum of inertia very large, then the energy of the flywheel becomes essentially independent of its rotational property  $E_{fly} = \frac{L^2}{2I} \approx 0$ . Varying the angular momentum changes  $E_{fly}$  very little, thus the two batteries can effectively operate independently of one another.

<sup>4</sup>One can imagine a ladder that is very high (orders of magnitude greater than the number of system levels). If one is in the centre of this ladder then for all practical purposes it is unbounded from above and below. Similarly, if the initial systems are  $d$ -dimensional then one can also use a finite ladder and avoid boundary effects by initialising it in a state whose support is greater than  $d$ -levels about the ground state.

<sup>5</sup>Unitaries are chosen as opposed to more general completely positive (CP) maps in order not to use external ancillas in non-thermal states as sources of work.

### 31.3.3 Applications

#### 31.3.3.1 Extracting Resources

In [24] it was shown that for commuting quantities  $[A, B] = 0$ , the second law (31.17) is *tight*. In order to demonstrate tightness one needs to provide an explicit unitary  $U$ . Let  $p_i$  represent the populations of the system, i.e., the probability of the system to occupy the  $i$ -th joint eigenstate of  $A$  and  $B$ . The effect of the unitary is to create a small change  $\delta p$  between two of the levels  $p'_0 = p_0 + \delta p$  and  $p'_1 = p_1 - \delta p$  of the system. One must also show that the change in free entropy of the bath due to this  $U$  is small  $\Delta\tilde{F}_b = O(\delta p^2)$ , as well as the fact that the system and bath remain effectively uncorrelated after the interaction  $\Delta S_s + \Delta S_b = O(\delta p^2)$ .

$$\beta_A \Delta W_A + \beta_B \Delta W_B = -\Delta\tilde{F}_s + O(\delta p^2) \quad (31.24)$$

i.e. that up to a correction of order  $O(\delta p^2)$ , the combination of conserved quantities extracted, which themselves are of order  $O(\delta p)$ , matches the change in free entropy of the system. The state of the system is now a little closer to thermal. Thus, by repeating the process  $O(\frac{1}{\delta p})$  times (each time taking  $N$  new bath states) one can implement a protocol which transforms  $\rho_s \rightarrow \tau_s(\beta_A, \beta_B)$ , whereby in each stage the population changes between two states by order  $O(\delta p)$ , and such that in the end

$$\beta_A \Delta W_A + \beta_B \Delta W_B = -\Delta\tilde{F}_s + O(\delta p). \quad (31.25)$$

Thus, by taking  $\delta p$  sufficiently small one can approach reversibility. In the same work the authors present a variant of the protocol which is *robust*. Robust, in this case means that should an experimenter have access to a generalised thermal bath  $\tau(\beta_A, \beta_B)$ , but they can only characterise the inverse temperatures to some finite precision, or ‘window’  $x_1 \leq \beta_A \leq x_2$  and  $y_1 \leq \beta_B \leq y_2$ , then there still exists a procedure which will saturate the second law.<sup>6</sup> These results are valid for commuting quantities  $A$  and  $B$ , and can be easily generalised to  $k$  quantities. For the case that they do not commute  $[A, B] \neq 0$  there is no known protocol to extract work from a quantum system, and it remains an open question to show whether or not it is possible to saturate the second law.

#### 31.3.3.2 Trading Resources

Using Corollary 7 one can arrive at one of the central results of this formalism, namely, that conserved quantities can be *traded*. In particular, for commuting quantities  $[A, B] = 0$  in the presence of a single bath one can show that there exists a unitary acting solely on the bath  $U_b$  (given in [24]) such that  $U_b \tau(\beta_A, \beta_B) U_b^\dagger$  results

---

<sup>6</sup>Up to a measure zero set of inverse temperatures which present ‘pathological’ cases.

**Table 31.1** Summary of the results for the ‘resource theory’ with multiple conserved observables. Here, ‘protocol’ means the existence and construction of a unitary transformation that demonstrates extraction and trade of resources. Explicit battery models can be split into those which conserve observables strictly and those which conserve them on average. \* indicates that a unitary has been found for explicit batteries that have continuous (i.e. not discrete) spectra.

		Commuting	Non-Commuting
Implicit batteries	2nd law	✓	✓
	protocol	✓	✓
Explicit batteries (strict cons.)	2nd law	✓	✓
	protocol	✓	?
Explicit batteries (ave. cons.)	2nd law	✓	✓
	protocol	✓	✓*

in changes in  $\Delta A_b$  and  $\Delta B_b$  that are very large compared with the change in free entropy.

$$\Delta \tilde{F}_b = \beta_A \Delta A_b + \beta_B \Delta B_b \approx \epsilon \quad \Rightarrow \quad \Delta A_b \approx -\frac{\beta_B}{\beta_A} \Delta_b B + \frac{\epsilon}{\beta_A}. \quad (31.26)$$

When  $|\frac{\Delta A}{\Delta \tilde{F}_b}|$  and  $|\frac{\Delta B}{\Delta \tilde{F}_b}|$  are sufficiently large and  $\epsilon$  is sufficiently small, we say that these quantities can be trade *reversibly*. The exchange rate for this trade is given by the ratio  $\beta_B/\beta_A$ .<sup>7</sup> Note that it is important that  $\Delta \tilde{F}_b \neq 0$ —since the thermal state is the unique state which minimises  $\tilde{F}_b$ , this would require that the bath is left completely unchanged, resulting in trivial changes  $\Delta A_b = \Delta B_b = 0$ . This is in stark contrast to the standard picture, where the thermal state is useless for all practical purposes. Here, the analogous Kelvin-Planck statement of the second law becomes ‘there is no way to extract the linear combination  $\beta_A A + \beta_B B$  from a single, generalised thermal bath’. This demonstrates the interconversion of resources, which is illustrated in the following example.

*Example 9 (Energy and angular momentum)* Imagine that a protocol has successfully effected the transformation  $\rho_s \otimes \tau(\beta_E, \beta_L)^{\otimes N} \rightarrow \tau(\beta_E, \beta_L) \otimes \tau(\beta_E, \beta_L)^{\otimes N}$ . The free entropy of the system is spent and it has now become thermal, an extra particle in the bath. Both energy and angular momentum have been extracted and consequently the weight has been raised to a certain height and the flywheel is spinning with some angular momentum. Equation (31.26) tells us that we can raise the weight even higher at the expense of slowing down the fly-wheel (or vice versa). The currency for this trade is given by the ratio  $\beta_E/\beta_L$ .

The existence and construction of unitary for trading quantities which do not commute  $[A, B] \neq 0$  remains an open problem. The results discussed in this section, as well as extensions are summarised in Table 31.1.

<sup>7</sup>Note that although  $U_b$  does not change the free entropy of the bath, it *does* change the state of the bath, such that the state after the interaction could be very far from  $\tau(\beta_A, \beta_B)$ .

### 31.3.3.3 Landauer with Multiple Charges

The topics of Landauer erasure [35], and the Szilard engine [36] illustrate subtle connections between information and thermodynamics. The most basic concept in information is that of a ‘bit’, which is simply the answer to some ‘yes/no’ question. In the case of quantum mechanics, these yes/no states are labeled as  $|0\rangle$  and  $|1\rangle$ . Such a system contains a single bit of information if it is in the (maximally) mixed state  $\rho_1 = \frac{1}{2}|0\rangle\langle 0| + \frac{1}{2}|1\rangle\langle 1|$ .

Landauer showed that logically irreversible processing, such as resetting a single bit to its  $|0\rangle$  state, necessarily incurs a corresponding entropy increase of the environment, which in turn causes the dissipation of  $kT \ln(2)$  heat [35]. This energy must be provided in the form of work; this observation provided fundamental insights to the thermodynamics of computing, and was instrumental to the exorcism of Maxwell’s demon (see [37, 38] and also Chaps. 39 and 40, for recent Maxwell demon experiments). It is therefore a natural question to ask whether this thermodynamic cost can be furnished in terms of other physical quantities: How does Landauer erasure behave in the context of multiple conserved quantities? Do quantum-mechanical effects, such as non-commutativity, affect this erasure? To address this we formulate erasure with multiple charges, and present a generalized Landauer result. This topic is discussed in more detail in Chap. 29, and in the works [10, 12, 13, 39]. Here we present a simple entropic account of erasure.

As before, we allow for an arbitrary number of conserved charges  $\{Q_1, \dots, Q_k\}$ , and make use of the generalized Gibbs state

$$\tau_b = \frac{1}{Z} e^{-\sum_i \beta_i Q_i}. \quad (31.27)$$

Then a general erasure procedure can be described by the unitary transformation  $\rho_s \otimes \tau_b \mapsto \rho'_{sb} := U(\rho_s \otimes \tau_b)U^\dagger$  for some unitary  $U$  acting on both systems. Now we can consider the mutual information between  $s$  and  $b$ , which is given by  $I(s : b) := S(\rho'_a) + S(\rho'_b) - S(\rho'_{sb})$ , where  $\rho'_s = \text{Tr}_b[\rho'_{sb}]$  and similarly for  $\rho'_b$ .

Since the von Neumann entropy is unitarily invariant we have that  $S(\rho'_{sb}) = S(\rho_s \otimes \tau_b) = S(\rho_s) + S(\tau_b)$  and so

$$\Delta S_s + \Delta S_b = I(s : b). \quad (31.28)$$

We now exploit the basic features of the generalized Gibbs state. It is readily seen that

$$\Delta S_b = \sum_i \beta_i \text{Tr}[Q_i(\rho'_b - \tau_b)] - D(\rho'_b || \tau_b), \quad (31.29)$$

where  $D(\rho || \sigma) = \text{Tr}[\rho \log \rho - \rho \log \sigma]$  is the relative entropy. We now assume that the generalized thermal bath is sufficiently large that it is unaffected in the thermodynamic process, and so  $\rho'_b \approx \tau_b$  which means the last term in Eq.(31.29) can be neglected. We now define a  $Q_i$  heat flow via  $\langle Q_i \rangle := \text{Tr}[Q_i(\rho'_b - \tau_b)]$ . Inserting

these into equation (31.28) gives us that

$$\sum_i \beta_i \langle Q_i \rangle = -\Delta S_s + I(s : b). \quad (31.30)$$

However the mutual information is always non-negative and so we deduce that  $\sum_k \beta_k \langle Q_k \rangle \geq -\Delta S_s$ . This is the generalized Landauer bound in the presence of arbitrary many conserved charges and where the erasure need not be perfect. For the case of complete erasure we have an initial state  $\rho_s$  with entropy  $\ln 2$  (a single bit) that is sent to some default state with zero entropy. Thus for complete erasure we have the general erasure bound,

$$\sum_i \beta_i \langle Q_i \rangle \geq \ln 2. \quad (31.31)$$

This relation again highlights the ability to trade the difference resources on an equal footing within a thermodynamic process. A key thing to notice however, is that nowhere did we use the commutation relations between the charges. In other words, the above Landauer bound applies equally well for commuting and non-commuting cases.

## 31.4 Outlook

A key aspect of quantum mechanics is the non-commutativity of observables (such as position and momentum), and the resultant complementarity which prohibits assigning definite values simultaneously to these observables. In this chapter, we have shown how multiple quantum observables that may possess non-trivial commutation relations, may be incorporated into a framework of quantum thermodynamics. Subtleties aside, non-commutativity does not create an obstacle to the generalized Gibbs ensemble playing the same role as in classical statistical mechanics.

That said, a key goal of the recent quantum thermodynamics program is precisely to identify quantum-mechanical signatures that signal a departure from classical physics. In this regard one would expect that non-commutativity should produce such a thermodynamic signature, however the analysis that has so far been under-taken has not revealed any. For example, the form for the generalized Landauer erasure involving multiple conserved charges  $\{Q_i\}$  does not differ if these charges commute or not. However there exist a range of reasons why one expects such a signature. The MaxEnt procedure [8, 9] singles out the generalized Gibbs state subject to constraints on the expectation value of the microscopically conserved observables  $\{\langle Q_1 \rangle, \langle Q_2 \rangle, \langle Q_3 \rangle, \dots\}$ . However it is known that the MaxEnt procedure possesses a *discontinuity* in the quantum-mechanical case: arbitrarily small changes in values of the  $\langle Q_i \rangle$  constraints can produce large changes in the associated generalized Gibbs state. This feature is due to non-commutativity [40, 41], and has connections

with quantum phase transitions in many-body quantum systems [42]. In contrast to the analysis conducted here, the way in which this non-commutativity is detected is through the varying of the external constraints (for example the switching of classical field strengths). Recent quantum information-theoretic approaches are very good at explicitly accounting for non-classical resources (such as quantum coherence), however this strength becomes a weakness when it comes to varying the constraining fields. This is because to do such a change necessarily involves a non-trivial use of coherence that must be accounted for thermodynamically. Such an analysis has been done in the case of an effective change in the energy eigenbasis [43], and so a similar approach could be taken for the case of multiple conserved observables.

Recent work has formulated a trade-off relation for energy and time in quantum thermodynamics [44], and a natural direction would be to extend such a relation to include non-commuting conserved charges. An alternative way to detecting the effects of non-commutativity would be to exploit the fact that the microscopically conserved charges have an associated symmetry group that explicitly depends on their commutation relations – therefore the structure of the state interconversions, admissible within the thermodynamic framework, must carry a signature of any non-commutativity. Also, recently a complete set of conditions for state interconversions for such a general scenario have been derived [45], however a detailed study of these conditions still remains to be done.

One other direction that deserves exploration is the approximate micro-canonical subspaces [23] and their precise relation to typicality in the case of non-commuting charges.

**Acknowledgements** EHM is funded by the EPSRC, DJ is supported by the Royal Society. YG acknowledges funding from the FWF START grant Y879-N27. PhF acknowledges support from the Swiss National Science Foundation (SNSF) through the Early PostDoc.Mobility Fellowship No. P2EZP2\_165239 hosted by the Institute for Quantum Information and Matter (IQIM) at Caltech, from the IQIM which is a National Science Foundation (NSF) Physics Frontiers Center (NSF Grant PHY-1733907), and from the Department of Energy Award DE-SC0018407.

## References

1. E.A. Guggenheim, The Thermodynamics of Magnetization, in *Proc. R. Soc. Lond. A: Math. Phys. Eng. Sci.* **155**(884), 70–101(1936). <https://doi.org/10.1098/rspa.1936.0085>
2. E.C. Stoner, Proc. R. Soc. Lond. A: Math. Phys. Eng. Sci. **165**, 372 (1938). <https://doi.org/10.1098/rspa.1938.0066>
3. H. Alloul, Thermodynamics of superconductors, in *Introduction to the Physics of Electrons in Solids* (Springer, Berlin, 2011), pp. 175–199. [https://doi.org/10.1007/978-3-642-13565-1\\_6](https://doi.org/10.1007/978-3-642-13565-1_6)
4. D.N. Page, Hawking radiation and black hole thermodynamics, *N. J. Phys.* **7**(1), 203 (2005). <https://doi.org/10.1088/1367-2630/7/1/203>
5. J.B. Ott, J. Boerio-Goates (eds.), *Chemical Thermodynamics: Principles and Applications* (Academic, London, 2000). <https://doi.org/10.1016/B978-0-12-530990-5.50017-1>
6. E. Schrödinger, R. Penrose, *What is Life?: With Mind and Matter and Autobiographical Sketches*, Canto (Cambridge University Press, Cambridge, 1992). <https://doi.org/10.1017/CBO9781139644129>

7. T.E. Ouldridge (2017), [arXiv:1702.00360](https://arxiv.org/abs/1702.00360) [quant-ph]
8. E.T. Jaynes, Information Theory and Statistical Mechanics, Phys. Rev. **106**(4), 620 (1957a). <https://doi.org/10.1103/PhysRev.106.620>
9. E.T. Jaynes, Information Theory and Statistical Mechanics. II, Phys. Rev. **108**(2), 171 (1957b). <https://doi.org/10.1103/PhysRev.108.171>
10. M. Lostaglio, D. Jennings, T. Rudolph, Thermodynamic resource theories, non-commutativity and maximum entropy principles, *N. J. Phys.* **19**(4), 043008 (2017). <https://doi.org/10.1088/1367-2630/aa617f>
11. N. Yunger Halpern, Beyond heat baths II: framework for generalized thermodynamic resource theories, *J. Phys. A: Math. Theor.* **51**(9), 094001 (2018). <https://doi.org/10.1088/1751-8121/aaa62f>
12. S.M. Barnett, J.A. Vaccaro, Beyond Landauer Erasure, *Entropy* **15**(11), 4956 (2013). <https://doi.org/10.3390/e15114956>
13. J.A. Vaccaro, S.M. Barnett, Information erasure without an energy cost, in *Proceedings of the Royal Society of London A: Mathematical, Physical and Engineering Sciences* (The Royal Society, 2011). <https://doi.org/10.1098/rspa.2010.0577>
14. F.G.S.L. Brandão, M. Horodecki, J. Oppenheim, J.M. Renes, R.W. Spekkens, Resource Theory of Quantum States Out of Thermal Equilibrium, Phys. Rev. Lett. **111**(25), 250404 (2013). <https://doi.org/10.1103/PhysRevLett.111.250404>
15. F. Brandão, M. Horodecki, N. Ng, J. Oppenheim, S. Wehner, Proc. Natl. Acad. Sci. **112**(11), 3275 (2015). <https://doi.org/10.1073/pnas.1411728112>
16. N. Yunger Halpern, J.M. Renes, Beyond heat baths: Generalized resource theories for small-scale thermodynamics, Phys. Rev. E **93**(2), 022126 (2016). <https://doi.org/10.1103/PhysRevE.93.022126>
17. M. Weilenmann, L. Kraemer, P. Faist, R. Renner, Axiomatic Relation between Thermodynamic and Information-Theoretic Entropies, Phys. Rev. Lett. **117**(26), 260601 (2016). <https://doi.org/10.1103/PhysRevLett.117.260601>
18. M. Rigol, V. Dunjko, V. Yurovsky, M. Olshanii, Relaxation in a Completely Integrable Many-Body Quantum System: An Ab Initio Study of the Dynamics of the Highly Excited States of 1D Lattice Hard-Core Bosons, Phys. Rev. Lett. **98**(5), 050405 (2007). <https://doi.org/10.1103/PhysRevLett.98.050405>
19. C. Gogolin, J. Eisert, Equilibration, thermalisation, and the emergence of statistical mechanics in closed quantum systems, Rep. Prog. Phys. **79**(5), 056001 (2016). <https://doi.org/10.1088/0034-4885/79/5/056001>
20. A.C. Cassidy, C.W. Clark, M. Rigol, Generalized Thermalization in an Integrable Lattice System, Phys. Rev. Lett. **106**(14), 140405 (2011). <https://doi.org/10.1103/PhysRevLett.106.140405>
21. T. Langen, S. Erne, R. Geiger, B. Rauer, T. Schweigler, M. Kuhnert, W. Rohringer, I.E. Mazets, T. Gasenzer, J. Schmiedmayer, Experimental observation of a generalized Gibbs ensemble, Science **348**(6231), 207 (2015). <https://doi.org/10.1126/science.1257026>
22. M. Perarnau-Llobet, A. Riera, R. Gallego, H. Wilming, J. Eisert, Work and entropy production in generalised Gibbs ensembles, N. J. Phys. **18**(12), 123035 (2016). <https://doi.org/10.1088/1367-2630/aa4fa6>
23. N. Yunger Halpern, P. Faist, J. Oppenheim, A. Winter, Microcanonical and resource-theoretic derivations of the thermal state of a quantum system with noncommuting charges, Nat. Commun. **7**, 12051 (2016). <https://doi.org/10.1038/ncomms12051>
24. Y. Guryanova, S. Popescu, A.J. Short, R. Silva, P. Skrzypczyk, Thermodynamics of quantum systems with multiple conserved quantities, Nat. Commun. **7**, 12049 (2016). <https://doi.org/10.1038/ncomms12049>
25. S. Goldstein, J.L. Lebowitz, R. Tumulka, N. Zanghi, Canonical Typicality, Phys. Rev. Lett. **96**(5), 050403 (2006a). <https://doi.org/10.1103/PhysRevLett.96.050403>

26. S. Popescu, A.J. Short, A. Winter, Entanglement and the foundations of statistical mechanics, *Nat. Phys.* **2**(11), 754EP (2006a). <https://doi.org/10.1038/nphys444>
27. Y. Ogata, Approximating macroscopic observables in quantum spin systems with commuting matrices, *J. Funct. Anal.* **264**(9), 2005 (2013). <https://doi.org/10.1016/j.jfa.2013.01.021>
28. A. Winter (2015), unpublished notes
29. S. Goldstein, J.L. Lebowitz, R. Tumulka, N. Zanghi, Canonical Typicality, *Phys. Rev. Lett.* **96**(5), 050403 (2006b). <https://doi.org/10.1103/PhysRevLett.96.050403>
30. S. Popescu, A.J. Short, A. Winter, Entanglement and the foundations of statistical mechanics, *Nat. Phys.* **2**(11), 754 (2006b). <https://doi.org/10.1038/nphys444>
31. N. Linden, S. Popescu, A. Short, A. Winter, Quantum mechanical evolution towards thermal equilibrium, *Phys. Rev. E* **79**(6) (2009). <https://doi.org/10.1103/PhysRevE.79.061103>
32. D. Janzing, P. Wocjan, R. Zeier, R. Geiss, T. Beth, Thermodynamic cost of reliability and low temperatures: tightening landauer's principle and the second law, *Int. J. Theor. Phys.* **39**(12), 2717 (2000). <https://doi.org/10.1023/A:1026422630734>
33. M. Horodecki, J. Oppenheim, Fundamental limitations for quantum and nanoscale thermodynamics, *Nat. Commun.* **4**, 2059 (2013). <https://doi.org/10.1038/ncomms3059>
34. Y.-K. Liu, Gibbs States and the Consistency of Local Density Matrices, (2006), [arXiv:quant-ph/0603012v1](https://arxiv.org/abs/quant-ph/0603012v1)
35. R. Landauer, Irreversibility and heat generation in the computing process, *IBM J. Res. Dev.* **5**(3), 183–191 (1961). <https://doi.org/10.1147/rd.53.0183>
36. L. Szilard, Über die Entropieverminderung in einem thermodynamischen System bei Eingriffen intelligenter Wesen, *Z. Phys.* **53**(11), 840 (1929). <https://doi.org/10.1007/BF01341281>
37. C.H. Bennett, The thermodynamics of computation—a review, *Int. J. Theor. Phys.* **21**(12), 905 (1982). <https://doi.org/10.1007/BF02084158>
38. C.H. Bennett, Notes on Landauer's principle, reversible computation and Maxwell's demon. *Stud. Hist. Philos. Mod. Phys.* **34**, 501 (2003). [https://doi.org/10.1016/S1352-2198\(03\)00039-X](https://doi.org/10.1016/S1352-2198(03)00039-X)
39. T. Croucher, S. Bedekhal, J.A. Vaccaro, Discrete Fluctuations in Memory Erasure without Energy Cost, *Phys. Rev. Lett.* **118**(6), 060602 (2017). <https://doi.org/10.1103/PhysRevLett.118.060602>
40. S. Weis, A. Knauf, Entropy distance: New quantum phenomena, *J. Math. Phys.* **53**(10), 102206 (2012). <https://doi.org/10.1063/1.4757652>
41. O. Barndorff-Nielsen, *Information and Exponential Families: In Statistical Theory* (Wiley, New York, 2014), pp. 1–8. <https://doi.org/10.1002/9781118857281.ch1>
42. J. Chen, Z. Ji, C.-K. Li, Y.-T. Poon, Y. Shen, N. Yu, B. Zeng, D. Zhou, Discontinuity of maximum entropy inference and quantum phase transitions, *N. J. Phys.* **17**(8), 083019 (2015). <https://doi.org/10.1088/1367-2630/17/8/083019>
43. K. Korzekwa, M. Lostaglio, J. Oppenheim, D. Jennings, The extraction of work from quantum coherence, *N. J. Phys.* **18**(2), 023045 (2016). <https://doi.org/10.1088/1367-2630/18/2/023045>
44. H. Kwon, H. Jeong, D. Jennings, B. Yadin, M. Kim (2017). <https://doi.org/10.1103/PhysRevLett.120.150602>
45. G. Gour, D. Jennings, F. Buscemi, R. Duan, I. Marvian, Quantum majorization and a complete set of entropic conditions for quantum thermodynamics, *Nat. Commun.* **9**(5352) (2018). <https://doi.org/10.1038/s41467-018-06261-7>

# Chapter 32

## Smooth Entropy in Axiomatic Thermodynamics



Mirjam Weilenmann, Lea Krämer and Renato Renner

### 32.1 Introduction

The thermodynamic behaviour of macroscopic systems is traditionally described according to either of two theories: we can take a phenomenological approach that refers to macroscopic quantities such as the volume and the pressure of a system, or we can take a statistical approach relying on the underlying microscopic constituents, for instance taking the position and momentum of individual particles into account. The two theories are fundamentally different, each referring to quantities that are not defined within the other, but at the same time they are known to lead to consistent descriptions regarding the behaviour of thermodynamic systems in equilibrium. More precisely, the two approaches are usually connected through the identification of appropriate quantities in the two theories such as the entropy. The standard textbook approach to justify this is to show that the quantities have similar properties. For example, it is usually shown that both the phenomenological and the statistical entropy are additive, extensive and increase under the removal of inhibitions.

In this chapter, we demonstrate how the phenomenological and the statistical approach can be treated in a common underlying framework. Rather than using similarities in (derived) quantities such as the entropy, we connect the two approaches on the level of their basic structure. We show that this relation extends from the macroscopic realm where we usually consider large (idealised) systems in thermodynamic equilibrium to scenarios for which imprecisions and errors are crucial, including very

---

M. Weilenmann (✉)

Department of Mathematics, University of York, York YO10 5DD, UK

e-mail: mirjam.weilenmann@york.ac.uk

L. Krämer

Institute for Theoretical Physics, ETH Zurich, 8093 Zurich, Switzerland

e-mail: leakraemer@gmail.com

R. Renner

Institute for Theoretical Physics, ETH Zurich, 8093 Zurich, Switzerland

e-mail: renner@phys.ethz.ch

small systems. In all regimes, we find that the quantities that characterise whether certain processes may occur (in the spirit of a second law) correspond to entropy measures from information theory when considered within the statistical approach.

To establish our results, we rely on a resource theoretic formulation of thermodynamics. There are several approaches to this, depending on which operations are considered to be the *free operations* of the resource theory. The most widespread approach relies on thermal operations [1–3], which are reviewed in Chap. 26. Instead, we consider *adiabatic processes* here, which are central to Lieb and Yngvason’s axiomatic approach to phenomenological thermodynamics [4–9]. Their approach follows a long tradition of formulating thermodynamics axiomatically [4–18], which has also been continued by recent work [19–23]. In an adiabatic process, a system interacts with a weight that can perform or extract work from the system without changing the environment. Contrary to the thermal operations, these processes do not impose any constraint regarding the conservation of energy. Instead, they forbid the equilibration with a reservoir, which would result in a change of the state of the system’s environment. We will introduce Lieb and Yngvason’s axiomatic framework for thermodynamics in Sect. 32.2 and then translate the notion of an adiabatic process into the statistical picture in Sect. 32.3. Based on this, we will present an axiomatic relation between the entropy measures relevant for thermodynamics in the phenomenological and in the statistical approach. This will essentially be a summary of results derived in Ref. [24].

Furthermore, we introduce a novel, error-tolerant axiomatic framework that allows us to realistically describe systems at any scale, including microscopic and macroscopic systems. (Previous approaches were typically concerned solely with macroscopic systems and did not take errors into account.) Our framework contributes to the current development of pushing resource theories towards more realistic regimes, which has been initiated through the consideration of probabilistic transformations [25] and finite size effects [26, 27] and which has recently also led to the consideration of imprecisions in specific resource theories [28–32]. Similar to our consideration of Lieb and Yngvason’s work, we present our new framework first phenomenologically in Sect. 32.4 and then from the statistical viewpoint in Sect. 32.5. This allows us to relate the quantities that characterise whether there exists an error-tolerant adiabatic process between certain states to smooth min and max entropies, which are known from single-shot information theory [33].

In the limit of large systems, our error-tolerant framework furthermore recovers the structure of a resource theory for macroscopic thermodynamics. Specifically, there is a single quantity, the entropy, that specifies whether a transformation between different equilibrium states of a macroscopic system is possible. In the spirit of the chapter, we present these results first according to the phenomenological approach in Sect. 32.6, followed by the statistical perspective in Sect. 32.7. The latter viewpoint allows us to recover the von Neumann entropy as the quantity that characterises the behaviour of so-called i.i.d. states under error-tolerant adiabatic processes and the Boltzmann entropy is recovered for microcanonical states. Through this consideration of macroscopic systems in equilibrium we relate our error-tolerant framework

to the framework for thermodynamics introduced by Lieb and Yngvason. Our elaborations regarding the error-tolerant axiomatic framework and its macroscopic limits are to a large extent based on [32].

## 32.2 Axiomatic Framework for Phenomenological Thermodynamics

In phenomenological thermodynamics, the state of a system in equilibrium is usually described in terms of a few real and positive parameters. For instance, the state of a gas in a box is often given in terms of its internal energy,  $U$ , and its volume,  $V$ . Such an equilibrium state  $X = (U, V)$  lives in the space of all equilibrium states of that system, denoted  $\Gamma_{\text{EQ}}$ . The description of the state of a system out of equilibrium is more involved; such states live in a larger state space  $\Gamma \supseteq \Gamma_{\text{EQ}}$ .

Thermodynamics is a resource theory, a perspective that is implicit in the axiomatic framework proposed by Lieb and Yngvason to derive the second law [4–8]. At the core of this framework lie the *adiabatic processes*. They are defined in [4–8] as those operations on a system that leave no trace on its environment, except for a change in the position of a weight. These processes are sometimes also called *work processes* [23]. They induce a preorder relation  $\prec$  on the state space  $\Gamma$  of a system that is called *adiabatic accessibility*. For two states  $X, Y \in \Gamma$ , there is an adiabatic process transforming  $X$  into  $Y$  if and only if  $X \prec Y$ .<sup>1</sup> States  $X, Y \in \Gamma$  that can be adiabatically interconverted, i.e., obey  $X \prec Y$  as well as  $Y \prec X$ , are denoted  $X \sim Y$ .

*Example 32.2.1* Let there be one mole of Helium gas in a box that is in a thermodynamic equilibrium state (which we may treat as an ideal monoatomic gas). Its state can be characterised by a tuple  $(U, V)$ , where  $U \geq 0$  is the internal energy and  $V \geq 0$  is the volume of the gas. Now assume that there are two states of the gas that differ in their internal energy, for instance  $X = (U, V)$  and  $Y = (2U, V)$ . Then we can find an adiabatic process transforming the state  $X$  into  $Y$ , namely we can use a weight to mechanically stir the gas up to increase its internal energy, hence  $X \prec Y$ . An adiabatic process that recovers  $X$  again from  $Y$  cannot be constructed. If we were to consider the state  $Z = (2U, V2^{-\frac{1}{2}})$  instead of  $Y$ , however, we could construct adiabatic processes that allow us to interconvert the two, i.e.,  $X \sim Z$ . Namely, we could compress the gas adiabatically to obtain the state  $Z$  (using a weight to quickly move a piston). To recover  $X$ , the gas could be decompressed changing nothing else in the environment than the position of a weight. This coincides with the textbook understanding of an adiabatic compression and decompression.

The state of a composed system is denoted as the Cartesian product of the individual states of the systems to be composed, for  $X \in \Gamma$  and  $X' \in \Gamma'$  it is

---

<sup>1</sup>Throughout this chapter, we follow Lieb and Yngvason's convention regarding the notation of the order relation, where  $X \prec Y$  means that  $X$  can be transformed into  $Y$  with an adiabatic process. Note that this is the reverse convention of what a reader acquainted with the literature on quantum resource theories might expect.

$(X, X') \in \Gamma \times \Gamma'$ .<sup>2</sup> Physically, composition is understood as bringing individual systems together to one without letting them interact (yet). The state of the composed system is therefore naturally characterised by the properties of its constituent systems.

The set of equilibrium states of a thermodynamic system,  $\Gamma_{\text{EQ}}$ , is central to the axiomatic framework and will be necessary for introducing an entropy function later as well as for deriving a second law. In the axiomatic framework, equilibrium states are distinct from other states in that they are assumed to be scalable, i.e., for any  $\alpha \in \mathbb{R}_{\geq 0}$  one can define a scaled version of an equilibrium state  $X \in \Gamma_{\text{EQ}}$ , denoted as  $\alpha X \in \alpha \Gamma_{\text{EQ}}$ .<sup>3</sup> Scaling a system by a factor  $\alpha$  means taking  $\alpha$  times the amount of substance of the original system. As is usual in phenomenological thermodynamics, we ignore the fact that the system is made up of a finite number of particles that cannot be subdivided and allow the scaling by any positive real number.

*Example 32.2.2* Let us consider two systems, one being a mole of Helium gas in an equilibrium state  $X = (U, V)$ , and the other two moles of Helium in another equilibrium state  $X' = (U', V')$ . The composition operation allows us to regard these as subsystems of a composed system in state  $(X, X')$ . Adiabatic operations may then either affect one of the individual subsystems or both of them. For instance, we may connect the two systems and allow them to equilibrate thermally by means of such an operation. Alternatively, removing the walls that separate the two subsystems is an adiabatic process on the composite system, which in this case would lead to a system containing three moles of Helium gas.

Scaling the state  $X$ , say by a factor of 3, leads to a state  $3X = (3U, 3V)$ , where the extensive properties of the state scale with the system size. Note that if the gas were not in an equilibrium state, for instance if it had a temperature gradient, it would not be clear how its properties scale with the amount of substance. The scaling operation is not defined for such a state.

For the order relation of adiabatic accessibility a few physically motivated properties shall be assumed [4–6]. For equilibrium states  $X, Y, Z \in \Gamma_{\text{EQ}}$  and  $X', Y', Z_0, Z_1 \in \Gamma'_{\text{EQ}}$ , these are:

- (E1) Reflexivity:  $X \sim X$ .
- (E2) Transitivity:  $X \prec Y$  and  $Y \prec Z \Rightarrow X \prec Z$ .
- (E3) Consistent composition:  $X \prec Y$  and  $X' \prec Y' \Rightarrow (X, X') \prec (Y, Y')$ .
- (E4) Scaling invariance:  $X \prec Y \Rightarrow \alpha X \prec \alpha Y, \forall \alpha > 0$ .
- (E5) Splitting and recombination: For  $0 < \alpha < 1$ ,  $X \sim (\alpha X, (1 - \alpha)X)$ .
- (E6) Stability: If  $(X, \alpha Z_0) \prec (Y, \alpha Z_1)$  for a sequence of scaling factors  $\alpha \in \mathbb{R}$  tending to zero, then  $X \prec Y$ .
- (CH) Comparison Hypothesis: For each  $0 \leq \alpha \leq 1$ , any two states in  $(1 - \alpha)\Gamma_{\text{EQ}} \times \alpha\Gamma_{\text{EQ}}$  can be related by means of  $\prec$ , i.e., for any  $X, Y \in (1 - \alpha)\Gamma_{\text{EQ}} \times \alpha\Gamma_{\text{EQ}}$  either  $X \prec Y$  or  $Y \prec X$  (or both).

---

<sup>2</sup>The composition operation is assumed to be associative and commutative.

<sup>3</sup>The scaling is taken to obey  $1X = X$  as well as  $\alpha_1(\alpha_2 X) = (\alpha_1 \alpha_2)X$ , thus  $1\Gamma_{\text{EQ}} = \Gamma_{\text{EQ}}$  and  $\alpha_1(\alpha_2 \Gamma_{\text{EQ}}) = (\alpha_1 \alpha_2)\Gamma_{\text{EQ}}$ .

Axioms (E1)–(E4) are naturally obeyed by any order relation  $\prec$  that is specified through a class of processes that can be composed sequentially as well as in parallel (on composed systems) and that respect a scaling operation. Notice that (E5) relates states on different spaces. In the example of a box of gas in an equilibrium state  $X$  an adiabatic process interconverting the two could be realised by inserting and removing a partition at a ratio  $\alpha : (1 - \alpha)$ . (E6) captures the physical intuition that arbitrarily small impurities in a large thermodynamic system should not affect the possible adiabatic transformations.

Note that in [4–6], (CH) is not stated as an axiom but rather derived from additional axioms about thermodynamic systems. For this derivation more structure is required, such as the definition of so-called simple systems, the state of which is an  $n$ -tuple with one distinguished energy coordinate. The discussion of these additional axioms for systems in phenomenological thermodynamics is beyond the scope of this chapter. That states considered from the statistical viewpoint obey (CH) is shown in the next section directly, without relying on any additional underlying axioms.

For any other states of a system, i.e., states in  $\Gamma$  that are not necessarily equilibrium states, the following axioms will be assumed [7].

- (N1) Axioms (E1), (E2), (E3) and (E6), with  $Z_0, Z_1 \in \Gamma_{\text{EQ}}$  in axiom (E6), hold for all states in  $\Gamma$ .
- (N2) For any  $X \in \Gamma$  there exist  $X_0$  and  $X_1 \in \Gamma_{\text{EQ}}$  with  $X_0 \prec X \prec X_1$ .

Axiom (N2) specifies that for any non-equilibrium state of a system to be considered there should exist an equilibrium state from which it can be generated by means of an adiabatic process and that each non-equilibrium state can be brought to equilibrium adiabatically. In the case of a box of gas, this could be achieved by letting the system equilibrate.

It is possible to assign values to the states of a system that quantify their use as a resource for performing tasks with adiabatic operations. Intuitively, a state  $X \in \Gamma$  is more valuable than another state  $Y \in \Gamma$  if it allows for the generation of  $Y$  with an adiabatic operation. More precisely, if the two states can be compared with  $\prec$ , then  $X$  is more valuable than  $Y$  if and only if  $X \prec Y$  and  $Y \not\prec X$ . The assignment of values to states should thus reflect this order.<sup>4</sup>

Lieb and Yngvason defined entropy functions as such value assignments. They showed that there is a (essentially) unique real valued function  $S$  on the space of all equilibrium states of a thermodynamic system that is additive, i.e., for any two states  $X \in \Gamma_{\text{EQ}}$  and  $X' \in \Gamma'_{\text{EQ}}$ ,  $S((X, X')) = S(X) + S(X')$ , extensive, i.e., for any  $\alpha > 0$  and any  $X \in \Gamma_{\text{EQ}}$ ,  $S(\alpha X) = \alpha S(X)$ , and monotonic, i.e., for two states  $X, Y \in \Gamma_{\text{EQ}}$  that are related by means of  $\prec$ ,  $X \prec Y$  holds if and only if  $S(X) \leq S(Y)$ . Hence, the lower the entropy, the more valuable the state in this resource theory.

**Theorem 32.2.1** (Lieb and Yngvason) *Provided that Axioms (E1) to (E6) as well as (CH) are fulfilled on  $\alpha\Gamma_{\text{EQ}} \times (1 - \alpha)\Gamma_{\text{EQ}}$  for any  $0 \leq \alpha \leq 1$ , there exists a function  $S$  that is additive under composition, extensive in the scaling and monotonic with*

---

<sup>4</sup>In general,  $\prec$  may not be a total preorder and the ordering of values assigned to states that cannot be compared by means of  $\prec$  may be ambiguous.

respect to  $\prec$ . Furthermore, this function  $S$  is unique up to a change of scale  $C_1 \cdot S + C_0$ , where  $C_0, C_1 \in \mathbb{R}$  with  $C_1 > 0$ .

For a state  $X \in \Gamma_{\text{EQ}}$ , the unique function  $S$  is given as

$$S(X) = \sup \{ \alpha \mid ((1 - \alpha)X_0, \alpha X_1) \prec X \}, \quad (32.1)$$

where the states  $X_0, X_1 \in \Gamma_{\text{EQ}}$  may be chosen freely as long as  $X_0 \prec X_1$  and  $X_1 \not\prec X_0$ . This choice only changes the constants  $C_0$  and  $C_1$ . In the case  $X_0 \prec X \prec X_1$ , (32.1) can be intuitively understood as the optimal ratio  $(1 - \alpha) : \alpha$  of  $X_0$  and  $X_1$  such that the state  $X$  can be created in an adiabatic process.<sup>5</sup>

Lieb and Yngvason derive equilibrium thermodynamics from the above axioms for equilibrium states and a few additional physically motivated properties, which also specify the geometric structure of the state space of thermodynamic systems a little more (for instance introducing convex combinations of states) [4–6]. Their considerations rely on the phenomenological description of systems (by referring to simple systems for instance). We refer to [9] for a textbook on thermodynamics formulated in this approach. In addition, Lieb and Yngvason derive bounds on any monotonic extensions of  $S$  from  $\Gamma_{\text{EQ}}$  to  $\Gamma$  under the condition that the above axioms for non-equilibrium states hold [7]. We consider here the following slight adaptations of their bounds<sup>6</sup>

$$S_-(X) = \sup \{ \alpha \mid ((1 - \alpha)X_0, \alpha X_1) \prec X \} \quad (32.5)$$

$$S_+(X) = \inf \{ \alpha \mid X \prec ((1 - \alpha)X_0, \alpha X_1) \}. \quad (32.6)$$

<sup>5</sup>This definition extends to states obeying  $X \prec X_0$  or  $X_1 \prec X$  [5], where it has to be interpreted slightly differently. To see this, note that the expression

$$((1 - \alpha)X_0, \alpha X_1) \prec X \quad (32.2)$$

is equivalent to  $((1 - \alpha)X_0, \alpha X_1), \alpha' X_1 \prec (X, \alpha' X_1)$  for any  $\alpha' \geq 0$  and hence also to  $((1 - \alpha)X_0, (\alpha' + \alpha)X_1) \prec (X, \alpha' X_1)$ . This allows us to consider negative  $\alpha$  (while still using only positive coefficients as scaling factors). If  $\alpha < 0$ , by choosing  $\alpha' = -\alpha$ , condition (32.2) is to be understood as a transformation  $((1 - \alpha)X_0) \prec (X, |\alpha|X_1)$ . A similar argument shows that for  $\alpha > 1$  the condition  $((1 - \alpha)X_0, \alpha X_1) \prec X$  can be understood as  $\alpha X_1 \prec ((\alpha - 1)X_0, X)$ .

<sup>6</sup>The bounds given in [7] are

$$S_-(X) = \sup \{ S(X') \mid X' \in \Gamma_{\text{EQ}}, X' \prec X \} \quad (32.3)$$

$$S_+(X) = \inf \{ S(X'') \mid X'' \in \Gamma_{\text{EQ}}, X \prec X'' \}. \quad (32.4)$$

In phenomenological thermodynamics, where equilibrium states are traditionally described in terms of continuous parameters (such as the internal energy and the volume for instance), there exists an equilibrium state  $X_\alpha$  for each  $((1 - \alpha)X_0, \alpha X_1)$  that obeys  $X_\alpha \sim ((1 - \alpha)X_0, \alpha X_1)$ . Under these circumstances the bounds (32.5) and (32.6) coincide with (32.3) and (32.4) respectively. This is, however, not implied by the axioms and may not hold if systems are described in a different way (e.g. in the statistical approach taken in Sect. 32.3). Note also that for (32.3) and (32.4) the inequality in (32.7) need not be strict.

$S_-$  specifies the maximal fraction of the system that may be in state  $X_1$  if  $X$  is formed by combining systems in states  $X_0$  and  $X_1$  scaled appropriately, giving a measure for the resources needed to produce  $X$ .  $S_+$  is the minimal portion of  $X_1$  that is generated from  $X$  when transforming it into a system composed of scaled copies of  $X_0$  and  $X_1$ . The difference  $S_-(X) - S_+(X) \leq 0$  can be viewed as a measure for the resources that are used up when producing  $X$  and decomposing it again (quantified in proportion of  $X_0$  and  $X_1$ ). For equilibrium states, where  $S_-(X) = S_+(X) = S(X)$ , this can be achieved without generating any overall resource loss.

$S_-$  and  $S_+$  also provide necessary conditions as well as sufficient conditions for state transformations between non-equilibrium states by means of adiabatic processes.

**Proposition 32.2.1** (Lieb and Yngvason) *Let  $X, Y \in \Gamma$ . Then, the following two conditions hold:*

$$S_+(X) < S_-(Y) \Rightarrow X \prec Y , \quad (32.7)$$

$$X \prec Y \Rightarrow S_-(X) \leq S_-(Y) \text{ and } S_+(X) \leq S_+(Y) . \quad (32.8)$$

Note that these conditions are closely related to the conditions we shall derive in the error-tolerant setting in Proposition 32.4.1.

### 32.3 Adiabatic Processes in the Statistical Approach

In this section, we show that the axiomatic framework that was introduced to describe systems phenomenologically applies also to a statistical description of systems: The phenomenologically-motivated axioms are satisfied by an order relation that is based on a statistical description of systems and of the adiabatic processes affecting them. In this sense, we can see the axiomatic framework as overarching these two approaches to thermodynamics.

Here, the state of a system is described in terms of a density function over the space of microscopic states. Classically this is a distribution over phase space. In the quantum case, which we consider here for generality, it is a density operator on a Hilbert space  $\mathcal{H}$ , denoted  $\rho \in \Gamma = \mathcal{S}(\mathcal{H})$ . An adiabatic process, which leaves no trace on the environment except for a change in the relative position of a weight, affects the microscopic degrees of freedom in the following way [24].

**Definition 32.3.1** An *adiabatic process* maps a state  $\rho \in \mathcal{S}(\mathcal{H}_S)$  to another state

$$\sigma = \text{tr}_A (U(\rho \otimes \tau)U^\dagger) , \quad (32.9)$$

where  $\tau \in \mathcal{S}(\mathcal{H}_A)$  is a *sharp state*, meaning a state for which all its non-zero eigenvalues are equal,  $U$  is an arbitrary unitary and the partial trace is taken over the subsystem  $A$ , where it is further required that

$$\mathrm{tr}_S(U(\rho \otimes \tau)U^\dagger) = \tau . \quad (32.10)$$

The evolution with an arbitrary unitary  $U$  (that does not have to commute with the Hamiltonian) is enabled by the weight system, which is assumed to contain coherence as a resource that can be used catalytically. We rely on a model introduced in [34], where the weight is in a superposition of energy eigenstates of a Hamiltonian with equally spaced energy levels. These may extend to infinity or (more physically) be bounded from below. Such a model could for instance be practically realised with a laser, which naturally emits light in a coherent state. There are other weight models that can be used and that lead to similar behaviour; for instance, a weight modelled through switching potentials on and off as considered in [35] also leads to the emergence of arbitrary unitary operations on the system (and environment  $\tau$ ). Intuitively, the weight can be understood as a work storage system that is able to supply or absorb any amount of work, eliminating the significance of energetic considerations for these processes from the framework. (For further details regarding the weight system, we refer to [24, 34].)

The state  $\tau$  represents the part of the environment that is affected by the interaction with the weight system. The condition (32.10) encodes the requirement that the operations leave no trace on the environment after the interaction (except for the change in the weight). The sharp states take the role of the equilibrium states of the framework. This is inspired by the fact that the microcanonical states have this property. However, here we apply our approach to systems of any size, including microscopic systems, and a notion of equilibration in terms of time evolution is not necessarily available. Nonetheless, there is a class of states that are equilibrium states in the sense that they obey all of the corresponding axioms, namely (E1)–(E6) and (CH). These are precisely the sharp states.

The preorder relation induced by the adiabatic processes of Definition 32.3.1 on the state space  $\Gamma = \mathcal{S}(\mathcal{H})$  is closely related to the mathematical notion of majorisation (as stated in Proposition 32.3.1 below).

**Definition 32.3.2** Let  $\rho, \sigma \in \mathcal{S}(\mathcal{H})$  with Hilbert space dimension  $\dim(\mathcal{H}) = n$  be two states with spectra  $\{\lambda_i(\rho)\}_i$  and  $\{\lambda_i(\sigma)\}_i$  respectively, ordered such that  $\lambda_1(\rho) \geq \lambda_2(\rho) \geq \dots \geq \lambda_n(\rho)$  and  $\lambda_1(\sigma) \geq \lambda_2(\sigma) \geq \dots \geq \lambda_n(\sigma)$ . Then  $\rho$  majorises  $\sigma$ , denoted  $\rho \prec_M \sigma$ ,<sup>7</sup> if for all  $1 \leq k \leq n$ ,

$$\sum_{i=1}^k \lambda_i(\rho) \geq \sum_{i=1}^k \lambda_i(\sigma) . \quad (32.11)$$

Mathematically,  $\prec_M$  is a *preorder*, meaning it is reflexive, and transitive. The following proposition specifies its relation to adiabatic processes, which was proven in [24] based on results concerning the resource theory of noisy operations [36–38].

**Proposition 32.3.1** For  $\rho, \sigma \in \mathcal{S}(\mathcal{H})$ ,  $\rho \prec_M \sigma$  if and only if  $\rho$  can be transformed into  $\sigma$  by an adiabatic operation.

---

<sup>7</sup>We alert the reader to the non-standard notation for the order relation (see also Footnote 1).

*Example 32.3.1* Consider the Helium gas from Example 32.2.1, where  $\rho_X = \frac{\Pi_{\Omega_{\text{micro}}(U,V)}}{\Omega_{\text{micro}}(U,V)}$  and  $\rho_Y = \frac{\Pi_{\Omega_{\text{micro}}(2U,V)}}{\Omega_{\text{micro}}(2U,V)}$  with  $\Omega_{\text{micro}}(U, V)$  the microcanonical partition function and  $\Pi_{\Omega_{\text{micro}}(U,V)}$  the projector onto its subspace. Then the two states obey  $\rho_X \prec_M \rho_Y$ .

The composition of two systems characterised by density operators  $\rho, \sigma \in \Gamma$  is defined as their tensor product (replacing the Cartesian product considered in the phenomenological setting), i.e.,  $(\rho, \sigma)$  means  $\rho \otimes \sigma$  here. Scaling a system in a sharp state (corresponding to an equilibrium state in the axiomatic framework) by a factor  $\alpha \in \mathbb{Z}_{\geq 0}$  corresponds to taking its tensor power,  $\alpha\rho = \rho^{\otimes \alpha}$ . This operation can be formally extended to arbitrary  $\alpha \in \mathbb{R}_{\geq 0}$ , which physically involves the consideration of processes on a larger system. For the details of this we refer to [24]. The following proposition relates the statistical description of adiabatic processes to the phenomenological approach introduced in Sect. 32.2.

**Proposition 32.3.2** *Consider adiabatic operations on states in  $\Gamma = \mathcal{S}(\mathcal{H})$ , with an equilibrium state space,  $\Gamma_{\text{EQ}}$ , made up of all sharp states. Then, the axioms (E1) to (E6), (CH) and (N1) and (N2) are obeyed. The corresponding entropy functions (according to (32.5) and (32.6)) are*

$$S_-(\rho) = H_{\min}(\rho) \quad (32.12)$$

$$S_+(\rho) = H_0(\rho), \quad (32.13)$$

where  $H_{\min}(\rho) = -\log \lambda_{\max}(\rho)$  and  $\lambda_{\max}(\rho)$  is the maximal eigenvalue of  $\rho$ , and where  $H_0(\rho) = \log \text{rank}(\rho)$ .

These entropies are generally known as *min* and *max entropies* and have initially been introduced in information theory. They have various applications, e.g. for characterising extractable randomness and the compressibility of data respectively [39, 40]. For  $\rho \in \Gamma_{\text{EQ}}$  these entropies coincide and they coincide with the unique additive and extensive entropy  $S$ . This establishes a connection between entropy in phenomenological thermodynamics and in the statistical approach by means of a general and rigorous framework. Note that the connection established by Proposition 32.3.2 is different from Jaynes' work [41, 42], which connects entropy in information theory to entropy in statistical physics (rather than phenomenological thermodynamics).

For microscopic systems, the question of whether there exists an (idealised) adiabatic operation achieving a transition between two (exact) microscopic states may not be meaningful in realistic situations where, due to experimental limitations, certain states may not be experimentally distinguishable, or in situations where one is satisfied with obtaining the desired states approximately.<sup>8</sup> To consider such situations, we now introduce an extended framework that can tackle such approximations. It furthermore does not rely on a continuous scaling operation, which (even though

---

<sup>8</sup>Notice that approximations are also relevant for macroscopic systems. However, we do not usually explicitly mention them there, as they are extremely accurate.

possible) is unnatural for microscopic systems. The reason is that processes that involve a scaling with non-integer factors often have to be physically interpreted as operations on a larger (potentially macroscopic) system [24].

## 32.4 Axiomatic Framework for Error-Tolerant Resource Theories

In this section, we extend the axiomatic framework described above to take approximations into account. This is important to make a resource theory practically useful. Indeed, it is often the case that an approximation of a desired output is good enough for an intended purpose, and, at the same time, much less costly (in terms of the required resources). For this reason, accounting for approximations is also usual in information theory. For example, in randomness extraction, allowing for a deviation from the desired uniformly random bit string usually enables the extraction of a much larger number of (close to) random bits from the same data.

Processes with error-tolerance could not be modelled in previously existing axiomatic frameworks. Error-tolerant frameworks differ in various fundamental ways from those earlier ones. An example illustrating this is the fact that, if two transformations, each with error-tolerance  $\epsilon$ , are composed (either sequentially or in parallel), then there may be no process with error-tolerance  $\epsilon$  that achieves the overall transformation: the errors of the separate processes may add up and there is generally no alternative process with a smaller error. Error-tolerant resource theories can therefore not be described with a transitive order relation. Instead, an error-tolerant resource theory introduces a family of order relations,  $\{\prec^\epsilon\}_\epsilon$ , one for each error-tolerance  $\epsilon$ : for  $X, Y \in \Gamma$  the relation  $X \prec^\epsilon Y$  expresses that a transformation from  $X$  to  $Y$  with error at most  $\epsilon$  is possible,  $X \sim^\epsilon Y$  means that  $X \prec^\epsilon Y$  as well as  $Y \prec^\epsilon X$ . We require  $\prec^\epsilon$  to satisfy a few natural axioms.

- (A1) Reflexivity: For any state  $X \in \Gamma$  and any  $\epsilon \geq 0$ ,  $X \prec^\epsilon X$ .
- (A2) Ordering of error-tolerances: For any  $X, Y \in \Gamma$  and any  $\epsilon' \geq \epsilon \geq 0$ ,  $X \prec^\epsilon Y \Rightarrow X \prec^{\epsilon'} Y$ .
- (A2) Additive transitivity: For any  $X, Y, Z \in \Gamma$  and any  $\epsilon, \delta \geq 0$ ,  $X \prec^\epsilon Y$  and  $Y \prec^\delta Z \Rightarrow X \prec^{\epsilon+\delta} Z$ .
- (A3) Consistent composition: For any  $X, Y \in \Gamma$ ,  $Z \in \Gamma'$  and any  $\epsilon \geq 0$ ,  $X \prec^\epsilon Y \Rightarrow (X, Z) \prec^\epsilon (Y, Z)$ .

Axioms (A1), (A3) and (A4) are adaptations of (E1), (E2) and (E3) to the error-tolerant setting. In particular, they recover the latter axioms in the error free case ( $\epsilon = 0$ ). The Axiom (A2) further relates the different  $\prec^\epsilon$ , it expresses that increasing the error-tolerance increases the set of possible transformations. That such an error-tolerant description allows us to describe scenarios that could not be treated previously is illustrated with the following toy example.

*Example 32.4.1* Consider a box containing a mole of Helium gas and let the states  $X$  and  $Z$  be given as in Example 32.2.1. Now assume that  $X$  and  $Z$  are used to encode information (they may for instance encode bit values 0 and 1 respectively) and that they are produced as the output of some computation that we know to yield either  $X$  or  $Z$  with probabilities  $p$  and  $(1 - p)$  respectively. We describe the output state of our computation as  $pX + (1 - p)Z$ , which corresponds to a state  $(pU + (1 - p)2U, pV + (1 - p)2^{-\frac{3}{2}}V)$ . This state can neither be transformed into  $X$  nor  $Z$  with an adiabatic operation. However, when considering error-tolerant adiabatic processes, an error probability of  $\epsilon = \frac{1}{2}$  is sufficient to enable a transformation from  $pX + (1 - p)Z$  to  $X$  for any  $p$ . If  $p \geq \frac{1}{2}$  this is achievable with the identity operation, if  $p < \frac{1}{2}$ , the adiabatic operation that transforms  $Z$  to  $X$  (and  $X$  to another state) achieves this with error probability  $\epsilon \leq \frac{1}{2}$ .

The statistical viewpoint on this will be provided in Example 32.5.1 below. There, we shall also quantify errors in a more rigorous manner, which will give us further insights.

### 32.4.1 Quantifying Resources in an Error-Tolerant Framework

We are interested in quantifying the value of the different states of a system as resources in an error-tolerant resource theory. In the error-free case, the relevant quantity is the position of the state in the state space with respect to the (transitive) preorder relation  $\prec$ . Tolerating an error of  $\epsilon > 0$  affects this value, making the same resource state more potent. This can be specified with the help of a *meter system*, which is characterised by a single parameter (as it essentially serves to specify the position of states in the ordering  $\prec$ ). We shall consider interactions between the system of interest and such a meter that simultaneously change the state of the system and of the meter, where the relative state change of the meter provides information about the system's state.

In Lieb and Yngvason's framework the subspace of equilibrium states of a thermodynamic system is such a meter system [8]. They have used this meter to specify the entropy of its own non-equilibrium states as well as that of the states of other systems whose state space does not have its own subspace of equilibrium states obeying the axioms, e.g. gravitating bodies [8]. The meter systems we shall introduce in the following are more general in the sense that we do not impose a continuous scaling operation on their state space. Instead, we allow a meter to be characterised by a parameter that may be discrete (rather than continuous) and have a finite (rather than infinite) range.

We consider a meter system with state space  $\Gamma_\lambda = \{\chi_\lambda\}_{\lambda \in \Lambda}$ , specified with a function

$$\begin{aligned}\chi : \Lambda &\rightarrow \Gamma_\lambda \\ \lambda &\mapsto \chi_\lambda\end{aligned}$$

with  $\Lambda \subseteq \mathbb{R}_{\geq 0}$ , where the parameter  $\lambda$  labels the different states. The change in  $\lambda$  produced during an interaction with a system shall specify the resource value of the system's states.

From now on, we shall quantify errors in terms of probabilities, i.e., we shall require  $0 \leq \epsilon, \delta \leq 1$ . Whenever we add two errors we understand this as  $\epsilon + \delta = \min \{\epsilon + \delta, 1\}$ . While the axiomatic framework does not rely on this restriction, the particular choice of the function  $f(\epsilon)$  below that specifies the resource-error tradeoff is motivated by the probabilistic interpretation of errors.

We assume a meter system to obey the following axioms.

- (M1) Reduction property: For any  $X, Y \in \Gamma$ , for any meter state  $\chi_\lambda \in \Gamma_\lambda$  and any  $\epsilon \geq 0$ ,  $(X, \chi_\lambda) \prec^\epsilon (Y, \chi_\lambda) \Rightarrow X \prec^\epsilon Y$ .
- (M2) Additivity of meter states: For any  $\chi_{\lambda_1}, \chi_{\lambda_2} \in \Gamma_\lambda$ ,  
 $\chi_\lambda \sim (\chi_{\lambda_1}, \chi_{\lambda_2}) \iff \lambda = \lambda_1 + \lambda_2$ .
- (M3) Ordering of meter states: A meter system has at least two inequivalent states and its states are labelled monotonically in  $\lambda$ , such that for any  $\chi_{\lambda_1}, \chi_{\lambda_2} \in \Gamma_\lambda$ ,  
 $\lambda_1 \leq \lambda_2 \iff \chi_{\lambda_1} \prec \chi_{\lambda_2}$ .
- (M4) Resource-error tradeoff: For any  $\lambda_1 > \lambda_2 \in \Lambda$  and any  $0 \leq \epsilon \leq 1$ ,  
 $\chi_{\lambda_1} \prec^\epsilon \chi_{\lambda_2} \Rightarrow \lambda_1 \leq \lambda_2 + f(\epsilon)$  with  $f(\epsilon) = -\log_2(1 - \epsilon)$ .

A meter system is supposed to measure the value of different resources. Axiom (M1) demands that it acts passively in the sense that it should not enable otherwise impossible state transformations. This property is also obeyed by the equilibrium states in Lieb and Yngvason's axiomatic framework, where it is known as the cancellation law [4, 5]. Axioms (M2) and (M3) concern merely the labelling of meter states; according to (M2) this should be additive under composition and according to (M3) monotonic with respect to the error-free ordering  $\prec$ . Note that (M3) also ensures that all states  $\chi_\lambda \in \Gamma_\lambda$  can be compared with  $\prec$ , i.e., for any such states  $\chi_{\lambda_1}, \chi_{\lambda_2} \in \Gamma_\lambda$  either  $\chi_{\lambda_1} \prec \chi_{\lambda_2}$  or  $\chi_{\lambda_2} \prec \chi_{\lambda_1}$ .

Axiom (M4) specifies the transformations on  $\Gamma_\lambda$  that are enabled by accepting imprecisions. According to Axiom (A2), a higher error-tolerance cannot prohibit any transformations but may enable more. A bound on these is specified on the meter in terms of the function  $f(\epsilon)$ , which is non-decreasing in  $\epsilon$  and obeys  $f(0) = 0$  (according to Axiom (M3)). Since we understand  $\epsilon$  as an error probability such that  $0 \leq \epsilon \leq 1$ , any state transformation should be possible in the extreme case of  $\epsilon = 1$ . Thus, in addition to  $f(0) = 0$ , we require  $\lim_{\epsilon \rightarrow 1} f(\epsilon) = \infty$  (as the allowed values for  $\lambda$  can be unbounded if we allow for the composition of an arbitrary number of meter systems). Furthermore, it should always be possible to run  $n$  independent instances of a process in parallel, in which case the success probabilities  $(1 - \epsilon)$  should multiply. In the case of a meter system we take it that there is also no alternative process with a lower error probability, i.e., we require that the process is possible if and only if the  $n$  parallel instances of that process are possible. We thus require that the existence of a process  $\chi_{\lambda_1} \prec^\epsilon \chi_{\lambda_2}$  implies that for any  $n \in \mathbb{N}_+$ ,

$$n \cdot \lambda_1 \leq n \cdot \lambda_2 + f(1 - (1 - \epsilon)^n). \quad (32.14)$$

This can be ensured with  $f(1 - (1 - \epsilon)^n) = n \cdot f(1 - (1 - \epsilon))$ , which implies that  $f(\epsilon) = -c \cdot \log_2(1 - \epsilon)$  (assuming continuity of  $f$ ). We choose  $c = 1$  for simplicity, which fixes a scale for the parameter  $\lambda$ . According to (M4), increasing the error-tolerance allows for an increase in  $\lambda_1 - \lambda_2$ ; we therefore call this axiom a resource-error tradeoff.

**Definition 32.4.1** A meter system with state space  $\Gamma_\lambda$  is *suitable* for measuring a system with state space  $\Gamma$  if it obeys (A1) to (A4) and the axioms for meter systems (Axioms (M1) to (M4)), and, if there exists a reference state denoted by  $X_{\text{ref}} \in \Gamma$  such that for any state  $X \in \Gamma$  there exist meter states  $\chi_{\lambda_1}(X), \chi_{\lambda_2}(X), \chi_{\lambda_3}(X), \chi_{\lambda_4}(X) \in \Gamma_\lambda$  such that  $(X_{\text{ref}}, \chi_{\lambda_1}(X)) \prec (X, \chi_{\lambda_2}(X))$  and  $(X, \chi_{\lambda_3}(X)) \prec (X_{\text{ref}}, \chi_{\lambda_4}(X))$  hold.

Relying on the notion of a suitable meter system, we define the following quantities.

**Definition 32.4.2** For an error-tolerant resource theory with state space  $\Gamma$  and a suitable meter system  $\Gamma_\lambda$  we define for each  $\epsilon \geq 0$  and for each  $X \in \Gamma$ ,

$$S_-^\epsilon(X) = \sup \{ \lambda_1 - \lambda_2 \mid (X_{\text{ref}}, \chi_{\lambda_1}) \prec^\epsilon (X, \chi_{\lambda_2}) \} \quad (32.15)$$

$$S_+^\epsilon(X) = \inf \{ \lambda_2 - \lambda_1 \mid (X, \chi_{\lambda_1}) \prec^\epsilon (X_{\text{ref}}, \chi_{\lambda_2}) \}, \quad (32.16)$$

where  $X_{\text{ref}} \in \Gamma$  is a fixed reference state and  $\chi_{\lambda_1}, \chi_{\lambda_2} \in \Gamma_\lambda$ .

Due to the suitability of the meter system,  $S_-^\epsilon$  and  $S_+^\epsilon$  are defined for all  $X \in \Gamma$ . In terms of these quantities, we can derive necessary conditions and sufficient conditions for state transformations. In the error-free case, i.e., if  $\epsilon = \epsilon' = \delta = 0$  in Proposition 32.4.1 below, the relations from Proposition 32.2.1 are recovered for  $S_-^0$  and  $S_+^0$ .

**Proposition 32.4.1** Consider an error-tolerant resource theory with state space  $\Gamma$  that obeys Axioms (A1) to (A4) and a suitable meter system. Then for any  $X, Y \in \Gamma$  and  $\epsilon, \epsilon' \geq 0$ , the following conditions hold:

$$S_+^\epsilon(X) < S_-^{\epsilon'}(Y) \Rightarrow X \prec^{\epsilon+\epsilon'} Y, \quad (32.17)$$

$$X \prec^\epsilon Y \Rightarrow S_-^\delta(X) \leq S_-^{\delta+\epsilon}(Y) \text{ and } S_+^{\delta+\epsilon}(X) \leq S_+^\delta(Y) \text{ for any } \delta \geq 0. \quad (32.18)$$

Because  $\prec^\epsilon$  is intransitive for  $\epsilon > 0$ ,  $S_-^\epsilon$  and  $S_+^\epsilon$  are not monotonic with respect to  $\prec^\epsilon$  (except for  $\epsilon = 0$ ). For the proof of this proposition and further properties of  $S_-^\epsilon$  and  $S_+^\epsilon$ , for instance the respective super- and sub-additivity that is expected for entropy measures, we refer the reader to Propositions 7.3.8 and 7.3.9 as well as the subsequent elaborations in [32].

## 32.5 Error-Tolerant Resource Theories in the Statistical Approach

In this section we treat states in the usual quantum-mechanical framework. This means that the state space is  $\Gamma = \mathcal{S}(\mathcal{H})$ , the set of density operators on a Hilbert space  $\mathcal{H}$ . Composition of states is defined as their tensor product and adiabatic operations on these states were introduced in Definition 32.3.1.

We will rely on a meter system for which the meter states  $\chi_\lambda \in \Gamma_\Lambda$  have eigenvalues  $2^{-\lambda}$  and 0 with multiplicities  $2^\lambda$  and  $\dim(S) - 2^\lambda$  respectively, where  $\dim(S)$  is the dimension of the Hilbert space  $\chi_\lambda$  acts on, in accordance with [24, 38, 43]. The spectrum of such a state can be conveniently written as a step function,

$$f_{\chi_\lambda}(x) = \begin{cases} 2^{-\lambda} & x \leq 2^\lambda, \\ 0 & 2^\lambda < x \leq \dim(S). \end{cases} \quad (32.19)$$

We let the parameter  $\lambda$  take values  $\lambda = \log_2(n)$  for  $n = 1, \dots, \dim(S)$ , where  $\dim(S) > 1$  and we assume that a meter system  $\Gamma_\Lambda$  with arbitrarily large dimension,  $\dim(S)$ , may be chosen. In the definition of  $S_-^\epsilon$  and  $S_+^\epsilon$  we shall optimise over meter systems of different sizes. We will compare this to another meter system in Example 32.5.2.

In a thermodynamic process, imprecisions may occur and be tolerated either in the input states to a process, its outputs, or both. Imprecise input states account for errors in the preparation of a system. When tolerating such errors, an error-tolerant transition is possible if a transition from an approximate input state to the target output can be achieved. In case of imprecisions in the output, an error-tolerant transformation is possible if a transformation could reach the output state approximately. These two types of errors can moreover be combined to an overall error  $\epsilon$ . We shall call these three ways of quantifying errors *smoothings*. They were previously considered in the context of resource theories in [28–32]. When quantified by means of the generalised trace distance, these smoothings are equivalent for adiabatic operations, meaning that they all lead to the same family of order relations  $\{\prec_M^\epsilon\}_\epsilon$  (adaptations of the majorisation relation). The equivalence of these three smoothings was proven in [29, 32], allowing us (without loss of generality) to state only one of the equivalent definitions in the following.

**Definition 32.5.1** The resource theory of *smooth adiabatic operations* is characterised by the family of order relations  $\{\prec_M^\epsilon\}_\epsilon$ , where  $\rho \prec_M^\epsilon \sigma$  if and only if  $\exists \rho', \sigma'$  and  $\epsilon', \epsilon''$  such that  $\rho' \prec_M \sigma'$  and  $\rho' \in \mathcal{B}^{\epsilon'}(\rho)$ ,  $\sigma' \in \mathcal{B}^{\epsilon''}(\sigma)$  with  $\epsilon' + \epsilon'' \leq \epsilon$ ;  $\mathcal{B}^\epsilon(\rho) = \{\rho' \in \mathcal{S}(\mathcal{H}) \mid D(\rho, \rho') \leq \epsilon\}$  denotes the set of all states that are  $\epsilon$ -close to the state  $\rho \in \mathcal{S}(\mathcal{H})$ , measured in terms of the generalised trace distance  $D(\cdot, \cdot)$  [44].<sup>9</sup>

The following example illustrates that the resource theory of smooth adiabatic operations allows us to analyse situations that could not be described within the

---

<sup>9</sup>For  $\epsilon = 0$  the usual majorisation relation is recovered.

resource theory of adiabatic processes. It is analogous to Example 32.4.1, but described from a statistical perspective.

*Example 32.5.1* Consider once more a mole of Helium gas with states  $\rho_X = \frac{\Pi_{\Omega_{\text{micro}}(U,V)}}{\Omega_{\text{micro}}(U,V)}$  and  $\rho_Z = \frac{\Pi_{\Omega_{\text{micro}}(2U,2^{-3/2}V)}}{\Omega_{\text{micro}}(2U,2^{-3/2}V)}$ . Now assume again that these states are used to encode information (they may for instance encode bit values 0 and 1 respectively) and that they are produced as the output of a computation that we know to yield either  $\rho_X$  or  $\rho_Z$  with probabilities  $p$  and  $(1 - p)$  respectively. We describe the output state of this computation as  $p\rho_X + (1 - p)\rho_Z$ , which cannot be transformed into  $\rho_X$  (or  $\rho_Z$ ) with an adiabatic operation. However, when considering error-tolerant adiabatic processes, an error-probability of  $\epsilon = \frac{1}{2}$  is sufficient to enable a transformation from  $p\rho_X + (1 - p)\rho_Z$  to  $\rho_X$  for any  $p$  (as  $p\rho_X + (1 - p)\rho_Z \prec_M^\epsilon \rho_X$ ). More generally, the required error probability to achieve this transformation is  $\epsilon = \min\{p, 1 - p\}$ . For smaller  $\epsilon$  additional resources would be required to recover  $\rho_X$ , which can be seen as an example of the resource-error tradeoff.

In the following we derive the quantities  $S_-^\epsilon$  and  $S_+^\epsilon$  that provide necessary conditions as well as sufficient conditions for the existence of smooth adiabatic operations between different states according to Proposition 32.4.1.

**Proposition 32.5.1** *The resource theory of smooth adiabatic operations with state space  $\Gamma = \mathcal{S}(\mathcal{H})$  and with composition of states defined as their tensor product obeys Axioms (A1) to (A4). The meter system  $\Gamma_\Lambda$  defined by (32.19) is suitable for measuring systems with a state space  $\Gamma = \mathcal{S}(\mathcal{H})$ . With reference state  $\rho_{\text{ref}} = |0\rangle\langle 0| \in \mathcal{S}(\mathcal{H})$ , we obtain*

$$S_-^\epsilon(\rho) = H_{\min}^\epsilon(\rho) \quad (32.20)$$

$$S_+^\epsilon(\rho) = H_H^{1-\epsilon}(\rho) + \log_2(1 - \epsilon), \quad (32.21)$$

where

$$H_{\min}^\epsilon(\rho) = \sup_{\rho' \in \mathcal{B}^\epsilon(\rho)} H_{\min}(\rho') \quad (32.22)$$

$$H_H^{1-\epsilon}(\rho) = \log \inf \left\{ \frac{1}{1 - \epsilon} \text{tr}(Q) : \text{tr}(Q\rho) \geq 1 - \epsilon \text{ and } 0 \leq Q \leq \mathbb{1} \right\}. \quad (32.23)$$

This is shown by means of Proposition 7.2.7, Lemma 7.3.12 and Proposition 7.3.13 in [32].  $H_{\min}^\epsilon$  is known as a *smooth min entropy* and  $H_H^{1-\epsilon}$  as a *smooth max entropy* in single-shot information theory [33]. Note further that for  $\epsilon = 0$  we recover the quantities  $S_-$  and  $S_+$  from Proposition 32.3.2.

Alternatively, we may consider other meter systems that are less fine-grained. An example is a meter system that consists of a number of small systems in two possible states, one of which is a resource state. The number of such resource states that is consumed (or gained) in the construction or destruction of a particular state is then a measure for the resourcefulness of that state. This type of meter system is also known as a *battery* in the literature, going back to ideas of Bennett [45].

*Example 32.5.2* Take the meter system to be an arbitrarily large collection of qubits that can each be either in a pure state  $\rho = |0\rangle\langle 0|$  or in a maximally mixed state  $\rho = \frac{1}{2}I$ . Thus, the spectrum of such a meter state  $\chi_\lambda \in \Gamma_\Lambda$  can be written as a step function

$$f_{\chi_\lambda}(x) = \begin{cases} 2^{-\lambda} & x \leq 2^\lambda, \\ 0 & 2^\lambda < x \leq \dim(S), \end{cases} \quad (32.24)$$

where  $\lambda \in \mathbb{Z}_{\geq 0}$  and  $\dim(S)$  is the dimension of the Hilbert space  $\chi_\lambda$  acts on. Compared to the previously considered one, this meter system leads to coarse-grained entropy measures that can only take integer values. More precisely, it leads to

$$S_-^\epsilon(\rho) = \lfloor H_{\min}^\epsilon(\rho) \rfloor \quad (32.25)$$

$$S_+^\epsilon(\rho) = \lceil H_H^{1-\epsilon}(\rho) + \log_2(1-\epsilon) \rceil. \quad (32.26)$$

With this meter system, larger classes of states  $\rho$  yield the same  $S_-^\epsilon(\rho)$  (and similar for  $S_+^\epsilon(\rho)$ ), i.e., the meter system is not fine-grained enough to distinguish them. For a qubit in a state  $\rho$ , for instance,  $S_-^\epsilon(\rho) = 0$  for all  $\rho$  with  $\frac{1}{2} < \lambda_{\max}(\rho) - \epsilon < 1$ , where  $\lambda_{\max}(\rho)$  is the larger eigenvalue of  $\rho$ .

Our framework also exhibits the phenomenon of embezzling, which is known from various resource theories [46–48]. We define a catalytic transformation as one that can be achieved with any catalyst. For instance, there is a *catalytic smooth adiabatic process* from a state  $\rho$  to  $\sigma$ , denoted as  $\rho \prec_{\text{cat}}^\epsilon \sigma$ , if and only if there exists a catalyst  $\rho_{\text{cat}}$  (a state on a finite dimensional Hilbert space) such that  $\rho \otimes \rho_{\text{cat}} \prec_M^\epsilon \sigma \otimes \rho_{\text{cat}}$ . In principle, by suitably engineering  $\rho_{\text{cat}}$  (allowing it to be an arbitrarily large system) we can achieve a transformation between any states  $\rho$  and  $\sigma$ . To show this, it is sufficient to consider transformations on the meter systems. It turns out that, provided the tolerated error probability  $\epsilon$  is strictly positive, any transformation on the meter system is enabled by a suitable catalyst [32].

**Proposition 32.5.2** *For any meter state  $\chi_\lambda \in \Gamma_\Lambda$  and for any  $\epsilon > 0$  we can find a quantum state  $\rho_{\text{cat}}$  such that*

$$\chi_\lambda \prec_{\text{cat}}^\epsilon \chi_0. \quad (32.27)$$

Figure 32.1 illustrates how a corresponding catalyst can be engineered. Notice that since  $\lambda > 0$  for all meter states (recall (32.19)) and according to (M3),  $\chi_0$  is the most valuable meter state in the resource theory from which all others can be generated with an adiabatic process.

That catalysts can enable any transformations may sound counter-intuitive at first. It is a phenomenon that, nonetheless, naturally occurs in experiments. Consider for instance an experiment in a laboratory, where we aim to excite an atom to a higher energetic state. The light present in the laboratory can be viewed as a large catalyst, that, if the atom is not properly isolated from it, may cause this transition without us perceiving any change in the laboratory's state. The part of this catalyst that is relevant for the transition is the light around a certain frequency, which we can model

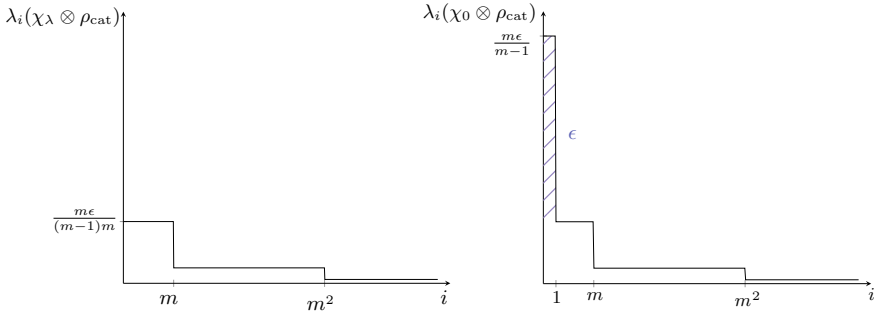


**Fig. 32.1** A transformation  $\chi_\lambda \prec_{\text{cat}}^\epsilon \chi_0$  is achieved with a catalyst  $\rho_{\text{cat}}$  with eigenvalues  $\lambda_i(\rho_{\text{cat}}) = \frac{m\epsilon}{m-1} \cdot m^{-\lceil \log_m i \rceil}$ , where  $m = 2^\lambda$  and where  $i$  ranges from 1 to the maximal value that leaves  $\rho_{\text{cat}}$  normalised (and where the last eigenvalue may be smaller than prescribed so that normalisation is achieved). On the left hand side we show the spectrum of  $\chi_\lambda \otimes \rho_{\text{cat}}$  and on the right hand side that of  $\chi_0 \otimes \rho_{\text{cat}}$ . They differ in the first eigenvalue (and in the last few, which is not visible in the plots), giving an overall trace distance of  $\epsilon$ .

as a distribution over the number of photons at the corresponding energy, expressing our knowledge of the probability that  $n$  photons of (approximately) that frequency are present. The absorption of one of these photons is enough to cause the transition, however, it changes our description of the catalyst only marginally (also without a supply of new photons).

If we were to impose restrictions on the type of system that can be used as a catalyst, for instance if in an experimental setup a system of a certain size is present, the processes the system could enable when considered as a catalyst would be more restrictive. This is illustrated with the following toy example.

*Example 32.5.3* Assume that we want to make the transformation  $\frac{\mathbb{I}_2}{2} \prec_{\text{cat}}^\epsilon |0\rangle\langle 0|$  and that we have only one additional qubit as a catalyst at our disposal. Let this qubit be  $\rho$  with spectrum  $(p, 1-p)$  where  $p \geq \frac{1}{2}$ . According to the majorisation condition,<sup>10</sup>  $\rho$  can be used as a catalyst that enables the transformation of  $\frac{\mathbb{I}_2}{2}$  to  $|0\rangle\langle 0|$ , if  $\frac{1}{2}p \leq \epsilon$  and  $1-p \leq \epsilon$ . Hence, if  $\epsilon < \frac{1}{3}$ , a qubit catalyst is not sufficient.

The size of the catalyst  $\rho$  that is needed to enable a transformation  $\chi_{\lambda_1} \prec_{\text{cat}}^\epsilon \chi_{\lambda_2}$  where  $\lambda_2 < \lambda_1$  is bounded by means of the following necessary condition for such a transformation: for  $\epsilon \text{rank}(\rho) < 1$ ,<sup>11</sup>

$$\lambda_1 - \lambda_2 \leq -\log_2 (1 - \epsilon \text{rank}(\rho)) . \quad (32.28)$$

<sup>10</sup>We aim to achieve the transformation  $\rho \otimes \frac{\mathbb{I}_2}{2} \prec_M^\epsilon \rho \otimes |0\rangle\langle 0|$ , where the ordered spectra of the two states are  $(\frac{p}{2}, \frac{p}{2}, \frac{1-p}{2}, \frac{1-p}{2})$  and  $(p, 1-p, 0, 0)$ .

<sup>11</sup>The largest eigenvalues of  $\rho \otimes \chi_{\lambda_1}$  and  $\rho \otimes \chi_{\lambda_2}$  are  $p2^{-\lambda_1}$  and  $p2^{-\lambda_2}$  respectively, where  $p$  is the maximal eigenvalue of  $\rho$ . Up to  $2^{\lambda_2}$ , the sums of the eigenvalues of the two states are  $p2^{\lambda_2-\lambda_1}$  and  $p$  respectively, thus the transition is only possible if  $p2^{\lambda_2-\lambda_1} \geq p - \epsilon$ .

For any given transformation on the meter system (i.e., for fixed  $\lambda_1 > \lambda_2$ ) this bound on the minimal catalyst size increases with decreasing error-tolerance  $\epsilon$ . The bound also shows that in the special case  $\epsilon = 0$  no transition with  $\lambda_1 > \lambda_2$  is possible.

Our axiomatic approach has the flexibility needed to describe different error types. We illustrate this in the following with the example of probabilistic transformations from [25]. A probabilistic transformation,  $\mathcal{E}$ , from a state  $\rho \in \mathcal{S}(\mathcal{H})$  to a state  $\sigma \in \mathcal{S}(\mathcal{H})$  with error probability  $\epsilon$ , is

$$\rho \rightarrow \mathcal{E}(\rho) = (1 - \epsilon)\sigma + \epsilon\xi, \quad (32.29)$$

where  $\xi$  is an arbitrary state. This expresses that the process, which aims to transform  $\rho$  to  $\sigma$ , succeeds with probability  $1 - \epsilon$ , whereas with probability  $\epsilon$  any output can be produced.

**Definition 32.5.2** The resource theory of *probabilistic adiabatic operations* is characterised by the order relations  $\{\prec_p^\epsilon\}_\epsilon$ , where for  $\rho, \sigma \in \mathcal{S}(\mathcal{H})$ ,  $\rho \prec_p^\epsilon \sigma$  if and only if  $\exists \xi \in \mathcal{S}(\mathcal{H})$  such that  $\rho \prec_M (1 - \epsilon)\sigma + \epsilon\xi$ .

Probabilistic adiabatic transformations are characterised by  $S_-^\epsilon$  and  $S_+^\epsilon$  given in the following proposition, which provide necessary conditions and sufficient conditions for state transformations with such processes (according to Proposition 32.4.1).

**Proposition 32.5.3** *Probabilistic adiabatic transformations on a state space  $\Gamma = \mathcal{S}(\mathcal{H})$ , where composition of states is defined as their tensor product, obey Axioms (A1) to (A4). The meter system  $\Gamma_\Lambda$  defined by (32.19) is suitable for measuring systems with a state space  $\Gamma = \mathcal{S}(\mathcal{H})$ . With reference state  $\rho_{\text{ref}} = |0\rangle\langle 0| \in \mathcal{S}(\mathcal{H})$ , we obtain*

$$S_-^\epsilon(\rho) = H_{\min}(\rho) + \log_2(1 - \epsilon) \quad (32.30)$$

$$S_+^\epsilon(\rho) = H_0(\rho) . \quad (32.31)$$

This has been proven as Lemma 7.4.1 and Proposition 7.4.2 in [32]. We remark here that  $\rho \prec_p^\epsilon \sigma$  and  $\sigma \prec_p^\delta \omega$  imply  $\rho \prec_p^{\epsilon+\delta-\epsilon\delta} \omega$ , which for  $\epsilon, \delta \neq 0$  is a strictly smaller error than the axiomatically required  $\epsilon + \delta$ .

The existence of a probabilistic adiabatic transformation from a state  $\rho$  to a state  $\sigma$  implies that there is also a smooth adiabatic transformation from  $\rho$  to  $\sigma$ , hence the state transformations enabled by adiabatic probabilistic transformations are a subset of the smooth adiabatic ones. We can see this by considering the output state of a probabilistic adiabatic process (see Definition 32.5.2), which obeys

$$D(\sigma, (1 - \epsilon)\sigma + \epsilon\xi) = \epsilon D(\sigma, \xi) \leq \epsilon, \quad (32.32)$$

because the trace distance of two states  $\sigma$  and  $\xi$  is bounded by 1. The converse statement is not true. This can be seen by considering the states  $\rho = \frac{1}{2}|0\rangle\langle 0| + \frac{1}{2}|1\rangle\langle 1|$  and  $\sigma = \frac{3}{4}|0\rangle\langle 0| + \frac{1}{4}|1\rangle\langle 1|$ . For an error-tolerance of  $\epsilon = \frac{1}{4}$  there is a smooth adiabatic

operation from  $\rho$  to  $\sigma$ , since  $\rho \prec_M^{1/4} \sigma$ , but there is no corresponding probabilistic adiabatic process,  $\rho \not\prec_p^{1/4} \sigma$ . Instead, an error-tolerance of (at least)  $\epsilon = \frac{1}{3}$  would be needed in the latter case.

## 32.6 Axiomatic Emergence of Macroscopic Thermodynamics

In the limit of large systems our error-tolerant framework leads to the emergence of an effective order relation that is characterised by a single entropic quantity for thermodynamic equilibrium states, as we shall explain in the following. Even though our considerations in this and the subsequent section are based on insights from Chap. 8 of [32], we take a slightly different approach here, where macroscopic states depend on a continuous parameter.

We first define the elements of a macroscopic state space as functions of a continuous parameter  $n \in \mathbb{R}_{\geq 0}$  that maps each  $n$  to a state  $X(n) \in \Gamma(n)$ , i.e., to a state in a state space  $\Gamma(n)$ . The set of all such macroscopic states is

$$\Gamma_\infty = \left\{ X_\infty \left| \begin{array}{l} X_\infty : \mathbb{R}_{\geq 0} \rightarrow \bigcup_n \Gamma(n) \\ n \mapsto X(n) \in \Gamma(n) \end{array} \right. \right\}. \quad (32.33)$$

One may think of  $n$  as encoding the amount of substance in a system (and the fact that it can take any value in a continuum corresponds to the usual approximation made in macroscopic thermodynamics). The states  $X_\infty$  that intuitively describe a physical system are those for which  $X(n')$  is the state of a subsystem of  $X(n)$  for all  $n' \leq n$ . Among them, the equilibrium states are those whose macroscopic properties scale linearly with the parameter  $n$ . Thinking for instance of the state of a gas in a box, a function that characterises such an equilibrium state is  $X_\infty$  such that  $X(n) = (nU, nV, nN)$  for all  $n \in \mathbb{R}_{\geq 0}$ , where  $nU$  is the internal energy,  $nV$  the volume and  $nN$  the matter content of a system. In order to introduce these intuitive notions into the formalism, we require a little more terminology and another axiom, which may be added to any error-tolerant resource theory.

- (A5) Let  $\Gamma$  be the state space of the resource theory and  $\Gamma_\lambda$  a meter system. Then there exists a state  $Z \in \Gamma$  that for any  $X, Y \in \Gamma$  obeys

$$X \prec^\epsilon Y \iff (X, Z) \prec^\epsilon (Y, Z) \quad (32.34)$$

and that for any meter states  $\chi_{\lambda_1}, \chi_{\lambda_2} \in \Gamma_\lambda$  obeys<sup>12</sup>

$$\chi_{\lambda_1} \prec^\epsilon \chi_{\lambda_2} \iff (\chi_{\lambda_1}, Z) \prec^\epsilon (\chi_{\lambda_2}, Z). \quad (32.35)$$

---

<sup>12</sup>This condition is independent of (32.34) only if  $\Gamma_\lambda \not\subseteq \Gamma$ ; if  $\Gamma_\lambda$  is chosen such that  $\Gamma_\lambda \subseteq \Gamma$  it is implied by (32.34).

The axiom encodes the requirement that a system should have at least one state that cannot be used as a catalyst with respect to the resource theory. It is conceivable that a ground state of a system should generally have this property. Taking a statistical viewpoint, there are usually many such states. For example, in the quantum resource theories considered before, the maximally mixed state for adiabatic processes (and the meter states in  $\Gamma_A$ ) and the Gibbs states for thermal operations have this property. From now on, whenever (A5) holds, we choose the reference state on the system,  $X_{\text{ref}} \in \Gamma$  (recall Definition 32.4.1), such that it has this property. This choice fixes the zero of the entropic quantities we shall consider below. We then define the following subset of  $\Gamma$ ,

$$\Gamma_M = \{\tau_\lambda \in \Gamma \mid S_-^0(\tau_\lambda) = S_+^0(\tau_\lambda) = \lambda\} \subseteq \Gamma. \quad (32.36)$$

From our choice of  $X_{\text{ref}}$ , it is easy to see that the set  $\Gamma_M$  contains at least this state, which obeys  $S_-^0(X_{\text{ref}}) = S_+^0(X_{\text{ref}}) = 0$ , i.e.,  $\tau_0 = X_{\text{ref}}$ . The label  $M$  stands for meter, as the states  $\tau_\lambda \in \Gamma_M$  behave like meter states, i.e., they obey Axioms (M1) to (M4).<sup>13</sup> Macroscopic states made up of states  $\tau_{\lambda_n} \in \Gamma_M(n)$  are denoted as  $\tau_{\lambda_\infty} \in \Gamma_M^\infty$ .

On  $\Gamma_\infty$ , we introduce an effective macroscopic order relation  $\prec_\infty$ : we write  $X_\infty \prec_\infty Y_\infty$  if for any  $\epsilon > 0$  there exists  $n_0$  such that for all  $n \geq n_0$ ,  $X(n) \prec^\epsilon Y(n)$ . Intuitively, equilibrium states have the property that their behaviour with respect to  $\prec_\infty$  is essentially characterised by a single quantity which we call  $\lambda_{X_\infty}$ , i.e., an equilibrium state  $X_\infty$  should essentially be interconvertible with a meter state that is characterised by this parameter in the sense that  $X(n)$  is roughly interconvertible with a  $\tau_{n\lambda_{X_\infty}}$ . The relation of equilibrium states to such macroscopic meter states concerns only their (approximate) behaviour, but they do not have to be meter states themselves (as opposed to [8]).

**Definition 32.6.1**  $X_\infty$  is a *thermodynamic equilibrium state* if there exists  $\lambda_{X_\infty}$  such that for any  $\delta > 0$  there exist meter states  $\tau_{\lambda_\infty^-}, \tau_{\lambda_\infty^\pm} \in \Gamma_M^\infty$  such that

$$\tau_{\lambda_\infty^-} \prec_\infty X_\infty \prec_\infty \tau_{\lambda_\infty^\pm} \quad (32.37)$$

and such that the parameters of the meter states  $\lambda_n^-$  and  $\lambda_n^+$  obey  $\lambda_n^- \geq n(\lambda_{X_\infty} - \delta)$  and  $\lambda_n^+ \leq n(\lambda_{X_\infty} + \delta)$  for large enough  $n$  respectively. The set of all thermodynamic equilibrium states is denoted  $\Gamma_\infty$ .

Thermodynamic equilibrium states are essentially characterised by a single entropic quantity, as shown with the following assertion that is based on Proposition 8.1.3 in [32].

**Proposition 32.6.1** *Let there be an error-tolerant resource theory on state spaces  $\Gamma(n)$  that obeys Axioms (A1) to (A4) and Axiom (A5) and let there be a suitable meter system on each of them. Furthermore, let  $X_\infty \in \Gamma_\infty$  be a thermodynamic equilibrium state. Then, for any  $0 < \epsilon < 1$ ,*

---

<sup>13</sup>Axiom (M1), for instance, follows since  $(X, \tau_\lambda) \prec^\epsilon (Y, \tau_\lambda)$  implies  $(X, \tau_\lambda, \chi_{\lambda_1}, \chi_{\lambda_2}) \prec^\epsilon (Y, \tau_\lambda, \chi_{\lambda_1}, \chi_{\lambda_2})$  by (A4) and since by applying (32.36) and the property (A5) for  $X_{\text{ref}}$  this can be shown to also imply  $X \prec^\epsilon Y$ . (M2), (M3) and (M4) also follow from (32.36) and the axioms.

$$S_\infty(X_\infty) = \lim_{n \rightarrow \infty} \frac{S_-^\epsilon(X(n))}{n} = \lim_{n \rightarrow \infty} \frac{S_+^\epsilon(X(n))}{n} = \lambda_{X_\infty}. \quad (32.38)$$

**Corollary 32.6.1** Consider states  $X \in \Gamma$  and macroscopic states  $X_\infty \in \Gamma_\infty$ , where  $X(n) = (X, \dots, X)$  is the composition of  $[n]$  copies of  $X$  for each  $n$ . If all such states  $X_\infty$  obey the requirements of Proposition 32.6.1, i.e., if the  $X(n)$  obey all axioms (including the consideration of suitable meter systems) and the  $X_\infty$  are thermodynamic equilibrium states, then

$$S_-^0(X) \leq S_\infty(X_\infty) \leq S_+^0(X). \quad (32.39)$$

The following shows how  $S_\infty$  is the quantity that generally provides necessary and sufficient conditions for state transformations in the macroscopic regime. It is based on Proposition 8.1.5 of [32].

**Proposition 32.6.2** Let there be an error-tolerant resource theory on state spaces  $\Gamma(n)$  that obeys Axioms (A1) to (A4) and Axiom (A5) and let there be a suitable meter system on each of them. Furthermore, let  $X_\infty, Y_\infty \in \Gamma_\infty$  be thermodynamic equilibrium states. Then, for any  $\delta > 0$ ,

$$S_\infty(X_\infty) + \delta \leq S_\infty(Y_\infty) \Rightarrow X_\infty \prec_\infty Y_\infty. \quad (32.40)$$

Furthermore, the converse holds for  $\delta = 0$ . More generally, if for some  $0 < \epsilon < 1$ , there exists an  $n_0$  such that for all  $n \geq n_0$ , the relation  $X(n) \prec^\epsilon Y(n)$  holds, then

$$S_\infty(X_\infty) \leq S_\infty(Y_\infty). \quad (32.41)$$

The proposition thus guarantees that  $S_\infty$  is monotonic with respect to  $\prec_\infty$  and that  $S_\infty(X_\infty) < S_\infty(Y_\infty)$  implies  $X_\infty \prec_\infty Y_\infty$ . The macroscopic transformations according to  $\prec_\infty$  are fully characterised by a necessary and sufficient condition in terms of  $S_\infty$  (except for pairs of states where  $S_\infty(X_\infty) = S_\infty(Y_\infty)$ ).

The relation  $\prec_\infty$  establishes the connection to the structure of traditional resource theories [1–3, 36, 37] and (with appropriate composition and scaling operations) to the resource theories for macroscopic equilibrium thermodynamics [4–6]. We will show this in the following. Let us define the composition of macroscopic states as

$$\Gamma_\infty \times \Gamma'_\infty = \left\{ (X_\infty, Y_\infty) \mid \begin{array}{l} (X_\infty, Y_\infty) : \mathbb{R}_{\geq 0} \rightarrow \bigcup_n \Gamma(n) \times \Gamma'(n) \\ n \mapsto (X(n), Y(n)) \in \Gamma(n) \times \Gamma'(n) \end{array} \right\}. \quad (32.42)$$

The scaling with a parameter  $\alpha \in \mathbb{R}_{\geq 0}$  leads to a state space  $\alpha\Gamma_\infty$ , obtained by scaling the parameter  $n$ . More precisely, a state  $\tilde{X}_\infty = \alpha X_\infty \in \alpha\Gamma_\infty$  is obtained from  $X_\infty \in \Gamma_\infty$  as the function that maps  $n$  to  $\tilde{X}(n) = X(\alpha n)$ . With these operations,  $\prec_\infty$  obeys Axioms (E1)–(E4), which follows directly from the definitions. In addition,  $S_\infty$  is extensive in the scaling and additive under composition, as stipulated for a thermodynamic entropy function. To see this, let there be an equilibrium state  $X_\infty$ ,

meaning that for any  $\delta > 0$  and  $\epsilon > 0$  there is a  $n_0$  such that for  $n \geq n_0$ ,

$$\tau_{\lambda_n^-} \prec^\epsilon X(n) \prec^\epsilon \tau_{\lambda_n^+} \quad (32.43)$$

with  $\lambda_n^- \geq n(\lambda_{X_\infty} - \delta)$  and  $\lambda_n^+ \leq n(\lambda_{X_\infty} + \delta)$ . This implies that for  $\alpha n \geq n_0$  also

$$\tau_{\lambda_{\alpha n}^-} \prec^\epsilon X(\alpha n) \prec^\epsilon \tau_{\lambda_{\alpha n}^+}, \quad (32.44)$$

which in turn implies that  $\alpha X_\infty$  is an equilibrium state with  $S_\infty(\alpha X_\infty) = \lambda_{\alpha X_\infty} = \alpha \lambda_{X_\infty}$  (and similarly  $S_\infty((1-\alpha)X_\infty) = \lambda_{(1-\alpha)X_\infty} = (1-\alpha) \cdot \lambda_{X_\infty}$ ). The additivity under composition follows since the states  $\tau_\lambda$  obey (M2). From this it also follows that for  $0 < \alpha < 1$ ,  $S_\infty(X_\infty) = S_\infty((\alpha X_\infty, (1-\alpha)X_\infty))$ .<sup>14</sup>

## 32.7 Emergence of Macroscopicity in the Statistical Approach

To identify the thermodynamic equilibrium states with respect to adiabatic processes, let us first consider the set  $\Gamma_M$  defined in (32.36), which is the set of all states  $\rho \in \mathcal{S}(\mathcal{H})$  that obey  $H_{\min}(\rho) = H_0(\rho)$  (see Proposition 32.3.2). Hence,  $\Gamma_M$  is the set of all states that obey  $\lambda_{\max}(\rho) = \frac{1}{\text{rank}(\rho)}$ , where  $\lambda_{\max}(\rho)$  denotes the maximal eigenvalue of  $\rho$ . These are the sharp states.

A class of thermodynamic equilibrium states with respect to the smooth adiabatic operations (and using the meter  $\Gamma_\Lambda$ ) are the microcanonical states,

$$\Gamma_\infty^{\text{micro}} = \left\{ \rho_\infty \left| \begin{array}{l} \rho_\infty : \mathbb{R}_{\geq 0} \rightarrow \bigcup_n \Gamma(n) \\ n \mapsto \rho(n) = \frac{\Pi_{\Omega_{\text{micro}}(nU, nV, n)}}{\Omega_{\text{micro}}(nU, nV, n)} \end{array} \right. \right\}, \quad (32.45)$$

where  $\Omega_{\text{micro}}$  is the microcanonical partition function and  $\Pi_{\Omega_{\text{micro}}}$  is the projector onto its subspace. For a microcanonical state  $\rho_\infty \in \Gamma_\infty^{\text{micro}}$ ,  $S_\infty$  is the entropy per particle known from statistical mechanics,  $S_\infty(\rho_\infty) = \lambda_{\rho_\infty} = \log_2(\Omega_{\text{micro}}(U, V, 1))$ .

In the following, we show that the so-called i.i.d. states are also a class of thermodynamic equilibrium states with respect to smooth adiabatic operations. The proposition is based on Lemma 8.2.1 from [32].

**Proposition 32.7.1** *For smooth adiabatic operations on quantum states with state space  $\Gamma = \mathcal{S}(\mathcal{H})$  and the meter system  $\Gamma_\Lambda$ ,*

$$\Gamma_\infty^{\text{i.i.d.}} = \left\{ \rho_\infty \left| \begin{array}{l} \rho_\infty : \mathbb{R}_{\geq 0} \rightarrow \bigcup_n \Gamma^{\otimes[n]} \\ n \mapsto \rho(n) = \rho^{\otimes[n]} \end{array} \right. \right\} \quad (32.46)$$

---

<sup>14</sup>Axiom (E5) is, however, not implied by this.

is a set of equilibrium states. Furthermore,  $\lambda_{\rho_\infty} = H(\rho)$  is the von Neumann entropy  $H(\rho) = -\text{tr}(\rho \log_2 \rho)$ .

This agrees with previous results regarding the asymptotic equipartition property for i.i.d. states [49], which recover the von Neumann entropy as the relevant quantity in the macroscopic regime.<sup>15</sup> Note that Corollary 32.6.1 implies that thus  $S_-^0(\rho) \leq S_+^0(\rho)$  for all  $\rho \in \mathcal{S}(\mathcal{H})$  (which we know to be true for  $H_{\min}(\rho)$  and  $H_0(\rho)$ ).

Notice that with respect to *probabilistic* adiabatic transformations, the set of i.i.d. states,  $\Gamma_\infty^{\text{i.i.d.}}$ , is not a set of thermodynamic equilibrium states according to Definition 32.6.1. To see this, let  $\epsilon \leq \frac{1}{4}$ , let  $\delta = \frac{1}{100}$  and take a state  $\rho = \frac{3}{4}|0\rangle\langle 0| + \frac{1}{4}|1\rangle\langle 1|$ . Then  $\rho^{\otimes n}$  has a maximal eigenvalue  $\lambda_{\max}(\rho^{\otimes n}) = \left(\frac{3}{4}\right)^n$  and its rank is  $\text{rank}(\rho^{\otimes n}) = 2^n$ . Now consider  $\tau_{\lambda_n^-} \prec_p^\epsilon \rho^{\otimes n}$  and  $\rho^{\otimes n} \prec_p^\epsilon \tau_{\lambda_n^+}$ , i.e.,

$$\tau_{\lambda_n^-} \rightarrow (1 - \epsilon)\rho^{\otimes n} + \epsilon\xi_1 \quad (32.47)$$

$$\rho^{\otimes n} \rightarrow (1 - \epsilon)\tau_{\lambda_n^+} + \epsilon\xi_2. \quad (32.48)$$

For there to be such transformations, the necessary conditions  $\lambda_n^- \leq n \log_2 \left(\frac{4}{3}\right) - \log_2(1 - \epsilon)$  and  $\lambda_n^+ \geq n \log_2(2)$  have to be met,<sup>16</sup> which imply that  $\lambda_n^+ - \lambda_n^- \geq n \log_2 \left(\frac{3}{2}\right) + \log_2(1 - \epsilon) > 2n\delta$ .

## 32.8 Conclusion

In this chapter, we have presented a unified axiomatic framework for thermodynamics. The phenomenological viewpoint taken to describe the transformations of thermodynamic systems in the axiomatic setting is complemented with microscopic models of these processes, leading to explicit entropic quantities that characterise state transformations. The connection between adiabatic processes according to Lieb and Yngvason and their analogue in the statistical approach is of conceptual interest, since it also connects entropy measures from information theory to their thermodynamic counterparts. It extends the well-known link between entropy in statistical physics and information theory [41, 42] (which are both based on microscopic descriptions of systems) to phenomenological thermodynamics.

Considering approximations and errors is necessary for the theoretical treatment of thermodynamics, even if these errors are so small that we do not usually notice them. The structure of our error-tolerant framework deviates from that of resource theories without this feature (including the latter as a zero-error case). The operationally significant quantities for characterising transformations under smooth adiabatic operations (the error-tolerant versions of adiabatic processes) are the smooth

<sup>15</sup>In [49] the max entropy  $H_0^\epsilon$  instead of  $H_H^{1-\epsilon}$  is considered, however, the relation has also been proven for the latter [33].

<sup>16</sup>This follows as the state  $\tau_{\lambda_n^-}$  has to be chosen such that it majorises  $(1 - \epsilon)\rho^{\otimes n}$ . Furthermore,  $\rho^{\otimes n}$  has to majorise  $(1 - \epsilon)\tau_{\lambda_n^+}$ , hence its rank has to be smaller than that of  $\tau_{\lambda_n^+}$ .

min and max entropies from the generalised entropy framework [33] (cf. Proposition 32.5.1). The emergence of macroscopic thermodynamics from our error-tolerant framework furthermore establishes the latter as a natural underlying structure. We recover the von Neumann entropy (for i.i.d. states) and the Boltzmann entropy (for microcanonical states) as the quantities that specify the existence of state transformations in the macroscopic regime.

Our error-tolerant axiomatic framework applies to systems of any size, including very small systems. By introducing entropy meters without a continuous parameter we furthermore provide an axiomatic basis for describing the thermodynamics of small systems without referring to large meter systems in order to specify their properties. In fact, the meter system could be of a size comparable to that of the (small) system of interest (which is usually accompanied with limitations in the precision).

Due to the axiomatic nature of our error-tolerant framework, it can also be applied to other resource theories. In particular, some preliminary work suggests that a resource theory of *smooth thermal operations* [28] also obeys our axioms. This implies that we can consider this resource theory in the same manner as the adiabatic processes and derive corresponding quantities  $S_-^\epsilon$  and  $S_+^\epsilon$ , which will be quantities that generalise the free energy. Whether our framework is naturally applicable beyond the realm of thermodynamics, for instance to the resource theory of asymmetry [50], remains an interesting open question.

So far, our axiomatic framework lacks the ability to describe situations where quantum side information about a system is accessible. It is known that this can lead to new types of phenomena such as a negative work cost for erasure [51]. The quantities that characterise the existence of state transformations in such cases would likely correspond to conditional entropies as known from information theory. An axiomatic framework that takes quantum side information into account would hence provide an axiomatic foundation for these entropies, paired with an operational meaning.

**Acknowledgements** Philippe Faist is not listed as an author for editorial reasons. MW is supported by the EPSRC (grant number EP/P016588/1). RR acknowledges contributions from the Swiss National Science Foundation via the NCCR QSIT as well as project No. 200020 165843.

## References

1. D. Janzing, P. Wocjan, R. Zeier, R. Geiss, T. Beth, Thermodynamic cost of reliability and low temperatures: tightening Landauer's principle and the second law. *Int. J. Theor. Phys.* **39**(12), 2717–2753 (2000). [arXiv:quant-ph/0002048](https://arxiv.org/abs/quant-ph/0002048)
2. M. Horodecki, J. Oppenheim, Fundamental limitations for quantum and nanoscale thermodynamics. *Nat. Commun.* **4**, 2059 (2013). <https://doi.org/10.1038/ncomms3059>
3. J.M. Renes, Work cost of thermal operations in quantum thermodynamics. *Eur. Phys. J. Plus* **129**(7), 153 (2014). <https://doi.org/10.1140/epjp/i2014-14153-8>
4. E.H. Lieb, J. Yngvason, A guide to entropy and the second law of thermodynamics. *Not. Am. Math. Soc. A* **58**1, 571–581 (1998). [arXiv:math-ph/9805005](https://arxiv.org/abs/math-ph/9805005)

5. E.H. Lieb, J. Yngvason, The physics and mathematics of the second law of thermodynamics. *Phys. Rep.* **310**, 1–96 (1999). [https://doi.org/10.1016/S0370-1573\(98\)00082-9](https://doi.org/10.1016/S0370-1573(98)00082-9)
6. E.H. Lieb, J. Yngvason, The mathematical structure of the second law of thermodynamics. in *Current Developments in Mathematics* (2001), pp. 89–129. <https://doi.org/10.4310/CDM.2001.v2001.n1.a3>
7. E.H. Lieb, J. Yngvason, The entropy concept for non-equilibrium states. *Proc. R. Soc. Math. Phys. Eng. Sci.* **469**(2158), 20130408 (2013). <https://doi.org/10.1098/rspa.2013.0408>
8. E.H. Lieb, J. Yngvason, Entropy meters and the entropy of non-extensive systems. *Proc. R. Soc. Math. Phys. Eng. Sci.* **470**(2167), 20140192 (2014). <https://doi.org/10.1098/rspa.2014.0192>
9. A. Thess, *The Entropy Principle* (Springer, Berlin Heidelberg, 2011). <https://doi.org/10.1007/978-3-642-13349-7>
10. C. Carathéodory, Untersuchungen über die Grundlagen der Thermodynamik. *Math. Ann.* **67**(3), 355–386 (1909). <https://doi.org/10.1007/BF01450409>
11. R. Giles, *Mathematical Foundations of Thermodynamics* (Elsevier, Amsterdam, 1964)
12. E.P. Gyftopoulos, G.P. Beretta, *Thermodynamics: Foundations and Applications* (Macmillian, New York, 1991)
13. G.P. Beretta, E. Zanchini, Rigorous and general definition of thermodynamic entropy. in *Thermodynamics*, ed. by M. Tadashi, Chapter 2, InTech (2011), pp. 23–50. <https://doi.org/10.5772/13371>
14. E. Zanchini, G.P. Beretta, Recent progress in the definition of thermodynamic entropy. *Entropy* **16**(3), 1547–1570 (2014). <https://doi.org/10.3390/e16031547>
15. G.N. Hatsopoulos, E.P. Gyftopoulos, A unified quantum theory of mechanics and thermodynamics. Part i. Postulates. *Found. Phys.* **6**(1), 15–31 (1976). <https://doi.org/10.1007/BF00708660>
16. G.N. Hatsopoulos, E.P. Gyftopoulos, A unified quantum theory of mechanics and thermodynamics. Part iiia. Available energy. *Found. Phys.* **6**(2), 127–141 (1976). <https://doi.org/10.1007/BF00708955>
17. G.N. Hatsopoulos, E.P. Gyftopoulos, A unified quantum theory of mechanics and thermodynamics. Part iib. Stable equilibrium states. *Found. Phys.* **6**(4), 439–455 (1976). <https://doi.org/10.1007/BF00715033>
18. G.N. Hatsopoulos, E.P. Gyftopoulos, A unified quantum theory of mechanics and thermodynamics. Part iii. Irreducible quantal dispersions. *Found. Phys.* **6**(5), 561–570 (1976). <https://doi.org/10.1007/BF00715108>
19. L. del Rio, Resource theories of knowledge, Ph.D. thesis, ETH Zürich, 2015. <https://doi.org/10.3929/ethz-a-010553983>
20. L.P. Krämer Gabriel, Restricted agents in thermodynamics and quantum information theory, Ph.D. thesis, ETH Zürich, 2016. <https://doi.org/10.3929/ethz-a-010858172>
21. A. Hulse, B. Schumacher, M. Westmoreland, Axiomatic information thermodynamics. *Entropy* **20**(4), 237 (2018). <https://doi.org/10.3390/e20040237>
22. P. Kammerlander, R. Renner, The zeroth law of thermodynamics is redundant (2018). E-print [arXiv:1804.09726](https://arxiv.org/abs/1804.09726)
23. T. Fritz, Resource convertibility and ordered commutative monoids. *Math. Struct. Comp. Sci.* **27**(6), 850–938 (2017). <https://doi.org/10.1017/S0960129515000444>
24. M. Weilenmann, L. Kraemer, P. Faist, R. Renner, Axiomatic relation between thermodynamic and information-theoretic entropies. *Phys. Rev. Lett.* **117**, 260601 (2016). <https://doi.org/10.1103/PhysRevLett.117.260601>
25. Á.M. Alhambra, J. Oppenheim, C. Perry, Fluctuating states: what is the probability of a thermodynamical transition? *Phys. Rev. X* **6**(4), 041016 (2016). <https://doi.org/10.1103/PhysRevX.6.041016>
26. J. Gemmer, M. Michel, Thermalization of quantum systems by finite baths. *Europhys. Lett.* **73**(1), 1 (2006). <https://doi.org/10.1209/epl/i2005-10363-0>
27. C. Sparaciari, J. Oppenheim, T. Fritz, Resource theory for work and heat. *Phys. Rev. A* **96**, 052112 (2017). <https://doi.org/10.1103/PhysRevA.96.052112>

28. R. van der Meer, N.H.Y. Ng, S. Wehner, Smoothed generalized free energies for thermodynamics (2017). E-print. <https://doi.org/10.1103/PhysRevA.96.062135>
29. M. Horodecki, J. Oppenheim, C. Sparaciari, Approximate majorization (2017). E-print. <https://doi.org/10.1088/1751-8121/aac87c>
30. E.P. Hanson, N. Datta, Maximum and minimum entropy states yielding local continuity bounds. *J. Math. Phys.* **59**(4), 042204 (2018). <https://doi.org/10.1063/1.5000120>
31. E.P. Hanson, N. Datta, Tight uniform continuity bound for a family of entropies (2017). E-print [arXiv:1707.04249](https://arxiv.org/abs/1707.04249)
32. M. Weilenmann, Quantum causal structure and quantum thermodynamics, Ph.D. thesis, University of York, 2017. Available at <http://etheses.whiterose.ac.uk/19454/>
33. F. Dupuis, L. Kraemer, P. Faist, J.M. Renes, R. Renner, Generalized entropies, in *XVIIth International Congress on Mathematical Physics* (2013), pp. 134–153. [https://doi.org/10.1142/9789814449243\\_0008](https://doi.org/10.1142/9789814449243_0008)
34. J. Åberg, Catalytic coherence. *Phys. Rev. Lett.* **113**(15), 150402 (2014). <https://doi.org/10.1103/PhysRevLett.113.150402>
35. A.E. Allahverdyan, R. Balian, T.M. Nieuwenhuizen, Maximal work extraction from finite quantum systems. *Europhys. Lett.* **67**(4), 565 (2004). <https://doi.org/10.1209/epl/i2004-10101-2>
36. M. Horodecki, P. Horodecki, J. Oppenheim, Reversible transformations from pure to mixed states and the unique measure of information. *Phys. Rev. A* **67**(6), 062104 (2003). <https://doi.org/10.1103/PhysRevA.67.062104>
37. M. Horodecki, K. Horodecki, P. Horodecki, R. Horodecki, J. Oppenheim, A. Sen De, U. Sen, Local information as a resource in distributed quantum systems. *Phys. Rev. Lett.* **90**(10), 100402 (2003). <https://doi.org/10.1103/PhysRevLett.90.100402>
38. G. Gour, M.P. Müller, V. Narasimhachar, R.W. Spekkens, N. Yunger Halpern, The resource theory of informational nonequilibrium in thermodynamics. *Phys. Rep.* **583**, 1–58 (2015). <https://doi.org/10.1016/j.physrep.2015.04.003>
39. R. Renner, S. Wolf, Simple and tight bounds for information reconciliation and privacy amplification, in *Advances in Cryptology - ASIACRYPT 2005* (Springer, Berlin, 2005), pp. 199–216. [https://doi.org/10.1007/11593447\\_11](https://doi.org/10.1007/11593447_11)
40. R. König, R. Renner, C. Schaffner, The operational meaning of min- and max-entropy. *IEEE Trans. Inf. Theory* **55**(9), 4337–4347 (2009). <https://doi.org/10.1109/TIT.2009.2025545>
41. E.T. Jaynes, Information theory and statistical mechanics. *Phys. Rev.* **106**(4), 620–630 (1957). <https://doi.org/10.1103/PhysRev.106.620>
42. E.T. Jaynes, Information theory and statistical mechanics ii. *Phys. Rev.* **108**, 171–190 (1957). <https://doi.org/10.1103/PhysRev.108.171>
43. L. Kraemer, L. del Rio, Currencies in resource theories (2016). E-print [arXiv:1605.01064](https://arxiv.org/abs/1605.01064)
44. M. Tomamichel, *Modeling quantum information, in Quantum Information Processing with Finite Resources* (Springer, Berlin, 2016), pp. 11–32. <https://doi.org/10.1007/978-3-319-21891-5>
45. C.H. Bennett, The thermodynamics of computation—a review. *Int. J. Theor. Phys.* **21**(12), 905–940 (1982). <https://doi.org/10.1007/BF02084158>
46. W. van Dam, P. Hayden, Universal entanglement transformations without communication. *Phys. Rev. A* **67**(6), 060302 (2003). <https://doi.org/10.1103/PhysRevA.67.060302>
47. N.H.Y. Ng, L. Mančinska, C. Cirtoiu, J. Eisert, S. Wehner, Limits to catalysis in quantum thermodynamics. *N. J. Phys.* **17**(8), 085004 (2015). <https://doi.org/10.1088/1367-2630/17/8/085004>
48. F.G.S.L. Brandão, G. Gour, Reversible framework for quantum resource theories. *Phys. Rev. Lett.* **115**(7), 070503 (2015). <https://doi.org/10.1103/PhysRevLett.115.070503>
49. M. Tomamichel, R. Colbeck, R. Renner, A fully quantum asymptotic equipartition property. *IEEE Trans. Inf. Theory* **55**(12), 5840–5847 (2009). <https://doi.org/10.1109/TIT.2009.2032797>
50. G. Gour, I. Marvian, R.W. Spekkens, Measuring the quality of a quantum reference frame: the relative entropy of frameness. *Phys. Rev. A* **80**(1), 012307 (2009). <https://doi.org/10.1103/PhysRevA.80.012307>
51. L. del Rio, J. Åberg, R. Renner, O. Dahlsten, V. Vedral, The thermodynamic meaning of negative entropy. *Nature* **474**(7349), 61–63 (2011). <https://doi.org/10.1038/nature10123>

# Chapter 33

## Thermodynamics from Information



Manabendra Nath Bera, Andreas Winter and Maciej Lewenstein

### 33.1 Introduction

Thermodynamics, being one of the most basic foundations of modern science, not only plays an important role in modern technologies, but also provides basic understanding of the vast range of natural phenomena. Initially, it was phenomenologically developed to address the issues related to heat engines, i.e., the question on how, and to what extent, heat could be converted into work. But, with the developments of statistical mechanics, relativity and quantum mechanics, thermodynamics has attained quite a formal and mathematically rigorous form [1] along with its fundamental laws. It plays important roles in understanding relativistic phenomena in astrophysics and cosmology, in microscopic systems with quantum effects, or in complex systems in biology and chemistry.

The inter-relation between information and thermodynamics [2] has been studied in the context of Maxwell's demon [3–6], Szilard's engine [7], and Landauer's principle [8–12]. The classical and quantum information theoretic approaches help us to explain thermodynamics for small systems [13–15]. Recently, information theory has played an important role to explore thermodynamics with inter-system and system-bath correlations [16–18], equilibration processes [19–22], and foundational aspects

---

M. N. Bera (✉) · M. Lewenstein

ICFO – Institut de Ciències Fotoniques, The Barcelona Institute of Science and Technology,  
08860 Castelldefels, Spain  
e-mail: mnbera@gmail.com

M. N. Bera

Max-Planck-Institut für Quantenoptik, 85748 Garching, Germany

A. Winter

Departament de Física: Grup d'Informació Quàntica, Universitat Autònoma de Barcelona,  
08193 Bellaterra, Barcelona, Spain

A. Winter · M. Lewenstein

ICREA, Pg. Lluis Companys 23, 08010 Barcelona, Spain

of statistical mechanics [23] in quantum mechanics. Inspired by information theory, a resource theoretic framework for thermodynamics [24] has been developed, which can reproduce standard thermodynamics in the asymptotic (or thermodynamic) limit. For small systems or in the finite copy limit (also known as one-shot limit), it reveals that the laws of thermodynamics require modifications to dictate the transformations on the quantum level [25–33].

In the following, we make an axiomatic construction of thermodynamics by elaborating on the inter-relations between information and thermodynamics, and identify the “information conservation”, measured by the von Neumann entropy, as the crucial underlying property for that. This has been formulated recently in [34]. We introduce the notion of *bound energy*, which is the amount of energy locked in a system that cannot be accessed (extracted) given a set of allowed operations. We recover standard thermodynamics as a spacial case, by assuming (i) global *entropy preserving (EP) operations* as the set of allowed operations and (ii) infinitely large thermal baths initially uncorrelated from the system.

All fundamental physical theories share a common property, that is information conservation. It implies that the underlying dynamics deterministically and bijectively map the set of possible configurations of a system between any two instants of time. A non-deterministic feature, in a classical world, appears due to ignorance of some degree of freedoms, leading to an apparent information loss. In contrast, this loss of information could be intrinsic in quantum mechanics, and occurs in measurement processes and in presence of non-local correlations [35]. The set of entropy preserving operations is larger than the set of unitary operations in the sense that they conserve entropy (coarse-grained information) but not the probabilities (fine-grained information). This is why we refer *coarse-grained* information conservation. Both coarse-grained and fine-grained information conservation become equivalent (see Sect. 33.2) in the asymptotic limit. Note that unitaries are the only linear operations that are entropy preserving for all states [36]. Except few specific example, To what extent a general coarse-grained information conserving operations can be implemented in the single-copy limit is yet to be understood.

Note that an alternative approach to tackle thermodynamics for finite quantum systems relies fluctuation theorems. The second law is obtained there as a consequence of reversible transformations on initially thermal states or states with a well defined temperature [37–39]. In contrast, the aim of our work is instead to generalize thermodynamics, that is valid for arbitrary environments, irrespective of being thermal, or considerably larger than the system. This is illustrated in the table below. Our formalism, which treats systems and environments on equal footing, results in a “temperature”-independent formulation of thermodynamics.

	<b>Unitaries (fine-grained IC*)</b>	<b>EP operations (coarse-grained IC)</b>
<b>Large thermal bath</b>	Resource theory of Thermo-dynamics	Standard Thermodynamics
<b>Arbitrary environment</b>	?	Our formalism

\*IC: Information Conservation

This “temperature”-independent thermodynamics is essential in contexts where the environment and the system are comparable in size, or the environment simply not being thermal. In the real experimental situations, environments are not necessarily thermal, but can even possess quantum properties, like coherence or correlations.

The entropy preserving operations allow us to represent all the states and thermodynamic processes in a simple energy-entropy diagram. It shows that all the states with equal energies and entropies thermodynamically equivalent. We give a diagrammatic representation for heat, work and other thermodynamic quantities, and exploit a geometric approach to understand their transformation under thermodynamics processes. This could enable us to reproduce several results in the literature, for example resource theory of work and heat in [40], and also to extend thermodynamics involving multiple conserved quantities [34] in terms of generalized Gibbs ensembles.

### 33.2 Entropy Preserving Operations, Entropic Equivalence Class and Intrinsic Temperature

We consider *entropy preserving (EP) operations* that arbitrarily change an initial state  $\rho$  without changing its entropy

$$\rho \rightarrow \sigma \quad : \quad S(\rho) = S(\sigma),$$

where  $S(\rho) := -\text{Tr}(\rho \log \rho)$  is the von Neumann entropy. Sometime we denote these operations as *iso-informatic* operations as well. Note, in general, these operations are not linear operations, i.e., an operation that acts on  $\rho$  and produces a state with the same entropy, not necessarily preserves entropy when acting on other states. As was shown in Ref. [36], a quantum channel  $\Lambda(\cdot)$  that preserves entropy as well as linearity, i.e.  $\Lambda(p\rho_1 + (1-p)\rho_2) = p\Lambda(\rho_1) + (1-p)\Lambda(\rho_2)$ , has to be unitary.

Given any two states  $\rho$  and  $\sigma$  with  $S(\rho) = S(\sigma)$ , and an ancillary system  $\eta$  of  $O(\sqrt{n \log n})$  qubits, there exists a global unitary  $U$  such that [40]

$$\lim_{n \rightarrow \infty} \|\text{Tr}_{\text{anc}}(U\rho^{\otimes n} \otimes \eta U^\dagger) - \sigma^{\otimes n}\|_1 = 0, \quad (33.1)$$

where the partial trace is performed on the ancillary system and  $\|\cdot\|_1$  is the one-norm. The reverse statement is also true, i.e. if two states respect Eq. (33.1), then they also have equal entropies.

For thermodynamics, it is important to restrict entropy preserving operations that are also be energy preserving. These operations can also be implemented. In Theorem 1 of Ref. [40], it is shown that if two states  $\rho$  and  $\sigma$  have equal entropies and energies, i.e. ( $S(\rho) = S(\sigma)$  and  $E(\rho) = E(\sigma)$ ), then there exists energy preserving  $U$  and an additional ancillary system  $A$  in some state  $\eta$  with  $O(\sqrt{n \log n})$  of qubits and Hamiltonian  $\|H_A\| \leq O(n^{2/3})$ , for which (33.1) is fulfilled. Note, in the large  $n$  limit, the amount of energy and entropy of the ancillary system per copy vanishes.

Let us introduce different equivalence classes of states, depending on their entropy, by which we establish a hierarchy of states depending on their information content.

**Definition 1** (*Entropic equivalence class*) For any quantum system of dimension  $d$ , two states  $\rho$  and  $\sigma$  are equivalent and belong to the same entropic equivalence class if and only if both have the same Von Neumann entropy,

$$\rho \sim \sigma \quad \text{iff} \quad S(\rho) = S(\sigma).$$

Assuming some fixed Hamiltonian  $H$ , the representative element of every class is the state that *minimizes* the energy within it, i.e.,

$$\gamma(\rho) := \arg \min_{\sigma : S(\sigma)=S(\rho)} E(\sigma),$$

where  $E(\sigma) := \text{Tr}(H\sigma)$  is the energy of the state  $\sigma$ .

Complementary to the maximum-entropy principle [41, 42], that identifies the thermal state as the state that maximizes the entropy for a given energy, one can show that, the thermal state also minimizes the energy for a given entropy. We refer to this latter property as *min-energy principle* [16, 43, 44], which identifies thermal states as the representative elements of every class as

$$\gamma(\rho) = \frac{e^{-\beta(\rho)H}}{\text{Tr}(e^{-\beta(\rho)H})}. \quad (33.2)$$

The  $\beta(\rho)$  is inverse temperature and labels the equivalence class, to which the state  $\rho$  belongs. This  $\beta(\rho)$  is denoted as the “intrinsic” inverse temperature associated to  $\rho$ . The state  $\gamma(\rho)$  is, also, referred to as the completely passive (CP) state [16] with the minimum internal energy, but with the same information content. These CP states, with the form  $\gamma(H_S, \beta_S)$ , has several interesting properties [43, 44]: (P1) It minimizes the energy, for a given entropy. (P2) With the decrease (increase) in  $\beta_S$ , both energy and entropy monotonically increase (decrease), and vice versa. (P3) For non-interacting Hamiltonians,  $H_T = \sum_{X=1}^N I^{\otimes X-1} \otimes H_X \otimes I^{\otimes N-X}$ , the joint complete passive state is tensor product of individual ones, i.e,  $\gamma(H_T, \beta_T) = \otimes_{X=1}^N \gamma(H_X, \beta_T)$ , with identical  $\beta_T$  [43, 44].

### 33.3 Bound and Free Energies: Energy-Entropy Diagram

Here we identify two relevant forms of internal energy: the free and the bound energy. Indeed, the notions depend on the set of allowed operations. While the latter is defined as the amount of internal energy that is accessible in the form of work. For entropy preserving operations, in which the entropic classes and CP states arise, it is quantified as in the following.

**Definition 2** (*Bound energy* [34]) The bound energy for a state  $\rho$  with the system Hamiltonian  $H$  is

$$B(\rho) := \min_{\sigma : S(\sigma)=S(\rho)} E(\sigma) = E(\gamma(\rho)), \quad (33.3)$$

where  $\gamma(\rho)$  is the state with minimum energy (CP), within the equivalence class of  $\rho$ .

As guaranteed by the min-energy principle,  $B(\rho)$  is the amount of energy that cannot be extracted further by performing any entropy preserving operations. Amount of bound energy is strongly related to the information content in the state. Only by allowing an outflow of information from the system, one could have access to this energy (in the form of work).

On other hand, the free energy is the accessible part of the internal energy:

**Definition 3** (*Free energy*) The free energy stored in a system  $\rho$ , with system Hamiltonian  $H_S$ , is given by

$$F(\rho) := E(\rho) - B(\rho), \quad (33.4)$$

where  $B(\rho)$  is the bound energy in  $\rho$ .

Note, the free energy does not rely on a predefined temperature, in contrast to the standard out of equilibrium Helmholtz free energy  $F_T(\rho) := E(\rho) - T S(\rho)$ , where  $T$  is the temperature of a thermal bath. The situation in which the free energy in Eq. (33.4) becomes equal to the accessible Helmholtz free energy is considered in Lemma 11. Nevertheless, with intrinsic temperature  $T(\rho) := \beta(\rho)^{-1}$  that labels the equivalence class that contains  $\rho$ , our definition of free energy identifies with the out of equilibrium free energy as

$$F(\rho) = F_{T(\rho)}(\rho) - F_{T(\rho)}(\gamma(\rho)).$$

Let us mention that, in the rest of the manuscript, we use  $F_\beta(\rho) := E(\rho) - \beta^{-1} S(\rho)$  to denote the standard out of equilibrium free energy, wherever we find it more convenient.

Beyond single systems, the notions of bound and free energy can be extended to multi-particle (multipartite) systems, where these quantities exhibit several interesting properties. They even can capture the presence of inter-party correlations. For bipartite system, the list of properties is given below.

**Lemma 4** ([34]) For a bipartite system, with non-interacting Hamiltonian  $H_A \otimes \mathbb{I} + \mathbb{I} \otimes H_B$ , in an arbitrary state  $\rho_{AB}$  and a product state  $\rho_A \otimes \rho_B$  with marginals  $\rho_{A/B} := \text{Tr}_{B/A}(\rho_{AB})$ , the bound and the free energy satisfy the following:

(P4) *Bound energy and correlations:*

$$B(\rho_{AB}) \leq B(\rho_A \otimes \rho_B). \quad (33.5)$$

(P5) *Bound energy of composite systems:*

$$B(\rho_A \otimes \rho_B) \leq B(\rho_A) + B(\rho_B). \quad (33.6)$$

(P6) *Free energy and correlations:*

$$F(\rho_A \otimes \rho_B) \leq F(\rho_{AB}). \quad (33.7)$$

(P7) *Free energy of composite systems:*

$$F(\rho_A) + F(\rho_B) \leq F(\rho_A \otimes \rho_B). \quad (33.8)$$

*Equations (33.5) and (33.7) are saturated if and only if A and B are uncorrelated  $\rho_{AB} = \rho_A \otimes \rho_B$ , and Eqs. (33.6) and (33.8) are saturated if and only if  $\beta(\rho_A) = \beta(\rho_B)$ .*

These properties give an additional operational meaning to the free energy  $F(\rho)$ . For a system in a state  $\rho$  and infinitely large bath at inverse temperature  $\beta$ , the extractable work under global entropy preserving operations is given by

$$W = F_\beta(\rho) - F_\beta(\gamma(\beta)), \quad (33.9)$$

where the standard free energy is  $F_\beta(\rho) = E(\rho) - \beta^{-1}S(\rho)$  and  $\gamma(\beta)$  is the thermal state with the inverse temperature  $\beta$ , which is the resultant state once the work has been extracted.

**Lemma 5** (Free energy versus  $\beta$ -free energy [34]) *The free energy  $F(\rho)$  is the one that corresponds to work extracted by attaching a bath at the worst possible temperature,*

$$F(\rho) = \min_{\beta} (F_\beta(\rho) - F_\beta(\gamma(\beta))).$$

*The minimization is achieved when inverse temperature becomes identical to the inverse intrinsic temperature  $\beta(\rho)$ .*

*Energy-entropy diagrams* are very useful in thermodynamics, where every point in the diagram is represented by energy and entropy. As shown in Fig. 33.1, a state  $\rho$  of a system with Hamiltonian  $H$  is represented by a point with coordinates  $x_\rho := (E(\rho), S(\rho))$ . All physical states are bounded in a region made of the horizontal axis (i.e.,  $S = 0$ , corresponding to the pure states) and the convex curve  $(E(\beta), S(\beta))$  correspond to the thermal states of both positive and negative temperatures which is denoted as the thermal boundary. The slope of the tangent line associated to a point on the thermal boundary is given by the inverse temperature, since  $\frac{dS(\beta)}{dE(\beta)} = \beta$ .

In general a point in the energy-entropy diagram could correspond to multiple states, as different quantum states can have identical entropy and energy. This conversely shows that the energy-entropy diagram establishes a link between the microscopic and the macroscopic thermodynamics, i.e. in the asymptotic limit all the

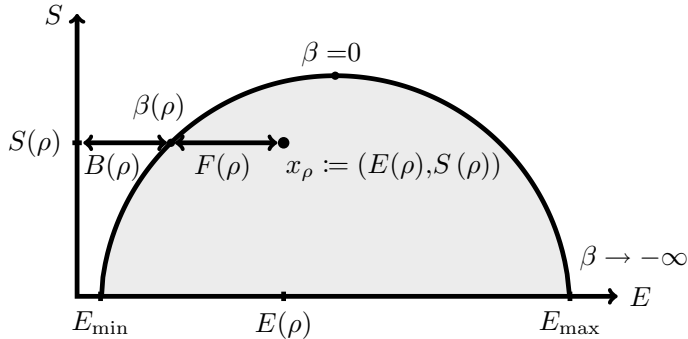


**Fig. 33.1** Energy-entropy diagram. Any quantum state  $\rho$  is represented in the diagram as a point with coordinates  $x_\rho := (E(\rho), S(\rho))$ . Note, since we consider average energy and coarse-grained entropy as the coordinates, a single point in this diagram represents not one but many quantum states. The free energy  $F(\rho)$ , of the state  $\rho$ , can be seen from the diagram as the horizontal distance from the thermal boundary. This is, in fact, the part of internal energy which is accessible without altering system's entropy. The bound energy  $B(\rho)$  is the horizontal distance between the thermal boundary and the energy reference. Contrary to the free energy, it cannot be extracted by means of entropy preserving operations. The slope of the tangent line on a point in the thermal boundary represents the intrinsic temperature,  $\beta(\rho)$ , of the state  $\rho$ .

thermodynamic quantities only rely on the energy and entropy per particle [40]. In fact, all the states with equal entropy and energy are thermodynamically equivalent in the sense that they can be inter-converted into each other in the limit of many copies  $n \rightarrow \infty$ , using energy conserving unitary operations with an ancilla of sub-linear size  $O(\sqrt{n \log n})$  and a Hamiltonian upper bounded by sub-linear bound  $O(n^{2/3})$  [40].

## 33.4 Temperature Independent Formulation of Thermodynamics

### 33.4.1 Equilibrium and Zeroth Law

In thermodynamics, the zeroth law establishes the absolute scaling of temperature and the notion of thermal equilibrium. It states that if systems  $A$  and  $B$  are in mutual thermal equilibrium,  $B$  and  $C$  are also in mutual thermal equilibrium, then  $A$  will also be in thermal equilibrium with  $C$ . All these systems, in mutual thermal equilibrium, are classified to thermodynamically equivalent class where each state in the class is assigned with a unique parameter called temperature and there is no spontaneous energy exchange in between them. When a non-thermal state is brought in contact with a large thermal bath, the system may exchange energy and entropy to acquire a thermally equilibrium state with the temperature of the bath. This is also known

as equilibration process, during which the system could exchange both energy and entropy with bath such that it minimizes its Helmholtz free energy.

However, such an equilibration process would be very different when the system cannot have access to a considerably large thermal bath or in absence of a thermal bath. A formal definition of equilibration, in that case, based on information preservation and intrinsic temperature can be given as in the following.

**Definition 6** (*Equilibrium and zeroth law* [34]) Given a collection of systems  $A_1, \dots, A_n$  with non-interacting Hamiltonians  $H_1, \dots, H_n$  in a joint state,  $\rho_{A_1 \dots A_n}$ , we call them to be mutually at equilibrium if and only if

$$F(\rho_{A_1 \dots A_n}) = 0,$$

i.e. they “jointly” minimize the free energy as defined in (33.4).

Two states  $\rho_A$  and  $\rho_B$ , with corresponding Hamiltonians  $H_A$  and  $H_B$ , achieve mutual equilibrium when they jointly attain an iso-informatic (i.e. iso-entropic) state with minimum possible energy. The resultant equilibrium state is indeed a completely passive (CP) state  $\gamma(H_{AB}, \beta_{AB})$  with the joint (non-interacting) Hamiltonian  $H_{AB} = H_A \otimes \mathbb{I} + \mathbb{I} \otimes H_B$ , it is

$$\gamma(H_{AB}, \beta_{AB}) = \gamma(H_A, \beta_{AB}) \otimes \gamma(H_B, \beta_{AB}), \quad (33.10)$$

where the local systems are also in completely passive states with the same  $\beta_{AB}$ . This follows from the property (P3). Note, we denote  $\gamma(H_X, \beta_Y) = e^{-\beta_Y H_X} / \text{Tr}(e^{-\beta_Y H_X})$ . As a corollary, it can be seen that if two CP states  $\gamma(H_A, \beta_A)$  and  $\gamma(H_B, \beta_B)$  are with  $\beta_A \neq \beta_B$ , then they can, still, jointly reduce bound-energy without altering the total information content and acquire their mutual equilibrium state  $\gamma(H_{AB}, \beta_{AB})$ . From the property (P5), this implies a unique  $\beta_{AB}$ , i.e.,

$$E(\gamma(H_A, \beta_A)) + E(\gamma(H_B, \beta_B)) > E(\gamma(H_{AB}, \beta_{AB})). \quad (33.11)$$

Moreover for  $\beta_A \geq \beta_B$ , the equilibrium temperature  $\beta_{AB}$  is bounded. This is expressed in Lemma 7 below and has been proven in [34].

**Lemma 7** ([34]) *Iso-informatic equilibration process between  $\gamma(H_A, \beta_A)$  and  $\gamma(H_B, \beta_B)$ , with  $\beta_A \geq \beta_B$ , results in a mutually equilibrium joint state  $\gamma(H_{AB}, \beta_{AB})$ , where  $\beta_{AB}$  satisfies*

$$\beta_A \geq \beta_{AB} \geq \beta_B,$$

*irrespective of non-interacting systems' Hamiltonians.*

Now with the notion of equilibration and equilibrium state as the global CP state, we could recast the *zeroth law*, in terms of intrinsic temperature. A global CP state assures that the individual states are not only CP states with vanishing inter-system

correlations but also they share identical intrinsic temperature, i.e.,  $\beta$ . In reverse, individual systems are in mutual equilibrium as long as they are locally in a CP state and share the same intrinsic temperature.

The traditional notion of thermal equilibrium, as well as, the zeroth law can also be recovered using the argument above. In traditional sense, the thermal baths are reasonably large, in comparison to the systems under consideration, with a predefined temperature. For a bath Hamiltonian  $H_B$ , a bath can be expressed as  $\gamma_B = e^{-\beta_B H_B} / \text{Tr}(e^{-\beta_B H_B})$ , where  $\beta_B$  is the inverse temperature and  $|\gamma_B| \rightarrow \infty$ . Note it is also a CP state. When a finite system in a state  $\rho_S$  (with  $|\rho_S| \ll |\gamma_B|$ ) with Hamiltonian  $H_S$  is brought in contact with a thermal bath, the global state, after reaching mutual thermal equilibrium, will be a CP state, i.e.,  $\gamma_B \otimes \rho_S \xrightarrow{\Lambda^{ep}} \gamma'_B \otimes \gamma_S$ , with a global inverse temperature  $\beta_e$ . It can be easily seen that  $\gamma'_B \rightarrow \gamma_B$ ,  $\beta_e \rightarrow \beta_B$  and  $\gamma_S \rightarrow e^{-\beta_B H_S} / \text{Tr}(e^{-\beta_B H_S})$ , in the limit  $|\gamma_B| \gg |\rho_S|$  and  $|\gamma_B| \rightarrow \infty$ .

### 33.4.2 Work, Heat and the First Law

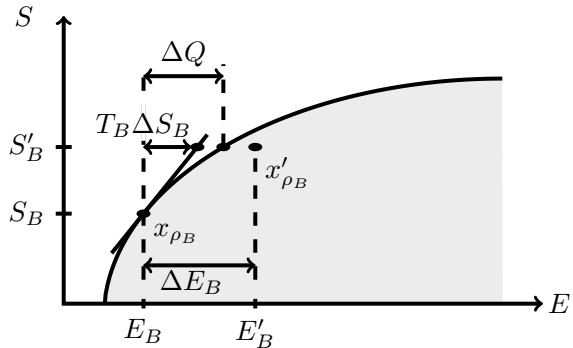
In thermodynamics, the conservation of energy is assured by the first law by taking into account the distribution of energy over work and heat, that are the two forms of energy transfer.

Consider a thermodynamic process that involves a system  $A$  and a bath  $B$  and a transformation  $\rho_{AB} \rightarrow \rho'_{AB}$  that respect conservation of the global entropy  $S(\rho_{AB}) = S(\rho'_{AB})$ . Traditionally, a bath is by definition assumed to be initially thermal and fully uncorrelated from the system. Then the heat dissipation is usually quantified as the internal energy change in the bath, i.e.  $\Delta Q = E(\rho'_B) - E(\rho_B)$  where the reduced state of the bath is  $\rho_B^{(0)} = \text{Tr}_A \rho_{AB}^{(0)}$ . This definition, however, has been shown to have limitations. A consistent definition has been discussed recently in [18] based on information theoretic approach. It has been suggested that heat has to be quantified as  $\Delta Q = T_B \Delta S_B$ , where  $T_B$  being the temperature and  $\Delta S_B = S(\rho'_B) - S(\rho_B)$  is the von Neumann entropy change in the bath. This definition can further be generalized to the situation where the system and bath are correlated, where  $\Delta S_B = -\Delta S(A|B)$  is also the conditional entropy change in system  $A$ , conditioned on the bath  $B$ , defined as  $S(A|B) = S(\rho_{AB}) - S(\rho_B)$ . Thus, in the presence of correlations, heat flow can be understood as the energy exchange due to information flow from the system to the bath.

However this definition will not be meaningful if the environment is athermal or not in the state of the Boltzmann-Gibbs form. For arbitrary environments, an alternative, and meaningful, quantification of heat exchange can still be given in terms of the change in bound energies.

**Definition 8 (Heat)** For a system  $A$  and environment  $B$ , the dissipated heat by the system  $A$  in the process  $\rho_{AB} \xrightarrow{\Lambda^{ep}} \rho'_{AB}$  is the change in bound energy of the environment  $B$ , i.e.

**Fig. 33.2** The different notions of heat can be understood using the energy-entropy diagram. They are **1**  $\Delta Q$  as change of the bound energy of the bath, **2**  $\Delta E_B$  as the change in internal energy, and **3**  $T_B \Delta S_B$ . In this example, the bath is initially thermal but this is not necessary.



$$\Delta Q := B(\rho'_B) - B(\rho_B). \quad (33.12)$$

Here  $B(\rho_B^{(i)})$  is the initial (final) bound energy of the bath  $B$ .

Clearly heat is a process dependent quantity. There might be many different processes, that transform the same initial to the same final marginal state for  $A$ , but with different marginal states for  $B$ . Since the global process is entropy preserving, for same marginal states for  $A$ , the global process could lead to different entropy change for  $B$  and also to a different amount of correlations between  $A$  and  $B$ , which is measured by the mutual information  $I(A : B) := S_A + S_B - S_{AB}$ . Note  $\Delta S_A + \Delta S_B = \Delta I(A : B)$ .

As special cases, this quantification of heat can give rise to other existing definitions [34]. In particular, for an initial thermal environment  $\rho_B = e^{-H_B/T} / \text{Tr}(e^{-H_B/T})$  with Hamiltonian  $H_B$  at temperature  $T$ , then the exchanged heat is upper and lower bounded by

$$T \Delta S_B \leq \Delta Q \leq \Delta E_B. \quad (33.13)$$

These three quantities have been schematically represented in the energy-entropy diagram in Fig. 33.2. The three definitions become equivalent in the limit of large thermal baths, as in that case, a small perturbation of the bath  $\rho'_B = \rho_B + \delta\rho_B$  leads to

$$T \Delta S_B + O(\delta\rho_B^2) = \Delta Q = \Delta E_B - O(\delta\rho_B^2), \quad (33.14)$$

and the second order contribution will vanish. With this consistent definition of heat, let us turn to define work.

**Definition 9 (Work)** For a system  $A$  and its environment  $B$ , and an arbitrary entropy preserving transformation  $\rho_{AB} \rightarrow \rho'_{AB}$ , with fixed non-interacting Hamiltonians  $H_A$  and  $H_B$ , the work performed on the system  $A$  is quantified as,

$$\Delta W_A := W - \Delta F_B$$

where the work cost implement the global transformation is  $W = \Delta E_A + \Delta E_B$  and  $\Delta F_B = F(\rho'_B) - F(\rho_B)$ .

Now equipped with the notions of heat and work, the first law takes the form of a mathematical identity.

**Lemma 10** (First law) *For a system A and its environment B with fixed non-interacting Hamiltonians  $H_A$  and  $H_B$ , and an arbitrary entropy preserving transformation  $\rho_{AB} \rightarrow \rho'_{AB}$ , the change in energy for system A is distributed as*

$$\Delta E_A = \Delta W_A - \Delta Q.$$

This can be deduced directly from the definitions of work and heat. Recall,  $-\Delta W_A$  is the amount of “pure” energy, i.e. work, and  $\Delta Q_A$  is the heat which is change in energy due to exchange of information with the system.

### 33.4.3 Second Law

The second law of thermodynamics can be expressed in several forms. These include an upper bound on the extracted work, or the impossibility of complete conversion of heat into work etc. Below we show how all existing formulations are a consequence of the principle of information conservation.

#### 33.4.3.1 Work Extraction

In thermodynamics, one of the main concerns is to convert heat into work, which is the “pure” form of energy and can be used for any application.

**Lemma 11** (Work extraction) *The extractable work from an arbitrary composite system  $\rho$ , by using entropy preserving process  $\rho \rightarrow \rho'$ , is upper-bounded by the free energy*

$$W \leq F(\rho),$$

where  $W = E(\rho) - E(\rho')$  and the equality is reached if and only if  $\rho' = \gamma(\rho)$ .

If the composite is a bipartite system with the form  $\rho = \rho_A \otimes \gamma_B(T_B)$ , where  $\gamma_B(T_B)$  is thermal at temperature  $T_B$ , then

$$W \leq F_{T_B}(\rho_A) - F_{T_B}(\gamma_A(T_B)) \tag{33.15}$$

where the standard out of equilibrium free energy is  $F_T(\cdot)$ . The equality is achieved in the limit of asymptotically large bath (or with infinite heat capacity).

The first part can be proven by seeing that  $E(\rho') \geq B(\rho')$  and therefore  $W = E(\rho) - E(\rho') \leq E(\rho) - B(\rho') = F(\rho)$ . Note, under iso-informative transformation,  $B(\rho') = B(\rho)$ . For bipartite composite case  $\rho = \rho_A \otimes \gamma_B(T_B)$ , we may write

$$\begin{aligned} F(\rho_A \otimes \gamma_B(T_B)) &= E(\rho_A) + E(\gamma_B(T_B)) \\ &\quad - (B(\gamma_A(T_{AB})) + B(\gamma_B(T_{AB}))) \end{aligned}$$

where  $T_{AB}$  is the intrinsic temperature of the composite  $\rho_A \otimes \gamma_B(T_B)$ . Recall that thermal states satisfy  $E(\gamma) = B(\gamma)$ . Now by reshuffling the terms, we recover the first law, i.e.

$$F(\rho_A \otimes \gamma_B(T_B)) = -\Delta E_A - \Delta Q_A$$

where we use  $\Delta E_A = E(\gamma_A(T_{AB})) - E(\rho_A)$  and  $\Delta Q_A = B(\gamma_B(T_{AB})) - B(\gamma_B(T_B))$ . Also we have  $\Delta Q \geq T_B \Delta S_B$  (see Eq.(33.13)). Since the whole process is entropy preserving and we restrict initial and final composite to be in product state forms, we have  $\Delta S_A = -\Delta S_B$ , and therefore,

$$F(\rho_A \otimes \gamma_B(T_B)) \leq -\Delta E_A - T_B \Delta S_B = -(\Delta E_A - T_B \Delta S_A) \quad (33.16)$$

which proves (33.15). Again, in the infinitely large bath limit, the final intrinsic temperature  $T_{AB}$  will become the bath temperature  $T_B$  and also  $\Delta Q = T_B \Delta S_B$ . Then the equality in Eq. (33.16) is achieved.

Now we turn to the question if heat can be converted into work. Traditionally, answer to this question leads to various other formulations of the second law in thermodynamics. They are the Clausius statement, Kelvin-Planck statement and Carnot statement, to mention a few. Indeed, similar question can be put forward in the framework considered here, in terms of bound energy, where one may not have access to large thermal bath. The analogous forms of second laws that consider this question both qualitatively and quantitatively, and they are outlined below.

### 33.4.3.2 Clausius Statement

Second law puts fundamental bound on extractable work, as well as dictates the direction of state transformations. Lets us first elaborate on the bounds on extractable work and thereby put forward the analogous versions of second law in this framework.

**Lemma 12** (Clausius statement) *For two systems A and B in an arbitrary states and with intrinsic temperatures  $T_A$  and  $T_B$  respectively, any iso-informatic process satisfy the inequality*

$$(T_B - T_A)\Delta S_A \geq \Delta F_A + \Delta F_B + T_B \Delta I(A : B) - W, \quad (33.17)$$

where the change in the free energy of the body A/B is  $\Delta F_{A/B}$  and  $\Delta I(A : B)$  is the change of mutual information before and after the process. The  $W = \Delta E_A + \Delta E_B$  is the amount of external work, which is performed on the global state. Note for initially uncorrelated state ( $I(A : B) = 0$ ), systems A and B are thermal ( $F_A = F_B = 0$ ), and no external work being performed ( $W = 0$ ), we have

$$(T_B - T_A)\Delta S_A \geq 0 \quad (33.18)$$

as a corollary. This implies that there exists no iso-informatic equilibration process whose **sole result is the transfer of heat from a cooler to a hotter body.**

The Clausius statement above can be proven as in the following. By definition, free and bound energies satisfy

$$W = \Delta F_A + \Delta F_B + \Delta Q_A + \Delta Q_B . \quad (33.19)$$

Recall, the heat is defines as the change of bound energy of the environment. Also, increase in bound energy implies increase in entropy, i.e.  $\text{sign}(\Delta B) = \text{sign}(\Delta S)$ . Now from Eq. (33.13) and with  $T_{A/B}$  as the initial intrinsic temperature of the systems A/B, we may write

$$\Delta Q_A + \Delta Q_B \geq T_B \Delta S_B + T_A \Delta S_A .$$

As a result of total entropy conservation, the change in mutual information is then  $\Delta I(A : B) = \Delta S_A + \Delta S_B$ . Now putting this in Eq. (33.19) gives raise to Eq. (33.17).

Note the standard Clausius statement (as in Eq. (33.18)) can be “apparently” violated, due to three reasons and that can be recovered from the general one in Eq. (33.17). Either the process not being spontaneous, which means external work is performed  $W > 0$ , or due to the presence initial free energy in the systems (i.e.  $F_A \neq 0$  or/and  $F_B \neq 0$ ) which is consumed during the process, or due to the presence of initial correlations, i.e.  $I(A : B) \neq 0$ , which could lead to  $\Delta I(A : B) < 0$  [18].

### 33.4.3.3 Kelvin–Planck Statement

While Clausius statement says that spontaneously heat cannot flow from a cooler to a hotter body, the Kelvin–Plank formulation of second law restricts it further stating that the heat flowing from a hotter to a colder body, cannot be transformed into work completely. A generalized form of that we present below.

**Lemma 13** (Kelvin–Planck statement) *For two systems A and B in arbitrary states, any iso-informatic process satisfies*

$$\Delta Q_B + \Delta Q_A = -(\Delta F_A + \Delta F_B) + W , \quad (33.20)$$

where  $\Delta F_{A/B}$  is the change in the free energy of the body A/B before and after the process,  $\Delta Q_{A/B}$  the heat exchanged by the body A/B. The  $W = \Delta E_A + \Delta E_B$  is the amount of external work invested, on the global state, to carry out the process.

For the case where the reduced states are thermal and the process is a work extracting one  $W < 0$ , then above equality reduces

$$\Delta Q_B + \Delta Q_A \leq W < 0 . \quad (33.21)$$

Further, in absence of initial correlations, Eq. (33.21) implies that there exists no iso-informatic process whose **sole** result is the absorption of bound energy (heat) from an equilibrium state and converting it into work completely.

The Eq. (33.20) is followed from the energy balance (33.19). The Eq. (33.21) is deduced from (33.20) by assuming reduced states that are initially in thermal states and therefore  $\Delta F_{A/B} \geq 0$ . The final statement is derived by noting that any entropy preserving process applied on initially uncorrelated systems fulfills  $\Delta S_A + \Delta S_B \geq 0$ , which together with (33.21) leads to  $\text{sign}(\Delta Q_A) = -\text{sign}(\Delta Q_B)$ .

### 33.4.3.4 Carnot Statement

Another version of second law is based on highest possible work conversion efficiency in an ideal heat engine, also known as Carnot statement.

Consider a heat engine consists of two heat baths  $A$  and  $B$ , with different temperatures  $T_A$  and  $T_B$  respectively. A working body  $S$  cyclically interacts with  $A$  and  $B$ . There is no restriction on how the working body interacts with the baths  $A$  and  $B$ , apart from the fact that the working body is left in its initial state and also uncorrelated with the bath(s) at the end of every cycle. This is to guarantee that the working body only absorbs heat from a bath and releases to the other one, without changing itself the end of the cycle.

Here, in contrast to standard situations, we go beyond the assumption that baths are infinitely large. Rather, we consider the possibility that a bath could be similar in size as the system, such that loss or gain of energy changes their (intrinsic) temperatures. Consider, two uncorrelated baths  $A$  and  $B$  at equilibrium with temperatures  $T_A$  and  $T_B$  respectively, and  $T_A < T_B$ , i.e.  $\rho_{AB} = \gamma_A \otimes \gamma_B$ . After one (or several complete) cycle(s) in the engine, the environments transformed to  $\rho_{AB} \rightarrow \rho'_{AB}$ .

The efficiency of work extraction in a heat engine, defined as the fraction of energy that is taken from the hot bath and then transformed into work, is expressed as

$$\eta := \frac{W}{-\Delta E_B}$$

where  $W$  is the amount of work extracted from the heat absorbed  $-\Delta E_B = E_B - E'_B > 0$  from the hot environment. Below, we go on to give upper bounds on the efficiency for any heat engine consist of arbitrary baths.

**Lemma 14** (Carnot statement) *For a heat engine working between two baths  $\gamma_A \otimes \gamma_B$  each of which in a local equilibrium state with intrinsic temperatures  $T_B > T_A$  and uncorrelated with each other, the bound on efficiency of work extraction is given by*

$$\eta \leq 1 - \frac{\Delta B_A}{-\Delta B_B}, \quad (33.22)$$

where the change in bound energies of the systems A and B are  $\Delta B_A$  and  $\Delta B_B$  respectively.

In the special case where baths are considerably large and engine operates under global entropy preserving operations, the Carnot efficiency is recovered,

$$\eta \leqslant 1 - \frac{T_A}{T_B}. \quad (33.23)$$

The statement above is respected for arbitrary baths, even for the ones with small sizes, and can be proven as follows. For a transformation  $\rho_{AB} \rightarrow \rho'_{AB}$ , the maximum extractable work is given by

$$W = F(\rho_{AB}) - F(\rho'_{AB}) = (-\Delta E_B) - \Delta E_A > 0.$$

Then the efficiency of conversion of heat into work becomes

$$\eta = 1 - \frac{\Delta E_A}{-\Delta E_B}.$$

If A being initially at equilibrium, then  $\Delta F_A \geqslant 0$  and  $\Delta E_A > \Delta B_A$ , which is also true for B. As a consequence,  $\eta \leqslant 1 - \frac{\Delta B_A}{-\Delta B_B}$ , which is Eq. (33.22). In the large bath limit i.e.  $\Delta B_A \ll B_A$ , bound energy change becomes  $\Delta B_A = T_A \Delta S_A$ . As a result,

$$\eta \leqslant 1 - \frac{T_A \Delta S_A}{-T_B \Delta S_B}. \quad (33.24)$$

For globally entropy preserving operations, the joint entropy remains unchanged, i.e.  $S'_{AB} = S_A + S_B$ , and  $\Delta S_A + \Delta S_B \geqslant 0$  or alternatively  $\Delta S_A \geqslant -\Delta S_B$ . Now this, together with (33.24), implies (33.23).

Note that efficiency, in (33.22), is derived with the consideration that the initial bath states are thermal. While the final states may or may not thermal after first cycle. The equality is achieved if the final states, after first cycle, are also thermal where temperature of the final states could be different form initial ones. If an engine cycle starts with non-thermal baths, the efficiency will be different from (33.22), which has been discussed in details in [34].

### 33.4.4 Third Law

In thermodynamics, the third law deals with the impossibility of attaining the absolute zero temperature. According to Nernst version, it states: “it is impossible to reduce the entropy of a system to its absolute-zero value in a finite number of operations”. Very recently, the third law of thermodynamics has been proven in Ref. [45], where it is shown to be a consequence of the unitarity character of the thermodynamic

transformations. For example, let us consider the transformation that cools (erases) system  $S$ , initially in a state  $\rho_S$ , in the presence of a bath  $B$

$$\rho_S \otimes \rho_B \rightarrow |0\rangle\langle 0| \otimes \rho'_B, \quad (33.25)$$

where  $\rho_B$  is a thermal state and  $\text{rank}(\rho_S) > 1$ . The dimension of the bath's Hilbert space,  $d_B$ , could be arbitrarily large but finite. Since bath  $\rho_B$ , by definition, is a full-rank state, the left hand side and the right hand side of Eq. (33.25) are of different ranks. Unitary operations preserve rank of states. Therefore the transformation cannot be carried out using a unitary operation, irrespective of work supply, where the system attains an absolute zero entropy state.

In access to infinitely large baths and a sufficient work supply, the zero entropy state can only be produced. However, if one assumes a locality structure for the bath's Hamiltonian, such a cooling (unitary) process would take an infinitely large amount time. In case of finite dimensional bath and a finite amount of resources (e.g. work, time), a quantitative bound on the achievable temperature can be given, as in [45].

Note that the framework considered here replies on set of entropy preserving operations and they are more powerful than unitaries. Clearly, transformation (33.25) is possible using entropy preserving operation, if

$$S(\rho_S) \leq \log d_B - S(\rho_B),$$

and an access to work  $W = F(|0\rangle\langle 0| \otimes \rho'_B) - F(\rho_S \otimes \rho_B)$  to implement the operation. Since entropy preserving operations can be implemented by using a global unitaries acting on infinitely many copies (see Sect. 33.2), the absolute zero entropy state can be achieved by means of entropy preserving operations. This is in agreement with [45], in the cases of infinitely large baths and unitary operations.

In conclusion, the third law of thermodynamics can be understood as a consequence of the microscopic reversibility (unitarity) of the transformation and is not necessarily respected by general entropy preserving operations.

### 33.5 State Transformations: A Temperature Independent Resource Theory of Thermodynamics

One of the important aspects this framework is that it can be exploited to provide a resource theory of thermodynamics, which is independent of temperature [34]. A similar formulation is also introduced in [40]. Here we briefly introduce that. The main ingredients of every resource theory are the resourceless state space, which are of vanishing resource, and a set of allowed state transformations. Here, CP states are resourceless and set of allowed operations, in general, are the ones that are energy non-increasing and entropy non-decreasing.

Let us first restrict to the set of operations that are entropy preserving regardless the energy. Consider two states  $\rho$  and  $\sigma$ , and without loss of generality  $S(\rho) \leq S(\sigma)$ . Then, there exists an  $n$ , for which

$$S(\rho^{\otimes n}) = S(\sigma^{\otimes m}). \quad (33.26)$$

Therefore, there is an entropy preserving operation that transforms  $n$ -copies of  $\rho$  to  $m$ -copies of  $\sigma$ , and vice versa. By such a trick, with access to arbitrary number of copies, the states  $\rho$  and  $\sigma$  with different entropies, can be brought to a same manifold of equal entropy. Note  $\rho^{\otimes n}$  and  $\sigma^{\otimes m}$  belong to the spaces of different dimension, and they can be made equal in dimensions by

$$\Lambda(\rho^{\otimes n}) = \sigma^m \otimes |0\rangle\langle 0|^{n-m}. \quad (33.27)$$

The  $\rho^{\otimes n}$  and  $\sigma^{\otimes m} \otimes |0\rangle\langle 0|^{n-m}$  live now in spaces of the same dimension. Equation (33.27) represents, in fact, a randomness compression process, in which the information in  $n$ -copies of  $\rho$  is compressed to  $m$ -copies of  $\sigma$ , and  $n - m$  systems are erased. If we are restricted to only entropy preserving operations, the rate of transformation, from (33.26), becomes

$$r := \frac{m}{n} = \frac{S(\rho)}{S(\sigma)}. \quad (33.28)$$

In thermodynamics, however, energy also plays important roles and thus must be taken into account. Otherwise, it could be possible that the process considered in (33.27) is not favorable energetically if  $E(\rho^{\otimes n}) < E(\sigma^{\otimes m})$ . Then, more copies of  $\rho$  are required such that the transformation becomes energetically favorable. Further, it creates states (with non-zero entropy),  $\phi$ , such that

$$\Lambda(\rho^{\otimes n}) = \sigma^{\otimes m} \otimes \phi^{\otimes n-m}.$$

The operation satisfies the energy and entropy conservation constraints, therefore

$$\begin{aligned} E(\rho^{\otimes n}) &= E(\sigma^{\otimes m} \otimes \phi^{\otimes n-m}), \\ S(\rho^{\otimes n}) &= S(\sigma^{\otimes m} \otimes \phi^{\otimes n-m}). \end{aligned}$$

In other form, they represent a geometric equation of the points  $x_\psi = (E(\psi), S(\psi))$  with  $\psi \in \{\rho, \sigma, \phi\}$

$$x_\rho = r x_\sigma + (1 - r) x_\phi, \quad (33.29)$$

in the energy-entropy diagram and  $r := m/n$  is the state conversion rate. Here the extensivity of both entropy and energy in the number of copies, e.g.  $E(\rho^{\otimes n}) = nE(\rho)$ , are used.

As shown in Fig. 33.3, the three points  $x_\rho$ ,  $x_\sigma$  and  $x_\phi$  lie on a straight line in the energy-entropy diagram, as a consequence of Eq. (33.29). Moreover,  $0 \leq r \leq 1$

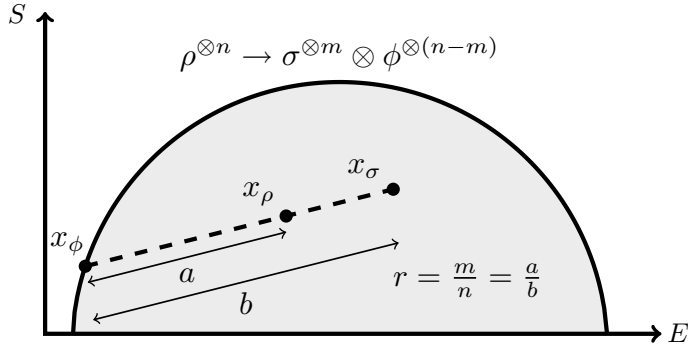


**Fig. 33.3** Representation in the energy-entropy diagram and role of operations respecting energy and entropy conservation constraints in the transformation  $\rho^{\otimes n} \rightarrow \sigma^{\otimes m} \otimes \phi^{\otimes(n-m)}$  imply  $x_\rho$ ,  $x_\sigma$  and  $x_\phi$  to be aligned and  $x_\rho$  to lie in between  $x_\sigma$  and  $x_\phi$ .

implies that  $x_\rho$  lies in between  $x_\sigma$  and  $x_\phi$ . The conversion rate  $r$  can be given a geometric interpretation and it is the Euclidean distance between  $x_\phi$  and  $x_\rho$  relative to the total Euclidean distance between  $x_\sigma$  and  $x_\phi$  (see Fig. 33.3).

The conversion rate  $r$ , from  $\rho$  and  $\sigma$ , becomes maximal when the state  $\phi$  lies on the boundary of the energy-entropy diagram. That means it would be either a thermal or a pure state. Quantitatively, the conversion rate  $r$  is maximized, when

$$\frac{S(\sigma) - S(\phi)}{S(\sigma) - S(\rho)} = \frac{E(\sigma) - E(\phi)}{E(\sigma) - E(\rho)},$$

and  $\phi$  is thermal state. Accordingly, the rate becomes

$$r = \frac{m}{n} = \frac{S(\rho) - S(\phi)}{S(\sigma) - S(\phi)}. \quad (33.30)$$

This can be easily seen, geometrically, in Fig. 33.3. The Eq. (33.28) is recovered in the case of  $\phi$  being pure (vanishing entropy). Let us note that, an alternative derivation of the transformation rate is obtained in [40]. However, they can be shown to be identical. The rate in Eq. (33.30) is more compact and less technical, compared to the one in [40].

We note that the resource theory of quantum thermodynamics, presented in Chap. 26, can be understood as a special case of our consideration above, where system is attached to an arbitrarily large bath at fixed temperature and allowed operations are global energy preserving unitaries, instead of more general global entropy preserving operations.

### 33.6 Discussion

Thermodynamics, and in particular work extraction from non-equilibrium states, has been studied in the quantum domain, in the recent years. It introduces radically new insights into quantum statistical and thermal processes. In much these studies, be it classical or quantum, thermal baths are assumed to be considerably large in size compared to systems under consideration. That is why, the baths remains always thermal, with same temperature, before and after it interacts with a system. Also, an equilibrated system always shares the same temperature with the bath. Indeed, the assumption large is not fulfilled in every situation. If the baths are finite and small systems, the standard formulation of thermodynamics breaks down. The first problem one would encounter is the inconsistency in the notion of temperature itself. A finite bath could go out of thermal equilibrium, by exchanging energy with a system. Such a situation is relevant for thermodynamics that applies to quantum regime, where system and bath could be small and comparable in size. To incorporate such scenarios, we need to develop a temperature independent thermodynamics, where the bath could be small or large and will not have a special status.

Here, we have introduced temperature independent formulation of thermodynamics as an exclusive consequence of (coarse-grained) information conservation. The information is measured in terms of von Neumann entropy. The formulation is relied on the fact that systems with same entropy can be inter-convertible using entropy preserving operations. Therefore, the states with same entropy forms a constant entropy manifold and there exists a state that possesses minimal amount of energy. This state with minimal energy are known as *a completely passive state*, which assumes a Boltzmann–Gibb’s canonical form with an intrinsic temperature. The energy of a completely passive state is defined as the bound energy, as this energy cannot be extracted by any entropy preserving operations. For any given state, the free energy is defined as the difference between the internal energy and the bound energy, as this amount of energy can be accessible by means of entropy preserving operations. As shown in [40], two different states possessing identical energy and entropy are thermodynamically equivalent. Such equivalence enables us to exploit energy-entropy diagram to understand bound, free energies geometrically.

With these machinery, we have introduced a completely new definition of heat in terms of bound energy, applicable for arbitrary systems and without any reference to a temperature. We have formulated the laws of thermodynamics accordingly and, as we have seen, they are a consequence of the reversible dynamics of the underlying physical theory. In particular:

- *Zeroth law* is a consequence of information conservation.
- *First and second laws* are a consequence of energy conservation, together with information conservation.
- *Third law* is a consequence of “strict” information conservation (i.e. microscopic reversibility or unitarity). There is no third law for processes that only respect “coarse-grained” information conservation.

We have applied our formalism to the heat engines that consist of finite bath and demonstrated that the maximum efficiency is in general less, compared to an ideal Carnot's engine. We have also introduced a resource theoretic framework for intrinsic temperature based thermodynamics. This approach enables us to address the problem of inter-state transformations and work extraction. These results are given a geometric meaning, in terms of the energy-entropy diagram.

The information conservation based framework for thermodynamics can be extended to multiple conserved quantities [34]. Analogously, charge-entropy and resource theory can be given in this scenario. The extraction of a generalized potential (i.e. linear combinations of charges), becomes analogous to the work extraction (the single charge case).

An immediate question arises is that to what extent the formalism can be extended beyond coarse-grained information conservation operations. This is an interesting open question, as in that case, there would be a different notion of bound energy and possibly many more equivalence classes of states. It is also far from clear if energy-entropy diagrams would be meaningful there.

**Acknowledgements** We acknowledge financial support from the European Commission (FETPRO QUIC H2020-FETPROACT-2014 No. 641122), the European Research Council (AdG OSYRIS and AdG IRQUAT), the Spanish MINECO (grants no. FIS2008-01236, FISICATEAMO FIS2016-79508-P, FIS2013-40627-P, FIS2016-86681-P, and Severo Ochoa Excellence Grant SEV-2015-0522) with the support of FEDER funds, the Generalitat de Catalunya (grants no. 2017 SGR 1341, and SGR 875 and 966), CERCA Program/Generalitat de Catalunya and Fundació Privada Cellex. MNB also thanks support from the ICFO-MPQ fellowship.

## References

1. J. Gemmer, M. Michel, G. Mahler, in *Quantum thermodynamics*. Lecture Notes in Physics, vol. 748 (Springer, Berlin, Heidelberg, 2009). <https://doi.org/10.1007/978-3-540-70510-9>
2. J.M.R. Parrondo, J.M. Horowitz, T. Sagawa, Nat. Phys. **11**, 131 (2015). <https://doi.org/10.1038/nphys3230>
3. J.C. Maxwell, *Theory of Heat* (Longmans, Green, and Co., London, New York, Bombay, 1908). <https://archive.org/details/theoryofheat00maxwrich/page/n8>
4. H.S. Leff, A.F. Rex, *Maxwell's Demon: Entropy, Information, Computing* (Taylor and Francis, London, 1990). <https://press.princeton.edu/titles/4731.html>
5. H.S. Leff, A.F. Rex, *Maxwell's Demon 2: Entropy, Classical and Quantum Information, Computing* (Taylor and Francis, London, 2002). <https://doi.org/10.1201/9781420033991>
6. K. Maruyama, F. Nori, V. Vedral, Rev. Modern Phys. **81**, 1 (2009). <https://doi.org/10.1103/RevModPhys.81.1>
7. L. Szilard, Z. Phys. **53**, 840 (1929). <https://doi.org/10.1007/BF01341281>
8. R. Landauer, IBM J. Res. Dev. **5**, 183 (1961). <https://doi.org/10.1147/rd.53.0183>
9. C.H. Bennett, Int. J. Theor. Phys. **21**, 905 (1982). <https://doi.org/10.1007/BF02084158>
10. M.B. Plenio, V. Vitelli, Contemp. Phys. **42**, 25 (2001). <https://doi.org/10.1080/00107510010018916>
11. L. del Rio, J. Åberg, R. Renner, O.C.O. Dahlsten, V. Vedral, Nature **474**, 61 (2011). <https://doi.org/10.1038/nature10123>
12. D. Reeb, M.M. Wolf, N. J. Phys. **16**, 103011 (2014). <https://doi.org/10.1088/1367-2630/16/10/103011>

13. C.E. Shannon, Bell Syst. Tech. J. **27**, 379 (1948). <https://doi.org/10.1002/j.1538-7305.1948.tb01338.x>
14. M.A. Nielsen, I.L. Chuang, *Quantum Computation and Quantum Information: 10th Anniversary Edition* (Cambridge University Press, Cambridge, 2010). <https://doi.org/10.1017/CBO9780511976667>
15. T.M. Cover, J.A. Thomas, *Elements of Information Theory*, 2nd edn. (Wiley, New York, 2005). <https://doi.org/10.1002/047174882X>
16. R. Alicki, M. Fannes, Phys. Rev. E **87**, 042123 (2013). <https://doi.org/10.1103/PhysRevE.87.042123>
17. M. Perarnau-Llobet, K.V. Hovhannisyan, M. Huber, P. Skrzypczyk, N. Brunner, A. Acín, Phys. Rev. X **5**, 041011 (2015). <https://doi.org/10.1103/PhysRevX.5.041011>
18. M.N. Bera, A. Riera, M. Lewenstein, A. Winter, Nat. Commun. **8**, 2180 (2017a). <https://doi.org/10.1038/s41467-017-02370-x>
19. A.J. Short, N. J. Phys. **13**, 053009 (2011). <https://doi.org/10.1088/1367-2630/13/5/053009>
20. J. Goold, M. Huber, A. Riera, L. del Rio, P. Skrzypczyk, J. Phys. A Math. Theor. **49**, 143001 (2016). <https://doi.org/10.1088/1751-8113/49/14/143001>
21. L. del Rio, A. Hutter, R. Renner, S. Wehner, Phys. Rev. E **94**, 022104 (2016). <https://doi.org/10.1103/PhysRevE.94.022104>
22. C. Gogolin, J. Eisert, Rep. Prog. Phys. **79**, 056001 (2016). <https://doi.org/10.1088/0034-4885/79/5/056001>
23. S. Popescu, A.J. Short, A. Winter, Nat. Phys. **2**, 745 (2006). <https://doi.org/10.1038/nphys444>
24. F.G.S.L. Brandão, M. Horodecki, J. Oppenheim, J.M. Renes, R.W. Spekkens, Phys. Rev. Lett. **111**, 250404 (2013). <https://doi.org/10.1103/PhysRevLett.111.250404>
25. O.C.O. Dahlsten, R. Renner, E. Rieper, V. Vedral, N. J. Phys. **13**, 053015 (2011). <https://doi.org/10.1088/1367-2630/13/5/053015>
26. J. Åberg, Nat. Commun. **4**, 2013 (1925). <https://doi.org/10.1038/ncomms2712>
27. M. Horodecki, J. Oppenheim, Nat. Commun. **4**, 2013 (2013). <https://doi.org/10.1038/ncomms3059>
28. P. Skrzypczyk, A.J. Short, S. Popescu, Nat. Commun. **5**, 4185 (2014). <https://doi.org/10.1038/ncomms5185>
29. F.G.S.L. Brandao, M. Horodecki, N. Ng, J. Oppenheim, S. Wehner, Proc. Natl. Acad. Sci. **112**, 3275 (2015). <https://doi.org/10.1073/pnas.1411728112>
30. P. Ćwikliński, M. Studziński, M. Horodecki, J. Oppenheim, Phys. Rev. Lett. **115**, 210403 (2015). <https://doi.org/10.1103/PhysRevLett.115.210403>
31. M. Lostaglio, K. Korzekwa, D. Jennings, T. Rudolph, Phys. Rev. X **5**, 021001 (2015a). <https://doi.org/10.1103/PhysRevX.5.021001>
32. D. Egloff, O.C.O. Dahlsten, R. Renner, V. Vedral, N. J. Phys. **17**, 073001 (2015). <https://doi.org/10.1088/1367-2630/17/7/073001>
33. M. Lostaglio, D. Jennings, T. Rudolph, Nat. Commun. **6**, 6383 (2015b). <https://doi.org/10.1038/ncomms7383>
34. M.N. Bera, A. Riera, M. Lewenstein, A. Winter (2017b), [arXiv:1707.01750](https://arxiv.org/abs/1707.01750)
35. M.N. Bera, A. Acín, M. Kuś, M. Mitchell, M. Lewenstein, Rep. Prog. Phys. **80**, 124001 (2017c). <https://doi.org/10.1088/1361-6633/aa8731>
36. F. Hulpke, U.V. Poulsen, A. Sanpera, A. Sen(De), U. Sen, M. Lewenstein, Found. Phys. **36**, 477 (2006). <https://doi.org/10.1007/s10701-005-9035-7>
37. C. Jarzynski, J. Stat. Phys. **98**, 77 (2000). <https://doi.org/10.1023/A:1018670721277>
38. M. Esposito, U. Harbola, S. Mukamel, Rev. Mod. Phys. **81**, 1665 (2009). <https://doi.org/10.1103/RevModPhys.81.1665>
39. T. Sagawa, Second law-like inequalities with quantum relative entropy: an introduction, in *Lectures on Quantum Computing, Thermodynamics and Statistical Physics*, vol. 8 (World Scientific, Singapore, 2012), pp. 125–190. [https://doi.org/10.1142/9789814425193\\_0003](https://doi.org/10.1142/9789814425193_0003)
40. C. Sparaciari, J. Oppenheim, T. Fritz, Phys. Rev. A **96**, 052112 (2017). <https://doi.org/10.1103/PhysRevA.96.052112>
41. E.T. Jaynes, Phys. Rev. **106**, 620 (1957a). <https://doi.org/10.1103/PhysRev.106.620>

42. E.T. Jaynes, Phys. Rev. **108**, 171 (1957b). <https://doi.org/10.1103/PhysRev.108.171>
43. W. Pusz, S.L. Woronowicz, Commun. Math. Phys. **58**, 273 (1978). <https://doi.org/10.1007/BF01614224>
44. A. Lenard, J. Stat. Phys. **19**, 575 (1978). <https://doi.org/10.1007/BF01011769>
45. L. Masanes, J. Oppenheim, Nat. Commun. **8**, 14538 (2017). <https://doi.org/10.1038/ncomms14538>

**Part VI**

**Experimental Platforms for Quantum  
Thermodynamics**

# Chapter 34

## One-Dimensional Atomic Superfluids as a Model System for Quantum Thermodynamics



Jörg Schmiedmayer

### 34.1 Introduction

Statistical mechanics provides a powerful connection between the microscopic dynamics of atoms and molecules and the macroscopic properties of matter [1]. We have a deep understanding of (thermal) equilibrium properties of a system, but the question of how equilibrium is reached or under which circumstances it can be reached at all is still unsolved. This problem is particularly challenging in quantum mechanics, where unitarity appears to render the very concept of thermalisation counterintuitive. The time-reversal symmetry that results from the unitarity of quantum mechanics seems to make the relaxation to thermal states impossible in an isolated system.

This question is usually avoided by ‘coupling the quantum system to a (macroscopic) bath’. If we assume that quantum mechanics is the fundamental description of nature, this procedure does NOT solve the fundamental question raised by the apparent contradiction of unitary evolution and thermalisation/equilibration. On the fundamental level the ‘bath’ has also to be described by quantum physics, and the system can always be enlarged to include the bath. Therefore the fundamental question to consider is:

*Does an isolated many-body quantum system relax/thermalise?*

It addresses the essentials of the fundamental relation between the macroscopic description of statistical mechanics and the microscopic quantum world and has been intensely discussed since the 1920s [2]. Important theoretical advances have been achieved over the years [3–9]. Variations of this question play important roles in such diverse fields as cosmology [10, 11] with the ultimate isolated quantum

---

J. Schmiedmayer (✉)

Vienna Center for Quantum Science and Technology (VCQ), Atominstitut, TU-Wien,  
Vienna, Austria

e-mail: schmiedmayer@atomchip.org

system being the whole universe, high-energy physics [12, 13] and condensed matter [14, 15].

A key insight to resolve this apparent contradiction between unitary quantum evolution and relaxation comes from the fact that the required resources to measure many-body eigenstates scale exponentially with system size. The best we can do is to measure (local) few-body observables  $\mathcal{O}$  and their correlations. A nice illustration of this is the growing complexity and computational effort when evaluating connected high order correlation functions [16] or when applying tomography to few qubit systems [17]. Since (local) few-body observables do not probe the whole system, one can view the ‘measurement’ as dividing the one closed system internally into degrees of freedom that are measured, and others that are not. This way, the observables  $\mathcal{O}$  one chooses to investigate automatically create a situation where the system is partitioned into a (reduced) system and an environment, i.e. it becomes its own environment. Changing the observable naturally leads to a different separation between what is measured and what constitutes the environment.

With the rapid experimental progress in the control and probing of ultra-cold quantum gases [18] these questions come within reach of detailed experimental investigations. Trapped atoms are almost perfectly isolated from the environment and the important time scales governing their dynamics are easily accessible. Powerful manipulation techniques allow for a large variety of systems to be implemented. For an overview on recent experiments exploring non equilibrium physics with isolated quantum systems using ultra-cold quantum gases, see [19, 20].

In this chapter we present, as an example, our experiments with ultra-cold one-dimensional Bose gases that realise several textbook non-equilibrium phenomena providing insights into these fundamental question and highlight some of the physics related to quantum thermodynamics and quantum machines which may be explored in the near future.

## 34.2 One-Dimensional Superfluids

Over the last years, one-dimensional (1D) Bose gases have proven to be a especially versatile testbed for the study of quantum many-body systems in and out of equilibrium. From the theorist’s perspective 1D Bose gases offer a rich variety of interesting many-body physics, while still being tractable with reasonable effort [21, 22]. Compared to 3D, significantly different physics arise in the 1D regime. The Mermin-Wagner theorem [23] tells us that no true off-diagonal long-range order can emerge due to the enhanced role of fluctuations in 1D and no true Bose-Einstein condensation is possible even at  $T = 0$ . Instead a large number of distinct degenerate regimes emerges [24, 25], which might share or not share some of the familiar features of a Bose-Einstein condensate. On the experimental side their realisation using cold atomic gases offers precise control over many system parameters, as well as highly-effective means to probe their dynamics [26].

### 34.2.1 Theoretical Description of 1D Systems

#### Lieb-Liniger Model

In the homogeneous limit an ideal 1D system of hard core interacting Bosons is described by [27]

$$\hat{H} = \frac{\hbar^2}{2m} \int dz \frac{\partial \hat{\Psi}^\dagger(z)}{\partial z} \frac{\partial \hat{\Psi}(z)}{\partial z} + \frac{g_{1D}}{2} \int dz dz' \hat{\Psi}^\dagger(z) \hat{\Psi}^\dagger(z') \delta(z - z') \hat{\Psi}(z') \hat{\Psi}(z), \quad (34.1)$$

where the  $\hat{\Psi}(z)$  denote bosonic field operators. The first term accounts for the kinetic energy and the second one for interactions, characterised by the 1D interaction strength  $g_{1D}$ . The Lieb-Lininger Hamiltonian (Eq. 34.1) is a prime example of an integrable model [27–30], solvable by Bethe Ansatz. Experiments with 1D Bose gases can thus provide a link between the deep insights from these mathematical models and physical reality. Most notably, the many conserved quantities have a profound influence on the non-equilibrium dynamics of these systems, which makes them particularly interesting for the study of relaxation and thermalisation processes [31, 32].

The interaction in Eq. 34.1 can be parameterised by the Lieb-Lininger parameter  $\gamma = mg_{1D}/\hbar^2 n_{1D}$ . Notably  $\gamma$  increases for decreasing particle densities  $n_{1D}$ . For  $\gamma \gg 1$  the gas is in the strongly-interacting Tonks-Girardeau regime [33–35] which was probed in [36, 37]. The experiments presented in this chapter are performed with  $\gamma \ll 1$ , where the gas is a weakly interacting quasi-condensate [24]. In this regime, density fluctuations are suppressed, however, the phase fluctuates strongly along the length of the system.

#### Luttinger Liquid Model

For low energies one can express the field operators  $\hat{\Psi}(z)$  in Eq. 34.1 in terms of density  $\hat{n}(z)$  and phase  $\hat{\theta}(z)$  operators:  $\hat{\Psi}(z) = e^{i\hat{\theta}(z)} \sqrt{n_{1D} + \hat{n}(z)}$ , which satisfy the bosonic commutation relation  $[\hat{n}(z), \hat{\theta}(z')] = i\delta(z - z')$ . Inserting this definition into Eq. 34.1 leads to a quadratic low energy effective field theory description [38], a Tomonaga–Luttinger liquid [39–41]:

$$\begin{aligned} \hat{H} &= \frac{\hbar c}{2} \int dz \left[ \frac{K}{\pi} \left( \frac{\partial \hat{\theta}(z)}{\partial z} \right)^2 + \frac{\pi}{K} \hat{n}(z)^2 \right] \\ &= \sum_k \hbar \omega_k \hat{a}_k^\dagger \hat{a}_k. \end{aligned} \quad (34.2)$$

where  $c = \sqrt{g_{1D} n_{1D} / m}$  is the speed of sound and  $K = \sqrt{n_{1D} (\hbar \pi)^2 / 4 g_{1D} m}$  is the Luttinger parameter. The corresponding eigenmodes are non-interacting phonons with momentum  $\hbar k$ , a linear dispersion relation  $\omega_k = ck$  and energies  $\hbar \omega_k$ . The

creation and annihilation operators  $\hat{a}_k$  and  $\hat{a}_k^\dagger$  define the phonon occupation number  $\hat{n}_k = \hat{a}_k^\dagger \hat{a}_k$ . They are directly related to the Fourier components of density and phase via

$$\begin{aligned}\hat{n}_k &\sim \left( \hat{a}_k(t) + \hat{a}_{-k}^\dagger(t) \right) \\ \hat{\theta}_k &\sim \left( \hat{a}_k(t) - \hat{a}_{-k}^\dagger(t) \right)\end{aligned}\quad (34.3)$$

In analogy to photon quantum optics  $\hat{\theta}_k$  represents the phase quadrature and  $\hat{n}_k$  the density quadrature related to a phonon with momentum  $\hbar k$ .

The Luttinger liquid description is only an approximate effective field theory describing the low energy physics of hard core bosons in 1D. For a detailed account of effects beyond the Luttinger Liquid description, see [42]. Finally, we note that, besides cold atoms, the Luttinger liquid Hamiltonian also plays an important role in both bosonic and fermionic condensed matter systems [43–46].

### **Two Tunnel-Coupled Superfluids: The Quantum Sine-Gordon Model**

A second fundamental model connected to 1D superfluids is the quantum Sine-Gordon model [47–50], relevant for a wide variety of disciplines from particle to condensed-matter physics [51, 52]. It has been proposed by Gritsev et al. [53] and experimentally verified in [16], that the relative degrees of freedom (phase  $\varphi(z)$  and density fluctuations  $\delta\rho(z)$ ) of two tunnel-coupled one-dimensional (1D) bosonic superfluids (tunnel-coupling strength  $J$ ) can be described by the sine-Gordon Hamiltonian:

$$\begin{aligned}H_{\text{SG}} = \int dz & \left[ g_{1\text{D}} \delta\rho^2 + \frac{\hbar^2 n_{1\text{D}}}{4m} (\partial_z \varphi)^2 \right] \\ & - \int dz 2\hbar J n_{1\text{D}} \cos(\varphi),\end{aligned}\quad (34.4)$$

The first term represents the well-known quadratic Tomonaga–Luttinger Hamiltonian Eq. 34.2, which can be solved using non-interacting phononic quasi-particles. The second term is non-quadratic and includes all powers of the field  $\varphi$ , which leads to many intriguing properties such as a tuneable gap, non-Gaussian fluctuations, non-trivial quasi-particles and topological excitations. The fields  $\varphi(z)$  and  $\delta\rho(z)$  represent canonically conjugate variables fulfilling appropriate commutation relations.

The system is characterized by two scales: The phase coherence length  $\lambda_T = 2\hbar^2 n_{1\text{D}} / (mk_B T)$  describing the randomisation of the phase due to temperature  $T$ , and the healing length of the relative phase (Spin healing length)  $\xi_J = \sqrt{\hbar / (4mJ)}$  determining restoration of the phase coherence through the tunnel coupling  $J$ . The relevance of the non-quadratic contributions to the Hamiltonian is characterized by the dimensionless ratio  $q = \lambda_T / \xi_J$ . By independently varying  $J$ ,  $T$  and  $n_{1\text{D}}$  the ratio  $q$  can be tuned over a large range to explore different regimes of the field theory [16].

### ***Breaking Integrability***

Both the Lieb-Liniger model and its low energy effective description the Luttinger Liquid are integrable models. In any realistic experimental setting this integrability will be broken at some level. The analysis of this scenario in the context of classical mechanics has culminated in the important Kolmogorov-Arnold-Moser (KAM) theorem [54]. No complete analogue of this theorem has so far been found in quantum mechanics [55]. For ultra-cold atoms in 1D traps key candidates for breaking integrability are the motion in the longitudinal confinement [56], virtual 3-body collisions [57–60] which ‘feel’ the transverse confinement even when the energy in the atom-atom collisions does not allow to excite transverse states, long range interactions [61], or simply a small addition of transversely excited atoms [62–64].

### ***34.2.2 Realising 1D Many-body Quantum Systems***

The experimental realisation of a 1D Bose gas follows the familiar procedure based on laser and evaporative cooling that is also used for the production of Bose-Einstein condensates in 3D. Creating an effectively 1D system in a 3D world requires extremely asymmetric traps with a tight confinement in the two transverse directions. To reach the 1D regime the energy splitting between the ground state and the first transverse excited state in the trap has to be larger than all other relevant energy scales.

For a tight transverse harmonic confinement characterised by  $\omega_{\perp}$  and  $a_{\perp} = \sqrt{\hbar/(m\omega_{\perp})}$  this translates into the requirement that both the temperature  $T$  and the chemical potential  $\mu = g_{1D}n_{1D}$ , which is the interaction energy per particle, both fulfil  $k_B T, \mu \ll \hbar\omega_{\perp}$ . In this situation the dynamics along the transverse directions can be integrated out leaving the dynamics along the weakly confined axial direction. The 1D interaction strength  $g_{1D}$  can then be related to the s-wave scattering length  $a_s$  in 3D by [35]

$$g_{1D} = \frac{2\hbar a_s \omega_{\perp}}{1 - 1.4603 a_s/a_{\perp}}. \quad (34.5)$$

Note that microscopic scattering processes always have a 3D character. In the weakly-interacting regime the s-wave scattering length  $a_s$  is small compared to the ground state width  $a_{\perp}$  of the tight transverse confinement, i.e.  $a_s \ll a_{\perp}$ . In that case Eq. 34.5 can be approximated to a very good approximation by  $g_{1D} = 2\hbar a_s \omega_{\perp}$ . Interesting effects like confinement-induced resonances can occur when this assumption is no longer valid [35, 65].

Highly anisotropic trap configurations can be created in strongly-focussed optical dipole traps [66–68], optical lattices [18, 36, 69, 70] or in magnetic micro traps [71, 72]. In our experiments we rely on the latter because micro traps, as we will see below, allow for a particularly precise and convenient preparation of non-equilibrium states by splitting a 1D gas. Typical trap frequencies in our setup are  $\omega_{\perp} = 2\pi \cdot 3 \text{ kHz}$  in the tightly-confining transverse directions and  $\omega_{\text{ax}} = 2\pi \cdot 5 \text{ Hz}$

in the weakly-confining axial direction. The 1D Bose gas of  $^{87}\text{Rb}$ -atoms is then created in this trap by evaporative cooling of an elongated 3D thermal cloud through the condensation crossover and then further into the 1D regime.

### **Cooling in 1D**

In 1D systems thermalising two body collisions are suppressed by  $\exp(-\frac{2\hbar\omega_{\perp}}{k_B T})$  [57], which renders standard evaporative cooling ineffective for  $k_B T \ll \hbar\omega_{\perp}$ . Nevertheless extremely low temperatures, far below  $\hbar\omega_{\perp}$  and far below the chemical potential  $\mu = g_{1\text{D}}n_{1\text{D}}$  are reported [73–75]. In experiments to study cooling mechanisms in 1D systems [76] we reach  $T \sim 0.1\hbar\omega_{\perp}$  and  $T \sim 0.25\mu$  which demonstrates that the above intuitive picture is incomplete. We developed a simple theoretical model based on the dynamics of an one-dimensional Bose gas [77]: Cooling can be modelled as a series of infinitesimal density quenches extracting energy from the density quadrature of the phononic excitations followed by many-body de-phasing. This process reduces the occupation number of each phonon mode, leading to a cooler system. Our simple model leads, in a harmonic trap, to a scaling relation  $T \propto N$ , which is confirmed in our experiments. It is interesting to note that the above simple model neglects the quantum noise coming from out-coupling of atoms. If included, the complete model [77] does not agree with the experimental observations [76].

### **Splitting a 1D Quantum Gas**

The magnetic micro traps on atom chips allow for a precise dynamical control over the trap parameters. Most notably, the initial transverse tight harmonic confinement can be transformed into a double well potential. This is realised by radio-frequency (RF) dressing of the magnetic sub-levels of the atoms [78–80]. The RF fields are applied through additional wires on the chip, which due to their proximity to the atoms allows for very high RF field amplitudes and a precise control over the field polarisation.

We use this technique to coherently split a single 1D Bose gas into two halves, thereby creating a non-equilibrium state [81–83]. If the splitting is performed fast compared to the axial dynamics in the system, that is  $t_{\text{split}} < \xi_n/c = \hbar/\mu$  ( $\xi_n = \hbar/mc$  is the healing length for the density  $n$ ), then no correlations can build up along the axial direction and the splitting happens independently at each point in the gas. In this case the process can be intuitively pictured as a local beam splitter where each atom is independently distributed into the left or right half of the new system. The corresponding probability distribution for the local number of particles  $N$  on each side is therefore binomial. If the splitting is slower, then correlations can build up along the system, and the local number fluctuations will not be independent. This results in such intriguing quantum phenomena as number squeezing or spin squeezing [84, 85]. Using optimal control to shape the splitting procedure one can speed up and enhance the squeezing [86–88].

### 34.2.3 Experimental Techniques for Probing the Quantum State

Information about the system and its dynamics is extracted using standard absorption [89, 90] or by fluorescence imaging [91] after releasing the atoms from the trap. If only a single gas is present it simply expands in time-of-flight (TOF), while a pair of condensates expands, overlaps and forms a matter-wave interference pattern. This detection method is destructive, therefore many identical realisations are necessary to probe a time evolution.

It is important to note that in the 1D regime the tight transversal confinement leads to a very rapid radial expansion suppressing any effects of interactions during time of flight. Consequently the obtained images enable comprehensive insights into the properties of the initial trapped system [92].

#### Density Ripples

A single quasi-condensate that is released and expands in TOF forms strong density speckles along the 1D axis (see Fig. 34.1). These speckles are a direct consequence of the fluctuating phase  $\theta(z)$  in the trapped system and are superposed on the average density profile. Analysing the correlations in these patterns and comparing them to simulated results obtained from an Ornstein-Uhlenbeck stochastic process allows us to determine the temperature of the gas [92, 93] as shown in Fig. 34.1. This powerful tool works as well for 2D systems [94]. In our experiments it is primarily used to characterise the initial gas before the splitting. However, it can also be used for the study of the evaporative cooling process [76] or thermalisation.

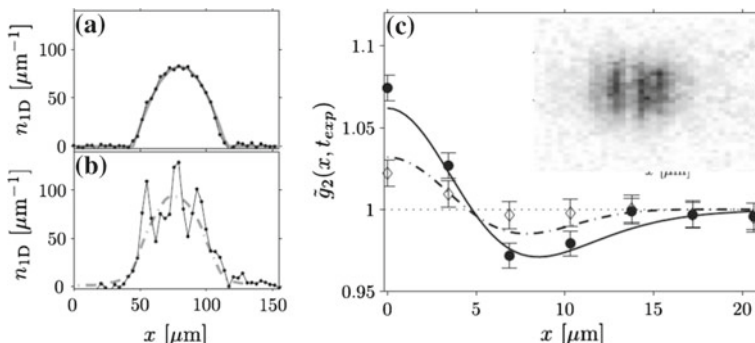


**Fig. 34.1 Density ripples.** The phase fluctuations in the individual realisation of a 1D quantum gas lead to a pronounced random speckle pattern in time of flight visible as the strong variations in the density profile shown as insert in (c) and the extracted individual density profile (b). The density profile averaged over  $> 100$  realisations is displayed in (a). (c) The density-density correlations of these speckles allow to characterise the phase fluctuations in the trapped 1D gas and with that its temperature. Black dots (open diamonds): Measured correlation function  $\tilde{g}_2(x)$  for 150 nK (60 nK). Figures adapted from [93].

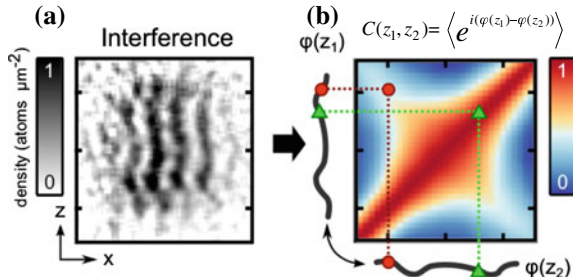


**Fig. 34.2 Phase correlations.** **a)** Typical interference pattern created by two 1D superfluids. The local relative phase  $\varphi(z)$  between the two 1D BEC can be extracted by fitting the interference pattern for each pixel row. **b)** From the measured relative phase profiles one can evaluate the non translation-invariant correlation function  $C(z_1, z_2) = \langle e^{i\hat{\phi}(z_1) - i\hat{\phi}(z_2)} \rangle$ . The central red diagonal is the trivial auto correlation  $C(z, z) = 1$ . Figures adapted from [97].

### Correlation Functions

Correlation functions are directly linked to the theoretical description of many-body systems and are a powerful tool to probe equilibrium and non-equilibrium physics. As pointed out by Schwinger [95, 96] the knowledge of all correlation functions of a system is equivalent to solving the corresponding many-body problem. If the relevant degrees of freedom are known, the knowledge of a finite set of basic correlation functions can be sufficient to construct a solution of the corresponding theory. For a first experimental implementation of this powerful theoretical concept, see Schweigler et al. [16].

For 1D systems the most relevant correlations are the ones directly connected to the theoretical models discussed in Sect. 34.2.1. These are density correlations and phase correlations (Fig. 34.2). Density correlations measured in situ have been used to characterise the temperature of 1D systems [74, 75], investigate analogues to ‘Hawking radiation’ emerging from acoustic horizons [98]. Density correlations in time of flight [99] have been used to study, for example, optical lattice systems [100, 101], the difference between Bosons and Fermions [102] or the transition from 1D to 3D [103].

Here we will concentrate mainly on the correlations of the phase (Fig. 34.2). The interference pattern of two 1D quasi-condensates is a direct measurement of the fluctuations in the relative phase along the length of the two 1D superfluids.

If density fluctuations can be neglected, which is a very good approximation in the quasi-condensate regime, the second order correlation function

$$\begin{aligned} C(z, z') &= \langle e^{i\hat{\phi}(z) - i\hat{\phi}(z')} \rangle \\ &\simeq \frac{\langle \hat{\Psi}_l^\dagger(z) \hat{\Psi}_r(z) \hat{\Psi}_r^\dagger(z') \hat{\Psi}_l(z') \rangle}{\langle |\Psi_r(z)|^2 \rangle \langle |\Psi_l(z')|^2 \rangle}. \end{aligned} \quad (34.6)$$

can be related to correlations in the field operators  $\hat{\Psi}_{l,r}$  of the left and right gas.  $z$  and  $z'$  are two points along the axial direction of the system. In a finite system the correlations  $C(z, z')$  are non translation-invariant. Equation 34.6 can easily be extended to higher order correlations [97]. In the experiment, the expectation value is measured by averaging over many identical realizations.

From the measured phase field  $\varphi(z)$  we can extract the equal-time Nth-order correlation functions of the phase directly [16]:

$$G^{(N)}(\mathbf{z}, \mathbf{z}') = \langle \Delta\varphi(z_1, z'_1) \dots \Delta\varphi(z_N, z'_N) \rangle, \quad (34.7)$$

where  $\Delta\varphi(z_i, z'_i) = \varphi(z_i) - \varphi(z'_i)$  are continuous (not restricted to  $2\pi$ ) phase differences of the unbound phase at different spatial points  $z_i, z'_i$ . The second order phase correlation function  $G^{(2)}(\mathbf{z}, \mathbf{z}')$  can be related to the creation and annihilation operators of the quasi-particles in the 1D system, the 4th-order  $G^{(4)}(\mathbf{z}, \mathbf{z}')$  to quasi-particle scattering and the higher order correlations to higher order interaction processes between the quasi-particles. The  $N$ th-order correlation functions can be decomposed

$$G^{(N)}(\mathbf{z}, \mathbf{z}') = G_{\text{con}}^{(N)}(\mathbf{z}, \mathbf{z}') + G_{\text{dis}}^{(N)}(\mathbf{z}, \mathbf{z}') \quad (34.8)$$

into an disconnected part  $G_{\text{dis}}^{(N)}$  which contains redundant information already present in lower-order correlations, and a connected part  $G_{\text{con}}^{(N)}$  which represents the genuine new information at order  $N$ . At the level of a field theory description of the many-body system to study  $G_{\text{con}}^{(N)}$  can be related to genuine  $\frac{N}{2}$  mode interactions that can not be decomposed into successive lower order interactions and are related to the non-perturbative sum off all diagrams of order  $N$ .

In a recent experiment [16] we have used high order phase correlations (Eq. 34.7) to demonstrate that two tunnel-coupled superfluids are a genuine quantum simulator for the quantum Sine-Gordon model. Analysing the phase correlation functions up to high order, and under which conditions they factorise allowed us to characterise the essential features of the model solely from our measurements, detect the relevant quasi-particles, their interactions and the topologically distinct vacuum states of the model. Analysing high order correlation functions and how they factorise thus provides a comprehensive and general method to analysing quantum many-body systems through experiments.

### **Full Distribution Functions**

Another powerful technique to analyse the properties of many-body states and their dynamics are the full distribution functions (FDF) of observables. The FDFs contain information about all order correlation functions. If they are Gaussian, then the correlations factorise.

From the interference pattern we can construct a variety of different full distribution functions. Filling phase and contrast in a polar plot (Fig. 34.3) allows to visualise the difference between de-coherence and de-phasing [104].

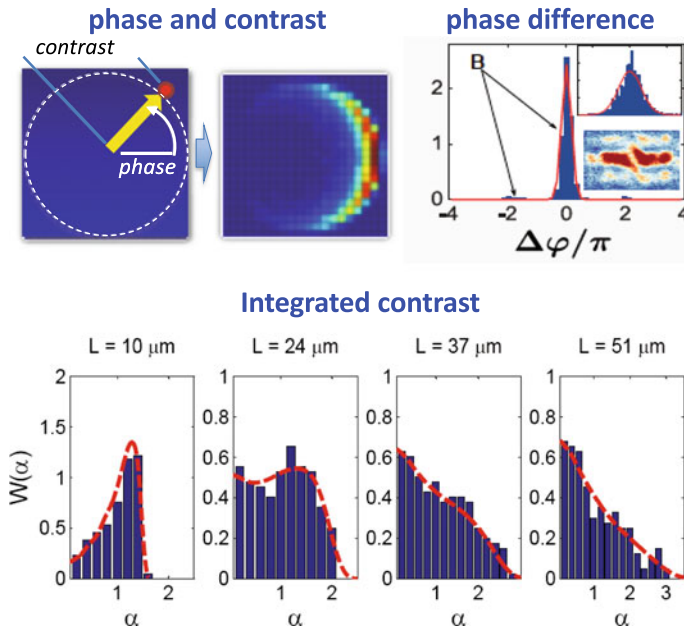


**Fig. 34.3 Full distribution functions.** From the evaluated phases one can construct the full distribution functions (FDF) of (left) phase and contrast [104] and (right) of phase difference [16]. The insert shows a direct image of a phase kink, the topological excitations of the Sine-Gordon model. The full distribution function of the integrated contrast (bottom). The measured FDF are in excellent agreement with FDF's calculated for thermal equilibrium [73].

A different FDF can be constructed from the contrast  $C(z) = \frac{I_{\max}(z) - I_{\min}(z)}{I_{\max}(z) + I_{\min}(z)}$  of the measured interference [73, 105, 106]. We define the operator  $\hat{A}(L) = \int_{-L/2}^{L/2} dz \hat{\Psi}_l^\dagger(z, t) \hat{\Psi}_l(z, t)$ . Its magnitude is related to the contrast  $C(L)$  of the interference pattern integrated over length  $L$  by  $\langle C^2(L) \rangle = \langle |\hat{A}(L)|^2 \rangle / n_{1D}^2 L^2$ . Experimentally the distribution of the squared contrast normalised by the mean squared contrast  $\alpha = C^2 / \langle |C|^2 \rangle$  is less prone to systematic errors and therefore favourable. Recording the shot-to-shot fluctuations of this quantity gives us the full distribution function  $W(\alpha)d\alpha$  of the probability to observe a contrast in the interval  $\alpha + d\alpha$ .

Similarly, the full distribution functions of the phase difference  $\Delta\varphi = \varphi(z_1) - \varphi(z_2)$  can reveal details about the excitations in a system [16]. Figure 34.3 (top, left) shows the triple peaked FDF of  $\Delta\varphi$  in the quantum Sine-Gordon model identifying sine-Gordon Solitons (or kinks), the topological excitations of this model.

### 34.3 Non-Equilibrium Dynamics and Relaxation in 1D Superfluids

We now give a schematic overview of our experiments investigating the non equilibrium dynamics of 1D superfluids. For details we refer to the original publications.

#### 34.3.1 Creating a Non-equilibrium State

Coherently splitting a single 1D Bose gas into two creates a non-equilibrium state [81, 82] (Fig. 34.4). The process of splitting is performed fast compared to the axial dynamics in the system ( $t_{\text{split}} < \xi_h/c$ ), which assures that no correlations can build up along the axial direction, consequently the splitting happens independently at each point in the gas. The process can be intuitively pictured as a local beam splitter where each atom is independently distributed into the left or right half of the new system. The corresponding probability distribution for the local number of particles  $N$  on each side is therefore binomial

$$P(N_l, N_r) = \binom{N_l + N_r}{N_l} p_1^{N_l} (1 - p_1)^{N_r}, \quad (34.9)$$

with  $p_1 = 1/2$  for a balanced splitting process. The resulting fluctuations in one half of the system are thus given by  $\text{Var}[N_{l,r}] = N p_1 (1 - p_1)$ , which translates into  $\langle |\Delta N|^2 \rangle = N/4$  for  $\Delta N = (N_l - N_r)/2$  in the balanced case.

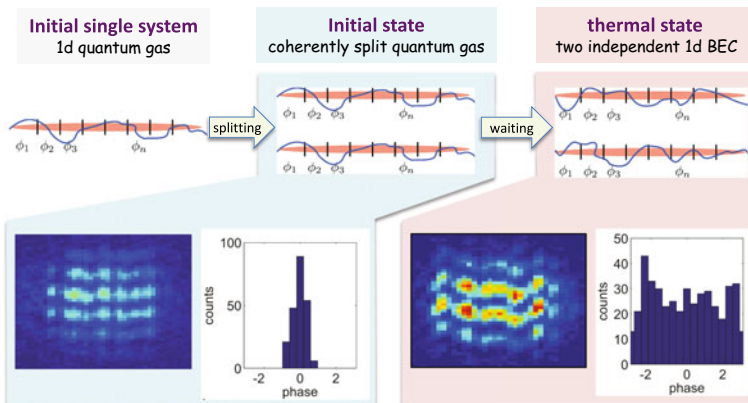


**Fig. 34.4 Creating a non equilibrium state.** We create a non equilibrium state by coherently splitting a 1D quantum gas. The coherently split state is characterised by straight fringes and  $\varphi(z) \sim 0$ . The final thermal state can be created by cooling two separate atom clouds into the two sides of the double well [79]. The resulting interference pattern shows strong phase fluctuations and a random global phase.

Once we can speak of two spatially separated systems we can perform a variable transformation to anti-symmetric and symmetric degrees of freedom, which will help us to better describe the quantum state after the splitting. In the following these will also be referred to as relative and common degrees of freedom (modes). Starting from the density and phase fluctuations in the left and right halves (denoted by  $\hat{n}_{l,r}(z)$  and  $\hat{\theta}_{l,r}(z)$ , respectively) we find for the anti-symmetric and symmetric degrees of freedom of the phase:

$$\begin{aligned}\hat{\phi}_{\text{as}}(z) &= \hat{\theta}_r(z) - \hat{\theta}_l(z) \\ \hat{\phi}_{\text{sy}}(z) &= \frac{\hat{\theta}_r(z) + \hat{\theta}_l(z)}{2}\end{aligned}\quad (34.10)$$

and for the density:

$$\begin{aligned}\hat{\nu}_{\text{as}}(z) &= \frac{\hat{n}_r(z) - \hat{n}_l(z)}{2} \\ \hat{\nu}_{\text{sy}}(z) &= \hat{n}_r(z) + \hat{n}_l(z)\end{aligned}\quad (34.11)$$

The usefulness of this approach becomes clear as we return to the shot noise, which now only enters in the relative number fluctuations

$$\langle \hat{\nu}_{\text{as}}(z) \hat{\nu}_{\text{as}}(z') \rangle = \frac{n_{\text{1D}}}{2} \delta(z - z'). \quad (34.12)$$

Here,  $n_{\text{1D}}$  denotes the mean density in a single gas after splitting. The corresponding shot-noise introduced to the phase quadrature of the relative modes goes with  $1/n_{\text{1D}}$  and is therefore negligible.

Returning to the Luttinger Hamiltonian (Eq. 34.2) we can identify the amount of energy  $\Delta E_{\text{quench}}$  that is introduced into each individual phononic mode during the splitting process as

$$\Delta E_{\text{quench}} = \frac{g_{\text{1D}} n_{\text{1D}}}{2} \quad (34.13)$$

which is typically smaller than the thermal energy of the initial gas. Moreover, this energy is only stored in the density quadrature of the relative degrees of freedom, while it should be equipartitioned between phase and density quadrature in thermal equilibrium.

The situation is different for the common degrees of freedom, which inherit all thermal excitations that were present in the initial gas before the splitting. The state created by splitting is thus also out of equilibrium. The common degrees of freedom contain the initial thermal energy, while the relative degrees of freedom contain only quantum shot-noise. In equilibrium both should be equally and thermally populated.

In experiment, the equilibrium situation can be realised by the transforming the harmonic trap into a double well while the Bose gas is still non degenerate.

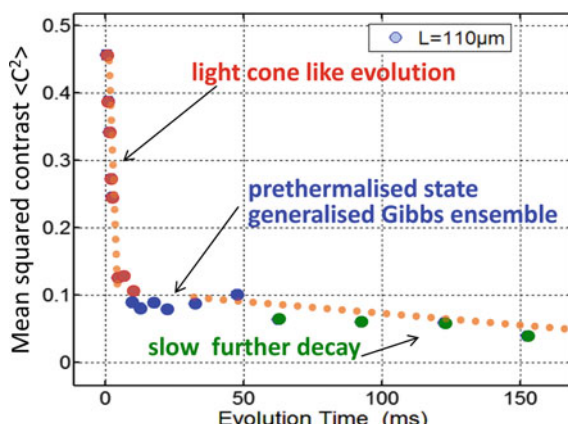
Subsequent evaporative cooling in both wells then results in two degenerate gases with no knowledge of each other, which corresponds exactly to thermal equilibrium. The experiment thus enables the unique possibility to contrast non-equilibrium and thermal states in identical settings.

It is interesting to note, that splitting a low dimensional system along the strongly confining transversal direction allows to study modes of a many body system that were initially empty, i.e. populated only by vacuum noise, corresponding to temperature  $T = 0$ . This is easily seen by looking at the evolution of the transverse excited states during the splitting of a double well. The ground state is directly connected to the symmetric mode of the double well, the first excited state to the anti-symmetric mode. In a 1D system of bosons at low enough temperature the first transverse excited state is not populated and therefore the anti symmetric mode in the double well is initially empty. This allows us to clearly see the quantum noise introduced by the quench.

### 34.3.2 Relaxation in a Isolated 1D Superfluid

We now describe our basic observations that lead to relaxation (Fig. 34.5) when bringing a 1D superfluid out of equilibrium by splitting (Fig. 34.4). For our experiments we implement a splitting quench as discussed above. This introduces quantum shot noise into the density quadrature  $\hat{\nu}_{\text{as}}(z)$  of the anti-symmetric degrees of freedom of the newly formed double wells. Our 1D superfluids are at the microscopic scale an interacting system. These fluctuations in the density add additional energy. This brings the system out of equilibrium and starts a de-phasing dynamics that leads to relaxation. This is best seen by looking at the excited modes in the anti-symmetric combination of the two 1D superfluids. The splitting excites phonons in the anti-symmetric degrees of freedom of the two 1D superfluids. These phonons are created

**Fig. 34.5 Relaxation of a split 1D quantum gas.** The basic features of the relaxation process after coherent splitting is best illustrated by looking at the contrast of the interference pattern integrated over the central 110  $\mu\text{m}$ . The coherence shows a fast decay towards the pre-thermalised quasi steady state and then a slow further evolution.



in the density quadrature (the fluctuations of the relative phase are minimal). Following a Luttinger liquid description these phonons will now evolve independently. A phonon of wave vector  $k$  and energy  $\hbar\omega_k$  rotates between density and phase quadrature with an frequency  $\omega_k$ . This will lead to a de-phasing of the phonon modes, since for each phonon the quadrature rotation between density and phase will proceed at a different speed. In interference experiments, we observe the phase quadrature of the phonons. The de-phasing of the phonons lead directly to a de-phasing and a loss of contrast in the observed interference pattern. A detailed theoretical derivation and discussion of these processes can be found in [81, 82], an application to a real world 1D superfluid in a harmonic longitudinal confinement in [107].

### Pre-thermlisation

We first discuss the state two 1D superfluids will relax to due to the de-phasing of the phonons introduced by the quantum noise of the splitting quench. A study of the full counting statistics of the interference contrast revealed that instead of relaxing to thermal equilibrium, the system relaxed to a long-lived pre-thermalised state [83]. In this quasi steady state, the system already shows thermal features characterised by an exponential decaying phase correlation function and thermal full distribution functions of contrast. This allows us to assign a temperature. Most remarkably this effective temperature  $T_{\text{eff}}$  is much lower then the initial temperature  $T_i$  of the 1D superfluid before splitting. This indicates that the relaxed state is still markedly different from thermal equilibrium.

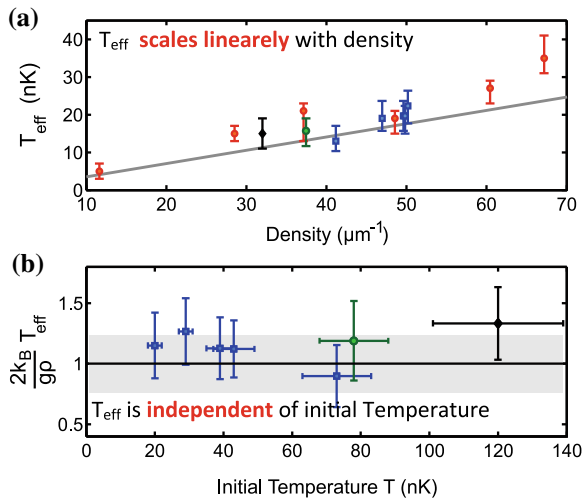
Following [81, 82] we find that the equipartition of energy between the  $k$ -modes introduced by the fast splitting, results in the relaxed quasi-steady state being indistinguishable from thermal equilibrium at some effective temperature

$$k_B T_{\text{eff}} = \frac{g_{1\text{D}} n_{1\text{D}}}{2}, \quad (34.14)$$

which is determined by the energy given to the relative degrees of freedom by the quantum shot noise introduced in the splitting. Remarkably  $T_{\text{eff}}$  only depends on the 1D density  $n_{1\text{D}}$  and is independent of the initial temperature  $T_i$ , as can be seen in Fig. 34.6a, b.

Looking at the system on different length scales reveals two regimes [104]. For short lengths  $L$ , the sparsely populated high momentum modes ( $k > 2\pi/L$ ) do not lead to a reduction of the interference contrast. This regime corresponds to phase-diffusion (spin diffusion, magnetisation diffusion). For large  $L$ , many modes satisfying  $k > 2\pi/L$  are populated and their dynamics leads to a scrambling of  $\phi(z)$  *within* the probed integration length, resulting in a significant reduction of the interference contrast. This is the contrast-decay (spin decay, magnetisation decay) regime. Between the two regimes there is a cross over length scale  $\lambda_{\text{eff}}$  which can be associated with the effective temperature  $T_{\text{eff}}$  by  $\lambda_{\text{eff}} = \hbar^2 \rho / m k_B T_{\text{eff}}$ .

**Fig. 34.6 Pre-thermalised state** **a)** The effective temperature  $T_{\text{eff}}$  of the pre-thermalised quasi steady state scales linearly with the initial 1D density. **b)** The effective temperature  $T_{\text{eff}}$  is independent of the initial temperature of the system before the splitting quench. Figure adapted from [83].



### Light-Cone Spreading of ‘de-coherence’

The pre-thermalised state emerges by de-phasing of the phonon modes created in their density quadrature by the splitting quench. This de-phasing and the emergence of the pre-thermal state can be seen best by looking at the phase correlation function  $C(z, z') = \langle e^{i\hat{\phi}(z) - i\hat{\phi}(z')} \rangle$ . The final pre-thermlised exponential decaying  $C(z - z')$  emerges locally and spreads throughout the system with the sound velocity as shown in Fig. 34.7. Outside this ‘horizon’ the long range order imprinted by the coherent splitting persists. This light-cone-like evolution was predicted by Calabrese and Cardy [108] and illustrates the spreading of correlations with a characteristic velocity and is directly connected to Lieb-Robinson bounds [109].

This light-cone like emergence of phase fluctuations after the splitting quench in our 1D system is analogous to the emergence of density fluctuations (Sacharov oscillations) after cosmic inflation. In the 1D superfluid the quench introduces density fluctuations which de-phase a uniform phase, in the case of Sacharov oscillations [110] the fluctuations introduced into the phase of a system with uniform density leads to the growth of density fluctuations by an analogous de-phasing.

### Generalized Gibbs Ensemble

Let us now turn to the statistical mechanics description of the relaxed state. It has been conjectured that the state which integrable systems relax to is a maximum entropy state under the constraints of the many conserved charges [112, 113]. Its associated density matrix is given by a generalized Gibbs ensemble (GGE) [31]

$$\hat{\rho} = \frac{1}{Z} e^{-\sum \lambda_j \hat{l}_j}. \quad (34.15)$$

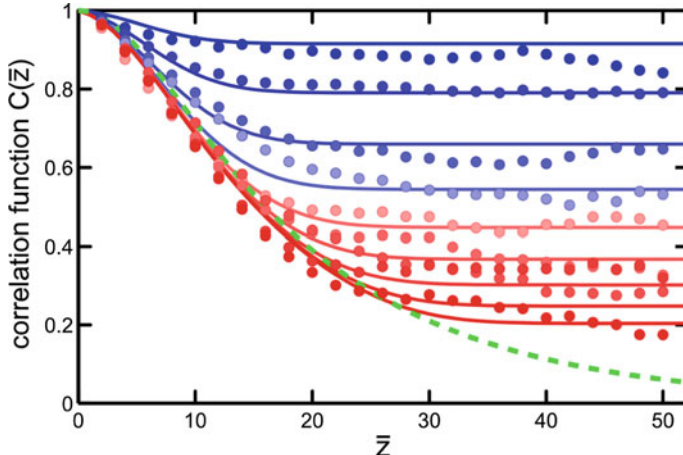


**Fig. 34.7 Light-cone like spreading of de-coherence:** The phase correlation function  $C(\bar{z}) = \langle e^{i\hat{\phi}(z)} - i\hat{\phi}(z+\bar{z}) \rangle$  characteristic for the pre-thermalised state appears locally in its final form and spreads throughout the system with a relaxation horizon. Outside the light-cone the long range order from the initially coherent splitting persist [111].  $C(\bar{z})$  is plotted for the first 1–9 ms of evolution (blue → red). Dots are the measurements, the lines depict the theoretical model convoluted with experimental resolution. Dashed green line represents the final prethermal correlations.

Here,  $Z$  is the partition function,  $\hat{I}_j$  are the operators of the conserved quantities and  $\lambda_j$  the corresponding Lagrange multipliers. If only energy is conserved this density matrix reduces to the well-known canonical or Gibbs ensemble, with  $\beta = 1/k_B T$  being the only Lagrange multiplier. If many more conserved quantities exist like the phonon occupations in the Luttinger liquid model describing the 1D superfluids, many Lagrange multipliers, one for each conserved quantity, restrict the possible ways in which entropy can be maximized.

The pre-thermalised state described above is a special case. The equipartition created by the fast splitting quench creates  $\lambda_j$  that can all be associated with the same effective temperature  $T_{\text{eff}}$ . Nevertheless the appearance of different temperatures in the common mode ( $T_{\text{com}}$  associated with the initial temperature  $T_i$ ) and the anti-symmetric mode ( $T_{\text{eff}}$ ) requires a GGE to describe the complete density matrix of the pre-thermalised system.

To illustrate the presence of a GGE directly it is necessary to change mode occupation numbers created by the splitting. That can be achieved by introducing a different splitting process. The non translation-invariant phase correlation function  $C(z_1, z_2) = \langle e^{i\hat{\phi}(z_1) - i\hat{\phi}(z_2)} \rangle$  characterises the system. A detailed analysis allows to extract the mode occupations that are necessary to describe the state [97]. Given these extracted occupation numbers the de-phasing model also provides a detailed description of the dynamics, which proves that the conserved quantities were indeed set during the splitting process. As seen in Fig. 34.8, the odd phonon modes have occupations that are significantly below the quantum shot noise of the pre-thermalised state, indicating strong squeezing of phonon modes created by the slower splitting.

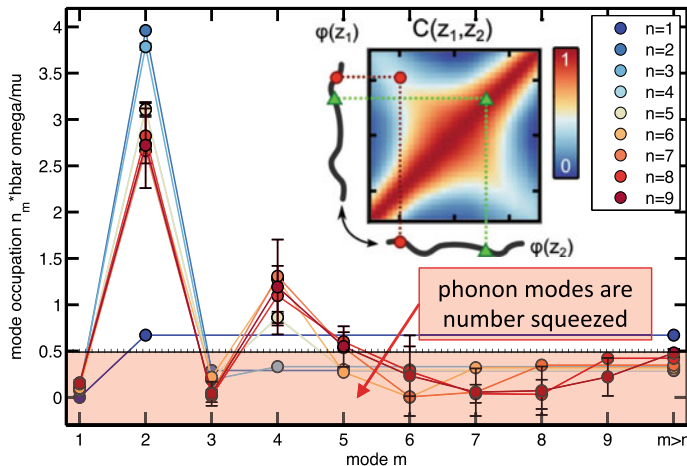


**Fig. 34.8 Generalised Gibbs ensemble:** Phonon occupation numbers normalised to the quantum noise of a fast (instantaneous) splitting as extracted from the non translation-invariant phase correlation function  $C(z_1, z_2) = \langle e^{i\hat{\phi}(z_1)-i\hat{\phi}(z_2)} \rangle$  shown as insert. The central red diagonal is the trivial auto correlation  $C(z, z) = 1$ . The two orthogonal lobes show enhanced correlations which are a direct consequence of the quantum state to be imprinted by the quench. The occupations of the lowest 9 modes can be extracted with statistical significance. Phonon modes with populations below the quantum shot noise are number squeezed. Figure adapted from [97].

These observations illustrate how the unitary evolution of our quantum many-body system can lead to the establishment of thermal properties. This does not mean that a true thermal state was reached, but rather that the expectation values of certain observables became indistinguishable from the corresponding thermal values. In this way the predictions of statistical and quantum mechanics are reconciled.

### Dynamics Beyond Pre-thermalisation

As demonstrated above, the 1D Bose gas, as an example of an integrable system, does not relax to thermal equilibrium but to a pre-thermalised state that can be described by a GGE. However, the 1D Bose gas, as realised in the experiments, is only nearly-integrable. In any realistic experimental setting this integrability will be broken at some level. In this case the observed pre-thermalised state is only an intermediate steady state on the way to thermal equilibrium. Experimental investigations into this effect are ongoing in our and other groups [115].

### 34.3.3 Recurrences

Poincaré and Zermelo, conjectured that a *finite* isolated physical system will recur arbitrarily close to its initial state after a sufficiently long but finite time [116, 117]. In quantum mechanics a general recurrence theorem has been proven [118, 119], explicitly showing that an arbitrary wave function  $\Psi(t) = \sum C_n e^{\frac{E_n}{\hbar} t} \Phi_n$  returns arbitrary close to its initial state ( $\Phi_n$  is the  $n$ th eigenfunction with energy  $E_n$ ).

A beautiful example of recurrences in a simple quantum system is the collapse and revivals in the Jaynes–Cummings model of a single atom interacting with a coherent radiation field [120, 121]. In interacting few-body systems collapse and revivals were observed for small samples of a few atoms trapped in optical lattices [122, 123]. For larger systems however, the complexity of the spectrum of eigenstates  $\{E_n\}$  leads to exceedingly long recurrence times, in general prohibiting their observation.

For many-body systems it becomes exponentially difficult to observe the eigenstates, and one probes them through much simpler (local) few-body observables  $\mathcal{O}$ . This suggests that the system does not have to come back close to the *exact* initial configuration of many-body states, but only needs to give the same measurement results under the evaluation of  $\mathcal{O}$ . Choosing an observable  $\mathcal{O}$  that connects to the collective degrees of freedom of an underlying effective quantum field theory description of the many body system dramatically reduces the complexity of the problem. Instead of dealing with a large number of constituents, one observes a much smaller number of populated modes. Designing the system such that the collective excitations have commensurate energies, the observation of recurrences becomes feasible even for many-body systems containing thousands of interacting particles [114].

In a 1D superfluid with harmonic longitudinal confinement  $\omega_{\parallel}$  the phonon modes are described by Legendre polynomials [124] and the  $j$ th mode oscillates with frequency  $\omega_j = \omega_{\parallel} \sqrt{j(j+1)/2}$  which shifts recurrences to very long times. For a 1D superfluid in a box like longitudinal confinement the phonon frequencies become commensurate  $\omega_j = \pi \frac{c}{L} j$  and the time between recurrences becomes  $t_{\text{rec}} = \frac{L}{c}$  [107]. Figure 34.9 shows the observation of recurrences by the reappearance of long range order in the phase correlation function [114].

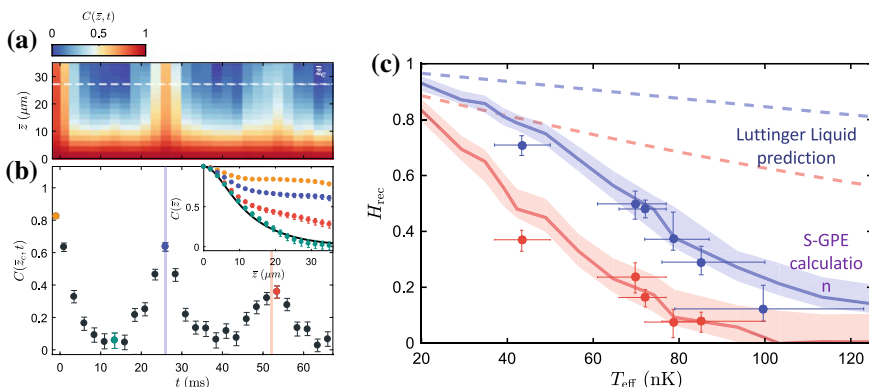


**Fig. 34.9 Observation of recurrences in long range order** **a)** The recurrence is seen by the recovery of long range order ( $C$  close to 1 over the whole distance). **b)** The lower graph shows the correlations at  $30 \mu\text{m}$ . The inset shows the full correlation function at selected points as indicated by the colour of the symbols. **c)** The recurrences decay faster than predicted from the Luttinger liquid with averaging about the measured initial state distribution. The decay is well described by a stochastic GPE calculation which naturally includes the interaction between the excited modes. The decay of recurrences is faster with higher temperature. Figures adapted from [114].

### 34.3.4 Outlook on Non-equilibrium Dynamics

Up to now each system is treated individually, and each time one works with a different system one has to start new to develop a model. One of the key challenges in non equilibrium many-body quantum physics is therefore to find universal descriptions that would allow us to characterise a whole class of systems. One intriguing description of non-equilibrium dynamics that surfaced in the last years relates to *non-thermal fixed points* of a Renormalisation Group (RG) evolution [125–127]. This is reminiscent of the description of second order phase transitions by the RG fixed-points [128]. The universal scaling connected to non-thermal fixed points was recently observed [129, 130].

We conjecture that the relaxation observed in 1D superfluids is universal for a large class of many-body systems: those where the relevant physics can be described by a set of ‘long lived’ collective modes and can be associated with a Gaussian non-thermal fix-point in the non-equilibrium evolution of a bosonic Luttinger liquid. The time window where the ‘close to integrable’ dynamics can be observed is given by the ‘lifetime’ of the quasi-particles associated with the collective modes. From a quantum field theory perspective, one can view such a many-body quantum system at  $T = 0$  as ‘vacuum’ and its ‘long lived’ collective modes as the excitations (particles) as the laboratory to experiment with.

## 34.4 Implementing Thermal Machines in 1D Superfluids

A 1D superfluid and its excitations are a very interesting model system for the interplay between quantum science and statistical mechanics. We will now give a brief outline, how one-dimensional superfluids will allow to implement simple thermal machines and thereby help to explore some of the intriguing effects of quantum physics on their workings. The essential new input is to deliberately structure and manipulate the 1D superfluid along its longitudinal directions to create different quantum systems that can be connected, disconnected and manipulated.

### 34.4.1 Implementing Arbitrary Designed Longitudinal Confinements

The longitudinal trapping potential can be designed and manipulated by applying an additional structured dipole potential to the existing atom chip trap which will still perform the transverse trapping and manipulation. A far blue detuned light field will create a conservative repulsive potential for the atoms. Applying the light field from a direction orthogonal to the 1D chip trap and structuring the applied light field will allow us to create a nearly arbitrary potential landscape along the trapped 1D

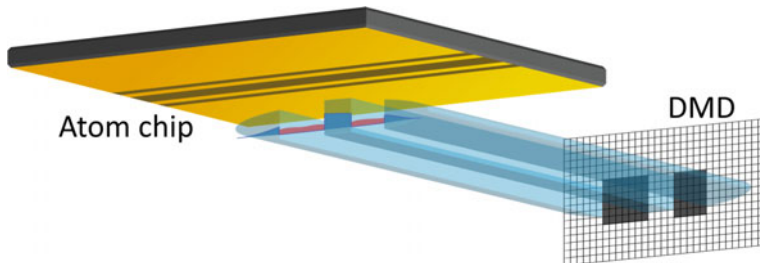


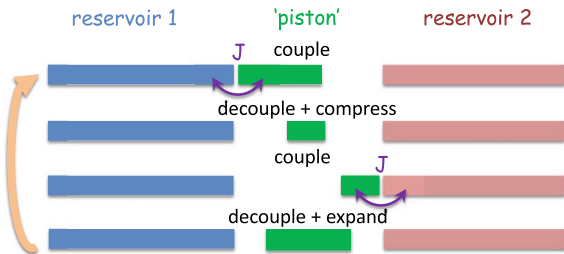
**Fig. 34.10 Controlled longitudinal potentials:** A designed light profile of a far detuned laser modifies the longitudinal confinement of the atom chip trap. The intensity profile at the chip trap is created by imaging a pattern created at a Digital Mirror Device (DMD).

superfluid (see Fig. 34.10). Using a far blue detuned light has the advantage that atoms are repelled from the light field and sit at low intensity regions which minimises the small remaining spontaneous light scattering (which would destroy coherence). In addition, the obtainable structure size is smaller for shorter wavelength. Moreover, the applied potentials can be small when compared to standard optical traps. We use these dipole potentials to ‘shape’ or ‘add’ features to the existing magnetic trap. Consequently, the applied potentials just have to be comparable to the interaction energy on the 1D superfluid. For example using a few 100 mW of 660 nm light (120 nm blue detuned from the Rb optical transitions at 780 nm) one can design 1D potential landscapes for a Rb quantum gas up to 1 mm long with negligible decoherence from spontaneous scattering.

Creating the dipole trap light fields to control an arbitrary 1D potential landscape requires beam shaping along a single spatial dimension. To realise this, the intensity (or the phase) of the light field has to be modified using a spatial light modulator (SLM). There are different kinds of SLMs to choose from. Our choice fell on the Digital Micro-mirror Device (DMD) which is a reflective SLM. DMDs are used in commercial projection devices and have sufficient spatial and intensity resolution to create up to 1 mm long potential landscapes in our experimental settings. The update timescale of 32  $\mu$ s is also much faster than the typical timescales associated with the excitations in the 1D superfluids ( $> 1$  ms). Examples where DMDs have been used successfully already to manipulate potential landscapes can be found in [131–135].

With this *dipole painting* we can deliberately structure the 1D superfluid along its longitudinal directions. This will allow us to create separate quantum systems that can take the role of the different components of a thermal machine (Fig. 34.11) like a *reservoir* or a *working fluid*. (Adiabatically) expanding them will cool them, (adiabatically) compressing will heat them. Coupling between different parts of a thermal machine can be achieved by connecting them or by a tunnel barrier. The strength of the coupling can be precisely adjusted by adjusting tunnel coupling  $J$  through the height and width of the barrier. This will allow us to build a series of different thermal processes and thermal machines for the quantum excitations in the 1D superfluids.

**Fig. 34.11 Implementing thermal machines in 1D superfluids:** Typical schema of decoupling, manipulation and recoupling a quantum working fluid (piston) to two reservoirs created by the light fields of the DMD.



### 34.4.2 Quantum Aspects in 1D Superfluid Machines

The experimental setting outlined above opens up a pathway to the study of novel thermodynamic schemes in many-body quantum systems. A specially interesting point is that the 1D superfluids used are close to an integrable point, where common assumptions on complete thermalisation are challenged.

**Non-Markovianity:** Integrable (non thermalising) systems keep a memory of their initial state and are therefore ideal candidates to implement aspects of non-markovianity. Our observation of recurrences in a many-body system of thousands of particles [114] points to a special interesting way to exploit this. Let us illustrate that with an example: If a system is decoupled at time  $t = 0$  from an 1D-reservoir then the role of the reservoir in a thermal machine cycle will strongly depend when the next ‘contact’ takes place. If the re-coupling is in between recurrences, the reservoir will be completely de-phased and have no memory of what happened during the last cycle. If the re-coupling is at the time of the recurrence, the reservoir will have (full) memory of what happened during the last cycle, and will behave maximally non-Markovian. Designing the longitudinal confinement in each part of the thermal machine will allow us to have (nearly) full control of the memory of selected states in the thermal machine at later times. This will allow us to design and probe a large variety of interesting Markovian and non-Markovian situations [136–139].

**Strong Coupling:** The coupling and de-coupling of two interacting many-body systems can be precisely controlled by the barrier between the two systems. On one hand weak coupling can be implemented by a small tunnel-coupling between the two superfluids. On the other maximally strong coupling is achieved by removing the barrier at all, that is joining the two systems. This will allow us to implement and probe a large variety of interesting coupling situations and their role in thermal processes and thermal machines [139–141].

**Entanglement:** The coupling and de-coupling of two interacting many-body systems is a direct way to entangle the two. The canonical system is the double well. When the de-coupling is slower than the time scale given by the interaction energy, the two systems will build up quantum correlations between them, which persist even if they are separated [84, 85, 142]. An indication that this also works for excitations in a many-body system is the observation of number squeezing in the modes created by

slow splitting in the GGE experiment [97] (see Fig. 34.8). This will allow us to probe things like anomalous heat flow [143–145].

**Quantum Noise:** Another distinct observation from our experiments is that disconnecting two systems creates quantum noise. Since this noise and the associated energy put into the system scales with  $\sqrt{N}$  it can be safely neglected in the thermodynamic limit. But for finite systems this additional energy will be visible, and might have a significant effect on efficiencies of quantum thermodynamic processes. If one reduces this noise, one automatically introduces quantum correlations and entanglement between the two systems.

**Role of knowledge in Thermodynamic Processes:** If we could measure the many-body eigenstates of our complete machine, we would have complete control. For any sizeable system of more than a few particles (or spins) this becomes impractical and we have to restrict ourselves to (local) few-body observables and a finite set of their correlations. This will define what we know and what we can use and what we don't know, we need to ignore. The first can in the widest sense be related to *work*, the latter to *heat* and entropy. Since we can choose what we measure, we can illuminate the role of knowledge in what is work and what is heat. In fact what is work and what is heat in a fully quantum sense of a unitary (many-body) machine will depend on the resources one can (want to) invest. Whether a system is a heat reservoir or a work reservoir just depends on what you personally know about it [8, 9, 146, 147]. The manipulation of 1D superfluids in simple (quantum) thermodynamic processes is an ideal testbed for these questions.

**Operating Two Parallel Machines:** The design and manipulation of the longitudinal confinement with the designed dipole trap works for both a single 1D system, and two 1D systems in our double well on the atom chip. This opens up the possibility to directly compare the operation of two identical machines. The initial states of these two systems can be: (i) Two completely independent systems created by cooling two separate cold atomic clouds into the two wells of the double well. (ii) Two systems that are de-phased in a pre-thermlised state, that is their relative phase temperature is given by the interaction energy and not the cooling. (iii) two systems with (nearly) identical phonon modes with the quantum noise in the anti-symmetric mode strongly suppressed. Such states have been achieved in our experiments [85, 97] and can be significantly improved by optimal control of the splitting process [87]. Such a setting would allow to directly probe the quantum noise introduced in the thermal processes.

**Quantum Sine-Gordon Model:** We can also implement the thermodynamic processes in two tunnel-coupled superfluids. Then the underlying quantum field theory model ins not a Luttinger liquid, but the quantum Sine-Gordon model. This will allow us to carry the studies of thermal machines in a wide range of settings, ranging from a free system of non interacting modes to very strongly correlated quantum systems which also exhibit topological excitations [16].

Over all experimenting with 1D atomic superfluids arbitrary controlled longitudinal confinement will open up a large variety of new experimental possibilities to implement on one hand the ‘classical’ thermal machines like a Otto cycle, a Carnot

machine or a refrigerator in well controlled many-body quantum systems, and on the other hand let us explore many more predicted novel quantum phenomena like anomalous heat flow etc . . . and hopefully find new ones.

### 34.5 Conclusion

Experiments with ultra-cold quantum gases (in general) and 1D Bose gases (in particular) allow the realisation and manipulation of well-controlled and truly isolated quantum systems. As we have shown, this provides unique opportunities to study and understand non-equilibrium phenomena. For example, the results discussed in these notes demonstrate for the first time several characteristic aspects of these dynamics, including the existence of a stable, thermal-like pre-thermalised state and its dynamical, light-cone-like emergence. Furthermore, the connection of the pre-thermalised state with generalised statistical ensembles highlights the connection between unitary quantum evolution and statistical mechanics.

Extending these experiments to arbitrary designing and manipulating the longitudinal confinement will open up many new possibilities to build thermodynamic processes and machines from nearly integrable quantum many-body systems. This will allow us to further probe and explore the role of quantum physics in (quantum) thermodynamic processes.

**Acknowledgements** I would like to thank all my collaborators during the last years for many illuminating discussions, especially the theory in Heidelberg: J. Berges, S. Erne, V. Kasper, and Th. Gasenzer, and my long term collaborators E. Demler and J. Eisert. M. Huber provided invaluable insight into the quantum to classical transition and towards the implementation of thermal machines with 1D superfluids. None of this would have been possible without the fatalistic effort of my group at the Atominstitut, special thanks to I. Mazets for keeping me on track in theoretical matters, T. Langen, B. Rauer and Th. Schweigler for making the experiments work and their deep insight into the related physics and Joao Sabino for help with the manuscript. This work was supported by the FWF through the SFB FoQuS, the DFG-FWF Forschergruppe 2427:Thermal machines in the quantum world and by the EU through the ERC advanced grant *Quantum-Relax*. JS acknowledges the hospitality of the Erwin Schrödinger Institut in the framework of their thematic program *Quantum Paths* which enabled many discussions shaping this article. Part of the research reviewed in this chapter was made possible by the COST MP1209 network *Thermodynamics in the quantum regime*.

## References

1. L. Boltzmann, Sitzungsberichte Akademie der Wissenschaften **66**, 275 (1872). [https://doi.org/10.1142/9781848161337\\_0015](https://doi.org/10.1142/9781848161337_0015)
2. J.V. Neumann, Z. Phys. **57**, 30 (1929). <https://doi.org/10.1007/BF01339852>
3. M. Srednicki, Phys. Rev. E **50**, 888 (1994). <https://doi.org/10.1103/PhysRevE.50.888>
4. M. Rigol, V. Dunjko, M. Olshanii, Nature **452**, 854 (2008). <https://doi.org/10.1038/nature06838>

5. A. Polkovnikov, K. Sengupta, A. Silva, M. Vengalattore, Rev. Mod Phys **83**, 863 (2011). <https://doi.org/10.1103/RevModPhys.83.863>
6. J. Eisert, M. Friesdorf, C. Gogolin, Nat. Phys. **11**, 124 (2015). <https://doi.org/10.1038/nphys3215>
7. C. Gogolin, J. Eisert, Rep. Prog. Phys. **79**, 56001 (2016). <https://doi.org/10.1088/0034-4885/79/5/056001>
8. J. Goold, M. Huber, A. Riera, L. del Rio, P. Skrzypczyk, J. Phys. A Math. Theor. **49**, 143001 (2016). <https://doi.org/10.1088/1751-8113/49/14/143001>
9. L. del Rio, L. Kraemer, R. Renner (2015). [arXiv:1511.08818](https://arxiv.org/abs/1511.08818)
10. L. Kofman, A. Linde, A. Starobinsky, Phys. Rev. Lett. **73**, 3195 (1994). <https://doi.org/10.1103/PhysRevLett.73.3195>
11. D. Podolsky, G.N. Felder, L. Kofman, M. Peloso, Phys. Rev. D **73**, 023501 (2006). <https://doi.org/10.1103/PhysRevD.73.023501>
12. P. Braun-Munzinger, D. Magestro, K. Redlich, J. Stachel, Phys. Lett. B **518**, 41 (2001). [https://doi.org/10.1016/S0370-2693\(01\)01069-3](https://doi.org/10.1016/S0370-2693(01)01069-3)
13. J. Berges, S. Borsányi, C. Wetterich, Phys. Rev. Lett. **93**, 142002 (2004). <https://doi.org/10.1103/PhysRevLett.93.142002>
14. M. Eckstein, M. Kollar, P. Werner, Phys. Rev. Lett. **103**, 056403 (2009). <https://doi.org/10.1103/PhysRevLett.103.056403>
15. M. Moeckel, St. Kehrein, New J. Phys. **12**, 055016 (2010). <https://doi.org/10.1088/1367-2630/12/5/055016>
16. T. Schweigler, V. Kasper, S. Erne, I. Mazets, B. Rauer, F. Cataldini, T. Langen, T. Gasenzer, J. Berges, J. Schmiedmayer, Nature **545**, 323 (2017). <https://doi.org/10.1038/nature22310>
17. B.P. Lanyon, C. Maier, M. Holzapfel, T. Baumgratz, C. Hempel, P. Jurcevic, I. Dhand, A.S. Buyskikh, A.J. Daley, M. Cramer, M.B. Plenio, R. Blatt, C.F. Roos, Nat. Phys. **13**, 1158 (2017). <https://doi.org/10.1038/NPHYS4244>
18. I. Bloch, J. Dalibard, W. Zwerger, Rev. Mod. Phys. **80**, 885 (2008). <https://doi.org/10.1103/RevModPhys.80.885>
19. T. Giamarchi, A.J. Millis, O. Parcollet, H. Saleur, L.F. Cugliandolo, *Strongly Interacting Quantum Systems out of Equilibrium: Lecture Notes of the Les Houches Summer School: Volume 99, August 2012*, vol. 99 (Oxford University Press, 2016). <https://doi.org/10.1093/acprof:oso/9780198768166.001.0001>
20. T. Langen, R. Geiger, J. Schmiedmayer, Ann. Rev. Cond. Mat. Phys. **6**, 201 (2015). <https://doi.org/10.1146/annurev-conmatphys-031214-014548>
21. T. Giamarchi, *Quantum Physics in One Dimension* (Clarendon Press, Oxford, 2004). <https://doi.org/10.1093/acprof:oso/9780198525004.001.0001>
22. M.A. Cazalilla, R. Citro, T. Giamarchi, E. Orignac, M. Rigol, Rev. Mod. Phys. **83**, 1405 (2011). <https://doi.org/10.1103/RevModPhys.83.1405>
23. N.D. Mermin, H. Wagner, Phys. Rev. Lett. **17**, 1133 (1966). <https://doi.org/10.1103/PhysRevLett.17.1133>
24. D.S. Petrov, G.V. Shlyapnikov, J.T.M. Walraven, Phys. Rev. Lett. **85**, 3745 (2000). <https://doi.org/10.1103/PhysRevLett.85.3745>
25. K.V. Kheruntsyan, D.M. Gangardt, P.D. Drummond, G.V. Shlyapnikov, Phys. Rev. Lett. **91**, 040403 (2003). <https://doi.org/10.1103/PhysRevLett.91.040403>
26. T. Langen, Non-equilibrium dynamics of one-dimensional bose gases, Ph.D. thesis, Vienna University of Technology (2013)
27. E.H. Lieb, W. Liniger, Phys. Rev. **130**, 1605 (1963). <https://doi.org/10.1103/PhysRev.130.1605>
28. E.H. Lieb, Phys. Rev. **130**, 1616 (1963). <https://doi.org/10.1103/PhysRev.130.1616>
29. C.N. Yang, J. Mat. Phys. **10**, 1115 (1969). <https://doi.org/10.1063/1.1664947>
30. B. Sutherland, *Beautiful Models: 70 Years of Exactly Solved Quantum Many-body Problems* (World Scientific, 2004). <https://doi.org/10.1142/5552>
31. M. Rigol, V. Dunjko, V. Yurovsky, M. Olshanii, Phys. Rev. Lett. **98**, (2007). <https://doi.org/10.1103/PhysRevLett.98.050405>

32. J.-S. Caux, F.H.L. Essler, Phys. Rev. Lett. **110**, 257203 (2013). <https://doi.org/10.1103/PhysRevLett.110.257203>
33. L. Tonks, Phys. Rev. **50**, 955 (1936). <https://doi.org/10.1103/PhysRev.50.955>
34. M. Girardeau, J. Math. Phys. **1**, 516 (1960). <https://doi.org/10.1063/1.1703687>
35. M. Olshanii, Phys. Rev. Lett. **81**, 938 (1998). <https://doi.org/10.1103/PhysRevLett.81.938>
36. B. Paredes, A. Widera, V. Murg, O. Mandel, S. Fölling, I. Cirac, G.V. Shlyapnikov, T.W. Hänsch, I. Bloch, Nature **429**, 277 (2004). <https://doi.org/10.1038/nature02530>
37. T. Kinoshita, T. Wenger, D.S. Weiss, Science **305**, 1125 (2004). <https://doi.org/10.1126/science.1100700>
38. F.D.M. Haldane, Phys. Rev. Lett. **47**, 1840 (1981). <https://doi.org/10.1103/PhysRevLett.47.1840>
39. S.-I. Tomonaga, Prog. Theor. Phys. **5**, 544 (1950). <https://doi.org/10.1143/ptp/5.4.544>
40. J.M. Luttinger, J. Math. Phys. **4**, 1154 (1963). <https://doi.org/10.1063/1.1704046>
41. D.C. Mattis, E.H. Lieb, J. Math. Phys. **6**, 304 (1965). <https://doi.org/10.1063/1.1704281>
42. A. Imambekov, T.L. Schmidt, L.I. Glazman, Rev. Mod. Phys. **84**, 1253 (2012). <https://doi.org/10.1103/RevModPhys.84.1253>
43. M. Bockrath, D.H. Cobden, J. Lu, A.G. Rinzler, R.E. Smalley, L. Balents, P.L. McEuen, Nature **397**, 598 (1999). <https://doi.org/10.1038/17569>
44. C. Blumenstein, J. Schäfer, S. Mietke, S. Meyer, A. Dollinger, M. Lochner, X.Y. Cui, L. Patthey, R. Matzdorf, R. Claessen, Nat. Phys. **7**, 76 (2011). <https://doi.org/10.1038/nphys2051>
45. Y. Jompol, C. Ford, J. Griffiths, I. Farrer, G. Jones, D. Anderson, D. Ritchie, T. Silk, A. Schofield, Science **325**, 597 (2009). <https://doi.org/10.1126/science.1171769>
46. V.V. Deshpande, M. Bockrath, L.I. Glazman, A. Yacoby, Nature **464**, 209 (2010). <https://doi.org/10.1038/nature08918>
47. S. Coleman, Phys. Rev. D **11**, 2088 (1975). <https://doi.org/10.1103/PhysRevD.11.2088>
48. S. Mandelstam, Phys. Rev. D **11**, 3026 (1975). <https://doi.org/10.1103/PhysRevD.11.3026>
49. W.E. Thirring, Ann. Phys. **3**, 91 (1958). [https://doi.org/10.1016/0003-4916\(58\)90015-0](https://doi.org/10.1016/0003-4916(58)90015-0)
50. L.D. Faddeev, V.E. Korepin, Phys. Rep. **42**, 1 (1978). [https://doi.org/10.1016/0370-1573\(78\)90058-3](https://doi.org/10.1016/0370-1573(78)90058-3)
51. J. Cuevas-Maraver, P.G. Kevrekidis, F. Williams (eds.), *The Sine-Gordon Model and its Applications*, Nonlinear systems and complexity (Springer International Publishing, Switzerland, 2014). <https://doi.org/10.1007/978-3-319-06722-3>
52. M.B. Fogel, S.E. Trullinger, A.R. Bishop, J.A. Krumhansl, Phys. Rev. B **15**, 1578 (1977). <https://doi.org/10.1103/PhysRevB.15.1578>
53. V. Gritsev, A. Polkovnikov, E. Demler, Phys. Rev. B **75**, 174511 (2007). <https://doi.org/10.1103/PhysRevB.75.174511>
54. A.N. Kolmogorov, Dokl. Akad. Nauk SSSR **98**, 527 (1954), <http://cds.cern.ch/record/430016>
55. G.P. Brandino, J.-S. Caux, R.M. Konik, Phys. Rev. X **5**, 041043 (2015). <https://doi.org/10.1103/PhysRevX.5.041043>
56. I.E. Mazets, Eur. Phys. J. D **65**, 43 (2011). <https://doi.org/10.1140/epjd/e2010-10637-5>
57. I.E. Mazets, T. Schumm, J. Schmiedmayer, Phys. Rev. Lett. **100**, 210403 (2008). <https://doi.org/10.1103/PhysRevLett.100.210403>
58. I.E. Mazets, J. Schmiedmayer, Phys. Rev. A **79**, 061603 (2009). <https://doi.org/10.1103/PhysRevA.79.061603>
59. I.E. Mazets, J. Schmiedmayer, New J. Phys. **12**, 055023 (2010). <https://doi.org/10.1088/1367-2630/12/5/055023>
60. S. Tan, M. Pustilnik, L.I. Glazman, Phys. Rev. Lett. **105**, 090404 (2010). <https://doi.org/10.1103/PhysRevLett.105.090404>
61. Y. Tang, W. Kao, K.-Y. Li, S. Seo, K. Mallayya, M. Rigol, S. Gopalakrishnan, B.L. Lev, Phys. Rev. X **8**, 021030 (2018). <https://doi.org/10.1103/PhysRevX.8.021030>
62. P. Krüger, S. Hofferberth, I.E. Mazets, I. Lesanovsky, J. Schmiedmayer, Phys. Rev. Lett. **105**, 265302 (2010). <https://doi.org/10.1103/PhysRevLett.105.265302>
63. J.-F. Riou, L.A. Zundel, A. Reinhard, D.S. Weiss, Phys. Rev. A **90**, 033401 (2014). <https://doi.org/10.1103/PhysRevA.90.033401>

64. C. Li, T. Zhou, I. Mazets, H.-P. Stimming, Z. Zhu, Y. Zhai, W. Xiong, X. Zhou, X. Chen, J. Schmiedmayer (2018). [arXiv:1804.01969](https://arxiv.org/abs/1804.01969)
65. E. Haller, M. Mark, R. Hart, J.G. Danzl, L. Reichsöllner, V. Melezik, P. Schmelcher, H.-C. Nägerl, Phys. Rev. Lett. **104**, 153203 (2010). <https://doi.org/10.1103/PhysRevLett.104.153203>
66. S. Dettmer, D. Hellweg, P. Ryytty, J. Arlt, W. Ertmer, K. Sengstock, D.S. Petrov, G. Shlyapnikov, H. Kreutzmann, L. Santos, M. Lewenstein, Phys. Rev. Lett. **87**, 160406 (2001). <https://doi.org/10.1103/PhysRevLett.87.160406>
67. J. Billy, V. Josse, Z. Zuo, A. Bernard, B. Hambrecht, P. Lugan, D. Clément, L. Sanchez-Palencia, P. Bouyer, A. Aspect, Nature **453**, 891 (2008). <https://doi.org/10.1038/nature07000>
68. F. Serwane, G. Zürn, T. Lompe, T.B. Ottenstein, A.N. Wenz, S. Jochim, Science **322**, 336 (2011). <https://doi.org/10.1126/science.1201351>
69. T. Kinoshita, T. Wenger, D. Weiss, Nature **440**, 900 (2006). <https://doi.org/10.1038/nature04693>
70. O. Morsch, M. Oberthaler, Rev. Mod. Phys. **78**, 179 (2006). <https://doi.org/10.1103/RevModPhys.78.179>
71. R. Folman, P. Kruger, J. Schmiedmayer, J. Denschlag, C. Henkel, Adv. At. Mol. Opt. Phys. **48**, 263 (2002). [https://doi.org/10.1016/S1049-250X\(02\)80011-8](https://doi.org/10.1016/S1049-250X(02)80011-8)
72. J. Reichel, V. Vuletić (eds.), *Atom Chips* (Wiley, VCH, 2011). <https://doi.org/10.1002/9783527633357>
73. S. Hofferberth, I. Lesanovsky, T. Schumm, A. Imambeikov, V. Gritsev, E. Demler, J. Schmiedmayer, Nat. Phys. **4**, 489 (2008). <https://doi.org/10.1038/nphys941>
74. T. Jacqmin, J. Armijo, T. Berrada, K.V. Kheruntsyan, I. Bouchoule, Phys. Rev. Lett. **106**, 230405 (2011). <https://doi.org/10.1103/PhysRevLett.106.230405>
75. R. Schley, A. Berkovitz, S. Rinott, I. Shammass, A. Blumkin, J. Steinhauer, Phy. Rev. Lett. **111**, 055301 (2013). <https://doi.org/10.1103/PhysRevLett.111.055301>
76. B. Rauer, P. Grisins, I.E. Mazets, T. Schweigler, W. Rohringer, R. Geiger, T. Langen, J. Schmiedmayer, Phys. Rev. Lett. **116**, 030402 (2016). <https://doi.org/10.1103/PhysRevLett.116.030402>
77. P. Grisins, B. Rauer, T. Langen, J. Schmiedmayer, I.E. Mazets, Phys. Rev. A **93**, 033634 (2016). <https://doi.org/10.1103/PhysRevA.93.033634>
78. T. Schumm, S. Hofferberth, L.M. Andersson, S. Wildermuth, S. Groth, I. Bar-Joseph, J. Schmiedmayer, P. Kruger, Nat. Phys. **1**, 57 (2005). <https://doi.org/10.1038/nphys125>
79. S. Hofferberth, I. Lesanovsky, B. Fischer, J. Verdu, J. Schmiedmayer, Nat. Phys. **2**, 710 (2006). <https://doi.org/10.1038/nphys420>
80. I. Lesanovsky, T. Schumm, S. Hofferberth, L.M. Andersson, P. Krüger, J. Schmiedmayer, Phys. Rev. A **73**, 033619 (2006). <https://doi.org/10.1103/PhysRevA.73.033619>
81. T. Kitagawa, S. Pielawa, A. Imambeikov, J. Schmiedmayer, V. Gritsev, E. Demler, Phys. Rev. Lett. **104**, 255302 (2010). <https://doi.org/10.1103/PhysRevLett.104.255302>
82. T. Kitagawa, A. Imambeikov, J. Schmiedmayer, E. Demler, New. J. Phys. **13**, 073018 (2011). <https://doi.org/10.1088/1367-2630/13/7/073018>
83. M. Gring, M. Kuhnert, T. Langen, T. Kitagawa, B. Rauer, M. Schreitl, I.E. Mazets, D.A. Smith, E. Demler, J. Schmiedmayer, Science **337**, 1318 (2012). <https://doi.org/10.1126/science.1224953>
84. J. Estève, C. Gross, A. Weller, S. Giovanazzi, M.K. Oberthaler, Nature **455**, 1216 (2008). <https://doi.org/10.1038/nature07332>
85. T. Berrada, S.V. Frank, R. Bücker, T. Schumm, J.-F. Schaff, J. Schmiedmayer, Nat. Commun. 2077 (2013). <https://doi.org/10.1038/ncomms3077>
86. U. Hohenester, P.K. Rekdal, A. Borzì, J. Schmiedmayer, Phys. Rev. A **75**, 023602 (2007). <https://doi.org/10.1103/PhysRevA.75.023602>
87. J. Grond, J. Schmiedmayer, U. Hohenester, Phys. Rev. A **79**, 021603 (2009a). <https://doi.org/10.1103/PhysRevA.79.021603>
88. J. Grond, G. von Winckel, J. Schmiedmayer, U. Hohenester, Phys. Rev. A **80**, 053625 (2009b). <https://doi.org/10.1103/PhysRevA.80.053625>

89. W. Ketterle, D. Durfee, D. Stamper-Kurn, Bose-Einstein condensation in atomic gases, in *Proceedings of the International School of Physics Enrico Fermi*
90. D.A. Smith, S. Aigner, S. Hofferberth, M. Gring, M. Andersson, S. Wildermuth, P. Krüger, S. Schneider, T. Schumm, J. Schmiedmayer, Opt. Express **19**, 8471 (2011). <https://doi.org/10.1364/OE.19.008471>
91. R. Bücker, A. Perrin, S. Manz, T. Betz, C. Koller, T. Plisson, J. Rottmann, T. Schumm, J. Schmiedmayer, New J. Phys. **11**, 103039 (2009). <https://doi.org/10.1088/1367-2630/11/10/103039>
92. A. Imambekov, I.E. Mazets, D.S. Petrov, V. Gritsev, S. Manz, S. Hofferberth, T. Schumm, E. Demler, J. Schmiedmayer, Phys. Rev. A **80**, 033604 (2009). <https://doi.org/10.1103/PhysRevA.80.033604>
93. S. Manz, R. Bücker, T. Betz, C. Koller, S. Hofferberth, I.E. Mazets, A. Imambekov, E. Demler, A. Perrin, J. Schmiedmayer, T. Schumm, Phys. Rev. A **81**, 031610 (2010). <https://doi.org/10.1103/PhysRevA.81.031610>
94. I.E. Mazets, Phys. Rev. A **86**, 055603 (2012). <https://doi.org/10.1103/PhysRevA.86.055603>
95. J. Schwinger, Proc. Natl. Acad. Sci. **37**, 452 (1951a). <https://doi.org/10.1073/pnas.37.7.452>
96. J. Schwinger, Proc. Natl. Acad. Sci. **37**, 455 (1951b). <https://doi.org/10.1073/pnas.37.7.455>
97. T. Langen, S. Erne, R. Geiger, B. Rauer, T. Schweigler, M. Kuhnert, W. Rohringer, I.E. Mazets, T. Gasenzer, J. Schmiedmayer, Science **348**, 207 (2015b). <https://doi.org/10.1126/science.1257026>
98. J. Steinhauer, Nat. Phys. **12**, 959 (2016). <https://doi.org/10.1038/nphys3863>
99. E. Altman, E. Demler, M.D. Lukin, Phys. Rev. A **70**, 013603 (2004). <https://doi.org/10.1103/PhysRevA.70.013603>
100. S. Fölling, F. Gerbier, A. Widera, O. Mandel, T. Gericke, I. Bloch, Nature **434**, 481 (2005). <https://doi.org/10.1038/nature03500>
101. T. Rom, T. Best, D. van Oosten, U. Schneider, S. Fölling, B. Paredes, I. Bloch, Nature **444**, 733 (2006). <https://doi.org/10.1038/nature05319>
102. T. Jeltes, J.M. McNamara, W. Hogervorst, W. Vassen, V. Krachmalnicoff, M. Schellekens, A. Perrin, H. Chang, D. Boiron, A. Aspect, C.I. Westbrook, Nature **445**, 402 (2007). <https://doi.org/10.1038/nature05513>
103. A. Perrin, R. Bücker, S. Manz, T. Betz, C. Koller, T. Plisson, T. Schumm, J. Schmiedmayer, Nat. Phys. **8**, 195 (2012). <https://doi.org/10.1038/nphys2212>
104. M. Kuhnert, R. Geiger, T. Langen, M. Gring, B. Rauer, T. Kitagawa, E. Demler, D. Adu Smith, J. Schmiedmayer, Phys. Rev. Lett. **110**, 090405 (2013). <https://doi.org/10.1103/PhysRevLett.110.090405>
105. V. Gritsev, E. Altman, E. Demler, A. Polkovnikov, Nat. Phys. **2**, 705 (2006). <https://doi.org/10.1038/nphys410>
106. A. Polkovnikov, E. Altman, E. Demler, Proc. Natl. Acad. Sci. **103**, 6125 (2006). <https://doi.org/10.1073/pnas.0510276103>
107. R. Geiger, T. Langen, I. Mazets, J. Schmiedmayer, New J. Phys. **16**, 053034 (2014). <https://doi.org/10.1088/1367-2630/16/5/053034>
108. P. Calabrese, J. Cardy, Phys. Rev. Lett. **96**, 136801 (2006). <https://doi.org/10.1103/PhysRevLett.96.136801>
109. E.H. Lieb, D.W. Robinson, Commun. Math. Phys. **28**, 251 (1972). <https://doi.org/10.1007/BF01645779>
110. C.-L. Hung, V. Gurarie, C. Chin, Science **341**, 1213 (2013). <https://doi.org/10.1126/science.1237557>
111. T. Langen, R. Geiger, M. Kuhnert, B. Rauer, J. Schmiedmayer, Nat. Phys. **9**, 640 (2013). <https://doi.org/10.1038/nphys2739>
112. E.T. Jaynes, Phys. Rev. **106**, 620 (1957a). <https://doi.org/10.1103/PhysRev.106.620>
113. E.T. Jaynes, Phys. Rev. **108**, 171 (1957b). <https://doi.org/10.1103/PhysRev.108.171>
114. B. Rauer, S. Erne, T. Schweigler, F. Cataldini, M. Tajik, J. Schmiedmayer, Science **359**, (2018). <https://doi.org/10.1126/science.aan7938>
115. D. Weiss (private communication)

116. H. Poincaré, Acta Math. **13**, 1 (1890). <https://doi.org/10.1007/BF02392506>
117. E. Zermelo, Annalen der Physik **293**, 485 (1896). <https://doi.org/10.1002/andp.18962930314>
118. P. Bocchieri, A. Loinger, Phys. Rev. **107**, 337 (1957). <https://doi.org/10.1103/PhysRev.107.337>
119. I.C. Percival, J. Math. Phys. **2**, 235 (1961). <https://doi.org/10.1063/1.1703705>
120. F.W. Cummings, Phys. Rev. **140**, A1051 (1965). <https://doi.org/10.1103/PhysRev.140.A1051>
121. G. Rempe, H. Walther, N. Klein, Phys. Rev. Lett. **58**, 353 (1987). <https://doi.org/10.1103/PhysRevLett.58.353>
122. M. Greiner, O. Mandel, T. Hänsch, I. Bloch, Nature **419**, 51 (2002). <https://doi.org/10.1038/nature00968>
123. S. Will, T. Best, U. Schneider, L. Hackermüller, D.-S. Lühmann, I. Bloch, Nature **465**, 197 (2010). <https://doi.org/10.1038/nature09036>
124. D.S. Petrov, D.M. Gangardt, G.V. Shlyapnikov, J. Phys. IV France **116**, 5 (2004). <https://doi.org/10.1051/jp4:2004116001>
125. J. Berges, A. Rothkopf, J. Schmidt, Phys. Rev. Lett. **101**, 041603 (2008). <https://doi.org/10.1103/PhysRevLett.101.041603>
126. M. Schmidt, S. Erne, B. Nowak, D. Sexty, T. Gasenzer, New J. Phys. **14**, 075005 (2012). <https://doi.org/10.1088/1367-2630/14/7/075005>
127. B. Nowak, S. Erne, M. Karl, J. Schole, D. Sexty, T. Gasenzer, Strongly interacting quantum systems out of equilibrium. Lecture Notes of the Les Houches Summer School, **99** (2013). [arXiv:1302.1448](https://arxiv.org/abs/1302.1448)
128. J. Zinn-Justin, *Quantum Field Theory and Critical Phenomena*, International series of monographs on physics (2002). <https://doi.org/10.1093/acprof:oso/9780198509233.001.0001>
129. M. Prüfer et al., Observation of universal quantum dynamics far from equilibrium. Nature **563**, 217–220 (2018). <https://doi.org/10.1038/s41586-018-0659-0>
130. S. Erne, R. Bücker, T. Gasenzer, J. Berges, J. Schmiedmayer, Observation of universal dynamics in an isolated one-dimensional Bose gas far from equilibrium. Nature **563**, 225 (2018). <https://doi.org/10.1038/s41586-018-0667-0>
131. L.-C. Ha, L.W. Clark, C.V. Parker, B.M. Anderson, C. Chin, Phys. Rev. Lett. **114**, 055301 (2015). <https://doi.org/10.1103/PhysRevLett.114.055301>
132. G. Gauthier, I. Lenton, N. McKay Parry, M. Baker, M.J. Davis, H. Rubinsztein-Dunlop, T.W. Neely, Optica **3**, 1136 (2016). <https://doi.org/10.1364/OPTICA.3.001136>
133. P. Zupancic, P.M. Preiss, R. Ma, A. Lukin, M.E. Tai, M. Rispoli, R. Islam, M. Greiner, Opt. Express **24**, 13881 (2016). <https://doi.org/10.1364/OE.24.013881>
134. M. Aidelsburger, J.L. Ville, R. Saint-Jalm, S. Nascimbène, J. Dalibard, J. Beugnon, Phys. Rev. Lett. **119**, 190403 (2017). <https://doi.org/10.1103/PhysRevLett.119.190403>
135. A.L. Gaunt, T.F. Schmidutz, I. Gotlibovich, R.P. Smith, Z. Hadzibabic, Phys. Rev. Lett. **110**, 200406 (2013). <https://doi.org/10.1103/PhysRevLett.110.200406>
136. M. Pezzutto, M. Paternostro, Y. Omar, New J. Phys. **18**, 123018 (2016). <https://doi.org/10.1088/1367-2630/18/12/123018>
137. P.P. Hofer, M. Perarnau-Llobet, L.D.M. Miranda, G. Haack, R. Silva, J.B. Brask, N. Brunner, New J. Phys. **19**, 123037 (2017). <https://doi.org/10.1088/1367-2630/aa964f>
138. J.O. González, L.A. Correa, G. Nocerino, J.P. Palao, D. Alonso, G. Adesso, Open Syst. Inf. Dyn. **24**, 1740010 (2017). <https://doi.org/10.1142/S1230161217400108>
139. R. Uzdin, A. Levy, R. Kosloff, Entropy **18**, 124 (2016). <https://doi.org/10.3390/e18040124>
140. M. Perarnau-Llobet, H. Wilming, A. Riera, R. Gallego, J. Eisert, Phys. Rev. Lett. **120**, 120602 (2018). <https://doi.org/10.1103/PhysRevLett.120.120602>
141. S. Seah, S. Nimmrichter, V. Scarani, Phys. Rev. E **98**, 012131 (2018). <https://doi.org/10.1103/PhysRevE.98.012131>
142. G.-B. Jo, Y. Shin, S. Will, T.A. Pasquini, M. Saba, W. Ketterle, D.E. Pritchard, M. Bengalattore, M. Prentiss, Phys. Rev. Lett. **98**, 030407 (2007). <https://doi.org/10.1103/PhysRevLett.98.030407>
143. D. Jennings, T. Rudolph, Phys. Rev. E **81**, 061130 (2010). <https://doi.org/10.1103/PhysRevE.81.061130>

144. S. Jevtic, D. Jennings, T. Rudolph, Phys. Rev. Lett. **108**, 110403 (2012). <https://doi.org/10.1103/PhysRevLett.108.110403>
145. L. del Rio, A. Hutter, R. Renner, S. Wehner, Phys. Rev. E **94**, 022104 (2016). <https://doi.org/10.1103/PhysRevE.94.022104>
146. M. Perarnau-Llobet, K.V. Hovhannisyan, M. Huber, P. Skrzypczyk, N. Brunner, A. Acín, Phys. Rev. X **5**, 041011 (2015). <https://doi.org/10.1103/PhysRevX.5.041011>
147. N. Brunner, M. Huber, N. Linden, S. Popescu, R. Silva, P. Skrzypczyk, Phys. Rev. E **89**, 032115 (2014). <https://doi.org/10.1103/PhysRevE.89.032115>

# Chapter 35

## Single Particle Thermodynamics with Levitated Nanoparticles



James Millen and Jan Gieseler

### Introduction

The first demonstration of the stable 3D optical trapping of micron-scale particles was in the 1980s [1], and since then there has been an explosion of research using “optical tweezers”, to the point that they are an off-the-shelf tool for physical and biological scientists. Using this system, it is possible to control and track the motion of mesoscopic objects with astounding precision. The first investigation of a microscopic thermodynamic process with an optically trapped particle was the realization of a Brownian ratchet [2] and there was a strong increase of activity following the foundation of stochastic thermodynamics [3] and the discovery of fluctuation theorems such as the Jarzynski equality, with Seifert describing trapped colloidal particles as “*the paradigm for the field (of stochastic thermodynamics)*”.

So, what makes the trapped microparticle such a good platform for thermodynamic studies? First and foremost, its characteristic energy is comparable to that of the thermal fluctuations of the bath  $\sim k_B T_{\text{env}}$ . These small particles in harmonic optical potentials are simple, and considering only the centre-of-mass motion is for most cases sufficient to fully describe their behaviour.<sup>1</sup> Having few degrees of freedom enhances the relative role of thermal fluctuations via the central limit theorem: energy

---

<sup>1</sup>Recent work with levitated nanoparticles also considers rotational degrees of freedom [4].

J. Millen (✉)  
Department of Physics, King’s College London, Strand, London WC2R  
2LS, UK  
e-mail: james.millen@kcl.ac.uk

J. Gieseler  
Department of Physics, Harvard University, 17 Oxford Street,  
Cambridge, MA 02138, USA  
e-mail: jgieseler@fas.harvard.edu

fluctuations of a system with  $N$  degrees of freedom can be quantified by comparing the variance  $\sigma^2 \propto N$  to the mean  $\langle U \rangle \propto N$  of an extensive macroscopic quantity  $U$ , such as the total energy. For large  $N$ ,  $\langle U \rangle \gg \sigma$ , whereas for small  $N$ ,  $\langle U \rangle \sim \sigma$  [5], illustrating the dominant role of fluctuations in systems with few degrees of freedom.

Thus, with optical trap depths  $> 10^4$  K and optical spring constants of  $\sim$ pN/ $\mu\text{m}$ , the motion of micron-sized particles is sensitive to thermal fluctuations, but not destructively so. The ability to dynamically alter the potential landscape in which the particle moves is also key to their application in studying thermodynamics. This can involve changing the depth of the optical potential, to realize compression stages in heat engines [6] or to speed-up equilibration [7], or creating geometries with multiple stable trapping sites to test information thermodynamics [8].

The majority of thermodynamic studies with optically trapped particles involve *colloidal* particles: objects suspended in a liquid. In contrast, this chapter will consider *levitated* nanoparticles, that is particles trapped in a gas or vacuum. It is somewhat experimentally more challenging than working in liquid, requiring deeper optical potentials due to reduced viscous damping, and loss of the particles from the trap at low pressures is a common problem.

Why work in this challenging regime at all, if the colloidal system has been so successful? Firstly, working in a gaseous environment gives us access to *underdamped* dynamics, as opposed to the overdamped dynamics typically observed in a liquid. The underdamped regime is of fundamental interest, since the inertia of a particle plays a role in the dynamics, whereas it can be mostly ignored in overdamped systems. Secondly, and motivated by the subject matter of this book, the underdamped regime allows one to make the connection to the even more fundamental unitary evolution of quantum mechanical systems. In addition, there is the potential to study quantum physics with these mesoscopic objects [9]. The observation of quantum phenomena with levitated nanoparticles absolutely requires working in a good vacuum, since collisions with gas molecules cause rapid heating and decoherence.

This chapter is intended as a pedagogical introduction to the dynamics of optically levitated nanoparticles with a focus on the study of single particle thermodynamics. Much of the work studying thermodynamics with nano- and micro-particles has taken place in liquid, and this chapter will avoid reviewing this impressive body of work, focussing instead on studies of thermodynamics with nanoparticles levitated in a gas. For a recent literature review we refer the reader to Ref. [10]. The authors will discuss extensions into the quantum regime where relevant throughout the chapter.

Section 35.1 gives a detailed review of the stochastic and deterministic forces acting on an optically levitated nanoparticle, including a discussion of heating due to optical absorption. Section 35.2 describes the Brownian motion of a levitated particle, which will highlight the role of this system as a paradigm for studying stochastic thermodynamics. Section 35.3 will detail the utility of sculpting time-dependent potentials for trapped particles, in particular the ability to create effective baths and non-thermal states. Finally, Sect. 35.4 will review and discuss recent experimental progress in realising important thermodynamics processes with levitated nanoparticles.

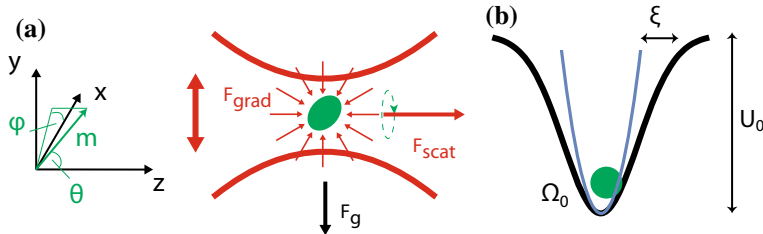


**Fig. 35.1** **a** An optical trap is formed by a tightly focused laser beam. In a single beam trap, the laser propagates along  $z$ . The non-conservative scattering force  $\mathbf{F}_{\text{scat}}$  acts along  $z$  while the gradient force points towards the maximum laser intensity, where the thick red lines on the figure represent the profile of a focussed light beam. In addition, the particle can experience torque and rotate in the trap. The orientation of a particle with a single symmetry axis is characterized by the two angles  $\phi$  and  $\theta$ . The particle also feels a force  $\mathbf{F}_g$  due to gravity. **b** The gradient force forms an optical potential with depth  $U_0$ . The particle is trapped at the bottom of the potential and oscillates at frequency  $\Omega_0$ . For large oscillation amplitudes, the nonlinearity of the potential is characterized by the Duffing parameter  $\xi$ .

### 35.1 The Trapped Nanoparticle System

A particle with radius  $a \sim 100$  nm has, generally speaking, of order  $(a/a_o)^3 \approx 10^{10}$  degrees of freedom, where  $a_o$  is the size of the atoms making up the particle. However, for most practical purposes we characterize excitations within the particle by its internal temperature  $T_{\text{int}}$  and the particle's external degrees of freedom, like its position  $\mathbf{r}$ , which describes its centre-of-mass motion, and its orientation. In the context of single particle thermodynamics, the most relevant degree of freedom is the particle's position. Thus, we will focus our attention on this degree of freedom and only briefly mention the others in their relationship to the center-of-mass motion.

The equations of motion for the centre-of-mass can be well described classically and are given by Newton's second law

$$\ddot{\mathbf{r}}(t) + \Gamma_{\text{CM}} \dot{\mathbf{r}} = \frac{1}{m} [\mathcal{F}_{\text{fluct}}(t) + \mathbf{F}_{\text{det}}(\mathbf{r}, t)], \quad (35.1)$$

where  $m$  is the particle's mass and  $\Gamma_{\text{CM}}$  the momentum damping rate, as discussed in detail below. We have isolated the contributions to the forces that act on the particle into stochastic forces  $\mathcal{F}_{\text{fluct}}$  and deterministic forces  $\mathbf{F}_{\text{det}}$ .

In the following section we discuss the origin of these forces and how they can be controlled in an experiment. This will lead to an effective description of the particle as a Brownian particle in a potential landscape, where the shape of the potential and the thermal bath can be controlled experimentally. This model is at the heart of many stochastic processes, which can therefore be simulated with this platform.

### 35.1.1 Stochastic Forces

The interaction of the particle with its environment has mechanical (collisions with air molecules) and radiative (blackbody and scattering) contributions. These interactions lead to dissipation acting on the center-of-mass motion  $\Gamma_{\text{CM}}^n$  and are the source of the random forces acting on the particle. The strength of the random forces is characterized by their power spectral densities  $S_{\text{ff}}^n$ . For most practical purposes, they can be considered as frequency independent (white noise), that is the autocorrelation functions of the stochastic forces are  $\langle \mathcal{F}_n(t)\mathcal{F}_n(t') \rangle = 2\pi S_{\text{ff}}^n \delta(t - t')$ . After a time  $\approx 1/\Gamma_{\text{CM}}$ , where  $\Gamma_{\text{CM}} = \sum_n \Gamma_n$  is the total damping rate, the center-of-mass motion of the particle reaches an effective thermal equilibrium, which is characterized by an effective temperature through the fluctuation-dissipation relation:

$$T_{\text{CM}} = \frac{\pi S_{\text{ff}}}{k_B m \Gamma_{\text{CM}}}, \quad (35.2)$$

where  $S_{\text{ff}} = \sum_n S_{\text{ff}}^n$  is the total force spectral density,  $m$  the mass of the particle, and  $k_B$  is Boltzmann's constant. Below we describe the individual contributions. They are: collisions with air molecules ( $n = \text{gas}$ ), radiation damping ( $n = \text{rad}$ ), feedback or cavity damping ( $n = \text{fb}$ ), stochastic driving ( $n = \text{drive}$ ), and in the quantum regime noise driving wavefunction collapse ( $n = \text{CSL}$ ).

#### 35.1.1.1 Gas Damping

For pressures higher than  $\sim 10^{-6}$  mbar, the dominant contribution to the stochastic forces is due to collisions with surrounding air molecules, and the damping rate is given by [11]

$$\frac{\Gamma_{\text{gas}}}{2\pi} = 3\mu_v \frac{a}{m} \frac{0.619}{0.619 + \text{Kn}} (1 + c_K), \quad S_{\text{ff}}^{\text{gas}} = \frac{m k_B T_{\text{gas}}}{\pi} \Gamma_{\text{gas}}, \quad (35.3)$$

where  $c_K = 0.31 \text{Kn} / (0.785 + 1.152 \text{Kn} + \text{Kn}^2)$ ,  $\mu_v$  is the viscosity coefficient, which for a dilute gas is  $\mu_v = 2\sqrt{m_{\text{gas}} k_B T_{\text{gas}}} / 3\sqrt{\pi} \sigma_{\text{gas}}$  and  $\text{Kn} = \bar{l}/a$  is the Knudsen number for the mean free path  $\bar{l} = k_B T_{\text{gas}} / (\sqrt{2} \sigma_{\text{gas}} P_{\text{gas}})$ ,  $\sigma_{\text{gas}} = \pi d_m^2$ ,  $d_m = 0.372$  nm is the diameter of the air molecules and  $m_{\text{gas}}$  their mass.

For high pressures (where  $\text{Kn} \ll 1$ ), the interaction with the gas is so strong that the particle motion is heavily damped and its internal temperature  $T_{\text{int}}$  and centre-of-mass temperature  $T_{\text{CM}}$  quickly thermalize with the gas temperature  $T_{\text{gas}}$ . In this regime, the damping becomes independent of pressure  $\Gamma_{\text{CM}}/2\pi \approx 3a\mu_v/m$ , as predicted by Stokes' law.

For decreasing pressure, the mean free path of the gas molecules increases (e.g.  $\bar{l} \sim 60$  μm at 1 mbar). As a consequence, the particle no longer thermalizes with the gas since the impinging gas molecules no longer carry away enough thermal power to balance the optical absorption from the trapping laser. Due to the increased

internal temperature  $T_{\text{int}}$  of the particle, the average energy of the gas molecule after a collision with the particle increases. The process by which a surface exchanges thermal energy with a gas is called accommodation, which is characterized by the accommodation coefficient,

$$c_{\text{acc}} = \frac{T_{\text{em}} - T_{\text{gas}}}{T_{\text{int}} - T_{\text{gas}}}, \quad (35.4)$$

where  $T_{\text{int}}$  is the temperature of the surface,  $T_{\text{gas}}$  the temperature of the impinging gas molecules and  $T_{\text{em}}$  the temperature of the gas molecules emitted from the surface. Accommodation quantifies the fraction of the thermal energy that the colliding gas molecule removes from the surface, such that  $c_{\text{acc}} = 1$  means that the molecule fully thermalizes with the surface. Since the mean free path in a dilute gas is long, one can safely assume that a molecule that comes from the particle surface will not interact again with the particle before thermalizing with the environment. Consequently, we can consider the particles that impinge on the particle surface and those that leave the surface as being in equilibrium with two different baths with temperatures corresponding to the temperature of the environment and the particle surface, respectively. Therefore, we get an additional contribution to the damping from the emerging hot molecules

$$\frac{\Gamma_{\text{em}}}{2\pi} = \frac{1}{16} \sqrt{\frac{T_{\text{em}}}{T_{\text{gas}}}} \Gamma_{\text{gas}}, \quad S_{\text{ff}}^{\text{em}} = \frac{m k_B}{\pi} [c_{\text{acc}} T_{\text{int}} + (1 - c_{\text{acc}}) T_{\text{gas}}] \Gamma_{\text{em}}, \quad (35.5)$$

as experimentally observed by Millen et al. [12]. Note that  $T_{\text{em}}$  can be calculated using Eq. (35.4). In addition to this noise contribution, the internal temperature of the particle can also cause deterministic forces to act on the particle's centre-of-mass motion through the photophoretic effect, where absorbing particles are repelled from the optical intensity maxima [13]. However, since photophoretic forces require a temperature gradient across the particle, they vanish for sub-wavelength particles, which are mostly used in vacuum trapping experiments (typical trapping laser wavelengths range from 532 to 1550 nm).

For pressures below  $P_{\text{gas}} = 0.57 k_B T_{\text{gas}} / \sigma_{\text{gas}} a \approx 54.4 \text{ mbar} \times (a/\mu\text{m})^{-1}$ , where the mean free path is much larger than the radius of the particle ( $\text{Kn} \gg 1$ ), the damping becomes linear in pressure

$$\frac{\Gamma_{\text{gas}}}{2\pi} = \frac{3}{\pi\sqrt{2}} \frac{\mu_v \sigma_{\text{gas}}}{k_B T_{\text{gas}} \rho} \frac{P_{\text{gas}}}{a}, \quad (35.6)$$

where  $\rho$  is the density of the particle. The two expressions Eqs. (35.3) and (35.6) differ by less than 10% for  $\text{Kn} \gg 1$ , with the discrepancy due to numerical accuracy when calculating the constant factors in Eq. (35.3) [11]. The total damping due to the hot particle with the gas environment is  $\Gamma_{\text{em}} + \Gamma_{\text{gas}} = 2\pi c_P P_{\text{gas}}/a$ , where typically  $c_P \approx 50 \text{ Hz}(\mu\text{m}/\text{mbar})$ . When considering operation in the quantum regime, it is

absolutely necessary to work under extremely good vacuum conditions, as collisions with gas molecules cause rapid decoherence and heating out of the ground state. As an example, a 100 nm radius silica nanosphere in a room temperature gas experiences  $\Gamma_{\text{gas}} \sim \text{MHz}$  at atmospheric pressures, and  $\Gamma_{\text{gas}} \sim \text{mHz}$  at  $10^{-6}$  mbar pressures.

So far, we have considered spherical particles with translational degrees of freedom. However, in general the particle has some anisotropy and is free to rotate within the trap. The orientation of the particle with respect to the trap (see Fig. 35.1) is described by the angles  $(\phi, \theta)$ , where  $\phi$  is the angle between the  $x$ -axis and the projection onto the  $x - y$  plane, and  $\theta$  is the angle between the particle axis and the  $z$ -axis. The particle axis is usually defined along its symmetry axis and represented here by the vector  $\mathbf{m}$ . For anisotropic particles, e.g. a cylinder, the friction term is different along each of the axes, and depends upon the alignment  $\mathbf{m}$  of the particle. As a consequence, the friction coefficient has to be replaced by a tensor  $\boldsymbol{\Gamma}$  and the damping in a direction  $\mathbf{s}$  is given by  $\boldsymbol{\Gamma} \cdot \mathbf{s}$ . In the low pressure regime, the friction tensor of the translational degrees of freedom for a particle with a single symmetry axis can be derived analytically [14]. As an example, for a cylinder of diameter  $d$

$$\frac{\boldsymbol{\Gamma}_{\text{trans}}}{2\pi} = 6\sqrt{2} \frac{\mu_v \sigma_{\text{gas}}}{k_B T_{\text{gas}} \rho} \frac{P_{\text{gas}}}{d} \left( 2 - \frac{1}{2} c_{\text{acc}} + \frac{\pi}{4} c_{\text{acc}} \right) \left( \mathbb{I} - \frac{8 - 6c_{\text{acc}} + \pi c_{\text{acc}}}{8 - 2c_{\text{acc}} + \pi c_{\text{acc}}} \mathbf{m} \otimes \mathbf{m} \right). \quad (35.7)$$

For the rotational degrees of freedom we find that the damping is isotropic and given by

$$\frac{\boldsymbol{\Gamma}_{\text{rot}}^{\text{sphere}}}{2\pi} = \frac{30c_{\text{acc}}}{8\pi\sqrt{2}} \frac{\mu_v \sigma_{\text{gas}}}{k_B T_{\text{gas}} \rho} \frac{P_{\text{gas}}}{a}, \quad (35.8a)$$

for a sphere and

$$\frac{\boldsymbol{\Gamma}_{\text{rot}}^{\text{cyl}}}{2\pi} = 6\sqrt{2} \frac{\mu_v \sigma_{\text{gas}}}{k_B T_{\text{gas}} \rho} \frac{P_{\text{gas}}}{d} \left( 2 - \frac{1}{2} c_{\text{acc}} + \frac{\pi}{4} c_{\text{acc}} \right), \quad (35.8b)$$

for a cylinder.

### 35.1.1.2 Noise From Optical Fields

At very low pressure ( $\leq 10^{-6}$  mbar), gas damping rates become extremely small and photon shot noise starts to dominate [15]. Photon shot noise is a consequence of the particulate nature of light. Photons arrive at discrete times, where the number of photons arriving per time interval  $\Delta t$  is given by  $\sqrt{\Delta t P_{\text{opt}} / \hbar \omega_L}$ , where  $P_{\text{opt}}$  and  $\omega_L$  are the optical power and frequency, respectively. The recoil from the fluctuating number of phonons impinging on the nanoparticle can be modelled as an effective bath with the characteristics

$$\frac{\Gamma_{\text{rad}}}{2\pi} = c_{\text{dp}} \frac{P_{\text{scat}}}{2\pi mc^2} \quad \text{and} \quad S_{\text{ff}}^{\text{rad}} = c_{\text{dp}} \frac{\hbar\omega P_{\text{scat}}}{2\pi c^2}, \quad (35.9)$$

where  $c_{\text{dp}}$  depends on the direction of motion of the particle with respect to the polarization of the laser and is  $c_{\text{dp}} = 2/5$  for motion along the direction of polarization and  $c_{\text{dp}} = 4/5$  for motion perpendicular to the polarization. The scattered power is  $P_{\text{scat}} = \sigma_{\text{scat}} I_{\text{opt}}$ , where  $\sigma_{\text{scat}} = |\alpha|^2 k_{\text{L}}^4 / 6\pi\epsilon_0^2$  with  $\alpha$  the particle polarizability, and  $I_{\text{opt}}$  is the laser intensity. The effective temperature of this bath can be calculated via Eq. (35.2).

The noise processes described so far are present in any experiment with optically levitated nanoparticles in high vacuum. In addition, random forces and damping can be introduced through external fields that are under experimental control. Importantly, since energy can be injected or extracted from the particle, i.e. it is not in a thermal equilibrium, the fluctuation-dissipation relation does not have to hold and the effective damping and temperatures can be controlled independently.

For instance, by parametric feedback damping (see also Sect. 35.3.1.1), the temperature alone is not sufficient to give a full description of the bath. Ideal feedback cooling damps the particle motion at a rate  $\Gamma_{\text{fb}}$  without adding any fluctuating forces, thus  $S_{\text{ff}}^{\text{fb}} = 0$  and it is therefore referred to as cold damping. Similarly, cavity cooling up-converts the particle energy to optical frequencies, which are effectively at zero temperature because  $\hbar\omega \gg k_{\text{B}}T_{\text{env}}$  in a room temperature environment. Conversely, fluctuations of the trapping or additional control fields only add fluctuating forces without providing damping. Hence,  $\Gamma_{\text{drive}} = 0$  and  $S_{\text{ff}}^{\text{drive}} = q^2 S_{\text{qq}}$ , where  $q$  is the coupling parameter to the control field and  $S_{\text{qq}}$  its spectral density. This can be realized for example with fluctuating electric fields, where  $q$  corresponds to the charge on the particle. A real feedback signal is noisy, since any measurement is accompanied by noise, and this will heat the particle motion without providing additional damping. In addition, one has to consider correlations between the measurement signal and the particle motion when interpreting the measurement result, in particular when using a linear feedback signal.

### 35.1.1.3 Noise Due to Wavefunction Collapse

There are a class of theories, called *collapse models*, which aim to phenomenologically explain why we do not observe superposition states of macroscopic objects [16]. These models invoke a (classical) noise field, which acts upon particles in a mass-dependent way, to ensure localization of the wavefunction. There are various proposed forms of the noise, including white noise fields which violate conservation of energy, to coloured and dissipative noise with a finite temperature (suggested to be between 0.1–10 K). The noise induces a type of Brownian motion on the centre-of-mass or alignment of the particle, which in principle can be observed. For example, a model of wavefunction collapse known as Continuous Spontaneous Localization (CSL), predicts a random force with  $S_{\text{ff}}^{\text{CSL}} = \lambda_{\text{CSL}} (\hbar/r_{\text{CSL}})^2 \alpha_{\text{CSL}}$ , where the parameters  $\lambda_{\text{CSL}}$  and  $r_{\text{CSL}}$  are a phenomenological rate and length scale, respectively. The

factor  $\alpha_{\text{CSL}}$  is mass and geometry dependent, and as an example is proportional to the mass  $m^{2/3}$  for a sphere. For a thorough discussion of this process, see the review by Bassi et al. [16].

### 35.1.2 Deterministic Forces

In addition to stochastic forces, which we described in Sect. 35.1.1, the particle is also subject to deterministic forces. They are gravity  $\mathbf{F}_g = m\mathbf{g}$ , electric forces  $\mathbf{F}_e = q\mathbf{E}$  if the particle carries a charge  $q$ , magnetic forces  $\mathbf{F}_{\text{mag}} = \nabla(\boldsymbol{\mu} \cdot \mathbf{B})$  if the particle has a magnetic dipole moment  $\boldsymbol{\mu}$  and optical forces  $\mathbf{F}_{\text{opt}}$ . Most experiments with levitated particles in vacuum use optical forces to create a stable trap. This gives a great deal of flexibility since optical fields can be controlled very well in both intensity and position, allowing the creation of almost arbitrary fluctuating force fields. Particles that are much smaller than the wavelength  $\lambda_L$  of the trapping laser  $ak_L \ll 1$ , where  $k_L = 2\pi/\lambda_L$ , can be treated as dipoles in the Rayleigh approximation. The polarizability for a particle with volume  $V$  is thereby given by

$$\alpha_0 = \epsilon_0 V \chi, \quad (35.10)$$

where the total susceptibility of the particle  $\chi = \chi_e (1 + N\chi_e)^{-1}$  depends on the material via the material susceptibility  $\chi_e$  and on its geometry through the depolarization tensor  $N$ , which in general are both rank-2 tensors. However, for isotropic materials, the material susceptibility simplifies to a scalar  $\chi_e$  and similarly for a sphere the depolarization tensor is isotropic and simplifies to a scalar  $N = 1/3$ . Thus, for a sphere we recover the Clausius–Mossotti relation  $\chi = 3(\epsilon_p - 1)/(\epsilon_p + 2)$ , where we use  $\epsilon_p = 1 + \chi_e$ .

For a particle with a uniaxial anisotropy, e.g. a cylinder, the susceptibility  $\chi = \text{diag}(\chi_{\parallel}, \chi_{\perp}, \chi_{\perp})$ , has a component  $\chi_{\parallel}$  parallel and a component  $\chi_{\perp}$  perpendicular to the symmetry axis. For example, the depolarization tensor of a cylinder is  $N = \text{diag}(0, 1/2, 1/2)$  in the frame of the cylinder, where the cylinder axis is along the  $x$ -axis. Consequently,  $\chi_{\parallel} = \epsilon_r - 1$ ,  $\chi_{\perp} = 2(\epsilon_r - 1)/(\epsilon_r + 1)$  for a cylinder with isotropic  $\epsilon_r$ . This means the maximal polarizability of a cylinder is  $(\epsilon_r + 2)/3$  times higher than for a sphere of the equivalent volume. For silica, this is a factor of 2, whereas it is a factor of 4.6 for silicon.

In general, the particle reacts to the total field, that is the sum of the incident and the scattered field. The total field is the self consistent solution to Maxwell's equations and has to be calculated generally with numerical methods. However, for a spherical particle, the modified polarizability

$$\alpha = \alpha_0 \left( 1 - i \frac{k_L^3 \alpha_0}{6\pi\epsilon_0} \right)^{-1}, \quad (35.11)$$

accounts for the radiation reaction of the particle to its own scattered field, such that the induced polarization due to a field  $\mathbf{E}_0$  is  $\mathbf{P} = \alpha\mathbf{E}_0$ . We introduce  $\alpha'$  and  $\alpha''$  to refer to the real and imaginary part of the polarisability, respectively.

Knowing the polarizability, we can calculate the optical force for sub-wavelength particles in the Rayleigh approximation. The optical force has conservative and non-conservative contributions

$$\mathbf{F}_{\text{opt}} = \alpha' \nabla I_0 / 4 + \sigma_{\text{tot}} [\mathbf{S}/c + c \nabla \times \mathbf{L}], \quad (35.12)$$

where the total cross-section  $\sigma_{\text{tot}} = \alpha'' k_L / \epsilon_0$  is the sum of the absorption and scattering cross-sections. The optical intensity at the field maximum  $I_0$  is related to the field  $E_0$  through  $I_0 = c\epsilon_0 E_0^2 / 4$ . The first term in Eq. (35.12) is a conservative force. It pulls particles with a high refractive index relative to their surroundings toward the region of maximum light intensity. In an optical tweezers, this is the focal volume of the light beam.

The second term is the non-conservative scattering force, which has two contributions: the radiation pressure term, which is proportional to the time averaged Poynting vector  $\mathbf{S} = \langle \mathbf{E} \times \mathbf{H}^* \rangle$ ,  $\mathbf{H}$  being the magnetic field, and a curl force associated to the non-uniform distribution of the time averaged spin density of the light field  $\mathbf{L} = -i\epsilon_0 \langle \mathbf{E} \times \mathbf{E}^* \rangle / 4\omega_L$ ,  $\langle \dots \rangle$  being a time average. The curl force is zero for a plane wave but can be significant for a tightly focused beam in an optical tweezers.<sup>2</sup> However, since  $\alpha''/\alpha' \propto a^3$ , the non-conservative forces vanish for small particles and we will neglect them in the following discussion.

### 35.1.2.1 Optical Potential

The conservative force in Eq. (35.12) can be expressed as the gradient of a potential  $\mathbf{F}_{\text{opt}} = -\nabla U_{\text{opt}}$ . Even for a tightly focused laser beam, the optical intensity distribution is to a good approximation described by a transverse Gaussian profile and a Lorentzian profile along the direction of beam propagation. Thus, for a single focused laser beam the optical potential reads

$$U_{\text{opt}}(\mathbf{r}) = \frac{-U_{\text{opt}}}{1 + (z/z_0)^2} \exp \left[ -\frac{2}{1 + (z/z_0)^2} \left( \frac{x^2}{w_x^2} + \frac{y^2}{w_y^2} \right) \right], \quad (35.13)$$

where  $U_{\text{opt}} = \alpha' E_0^2 / 4$  is the potential depth,  $\mathbf{r}$  is the position of the particle,  $w_x, w_y$  denote the transverse extent of the focus, and we define a longitudinal waist  $w_z$  via the Rayleigh range  $z_0 = w_z / \sqrt{2} \approx \pi w_0^2 / \lambda_L$ , which gives the depth of focus. Note that for tightly focused laser beams, as are commonly used in optical trapping, the field distribution is slightly elongated along the direction of polarization of the incident field. Integrating the Poynting vector over a cross-section that is transverse to the

---

<sup>2</sup>For a Gaussian beam with waist  $w_0$ , we estimate the curl force as  $F_{\text{curl}} \approx -2F_{\text{scat}} / w_0^2 k_L^2$ , where  $F_{\text{scat}} \sim \sigma_{\text{tot}} P_{\text{opt}} / w_0^2 c$ .

direction of propagation allows us to relate the field intensity at the centre of the focus  $E_0^2$  to the optical power of the trapping laser  $P_{\text{opt}} = \int_s \langle \mathbf{S} \rangle d\mathbf{s} = \pi c \epsilon_0 w_0^2 E_0^2 / 4$ , where  $w_0^2 = w_y w_x$ . At the bottom of the potential, the centre-of-mass motion is harmonic, with frequencies

$$\Omega_i = 2 \sqrt{\frac{\chi}{c\pi\rho} \frac{\sqrt{P_{\text{opt}}}}{w_0 w_i}}, \quad (35.14)$$

along the three directions ( $q = x, y, z$ ). For larger oscillation amplitudes, the motion becomes anharmonic, and the nonlinear coefficients can be obtained from higher derivatives of the optical potential (see Sect. 35.2.3).

### 35.1.2.2 Rotation

As we have already seen in Sect. 35.1.1, the light matter interaction is more complicated for anisotropic particles, since it depends upon the alignment of the object relative to the polarization axis of the field.<sup>3</sup> The induced polarization is  $\mathbf{P} = \alpha \mathbf{E}$ . Consequently, the particle experiences an optical torque

$$\mathbf{N}_{\text{opt}} = \langle \mathbf{P} \times \mathbf{E}^* \rangle, \quad (35.15)$$

which aligns the particle along the polarization axis. For small deflections from the polarization axis the angular motion is harmonic. For a cylinder of length  $l$  the frequencies are

$$\Omega_\theta = \sqrt{\frac{24 P_{\text{opt}} \chi_{\parallel}}{\pi \rho c w_0^2 l^2} \left( \frac{\Delta \chi}{\chi_{\parallel}} + \frac{(k_L l)^2}{12} \right)}, \quad \Omega_\phi = \sqrt{\frac{24 P_{\text{opt}} \Delta \chi}{\pi \rho c w_0^2 l^2}}, \quad (35.16)$$

where the term  $(k_L l)^2/12$  is a correction term that accounts for the particle's finite extension.

In contrast to linearly polarized light, the polarization axis of circularly polarized light rotates at the optical frequency. This is too fast for the particle to follow. Nonetheless, light scattering transfers the angular momentum of the light to a particle with polarization anisotropy, which can originate from the intrinsic birefringence of the particle or from the anisotropic shape of the particle (c.f. Eq. (35.10)). The torque that results from angular momentum transfer is for a cylinder [4]:

$$N_\phi = \frac{\Delta \chi l^2 d^4 k_L^3}{96 c w_0^2} [\Delta \chi \eta_1(k_L l) + \chi_{\perp} \eta_2(k_L l)] P_{\text{opt}}, \quad (35.17)$$

---

<sup>3</sup>For a thorough treatment, including optical scattering, see [4] and references therein.

where the functions  $\eta_{1,2}(k_L l)$  are given by

$$\begin{aligned}\eta_1(k_L l) &= \frac{3}{4} \int_{-1}^1 ds (1 - s^2) \text{sinc}^2\left(\frac{k_L l s}{2}\right), \\ \eta_2(k_L l) &= \frac{3}{8} \int_{-1}^1 ds (1 - 3s^2) \text{sinc}^2\left(\frac{k_L l s}{2}\right).\end{aligned}\quad (35.18)$$

For short rods,  $k_L l \ll 1$ , one has  $\eta_1 \simeq 1$  while  $\eta_2 \simeq 0$ . The rotational frequency  $\Omega_{\text{rot}}$  is given by the balance between the torque  $N_\phi$  and the damping  $\Gamma_{\text{rot}}^{\text{cyl}}$ , such that  $\Omega_{\text{rot}} = N_\phi / (I \Gamma_{\text{rot}}^{\text{cyl}})$ , where  $I$  is the moment of inertia  $I = ml^2/12$ . We note that this analysis is true in the Rayleigh-Gans approximation, where  $k_L l (\epsilon_r - 1) \ll 1$  and  $\pi k_L^2 d^2 (\epsilon_r - 1) \ll 1$ .

### 35.1.3 Internal Temperature

In the previous section we discussed the behaviour of a hot sphere levitated in gas and how its internal temperature  $T_{\text{int}}$  couples to the centre-of-mass motion, which we characterized by its centre-of-mass temperature  $T_{\text{CM}}$ . In this section we will consider the process by which an optically levitated nanoparticle heats up.

Following Bateman et al. [17] and Chang et al. [9], the interaction between a sub-wavelength ( $a < \lambda_L$ ) sphere of radius  $a$  and a light field of frequency  $\omega_L$ , is governed by the complex polarisability  $\alpha$ . The frequency dependent permittivity is related to the complex refractive index through  $\epsilon(\omega) = n(\omega)^2$ . While  $\alpha'_0$  determines the optical potential,  $\alpha''_0$  determines optical absorption, with absorption cross-section  $\sigma_{\text{abs}} = \alpha''_0 k_L / \epsilon_0$ . The bulk temperature depends on several competing processes: heating through absorption of the trapping light  $\omega_L$ , optical absorption of blackbody radiation with a spectral absorption rate  $\rho_{\text{abs}}$ , and cooling through blackbody emission at a spectral emission rate  $\rho_{\text{emis}}$  and through energy exchange with the background gas. The blackbody spectral rates are given by:

$$\begin{aligned}\rho_{\text{abs}}(\omega_{\text{bb}}) &= \frac{(\omega_{\text{bb}}/(\pi c))^2 \sigma_{\text{abs}}(\omega_{\text{bb}})}{\exp(\hbar\omega_{\text{bb}}/(k_B T_{\text{env}})) - 1}, \\ \rho_{\text{emis}}(\omega_{\text{bb}}, T_{\text{int}}) &= \left(\frac{\omega_{\text{bb}}}{\pi c}\right)^2 \sigma_{\text{abs}}(\omega_{\text{bb}}) \exp\left(-\frac{\hbar\omega_{\text{bb}}}{k_B T_{\text{int}}}\right),\end{aligned}\quad (35.19)$$

where  $T_{\text{env}}$  is the ambient temperature of the environment, and  $T_{\text{int}}$  the surface temperature of the sphere (which we assume is equal to the bulk temperature). Following Chang et al. [9], we can integrate across the blackbody spectrum to find the rate at which the sphere absorbs or emits blackbody energy:

$$\begin{aligned}\dot{E}_{\text{abs}}^{\text{bb}} &= \frac{24\xi_R(5)}{\pi^2\epsilon_0 c^3 \hbar^4} \alpha''_{\text{bb}} (\text{k}_B T_{\text{env}})^5 \\ \dot{E}_{\text{emis}}^{\text{bb}} &= -\frac{24\xi_R(5)}{\pi^2\epsilon_0 c^3 \hbar^4} \alpha''_{\text{bb}} (\text{k}_B T_{\text{int}})^5,\end{aligned}\quad (35.20)$$

where  $\xi_R(5) \approx 1.04$  is the Riemann zeta function, and  $\alpha_{\text{bb}}$  is averaged over the blackbody spectrum, such that for silica, which is the material most commonly used in optical levitation experiments,  $\alpha''_{\text{bb}} \approx 4\pi\epsilon_0 a^3 \times 0.1$  [9]. These energy absorption and emission processes lead to decoherence when operating in the quantum regime, and for this reason it may be desirable to work in a cryogenic environment, or to work with internally cold particles.

Next we consider the cooling power due to collisions with gas molecules, again following [9]:

$$\dot{E}_{\text{gas}} = -c_{\text{acc}} \sqrt{\frac{2}{3\pi}} (\pi a^2) v_{\text{th}} \frac{\gamma_{\text{sh}} + 1}{\gamma_{\text{sh}} - 1} \left( \frac{T_{\text{int}}}{T_{\text{gas}}} - 1 \right) P_{\text{gas}}, \quad (35.21)$$

where  $v_{\text{th}}$  is the mean thermal velocity of the impinging gas molecules,  $\gamma_{\text{sh}} = 7/5$  is the specific heat ratio of a diatomic gas, and for most experiments  $T_{\text{gas}} \equiv T_{\text{env}}$ . This expression holds in the Knudsen regime ( $\bar{l} \gg a$ ). Combining all of these leads to a rate equation that describes  $T_{\text{int}}$ :

$$mc_{\text{HC}} \frac{dT_{\text{int}}}{dt} = I_{\text{opt}} \sigma_{\text{abs}} + \dot{E}_{\text{gas}} + \dot{E}_{\text{abs}}^{\text{bb}} + \dot{E}_{\text{emis}}^{\text{bb}}, \quad (35.22)$$

where  $c_{\text{HC}}$  is the specific heat capacity for the particle material and  $I_{\text{opt}}$  is the light intensity. Using Eq. (35.22), one can calculate the steady-state temperature of a sphere levitated in vacuum. It is also the case that the refractive index  $n(\omega)$ , and hence the permittivity  $\epsilon(\omega)$ , of the levitated particle varies with the bulk temperature, but since for silica it varies by only 1% over 2000 K, we ignore this effect here. To avoid absorption, pairings of nanoparticle material and trapping wavelengths should be carefully chosen, for example working with pure silicon particles and telecom wavelengths ( $\sim 1500$  nm).

In Fig. 35.2, the variation in  $T_{\text{int}}$  and  $T_{\text{CM}}$  with pressure is shown, for silica spheres trapped in an optical tweezer under realistic experimental conditions. We can identify three regimes: At high pressures, the cooling power of the surrounding gas is sufficient to counter any heating due to optical absorption, and the particle surface and centre-of-mass temperatures thermalize to the environmental temperature. At low pressures, the surface temperature increases, due to reduced gas cooling power (Eq. (35.21)) and at ultra low pressure, the centre-of-mass motion thermalizes with the photon shot noise [15].

It should be noted that all centre-of-mass heating mechanisms pose a problem to operating in the quantum regime. Because of this, most proposals for testing quantum physics with optically trapped particles involve switching off the light fields after state-preparation, and letting the particle drop. This may not be desirable for thermodynamics experiments which require long interrogation times. For this reason, some proposals consider magnetic or electric levitation, and even operation in space.

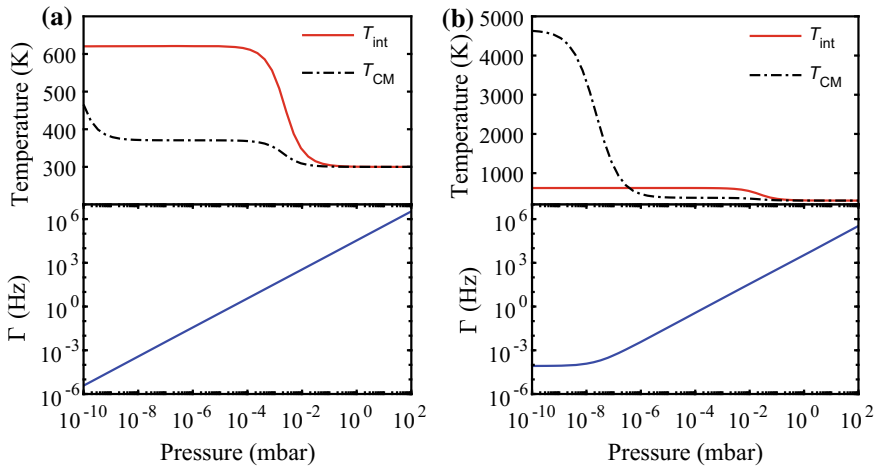


**Fig. 35.2 The variation in particle dynamics with pressure.** Variation in the surface temperature  $T_{\text{int}}$ , centre-of-mass temperature  $T_{\text{CM}}$ , and damping rate  $\Gamma_{\text{CM}}$  with pressure for **a**  $a = 10\text{ nm}$ , and **b**  $a = 100\text{ nm}$  silica spheres, with  $T_{\text{gas}} \equiv T_{\text{env}} = 300\text{ K}$ . These dynamics are due to the balance between optical absorption, blackbody absorption and emission (Eq. (35.20)), photon recoil heating (Eq. (35.9)), and cooling due to collisions with gas molecules (Eq. (35.21)). This figure assumes a sphere trapped with a realistic laser intensity of  $6 \times 10^{11}\text{ W m}^{-2}$  with a wavelength of 1550nm. The optical trap depth is a)  $U_0/k_B = 520\text{ K}$  and b)  $U_0/k_B = 5 \times 10^5\text{ K}$ . For silica we use a complex refractive index  $n = 1.45 + (2.5 \times 10^{-9})i$  [17], material density  $\rho = 2198\text{ kg m}^{-3}$ , and we assume the surrounding gas is  $N_2$ , with a corresponding surface accommodation coefficient  $c_{\text{acc}} = 0.65$ .

## 35.2 Brownian Motion

Besides its important role in the development of the foundations of physics, today the Brownian particle serves as an exemplary model to describe a variety of stochastic processes in many fields, including physics, finance and biology. Brownian motion in non-equilibrium systems is of particular interest because it is directly related to the transport of molecules and cells in biological systems. Important examples include Brownian motors, active Brownian motion of self-propelled particles, hot Brownian motion, and Brownian motion in shear flows. Despite its importance, the first experimental observation of ballistic Brownian motion had to wait a century until Li et al.'s seminal work with optically levitated microparticles [18]. This result already highlights the importance of the levitated particle system for studying thermodynamics.

In this section we will discuss the basics of Brownian motion. We will mainly treat the aspects that are necessary for understanding the following discussion of thermodynamics with levitated nanoparticles. For details on the theory of Brownian motion we refer the reader to the work of Ornstein, Uhlenbeck and Wang [19, 20]. First we will consider the motion of a free Brownian particle. Then we will add the confining potential and discuss important concepts such as a the power spectral density. Then we will include higher order (nonlinear) terms of the trapping potentials

and discuss how they impact the power spectra. Finally, we go to the opposite extreme case where the particle is cooled to extremely low energies such that quantum effects have to be included.

### 35.2.1 Free Brownian Motion

The three motional degrees of freedom of a free particle are decoupled and without loss of generality it suffices to discuss a single coordinate  $q(t)$  ( $q = x, y, z$ ). When coupled to a thermal bath at temperature  $T_{\text{CM}}$  with rate  $\Gamma_{\text{CM}}$ , the equation of motion is given by the Langevin equation

$$\ddot{q} + \Gamma_{\text{CM}} \dot{q} = \mathcal{F}_q(t)/m, \quad (35.23)$$

where  $\mathcal{F}_q(t)/m = \sqrt{2k_B T_{\text{CM}} \Gamma_{\text{CM}}/m} \Xi(t)$  and  $\Xi(t)$  is a normalised white-noise process with  $\langle \Xi(t) \rangle = 0$ ,  $\langle \Xi(t) \Xi'(t') \rangle = \delta(t - t')$ . Here  $\delta(t - t')$  is the Dirac delta function. Since  $\mathcal{F}_q(t)$  is a random process,  $q(t)$  is also a random variable, such that each trajectory starting from the same initial conditions is different. However, the mean and variance for an ensemble of particles are well defined and are identical to the values for a single particle measured over a long time by virtue of the ergodic theorem.

Since the average force is zero, the mean particle position is also zero  $\langle q(t) \rangle = 0$ . Its variance, or mean-square displacement, is given by

$$\sigma_q^2(t) = \langle [q(t) - q(0)]^2 \rangle = \frac{2k_B T_{\text{CM}}}{m \Gamma_{\text{CM}}^2} [\Gamma_{\text{CM}} t - 1 + e^{-\Gamma_{\text{CM}} t}]. \quad (35.24)$$

At long time scales ( $t \gg 1/\Gamma_{\text{CM}}$ ), the variance is the same as that predicted by Einstein's theory of diffusion  $\sigma_q^2(t) = 2Dt$  where  $D = k_B T_{\text{CM}}/m \Gamma_{\text{CM}}$  is the diffusion coefficient. This regime is truly random in the sense that the particle trajectory is fractal and, therefore, is continuous but not differentiable. At short time scales ( $t \ll 1/\Gamma_{\text{CM}}$ ), the dynamics of a Brownian particle is dominated by its inertia and its trajectory is ballistic. In this regime, the variance grows quadratically in time  $\sigma_q^2(t) = (k_B T_{\text{CM}}/m)t^2$  as expected for a free particle.

### 35.2.2 Harmonic Brownian Motion

Under the influence of trapping forces, the particle will be localised about its equilibrium position. For small displacements, the trap can be approximated by a three-dimensional harmonic potential. As before, we limit our discussion to a single coordinate. The equation of motion for a harmonically trapped Brownian particle is [20]

$$\ddot{q} + \Gamma_{\text{CM}} \dot{q} + \Omega_0^2 q = \sqrt{2k_B T_{\text{CM}} \Gamma_{\text{CM}} / m} \Xi(t). \quad (35.25)$$

Due to the confinement provided by the trap the variance does not grow unbounded. Instead, the particle oscillates in the trap at the characteristic frequency  $\tilde{\Omega} = \sqrt{\Omega_0^2 - \Gamma_{\text{CM}}^2 / 4}$ . For the optical potential equation (35.13), the trap frequency  $\Omega_0$  is given by Eq. (35.14).

We distinguish between three cases, the overdamped ( $\Omega_0 \ll \Gamma_{\text{CM}}$ ), the critically damped ( $\Omega_0 \approx \Gamma_{\text{CM}}$ ) and underdamped case ( $\Omega_0 \gg \Gamma_{\text{CM}}$ ). This stochastic equation of motion has been studied in detail by Ornstein and Uhlenbeck [19] and we summarise their results here. The variance of the position of a Brownian particle in an under-damped harmonic trap is

$$\sigma_q^2(t) = \frac{2k_B T_{\text{CM}}}{m \Omega_0^2} \left[ 1 - e^{-\frac{1}{2}\Gamma_{\text{CM}}t} \left( \cos(\tilde{\Omega}t) + \frac{\Gamma_{\text{CM}}}{2\tilde{\Omega}} \sin(\tilde{\Omega}t) \right) \right]. \quad (35.26)$$

In the over-damped harmonic trap, set  $\tilde{\Omega} \rightarrow i\tilde{\Omega}$ . In a critically damped harmonic trap, set  $\tilde{\Omega} \rightarrow 0$ . The position autocorrelation function is related to the variance as follows

$$\langle q(t)q(0) \rangle = \frac{k_B T_{\text{CM}}}{m \Omega_0^2} - \frac{1}{2} \sigma_q^2(t) \quad (35.27)$$

The velocity autocorrelation function is given by

$$\langle v(t)v(0) \rangle = \frac{k_B T_{\text{CM}}}{m} e^{-\frac{1}{2}\Gamma_{\text{CM}}t} \left( \cos(\tilde{\Omega}t) - \frac{\Gamma_{\text{CM}}}{2\tilde{\Omega}} \sin(\tilde{\Omega}t) \right), \quad (35.28)$$

and an experimental verification of this form is shown in Fig. 35.3. In addition, position and velocity are correlated and the position-velocity correlation function is given by

$$\langle q(t)v(0) \rangle = \langle v(t)q(0) \rangle = \frac{k_B T_{\text{CM}}}{m \tilde{\Omega}} e^{-\frac{1}{2}\Gamma_{\text{CM}}t} \sin(\tilde{\Omega}t). \quad (35.29)$$

According to the Wiener–Khinchin theorem, the position autocorrelation function is the Fourier transform of the power spectral density  $S_{qq}(\Omega) = \int_{-\infty}^{\infty} \langle q(t)q(0) \rangle e^{i\Omega t} dt$ , which for Eq. (35.25) is given by

$$S_{qq}(\Omega) = |\chi(\Omega)|^2 S_{ff}(\Omega) = \frac{\Gamma_{\text{CM}} k_B T_{\text{CM}} / \pi m}{(\Omega^2 - \Omega_0^2)^2 + \Gamma_{\text{CM}}^2 \Omega^2} \quad (35.30)$$

where  $\chi(\Omega) = m^{-1} [\Omega^2 - \Omega_0^2 + i\Gamma_{\text{CM}}\Omega]^{-1}$  is the response function or susceptibility of a harmonic oscillator. In the underdamped regime, the frequency spectrum of the autocorrelation function is strongly peaked around the trap frequency  $\Omega_0$ , whereas when overdamped the frequency spectrum is broad, as shown in Fig. 35.4a. The power spectral density (PSD) is a useful tool in experiments with harmonic oscillators,

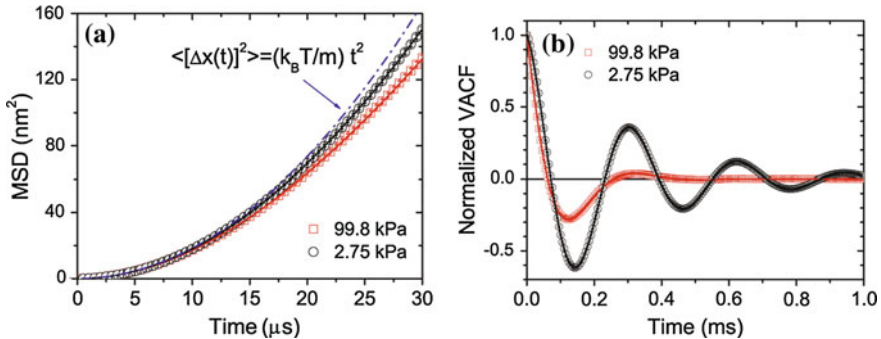


**Fig. 35.3 First experimental observation of the instantaneous velocity of a Brownian particle.** **a** The mean-square displacement for short times is proportional to  $t^2$ , a signature of ballistic motion. **b** The normalized velocity autocorrelation functions for different pressures in perfect agreement with Eq. (35.28). Figures taken from [18] with permission from Science.

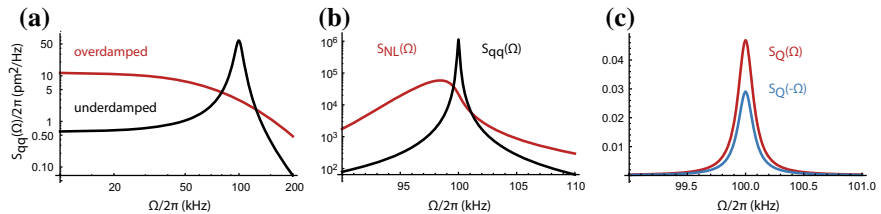


**Fig. 35.4 Position power spectral densities (PSD) in different regimes.** **a** In the overdamped regime (quality factor  $Q = \Omega / \Gamma_{cm} = 1/2$ , red) the PSD has its maximum at  $\Omega = 0$  and falls off for higher frequencies. In the underdamped regime ( $Q = 10$ , black), the PSD is peaked around the resonance frequency  $\Omega_0$  and has a linewidth of  $\Gamma \approx \Omega_0 / Q$ . **b** For even higher  $Q$ , nonlinear effects can broaden the linewidth and instead of the expected narrow harmonic oscillator PSD (black,  $Q = 100$ , Eq. (35.30)), the observed PSD is highly asymmetric (red,  $\xi = 5 \mu\text{m}^{-2}$ ,  $T = 300 \text{ K}$  Eq. (35.34)). **c** When the motion is cooled near the quantum ground state (here  $T_{CM} = 10 \mu\text{K}$ ), nonlinear effects are negligible. Instead, quantum features lead to an asymmetric PSD, where the PSD at positive frequencies (red) is by a factor  $\exp(\hbar\Omega_0/k_B T_{CM})$  higher than the PSD at negative frequencies (blue).

since the dynamics of the oscillator can be separated from (spectrally distant) noise. An analysis of the power spectral density allows one to extract the center of mass temperature of the oscillator and the damping rate, as is clear from Eq. (35.30).

### 35.2.3 Nonlinear Brownian Motion

Until now, we have only considered small deviations from the equilibrium position, where the potential is harmonic. However, the actual trapping potential is nonlinear. For the transverse directions, the lowest order nonlinear term is a cubic or Duffing nonlinearity in the equation of motion due to the symmetry of the trap. Along the

direction of propagation of the trapping laser, the scattering force breaks the symmetry and we also get a quadratic term. Similarly, gravity breaks the symmetry along the  $y$ -axis (see Fig. 35.1). However, due to the smallness of the quadratic nonlinearity we will neglect it and focus our discussion on the Duffing term. Including the latter, the equation of motion for a single coordinate reads

$$\ddot{q}_i + \Gamma_i \dot{q}_i + \Omega_i^2 q_i + \Omega_i^2 \left( \sum_j \xi_{ij} q_j^2 \right) q_i = \sqrt{2k_B T_{CM} \Gamma_i / m} \Xi(t), \quad (35.31)$$

where we have re-introduced the indices for a clearer notation. From the optical potential equation (35.13) we find that  $\xi_{ij} \sim -w_j^{-2}$ . As a consequence, the oscillation frequency becomes a function of the oscillation amplitude and is red shifted by [21]

$$\Delta\Omega_i = \frac{3}{8} \Omega_i \sum_j \xi_{ij} A_j^2, \quad (35.32)$$

where  $A_i$  is the instantaneous oscillation amplitude. In the low damping regime ( $\Omega \gg \Gamma_{CM}$ ), the amplitude  $A_i$  and phase  $\phi_i$  are quasi-static over many oscillation periods  $2\pi/\Omega$  and only change significantly over times scales on the order of the relaxation time  $2\pi/\Gamma_{CM}$ . Hence, the position can be written as  $q_i(t) = A_i(\tau) \cos [\Omega t + \phi_i(\tau)]$ , with  $2\pi/\Omega \ll \tau \ll 2\pi/\Gamma_{CM}$ , where  $\tau$  represents the slow timescale of the amplitude and phase evolution. The frequency shift due to changes in the oscillation amplitudes is also known as self-phase modulation ( $j = i$ ) and cross-phase modulation ( $j \neq i$ ). To resolve the nonlinear frequency shift originating from thermal motion, the nonlinear contribution must be larger than the linear one, resulting in the condition

$$\mathcal{R} = \frac{\Delta\Omega_{NL}}{\Gamma_{CM}} = \frac{3\xi Q k_B T_{CM}}{4\Omega^2 m} \gg 1, \quad (35.33)$$

where  $Q = \Omega / \Gamma_{cm}$  is the quality factor. If this condition is fulfilled, the power spectral density (PSD) is no longer given by Eq. (35.30). Instead, the harmonic oscillator PSD is now weighted with the probability to find the particle with a certain energy  $E$  and the resulting PSD

$$S_{NL}(\Omega) = \int_0^\infty \rho(E) S_L(\Omega, E) dE, \quad (35.34)$$

is no longer symmetric, as shown in Fig. 35.4b. The energy distribution is given by the Gibbs distribution  $\rho(E) = Z^{-1} \exp(-E/k_B T_{CM})$  with  $Z = \int \rho(E) dE = k_B T_{CM}$  and the spectra  $S_L(\Omega, E) = E \Gamma_{CM} / \pi m \Omega_0^2 [(\Omega^2 - \hat{\Omega}(E)^2)^2 + \Gamma_{CM}^2 \Omega^2]^{-1}$  are shifted to  $\hat{\Omega}_0(E) = \Omega_0 + 3\xi/(4m\Omega_0)E$ . Notably, due to the Gibbs distribution weighting term, the symmetry of the thermally driven spectra is opposite to the frequency response of the driven Duffing oscillator.

### 35.2.4 Quantum Brownian Motion

While the nonlinear aspects of the potential are only relevant for large excitations, the opposite extreme, when the center of mass temperature is of the order of a single quantum of motion  $k_B T_{CM} \approx \hbar\Omega_0$ , is of particular importance since quantum effects can no longer be neglected. In the quantum regime, the position autocorrelation Eq. (35.27) contains the product of time-evolved operators  $\langle \hat{q}(t)\hat{q}(0) \rangle$ , which do not commute. As a result, the spectrum

$$S_Q(\Omega) = \frac{\hbar/\pi}{1 - \exp\left(-\frac{\hbar\Omega}{k_B T_{CM}}\right)} \text{Im}\chi(\Omega) = \frac{\hbar\Omega m \Gamma_{eff}/\pi}{1 - \exp\left(-\frac{\hbar\Omega}{k_B T_{eff}}\right)} |\chi(\Omega)|^2 \quad (35.35)$$

is asymmetric in frequency, where the PSD at positive frequencies is a factor  $\exp(\hbar\Omega_0/k_B T_{CM})$  higher than the PSD at negative frequencies, as shown in Fig. 35.4c. The positive-frequency part of the spectral density is a measure of the ability of the oscillator to absorb energy, while the negative-frequency part is a measure of the ability of the oscillator to emit energy. Therefore, we can understand the positive frequency part of the spectral density as being related to stimulated emission of energy into the oscillator, while the negative-frequency part is related to the emission of energy by the oscillator.

Typically, the motional frequencies of a levitated particle are  $\sim 100$  kHz. Therefore, the required temperature is a few micro-kelvin and therefore out of reach for cryogenic techniques and one has to resort to active cooling techniques. Recent experiments using feedback cooling have already attained motional occupations of a few tens of phonons [15].

## 35.3 Time Dependent Potentials

So far we have considered only static trapping potentials  $U_{opt} \equiv U_{opt}(\mathbf{r})$ , where the trapping laser power is constant. However, through modulation of the trapping beam intensity, we can make the optical potential time-dependent. This is particularly useful when studying non-equilibrium dynamics. From Eq. (35.14) it follows that a change in optical power  $\delta P_{opt}(t)$  changes the trap frequency by  $\Omega = \Omega_0(1 + \zeta(t)/2)$ , where  $\zeta(t) = \delta P_{opt}(t) / \bar{P}_{opt}$  and  $\bar{P}_{opt}$  is the mean optical power. The equation of motion under this parametric modulation is given by

$$\ddot{q} + \Gamma_{CM}\dot{q} + \Omega_0^2 [1 + \zeta_0 \cos(\Omega_{mod}t) + \xi q^2] q = \sqrt{2k_B T_{CM} \Gamma_{CM}/m} \Xi(t). \quad (35.36)$$

Energy is most effectively exchanged between the trapping laser and the particle if the modulation  $\zeta(t) = \zeta_0 \cos(\Omega_{mod}t)$  occurs at twice the trapping frequency

$\Omega_{\text{mod}} \approx 2\Omega_0$ . The flow of energy is thereby determined by the relative phase  $\phi_{\text{mod}}$  between the particle oscillation and the laser intensity modulation.<sup>4</sup> If the modulation is in-phase, energy is extracted (cooling), while the motion is excited when the modulation is out-of-phase (heating). For  $\zeta_0 > 1/2Q$ , where  $Q = \omega_0/\Gamma_{\text{cm}}$  is the motional quality factor, energy is pumped into the system faster than can be extracted through dissipation. For a harmonic trap this would lead to a steady increase in energy. However, due to the nonlinear Duffing term, the oscillation frequency of the particle shifts away from the energy matching condition, which limits the maximum oscillation amplitude. Without active stabilization of the modulation phase with respect to the particle motion, the relative phase is random. Therefore, to achieve cooling the phase needs to be actively stabilized, for instance with a phase-locked-loop [15].

### 35.3.1 Effective Potentials and Non-equilibrium Steady States

As we discussed in Sect. 35.2.3, the particle motion is described by a slowly varying evolution of the phase and amplitude and a fast modulation at frequency  $\Omega$ . In many cases we are primarily interested in the slow evolution of the energy or amplitude and it is, thus, advantageous to work with the effective equations of motion for the energy instead of considering full particle dynamics. This strategy allows us to define effective potentials for the energy and to derive an effective temperature for the particle center-of-mass motion.

For convenience we introduce the position  $q$  and momentum  $p = m\dot{q}$  differential equations of motion for a particle in a time-dependent potential [22]

$$dq = \frac{p}{m} dt, \quad (35.37a)$$

$$dp = [-m\Omega_0^2 q - \Gamma_{\text{CM}} p + \zeta_0 m\Omega_0^2 \cos(\Omega_{\text{mod}} t) q] dt + \sqrt{2m\Gamma_{\text{CM}}k_B T_{\text{CM}}} dW. \quad (35.37b)$$

Here,  $W(t)$  is the Wiener process with  $\langle W(t) \rangle = 0$ ,  $\langle W(t)W(t') \rangle = t' - t$ . Note that  $\langle W^2(t) \rangle = t$  for any time  $t \geq 0$  and, thus, for an infinitesimal time interval  $dt$  one has  $\langle (dW)^2 \rangle = dt$ . The white noise  $\Xi(t)$  appearing in the random force can be viewed as the time derivative of the Wiener process,  $\Xi(t) = dW(t)/dt$ . The total energy of the particle in one dimension is given by

$$E(q, p) = \frac{1}{2}m\Omega_0^2 q^2 + \frac{p^2}{2m} + \frac{1}{4}\xi m\Omega_0^2 q^4. \quad (35.38)$$

To avoid multiplicative noise, i.e. a noise term that depends on the current value of the energy, we consider the square root of the energy rather than the energy itself,

---

<sup>4</sup>Note that  $\phi_{\text{mod}}$  doesn't appear in the expression for  $\zeta(t)$ , since the modulation serves as the time reference and  $\phi_{\text{mod}}$  is the phase of the particle with respect to the modulation.

$$\varepsilon(q, p) = \sqrt{E(q, p)}. \quad (35.39)$$

At low friction, the amplitude  $A$  and phase  $\phi_{\text{mod}}$  with respect to the driving force are quasi-constant, and the particle performs an undisturbed harmonic oscillation evolving according to

$$q(t) = A \cos(\Omega t + \phi_{\text{mod}}) \quad p(t) = -m\Omega A \sin(\Omega t + \phi_{\text{mod}}), \quad (35.40)$$

where the amplitude of the oscillation is related to  $\varepsilon$  by  $A = \sqrt{2/m}(\varepsilon/\Omega)$ . Note that the oscillation frequency  $\Omega$  is not necessarily the same as the frequency  $\Omega_0$  of the unperturbed harmonic oscillator. For instance, for strong modulation the particle motion entrains with the modulation and  $\Omega \approx \Omega_{\text{mod}}/2$  [23].

Applying Ito's formula for the change of variables to  $\varepsilon(q, p)$  and integrating over an oscillation period, we find that the change  $d\varepsilon$  during a short time interval is given by a Langevin equation for a *fictitious* overdamped Brownian particle

$$d\varepsilon = \tilde{\Gamma}^{-1} f(\varepsilon) dt + \sqrt{2k_B T_{\text{CM}} / \tilde{\Gamma}} dW \quad (35.41)$$

with damping  $\tilde{\Gamma} = 4/\Gamma_{\text{CM}}$ , moving through an effective potential

$$U_{\text{eff}}(\varepsilon) = \varepsilon^2 - k_B T_{\text{CM}} \ln \varepsilon + \frac{\varepsilon^2 \zeta_0 \Omega_0^2 \sin(2\phi_{\text{mod}})}{2\Gamma_{\text{CM}} \Omega}, \quad (35.42)$$

under the influence of an external force  $f(\varepsilon) = -dU_{\text{eff}}(\varepsilon)/d\varepsilon$ . Note that due to the integration over one oscillation period, this equation has  $\varepsilon$  as its only time dependent variable, while the dependence on other variables has been removed. By virtue of this isomorphism with over-damped Brownian motion, one can then immediately infer that Eq. (35.41) samples the distribution  $P_\varepsilon(\varepsilon) \propto \exp\{-\beta U_{\text{eff}}(\varepsilon)\}$ , where  $\beta = 1/k_B T_{\text{CM}}$ . Equation (35.41) implies that the time evolution of  $\varepsilon$  can be viewed as a Brownian motion in the high friction limit. A small real friction  $\Gamma_{\text{CM}}$  corresponds to large effective friction  $\tilde{\Gamma}$  determining the time evolution of  $\varepsilon$  and, thus, the energy  $E$  of the oscillator. Interestingly, the *fictitious* Brownian particle of the *time-dependent* optical potential can exhibit similar dynamics to the *real* Brownian particle in a *static* optical potential [24].

Changing variables from  $\varepsilon$  to  $E = \varepsilon^2$  and applying Ito's formula, we finally obtain the probability density function of the energy,  $P_E(E) = \frac{1}{Z} \exp\{-\beta'E\}$ , where  $\beta' = 1/k_B T'_{\text{CM}}$  with effective temperature

$$T'_{\text{CM}} = T_{\text{CM}} \left( 1 + \frac{\zeta_0 \Omega_0^2 \sin(2\phi_{\text{mod}})}{2\Gamma_{\text{CM}} \Omega} \right)^{-1}. \quad (35.43)$$

Equation (35.43) states that parametric modulation of the trapping potential results in an effective temperature change of the environment, where the particle centre-of-mass temperature changes from  $T_{\text{CM}}$  to  $T'_{\text{CM}}$ . For  $-\pi/2 < \phi_{\text{mod}} < 0$ ,  $T'_{\text{CM}} > T_{\text{CM}}$ ,

that is the particle motion is heated, while for  $0 < \phi_{\text{mod}} < \pi/2$ ,  $T'_{\text{CM}} < T_{\text{CM}}$  and the particle motion is cooled. The rate at which the particle thermalizes with this effective bath is  $\Gamma'_{\text{CM}} = \Gamma_{\text{CM}} (T_{\text{CM}}/T'_{\text{CM}} - 1)$ , where the largest rates are achieved at  $\phi_{\text{mod}} = -\pi/4$  and  $\phi_{\text{mod}} = \pi/4$ , for heating and cooling respectively. If the relative phase between the particle motion and the modulation  $\phi_{\text{mod}}$  is not stabilized actively, for example through implementing a phase-locked loop fed back onto the trapping laser intensity, the particle motion will self-lock to  $\phi_{\text{mod}} = -\pi/4$ . Thus, an effective hot bath can be implemented easily by a simple modulation of the trapping laser at  $\Omega_{\text{mod}} \approx 2\Omega_0$ .

The change of variables also yields the corresponding stochastic differential equation for the energy

$$dE = \left[ -\Gamma_{\text{CM}}(E - k_B T_{\text{CM}}) - \frac{\eta \Omega_0 E^2}{2m\Omega^2} - \frac{E \zeta \Omega_0^2 \sin(2\phi)}{2\Omega} \right] dt + \sqrt{2E\Gamma_{\text{CM}}k_B T_{\text{CM}}} dW. \quad (35.44)$$

In contrast to the stochastic equation of motion for  $\varepsilon$ , here the noise is multiplicative, i.e., its amplitude is energy dependent.

Using the active feedback cooling discussed here  $\sim 100 \mu K$  temperatures have been achieved, corresponding to a phonon occupancy of  $\sim 20$  [15]. Another method to use is the passive feedback provided by optical cavity cooling, with firm predictions of reaching the quantum ground-state [9]. The thermal occupation of an optical cavity at room temperature is extremely low, with a photon occupation of  $n_{\text{ph}} = \sqrt{k_B T_{\text{env}}/\hbar\omega_L} \ll 1$ , which forms the effective low temperature bath.

### 35.3.1.1 Non-thermal States

The modulation of the trapping potential gives rise to a non-conservative force that allows us to inject and extract energy from the particle. Since there is a continuous flow of energy, the particle is no longer in thermal equilibrium. Surprisingly, under the appropriate conditions we can describe the particle as in thermal equilibrium with an effective bath (c.f. Eq. (35.43)). However, this description breaks down when we heat the particle ( $\phi_{\text{mod}} = -\pi/4$ ) above the threshold condition  $\zeta > 2Q^{-1}\sqrt{1+Q^2(2-\Omega_{\text{mod}}/\Omega_0)^2} \approx 2Q^{-1}$ , where the approximation is exact at parametric resonance  $\Omega_{\text{mod}} = 2\Omega_0$ . Then the effective temperature diverges and the motion transitions from a thermal state to a coherent oscillation, which is phase-locked to the modulation source, similar to the lasing condition of an optical oscillator.

A more subtle non-equilibrium steady state, which can no longer be described as an effective thermal bath can be achieved by parametric feedback modulation of the form  $\zeta_{\text{fb}}(t) = -(\eta/\Omega_0)q(t)\dot{q}(t)$ , where  $\eta$  parametrizes the feedback strength. This leads to a parametric modulation at the parametric resonance condition, while ensuring a phase that is optimized for extracting energy from the mechanical mode. However, in contrast to the previous case with constant modulation amplitude, here

the modulation amplitude is proportional to the particle energy  $\zeta_0 \propto A^2 \propto E$ . As a consequence, the particle feels a nonlinear friction force with  $\Gamma_{\text{NL}} \propto E$ .

The probability distribution for the energy, including the position dependent feedback term  $\eta$  and parametric modulation with constant amplitude  $\zeta_0$ , is then given by [22]

$$P_E(E) = \frac{1}{Z} \exp \left\{ -\beta \left[ \left( 1 + \frac{\zeta_0 \Omega_0^2 \sin(2\phi_{\text{mod}})}{2\Gamma_{\text{CM}}\Omega} \right) E + \frac{\eta\Omega_0}{4m\Gamma_{\text{CM}}\Omega^2} E^2 \right] \right\}, \quad (35.45)$$

where the normalization factor  $Z = \int P_E(E) dE$  is given by

$$Z = \sqrt{\frac{\pi m \Gamma_{\text{CM}} \Omega^2}{\beta \eta \Omega_0}} h \left( \sqrt{\frac{\beta m \Gamma_{\text{CM}} \Omega^2}{\eta \Omega_0}} \left( 1 + \frac{\zeta_0 \Omega_0^2 \sin(2\phi_{\text{mod}})}{2\Gamma_{\text{CM}}\Omega} \right) \right), \quad (35.46)$$

and the function  $h(x)$  is defined as  $h(x) = \exp(x^2) \text{erfc}(x)$  and  $\text{erfc}(x)$  is the complementary error function. Thus, the energy distribution is that of an equilibrium system with effective energy

$$H = \left[ 1 + \frac{\zeta_0 \Omega_0^2 \sin(2\phi_{\text{mod}})}{2\Gamma_{\text{CM}}\Omega} \right] E + \frac{\eta\Omega_0}{4m\Gamma_{\text{CM}}\Omega^2} E^2. \quad (35.47)$$

While the term proportional to  $E^2$  is caused by the feedback cooling, the term proportional to  $E$  is affected only by the parametric modulation.

For low friction, the energy of the oscillator is essentially constant over many oscillation periods, the full phase-space density  $P_{q,p}$  can be obtained by averaging the micro-canonical distribution  $P_m(q, p; \tilde{E}) = g^{-1}(\tilde{E}) \delta[E(q, p) - \tilde{E}]$  over the energy distribution Eq. (35.45). For low friction constants and small feedback strength, this linear superposition of micro-canonical distributions is valid even under non-equilibrium conditions and we obtain

$$P_{q,p}(q, p) = \frac{\Omega_0}{2\pi} P_E(E(q, p)), \quad (35.48)$$

where the  $E(q, p)$  is given by Eq. (35.38), and we approximated the micro-canonical density of states with the density of states for the harmonic oscillator  $g(\tilde{E}) \approx 2\pi/\Omega_0$ , that is we neglect the Duffing term of the potential in  $g(\tilde{E})$ . Note, however, that while we have neglected the Duffing term in the expression for the density of states, it is included in the energy appearing in the argument of the exponential on the right-hand side of the above Eq. (35.45).

### 35.3.1.2 Thermal Squeezing

A big advantage when using an optically levitated oscillator over conventional nanomechanical oscillators is that the mechanical frequency can be changed by changing the power of the trapping laser. This allows one to perform unconfined time-of-flight measurements, to create physically large superposition states [17], and to prepare squeezed states. In the quantum regime, squeezing enables one to push the fundamental quantum uncertainty below the standard quantum limit. A thermal state can be squeezed to reduce the uncertainty in one of the quadratures at the expense of anti-squeezing the other. While classical thermal squeezing of a levitated particle has been observed experimentally [25], squeezing below the standard quantum limit remains elusive. In the following we discuss how a change in laser power leads to squeezing.

A sudden change, or quench, in power of the trapping beam changes the mechanical frequency to a new value  $\Omega \rightarrow \Omega_s$ . Thus, the time evolution of the position and momentum of the harmonic oscillator is given by

$$q(\tau\Omega_s) = X_Q \cos(\Omega_s\tau) + P_Q \frac{\Omega}{\Omega_s} \sin(\Omega_s\tau) \quad (35.49a)$$

$$p(\tau\Omega_s) = m P_Q \Omega \cos(\Omega_s\tau) - m X_Q \Omega_s \sin(\Omega_s\tau), \quad (35.49b)$$

where we introduced the position and momentum quadratures  $X_Q = q(0)$  and  $P_Q = -\dot{q}(0)/\Omega$  to denote the position and velocity at the time of the quench. After a time  $\tau$ , the power is switched back to its original value and we find that the phase space distribution for position and momentum is

$$\begin{aligned} P_{q,p}^{\text{sq}}(q, p, \tau) &= \frac{\Omega\beta}{2\pi} \times \\ &\exp \left[ -\beta \frac{1}{2} m \Omega^2 \left( [X_Q \cos(\Omega_s\tau) + e^{2r} P_Q \sin(\Omega_s\tau)]^2 \right. \right. \\ &\quad \left. \left. + [P_Q \cos(\Omega_s\tau) - e^{-2r} X_Q \sin(\Omega_s\tau)]^2 \right) \right] \end{aligned} \quad (35.50)$$

where we introduced the squeezing parameter  $r = \frac{1}{2} \log(\Omega/\Omega_s)$ . Therefore, the squeezing pulse of duration  $\tau$  leads to a non-Gaussian state, with correlations between position and momentum. However, at times  $\tau = \pi/2\Omega_s$ , the exponent in Eq. (35.50) simplifies and we find that the position quadrature is squeezed by a factor  $\exp(-2r)$ , while the momentum quadrature is anti-squeezed by  $\exp(2r)$ . Due to the reduced width of the squeezed distribution along a particular direction, this kind of state preparation allows one to reduce the measurement uncertainty. However, to be actually useful, the error introduced by the anti-squeezing of the momentum quadrature should not overwhelm the squeezing of the position quadrature. Note that in contrast to the distribution Eq. (35.48), which describes a steady state distribution, i.e. it does

not depend on the observation time, Eq.(35.50) is defined at a specific time (right after the application of the squeezing pulse). From this distribution, the system will relax back into thermal equilibrium as described in Sect.35.4.2.

## 35.4 Thermodynamics

In this final section we will discuss the application of levitated nanoparticles to problems in stochastic thermodynamics and highlight some relevant experimental results.

### 35.4.1 Kramers Escape and Turnover

We have discussed the dynamics of a particle confined within a potential, and subject to fluctuating forces from the environment. Due to the stochastic nature of the imparted force, there is a probability that the particle will gain enough energy to escape the potential, even when it is confined by a potential much deeper than  $k_B T_{CM}$ , in a process known as Kramers escape. This form of “classical tunnelling” appears in a diverse range of physical systems, importantly including chemical reaction rates, protein folding, atomic transport in optical lattices and molecular diffusion at solid-liquid interfaces [26].

The Kramers’ escape rate is given by

$$R_K = R_0 \exp\left(-\frac{U_{opt}}{k_B T_{CM}}\right) \quad (35.51)$$

where  $R_0$  is the attempt frequency and  $U_{opt}$  is the barrier height. From the Boltzmann factor in Eq.(35.51) it follows that such a transition is exponentially suppressed if the potential is much deeper than the thermal energy  $U_{opt} \gg k_B T_{CM}$ . Closely related to the Kramers escape is the Kramers turnover problem, which describes the tunnelling between two potential minima as the friction is varied. This is often more relevant in physical situations, describing the transitions between two protein configurations, for example. Kramers found [27] that in the underdamped regime, the transition rate increases with *increasing* friction, and that in the overdamped regime the transition rate increases with *decreasing* friction, with the transition region labelled the turnover. Fifty years later, a theory was developed that linked the two regimes [28]. The first quantitative measurement of Kramers turnover was achieved using a levitated nanoparticle hopping between two potential wells formed by focussed laser beams. In this experiment, the friction rate was varied over many orders of magnitude through a change in the gas pressure  $P_{gas}$  [26].

We consider the hopping between two metastable potential wells that are separated by a barrier. The local principal axes are labeled  $i = x', y', z'$  and the potential

extrema are labeled  $p = A, B, C$ , as illustrated in Fig. 35.5a. Since the particle is not lost but recaptured in the second well, this problem is much more convenient to study experimentally than stochastic escape. A double well potential can be created by using two tightly focused laser beams, where the intensity and exact relative position of the two foci determines the height of the barrier. The hopping rates between the two wells is determined by the local curvatures of the potential at the extrema.

In the overdamped regime, the hopping from well  $A$  to well  $C$  via the barrier  $B$  is given by Kramers' law. For a three-dimensional optical potential its dependency on the potential parameters is given by

$$R_{A \rightarrow C}^{\text{HD}} = \frac{1}{2\pi} \prod_{i \in \{x', y', z'\}} \frac{\Omega_i^A}{|\Omega_i^B|} \left[ \sqrt{|\Omega_B^S|^2 + \frac{\Gamma_{\text{CM}}^2}{4}} - \frac{\Gamma_{\text{CM}}}{2} \right] e^{-\frac{U^A}{k_B T_{\text{CM}}}} \approx \frac{1}{2\pi} \frac{\Omega^A \Omega^B}{\Gamma_{\text{CM}}} e^{-\frac{U^A}{k_B T_{\text{CM}}}}, \quad (35.52)$$

where  $\Omega_i^p$  are the three frequencies at the three extrema along the local principal axis  $(x', y', z')$  and  $\Omega_B^S$  is the purely imaginary frequency of the saddle point [26]. The approximation holds in the limit of high damping  $\Gamma_{\text{CM}} \gg \Omega_B$  and one dimensional motion.

In the underdamped regime, on the other hand, the rate is limited by the slow transfer of energy between the particle and its environment. This leads to a hopping rate that is proportional to  $\Gamma_{\text{CM}}$

$$R_{A \rightarrow C}^{\text{LD}} = \frac{\Gamma_{\text{CM}} S^A}{2\pi} \frac{\Omega^A}{k_B T_{\text{CM}}} e^{-\frac{U^A}{k_B T_{\text{CM}}}}. \quad (35.53)$$

where  $S^p = 4 \int_{r_p}^{r_B} \sqrt{2m(U_B - U(\mathbf{r}))} dr$  is the particle action over one oscillation period in well  $p$  and is measured along the minimum energy path of the potential. These two limiting cases were already derived by Kramers [27]. In the transition region, such a simple analytical formula does not exist. Instead the rates depend on the depopulation factor

$$\Upsilon(\delta) = \exp \left[ \frac{1}{\pi} \int_0^\infty \ln \left\{ 1 - \exp \left[ -\frac{\delta}{k_B T} \left( x^2 + \frac{1}{4} \right) \right] \right\} \frac{dx}{x^2 + \frac{1}{4}} \right], \quad (35.54)$$

where  $\delta$  is the energy loss parameter. Generally, the estimation of the energy loss parameter is quite challenging. However, for memory-free friction, the energy loss is well approximated by  $\delta = \Gamma_{\text{CM}} S_p$ .

To account for the difference in transition rates from well  $A$  to  $C$  versus well  $C$  to  $A$  we need to multiply the transition rates by a factor  $\prod_{p=A,B} \Upsilon(\Gamma_{\text{CM}} S^p) / \sum_{p=A,B} \Upsilon(\Gamma_{\text{CM}} S^p)$  and arrive at the general expression for the hopping rate

$$R(\Gamma_{\text{CM}}) = \frac{\Upsilon(\Gamma_{\text{CM}} S^A) \Upsilon(\Gamma_{\text{CM}} S^C)}{\Upsilon(\Gamma_{\text{CM}} S^A + \Gamma_{\text{CM}} S^C)} [R_{A \rightarrow C}^{\text{HD}} + R_{C \rightarrow A}^{\text{HD}}]. \quad (35.55)$$

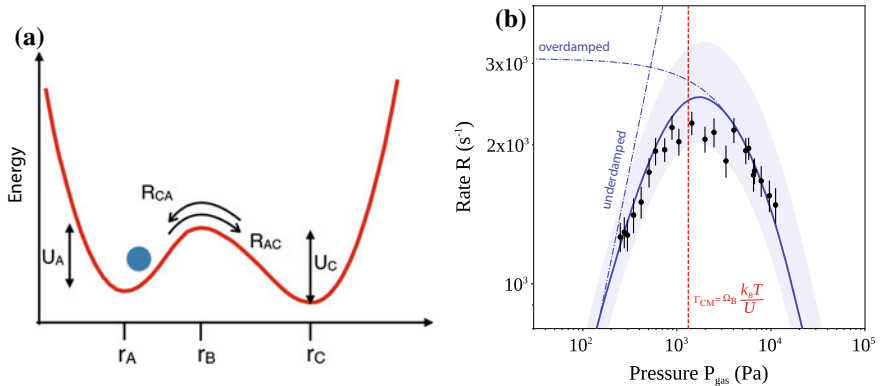


**Fig. 35.5 Measurement of the Kramers turnover with a levitated nanoparticle.** **a** Illustration of a particle in a (generally asymmetric) bistable potential. The hopping rate  $R$  between the wells  $A, C$  depends upon the local potential  $U$ , and the background pressure  $P_{\text{gas}}$ . **b** Data illustrating the first experimental observation of Kramers' turnover, reproduced with permission from *Nature Nanotechnology* [26]. Also marked is the full theory from [28] (solid line), the turnover point which depends on the comparison of the damping rate  $\Gamma_{\text{CM}}$  and the harmonic trap frequency at the crossing point  $\Omega_B$  (dashed line), and the limiting cases as predicted by Kramers [27] (dot-dashed lines).

Figure 35.5b shows the limiting cases in the high and low damping regime, and the full solution for arbitrary damping. In addition, the figure includes experimental data from Rondin et al. which, using an optically levitated nanoparticle, presents the first quantitative measurement of the Kramers rate across the turnover [26].

### 35.4.2 Relaxation

In the steady-state, a trapped particle samples the distribution Eq. (35.45), which depends on experimental parameters, such as the average power of the trapping laser, and the rate and depth of any modulation of the optical potential. Hence, under a non-adiabatic change of the parameters, the system relaxes into a new steady state.

The Fokker–Planck equation that describes the time evolution of the probability density function  $P_E(E, t)$ , including feedback and modulation, is given by

$$\begin{aligned} \frac{\partial P_E(E, t)}{\partial t} = & \frac{\partial}{\partial E} \left[ \Gamma_{\text{CM}}(E - k_B T) + \frac{\eta \Omega_0 E^2}{2m \Omega^2} + \frac{E \zeta_0 \Omega_0^2 \sin(2\phi_{\text{mod}})}{2\Omega} \right] \\ & \times P_E(E, t) + \Gamma_{\text{CM}} k_B T \frac{\partial^2}{\partial E^2} E P_E(E, t). \end{aligned} \quad (35.56)$$

In general it is non-trivial to find an analytic solution to Eq. (35.56). Amazingly, in the absence of feedback cooling ( $\eta = 0$ ), the equation of motion for the energy

corresponds to the Cox–Ingersoll–Ross model for interest rates, for which the exact analytical solution is given by the Noncentral Chi-squared distribution [29]

$$P_E(E|E_0, t) = c_t e^{-c_t(E+E_0 e^{-\Gamma_{CM} t})} I_0(2c_t \sqrt{E E_0 e^{-\Gamma_{CM} t}}), \quad (35.57)$$

where  $c_t = \beta (1 - e^{-\Gamma_{CM} t})^{-1}$ ,  $I_0(x)$  is the modified Bessel function of the first kind and  $E_0$  is the initial energy, i.e.  $P_0(E|E_0) = \delta(E - E_0)$ . As expected, the equilibrium distribution  $P_\infty(E|E_0) = \beta \exp(-\beta E)$  does not depend on the initial conditions and is given by the Maxwell–Boltzmann distribution at temperature  $T_{CM} = 1/(k_B \beta)$ . If the system is initially prepared at  $t = 0$  in a steady state with energy distribution  $P_0(E_0)$ , the energy distribution after time  $t$  is

$$P_E(E, t) = \int_0^\infty P_E(E|E_0, t) P_0(E_0) dE_0. \quad (35.58)$$

For an initial Maxwell–Boltzmann distribution, corresponding to a thermal equilibrium distribution at temperature  $T_{init}$ , the energy distribution at time  $t$  is also a Maxwell–Boltzmann distribution

$$P_E^{\text{MB}}(E, t) = \beta(t) e^{-\beta(t)E}, \quad (35.59)$$

with time dependent temperature

$$T_{CM}(t) = T_\infty + (T_{init} - T_\infty) e^{-\Gamma_{CM} t}. \quad (35.60)$$

Note that the initial temperature  $T_{init}$  and final temperature  $T_\infty$  can be controlled in the experiment by modulation of the trapping laser (feedback cooling), as discussed in Sect. 35.3.1.1 and demonstrated by Gieseler et al. [5]. Explicitly, a levitated nanoparticle can be cooled via feedback to a centre-of-mass temperature  $T_{CM}$  far below the ambient temperature  $T_{env}$ . Once the feedback modulation is switched off, the particle will thermalize with the environment (in general via collisions with surrounding gas), at an average rate  $\Gamma_{CM}$ , which can be controlled by varying the gas pressure. The rate at which the particle relaxes to the new equilibrium state can also be accelerated by using time-dependent potentials [7].

### 35.4.3 Fluctuation Theorems

As a system relaxes to a thermal equilibrium, the dynamics satisfy detailed balance with respect to the equilibrium distribution, and the time reversibility of the underlying dynamics implies that the transient fluctuation theorem

$$\frac{P(-\Delta S)}{P(\Delta S)} = e^{-\Delta S}, \quad (35.61)$$

for the relative entropy change  $\Delta\mathcal{S} = \beta\mathcal{Q} + \Delta\Phi$  (or Kullback–Leibler divergence) holds. The quantity  $\Delta\Phi = \Phi(t) - \Phi(0)$  is the difference in trajectory dependent entropy  $\Phi(t) = -\ln P_0(u(t))$  between the initial and the final states of the trajectory  $u(t)$ . The relative entropy change  $\Delta\mathcal{S}$  is defined as the logarithmic ratio of the probability  $P[u(t)]$  to observe a certain trajectory  $u(t)$  and the probability  $P[u^*(t)]$  of the time reversed trajectory  $u^*(t)$ ,

$$\Delta\mathcal{S} = \ln \frac{P[u(t)]}{P[u^*(t)]}. \quad (35.62)$$

Here,  $u(t)$  denotes an entire trajectory of length  $t$  including position and momentum of the oscillator and  $u^*(t)$  denotes the trajectory that consists of the same states visited in reverse order with inverted momenta.  $\mathcal{Q}$  is the heat absorbed by the bath at reciprocal temperature  $\beta$ . Because no work is done on the system, the heat  $\mathcal{Q}$  exchanged along a trajectory equals the energy lost by the system,  $\mathcal{Q} = -(E_t - E_0)$  where  $E_0$  and  $E_t$  are the energy at the beginning and at the end of the stochastic trajectory. Note that the fluctuation theorem holds for any time  $t$  at which  $\Delta\mathcal{S}$  is evaluated, and it is not required that the system has reached the equilibrium distribution at time  $t$ .

In general, the steady distribution  $P_0(u(t))$  necessary to compute  $\Delta\Phi$  is unknown. However, from the distribution derived for our model Eq. (35.48), we find that for the relaxation from a non-equilibrium steady state generated by nonlinear feedback of strength  $\eta$  and parametric modulation of strength  $\zeta$ , the relative entropy change is given by

$$\Delta\mathcal{S} = -\beta \frac{\zeta \Omega_0^2 \sin(2\phi_{\text{mod}})}{2\Gamma\Omega} [E_t - E_0] - \beta \frac{\eta \Omega_0}{4m\Gamma\Omega^2} [E_t^2 - E_0^2]. \quad (35.63)$$

Thus, our stochastic model allows us to express the relative entropy change during a relaxation trajectory in terms of the energy at the beginning and the end of that trajectory. This model was verified using a levitated nanoparticle by Gieseler et al. [5], when starting from a variety of non-equilibrium steady states.

In addition to the fluctuation statistics during relaxation between steady states, one can also consider fluctuations during different protocols, e.g. during a full thermodynamic cycle or while driving the particle with an external force  $f(t)$  as was done by Hoang et al. [30], who verified a differential fluctuation theorem for the work  $W = -\int_0^\tau \dot{f}(t)q(t)dt$

$$\frac{P(-W, u^*(t))}{P(W, u(t))} = e^{-\beta(W - \Delta F)}. \quad (35.64)$$

The differential fluctuation theorems can be integrated to yield a series of well known fluctuation theorems, such as the Jarzynski equality, the Crooks fluctuation theorem and the Hummer–Szabo relation. Thus, by verifying the underlying

differential fluctuation theorem, the validity of the integral fluctuation theorem is implied. Importantly, the fluctuation theorems are valid for arbitrarily-far-from-equilibrium processes. Both detailed and integral fluctuation theorems allow the estimation of equilibrium free energy changes from nonequilibrium protocols and have found applications in determining the free energies of DNA molecules. For a detailed review, see Ref. [3].

### 35.4.4 Heat Engines

Technology is continuously miniaturizing, but as we pass below the micro-scale the challenge is not limited to the difficulty in constructing small devices. Once the work performed per duty cycle of an engine becomes comparable to the thermal energy of the piston, it is possible for the engine to run in reverse for short times, due to the fluctuating nature of energy transfer with the heat bath. This is exactly the scale at which biological systems operate, and a regime which levitated nano- and micro-particles have access to.

To apply work to a trapped particle, one must either change (via a control parameter  $\lambda_c(t)$ ) the trapping potential  $U(q, \lambda_c)$ , or apply an external force  $f(q, \lambda_c)$ , in which case the incremental work  $d\mathcal{W}$  reads:

$$d\mathcal{W} = (\partial U / \partial \lambda_c) d\lambda_c + f dq, \quad (35.65)$$

with an associated heat increment:

$$d\mathcal{Q} = F dq, \quad (35.66)$$

where  $F(q, \lambda_c) = -(\partial U / \partial q) + f$  is the total force acting on the particle, due to both the potential  $U$  and the external force  $f$ . Importantly, the external force  $f$  accounts for deterministic and stochastic contributions. Hence, along a trajectory  $u(0) \rightarrow u(\tau)$ :

$$\begin{aligned} \mathcal{W}(q(t)) &= \int_0^\tau [(\partial U / \partial \lambda_c) \dot{\lambda}_c + f \dot{q}] dt \\ \mathcal{Q}(q(t)) &= \int_0^\tau \dot{\mathcal{Q}} dt = \int_0^\tau F \dot{q} dt. \end{aligned} \quad (35.67)$$

Next, we will explicitly apply this to the case of a heat engine. We discuss heat engines since they are an extremely useful machine. An engine, or motor, converts one type of energy into mechanical work, and a heat engine specifically converts heat flow between two reservoirs into mechanical work, particularly useful since heat is often generated as a waste product. Schmiedl and Seifert gave the first full description of a colloidal stochastic heat engine [6], which was realized by Blickle and Bechinger a few years later [32]. The engine operates under the following cyclic process (as illustrated in Fig. 35.6): (1) an isothermal transition at temperature  $T_H$  with a time

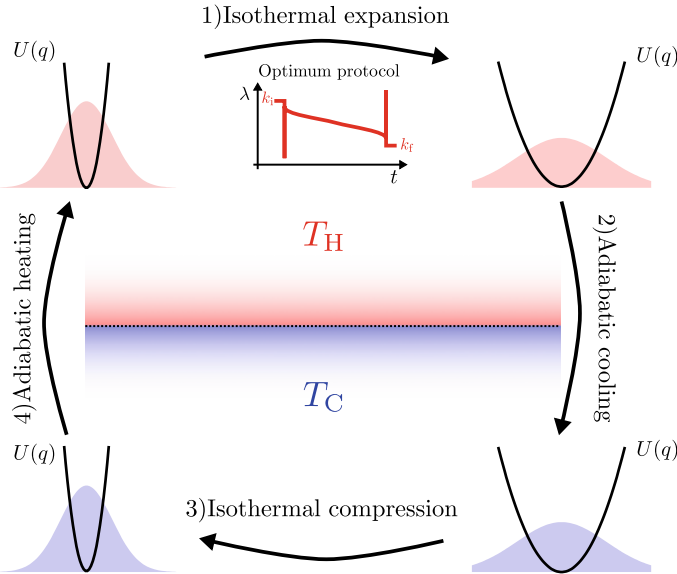


**Fig. 35.6 Stochastic heat engine.** This figure illustrates an engine cycle to realize a stochastic heat engine. A particle is confined by a potential  $U(q, \lambda_c)$ , and coupled to a hot/cold heat bath of temperature  $T_{\text{H/C}}$ . The shaded curves illustrate the position probability distribution of the particle. The cycle is explained in the text. The inset below (1) illustrates an example optimum protocol for realising the compression step for an underdamped heat engine. The trap is expanded by lowering the spring constant from a value  $k_i$  to  $k_f$ , with the most efficient protocol involving sharp parameter variations (adapted from [31]).

dependent variation of  $U(q, t)$  to extract work  $\mathcal{W} < 0$ ; (2) an instantaneous reduction in temperature  $T_{\text{H}} \rightarrow T_{\text{C}}$ , where no heat is exchanged with the bath (adiabatic); (3) an isothermal transition at  $T_{\text{C}}$  with a time dependent variation of  $U(q, t)$  and  $\mathcal{W} > 0$ ; (4) an instantaneous increase in temperature  $T_{\text{C}} \rightarrow T_{\text{H}}$ .

For a harmonically confined particle  $U(q, t) = k(t)q(t)^2/2$ , where  $k$  is the trap stiffness, our control parameter  $\lambda_c(t) \equiv k(t)$ . Other choices of  $\lambda_c$  could include a movement of the trap centre. Reducing  $k$  corresponds to an expansion  $\langle W \rangle < 0$ , as the confinement is weakened. Following references [6, 33], it is convenient to analyse this scenario by considering the equations of motion for the variance  $\sigma_q^2(t) \equiv \langle q^2(t) \rangle$ , with the equation of motion:

$$\dot{\sigma}_q^2 = -m\mu\ddot{\sigma}_q^2 - 2\mu k(t)\sigma_q^2 + 2m\mu\sigma_v^2, \quad (35.68)$$

where  $\mu = 1/(m\Gamma_{\text{CM}})$ ,  $\sigma_v^2(t) \equiv \langle \dot{q}^2(t) \rangle$ , and also noting for the harmonic oscillator that the frequency  $\Omega(t) = \sqrt{k(t)/m}$ . This can be simplified in the overdamped regime  $\Gamma_{\text{CM}} \gg \Omega$ , first by removing the inertial term  $\propto \ddot{\sigma}_q^2$ , and secondly by assuming that the state is always thermal  $\sigma_v^2 = k_B T_{\text{CM}}/m$  [33]. This yields the overdamped equation of motion,

$$\dot{\sigma}_q^2 = -2\mu k(t)\sigma_q^2 + 2\mu k_B T_{CM}. \quad (35.69)$$

Using Eq. (35.67) we find for the total work  $\mathcal{W}$  along an isothermal trajectory at  $T_{CM}$  from time  $t_i \rightarrow t_f$ ,

$$\mathcal{W}(k(t)) = \int_{t_i}^{t_f} \dot{k} \frac{\sigma_q^2}{2} dt, \quad (35.70)$$

where it is evident that the work done on the particle depends on the rate at which the potential is changed. For an instantaneous change in spring constant, where the position distribution of the particle does not have time to change, the work done is simply  $\Delta\mathcal{W} = \frac{1}{2}[k(t_f) - k(t_i)]q(t_i)^2$ . More generally, through solving Eq. (35.69) for  $k(t)$  one finds the full expression for the work along the trajectory:

$$\mathcal{W}(k(t)) = \frac{1}{4\mu} \int_{t_i}^{t_f} \frac{(\dot{\sigma}_q^2)^2}{\sigma_q^2} - \frac{1}{2} T_{CM} [\ln \sigma_x^2]_{t_i}^{t_f} + \frac{1}{2} [k(t)\sigma_q^2]_{t_i}^{t_f}. \quad (35.71)$$

Hence, using this expression, by monitoring the motion of a colloidal particle as it undergoes the cyclic heat engine, one can extract the work statistics. We leave a full discussion of the heat and entropy statistics to other sources, for example Spinney and Ford [34].

How does this discussion of heat engines change in the underdamped regime? In Eq. (35.69) we simplified the equation of motion in the overdamped regime, such that the position was independent of the velocity. This simplification allows one to analytically construct protocols (the way in which  $\lambda_c$  changes over time) that maximize the efficiency of a stochastic heat engine [6]. The overdamped efficiency of a microscopic heat engine can even exceed the Curzon-Ahlborn efficiency-at-maximum-power limit  $\eta^* = 1 - \sqrt{T_C/T_H}$  for macroscopic engines [6].

An analytic solution is not known in the underdamped case, where the position and velocity variables cannot be separated, and numerical methods must be used, which find that the efficiency of the underdamped stochastic heat engine is bounded by  $\eta^*$  [35]. In both regimes, the optimum protocols call for instantaneous jumps in the control parameter<sup>5</sup>  $\lambda_c$ , as illustrated in the inset to Fig. 35.6. In the overdamped regime, a particle reacts slowly to changes in  $\lambda_c$ , whereas in the underdamped regime it reacts rapidly. Hence, although in theory the overdamped efficiency may be higher, practically it may be easier to realize optimum work extraction cycles with an underdamped engine.

To realize an underdamped heat engine, one has to engineer a coupling to an effective heat bath (since by definition an underdamped system is weakly coupled to the environment). Such a coupling is described in detail in Sect. 35.3.1. Dechant et al. [31] propose to realize an underdamped heat engine through a combination of

---

<sup>5</sup>Instantaneous changes minimize work dissipation, since they minimize the time over which a particle is accelerating [35].

optical cavity cooling and thermalization with residual gas. Another option would be to levitate a charged particle in a Paul trap and provide the heat bath via noise applied to nearby electrodes [36, 37], which may be more suitable for operation in the quantum regime.

## References

1. A. Ashkin, J.M. Dziedzic, J.E. Bjorkholm, S. Chu, Observation of a single-beam gradient force optical trap for dielectric particles. *Opt. Lett.* **11**(5), 288–290 (1986). <https://doi.org/10.1364/OL.11.000288>
2. L.P. Faucheux, L.S. Bourdieu, P.D. Kaplan, A.J. Libchaber, Optical thermal ratchet. *Phys. Rev. Lett.* **74**, 1504–1507 (1995). <https://doi.org/10.1103/PhysRevLett.74.1504>
3. U. Seifert, Stochastic thermodynamics, fluctuation theorems and molecular machines. *Rep. Prog. Phys.* **75**(12), 126001 (2012). <https://doi.org/10.1088/0034-4885/75/12/126001>
4. S. Kuhn, A. Kosloff, B.A. Stickler, F. Patolsky, K. Hornberger, M. Arndt, J. Millen, Full rotational control of levitated silicon nanorods. *Optica* **4**(3), 356 (2017). <https://doi.org/10.1364/OPTICA.4.000356>
5. J. Gieseler, R. Quidant, C. Dellago, L. Novotny, Dynamic relaxation of a levitated nanoparticle from a non-equilibrium steady state. *Nat. Nanotechnol.* **9**, 358 EP (2014). <https://doi.org/10.1038/NNANO.2014.40>
6. T. Schmiedl, U. Seifert, Efficiency at maximum power: an analytically solvable model for stochastic heat engines. *EPL (Europhys. Lett.)* **81**(2), 20003 (2008). <https://doi.org/10.1209/0295-5075/81/20003>
7. I.A. Martínez, A. Petrosyan, D. Guéry-Odelin, E. Trizac, S. Ciliberto, Engineered swift equilibration of a brownian particle. *Nat. Phys.* **12**, 843 EP (2016). <https://doi.org/10.1038/nphys3758>
8. A. Bérut, A. Arakelyan, A. Petrosyan, S. Ciliberto, R. Dillenschneider, E. Lutz, Experimental verification of Landauer's principle linking information and thermodynamics. *Nature* **483**, 187 EP (2012). <https://doi.org/10.1038/nature10872>
9. D.E. Chang, C.A. Regal, S.B. Papp, D.J. Wilson, J. Ye, O. Painter, H.J. Kimble, P. Zoller, Cavity opto-mechanics using an optically levitated nanosphere. *Proc. Natl. Acad. Sci.* **107**(3), 1005–1010 (2010). <https://doi.org/10.1073/pnas.0912969107>
10. J. Gieseler, J. Millen, Levitated nanoparticles for microscopic thermodynamics - a review, *Entropy* (2018). <https://doi.org/10.3390/e20050326>
11. S.A. Beresnev, V.G. Chernyak, G.A. Fomyagin, Motion of a spherical particle in a rarefied gas. part 2. drag and thermal polarization. *J. Fluid Mech.* **219**(1), 405–421 (1990). <https://doi.org/10.1017/S0022112090003007>
12. J. Millen, T. Deesawan, P. Barker, J. Anders, Nanoscale temperature measurements using non-equilibrium brownian dynamics of a levitated nanosphere. *Nat. Nanotechnol.* **9**, 425–429 (2014). <https://doi.org/10.1038/nnano.2014.82>
13. M. Lewittes, S. Arnold, G. Oster, Radiometric levitation of micron sized spheres. *Appl. Phys. Lett.* **40**(6), 455–457 (1982). <https://doi.org/10.1063/1.93146>
14. L. Martinetz, K. Hornberger, B.A. Stickler, Gas-induced friction and diffusion of rigid rotors. *Phys. Rev. E* **97**, 052112 (2018). <https://doi.org/10.1103/PhysRevE.97.052112>
15. V. Jain, J. Gieseler, C. Moritz, C. Dellago, R. Quidant, L. Novotny, Direct measurement of photon recoil from a levitated nanoparticle. *Phys. Rev. Lett.* **116**, 243601 (2016). <https://doi.org/10.1103/PhysRevLett.116.243601>
16. A. Bassi, K. Lochan, S. Satin, T.P. Singh, H. Ulbricht, Models of wave-function collapse, underlying theories, and experimental tests. *Rev. Mod. Phys.* **85**, 471–527 (2013). <https://doi.org/10.1103/RevModPhys.85.471>

17. J. Bateman, S. Nimmrichter, K. Hornberger, H. Ulbricht, Near-field interferometry of a free-falling nanoparticle from a point-like source. *Nat. Commun.* **5**, 4788 EP (2014). <https://doi.org/10.1038/ncomms5788>
18. T. Li, S. Kheifets, D. Medellin, M.G. Raizen, Measurement of the instantaneous velocity of a brownian particle. *Science* **328**(5986), 1673–1675 (2010). <https://doi.org/10.1126/science.1189403>
19. G.E. Uhlenbeck, L.S. Ornstein, On the theory of the brownian motion. *Phys. Rev.* **36**(5), 823–841 (1930). <https://doi.org/10.1103/PhysRev.36.823>
20. M.C. Wang, G.E. Uhlenbeck, On the theory of the brownian motion II. *Rev. Mod. Phys.* **17**(2–3), 323–342 (1945). <https://doi.org/10.1103/RevModPhys.17.323>
21. J. Gieseler, L. Novotny, R. Quidant, Thermal nonlinearities in a nanomechanical oscillator. *Nat. Phys.* **9**, 806 EP (2013). <https://doi.org/10.1038/nphys2798>
22. J. Gieseler et al., Non-equilibrium steady state of a driven levitated particle with feedback cooling. *New J. Phys.* **17**(4), 045011 (2015). <https://doi.org/10.1088/1367-2630/17/4/045011>
23. J. Gieseler, M. Spasenović, L. Novotny, R. Quidant, Nonlinear mode coupling and synchronization of a vacuum-trapped nanoparticle. *Phys. Rev. Lett.* **112**(10), 103603 (2014). <https://doi.org/10.1103/PhysRevLett.112.103603>
24. F. Ricci, R.A. Rica, M. Spasenovic, J. Gieseler, L. Rondin, L. Novotny, R. Quidant, Optically levitated nanoparticle as a model system for stochastic bistable dynamics. *Nat. Commun.* **8**, 15141 (2017). <https://doi.org/10.1038/ncomms15141>
25. M. Rashid, T. Tufarelli, J. Bateman, J. Vovrosh, D. Hempston, M.S. Kim, H. Ulbricht, Experimental realization of a thermal squeezed state of levitated optomechanics. *Phys. Rev. Lett.* **117**(27), 273601–5 (2016). <https://doi.org/10.1103/PhysRevLett.117.273601>
26. L. Rondin, J. Gieseler, F. Ricci, R. Quidant, C. Dellago, L. Novotny, Direct measurement of Kramers turnover with a levitated nanoparticle. *Nat. Nanotechnol.* **12**, 1130 EP (2017). <https://doi.org/10.1038/nnano.2017.198>
27. H.A. Kramers, Brownian motion in a field of force and the diffusion model of chemical reactions. *Physica* **7**(4), 284–304 (1940). [https://doi.org/10.1016/S0031-8914\(40\)90098-2](https://doi.org/10.1016/S0031-8914(40)90098-2)
28. V.I. Mel'nikov, The Kramers problem: fifty years of development. *Phys. Rep.* **209**(1), 1–71 (1991). [https://doi.org/10.1016/0370-1573\(91\)90108-X](https://doi.org/10.1016/0370-1573(91)90108-X)
29. D.S.P. Salazar, S.A. Lira, Exactly solvable nonequilibrium Langevin relaxation of a trapped nanoparticle. *J. Phys. A Math. Theor.* **49**(46), 465001–18 (2016). <https://doi.org/10.1088/1751-8113/49/46/465001>
30. T.M. Hoang, R. Pan, J. Ahn, J. Bang, H.T. Quan, T. Li, Experimental test of the differential fluctuation theorem and a generalized Jarzynski equality for arbitrary initial states. *Phys. Rev. Lett.* **120**(8), 080602 (2018). <https://doi.org/10.1103/PhysRevLett.120.080602>
31. A. Dechant, N. Kiesel, E. Lutz, All-optical nanomechanical heat engine. *Phys. Rev. Lett.* **114**, 183602 (2015). <https://doi.org/10.1103/PhysRevLett.114.183602>
32. V. Blickle, C. Bechinger, Realization of a micrometre-sized stochastic heat engine. *Nat. Phys.* **8**, 143 (2011). <https://doi.org/10.1038/nphys2163>
33. A. Dechant, N. Kiesel, E. Lutz, Underdamped stochastic heat engine at maximum efficiency. *EPL (Europhys. Lett.)* **119**(5), 50003 (2017). <https://doi.org/10.1209/0295-5075/119/50003>
34. R.E. Spinney, I.J. Ford, in *Fluctuation relations: a pedagogical overview*, ed. by R. Klages, W. Just, C. Jarzynski. *Nonequilibrium Statistical Physics of Small Systems: Fluctuation Relations and Beyond* (Wiley-VCH, Weinheim, 2012, ISBN 978-3-527-41094-1). [arXiv:1201.6381](https://arxiv.org/abs/1201.6381)
35. A. Gomez-Marin, T. Schmiedl, U. Seifert, Optimal protocols for minimal work processes in underdamped stochastic thermodynamics. *J. Chem. Phys.* **129**(2), 024114 (2008). <https://doi.org/10.1063/1.2948948>
36. I.A. Martínez, É. Roldán, L. Dinis, D. Petrov, R.A. Rica, Adiabatic processes realized with a trapped brownian particle. *Phys. Rev. Lett.* **114**, 120601 (2015). <https://doi.org/10.1103/PhysRevLett.114.120601>
37. D. Goldwater, B.A. Stickler, K. Hornberger, T. Northup, J. Millen, Levitated electromechanics: all-electrical cooling of charged nano- and micro-particles. *Quantum Sci. Technol.* **4**, 024003 (2019). <https://doi.org/10.1088/2058-9565/aaf5f3>

# Chapter 36

## Single Atom Heat Engine in a Tapered Ion Trap



Samuel T. Dawkins, Obinna Abah, Kilian Singer and Sebastian Deffner

### 36.1 Introduction

A recent demonstration of a single atom heat engine [1] has extended a long trend of miniaturisation of thermal machines [2–7] to the level of a single particle. This result was achieved by confining a calcium ion in a linear Paul trap featuring tapered radial confinement. Ion traps feature both exquisite control of ions and a toolbox of laser-based optical techniques to interact with the ion. In the case of the single atom heat engine, these tools allowed for the creation and control of thermal reservoirs, plus the ability to observe the temperature and motion of the ion. The additional feature of tapered confinement provided the means to convert between thermal fluctuations and coherent motion, the essential mechanism of a heat engine.

The primary result of the single atom heat engine is a demonstration of machines at the lowest level, as Feynman had envisaged [8]. Whilst this is fascinating in its own right, the idea of incorporating the phenomena of the quantum world into such machines has attracted a great deal of interest. A collection of various quantum devices have been proposed such as quantum refrigerators, quantum amplifiers and quantum heat pumps [9–17]. Approaching the quantum regime also leads to

---

S. T. Dawkins (✉) · K. Singer  
Experimentalphysik I, Universität Kassel, 34132 Kassel, Germany  
e-mail: samdawkins@gmail.com

K. Singer  
e-mail: ks@uni-kassel.de

O. Abah  
Centre for Theoretical Atomic, Molecular and Optical Physics, Queen's University Belfast,  
Belfast BT7 1NN, UK  
e-mail: abahobinna@gmail.com

S. Deffner  
Department of Physics, University of Maryland Baltimore County,  
Baltimore, MD 21250, USA  
e-mail: deffner@umbc.edu

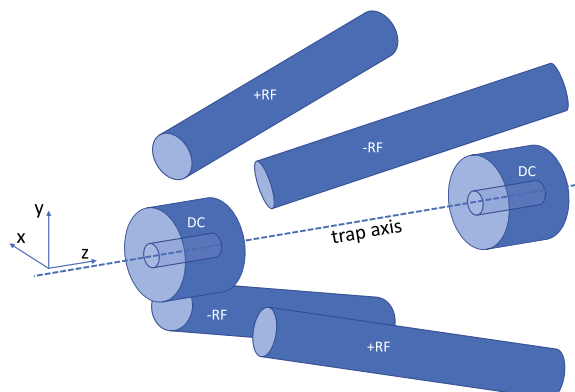
the question: What thermodynamic limits does nature impose on the performance of quantum mechanical devices, in particular thermal machines? Substantial theoretical and experimental effort has been devoted to answering this question [4, 13, 18–29] along with studying the equilibration and thermalisation of quantum systems [30] and more specifically the quantum thermodynamics of heat engines [14, 17–19, 30–38]. Various experimental platforms for investigating these themes include ultracold bosonic atoms [21], quantum dots [32], quantum optomechanical systems [23] and solid state implementations [29]. The tapered trap platform described here provides a powerful system for studying novel thermal devices at ultra-low temperatures at the nanoscale and thus also for addressing open questions of quantum thermodynamics.

## 36.2 Platform

Ions confined in linear Paul traps have been used extensively for experiments in the quantum regime, in particular in the quest to develop a functional quantum processor [39]. This technology employs a three-dimensional confining harmonic potential composed of DC and radio-frequency potentials. Together with optical interactions with laser beams, the platform provides a low-noise environment and affords exquisite control of ion position, temperature and internal states.

Here, the particular variant is a Paul trap with tapered radial confinement. This can be achieved by tilting the electrodes of a standard linear Paul trap, i.e., the distance of the electrodes from the central trap axis scales linearly with the axial position (see Fig. 36.1). It is also conceivable that one could achieve the same effect, or possibly even more complex confinement profiles, by other means, such as via segmented microstructure Paul traps. Note that, in contrast to the standard configuration of Paul traps, the tapered trap features a symmetric rf-drive in order to avoid the detrimental effects of axial micromotion that would arise in a tapered configuration.

**Fig. 36.1** Depiction of the tapered rod electrodes with symmetric radiofrequency drive for radial confinement and the two DC endcap electrodes for axial confinement. The trap axis is in the  $z$ -direction, and  $x$  and  $y$  are the radial directions.



In the case of a single trapped ion, this tapered geometry results in a harmonic pseudopotential with a local radial trapping frequency of the form:

$$\omega(z) = \frac{\omega_0}{(1 + z \tan(\theta)/r_0)^2}, \quad (36.1)$$

where  $\theta$  is the electrode angle and  $\omega_0$  and  $r_0$  are the trap frequency and the radial distance of the electrode respectively, at axial position  $z = 0$ . For limited axial extents, this form can be approximated to be linear, but other functional forms might be designed in order to, for example, implement shortcuts to adiabaticity [19].

The goal of the heat engine is to generate coherent motion in the axial direction from thermal motion in the radial direction. Here, the axial motion is confined by a harmonic potential, which conveniently allows for accumulation of coherent motional energy, much like a flywheel (note that the concept of a flywheel has also been extended to the quantum domain [40]). This axial confinement is chosen to be weaker than the radial confinement such that coherent motion generated in the axial direction has a long oscillation period compared to timescales of the thermal motion in the radial direction. In this way, the total potential energy of the ion results from its radial distribution within the pseudopotential, in addition to its position in the axial harmonic potential. Thus, potential energy can be exchanged between the radial and axial directions, in particular if the extent of the radial distribution is changed. For example, with increasing width of the radial distribution, the averaged radial potential energy is minimised if the ion climbs the axial potential towards a region with smaller radial confinement. As a result, an ion will experience a force in the axial direction which increases with the magnitude of the radial position variance. Note that this force depends on the radial distribution of motion, which is why incoherent radial motion can be converted into coherent axial motion.

### 36.3 Work Bench for Classical Thermodynamics

Ions in harmonic potentials are excellent subjects for performing thermodynamic experiments (see Chap. 38). When the ion interacts with a thermal reservoir (e.g. via a thermal noise mechanism or deliberately engineered perturbations), the motion is described by a thermal state, where the temperature is defined ergodically as the statistical characterisation of the ensemble of external interactions over time. In this way, the external interaction mechanism acts as a thermal reservoir, including some freedom to tune the characteristics of the thermal distribution. In the case of the single atom heat engine, the ion is simultaneously laser-cooled and perturbed by (bandwidth-limited) white noise in the electric field, where both mechanisms contribute to the thermal state of the ion and allow for control of the reservoir temperature.

The addition of the tapered confinement introduces some interesting thermodynamic mechanisms. The tapered potential landscape described above gives rise

to a temperature-dependent averaged force in the axial direction; the temperature determines the radial distribution of the ion and thus the magnitude of the force. Thus, for any non-zero temperature, the ion will equilibrate away from the DC potential minimum in the direction of weaker radial confinement towards the more open end of the taper. A further increase to this temperature will push it even further, and vice versa.

It can be useful to consider the analogy of gas in a container, such as is typically modelled with the equation of state for an ideal gas. The ergodic average of the ion plays the role of a many-particle gas ensemble, and has a corresponding temperature. The radial confinement of the ion plays the role of the volume of the container, where the relevant parameter is the local confining frequency. The force that results in the axial direction is the equivalent of pressure, where rather than integrate an ensemble of particle forces over a wall area (of a piston for example), the force is derived from an integration over time.

Therefore, we can consider the system as having a suite of familiar classical thermodynamic processes. Motion of the ion towards the taper constitutes a compression; motion away from the taper constitutes an expansion. Forces in the axial direction can do work on the ion. Interaction with the engineered reservoir can add or remove thermal energy. Adiabatic processes can be implemented by turning off all reservoir interactions. In this way, one can conceive of all kinds of classical thermodynamic processes such as adiabatic (no reservoir interaction), isothermal (constant temperature), isochoric (constant radial trap frequency) compression/expansion and so on (for quantum analogs, see Chap. 3). By combining these processes, one can construct familiar thermodynamic cycles. An Otto cycle for example involves four strokes: 1. an isentropic compression, 2. a hot isochore, 3. an isentropic expansion, and 4. a cold isochore [37]. In the case of the single atom heat engine, the cycle period is designed to be resonant with the axial trap frequency, and thus the build-up of axial motion becomes dominated by the energy stored in the oscillation mode, rather than the work being generated in each cycle. Thus, the shape of the cycle has a strong sinusoidal component, which combined with the reservoir coupling being continuously on, results in a cycle resembling a Stirling cycle [1].

## 36.4 Entering the Quantum Regime

The single atom heat engine employs thermal states with relatively high temperatures, which is well described by classical thermodynamics. However, the trapped ion platform is commonly taken to the quantum regime via laser-based dissipative state preparation of the motional degrees of freedom. This then allows one to create non-classical motional states such as the ground state, Fock states or squeezed states [41]. In this regime, quantum effects become predominant and have to be fully taken into consideration in the thermodynamic analysis.

Furthermore, non-classical reservoirs could be engineered with quantum effects such as coherence [17], correlations [36], and squeezing [42–44]. Recently, a heat engine whose working medium is a mechanical resonator in contact with a squeezed thermal reservoir [44] has been experimentally demonstrated. In a related development, active bacteria suspensions have been employed to construct a Stirling engine operating between equilibrium and non-equilibrium reservoirs [45]. In addition, motivated by the advances in reservoir engineering techniques in quantum optical systems, such as ion traps [46, 47] and microwave cavities [48], the single atom engine can be used to explore non-equilibrium effects.

## 36.5 Quantum Mechanical Description

We describe the working medium—a single ion in a harmonic pseudopotential oscillating in the radial  $x$ -direction—as a quantum harmonic oscillator, with Hamiltonian  $\hat{H} = \hat{p}^2/2m + m\omega^2\hat{x}^2/2$ , where  $m$ ,  $\hat{p}$  and  $\hat{x}$  are the mass of the ion, the momentum operator and the position operator respectively, which obey the commutation relation,  $[\hat{x}, \hat{p}] = i\hbar$ . For this treatment, we assume a classical thermal reservoir which can be considered as a distribution of infinitely many harmonic oscillators, characterised by the inverse temperature of the reservoir  $\beta = 1/k_B T$ , where  $k_B$  is the Boltzmann constant.

A particularly convenient representation of quantum states is given by the Wigner function [49, 50],

$$W(x, p) = \frac{1}{2\pi\hbar} \int dy \exp\left(-\frac{i}{\hbar} py\right) \langle x + \frac{y}{2} | \rho | x - \frac{y}{2} \rangle. \quad (36.2)$$

The Wigner function contains the full classical information, and its marginals are the probability distributions for the position  $x$  and the momentum  $p$ , respectively. In addition,  $W(x, p)$  contains the full quantum information about a state including coherence, which is signified by areas in phase space where  $W(x, p)$  takes negative values. It can also model quantum effects such as squeezing [19].

The dynamics of an ion in a tapered trap can then be described by a Fokker–Planck equation for  $W(x, p, t)$ , and we have [51, 52]

$$\frac{\partial}{\partial t} W(x, p, t) = \left[ -\frac{p}{m} \frac{\partial}{\partial x} + \frac{\partial}{\partial p} (\gamma p + m\omega^2 x) + D_{pp}(x, t) \frac{\partial^2}{\partial p^2} + D_{xp}(x, t) \frac{\partial^2}{\partial x \partial p} \right] W(x, p, t), \quad (36.3)$$

where  $\gamma$  is the coupling coefficient to the environment. A detailed discussion of the properties of the diffusion coefficients  $D_{pp}$  and  $D_{xp}$  can be found in Ref. [53, 54], but for the present purposes it will suffice to consider a high-temperature, semi-classical expansion. For  $\hbar\beta\omega \ll 1$  the two diffusion coefficients can be written as,  $D_{pp} = m\gamma/\beta + m\beta\gamma\hbar^2(\omega^2 - \gamma^2)/12$ , and  $D_{xp} = \beta\gamma^2\hbar^2/12$ . In this case, the stationary solution simply becomes [51],

$$W_{\text{stat}}(x, p) = \frac{m\gamma\omega}{2\pi} \frac{1}{\sqrt{D_{pp}(D_{pp} + m\gamma D_{xp})}} \exp\left(-\frac{\gamma}{2}\left(\frac{p^2}{D_{pp}} + \frac{m^2\omega^2 x^2}{D_{pp} + m\gamma D_{xp}}\right)\right). \quad (36.4)$$

Thus, we immediately observe that in the limit  $\hbar \rightarrow 0$  Eq. (36.3) reduces to the classical Klein-Kramers equation, and  $W_{\text{stat}}(x, p)$  becomes the classical Maxwell-Boltzmann distribution.

## 36.6 Example: Stirling Cycle

In the single atom heat engine, the cycle can be approximated by the classical Stirling cycle. The Stirling cycle consists of two isothermal processes during which the frequency is varied between  $\omega_1$  and  $\omega_2$ , plus two isochoric (constant frequency) processes during which the oscillator is alternately brought in contact with two different heat reservoirs at inverse temperatures  $\beta_i = 1/(k_B T_i)$  ( $i = 1, 2$ ).

In what follows, we analyse the heat engine performance by evaluating quantum mechanically the average thermodynamic quantities for each of the four consecutive steps of the Stirling cycle (see Fig. 36.2):

- (1) *Isothermal compression A( $\omega_1, \beta_1$ ) → B( $\omega_2, \beta_1$ )*: the frequency is varied while the system is in contact with a reservoir at inverse temperature  $\beta_1$ . The coupling coefficient  $\gamma$  is constant. The system absorbs heat at inverse temperature  $\beta_1$  and performs work according to

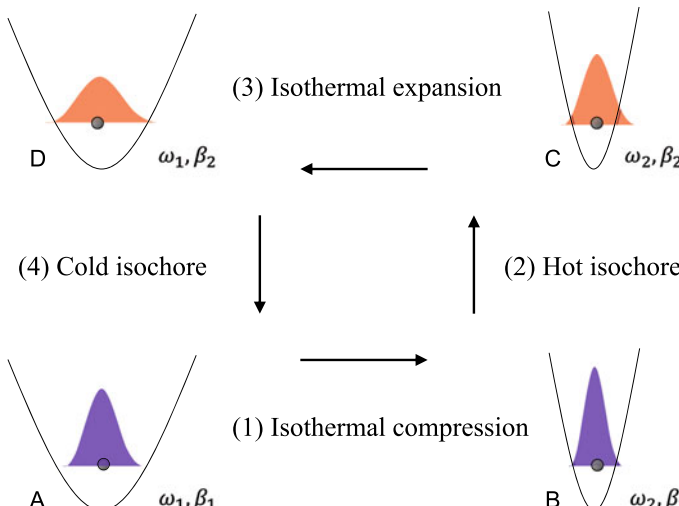


**Fig. 36.2** Stirling cycle of a harmonic oscillator with time-dependent frequency. The thermodynamic cycle consists of two isothermal (compression and expansion steps 1 and 3) and two isochoric processes (heating and cooling steps 2 and 3).

$$\mathcal{W}_{12} = \int_{\omega_1}^{\omega_2} \left\langle \frac{\partial H}{\partial \omega} \right\rangle d\omega = \int_{\omega_1}^{\omega_2} m\omega \langle x^2 \rangle d\omega, \quad (36.5)$$

where  $H$  is the Wigner–Weyl transform of the Hamiltonian.<sup>1</sup> The right-hand-side can be computed explicitly, if we assume that the cycle operates much slower than the equilibration time with the reservoir, which corresponds to the experiment [1]. Thus, we can compute the average with respect to  $W_{\text{stat}}(x, p)$  (36.4), and we obtain

$$\mathcal{W}_{12} = \int_{\omega_1}^{\omega_2} \frac{D_{pp} + D_{xp}m\gamma}{m\gamma\omega} d\omega = \frac{1}{\beta_1} \ln \left( \frac{\omega_2}{\omega_1} \right) + \frac{\beta_1}{24} \hbar^2 (\omega_2^2 - \omega_1^2). \quad (36.6)$$

In this process, the change in internal energy is zero and thus,  $\mathcal{Q}_{12} = -\mathcal{W}_{12}$

- (2) *Hot isochore* B( $\omega_2, \beta_1$ )  $\rightarrow$  C( $\omega_2, \beta_2$ ): the oscillator is held at frequency  $\omega_2$  and instantaneously coupled to a reservoir at inverse temperature  $\beta_2$ . In this process, no work is performed, but heat is exchanged between the ion and the environment. This heat is simply given by the change in the internal energy of the quantum oscillator,

$$\mathcal{U} = \int H(\Gamma) W_{\text{stat}}(\Gamma) d\Gamma = \frac{D_{pp}}{m\gamma} + \frac{D_{xp}}{2} \quad (36.7)$$

with  $\Gamma = (x, p)$ . Thus, we have

$$\mathcal{Q}_{23} = \mathcal{U}_{23} = \left( \frac{1}{\beta_2} - \frac{1}{\beta_1} \right) - \frac{1}{24} \hbar^2 (\gamma^2 - 2\omega_2^2) (\beta_2 - \beta_1) \quad (36.8)$$

- (3) *Isothermal expansion* C( $\omega_2, \beta_2$ )  $\rightarrow$  D( $\omega_1, \beta_2$ ): the frequency is changed back to its initial value at a constant inverse temperature  $\beta_2$ . The change in the internal energy is zero and the work is performed on the system is

$$\mathcal{W}_{34} = \int_{\omega_2}^{\omega_1} \left\langle \frac{\partial H}{\partial \omega} \right\rangle d\omega = \frac{1}{\beta_2} \ln \left( \frac{\omega_1}{\omega_2} \right) + \frac{\beta_2}{24} \hbar^2 (\omega_1^2 - \omega_2^2). \quad (36.9)$$

- (4) *Cold isochore* D( $\omega_1, \beta_2$ )  $\rightarrow$  A( $\omega_1, \beta_1$ ): the system is suddenly coupled back to a reservoir at inverse temperature  $\beta_1$  and quickly relaxes to the initial thermal state A. The frequency is again kept constant. The amount of heat extracted from the system is

$$\mathcal{Q}_{41} = \left( \frac{1}{\beta_1} - \frac{1}{\beta_2} \right) - \frac{1}{24} \hbar^2 (\gamma^2 - 2\omega_1^2) (\beta_1 - \beta_2) \quad (36.10)$$

---

<sup>1</sup>Note that here the Wigner–Weyl transform of the Hamiltonian is identical to the classical Hamiltonian function.

The efficiency of a thermodynamic heat engine is defined as the ratio of the total work per cycle and the heat received from the hot reservoir. In the present case, the Stirling heat engine efficiency reads

$$\eta = -\frac{\langle \mathcal{W}_{12} \rangle + \langle \mathcal{W}_{34} \rangle}{\langle \mathcal{Q}_{34} \rangle + \langle \mathcal{Q}_{23} \rangle}. \quad (36.11)$$

In the high temperature regime,  $\beta_i \hbar \omega_i \ll 1$ , the efficiency then simplifies to

$$\eta = \frac{\eta_C}{1 + \eta_C / \ln(\omega_2 / \omega_1)}, \quad (36.12)$$

which is always below the classical Carnot efficiency.

## 36.7 Conclusion

The tapered trap represents an attractive platform for investigating thermal machines and their corresponding thermodynamics at the single particle level, as demonstrated by the single atom heat engine. Cooling to the ground state and harnessing quantum phenomena, will allow for investigating ideas for engines such as feedback control, squeezed states, performance in the low-temperature limit, shortcuts to adiabaticity and avoiding dissipation. As such, this represents one possible route towards elucidating the fascinating realm of quantum thermodynamics and quantum thermal machines.

**Acknowledgements** S.T.D. and K.S. acknowledge support from the German Research Foundation (grant Einzelionen- wärmekraftmaschine), the Volkswagen Foundation (grant Atomic Nano-Assembler) and European Union (EU) COST action MP1209. O.A. is supported by the Royal Society Newton International Fellowship (grant number NF160966) and the Royal Commission for the 1851 Exhibition. S.D. acknowledges support from the U.S. National Science Foundation under Grant No. CHE-1648973.

## References

1. J. Roßnagel, S.T. Dawkins, K.N. Tolazzi, O. Abah, E. Lutz, F. Schmidt-Kaler, K. Singer, *Science* **352**, 6283 (2016). <https://doi.org/10.1126/science.aad6320>
2. S. Whalen, M. Thompson, D. Bahr, C. Richards, R. Richards, *Sens. Actuators A* **104**, 290–298 (2003). [https://doi.org/10.1016/S0924-4247\(03\)00032-3](https://doi.org/10.1016/S0924-4247(03)00032-3)
3. P. Steeneken, *Nat. Phys.* **7**, 354–359 (2011). <https://doi.org/10.1038/NPHYS1871>
4. J.P. Brantut, C. Grenier, J. Meineke, D. Stadler, S. Krinner, C. Kollath, T. Esslinger, A. Georges, *Science* **342**, 713 (2013). <https://doi.org/10.1126/science.1242308>
5. V. Blickle, C. Bechinger, *Nat. Phys.* **8**, 143 (2012). <https://doi.org/10.1038/nphys2163>
6. I.A. Martínez, *Nat. Phys.* **12**, 67–70 (2016). <https://doi.org/10.1038/nphys3518>
7. T. Hugel, *Science* **296**, 1103–1106 (2002). <https://doi.org/10.1126/science.1069856>

8. R.P. Feynman, Eng. Sci. **23**, 5 (1960). <http://resolver.caltech.edu/CaltechES:23.5.1960Bottom>
9. J. He, J. Chen, B. Hua, Phys. Rev. E **65**, 036145 (2002). <https://doi.org/10.1103/PhysRevE.65.036145>
10. F. Tonner, G. Mahler, Phys. Rev. E **72**, 066118 (2005). <https://doi.org/10.1103/PhysRevE.72.066118>
11. R. Kosloff, A. Levy, Annu. Rev. Phys. Chem. **65**, 365 (2014). <https://doi.org/10.1146/annurev-physchem-040513-103724>
12. E. Boukobza, D.J. Tannor, Phys. Rev. A **74**, 063822 (2006). <https://doi.org/10.1103/PhysRevA.74.063822>
13. R. Alicki, J. Phys. A **5**, L103 (1979). <https://doi.org/10.1088/0305-4470/12/5/007>
14. Y. Rezek, R. Kosloff, New J. Phys. **8**, 83 (2006). <https://doi.org/10.1088/1367-2630/8/5/083>
15. N. Linden, S. Popescu, P. Skrzypczyk, Phys. Rev. Lett. **105**, 130401 (2010). <https://doi.org/10.1103/PhysRevLett.105.130401>
16. H.T. Quan, Y.X. Liu, C.P. Sun, F. Nori, Phys. Rev. E **031105** (2007). <https://doi.org/10.1103/PhysRevE.76.031105>
17. M.O. Scully, M.S. Zubairy, G.S. Agarwal, H. Walther, Science **299**, 862 (2003). <https://doi.org/10.1126/science.1078955>
18. M.J. Henrich, G. Mahler, M. Michel, Phys. Rev. E **75**, 051118 (2007). <https://doi.org/10.1103/PhysRevE.75.051118>
19. R. Kosloff, Y. Rezek, Entropy **19**, 136 (2017). <https://doi.org/10.3390/e19040136>
20. E. Geva, R. Kosloff, J. Chem. Phys. **104**, 7691 (1996). <https://doi.org/10.1063/1.471453>
21. O. Fialko, D.W. Hallwood, Phys. Rev. Lett. **108**, 085303 (2012). <https://doi.org/10.1103/PhysRevLett.108.085303>
22. M. Esposito, R. Kawai, K. Lindenberg, C. Van den Broeck, Phys. Rev. E **81**, 041106 (2010). <https://doi.org/10.1103/PhysRevE.81.041106>
23. K. Zhang, F. Bariani, P. Meystre, Phys. Rev. A **90**, 023819 (2014). <https://doi.org/10.1103/PhysRevA.90.023819>
24. A. Dechant, N. Kiesel, E. Lutz, Phys. Rev. Lett. **114**, 183602 (2015). <https://doi.org/10.1103/PhysRevLett.114.183602>
25. J. Gemmer, M. Michel, G. Mahler, *Quantum Thermodynamics*, (Springer, Berlin, 2009). <https://doi.org/10.1007/978-3-540-70510-9>
26. D. Gelbwaser-Klimovsky, W. Niedenzu, G. Kurizki, *Advances in Atomic, Molecular, and Optical Physics*, vol. 64, (2015), pp. 329–407. <https://doi.org/10.1016/bs.aamop.2015.07.002>
27. K. Brander, K. Saito, U. Seifert, Phys. Rev. X **5**, 031019 (2015). <https://doi.org/10.1103/PhysRevX.5.031019>
28. H.E.D. Scovil, E.O. Schulz-DuBois, Phys. Rev. Lett. **2**, 262 (1959). <https://doi.org/10.1103/PhysRevLett.2.262>
29. M. Campisi, J. Pekola, R. Fazio, New J. Phys. **17**, 035012 (2015). <https://doi.org/10.1088/1367-2630/17/3/035012>
30. S. Vinjanampathy, J. Anders, Contemp. Phys. **57**, 545 (2016). <https://doi.org/10.1080/00107514.2016.1201896>
31. B. Gardas, S. Deffner, Phys. Rev. E **92**, 042126 (2015). <https://doi.org/10.1103/PhysRevE.92.042126>
32. C. Bergenfeldt, P. Samuelsson, B. Sothmann, C. Flindt, M. Bittiker, Hybrid microwave-cavity heat engine. Phys. Rev. Lett. **112**, 076803 (2014). <https://doi.org/10.1103/PhysRevLett.112.076803>
33. R. Kosloff, J. Chem. Phys. **80**, 1625 (1984). <https://doi.org/10.1063/1.446862>
34. E. Geva, R. Kosloff, J. Chem. Phys. **96**, 3054 (1992). <https://doi.org/10.1063/1.461951>
35. T.D. Kieu, Phys. Rev. Lett. **93**, 140403 (2004). <https://doi.org/10.1103/PhysRevLett.93.140403>
36. R. Dillenschneider, E. Lutz, Europhys. Lett. **88**, 50003 (2009). <https://doi.org/10.1209/0295-5075/88/50003>
37. O. Abah, J. Roßnagel, G. Jacob, S. Deffner, F. Schmidt-Kaler, K. Singer, E. Lutz, Phys. Rev. Lett. **109**, 203006 (2012). <https://doi.org/10.1103/PhysRevLett.109.203006>

38. A. Friedenberger, E. Lutz, *Europhys. Lett.* **120**, 10002 (2017). <https://doi.org/10.1209/0295-5075/120/10002>
39. K. Brown, J. Kim, C. Monroe, *NPJ Quantum Inf.* **2**, 16034 (2016). <https://doi.org/10.1038/npjqi.2016.34>
40. A. Levy, L. Disi, R. Kosloff, *Phys. Rev. A* **93**, 052119 (2016). <https://doi.org/10.1103/PhysRevA.93.052119>
41. D. Kienzler, *Science* **347**, 53 (2015). <https://doi.org/10.1126/science.1261033>
42. J. Roßnagel, O. Abah, F. Schmidt-Kaler, K. Singer, E. Lutz, *Phys. Rev. Lett.* **112**, 030602 (2014). <https://doi.org/10.1103/PhysRevLett.112.030602>
43. O. Abah, E. Lutz, *Europhys. Lett.* **106**, 20001 (2014). <https://doi.org/10.1209/0295-5075/106/20001>
44. J. Klaers, S. Faelt, A. Imamoglu, E. Togan, *Phys. Rev. X* **7**, 031044 (2017). <https://doi.org/10.1103/PhysRevX.7.031044>
45. S. Krishnamurthy, S. Ghosh, D. Chatterji, R. Ganapathy, A.K. Sood, *Nat. Phys.* **12**, 1134 (2016). <https://doi.org/10.1038/nphys3870>
46. J.F. Poyatos, J.I. Cirac, P. Zoller, *Phys. Rev. Lett.* **77**, 4728 (1996). <https://doi.org/10.1103/PhysRevLett.77.4728>
47. C.J. Myatt, B.E. King, Q.A. Turchette, C.A. Sackett, D. Kielpinski, W.M. Itano, C. Monroe, D.J. Wineland, *Nature (London)* **403**, 269 (2000). <https://doi.org/10.1038/35002001>
48. A. Sarlette, J.M. Raimond, M. Brune, P. Rouchon, *Phys. Rev. Lett.* **107**, 010402 (2011). <https://doi.org/10.1103/PhysRevLett.107.010402>
49. E. Wigner, *Phys. Rev.* **40**, 749 (1932). <https://doi.org/10.1103/PhysRev.40.749>
50. W.P. Schleich, *Quantum Optics in Phase Space* (Wiley, Weinheim, 2001). <https://doi.org/10.1002/3527602976>
51. S. Deffner, *Europhys. Lett.* **103**, 30001 (2013). <https://doi.org/10.1209/0295-5075/103/30001>
52. R. Dillenschneider, E. Lutz, *Phys. Rev. E* **80**, 042101 (2009). <https://doi.org/10.1103/PhysRevE.80.042101>
53. H.-P. Breuer, F. Petruccione, *The Theory of Open Quantum Systems* (Oxford University Press, New York, 2002). <https://doi.org/10.1093/acprof:oso/9780199213900.001.0001>
54. B.L. Hu, J.P. Paz, Y. Zhang, *Phys. Rev. D* **45**, 2843 (1992). <https://doi.org/10.1103/PhysRevD.45.2843>

# Chapter 37

## Quantum Thermodynamics in a Single-Electron Box



Jonne V. Koski and Jukka P. Pekola

In an electronic system, the thermodynamic quantities of heat and entropy are transferred by electrons, while work is done on the system by externally applied potentials. These systems are very well defined with a simple, easily controllable Hamiltonian. The crucial ingredients to conduct the experiments are the ability to track the transitions of single electrons, or to infer the transferred heat from a change in local electronic temperature. The immediate benefit of an electronic setup is the robustness of the device, permitting hundreds of thousands of repetitions and therefore reliable statistics of the chosen thermodynamic process in contrast to experiments with molecular or colloidal particles, where the number of repetitions is typically limited to hundreds.

The chapter is outlined as follows. The first four sections give the principles and methods required to design and execute thermodynamic experiments with a single-electron box. The last four sections review the recent thermodynamic experiments conducted in that setting.

### 37.1 Heat in Electronic Systems

In this chapter we are mainly concerned with systems where finite heat baths are formed of electrons in an island of normal metal [1]. In practise these reservoirs are thin film metals fabricated by electron-beam lithography. Due to manufacturing

---

J. V. Koski (✉)

Department of Physics, ETH Zurich, CH-8093 Zurich, Switzerland  
e-mail: koskij@phys.ethz.ch

J. P. Pekola

QTF Centre of Excellence, Department of Applied Physics, Aalto University School of Science, P.O. Box 13500, 00076 Aalto, Finland  
e-mail: jukka.pekola@aalto.fi

constraints, the islands have typically a volume of  $10^{-3} \mu\text{m}^3$  or larger, which means that there are of the order of or more than  $10^9$  conduction electrons in this system. Thus it is fair to say that such an island serves as a body to which temperature can be assigned, at least in equilibrium. Thermal electrons in this dot are only weakly coupled to the rest of the circuit. Typically this is made possible by embedding it in a low temperature ( $\ll 1$  K) environment, where coupling to phonons, which typically scales with temperature as  $T^5$  [2], is extremely weak. For many experiments to be presented below, namely the ones based on electron counting, this weakness of the coupling is not essential though. In all the experiments and their analysis, it is, however, important that the relevant relaxation timescales have a certain hierarchy. In particular, it is essential that the electron-electron (e-e) relaxation time is the fastest one in the system. For standard metallic structures, this relaxation time is  $10^{-9}$  s or shorter [3], which makes it about four orders of magnitude faster at the said temperatures than the electron-phonon (e-p) relaxation time [2], the other fundamental relaxation process in this system. If furthermore the external drive of the system is slow in comparison to the e-e relaxation rate, one may always assume that the electrons in the normal metal form a heat bath with well-defined local temperature at all instants of time.

## 37.2 Charge and Heat Transport Across a Tunnel Junction

In stochastic thermodynamics experiments performed up to now, heat has been measured by indirect means [4]. In other words, one typically relies on measurement of charges, voltages or currents in electrical circuits or on positions or momenta in mechanical systems, which allow one to evaluate the heat via a model applicable to the system in question. Direct measurement of stochastic heat is still elusive, although it looks feasible at least in a low temperature experiment on electric circuits as presented here [5]. Single-electron systems, in particular a single-electron box (SEB), see next chapter, provide a well characterized set-up to investigate stochastic thermodynamics either by indirect means but also by direct measurement of heat in the future.

A basic element in (single-)electronic circuits is a tunnel barrier, which in our metallic systems separates two Fermi seas of electrons, see Fig. 37.1. A chemical potential difference  $\Delta\mu = eV$  given by the voltage difference  $V = V_L - V_R$  is applied across the barrier between reservoirs  $L$  and  $R$ . Under these conditions, a tunneling event through the barrier leads to dissipation. If the electron tunneling from the left lead has energy  $E$  with respect to the Fermi level at  $eV_L$ , the energy deposited to this reservoir equals  $Q_L = eV_L - E$ . Now assuming an elastic process, with no exchange of energy by the electron in the process (horizontal arrow in Fig. 37.1), the electron lands on the right reservoir at the energy  $E - eV_R$ , which is also the energy input  $Q_R$  to this lead. Although the energies deposited to  $L$  and  $R$  vary stochastically depending on the energy  $E$  of the tunneling electron, the total heat input to the system formed of the left and right sides of the junction is

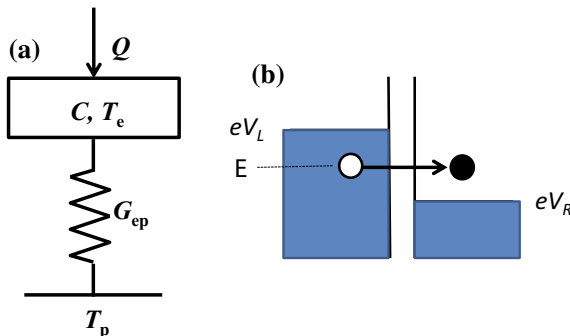


**Fig. 37.1** Schematics of the systems discussed. **a** Typically a finite electron system (metal conduction electrons) with heat capacity  $C$  and at temperature  $T_e$  interacts weakly with the phonon bath at temperature  $T_p$  via thermal conductance  $G_{ep}$ . Electrons themselves interact to establish internal thermal equilibrium. The electron system is subject to various heat inputs  $Q$ . **b** A tunnel barrier with chemical potential difference  $eV$ , where  $V = V_L - V_R$ . An electron tunnels at energy  $E$ , creating an excitation (heating) in both electrodes.

constant equal to  $Q = Q_L + Q_R = e(V_L - V_R) = eV$ , as one would naively expect. In terms of the total heat  $Q$ , the stochasticity of the process is then determined by the number of electrons tunneling during the observation time [6]. Alternatively, under time-dependent driving protocols, it is determined by the instantaneous value of  $V(t)$  at the time instant when the electron tunnels [7].

The rate of tunneling from  $L$  to  $R$  is given by a golden- rule based expression

$$\Gamma = \frac{1}{e^2 R_T} \int_{-\infty}^{\infty} dE n_L(E - eV_L) n_R(E - eV_R) f_L(E - eV_L) [1 - f_R(E - eV_R)], \quad (37.1)$$

where  $R_T$  is the tunnel resistance of the barrier (determined by the properties of the junction),  $n_i(E)$  is the (normalized) density of states of electrons, and  $f_i(E)$  the distribution of electrons in lead  $i = L, R$ . The two types of conductors considered in this chapter are normal metal (N, copper), for which  $n_N(E) = 1$ , and a superconductor (S, aluminum), for which  $n_S(E) = \text{Re}(|E|/\sqrt{(E)^2 - \Delta^2})$ , where  $\Delta$  is the superconductor energy gap [8]. The main feature of  $n_S(E)$  is that the density is zero for the energy range  $-\Delta \leq E \leq \Delta$ . If electrons in each lead are internally in equilibrium, they form a Fermi-Dirac distribution  $f_i(E) = 1/(1 + e^{E/k_B T_i})$ , where the temperatures of the two leads are given by  $T_L$  and  $T_R$ , respectively. Tunneling given by Eq. (37.1) is stochastic, and in the case of no correlations and assuming a fixed chemical potential difference  $eV$  across the barrier, it is a Poisson process.

For a more general description, it is convenient to view the transition rate for a specific energy cost  $\Delta E$ , that is, the difference in energy between the final and initial state. In the case of a voltage  $V$  biased tunnel junction where the electron is

initially at potential  $V_L$  and finally at potential  $V_R$ , we have  $\Delta E = eV_R - eV_L$ . This translates the tunneling rate by Eq. (37.1) to

$$\Gamma_{L \rightarrow R}(\Delta E) = \frac{1}{e^2 R_T} \int_{-\infty}^{\infty} dE n_L(E) n_R(E - \Delta E) f_L(E) [1 - f_R(E - \Delta E)]. \quad (37.2)$$

In accordance to thermodynamic principles, when the two leads are at equal temperatures  $T_L = T_R = T$ , the tunneling rate obeys detailed balance  $\Gamma_{L \rightarrow R}(\Delta E)/\Gamma_{R \rightarrow L}(-\Delta E) = \exp(-\Delta E/k_B T)$ .

### 37.3 Single-Electron Effects

As covered in the previous section, heat is primarily transported in nanoelectronic circuits by electrons. Those electrons are subject to mutual Coulomb interaction that can influence the properties of the device dynamics. As discussed below, when the size scale and the temperature of the circuit is small, this interaction becomes the dominant effect and the total electron number in the system is critical at the precision of one electron. Such devices are in general known as single-electron devices, of which the most relevant for this chapter are the single-electron box and the single-electron transistor.

A single-electron box (SEB) consists of a single piece of metal - an ‘island’ - connected to a grounded metallic lead by a tunnel junction and coupled to a gate electrode with capacitance  $C_g$ . The tunnel junction allows electrons to tunnel into and out of the island, changing the total charge of the island by  $\pm e$ . When an electron tunnels to the island, further electrons that would follow are repelled by the previously added negative charge. This effect is characterized by charging energy  $E_{ch} = \frac{(-en)^2}{2C} \equiv E_C n^2$ , where the net charge on the island is  $-en$  for  $n$  electrons, and  $C$  is the total capacitance of the island. The charging energy for a single-electron,  $E_C = e^2/2C$ , is the characteristic energy scale of the SEB. The island charge can be manipulated by gating, i.e. by tuning the gate electrode potential  $V_g$ . If the applied potential is positive, it will attract a negative charge equal to  $-C_g V_g$  to the island. This corresponds to an effective gate number  $n_g = C_g V_g/e$  that can be non-integer as it describes charge rearrangement on the island adapting to the surrounding potential rather than actual number of electrons. The Hamiltonian of the SEB is then

$$H = E_C(n - n_g)^2. \quad (37.3)$$

An SEB constitutes a controllable two-level system as follows. The system degree of freedom is  $n$  and the control parameter is  $n_g$ . If the charging energy is substantially larger than thermal energy,  $E_C \gg k_B T$ , only the lowest energy states need to be considered. Note that the charging energy by Eq.(37.3) remains constant if both  $n$  and  $n_g$  are offset by an integer. We can therefore consider  $n_g$  to be operated in the range 0...1, such that the single-electron box forms a two-level system with

possible states  $n = 0$  or  $n = 1$ . The energy difference between the two states can be readily controlled with  $V_g$  and is given by Eq. (37.3) as  $\Delta E = H_{n=1} - H_{n=0} = -2E_C(n_g - 0.5)$ .  $\Delta E$  directly determines the transition rate for the event  $n : 0 \rightarrow 1$  (an electron enters the island, changing the number of electrons from 0 to 1) as  $\Gamma_{L \rightarrow R}(\Delta E) \equiv \Gamma_{0 \rightarrow 1}$ , and for  $n : 1 \rightarrow 0$  as  $\Gamma_{R \rightarrow L}(-\Delta E) \equiv \Gamma_{1 \rightarrow 0}$  from Eq. (37.2). The control parameter value  $n_g = 0.5$  sets the two states to have equal energy, and is often referred to as the degeneracy point. As thermal fluctuations are relevant when  $|\Delta E| \lesssim k_B T$ , most thermodynamic processes take place around this point.

Next we consider the validity of the two-level condition, i.e. the criterion  $E_C \gg k_B T$ , for practical nanoscale devices. If the SEB island with a maximum length scale of  $l = 1 \mu\text{m}$  lies on a silicon/silicon oxide substrate (self capacitance  $C_0 \sim (\epsilon_{\text{Si}} + \epsilon_0)l/2 \approx 50 \text{ aF}$ ) and is tunnel coupled to a metallic lead through an aluminum oxide insulator layer with a thickness of  $d = 2 \text{ nm}$  and a cross section area of  $A = 100 \times 100 \text{ nm}^2$  (capacitance  $C_J = \epsilon_{\text{Al}_2\text{O}_3}A/d \approx 440 \text{ aF}$ ), the single electron charging energy is  $E_C = e^2/2(C_0 + C_J) \approx k_B \times 2 \text{ K}$ . Dilution cryostats can routinely reach temperatures of  $T \ll 50 \text{ mK}$  well ascertaining the condition  $E_C \gg k_B T$ . A standard SEB therefore realizes a two-level system as the probability to be in a state other than  $n = 0$  or  $n = 1$  is  $P < 10^{-17}$ .

A single-electron transistor (SET) is similar to an SEB, with the distinction that the island is connected to two (or more) metallic leads. An example device is shown in Fig. 37.2. The two leads can further have potentials  $V_L = V/2$  and  $V_R = -V/2$ , where L(R) refers to the left (right) lead and  $V$  is the potential bias. The charge current from the left to the right lead occurs under a finite bias  $V$  and is controlled with the gate voltage  $V_g$ , as seen in Fig. 37.2. When  $|\Delta E| > eV/2$ , charge transport is suppressed as Coulomb blockade prevents electrons from tunneling into (out of) the island, while with  $|\Delta E| < eV/2$ , electrons can consecutively tunnel in from the left lead, and out to the right lead. In general, the full dynamics can be modeled with a rate equation,

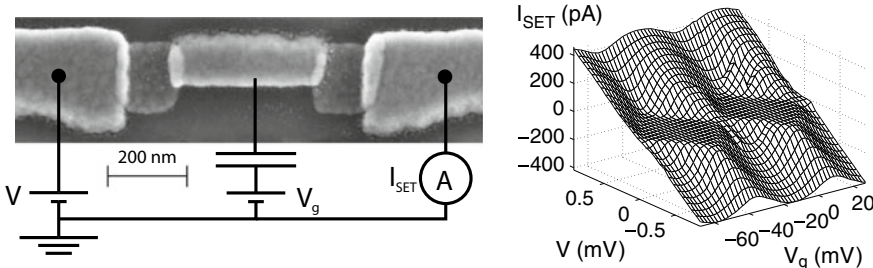


**Fig. 37.2** Left panel: An example of a single-electron transistor. A metallic island (structure in the middle) is connected to two metallic leads by tunnel junctions. The SET is voltage  $V$  biased, and the current  $I_{\text{SET}}$  is manipulated by the gate voltage  $V_g$ . Right panel: Measured current through the SET as a function of  $V$  and  $V_g$ . Reproduced from [9], with permission from AIP Publishing.

$$dP_n/dt = \Gamma_{n+1 \rightarrow n}^{\text{out}} P_{n+1} + \Gamma_{n-1 \rightarrow n}^{\text{in}} P_{n-1} - (\Gamma_{n \rightarrow n-1}^{\text{out}} + \Gamma_{n \rightarrow n+1}^{\text{in}}) P_n, \quad (37.4)$$

where  $P_n$  is the probability to occupy state  $n$ , and  $\Gamma_{n \rightarrow n \pm 1}^{\text{in}(\text{out})}$  is the transition rate in (out) from the island, changing the state from  $n$  to  $n \pm 1$ . The probability distribution  $P_n$  can be solved under steady state  $dP_n/dt = 0$  and normalization  $\sum P_n = 1$ . The current to lead R is then given by

$$I_R = \sum_n \Gamma_{n \rightarrow n+1}^{\text{out}, R} P_{n+1} - \Gamma_{n+1 \rightarrow n}^{\text{in}, R} P_n, \quad (37.5)$$

where the superscript R refers to transitions occurring by tunneling events through the right junction. Note that at steady state, the current to lead L,  $I_L = -I_R$ .

### 37.4 Detecting the Charge in a Single-Electron Box

An SEB provides a controllable two-level system, however an ability to time-dependently resolve its charge state is essential for the execution of thermodynamic experiments. This is realized with a charge detector in form of an SET by coupling the islands of the two devices with capacitance  $C_{\text{int}}$ , as illustrated in Fig. 37.3. The two coupled devices follow a Hamiltonian

$$H = E_C(n - n_g)^2 + E_C^{\text{det}}(n^{\text{det}} - n_g^{\text{det}})^2 + J(n - n_g)(n^{\text{det}} - n_g^{\text{det}}). \quad (37.6)$$

Here, the superscript ‘det’ refers to the SET, and  $J = e^2 C_{\text{int}} / (CC_{\text{det}} - C_{\text{int}}^2)$  describes the mutual Coulomb interaction between the electrons in the two islands. An electron tunneling in the SEB ( $\Delta n = \pm 1$ ) effectively acts as a gate voltage change  $\Delta n_{g,\text{eff}}^{\text{det}} = -J \Delta n / (2E_C^{\text{det}})$  on the SET. Therefore, when the SET is voltage  $V$  biased and operated in a regime of finite current flow, its current switches between two values  $I_0$  and  $I_1$  that correspond to the two states  $n = 0$  or  $n = 1$  whenever an electron tunnels in the SEB. By measuring a time trace of the current through the SET during a thermodynamic process, the evolution of the system state  $n$  is determined in real time as demonstrated in Fig. 37.3.

Practical charge detection schemes are limited by the bandwidth of the detector. This is typically set by the cut-off frequency of a low-pass filter, either determined by the measurement setup, or by noise that has to be averaged out to reach a sufficient signal-to-noise ratio for exact determination of the charge state. For a standard SET charge detector, a typical bandwidth is up to 1 kHz, and the frequency of tunneling events in the system should be lower for an accurate time-resolved determination of the system state evolution. A typical tunnel junction resistance is of the order of 100 kΩ, which means that a fully normal metallic SEB would not qualify for these experiments. At 50 mK temperature, a normal metallic SEB would give a tunnel rate by Eq. (37.2) of 300 MHz at the degeneracy point, significantly exceeding the detection bandwidth. However, by fabricating either the SEB island or the lead (or,

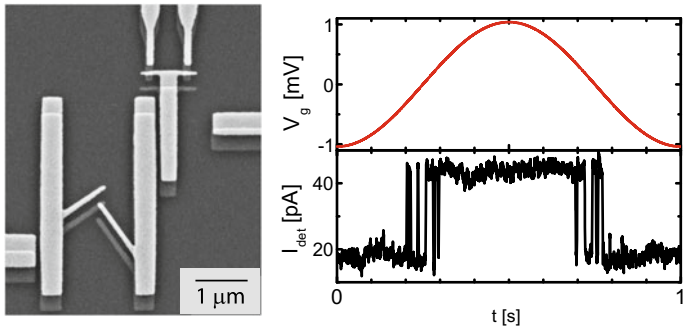


**Fig. 37.3** Left panel: A scanning electron micrograph of a single-electron box coupled to a single-electron transistor. The light gray features are copper, and the gray ‘shadows’ of the same features are aluminum covered by an insulating aluminum oxide layer. The H-shaped SEB has a charging energy of  $E_C \approx 2$  K and is cooled down to 200 mK and below, ensuring that it behaves as a two-level system. A tunnel junction is connecting the two halves of the “H”. The SET, which is the fork-shaped structure on the top, lies close to the SEB, resulting in capacitive coupling that facilitates charge detection. Right panel: modulating the gate voltage  $V_g$  triggers an evolution of the charge state  $n(t)$  observed as jumps in the detector current  $I_{\text{det}}$ . Reproduced figure with permission from [7]. Copyright 2012 by the American Physical Society.

in case of a two-island SEB, one of the islands) out of aluminum (superconducting below 1 K), the superconductor energy gap  $\Delta \simeq 200$   $\mu$ eV drastically suppresses the tunneling rates to 1–1000 Hz level around the degeneracy point, bringing the events to a detectable range. This method is used in the experiments reviewed in the next three sections.

With the charge detection scheme discussed above, the system state as a function of time,  $n(t)$ , can be resolved. Other thermodynamically relevant quantities, namely the state occupation probability and transition rates for a given control parameter  $n_g$ , are determined from long time traces of  $n(t)$  for a stationary  $n_g$ . The trace duration  $T$  should cover a sufficient number of tunneling events to gain reasonable statistical reliability. Then the steady state occupation probability  $P_n(n_g)$  is determined from the total time  $T_n$  spent on the state  $n$  as  $P_n(n_g) = T_n/T$ .

The tunneling rates  $\Gamma_{0 \rightarrow 1}$  and  $\Gamma_{1 \rightarrow 0}$  are extracted by determining the lifetime of states 0 and 1, that is, the average time that the system spends in state 0 or 1 before transitioning to the other state. First, the time instants and the initial and final states of tunneling events are extracted from a time trace with stationary  $n_g$ . For each recorded tunneling event, the time spent on the state  $n$  to which the event brought the system is determined as the time  $\tau_n$  until the next tunneling event occurs. The lifetime of state  $n$  is the average  $\langle \tau_n \rangle$ . The corresponding tunneling rate is then determined as  $\Gamma_{n \rightarrow (1-n)} = 1/\langle \tau_n \rangle$ . For a given  $\Delta E$  as determined by the control parameter  $n_g$  and at uniform electronic temperature  $T_e$ , the tunneling rates follow detailed balance,  $\ln(\Gamma_{0 \rightarrow 1}/\Gamma_{1 \rightarrow 0}) = -\Delta E/k_B T_e$ . Assuming that the SEB electrodes are well thermalized to the cryostat temperature so that  $T_e$  is known, the calibration for  $\Delta E(V_g)$  is obtained from the detailed balance condition.

### 37.5 Single-Electron Box as a Testbed for Quantum Thermodynamics

This section gives a brief overview of the experimental test in [7] on Jarzynski equality [10] ( $\exp(-W/k_B T) = \exp(-\Delta F/k_B T)$ ), where  $W$  is the applied work and  $\Delta F$  is the free energy difference, and Crooks relation [11],  $\ln(P(W)/P_R(-W)) = (W - \Delta F)/k_B T$ , where  $P(W)$  is the probability to apply work  $W$  in the forward process and  $P_R(-W)$  is the probability for negative work in the reverse process. The test is carried out by introducing a drive protocol to the SEB that transfers an electron from the left island to the right, and a reverse protocol that does the opposite. Each realization of the protocol requires work and generates heat stochastically. The statistics of those quantities are studied by performing multiple realizations of the drive protocol.

More specifically, the SEB shown in Fig. 37.3, is driven by modulating the control parameter as  $n_g(t) = 1/2 - \cos(2\pi f t)/2$  while continuously monitoring the charge state  $n(t)$  with a nearby SET. This drive is symmetric around the degeneracy point  $n_g = 1/2$ . A single realization of the drive protocol is taken from  $t = 0$  to  $t = 1/(2f)$ , during which the system is driven across the degeneracy point from  $\Delta E = E_C$  where  $n = 0$  is the ground state to  $\Delta E = -E_C$  where  $n = 1$  is the ground state. The reverse process takes place from  $t = 1/(2f)$  to  $t = 1/f$  bringing the state from  $n = 1$  to  $n = 0$ . Thus each period of drive consists of two identical realizations of the protocol. One of the initial criteria to test JE is to start from thermal equilibrium, which is the case in the experiment since the system always starts from the ground state under the given experimental conditions.

For each realization of the drive protocol the relevant thermodynamic quantities, work and heat, are determined from the measured trace  $n(t)$  as follows. As mentioned in Sect. 37.2, heat is generated at every electron tunneling event that takes place during the process as an electron carries an energy  $E$  from source to target electrode, and the excess energy is distributed to the reservoirs as heat. Correspondingly, in a tunneling event, the energy of the system changes by  $\Delta E$  as determined by the control parameter  $n_g$ . Energy conservation requires that the energy added to the system must originate from the heat baths, generating heat  $Q = -\Delta E(n_g)$ . If a single trace has multiple tunneling events, indexed with  $i$ , the total heat generated is

$$Q = - \sum_i \Delta n_i \Delta E(n_{g,i}), \quad (37.7)$$

where  $\Delta n_i$  is the electron number change in tunneling event  $i$  (+1 for  $n : 0 \rightarrow 1$  and -1 for  $n : 1 \rightarrow 0$ ), and  $n_{g,i}$  is the value of the control parameter at the given time instant of the tunneling event. Work, in contrast, is applied when the drive changes the system energy  $H$  by Eq. (37.3). For a single trace of duration  $T$ , work is evaluated as

$$W = \int_0^T 2E_C(n_g(t) - n(t)) \frac{dn_g(t)}{dt} dt. \quad (37.8)$$

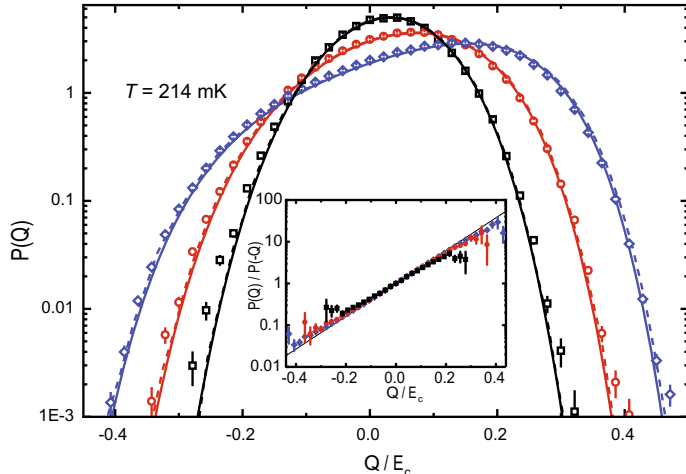


**Fig. 37.4** Measured probability distributions for dissipated heat, i.e. histograms of measured  $Q$  for drive frequencies  $f = 1\text{ Hz}$  (black, squares),  $2\text{ Hz}$  (red, circles), and  $4\text{ Hz}$  (blue, diamonds). Symbols show measured data, solid lines give theoretical predictions, and dashed lines include a finite detector bandwidth in the model. Inset: The test of Crooks relation. Reproduced figure with permission from [7]. Copyright 2012 by the American Physical Society.

We note that since the processes practically always start and end in fixed states and the free energy change in the process is zero, work and heat are equal.

The experiments were carried out at various driving frequencies and at a few temperatures, and under each experimental condition more than  $10^5$  repetitions of the protocol were realized. The probability distributions for  $Q$  as extracted by Eq. (37.7) from the ensemble of traces are shown in Fig. 37.4. It was found that the Jarzynski equality is valid within 3% and that the distributions obey Crooks relation. The main uncertainty stems from the finite bandwidth of the detector leading to unregistered transitions.

### 37.6 Test of Fluctuation Relations for Two Heat Baths

The temperature of a well thermalized system is uniform. However, with an SEB, it is relatively straightforward to form a system with two unequal temperatures by maintaining a temperature difference between the two electrodes. This system allows investigation of fluctuation relations in the presence of multiple heat baths. Jarzynski equality is defined for single temperature systems and thus is not expected to hold, however, fluctuation relations for entropy production can be tested also in this situation [11, 13–15].

For the experiment [12] described here, a temperature difference between the two electrodes is achieved by suppressing the thermalization mechanism of the

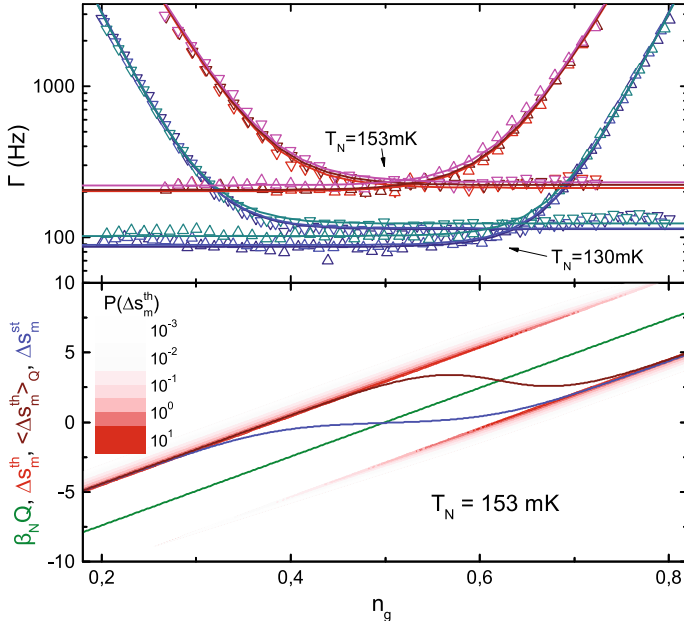


**Fig. 37.5** Top panel: Measured tunneling rates for  $n : 0 \rightarrow 1$  transitions (triangles pointing up) and  $n : 1 \rightarrow 0$  transitions (triangles pointing down) as functions of  $n_g$  at two bath temperatures  $T_N$ . Solid lines show corresponding fits of Eq. (37.2), yielding a superconductor temperature  $T_S = 175\text{ mK}$  when  $T_N = 130\text{ mK}$ , and  $T_S = 185\text{ mK}$  when  $T_N = 153\text{ mK}$ . Bottom panel: thermodynamic or stochastic entropy produced in a single  $n : 0 \rightarrow 1$  tunneling event as a function of  $n_g$  at the time instant of the event. The thermodynamic entropy  $\Delta s_m^{\text{th}}$  given by Eq. (37.9) follows a probability distribution shown in red along the y-axis (in logarithmic scale) and determined by Eq. (37.10). The average value  $\langle \Delta s_m^{\text{th}} \rangle$  is shown in brown. The corresponding stochastic entropy production  $\Delta s_m^{\text{st}}$  determined by Eq. (37.11) is shown in blue. For reference, the entropy  $\Delta s_m = -\Delta E/k_B T_N$  is shown in green. For both panels, the superconductor energy gap is  $\Delta \simeq 224\text{ }\mu\text{eV}$ , the charging energy is  $E_C \simeq 162\text{ }\mu\text{eV}$ , and the tunneling resistance is  $R_T \simeq 1.3\text{ M}\Omega$ . Reproduced figure from [12].

aluminum electrode. Unlike in the SEB shown in Fig. 37.3, here the aluminum island is not covered by a normal metal shadow that would otherwise thermalize it. The only remaining channel is electron-phonon relaxation that takes place in a superconductor only via the unpaired quasiparticles. It is typical for a superconducting aluminum island at a temperature of 150 mK to host only of the order of ten unpaired quasiparticles [16] and it therefore has a very weak phonon thermalization in contrast to normal metallic electrodes. The high temperature of the superconductor is verified from the measured transition rates  $\Gamma_{0 \rightarrow 1}$  and  $\Gamma_{1 \rightarrow 0}$ , shown in Fig. 37.5. By changing the cryostat bath temperature and assuming that it is the same as that of the normal metal electrode, the fits to the transition rates by Eq. (37.2) indicate that the superconductor is consistently at a temperature of approximately 180 mK.

For the present experiment, the drive protocol is identical to the one in the previous section. However, the feature of two unequal temperatures prompts to revise the thermodynamic quantities extracted from the measurement. First, we consider what we call 'thermodynamic' (dimensionless) entropy generated in the medium, namely

$$\Delta s_m^{\text{th}} = Q_N/(k_B T_N) + Q_S/(k_B T_S), \quad (37.9)$$

where  $Q_N + Q_S = -\Delta E$ . For unequal  $T_N$  and  $T_S$ , the magnitudes of both  $Q_N$  and  $Q_S$  are relevant. As our detection scheme only allows to determine  $\Delta E$  directly, we assign a probability density for heat generated in the normal electrode. For example, if we assume that an electron tunnels from the normal (N) to the superconducting (S) electrode, the probability distribution is given by

$$P(Q_N = -\epsilon \mid \Delta E) = \frac{f_N(\epsilon)n_S(\epsilon - \Delta E)(1 - f_S(\epsilon - \Delta E))}{\int d\epsilon f_N(\epsilon)n_S(\epsilon - \Delta E)(1 - f_S(\epsilon - \Delta E))}. \quad (37.10)$$

The resulting probability distribution for thermodynamic entropy production as a function of  $n_g$  for a tunneling event is shown in Fig. 37.5. The distribution shows two distinct peaks for each  $n_g$ . Qualitatively, this can be understood from the energy gap  $\Delta$  in the superconductor density of states which dictates that electrons tunneling into or out of the superconductor can either satisfy  $Q_S \gtrsim \Delta$  or  $Q_S \lesssim -\Delta$ .

Next, we consider what we call 'stochastic' dimensionless entropy defined in [13], which for a single transition is given by

$$\Delta s_m^{\text{st}} = \ln \left( \frac{\Gamma_{0 \rightarrow 1}(n_g)}{\Gamma_{1 \rightarrow 0}(n_g)} \right). \quad (37.11)$$

As seen in Fig. 37.5, the stochastic entropy has the same value irrespective of the energy of the tunneling electron. As such, one can view this entropy as the one observed where the electron energy degree of freedom is coarse-grained. The two definitions satisfy

$$\langle e^{-\Delta s_m^{\text{th}}} \rangle_{Q_N} = e^{-\Delta s_m^{\text{st}}}, \quad (37.12)$$

where the  $\langle \dots \rangle_{Q_N}$  denotes averaging over all possible  $Q_N$  with the constraint that  $\Delta E$  is determined by  $n_g$ , and  $Q_S = -\Delta E - Q_N$ . From Eq. (37.12) it immediately follows that  $\langle \Delta s_m^{\text{th}} \rangle \geq \Delta s_m^{\text{st}}$ , which is also captured in Fig. 37.5. The total entropy produced over a trajectory is the sum over those produced in the transitions during a process, similarly as presented for the heat  $Q$  in the previous section. For driven processes where both the initial and the final state follows thermal equilibrium, both definitions of entropy production are expected to follow fluctuation relations [13].

Figure 37.6 shows the measured distributions of stochastic entropy, thermodynamic entropy for single-jump trajectories, and a distribution that 'tests' JE by assuming that both electrodes are at temperature  $T_N$ . As expected, the JE does not hold in a system with two unequal temperatures, for the exponential average of the

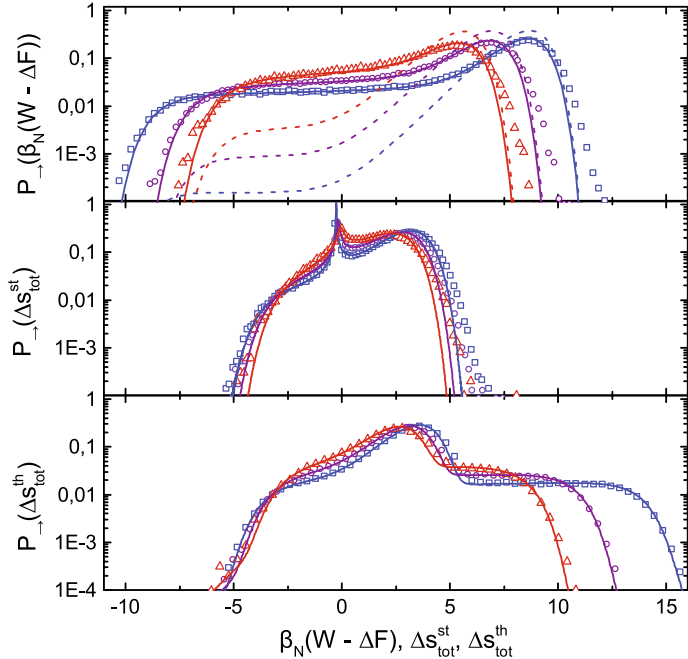


**Fig. 37.6** Top panel: Measured probability distribution for  $W/k_B T_N$ . Middle panel: measured distribution for stochastic entropy production given by Eq. (37.11). Bottom panel: distribution for thermodynamic entropy production given by Eqs. (37.9) and (37.10) for the recorded single-jump trajectories. In all panels, data measured at  $T_N = 130$  mK are shown in blue (squares),  $T_N = 142$  mK in purple (circles), and  $T_N = 153$  mK in red (triangles). Symbols show measured values, solid lines show theoretical predictions, and in the top panel, dashed lines show the predicted distributions for  $T_S = T_N$ . Reproduced figure from [12].

distribution yields  $\langle \exp(-W/k_B T_{N/S}) \rangle \geq 10$ . However, we find that both the stochastic and thermodynamic entropy distributions do satisfy the fluctuation relations, as the exponential average for both  $\langle \exp(-\sum \Delta s_{\text{th}}^{\text{m}}) \rangle \simeq 1$  and  $\langle \exp(-\sum \Delta s_{\text{st}}^{\text{m}}) \rangle \simeq 1$ .

## 37.7 Single-Electron Box in Information Thermodynamics

The ability to track individual electron tunneling events in a SEB gives access to information thermodynamic experiments with processes under feedback-control. A feedback-control protocol consists of a sequence of measurements, which determine the instantaneous system state, followed by a routine which depends on the previously measured state but is otherwise pre-determined [17, 18]. We consider in [19] a simple protocol consisting of a single measurement followed by a feedback drive. The measurement obtains one bit of information from the system ( $n = 0$  or  $n = 1$ )

which, according to the thought experiment by Szilard [20] and Landauer's principle [21], can be converted to a fundamental amount of  $k_B T \ln(2)$  energy. Here,  $k_B \ln(2)$  is the maximum amount of entropy for one bit of information corresponding to a case where both states have an equal probability. Indeed, Landauer's erasure principle has been demonstrated with a colloidal particle in a two-well potential [22, 23] by showing that erasing one bit of information expends a minimum amount of work  $k_B T \ln(2)$ .

The drive protocol for the SEB considered here is the counterpart of erasure, namely using the one bit of information obtained from the electron position to extract  $k_B T \ln(2)$  directly from the heat bath. Example traces of the protocol are shown in Fig. 37.7. The cycle is similar to a Szilard's engine [20] by starting from the degeneracy point at thermal equilibrium, where an excess electron can reside either inside ( $n = 1$ ) or outside ( $n = 0$ ) of the SEB island with equal probability. The electron position is established from the detector current with threshold detection yielding a measurement outcome  $m$ . The feedback takes place as follows: if  $m = 0$  was measured,  $n_g$  is rapidly driven to introduce a positive energy difference  $\Delta E = E_{fb}$  that effectively traps the electron to the  $n = 0$  state. If  $m = 1$  was measured, the energy difference is driven to be negative,  $\Delta E = -E_{fb}$ , trapping the electron to the  $n = 1$  state. We refer to this first step as the 'fast drive'. Both protocols finish by slowly returning back to the degeneracy point, allowing thermal expansion of the electron. In the ideal limit of a perfect measurement and response, infinite  $E_{fb}$ , and infinitesimally slow drive, the work extracted in the cycle is  $k_B T \ln(2)$  produced by the thermal excitations during the slow drive. In a practical experiment [19], we extract 75% of this fundamental maximum.

For a practical experimental scheme, the measurement outcome  $m$  has a strong but not perfect correlation to the actual charge state  $n$ . This is described by the probability  $P(n = m) = 1 - \varepsilon$ , where  $\varepsilon$  is the error probability  $P(n \neq m) = \varepsilon$ , i.e. the probability to get an incorrect outcome. An important parameter that characterizes the maximum energy available is mutual information  $I_m(n, m) = \ln(P(n|m)) - \ln(P(n))$ . In a cyclic process with  $\Delta F = 0$ , the maximum work that can be extracted is  $\langle -W \rangle \leq k_B T \langle I_m(n, m) \rangle$  [17]. Furthermore, irreversible feedback processes are described by Sagawa-Ueda equality [17] (see also Chap. 10). The equality reads  $\langle e^{-(W-\Delta F)/k_B T - I_m} \rangle = 1$ . With a finite error probability, it is no longer optimal to drive with infinite  $E_{fb}$ . Every time the SEB is driven incorrectly, the fast drive excites the system leading to immediate relaxation and dissipation of  $E_{fb}$ . This is illustrated in the insets of Fig. 37.7 and explains the instances of positive work in the measured work distribution. The optimal  $E_{fb}$  [24] can be found by requiring that after the fast drive, the system is at thermal equilibrium. For example, if  $m = 0$  was measured, the occupation probabilities are  $P(0) = 1 - \varepsilon$  and  $P(1) = \varepsilon$ , which corresponds to the thermal equilibrium distribution with  $\Delta E = k_B T \ln((1 - \varepsilon)/\varepsilon) \equiv E_{fb, opt}$  setting the optimal  $E_{fb, opt}$ .

In [25], we consider a fixed  $E_{fb}$  while the magnitude of error probability  $\varepsilon$  is varied by changing the amount of detector signal averaging for the pre-feedback measurement. The error probability was estimated in a post-analysis, similar to the method of extracting the occupation probability as discussed in the third section of

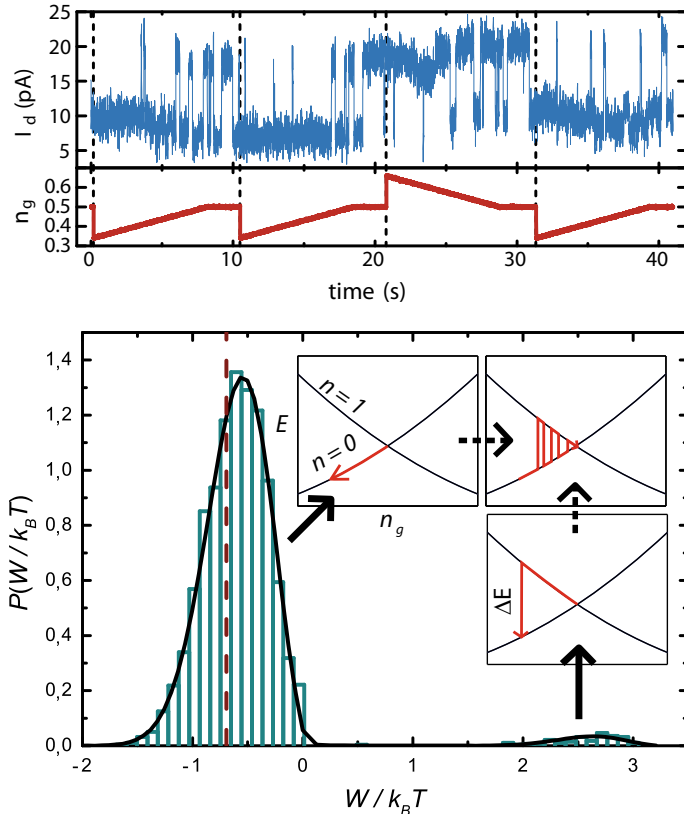


**Fig. 37.7** Top panel: A time trace of a Szilard's engine [20] with four realizations of the feedback control protocol. The vertical dashed lines mark the time instants for measuring the system state by observing the detector current  $I_d$ . Based on the measured  $I_d$ , the feedback drive rapidly changes  $n_g$  to set the energy difference to  $\Delta E \approx \pm 3.2 k_B T$ , where the sign is determined by the measurement outcome. Bottom panel: A histogram displaying the work done in about 3000 cycles of the Szilard's engine. The main peak at negative energies ( $W \approx -k_B T \ln(2)$ ) is due to successful cycles whereas the weaker positive peak represents measurement and feedback errors. These errors counterbalance partly the successful ones leading eventually to about 75% of the ideal work extraction of  $k_B T \ln(2)$  on the average. Figure adapted from [19], Copyright 2014 National Academy of Sciences, USA.

this chapter. The extracted work  $W$  increases linearly with decreasing error probability  $\varepsilon$ . However, the 'feedback efficiency'  $\eta \equiv \langle -W \rangle / k_B T \langle I_m(n, m) \rangle$  exhibits a maximum in  $\varepsilon$ . This implies that the feedback process could be further improved by adjusting  $E_{fb}$  accordingly. Furthermore, we find that for all  $\varepsilon$ , the Sagawa-Ueda relation holds.

### 37.8 Single-Electron Box as an Autonomous Maxwell's Demon

An autonomous Maxwell's demon is a configuration where both the controlled system and the demon performing the measurements and the feedback are present [26–30]. In this section, we review the first experimental realization of an autonomous Maxwell's demon [31] by employing an SEB as the measurement and feedback control unit (the demon) for an SET. The demon is designed to apply a positive potential to the SET island when an electron is in there in order to trap it, and apply a negative potential to repel electrons from entering the island when an electron is not there. A small potential bias is applied to the SET to trigger charge transport, however due to the aforementioned feedback control by the demon, the SET cools down as all electron tunneling events cost energy, an effect that is verified by thermometry. A notable feature of this experiment on a Maxwell's demon is that its performance and heat flow is measured directly by observing a temperature change in the device. The operation principle is similar to the proposal in [28] and is illustrated in Fig. 37.8. The two devices are gated such that the lowest energy configuration has a total of one electron in the whole system, i.e. an electron either in the SET or the SEB island, while excess negative charge (one electron in each island) and positive charge (zero electrons in each island) both have a higher energy equal to the mutual Coulomb interaction  $J$  from Eq. (37.6). This is achieved with  $n_g = n_g^{\text{det}} = 0.5$ , where  $n_g$  now refers to the SET gate and  $n_g^{\text{det}}$  to the demon gate. A similar configuration based on quantum dots has been used to realize an energy harvester [32] and a Maxwell's demon operating as a power generator [33].

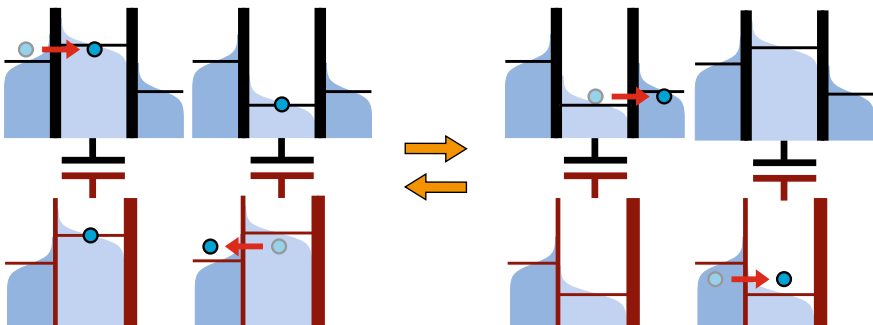


**Fig. 37.8** The operation principle of the autonomous Maxwell's demon. The top row shows the energy levels of the feedback-controlled SET, and the bottom row shows those for the SEB acting as a Maxwell's demon. The first and third steps show an electron tunneling in the SET, which are processes that cost energy and therefore cool the system. The second and fourth step show an electron tunneling in the SEB, which are processes that release energy and heat up the demon. When the SET is voltage biased and the demon is designed to have a lower tunneling resistance, the illustrated cycle is the most preferred one.

We now consider the process cycle in Fig. 37.8, starting with one electron in the SEB and none in the SET, which is one of the degenerate ground states. The SET is voltage biased to trigger charge transport under condition  $eV < J$  to ensure Coulomb blockade. An electron tunnels into the SET island from the source electrode with an energy cost  $J/2 - eV/2$  that is provided by thermal excitations. The process costs energy, because the electron already present in the SEB island is repelling any electron that would enter the SET island. The SEB is designed to have a low tunneling resistance, i.e. a fast reaction time. This way, it can act as a Maxwell's demon with an electron tunneling out of the island in response to the transition in the SET. At this point, one electron is trapped in the SET and, similarly to the initial setup, it can tunnel out to the drain electrode with an energy cost  $J/2 - eV/2$ . When it does, the demon reacts by an electron tunneling to the island, resuming back to the initial state and closing the operation cycle. During the cycle, the SET has been cooled down by an energy  $J - eV$  due to the feedback-control of the demon. The thermodynamic cost of the cycle is the heat  $J$  dissipated in the demon, restoring an agreement with Joule's law (total heat  $Q = eV$ ) and the second law of thermodynamics.

Note that the operation described above takes place internally in the circuit (autonomous operation), therefore there is no need to measure the system state with a charge detector. Furthermore, external feedback is not required, rather all external control parameters are constant. However, the device should be designed to have certain properties in order to optimize and observe the operation. First, the devices are designed to be fully normal metallic, introducing fast tunneling rates and enhanced cooling power to the device. The normal metallic junctions are realized by using the technique presented in [9]. Second, the tunnel junction of the SEB is designed to have a lower tunneling resistance than the SET junctions to ensure fast feedback to the SET transitions. However, the resistances are designed to be higher than the quantum resistance  $R_K = h/e^2 \approx 26$  k $\Omega$  to minimize the detrimental effects of cotunneling [34, 35]. Third, the leads of both devices are thermally isolated while still permitting charge transport by interrupting them with superconducting aluminum leads [36, 37]. Finally, the temperatures of the system and the demon are readout with normal metal - insulator - superconductor thermometers [38].

Figure 37.9 shows the key results of the device operation. The data in Fig. 37.9a are obtained when the full feedback cycle described above takes place. We observe that even though heating would naively be expected from Joule's law as a finite charge current flows through the SET in the direction of voltage bias, both leads of the SET cool down as a result of the feedback control by the demon. The feedback control has a thermodynamic expense of heating the demon, apparent as a measured temperature rise. The total heat in the SET and the demon are in agreement with Joule's law. For comparison, the data from a reference measurement with the demon deactivated ( $n_g^{\text{det}} = 0$  for the demon) is shown in Fig. 37.9b. While one-sided cooling in the SET is observed, the total heat generated in the system is always positive in the absence of feedback control. Furthermore, the temperature of the demon does not change. This concludes that in the feedback-controlled configuration (Fig. 37.9a) all the heat produced in the demon is a result of tunneling events and not of direct heat flow between the two devices.

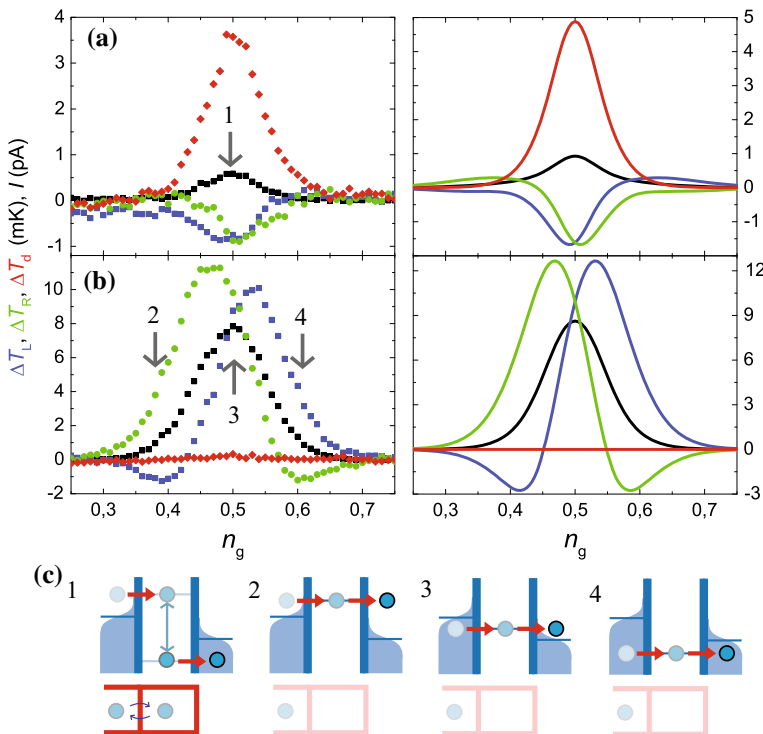


**Fig. 37.9** **a–b** Current through the SET (black), temperature of its left (blue) and right (green) electrode, and the temperature of the demon (red) as a function of the SET control parameter. Left panel shows measured data and the right shows calculated values. **a** shows the case where the SEB is allowed to operate as a demon, while in **b**, the demon is deactivated by setting its control parameter to zero (the electron in the demon is trapped to the lead). **c** shows the schematics of the device operation at the settings indicated with arrows in **a** and **b**. Reproduced figure with permission from [31]. Copyright 2015 by the American Physical Society.

**Acknowledgements** We acknowledge financial support from Academy of Finland contract number 312057.

## References

1. F. Giazotto, T.T. Heikkilä, A. Luukanen, A.M. Savin, J.P. Pekola, Rev. Mod. Phys. **78**, 217 (2006). <https://doi.org/10.1103/RevModPhys.78.217>
2. F.C. Wellstood, C. Urbina, J. Clarke, Phys. Rev. B **49**, 5942 (1994). <https://doi.org/10.1103/PhysRevB.49.5942>
3. H. Pothier, S. Gueron, N.O. Birge, D. Esteve, M.H. Devoret, Phys. Rev. Lett. **79**, 3490 (1997). <https://doi.org/10.1103/PhysRevLett.79.3490>
4. J.P. Pekola, Nat. Phys. **11**, 118 (2015). <https://doi.org/10.1038/nphys3169>

5. J.P. Pekola, P. Solinas, A. Shnirman, D.V. Averin, New J. Phys. **15**, 115006 (2013). <https://doi.org/10.1088/1367-2630/15/11/115006>
6. B. Kung, C. Rössler, M. Beck, M. Marthaler, D.S. Golubev, Y. Utsumi, T. Ihn, K. Ensslin, Phys. Rev. X **2**, 011001 (2012). <https://doi.org/10.1103/PhysRevX.2.011001>
7. O.-P. Saira, Y. Yoon, T. Tanttu, M. Möttönen, D.V. Averin, J.P. Pekola, Phys. Rev. Lett. **109**, 180601 (2012). <https://doi.org/10.1103/PhysRevLett.109.180601>
8. J. Bardeen, L.N. Cooper, J.R. Schrieffer, Phys. Rev. **108**, 1175 (1957). <https://doi.org/10.1103/PhysRev.108.1175>
9. J.V. Koski, J.T. Peltonen, M. Meschke, J.P. Pekola, Appl. Phys. Lett. **98**, 203501 (2011). <https://doi.org/10.1063/1.3590922>
10. C. Jarzynski, Phys. Rev. Lett. **78**, 2690 (1997). <https://doi.org/10.1103/PhysRevLett.78.2690>
11. G.E. Crooks, Phys. Rev. E **60**, 2721 (1999). <https://doi.org/10.1103/PhysRevE.60.2721>
12. J.V. Koski, T. Sagawa, O.-P. Saira, Y. Yoon, A. Kutvonen, P. Solinas, M. Möttönen, T. Ala-Nissila, J.P. Pekola, Nat. Phys. **9**, 644 (2013). <https://doi.org/10.1038/NPHYS2711>
13. U. Seifert, Phys. Rev. Lett. **95**, 040602 (2005). <https://doi.org/10.1103/PhysRevLett.95.040602>
14. S. Schuler, T. Speck, C. Tietz, J. Wrachtrup, U. Seifert, Phys. Rev. Lett. **94**, 180602 (2005). <https://doi.org/10.1103/PhysRevLett.94.180602>
15. C. Tietz, S. Schuler, T. Speck, U. Seifert, J. Wrachtrup, Phys. Rev. Lett. **97**, 050602 (2006). <https://doi.org/10.1103/PhysRevLett.97.050602>
16. V.F. Maisi, S.V. Lotkhov, A. Kemppinen, A. Heimes, J.T. Muhonen, J.P. Pekola, Phys. Rev. Lett. **111**, 147001 (2013). <https://doi.org/10.1103/PhysRevLett.111.147001>
17. T. Sagawa, M. Ueda, Phys. Rev. Lett. **104**, 090602 (2010). <https://doi.org/10.1103/PhysRevLett.104.090602>
18. S. Toyabe, T. Sagawa, M. Ueda, E. Muneyuki, M. Sano, Nat. Phys. **6**, 988 (2010). <https://doi.org/10.1038/nphys1821>
19. J.V. Koski, V.F. Maisi, J.P. Pekola, D.V. Averin, PNAS **111**, 13786 (2014). <https://doi.org/10.1073/pnas.1406966111>
20. L. Szilard, Z. Phys. **53**, 840 (1929). <https://doi.org/10.1007/BF01341281>
21. R. Landauer, IBM, J. Res. Develop. **5**, 183 (1961). <https://doi.org/10.1147/rd.53.0183>
22. A. Bérut, A. Arakelyan, A. Petrosyan, S. Ciliberto, R. Dillenschneider, E. Lutz, Nature **483**, 187 (2012). <https://doi.org/10.1038/nature10872>
23. Y. Jun, M. Gavrilov, J. Bechhoefer, Phys. Rev. Lett. **113**, 190601 (2014). <https://doi.org/10.1103/PhysRevLett.113.190601>
24. J.M. Horowitz, J.M.R. Parrondo, Euro. Phys. Lett. **95**, 10005 (2011). <https://doi.org/10.1209/0295-5075/95/10005>
25. J.V. Koski, V.F. Maisi, T. Sagawa, J.P. Pekola, Phys. Rev. Lett. **113**, 030601 (2014). <https://doi.org/10.1103/PhysRevLett.113.030601>
26. D. Mandal, C. Jarzynski, Proc. Nat. Acad. Sci. **109**, 11641 (2012). <https://doi.org/10.1073/pnas.1204263109>
27. A.C. Barato, U. Seifert, Europhys. Lett. **101**, 60001 (2013). <https://doi.org/10.1209/0295-5075/101/60001>
28. P. Strasberg, G. Schaller, T. Brandes, M. Esposito, Phys. Rev. Lett. **110**, 040601 (2013). <https://doi.org/10.1103/PhysRevLett.110.040601>
29. J.M. Horowitz, M. Esposito, Phys. Rev. X **4**, 031015 (2014). <https://doi.org/10.1103/PhysRevX.4.031015>
30. A. Kutvonen, J.V. Koski, T. Ala-Nissila, Sci. Rep. **6**, 21126 (2016). <https://doi.org/10.1038/srep21126>
31. J.V. Koski, A. Kutvonen, I.M. Khaymovich, T. Ala-Nissila, J.P. Pekola, Phys. Rev. Lett. **115**, 260602 (2015). <https://doi.org/10.1103/PhysRevLett.115.260602>
32. H. Thierschmann, R. Sánchez, B. Sothmann, F. Arnold, C. Heyn, W. Hansen, H. Buhmann, L.W. Molenkamp, Nat. Nano. **10**, 854 (2015). <https://doi.org/10.1038/nnano.2015.176>
33. K. Chida, S. Desai, K. Nishiguchi, A. Fujiwara, Nat. Commun. **8**, 15310 (2017). <https://doi.org/10.1038/ncomms15301>

34. D.V. Averin, Y.V. Nazarov, Phys. Rev. Lett. **65**, 2446 (1990). <https://doi.org/10.1103/PhysRevLett.65.2446>
35. N. Walldorf, A.-P. Jauho, K. Kaasbjerg, Phys. Rev. B **96**, 115415 (2017). <https://doi.org/10.1103/PhysRevB.96.115415>
36. J. Bardeen, G. Rickayzen, L. Tewordt, Phys. Rev. **113**, 982 (1959). <https://doi.org/10.1103/PhysRev.113.982>
37. A.V. Timofeev, M. Helle, M. Meschke, M. Möttönen, J.P. Pekola, Phys. Rev. Lett. **102**, 200801 (2009). <https://doi.org/10.1103/PhysRevLett.102.200801>
38. M. Nahum, T.M. Eiles, J.M. Martinis, Appl. Phys. Lett. **65**, 3123 (1994). <https://doi.org/10.1063/1.112456>

# Chapter 38

## Probing Quantum Fluctuations of Work with a Trapped Ion



**Yao Lu, Shuoming An, Jing-Ning Zhang and Kihwan Kim**

### 38.1 Introduction

The technologies of nano/micro scale have been rapidly developed [1–3]. On the nano/micro scale, quantum fluctuations become important and such quantum effects should be fully taken into account to properly understand and manipulate nano/micro systems [1–9]. The extension of the principles of thermodynamics [10, 11] to the quantum regime has been the subject of extensive theoretical studies in the last decades [12–19]. As nano/micro technologies develop, there has been growing interest in experimentally testing the principles of quantum thermodynamics, which would be a solid foundation for further development of technologies in the quantum regime.

Among diverse physical platforms, a trapped ion system is particularly interesting to test quantum thermodynamics [20–24]. One important feature in a quantum system, which distinguishes from classical macroscopic systems, is energy quantization. Historically, the finding of discretized energy levels of an atom has led to the birth of quantum mechanics [25] and the electron shelving technique can distinguish internal states of the trapped ion with near-perfect detection efficiency [26–30]. For the external degree of freedom of the atomic ion trapped in a harmonic potential, the technology of cooling to the ground state of the trap has been developed and the quantized energy levels of motion have been observed and manipulated through the

---

Y. Lu · S. An · J.-N. Zhang · K. Kim (✉)

Center for Quantum Information, Institute for Interdisciplinary  
Information Sciences, Tsinghua University, Beijing 100084, P. R. China  
e-mail: kimkihwan@mail.tsinghua.edu.cn

Y. Lu  
e-mail: luyao\_physics@163.com

S. An  
e-mail: anshuoming-hn@163.com

J.-N. Zhang  
e-mail: jnzhang13@mail.tsinghua.edu.cn

resolved Raman laser technique [31–36]. The single trapped atomic ion can be considered as the most fundamental and the simplest system, which can be manipulated and measured with high precision enough to experimentally verify the principles of quantum thermodynamics.

Generally, the principles of non-equilibrium thermodynamics are expressed as inequalities. For example, the work performed on a system in contact with a heat reservoir during an arbitrary drive of the system is lower bounded by the net change in its free energy:  $\langle W \rangle \geq \Delta F$ , where the equality holds for equilibrium processes. When statistical fluctuations are properly incorporated in exponential form, the inequality is reformulated as equality, which is known as the Jarzynski equality [10],

$$\langle e^{-W/k_B T} \rangle = e^{-\Delta F/k_B T}, \quad (38.1)$$

where  $T$  is the temperature of the environment and the brackets  $\langle \cdot \rangle$  denote an average over repetitions of the process. For classical systems, this prediction and related fluctuation theorems have been extensively studied both theoretically [37–39] and experimentally [2–9].

However, it has been shown that extending these advances to quantum systems is challenging. One main difficulty is to measure work and work distributions in a quantum system [40]. In classical systems, work can be obtained by measuring work trajectories, which cannot be determined in quantum regime. For closed quantum systems with no heat transfer to or from the system, the difficulty can be avoided and the work can be obtained by measuring the difference of the initial and the final energies [12–14], which has been demonstrated experimentally [22, 41]. However, it still remains as the challenge to extend the equality and the theorem to open quantum systems [42]. Recently, for the restricted open environment that induces only dephasing not dissipation, it was pointed out that the equality would hold in quantum regime [24].

In this chapter, we present the experimental tests of the Jarzynski equality for both closed and quasi-open quantum systems based on trapped ion systems [22, 24]. In the following section, we provide a basic introduction of the trapped ion system, then present the theoretical framework for the experimental test. Finally we discuss the examples of experimental tests of the Jarzynski equality and conclude the chapter.

## 38.2 Trapped-Ion System

### 38.2.1 Free Hamiltonian

As one of the most promising platforms for quantum simulation [43, 44] and quantum computation [45, 46], the trapped-ion system is famous for its unprecedented stability and controllability. A typical trapped-ion system is shown in Fig. 38.1a, where a single atomic ion is confined in a harmonic potential produced by oscillating

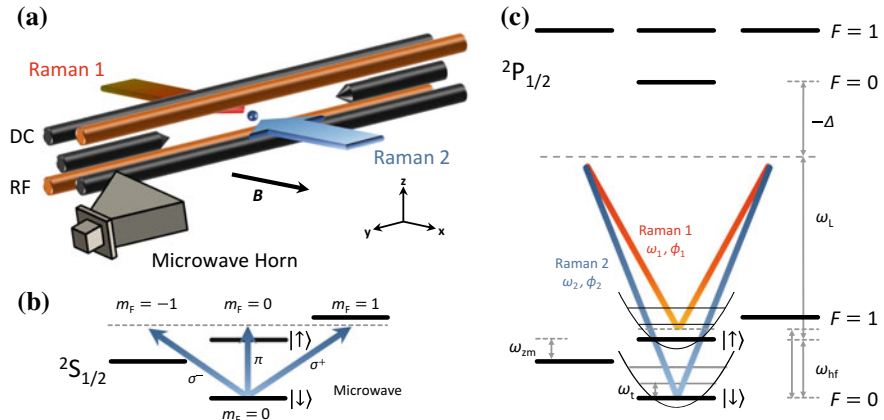


**Fig. 38.1** Trapping and manipulation of the  $^{171}\text{Yb}^+$  ion. **a** Schematic plot of a four-rod trap. The ion is trapped at the center of the four-rod trap, and manipulated either by microwave from the microwave horn or by a pair of counter-propagating Raman beams along the  $X$ -direction. The external magnetic field is applied along the  $X$  direction. **b** Microwave manipulation and relevant energy level diagram. The internal states in the ground state  $^2\text{S}_{1/2}$  manifold are manipulated by the microwave radiation. To target transitions between different states, we first introduce an external magnetic field to induce the linear Zeeman splitting  $\omega_{\text{zm}}$  of the  $F = 1$  manifold, and then tune the frequency of the microwave to the desired resonance. **c** Raman manipulation and relevant energy level diagram. The stimulated Raman process, which is implemented by two laser beams coupling to the  $^2\text{P}_{1/2}$  states with a large detuning  $-\Delta$ , has the ability to couple the internal and external degrees of freedom. Thus the lower part of the energy spectrum can be viewed as a harmonic oscillator superposed on a two-level system. By tuning the frequency difference  $\delta\omega$  of the two Raman beams around the hyperfine splitting  $\omega_{\text{hf}} = 2\pi \times 12.6$  GHz, we can selectively excite or deexcite the motional states when manipulating the internal states.

radio-frequency electric field [35, 47]. The state of the trapped-ion system belongs to the product of the internal and the external Hilbert spaces. The internal space is expanded by a selection of electronic energy levels. In our setup with  $^{171}\text{Yb}^+$ , the basis of the internal space is defined by a pair of hyperfine states of the ground state manifold  $^2\text{S}_{1/2}$ . For instance  $|F = 0, m_F = 0\rangle = |\downarrow\rangle$  and  $|F = 1, m_F = 0\rangle = |\uparrow\rangle$  shown in Fig. 38.1(b, c), known as the clock states, are a good choice of basis because of the long coherence time [48]. Sometimes the upper state  $|\uparrow\rangle$  is encoded with  $|F = 1, m_F = \pm 1\rangle$  for a certain purpose. Note that the internal state of a single trapped ion can be represented by the Pauli matrices  $\hat{\sigma}_{x,y,z}$  and the identity  $\hat{\mathbb{I}}$ , known as the Bloch representation.

The other part of the Hilbert space is related to the motion of the ion, which can be modeled by a harmonic oscillator. In this case, a set of the Fock number states  $\{|n\rangle, n = 0, 1, 2 \dots\}$ , also known as the phonon number states, could be chosen as a complete orthonormal basis of this space. The free Hamiltonian of a single trapped-ion system can be written as

$$\hat{H}_0 = \frac{\hbar\omega_0}{2}\hat{\sigma}_z + \hbar\omega_t \left( \hat{a}^\dagger \hat{a} + \frac{1}{2} \right), \quad (38.2)$$

where  $\omega_0$  is the internal energy splitting, and  $\hat{a}$  ( $\hat{a}^\dagger$ ) is the annihilation (creation) operator for the harmonic oscillator with the trapping frequency  $\omega_t$ . As shown in Fig. 38.1b, c, depending on the choice of the electronic states to encode the two-level system, the internal energy splitting is  $\omega_0 = \omega_{\text{hf}} + \Delta_{m_F} \omega_{\text{zm}}$ , where  $\omega_{\text{hf}}$  is the hyperfine splitting,  $\Delta_{m_F} = 0, \pm 1$  is the difference of the magnetic quantum numbers, and  $\omega_{\text{zm}}$  is the first-order Zeeman splitting of the  $F=1$  hyperfine manifold.

### 38.2.2 Quantum Manipulation

In order to manipulate the quantum state of the trapped-ion system, either microwaves or laser beams should be applied to the  $^{171}\text{Yb}^+$  ion. For the magnetic dipole interaction induced by the microwave shown in Fig. 38.1b, the interaction Hamiltonian can be written as

$$\hat{H}_i^\mu = \hbar\Omega\hat{\sigma}_x \cos(\omega t - \phi), \quad (38.3)$$

where  $\Omega$  is the Rabi oscillation frequency,  $\omega$  and  $\phi$  are the frequency and the initial phase of the applied microwave, respectively. Using the time evolution operator  $\hat{U}_0 = \exp[-(i/\hbar)\hat{H}_0 t]$ ,  $\hat{H}_i^\mu$  can be transformed into the interaction picture

$$\begin{aligned} \hat{H}_i^\mu &= \hat{U}_0^\dagger \hat{H}_i^\mu \hat{U}_0 \\ &= \frac{\hbar\Omega}{2} [\hat{\sigma}_x \cos(\delta t - \phi) + \hat{\sigma}_y \sin(\delta t - \phi)], \end{aligned} \quad (38.4)$$

where  $\delta = \omega - \omega_0$  is the frequency difference between the microwave and the energy splitting of the internal two-level system.

The electric dipole interaction induced by light fields is relatively complicated because the coupling to the motional degrees of freedom cannot be neglected. The Hamiltonian is written as follows,

$$\hat{H}_i^L = \hbar\Omega\hat{\sigma}_x \cos(k\hat{x} - \omega t + \phi), \quad (38.5)$$

where  $k$  is the effective component of the momentum along the  $X$ -axis and  $\hat{x} = \sqrt{\frac{\hbar}{2M\omega_t}} (\hat{a} + \hat{a}^\dagger)$  is the  $X$ -component of the position operator of the ion and  $M$  is the mass of the single  $^{171}\text{Yb}^+$  ion. In the  $^{171}\text{Yb}^+$  system, we off-resonantly couple the  $|\uparrow\rangle$  and the  $|\downarrow\rangle$  states to the excited  $^2P$  manifold, constructing a  $\Lambda$ -type Raman transition as shown in Fig. 38.1c, to realize the laser-ion interaction described by Eq. (38.5). By tuning the frequency difference  $\omega = \omega_2 - \omega_1$  (assuming  $\omega_2 > \omega_1$ ) of two Raman lasers, several kinds of the resonant transitions can be realized in the interaction picture, for example,

- The carrier transition with  $\omega = \omega_0$ ,

$$\hat{H}_c = \frac{\hbar\Omega_{\text{eff}}}{2}(\hat{\sigma}_+ e^{i\phi} + \hat{\sigma}_- e^{-i\phi}). \quad (38.6)$$

- The red-sideband transition with  $\omega = \omega_0 - \omega_t$ ,

$$\hat{H}_{\text{rsb}} = \frac{\hbar\eta\Omega_{\text{eff}}}{2}(\hat{\sigma}_+ \hat{a} e^{i\phi} + \hat{\sigma}_- \hat{a}^\dagger e^{-i\phi}). \quad (38.7)$$

- The blue-sideband transition with  $\omega = \omega_0 + \omega_t$ ,

$$\hat{H}_{\text{bsb}} = \frac{\hbar\eta\Omega_{\text{eff}}}{2}(\hat{\sigma}_+ \hat{a}^\dagger e^{i\phi} + \hat{\sigma}_- \hat{a} e^{-i\phi}). \quad (38.8)$$

Here,  $\hat{\sigma}_\pm$  is spin raising (lowering) operator,  $\eta = k\sqrt{\hbar/(2M\omega_t)}$  is the Lamb-Dicke parameter with  $k$  being the component of the momentum difference of the two Raman beams along the  $X$ -axis, while  $\phi = \phi_2 - \phi_1$  and  $\Omega_{\text{eff}}$  are the relative phase between two light fields and the effective coupling strength of the Raman transition, respectively.

### 38.2.3 Initialization and Measurement

#### 38.2.3.1 State Initialization

The quantum state initialization is the first step for typical experimental protocols with the trapped ion system. Depending on the requirement of Hilbert space in the protocols, we initialize only the internal state or both of the internal and the motional state. The initialization of the internal state is performed by utilizing optical pumping. In the  $^{171}\text{Yb}^+$  ion, the optical transition between  $|^2S_{1/2}, F=1\rangle$  and  $|^2P_{1/2}, F=1\rangle$  leaves the population in the  $|\downarrow\rangle$  state [49].

As to the motional state, we introduce a two-stage cooling protocol to prepare the ground state of the harmonic oscillator. We first perform the standard Doppler cooling through the transition from  $^2S_{1/2}$  to  $^2P_{1/2}$  with a red detuning, and cool the motion of the ion to an average phonon number of 15. To further lower the ion's temperature, we continue to perform the resolved sideband cooling. Specifically, we alternately apply the red sideband transition and the optical pumping sequences for around hundred times. The final state has an average phonon number of around 0.02, which is the ground state within experimental precision.

#### 38.2.3.2 Measurement of State

The quantum measurement for trapped-ion systems includes the measurements of the internal states and the motional states. The internal states are measured by the state-dependent fluorescence detection [49]. For  $^{171}\text{Yb}^+$ , the detection of the internal

state is realized by applying a resonant laser to drive the cycling transition between  $|^2S_{1/2}, F = 1\rangle$  and  $|^2P_{1/2}, F = 0\rangle$  for a certain duration and counting the fluorescent photons during this time. Almost no photons are detected if the internal state collapses to the down state  $|\downarrow\rangle$ , while lots of photons are detected if the upper state  $|\uparrow\rangle$  is projected. We repeat the sequence of the state detection for a certain number of times and measure  $P_\uparrow$ , the probability of being in the  $|\uparrow\rangle$  state, as the ratio of the number of the fluorescent cases to the total number of repetitions.

For the motional state detection, we map the information of a motional state to the internal state [35]. By driving the resonant blue-sideband transition on a motional state  $|\downarrow\rangle \otimes \sum_{n=0}^{\infty} c_n |n\rangle$  for varied interaction duration  $\tau$ , we measure the upper state probability,

$$P_\uparrow(\tau) = \frac{1}{2}[1 - \sum_{n=0}^{\infty} |c_n|^2 \cos(\sqrt{n+1}\Omega_{\text{eff}}\tau)], \quad (38.9)$$

which oscillates with the duration of the blue-sideband transition  $\tau$ . By applying the Fourier transform to the output signal, we can resolve the phonon distributions  $\{|c_n|^2, n = 0, 1, 2, 3, \dots\}$ . We note that for the test of quantum fluctuation theorems, the above ensemble measurement of motional degrees of freedom is not sufficient. We need the projective measurement of phonons to determine the phonon number in each sequence, which will be discussed later.

### 38.3 Experimental Framework

We have shown that the trapped-ion systems are of great controllability, in a sense that state preparation, versatile operations, and state measurements be reliably performed in this platform. Thus the trapped-ion platform is an excellent experimental candidate for exploiting and verifying the foundations of the interdisciplinary field of thermodynamics and quantum mechanics, i.e. quantum thermodynamics.

Internal energy, work and heat belong to the set of the most fundamental concepts in classical thermodynamics, which are related by the first law of thermodynamics. However, the generalization of these classical concepts to the quantum region is not straightforward, where the state of the system is in general a coherent superposition, instead of a mixture, of the energy eigenstates. What's more, these energy eigenstates form a discrete energy spectrum in the deep quantum realm. These intrinsic differences render rich and exotic insights in quantum thermodynamic processes, which have attracted great interest in recent years.

As a starting point, we begin by considering closed and quasi-open quantum systems. In the former case, with the exception of a time-dependent parameter to model the external control, the system does not interact with the environment. Meanwhile, in the latter cases, the system is interacting with a special type of environment, i.e. a dephasing environment, which only eliminates quantum coherence with respect to

the energy eigenbasis. In this case, it can be strictly proved that there is no heat transfer during the process [24].

In the following, we first introduce the effective models which are feasible in the trapped-ion system. Then we investigate the concept of quantum work in our limited configurations, from both theoretic and experimental perspectives.

### 38.3.1 Effective Models in Rotating Frames

Recall that by irradiation of electromagnetic fields with suitable frequencies, two of the internal states and/or one of the external modes can be coherently coupled to each other. Here in this section, we show that the parameters of the effective models can be controlled to evolve according to designed time-dependent functions by tuning the intensity and the relative phase of the Raman laser beams. In this manner, we are able to simulate far-from-equilibrium thermodynamic processes in properly chosen rotating frames. Specifically, we deal with two kinds of effective models: (1) the dragged quantum harmonic oscillator and (2) the driven quantum two-level system with the dephasing bath.

#### 38.3.1.1 The Rotating Frame

A natural and widely adopted rotating frame in a trapped ion system is with respect to the free Hamiltonian  $\hat{H}_0$ . In order to gain more flexibility, we introduce a different rotating frame with respect to

$$\hat{H}'_0(\omega_z, \nu) = \frac{\hbar(\omega_0 - \omega_z)}{2} \hat{\sigma}_z + \hbar(\omega_t - \nu) \left( \hat{a}^\dagger \hat{a} + \frac{1}{2} \right), \quad (38.10)$$

where the interaction-picture Hamiltonian becomes

$$\hat{H}_I = \frac{\hbar\omega_z}{2} \hat{\sigma}_z + \hbar\nu \left( \hat{a}^\dagger \hat{a} + \frac{1}{2} \right). \quad (38.11)$$

It is worth bearing in mind that  $\omega_z$  and  $\nu$  are completely determined by the choice of the rotating frame, which is a purely mathematical operation.

#### 38.3.1.2 Dragged Quantum Harmonic Oscillators

The key ingredient needed to construct the model Hamiltonian of a dragged quantum harmonic oscillator is the interaction between the trapped ion and a bichromatic laser field with detuned first red- and blue-sideband frequencies  $\omega_{\pm} = \omega_0 \pm (\omega_t - \nu)$ . In

the rotating frame with respect to  $\hat{H}'_0(0, \nu)$  and after the rotating-wave approximation (RWA), the interaction-picture Hamiltonian is

$$\hat{H}_I(t) = \hbar\nu \left( \hat{a}^\dagger \hat{a} + \frac{1}{2} \right) + \frac{\hbar\Omega(t)}{2} (\hat{a} + \hat{a}^\dagger) \hat{\sigma}_x, \quad (38.12)$$

where the Rabi coupling strength  $\Omega(t) \equiv \eta\Omega_\pm(t)$  can be varied by tuning the intensity of the bichromatic laser field.

Inspecting the Hamiltonian in Eq. (38.12), one can easily find that by setting the initial state of the two-level system to the eigenstate of  $\hat{\sigma}_x$  with the eigenvalue +1, the two-level system can be factored out and the system reduced to a dragged quantum harmonic oscillator. Rewritten in the first quantized operators, the time-dependent system Hamiltonian becomes

$$\hat{H}_S(t) = \frac{\hat{P}^2}{2M_e} + \frac{1}{2}M_e\nu^2\hat{X}^2 + f(t)\hat{X}, \quad (38.13)$$

where the momentum operator  $\hat{P}$  and the position operator  $\hat{X}$  are defined as

$$\begin{aligned} \hat{P} &= i\sqrt{\frac{\hbar M_e \nu}{2}} (\hat{a}^\dagger - \hat{a}), \\ \hat{X} &= \sqrt{\frac{\hbar}{2M_e \nu}} (\hat{a}^\dagger + \hat{a}), \end{aligned} \quad (38.14)$$

with the effective mass  $M_e = \frac{\omega_1}{\nu} M$  and the effective dragging force  $f(t) = \frac{\hbar}{2}k\Omega(t)$ .

Here we have shown how to generate the effective Hamiltonian of a dragged quantum harmonic oscillator by the ion-laser interaction. Furthermore, with more complicated setting of lasers, it is also possible to realize the effective Hamiltonian of a quantum harmonic oscillator with time-dependent frequency in the rotating frame in a pretty similar manner [50].

### 38.3.1.3 Driven Quantum Two-Level Systems

Alternatively, we can use the two-level system to explore the quantum fluctuation theorems. Compared to the dragged harmonic oscillator case, the advantage of this scenario is that it allows us to investigate the effect of the coupling to a special kind of environment, namely the dephasing environment.

In order to simulate the quantum dynamics of a driven quantum two-level system, we irradiate the trapped ion by a microwave field with the resonant carrier frequency  $\omega_0$ . Note that the Lamb–Dicke parameter, which couples the internal and motional degrees of freedom, of a microwave is negligibly small, thus the motional mode is

irrelevant and can be omitted in this case. The effective Hamiltonian in the rotating frame with respect to  $\hat{H}_0$  is written as follows,

$$\hat{H}_S(t) = \frac{\hbar\Omega(t)}{2} [\hat{\sigma}_x \cos \phi(t) + \hat{\sigma}_y \sin \phi(t)], \quad (38.15)$$

where the Rabi coupling  $\Omega(t)$  and phase  $\phi(t)$  can be varied by tuning the intensity and phase of the microwave field.

### 38.3.1.4 Dephasing Environment

The general coupling to a thermal environment results in non-unitary evolution of the system, whose effect can be phenomenologically classified into two kinds of decohering effects: dissipation and dephasing. The former induces energy transfer between the system and the environment, while the latter only attenuates the quantum coherence of the state, which is quantified by the off-diagonal matrix element of the density operator in the energy eigenbasis. Note that the term “decoherence” in Ref. [24] is used with the same meaning as the term “dephasing” here. Although it is possible to have both decohering effects in the trapped-ion system, we only focus on the dephasing effect, because there is no energy transfer between the system and the environment and the definition of work through energy difference is still valid in this case.

With the existence of a purely dephasing environment, the quantum dynamics of the system is described by the following master equation,

$$\frac{d\hat{\rho}}{dt} = -\frac{i}{\hbar} [\hat{H}_S(t), \hat{\rho}] - \sum_{i \neq j} \gamma_{ij} \rho_{ij} |i\rangle \langle j|, \quad (38.16)$$

where  $\rho$  is the density operator of the system,  $\{|i\rangle\}$  is the instantaneous energy eigenbasis of  $\hat{H}_S(t)$ , and  $\rho_{ij}$  and  $\gamma_{ij}$  are the matrix element of  $\hat{\rho}$  in the instantaneous energy eigenbasis and corresponding phenomenological dephasing strength.

In the trapped-ion setup, we introduce the pure dephasing with respect to the instantaneous energy eigenbasis by adding Gaussian white noise into the intensity of the microwave field. The net effect of this operation is the substitution  $\Omega(t) \rightarrow \Omega(t) + \Omega_0 \xi(t)$ , with  $\Omega_0 \equiv \Omega(t=0)$  and  $\xi(t)$  satisfying

$$\langle \xi(t) \rangle = 0, \quad \langle \xi(t) \xi(t+\tau) \rangle = \sigma^2 \delta(\tau), \quad (38.17)$$

with  $\sigma$  characterizing the standard deviation of the noise fluctuations, which can be controlled by changing the intensity of the Gaussian white noise and is related to the strength of the dephasing effect [51, 52].

### 38.3.2 Quantum Work

#### 38.3.2.1 Definition of Quantum Work

The definition of work in the quantum regime is tricky [15]. In classical systems, work can be obtained by measuring the force and the displacement, and then integrating the force over the displacement during the driving process. In the quantum regime, however, as a result of Heisenberg's uncertainty principle, we cannot determine the position and the momentum simultaneously thus invalidating the above approach.

We mainly consider the situations of the closed quantum system or the quasi-open quantum system undergoing dephasing. Because of the first law of thermodynamics, work equals the difference of the internal energy and the heat transferred between the system and the environment, namely

$$W = \Delta U - Q. \quad (38.18)$$

Since there is no heat in our consideration, work can be defined as the difference of internal energy before and after applying the work. The quantum work is defined as

$$W_{n \rightarrow m} = \epsilon_f^m - \epsilon_i^n, \quad (38.19)$$

where  $\epsilon_f^m$  is the  $m$ -th eigenenergy of the final system and  $\epsilon_i^n$  is the  $n$ -th eigenenergy of the initial system.

#### 38.3.2.2 Measurement of Quatum Work: Two-Point Measurement

The quantum work in a single realization defined as Eq. (38.19) can be obtained by performing the projective measurements over the energy eigenstates at the initial and final points of the process of applying work. We repeat the two-point projective measurements to determine the work distribution [42, 53]. In the trapped ion system, we choose to use either the spin or the motional states as the system that we apply the work on. For the spin system, we apply the  $\hat{\sigma}_z$  measurement along the instantaneous energy eigenbasis, which is equivalent to the energy measurement. For the motional or phonon system, we realize the phonon projective measurement for the first time to get the quantum work  $W_{n \rightarrow m}$  and its corresponding probability  $P_{n \rightarrow m}$ .

The system Hamiltonians in general do not commute with the projective measurements. Intuitively, this can be tackled by adiabatically transferring the probability distribution on the energy basis of the system Hamiltonians to the distribution on the basis of the projective measurements, which commutes with that of the lab frame. Practically, we introduce the technique referred to as the shortcut to adiabaticity to speed up the adiabatic process [54].

## 38.4 Examples: The Quantum Jarzynski Equality

The Jarzynski equality relates the free-energy difference  $\Delta F$  to the exponential average of the work  $W$  done on the system [10] as shown in Eq. (38.1). Its quantum version is introduced later in Ref. [42]. In the trapped ion system, we use the motional state of the ion to test the Jarzynski equality in the closed quantum system and the two-level system consisting of internal states to test that in equality the quasi-open quantum system with the dephasing effect.

The general experiment sequence for a single realization is summarized as [20]:

1. Prepare the initial thermal state at temperature  $T$  with respect to  $\hat{H}_S(0) = \sum_n \epsilon_i^n |n\rangle \langle n|_i$ ,

$$\begin{aligned}\hat{\rho}(T) &= \exp\left[-\frac{\hat{H}_S(0)}{k_B T}\right] / \mathcal{Z}_0 \\ &= \sum_n P_n^{\text{th}} |n\rangle \langle n|_i\end{aligned}$$

with the initial distribution probability  $P_n^{\text{th}} = \exp\left[-\frac{\epsilon_i^n}{k_B T}\right] / \mathcal{Z}_0$  and  $\mathcal{Z}_0 = \sum_n \exp\left[-\frac{\epsilon_i^n}{k_B T}\right]$  being the initial partition function.

2. Project to the energy eigenstate  $|n\rangle_i$  with the probability  $P_n^{\text{th}}$ ,
3. Apply work  $W$  on the system,
4. Project to the energy eigenstate  $|m\rangle_f$  of the final state with the probability  $P_{n \rightarrow m}$ .

The whole sequence is repeated many times to obtain statistics and we can construct the distribution of the work and the exponential average of the work as

$$\langle e^{-W/k_B T} \rangle = \sum P_n^{\text{th}} P_{n \rightarrow m} e^{-W_{n \rightarrow m}/k_B T}. \quad (38.20)$$

Finally we can verify the equality by comparing the Eq. (38.20) to the  $e^{-\Delta F/k_B T}$ . Here we will show the experimental realization step by step.

### 38.4.1 Experimental Verification in a Closed Quantum System

In the first example, we utilize the quantum dragged harmonic oscillator model in the previous section [22]. The Hamiltonian as the Eq. (38.13) can be realized in the interaction picture. In our setup, we use detuning  $\nu$  of  $2\pi \times 20$  kHz and the maximum of the Rabi coupling  $\Omega(t)$  is  $\Omega_{\max} = 2\pi \times 15$  kHz.

1. *Preparation of the initial thermal state.* The quantum Jarzynski equality requires the thermal state as the initial state. After the standard Doppler cooling and the

sideband cooling, the average phonon of the thermal state is about 0.03. When the ion is trapped in the pseudo-potential generated by the RF field, the ion also feels a DC field fluctuation. It has been theoretically proved that the DC noise plays a role of a high temperature thermal reservoir [55]. By waiting for 1 ms, we get a thermal state with average phonon number  $\langle n \rangle = 0.157$  ( $T_{\text{eff}} = 480$  nK) as shown in Fig. 38.2.

**2. The projective measurement.** The projective measurement is the key to realize the two-point measurement of the quantum work. The phonon projective measurement we use here was initially proposed for Boson sampling [56]. The basic operation is shown in Fig. 38.3.

We firstly use the combination of the carrier and the adiabatic blue-sideband pulses to transfer the populations on  $|\downarrow, n \geq 1\rangle$  to  $|\downarrow, n - 1\rangle$ , and then perform the state-dependent fluorescence detection to interrogate if the system is projected to  $|\downarrow, n = 0\rangle$ . The probability  $P_B^1$  that we see the fluorescence in the first detection sequence is the probability  $P_0 (= P_B^1)$  that the  $|n = 0\rangle$  state is projected. If we see no fluorescence, we repeat the carrier, the adiabatic blue-sideband and the detection until we see the fluorescence. If we see the first fluorescence at the  $(n + 1)$ -th detection, we know the state is projected to  $|n\rangle$  with the corresponding probability of  $P_n = P_D^1 \dots P_D^n P_B^{n+1}$ , where  $P_D^i$  is the probability of no fluorescence at the  $i$ -th detection sequence. Note that the internal state is distributed among all Zeeman levels after detecting fluorescence. As a result, after the first fluorescence at the  $(n + 1)$ -th interrogation, we prepare the motional state to the projected number state  $|n\rangle$ .

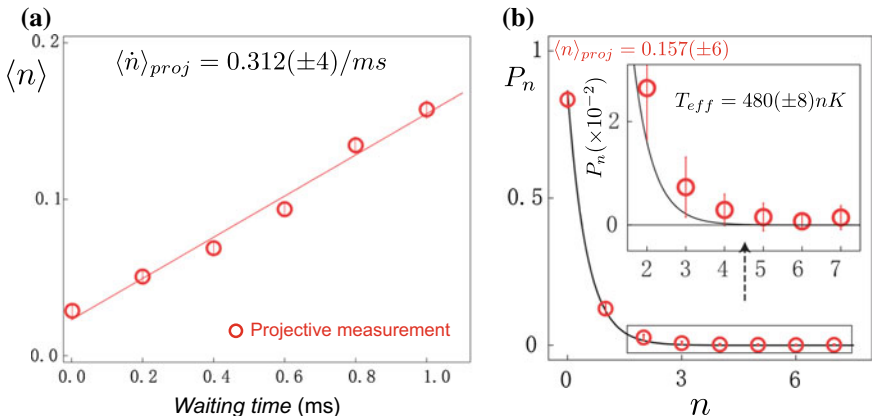


**Fig. 38.2** Preparation of the initial thermal state. **a** The averaged phonon number obtained by the phonon projective measurement as a function of the waiting time. After the side-band cooling, the motional state is cooled near to the ground state and the average phonon number  $\langle n \rangle$  increases linearly with the waiting time, and the slope of the fitted line is defined as the heating rate. **b** The phonon distribution (circles) measured by projective measurement at the waiting time of 1 ms. The circles are experimental data obtained by the projective measurement and the solid line is a fitted thermal distribution with  $P_n^{\text{th}} = \langle n \rangle^n / (\langle n \rangle + 1)^{n+1}$ . The inset shows the details of the phonon distribution for  $n$  larger than 2. The error bars represent one standard deviation of uncertainty.

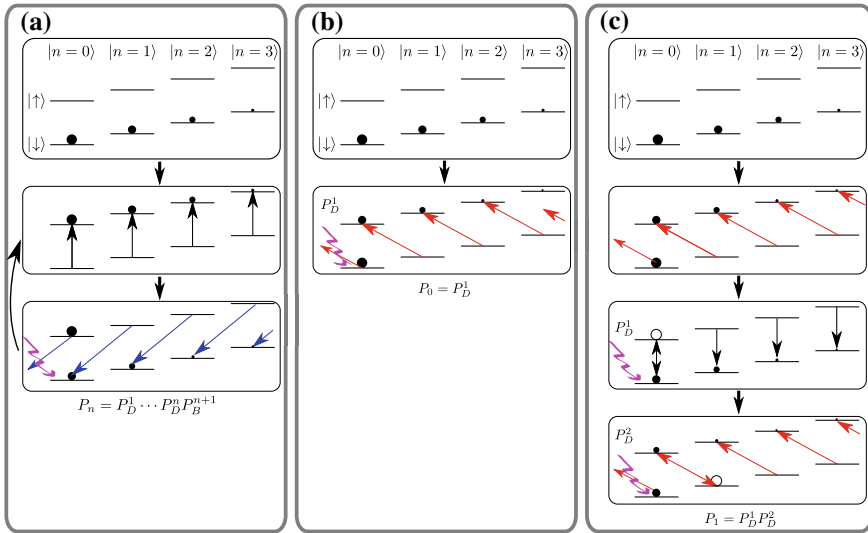


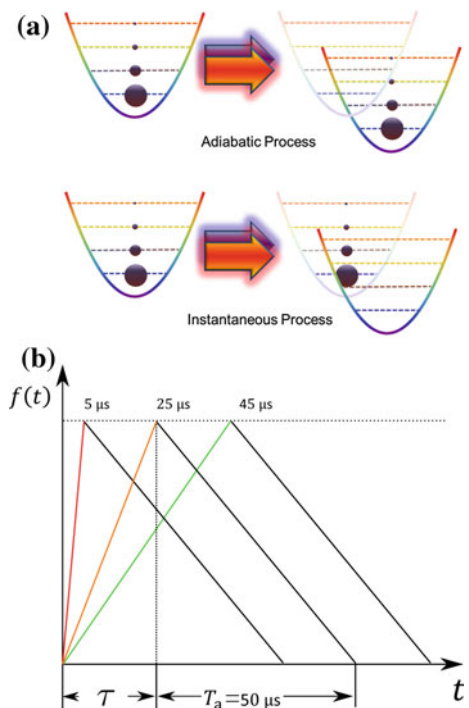
**Fig. 38.3** Experimental schemes for the projective measurement of the phonon state. **a** The fluorescence projective measurement that used in the actual experiments. After applying the pulses of carrier and the adiabatic blue-sideband and the sequence of detection, if we see the fluorescence, we know that the state is projected to  $|n=0\rangle$ . If there is no fluorescence, we continue. From the number of iterations and the probability that we detect the first fluorescence, we know the projected state and its corresponding probability, respectively. **b** The no-fluorescence projective measurement for  $|n=0\rangle$ . After applying the adiabatic red-sideband pulse and the detection sequence, we see no fluorescence with the probability  $P_D^1$ , which shows the state is projected to  $|n=0\rangle$  with its probability  $P_0 = P_D^1$ . **c** The no-fluorescence projective measurement for  $|n=1\rangle$ . We apply the adiabatic red-sideband, the carrier, the detection, the adiabatic red-sideband and the detection. If the two detections show no fluorescence, the  $|n=1\rangle$  state is projected with its probability  $P_1 = P_D^1 P_D^2$ . The empty circles mean the population has been excluded from the no-fluorescence detection. For larger  $|n\rangle$  states, we can design the similar pulse sequence, which detects no fluorescence for  $n+1$  times successively.

An alternative approach to the projective measurement of the phonon state is as follows. We may use pulses of the adiabatic red-sideband and the carrier. To project the  $|n=0\rangle$  state, we apply the adiabatic red sideband and then the detection. If we see no fluorescence with the probability  $P_D^1$ , the state is projected to the  $|n=0\rangle$  state and the corresponding probability is  $P_0 = P_D^1$ . For  $|n=1\rangle$ , we can use the combination of the adiabatic red-sideband, the carrier, the detection, the adiabatic red-sideband and the detection. If the two detections show no fluorescence, the state is projected to  $|n=1\rangle$  with its probability  $P_1 = P_D^1 P_D^2$  as shown in Fig. 38.3c. For larger  $n$ , we can design a similar pulse sequence. With no-fluorescence detection the state is not destroyed by the detection. The disadvantage is that the post-selection process decreases the efficiency of sampling data. Note that in the fluorescence projection method, every result of detection sequence contributes to the sampling data.

**3. Application of work.** After determining and preparing the projected energy eigenstate  $|n\rangle_i$ , we apply work to the system. Specifically, we linearly increase the dragging force to the same maximum value by applying a spin-dependent force on the prepared state for durations  $\tau = 5, 25$  and  $45 \mu\text{s}$ , as shown in Fig. 38.4. The fastest process of  $5 \mu\text{s}$  duration is regarded as a non-equilibrium process and the longest process with  $45 \mu\text{s}$  is treated as the adiabatic process.

**4. The second measurement of phonon state.** After the work process, we perform the second energy measurement to get the distribution of quantum work. However, with the dragging force, the final Hamiltonian does not commute with the phonon operator. Thus the energy measurement is not equivalent with the phonon number measurement. Naively, we can adiabatically turn off the laser that generates the spin-dependent force, which would take several tens of the oscillating periods ( $2\pi/\nu$ ) of the effective harmonic oscillator in Eq.(38.13) to satisfy the adiabatic criteria. In practice, we find this process is equivalent to an adiabatic process when we reduce the force linearly over a duration of integer multiples of the effective oscillating period. We can express the time evolution in the form of displacement operator  $\hat{D}(\alpha) = \exp(\alpha\hat{a}^\dagger - \alpha^*\hat{a})$  up to a global phase. When we increase the laser intensity in  $\tau$  and decrease in  $T_a$  linearly, the displacement in phase space is

**Fig. 38.4** The work-performing protocols. **a** The intuitive pictures of the adiabatic and the instantaneous processes for dragging a harmonic potential. The size of the black balls is indicatively proportional to the population probability of the eigenstate (dashed lines). **b** The dragging force as functions of time for protocols of different duration  $\tau$ . The dragging force is linearly increased to the same maximum value with  $t \in [0, \tau]$ . These work-performing procedures are followed by an effective adiabatic process with the duration of  $T_a = 50 \mu\text{s}$  (see text), which is one period of the effective harmonic oscillation.



$$\alpha = -i \frac{\Delta k x_0 \Omega_{\max}}{2} \left( \frac{e^{i\tau\nu}(1 - i\tau\nu) - 1}{\tau\nu^2} + \frac{e^{i\tau\nu}(1 - e^{iT_a\nu} + iT_a\nu)}{T_a\nu^2} \right).$$

The first term in the parentheses is the contribution from the working process and the second from the transferring process. Here, we can notice that the adiabatic evolution with  $T_a = +\infty$  is the same for the case with  $T_a = l \frac{2\pi}{\nu}$  ( $l = 1, 2, 3 \dots$ ). When we set  $T_a = \frac{2\pi}{\nu} = 50 \mu s$ , we can transfer the phonon distribution of the system Hamiltonian  $H_S(t = \tau)$  to the distribution of the phonon measurement. This fast adiabatic protocol is further developed systematically within the theory of the shortcut to adiabaticity as discussed in Ref. [23]. Finally we apply the blue-sideband transition to get the phonon distribution according to Eq. (38.9), which is the transition probability  $P_{n \rightarrow m}$ . The experimental dissipated quantum work,  $W_{\text{dis}} = W - \Delta F$ , distribution can be constructed by  $P(W_{\text{dis}}) = \sum_{n,m} P_n^{\text{th}} P_{n \rightarrow m} \delta(W_{\text{dis}} - \hbar\nu(m - n))$ .

The experimentally reconstructed work distributions for the initial thermal distribution with  $\langle n \rangle = 0.157$  ( $T_{\text{eff}} = 480 \text{ nK}$ ) are shown in Fig. 38.5a, based on which the quantum Jarzynski equality is verified within experimental precision. It is clear that the ramping of the force with duration  $\tau = 45 \mu s$  is close to an adiabatic process, as there is almost no change in the phonon distribution in the work process. Similar to the results for the classical regime, the mean value and the width of the distribution of the dissipated work increase with the ramping speed. The standard deviations of the dissipated work in the two fast-ramping protocols ( $\tau = 5 \mu s$  and  $\tau = 25 \mu s$ ) show negative dissipated work, as a manifestation of the microscopic violation of the second law. Note that in the classical version of our model, only a Gaussian profile of the distribution of dissipated work exists in an open system as well as in an isolated system regardless of the protocol. The non-Gaussian profile at the extremely low initial temperature  $\langle n \rangle < 1$  is a quantum manifestation. In Fig. 38.5b, we also show the Crooks relations [11] for all the three different cases. For the dragged harmonic oscillator model, the backward and the forward processes are identical. We can use the same dissipated work distribution for these forward and backward processes. We notice for the adiabatic case, the relatively large experimental errors at the large  $|\Delta n|$  distorted the linear relation.

### 38.4.2 Experimental Verification in a Quasi-open Quantum System

In this example we employ a driven quantum two-level system to verify the quantum Jarzynski equality in the presence of the dephasing effect [24]. A pair of the internal levels in the ground-state  ${}^2S_{1/2}$  manifold, which are  $|F = 1, m_F = -1\rangle = |\uparrow\rangle$  and  $|F = 0, m_F = 0\rangle = |\downarrow\rangle$ , are chosen as the two-level system. We modulate both the amplitude and the phase in Eq. (38.15), leading to a parameter  $\tau$ -dependent Hamiltonian

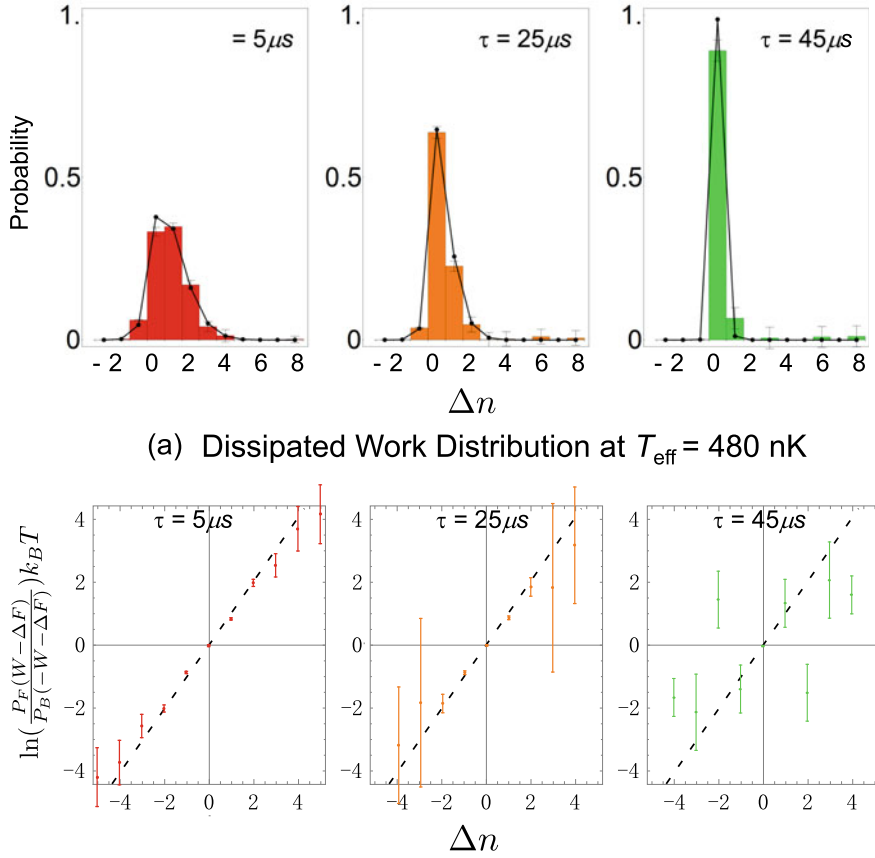


**Fig. 38.5** The experimental results. **a** For the fastest  $5 \mu\text{s}$  working process, we get the widest distribution. We can also notice the non-Gaussian feature here. For the slowest working process, we get a distribution close to the delta function. For all these working processes with different speeds, the exponential average of the dissipated work is one within the experimental error bars. **b** The Crooks relation for all the previous cases. When the fluctuation is relatively large, we can get a good linear relation for the  $\tau = 5 \mu\text{s}$ . When the processes are close to adiabatic, the dissipated work distributions are narrow and the work probabilities for large  $|\Delta n|$  become much smaller than the experimental uncertainties, which makes it difficult to clearly observe the Crooks relation. The dashed lines here are the predictions from the Crooks relation. Here  $P_F$  and  $P_B$  mean the dissipated work distributions for the forward and the backward processes.

$$\hat{H}_S(t) = \frac{\hbar\Omega_0}{2} \left(1 - \frac{t}{2\tau}\right) [\hat{\sigma}_x \cos(\frac{\pi t}{2\tau}) + \hat{\sigma}_y \sin(\frac{\pi t}{2\tau})]. \quad (38.21)$$

Here  $\Omega_0$  is the energy splitting of the initial Hamiltonian  $\hat{H}_S(0)$ , which is equal to  $2\pi \times 50$  kHz in the experiment, and the evolution time  $t$  varies from 0 to  $\tau$ .

*1. Preparation of the initial thermal state.* We utilize the strong decoherence of the Zeeman levels to create an effective thermal state. First we prepare the superposition state  $|c_{\downarrow}\downarrow\rangle + |c_{\uparrow}\uparrow\rangle$  through optical pumping followed by a resonant microwave transition for a certain duration. Because of the fluctuations of the external magnetic field, this pure state evolves into a mixed state  $|c_{\downarrow}|^2 |\downarrow\rangle\langle\downarrow| + |c_{\uparrow}|^2 |\uparrow\rangle\langle\uparrow|$  after waiting around ten times the coherence time, which is equivalent to the thermal state with the effective temperature

$$T_{\text{eff}} = \frac{\hbar\Omega_0}{k_B \ln(|c_{\downarrow}|^2/|c_{\uparrow}|^2)}. \quad (38.22)$$

In the example of our experiment, the effective temperature is  $T_{\text{eff}} = 5.63$  mK.

*2. The first projective measurement.* After preparing the effective thermal state in the basis of  $\hat{\sigma}_z$ , we apply the first projective measurement on the internal state. Then this projected state is adiabatically transferred to the basis of the initial Hamiltonian [54], shown in Fig. 38.6a. We note that the first projective measurement includes

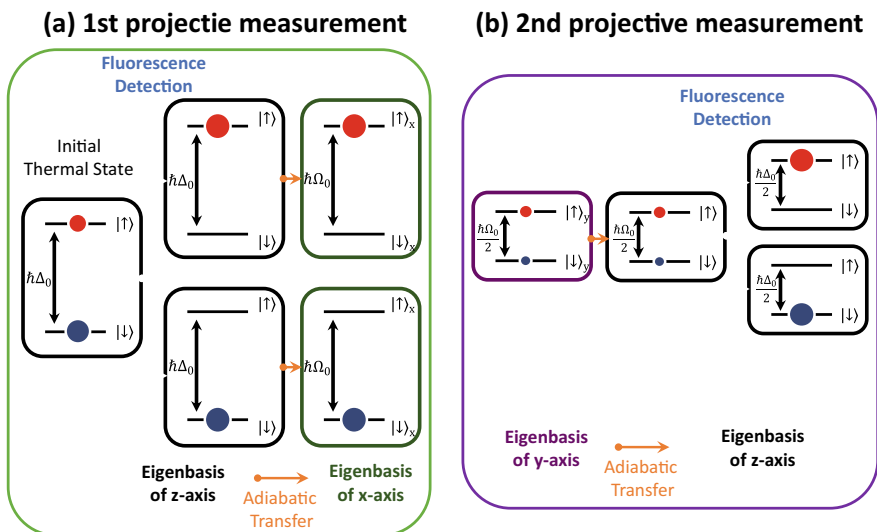


**Fig. 38.6** The projective measurements on the internal state. **a** We prepare the initial thermal state and apply the first projective measurement in the basis of  $\hat{\sigma}_z$ . Then the projected state is transferred to the basis of  $\hat{\sigma}_x$  in the adiabatic way. **b** For the second projective measurement, we adiabatically rotate the basis from  $\hat{\sigma}_y$  back to  $\hat{\sigma}_z$  then apply the state-dependent fluorescence detection to the system.

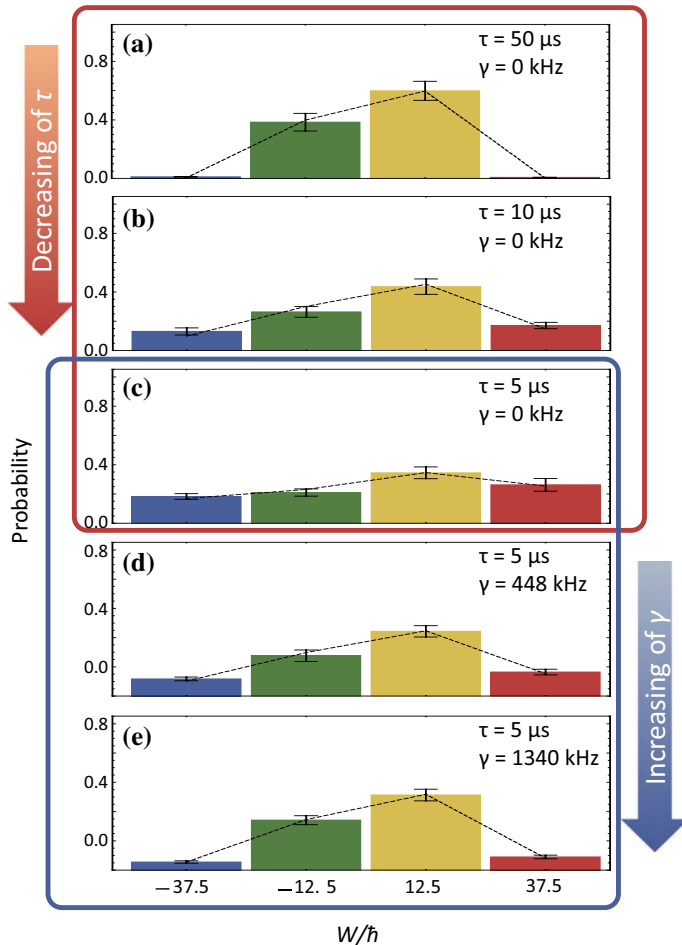
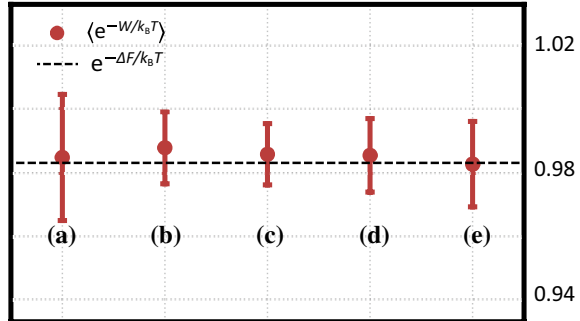


**Fig. 38.7** Work distributions for different combinations of the experimental parameters. For **a–c** we consider the cases without dephasing, while decreasing the duration of driving system from 50 to 5  $\mu\text{s}$ . For **c–e** we keep the duration  $\tau$  as 5  $\mu\text{s}$ , meanwhile increase the strength of dephasing effect from 0 to 1340 kHz.

the state-dependent fluorescence detection and the state re-preparation. If the upper state  $|\uparrow\rangle$  is detected, the system will be left in a mixed state of all the levels belong to  $|^2S_{1/2}, F=1\rangle$ . In this case we have to re-prepare the upper state using additional optical pumping followed by a microwave  $\pi$  pulse before continuing the experiment. Otherwise, if the outcome is  $|\downarrow\rangle$ , we can directly move to the next step.

*3. Application of work.* Our work protocol is modeled by the Hamiltonian in Eq. (38.21), which describes the rotation of the Hamiltonian from the initial  $\hat{\sigma}_x$  to the final  $\hat{\sigma}_y$ . The parameter  $\tau$  is the duration of driving the system. In the experiment we set this parameter to several values of 50, 10 and 5  $\mu\text{s}$ , corresponding to the near adiabatic, the moderate and the fast processes of driving the system. By simultaneously applying an additional stochastic Hamiltonian

**Fig. 38.8** Comparison between the exponential average of work for distributions (a–e) shown in Fig. 38.7 and the exponential of the calculated free energy difference.



$$\hat{H}_\xi(t) = \frac{\Omega_0 \xi(t)}{2} [\hat{\sigma}_x \cos(\frac{\pi t}{2\tau}) + \hat{\sigma}_y \sin(\frac{\pi t}{2\tau})], \quad (38.23)$$

where  $\xi(t)$  is the Gaussian white noise, we can simulate the work process undergoing dephasing, which is exactly the same as the evolution described in Eq. (38.16) [51, 52]. Here the dephasing strength  $\gamma$  of the Eq. (38.16) in the basis of the instantaneous Hamiltonian (38.21) is uniform and proportional to  $(\sigma \Omega_0)^2$ , where  $\sigma$  is defined in Eq. (38.17). In our experimental realization, the values of dephasing strength  $\gamma$  are set to 0, 448 and 1340 kHz by controlling the noise intensities.

*4. The second projective measurement.* This measurement is similar to the first one. We apply the fluorescence detection after adiabatically transferring state from the  $\hat{\sigma}_y$  to the  $\hat{\sigma}_z$  basis, shown in Fig. 38.6b. Because this is the final step of the experimental sequence, the re-preparation of the state is not necessary here.

We test five combinations of the dephasing strength  $\gamma$  and the driving duration  $\tau$ . The work distributions are summarized in Fig. 38.7. It is obvious that the dephasing effect plays a non-trivial role in the process of applying work. The final work distribution depends on the competition between the driving duration  $\tau$  and the dephasing strength  $\gamma$ . Decreasing parameter  $\tau$  broadens the work distribution, which means more work is done on the system as shown in Fig. 38.7a–c. However, increasing dephasing strength  $\gamma$  tends to narrow the work distribution, and brings it close to the case of the adiabatic process as shown in Fig. 38.7c–e. The experimental results reveal the similarity between the dephasing effect and the continuous measurements on the instantaneous basis of the system, which collapse the wave function of the system and effectively trap the system in one of the instantaneous eigenstates, known as the quantum Zeno effect.

Meanwhile, the quantum Jarzynski equality can be verified with all the work distributions as shown in Fig. 38.8. The quantity  $\langle e^{-W/k_B T} \rangle$  in the left hand of equation (38.1) is obtained by using the experimental work distribution as discussed in Eq. (38.20), while the right hand of equation (38.1) was calculated by the theoretical difference of the free energy between  $\hat{H}_S(\tau)$  and  $\hat{H}_S(0)$ . The experimental results are consistent with the theoretical predictions within the experimental errors.

## 38.5 Conclusion and Discussions

In this chapter, we present how to employ a single ion trapped in a harmonic potential for the experimental test of the quantum Jarzynski equality. Using projective measurements of the motional mode, we verify the equality for a closed quantum system. With the internal levels and properly designed noise, we perform the experimental test of the equality for a quasi-open quantum system. Together with further theoretical developments, these demonstrations would be important stepping stones to fully confirm the equality and the fluctuation theorem for open quantum systems [57, 58]. Besides being used in verifying the quantum Jarzynski equality, our experimental breakthrough could be applied to realize many other thought experiments in quantum thermodynamics. For example, it could be applied to the studies of quantum heat engines by experimentally exploring the relation between work and heat in thermodynamic cycles [59–62].

**Acknowledgements** This work was supported by the National Key Research and Development Program of China under Grants No. 2016YFA0301900 and No. 2016YFA0301901 and the National Natural Science Foundation of China Grants No. 11374178, No. 11574002, and No. 11504197.

## References

1. G. Hummer, A. Szabo, Proc. Natl. Acad. Sci. USA **98**, 3658 (2001). <https://doi.org/10.1073/pnas.071034098>
2. J. Liphardt, S. Dumont, S.B. Smith, I. Tinoco Jr., C. Bustamante, Science **296**, 1832 (2002). <https://doi.org/10.1126/science.1071152>
3. D. Collin, F. Ritort, C. Jarzynski, S.B. Smith, I. Tinoco Jr., C. Bustamante, Nature **437**, 231 (2005). <https://doi.org/10.1038/nature04061>
4. F. Douarché, S. Ciliberto, A. Petrosyan, I. Rabbiosi, Europhys. Lett. **70**, 593 (2005). <https://doi.org/10.1209/epl/i2005-10024-4>
5. V. Bickle, T. Speck, L. Helden, U. Seifert, C. Bechinger, Phys. Rev. Lett. **96**, 070603 (2006). <https://doi.org/10.1103/PhysRevLett.96.070603>
6. N.C. Harris, Y. Song, C.-H. Kiang, Phys. Rev. Lett. **99**, 068101 (2007). <https://doi.org/10.1103/PhysRevLett.99.068101>
7. I. Junier, A. Mossa, M. Manosas, F. Ritort, Phys. Rev. Lett. **102**, 070602 (2009). <https://doi.org/10.1103/PhysRevLett.102.070602>
8. E.A. Shank, C. Cecconi, J.W. Dill, S. Marqusee, C. Bustamante, Nature **465**, 637 (2010). <https://doi.org/10.1038/nature09021>
9. O.-P. Saira, Y. Yoon, T. Tanttu, M. Möttönen, D. Averin, J. Pekola, Phys. Rev. Lett. **109**, 180601 (2012). <https://doi.org/10.1103/PhysRevLett.109.180601>
10. C. Jarzynski, Phys. Rev. Lett. **78**, 2690 (1997). <https://doi.org/10.1103/PhysRevLett.78.2690>
11. G.E. Crooks, Phys. Rev. E **60**, 2721 (1999). <https://doi.org/10.1103/PhysRevE.60.2721>
12. J. Kurchan, A quantum fluctuation theorem (2000), arXiv:cond-mat/0007360v2
13. H. Tasaki, Jarzynski relations for quantum systems and some applications (2000), arXiv:cond-mat/0009244
14. S. Mukamel, Phys. Rev. Lett. **90**, 170604 (2003). <https://doi.org/10.1103/PhysRevLett.90.170604>
15. M. Campisi, P. Hänggi, P. Talkner, Rev. Mod. Phys. **83**, 771 (2011). <https://doi.org/10.1103/RevModPhys.83.771>

16. M. Heyl, S. Kehrein, Phys. Rev. Lett. **108**, 190601 (2012). <https://doi.org/10.1103/PhysRevLett.108.190601>
17. R. Dorner, S.R. Clark, L. Heaney, R. Fazio, J. Goold, V. Vedral, Phys. Rev. Lett. **110**, 230601 (2013). <https://doi.org/10.1103/PhysRevLett.110.230601>
18. L. Mazzola, G. De Chiara, M. Paternostro, Phys. Rev. Lett. **110**, 230602 (2013). <https://doi.org/10.1103/PhysRevLett.110.230602>
19. P. Hänggi, P. Talkner, Nat. Phys. **11**, 108 (2015). <https://doi.org/10.1038/nphys3167>
20. G. Huber, F. Schmidt-Kaler, S. Deffner, E. Lutz, Phys. Rev. Lett. **101**, 070403 (2008). <https://doi.org/10.1103/PhysRevLett.101.070403>
21. G.T. Huber, Ph.D. thesis, Universität Ulm, 2010
22. S. An, J.-N. Zhang, M. Um, D. Lv, Y. Lu, J. Zhang, Z.-Q. Yin, H.T. Quan, K. Kim, Nat. Phys. **11**, 193 (2015). <https://doi.org/10.1038/nphys3197>
23. S. An, D. Lv, A. del Campo, K. Kim, Nat. Commun. **7**, 12999 (2016). <https://doi.org/10.1038/ncomms12999>
24. A. Smith, Y. Lu, S. An, X. Zhang, J.-N. Zhang, Z. Gong, H. Quan, C. Jarzynski, K. Kim, N. J. Phys. **20**, 013008 (2018). <https://doi.org/10.1088/1367-2630/aa9cd6>
25. P. Dirac, *The Principles of Quantum Mechanics* (Clarendon Press, Oxford, 1930)
26. H. Dehmelt, P. Toschek, Bull. Am. Phys. Soc. **20**, 61 (1975)
27. J.C. Bergquist, R.G. Hulet, W.M. Itano, D.J. Wineland, Phys. Rev. Lett. **57**, 1699 (1986). <https://doi.org/10.1103/PhysRevLett.57.1699>
28. W. Nagourney, J. Sandberg, H. Dehmelt, Phys. Rev. Lett. **56**, 2797 (1986). <https://doi.org/10.1103/PhysRevLett.56.2797>
29. T. Sauter, W. Neuhauser, R. Blatt, P.E. Toschek, Phys. Rev. Lett. **57**, 1696 (1986). <https://doi.org/10.1103/PhysRevLett.57.1696>
30. R. Blatt, P. Zoller, Eur. J. Phys. **9**, 250 (1988). <https://doi.org/10.1088/0143-0807/9/4/002>
31. D.J. Wineland, H. Dehmelt, Bull. Am. Phys. Soc. **20**, 637 (1975)
32. D.J. Wineland, R.E. Drullinger, F.L. Walls, Phys. Rev. Lett. **40**, 1639 (1978). <https://doi.org/10.1103/PhysRevLett.40.1639>
33. W. Neuhauser, M. Hohenstatt, P. Toschek, H. Dehmelt, Phys. Rev. Lett. **41**, 233 (1978). <https://doi.org/10.1103/PhysRevLett.41.233>
34. F. Diedrich, J.C. Bergquist, W.M. Itano, D.J. Wineland, Phys. Rev. Lett. **62**, 403 (1989). <https://doi.org/10.1103/PhysRevLett.62.403>
35. D. Leibfried, R. Blatt, C. Monroe, D. Wineland, Rev. Mod. Phys. **75**, 281 (2003). <https://doi.org/10.1103/RevModPhys.75.281>
36. H. Häffner, C.F. Roos, R. Blatt, Phys. Rep. **469**, (2008). <https://doi.org/10.1016/j.physrep.2008.09.003>
37. C. Chipot, A. Pohorille, *Free Energy Calculations* (Springer, Berlin, 2007). <https://doi.org/10.1007/978-3-540-38448-9>
38. A. Pohorille, C. Jarzynski, C. Chipot, J. Chem. Phys. B **114**, 10235 (2010). <https://doi.org/10.1021/jp102971x>
39. C. Jarzynski, Annu. Rev. Condens. Matter Phys. **2**, 329 (2011). <https://doi.org/10.1146/annurev-conmatphys-062910-140506>
40. P. Talkner, E. Lutz, P. Hänggi, Phys. Rev. E **75**, 050102(R) (2007a). <https://doi.org/10.1103/PhysRevE.75.050102>
41. T.B. Batalhao, A.M. Souza, L. Mazzola, R. Auccaise, R.S. Sarthour, I.S. Oliveira, J. Goold, G.D. Chiara, M. Paternostro, R.M. Serra, Phys. Rev. Lett. **113**, 140601 (2014). <https://doi.org/10.1103/PhysRevLett.113.140601>
42. M. Esposito, U. Harbola, S. Mukamel, Rev. Mod. Phys. **81**, 1665 (2009). <https://doi.org/10.1103/RevModPhys.81.1665>
43. J. Zhang, P. Hess, A. Kyprianidis, P. Becker, A. Lee, J. Smith, G. Pagano, I.-D. Potirniche, A.C. Potter, A. Vishwanath et al., Nature **543**, 217 (2017a). <https://doi.org/10.1038/nature21413>
44. J. Zhang, G. Pagano, P.W. Hess, A. Kyprianidis, P. Becker, H. Kaplan, A.V. Gorshkov, Z.-X. Gong, C. Monroe, Nature **551**, 601 (2017b). <https://doi.org/10.1038/nature24654>

45. S. Debnath, N.M. Linke, C. Figgatt, K.A. Landsman, K. Wright, C. Monroe, *Nature* **536**, 63 (2016). <https://doi.org/10.1038/nature18648>
46. T. Monz, D. Nigg, E.A. Martinez, M.F. Brundl, P. Schindler, R. Rines, S.X. Wang, I.L. Chuang, R. Blatt, *Science* **351**, 1068 (2016). <https://doi.org/10.1126/science.aad9480>
47. W. Paul, *Rev. Mod. Phys.* **62**, 531 (1990). <https://doi.org/10.1103/RevModPhys.62.531>
48. Y. Wang, M. Um, J. Zhang, S. An, M. Lyu, J.-N. Zhang, L.-M. Duan, D. Yum, K. Kim, *Nat. Photonics* **11**, 646 (2017). <https://doi.org/10.1038/s41566-017-0007-1>
49. S. Olmschenk, K.C. Younge, D.L. Moehring, D.N. Matsukevich, P. Maunz, C. Monroe, *Phys. Rev. A* **76**, 052314 (2007). <https://doi.org/10.1103/PhysRevA.76.052314>
50. K. Funo, J.-N. Zhang, C. Chatou, K. Kim, M. Ueda, A. del Campo, *Phys. Rev. Lett.* **118**, 100602 (2017). <https://doi.org/10.1103/PhysRevLett.118.100602>
51. F.N. Loret, A.B. Balantekin, *Phys. Rev. D* **50**, 4762 (1994). <https://doi.org/10.1103/PhysRevD.50.4762>
52. N.G.V. Kampen, *Stochastic Processes in Physics and Chemistry* (Elsevier, Amsterdam, 2007)
53. P. Talkner, E. Lutz, P. Hänggi, *Phys. Rev. E* **75**, 050102 (2007b). <https://doi.org/10.1103/PhysRevE.75.050102>
54. M.V. Berry, *J. Phys. A Math. Theor.* **42**, 365303 (2009). <https://doi.org/10.1088/1751-8113/42/36/365303>
55. Q. Turchette, B. King, D. Leibfried, D. Meekhof, C. Myatt, M. Rowe, C. Sackett, C. Wood, W. Itano, C. Monroe et al., *Phys. Rev. A* **61**, 063418 (2000). <https://doi.org/10.1103/PhysRevA.61.063418>
56. C. Shen, Z. Zhang, L.-M. Duan, *Phys. Rev. Lett.* **112**, 050504 (2014). <https://doi.org/10.1103/PhysRevLett.112.050504>
57. F. Petruccione, H.P. Breuer, *The Theory of Open Quantum Systems* (Oxford University Press, London, 2002)
58. S. Pigeon, L. Fusco, A. Xuereb, G.D. Chiara, M. Paternostro, *N. J. Phys.* **18**, 013009 (2016). <https://doi.org/10.1088/1367-2630/18/1/013009>
59. H.T. Quan, Y.X. Liu, C.P. Sun, F. Nori, *Phys. Rev. E* **76**, 031105 (2007). <https://doi.org/10.1103/PhysRevE.76.031105>
60. O. Abah, J. Ronßagel, G. Jacob, S. Deffner, F. Schmidt-Kaler, K. Singer, E. Lutz, *Phys. Rev. Lett.* **109**, 203006 (2012). <https://doi.org/10.1103/PhysRevLett.109.203006>
61. J. Roßnagel, S.T. Dawkins, K.N. Tolazzi, O. Abah, E. Lutz, F. Schmidt-Kaler, K. Singer, *Science* **352**, 325 (2016). <https://doi.org/10.1126/science.aad6320>
62. G. Maslennikov, S. Ding, R. Hablitzel, J. Gan, A. Roulet, S. Nimmrichter, J. Dai, V. Scarani, D. Matsukevich (2017). <https://doi.org/10.1038/s41467-018-08090-0>

# Chapter 39

## Maxwell's Demon in Photonic Systems



**Luca Mancino, Mario A. Ciampini, Mihai D. Vidrighin, Marco Sbroscia,  
Ilaria Gianani and Marco Barbieri**

### 39.1 Introduction

The second law of thermodynamics states that natural phenomena are irreversible: a spontaneous process always results in a state with increased entropy. The reversed process is never observed, even if it would obey the first law of thermodynamics. The second law was initially an empirical discovery and, later, its emergence from the microscopic laws was explained by statistical thermodynamics. However, it is also widely considered one of the fundamental principles of Physics and a pass-or-fail test for new physical theories. The law has been the subject of some historic debates.

Rudolf Clausius gave a formulation of the second law of thermodynamics in terms of heat transfer and work: “*It is impossible to devise an engine which, working in a*

---

L. Mancino · M. Sbroscia · I. Gianani · M. Barbieri (✉)  
Dipartimento di Scienze, Università degli Studi Roma Tre,  
Via della Vasca Navale 84, 00146 Rome, Italy  
e-mail: marco.barbieri@uniroma3.it

L. Mancino  
e-mail: luca.mancino@uniroma3.it

M. Sbroscia  
e-mail: marco.sbroscia@uniroma3.it

I. Gianani  
e-mail: ilaria.gianani@uniroma3.it

M. A. Ciampini  
Quantum Optics, Quantum Nanophysics and Quantum Information,  
Faculty of Physics, University of Vienna, Boltzmanngasse 5, 1090 Vienna, Austria  
e-mail: mario.arnolfo.ciampini@univie.ac.at

M. D. Vidrighin  
Formerly at Imperial College London, London SW7 2BW, UK  
e-mail: mihai.vidrighin@gmail.com

M. Barbieri  
Istituto Nazionale di Ottica - CNR, Largo Enrico Fermi 6, 50125 Florence, Italy

*cycle, shall produce no effect other than the heat transfer from a colder to a hotter body”* [1]. James Clerk Maxwell’s reflections on the implications of a material’s discrete structure for heat exchange, from 1871, introduced the paradox now known as Maxwell’s demon [2, 3]. Maxwell wrote that the second law is “*undoubtedly true*” if restricted to situations where we “*have no power of perceiving or handling the separate molecules.*” However, a being can be conceived “*whose attributes are still as essentially finite as our own*” that by close monitoring of each molecular constituent of a system can achieve violations of the second law. Maxwell’s demon, “*a being whose faculties are so sharpened that he can follow every molecule in its course*”, can use sharp observations to modify an otherwise inert material, and turn it into a working medium, without applying work to it, suggesting “*limitations of the second law of thermodynamics*” [4].”

Maxwell proposed the following thought experiment: a gas is contained in a vessel of volume  $V$ , divided in two parts, A and B, of equal volume, by a fixed splitter door on which a smart agent, the demon, can operate. This system is prepared in thermodynamic equilibrium, with temperature  $T$  over the entire volume of the vessel. Thus, the average speed of the gas particles,  $\langle v \rangle_T$ , is a characteristic parameter of the system. The demon observes the particles on the left (B) side of the vessel, and opens the splitting door to let the particles with a speed exceeding  $\langle v \rangle_T$  go to the right (A) side of the box; similarly, it can open the splitting door to let the particles with a speed lower than  $\langle v \rangle_T$  move to the left (B) side. The demon is able to act on the system with no work expenditure. As a result [3], “*the energy in A is increased and that in B diminished, and yet no work has been done: only the intelligence of a very observant and neatfingered being has been employed*”.

Maxwell’s argument may be looked upon with suspicion from a practical point of view: the original paradox starts from ideal considerations which may hardly be satisfied under real conditions. However, no fundamental link arises between the extracted work and the work that the demon needs to apply: the demon may in principle gain some work, less than the ideal amount, by acting based on its observations. The real exorcism of the Maxwell’s demon paradox started in 1929, when Leo Szilard discussed a simplified version of the problem, known as *Szilard’s engine*, where the gas is reduced to a single molecule and the demon to a mechanical apparatus. Szilard’s engine has four stages, as depicted in Fig. 39.1 (left panel): (i) the single gas molecule occupies a volume  $V$ ; (ii) an adiabatic partition is inserted into the vessel, and it divides the latter in two parts of equal volume  $V/2$ ; (iii) the position of the molecule, either on the right or on the left side of the partition, is measured and recorded. Depending on the result of the measurement, the demon attaches a weight using a pulley, on the same side as the molecule; (iv) the whole system is kept at a constant temperature  $T$  by interaction with an external thermal bath, while the single-molecule gas undergoes a quasistatic isothermal expansion. After this transformation, the thermodynamic cycle is closed as the single-particle gas is free to move anywhere in the vessel, as it was in step (i). During the expansion, an amount of heat  $Q$  is extracted from the thermal bath, and converted to an equal amount of mechanical work  $W$ , stored in a displacement of the weight. The extracted work is given by

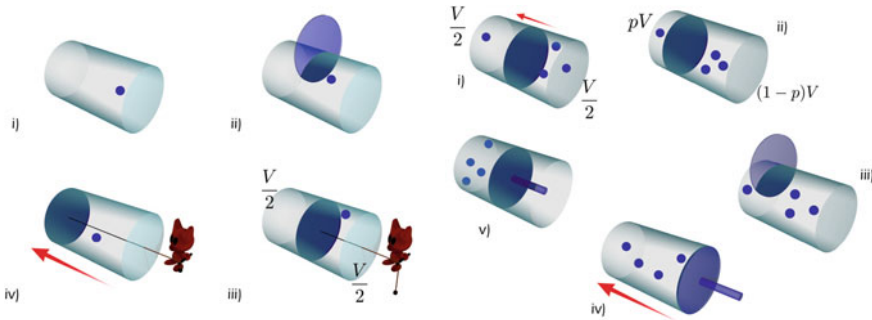


**Fig. 39.1** Schematics of Szilard's engine (left panel), and of the erasure of the Demon's memory (right panel).

$$W = \int_{\frac{V}{2}}^V p dV = k_B T \int_{\frac{V}{2}}^V \frac{1}{V} dV = k_B T \ln 2, \quad (39.1)$$

where  $k_B$  is Boltzmann's constant. In (39.1), the single-particle gas has been assumed to be ideal. This approach can be justified considering an ensemble of single-particle gases: each physical quantity can be evaluated by taking averages over the ensemble, as if considering an ideal gas with a large number of non-interacting constituents. Therefore, work is produced, while the entropy of the external thermal bath is decreased by  $Q/T = k_B \ln 2$ , and the system is back to its original state.

The caveat here is that the entire system, including the demon, does not actually return to the initial state. In Szilard's engine, the measurement outcome is a single bit of information: the molecule is either in volume A or in volume B. In order to record this bit of information, the demon's memory must be prepared, to start with, in a well defined state. After the measurement, one bit of memory is occupied, and it must be reset for truly cyclic operation. In 1961, Rolf Landauer drew a connection between *logical* and *physical* operations: every time a bit of information is irreversibly lost, thermodynamic irreversibility occurs [5]. Thus “*the dissipation required to save the second law comes from the subsequent resetting of that apparatus*” [6], i.e. the memory. This represents a cornerstone of information-thermodynamics, as “*measures of information arise as the answers to fundamental questions about the physical resources required to solve some information processing problems*” [7].

One way to model the demon's memory is as another partitioned vessel, with a single particle occupying one of the two sides e.g. the same side as the observed particle. The blank state of the memory corresponds to the particle occupying a predetermined side. With this model, we can explore the thermodynamics of information erasure. Such a process (moving the memory particle to a predetermined side independent on the initial state) is realized by removing the partition between the vessels and recompressing the gas from volume  $V$  to volume  $V/2$ . This procedure allows for an irreversible formatting of all the memories, as no track of the previous informations can be recovered. The amount of work the Demon needs to spend to format a single

ideal memory is equal in absolute value to the extractable work,  $W^{eras} = -k_B T \ln 2$ . This saves the second law of thermodynamics. In general, the demon's measurement output may be biased. From an ensemble of  $\mathcal{N}$  Szilard's engines,  $\mathcal{M}$  of the memory particles may be set to the left, and  $\mathcal{N} - \mathcal{M}$  to the right. The average ratio is given by the probability to measure the work particle on the left side,  $p = \langle \mathcal{M}/\mathcal{N} \rangle$ . The memory particles can be taken to constitute an ideal gas, thus one can consider them all together in a single vessel. This state of the memory is not in equilibrium, due to the pressure unbalance between the two halves. One lets it expand isothermally: work can be extracted via this transformation before erasing the memory content. Defining  $p_A$ ,  $p_B$ , and  $V_B$  as the pressure in the A and the B side of the box, and the volume of the right side of the vessel, the work done by letting the memory equilibrate ( $W'$ ) is:

$$W' = \int_{V/2}^{pV} (p_B - p_A) dV_B = k_B T \int_{V/2}^{pV} \left( \frac{p}{V_B} - \frac{1-p}{V-V_B} \right) dV_B = k_B T \ln 2 (1 - H(p)). \quad (39.2)$$

Here,  $H(p)$  is the binary Shannon entropy, which quantifies the amount of information extracted by the measurements [7]:

$$H(p) = -p \log_2 p - (1-p) \log_2 (1-p). \quad (39.3)$$

This leads to  $W^{eras} = W' - k_B T \ln 2 = -k_B T \ln 2 H(p)$  for the erasure work required in the general scenario.<sup>1</sup> The profound meaning of this equality resides in the fact that it provides a direct link between the information acquired by measurement and the presence of extractable work. One can then make use of these ideas to analyse experiments in which resources are prepared and modified by means of measurements: if information is acquired, work is made available somewhere else in the system. This chapter will be dedicated to the development of these ideas in a photonics setting. While it looks difficult to apply thermodynamics directly to photons, one can retain the fundamental idea: trading information for work and vice versa. In the next sections, we will detail how this has been applied with two examples.

## 39.2 Information Thermodynamics of Photon Subtraction

The first of the two examples shows how the manipulation of photon statistics can be interpreted in terms of information thermodynamics, in the spirit of Maxwell's original conception. In the work pursued by M. D. Vidrighin and co-workers [8], an optical device in a conditional operation scheme is proposed as a physical scenario analogous to Maxwell's demon, with light as the working medium. Instead of the two boxes occupied by gas molecules, two optical modes are prepared in thermal equilibrium. The thermal state of an optical mode is described by the density matrix:

---

<sup>1</sup>Here, we always consider the work performed by the system. Our sign convention is that  $W < 0$  if this has to be performed from the outside, while  $W > 0$  if this is extracted. This explains some discrepancies between our formulas and those often reported in the literature.

$$\rho = (1 - e^{-\beta h\nu}) \sum_{n=0}^{\infty} e^{-\beta h\nu n} |n\rangle \langle n|, \quad (39.4)$$

where  $n$  denotes photon number,  $h\nu$  is the photon energy and  $\beta = 1/(k_B T)$ . This state describes a mode of light generated by a collection of narrow-band emitters at fixed temperature  $T$ .

Thermal fluctuations can be resolved with detection faster than the thermal source's coherence time. However, optical thermal sources are generally very weak. A solution is to use the following trick: one can adopt a laser source and vary its average intensity over time in order to attain the super-Poissonian photon number distribution given in (39.4). Precisely this is achieved by collecting a single coherence area in a time-varying laser speckle pattern, which can be produced using a spinning glass diffuser (Arechi's wheel) [9]. A convenient choice is to adopt light pulses at a given repetition rate: the detection system can then work at such rate, and each pulse represents a realization of the system. It has been shown that photon subtraction [10, 11] from a thermal light mode updates its state to one with higher average energy. The information gained by successfully subtracting a photon effectively increases the energy of the mixed state by a factor of 2 [12]. A demon can use this type of operation to perform work extraction.

As Maxwell's thought experiment considers two partitions at the same temperature, two thermal light modes are selected, using two different spatial modes produced by the same glass diffuser (see Fig. 39.2). The thermal modes have the same average energy. However, if a demon can gain access to the energy fluctuations, it can extract work by an appropriate selection of microstates with different energy in the two modes. Taking inspiration from photon subtraction, each mode propagates through a high-transmittance beam splitter from which the reflected light is coupled to a highly sensitive avalanche photo-diode (APD). One may picture the demon hidden behind a mirror on which the thermal light is reflected, monitoring the leaked light with an APD detector. This measurement has a binary output for each mode, as an APD simply heralds the detection of one or more photons by producing a "click", or otherwise remains in its default state. In the limit of small click probability, the operation conditioned by a click is precisely single photon subtraction, which has been used extensively for preparing non-classical states of light. In the work discussed here, the measurement is not restricted to small click probabilities. Instead, it is tuned by choosing how much light gets sent to the APDs. Thus, the information extracted by the demon can be changed. In general for this measurement, when the detector clicks, the expected average number of photons is updated to a higher value if the input state has super-Poissonian fluctuations of the photon number (as thermal light does), and to a lower value in the sub-Poissonian case. The energy used to perform the measurement is considered as belonging to the demon's resources, and is kept out of the overall balance. If an observer has no access to the information from the APDs, the state of the light bears almost no differences before and after the measurement: the average effect amounts to a negligibly small loss introduced by the high transmittance beam splitters.

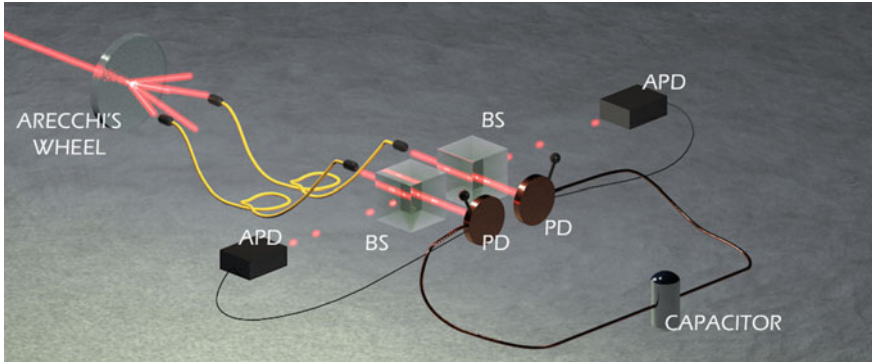


**Fig. 39.2** Essential elements of the experimental photonic Maxwell's Demon. APD: avalanche photodiode, PD: photodiode, BS: beamsplitter.

For work extraction, the transmitted light falls on two photodiodes, connected with opposing polarities such that on average they produce zero voltage ( $U = 0$ ) when the two light modes are balanced. This photodiode circuit charges a capacitor according to the fluctuating energy difference between the two light modes. If an asymmetry is produced by a feed-forward operation based on the demon's APD measurement outcomes, the capacitor gains a non-zero average voltage. For instance, the demon's measured outcomes may be used to switch the thermal modes, such that the more energetic one ends always on the same side of the capacitor. In a proof-of-principle demonstration, it is equivalent to change the sign of the measured capacitor voltage conditioned on the APD signals instead of actually performing a feed-forward operation. More details on the interpretation of work extraction are given in the Appendix.

Experimental results are reported in Fig. 39.3. This shows histograms of the measured voltage drop  $U$  across the capacitor. When the outcomes of the measurements are ignored, the average drop is zero. If the information from the APDs is considered to realize an effective feedback control, the average voltage can be made significantly different from zero. This is linked to the work which can be extracted on average from observing the details of the system.

The principle that information is connected to extractable work is thus demonstrated but the connection is not yet quantified. One can consider the equality due to T. Sagawa and M. Ueda (see Chap. 10), [14],

$$\langle e^{\beta(W+\Delta F)-I} \rangle = 1, \quad (39.5)$$

which establishes a link between the extracted work  $W$ , the mutual information between the system and the measurement apparatus,  $I$ , and the variation of the Helmholtz free energy,  $\Delta F$  between pre- and post-measurement states of the system. This does not apply directly to this experiment, as Eq. (39.5) only holds for transformations that occur in contact with a single thermal bath, which is not the

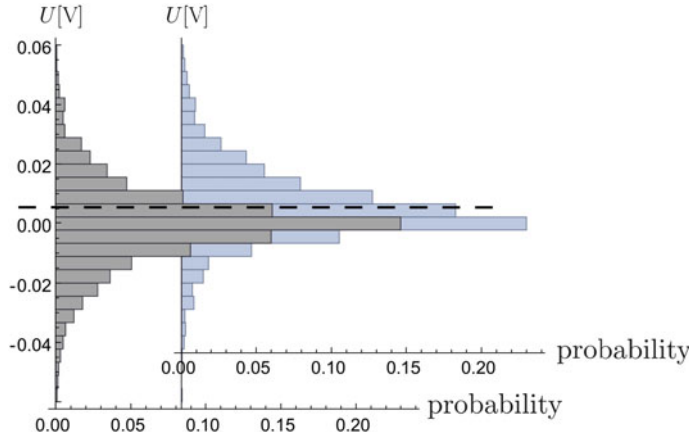


**Fig. 39.3** Observing the average effect of measurement and feedback on the capacity voltage. Top, histogram of the measured values in the case when no feedback is applied, when the average is close to 0. Bottom: same histogram the sign of the voltage is flipped if the measurement outcome is “click” in one arm “no click” in the other. The dashed horizontal line shows the average value for the second distribution, significantly displaced from 0. The detection rates for the two APDs were  $p_1 = 0.702 \pm 0.008$  clicks/pulse for one arm, and  $p_2 = 0.311 \pm 0.008$  clicks/pulse for the second. Reproduced from [13].

case here. However, it is a valid starting point to look for similar quantitative analysis. The appropriate modification is found to be

$$\langle e^{-\beta W - I} \rangle_f = \langle e^{-\beta W} \rangle_0, \quad (39.6)$$

where the average  $\langle \cdot \rangle_f$  considers the effect of the feedback control, while  $\langle \cdot \rangle_0$  refers to the state with no feedback applied. The proof of this equality is given in the Appendix, and relies on the following conditions: the measurement and feedback are applied to a system initially in thermal equilibrium with the inverse temperature appearing as  $\beta$  in (39.6); the feedback operation is unitary and energy conserving (such as swapping modes, in this case); the system and energy reservoir suffer decoherence after the energy transfer takes place. In addition, a particular non-disturbance condition (detailed in the Appendix) needs to be satisfied, as is the case for the measurement described here.

A more useful relation is obtained using Jensen’s inequality. For the particular experiment discussed here, this leads to a bound on the distribution of the capacitor voltage (which is proportional to extractable work) in terms of mutual information:

$$\begin{aligned} \langle U \rangle_f - \langle U \rangle_0 &< \min_{\xi} \left\{ \frac{1}{\xi} \langle I \rangle + \xi [\sigma(\xi, U)]^2 / 2 \right\}, \\ \sigma(\beta, U) &\equiv \sqrt{2 \beta^{-2} \log \langle e^{\beta(U - \langle W \rangle_0)} \rangle_0}. \end{aligned} \quad (39.7)$$

where the latter quantity is a measure of fluctuations, and coincides with the standard deviation if the distribution is Gaussian. For a Gaussian work distribution, the expression above can be put in the simpler form:

$$\frac{|\langle W \rangle_f - \langle W \rangle_0|}{\sigma(W)_0} < \sqrt{2\langle I \rangle}. \quad (39.8)$$

Since  $W$  is proportional to  $U$ , (39.7) is effectively a bound on the extractable work based on the extracted information. The physical meaning of this inequality is that the efficiency of the work extraction protocol is governed by the information collected and by the presence of fluctuations. Indeed, the distinguishability of work distributions with and without a feedback operation based on a measurement of a thermal system is limited by the mutual information characterizing that measurement. The figure of merit that quantifies the effect on the work distributions includes normalization to the variance: this is related to the concept of “strength of the work”, introduced in [15]. This relation approaches the regime of Landauer’s bound [5], when the work fluctuations are of the same order as the characteristic thermal energy of the equilibrium system on which measurement and feedback are applied. All quantities in (39.7) can be measured: experimental results are shown in Fig. 39.4 together with the thermodynamic bound (39.7). The bound is clearly satisfied, however, it is not tight, due in part to the use of Jensen’s inequality.

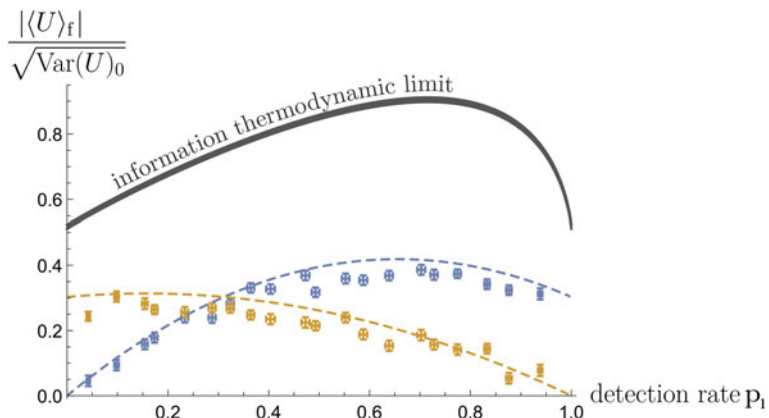


**Fig. 39.4** Extracted work bounded by information. The quantity  $|\langle U \rangle_f|/\sqrt{\text{Var}(U)_0}$ , introduced in [13], is reported as a function of the detection rate  $p_1$  on the first arm, with the other held fixed at  $0.311 \pm 0.008$  clicks/pulse. This effectively tunes the effect of the measurement as well as the extracted information. Blue and yellow points correspond to two feedback strategies: changing the polarity of  $C$  when the measurement yields click/no-click (blue) or no-click/click (yellow). The black line gives the bound established in terms of mutual information. The width of the line represents the uncertainty with which the bound is determined using the measured voltage distribution (two times the standard deviation). Dashed lines give predictions based on the average photon number difference between the two light modes after feedback. Reproduced from [13].

This result is an information-theoretic equality which describes the transfer of energy, showing the two descriptions can be interwoven [16]. The main advantage of investigating this concepts in an optical platform is the ability of addressing both the single-photon and the intense-field regimes in the same experiment. Similar single-particle measurement can also be applied in other contexts, such as optomechanics [17] and spin-ensemble systems [18] to investigate how weak probing affects the dynamics of open systems. The capabilities of work extraction for light modes showing photon number correlation have been considered in Ref. [19]: the presence of positive correlations reduces the power of the demon, while anti-correlations can provide an enhancement.

### 39.3 Asking Maxwell's Demons to Measure Nonclassicality

The second example considers how Maxwell's Demon can serve as a witness of the presence of nonclassical correlations between two qubits, coded, in this case, in the polarization of two single photons. The idea is now that information is not used to actually gain work, but instead of looking at optical properties, to assess the quantum nature of the correlations.

Szilard's engine, as described in the introduction, considers a single-particle gas in a split vessel, and a memory storing information on the position of the particle. The latter can be used to extract some work, according to the work-information relation (39.2). When moving to the quantum domain, the particle is now allowed to be in an arbitrary superposition of the two partitions: the memory will now keep track of the result obtained from the measurement of a generic observable  $\hat{A}_\theta$ . The Shannon entropy associated to the statistics of its outcomes is  $H(A_\theta)$ , which, in turn, determines what is the work that the Demon can extract from its memory. Imagine this system is correlated to a second qubit, accessible to a second Demon, as depicted schematically in Fig. 39.5. A measurement of the observable  $\hat{B}_{\theta'}$  can then deliver some information on the first qubit, hence on the result of  $\hat{A}_\theta$ . In informational terms, the entropy of the first Demon can be decreased from  $H(A_\theta)$  to the conditional expression  $H(A_\theta|B_{\theta'})$  (refer to the Appendix for the definition of the conditional Shannon entropy). The reverse argument will clearly hold as well. As far

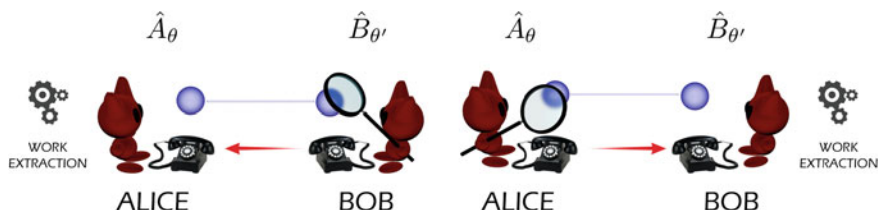


**Fig. 39.5** Schematic representation of the two-qubit work extraction protocol.

as the two Demons look at selected observable, they can gain information about the correlation pertaining to the state they are sharing. In order to rule out the presence of solely classical correlations, they have to measure different observables on each side: if correlation between the outcomes is still present, stronger than classical correlations, i.e. quantum, occur. A protocol can be devised in this quantum scenario by considering two Demons, Alice and Bob, whose goal is to extract the largest amount of work using their two-qubit system. Notice that work is actually extracted from classical memories, and not directly from the quantum systems. These only serve as means to prepare the memories in classically correlated states: the stronger the quantum correlation within the system, the stronger the classical correlation between the memories, thus the larger the extractable work.

The Demons proceed as follows: (i) Alice and Bob share an ensemble of qubit pairs. All of the pairs are prepared in the same state  $\rho$ , and each Demon can only access one of the particles; (ii) the two parties agree on a fixed set of measurements they implement:  $\hat{A}_\theta, \hat{B}_\theta$ , where  $\hat{A}$  ( $\hat{B}$ ) is the set of operator associated to Alice (Bob), and  $\theta$  indicates a parametrization of the observables; (iii) Alice measures part of her qubits, selecting an operator from her set, and communicates the result of her measurement to Bob, who, in turn, evaluates the extractable work using the gathered information, as

$$W_{A \rightarrow B} = k_B T \ln 2 (1 - H(B_\theta | A_\theta)), \quad (39.9)$$

as if he were applying a Szilard's scheme. Here  $T$  is the temperature of an external heat reservoir connected to the system in the sense of a Szilard's engine [20], and not a characteristic parameter of the state; (iv) the protocol has to be performed again, switching Alice's and Bob's roles. The average value of extractable work then becomes:

$$w(A_\theta, B_\theta) = \frac{1}{2}(W_{A \rightarrow B} + W_{B \rightarrow A}) = k_B T \ln 2 [1 - H(A_\theta, B_\theta) + \frac{1}{2}(H(A_\theta) + H(B_\theta))], \quad (39.10)$$

where  $H(\cdot, \cdot)$  is the joint entropy between two variables; (v) the protocol is repeated for every choice of measurements, taking  $\theta$  as the angle position over the great circle of the Bloch sphere. The amount of extractable work, averaged over all the possible choices of the measurements, is computed:

$$W(\rho) = \max_{\phi} \frac{1}{2\pi} \int_0^{2\pi} d\theta w(A_\theta, B_\theta), \quad (39.11)$$

where  $\phi$  is the azimuthal angle; (vi) in order to obtain a suitable bound, one has to search for the maximum value of (39.11) over the set of the separable states:

$$W(\rho) \leq W_0 k_B T \ln 2. \quad (39.12)$$

The maximum work  $W_0$ , in units of  $k_B T \ln 2$ , corresponds to pure separable states, due to the concavity of the Shannon entropy; its value is found numerically as  $W_0 = 0.4427$  [21, 22]. If this bound is violated, the surplus of extractable work

can be due only to the presence of non classical correlations shared between the two parties: Eq. (39.12), therefore, can be used as a witness for entanglement, derived from thermodynamically rooted considerations.

The experimenter has two choices for testing the failure of the bound (39.12). They can either perform Szilard's scheme by putting their memory in contact with a reservoir, or, they can, so to speak, throw away the ladder, after they have climbed up on it [23]: they can retain the considerations on the entropy, hence considering only the measurement statistics of the observables  $\hat{A}_\theta$  and  $\hat{B}_\theta$ ; in this case,  $k_B T \ln 2$  is just a scale factor, and can be set equal to 1. M.A. Ciampini and coworkers [24] used this second approach to evaluate and characterize entanglement in a two-qubit photonic system, relating it to the violation of Bell's inequality.

The qubit is coded by taking the horizontal  $H$  and vertical  $V$  polarizations as the basis; these two components can be easily separated by a polarizing beam splitter (PBS), that directs the photons to either of its two output modes depending on its polarization. Two APDs placed on the modes then signal which outcome has been taken. In order to access the full great circle, an optical element has to be included to rotate the initial polarization, namely a half wave plate (HWP). This introduces a phase delay  $\pi$  between two linear polarizations, due to the birefringence of its material, which corresponds to the geometrical reflection of the polarisation with respect to a characteristic axis of the plate. Setting the axis at an angle  $\vartheta$  corresponds to  $\theta = 4\vartheta$  on the Bloch sphere.

The experimental platform is shown in Fig. 39.6. The entanglement source is the one described in [25], and produces photon pairs in the state  $|\Phi\rangle = \cos \varphi |HH\rangle + \sin \varphi |VV\rangle$ ;  $\varphi$  is a parameter defining the level of entanglement, and can be set experimentally. Since one is interested in describing nonclassical correlations as a resource for work extraction, it is natural to ask the question on how these get degraded when noise is present. In detail, one considers the effect of depolarization: this is defined as the operation that brings the initial state from the pure state  $|\Phi\rangle$  to the mixture  $\rho = \mu |\Phi\rangle\langle\Phi| + (1 - \mu) \mathbb{I}/4$ ; These states become separable for  $\mu \leq 1/3$  [26]. In the experiment, this operation is implemented by means of two liquid crystal plates on the path of one of the photons. By varying the birefringence of the plates via an applied voltage during the acquisition time, an average over different polarization states is carried out, which returns the measurement statistics of the state  $\rho$  [27, 28]. A delicate point is that the bound is strictly valid only in the limit of an infinite number of measurements covering all the great circle: the experimenter needs to verify that the unavoidable discretization is dense enough for the bound to be still meaningful.

Figure 39.7 shows the experimental results of the extractable work  $W$  in (39.11) obtained from measurements acted on the initial state  $|\Phi\rangle$  with  $\cos \varphi = 0.62$ , close to maximal entanglement. For each value of  $\mu$ , the conditional entropies have been evaluated from the photon counting frequencies associated to the setting  $\theta$ , and then averaged over all measurements. The test is able to detect the presence of nonclassical correlations when the purity of the state is high: this criterion is quite demanding. It is then interesting to compare this test with the similarly demanding violation of Bell's inequality:  $S < 2$ , where  $S$  is a quantifier of the level of correlation

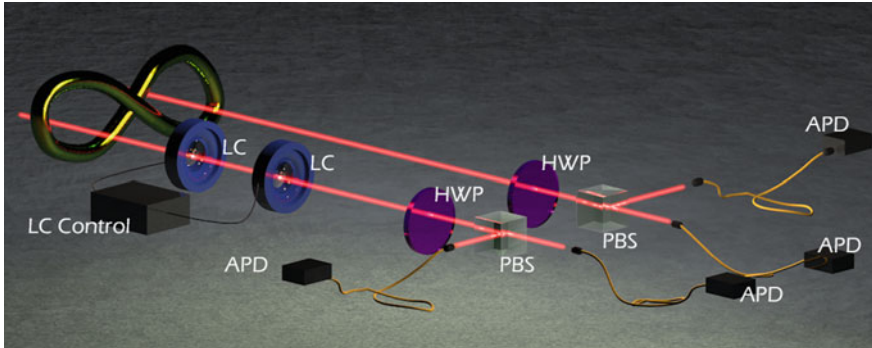


**Fig. 39.6** Essential elements of the setup for measuring the nonclassicality witness based on the extractable work. LC: liquid crystal, APD: avalanche photodiode, HWP: half wave plate, PBS: polarizing beam splitter.

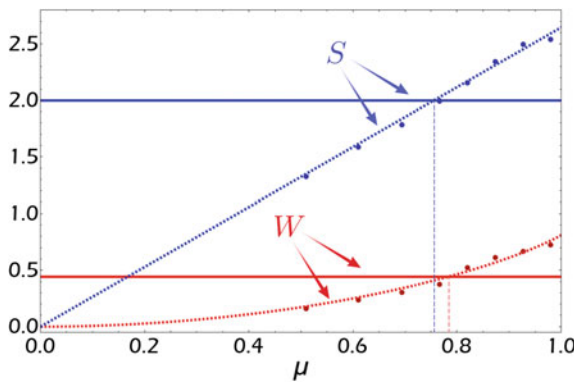


**Fig. 39.7** Results of the two-qubit work extraction protocol, and comparison with Bell's nonlocality. The extractable work  $W$  (red) and Bell's parameter  $S$  (blue) are derived from the counting statistics of the experiment, for different values of the depolarization strength  $\mu$  to which the state is subject. The solid lines are predictions under ideal conditions, while the dotted lines indicate the values of the strength for which the violation of the bound (39.12) ceases. Adapted from [24].

between the two qubits of the state, and can be assessed experimentally [29]. This aims at disproving the possibility of explaining the results of the measurements by means of pre-determined local values, hence it derives from an unrelated question. There exist a region where the violation of the bound (39.12) is lost, but a Bell's inequality is violated. This property holds true for this particular class of states, but it is not general. Indeed, counterexamples of quantum states can be found where the thermal separability criterion is violated, while Bell nonlocality is absent [24]: this demonstrates that considerations on the extractable work do introduce a different nonclassicality criterion, inequivalent to those established so far. Such a criterion can be extended to the case of three-qubit systems [22, 24], and continuous-variable systems [30].

## 39.4 Conclusions

We have illustrated how a connection can be made between Maxwell's Demon and optics, using two examples from recent literature. The first example shows how thermodynamic consideration describe quantitatively the effect of subtracting a photon from a thermal state, by interpreting the results in the light of the information gain from the photon detection. The second concerns how to use a work extraction protocol to infer the presence of nonclassical correlations in a two-qubit system. All things considered, these are actually two instances of physically-motivated manipulation of the information content of the state, where thermodynamics has acted as a guide for reaching interesting conclusions, and valid quantifiers. This extends the usefulness of thermodynamics to a broader class of problems, for which it was not initially intended.

These considerations will also inform future investigations at the intersection of optics and thermodynamics. It is unlikely that photonics could ever be used for direct demonstrations of thermodynamics processes; however, it can keep serving as a platform to study the interplay between information and thermodynamics by means of simulators. This has attracted some interest recently in the context of mixed state discrimination [31], interpreted as a simple thermometry protocol, and simulated by means of linear optics [32, 33]. Further investigations have also looked at entropy production in open quantum systems, supported by photonics simulations [34].

**Acknowledgements** We thank Mauro Paternostro, Paolo Mataloni, Oscar Dahlsten, Ian Walmsley, M.S Kim, Vlatko Vedral, Emanuele Roccia and Valeria Cimini for discussion and encouragement.

## Appendix

In this appendix we revise the demonstrations of the results (39.6), (39.8), and (39.12) which have been stated in this chapter.

**Derivation of the work-information equality** The work-information theorem by Sagawa and Ueda (see Chap. 10), [14] assumes interaction with a single thermal bath, but this is not the case for the photonic Maxwell's demon experiment. However, in [8], a relation similar to that of Sagawa and Ueda is derived to describe this scenario. This work-information relation connects the work extraction with and without an action by the demon. The cases are denoted by the subscripts “0” for the unperturbed state, and “ $f$ ” when including measurement and feedback.

The language adopted to describe the model is that of quantum mechanics for the sake of generality, but it also applies to states and operations with a valid classical counterpart. Three parts can be distinguished: (i) the system  $\mathcal{S}$ , starting in thermal equilibrium with inverse temperature  $\beta$ , representing the working medium (i.e. the two thermal light modes). Its initial and final energy eigenstates are  $|s\rangle$  and  $|S\rangle$  respectively, and its Hamiltonian is  $\hat{H}_S$ . This is the only part on which measurement and feedback operate. The measurement outcomes are indicated by  $m$ , associated to the measurement operator  $\hat{M}_j^{(m)}$ , with an extra index  $j$  due to the possibility

of several measurement operators associated with a single measurement outcome (e.g. APD click). The measurement operators must sum to the identity operator:  $\sum_{m,j} \hat{M}_j^{(m)\dagger} \hat{M}_j^{(m)} = \hat{1}$ . The feed-forward operation is described by  $\hat{U}_m$ . (ii) The work reservoir, which in the experiment is a battery  $\mathcal{B}$  which provides an initial voltage drop  $U_0$  across the capacitor. Its initial and final energy levels are  $|b\rangle$  and  $|B\rangle$  with energies  $E_b$  and  $E_B$ , respectively. Its Hamiltonian is  $\hat{H}_{\mathcal{B}}$ . The extracted work is defined as the energy increase of this system:  $W = E_B - E_b$ . (iii) All the remaining ancillary systems as well as the environment: these are collectively denoted as the rest,  $\mathcal{R}$ . The Hamiltonian is  $\hat{H}_{\mathcal{R}}$ , giving initial and final energy levels  $r$  and  $R$  respectively. The final joint energy of  $\mathcal{S}$  and  $\mathcal{R}$  is  $E_{SR} \equiv E_S + E_R$ . The set of random variables of interest is given by  $v \equiv \{s, b, r, m, SR\}$ .

Owing to decoherence, the total initial state can be assumed to be diagonal in the product basis of the free Hamiltonians: the initial energies of the three systems then represent classical variables. The work reservoir undergoes decoherence in its energy eigenbasis at the end, hence its final energy is well defined. A priori, the sum of the free-Hamiltonian energies of the systems is not necessarily conserved: however, by modelling light-matter interaction with the Jaynes–Cummings interaction Hamiltonian plus decoherence in the energy eigenbasis, energy conservation is ensured. Furthermore, connecting or disconnecting the capacitor from the battery requires in principle no energy. These conditions lead to  $E_s + E_b + E_r = E_S + E_B + E_R$ , which, in turn, implies that  $W = E_s + E_r - E_{SR}$ .

The left hand side of (39.6) is given by

$$\langle e^{\beta W - I} \rangle_f = \sum_v p(s, b, r, m, SR) e^{\beta W - I} = \sum_v p(m, SR|s, b, r) p(s, b, r) e^{\beta W - I}, \quad (39.13)$$

where Bayes' theorem has been used in the second step. The probabilities for the initial system is given by the thermal distribution  $p(s, b, r) = \frac{1}{Z} e^{-\beta E_s} p(b, r)$ , where  $Z$  is the partition function. If the expressions for  $W$  and  $I = \log [p(m|s)] - \log [m]$  are introduced one gets

$$\begin{aligned} \langle e^{\beta W - I} \rangle_{m+f} &= \sum_v p(m, SR|s, b, r) \frac{1}{Z} e^{-\beta E_s} p(b, r) e^{\beta(E_s + E_r - E_{SR})} \frac{p(m)}{p(m|s)} \\ &= \sum_v p(m, SR|s, b, r) \frac{p(m)}{p(m|s)} \frac{1}{Z} p(b, r) e^{\beta(E_r - E_{SR})}. \end{aligned} \quad (39.14)$$

If the sum over the initial states  $s$  is isolated, one gets

$$\begin{aligned} \sum_s p(m, SR|s, b, r) / p(m|s) &= \\ \text{Tr} \left[ |SR\rangle \langle SR| \hat{V} \left( \hat{U}_m \left( \sum_s \frac{\sum_j \hat{M}_j^{(m)} |s\rangle \langle s| \hat{M}_j^{(m)\dagger}}{p(m|s)} \right) \hat{U}_m^\dagger \otimes |b r\rangle \langle b r| \right) \hat{V}^\dagger \right], \end{aligned} \quad (39.15)$$

where the fact that system is closed, hence its evolution is described by the unitary  $\hat{V}$ , has been made explicit. The sum over  $s$  contains all normalized states produced by the demon's measurement, for a sharp energy input. A non-disturbing measurement would leave the state  $|s\rangle\langle s|$  unchanged: in this limit the sum would reduce to the identity. The measurement of the demon does not meet this requirement, however, it can be shown to satisfy the relation [8]:

$$\sum_s \sum_j \frac{\hat{M}_j^{(m)} |s\rangle\langle s| \hat{M}_j^{(m)\dagger}}{p(m|s)} = \hat{1}, \quad (39.16)$$

which can be taken as a generalization of the notion of non-disturbance. Invoking this and  $\hat{U}_m \hat{U}_m^\dagger = \hat{1}$ , one gets

$$\sum_s p(m, SR|s, b, r) / p(m|s) = \text{Tr} \left[ |SR\rangle\langle SR| \hat{V} (\hat{I} \otimes |b r\rangle\langle b r|) \hat{V}^\dagger \right] = \sum_s p_0(SR|s, b, r) \quad (39.17)$$

where  $p_0$  is the probability distribution for the free evolution of the systems, i.e. without implementing measurement and conditional operations. The final result is obtained:

$$\langle e^{\beta W - I} \rangle_f = \sum_v p_0(SR|s, b, r) p(s, b, r) e^{\beta W} = \langle e^{\beta W} \rangle_0. \quad (39.18)$$

**Informational bound on work extraction** The bound (39.6) is hard to relate directly to measurable quantities. For this purpose, one can apply the concave log function to both sides of the equation, and use Jensen's inequality:

$$\beta \langle W \rangle_f - \langle I \rangle < \log \langle e^{\beta W} \rangle_0. \quad (39.19)$$

It is convenient to act with the substitution  $\langle e^{\beta W} \rangle_0 = e^{\beta \langle W \rangle_0} \langle e^{\beta(W - \langle W \rangle_0)} \rangle_0$  to manipulate the expression above:

$$\langle W \rangle_f - \langle W \rangle_0 < \beta^{-1} \langle I \rangle + \beta^{-1} \log \langle e^{\beta(W - \langle W \rangle_0)} \rangle_0. \quad (39.20)$$

In order to develop an intuition on these quantities, one can perform an expansion up to second order in  $\beta$ :

$$\log \langle e^{\beta(W - \langle W \rangle_0)} \rangle_0 = \beta^2 / 2 \text{Var}(W)_0 + \mathcal{O}(\beta^3), \quad (39.21)$$

which is exact for Gaussian work distributions. This leads to the definition:

$$\sigma(\beta, W) \equiv \sqrt{2 \beta^{-2} \log \langle e^{\beta(W - \langle W \rangle_0)} \rangle_0}. \quad (39.22)$$

This coincides with the standard deviation of  $W$  for a Gaussian distribution, and it is an approximation up to first order in  $\beta$  for the general case. Equation (39.20) can then be rewritten as:

$$\langle W \rangle_f - \langle W \rangle_0 < \beta^{-1} \langle I \rangle + \beta [\sigma(\beta, W)]^2 / 2. \quad (39.23)$$

Statistical considerations are drawn by taking into account  $N$  runs of the experiment. Let  $U_k$  denote the voltage created across the capacitor  $C$  in the  $k^{\text{th}}$  iteration: work extraction relies on storing the energy accumulated in the capacitor in a work reservoir. The capacitor is connected to a battery with voltage  $U_0$ : the charge  $C(U_k - U_0)$  is transferred to the battery, increasing its energy by  $CU_0(U_k - U_0)$ . The voltage  $U_0$  can be held as constant, since  $U_k$  can be made arbitrarily small. The capacitor then relaxes to 0 voltage. Over the  $N$  cycles the work extracted is  $W^{(N)} = CU_0 \sum_k^N (U_k - U_0)$ , while the mutual information gain is  $I^{(N)} \equiv \sum_k^N I_k$ . Consequently, the sum of voltages across the capacitor over  $N$  runs is  $U^{(N)} \equiv \sum_k^N U_k$ . The energy scale with respect to the temperature is indicated by the parameter  $\xi \equiv \beta C U_0$ . If these expressions are inserted in (39.6), Jensen's inequality is applied as above, one obtains:

$$\langle U^{(N)} \rangle_f - \langle U^{(N)} \rangle_0 < \xi^{-1} \langle I^{(N)} \rangle + \xi [\sigma(\xi, U^{(N)})]^2 / 2. \quad (39.24)$$

The voltages  $U_k$  are independently and identically distributed, implying:

$$\langle e^{x U^{(N)}} \rangle_0 = \langle e^{x U} \rangle_0^N, \quad (39.25)$$

a general property of the moment generating function. Equation (39.22) results in the fact that  $[\sigma(\xi, U^{(N)})]^2 = N[\sigma(\xi, U)]^2$ . Furthermore, the properties hold:  $\langle U^{(N)} \rangle = N \langle U \rangle$  and  $\langle I^{(N)} \rangle = N \langle I \rangle$ . Equation (39.24) then becomes

$$\langle U \rangle_f - \langle U \rangle_0 < \frac{1}{\xi} \langle I \rangle + \xi [\sigma(\xi, U)]^2 / 2. \quad (39.26)$$

Since this holds for arbitrary  $U_0$ , minimization of the right-hand term of the inequality can be performed with respect to  $\xi$ , delivering the tightest bound:

$$\langle U \rangle_f - \langle U \rangle_0 < \min_{\xi} \left\{ \frac{1}{\xi} \langle I \rangle + \xi [\sigma(\xi, U)]^2 / 2 \right\}. \quad (39.27)$$

For a Gaussian distribution of  $U$ , one has that  $[\sigma(\xi, U)] = \sqrt{\text{Var}(U_0)}$ , thus  $\min_{\xi} \left\{ \frac{1}{\xi} \langle I \rangle + \xi [\sigma(\xi, U)]^2 / 2 \right\} = \sqrt{2I} \sqrt{\text{Var}(U_0)}$ . This yields the bound

$$\frac{|\langle U \rangle_f - \langle U \rangle_0|}{\sqrt{\text{Var}(U_0)}} < \sqrt{2 \langle I \rangle} \quad (39.28)$$

and, using the definition of work in the setup

$$\frac{|\langle W \rangle_f - \langle W \rangle_0|}{\sqrt{\text{Var}(W)_0}} < \sqrt{2\langle I \rangle}. \quad (39.29)$$

The bound given by (39.28) is a stronger version of in (39.27), which is valid for small values of  $\langle I \rangle$ .

**Bounding the extractable work by separable quantum state** We start by considering a generic separable quantum state in the form  $\rho = \sum_i p_i \rho_i^A \otimes \rho_i^B$ , where  $\rho_i^A$  and  $\rho_i^B$  are a set of local state at Alice's and Bob's locations, jointly showing with probability  $p_i$ . When measuring the observables  $\hat{A}$  and  $\hat{B}$ , one can introduce two operators  $\hat{A}^1$  and  $\hat{A}^0$  such that the probabilities for Alice to get the outcome  $j$  are given by  $p_j^A = \sum_i p_i \text{Tr}[\hat{A}_j \rho_i^A]$ , and similarly for Bob's side. This allows to express the conditional entropy in terms of the conditional probabilities  $p(B^0|A^j)$  as  $H(B|A) = \sum_j p_j^A H(p(B^0|A^j))$ . Bayes' theorem can be invoked to find the conditional probability as:

$$\begin{aligned} p(B^0|A^j) &= \frac{p(A^j, B^0)}{p_j^A} = \frac{\sum_i p_i \text{Tr}[A^j \rho_i^A] \text{Tr}[B^0 \rho_i^B]}{p_j^A} \\ &= \frac{\sum_i p_i p_{j,i}^A p_{0,i}^B}{p_j^A}, \end{aligned} \quad (39.30)$$

where the shorthand notation has been introduced  $p_{j,i}^A = \text{Tr}[A^j \rho_i^A]$  for Alice, and similarly for Bob. This leads to

$$\begin{aligned} H(B|A) &= \sum_j p_j^A H\left(\frac{\sum_i p_i p_{j,i}^A p_{0,i}^B}{p_j^A}\right) \\ &\geq \sum_j \sum_i p_i p_{j,i}^A H(p_{0,i}^B) = \sum_i p_i H(p_{0,i}^B), \end{aligned} \quad (39.31)$$

due to the concavity of Shannon entropy. The inequality is saturated when a single component is present:  $\rho = \rho_0^A \otimes \rho_0^B$ , and  $H(p_{0,0}^B)$  is minimal for a pure state. QED.

## References

1. K. Maruyama, F. Nori, V. Vedral, Colloquium: the physics of Maxwell's demon and information. Rev. Mod. Phys., American Physical Society **81**(1), 1–23 (2009). <https://doi.org/10.1103/RevModPhys.81.1>
2. J.C. Maxwell, *Theory of Heat* (D. Appleton and Co, New York, 1872)
3. H. Leff, A.F. Rex, *Maxwell's demon 2, entropy, classical and quantum information computing*, CRC Press, 2002). <https://doi.org/10.1201/9781420033991>
4. J.C. Maxwell, *Letter to P.G. Tait* (Cambridge University Press, London, 1911)

5. R. Landauer, Irreversibility and heat generation in the computing process. *IBM J. Res. Dev.* **5**(3), 183–191 (1961). <https://doi.org/10.1147/rd.53.0183>
6. R. Landauer, Information is physical. *Phys. Today* **44**(5), 23 (1991). <https://doi.org/10.1063/1.881299>
7. M.A. Nielsen, I.L. Chuang, *Quantum Computation and Quantum Information* (Cambridge University Press, New York, 2000)
8. M.D. Vidrighin, O. Dahlsten, M. Barbieri, M.S. Kim, V. Vedral, I.A. Walmsley, Photonic Maxwell’s demon. *Phys. Rev. Lett.*, American Physical Society **116**(5), 050401 (2016). <https://doi.org/10.1103/PhysRevLett.116.050401>
9. F.T. Arecchi, Measurement of the statistical distribution of Gaussian and laser sources. *Phys. Rev. Lett.*, American Physical Society **15**(24), 912–916 (1965). <https://doi.org/10.1103/PhysRevLett.15.912>
10. A. Zavatta, V. Parigi, M.S. Kim, M. Bellini, Subtracting photons from arbitrary light fields: experimental test of coherent state invariance by single-photon annihilation. *N. J. Phys.* **10**(12), 123006 (2008). <https://doi.org/10.1088/1367-2630/10/12/123006>
11. V. Parigi, A. Zavatta, M. Bellini, Implementation of single-photon creation and annihilation operators: experimental issues in their application to thermal states of light. *J. Phys. B : Atomic, Molecular and Optical Phys.* **42**(11), 114005 (2009). <https://doi.org/10.1088/0953-4075/42/11/114005>
12. M. Ueda, N. Imoto, T. Ogawa, Quantum theory for continuous photodetection process. *Phys. Rev. A*, American Physical Society **41**(7), 3891–3904 (1990). <https://doi.org/10.1103/PhysRevA.41.3891>
13. M.D. Vidrighin, Quantum optical measurements for practical estimation and information thermodynamics, Ph.D. thesis, Imperial College London (2017)
14. T. Sagawa, M. Ueda, Generalized Jarzynski equality under nonequilibrium feedback control. *Phys. Rev. Lett.*, American Physical Society **104**(9), 090602 (2010). <https://doi.org/10.1103/PhysRevLett.104.090602>
15. N. Brunner, N. Linden, S. Popescu, P. Skrzypczyk, Virtual qubits, virtual temperatures, and the foundations of thermodynamics. *Phys. Rev. E*, American Physical Society **85**(5), 14 051117 (2012). <https://doi.org/10.1103/PhysRevE.85.051117>
16. V. Vedral, An information-theoretic equality implying the Jarzynski relation. *J. Phys. A: Mathematical and Theoretical* **45**(27), 272001 (2012). <https://doi.org/10.1088/1751-8113/45/27/272001>
17. M.R. Vanner, M. Aspelmeyer, M.S. Kim, Quantum state orthogonalization and a toolset for quantum optomechanical phonon control. *Phys. Rev. Lett.*, American Physical Society **110**(1), 010504 (2013). <https://doi.org/10.1103/PhysRevLett.110.010504>
18. R. McConnell, H. Zhang, J. Hu, S. Ćuk, V. Vuletić, Entanglement with negative Wigner function of almost 3,000 atoms heralded by one photon. *Nature*, Nature Publishing Group, a division of Macmillan Publishers Limited **519**, 439442 (2015). <https://doi.org/10.1038/nature14293>
19. A. Shu, J. Dai, V. Scarani, Power of an optical Maxwell’s demon in the presence of photon-number correlations. *Phys. Rev. A* **95**(2), 022123 (2017). <https://doi.org/10.1103/PhysRevA.95.022123>
20. L. Szilard, On the decrease of entropy in a thermodynamic system by the intervention of intelligent beings. *Behav. Sci.* **9**(4), 301–310 (1929). <https://doi.org/10.1002/bs.3830090402>
21. K. Maruyama, F. Morikoshi, V. Vedral, Thermodynamical detection of entanglement by Maxwell’s Demons. *Phys. Rev. A*, American Physical Society **71**(1), 012108 (2005). <https://doi.org/10.1103/PhysRevA.71.012108>
22. V. Viguié, K. Maruyama, V. Vedral, Work extraction from tripartite entanglement. *N. J. Phys.* **7**(1), 195 (2005). <https://doi.org/10.1088/1367-2630/7/1/195>
23. L. Wittgenstein, *Tractatus Logico-Philosophicus*, Harcourt, Brace and Co. proposition 6.54 (1922)
24. M.A. Ciampini, L. Mancino, A. Orieux, C. Vigliar, P. Mataloni, M. Paternostro, M. Barbieri, Experimental extractable work-based multipartite separability criteria. *npj Quantum Inf.* **3**(1), 10 (2017). <https://doi.org/10.1038/s41534-017-0011-9>

25. C. Cinelli, G. Di Nepi, F. De Martini, M. Barbieri, P. Mataloni, Parametric source of two-photon states with a tunable degree of entanglement and mixing: experimental preparation of Werner states and maximally entangled mixed states. *Phys. Rev. A, American Physical Society* **70**(2), 022321 (2004). <https://doi.org/10.1103/PhysRevA.70.022321>
26. R.F. Werner, Quantum states with Einstein–Podolsky–Rosen correlations admitting a hidden-variable model. *Phys. Rev. A, American Physical Society* **40**(8), 4277–4281 (1989). <https://doi.org/10.1103/PhysRevA.40.4277>
27. A. Chiuri, V. Rosati, G. Vallone, S. Padua, H. Imai, S. Giacomini, C. Macchiavello, P. Mataloni, Experimental realization of optimal noise estimation for a general Pauli channel. *Phys. Rev. Lett., American Physical Society* **107**(25), 253602 (2011). <https://doi.org/10.1103/PhysRevLett.107.253602>
28. A. Chiuri, S. Giacomini, C. Macchiavello, P. Mataloni, Experimental achievement of the entanglement-assisted capacity for the depolarizing channel. *Phys. Rev. A, American Physical Society* **87**(2), 022333 (2013). <https://doi.org/10.1103/PhysRevA.87.022333>
29. J.F. Clauser, M.A. Horne, A. Shimony, R.A. Holt, Proposed experiment to test local hidden-variable theories. *Phys. Rev. Lett.* **23**(15), 880–884 (1969). <https://doi.org/10.1103/PhysRevLett.23.880>
30. M. Brunelli, M.G. Genoni, M. Barbieri, M. Paternostro, Detecting Gaussian entanglement via extractable work. *Phys. Rev. A, American Physical Society* **96**(6), 062311 (2017). <https://doi.org/10.1103/PhysRevA.96.062311>
31. S. Jevtic, D. Newman, T. Rudolph, T.M. Stace, Single-qubit thermometry. *Phys. Rev. A* **91**(1), 012331 (2015). <https://doi.org/10.1103/PhysRevA.91.012331>
32. W.K. Tham, H. Ferretti, A.V. Sadashivan, A.M. Steinberg, Simulating and optimising quantum thermometry using single photons. *Sci. Rep.* **6**, 38822 (2016). <https://doi.org/10.1038/srep38822>
33. L. Mancino, M. Sbroscia, I. Gianani, E. Roccia, M. Barbieri, Quantum simulation of single-qubit thermometry using linear optics. *Phys. Rev. Lett., American Physical Society* **118**(13), 130502 (2017). <https://doi.org/10.1103/PhysRevLett.118.130502>
34. L. Mancino, et al., Geometrical bounds on irreversibility in open quantum systems, *Phys. Rev. Lett.* **121**(16) 160602 (2018). <https://doi.org/10.1103/PhysRevLett.121.160602>

# Chapter 40

## Maxwell’s Demon in Superconducting Circuits



Nathanaël Cottet and Benjamin Huard

### 40.1 Introduction

The past decades have seen the development of superconducting circuits based on Josephson junctions as one of the most promising platforms for quantum information processing [1]. Owing to their high level of control in both their design and their manipulation, they naturally constitute a convenient testbed of fundamental properties of quantum mechanics. Superconducting circuits reach strong coupling with microwave light, allowing quantum-limited amplification [2], strong Quantum Non Demolition measurement [3], weak measurement [4, 5], quantum feedback [6], and the observation of quantum trajectories [7]. From a quantum thermodynamics point of view, this high level of control gives full access to the dynamics of energy and entropy flows between the different parts of the experimental system. Up to now, three experimental realizations of a Maxwell’s demon have been achieved using superconducting circuits in the quantum regime [8–10]. They all consist of a 3D-transmon qubit dispersively coupled to a 3D cavity waveguide measured at cryogenic temperatures around 20 mK [11]. The characteristic frequencies of such systems are in the microwave range.

Szilard reformulated the original Maxwell’s demon gedanken experiment in the case of a single molecule in a two sided box [12, 13]. In general, one can cast the experiment in terms of five components with different roles: system, demon, two thermal baths and battery. At the beginning of each thermodynamic cycle, the system is thermalized to its thermal bath. The demon then acquires information on

---

N. Cottet · B. Huard (✉)

Laboratoire Pierre Aigrain, École normale supérieure, PSL Research University,  
CNRS, Université Pierre et Marie Curie, Sorbonne Université, Université Paris Diderot,  
Sorbonne Paris-Cité, 24 rue Lhomond, 75231 Paris Cedex 05, France  
e-mail: benjamin.huard@ens-lyon.fr

B. Huard

Université Lyon, ENS de Lyon, Université Claude Bernard Lyon 1,  
CNRS, Laboratoire de Physique, 69342 Lyon, France

the system to extract work, which can then charge a battery. The apparent possibility to extract work out of a single heat bath vanishes when considering the need to reset the demon state in order to close the thermodynamic cycle [14, 15]. One way to reset the demon state consists in thermalizing it with a hidden thermal bath at the end of the cycle, or by actively resetting its state at the expense of external work. There are plenty of ways to transfer information, extract work and thermalize the system. From an experimental perspective, the manner work and entropy flows are measured or inferred is also crucial since the measurement of a quantum system is inherently invasive. This chapter will therefore focus on the existing experimental realizations that illustrate what superconducting circuits can bring to quantum thermodynamics. The chapter is organized as follows. We first introduce the reader to the field of circuit Quantum Electro-Dynamics. Then we present the spirit of the three existing experiments before describing the particular experimental realizations in details.

### 40.1.1 Introduction to Circuit-QED

In this section, we provide a brief introduction to circuit-QED. The interested reader is advised to look into a recent review on the subject [16, 17].

A superconducting qubit that is coupled to a cavity can reach two main regimes of interest. First, close to resonance, they can swap excitations, which results in vacuum Rabi splitting. In this chapter, we focus on the opposite regime, where the cavity-qubit detuning is much larger than their coupling rate. This so called dispersive regime can be described by the Hamiltonian [18]

$$H_{\text{disp}} = \frac{\hbar\omega_q}{2}\sigma_z + \hbar\omega_c a^\dagger a - \hbar\frac{\chi}{2}a^\dagger a\sigma_z, \quad (40.1)$$

where  $a$  is the annihilation operator of a photon in the cavity,  $\omega_q$  (respectively  $\omega_c$ ) the frequency of the qubit (resp. cavity), and  $\sigma_z$  the Pauli matrix of the qubit along  $z$ . The two first terms represent the Hamiltonians of the qubit and cavity, while the last term describes the coupling between them. Compared to the case of the ground state of both qubit and cavity, the interaction induces a frequency shift  $-\chi$  of the cavity when the qubit is excited while the qubit frequency is shifted by  $-N\chi$  when the cavity hosts  $N$  photons. Thanks to this coupling term it is possible to entangle the qubit and the cavity and hence to transfer information between the two. Moreover, when the cavity is coupled to a transmission line, this information can be either dissipated in the environment or collected into a measurement apparatus.

The state of the qubit and cavity is controlled using microwave drives on or near resonance with either the qubit or the cavity. Let us consider first a drive near qubit frequency at  $\omega_q - \delta$ . Without loss of generality one can set the phase of the drive so that it is along the  $y$ -axis of the Bloch sphere. In the rotating frame of the drive and only keeping the slowly rotating terms (rotating wave approximation) the Hamiltonian becomes

$$H_{\text{driven}}^q = \frac{\hbar}{2}(\delta - \chi a^\dagger a)\sigma_z + \Omega_q \sigma_y, \quad (40.2)$$

where  $\Omega_q$  is proportional to the amplitude of the drive. This Hamiltonian induces Rabi oscillations of the qubit around an axis, which depends on the number of photons in the cavity. Energetically the qubit undergoes cycles of absorption where work is absorbed from the drive and stimulated emission where work is emitted in the drive. Similarly a drive near cavity frequency at  $\omega_c - \Delta$  gives the following Hamiltonian

$$H_{\text{driven}}^c = \hbar \left( \Delta - \frac{\chi}{2} \sigma_z \right) a^\dagger a + \Omega_c (a + a^\dagger), \quad (40.3)$$

where the complex drive amplitude, proportional to  $\Omega_c$ , is here chosen to be positive. The result is a displacement of the cavity field that depends on the state of the qubit. Assuming the cavity is initially in vacuum it results in the preparation of a coherent state  $|\alpha_g\rangle$  (respectively  $|\alpha_e\rangle$ ) in the cavity when the qubit is in the ground (respectively excited) state. Note that two coherent states are never fully orthogonal ( $\langle \alpha_e | \alpha_g \rangle \neq 0$ ) so that they cannot perfectly encode the qubit state.

All the processes described so far are unitary. In the Zurek description of a quantum measurement [19], driving the cavity corresponds to a *premeasurement* of the qubit state. The information stored in the cavity eventually escapes towards the transmission line, and can therefore be amplified and detected by classical detectors hence terminating the measurement process of the qubit's state. In the dispersive regime, the observable  $\sigma_z$  commutes with the qubit-cavity Hamiltonian (40.1), ensuring that the measurement is Quantum Non Demolition.

### 40.1.2 Description of the Existing Experiments

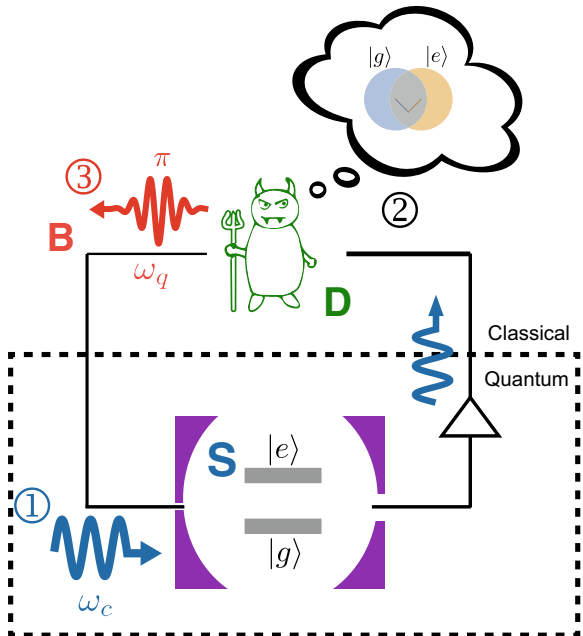
All three experimental realizations presented in this chapter share the common feature of using the qubit as the system. Its state is measured by the demon (of different nature depending on the experiments) thanks to the coupling term of the dispersive Hamiltonian (40.1). Work is extracted through a pulse on resonance with the qubit that induces a rotation of the qubit. The pulse acts as the battery<sup>1</sup> and is powered-up when the qubit is flipped from a high-energy state to a lower-energy one.

Masuyama et al. [8] base their Maxwell's demon on a measurement-based feedback scheme. After initialization, the qubit is measured and feedback control is used conditionally on the result of the measurement in the following way: whenever the qubit is measured in  $|e\rangle$ , a  $\pi$ -pulse flips it back to the ground state and transfers one

---

<sup>1</sup>Strictly speaking, the battery is the propagating electromagnetic mode that contains the pulse. It can both store and use the energy it contains, hence qualifying as a battery. Indeed, it can store the excitation of a qubit or of a classical cavity field as described in the text. Moreover, if it interacts with an other distant ancillary qubit or cavity in its ground state, it can provide work to excite it. In the text, the qubit extracted work is used to amplify the pulse in the battery.

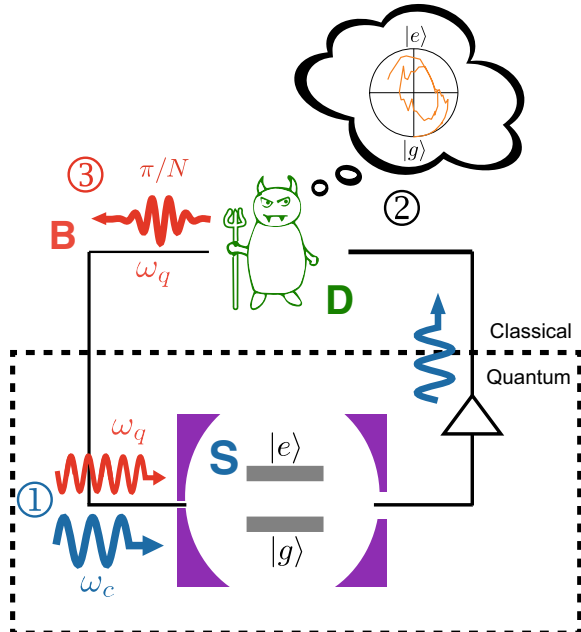
**Fig. 40.1** Demon whose action is based on a single measurement. ① After qubit initialization, a pulse at cavity frequency is transmitted through the cavity so that its phase encodes the state of the qubit. ② This information is recorded by a classical measurement apparatus acting as the demon. ③ A feedback  $\pi$ -pulse is applied conditioned on the measurement outcome in order to extract work.



quantum of work to the battery. In contrast when the qubit is measured in  $|g\rangle$  no pulse is applied. The operation time of the sequence is much faster than the thermalization time of the qubit with the rest of the environment so that the whole process can be considered adiabatic. In this experiment the demon is therefore the classical measurement apparatus and information is acquired and stored into a classical memory (Fig. 40.1). An interesting twist is added by the possibility to use a weak measurement for the feedback control input. Masuyama et al. are then able to demonstrate the role of mutual information in the second law for quantum systems.

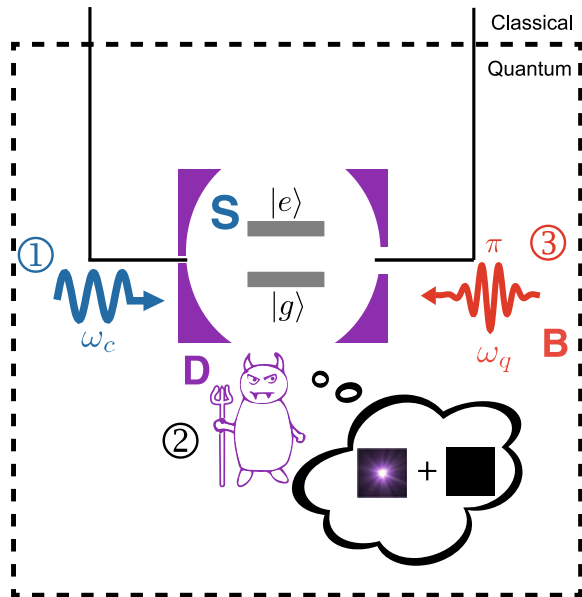
Naghiloo et al. [9] also present a Maxwell's demon based on a classical detector. In their case the demon tracks the quantum trajectory of the qubit thanks to time-resolved measurement records. In this case, after initialization, the qubit is driven on resonance while a weak measurement tone is applied at cavity frequency. The qubit state is then reconstructed using the measurement records based on the stochastic master equation (see Appendix). This classical detector acts as a demon that uses its knowledge on both the qubit excitation and coherences to apply an optimal feedback pulse that flips the qubit to the ground state hence extracting work out of the qubit (Fig. 40.2). Importantly in this experiment, the qubit exchanges work with the qubit drive during the measurement process. Using the quantum trajectory, one can determine how much work is exchanged at each time step. Interestingly, this amount of work cannot be controlled and present a stochastic behavior (see Chap. 15). This experiment confirms the crucial role of mutual information in the second law for quantum systems.

**Fig. 40.2** Trajectory based demon. ① After initialization, the qubit is driven at  $\omega_q$  while a weak tone at  $\omega_c$  measures its state. ② The information is recorded in a time-resolved way, allowing the demon to reconstruct the quantum trajectory of the qubit in the  $XZ$  plane of the Bloch sphere. ③ Based on this information, an optimized feedback pulse is applied to flip down the qubit to the ground state and extract work.



In the previous experiments, the demon is a classical black box. The resolution of the paradox of the Maxwell demon involves the acknowledgment of the demon's information as a physical object. In order to analyze the inner dynamics of the demon and even probe its quantum coherence, Cottet, Jezouin et al. [10] demonstrated an autonomous Maxwell's demon in the quantum regime (classical autonomous demons using single electron transistors are discussed in Chap. 37). After initialization in a thermal or a superposed state, a pulse at  $\omega_c$  is applied on the cavity and displaces it conditioned on the qubit being in the ground state. It is followed by a  $\pi$ -pulse at  $\omega_q$  that flips the qubit conditioned to the cavity hosting 0 photon. This sequence is realized in a time smaller than the lifetimes of both the qubit and cavity so that the information stored in the cavity does not have the time to escape into the transmission line. Therefore the demon is here the cavity whose quantum state could be measured in a quantum state that exhibits quantum coherences (Fig. 40.3). Another particularity of this experiment is the direct measurement of the work extracted into the battery. The other experiments use a Two Point Measurement protocol, which is described below.

**Fig. 40.3** Autonomous quantum demon. ① After initialization the cavity is populated conditioned to the qubit being in  $|g\rangle$  using a drive at  $\omega_c$ . ② The cavity state reflects the qubit state, hence acting as the demon and possibly exhibiting quantum coherences. ③ A  $\pi$ -pulse at  $\omega_q$  extracts work conditioned to the cavity being in the vacuum state. Importantly, the information never leaves the quantum world during the whole process.



## 40.2 Quantum-Classical Demon

### 40.2.1 Inferring Work and Tuning the Measurement Strength

Before detailing how fluctuation relations can be investigated using superconducting circuit based quantum-classical demons, we discuss two key tools for the realization of these experiments.

#### 40.2.1.1 Inferring Work from Two Point Measurement

Acquiring information on a quantum system is known to be invasive: if the quantum system is not in an eigenstate of the measured observable, the outcome of the measurement is non deterministic and the system state changes following measurement. Work is not an observable [20]. Therefore quantifying the work done on a quantum system is subject to interpretation. However, there is one case that does not suffer from these inconsistencies. It is the work done on a system that starts from an eigenstate of the Hamiltonian, evolves adiabatically and ends up in an eigenstate of the Hamiltonian. In the Two-Point Measurement (TPM) scheme [21, 22], the adiabatic evolution takes place between two projective measurements of the Hamiltonian at times  $t_i$  and  $t_f$  leading to measurement outcomes indicating the energies  $E(t_i)$  and  $E(t_f)$  so that the extracted work (positive when the system provides work) is defined by the change of energy  $W = E(t_i) - E(t_f)$ . Note that lifting the adiabatic

assumption leads to an additional contribution in the change of energy coming from the exchange heat. This TPM scheme allows to recover thermodynamics fluctuation relations such as the Jarzynski equality in the case of classical information acquired on a quantum system.

The two experiments of Masuyama et al. [8] and Naghiloo et al. [9] both use a TPM scheme to infer the work exchanged between the qubit and the battery. Note that a strong assumption of this TPM scheme is the adiabatic nature of the evolution between projective measurements. For the above experiments, it requires that the operation time (about 0.01–1  $\mu\text{s}$ ) is much smaller than the thermalization time of the qubit, which is given by the qubit lifetime  $T_1$  (about 10–100  $\mu\text{s}$ ).

#### 40.2.1.2 Weak and Strong Measurements

We have discussed in the introduction on circuit-QED the way dispersive measurement operates. A big asset of circuit-QED for implementing a Maxwell demon is the possibility to arbitrarily tune the amount of information that the demon extracts from the qubit. This skill arises from the fact that the two cavity coherent states  $|\alpha_{g,e}\rangle$  corresponding to the qubit in  $|g\rangle$  or  $|e\rangle$  are not orthogonal. More precisely, their overlap is  $|\langle\alpha_e|\alpha_g\rangle| = e^{-|\alpha_e-\alpha_g|^2/2}$ . When the cavity is coupled to a transmission line at a rate  $\kappa$ , the measurement rate [23], i.e. the rate at which information about the qubit state leaks towards the transmission line, is given by  $\Gamma_m = \kappa|\alpha_e - \alpha_g|^2/2 \propto \Omega_c^2$  where  $\Omega_c$  is a drive strength that appears in Eq. (40.3) and is proportional to the drive amplitude. The measurement rate does not necessarily quantifies how much information is effectively acquired by the measurement apparatus at the other end of the transmission line. It just sets an upper bound by describing the case of a perfect measurement, and thus corresponds to the measurement induced dephasing rate. Taking into account the finite efficiency  $0 \leq \eta \leq 1$  with which information is transmitted between the transmission line input and the final detector, one can more generally write the effective rate at which information about the qubit is acquired by the detector  $\Gamma_m^{\text{eff}} = \eta\Gamma_m$ . For a given measurement duration  $t_m$ , the measurement is said to be weak (respectively projective) when  $\Gamma_m t_m < 1$  (resp.  $\Gamma_m t_m \gg 1$ ). The strength of the measurement can be experimentally tuned by choosing the drive strength  $\Omega_c$  (see Fig. 40.4).

#### 40.2.2 Probing Quantum Fluctuation Theorems with Weak Measurements

##### 40.2.2.1 Jarzynski for a Discrete Weak Quantum Measurement

One of the main interest of the experiment of Masuyama et al. is that it puts to the test [8] the Sagawa-Ueda quantum generalization of the Jarzynski equality where a so-called Quantum-to-Classical mutual information plays a key role (see Ref. [24]

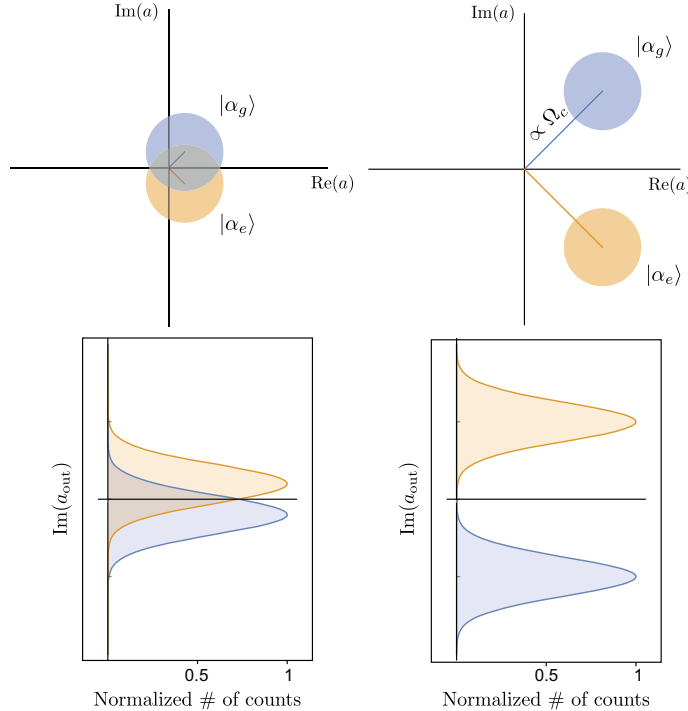


**Fig. 40.4** Weak to strong measurement of a qubit. (top) When driven at resonance, the cavity hosts a coherent state  $|\alpha_{g,e}\rangle$  that depends on the qubit state. Each disk represents the Gaussian distribution of the Wigner function of states  $|\alpha_{g,e}\rangle$  in the phase space of the cavity mode quadratures. The disk radius corresponds to the vacuum fluctuations. (bottom) Histograms of the measurement outcomes for a detector that is sensitive to the quadrature encoding the qubit state in the cavity output field. When the drive amplitude  $\Omega_c$  is small enough (left) the two states strongly overlap and the histograms are not well separated leading to a weak measurement. At larger  $\Omega_c$  (right) the states and histograms are well separated and the measurement is strong.

and Chap. 10). Varying the measurement strength at which the demon extracts information about the system allows them to tune this mutual information and provides a relevant test of the equality. The demon first performs a weak or strong measurement that leads to a measurement outcome  $k$ . A projective measurement is then performed, leading to some outcome  $y$ , right afterwards so that the system gets either to the ground or to the excited state. Based on the outcome  $k$  alone, the demon then sends a feedback pulse to the qubit in order to try to extract a quantum of work out of it. Following the work of Funo, Watanabe and Ueda (see Ref. [24] and Chap. 10) the quantity of information acquired by the demon during the measurement of outcome  $k$  is given by the stochastic Quantum-to-Classical mutual information

$$I_{\text{QC}}(i, k, y) = \ln p(y|k) - \ln p(i), \quad (40.4)$$

where  $p(i)$  is the probability to get the outcome  $i$  during the first projective measurement of the TPM that surrounds the whole pulse sequence,  $p(y|k)$  is the probability to measure the outcome  $y$  during the projective measurement conditioned on  $k$ .  $I_{\text{Sh}}(i) = -\ln p(i)$  is the stochastic Shannon entropy of the initially thermalized qubit. In the limit where the first measurement is strong and in the absence of decay of the qubit the two outcomes  $k$  and  $y$  match, therefore  $p(y|k) = \delta_{y,k}$  and the stochastic mutual information  $I_{\text{QC}}(i, k, y)$  is simply given by the stochastic Shannon entropy corresponding to the first measurement of the TPM.

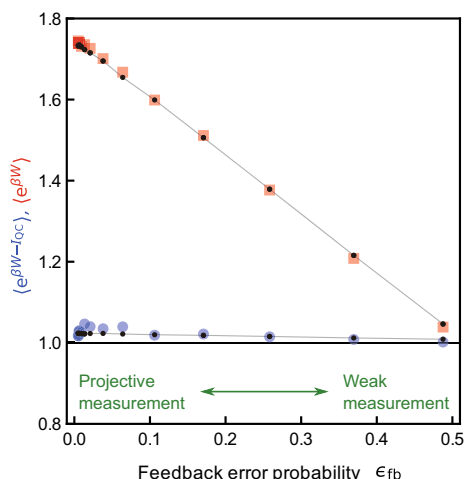
In presence of feedback and when the initial and final Hamiltonian are identical, the work  $W$  and the information  $I_{\text{QC}}$  extracted from the system by the demon verify the following generalized Jarzynski equality (see Chap. 10)

$$\langle e^{\beta W - I_{\text{QC}}} \rangle = 1 - \lambda_{\text{fb}} \quad (40.5)$$

with  $\beta = 1/k_B T$  the inverse temperature. This equality takes into account the absolute irreversibility induced by the measurement operation of the demon. It is done via the probability  $\lambda_{\text{fb}}$  of irreversible events owing to the measurement. In the case of weak measurements irreversible events disappear because any forward events become possible, as unlikely as they can be. As a result  $\lambda_{\text{fb}} = 0$  for weak measurements. The usual Jarzynski equality  $\langle e^{\beta W} \rangle = 1$  can thus be simply generalized to the case of non zero stochastic mutual information by replacing  $W$  by  $W - k_B T I_{\text{QC}}$  in the equality.

Figure 40.5 shows experimental data of  $\langle e^{\beta W - I_{\text{QC}}} \rangle$  and  $\langle e^{\beta W} \rangle$  as a function of the feedback error probability  $\epsilon_{\text{fb}}$  for a qubit initialized with approximatively 10% of excited state (from [8]). It is defined as the probability that the projective measurement outcome  $y$  does not match the weak measurement outcome  $k$ :  $\epsilon_{\text{fb}} = p(y = e|k = g) + p(y = g|k = e)$ . For strong measurement, the feedback process is almost error

**Fig. 40.5** (Adapted from Ref. [8]) Jarzynski equality is verified for any measurement strength only when the mutual information  $I_{\text{QC}}$  is taken into account. Here the blue dots correspond to the measured  $\langle e^{\beta W - I_{\text{QC}}} \rangle$  as a function of feedback error probability while red squares correspond to  $\langle e^{\beta W} \rangle$ .



free ( $\epsilon_{fb} \ll 1$ ), while when the measurement gets weaker and weaker, the error goes towards  $\epsilon_{fb} = 50\%$ . The latter value corresponds to the limit where the demon acts completely erratically because of its lack of information. The experiment shows that  $\langle e^{\beta W - I_{QC}} \rangle$  (blue dots) is almost equal to 1 no matter the strength of the measurement, while the uncorrected Jarzynski expression  $\langle e^{\beta W} \rangle$  (red squares) only reaches 1 when the feedback reaches its highest error probability. This effect can be simply understood by the fact that a 50% error probability means that no information is acquired by the demon and therefore  $I_{QC} = 0$ . In contrast, the situation when the measurement is so strong that it can be considered as projective might look surprising. According to Eq. (40.5), when the feedback measurement is projective, one should expect irreversible events to appear, yielding  $\lambda_{fb} > 0$  and implying  $\langle e^{\beta W - I_{QC}} \rangle < 1$ . Yet experimental data suggest otherwise, showing an average above one. The reason is to be found in qubit decay. First, as highlighted previously, the work has been assimilated to the energy change of the qubit in the TPM, resulting in a small overestimation of the work extracted from the qubit when it decays. Second, the qubit decay between the first TPM measurement and the two measurements  $k$  and  $y$  does not restrict forward processes and  $\lambda_{fb}$  stays null even in the strong measurement limit. Equivalently the qubit decay means that  $p(y|k)$  is never strictly equal to  $\delta_{y,k}$ , and hence  $I_{QC}$  does not equal  $I_{Sh}$  even in the strong measurement limit.

#### 40.2.2.2 Jarzynski for Continuous Quantum Measurements

In the previous part, the weak measurement provides a single measurement outcome  $k$  on which the feedback is conditioned. In all generality, the measurement record can be a continuous signal  $\{V(t)\}_{0 < t < t_m}$  that lasts for some total duration  $t_m$ . Then how can the demon optimally extract work from the system and how to quantify the knowledge of the demon about the system? This is what the experiment of Naghiloo et al. [9] addresses. It is in fact possible to infer the qubit state  $\rho_t$  at any time conditioned on the continuous measurement record (see Appendix and Ref. [25]). This is called a quantum trajectory. Importantly, the conditional density matrix  $\rho_{t_m}$  at the end of the measurement encodes everything one needs to know to predict the statistics of any following measurement on the qubit. In their experiment, Naghiloo et al. chose to drive the qubit during the measurement so that  $\sigma_X$  is non zero during the quantum trajectory. The information acquired by the demon then takes into account the fact that the demon not only has knowledge on the qubit energy expectation in  $\sigma_Z$  as in the previous experiment but also in the qubit coherence in  $\sigma_X$ . The density matrix can always be written as  $\rho_{t_m} = p_1 |\psi_{t_m}\rangle\langle\psi_{t_m}| + p_0 |\psi_{t_m}^\perp\rangle\langle\psi_{t_m}^\perp|$  for one particular pure qubit state  $|\psi_{t_m}\rangle$  and its orthogonal one  $|\psi_{t_m}^\perp\rangle$ . Note that due to the limited efficiency of the detector (here  $\eta = 30\%$ ), the quantum states are mixed and  $p_1, p_0 < 1$ . In order to optimally extract work out of the qubit, the demon needs to perform a pulse at the qubit frequency that brings  $\rho_{t_m}$  to  $\max(p_0, p_1)|g\rangle\langle g| + \min(p_0, p_1)|e\rangle\langle e|$ . In their experiment, Naghiloo et al. [9] avoid the complexity of calculating the proper

pulse to send in real time by performing rotations around the  $y$  axis of the Bloch sphere with a random angle and then postselecting the right ones by postprocessing.

As we have seen above, in the case of a quantum system and a classical demon such as here, the fluctuation relation needs to take into account the stochastic mutual information  $I_{QC}$ . This quantity is determined in a slightly different manner from for a discrete weak measurement. If one were to perform an ideal projective measurement at time  $t_m$  of the observable  $|\psi_{t_m}\rangle\langle\psi_{t_m}|$ , one would get an outcome  $z' = 1$  with probability  $p_{t_m}(z' = 1) = p_1$  and  $z' = 0$  with probability  $p_{t_m}(z' = 0) = p_0$ . With similar notations, a projective measurement of the observable  $|e\rangle\langle e|$  after the qubit is thermalized at the beginning of the experiment (time 0) leads to an outcome  $z = 1$  with probability  $p_0(z = 1) = (1 + e^{\beta\hbar\omega_q})^{-1}$  and  $z = 0$  with probability  $p_0(z = 0) = (1 + e^{-\beta\hbar\omega_q})^{-1}$ . The stochastic mutual information [24] can then be written as

$$I_{QC}(z, z') = \ln p_{t_m}(z') - \ln p_0(z). \quad (40.6)$$

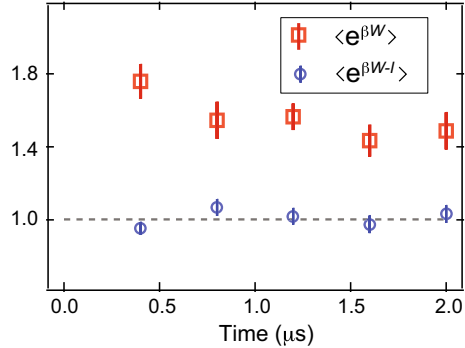
The above expression is very similar to Eq. (40.4). This illustrates that the main difference between the experiments of Masuyama et al. and Naghiloo et al. is not so much in the discrete versus continuous measurement approach since in the end only the last quantum state  $\rho_{t_m}$  matters. It is in the fact that the first focuses on states that do not have any quantum coherence while the second extends the experiment to finite coherences by adding a drive during the measurement.

Concretely, after initialization in a thermal state, Naghiloo et al. perform the first TPM projective measurement and measure continuously and dispersively the qubit state while a drive resonating at the qubit frequency induces a rotation of the qubit in the Bloch sphere. A feedback pulse is then applied by a postselection based on the reconstructed quantum trajectory. The sequence is terminated by the second TPM measurement. While the strength of the measurement allowed to tune the stochastic mutual information in the work of Masuyama et al., here the authors decided to keep a constant measurement rate and vary the duration  $t_m$  of the measurement. Noting that the free energy difference between the initial and final states is zero because the Hamiltonian is the same, the extracted work  $W$  and demon information verify:

$$\begin{aligned} & \sum_{z, z' \in \{0, 1\}} p_0(z) p_{t_m}(z') e^{\beta\hbar\omega_q(z-z') - I_{QC}(z, z')} \\ &= \langle e^{\beta W - I_{QC}} \rangle = 1. \end{aligned} \quad (40.7)$$

Experimentally, the work  $W$  that is extracted both during the measurement under a drive and during the feedback pulse is determined using the TPM protocol. The inferred evolution of  $\langle e^{\beta W - I} \rangle$  and  $\langle e^{\beta W} \rangle$  are represented in Fig. 40.6 as a function of the measurement duration  $t_m$  for a qubit initially at equilibrium at a temperature  $\hbar\omega_q/4k_B$ . As in the experiment by Masuyama et al., the generalized Jarzynski equality is indeed verified. This demonstrates that the feedback pulse is indeed applied the right way and validates the definition of information.

**Fig. 40.6** (Adapted from Ref. [9]) Jarzynski equality is verified for any measurement time only when the mutual information  $I_{QC}$  is taken into account. Here the blue dots correspond to the experimentally inferred  $\langle e^{\beta W - I_{QC}} \rangle$  as a function of measurement time  $t_m$  while red squares correspond to  $\langle e^{\beta W} \rangle$ .



### 40.2.3 Information Loss During Weak Measurements

Beyond Jarzynski equalities, the information acquired by the demon exposes the differences between a weak measurement in the  $Z$  direction with or without a drive at the qubit frequency.

Masuyama et al. show the evolution of  $\langle I_{QC} \rangle$  as a function of the feedback error probability  $\epsilon_{fb}$ . When the collected information is maximal (or equivalently the feedback error probability is zero) the mutual information does not quite reach  $\langle I_{Sh} \rangle$  due to the finite decay of the qubit. As expected the average of the demon information decays to zero as the feedback error probability goes up.

Similarly Naghiloo et al. compute the information acquired by the demon in the case of a continuous measurement when the qubit starts in a thermal state  $\rho_0$ . Since the qubit is not actually projectively measured after time  $t_m$ , one needs to sum over the different possible outcomes  $z$  and  $z'$  and gets for a single measurement record  $\{V(t)\}_t$

$$\begin{aligned} \langle I_{QC} \rangle_{\{V(t)\}_t} &= \sum_{z, z' \in \{0; 1\}} p_0(z) p_{t_m}(z') I_{QC}(z, z') \\ &= S(\rho_0) - S(\rho_{t_m}). \end{aligned} \quad (40.8)$$

where  $S(\rho) = -\text{Tr}(\rho \ln \rho)$  denotes the Von Neumann entropy. The information acquired by the demon over a trajectory is hence simply the difference between the initial and final entropies of the qubit. When the quantum efficiency  $\eta$  is 1, no information about the system is lost during the continuous measurement. The qubit state that is reconstructed from the measurement records using the stochastic master Eq. (40.11) conserves its initial purity. Since experimentally  $\eta \approx 30\%$ , information is lost in the environment. If the lost information is larger than the gained information during the measurement one gets  $\langle I_{QC} \rangle_{\{V(t)\}_t} < 0$ . This is the case when the initial state is close to a pure state: during the trajectory the state loses its coherence and hence purity because of the imperfection of the measurement, increasing its entropy. On the other hand when the initial state is close to the most entropic state, the measurement purifies the state of the qubit and the final entropy becomes smaller than

the initial one. This transition has been experimentally observed and can be seen in Ref. [9] where the mutual information goes from positive to negative values.

## 40.3 Autonomous Demon

### 40.3.1 Coherent Information Transfer and Work Extraction

In the two experiments presented previously the information has to leave the quantum world to be recorded and used in the feedback process of the demon. Yet, it is possible to realize a fully quantum experiment where the demon itself is a quantum system. This is a case where the control is deterministic and unconditional hence without any feedback based on measurement. Instead built-in conditional operations need to be designed for the demon to operate by autonomous feedback. In the dispersive Hamiltonian (40.1), when  $\chi$  is larger than the linewidths of both the qubit and cavity, a regime known as *photon-resolved* [26], it becomes possible for a pulse at a given frequency to excite the cavity (respectively qubit) conditionally on the number of excitations in the qubit (respectively cavity). More precisely a drive at  $\omega_c$  displaces the cavity only if the qubit is in its ground state, while a drive at  $\omega_q - N\chi$  flips the qubit only when the cavity hosts exactly  $N$  photons.

This autonomous quantum Maxwell demon was realized in Ref. [10]. Initially we assume the cavity to be in the vacuum state  $|0\rangle$  as thermal excitations can be neglected. After initialization of the qubit in a thermal or in a superposition of energy eigenstates, a pulse at  $\omega_c$  is applied with a duration chosen to be larger than  $\chi^{-1}$  to ensure selectivity. The cavity thus ends up either in  $|\alpha_e\rangle = |0\rangle$  if the qubit is excited, or ideally in a coherent state  $|\alpha_g\rangle = |\alpha\rangle$  if the qubit is in the ground state. Since the process follows a unitary evolution, an initial superposed state like  $(|e\rangle + |g\rangle)/\sqrt{2}$  results in an entangled state  $(|e\rangle|0\rangle + |g\rangle|\alpha\rangle)/\sqrt{2}$ . Consecutively, a  $\pi$ -pulse at  $\omega_q$  flips the qubit only if the cavity hosts 0 photon. It is always the case when the qubit is excited, and it happens with a probability  $|\langle 0|\alpha\rangle|^2 = \exp(-|\alpha|^2)$  when the qubit is in the ground state. If  $\alpha \gg 1$ , the demon distinguishes well between ground and excited states and the qubit always ends up in the ground state. Consequently, the information about the qubit state makes the energy exchange of 1 quantum of work between the drive pulse and the qubit unidirectional: the drive is either reflected without loss of energy (if the qubit has no energy to offer) or contains one extra stimulated-emitted photon (if the qubit is in  $|e\rangle$ ). A positive net extraction of work is thus ensured at  $\alpha \gg 1$ . In the case of an initially superposed qubit, the conditional  $\pi$ -pulse disentangles the qubit and the cavity so that the cavity ends up a state  $(|0\rangle + |\alpha\rangle)/\sqrt{N}$ . Therefore the conjugation of conditional displacement and  $\pi$ -pulse swaps the qubit and cavity states and performs a coherent information transfer from the qubit to the cavity. On the other hand if  $\alpha$  is not large enough, the conditional  $\pi$ -pulse does not fully disentangle the qubit and the cavity, the information transfer is imperfect and as a result the work extracted is smaller. Similarly to what has been done in Ref. [8],

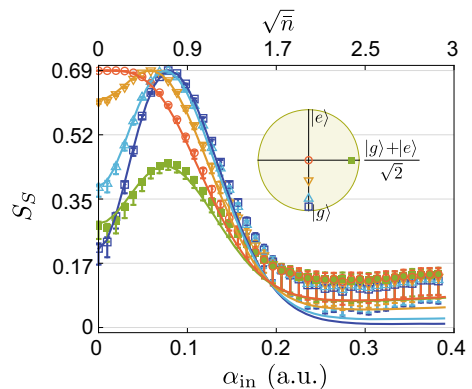
the quantity of information transferred to the demon can be tuned by varying the amplitude of the displacement  $\Omega_c$  or, equivalently, the mean number of photons in the cavity  $\bar{n}$ .

### 40.3.2 Information Transfer

In our work [10], the whole sequence is terminated by a full tomography of the final qubit (system) state  $\rho_S$  using a set of projective measurements. The evolution of the final Von Neumann entropy of the qubit  $S_S = -\text{Tr}(\rho_S \ln \rho_S)$  with  $\sqrt{\bar{n}}$  is represented in Fig. 40.7 for various initial states of the qubit, either in a thermal or superposed state. Its evolution exhibits a clear quantum feature that highlights the quantumness of the demon. The entropy of the qubit first goes to a maximum before eventually decreasing. This increase of entropy manifests the residual presence of entanglement between the qubit and the cavity after the work extraction pulse: when measuring the state of the qubit only, one discards the information encoded in the cavity and gets a more entropic qubit. Within the interpretation of the experiment in terms of Maxwell's demon, this large qubit entropy means that the demon operates erratically due to the partial quantum information it gets on the qubit. It is not the case when  $\bar{n} \ll 1$ , because then the conditional  $\pi$ -pulse at  $\omega_q$  is always on resonance. The behavior of the demon becomes perfectly predictable and does not affect the entropy of the qubit. In the limit of large  $\bar{n}$  however, the information transfer is large enough so that the demon lowers the entropy of the qubit. The residual entropy is mostly due to the parasitic thermalization of the qubit with the environment during the sequence.

When the demon's memory is a quantum system, such as the cavity here, it becomes possible to realize a full quantum tomography of its state and to uncover its quantum coherences. In our experiment [10], we used the qubit to perform a tomography of the cavity at the end of the sequence based on generalized Husimi Q-functions measurement and state reconstruction [27]. Because we used a single

**Fig. 40.7** (Figure from Ref. [10]) Final measured Von Neumann entropy of the system as a function of the amplitude of the cavity displacement drive amplitude (labeled  $\alpha_{in}$ ), which tunes the information quantity that the demon extracts from the qubit.



qubit as the system and as a tomographic tool, it is necessary to be certain that the qubit is in the ground state before starting the tomography. For that reason, the range of cavity displacement amplitudes where one can reconstruct the state of the cavity is limited to the cases where the demon cools efficiently the qubit close to its ground state. In particular, the technique does not allow us to measure the variations of the demon's information with the displacement drive amplitude. Such a measurement would be possible if one would use another ancillary qubit just to perform the cavity tomography (for instance with an architecture as in Ref. [28]). The magnitude of the elements of the reconstructed density matrix of the cavity  $\rho_D$  is represented in Fig. 40.8 in the Fock state basis for 4 different initial qubit states: (a) ground, (b) excited, (c) superposed and (d) thermal at infinite temperature. As expected, the cavity contains a large number of photons when the qubit is initially in the ground state ( $\bar{n} \approx 4.6$ ) and stays in vacuum when the qubit is initialized in the excited state. The coherence of the process arises when comparing the superposed case and the thermal one. When the qubit is initially superposed, the cavity ends up with non-zero

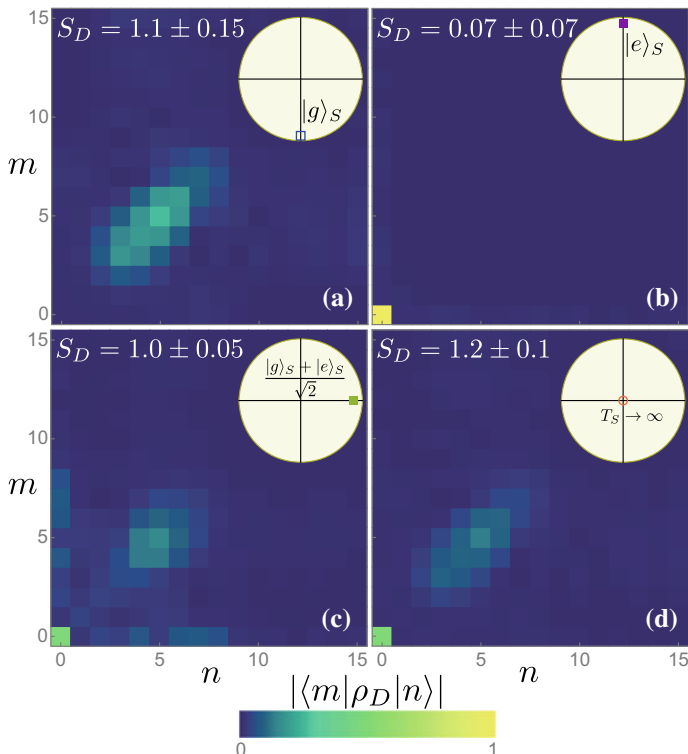


**Fig. 40.8** (Figure from Ref. [10]) Amplitude of the elements of the reconstructed density matrix of the cavity (demon's memory) in the Fock states basis after the sequence for a qubit initialized in the (a) ground state, (b) excited state, (c) superposed state and (d) thermal state at infinite temperature.

off-diagonal terms of the form  $\langle 0 | \rho_D | m \rangle$ ,  $m \in \mathbb{N}^*$ , showing coherences between the vacuum and the displaced state. These off-diagonal terms are zero in the thermal case.

From the reconstructed density matrix of the demon  $\rho_D$  one can infer its Von Neumann entropy in an attempt to quantify the amount of information stored in the cavity. It is indicated on Fig. 40.8. Surprisingly its state is very entropic except when it is in vacuum. This is due to the conjugated effect of the unwanted qubit induced non-linearity in the cavity and of dissipation. As a result the displacement produces an entropic state instead of a coherent state. Yet, the comparison of the superposed and thermal cases shows that the cavity entropy in this case indeed reflects the initial entropy of the qubit, with the superposed state resulting in a less-entropic cavity than the thermal one. However, besides highlighting quantum effects in the transfer of information, it is not possible to perform an information balance between the qubit and the cavity. This is only due to the fact that the information on the two-dimensional qubit is encoded in a multi-level system, the cavity, which does not remains pure due to the aforementioned parasitic nonlinearities. With this type of encoding, the only relevant information for the demon to operate efficiently is whether or not the cavity is in  $|0\rangle$ . Therefore, one could think of a better definition for the stored information in such a way that it would eliminate the irrelevant contribution of entropy in the excited states of the cavity.

### 40.3.3 Direct Work Measurement

Interestingly, it is possible to perform a direct measurement of the work extracted by the demon without resorting to the TPM process. It is done by directly recording the power contained in the reflected  $\pi$ -pulse. Given the small energy of a single microwave photon, the use of quantum limited Jopsephson amplifiers was instrumental [2]. To do so in Ref. [10], we amplify the reflected pulse by a Josephson Parametric Converter (JPC) [29]. It amplifies the two field quadratures by the same amount and as a result acts as a *phase-preserving* amplifier. After amplification the field is digitized and the average instantaneous power at  $\omega_q$  is extracted. Denoting as  $a_{\text{in,out}}$  the annihilation operator of a photon propagating in the transmission line towards (respectively from) the cavity, one can simply express the power extracted from the qubit  $P_{\text{ext}}$  by the difference between the photon rate that is sent and the one that is reflected  $P_{\text{ext}} = \hbar\omega_q(\langle a_{\text{out}}^\dagger a_{\text{out}} \rangle - \langle a_{\text{in}}^\dagger a_{\text{in}} \rangle)$ . Besides one can write the propagating number of photons in the transmission line in terms of qubit operators [30]

$$\frac{P_{\text{ext}}}{\hbar\omega_q} = \gamma_a \frac{1 + \langle \sigma_z \rangle}{2} + \frac{\Omega_q}{2} \langle \sigma_x \rangle, \quad (40.9)$$

where  $\gamma_a$  is the emission rate of the qubit towards the transmission line and  $\Omega_q$  is the Rabi frequency as defined in Eq. 40.2. The first term is proportional to the probability to find the qubit in the excited state and thus corresponds to spontaneous emission of the qubit. To understand the second one, let us integrate it over half a Rabi oscillation.

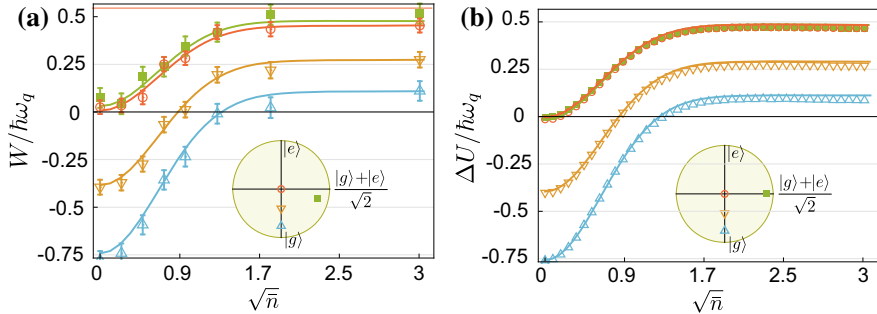


**Fig. 40.9** (Adapted from [10]) (a) Directly measured extracted work from the qubit by the autonomous demon for various initial thermal or superposed states. The direct measurement perfectly agrees with the (b) independent measurement of the variation of energy of the qubit between two projective measurements (TPM).

In the absence of losses ( $\Omega_q \gg \gamma_a$ ), if the qubit goes from  $|g\rangle$  to  $|e\rangle$ , one would find  $-1$ , and  $+1$  for a qubit going from  $|e\rangle$  to  $|g\rangle$ . Therefore, in case of negligible loss during the pulse, this term quantifies the coherent energy exchanges between the drive and the qubit through absorption/stimulated emission cycles.

Experimentally the reflected signal is decomposed into short time bins and integrated to get the extracted work  $W = \int_0^{\pi/\Omega_q} P_{\text{ext}} dt$ . The evolution of the extracted work with the number of photons contained in the demon is represented in Fig. 40.9 as well as the variation of the qubit internal energy  $\Delta U = E(t_i) - E(t_f)$  obtained from the qubit tomography, which is equivalent to a TPM in the case of projective measurement along  $\sigma_Z$ . As expected the extracted work is negative when the demon does not distinguish the ground from the excited state, and becomes positive as the number of photons in the cavity increases. The direct work measurement and the qubit energy change measurement are not obtained for the exact same pulse sequences due to technical issues in the work measurement (see supplementary material of [10]). A consequence is that the superposed state prepared in the two cases is not exactly the same, as represented in the Bloch sphere projections in the  $XZ$ -plane in insets. Nevertheless the agreement between the two independent measurements is remarkable.

## 40.4 Conclusion

### 40.4.1 Summary on Already Realized Experiments

The three experimental realizations of a quantum Maxwell's demon presented in this chapter demonstrate that superconducting circuits constitute a useful and versatile testbed for quantum thermodynamics. They make possible the experimental

**Table 40.1** Status of the three existing experiments on quantum Maxwell's demon using superconducting circuits at the time of this writing.

	Masuyama et al. [8]	Naghiloo et al. [9]	Cottet, Jezouin et al. [10]
Nature of the demon	Classical	Classical	Quantum
Mutual information knob	Cavity drive amplitude	Measurement duration	Cavity drive amplitude
Work determination	Inferred from TPM	Inferred from TPM	Direct power measurement
Fluctuation relation	Sagawa-Ueda equality for weak to strong measurement	Jarzynski equality with quantum trajectories	No measure of mutual information
Information evolution	Classical information	Information loss causing $\langle I \rangle \leq 0$	Differing demon entropies for thermal and quantum cases

validation of thermodynamical equalities in the context of various measurements: strong, weak, quantum trajectories or coherent transfer to an ancillary quantum system. The main features of these three experiments are shown in Table 40.1. On the basis of this table, we can foresee directions towards which future experimental realizations with superconducting circuits could go. A direct work measurement (using direct microwave measurement of the released energy [10], calorimeters [31] or other techniques) coupled to a demon using classical information would give access to the influence of irreversible events and how they arise when the measurement becomes strong. Coupled to quantum trajectory measurements, a direct work measurement through fluorescence would allow one to precisely quantify and separate the flows of heat and work during the trajectory and the feedback pulse. Finally in the case of quantum demon memories, the use of an ancillary qubit would allow one to perform joint measurements of the states of the qubit and cavity, and hence to quantify the mutual information between them at any measurement strength. This would lead to the experimental measurement of a fully quantum Jarzynski equality in the presence of quantum coherence.

#### 40.4.2 Theoretical Proposals

Over the past ten years few theoretical proposals have designed experiments based on superconducting circuits to probe further the physics of Maxwell's demon in quantum mechanics. First, it has been suggested to use superconducting circuits to realize a quantum Otto engine [32, 33], by using the tunability of the coupling between two charge qubits. A second important use of superconducting circuits is the possibility to quickly tune their frequency, allowing a demon to extract work from the system up to the Landauer bound  $k_B T \ln 2$ . Such a scheme was proposed by

Pekola et al. [34] for a single qubit using Landau-Zener transitions and measurement based feedback. In the three existing experiments, the energy levels of the qubit were fixed and it was thus impossible to saturate the bound. More precisely the maximal work extracted by the demon from a fixed-frequency qubit is equal to the initial mean energy of the qubit:  $W_{\max} = \hbar\omega_q p_e$  where  $p_e$  denotes the initial probability to find the qubit in the excited state. At thermal equilibrium at temperature  $T$  it reads  $p_e = 1/(1 + \exp(\hbar\omega_q/k_B T))$  and the ratio of work over Landauer bound reads at best

$$\frac{W_{\max}}{k_B T \ln 2} = \frac{\hbar\omega_q/k_B T}{\ln 2(1 + e^{\hbar\omega_q/k_B T})} \quad (40.10)$$

and reaches a maximum determined numerically around 40%. However allowing to tune the energy levels of the qubit during the sequence leads to saturating the bound. First, the initial sequence is left unchanged: the qubit is thermalized at fixed frequency  $\omega_1$ , then measured and flipped to the ground state (whether or not the demon is classical does not change the energy balance here). As already stated, this technique extracts at best a work  $W_1 = \hbar\omega_1 p_e$ . Second, the energy levels are shifted adiabatically to a frequency  $\omega_2$  so that  $\hbar\omega_2 \gg k_B T$ . Since the qubit is in the ground state, this process can be done without any expense of external work. Third, the energy levels are brought back quasi-statically to the initial frequency  $\omega_1$ . This has to be done slowly enough so that the qubit is always at equilibrium with the heat bath at temperature  $T$ . This process extracts a work  $k_B T \ln 2 - W_1$  and hence the total work extracted from the qubit reaches the bound. More generally, using tunable qubits leads to designing thermal machines able to operate at the Carnot efficiency. Josephson junction circuits offer such a tunability by the application of an external magnetic flux through a loop of two junctions [16, 17]. Various theoretical proposals suggest to use this tunability to perform Otto thermal machines operating either as engines or refrigerators [35, 36]. Owing to the possibility to perform single-shot measurements, superconducting circuits could exhibit the role of information transfers in such systems.

In most of proposed realizations of Maxwell's demon, the information about the system is used to extract work from a single heat bath. This process is not the only apparent violation of the second principle: an information-powered refrigerator would apparently violate the second principle as well. Campisi et al. [37] proposed to use superconducting circuits coupled to calorimetric measurements to generate an inverse heat flow from a cold bath to a hot one. Each bath is modeled as an RLC resonator with a frequency that can be tuned by an external flux and at temperatures  $T_{h,c}$ , with  $T_c < T_h$ . Both resonators are inductively coupled to the same superconducting qubit. Recently developed calorimeters [38–40] allow to detect when an excitation leaves or enters each resistor, and provide the information acquired by the demon. Initially the cold bath and the qubit in its ground state are on resonance and the hot bath is far from resonance, inhibiting the effective coupling between the bath and the qubit. A calorimeter can detect the transfer of an excitation from the cold bath to the qubit. Such an event triggers, by measurement based feedback, pulses on two control fluxes that bring the hot bath in resonance with the qubit and put the cold

bath out of resonance. The qubit eventually releases its excitation into the hot bath. This event is detected by the heating of the hot resistor through a second calorimeter and a second feedback control is applied to bring the system back to its initial state, hence closing the thermodynamic cycle.

When measuring the state of the qubit, it is interesting to consider cases where the demon does not measure its state in the energy basis, i.e. along the  $z$ -axis of the Bloch sphere. A measurement that would project the qubit in a coherent superposition [41, 42] would instead allow for more work extraction than classically allowed, by using the quantum coherence as a resource. Elouard et al. [43] studied the case of a demon measuring the state of a superconducting circuit in the  $x$ -direction. The qubit is initialized in  $(|g\rangle + |e\rangle)/\sqrt{2}$  then measured strongly along the  $x$ -axis in a stroboscopic way, and as a result is projected each time onto  $(|g\rangle \pm |e\rangle)/\sqrt{2}$ . Between the measurements the qubit is driven on resonance during a time  $\tau$  with a Rabi frequency  $\Omega_q$  and extracts positive work from the qubit if it was initially in  $(|g\rangle + |e\rangle)/\sqrt{2}$ . In the limit where  $\Omega_q\tau \ll 1$ , the qubit has almost not evolved between two consecutive measurements and is re-projected with a very high probability on  $(|g\rangle + |e\rangle)/\sqrt{2}$  by Zeno effect. Therefore the external pulse is continuously powered-up by the projective measurement of the qubit along  $x$ . Importantly, such a heat engine can be done in the absence of an external cold bath: the energy is here provided by the back-action of the measurement apparatus.

#### **40.4.3 Perspectives**

The first experimental realizations of quantum Maxwell's demons in this platform illustrate the many possibilities offered by superconducting circuits. They pave the way to various more experiments that will explore the intimate link between information and thermodynamics in the quantum regime. With this goal in mind, one could think of using other kinds of systems than transmon qubits as working agents. Among them, fluxonium qubits [44] appear as an extremely promising platform because they offer a whole zoology of transitions. Their transition frequency can be tuned from hundreds of MHz to about 20 GHz using an external magnetic flux, offering the possibility to study regimes where the system dynamically goes from  $\hbar\omega \gg k_B T$  to  $\hbar\omega \ll k_B T$ . Moreover the coupling rates of fluxonium qubits with their environment can vary over 5 orders of magnitude, allowing one to finely engineer the heat exchanges with the baths. Superconducting circuits can also provide components of more sophisticated experiments that would use heat switches [45]. In a broader picture, the use of hybrid systems formed by superconducting circuits coupled to mechanical resonators appears as extremely promising. It would allow one to proceed to a work extraction that would indeed be used to lift a small mass, as in the first early descriptions of Maxwell's gedanken experiment. This could be interesting to solve controversies about the nature of heat and work in quantum systems. Superconducting circuits are also a promising platform for realizing entanglement

between two qubits by the use of thermal baths only and in the absence of any coherent drive [46]. With the steady improvement of superconducting qubits, there is no doubt that these systems offer a growing number of possibilities to test quantum thermodynamic properties and implement potential applications.

**Acknowledgements** This work was funded by Agence Nationale de la Recherche under the grant ANR-17-ERC2-0001-01. Part of the research reviewed in this chapter was made possible by the COST MP1209 network “Thermodynamics in the quantum regime”.

## Appendix

### Quantum Trajectories

We describe here how one can determine the quantum state  $\rho_t$  in the experiment of Naghiloo et al. [9]. The signal  $V(t)$  carrying the information being continuous, one can decompose the information into time bins and get a time-resolved measurement. In order to observe non negligible effects of measurement backaction, it is crucial to minimize the amount of information that is lost between the cavity and the measurement apparatus, i.e. to maximize the quantum efficiency  $\eta$ . This process is done using quantum-limited amplification right after the cavity, a process that adds the minimal amount of noise allowed by quantum mechanics [47]. In their quantum trajectories experiment, Naghiloo et al. use a Josephson Parametric Amplifier (JPA) [48] that amplifies one of the two quadratures of the field (equivalent to the position and momentum operators of a mechanical linear oscillator) and as such operates as a *phase-sensitive* amplifier allowing to reach a state of the art quantum efficiency of about  $\eta = 30\%$ . Denoting as  $dt$  the time interval between two successive records, the measurement record at time  $t$  is given by  $dV(t) = \sqrt{2\eta\Gamma_m}\langle\sigma_z\rangle_{\rho_t}dt + dW_t$  where  $dW_t$  a zero-mean Wiener process whose variance is  $dt$  and which represents the quantum and technical noise. Note that here the expectation value  $\langle\sigma_z\rangle_{\rho_t} = \text{Tr}(\rho_t\sigma_z)$  depends on the particular realization of the trajectory and thus on the measurement record  $\{V(\tau)\}_\tau$  at all times  $\tau < t$ . The density matrix of the qubit is then reconstructed using the Stochastic Master Equation (SME) [49]

$$d\rho_t = -dt \frac{i}{\hbar}[H, \rho_t] + dt \frac{\Gamma_m}{2}\mathcal{D}[\sigma_z]\rho_t + dW_t \sqrt{2\eta\Gamma_m}\mathcal{M}[\sigma_z]\rho_t, \quad (40.11)$$

where  $\mathcal{D}$  is the Lindblad super operator and  $\mathcal{M}$  the measurement super operator  $\mathcal{M}[c]\rho = \frac{1}{2}((c) - \langle c \rangle)\rho + \rho(c^\dagger - \langle c^\dagger \rangle)$ . The two first terms correspond to a Lindbladian evolution of the qubit dephased by the measurement drive (for the seek of simplicity other decoherence channels as spontaneous decay of the qubit have been omitted). The last one represents the measurement backaction: at each  $dt$  the state is kicked depending on the measurement record, possibly changing the mean energy of the qubit. The inherent stochasticity of the SME highlights the profound link between

information and energy in quantum mechanics and has triggered recent works on the subject, including in the field of superconducting circuits. The reader can refer to the Chaps. 15, 29 and 33 for a more precise treatment of the subject.

## References

1. M.H. Devoret, R.J. Schoelkopf, *Science* **339**, 1169 (2013). <https://doi.org/10.1126/science.1231930>
2. A. Roy, M. Devoret, *Comptes Rendus Physique* **17**, 740 (2016). <https://doi.org/10.1016/j.crhy.2016.07.012>
3. F. Mallet, F.R. Ong, A. Palacios-Laloy, F. Nguyen, P. Bertet, D. Vion, D. Esteve, *Nat. Phys.* **5**, 791 (2009). <https://doi.org/10.1038/nphys1400>
4. K.W. Murch, S.J. Weber, C. Macklin, I. Siddiqi, *Nature* **502**, 211 (2013). <https://doi.org/10.1038/nature12539>
5. M. Hatridge, S. Shankar, M. Mirrahimi, F. Schackert, K. Geerlings, T. Brecht, K.M. Sliwa, B. Abdo, L. Frunzio, S.M. Girvin, R.J. Schoelkopf, M.H. Devoret, *Science* **339**, 178 (2013). <https://doi.org/10.1126/science.1226897>
6. R. Vijay, C. Macklin, D.H. Slichter, S.J. Weber, K.W. Murch, R. Naik, A.N. Korotkov, I. Siddiqi, *Nature* **490**, 77 (2012). <https://doi.org/10.1038/nature11505>
7. S.J. Weber, K.W. Murch, M.E. Kimchi-Schwartz, N. Roch, I. Siddiqi, *Comptes Rendus Physique* **17**, 766 (2016). <https://doi.org/10.1016/j.crhy.2016.07.007>
8. Y. Masuyama, K. Funo, Y. Murashita, A. Noguchi, S. Kono, Y. Tabuchi, R. Yamazaki, M. Ueda, Y. Nakamura, *Nat. Commun.* **9**, 1291 (2018). <https://doi.org/10.1038/s41467-018-03686-y>
9. M. Naghiloo, J.J. Alonso, A. Romito, E. Lutz, K.W. Murch (2018). <https://doi.org/10.1103/PhysRevLett.121.030604>
10. N. Cottet, S. Jezouin, L. Bretheau, P. Campagne-Ibarcq, Q. Ficheux, J. Anders, A. Auffèves, R. Azouit, P. Rouchon, B. Huard, *Proc. Natl. Acad. Sci.* **114**, 7561 (2017). <https://doi.org/10.1073/pnas.1704827114>
11. H. Paik, D.I. Schuster, L.S. Bishop, G. Kirchmair, G. Catelani, A.P. Sears, B.R. Johnson, M.J. Reagor, L. Frunzio, L.I. Glazman, S.M. Girvin, M.H. Devoret, R.J. Schoelkopf, *Physical Review Letters* **107**, 240501 (2011). <https://doi.org/10.1103/PhysRevLett.107.240501>
12. L. Szilard, *Behav. Sci.* **9**, 301 (1964). <https://doi.org/10.1002/bs.3830090402>
13. K. Maruyama, F. Nori, V. Vedral, *Rev. Mod. Phys.* **81**, 1 (2009). <https://doi.org/10.1103/RevModPhys.81.1>
14. R. Landauer, *IBM J. Res. Dev.* **5**, 183 (1961). <https://doi.org/10.1147/rd.53.0183>
15. C.H. Bennett, *Int. J. Theor. Phys.* **21**, 905 (1982). <https://doi.org/10.1007/BF02084158>
16. G. Wedin, *Rep. Prog. Phys.* **80**, 106001 (2017). <https://doi.org/10.1088/1361-6633/aa7e1a>
17. X. Gu, A.F. Kockum, A. Miranowicz, Y.-x. Liu, F. Nori, *Physics Reports* **718-719**, 1 (2017). <https://doi.org/10.1016/j.physrep.2017.10.002>
18. A. Blais, R.S. Huang, A. Wallraff, S.M. Girvin, R.J. Schoelkopf, *Phys. Rev. A* **69**, 62320 (2004). <https://doi.org/10.1103/PhysRevA.69.062320>
19. W.H. Zurek, *Rev. Mod. Phys.* **75**, 715 (2003). <https://doi.org/10.1103/RevModPhys.75.715>
20. P. Talkner, E. Lutz, P. Hänggi, *Phys. Rev. E* **75**, 050102 (2007). <https://doi.org/10.1103/PhysRevE.75.050102>
21. J. Kurchan (2000). [arXiv:cond-mat/0007360](https://arxiv.org/abs/cond-mat/0007360)
22. H. Tasaki (2000). [arXiv:cond-mat/0009244](https://arxiv.org/abs/cond-mat/0009244)
23. A.A. Clerk, M.H. Devoret, S.M. Girvin, F. Marquardt, R.J. Schoelkopf, *Revi. Mod. Phys.* **82**, 1155 (2010). <https://doi.org/10.1103/RevModPhys.82.1155>
24. K. Funo, Y. Watanabe, M. Ueda, *Phys. Rev. A* **88**, 052319 (2013). <https://doi.org/10.1103/PhysRevA.88.052319>

25. P. Campagne-Ibarcq, *Measurement back action and feedback in superconducting circuits*, Thesis, Ecole Normale Supérieure (ENS) (2015). <https://hal.archives-ouvertes.fr/tel-01248789>
26. D.I. Schuster, A.A. Houck, J.A. Schreier, A. Wallraff, J.M. Gambetta, A. Blais, L. Frunzio, J. Majer, B. Johnson, M.H. Devoret, S.M. Girvin, R.J. Schoelkopf, *Nature* **445**, 515 (2007). <https://doi.org/10.1038/nature05461>
27. G. Kirchmair, B. Vlastakis, Z. Leghtas, S.E. Nigg, H. Paik, E. Ginossar, M. Mirrahimi, L. Frunzio, S.M. Girvin, R.J. Schoelkopf, *Nature* **495**, 205 (2013). <https://doi.org/10.1038/nature11902>
28. J.Z. Blumoff, K. Chou, C. Shen, M. Reagor, C. Axline, R.T. Brierley, M.P. Silveri, C. Wang, B. Vlastakis, S.E. Nigg, L. Frunzio, M.H. Devoret, L. Jiang, S.M. Girvin, R.J. Schoelkopf, *Phys. Rev. X* **6**, 031041 (2016). <https://doi.org/10.1103/PhysRevX.6.031041>
29. N. Roch, E. Flurin, F. Nguyen, P. Morfin, P. Campagne-Ibarcq, M.H. Devoret, B. Huard, *Phys. Rev. Lett.* **108**, 147701 (2012). <https://doi.org/10.1103/PhysRevLett.108.147701>
30. C. Cohen-Tannoudji, J. Dupont-Roc, G. Grynberg, *Atom-Photon Interactions: Basic Processes and Applications* (2001). <https://doi.org/10.1002/9783527617197>
31. J.P. Pekola, P. Solinas, A. Shnirman, D.V. Averin, *New J. Phys.* **15**, 115006 (2013). <https://doi.org/10.1088/1367-2630/15/11/115006>
32. H. Quan, Y. Wang, Y.-X. Liu, C. Sun, F. Nori, *Phys. Rev. Lett.* **97**, 180402 (2006). <https://doi.org/10.1103/PhysRevLett.97.180402>
33. H. Quan, Y.-X. Liu, C. Sun, F. Nori, *Phys. Rev. E* **76**, 031105 (2007). <https://doi.org/10.1103/PhysRevE.76.031105>
34. J.P. Pekola, D.S. Golubev, D.V. Averin, *Phys. Rev. B* **93**, 024501 (2016). <https://doi.org/10.1103/PhysRevB.93.024501>
35. A.O. Niskanen, Y. Nakamura, J.P. Pekola, *Phys. Rev. B* **76**, 174523 (2007). <https://doi.org/10.1103/PhysRevB.76.174523>
36. B. Karimi, J.P. Pekola, *Phys. Rev. B* **94**, 184503 (2016). <https://doi.org/10.1103/PhysRevB.94.184503>
37. M. Campisi, J. Pekola, R. Fazio, *New J. Phys.* **19**, 053027 (2017). <https://doi.org/10.1088/1367-2630/aa6acb>
38. J.P. Pekola, V. Brosco, M. Möttönen, P. Solinas, A. Shnirman, *Phys. Rev. Lett.* **105**, 030401 (2010). <https://doi.org/10.1103/PhysRevLett.105.030401>
39. J. Govenius, R.E. Lake, K.Y. Tan, V. Pietilä, J.K. Julin, I.J. Maasilta, P. Virtanen, M. Möttönen, *Phys. Rev. B* **90**, 064505 (2014). <https://doi.org/10.1103/PhysRevB.90.064505>
40. S. Gasparinetti, K.L. Viisanen, O.-P. Saira, T. Faivre, M. Arzeo, M. Meschke, J.P. Pekola, *Phys. Rev. Appl.* **3**, 014007 (2015). <https://doi.org/10.1103/PhysRevApplied.3.014007>
41. S. Hacohen-Gourgy, L.S. Martin, E. Flurin, V.V. Ramasesh, K.B. Whaley, I. Siddiqi, *Nature* **538**, 491 (2016). <https://doi.org/10.1038/nature19762>
42. U. Vool, S. Shankar, S.O. Mundhada, N. Ofek, A. Narla, K. Sliwa, E. Zalys-Geller, Y. Liu, L. Frunzio, R.J. Schoelkopf, S.M. Girvin, M.H. Devoret, *Phys. Rev. Lett.* **117**, 133601 (2016). <https://doi.org/10.1103/PhysRevLett.117.133601>
43. C. Elouard, D. Herrera-Martí, B. Huard, A. Auffèves, *Phys. Rev. Lett.* **118**, 260603 (2017). <https://doi.org/10.1103/PhysRevLett.118.260603>
44. V.E. Manucharyan, J. Koch, L.I. Glazman, M.H. Devoret, *Science* **326**, 113 (2009). <https://doi.org/10.1126/science.1175552>
45. A. Ronzani, B. Karimi, J. Senior, Y.-C. Chang, J.T. Peltonen, C. Chen, J.P. Pekola, *Nat. Phys.* **14**, 991–995 (2018). <https://doi.org/10.1038/s41567-018-0199-4>
46. J.B. Brask, G. Haack, N. Brunner, M. Huber, *New J. Phys.* **17**, 113029 (2015). <https://doi.org/10.1088/1367-2630/17/11/113029>
47. C.M. Caves, J. Combes, Z. Jiang, S. Pandey, *Phys. Rev. A* **86**, 063802 (2012). <https://doi.org/10.1103/PhysRevA.86.063802>
48. M.A. Castellanos-Beltran, K.W. Lehnert, *Appl. Phys. Lett.* **91**, 083509 (2007). <https://doi.org/10.1063/1.2773988>
49. Q. Ficheux, S. Jezouin, Z. Leghtas, B. Huard, *Nat. Commun.* **9**, 1926 (2018). <https://doi.org/10.1038/s41467-018-04372-9>

# Chapter 41

## NV Color Centers in Diamond as a Platform for Quantum Thermodynamics



Nir Bar-Gill

This chapter focuses on the nitrogen-vacancy (NV) center in diamond and outlines its special relevance for experimental realizations of quantum thermodynamic scenarios, as a quantum spin coupled to naturally occurring spin baths. We detail the basic properties and control methods available for NVs, including the relatively long coherence times of the NVs and of the nuclear spin baths, the optical cooling cycle of the NV spin degree of freedom and the coherent control over the coupling between these systems, demonstrate their application in quantum thermodynamic machines, and present prospects for future research directions.

### 41.1 Introduction to NV Centers in Diamond

The nitrogen-vacancy (NV) center is a point defect in a diamond's lattice with  $C_{3v}$  symmetry. It consists of a substitutional nitrogen atom (N) adjacent to a carbon atom vacancy (V) that is oriented along one of the four crystalline directions ( $[11\bar{1}]$ ,  $[\bar{1}\bar{1}1]$ ,  $[\bar{1}11]$  and  $[1\bar{1}\bar{1}]$ ) (Fig. 41.1a). The electronic structure of the negatively charged NV center has a spin-triplet ground state, where the  $|m_s = \pm 1\rangle$  sublevels experience a zero-field splitting ( $\sim 2.87$  GHz) from the  $|m_s = 0\rangle$  sublevel due to spin-spin interactions (Fig. 41.1b). When an external static magnetic field is applied along the NV symmetry axis, the degeneracy of the  $m_s = \pm 1$  energy levels is lifted linearly via Zeeman splitting [1]. As described below, the NV is an attractive experimental platform, since as opposed to most solid-state defects its spin state can be initialized in the  $|m_s = 0\rangle$  state with off-resonant laser excitation, coherently

---

N. Bar-Gill (✉)

Department of Applied Physics and Physics, Hebrew University of Jerusalem,  
9190401 Jerusalem, Israel  
e-mail: bargill@phys.huji.ac.il

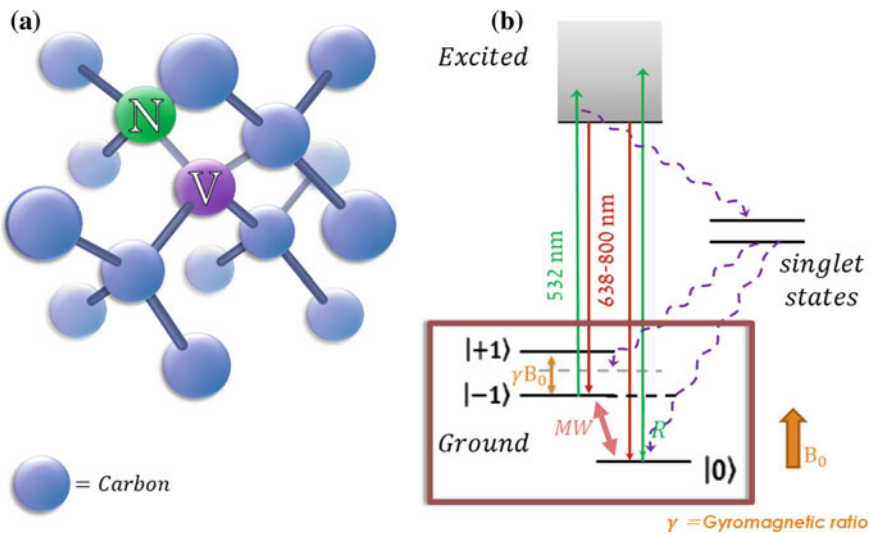


**Fig. 41.1** **a** Illustration of the nitrogen-vacancy (NV) defect within a diamond lattice. **b** Energy level diagram of the NV center. The ground-state “quantum spin” consists of 3 sub-levels, with  $|m_s = \pm 1\rangle$  separated from  $|m_s = 0\rangle$  by a zero-field splitting, and further split in the presence of an external magnetic field  $B_0$  due to the Zeeman effect. Off-resonant 532 nm light is used to excite the NV, which then emits in a red sideband (638–800 nm). Non-radiative transition through a pair of singlet states results in spin-dependent fluorescence and optical spin initialization to  $|m_s = 0\rangle$ .

manipulated with resonant microwave (MW) pulses, and read-out optically via its emitted spin-state-dependent fluorescence intensity [2].

## 41.2 NV Control Toolbox

In the context of quantum thermodynamics, the NV platform naturally provides a relevant test-bed, with the quantum NV spin exhibiting long coherence times in the order of milliseconds even at room temperature. The NV is surrounded by two spin baths: nuclear spins of the  $^{13}\text{C}$  isotopes (spin half, with a natural abundance of  $\sim 1.1\%$ ) (Fig. 41.2) and electronic spins of N defects (usually at a density exceeding that of the NVs themselves). Therefore, the NV system is relevant for studying various quantum thermodynamic scenarios, e.g., coherence effects in cooling processes, coupling of a quantum system to two different baths and coupling quantum systems through a common bath.

The optical pumping process (Fig. 41.1b) initializes the NV in the  $|m_s = 0\rangle$  sub-level of the ground-state manifold through spin-dependent non-radiative transitions from the excited states to the singlet states, preferring transitions from  $|m_s = \pm 1\rangle$  over transitions from  $|m_s = 0\rangle$  by over an order-of magnitude, while the radiative

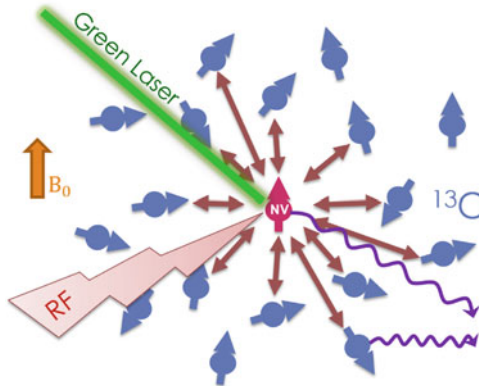


**Fig. 41.2** Illustration of an NV coupled to the nuclear spin bath ( $^{13}\text{C}$ ). RF (Radio Frequency) and MW (microwave) are used to coherently control the NV and bath spins, while green light is used to initialize and measure the NV spin state.  $B_0$  is an externally applied magnetic field.

transitions are nearly perfectly spin-preserving (with a slight spin-mixing of  $\sim 1 - 2\%$ ) [1]. This optical pumping process is an extremely useful element of the NV toolbox since it serves as an effective cooling mechanism for the NV spin degree of freedom through efficient population of the  $|m_s = 0\rangle$  ground-state to  $\sim 95\%$  (which based on the Boltzmann factor corresponds to an effective spin temperature of  $\sim 7$  mK, at zero magnetic field). In addition, on a short timescale determined by the lifetime of the singlet states (on the order of  $\sim 300$  ns), before the NV spin-state is initialized, the non-radiative transitions from the excited state result in spin-dependent fluorescence intensities, thus allowing for optical spin-state readout.

The energy scales relevant for the NV spin, as well as for the environment spins, provide a convenient handle for coherent control of these degrees of freedom, using readily-available irradiation sources in RF (radio-frequency)-MW (microwave) regimes. Advanced modulation capabilities (e.g. through combinations of arbitrary frequency, amplitude and phase modulations) enable complex coherent control schemes, including continuous-wave (CW) and pulsed approaches. In general, the complete dynamics of the NV-environment system (in the weak-coupling, Markovian limit) can be described by a master equation, containing coherent Hamiltonian evolution as well as Lindbladian dissipative terms:

$$\begin{aligned} \frac{\partial}{\partial t}\rho &= -i[H, \rho] + \Gamma + R \\ \Gamma &= \frac{\gamma_1}{2}\mathcal{D}[S^-]\rho \\ R &= \frac{\gamma_2}{2}\mathcal{D}[S_z], \end{aligned} \tag{41.1}$$

where  $H$  contains the coherent Hamiltonian dynamics,  $\Gamma$  describes effective spin decay due to optical pumping, and  $R$  features bath-induced dephasing. Below we detail an example of polarization transfer dynamics in such a system. In certain cases, the interaction of the NV with the driving microwave field can be cast in a quantum thermodynamic context, as a heat engine [3].

While we focus here on coupling of the NV to spin baths, the system is relevant for coupling to bosonic baths as well, such as phonons. In most cases bulk phonons constitute a relatively uncontrolled environment but more elaborate setups, for example diamond nano-mechanical cantilevers [4, 5] and surface acoustic waves [6, 7], can couple to the NV spin through strain and expand the NV-based quantum thermodynamics platform, e.g. by providing a partially controlled and bandwidth limited bosonic environment.

### ***41.2.1 Relevance to Thermodynamic Measures***

The toolbox presented above, together with the techniques described below, form a versatile platform for various aspects of quantum thermodynamics, specifically in the context of spin baths and the central spin problem.

A straightforward application of these techniques utilizes the NV optical pumping process as a means to effectively cool the NV spin degree of freedom (through initialization to the  $|m_s = 0\rangle$  state in the ground-state manifold), and thus realize a refrigerator. Combining polarization transfer stages between the NV and the surrounding spin bath, along with repeated optical pumping stages (to “re-cool” the NV spin), results in an effective cooling process of the spin bath (as detailed below). This experimental setup is relevant for considering thermodynamic properties such as the cooling efficiency in such a system, the temperature dependence of the cooling rate, and the lowest attainable temperature [8, 9]. Moreover, sustaining coherence of the NV central spin throughout the process can shed light on the thermodynamic implications of this resource [10].

Beyond these experiments we note that, in certain scenarios, non-trivial properties of the bath might become important. First, strong coupling between the NV spin and the bath spins is realistic in relatively high-density samples (regarding the N spin bath) or for nearby nuclear spins [10, 11]. Second, slow dephasing of the bath spins could lead to the formation of coherent, entangled states of the bath spins, departing from the limits of thermal states (see below). Finally, interactions with a limited number of nuclear spins (based on a close, strongly interacting sub-ensemble), or with a mesoscopic ensemble of electronic spins (through localized implantation of nitrogen ions), could provide access to non-Markovian dynamics [10, 11].

## 41.3 Transferring Polarization (Cooling) to Surrounding Spin Baths

The NV spin, combining relatively long quantum coherence times together with an effective cooling mechanism of its spin degree-of-freedom through the optical pumping process presented above, provides a unique platform for studying quantum thermodynamic refrigerators, with the surrounding spin baths (nuclear and/or electronic) serving as a non-trivial environment to be cooled.

The coupling between the NV and the surrounding spin baths is generally dipolar, although nuclear spins in close vicinity to the NVs can have a non-negligible contact hyperfine interaction [12]. Accordingly, this includes both dephasing terms ( $S_z$  coupling) and population transfer terms ( $S_{\pm}$ , also referred to as polarization transfer terms, or flip-flop terms). Normally, given that the different spin species have disparate resonant energies (resulting from their different gyromagnetic ratios, or from significant zero-field splitting, as is the case for NVs), the dominant interaction (in the secular approximation) originates from the dephasing terms. While this interaction has attracted significant attention in the context of quantum information processing and quantum sensing, for many aspects of quantum thermodynamics we are interested in polarization (or population) transfer, which underlies the realization of “machines”, such as refrigerators or engines, as it allows energy transfer between the system (the NV) and the environment (the surrounding spin bath).

Note that these spins are integrated within a solid structure (a diamond) and are thus coupled to lattice vibrations (phonons) that eventually lead to thermalization of the spin population. However, since this relaxation is relatively slow (usually milliseconds for the electronic spins and longer, could be hours, for nuclear spins [13]), we neglect it in this chapter and infer from the steady-state spin populations an “effective spin temperature”. This approximation can still be valid even for slower dynamics, simply through cooling of the diamond substrate, a process that efficiently suppresses phononic relaxation [14]. Nevertheless, we stress that the use of the term “spin temperature” is considered here loosely, as the steady-state does not necessarily correspond to a thermal equilibrium state, since it originates from an optical pumping process and not from coupling to a thermal reservoir (and thus, e.g., the populations of the  $|m_s = \pm 1\rangle$  states will be approximately equal, even if their energies are split by an external magnetic field).

Below we describe techniques utilized to enable polarization transfer in such spin systems, demonstrate their application with NVs, and suggest related schemes for measuring the bath polarization (or “effective spin temperature”).

### 41.3.1 *Polarization Transfer Schemes*

The essence of dressed-state resonant coupling is illustrated in Fig. 41.3 [15]. Two types of spins, A and B, with different gyromagnetic ratios ( $\gamma_A, \gamma_B$ ) have unequal

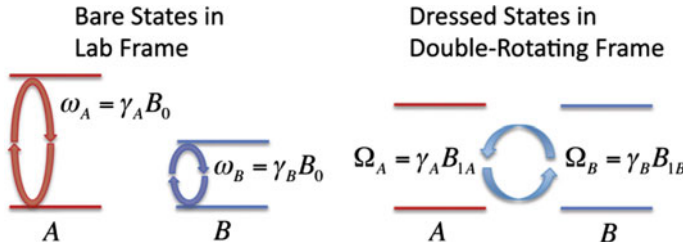


**Fig. 41.3** Illustration of dressed-state resonant coupling and energy-level diagrams. **a** Two spins with dissimilar Zeeman splitting cannot exchange energy in the lab frame. When driven resonantly (red and blue circular arrows), energy exchange becomes possible. Dressed states in the double-rotating frame are separated by the spin Rabi frequencies controlled by the respective driving fields  $B_{1A,B}$ . When the Rabi frequencies are matched, i.e.,  $\Omega_A = \Omega_B$ , energy conserving spin flip-flops can occur.

Zeeman splittings when placed in an external magnetic field ( $B_0$ ) and therefore cannot exchange energy in the lab frame. However, if both sets of spins are driven resonantly at their respective Larmor frequencies with transverse oscillating magnetic fields ( $B_{1A}$  and  $B_{1B}$ ) such that their Rabi frequencies are equal (analogous to the Hartmann-Hahn matching condition [16]), then in a double-rotating frame the dressed states of the two spins have equal energy separation and energy transfer becomes possible. A different but equivalent view of this is that the drive photons compensate for the energy mismatch, such that these photons act as the work repository. If one of the species is spin polarized, this polarization may be transferred to the other species by means of a resonant flip-flop process in the double-rotating frame mediated by their mutual magnetic coupling. Dressed-state coupling has been studied for nuclear spins in bulk as well as nanoscale ensembles [17]. Modified dressed-state schemes have also been used to transfer thermal polarization from electronic to nuclear spins in bulk ensembles [18].

#### 41.3.1.1 Transfer Scheme 1: Coupling to an Electronic Spin Bath

If the dark (i.e. not optically active), thermally mixed N spins (electronic spins associated with an N defect) are brought into resonance with spin-polarized NVs, then polarization can be transferred from NVs to N's mediated by the magnetic dipolar coupling with the Hamiltonian

$$H_{dip} = D_{NV,N} \left[ S_z^{NV} S_z^N - \frac{1}{4\sqrt{2}} (S_+^{NV} S_-^N + S_-^{NV} S_+^N) \right]. \quad (41.2)$$

Here  $S^{NV}$  and  $S^N$  are the spin operators for the NV and N spins, respectively,  $D_{NV,N} = \mu_0 \gamma_{NV} \gamma_N \hbar^2 (1 - -3 \cos^2(\theta)/4\pi r^3)$ , where  $r$  and  $\theta$  are coordinates of the position vector connecting the spins, and  $\gamma_{NV} \simeq \gamma_N = 2\pi \times 2.8$  MHz/Gauss. One

method to bring the N and NV spins into resonance is to tune the static magnetic field to  $B_0 = 512$  gauss. At this value of the field, the energy difference between the  $|m_s = 0\rangle$  and  $|m_s = -1\rangle$  NV spin states is equal to that between the  $|m_s = -1/2, m_I = 0\rangle$  and  $|m_s = 1/2, m_I = 0\rangle$  N spin states, and thus the second term of  $H_{dip}$  induces a resonant flip-flop process. However, this tuned  $B_0$  technique fails when several N spins are strongly coupled to each NV (there are 10 to 1000 nitrogens per NV in typical diamond samples) because, at a given  $B_0$  field, only one of the five N hyperfine transitions is in resonance with the NV. For the more generally applicable dressed-state scheme introduced here, the NV and N spins are locked in a direction transverse to the static  $B_0$  field by controllable, continuous driving at microwave and RF frequencies, respectively. When the drive Rabi frequencies are matched, the NV and N spins are brought into resonance in a double-rotating frame, such that the dipolar Hamiltonian consists of only the first term of Eq. (41.2) [19]. This term  $\sim S_z^{NV} S_z^N$  is perpendicular to the spin-locking direction and can therefore induce flip-flops between the N and NV spins. The primary advantage of dressed-state resonant coupling is that by driving each N hyperfine transition in resonance with a multifrequency radiofrequency field, all the different N hyperfine-split transitions (5 in this case) can be simultaneously brought into resonance with the NV in the rotating frame, allowing coupling and polarization transfer from the NV to all N spins. By direct analogy, bright (optically active) NV spins can be coupled to other dark (nuclear or electronic) spins with different Zeeman energies by driving each spin transition in resonance, simultaneously, and with matched Rabi frequencies. Other advantages of dressed-state resonant coupling include (i) the ability to switch on and off the coupling and polarization transfer mechanism on nanosecond time scales (by rapid switching of the RF and/or microwave fields), and (ii) the ability to couple bright and dark spins at any value of  $B_0$ .

The pulse sequence employed for dressed-state resonant coupling is shown in Fig. 41.4a. The microwave power was adjusted to give a NV Rabi frequency of 8 MHz (matched to the N Rabi frequency). Measuring the NV spin-lock signal as a function of the duration of the spin-lock pulse with no RF signal applied, produces the rotating-frame spin-lattice relaxation time  $T_{1,\rho} = 290(50)$   $\mu$ s. The blue trace of Fig. 41.4b shows the first 50  $\mu$ s of this measured NV spin-lock signal. When the N spin bath was driven such that the collective Rabi frequency was also 8 MHz, a 100 times faster decay of the NV spin-lock signal was observed, for a rotating-frame spin lattice relaxation time under resonant-coupling conditions  $T_{1,\rho}^{RC} = 2.0(4)$   $\mu$ s, as shown by the red line of Fig. 41.4b. This dramatic effect demonstrates that the NV spins are much more strongly coupled to the N spin bath under the condition of matched N and NV Rabi frequencies. At dressed-state resonance, polarization may be transferred back and forth between the NV and the bath several times before the NV is completely depolarized. Thus while the time scale for each energy-conserving flip-flop is  $\sim T_2^*$ , the depolarization time scale can be much longer. Experimentally, depolarization was observed at a time scale  $T_{1,\rho}^{RC}$ , which is approximately equal to  $T_2$  in the lab (non-rotating) frame. Therefore, this scheme presents a useful experimental technique for cooling the N electronic spin bath using the NV as a refrigerator.

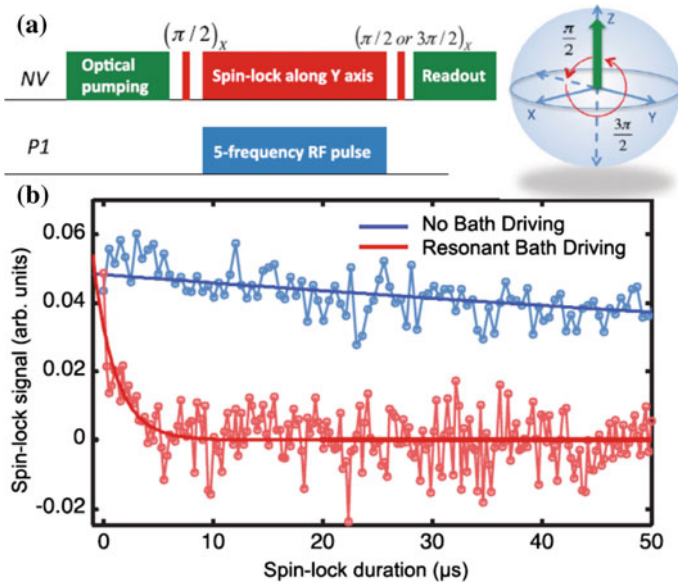
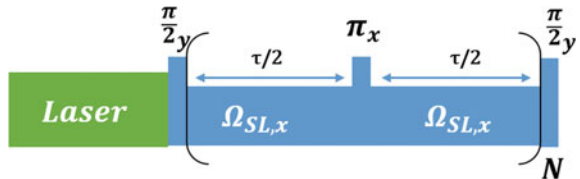


**Fig. 41.4** Measured dressed-state NV-N resonant coupling. **a** NV optical and microwave spin-lock sequence, and timing of five-frequency RF pulse to drive the N spin bath. After initializing NVs to the  $|m_s = 0\rangle$  state (Z axis) with a  $2\ \mu\text{s}$  optical pumping pulse,  $\pi/2$  and  $3\pi/2$  microwave pulses are applied along the X axis to rotate the spin to or from the equator of the Bloch sphere, and a microwave spin-locking pulse of variable duration is applied along the Y axis. To bring the N bath into a dressed-state resonance with the NV spins, a five-frequency RF pulse is applied during the spin-lock duration. **b** Measured decay of NV spin-lock signal as a function of spin-lock duration. When the N bath is not driven we recorded the blue trace. Driving the N bath simultaneously at all five electron spin resonances such that the collective N-bath Rabi frequency equals the NV Rabi frequency (8 MHz) produces the red trace, indicating strong NV spin depolarization caused by NV-N resonant coupling. The solid lines represent fits to decaying exponentials.

#### 41.3.1.2 Transfer Scheme 2: Coupling to a Nuclear Spin Bath

The ability to couple to more than one bath, i.e. to a nuclear spin bath in addition to the electronic spin bath presented above, strengthens the versatility of the NV platform in the context of quantum thermodynamic experiments, e.g. for studying the simultaneous coupling of a single quantum system to two different environments. There is an inherent difference between the cooling schemes relevant for electronic spins vs. nuclear spins, which stems from the very small gyromagnetic ratio of the nuclear spin compared to the electronic spin (approximately a factor of 1000 smaller). This weak magnetic interaction renders driving of the nuclear spins nearly impractical, and therefore the approach presented in the previous section for electronic spins is no longer viable. In this section other advanced control schemes are presented, allowing efficient polarization transfer from the NV to the nuclear spins, without requiring direct driving of these weakly coupled spins.

**Fig. 41.5** Schematic representation of the refocused-NOVEL sequence, as described in the main text.



NV based polarization of  $^{13}\text{C}$  nuclei in diamond can be achieved using the NOVEL (nuclear orientation via electron spin locking) scheme [20, 21], allowing for nuclear sensing [22] and bulk polarization [23]. During this sequence a spin lock [19] (SL) is applied on the NV spin with a SL Rabi frequency equal to the nuclear Larmor frequency, resulting in the rotating-frame or lab-frame Hartmann-Hahn polarization transfer condition. These NV based experiments are normally performed at relatively high fields (around 5000 G) to allow for efficient SL noise decoupling together with the Hartmann-Hahn condition. However, this relatively high magnetic field requires precise alignment of the field direction to that of the NV axis, in order to allow for the laser induced NV spin polarization to take place. NV based polarization transfer can also be obtained using an aligned magnetic field of 514 G [24], for which NV-nuclear state mixing occurs in the excited state, or at arbitrarily aligned fields, but based on the interaction of the NV to its close neighboring  $^{13}\text{C}$  nuclei [25].

A recently presented method [26] allows for coherent polarization transfer to remote nuclei (and therefore possibly also to nuclei outside of a diamond) at low fields ( $\ll 500$  G), for which field alignment is less demanding. This approach is important for quantum thermodynamic scenarios in which the central spin (the NV) is coupled to two spin baths, i.e. both an electronic spin bath (of N impurities) and a nuclear spin bath (of  $^{13}\text{C}$ ). Moreover, this scheme can be used for detecting the polarization of the bath, which can then be translated into its “effective spin temperature”. The relevant sequence is shown in Fig. 41.5. It is composed of three parts: (1) initialization, which includes a laser pulse for NV polarization and spin state detection, and a  $(\pi/2)$  preparation pulse; (2) the refocused-NOVEL (rNOVEL) sequence, which is composed of  $N$  repetitions of two SL pulses of duration  $(\tau/2)$ , separated by a  $\pi$  pulse of the same phase (unlike the refocused continuous-wave decoupling sequence [27, 28]); and (3), a detection  $(\pi/2)$  pulse, which can be added at different phases for optical detection of the NV polarization.

In order to describe the effect of this sequence we can consider a simple model spin system composed of the  $S = 1$  NV electron, limited to its  $|0\rangle, |-1\rangle$  subspace, and a spin  $I = \frac{1}{2}$  nucleus. The Hamiltonian of this system in the electronic rotating frame is given, assuming ideal  $\pi$  pulses for simplicity, by [19]:

$$H = \Delta_e S_z - \omega_n^0 I_z + A_{\parallel} S_z I_z + \frac{1}{2} S_z (A_{\perp} I^+ + A_{\perp}^* I^-) + b(t) S_z + \frac{1}{\sqrt{2}} \Omega_{SL} S_x + \sum_{k=1,3,5,\dots}^N \delta \left( t - \frac{1}{2} k \tau \right) \pi_x. \quad (41.3)$$

The above Hamiltonian includes the off-resonant irradiation on the electronic spin  $\Delta_e$ , the nuclear Larmor precession frequency  $\omega_n^0$ , the secular and pseudosecular terms of the hyperfine interaction  $A_{\parallel}$  and  $A_{\perp}$  respectively, external pure dephasing noise  $b(t)$ , and the MW irradiation term, given by the SL term with an amplitude of  $\Omega_{SL}$  and the ideal  $\pi_x$  pulses.

We can next transfer to the interaction frame of the ideal  $\pi$  pulses. This is given, for an even N, by a unitary transformation of the form  $U(t) = e^{\int_0^t dt i(\pi/\sqrt{2}) \sum_k \delta(t'-k\tau) S_x}$ . The resulting Hamiltonian is given by:

$$H^I = s(t) \left[ \Delta_e + A_{\parallel} I_z + \frac{1}{2}(A_{\perp} I^+ + A_{\perp}^* I^-) + b(t) \right] S_z - \omega_n^0 I_z + \Omega_{SL} S_x, \quad (41.4)$$

$$s(t) = \begin{cases} 1, & 0 \leq \text{mod}(t, 2\tau) < \frac{1}{2}\tau \\ -1, & \frac{1}{2}\tau \leq \text{mod}(t, 2\tau) < \frac{3}{2}\tau \\ 1, & \frac{3}{2}\tau \leq \text{mod}(t, 2\tau) < 2\tau \end{cases},$$

where  $s(t)$  is a periodic square wave, with a frequency of  $\omega_f = \pi/\tau$  (as in CPMG [29] and similar sequences) that can be expanded in terms of a Fourier Series:

$$s(t) = \sum_k s_k e^{ik\omega_f t}, \quad (41.5)$$

$$s_k = 2 \frac{(-1)^{\frac{k-1}{2}}}{\pi k},$$

with  $k = \pm 1, \pm 3, \dots$ . As can be seen,  $s_k$  decreases with increasing  $|k|$ .

In order to simplify the form of  $H^I$ , we can transfer to a rotating frame in  $S_x$ , with a frequency of  $k'\omega_f$ . Assuming that  $\omega_f \gg |\Delta_e + \frac{1}{2}A_{\parallel}| + b(t)|, |A_{\perp}|$  (at all times), we can neglect all the  $k \neq k'$  time-dependent terms. As such, the Hamiltonian can be written as:

$$H^R \approx s'_k \left[ \Delta' S_z + \frac{1}{2}(A_{\perp} I^+ + A_{\perp}^* I^-) S_z \right] - \omega_n^0 I_z + \Omega_k S_x, \quad (41.6)$$

where  $\Delta' = \Delta_e + A_{\parallel} I_z + b(t)$ , and  $\Omega_k = \Omega_{SL} - k'\omega_f$ . This reduces the Hamiltonian to a familiar form, with  $\Delta'$  and  $\Omega_k$  serving as effective detuning and irradiation terms on the  $S$  spin. As such,  $\Delta'$  will have little effect on the spin dynamics when  $s'_k \Delta' \ll \Omega_k$ , resulting in a decoupling of the undesired off resonance and noise effects. In addition, when  $\Omega_k \approx \pm \omega_n$ , with  $\omega_n = \omega_n^0 + \frac{1}{2}A_{\parallel}$  to first order, the NOVEL Hartmann-Hahn condition is met, and the  $A_{\perp}$  part of the hyperfine interaction will result in a polarization transfer between the electron and nucleus [21]. Higher  $k'$  values will lead to higher quenching of the interactions, resulting in narrower resonance conditions, lower dephasing and slower polarization transfer. We note that in the extreme case of  $\Omega_{SL} = 0$  or  $\omega_f \rightarrow 0$  (i.e. no  $\pi$  pulses), these conditions are identical to the ones used for CPMG based sensing [30] and spin-lock/NOVEL experiments, respectively.

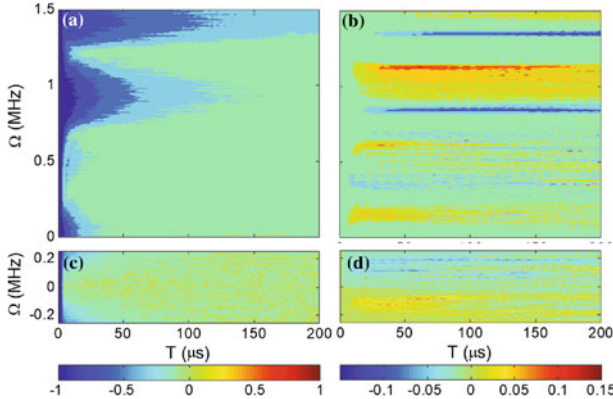


**Fig. 41.6** **a, c**  $\langle S_z \rangle$  and **b, d**  $\langle I_z \rangle$  as a function of  $N$  and  $\Omega_{SL}$  under dephasing noise, for the rNOVEL (**a, b**) and NOVEL (**c, d**) sequences.  $\tau = 2 \mu\text{s}$  was used, resulting in a total sequence duration of  $T = 2N \mu\text{s}$ . The noise source was modeled using correlation times of  $\tau_c = 11$  and  $150 \mu\text{s}$ , and  $\Delta_{\text{noise}}$  of  $0.5 \text{ MHz}$ . The value of  $b(t)$  was changed every  $0.1 \mu\text{s}$ , as described in the SM, and the plotted  $\langle S_z \rangle$  and  $\langle I_z \rangle$  values were obtained by averaging over 100 realizations of the noise. The simulation was performed using  $N = 60$ , on an NV- $^{13}\text{C}$  model system with  $A_{\parallel} = 30 \text{ kHz}$ ,  $A_{\perp}$ ,  $\Delta_e = 40 \text{ kHz}$ , and an external field of 80 Gauss.  $\tau = 2 \mu\text{s}$  was used, resulting in a total sequence duration of  $T = 2N \mu\text{s}$ .

Next we introduce the dephasing noise, including fast and slow noise components, characterized by correlation times  $\tau_c$  of  $11$  and  $150 \mu\text{s}$ , and with a coupling strength to the NV of  $\Delta_{\text{noise}} = 0.5 \text{ MHz}$  used in both cases. The resulting NV and nuclear polarizations are plotted in Fig. 41.6, using the same spin system as before, for the rNOVEL (**a, b**) and NOVEL (**c, d**) sequences.

In the NOVEL case, the low  $\Omega_{SL}$  power needed to polarize the nucleus is insufficiently strong to remove the effect of the decoherence noise. This results in a loss of NV polarization, leading to only  $\sim 6\%$  maximal polarization. In the rNOVEL sequence the effect of the noise on the NV polarization is reduced with  $k$ , as can be seen in Fig. 41.6a when comparing the different  $k$  conditions. This results in as much as  $\sim 13\%$  nuclear polarization, a factor of 2 higher than for the NOVEL case but still lower than in the ideal scenario, in which noise was not considered. Enhanced polarization could clearly benefit various applications such as in sensing [30] and cooling [22], and the high spectral resolution could contribute to selective addressing [31].

The limited nuclear polarization, as shown in Fig. 41.6, can be further increased by repeating the full sequence (Fig. 41.5)  $N$  times. As a result the maximal nuclear polarization (and the polarization rate) increases initially with  $N$ . However, using higher values result in a decrease in the maximal polarization. This can be explained by a decrease in the  $|\langle S_z \rangle|$  polarization, which remains mostly unchanged by the increasing nuclear polarization and is therefore governed mainly by the dephasing term in the Hamiltonian. For the NOVEL sequence the maximal nuclear polarization decreases with  $N$ , again due to the loss of NV polarization. This results in lower

maximal polarization when compared with the rNOVEL case. This highlights the advantage of the rNOVEL sequence over NOVEL due to its ability to tune down the effect of the dephasing noise value, therefore allowing for higher nuclear polarizations under noisy conditions.

### 41.3.2 Coherent Effects

The above-mentioned cooling processes might depart from regular thermodynamic considerations, specifically in the case of persistent coherence within the spin bath. For example, this is a realistic scenario for a nuclear spin bath since nuclear spins experience relatively slow dephasing and thus can maintain coherence for a significant duration.

Sustained coherence within the bath results in a build-up of non-classical, entangled states, which limits polarization transfer into the bath [32]. Intuitively, polarization transfer processes as described above, aimed at using the NV as a refrigerator to cool the spin bath, introduce a single decay channel for the NV-bath system, namely the NV optical pumping process. The existence of a single decay channel leads to the formation of coherent “dark states”, which eventually decouple from this decay and thus limit polarization transfer. For the special case of equal couplings between the NV and all bath spins, these dark states constitute the extreme angular states of the different Dicke State manifolds [33].

While such non-classical states could be of interest in their own right, they might hinder thermalization and the realization of quantum thermodynamic measurements. Nevertheless, they could be avoided through a modified polarization sequence in which each resonant polarization step is followed by a dispersive step, essentially suppressing the spin-lock to create  $I_z$  decoherence:

$$\begin{aligned} H_{res} &= \sum_k g_k^x (S^+ I_k^- + S^- I_k^+) \\ H_{disp} &= S^z \sum_k g_k^z I_k^z. \end{aligned} \quad (41.7)$$

Here  $S$  denotes NV operators and  $I_k$  denote operators of the  $k^{th}$  nuclear spin, and  $g_k^x$  is the flip-flop coupling of the NV to the  $k^{th}$  nuclear spin, while  $g_k^z$  is the corresponding dephasing coupling (Fig. 41.7a).

Figure 41.7b depicts the achieved polarization level in the nuclear spin bath as a function of the number of cooling steps, both for the regular polarization transfer process (red-dashed), and for the modified sequence including dispersive, decoherence steps (blue-solid).

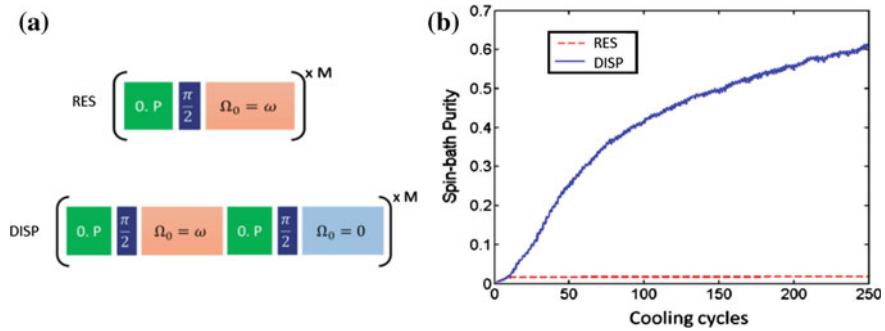


**Fig. 41.7** **a** The polarization transfer sequences (repeated  $M$ -times), depicted both for resonant coupling (top) and for interlaced dispersive coupling (bottom). **b** Spin-bath purity (polarization) as a function of cooling cycles for both resonant coupling (red-dashed) and dispersive (blue-solid) processes.

## 41.4 Prospects for Studies into Quantum Thermodynamics

The NV platform and the schemes presented above present prospects for novel research directions in the context of quantum thermodynamics. A few examples of such future directions are described below, demonstrating the potential of this experimental system to contribute to research in quantum thermodynamics.

### 41.4.1 Coupling to Two Spin Baths

The NV is naturally coupled to two disparate spin baths: the nitrogen electronic spins and the  $^{13}\text{C}$  nuclear spins. While coupling the NV selectively to each spin bath separately has been demonstrated [15, 22], experiments involving controlled coupling to both baths have not yet been realized. Such experiments could provide unique access to the thermodynamic scenario of coupling a quantum system (the NV spin) to two spin baths with different properties, with the capability of controlling these baths and the coupling separately. Clearly, such a system could be relevant for studying various thermodynamic machines, common cycles (such as Carnot), and expanded to explore non-trivial bath properties, such as memory and back-action.

### 41.4.2 Coupling Quantum Spins Through a Bath

The spin baths described in this chapter offer various levels of control, even at the level of sample fabrication. On the one hand, the nuclear spin bath naturally exhibits relatively weak interactions and slow decoherence times, thus providing sub-ensembles

with non-negligible memory effects. On the other hand, the nitrogen electronic spin bath can be “engineered” at the diamond sample fabrication level, e.g. by implanting nitrogen ions into an initial high-purity sample through nanometric masks, in order to create a spatially confined mesoscopic bath [34, 35]. This level of control paves the way for studies of quantum coupling between the NV quantum spin and the bath spins and beyond that, of coherent coupling between two or more NVs mediated by the bath. Such experiments could address questions related to non-Markovian bath dynamics, quantum state transfer [36], quantum dissipative dynamics and robust entanglement generation [37, 38], and more.

#### **41.4.3 Many-Body Effects: Many-Body Localization (MBL), Non-thermalizing States**

Ensembles of NV centers present a non-trivial spin bath with advantageous quantum properties, including efficient optical cooling (initialization) and long coherence times. High-density NV ensembles could provide access to the regime of coherent, many-body spin systems, if the timescale for interactions between NVs exceeds the NV decoherence time. In this regime the NV ensemble constitutes a quantum interacting many-body spin system, relevant for studies of open questions regarding the dynamics of such a system and its interaction with the environment. For example, the random distribution of NVs in the ensemble leads to an interplay between interactions and disorder, corresponding to the scenario of many-body localization (MBL) [39], which might lead to non-thermalizing states and insights into fundamental differences between classical and quantum thermodynamics.

**Acknowledgements** I gratefully acknowledge insights and valuable discussions with Ronald Walsworth, Chinmay Belthangady, Linh Pham, Fedor Jelezko, Paz London, Alex Retzker, Yonatan Hovav, Boris Naydenov and Demitry Farfurnik. I acknowledge support from the Minerva ARCHES award, the EU ERC Starting Grant (Project ID: 714005), the CIFAR-Azrieli Global Scholars program, Israel Ministry of Science, Technology and Space, and the Israel Science Foundation (Grant No. 750/14).

## **References**

1. M.W. Doherty, N.B. Manson, P. Delaney, J. Jelezko, L. Wrachtrup, L. Hollenberg, Phys. Rep. **528**(1) (2013). <https://doi.org/10.1016/j.physrep.2013.02.001>
2. J.M. Taylor, P. Cappellaro, L. Childress, L. Jiang, D. Budker, P.R. Hemmer, A. Yacoby, R. Walsworth, M.D. Lukin, Nat. Phys. **4** 810 (2008). <https://doi.org/10.1038/nphys1075>
3. J. Klatzow, J.N. Becker, P.M. Ledingham, C. Weinzel, K.T. Kaczmarek, D.J. Saunders, J. Nunn, I.A. Walmsley, R. Uzdin, E. Poem, [arXiv:1710.08716](https://arxiv.org/abs/1710.08716)
4. A. Barfuss, J. Teissier, E. Neu, A. Nunnenkamp, P. Maletinsky, Nat. Phys. **11**, 820 (2015). <https://doi.org/10.1038/nphys3411>

5. D.D.B. Rao, S.A. Momenzadeh, J. Wrachtrup, Phys. Rev. Lett. **117**, 077203 (2016). <https://doi.org/10.1103/PhysRevLett.117.077203>
6. M.J.A. Schuetz, E.M. Kessler, G. Giedke, L.M.K. Vandersypen, M.D. Lukin, J.I. Cirac, Phys. Rev. X **5**, 031031 (2015). <https://doi.org/10.1103/PhysRevX.5.031031>
7. D.A. Golter, T. Oo, M. Amezcua, I. Lekavicius, K.A. Stewart, H. Wang, Phys. Rev. X **6**, 041060 (2016). <https://doi.org/10.1103/PhysRevX.6.041060>
8. M. Kolář, D. Gelbwaser-Klimovsky, R. Alicki, G. Kurizki, Phys. Rev. Lett. **109**, 090601 (2012). <https://doi.org/10.1103/PhysRevLett.109.090601>
9. A. Levy, R. Alicki, R. Kosloff, Phys. Rev. E **85**, 061126 (2012). <https://doi.org/10.1103/PhysRevE.85.061126>
10. W.-L. Ma, G. Wolfowicz, N. Zhao, S.-S. Li, J.J.L. Morton, R.-B. Liu, Nat. Commun. **5**, 4822 (2014). <https://doi.org/10.1038/ncomms5822>
11. F. Reinhard, F. Shi, N. Zhao, F. Rempp, B. Naydenov, J. Meijer, L.T. Hall, L. Hollenberg, J. Du, R.-B. Liu, J. Wrachtrup, Phys. Rev. Lett. **108**, 200402 (2012). <https://doi.org/10.1103/PhysRevLett.108.200402>
12. B. Smeltzer, L. Childress, A. Gali, New J. Phys. **13**, 025021 (2011). <https://doi.org/10.1088/1367-2630/13/2/025021>
13. E. Reynhardt, G. High, Prog. Nucl. Magn. Reson. Spectrosc. **38**, 37 (2001). [https://doi.org/10.1016/S0079-6565\(00\)00025-X](https://doi.org/10.1016/S0079-6565(00)00025-X)
14. A. Jarmola, V.M. Acosta, K. Jensen, S. Chemerisov, D. Budker, Phys. Rev. Lett. **108**(197601) (2012). <https://doi.org/10.1103/PhysRevLett.108.197601>
15. C. Belthangady, N. Bar-Gill, L.M. Pham, K. Arai, D. Le Sage, P. Cappellaro, R.L. Walsworth, Phys. Rev. Lett. **110**, 157601 (2013). <https://doi.org/10.1103/PhysRevLett.110.157601>
16. E.L. Hahn, Phys. Rev. **80**, 580 (1950). <https://doi.org/10.1103/PhysRev.80.580>
17. M. Poggio, H.J. Mamin, C.L. Degen, M.H. Sherwood, D. Rugar, Phys. Rev. Lett. **102**, 087604 (2009). <https://doi.org/10.1103/PhysRevLett.102.087604>
18. E.C. Reynhardt, G.L. High, J. Chem. Phys. **109**, 4100 (1998). <https://doi.org/10.1063/1.477010>
19. C.P. Slichter, *Principles of Magnetic Resonance*, 3rd edn. (Springer, Heidelberg, 1990). <https://doi.org/10.1007/978-3-662-09441-9>
20. H. Brunner, R.H. Fritsch, K.H. Hausser, Zeitschrift für Naturforschung. J. phys. Sci. **42**, 1456 (1987)
21. A. Henstra, W.T. Wenckebach, Mol. Phys. **106**, 859 (2008). <https://doi.org/10.1080/00268970801998262>
22. P. London, J. Scheuer, J.-M. Cai, I. Schwarz, A. Retzker, M.B. Plenio, M. Katagiri, T. Teraji, S. Koizumi, J. Isoya, R. Fischer, L.P. McGuinness, B. Naydenov, F. Jelezko, Phys. Rev. Lett. **111**, 067601 (2013). <https://doi.org/10.1103/PhysRevLett.111.067601>
23. J. Scheuer, I. Schwartz, Q. Chen, D. Schulze-Sünninghausen, P. Carl, P. Höfer, A. Retzker, H. Sumiya, J. Isoya, B. Luy, M.B. Plenio, B. Naydenov, F. Jelezko, New J. Phys. **18**, 013040 (2016). <https://doi.org/10.1088/1367-2630/18/1/013040>
24. R. Fischer, C.O. Bretschneider, P. London, D. Budker, D. Gershoni, L. Frydman, Phys. Rev. Lett. **111**, 057601 (2013). <https://doi.org/10.1103/PhysRevLett.111.057601>
25. G.A. Álvarez, C.O. Bretschneider, R. Fischer, P. London, H. Kanda, S. Onoda, J. Isoya, D. Gershoni, L. Frydman, Nat. Commun. **6**, 8456 (2015). <https://doi.org/10.1038/ncomms9456>
26. Y. Hovav, B. Naydenov, F. Jelezko, N. Bar-Gill, Phys. Rev. Lett. **120**, 060405 (2018). <https://doi.org/10.1103/PhysRevLett.120.060405>
27. J.M. Vinther, A.B. Nielsen, M. Bjerring, E.R.H. van Eck, A.P.M. Kentgens, N. Khaneja, N.C. Nielsen, J. Chem. Phys. **137**, 214202 (2012). <https://doi.org/10.1063/1.4768953>
28. J.M. Vinther, N. Khaneja, N.C. Nielsen, J. Magn. Reson. **226**, 88 (2013). <https://doi.org/10.1016/j.jmr.2012.11.003>
29. S. Meiboom, D. Gill, Rev. Sci. Instrum. **29**, 688 (1958). <https://doi.org/10.1063/1.1716296>
30. S.J. DeVience, L.M. Pham, I. Lovchinsky, A.O. Sushkov, N. Bar-Gill, C. Belthangady, F. Casola, M. Corbett, H. Zhang, M. Lukin, H. Park, A. Yacoby, R.L. Walsworth, Nat. Nanotechnol. **10**, 129 (2015). <https://doi.org/10.1038/nnano.2014.313>

31. A. Ajoy, U. Bissbort, M.D. Lukin, R.L. Walsworth, P. Cappellaro, Phys. Rev. X **5**, 011001 (2015). <https://doi.org/10.1103/PhysRevX.5.011001>
32. D.D.B. Rao, D. Gelbwaser-Klimovsky, A. Ghosh, N. Bar-Gill, G. Kurizki, In Preparation (2018)
33. R.H. Dicke, Phys. Rev. **93**, 99 (1954). <https://doi.org/10.1103/PhysRev.93.99>
34. G. Jacob, K. Groot-Berning, S. Wolf, S. Ulm, L. Couturier, S.T. Dawkins, U.G. Poschinger, F. Schmidt-Kaler, K. Singer, Phys. Rev. Lett. **117**, 043001 (2016). <https://doi.org/10.1103/PhysRevLett.117.043001>
35. S. Pezzagna, D. Rogalla, H.-W. Becker, I. Jakobi, F. Dolde, B. Naydenov, J. Wrachtrup, F. Jelezko, C. Trautmann, J. Meijer, Physica Status Solidi (a) **208**, 2017 (2011). <https://doi.org/10.1002/pssa.201100455>
36. A. Ajoy, P. Cappellaro, Phys. Rev. Lett. **110**, 220503 (2013). <https://doi.org/10.1103/PhysRevLett.110.220503>
37. Y. Lin, J.P. Gaebler, F. Reiter, T.R. Tan, R. Bowler, A.S. Sørensen, D. Leibfried, D.J. Wineland, Nature **504**, 415 (2013). <https://doi.org/10.1038/nature12801>
38. S. Shankar, M. Hatridge, Z. Leghtas, K.M. Sliwa, A. Narla, U. Vool, S.M. Girvin, L. Frunzio, M. Mirrahimi, M.H. Devoret, Nature **504**, 419 (2013). <https://doi.org/10.1038/nature12802>
39. N.Y. Yao, C.R. Laumann, S. Gopalakrishnan, M. Knap, M. Müller, E.A. Demler, M.D. Lukin, Phys. Rev. Lett. **113**, 243002 (2014). <https://doi.org/10.1103/PhysRevLett.113.243002>